PROCEEDINGS OF THE IRE

Published Monthly by

The Institute of Radio Engineers, Inc.

VOLUME 43 — *October, 1955* — NUMBER 10

CONTENTS

Contents continued on following page

THE COVER—with this special SCATTER PROPAGATION issue, PROCEEDINGS OF THE IRE launches a brand new cover; a cover with a "Forward Look" to appear on each issue from this month on.

This month's cover shows two large high-gain antennas used by the Lincoln Laboratory of MIT for long-range scatter propagation tests. The paraboloidal antenna is employed for point-to-point uhf tropospheric transmission over distances of 620 miles. It measures 60 feet in diameter and has a gain of 34 db at 425 mc. Outlined in white is a 50 kw corner-reflector array used in vhf ionospheric propagation tests at 50 mc over a 1000-mile path between Round Hill, Mass., and Cedar Rapids, Iowa. The array, consisting of sixteen 90° corners mounted in two rows, stands 130 feet high and has a gain of 28 db.

MEMBER AUDIT BUREAU OF CIRCULATIONS

Change of address (with 15 days advance notice) and letters regarding subscriptions and payments should be mailed to the Secretary of the IRE, 1 East 79 Street, New York 21, N. Y.

PROCEEDINGS OF THE IRE

Published Monthly by

The Institute of Radio Engineers, Inc.

(*Continued*)

Advertising Section

FOREWORD

Four years ago this month the IRE inaugurated the practice of occasionally publishing a special issue of PROCEEDINGS devoted entirely to one topic of unusual importance and timeliness. These special issues have served to single out for PROCEEDINGS readers the major technical developments of our time and to provide them with an unusually valuable and comprehensive reference on these important subjects.

One such outstanding development has just recently emerged and, because of its great importance to the art of communications, it has been selected as the topic for this special issue—Scatter Propagation. The nature of scatter propagation and its practical significance are fully described in the following pages. Suffice it to note here that the material in these pages, released for publication just in the last three or four months, presents the results of over four years of intensive work on the subject.

Publication of this issue was undertaken under the joint sponsorship of the IRE Professional Group on Antennas and Propagation and the Scatter Communications Subcommittee of the Joint Technical Advisory Committee. We are most grateful to these organizations for their support and for the valuable assistance many of their members rendered individually to make this issue possible.

A special vote of thanks goes to Jerome B. Wiesner, Director of the Research Laboratory of Electronics at MIT, on whose shoulders fell the formidable task of organizing this issue, and to Kenneth A. Norton, Chief of the Radio Propagation Engineering Division of the Boulder laboratories of the National Bureau of Standards, who shared the heavy burden of planning the contents and procuring, reviewing, and selecting the material. Their competent and energetic efforts have produced a major and lasting contribution to the technical literature.

—*The Editor*

The Scatter Propagation Issue

In selecting papers for this issue, we have attempted to present an over-all picture of the present theoretical and experimental state of the techniques of scatter propagation. Particular emphasis has been laid on information that will facilitate system design employing these new propagation techniques. Recent experiments have demonstrated that it is possible to achieve very reliable "beyond-the-horizon" (scatter) radio communication in both the vhf and uhf regions of the spectrum. There has been, therefore, extensive re-examination of existing data, as well as increasing propagation research, primarily to provide necessary information for the design of scatter communication systems.

This collection of papers discusses two distinctly different modes of transmission which have been announced recently. The first mode, *ionospheric*, is communication by means of radio waves scattered, it is believed, from the lower *E*-layer of the ionosphere. This phenomenon permits communication in the frequency range from 25 to approximately 60 mc, and over distances extending from approximately 600 to 1,200 miles. Such circuits have so far been limited to use with teletype or voice intelligence. The second mode, *tropospheric*, is propagation by means of the scattering of electromagnetic waves by the troposphere. This phenomenon is, to a first approximation, independent of frequency; it appears to be useful for communication purposes over the frequency band extending from 100 to at least 10,000 mc.

Although it has been commonly believed that vhf and uhf radio transmission were limited to the line-of-sight distances, evidence to the contrary had been noted by early workers. In retrospect, Eckersley's work anticipated the ionospheric scatter effect, and Marconi found evidence in his short-wave experiments which led him to believe that with adequate power and a more sensitive receiver he could transmit beyond the optical line of sight. In 1932 Marconi wrote, in a paper published in the Proceedings of the Royal Institution of Great Britain, "*In regard to the limited range of propagation of these microwaves, the last word has not yet been said. It has already been shown that they can travel round a portion of the earth's curvature, to distances greater than had been expected, and I cannot help reminding you that at the very time when I first succeeded in proving that electric waves could be sent and received across the Atlantic Ocean in 1901, distinguished mathematicians were of the opinion that the distance of communications, by means of electric waves, would be limited to a distance of only about 165 miles.*" The propagation field has now caught up with Marconi's vision.

Speculations which led to the discovery of the ionospheric scatter communication were actually stimulated by discussions in 1950 regarding the use of tropospherically scattered signals. Thus the two completely separate techniques developed simultaneously. This has resulted unfortunately in a continuing confusion of the two techniques. Readers are therefore cautioned to note carefully the very different natures, capabilities, and limitations of the two phenomena involved.

Even though the existence of the scatter signals at great distances is well established, common agreement is lacking on the physical mechanism by which they are propagated. In the case of the tropospherically propagated uhf signals, most investigators attribute the presence of these fields, whose strengths greatly exceed the expected diffraction fields, to scattering from turbulent "blobs" in the atmosphere. However, some theorists believe that a partial reflection from a smooth atmosphere, the density of which varies with height, would by itself account for such signals. Unfortunately, the mathematical problems involved in obtaining an analytical solution of this model present great difficulty, and the conflict between these two points of view has not been completely resolved.

In the case of the ionospherically propagated waves, the same two explanations have been proposed; in addition, a third has been offered. Some investigators maintain that the fields detected at great distances are due to forward scattering of radio waves by meteor trails at *E*-layer height, trails caused, according to this theory, by cosmic dust that bombards the earth in great quantities.

The newly exploited propagation techniques discussed in these papers make possible extremely reliable communication over distances of 100 to 1,000 miles, distances formerly considered too short for good ionospheric propagation and too long for conventional vhf or uhf transmission.

—Kenneth A. Norton and Jerome B. Wiesner

Characteristics of Beyond-the-Horizon Radio Transmission*

KENNETH BULLINGTON†, FELLOW, IRE

Summary—**This paper summarizes the principal characteristics of tropospheric transmission beyond the horizon and compares them with some of the properties of ionospheric scatter transmission. Quantitative results are given on the dependence of the average signal level on distance and frequency, fading phenomena, bandwidth capabilities and realizable antenna gain. A short historical summary of beyond-horizon tropospheric transmission is also included.**

Introduction

DURING THE past five years, it has been definitely established that useful radio signals at all frequencies can be received consistently at distances far beyond the horizon. These facts have forced a considerable modification of the theories, concepts, and charts found in most textbooks and handbooks. Even more important, these facts have opened up many interesting radio possibilities, particularly in the field of fixed point-to-point communication.

This relatively long distance transmission has been called by various names, such as beyond-the-horizon or extended range transmission, but perhaps it is most generally known by the term, "scatter." It is important to note that the word "scatter" is used in a specialized sense which is actually closer to the layman's concept of reflection than it is to the opposite concept of scattering in all directions. More recently, the term, "forward scatter" has been used in an attempt to minimize this language difficulty. In this paper, the phrase "beyond-the-horizon transmission" will ordinarily be used because it is a descriptive term which does not imply a mechanism.

The situation in beyond-horizon transmission is similar to the old argument about an irresistible force and an immovable body. Until a few years ago, the general feeling was that the barrier to beyond-the-horizon transmission was immovable, so why try? Now we know that this obstruction, although difficult, is not impossible to overcome and the race is on for higher power and larger antennas.

There are two different types of beyond-horizon or scatter transmission. One type is the ionospheric scatter which is useful for telegraph signals at frequencies below about 50 mc for distances up to a thousand miles or more. The second type is tropospheric transmission which is useful over a very wide band of frequencies but is limited in distance to a few hundred miles.

* Original manuscript received by the IRE June 21, 1955; revised manuscript received, July 27, 1955. This paper was presented at the IRE Convention, March 23, 1955.

† Bell Telephone Labs., Inc., New York, N. Y.

This paper compares the two types but is concerned primarily with the second type, that is, tropospheric transmission. The available experimental data are summarized with a minimum of theoretical interpretation. It is shown that the phenomena observed beyond the horizon are a logical extension of well-known phenomena observed on line-of-sight paths. In other words, nature is continuous and perhaps more can be learned by looking at the similarities than by assuming that line-of-sight and beyond-the-horizon transmission are essentially separate phenomena.

History of Tropospheric Transmission Beyond-the-Horizon

The problem of diffraction of radio waves around a smooth spherical earth was first solved mathematically by Watson in 1919 but it was nearly 20 years before it was put in a form suitable for numerical computations by Van der Pol and Bremmer.[1,2] The smooth sphere theory predicts an exponential decrease in signal level beyond the horizon of about 1.2 db per mile at 500 mc and 2.4 db per mile at 4,000 mc. In the experimental side, Marconi talked over a distance of 168 miles at about 500 megacycles in 1932.[3] However, this circuit was not reliable because of its low power and small antennas and such reports of occasional long distance transmission were assumed to be unusual phenomena like mirages in the case of light.

By the early 1940's the smooth sphere theory was generally accepted but it had not been proved for points far beyond the horizon. The basic assumptions of the smooth sphere theory (outside of mathematical approximations) are that the earth is a perfectly smooth sphere and that the atmosphere is perfectly uniform. In addition, it is assumed that the use of an effective earth's radius (such as 4/3 of the true earth radius) to correct for average atmospheric refraction does not affect the accuracy of the basic theory.

Although the smooth sphere theory was generally accepted, experimental observations by several independent investigators indicated that vhf signals re-

[1] G. N. Watson, "The diffraction of electric waves by the earth," *Proc. Roy. Soc.*, London, A, vol. 95, pp. 83–89; October, 1918; and pp. 546–563; July, 1919.

[2] B. Van der Pol and H. Bremmer, "The diffraction of electromagnetic waves from an electrical point source round a finitely conducting sphere, with applications to radio telegraphy and the theory of the rainbow," *Phil. Mag.*, ser. 7, vol. 24, pp. 141–175; July, 1937; pp. 825–864; November supplement, 1937; also vol. 25, pp. 817–834; June supplement, 1938; and vol. 27, pp. 261–275; March, 1939.

[3] G. Marconi, "Radio communication by means of very short electric waves," *Proc. Roy. Inst. Great Britain*; December, 1932.

ceived at points far beyond the horizon faded over wide ranges.[4–6] This fading was generally attributed at the time to the presence of signals reflected from sharp gradients in the refractive index of the troposphere. The existence of such vhf tropospheric waves was sufficiently well known by 1940 that predictions of the field intensity to be expected by reflections from tropospheric layers were presented to the Federal Communication Commission at the same time as the smooth sphere theory.[7] Also at the same hearing, short term measurements on a number of paths at frequencies in the 40–50 mc band were presented to show the departures from the smooth sphere predictions.

During the war years, higher power tubes and larger antennas were developed at increasingly higher frequencies. Radar ranges much greater than expected were occasionally observed at both hundreds and thousands of megacycles. At the same time communication equipment, working primarily at frequencies below 100 megacycles, also showed greater range than would have been predicted by the smooth sphere theory. The concept of an atmospheric duct or waveguide caused by special meteorological conditions (mirages) was introduced to explain these effects. As more and more observations were reported it became clear that long distance transmission occurred much more frequently than the meteorological effects required by the duct theory.

Also during the war years and immediately thereafter, numerous long term tests were conducted in the frequencies of the 40–50 mc band.[8] Most of these data were collected by the FCC and made generally available in 1948.[9] A general review of results in the 40–100 mc band was given in 1948 in which it was postulated that the persistent tropospheric fields unexplainable in terms of duct propagation were caused by reflections from many small discontinuities in the refractive index of the atmosphere.[10] It was also pointed out that the median signal received at points far beyond the horizon could not be explained by modifying the effective earth radius since the data could not be fitted to an exponential law.[11]

At frequencies in the thousands of megacycles short term measurements over sea-water showed relatively strong signals even when no ducts were present.[12,13] Unpublished reports of 1948 investigations of interference between microwave radio relay stations showed a similar long distance transmission phenomenon over land.

Until the late 1940's there was little expectation that this long distance transmission could be used for reliable communication purposes; rather it was looked upon primarily as a source of interference. One sign of the times was the 1949 "freeze" on new television stations which was brought about because the co-channel interference proved to be much greater than had been expected from the allocation plan based on the smooth sphere theory.

While most of the data available by 1950 were in the lower vhf or shf ranges, similar long distance results had also been obtained in the intermediate range around 400 mc.[14] Each bit of data taken by itself seemed erratic and baffling. However, taken collectively all the data from 40 to 4,000 mc showed that the received signal was much stronger than could be accounted for by the existing theories and the long term data in the 40–50 mc band showed that the lower frequencies at least could be received consistently at distances of 200–300 miles. The implications of these results throughout the frequency spectrum led in 1950 to a definite program to investigate the usefulness and reliability of microwave transmission beyond the horizon.[15] The conclusions of this investigation were presented at the 1952 IRE Convention and have proved useful for subsequent engineering purposes.[16]

Many individuals and several organizations including National Bureau of Standards, Lincoln Laboratory of MIT and Bell Telephone Laboratories among others have been active in this field. Nevertheless, experimental data have accumulated relatively slowly because such tests require high power, large antennas and a relatively long and expensive testing program. On the other hand, theoretical speculation is relatively inexpensive and it was inevitable that similar or related ideas occurred in a relatively short time to many individuals working independently. For this reason it is very difficult to write a history of this period that provides proper individual credit.

On the theoretical side, the basic assumption of a perfectly smooth sphere has been questioned many times, but the mathematical difficulties in estimating

[4] Ross Hull, *Q.S.T.*, vol. 21, p. 16; May, 1937.

[5] C. R. Englund, A. B. Crawford, and W. W. Mumford, *Bell. Sys. Tech. Jour.*, vol. 17, pp. 489–519; October, 1938.

[6] K. G. Maclean and G. S. Wickizer, "Notes on the random fading of 50 mc signals over nonoptical paths," PROC. IRE, vol. 27, pp. 501–506; August, 1939.

[7] K. A. Norton, "A theory of tropospheric wave propagation," and "The calculation of ground wave field intensity over a finitely conducting spherical earth."

K. A. Norton and E. W. Chepin, "Field intensity survey of ultra high frequency broadcasting stations," FCC Hearing on Matter of Aural Broadcasting on Frequencies Above 25,000 Kilocycles; March 18, 1940.

[8] G. N. Pickard and H. T. Stetson, "Tropospheric reception at 42.8 mc and meteorological conditions," PROC. IRE, vol. 35, pp. 1445–1450; December, 1947.

[9] TID Report 2.4.5, "Summary of Tropospheric Propagation Measurements and the Development of Empirical Propagation Charts." FCC (27989); October 20, 1948.

[10] K. A. Norton, "Propagation in the FM Broadcast Band," Advances in Electronics, Academic Press, vol. I, pp. 381–421, 1948.

[11] K. Bullington, "Radio propagation variations at vhf and uhf," PROC. IRE, vol. 38, pp. 27–32; January, 1950.

[12] M. Katzin, R. W. Bauchman and W. Binnian, "3- and 9-centimeter propagation in low ocean ducts," PROC. IRE, vol. 35, pp. 891–905; September, 1947.

[13] E. C. S. Megaw, "Scattering of electromagnetic waves by atmospheric turbulence," *Nature*, vol. 166, p. 1100; December, 1950.

[14] I. H. Gerks, "Propagation at 412 megacycles from a high-power transmitter," PROC. IRE, vol. 39, pp. 1374–1382, November, 1951.

[15] K. Bullington, "Propagation of uhf and shf waves beyond the horizon," PROC. IRE, vol. 38, pp. 1221–1222; October, 1950.

[16] K. Bullington, "Radio transmission beyond the horizon in the 40- to 4,000-mc Band," PROC. IRE, vol. 41; pp. 132–135; January, 1953.

the effects of roughness have not been solved. It is interesting to note that the experimental data fall in between two diverging theoretical curves which give the diffraction loss over either a smooth sphere or a knife edge. At points far beyond the horizon the two diffraction losses differ by tens and even hundreds of decibels, so the two computations serve only to emphasize that diffraction calculations depend very critically on the assumed path profile. The most recent application of the knife edge diffraction curve has been in the "obstacle gain" theory, which fits the exceptional path where the profile approaches a knife edge but which cannot be expected to fit the average or typical path.[17]

The basic assumption of a uniform atmosphere has been questioned by the scattering theories.[18–23] The index of refraction of the atmosphere is slightly greater than unity near the surface of the earth, and must be equal to unity at very high elevation. The uniform decrease in refraction with height is accounted for by the concept of an effective earth's radius of 4/3 times the true earth's radius. However, the turbulence of the air superimposes many random irregularities which have been called scatterers, "blobs," or radio clouds. At first it was assumed that the blobs were small compared with the wavelength. However, it was soon recognized that the size of the blobs must be large compared with the wavelength in order to explain the vhf as well as the shf results, and measurements of the index of refraction have tended to confirm this assumption.[24,25] In addition to the physical size of the blobs, the magnitude of the change in the index of refraction and the distribution of the size, number and magnitude of the blobs in both space and time are needed to calculate radio transmission phenomena.

The third basic assumption in the application of the smooth sphere theory is that the use of an effective earth radius to account for the average refraction in the earth's atmosphere does not change the basic accuracy of the theory. This assumption is questioned in the internal reflection theory which maintains that the decrease in air density due to gravity not only refracts the radio waves but also reflects a small portion of this energy back to earth.[26–28] It is maintained that these internal reflected signals add in a more favorable manner than does the normally diffracted signal (around a perfect sphere) so that the internal reflected components become controlling at points far beyond the horizon. Internal reflections do occur in a stratified medium with sharp discontinuities. Whether or not such reflections occur in a continuously varying medium involves a mathematical controversy that has not yet been completely resolved.

The fading in signal level with time must be caused by variations in the atmosphere. On the other hand, the theoretical explanation of the average signal level has not yet been definitely established, but considerable experimental data are now available for engineering purposes.

Variations with Distance and Frequency

The variation of average signal level with distance is shown on Fig. 1. The ordinate is in terms of db below the value that would be expected at the same distance in free space with the same power and same antennas.

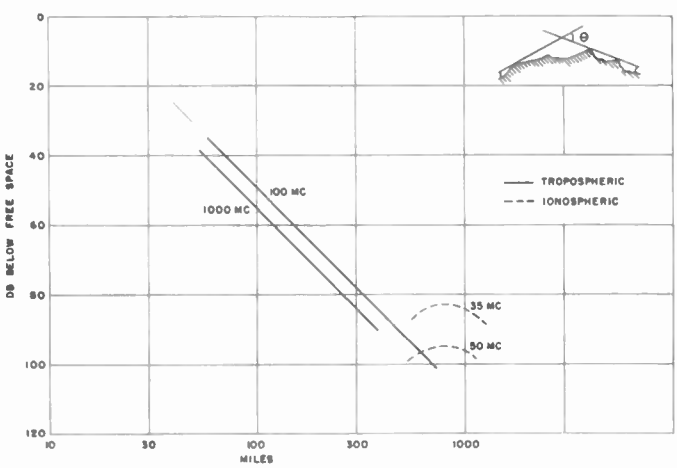

Fig. 1—Beyond-horizon transmission, median signal level vs distance.

At distances less than about 300–400 miles, the transmission is definitely tropospheric. The strongest signals are obtained by pointing the antennas at the horizon

[17] F. H. Dickson, J. J. Egli, J. W. Herbstreit and G. S. Wickizer, "Large reductions of vhf transmission loss and fading by the presence of a mountain obstacle in beyond-line-of-sight paths," Proc. IRE, vol. 41, pp. 967–9; August, 1953.

[18] C. L. Pekeris, "Note on scattering in an inhomogeneous medium," *Phys. Rev.*, vol. 71, p. 268; February, 1947.

[19] H. G. Booker and W. E. Gordon, "Theory of radio scattering in the troposphere," Proc. IRE, vol. 38, pp. 401–412; April, 1950.

[20] Harold Staras, "Scattering of Electromagnetic Energy in a Randomly Inhomogeneous Atmosphere," *Jour. Appl. Phys.*, vol. 23, p. 1152; October, 1952.

[21] S. O. Rice, "Radio field strength statistical fluctuations beyond the horizon," Proc. IRE, vol. 41, pp. 274–281; February, 1953.

[22] J. W. Herbstreit, K. A. Norton, P. L. Rice, and G. E. Schafer, "Radio wave scattering in tropospheric propagation," 1953 Convention Record of the IRE, Part II, "Antennas and Communications," pp. 85–93.

[23] W. E. Gordon, "Radio scattering in the troposphere," Proc. IRE, vol. 43, pp. 23–28, January, 1955.

[24] C. M. Crain, A. W. Straiton and C. E. von Rosenberg, "Atmospheric refractive-index fluctuations as recorded by an airborne microwave refractometer," Trans. IRE, vol. AP-1, pp. 43–46; October, 1953.

[25] H. E. Bussey and G. Birnbaum, "Measurement of variations in atmospheric refractive index with an airborne microwave refractometer," *Jour. Res. Nat. Bur. of Standards*, vol. 51, pp. 171–178; October, 1953.

[26] J. Feinstein, "Tropospheric propagation beyond the horizon," *Jour. Appl. Phys.*, vol. 22, pp. 1292–1293; October, 1951. An early suggestion that internal reflections might explain beyond-the-horizon transmissions was made in this article, but Feinstein later abandoned this theory, as may be seen below.

[27] J. Feinstein, "Gradient reflections from the atmosphere," Trans. IRE, vol. AP-4, pp. 2–13; December, 1952.

[28] T. J. Carroll and R. M. Ring, "Propagation of short radio waves in the normally stratified troposphere," presented at the General Assembly of the International Scientific Radio Union (URSI), Commission II, The Hague, Netherlands, August 23–September 2, 1954

along the great circle route. At distances greater than about 600 miles, the ionospheric and meteoric components seem to dominate, at least in the lower vnf band. The principal feature is that the tropospheric transmission decreases rapidly with increasing distance while the ionospheric transmission is weak but relatively independent of distance. With regard to frequency, the situation is reversed. Tropospheric transmission decreases relatively slowly with increasing frequency, while in the ionospheric case there is a big difference between 35 and 50 mc and frequencies greater than 60–70 megacycles are not likely to prove useful. The transition from one type to another is a gradual one and no drop-outs have been found at the intermediate distances around 500 miles. The figures shown on this chart are average values and it is necessary to point out that substantial variations are to be expected from hour to hour as well as with location, climate and season. The basic data supporting these generalizations have been obtained from many sources. The variations caused by terrain can be reduced by plotting the results as a function of the angle between the major lobes of the transmitting and receiving antennas as illustrated in Fig. 1.[29] However, for the present purpose the simpler coordinate of distance is easier to interpret.

This same information is shown as a function of frequency on Fig. 2. In this case the ionospheric transmission is shown on the left. At low frequencies, the level

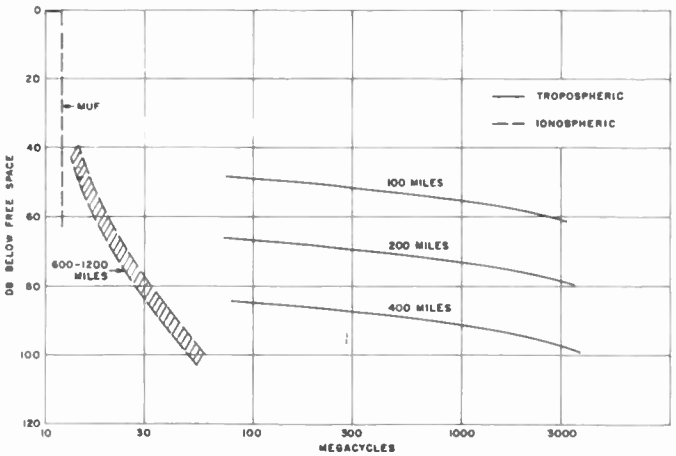

Fig. 2—Beyond-horizon transmission, median signal level vs frequency.

of the ionospheric (sky-wave) signals are close to the free space values. As the frequency is raised above the maximum usable sky wave frequency, (muf), the signal level drops rapidly. The early assumption was that the signal dropped out completely. Now we know that this curve is not discontinuous but that there is a floor below which the signal does not fall. The floor is now known as ionospheric scatter transmission. This type of transmission is discussed more completely elsewhere and the remainder of this paper will be limited to tropospheric transmission.

The information on tropospheric transmission shown on the right of Fig. 2 indicates once again that these signals depend on distance but decrease relatively slowly with frequency.

Fading Phenomena

The fading of tropospheric radio signals can be divided into two principal types: fast fading and slow fading. The fast fading is caused by multipath transmission in the atmosphere and the rate of this fading increases as either the frequency or distance is increased. The depth of fading ordinarily does not exceed the Rayleigh distribution, which is shown by the solid line

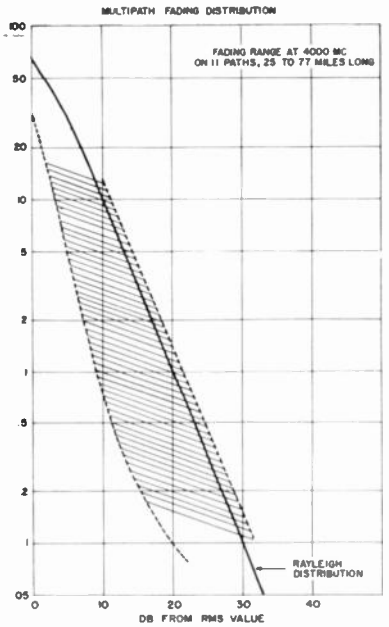

Fig. 3—Multipath fading distribution.

on Fig. 3. For example, a 20-db fade is expected about one per cent of the time and a 30-db fade for only one-tenth of one per cent of the time. The multipath or fast fading characteristic is one of the principal reasons why this type of transmission has been called "scatter." However, multipath transmission is also the principal cause of fading on good line-of-sight paths. The cross-hatched area on the chart shows the range of monthly fading distributions at 4,000 megacycles on eleven typical line-of-sight paths ranging from 25 to 77 miles in length. At frequencies below 4,000 megacycles, the fading rate on good optical paths becomes progressively slower until it is difficult to distinguish it from the second general type of fading that has been called slow fading.

Slow fading means variations in signal level over a period of hours or longer and it occurs within the horizon

[29] K. A. Norton, "The role of angular distance in tropospheric radio wave propagation," presented at the Western Electronic Show and Convention, San Francisco, Calif.; August 19–21, 1953.

as well as on paths beyond-the-horizon. This type of fading is almost independent of frequency and seems to be associated with changes in the average refraction in the atmosphere. Forty db fades of this type are rare on a good optical path but they have occurred. At points far beyond the horizon the variation in hourly median values follows a normal probability law in decibels with a standard deviation of about 8 db; it is also true, however, that larger variations occur on paths that are more nearly grazing.

Echo Delay—Useful Bandwidth

The fast fading or multipath phenomena mean that the signal contains one or more echoes. Echoes cause selective fading, which in turn causes distortion in telephone channels or ghosts in television pictures. However, these effects are not troublesome as long as the echo time delays are very short in comparison with one cycle of the highest baseband frequency to be transmitted.

It turns out that for the same size antennas, the useful bandwidth at points far beyond the horizon is at least one-tenth of the corresponding bandwidth for 30-mile line-of-sight path. By using narrow beam antennas, which are needed anyway for gain purposes, useful bandwidths of several megacycles can be obtained. This is illustrated on Fig. 4. The ordinate shows the maximum delay to be expected for strong echoes in free space. The delay time shown is the difference in travel time between the direct ray and a delayed signal that leaves the transmitting antenna and enters the receiving antenna at the 3 db points on their respective antenna patterns. For example, on a 30-mile path with 40-db antennas, the maximum computed time delay for strong echoes is about 16 millimicroseconds. Measurements of selective fading under these conditions are in good agreement with these values and have shown that the maximum delay (of strong echoes) does not exceed 6 to 10 millimicroseconds. The experimental values are shown by the crosses on the chart.[30,31] These conditions are typical of the various links along the transcontinental microwave radio relay system which is now providing an acceptable service of transcontinental television. In other words, echo delays of at least 10 millimicroseconds can be tolerated for the transmission bandwidths now in use. The corresponding frequency separation needed for adequate frequency diversity is shown on the right side of Fig. 4.

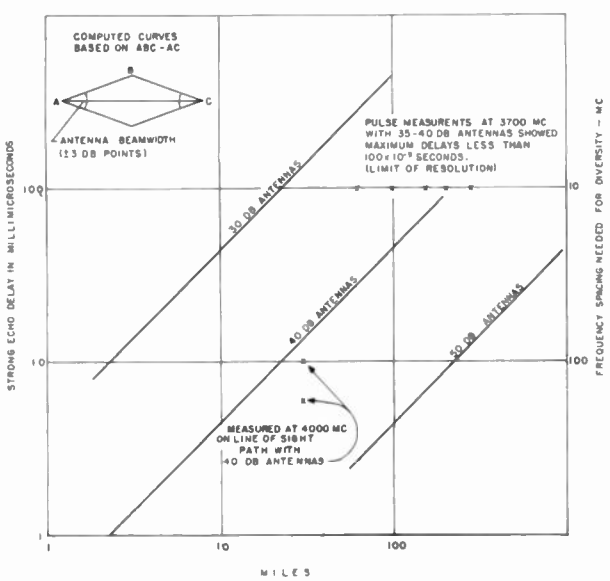

Fig. 4—Maximum delay of strong echoes (<6 db below principal component)

As the distance increases, the maximum echo delay will increase for a given size antenna. In going beyond the horizon, the delay may increase even more rapidly than this simple picture indicates. This more rapid increase was predicted in a recent paper by deBettencourt and Booker.[32] Nevertheless, pulse tests at distances of 75–200 miles have shown that the maximum delays of strong echoes are less than the resolution capability of the equipment which was approximately 100 millimicroseconds. Moreover, these results were obtained with 35–40 db antennas, which indicates that the maximum delay on 150-mile path is less than ten times that observed on good line-of-sight paths. The high gain antennas that are needed for gain purposes in beyond-the-horizon transmission will tend to reduce the delay time. Consequently, it is expected that useful bandwidths of several megacycles can be obtained beyond the horizon with 45–50 db antennas.

The actual situation is complicated by aircraft reflections and other factors not included in this simple picture, but the essential point is that transmission beyond the horizon does not automatically mean a drastic reduction in useful bandwidths. Some pictures of television transmission on a 188 mile path at 5,000 mc are shown in a companion paper.[33]

Antenna Gain

Another problem that is important in beyond-the-horizon transmission concerns the amount of antenna gain that can be realized. The presence of multipath fading indicates that the phase front of the radio signal is not uniform. When these variations are appreciable over the face of the antenna, it cannot deliver its full theoretical gain. This problem also exists on line-of-sight paths although to a lesser degree. Angle of arrival measurements on optical paths have shown some com-

[30] A. B. Crawford and W. C. Jakes, "Selective fading of microwaves," *Bell Sys. Tech. Jour.*, vol. 31, pp. 68–90; January, 1952.

[31] R. L. Kaylor, "A statistical study of selective fading of super high frequency radio signals," *Bell Sys. Tech. Jour.*, vol. 32, pp. 1187–1202; September, 1953.

[32] H. G. Booker and J. T. deBettencourt, "Theory of radio transmission by tropospheric scattering using very narrow beams," Proc. IRE, vol. 43, pp. 281–290; March, 1955.

[33] W. H. Tidd, "Demonstration of bandwidth capabilities of beyond-horizon tropospheric radio propagation," pp. 1297–1299, this issue.

ponents of the signal arriving at angles as much as 0.75 degrees from the expected direction.[34,35] This variation is comparable to the beamwidth of a 40-db antenna. In other words, even on a line-of-sight path, an antenna whose gain is considerably greater than 40 db will lose some of its theoretical gain during fading conditions. This experimental fact was one consideration in the choice of 40-db antennas for the transcontinental microwave radio relay system.

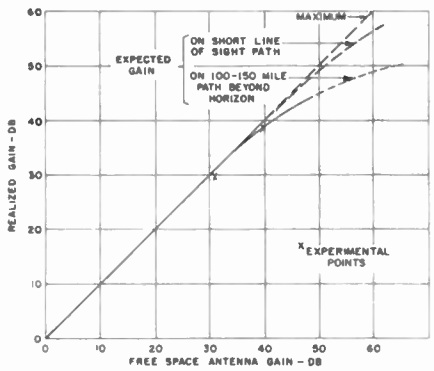

Fig. 5—Median antenna gain realized on paths with adequate foreground clearance.

On paths beyond the horizon, the fading exists all the time and high-gain, narrow-beam antennas may not be as efficient as on a short line-of-sight path. However, experimental data on 150–200 mile paths show that a 40-db antenna does not, on the average, lose more than 1 or 2 db of its theoretical gain. The estimated gain that can be realized on a long path is compared on Fig. 5 with the gain of the same antenna on a very short free space path. For large antennas, the average realized gain is expected to increase more slowly than the theoretical gain as shown by the dash line on the chart. For example, an antenna that provides 50-db gain on a short line-of-sight path may realize only about 45 db on a 200-mile path.

[34] W. M. Sharpless, "Measurements of the angle of arrival of microwaves," PROC. IRE, vol. 34, pp. 837–845; November, 1946.
[35] A. B. Crawford and W. M. Sharpless, "Further observations of the angle of arrival of microwaves," PROC. IRE, vol. 34, pp. 845–848; November, 1946.

CONCLUSION

This review of the principal characteristics of tropospheric transmission indicates that the differences between line-of-sight and beyond-the-horizon transmission are not as great as has been commonly believed. Until a few years ago, the general expectations were that, first, the beyond-horizon signal would not be reliable, second, it could not be used effectively because antennas would not realize their free space gain, and, third, the useful bandwidth would be very small. All of these doubts had a logical basis and contained an element of truth, but these fears have been exaggerated. Beyond horizon circuits can be made reliable with adequate engineering. The maximum useful antenna size is determined at the present time more by mechanical and economic factors than it is by radio propagation. The useful bandwidth can be several megacycles and is limited at the present time more by first circuit noise than it is by echo or scattering phenomena.

These new techniques open up new possibilities, particularly for point-to-point circuits over difficult terrain. It is expected that the use of beyond horizon circuits will supplement but not replace line-of-sight systems. It is now clear that reliable point-to-point radio circuits can be engineered for path lengths of 150 miles or more to provide good quality multichannel voice circuits or possibly even television for radio relay purposes. Such circuits require high power and large antennas but they are technically feasible.

Radio Transmission at VHF by Scattering and other Processes in the Lower Ionosphere*

D. K. BAILEY†, R. BATEMAN†, MEMBER, IRE, AND R. C. KIRBY†, SENIOR MEMBER, IRE

Summary—The results of a program extending over the last four and one-half years to investigate the nature and characteristics of high-loss regular VHF propagation by means of the lower ionosphere are presented. For the most part continuous-wave transmissions are employed, with the result that the effects of the different elements in the propagation are superposed. Three different ionizing agents operating in the lower ionosphere can be distinguished by means of their differing effects on the behavior of the signal, after the exclusion of behavior associated with sporadic-*E* propagation. They are solar radiation, corpuscular radiation presumably of solar origin, and meteors. The part played by each of these is discussed in the account and interpretation of the principal results obtained. Both short- and long-term characteristics of the observed composite signals are described, as well as the results of experiments with spaced and other antenna arrangements. The intensity and nature of the signals are discussed as a function of time of day, season, geographical position of the transmission path, and level of solar activity. The dependence of the strength of the signals on path length, on frequency, and on scattering angle has been studied. In the latter connection, pulse experiments were performed with equipment permitting fairly direct height determinations, which are found to be in satisfactory agreement with earlier less direct height determinations. Attempts to compare the observations with various existing theories designed to account for the propagation as a scattering process have been made. The results are not entirely satisfactory. The role of antennas in determining the behavior of received signals is examined from the point of view of geometrical concepts of scattering beamwidth, effective scattering volume, and signal coherence. Results of measurements of the realized gain of directive antenna systems are interpreted in relation to parameters involved in the scattering geometry, the influence of meteoric ionization, and the existence of large scale inhomogeneities in the ionosphere. A discussion is given of the possibilities for application of this type of propagation to communication systems operating over distances from about 1,000 to 2,300 kilometers. Design considerations for antenna systems including siting, choice of polarization, and space diversity are given. The useful range of frequencies and certain modulation techniques are discussed. Attention is given to multipath effects associated with the scattering process, and with the presence of meteoric and auroral ionization. Reliability of performance of typical systems is estimated.

Part I. Propagation Studies

Introduction

AN EARLY allusion to the possibility of radio-wave scattering in the lower ionosphere was made by Kennelly in 1913.[1] Little further thought seems to have been given to this matter until high-frequency communication came into general use, when Eckersley[2] began to investigate the possibility that *E*-region scattering from cloud-like electron concentrations could account for certain special effects which he and others had been observing. Eckersley proposed a theory of scattering[3] in the *E* region to account for his observations. The rapid further development of hf communications in the years that followed diverted attention to other matters, including ground scattering, and considerable time elapsed before further systematic propagation studies such as those now reported were undertaken.

In an earlier paper[4] the preliminary results of the experimental radio transmission at 49.8 Mc/s from Cedar Rapids, Iowa, to Sterling, Va., were described. Continuously present signals were found which exhibited interesting and promising behavior during SID's and during ionospheric disturbance. A program for further experimentation was formulated at that time by the National Bureau of Standards. The results of the program, which was subsequently enlarged in various ways, are now presented together with as much interpretation as seems warranted in view of the unresolved position which exists at present in connection with various theories which have been proposed to explain the propagation.

Throughout the investigations comprising the Bureau program there has existed the dual objective of improving understanding of the propagation, and of providing directly the necessary information for the design and construction of communication systems.

Scattering Theories

A limited account of some of the available scattering theories is presented at this time in order to facilitate the discussion and interpretation of certain of the observations and experiments. It is unfortunate that methods of experimentation and observation have not been found which permit a clear-cut separation in the observations of purely propagational effects from effects related to the antenna systems employed. The various theories of scattering which have been proposed to account for the observations express, or can be used to express the scattering cross section. The scattering cross section is defined as the power scattered per unit incident power density per unit solid angle in some direction γ with respect to the direction of incidence, per unit macroscopic element of volume of the scattering medium. In proceeding from expressions for scattering

* Original manuscript received by the IRE, August 8, 1955; revised manuscript released for publication September 6, 1955, by the Director, National Bureau of Standards.

† National Bureau of Standards, Washington, D. C.

[1] A. E. Kennelly, "The daylight effect in radio telegraphy," PROC. IRE, vol. 1, pp. 39–62; July, 1913.

[2] T. L. Eckersley, "An investigation of short waves," *Jour. IEE*, vol. 67, pp. 992–1032; August, 1929.

[3] T. L. Eckersley, "Studies in radio transmission," *Jour. IEE*, vol. 71, pp. 405–454; September, 1932.

[4] D. K. Bailey, R. Bateman, *et al.*, "A new kind of radio propagation at very high frequencies observable over long distances," *Phys. Rev.*, vol. 86, pp. 141–145; April 15, 1952.

cross section to transmission equations applicable to experimental situations, it has been generally assumed that only the power in the main lobe of the transmitting antenna is useful, and that the power is so sharply beamed at a small scattering volume containing the path midpoint, as shown in Fig. 1, that variations in distance and scattering angle throughout the volume are of negligible importance at the receiving location. This assumption leads to transmission equations which are independent of the transmitting antenna gain or aperture and avoids the difficult practical problem of how to perform the integration, actually required for rigor, over the entire scattering volume visible in common from the receiver and the transmitter. The fact that observed signal intensity behavior differs, and in some respects differs systematically, according to the antenna directivity used, provides observational confirmation of the importance of this difficulty. The various theories, while used to express transmission equations for very sharp transmitting beams, have nevertheless provided valuable assistance in the experimental program.

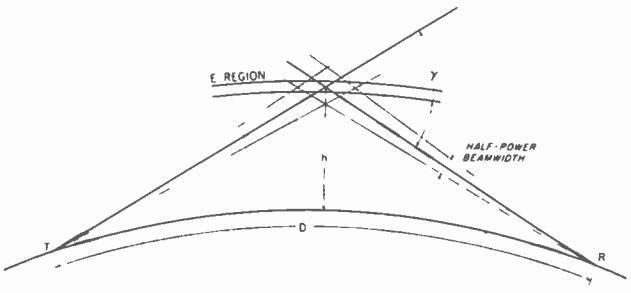

Fig. 1—Geometry of *E*-region scattering.

The parameters which enter all such transmission equations fall into three broad classes. First there are parameters which describe the scattering region, and with them may conveniently be included a parameter expressing the thickness of the scattering stratum. The thickness is always, and apparently correctly, taken to be small compared with the height at which scattering takes place. The disentanglement and evaluation of the parameters belonging to this class is both difficult and uncertain and has not yet been seriously attempted. In any case such attempts would be of doubtful value if the scattering theories should prove unsatisfactory when tested by means of less difficult experiments involving variation in a known manner of the geometric parameters characterizing the path of propagation. If the frequency used and the plasma frequency corresponding to the mean electron density of the scattering region are included for convenience with the purely geometric parameters such as ray-length and scattering angle, a second class of parameter is defined. Included implicitly in this class is the height at which the scattering takes place. The final class of parameters involves the terminal installations and includes the power radiated, the directivity of the transmitting antenna, the polarization employed, and the aperture of the receiving antenna.

Ideally to evaluate the effect on transmission of a particular parameter in the transmission equation it should be caused or allowed to vary in a known manner while all other parameters are held constant. This is not possible in the case of the parameters descriptive of the ionospheric stratum responsible for the received signals, and knowledge of them is therefore rather difficult to obtain. On the other hand, by making observations and performing experiments with sufficient simultaneity and using whenever possible the same scattering volume, it is possible to investigate the dependence of the scattering on the geometric variables. and the frequency. By using this investigating principle, the effects of the unknown but identical or nearly identical ionospheric parameters are minimized in the ratios of observations which are used. It is through systematic exploitation of this technique that much of the information about the height of the scattering stratum and the dependence of the strength of the received signals on frequency and scattering angle has been obtained.

In examining the various theories available in the literature, which may be called upon in connection with the interpretation of the observations, it is useful first to define the following quantities:

P_r = the received available power,
P_t = the power radiated by the transmitting antenna,
l = the ray distance from the path midpoint in the scattering stratum to the receiver,
f = the frequency of the transmitted wave,
f_N = the plasma frequency corresponding to the mean electron density, N, in the scattering volume,
γ = the scattering angle, defined as the difference in the direction of the incident wave and the received scattered wave,
A = the aperture of the receiving antenna, and
χ = the angle between the incident electric vector and the direction of the scattered wave.

Utilizing these quantities, transmission relations can be indicated. Application of the Booker-Gordon scattering theory[5] to the ionosphere[4] leads to the following:

$$\frac{P_r}{P_t} \propto \left(\frac{f_N}{f}\right)^4 \frac{A \sin^2 \chi}{l^2 \left(\sin \frac{\gamma}{2}\right)^5}. \tag{1}$$

On the other hand an extension of Eckersley's earlier *E*-region scattering model[3] leads to a transmission relation of the form:

$$\frac{P_r}{P_t} \propto \frac{f_N^4}{f^8} \frac{A \sin^2 \chi}{l^2 \left(\sin \frac{\gamma}{2}\right)^9}. \tag{2}$$

[5] H. G. Booker and W. E. Gordon, "A theory of radio scattering in the troposphere," PROC. IRE, vol. 38, pp. 401–412; April, 1950.

The geometric behavior of these two transmission equations is displayed as a function of path length in Fig. 2, in which the effect of the height of the scattering

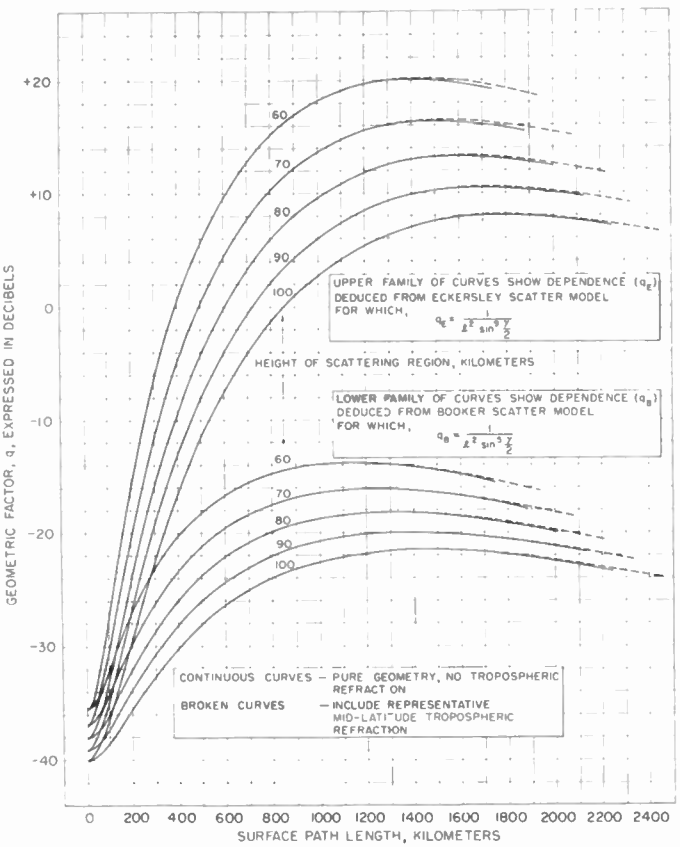

Fig. 2—Geometric factor q for midpoint scattering.

stratum is also shown. For this purpose geometric factors, q, are defined as follows:

$$q_B = \frac{1}{l^2\left(\sin\frac{\gamma}{2}\right)^5}, \tag{3}$$

and

$$q_E = \frac{1}{l^2\left(\sin\frac{\gamma}{2}\right)^9}. \tag{4}$$

Turning now to that portion of the more recent work of Villars and Weisskopf[6] which applies a theory of homogeneous turbulence to the lower ionosphere, the following approximate transmission relations can be obtained as limiting cases:

$$\frac{P_r}{P_t} \propto \frac{f_N^4}{f^{13/3}} \frac{A \sin^2\chi}{l^2\left(\sin\frac{\gamma}{2}\right)^{16/3}}, \tag{5}$$

and

$$\frac{P_r}{P_t} \propto \frac{f_N^4}{f^{11}} \frac{A \sin^2\chi}{l^2\left(\sin\frac{\gamma}{2}\right)^{12}}. \tag{6}$$

When f is small (5) applies, and as a practical matter (5) differs but slightly from (1). As f becomes greater the transmission is described by a transition relationship which in the limit for large values of f becomes (6). The meaning of small and large f will be discussed later.

Eq. (1) was developed on the basis of evidence of irregular distribution and irregular motion of ionization in the lower ionosphere taken from such observations as the fading of single reflected waves, the optically observed behavior of long-enduring meteor trails, and the known presence of a strong temperature inversion in the lower E region. The exponential autocorrelation function chosen originally to describe the isotropy of tropospheric turbulence, though not necessarily implausible, is arbitrary and was selected in part for its mathematical convenience. The application to the ionosphere is even more arbitrary and perhaps less plausible. On the other hand the model used for (2) originated many years earlier and was arrived at by means of a wave-mechanical analogy with α-particle scattering. Eq. (2) illustrates nicely what different results can be obtained with different models, a matter which has been pointed out by Staras.[7] Eqs. (1) and (2) predict a constant but different frequency dependence and from them the q-curves of Fig. 2 have been constructed. The exactness implied by them has not been observed, but the difference between them and the results of observation has been a stimulating influence in the interpretation of the observations. Eqs. (5) and (6), based on recent work on the statistical theory of homogeneous turbulence, provide more flexibility in making comparisons with observations since they indicate that both frequency and angle dependence are variable according to the frequency and the state of the scattering region. As will be seen below, it is the latter situation which corresponds more closely albeit nebulously, to the observational results. It is of interest to note that the quantity f_N enters all the transmission equations in the same way. It is this quantity which is supposed to be related directly to the intensity of the solar ultraviolet ionization of the lower E region, and which should respond to long-term changes in the level of solar activity, as well as to such short-term events as SID's.

In addition to the scattering theories discussed above, theories involving partial reflection associated with steep gradients of ionization have been advanced to account for the observations.[8,9] In order for these to

[6] F. Villars and V. F. Weisskopf, "The scattering of electromagnetic waves by turbulent atmospheric fluctuations," *Phys. Rev.*, vol. 94, pp. 232–240; April 15, 1954.

[7] H. Staras, "Scattering of electromagnetic energy in a randomly inhomogeneous atmosphere," *Jour. Appl. Phys.*, vol. 23, pp. 1152–1156; October, 1952.

[8] J. Feinstein and C. Salzberg, private communication, July, 1952.

[9] E. V. Appleton and W. J. G. Beynon, "An ionospheric attenuation equivalence theorem," *Jour. Atmos. Terr. Phys.*, vol. 6, pp. 141–148; March, 1955.

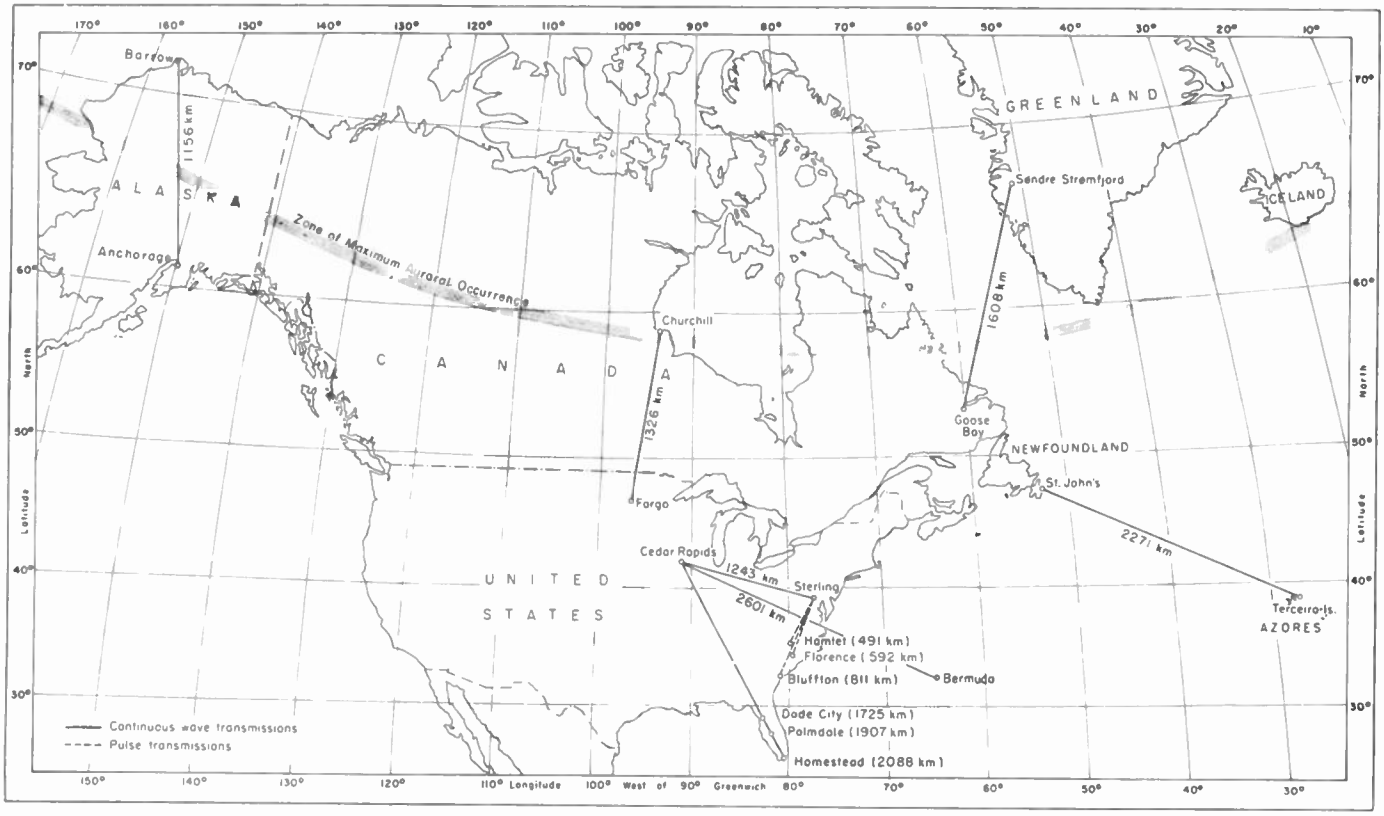

Fig. 3—Locations of experimental paths.

explain the observed fading characteristics, however, it is necessary to introduce either a fine structure of moving and changing irregularities in the gradients or to assign to some of the "constants" of gradient reflection theory an irregular time and space variation. Thus application of partial-reflection theories needs addition of features which can give rise to scattering.

Yet another school of thought exists which accounts for the observations as primarily or entirely the consequence of reflection or scattering at oblique incidence from many meteor trails, in the common volume, overlapping in time.[10–12] Such a view is based on experiments having either very different path geometry or employing much lower frequencies and using less directive antennas. Meteors are one of three major influences on the signals observed and their role will be discussed in due course. The presence of meteoric signals unfortunately adds further complications to the interpretation of the measurements.

As indicated in an earlier paper[4] the received signals are complex and it is certain that meteoric events, at times, and under certain circumstances make an important contribution to the mean signal level. Caution is therefore required in the interpretation of observational results, since none of the above transmission equations is applicable to the more easily recognizable meteoric components of the signal.

Experimental Arrangements

Much of the program has consisted in nearly continuous recording of horizontally polarized continuous-wave transmissions. This has involved several different paths (shown in Fig. 3 above) and operation at several different frequencies. Details are in Table I (facing). For the most part they have been operated at about 40 kilowatts input and all the signal-intensity data presently exhibited have been adjusted for a power level of 30 kilowatts at the transmitting antenna. In general identical rhombic antennas for each path have been used for transmitting and receiving. These antennas, of extreme design, were based on Harper's work.[13] Their plane-wave gains have been of the order of 17 to 20 decibels with reference to horizontal half-wave dipoles at the same height. Exceptions to this arrangement have existed. For the two-frequency comparisons on the Anchorage to Barrow path, horizontal five-element Yagi antennas were employed because of space limitations. For the test path from Goose Bay to Sondre Stromfjord, where vertical polarization was experimented with, vertical half-rhombics, vertical dual corner reflectors, and vertical full rhombics were variously employed.[14] From this latter path, because of the fre-

[10] D. W. R. McKinley, "Dependence of integrated duration of meteor echoes on wavelength and sensitivity," *Can. Jour. Phys.*, vol. 32, pp. 450–467; July, 1954.

[11] V. R. Eshleman, L. A. Manning, A. M. Peterson, and O. G. Villard, Jr., "The role of meteors in extended-range VHF propagation," 1955 IRE Convention Record, Part 1, "Antennas and Propagation," pp. 61–62.

[12] V. R. Eshleman, L. A. Manning, A. M. Peterson, and O. G. Villard, Jr., "The Role of Meteoric Ionization in Extended-Range VHF Propagation," Talk presented at URSI-IRE Meetings, Washington, D. C.; May 4, 1955.

[13] A. E. Harper, "Rhombic Antenna Design," D. Van Nostrand Company, Inc., New York, N. Y., 1941.

[14] R. Bateman, D. K. Bailey, and J. A. Waldschmitt, private communication, August, 1955.

TABLE I

DETAILS OF EXPERIMENTAL PATHS

	Cedar Rapids–Sterling			Anchorage–Barrow			Fargo–Churchill	Goose Bay–Sondre Stromfjord	St. Johns–Terceira
Frequency, Mc/s	49.800[1]	107.800	27.775	48.870	48.870	24.325	49.700	48.020	36.000
Date of commencement	January 23, 1951	December 4, 1951	May 6, 1953	August 28, 1951	March 2, 1953	February 16, 1953	August 29, 1951	April 1, 1952	October 4, 1954
Date of termination	Continues in operation	January 31, 1953	Continues in operation part time	June 30, 1953	June 30, 1953	June 30, 1953	March 31, 1953	November 30, 1953	September 30, 1955
Transmitter location coordinates of site	Cedar Rapids, Iowa 41°52′N; 91°41′W	←Same	←Same	Anchorage, Alaska 61°17′N; 149°42′W	←Same	←Same	Fargo, North Dakota 46°55′N; 96°46′W	Goose Bay, Labrador 53°17′N; 60°25′W	St. Johns, Newfoundland 47°32′N; 52°42′W
Receiver location coordinates of site	Sterling, Virginia 38°59′N; 77°29′W	←Same	←Same	Barrow, Alaska 71°18′N; 156°45′W	←Same	←Same	Churchill, Manitoba 58°44′N; 94°05′W	Sondre Stromfjord, Greenland 66°58′N; 50°55′W	Terceira Island, The Azores 38°45′N; 27°14′W
Surface path length (great circle)	1,243 km. 773 st. mi.	←Same	←Same	1,156 km. 718 st. mi.	←Same	←Same	1,326 km. 824 st. mi.	1,608 km. 999 st. mi.	2,271 km. 1,411 st. mi.
Geographic coordinates of path midpoint	40°39′N; 84°26′W	←Same	←Same	66°20′N; 152°31′W	←Same	←Same	52°50′N; 95°36′W	60°12′N; 56°39′W	44°51′N; 40°54′W
Geomagnetic latitude of path midpoint	51°38′N	←Same	←Same	65°02′N	←Same	←Same	62°42′N	70°46′N	54°40′N
True azimuth of transmitter from receiver	289°30′	←Same	←Same	160°55′	←Same	←Same	188°56′	203°18′	303°44′
True azimuth of receiver from transmitter	100°17′	←Same	←Same	347°24′	←Same	←Same	6°47′	15°01′	106°07′
Type of antennas	Rhombic-Rhombic	←Same	←Same	←Same	Yagi-Yagi	←Same	Rhombic-Rhombic	Various	Pairs of Yagis Stacked Vertically
Elevation of maximum of main lobe, degrees	7.0	←Same	←Same	5.7[2]	6.4[2]	6.4[2]	5.4	—	T +0.44 R −0.15
Height, feet	41	19	73	50	45	90	52	—	T 880 R 2240
Leg length, feet	500	230	897	500	—	—	500	—	—
Plane-wave gain, relative to dipole at same height, decibels	18	18	18	18	9	9	18	—	12
Attenuation[3] relative to inverse-distance transmission represented by received signal intensity of 1.0 microvolt, decibels.	122	115	127	123	105	111	122	—	112

[1] 49.600 Mc/s used from January 17, 1952 through March 31, 1952.
[2] Includes effect of sloping site at Anchorage.
[3] Received open-circuit antenna voltage measured at 600 ohms impedance (−154 dbw). Reference power to transmitting antenna is 30 kw.

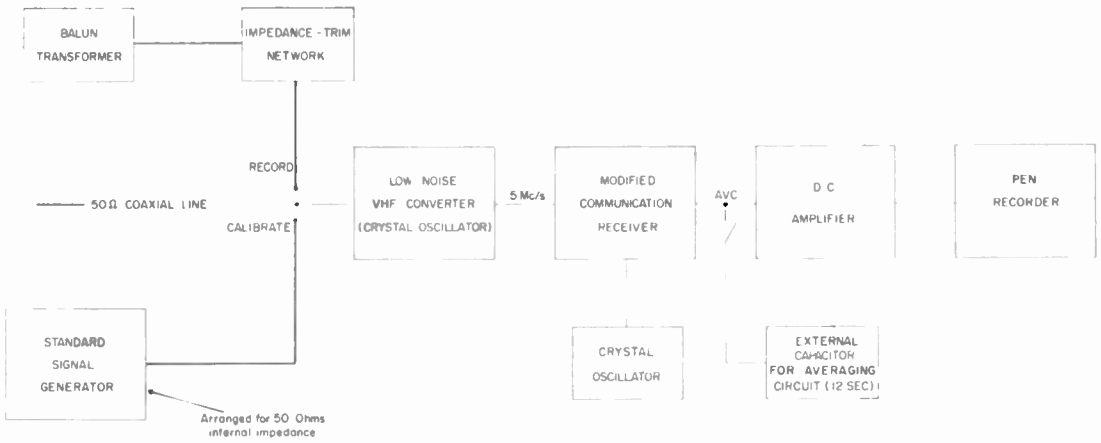

Fig. 4—Routine recording arrangement.

quent changes in the observing arrangements, only sporadic-E transmission data are presented. All antennas used were designed to have their first lobe maxima directed toward the E region at the path midpoint.

Routine reception and recording were performed in accordance with the receiving arrangement shown in Fig. 4, or with an equivalent arrangement. All data are adjusted for an equivalent lossless line impedance of 600 ohms, though later in the program reception was performed at 50 ohms. For the signal-intensity observations the continuous-wave emissions were recorded using a predetection receiver bandwidth of approximately 2 kc/s, and a post-detection RC averaging circuit having a time constant of 12 seconds. The recording receiver arrangement provided an output approximately proportional to the logarithm of the average input signal voltage. The 12-second time constant, while serving to smooth most of the rapid signal fluctuations and thereby facilitate the reduction of the observations, is short enough to allow the more intense meteor reflections or bursts to be indicated as sharp spikes on the record along with all slow variations in signal intensity. A special experiment was performed at Sterling simultaneously on the 49.8 and 107.8 Mc/s signals using an unusual receiving arrangement in order to measure power. This experiment established the validity of interpreting the routine intensity measurements as relative power measurements. Transmissions were interrupted twice each hour to permit the background external noise, mostly cosmic noise, to be recorded. These periodic noise observations provided a valuable check on the performance of the receiving system.

The observations of received signal intensity can be interpreted in terms of transmission loss[15] and loss relative to inverse-distance attenuation. For 30 kilowatts power to the transmitting antenna, a received open-circuit antenna voltage of 1.0 microvolt at 600 ohms impedance corresponds to a transmission loss of 199 decibels. The values of attenuation relative to inverse distance presented in Table I for the experimental paths are based on the assumption that the ground at each of the terminals and the ionosphere are perfectly reflecting planes. Received power for inverse-distance squared attenuation is calculated from the following equation:

$$P_r = \frac{P_t G_t G_r \lambda^2}{(8\pi l)^2}, \tag{7}$$

where G_r and G_t are power gains of the transmitting and receiving antenna systems, including the effects of perfect ground reflection, relative to an isotropic antenna in free space, and λ is the wavelength.

In addition to the routine observations and measurements, other experiments of relatively short duration having particular objectives in view were performed, for which pulse and other kinds of modulation were employed. Special antennas and receiving arrangements were often used. These experiments and their results are described below.

Characteristics of the Normal Signal

Short-Term Behavior

The characteristics of the normally received signals at about 50 Mc/s are substantially different from those observed over comparable paths at *HF*, *MF*, or *LF*. The signal levels reported in the measurement program are median values of the average open-circuit receiving antenna voltage resulting from reception of a transmitted unmodulated carrier. The instantaneous signal level may be above or below the average value by 20 decibels or more. Observations of signal behavior uninfluenced by the recording time constant lead to the impression that the total signal consists of a continuously present fluctuating component and transient components resulting from reflections or scattering from ionization associated with meteors.

During periods when the received signals are apparently unperturbed by meteor reflections the fading

[15] K. A. Norton, "Transmission loss in radio propagation," Proc. IRE, vol. 41, pp. 146–152; January, 1953.

rates, as observed in the output of a receiver having a bandwidth of two kilocycles, vary in a random manner principally in the range of 0.2 to 5 cycles per second. These variations of the signal level are considered to result from a scattering process in which the contributions of different elements within the effective scattering volume arrive at the receiver with relative phases that have been influenced by motions or changes of ionization. The changing relative phases at the receiver are responsible for the fading characteristics of the received signals. The fluctuation of the signal intensity when not obviously perturbed by meteoric events is adequately described by a Rayleigh distribution. There is thus always a finite probability that the signal intensity will be smaller than any specified value and that it will be smaller than this value for a finite fraction of the time over long periods. More detailed studies of the fading characteristics are presented elsewhere.[16,17]

There are two types of perturbations resulting from meteoric ionization which are easily distinguishable from the fluctuating background signal. First there are the Doppler frequencies which differ appreciably from the transmitted carrier frequency. These give rise to randomly occurring audio heterodyne whistles or beats in the output of a receiver designed for amplitude modulation reception. The heterodyne beats range in frequency from zero to several kilocycles. The Doppler frequency components are produced occasionally by reflections from the heads of ionization accompanying meteors, but much more frequently by scattering from rapidly lengthening meteor ionization trails during the process of their formation.[18,19] Special observations at Sterling have shown that considerably more than 90 per cent of the received Doppler frequencies are higher than the transmitter carrier frequency. It is also observed that most of the audio heterodyne frequencies decrease. Occasionally the Doppler frequencies pass through the carrier frequency from the high side resulting in audio heterodyne frequencies which decrease to zero beat and then increase. Relatively simple geometric considerations indicate that Doppler frequencies above the carrier should occur much more frequently and should be associated with descending audio heterodyne frequencies. Correspondingly the relatively rare ascending audio heterodyne frequencies should be associated with Doppler frequencies below the carrier frequency. A complete analysis of these observations involves much more than pure geometry and has not been attempted. The instantaneous amplitude of the Doppler components varies over a wide range relative to the background signal. At 49.8 Mc/s most, but not all, of the Doppler components have intensities which are small relative to the simultaneously received scattered component. An occasional Doppler component will have an intensity greater than that of the scattered component. During periods of high signal intensity such as during the summer day or during strong geomagnetic disturbances the effects of the Doppler components on the composite signal are markedly reduced. In these periods, occurrences of audio-frequency heterodyne whistles may be infrequent or unobserved when conventional receiving techniques are employed. Figs. 5 and 6 (above) show typical short-term behavior of the 49.8 Mc/s signals at Sterling.

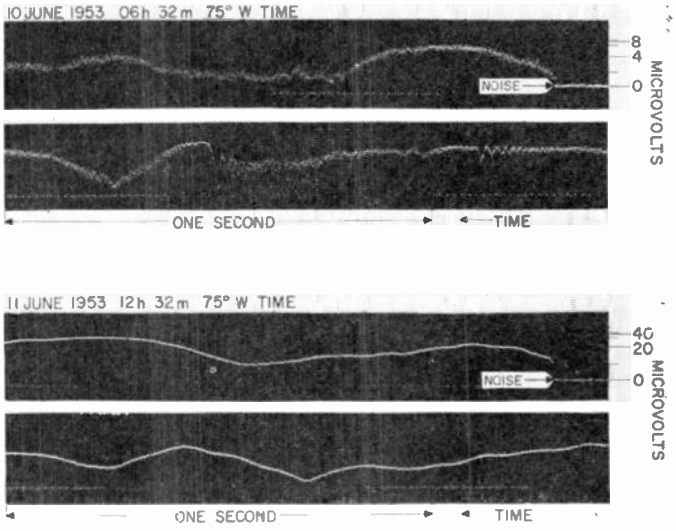

Fig. 5—Oscillograms showing typical short-term signal behavior for the Cedar Rapids to Sterling path at 49.8 Mc/s. System bandwidth is somewhat greater than 1,000 cps. Note in the early morning record interference patterns associated with meteoric reflections.

Fig. 6—Record of typical signal fading observed at Sterling at 49.8 Mc/s.

[16] G. R. Sugar, "Some fading characteristics of regular vhf ionospheric propagation," p. 1432 of this issue.

[17] R. A. Silverman and M. Balser, "Statistics of electromagnetic radiation scattered by a turbulent medium," *Phys. Rev.*, vol. 96, pp. 560–563; November 1, 1954.

[18] D. W. R. McKinley and P. M. Millman, "A phenomenological theory of radar echoes from meteors," PROC. IRE, vol. 37, pp. 364–375; April, 1949.

[19] L. C. Browne and T. R. Kaiser, "The radio echo from the head of meteor trails," *Jour. Atmos. Terr. Phys.*, vol. 4, pp. 1–4; September, 1953.

The second type of perturbation produced by meteors consists of transient but large signal enhancements resulting from reflection from columns of meteoric ionization so oriented as to present first Fresnel zones from which the scattering process more nearly resembles a specular reflection. These enhancements may exceed the fluctuating background signal by many decibels. They usually persist for periods of time ranging from a fraction of a second to several seconds. Occasionally durations of several minutes have been observed. An example occurs in a sample recording shown later in the paper. Drift velocities of meteor ionization trails are small compared to meteor velocities, and the received frequency during meteoric enhancements usually does not differ from the transmitted frequency by more than a few cycles per second.

The characteristics of the received signals are somewhat different at frequencies substantially higher or lower than 50 Mc/s. At the lower frequencies, the observed Doppler components appear to be few and smaller relative to the fluctuating background signal than at 50 Mc/s. Comparisons of recordings at 27.775, 49.8 and 107.8 Mc/s lead to the impression that the intensity of meteoric enhancements decreases more slowly with increasing frequency than does the intensity of the scattered component.

Long-Term Behavior—Middle Latitudes

In order to investigate the long-term behavior of the signals, the original propagation path of 1,243 kilometers from Cedar Rapids, Iowa, to Sterling, Va., operated at 49.8 Mc/s, has been kept in continuous service since early 1951 with routine recording performed as described above. For short periods of time 49.6 Mc/s has been used. Further details of this and other propagation-study paths are given in Fig. 3 and Table I. Over this period it has been found that the signals are always weakest in the evening period represented by about 19 to 21 hours local time at the path midpoint. This characteristic has also been found for all the other paths operated and appears to be a universal characteristic of the propagation. Despite the considerable variations in the hourly medians from day to day, the monthly medians by hours are more nearly the same for a given month from year to year, than are the monthly medians for adjacent months in the same year. Fig. 7 illustrates the diurnal variation of the monthly medians for December, March, June and September together with the upper and lower decile values in order to provide an indication of the day-to-day variation at a given hour. The strongest signals are received in the summer and the weakest at the equinoxes. The winter midday signals are about as strong as the summer midday signals, but are much weaker at other times of day. This behavior appears to be in part associated with the zenith distance of the sun. Fig. 8 (p. 1190) shows variation, by months for a period of several years, of signal intensities representative of three-hour periods centered about 00, 06, 12, and 18 hours local time at the path midpoint. The semi-annual period in the midday intensity is plainly evident, but is absent in the midnight intensities which show an annual period with a maximum in the summer. The winter midday maximum is thought to be closely connected with the winter daytime ionospheric absorption anomaly observed in mid-latitudes.

Fig. 9 (page 1191) shows the diurnal variation of very weak signal intensities observed during the period October, 1951 through September, 1952 as observed at 49.8 Mc/s for the Cedar Rapids to Sterling path. It will be noted that the diurnal minimum for these very low signal intensities also occurs during the period 19 to 21 hours local time at the path midpoint.

Fig. 10(a) (p. 1191) shows the cumulative distribution of the hourly median signal intensities throughout the year from October, 1951 through September, 1952.

Long-Term Behavior—High Latitudes

Following a short period of study of the early results from the Cedar Rapids to Sterling path it was decided to establish two further propagation study paths farther north in regions where hf communication is difficult. The path lengths were chosen to be as nearly the same as practicable as the Cedar Rapids to Sterling path, and similar frequencies were employed. The objective was to determine propagation differences associated with geographical position. The additional paths came into operation nearly simultaneously in late August, 1951 and employed antennas differing only slightly in design from those at Cedar Rapids and Sterling. The recording arrangements were identical. One of these paths, from Fargo, N. D., to Churchill, Manitoba, was somewhat longer than the Cedar Rapids to Sterling path and operated at 49.7 Mc/s. This path is subject to moderately severe auroral zone disturbance as its northern terminal lies practically at the zone of maximum auroral frequency. The other path from Anchorage to Barrow, Alaska, was somewhat shorter than the original path and operated at 48.87 Mc/s. The zone of maximum auroral occurrence crosses this path. For further details about these paths see Fig. 3 and Table I.

These new 50 Mc/s paths were found to exhibit short-term behavior of the kind described for the Cedar Rapids to Sterling path and as at Sterling the signals were found always to be present. With respect to long-term behavior, however, they revealed marked differences. In general the signal intensities were greater, and a number of special effects associated with auroras and severe geomagnetic disturbances were found. The diurnal minima were observed to occur in the evening period as

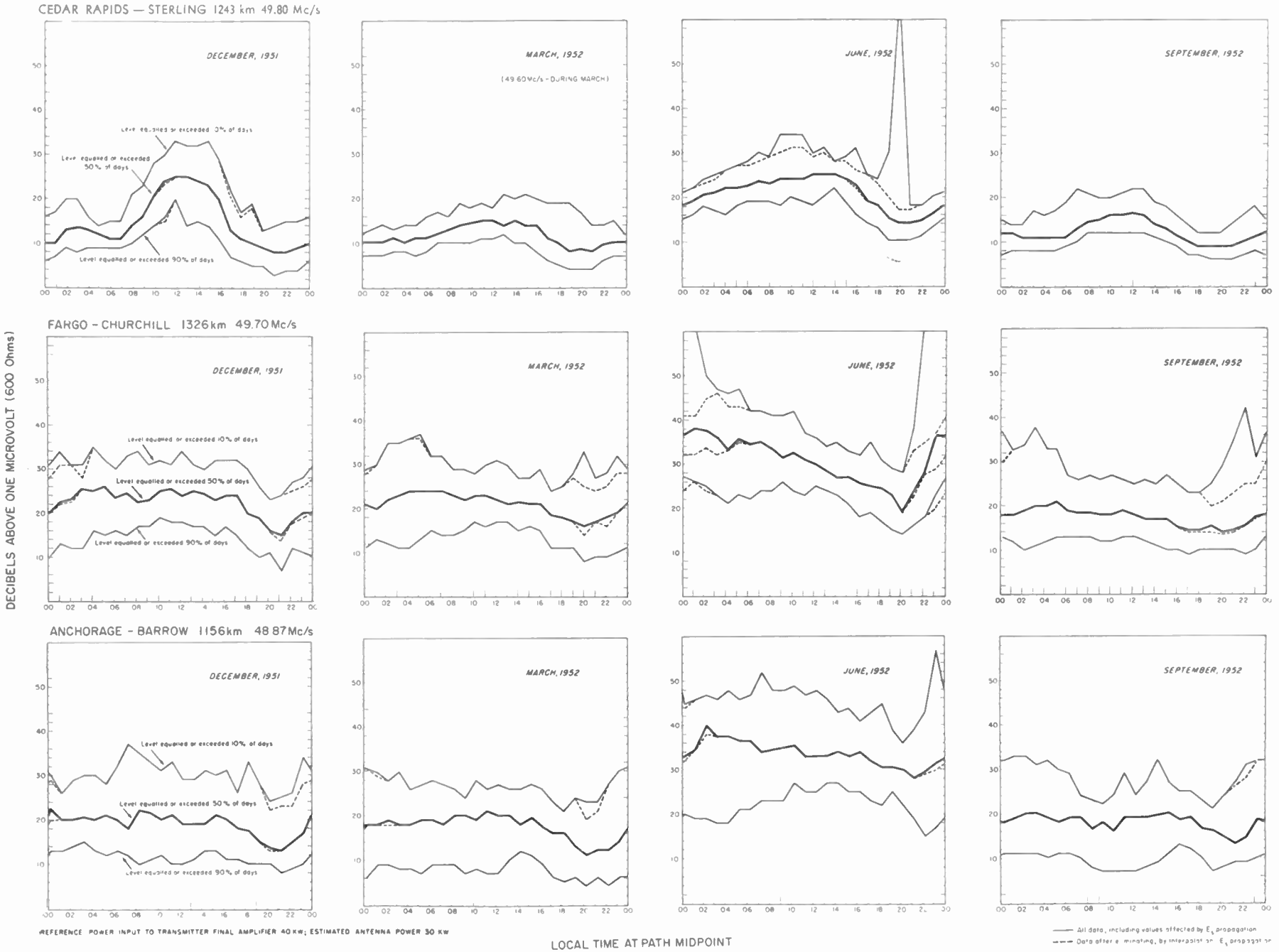

Fig. 7—Diurnal variation of signal intensity at different seasons.

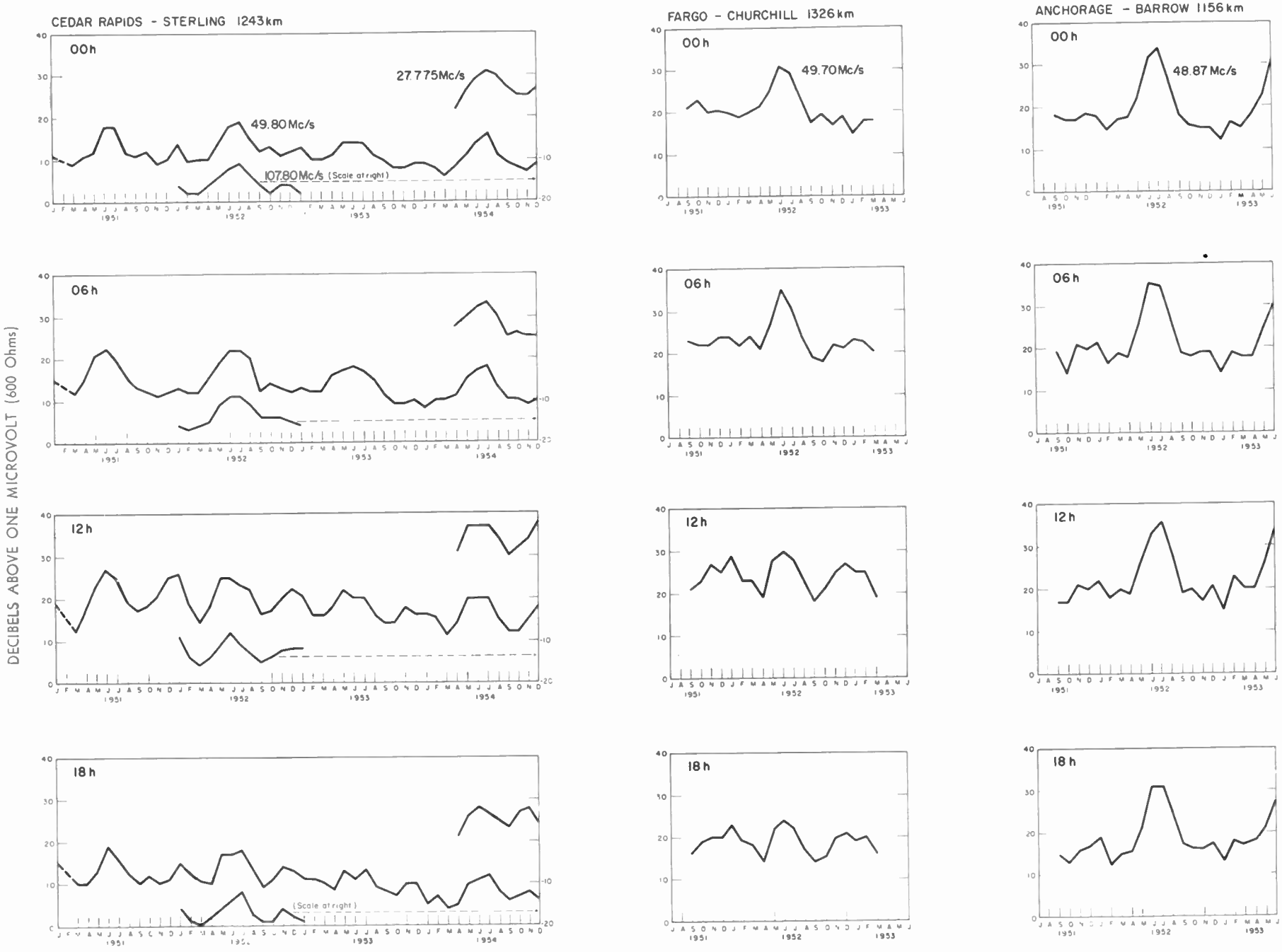

Fig. 8—Seasonal variation of signal intensity at different times of day.

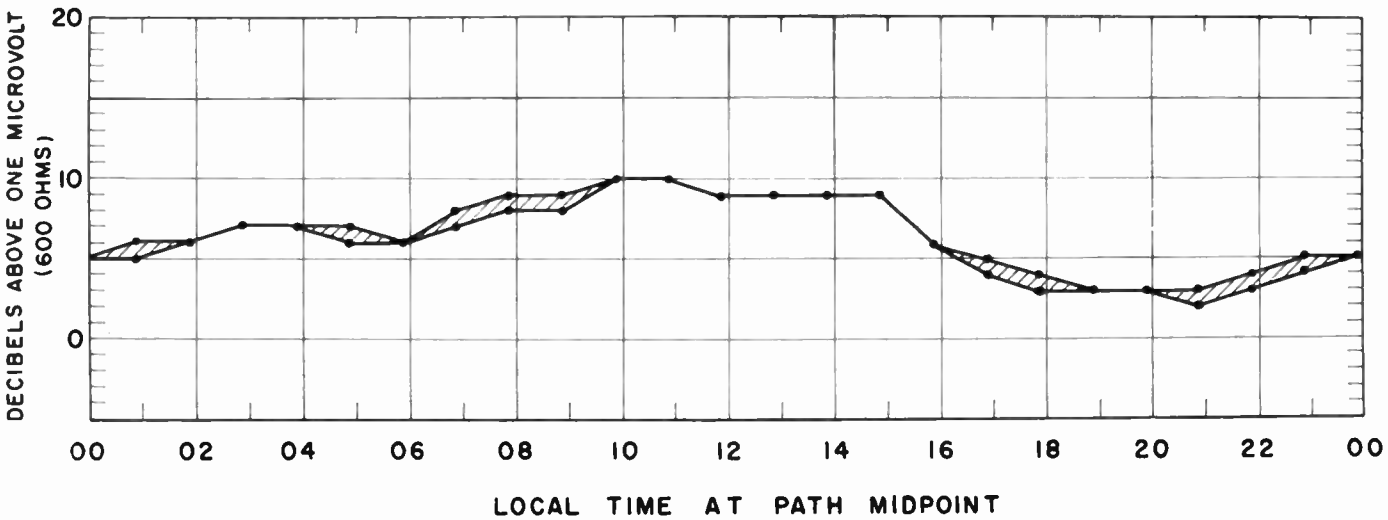

Fig. 9—Diurnal variation of very weak signal intensities observed at Sterling at 49.8 Mc/s for the year October 1951 through September 1952. The shaded areas contain the value of hourly median signal intensity equalled or exceeded 99 percent of the time for the hour shown.

at Sterling, but the hour-to-hour and day-to-day variations in median signal intensity were considerably greater. This is evident in the separation between the upper and lower deciles for December, March, June, and September shown with the corresponding monthly median signal intensities in Fig. 7. For both paths much the strongest signals were found to occur in the summer when the signals were very much stronger than at Sterling. The weakest signals occurred from February through early April, but at these times they were somewhat stronger than the minimum signals at Sterling. The times of day of maximum signal intensity were much less definite than for Sterling. Fig. 8 shows, as for the Sterling signals, the variation by months for the entire period of operation of these paths, of signal intensities representative of 00, 06, 12, and 18 hours local time. In presenting these data for comparison, the influence of sporadic-E propagation has been eliminated by interpolation when possible, and otherwise by omission. Note that the signal behavior of the two arctic paths is quite similar, but very different from that observed at Sterling. In the case of the Churchill observations for noon, some traces of the semiannual period remain.

Figs. 10(b) and 10(c) show for the arctic paths the cumulative distributions of the hourly median signal intensities from October, 1951 through September, 1952.

Distance Dependence—Ionospheric Heights

The maximum distance over which signals can be observed by means of scattering in the lower ionosphere is a matter of some interest both from the practical viewpoint of communication applications and from the more scientific viewpoint. In the latter connection it is to be noted that the scattering angle is least for the longest paths, and that the actual length of the longest path is determined by the curvature of the earth, the effects of tropospheric refraction on the upgoing and

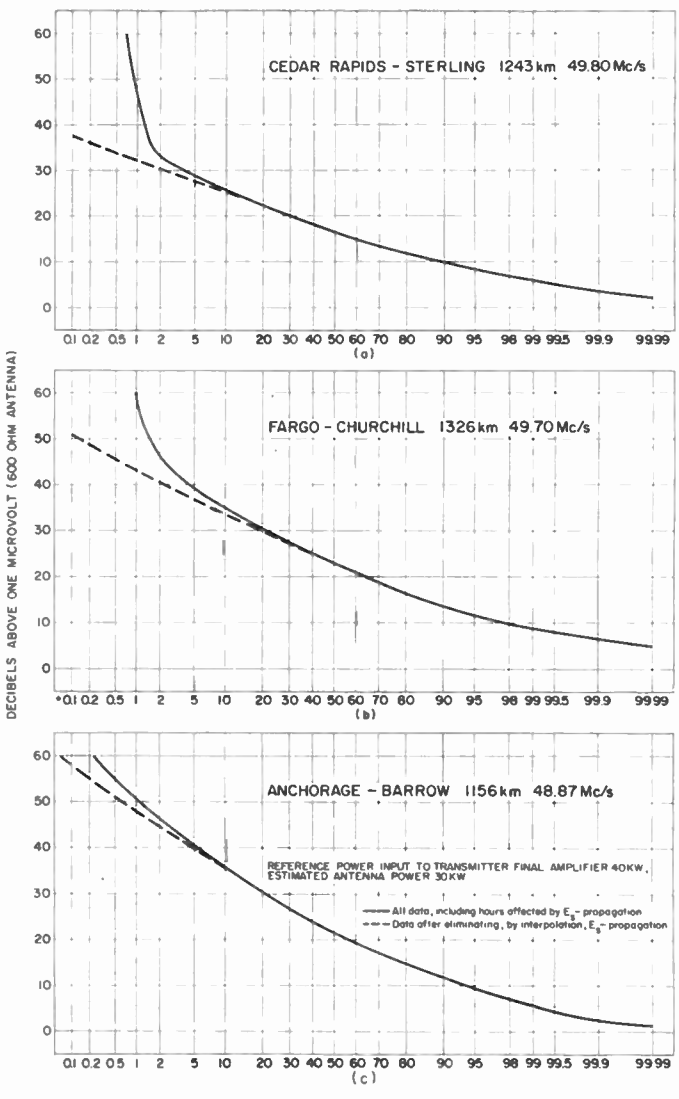

Fig. 10—Cumulative distributions of the hourly median signal intensities for the year from October, 1951 through September, 1952.

downcoming waves, and the height or range of heights from which the waves are returned. Fig. 11 illustrates for midpoint scattering the relationship of path length, angle of arrival or departure of the waves with respect to horizontal, and height of the scattering region for a range of scattering heights from 60 to 100 kilometers with and without allowance for tropospheric refraction. If very high antenna sites are available the maximum transmission path can be lengthened for a given ionospheric height by use of radiation which departs and arrives horizontally or at slightly negative angles with respect to horizontal.

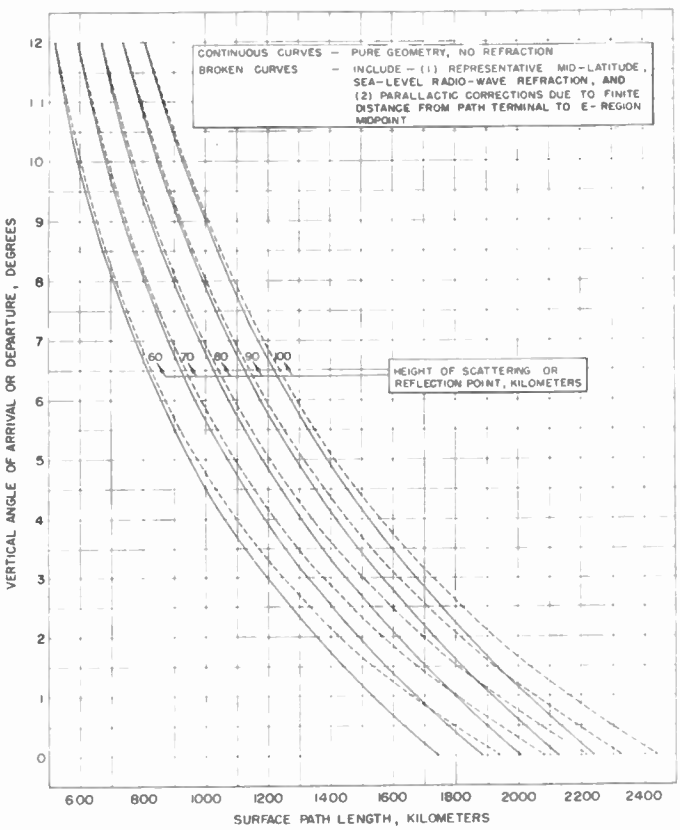

Fig. 11—Vertical angle of arrival or departure for midpoint scattering.

All distance-dependence tests are closely related to the identification of the height or range of heights above the surface of the earth responsible for returning the waves. From the beginning of observations at Sterling, it was assumed that the heights were ionospheric and specifically that the E region was involved. There were three arguments which supported this view. Firstly, the long- and short-term variations of the signal intensity were inconsistent with the known characteristics of long-distance tropospheric propagation. Secondly, the very early observations of signal enhancement during sudden ionospheric disturbances (SID's) and the less striking evidence at Sterling (subsequently observed to be more striking on the northern paths) that signal intensities tended to be unusually great during periods of severe geomagnetic disturbance, could only be explained in ionospheric terms. The third piece of early evidence was the results of the Bermuda observations of the 49.8 Mc/s signals from Cedar Rapids made during the summer of 1951 using a five-element Yagi antenna for reception. Most of the time no signals whatever were received.

Bermuda lies nearly along the Cedar Rapids to Sterling great circle at about twice the distance of Sterling as is shown in Fig. 3. The distance of Bermuda, 2,601 kilometers, from Cedar Rapids is well beyond any possibility of single-stage propagation from any height in the E region. Furthermore, the main lobe of the transmitting antenna at Cedar Rapids intensely illuminates the F region directly above the general vicinity of Sterling. It was thus possible to compare the occasional cases of weak reception at Bermuda, which could not be related to known cases of sporadic-E propagation between Cedar Rapids and Sterling, with the $h'f$ observations at Ft. Belvoir, Va., about 50 kilometers south of Sterling. No connection was found between Bermuda reception and any unusual conditions in the F region. In particular, no evidence could be found that the cases of "spread" or scattered F-region echoes at vertical incidence which occurred during the period of the Bermuda observations were in any way associated with the occasional weak reception at Bermuda. The occurrence characteristics of the latter could, in fact, be plausibly explained as cases of sporadic-E propagation at the midpoint of the second stage. This result was accepted for the time being as sufficient evidence that the E region was primarily responsible for the propagation observed regularly on the various test paths.

During the first half of 1952 some reception tests at 49.8 Mc/s at extreme range were made in Florida at locations shown in Fig. 3. These involved the occupation, in turn, of several sites along the great circle defined by the direction of the main lobe of a specially constructed long rhombic antenna at Cedar Rapids. This antenna had a plane-wave gain, compared with a half-wave dipole at the same height, of 19 decibels, and its first ground-reflection lobe maximum occurred at an angle of elevation of 2.4 degrees. Both the gain figure and the details of the first lobe were measured by means of an aircraft. At the various stations in Florida two five-element Yagi antennas were used at heights of 40 and 100 feet respectively. The ground-reflection lobe patterns at these two heights could be calculated with adequate precision for the flat and unobstructed Florida sites from earlier laboratory tests of the antenna. At each station observations of height gain for 100 vs 40 feet were made for limited periods, and continuous recording was made on one of the antennas, the 40-foot Yagi antenna at the nearer two of the three principal sites for which data are shown in Fig. 12 (next page), and at 100 feet at the most distant site where signals with the 40-foot Yagi antenna were usually too weak for measurement.

The single available transmitter at Cedar Rapids was connected for alternate half-hourly periods to the spe-

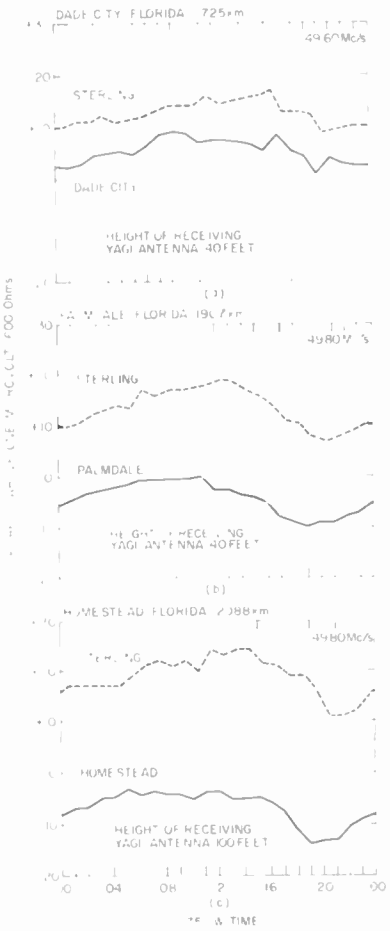

Fig. 12—Distance dependence observations in Florida—(a) Dade City, March 6–18, 1952, inclusive; (b) Palmdale, April 1–30, 1952, inclusive; (c) Homestead, May 21–June 2, 1952, inclusive. Sterling observations shown for corresponding periods.

cial rhombic antenna directed toward Florida, and to the rhombic antenna directed toward Sterling. The Sterling observations thus provided reference signal intensities, and the observed signal intensities in Florida could be expressed as a fraction of the Sterling intensities. This procedure permitted the results shown in Fig. 13 to be interpreted in terms of ionospheric height. The distances from Cedar Rapids to the three principal Florida sites were such that for *E*-region heights the angles of elevation of the path midpoints were all below the angles of elevation of the first ground-reflection lobes of the transmitting and receiving antennas. As should occur under these conditions for *E*-region scatter, the received signal power, relative to Sterling signals, decreased rapidly with increasing path length.

By regarding, for purposes of calculation, the received signals as coming from a point scatterer at the path midpoint, it is possible to compute from the known antenna patterns how the relative signal intensity should decrease with increasing path length for a series of trial heights of scatter. Into these calculations a standard inverse-distance squared factor must be inserted, and, in principle, a dependence on scatter angle should be used. Actually the scatter angle varies so little over the range of distances covered by the tests

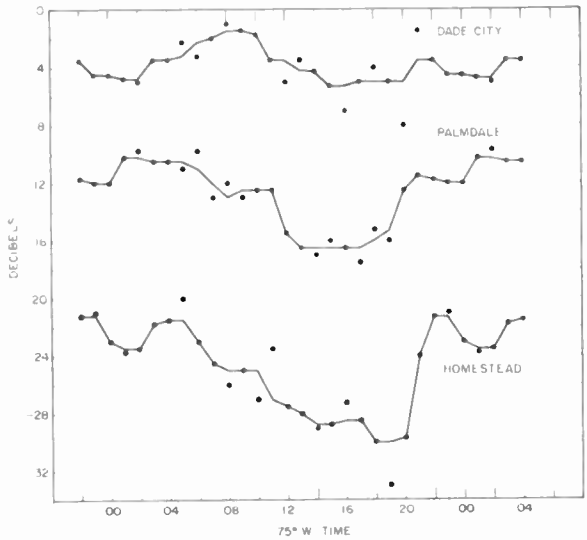

Fig. 13—Smoothed diurnal variation of the ratios of signal intensities received in Florida to those received at Sterling. Ratios shown for the shorter paths are adjusted by observed height gain to permit equivalent comparisons for reception at a height of 100 feet.

that any reasonable dependence may be used without significantly altering the result. The height is then deduced by comparing the predicted rates of decrease of relative signal intensity with distance, for the assumed heights, with the observed decreases relative to Sterling. This method of height finding, using continuous-wave signals, depends only on comparisons, and is quite insensitive to the form of the scattering transmission equation used. In fact the results are not affected significantly if the simple inverse distance squared term alone is used.

The results of these tests are summarized as follows. The heights by day and by night are different. Despite the changing seasons during the tests, the daytime heights lay between 75 and 80 kilometers, and the nighttime heights lay in the range from 85 to 90 kilometers. This day-night height difference received independent confirmation of a still different sort in the systematic differences in the observed height gains between day and night. The daytime height gains, corresponding to the lower height of scatter, were always greater, as would be expected for a smaller common volume associated with the lower midpoint height. At the greatest distance the height gains observed were very close to the theoretical plane-wave result of 8 decibels which would be anticipated if the common volume was small enough to approximate reasonably a point source. Table II summarizes these results. The

TABLE II

Reception Point in Florida	Distance from Cedar Rapids, kilometers	Height Gain, decibels 100 *versus* 40-foot Yagi	
		Day	Night
Dade City	1,725	3½	3
Palmdale	1,907	5	4
Homestead	2,088	8½	6½

method of height determination described above assumes that the scattering comes from a single stratum. As will be seen later this does not lead to significant error. It is to be added in connection with the height-gain results above, that at Sterling, distance 1,243 kilometers, no significant height-gain effect was found in a brief trial with a dipole whose height was varied from 12 to 80 feet.

In arriving at the height results given above, it was necessary to include the effects of tropospheric refraction. For this purpose the observations of astronomical refraction at 200 Mc/s made in Australia[20] were used after the application of suitable parallactic corrections for the finite distance of the scattering volume.[21] If tropospheric refraction had been neglected, the resulting heights would have come out some 10 kilometers higher.

In examining Fig. 12 which compares the median signals received in Florida with the median signals for the same period at Sterling, it will be observed that there are certain differences in the diurnal curves. The high midday maximum usually observed at Sterling, and now associated with the lower daytime scattering heights, is less prominent at the greater distances at which the antennas discriminate against the lower heights. This same sort of result has been found more recently in the tests at 36.0 Mc/s between St. Johns, Newfoundland, and Terceira Island in the Azores, a distance of 2,271 kilometers, for which very elevated but still height-limited antenna sites are used. Fig. 14 presents an example from these tests, showing the almost complete absence of a midday maximum as observed simultaneously at Sterling.

With these provisional height results it was possible to suggest that the maximum useful path length employing ionospheric scattering was likely to be about 2,000 kilometers under ordinary circumstances. This figure took account of the practical difficulties of antenna construction in flat country for the very low beam angles which would be required at such a distance. Since the period of minimum signal intensity occurs in the evening when the scattering heights are higher than in the daytime, it was concluded that an ionospheric midpoint height of 85 kilometers provided a useful compromise for designing antennas.

Distance dependence in the range of path lengths below 1,000 kilometers is closely related to angle dependence which is discussed below.

Height Determination by Pulse Methods

Successful ionospheric scattering observations with pulses, over distances short enough to permit simultaneous reception of tropospherically propagated reference pulses, require considerable power. For this purpose a pulse transmitter was constructed at Sterling for operation between about 48 and 52 Mc/s. It was capable of delivering to the antenna a peak power of one megawatt, at an average power somewhat in excess of one kilowatt, though it was generally operated, for the sake of reliable performance, at a somewhat lower power level.

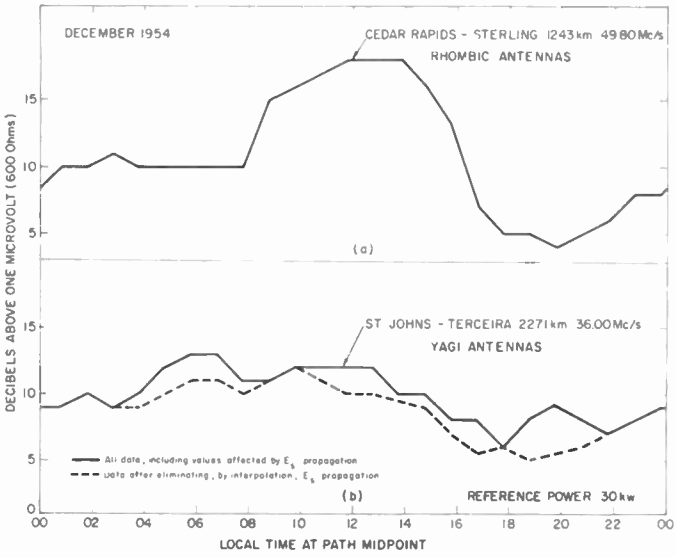

Fig. 14—Hourly median values of signal intensity observed on path from St. Johns to Terceira, compared with Cedar Rapids to Sterling path, December, 1954, to show absence of midday maximum for longer path.

Preliminary tests of the new transmitter at vertical incidence and over a path for which the scattering angle was 90 degrees were entirely negative. No scattered signals were observed, although meteor echoes were seen better on the oblique test. It was found, however, that the tropospheric signal was of sufficient strength to justify a considerable increase in the length of the test path, and useful observations were eventually made at Bluffton, S. C., a distance of 811 kilometers from Sterling. At this distance suitably designed horizontal rhombic antennas were used and the frequency employed was at different times either 49.7 or 49.8 Mc/s. At Bluffton the ionospheric and tropospheric signals were roughly of equal intensity, and both were weakly present for most of the time.

The first successful tests were conducted for a total period of about two weeks in the winter of 1952 to 1953, and confirmed the earlier continuous-wave results of the Florida distance-dependence tests. Again it was found that heights by day were lower than by night. The predominant nighttime scattering stratum appeared at about 88 kilometers, and while it sometimes persisted weakly during the daytime, it was generally replaced by a more strongly scattering stratum at about 70 kilometers. The results varied somewhat from day to day. The lowest height recorded, and recorded only for a short period, was 59 kilometers. Occasionally weak echoes were received from a height of about 105 kilometers which were considered to represent sporadic-

[20] L. L. McCready, J. L. Pawsey, and R. Payne-Scott, "Solar radiation at radio frequencies and its relation to sunspots," *Proc. Roy. Soc. A*, vol. 190, pp. 357–375; August 12, 1947.
[21] D. K. Bailey, private communication; February, 1947.

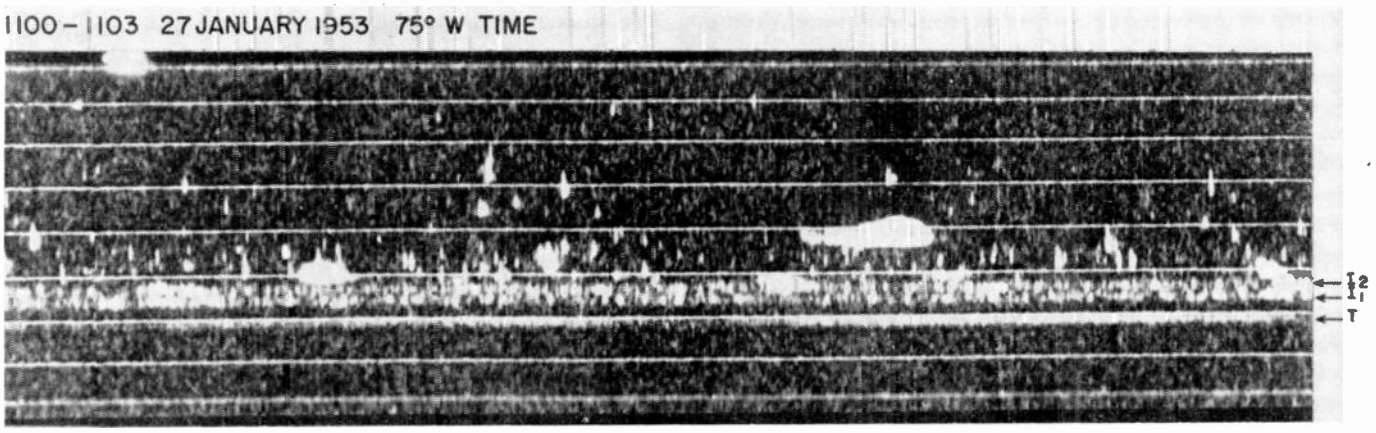

Fig. 15.—Oscillogram showing received pulse signals at 49.7 Mc/s on Sterling to Bluffton path, 811 km. T is tropospheric signal, and I_1 and I_2 are ionospheric signals with delays relative to the tropospheric pulses corresponding to heights of approximately 70 and 88 km. Time markers are at 100 microsecond intervals. The transmitted pulses are of approximately 30 microseconds duration, with a repetition rate of 50 per second.

E propagation. Often several strata were simultaneously active. Meteors were not seen at ranges less than that corresponding to the nighttime heights. Fig. 15 is a three-minute sample of the photographic record which shows two active scattering strata, some meteor echoes, and a fairly strong tropospheric signal. This record is typical in most respects for the season and hour except that usually only the lower scattering stratum was observable.

In the summer of 1954 the Bluffton site was reoccupied for ten days for some further height observations. This time the predominant daytime heights were somewhat greater—usually about 80 kilometers. The nighttime heights as in the winter lay mostly between 85 and 90 kilometers.

The agreement between the continuous-wave and pulse methods of height determination is satisfactory, and it only remains to discuss the possible sources of systematic error involved. Of these the most serious is thought to be concerned with the calculation of the travel time of the tropospheric pulses. Some more recent experiments,[22] with round-trip methods for both tropospheric and ionospheric pulses, suggest that the ionospheric heights deduced as described above may be too low by perhaps five kilometers or so. Also some winter observations made on a somewhat more northern path in the winter of 1953 to 1954 indicated that the daytime heights were more like 80 kilometers, though the same nighttime heights were found. This difference may be related to latitude or geographic position, and indicates a need for more extensive height observations. In connection with this work on scattering heights, attention is drawn to the recent work at vertical incidence at about 2 Mc/s by Gardner and Pawsey in Australia[23] which used special new techniques. Their height findings are in some respects so similar to those reported above as to suggest that the same part of the ionosphere is involved.

Angle Dependence

The dependence of the intensity of the signal on the scattering angle has been measured for the case when the transmitting and receiving antennas are directed at the ionospheric midpoint of the path. What has been determined is an approximate value for the exponent of $\sin \gamma/2$ which appears in the denominator of the various transmission equations discussed earlier. The experimental arrangement consisted of receiving signals simultaneously from Sterling at 49.7 Mc/s at three receiving stations placed along a single great circle at distances of 491, 592, and 811 kilometers respectively. These distances correspond to a range of path lengths for which the q-curves of Fig. 2 have the greatest difference in slope for different values of the exponent of $\sin \gamma/2$. The high-power pulse transmitter, used previously for the height observations, was used and the simultaneously present tropospheric signals were eliminated, by gating, from the measured intensities. The pulse intensities at the short distances used were very weak, and successful observations were only possible on a few summer days when the scattering was strong. The measurements were made during July, 1953.

The experiment was performed as follows. Separate transmitting rhombic antennas designed for each of the three path lengths were erected at Sterling, side by side, with sufficient space between them to avoid interaction. A single rhombic receiving antenna of identical design to the appropriate transmitting rhombic was erected at each of the three observing stations. The pulse transmitter was then connected in turn to each antenna for a period of about fifteen minutes once each hour during the period of the test. The signal intensity recorders were operated simultaneously and continuously at the three receiving locations. For each receiving station a curve was plotted showing the variation from hour to hour, of the received signal intensity when the station

[22] V. C. Pineo and W. G. Abel, private communication; 1955.
[23] F. F. Gardner and J. L. Pawsey, "Study of the ionospheric D-region using partial reflections," *Jour. Atmos. Terr. Phys.*, vol. 3, pp. 321–344; July, 1953.

was receiving signals from the transmitting antenna designed for its distance. By interpolation for the remaining periods of each hour at each station, it was possible to arrive at curves which permitted comparison of the intensity of the signals at the different distances.

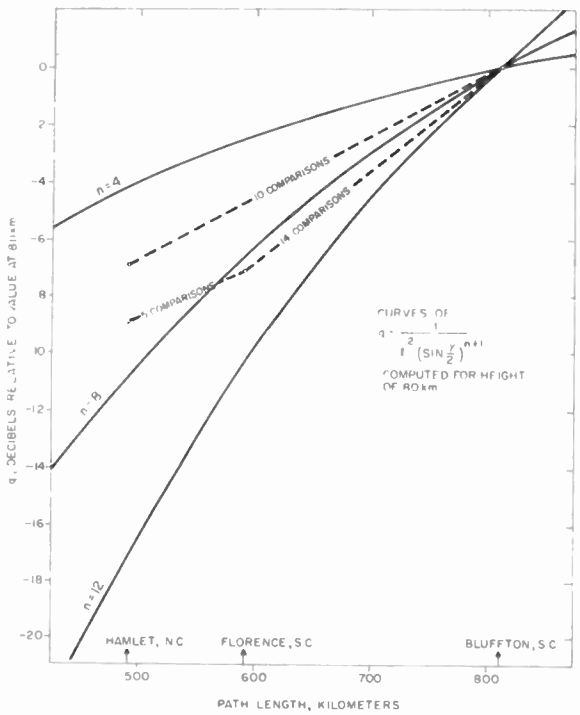

Fig. 16—Results of angle-dependence observations.

The results of these comparisons are given in Fig. 16 which shows comparisons between pairs of receiving stations in order to take account of situations where data are missing from one station. For reference, three q-curves corresponding to exponents of 4, 8, and 12 for a height of 80 kilometers are shown for the appropriate range of distances. It will be seen that the comparison between the two most distant stations indicates that the exponent n in $(\sin \gamma/2)^{n+1}$ is of the order of 8. The other comparisons involving the shortest path for which the observations are thought to be less reliable, indicate a somewhat lower exponent of the order of 4 to 6. All the comparisons are for daytime, and were possible on only three days. Measurements at night and during times of weaker signals will only be possible with much more power. Some further interpretation of these results is given in Part II.

Experiments designed to test the dependence of the intensity of the signals on angle of scatter, for receiving locations off the great circle defined by the principal lobe of the transmitting antenna, have been performed. Their interpretation is complicated by the presence of strong meteoric components which are emphasized in such experiments relative to the scattered signals.[24] As a consequence the signals observed do not fall off as rapidly as would be indicated by the exponent found in the above experiment. This matter will be discussed further below.

Attention is drawn, at this point in the account, to the relatively limited range of scattering angles available for study by the techniques under discussion. For the longest paths and lowest probable scattering height, values of γ as low as about 18 degrees at the path midpoint may be involved. For the shortest path length considered useful or easy to study, about 1,000 kilometers in length, and highest values of ionospheric scattering height, the largest value of γ at the path midpoint is about 25 degrees. With the extraordinary arrangements of the angle-dependence experiment, signals were occasionally observed at 491 kilometers coming from heights of 80 kilometers or higher. At this distance γ for midpoint scattering is about 40 degrees. If values of γ substantially smaller than 18 degrees were involved, care would be necessary in applying transmission equations of the form given above, since a term in the denominator has been omitted on the grounds that the term involving sin $\gamma/2$ is always much larger. For very small values of γ the received power does not increase indefinitely, but rather increases to a maximum nearly equal to the free-space value. As a result of the oblique-incidence $h'f$ observing program of the National Bureau of Standards,[25] it now appears that a means for observing ionospheric scattering at angles from zero to 5 degrees or more is available. This technique involves observing signals scattered through a small angle in the E region and subsequently reflected in the classical manner by the E or F region. These observations are possible with moderately directive antennas by using frequencies just a few per cent in excess of the classical F-region (or E-region) maximum usable frequency for the path.[26]

Frequency Dependence

According to the transmission relation originally applied to the Cedar Rapids to Sterling tests of 49.8 Mc/s, and given by (1), the received power should vary inversely as fourth power of operating frequency for constant values of ionospheric and system parameters.

The first opportunity to test the frequency dependence over the Cedar Rapids to Sterling path occurred in the autumn of 1951. The experiment was performed at 418 Mc/s with systems parameters which should just have permitted the successful detection of signal according to the original transmission equation. The systems parameters were as follows:

transmitter output power:	20 kw
transmitting antenna gain over isotropic radiator:	21 db

[24] V. R. Eshleman and L. A. Manning, "Radio communication by scattering from meteoric ionization," PROC. IRE, vol. 42, pp. 530–536; March, 1954.

[25] P. G. Sulzer, private communication; 1954.

[26] D. K. Bailey, "The Role of Ionospheric Forward Scatter in Oblique Incidence MUF," Talk presented at URSI-IRE Meetings, Washington, D. C.; May 4, 1955.

receiving antenna gain over isotropic radiator:	30 db
receiver noise figure:	4 db
receiver bandwidth:	1 kc/s.

The transmitting antenna was a pyramidal horn tilted to 7 degrees above horizontal in the direction of Sterling. The receiving antenna was a steerable 31-foot paraboloid. The observations made on September 26, September 28–29, and October 17, were disappointing. Only the very strong meteor bursts were observed. They were heard on an average of one every seven or eight minutes in a 24-hour period. This result did not appear sensitive to the angular elevation of the receiving antenna in the range of angles from zero to 30 degrees. At angles much above 30 degrees the burst rate decreased in accordance with expectation considering the beamwidth of the receiving antenna and the path geometry for meteor reflections. It was concluded from these tests that the received power must decline much more rapidly than inversely as the fourth power of frequency.

Routine frequency dependence observations have been made for both the Cedar Rapids to Sterling, and the Anchorage to Barrow paths using frequencies substantially lower than 418 Mc/s. As the results are similar, most of the discussion will deal with the Cedar Rapids to Sterling path, on which two new frequencies have, at different times, been used in addition to 49.8 Mc/s which has always provided a simultaneous reference. For a period of thirteen months continuous-wave transmissions at 107.8 Mc/s were available. Various difficulties with the recording, to some extent associated with the unexpected weakness of the signals, rendered a good part of the observational data of inferior reliability compared with the simultaneous data on 49.8 Mc/s. However, during the summer of 1952 when the signals were strong, good results were obtained, and for the last four months of the program the recording techniques were improved to the point at which it was possible to consider the data of nearly equal reliability to that taken at 49.8 Mc/s. In making comparisons of received signal intensities, representing received available power ratios, the data were adjusted for equal transmitter powers, and equivalent line losses. Also in order that the ionosphere should be illuminated in exactly the same way at the higher frequency, a scaled rhombic antenna was used. This means that the dimensions and height of the new antenna were simply those of the 49.8 Mc/s antenna reduced by the ratio of wavelengths. The 107.8 Mc/s antenna thus had the same lobe pattern and power gain at the maximum of its principal ground-reflection lobe. An identically scaled rhombic antenna was used for receiving at Sterling. In the receiving case, however, it is necessary to remember that the effective area of the 107.8 Mc/s antenna is smaller than that of the 49.8 Mc/s antenna by the wavelength ratio squared. If the frequency dependence is to be expressed on an equal or per unit aperture basis it is necessary to apply this correction before forming ratios. More recently it has been possible to compare 49.8 Mc/s signals with signals received simultaneously from Cedar Rapids at 27.775 Mc/s. Again scaled rhombic antennas have been used, and similar considerations apply.

If it is assumed, in accordance with the various transmission equations, that the received available power varies, after adjustment of the observations to conditions of equal radiated powers, equal apertures, and identical transmitting antenna patterns, as the reciprocal of the frequency to some power n, then a value of n can be obtained by direct comparison of the received signal intensities on two different frequencies. Such comparisons are usually made for simultaneous hourly or half-hourly samples, and the value of n thus determined is referred to as the effective frequency exponent. The word, effective, is intended to qualify the results as applicable only to the comparison of a particular pair of frequencies. In making comparisons, it is of course necessary to eliminate, to the extent possible, observations affected by such things as sporadic-E propagation, individual large meteoric enhancements, tropospheric propagation (very rare), and observations during any malfunctioning of the transmitting or receiving equipment.

With respect to the 107.8/49.8 Mc/s comparisons the following are found:

1. The effective exponent is not constant even when fullest possible allowances are made for experimental error; its extreme range of variation is from about 4 to about 12. (See Fig. 17, next page.)
2. Under conditions of strong signals, particularly in the midday and early afternoon period, as observed at the lower frequency, the median effective exponent tends to be of the order of 8.
3. Under conditions of weak signals, as observed for example at the lower frequency in the evening period and also for somewhat stronger signals in early and midmorning, the median effective exponent is smaller; values of 6 to 7 are typical, as shown in Fig. 18 (next page).
4. These systematic differences in effective exponent are about sufficient to account for certain systematic differences in the diurnal behavior of the median signal intensities observed at the two frequencies, so that no marked correlation can be found between the value of the effective exponent and the strength of the signals at the higher frequency.

This last point in particular is related to the problems of realizable gain and the performance of antennas. The whole question of the meaning of some of the diurnal variations in signal intensity will be discussed below in connection with the role of antennas. In addition to these points, the following special results are noted:

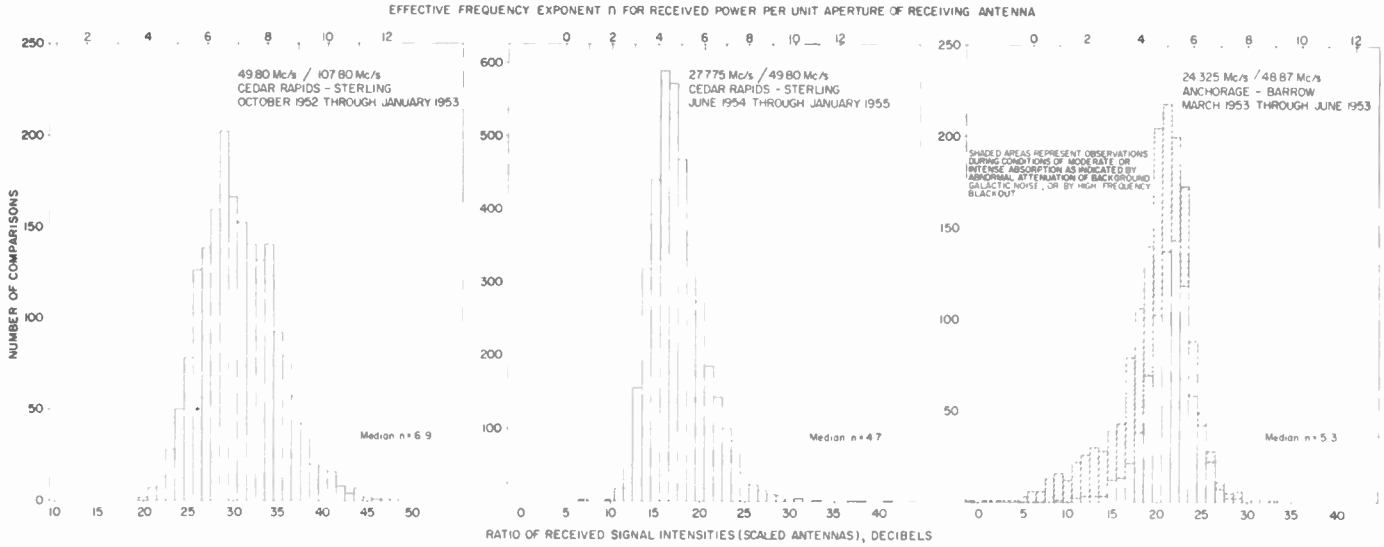

Fig. 17—Observed dependence of signal intensity on frequency.

5. During moderate or intense sudden ionospheric disturbances, associated with solar flares, and often with solar noise outbursts, approximately equal enhancements occur simultaneously on the two frequencies, so that the effective exponent is not appreciably affected.
6. During major meteor showers, which are readily identified by longer duration meteor bursts, the effective exponent as determined from the routine recordings is not appreciably affected.

Good standardized simultaneous recordings at Sterling of signals from Cedar Rapids at 27.775 Mc/s and 49.8 Mc/s covering a period of several months have been obtained. Again scaled rhombic antennas, directed along the great circle, are used, and all data are adjusted for equal transmitter powers, and equivalent line losses. As required, the data are also corrected for equal apertures. With frequencies as low as 27.775 Mc/s nondeviative *D*-region absorption may reduce the intensity of the signals as much as three decibels during midday. A correction for nondeviative absorption at 27.775 Mc/s has not been included in the data presented, since evidence that the scattering stratum might lie substantially above the absorbing layer was not obtained until recently. As in the earlier comparisons, the effective frequency exponent seems to vary as shown in Fig. 17. The following different results have been obtained.

1. Under conditions of strong signals as observed at the lower frequency, particularly in the midday and early afternoon period, the median effective exponent tends to be slightly greater than 5; if a rough allowance for absorption at the lower frequency is included, it may be as high as 6 to $6\frac{1}{2}$.
2. Under conditions of weak signals as observed at the lower frequency, the effective exponent is smaller—a value of 4 to $4\frac{1}{2}$ is representative.

A discussion of the 27.775 Mc/s signal behavior during an SID is reserved for another section below. The general long-term behavior observed for the 107.8 Mc/s and 27.775 Mc/s signals is shown in Fig. 8.

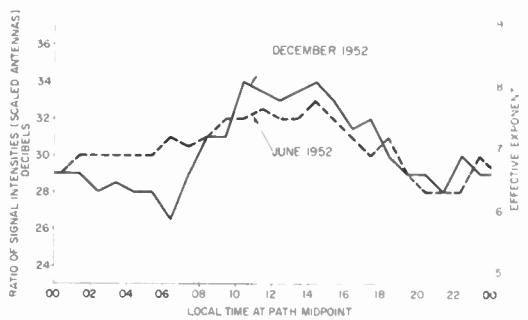

Fig. 18—Diurnal variation of frequency-dependence observed by comparing transmissions at 49.8 and 107.8 Mc/s.

For the last four months of the Barrow operation a second frequency, 24.325 Mc/s, was put on the air at Anchorage. Shortage of space for a scaled rhombic antenna at the Anchorage site led to the adoption of scaled five-element Yagi antennas at both terminals. In order to keep the continuity in the data taken with rhombic antennas at 48.87 Mc/s, the transmitter operating at this frequency was fed alternately for half-hourly periods into the original rhombic antenna and the Yagi. Reception at Barrow was performed simultaneously and separately with both a rhombic and a Yagi antenna. After the usual precautions and adjustments of the data, it was found that the effective frequency exponent was not constant but exhibited characteristics very much like those observed for the 27.775/49.8 Mc/s comparison at Sterling. In Alaska, where severe geomagnetic disturbance is common, the observed value of the effective exponent seemed often to be reduced as a result of nondeviative absorption,

which tended to reduce the intensity of the signals more at the lower frequency. This matter will be further discussed below in connection with special arctic behavior. Fig. 17 presents the results.

Since the effective frequency exponent is not constant for a given pair of frequencies, and differs systematically for a different pair, it would appear to be inappropriate to express the frequency dependence as a constant power of $1/f$. Fig. 19 is presented in an effort to show the frequency dependence in a different way which more directly represents the observations. Still another way of presenting the results is to determine an exponent of $1/f$ which is itself a function of frequency. The tests thus far represent only two substantially different comparisons, and two coefficients, A and B, can therefore be evaluated in an exponent expressed as $A+Bf$.

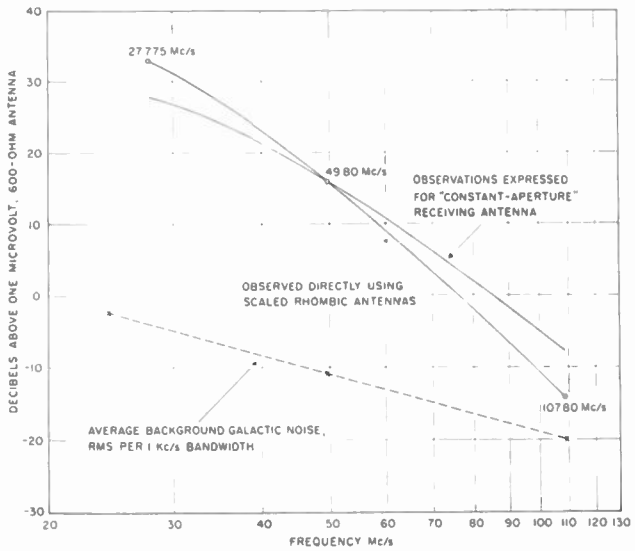

Fig. 19—Observed dependence of signal intensity and background galactic noise on frequency. Value plotted at 49.8 Mc/s is median of hourly signal intensity observations during the year from October, 1951 through September, 1952. Remainder of curve plotted through points representing median values of frequency-dependence ratios shown in Fig. 17.

Selected comparisons for constant aperture representing midday and early afternoon periods when the signal intensities appear to show a controlling solar influence, indicate effective frequency exponents of about 8 and $6\frac{1}{2}$ based on comparison of 107.8 and 27.775 Mc/s respectively with 49.8 Mc/s. Allowance has been made for the effect of nondeviative absorption in obtaining these particular effective frequency exponents. The coefficients A and B representing these selected data are found to be:

$$A = 5.3,$$

$$B = 0.0066,$$

for f expressed in megacycles per second.

A further look at the scattering theory of Villars and Weisskopf[6] is indicated. Their limiting cases of the transmission equation are controlled by a transition function $F(x)$ which enters the transmission equation as a factor $[F(x)]^2$ where $x=\lambda/L_s$. λ is the wavelength and L_s is a length describing the smallest eddy—taken to be about $2\frac{1}{2}$ meters. When $x \gg 1$ the function is of the order of unity and the transmission equation represented by (5) applies. When $x<1$ however the scattering decreases more rapidly with increasing frequency and scattering angle, and in the limit for $x \ll 1$, the transmission is described by (6). Now if λ is fixed as for the 49.8 Mc/s transmissions, the temporal variation in effective exponent must be associated, in the absence of any other mechanism contributing significantly to the net signal, with changes in L_s and therefore with the fine structure of the scattering medium. For a decrease in the exponent, L_s must in fact decrease at a fixed λ, or λ must increase for a fixed L_s. This would explain the lower exponents associated at all times with lower frequencies. It is of some interest to note that for much lower frequencies, the observed exponent would appear to be determined almost solely by the coefficient A and thus be 5.3 for the selected data. The exponent under similar conditions as given by Villars and Weisskopf is $4\frac{1}{3}$. It is difficult to say at this time whether the approximate agreement is significant.

Polarization Dependence

Each scatterer in the ionosphere may be thought of as a small radiating dipole oriented according to the direction of the incident electric vector. Its polar diagram is determined by the factor $\sin^2 \chi$ shown in the various transmission equations discussed earlier. Thus for midpoint scattering with horizontally polarized transmissions, $\chi=90°$ and $\sin^2 \chi=1$. For vertically polarized transmissions for midpoint scattering, $\chi=90°-\gamma$ and $\sin^2 \chi=\cos^2 \gamma$. A typical value of γ is about 20°, thus a loss of about half a decibel will result. To the extent that the received radiation comes from the general direction of the path midpoint, it will have predominantly the same polarization as the transmitted waves, and various experiments involving receiving antennas of opposite polarization have confirmed this. However signals received from scatterers far removed laterally from the path midpoint will, in general, have components of both polarizations, and complete suppression cannot therefore be effected by the use of receiving antennas which are crossed with respect to the transmitting antenna polarizations. There is room for some interesting investigations of the degree of suppression which can be achieved as a function, for example, of time of day and season, particularly if fairly broad-lobed antennas are used. If both crossed-polarization and split-beam techniques are used simultaneously, most of the scattered signal can be eliminated and other signal components can be isolated and investigated.

Important considerations connected with antennas indicate that horizontal polarization is generally to be preferred. This matter is discussed in more detail below.

Observations with Spaced Receiving Antennas

The microscopic structure of the downcoming signal at a receiving site is studied by making simultaneous observations of the signal with spaced receiving antennas. The correlation of the envelopes of scattered signals received on spaced antennas has been investigated at Sterling.[15] The regular transmissions at 49.8 Mc/s from Cedar Rapids were used. Three horizontal five-element Yagi antennas were used for simultaneous reception. The plane-wave gain of each was about 9 decibels with respect to a horizontal half-wave dipole at the same height. The three Yagi antennas were placed at the vertices of a right triangle. The antenna forming the right angle remained fixed and was the reference antenna. The other two were placed at variable spacings from the reference antenna, along the great-circle direction of Cedar Rapids, and normal to the direction of the transmitter respectively. Three voltages, proportional to the envelopes of the signals received by the three antennas, were simultaneously recorded for suitable sampling periods in each of several pairs of spacings. After editing to remove signals obviously strongly influenced by meteoric events, the data were analyzed to determine the envelope correlation coefficients as a function of antenna spacing. Periods of medium and strong signals were somewhat favored. Medians of the results for the different sets of observations made in January and April, 1953 are given in Fig. 20. It will be

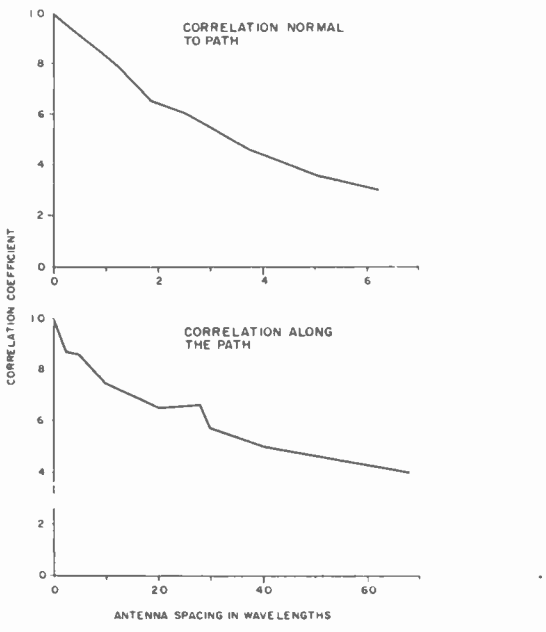

Fig. 20—Observed signal envelope correlation as a function of antenna spacing.

noted that the correlation coefficient falls to 0.5 for spacings of about 3.5 wavelengths normal to the path, and about 40 wavelengths along the path. The interpretation of these results is bound up not only with the scattering mechanism, but also with the beam-width of the transmitting antenna, as discussed in some detail later.

Abnormal Signal Behavior

Meteor Showers

Three well-known meteor showers are recognizable with ease in the routine signal-intensity recordings each year. Doubtless other lesser showers could also be recognized if the records were carefully studied with that objective. The three showers are the Perseids, the Geminids, and the Quadrantids. The shower meteors, which as a class are large meteors compared with the usual ever-present meteors, are recognized on the recordings by the great increase in general spikiness, and by the much longer durations of the bursts which characterize them. Some examples of recordings during a shower and normal recordings with comparable signal intensities are given in Fig. 21 (facing page) for reception at Sterling at 49.8 and 107.8 Mc/s. In these records it should be noticed that spikes associated with a particular meteor are often recognizable at both frequencies. Despite the more frequent and longer duration bursts during the great annual showers, it has not been possible to find any marked general enhancement of the signal intensities. This result is in striking contrast with the result obtained at Ottawa[27] where the signals at 49.8 Mc/s beamed toward Sterling were observed with a much less directive antenna than the rhombic. At Ottawa marked enhancements of the averaged signal intensity are observed during these showers. This result is now better understood as a result of the recent Carysbrook receiving tests which are described below in connection with the discussion of the role of antennas. The position of Ottawa with respect to the region of the ionosphere illuminated by the Cedar Rapids rhombic antenna is such that meteoric signals are enhanced relative to the scatter component. At Sterling the scatter components are greater than the meteoric signals or at times comparable. In the Arctic, events associated with geomagnetic phenomena occasionally lead to considerable enhancements of the scattered signal. If these events, usually having durations of an hour or so, occur during meteor showers or, at times of unusual spikiness in the records, they effectively mask the meteoric signals, as shown in Fig. 22 (facing page).

Sporadic-E Propagation

Occasionally for periods of time varying from a few minutes to several hours very strong signals are received which saturate the normal recorder. These events are considered to be the result of sporadic-*E* propagation, although the field intensities when measured with special auxiliary equipment, generally fall considerably short of inverse-distance values for the paths as shown in Table I. Usually the periods of sporadic-*E* propagation begin gradually and end gradually, though occasionally the beginnings and endings are abrupt. Ex-

[27] P. A. Forsyth and E. L. Vogan, "Forward scattering of radio waves by meteor trails," *Can. Jour. Phys.*, vol. 33, pp. 176–188; May, 1955.

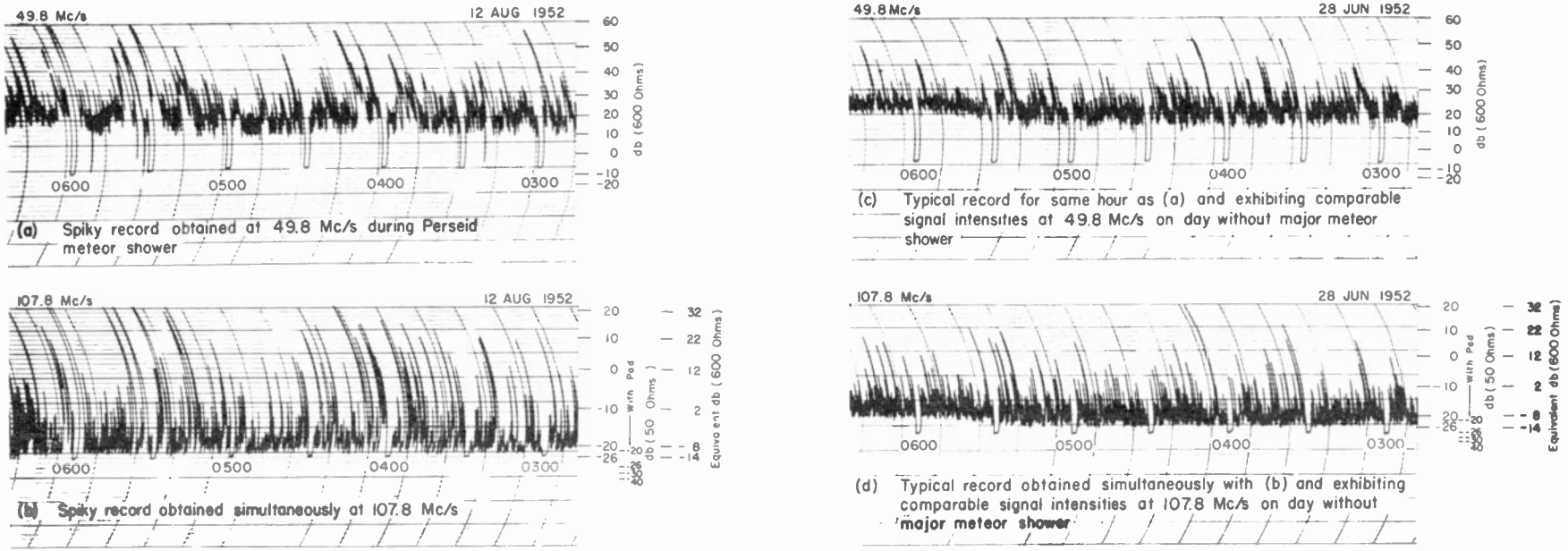

Fig. 21—Sample recordings illustrating effects of shower meteors observed at Sterling.

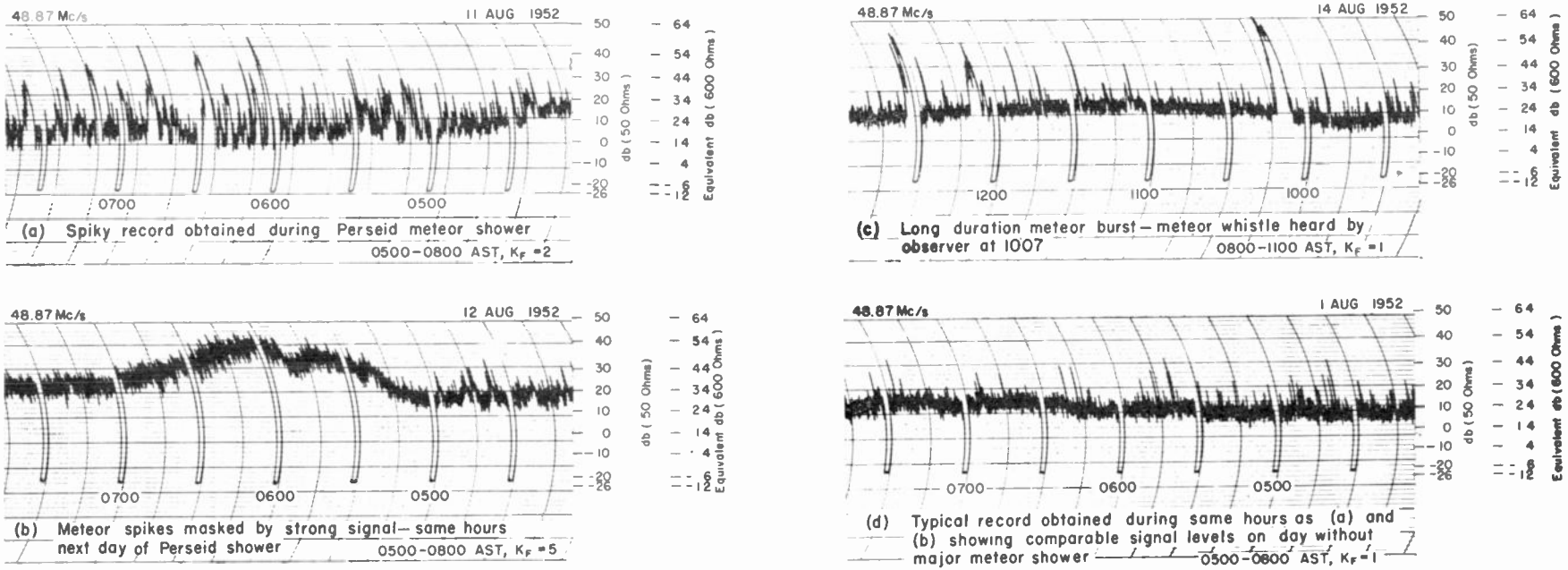

Fig. 22—Sample recordings illustrating effects of shower meteors observed at Barrow.

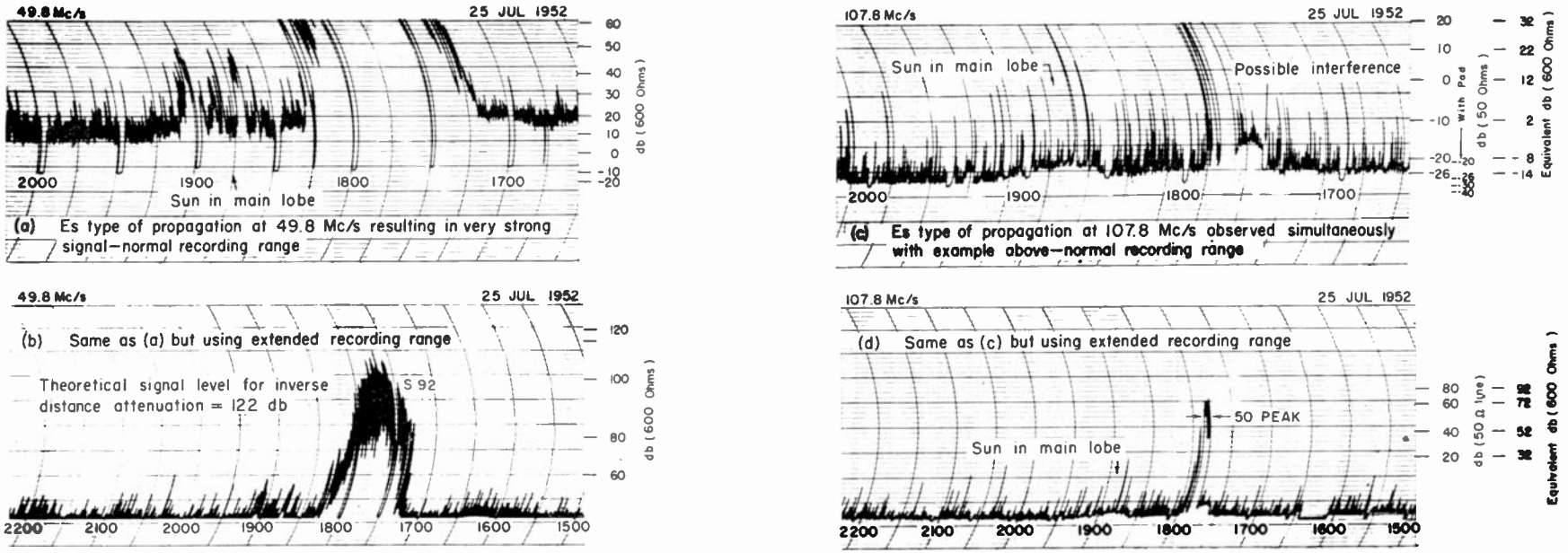

Fig. 23—Sample recordings illustrating effect of sporadic-*E* propagation at Sterling.

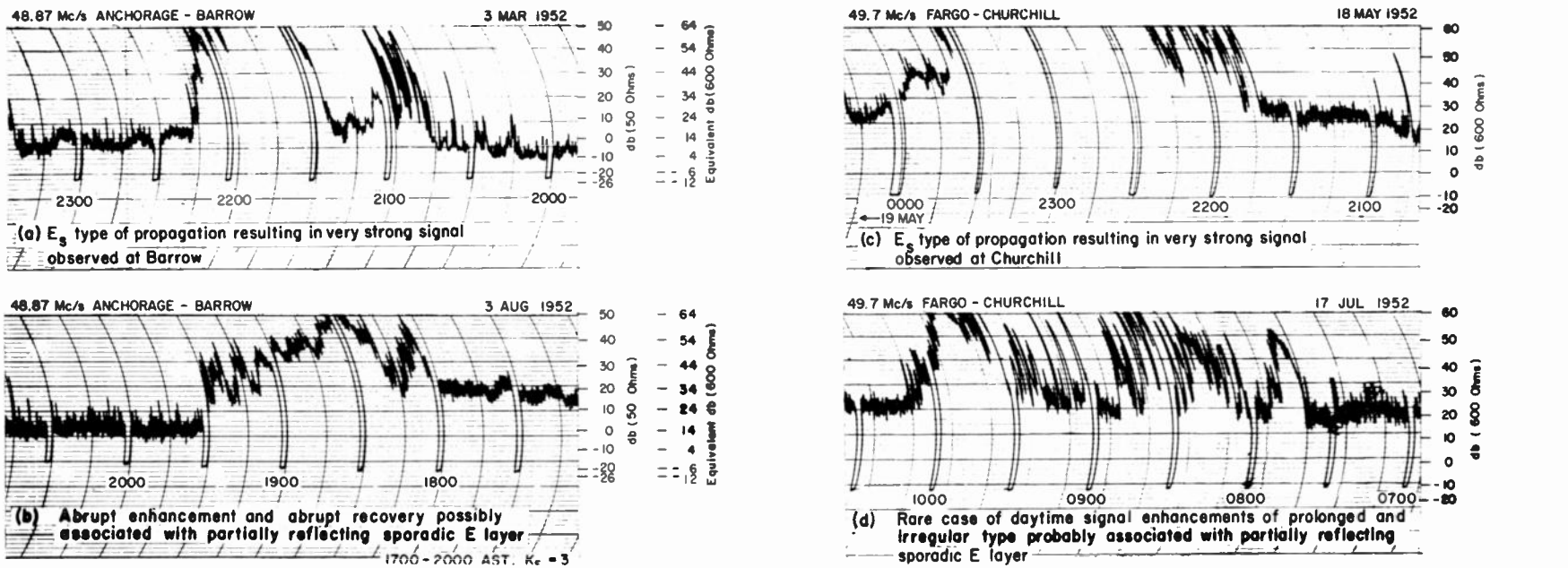

Fig. 24—Sample recordings illustrating effect of sporadic-*E* propagation on arctic paths.

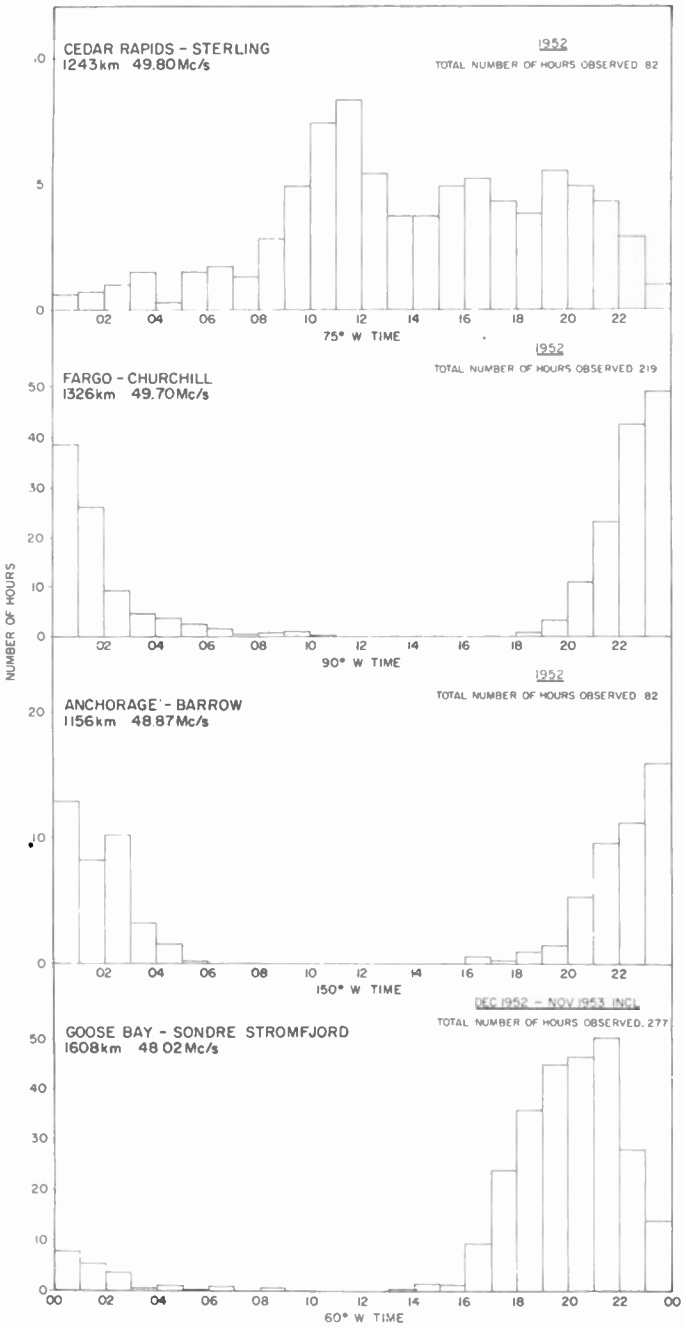

Fig. 25—Diurnal variation of occurrence of sporadic-*E* propagation for yearly periods indicated.

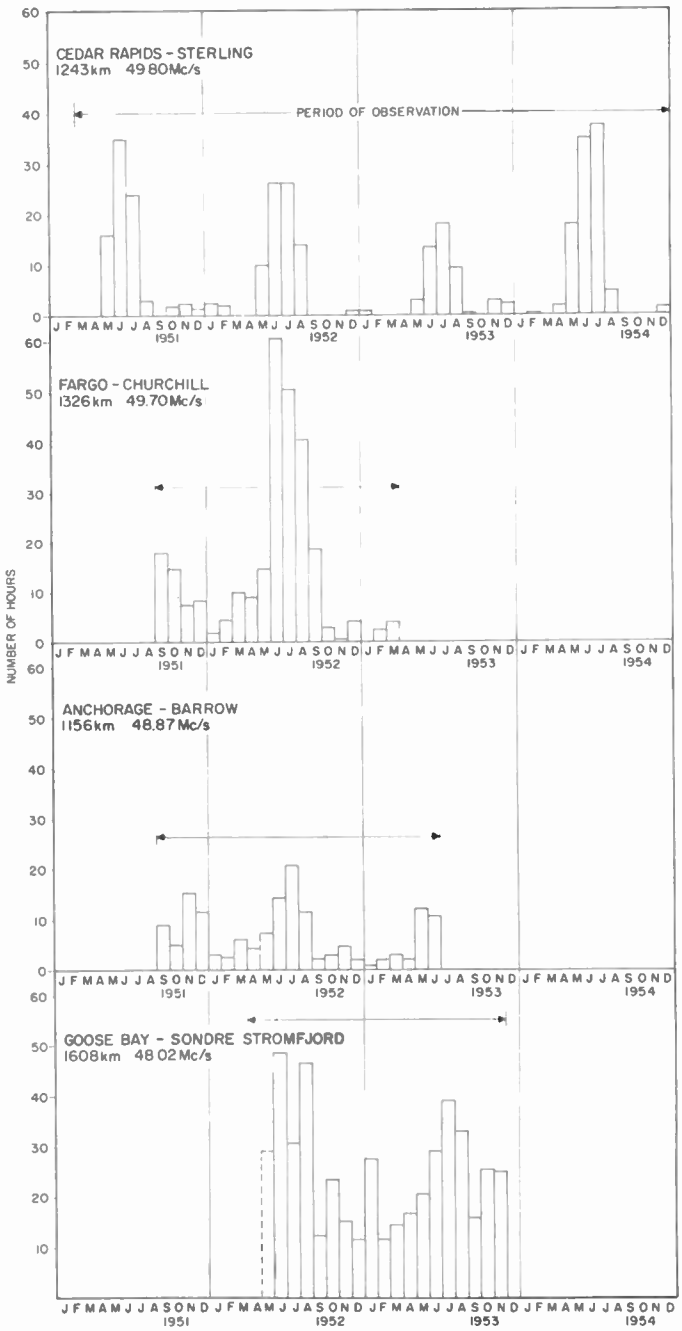

Fig. 26—Seasonal variation of occurrence of sporadic-*E* propagation.

amples of routine recordings illustrating such signals are in Figs. 23, 24 at left. Special records of these events have been kept in order to determine their diurnal and seasonal characteristics. Examples are considered in this analysis if, at some time during a period of at least twelve minutes during which the normal signal is masked, the signal levels exceed one millivolt for a reference impedance of 600 ohms. A criterion of this sort is necessary in order to eliminate the occasional long-duration meteor bursts. Whenever possible, interpolation through the sporadic-*E* event is performed in connection with the data analysis of the normal signals.

The sporadic-*E* observations are summarized in Figs. 25 and 26 for the paths operating at about 50 Mc/s. In these summaries are included the observations at 48.02 Mc/s for the experimental communication path from Goose Bay, Labrador, to Sondre Stromfjord, Greenland. For the temperate-zone path from Cedar Rapids to Sterling most of the sporadic-*E* propagation occurs during the summer season. It may occur at any time of day, but is more likely to occur during the daylight hours. A secondary but much weaker maximum occurs during the winter months, which may have somewhat different diurnal characteristics. Sporadic-*E*

propagation is not observed at this frequency over this path during the equinox months. These findings agree with other mid-latitude observations by other methods at lower frequencies. The characteristics observed on the arctic paths are totally different. Most of the sporadic-E propagation takes place between about 18 hours local time and about 02 hours. On the Goose Bay to Sondre Stromfjord path the diurnal maximum occurs about two hours earlier than on the other arctic paths. Sporadic-E propagation is almost completely absent during the late night and the daytime. This diurnal characteristic is observed in all months. There seems to be more sporadic-E propagation during the summer season, although the summer of 1953 had less sporadic-E propagation than the summer before. Nevertheless it cannot be said that these data show any certain solar cycle influence. The occurrence rates for a particular path were very sensitive to frequency, as would have been expected. At 107.8 Mc/s during the summer of 1952 only two brief occurrences were observed. They coincided with longer events at 49.8 Mc/s. At 27.775 Mc/s more events and a generally longer duration for specific events were observed. A similar result was found in Alaska at 24.325 Mc/s.

A connection between the aurora and sporadic-E propagation has long been suggested. At vertical incidence there appears to be a one-to-one correspondence between the zenith or near-zenith appearance of well-defined active auroral forms and $h'f$ observations of echoes from about 100 to 120 kilometers. On the other hand, nearly all attempts to associate the strong vhf signals of the type under discussion with the appearance of aurora in the illuminated common volume in the E region have proved unsatisfactory. Observations from the terminals of the Anchorage to Barrow path and for a briefer period from Fairbanks, where the path midpoint in the E region is more easily examined, failed to establish any significant connection. In the case of the Fargo to Churchill path the results are somewhat less negative though the connection sought is not very definite. Fig. 27 (facing page) shows an example where correlation between Es-influenced signal recordings and the presence of active auroral forms in the direction of the path midpoint is fairly direct. In this figure the auroral forms were actually photographed from the receiving hut and some of the poles of the receiving rhombic antenna can be seen. Fading twilight masks the observations at first. The discussion given below in connection with the sputter phenomenon should be borne in mind in any attempt to understand the relationship between Es-propagation and auroras.

Sudden Ionospheric Disturbances (SID's)

Signal enhancements at 49.8 Mc/s coinciding with SID's producing sky-wave fadeouts at hf have been observed from the beginning of the program and have already been reported. During 1952 when the 107.8 Mc/s signals from Cedar Rapids were also available at Sterling only a few occurred. They sufficed however to demonstrate that the enhancements were of the same amplitude at the two frequencies and that they occurred simultaneously. Best example obtained is in Fig. 28 (page 1206). Quite recently a moderately strong SID has occurred when signals were being recorded simultaneously at 27.775 and 49.8 Mc/s. In this case a good enhancement was observed at 49.8 Mc/s but the 27.775 Mc/s signal showed at first a trace of enhancement which was followed by a sharp decrease a few minutes after the start of the SID. This is interpreted as indicating that absorption associated with the sharp increase in ionization in the D region was more than enough to offset the enhancement once the event had become well developed. It further indicates that most of the scattering takes place in or above the absorbing layer during these events. At minimum the 27.775 Mc/s signal was still many decibels above the background noise level. It is a matter of some interest that the maximum absorption at 27.775 Mc/s occurred several minutes ahead of the maximum enhancement at 49.8 Mc/s. The details of this event are in Fig. 29 on page 1206.

In examining the routine records some care is necessary in identifying SID's. From time to time enhancements or signal variations of very similar appearance are observed which are not associated with unusual absorption. It is also observed that the weaker SID's produce no identifiable enhancement. The simultaneous recording of some distant hf station usually provides an excellent guide. Also whenever the received noise is predominantly cosmic noise and a transmission break occurs during the event, a significant decrease in the cosmic noise level is observed unless a simultaneous burst of solar noise contaminates the observation. The SID behavior is believed to be directly related to an increase in f_N, the plasma frequency corresponding to the mean electron density, N, in the scattering volume.

Polar Blackouts

The term polar blackout has been given to events occurring in regions of high auroral activity which are characterized by periods of very intense nondeviative ionospheric absorption lasting from somewhat less than an hour to six or more hours. These events, unlike SID's which are usually less than an hour in duration and can only occur during daylight, are observed at all hours though they are much less frequent in the evening period from about 18 hours local time to midnight. As with SID's they produce complete fadeouts at hf, but unlike SID's which occur simultaneously all over the sunlit hemisphere, polar blackouts are fairly local. By local it is meant that they occur over an area a few hundred miles wide, outside of which conditions may be fairly normal. They are thought to be associated in some complex way with the corpuscular radiation from

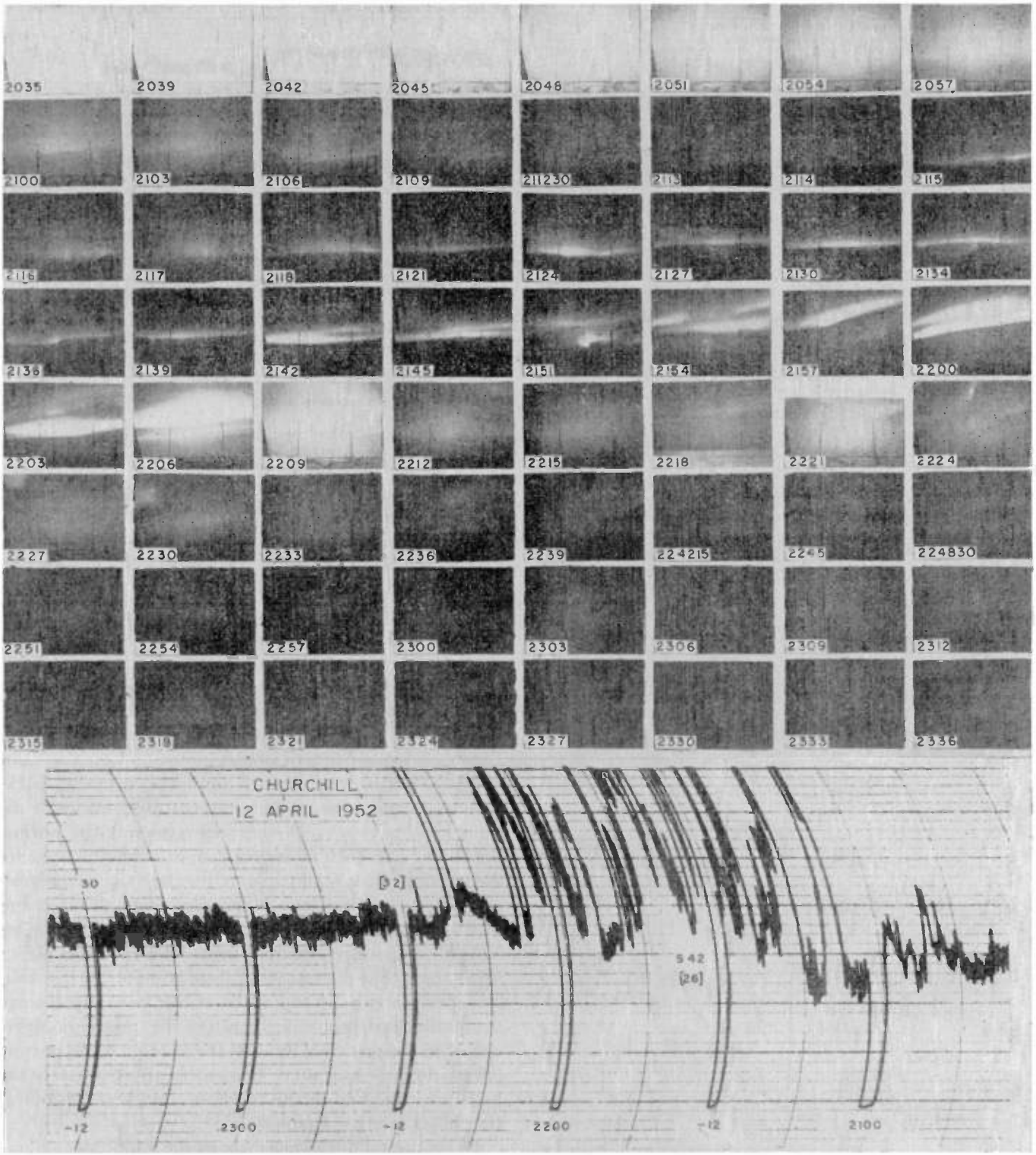

Fig. 27—Sample recording illustrating sporadic-*E* propagation observed at Churchill with accompanying photographs of aurorae in direction of path midpoint.

the sun. The characteristics of polar blackouts, determined from vertical-incidence *h'f* observations at Fairbanks, are well known.[28]

Polar blackouts are frequently much more intense than SID's. This result is derived from the observations of cosmic noise which show much greater absorption, at times, than has been observed during SID's. At 48.87 Mc/s at Barrow the more moderate blackouts produce signal enhancements, but if the blackout is very intense, the scatter signal may appear normal because the exces-

[28] H. W. Wells, "Polar radio disturbance during magnetic bays," *Terr. Mag.*, vol. 52, pp. 315–320; September, 1947.

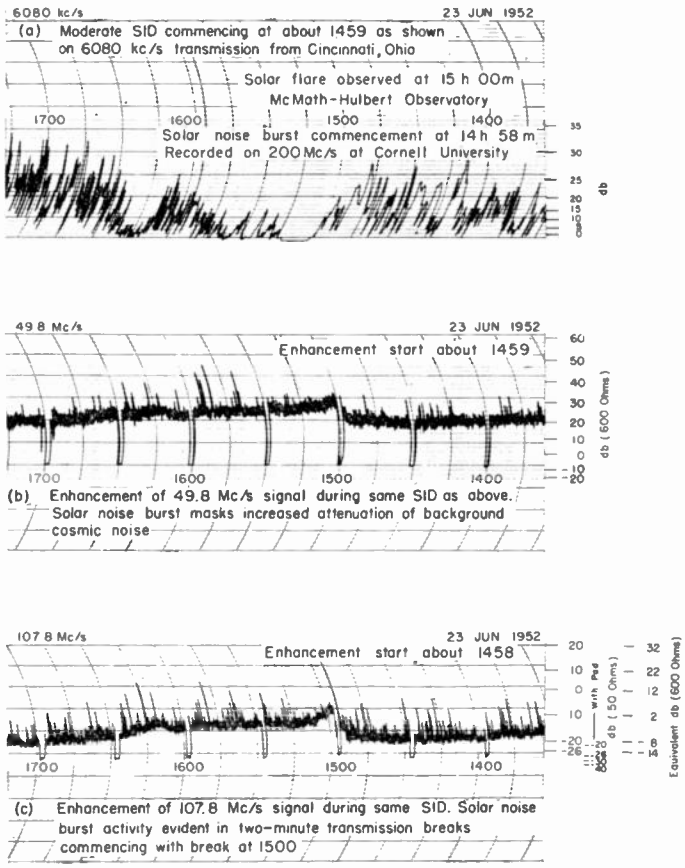

Fig. 28—Sample recordings illustrating simultaneous enhancements of vhf signal intensities observed at Sterling during an SID.

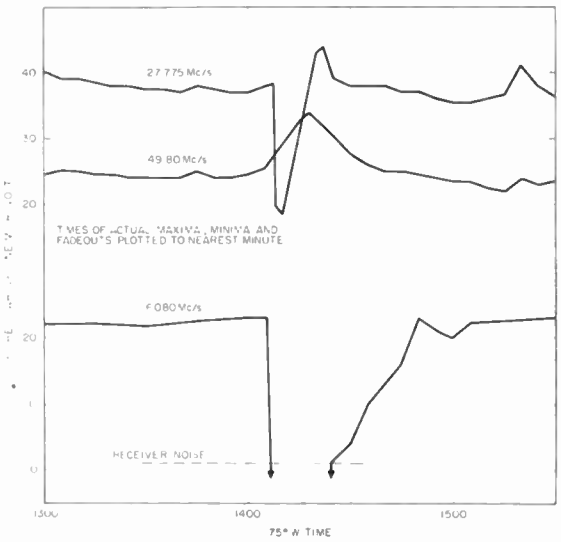

Fig. 29—Signal behavior during SID observed at Sterling on June 18, 1955.

sive absorption has compensated for the enhancement, and the decrease in cosmic-noise level serves as an indicator of the blackout condition. Examples of signal enhancement during intense arctic absorption are shown in Fig. 30.

As no direct pulse observations have been undertaken in high latitudes for height determination, it is of interest to consider what indirect evidence may be adduced about relative height from simultaneous observations on

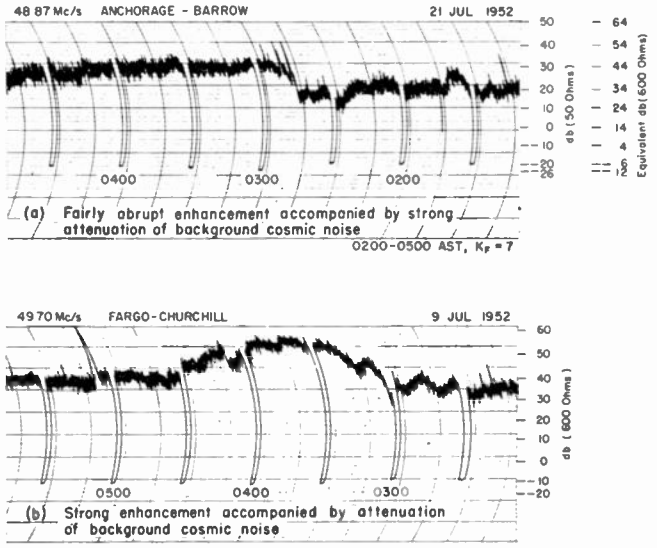

Fig. 30—Sample recordings illustrating typical effects of polar blackouts on arctic paths.

the Anchorage to Barrow path at 48.87 and 24.325 Mc/s during an intense and prolonged polar blackout. The basic observational material was obtained during the blackout of May 19, 1953 and it is presented in Fig. 31. The observations were made using scaled Yagi antennas for both transmitting and receiving. Four sets of simultaneous observations are shown. The variation of the scattered signal intensity as a function of time is shown for 24.325 and 48.87 Mc/s, together with a dashed curve representing, for each frequency, the normal behavior of the signal intensity during the same hours. Below these two sets of observations and on the same scale are shown the variations of the recorded background cosmic noise at the same two frequencies at the same time. Again dashed curves represent the normal behavior. The bottom curves cannot safely be used for direct absorption comparisons at the two frequencies because the cosmic noise is recorded from all directions in the sky according to the lobe patterns of the scaled Yagi antennas used, whereas from independent evidence it is known that the low-level absorption of the blackout was more intense to the south of Barrow. The absorption influenced primarily therefore the cosmic noise received in the principal lobes of the antenna. The bottom curves do, however, serve to identify approximately the beginning and end of the blackout, and give an indication of its relative intensity.

Examination of the behavior of the 48.87 Mc/s signal shows that some enhancement appears to have occurred at first, but as the absorption became more intense the strength of the scattered signals dropped to an appearance of normal. As the blackout wore off, the enhancement again appeared temporarily. From the observed signal-intensity and noise-intensity behavior, and judging by the behavior observed during many other blackout enhancements, it is estimated that the peak enhancement, in the absence of the excessive nondeviative absorption, would have resulted in signal intensities some 5 decibels or more above normal. At 24.325 Mc/s

the scattered signals showed a considerable decrease in intensity throughout the blackout. At the height of the absorption, the 24.325 Mc/s signal was about 16 decibels below normal. Now assume, as is reported above in connection with SID observations on higher frequencies, that the actual scattering enhancement is the same on the two frequencies. It then follows that an enhancement of about 5 decibels occurred in the strength of the scattering at 24.325 Mc/s, but that the observed strength of scattering, some 16 plus 5, or 21 decibels lower at the most intense phase of the blackout, was due to the nondeviative absorption occurring below the scattering stratum.

An independent check is available for the argument thus far. The frequencies involved are almost exactly in a one-to-two ratio. The different absorptions deduced for the two frequencies, 21 and 5 decibels respectively, correspond very nearly to an absorption ratio of four-to-one. The absorption in decibels would thus appear to vary inversely as the square of the frequency—a result in accordance with long-established theory, as verified by other kinds of measurements, for nondeviative absorption at frequencies well above the gyro-frequency.

Fig. 31—Signal and background cosmic noise behavior during a polar blackout observed at Barrow on May 19, 1953.

Next observe that the cosmic noise at 24.325 Mc/s decreased some 8 decibels during the maximum of the blackout. This figure represents a conservative estimate, for reasons already given, of the absorption in the direction of arrival of the scattered signals, for a single transit through the absorbing layer. For scattering from heights above the absorbing layer, two transits of the absorbing layer would occur, and the reduction in intensity of the scattered signals during the blackout would be expected to be in excess of 16 decibels. This conclusion is in sufficient accordance with the interpretation of the observations already given, to permit the further deduction that the scattering stratum during a blackout, at any rate, is substantially entirely above the absorbing layer. As with SID's the blackout enhancements are believed to be directly related to an increase in f_N, the plasma frequency indicated in the various transmission equations discussed earlier.

Sputter

Shortly after the commencement of operation of the arctic paths, Fargo to Churchill, and Anchorage to Barrow, occasions were observed when the received signal exhibited fading rates up to two or three hundred cycles per second, or about one hundred times normal. As a result, the signal sounded as if the transmitted wave was being noise-modulated, and the name *sputter* was used to describe the sound. Sputter represents a different propagation mechanism which occurs simultaneously with the regular scattering. If the sputter propagation is of comparable or greater intensity than the normal signal, it can be readily identified in the routine recordings by a characteristic thinning of the trace. Often sputter can be heard, if the audio gain is turned up, when it is too weak to affect the recordings. Since the receiving stations were not continuously manned, it has been necessary to study the occurrence of thinned trace as evidence of occurrence of moderate or strong sputter. Examples of thinned trace resulting from sputter are in Figs. 32 (next page) and 33 (page 1209). A seasonal and diurnal study of the occurrence of thinned trace has been made for Churchill and Barrow with results shown in Fig. 34 (page 1210). Sputter is much more frequent at Barrow. Its diurnal characteristics are similar at both places, and are considerably less distinct than those of sporadic *E*. But, it appears to occur most frequently between 16 hours local time and midnight. At Barrow a secondary maximum seems to occur between the hours of 04 and 08 local time. Sputter was not observed within an hour or so of midday at any season at Barrow and Churchill, nor was it observed during the summer when the normal signal levels were very high. A few cases of sputter at noon have, however, been recorded at Sondre Stromfjord at 48.02 Mc/s. To some extent the summer absence must be regarded as a masking effect, since it has been noticed on occasion when the audio gain has been turned up.

The connection between sputter and aurorae is now fairly well understood. To begin with, the five or six cases of sputter observed at Sterling during the past four and a half years have been associated with known auroral activity and with reports from radio amateurs of weak long-distance vhf communication in the 50 and 144 Mc/s bands. It should not be concluded that all auroras can give rise to sputter. Given suitable seeing conditions, aurora may be seen practically every night at Barrow and Fairbanks, but sputter is relatively infrequent. To produce sputter an aurora must be of the right kind, and must be situated in the correct place with respect to the vhf path. The aurora which can be observed with radar techniques such as those used by Canadian groups, University of Manchester workers,

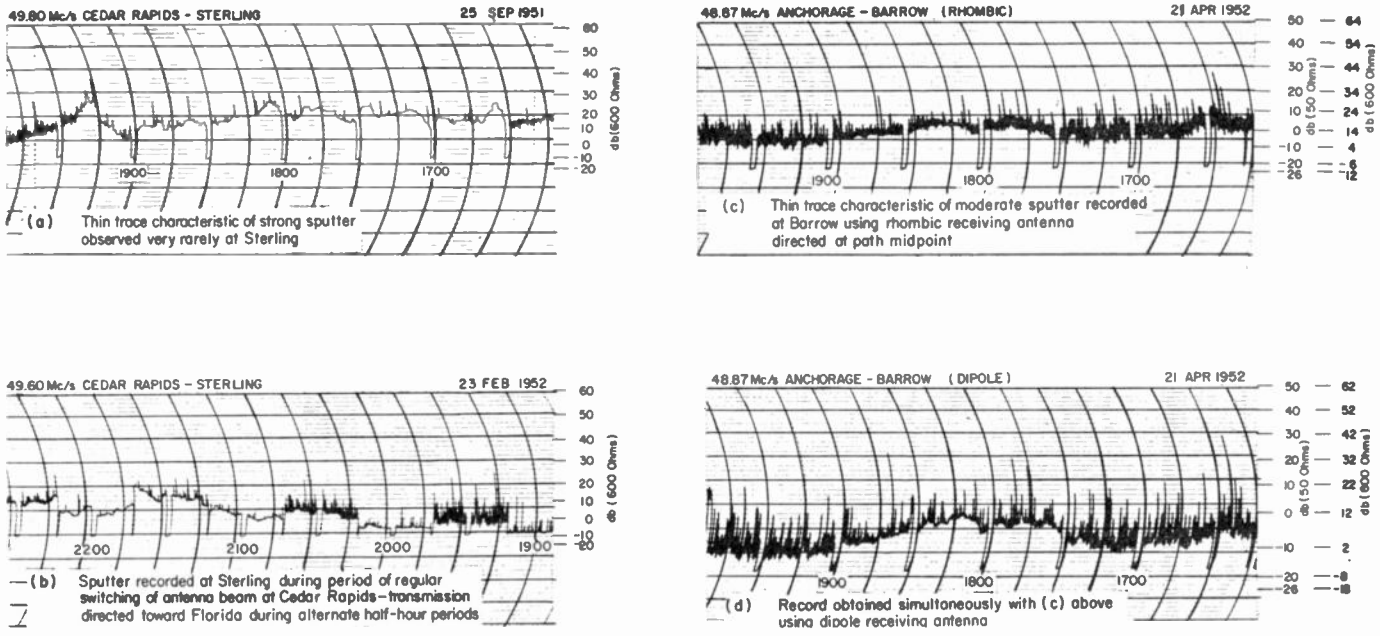

Fig. 32—Sample recordings illustrating the effects of sputter propagation.

and the group at Cornell University, has not been identified as the kind capable of giving rise to sputter. A recent paper by Booker, Gartlein, and Nichols[29] reviews the entire problem of radio reflections from the aurorae, and contains a full bibliography of this interesting subject. Chapman has made a thorough study of the geometry of radio echoes from aurora.[30]

A close analogy exists between meteors and aurorae as regards their study by radio techniques employing vhf. In both cases most of the work has been performed with radar techniques. In both cases the requirement for strong echoes has been found to be that the meteoric ionization column or the auroral ionization column should be viewed at normal or nearly normal incidence. In this connection it has been found that the auroral forms giving strong fairly discrete echoes consist of shafts or rays, rather than more diffuse forms. It is also fairly well established that the only part of an auroral ray or shaft capable of giving much of an echo is situated in the height region from about 80 to 120 kilometers—the same region in which meteors produce their ionization. In the case of meteors, the orientation of the ionization column is determined by astronomical considerations involving the orbit of the meteor and the motion of the earth; in the case of aurorae the orientation of the ionization columns is along the lines of the earth's magnetic field. As with meteors, the extension of the radar work to cases where the transmitter and receiver are widely separated leads to considerable geometric complication. In both cases the ionization columns must be so oriented with respect to the path that there exists a plane including the axis of the column of ionization from which the angles of incidence and reflection are about the same. The high rate of fading of the auroral signals is thought to be of Doppler origin and to be associated not only with the corpuscular velocities, which are greater than meteor velocities by factors of 50 to 100, but with rapid changes in the excitation. At any rate the practical effect is to spread a monochromatic transmission into a band two or three hundred cycles wide with weak wings extending much further.

In the light of the geometric conditions required for propagation by way of the aurorae, it is now possible to understand why there is more sputter observed at Barrow than at Churchill. It is also possible to deduce that long paths should exhibit less sputter than short ones. Indirect confirmation of this lies in the observation at Barrow illustrated in Fig. 32 that more sputter is observed when less directive antennas are used. It now seems inappropriate to apply the concepts of frequency and angle dependence, as used for forward scattering, to sputter.

In connection with the analysis of the Barrow observations of sputter, and in connection with studies of the relationship between the strength of the vhf signals and geomagnetic disturbance, many $h'f$ records taken at the same time at Anchorage, Fairbanks, and Barrow were examined. Some of these results are reported in the next section. As a result of this study, however, it is now possible to recognize in regular $h'f$ observations the presence of aurora of the type which gives rise to sputter. Fig. 33 presents examples of the $h'f$ observations at Fairbanks during an event consisting first of a short polar blackout, followed by sputter. As the fadeout wears off, it will be seen that E-region echoes of an unusual type appear. The observation at 04h 15m is particularly typical. As the frequency increases the echo heights are

[29] H. G. Booker, C. W. Gartlein, and B. Nichols, "Interpretations of radio reflections from the aurora," *Jour. Geophys. Res.*, vol. 60, pp. 1–22; March, 1955.

[30] S. Chapman, "The geometry of radio echoes from aurorae," *Jour. Atmos. Terr. Phys.*, vol. 3, pp. 1–29; January, 1953.

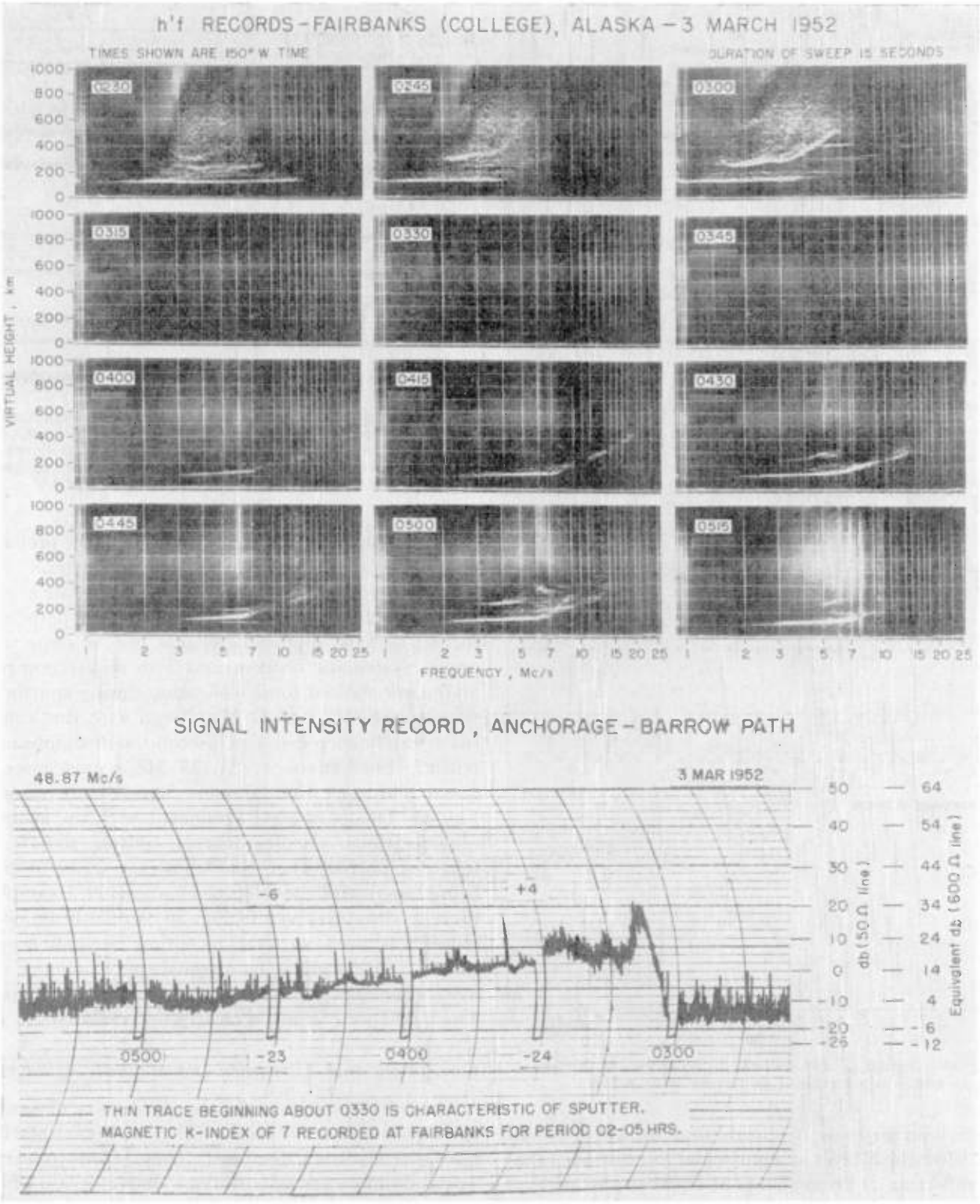

Fig. 33—Sample recording illustrating polar blackout followed by sputter observed at Barrow with accompanying *h'f* observations made at Fairbanks near the path midpoint.

at first normal, then a steady increase in height with frequency is observed with the echoes disappearing at delays corresponding to heights at vertical incidence of about 450 kilometers. *E*-layer traces of this type are usually referred to as "slant *E*." Their interpretation is thought to be about as follows. Until the vertical-incidence critical frequency, about 8 Mc/s in the record cited above, is reached, the *E*-region trace is normal for the Arctic. At frequencies above the vertical-incidence critical frequency the propagation path is triangular. The first leg is sufficiently oblique for *E*-layer reflection to take place. The second leg consists of a downcoming

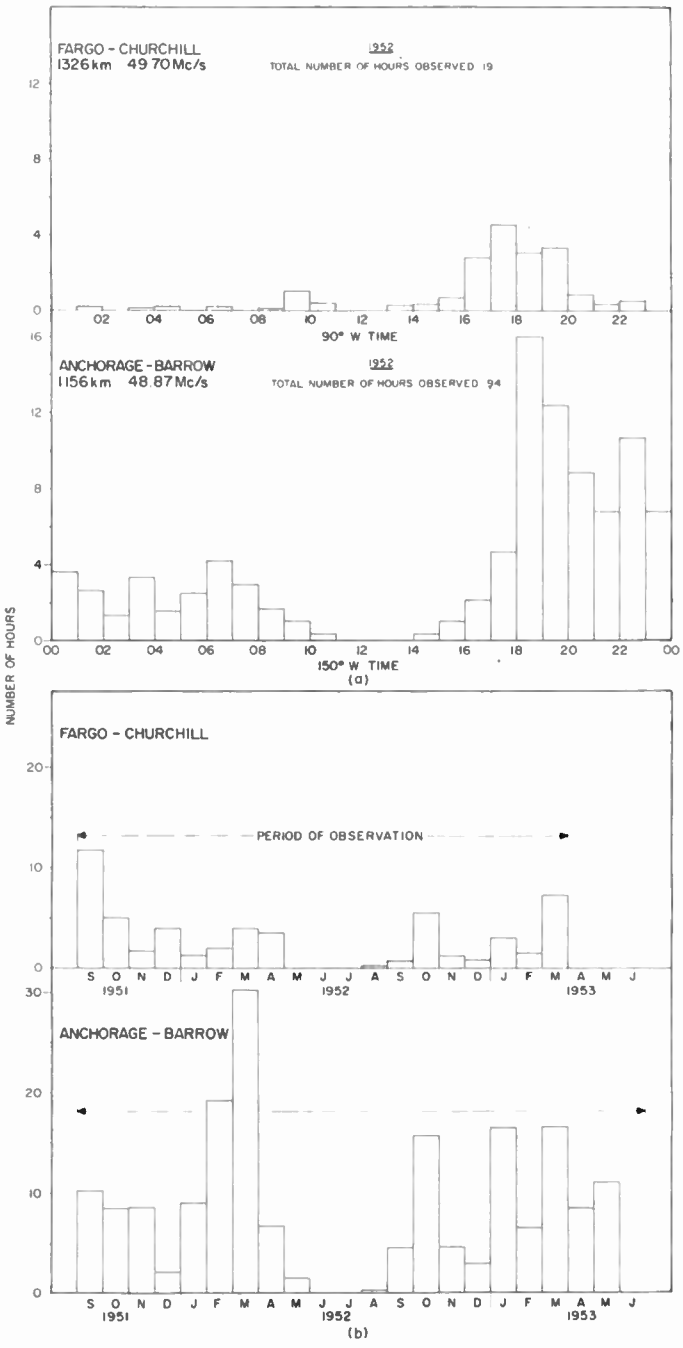

Fig. 34—Diurnal (a) and seasonal (b) occurrence of thinned trace characteristic of sputter for arctic paths.

ray which impinges on an auroral shaft or part of a shaft lying below the E layer at a particular location such that after reflection at an angle about equal to the angle of incidence, the ray on its third leg is returned to the $h'f$ receiver. Energy may traverse this course in either direction. As the sounding frequency is raised the E-layer reflection becomes more and more oblique; hence different and more distant auroral shafts must be responsible for the echoes observed. Gaps in slant-E records can be due either to an absence of auroral shafts in a suitable position, or to nulls in the antenna patterns in the directions and at the vertical angles required. Systematic observation of slant E at ionospheric stations in the

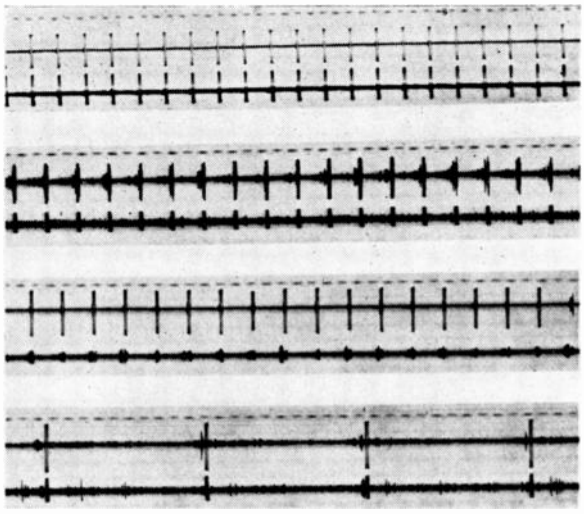

Fig. 35—Reception at Barrow of pulse transmissions from Anchorage at 24.325 Mc/s (upper trace) and 48.87 Mc/s (lower trace), during normal conditions (top frame) and during sputter (lower three frames) showing pulse elongations at either or both frequencies. Pulse duration slightly greater than one millisecond.

Arctic will thus give much information of the prevalence of aurorae of the type associated with sputter.

As the propagation path for sputter signals is generally quite different from the propagation path of the regular signals, multipath effects can be expected to occur. Systematic observations with millisecond pulses at Barrow showed some elongation during sputter, but the elongations at 48.87 Mc/s even with the Yagi antenna rarely exceeded a millisecond with significant intensity. Elongations at 24.325 Mc/s were more frequent and somewhat greater. Samples are shown in Fig. 35. This is in good agreement with the geometric considerations. Oscillograms of sputter signals were taken at Barrow when the Anchorage transmitter was being keyed with the teletype character R. Examples of these records are given in Fig. 36. A dual-beam oscilloscope was used so that reception on two separate rhombic antennas having a transverse spacing of about 300 feet and other pairs of antennas could be compared. The high-speed fading is clearly uncorrelated.

Correlations with Absorption and Magnetic Activity

The enhancements of the signal intensity observed at 50 Mc/s which occur during SID's and polar blackouts have already been discussed. They represent extreme cases of a more general behavior characteristic which is that departures of the signal intensity from normal, as measured, for example by the monthly medians, are closely correlated with amount of nondeviative absorption relative to the monthly median. This result is demonstrated in Fig. 37 in which absorption conditions at Fairbanks near the middle of the Anchorage to Barrow path have been determined from the $h'f$ observations. The procedure is to divide the $h'f$ observations taken at the middle of each hour for which medians of the vhf signal intensity are taken into four classes according

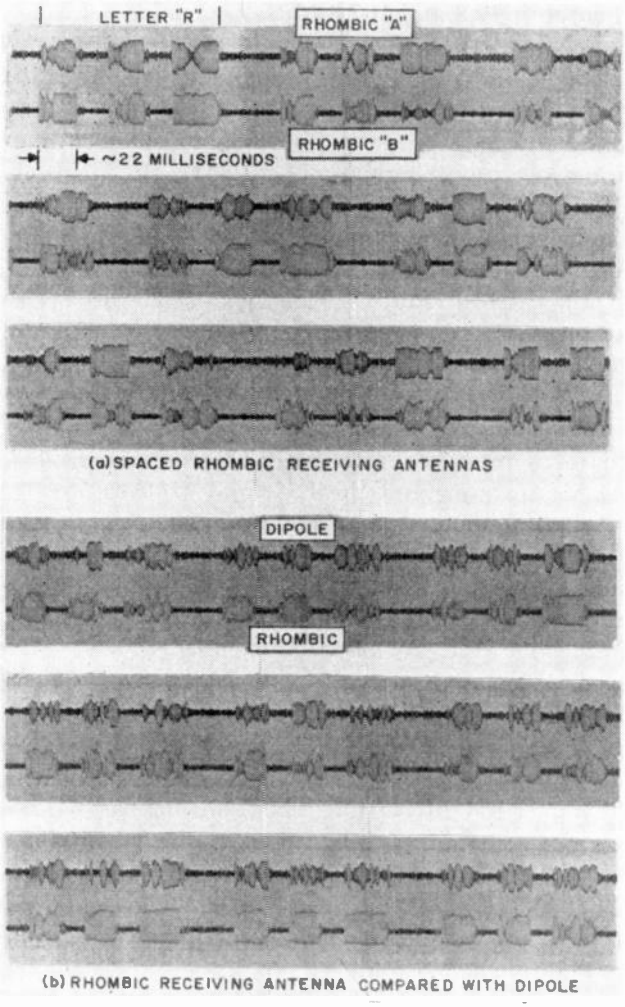

Fig. 36—Oscillograms illustrating radioteletype transmissions observed at Barrow during sputter.

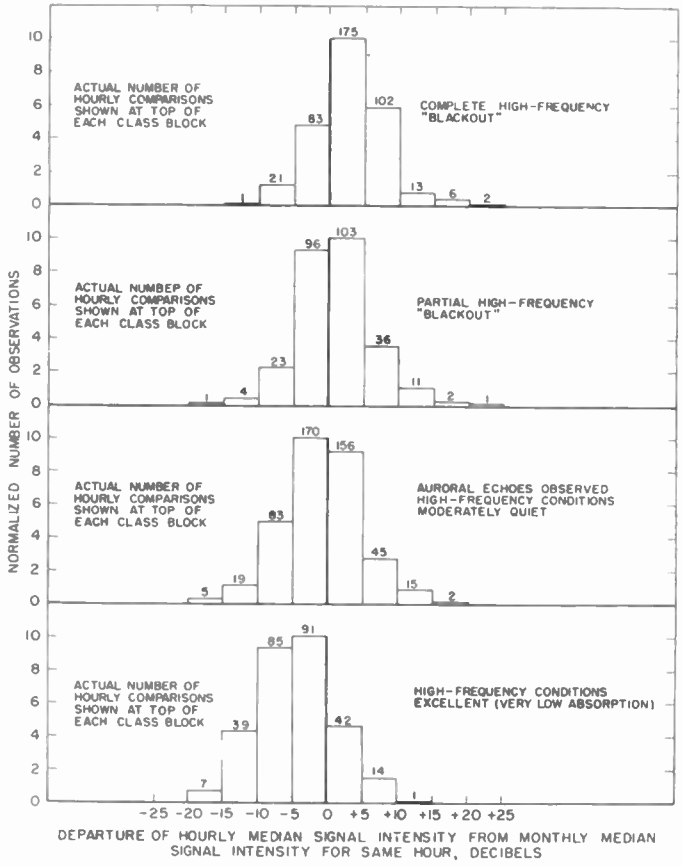

Fig. 37—Correlation of ionospheric absorption observed at hf with vhf signal intensities observed at Barrow.

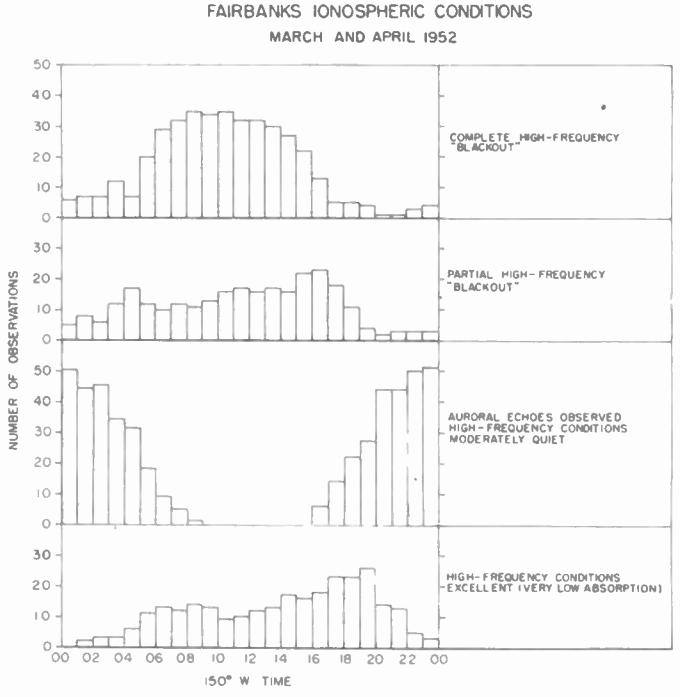

Fig. 38—Diurnal variation of occurrence of hf absorption classes for same period as used for Fig. 37.

to the absorption they indicate. The first class corresponds to a complete hf blackout and no echoes are observed. The second class represents conditions of partial blackout when weak echoes are observed at frequencies well above the normal lower frequency limit. The third class represents fairly quiet conditions when auroral echoes of a type usually not associated with sputter and slant-E are seen.[31] The fourth class corresponds to very quiet ionospheric conditions, when absorption is low, and hf propagation conditions are good. The distributions of departures of the individual hourly medians of the vhf signal intensities from the monthly medians for the same hours are then defined according to the absorption class as shown. In Fig. 38 the diurnal variation in the occurrence of the absorption classes for the same period of time is shown. From these figures it will be seen that as a general rule the signal intensity is stronger than normal when the absorption is greater than normal, and vice versa. It is also of some interest to note that the periods of partial and complete blackout occur mostly between about 05 and 17 hours local time, a period corresponding to strong signals according

[31] R. W. Knecht, "Relationships Between Aurorae and Sporadic E Echoes," Talk presented at URSI-IRE Meetings, Washington, D. C.; April 24, 1952.

to the monthly medians for the same months. During the universal period of minimum signal intensity in the evening around 20 hours local time, cases of very low absorption were most frequently observed.

A similar sort of analysis has been made in which the departures of the signal intensities observed at Barrow from the monthly median have been compared with the magnetic K-indexes observed at Fairbanks over a period of thirteen months. Result of this analysis is in Fig. 39. Black dots represent the median signal-intensity departures for each class interval in K-index and vertical lines at their limits show upper and lower decile values.

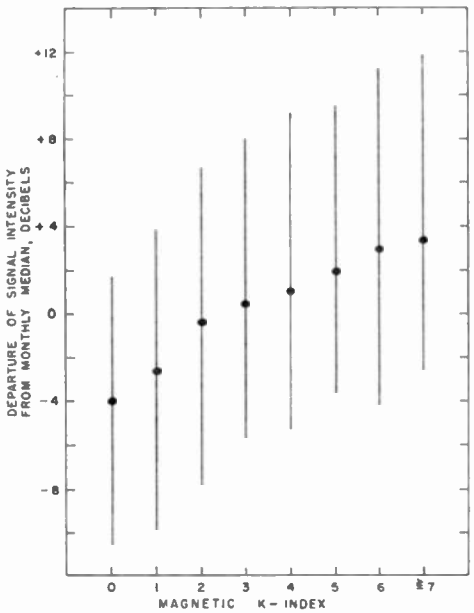

Fig. 39—Correlation of magnetic K-indexes observed at Fairbanks with signal intensities observed at Barrow.

These correlations are not on a one-to-one basis by any means but serve to demonstrate in a definite manner the statistical relationship between the strength of the vhf signals and ionospheric and magnetic conditions. It is the observation that the vhf signals tend to be stronger than normal during periods of heavy hf absorption or complete blackout that makes the vhf propagation attractive for arctic communications.

Tropospheric Propagation

While the various observations of the pulse transmitter located at Sterling have generally shown a "ground wave" even at the greatest distance tried, 811 kilometers, the intensity of the "ground wave" or tropospheric wave was weak, and decreased as the distance increased. There is therefore little reason to suppose that the continuous-wave observations at 49.8 Mc/s at Sterling have been contaminated to any significant extent by tropospheric propagation. This is more especially so because the rhombic antennas used have very poor radiation characteristics at the angles supposed to be of importance for tropospheric propagation. Nevertheless during the late part of the summer of 1952 when both 49.8 and 107.8 Mc/s transmissions were being recorded at Sterling, meteorological conditions were favorable and sufficiently stable for tropospheric ducts to form. During this period the Cedar Rapids transmissions were received for several hours at a time by means of tropospheric propagation with an intensity sufficient to affect and at times dominate the recordings. The most conspicuous sign of the tropospheric propagation was a thinning of the trace, somewhat resembling certain cases of sputter. The signals on this occasion exhibited a rolling type of slow intensity fluctuation characteristic of certain types of tropospheric propagation. Independent evidence of the widespread character of the meteorological situation was received from radio amateurs reporting near record-breaking contacts at 144 Mc/s throughout the East and Midwest.

Tropospheric propagation was observed at that time at both 49.8 and 107.8 Mc/s, though more frequently and conspicuously at the higher frequency. It is suggested that some of the occasions during the summer of 1952 when the 107.8 Mc/s signals seemed unduly strong compared with the 49.8 Mc/s signals, with a resulting small effective exponent for frequency dependence, may have resulted from tropospheric propagation of a type strong enough to affect the measured value of signal intensity without showing as a conspicuous alteration in the character of the trace. Fig. 40 shows simultaneous samples of recordings at 49.8 and 107.8 Mc/s illustrating the influence of tropospheric propagation at 49.8 Mc/s and dominant tropospheric propagation at 107.8 Mc/s.

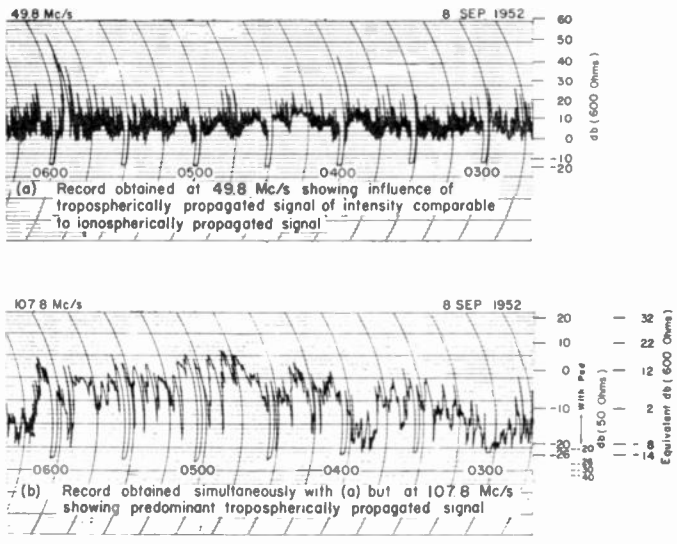

Fig. 40—Sample recordings at Sterling showing influence of unusual tropospheric propagation from Cedar Rapids.

Evidence of tropospheric propagation has not been found again at Sterling, nor has it been found at any time at any of the northern receiving terminals.

Background Noise Observations

Throughout the recording program the transmissions have been interrupted twice each hour in order to observe the level of background noise. Most of these ob-

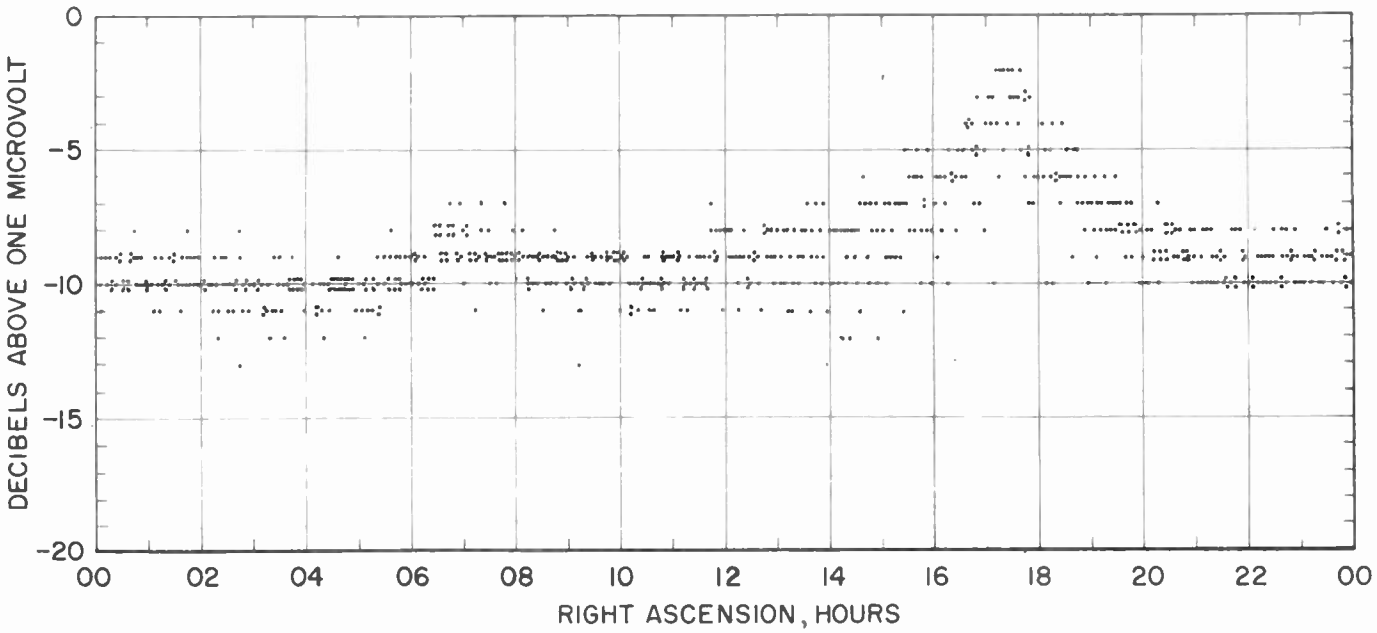

Fig. 41—Cosmic noise intensity observed hourly at Churchill in a 2 kc/s noise band, during December, 1951.

servations have been of cosmic noise. Fig. 41 is a mass plot of the measured noise intensities in a 2 kc/s noise bandwidth at Churchill during December, 1951. The observations are plotted against the right ascension of the direction of the receiving lobe maximum. The declination observed was about 26 degrees south. Two well-defined maxima are observed corresponding to the passage of the plane of the galaxy through the lobe. The greater maximum corresponds closely to the direction of the galactic center. Similar results have been obtained at the other receiving terminals, though they differ in detail owing to the different declinations viewed.

The twice-hourly noise observations soon proved to have definite value in the observing program. In the first place, for most kinds of changes in the receiving antenna or receiving system, drifts or discontinuities in the noise intensities gave a sensitive and valuable warning. Frequently drifts could be compensated for in the data analysis by knowing how much the noise observation was in error. In the second place, the noise levels at 50 Mc/s proved to be moderately sensitive indicators of the presence of unusual ionospheric absorption. A case in point has already been given in connection with the polar blackout illustrated in Fig. 31.

Apart from cosmic or galactic noise, solar noise was occasionally observed. The declination viewed by the Sterling rhombics was about 20 degrees north, and by the Barrow rhombics 11 degrees south. The sun therefore passed directly through these main lobes each day for a period of a few days twice each year. On these occasions solar noise was observed, usually of the quiet background kind, but occasionally of the active outburst kind. The latter was sometimes strong enough to be observed in the side lobes at other times of the year.

At various times noise of terrestrial origin was observed, as for example when active electrical storms were in progress near the receiving locations. Ignition noise, and power line noise have also been observed. At Sterling the precipitation noise levels were frequently high during certain rainstorms. At Churchill and Barrow, snow or drifting ice crystals during blizzard conditions gave rise to high noise levels. In one case at Barrow during a very severe blizzard, the precipitation noise rose to levels exceeding the signal level. During this event the noise level could be closely correlated with the wind velocities as observed at a U. S. Weather Bureau station about a mile away. Fig. 42 illustrates the noise behavior during this blizzard.

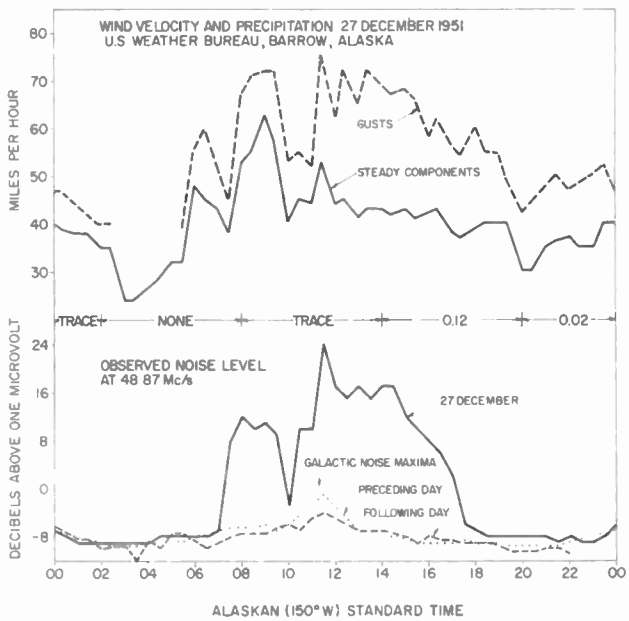

Fig. 42—Precipitation noise at Barrow during a severe blizzard.

If the antennas and receiving equipment are operated correctly and are properly designed, receiver noise is never a limiting factor at 50 Mc/s, though it influences, significantly at times, the observations of background cosmic noise at 107.8 Mc/s.

Part II. The Role of the Antennas

Introduction

In the preceding account it has been repeatedly emphasized that the behavior of the observations and the interpretations of this behavior cannot be divorced from consideration of the antennas actually used. In the sections that follow the part played by the antennas in the propagation studies will be examined more closely and from several points of view.

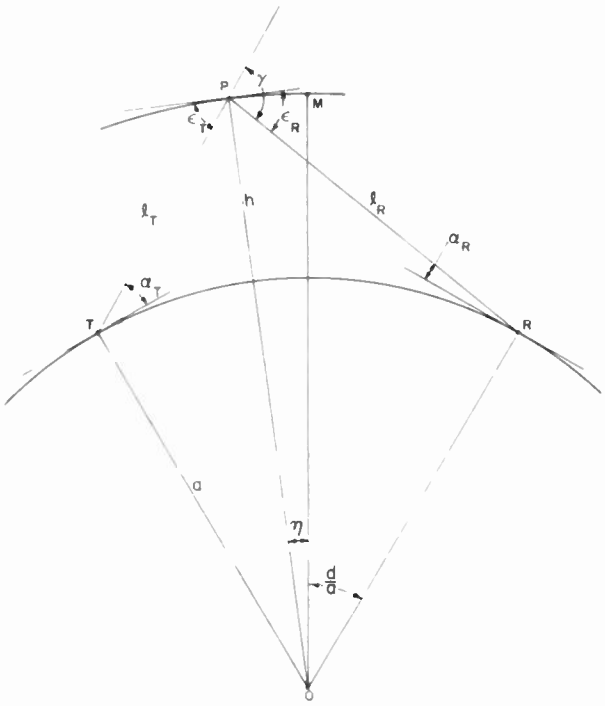

Fig. 43—Geometry for Case I scattering.

Geometric Considerations

Some generalization of the concept of the geometric factors, q, defined in a particular sense by (3) and (4), is indicated. Consider Fig. 43 where P represents the position of an elementary macroscopic volume of the scattering medium which is presumed to be distributed in a shell concentric with the earth, having a thickness b, small compared with its height h above earth. Let

M = midpoint of the path in the scattering medium,
P = a point in the scattering shell displaced from M in the plane containing the transmitter T, receiver R, and center of the earth O,
η = the angular position of P with respect to M measured at the center of the earth,
α_T, α_R = the angular elevation of P as seen from T and R respectively,
l_T, l_R = the ray lengths to P from T and R respectively,
ϵ_T, ϵ_R = the angles between l_T and l_R respectively, and the tangent plane to the scattering shell at P,
γ = the scattering angle,
$2d$ = surface distance from T to R,
a = radius of the earth, and
h = height of the thin scattering stratum.

The following relations may be used to determine the α's, l's, ϵ's, and γ as a function of the displacement of P from M as measured by η according to the conventions of Fig. 43:

$$\tan \alpha_T = \frac{\cos\left(\frac{d}{a} - \eta\right) - \frac{a}{a+h}}{\sin\left(\frac{d}{a} - \eta\right)}, \tag{8}$$

$$\tan \alpha_R = \frac{\cos\left(\frac{d}{a} + \eta\right) - \frac{a}{a+h}}{\sin\left(\frac{d}{a} + \eta\right)}, \tag{9}$$

$$l_T = \frac{(a+h)\sin\left(\frac{d}{a} - \eta\right)}{\cos \alpha_T}, \tag{10}$$

$$l_R = \frac{(a+h)\sin\left(\frac{d}{a} + \eta\right)}{\cos \alpha_R}, \tag{11}$$

$$\cos \epsilon_T = \frac{a}{a+h}\cos \alpha_T, \tag{12}$$

$$\cos \epsilon_R = \frac{a}{a+h}\cos \alpha_R. \tag{13}$$

and finally

$$\gamma = \alpha_T + \alpha_R + 2\frac{d}{a}, \tag{14}$$

or

$$\gamma = \epsilon_T + \epsilon_R. \tag{15}$$

If horizontal polarization is used the angle χ previously discussed is 90°. In vertical polarization $\chi = 90° - \gamma$. Displacements of P from M of the type illustrated by Fig. 43 will be referred to as Case I.

Now consider Case II, as represented by Fig. 44 in which P is displaced from M in a direction forming a right angle at the midpoint with the displacements of Case I. That is to say, P is displaced from M in such a way that $\alpha_T = \alpha_R = \alpha$, $l_T = l_R = l$, and $\epsilon_T = \epsilon_R = \epsilon$. As shown in Fig. 44 let ζ represent the angular position of P with respect to M measured at the center of the earth. It is necessary for Case II to define an azimuth β as the direction of P as seen from T or R with respect to the great-circle path connecting T and R. The following relations may now be used to calculate the principal geometric quantities, as a function of the displacement of P from M as measured by ζ:

$$l^2 = (a+h)^2 + a^2 - 2a(a+h)\cos\frac{d}{a}\cos\zeta, \tag{16}$$

$$\cos\gamma = \frac{2a^2 \sin^2 \frac{d}{a} - l^2}{l^2}, \tag{17}$$

$$\sin\alpha = \frac{(a+h)\cos\frac{d}{a}\cos\zeta - a}{l}, \tag{18}$$

$$\sin\beta = \frac{(a+h)\sin\zeta}{l\cos\alpha}, \tag{19}$$

and

$$\sin\epsilon = \frac{(a+h) - a\cos\frac{d}{a}\cos\zeta}{l}. \tag{20}$$

In Case II if horizontal polarization is used at T, the downcoming signal at R from P will contain both vertically and horizontally polarized components when $\zeta \neq 0$. The power received at R from P with a horizontal antenna is measured by $\sin^4\chi$, and with a vertical antenna by $\sin^2\chi\cos^2\chi$.

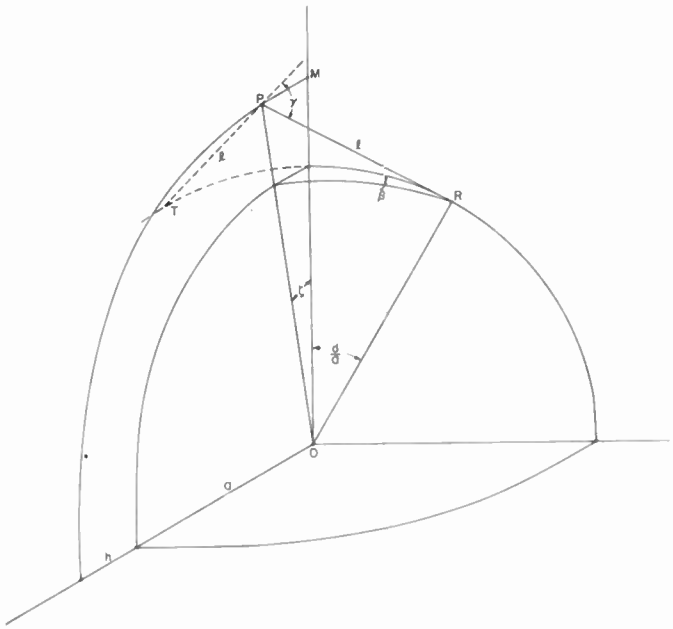

Fig. 44—Geometry for Case II scattering.

To obtain χ the following relationship is used,

$$\cos\chi = \frac{2a}{l} \frac{\sin\frac{d}{a}\cos\frac{d}{a}\sin\zeta}{\sqrt{1 - \cos^2\frac{d}{a}\cos^2\zeta}}, \tag{21}$$

or

$$\cos\chi = \frac{a}{l}\sin\frac{2d}{a}\sin\beta. \tag{22}$$

With the relations above it is possible to compute the geometric quantities required for certain idealized beam swinging transmission arrangements, which are chosen to give further insight into the interpretation of the observations made with less than ideal arrangements.

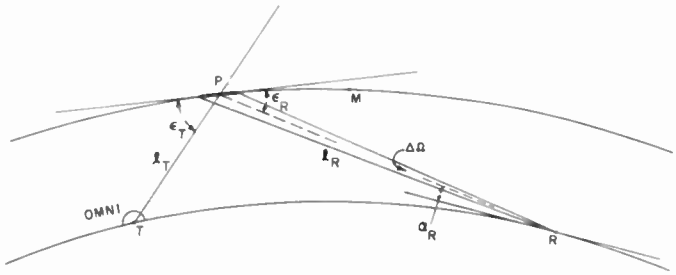

Fig. 45—Geometry for first beam swinging model—"omni to beam."

First Beam Swinging Model—"Omni to Beam"

As a first trial consider Fig. 45, which represents Case I geometry. The transmitter at T is connected to an omnidirectional antenna having an aperture A_0 and the receiver R is connected to a highly directional antenna having a single lobe of solid angle $\Delta\Omega$ which is inversely proportional to its aperture A_D. The receiving antenna is so directive that its beam $\Delta\Omega$ is formed independently of the ground no matter how it is steered as long as the lower edge of the beam is above the horizon. The directivity $\Delta\Omega$ is such that throughout the intercepted elementary macroscopic volume of the scattering medium, the values of the l's and γ may be regarded as constant to a high order of approximation. The position of the intercepted scattering volume may thus be represented by the point P as shown in Fig. 45. The received power is now expressed as a function of the position of P in the plane represented by Fig. 43, that is to say in a Case I manner. In accordance with the definition of the scatter cross section, the following relation can be written

$$P_r \propto \underbrace{\frac{P_t}{l_T^2}}_{(a)} \cdot \underbrace{\frac{bl_R^2\Delta\Omega}{\sin\epsilon_R}}_{(b)} \cdot \underbrace{\frac{\sin^2\chi}{\left(\sin\frac{\gamma}{2}\right)^n}}_{(c)} \cdot \underbrace{\frac{A_D}{l_R^2}}_{(d)}, \tag{23}$$

where

(a) is proportional to the incident power density,
(b) is the macroscopic element of volume illuminated by T seen by the receiving antenna,
(c) is proportional to the scatter function,
(d) is the solid angle intercepted at R,

but $A_D \propto 1/\Delta\Omega$, so that the geometric aspects of the transmission may be expressed by:

$$\frac{P_r}{P_t} \propto \frac{b\sin^2\chi}{l_T^2\sin\epsilon_R\left(\sin\frac{\gamma}{2}\right)^n}, \tag{24}$$

and a geometric factor, q, generalized in this manner

may be defined as

$$q = \frac{1}{l_T^2 \sin \epsilon_R \left(\sin \frac{\gamma}{2}\right)^n}. \tag{25}$$

If the beam $\Delta\Omega$ is swung according to Case II, the analogous generalized geometric factor is:

$$q = \frac{1}{l^2 \sin \epsilon \left(\sin \frac{\gamma}{2}\right)^n}. \tag{26}$$

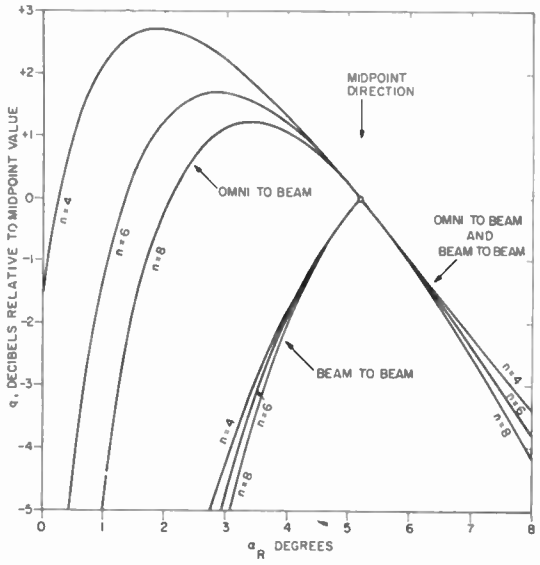

Fig. 46—Generalized q factor for Case I geometry for Cedar Rapids to Sterling distance.

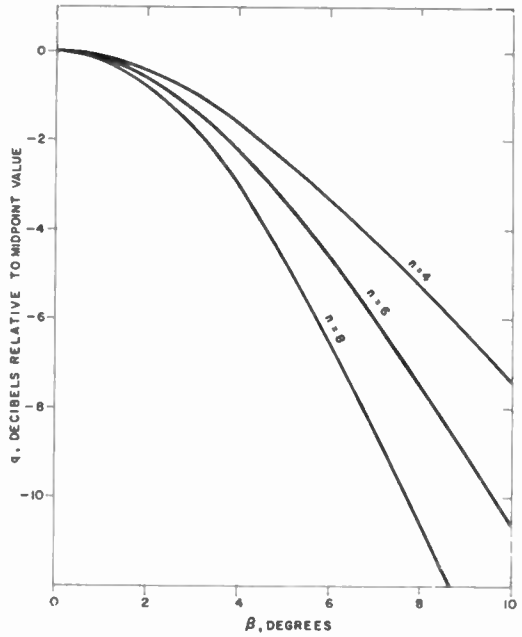

Fig. 47—Generalized q factor for Case II geometry for "omni to beam" model for Cedar Rapids to Sterling distance.

Figs. 46 and 47 illustrate the approximate behavior of (25) and (26) respectively in the vicinity of the path midpoint for the Sterling–Cedar Rapids path for $n=4$, 6, and 8. Fig. 46 shows q as a function of α_R. In Fig. 47 q is plotted as a function of β. For higher values of n the q curves fall more steeply from their maximum values, and the position of the maximum for Case I beam swinging is displaced in the direction of the path midpoint. In Fig. 47 the polarization correction $\sin^4 \chi$ corresponding to horizontal antenna elements at both terminals has been included.

The symmetrical properties of the q for Case I above may be easily established by interchanging T and R and by swinging the beam to a point displaced by an equal value of η in the direction of R.

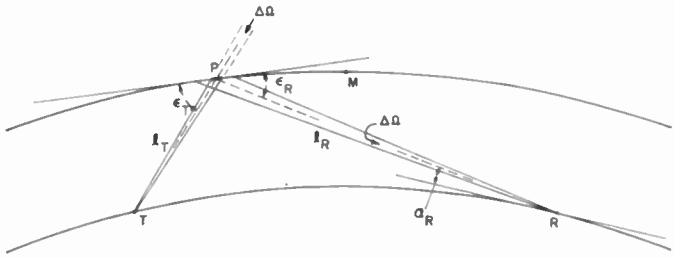

Fig. 48—Geometry for second beam swinging model—"beam to beam."

Second Beam Swinging Model—"Beam to Beam"

For this trial consider Fig. 48 which represents Case I geometry. Both T and R are connected with identical highly directional antennas of the kind used for receiving in the previous example. The two beams are directed toward P. The received power is now expressed as a function of the position of P as it varies in the plane represented by Fig. 43. As before the following relation may be written for P closer to T:

$$P_r \propto \underbrace{\frac{P_t}{l_T^2 \Delta\Omega}}_{(a)} \cdot \underbrace{\frac{b l_T^2 \Delta\Omega}{\sin \epsilon_T}}_{(b)} \cdot \underbrace{\frac{\sin^2 \chi}{\left(\sin \frac{\gamma}{2}\right)^n}}_{(c)} \cdot \underbrace{\frac{A_D}{l_R^2}}_{(d)}, \tag{27}$$

where (a), (b), (c), and (d) have the same meanings as before. Thus:

$$\frac{P_r}{P_t} \propto \frac{A_D b \sin^2 \chi}{l_R^2 \sin \epsilon_T \left(\sin \frac{\gamma}{2}\right)^n}. \tag{28}$$

If P is closer to R, the result corresponding to (28) is:

$$\frac{P_r}{P_t} \propto \frac{A_D b \sin^2 \chi}{l_T^2 \sin \epsilon_R \left(\sin \frac{\gamma}{2}\right)^n}. \tag{29}$$

In both cases the denominator contains the larger l and larger ϵ. If l_l and ϵ_l are written for the larger values of l and ϵ according to the position of P for Case I geometry, the generalized geometric factor q may be defined as:

$$q = \frac{1}{l_l^2 \sin \epsilon_l \left(\sin \frac{\gamma}{2}\right)^n}. \tag{30}$$

If the beams are now swung in azimuth corresponding to Case II geometry, the intersection of one beam with the scattering shell no longer entirely contains the other beam and a further factor is required in the generalized q. Since it is always assumed that the thickness of the scattering shell is small compared with its height, the scattering volume can again be written as the area of the thin shell illuminated multiplied by its thickness. Thus the volume illuminated by the transmitting beam is

$$V = \frac{bl^2\Delta\Omega}{\sin\epsilon}, \tag{31}$$

and if V_c is defined as that part of the illuminated volume within the receiving beam, then the further factor in the generalized q for Case II geometry is V_c/V, and

$$q = \left(\frac{V_c}{V}\right)\frac{1}{l^2\sin\epsilon\left(\sin\frac{\gamma}{2}\right)^n}. \tag{32}$$

The factor V_c/V can be approximated as follows. Define 2τ as the exterior angle between the two beam directions projected on a tangent plane at P. τ may be obtained from the following relation:

$$\cos\tau = \frac{\sin\frac{d}{a}}{\sqrt{1-\cos^2\frac{d}{a}\cos^2\zeta}}, \tag{33}$$

or

$$\cos\tau = \frac{\sin\beta}{\sin\zeta}\sin\frac{d}{a}. \tag{34}$$

Then as long as $2\tau \leqq \epsilon$, which includes the region of principal interest:

$$\frac{V_c}{V} \approx 1 - \frac{\sin 2\tau}{\pi\sin\epsilon}. \tag{35}$$

A less convenient approximation for V_c/V which is usable for all possible values of τ is

$$\frac{V_c}{V} \approx \frac{2}{\pi}\left[\arctan\left(-\frac{\cot\tau}{\sin\epsilon}\right) - \arctan\left(\frac{\tan\tau}{\sin\epsilon}\right)\right]. \tag{36}$$

The two arc tangents represent 2nd and 1st quadrant angles respectively. This expression is exact for beams of circular cross section in the limit as $\Delta\Omega \to 0$. Figs. 46 and 47 illustrate the behavior of (30) and (32) respectively for $n = 4$, 6, and 8 in the vicinity of the path midpoint for the Cedar Rapids to Sterling path. Fig. 49 includes the polarization correction $\sin^4\chi$ corresponding to horizontal antenna elements at both terminals. It will be seen that the maximum transmission takes place when the two beams are directed at the path midpoint. The two beams are then matched exactly in the scattering medium. As before if a greater value of n is selected the curves fall away more steeply.

The Beamwidth of the Scattering Mechanism

In general there will be an angular width in azimuth ϕ and an angular width in elevation ψ, which together define the range of directions from which the power received mainly arrives. With the aid of the foregoing beam swinging models it is possible to examine what may be termed the natural beamwidth of the scattering medium. The natural horizontal beamwidth associated with the scatter mechanism is called ϕ_m and is defined by the angular distance between the points three decibels below the maximum q's for Case II geometry. Table III shows values of ϕ_m obtained from Figs. 47 and 49 for typical values of n. It will be noted that ϕ_m does not vary greatly with extreme variations in the beamwidth of the transmitting antenna. The values in Table III are representative for all practical path lengths. At the greater distances beyond 1,800 kilometers, the ϕ_m's are about one degree narrower, and for the shortest distances of practical interest, about 1,000 kilometers, the ϕ_m's are about one degree wider.

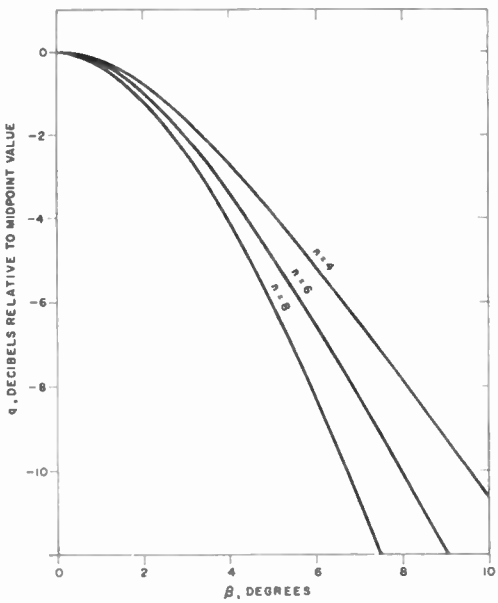

Fig. 49—Generalized q factor for Case II geometry for "beam to beam" model for Cedar Rapids to Sterling distance.

TABLE III

ϕ_m, Degrees, Cedar Rapids to Sterling Path

n	Omni to beam	Beam to beam
4	11.3	8.6
6	9.4	7.5
8	8.0	6.8

In the case of the vertical plane, as represented by Case I geometry, what may be termed the natural beamwidth ψ_m is defined as the angular distance between points three decibels below the maxima shown in Fig. 46. It is to be noted that the transmitting antenna plays a significant part in determining the angular elevation at the receiver of the upper and lower limits

of ψ_m. The case of the omnidirectional antenna to beam antenna represents an extreme condition exceeding any found in practice. The beam to beam case comes closer to practice. Table IV shows values of ψ_m obtained from Fig. 46 for typical values of n.

TABLE IV

ψ_m, DEGREES, CEDAR RAPIDS TO STERLING PATH

n	Omni to beam	Beam to beam
4	5.2	4.2
6	5.2	3.9
8	5.0	3.7

These results are discussed below in connection with problems associated with practical antennas.

EFFECTIVE VOLUME FOR SCATTERING

In practical situations, the transmitting antenna will have considerable directivity. If the transmitting antenna beamwidths, ϕ_a and ψ_a, in azimuth and elevation respectively, are substantially smaller than ϕ_m and ψ_m, ϕ and ψ will be largely determined by ϕ_a and ψ_a. For the longer paths, the common volume geometry shown in Fig. 50 will be the limiting factor in determining ψ.

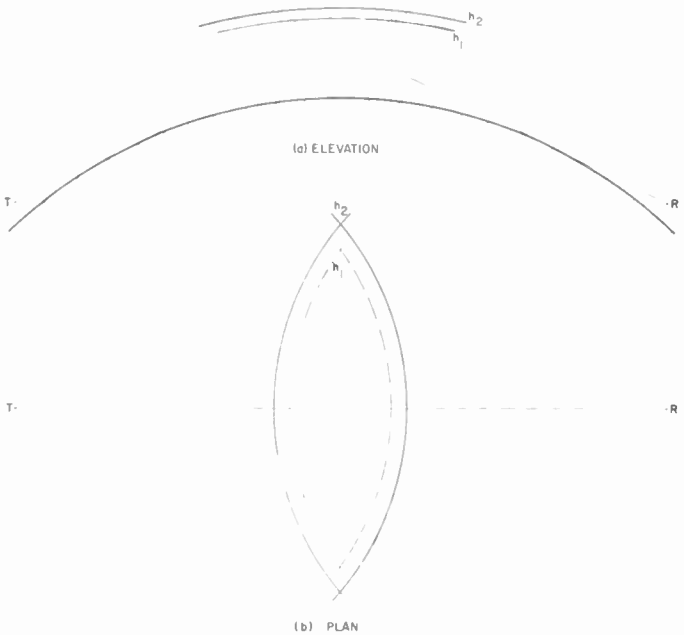

Fig. 50—Common volume geometry.

In this case ψ is approximately determined by the intersection of two planes tangent to the earth at the path terminals with the scattering stratum in the vertical plane passing through the terminals and the path midpoint. ψ thus limited is called ψ_c, and its value is given as a function of path length and scattering height in Fig. 51. For very long paths for which elevated antenna sites must be used ψ_c is greater than the values shown by Fig. 51 approximately by the sum of the dips of the radio horizons at the two terminals. As a practical matter, ϕ will not be limited by common volume geometry effects even for very long paths as can be seen

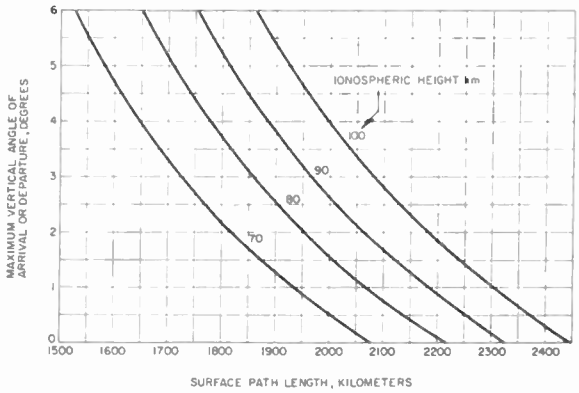

Fig. 51—Limiting effect of common volume geometry on maximum vertical angle of arrival or departure for Case I geometry for antennas at zero height, including effects of representative mid-latitude refraction.

from Fig. 52 and consideration of the influence of path length on ψ_m as discussed earlier. The cone widths ϕ and ψ as influenced by ϕ_m and ϕ_a, and ψ_m, ψ_a, and ψ_c, respectively, determine in a rough way what may be termed an effective volume in the height range over which scattering takes place.

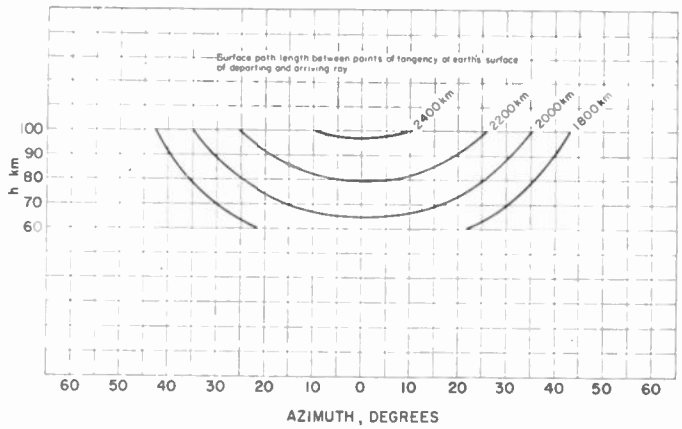

Fig. 52—Limiting effect of common volume geometry on maximum azimuthal angle of arrival or departure for Case II geometry, including effects of representative mid-latitude refraction.

It is useful to consider the influence of the effective volume in the design of antennas for use in transmission by ionospheric scattering. When the transmitting and receiving beamwidths both vertically and horizontally are substantially larger than, and include, the cone of angles associated with the effective volume, the received power will increase as the directivity of the antennas is increased in approximate proportion to the product of the plane-wave gains of the antennas. Under these circumstances increased transmitting directivity produces more intense illumination of the effective volume and, in reception, power from the effective

volume is received with a larger aperture resulting in a further increase of received power. If, however, the antenna beamwidths are smaller than the cone of angles determined by ϕ_m, and ψ_m or ψ_e whichever is smaller, the received power will increase more slowly with increasing antenna directivities. For this condition, the power received from the central portion of the effective volume, resulting from the increased intensity of illumination in the maximum of the transmitting antenna beam, and the more effective scattering in the vicinity of the path midpoint, more than offsets the loss of received power resulting from the reduction of the effective volume imposed by the smaller beamwidths. When the antenna beamwidths are approximately equal to ϕ_m, and ψ_m or ψ_e whichever is smaller, the effective volume will just fill the beams and the antenna beamwidths may be said to match the effective volume. The plane-wave gains of transmitting and receiving antennas should in these circumstances be largely realized.

Realized Gains of the Antennas

From early in the experimental program it has been apparent that antenna characteristics have an important influence on the received signal levels and on the diurnal variations of these levels. Fig. 53 shows the computed directivity of the transmitting and receiving

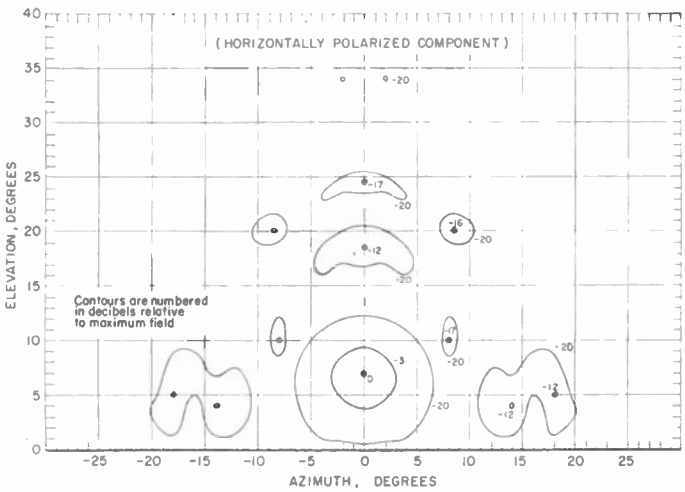

Fig. 53—Computed directivity of rhombic antennas used for the Cedar Rapids to Sterling path.

rhombics used for the routine signal intensity recording program on the Cedar Rapids–Sterling path. When antennas of lower directivity are used at Sterling for receiving it is found that the average signal intensities available from these antennas are generally lower than those available from the rhombic antenna but that the ratios of the powers received on the rhombic antenna to those received on the less directive antennas vary characteristically with local time. These effects are illustrated in Fig. 54 which displays the received intensities at 49.8 Mc/s on the rhombic antenna and on a five-element horizontal Yagi antenna. The free-space, half-power beamwidths of the Yagi antenna were approximately 65 degrees in the plane of the elements and 52 degrees in the plane normal to the elements. The plane-wave gains of the rhombic and the Yagi antennas in the beam maxima are approximately 18 db and 9 db respectively, relative to a horizontal half-wave dipole at the same height above ground. Comparisons of received

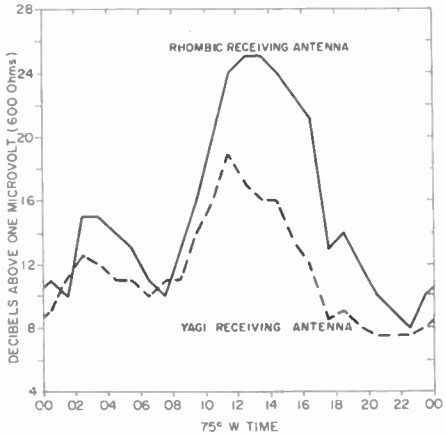

Fig. 54—Median signal intensities observed at 49.8 Mc/s at Sterling with rhombic and Yagi receiving antennas for a 19-day period in December, 1951. Rhombic transmitting antenna used at Cedar Rapids.

signal intensities using rhombic transmitting and receiving antennas and five-element Yagi transmitting and receiving antennas were made on the Anchorage to Barrow path at 48.87 Mc/s in March, 1953. Results of experiment are in Fig. 55. Fig. 56, page 1220, shows

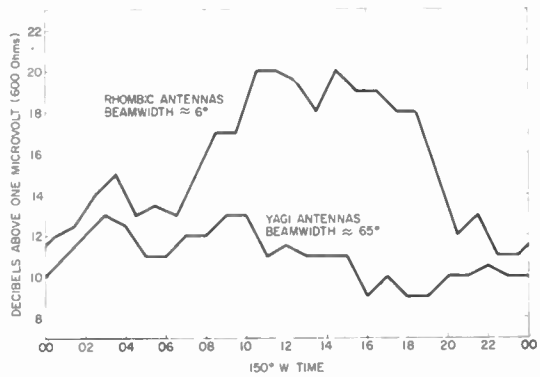

Fig. 55—Median signal intensities observed during March, 1953 at 48.87 Mc/s at Barrow with rhombic to rhombic and Yagi to Yagi antenna arrangements.

distributions of realized gain for rhombic-to-rhombic antenna systems used in the routine recording program as compared with dipole to dipole transmission. The realized gain of an antenna is defined here as the ratio of the signal intensity observed when the antenna is used to that observed when a reference or comparison antenna is used during the same period of time. In stating results of observations of realized gain it is necessary to specify the antenna arrangements used at both terminals. Measurements of realized gain were made on all of the 50 Mc/s test paths by means of alternate half-hourly transmissions on a rhombic antenna and on a reference dipole, with reception performed

simultaneously with a rhombic antenna and a dipole. Table V summarizes the results for the Fargo to Churchill path for a three-day period. It is evident that

TABLE V

REALIZED GAIN, DECIBELS

Per Cent of Comparisons in Which Gain Equals or Exceeds Value Shown	Transmitting Rhombic Antenna		Receiving Rhombic Antenna	
	Measured with Receiving Rhombic	Measured with Receiving Dipole	Measured While Transmitting on Rhombic	Measured While Transmitting on Dipole
5	19	14	19	17
10	18	13	18	15
50	14	9	15	10
90	10	4	11	3
95	9	2	10	1

the realized gain of a directive antenna is a function of the directivity of the antenna used at the opposite terminal and is influenced strongly by diurnal variations in the propagation mechanism or mechanisms. It is convenient to discuss this behavior by considering the case of a receiving antenna. The controlling factor in determining the realized gain of a receiving antenna is the angular size of the cone of angles from which power mainly arrives at the receiving location in relation to the angular dimensions of the receiving beam. The observed greater realized gain of the rhombic receiving antenna shown in Fig. 54 during the daylight hours suggests that most of the received power is arriving from a cone of angles determined largely by the directivity of the transmitting antenna or by a highly directive scattering mechanism. On the other hand, the behavior at other times when the realized gain is low suggests that a larger cone of angles exists from which power is effectively receivable. Table V further illustrates these effects.

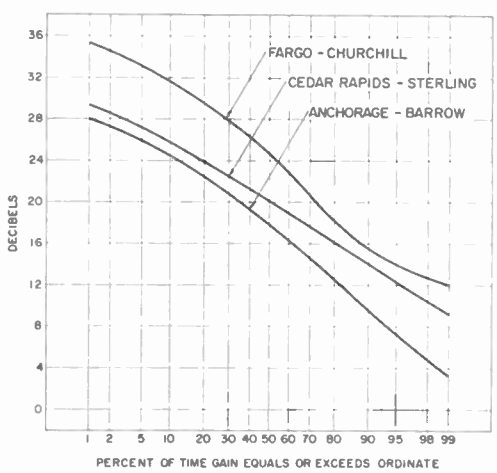

Fig. 56—Cumulative distributions of realized gain at about 50 Mc/s of rhombic to rhombic antenna arrangement over dipole to dipole arrangement, observed for 3-day period for each path.

Factors which can give rise to an increased angular size of the cone during these periods are decreases in the angle dependence of the scattering mechanism, large scale irregularities in the efficiency of scattering over the extent of the common volume, and contributions to the integrated signal intensities produced by reflections from meteor ionization which lies outside the effective volume as determined by ϕ_m, ϕ_a, ψ_m, ψ_a, and ψ_c. The first of these factors, in view of the frequency dependence measurements, and the calculated values of ϕ_m and ψ_m appears to be incapable of producing the observed wide variations in realized gain. Little detailed information is available concerning the nature and behavior of the large scale irregularities in scattering efficiency throughout the common volume, but there is hardly any doubt of their existence. Influence of meteoric ionization is probably most important single factor in causing observed variations in realized gain.

Influence of Meteoric Ionization

Much of the preceding discussion has been based on the assumption that a scattering mechanism is effective in propagating the received signals. To the extent that the received signals are appreciably contaminated by the presence of components resulting from meteoric ionization, the principal influence on the behavior of highly directive antennas will be a reduction in their realized gains as determined by the larger cone of angles associated with the meteoric components. If, however, the contributions from meteoric ionization are dominant, greater signal intensities could be received if different antennas were used.[11,12]

In an earlier paper the[4] possibility was suggested that the diurnal variation of observed signal intensity could be interpreted as the resultant of a solar ultra-violet influence having a maximum at midday, and a meteroic influence having a maximum at about 06 hours and a minimum at about 18 hours local time. To illustrate this suggestion the hourly median signal intensities observed at 49.8 Mc/s at Sterling were shown for April, 1951. Observations of the rate of occurrence of Doppler components differing from the carrier frequency by at least 200 cycles per second have been made at Sterling at 49.8 Mc/s over a long period. The resulting average rates for the month of April, 1955 are shown in Fig. 57

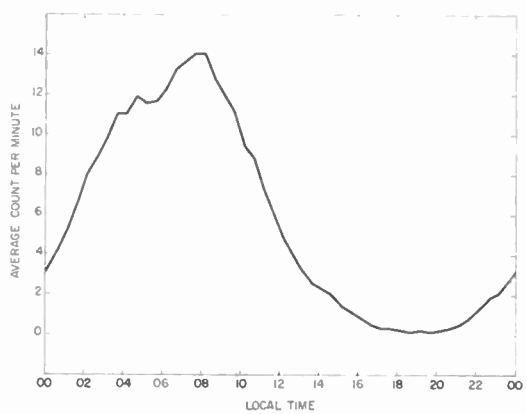

Fig. 57—Diurnal variation of the average rate of occurrence of meteor Doppler components observed at Sterling at 49.8 Mc/s during April, 1955.

for Doppler components having intensities exceeding 0.25 microvolt, open circuit voltage at 50 ohms. The maximum and minimum rates are seen to occur one to two hours later than 06 hours and 18 hours local time at the path midpoint. The secondary maximum at about 0430 is believed to be genuine.

The principal results of an experiment designed to establish more clearly the relationship between contributions resulting from a scattering mechanism and those resulting from meteoric components are now described. In this experiment, 49.8 Mc/s transmissions beamed towards Sterling, were simultaneously received at Sterling and at a site selected as being nearly optimum for reception of the meteoric components. This

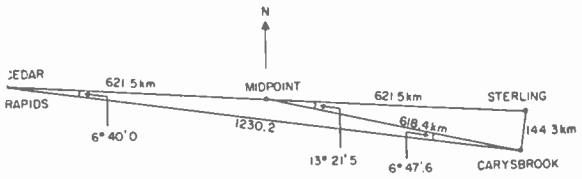

Fig. 58—Geometry for Carysbrook experiment.

site was near Carysbrook, Va., at a distance of 144.3 kilometers from Sterling in a southerly direction as shown in Fig. 58. At Sterling, the rhombic antenna normally used in the recording program was employed. An identical rhombic antenna was erected at Carysbrook, and directed toward the midpoint of the Cedar Rapids to Sterling path. Fig. 59 displays the hourly median signal intensities received simultaneously at Sterling and at Carysbrook during the course of the experiment. The integrated intensities were observed to be higher at Carysbrook between 23 hours and 04 hours local time at the path midpoint. During these hours the results would thus appear to be consistent with the theory that the meteor ionization trails contributing most effectively to the integrated signal intensity occur on one side of the great circle path between the transmitter and the receiver.[24] On the other hand, the existence of greater signal intensities on the Cedar Rapids to Sterling path most of the time provides further support of the view that the observed signals are the result of more than one propagation mechanism.[32] For the conditions under which the experiment was performed, it is concluded that systems designed to work through the universally observed periods of low signal intensity occurring at about 20 hours local time should employ antennas directed along the great circle bearing between the transmitter and receiver. It should be pointed out that the rhombic antennas used on the Cedar Rapids to Sterling path since the beginning of the experimental program were designed for an assumed midpoint height of about 105 kilometers for the scattering region. In the light of the knowledge acquired later concerning the heights at which scattering occurs, it would have been more appropriate to direct the beam maxima toward a midpoint height of about 85 kilometers. Consequently, it is thought that the experimental results throughout the observing program at Sterling including the results presented in Fig. 59 are biased to some extent in favor of the meteoric components.

Further experimentation of the kind above is desirable in order to obtain information on the relative contributions of the scattered components and the meteoric components at other times of year and for other path orientations. Some specific suggestions for related experimentation were made earlier in connection with polarization dependence.

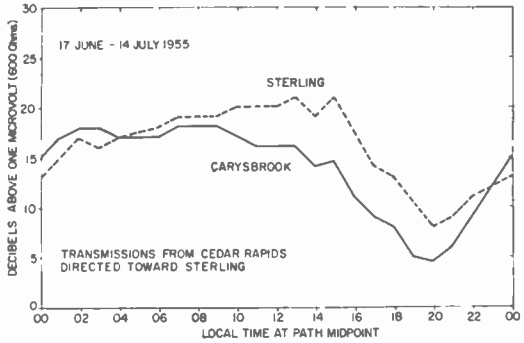

Fig. 59—Diurnal variation of hourly median signal intensities observed simultaneously at Sterling and at Carysbrook, at 49.8 Mc/s.

Diversity Considerations

In an earlier section the measurements of the correlation between the envelopes of signals received on spaced Yagi antennas were described. Fig. 20 illustrates the observed behavior for spacings along and transverse to the path. Envelope correlation coefficients of 0.5 were observed for spacings of about 3.5 wavelengths transverse to the path and about 40 wavelengths along the path. A practical implication of these results is that smaller antenna spacings will suffice for effective diversity action if the diversity antennas are disposed in a line normal to the path rather than along the path.

Gordon[33] has studied the effects of the tropospheric scattering mechanism in relation to the correlation expected between spaced antennas for diversity action. Using somewhat similar, but not identical arguments diversity spacings for transmission by ionospheric scattering can be estimated. While the precise calculations would be involved, important features can be seen from some very simplified considerations. As such consider that the antenna spacing required to produce a low envelope correlation is that necessary to give a difference of one wavelength in the paths of the signals from opposite boundaries of the effective scattering

[32] It is of interest to calculate the expected intensity of the Carysbrook signals relative to the simultaneously observed signal intensities at Sterling on the assumption that propagation is predominantly by a scattering mechanism, as might be expected during the afternoon. Previously given geometric considerations are employed and for angle dependence it is assumed that $n=6$. The loss resulting from the larger scattering angle at Carysbrook is found to be about 4 decibels. In addition a further loss of 1½ to 2 decibels, affecting the Carysbrook observations, is associated with V_c/V as given by (36). Finally there is a loss of about ¼ decibel associated with the use of horizontal polarization, because $\chi=90°$ at Carysbrook. A net loss at Carysbrook relative to Sterling of about 6 decibels is therefore predicted for propagation by scattering uncontaminated by meteoric or other components. This result is seen to be in fair agreement with Fig. 59, during the midafternoon period.

[33] W. E. Gordon, "Radio scattering in the troposphere," Proc. IRE, vol. 43, pp. 23–28; January, 1955.

volume. Fig. 60 illustrates the usual diversity arrangement in which diversity action is obtained by spacing the receiving antennas transverse to the great circle path at a constant height. The angle ϕ in Fig. 60 is the width of the cone of angles over which most of the power is received. The diversity distance S_t is defined to be the distance through which a receiving antenna must be moved to produce a change in the difference between the ray path lengths l_1 and l_2 of one wavelength. The ray lengths, l_1 and l_1', and l_2 and l_2', are much greater than S_t so that they may be considered to be parallel.

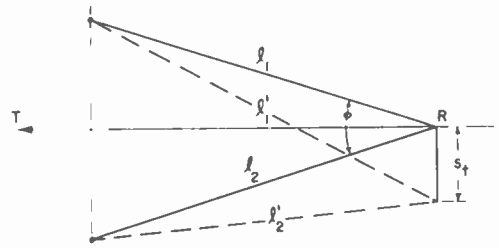

Fig. 60—Geometry for transverse spaced-antenna diversity.

From simple geometrical considerations,

$$l_1' - l_1 = S_t \sin \frac{\phi}{2}, \tag{37}$$

$$l_2' - l_2 = -S_t \sin \frac{\phi}{2}, \tag{38}$$

and the diversity distance is:

$$S_t = \frac{\lambda}{2 \sin \frac{\phi}{2}}. \tag{39}$$

The smaller of the cone widths, ϕ_m and ϕ_a is used with (39) for estimating appropriate spacing of the antennas for diversity action.

The diversity distance in a vertical direction at the receiver is, on the basis of similar considerations,[34]

$$S_v = \frac{\lambda}{2 \sin \frac{\psi}{2}}. \tag{40}$$

The smallest of the cone angles, ψ_m, ψ_a, and ψ_c, is used for ψ in computing an appropriate diversity distance S_v.

The longitudinal diversity distance S_l along the path and parallel to the tangent plane to the earth under the receiver is influenced by both cone angles ϕ and ψ. It is convenient to state the results separately. For ϕ,

$$S_l(\phi) = \frac{\lambda}{2 \sin^2 \frac{\phi}{4}}, \tag{41}$$

and for ψ,

$$S_l(\psi) = \frac{\lambda}{2 \sin \frac{\psi}{2} \sin \theta}, \tag{42}$$

where θ is the angle between the tangent plane at the receiver and the center of the cone width ψ. When the combined effects of ϕ and ψ are taken into account, the appropriate diversity spacings will be intermediate between the values determined separately. This matter has not been further explored since even the smaller of the diversity distances obtained from the above expressions will, in practice, be many times the diversity distance S_t required for spacings transverse to the path. For this reason longitudinal diversity is not convenient in practice.

As will be discussed in Part III, a useful siting procedure is to align the transmitting and receiving beams on the ionospheric midpoint height by putting the antennas at a height z above a smooth reflecting surface, as determined by,

$$z = \frac{\lambda}{4 \sin \alpha}, \tag{43}$$

where α is the angle of elevation of the path midpoint for the design height of scattering. For the shorter paths in which the antennas are sited in accordance with (43), α will be roughly the same size as ψ. With this in mind, and comparing (43) with (40) it will be seen that for small α and ψ, S_v will be roughly twice as great as $2z$, the distance between the antenna and its image. Accordingly, the correlation between the antenna and its image will be rather poor, and coherent gain will be realized only for the contributions arriving from the central portion of the effective volume. The net increase in signal power resulting from the presence of the image receiving antenna when both transmitting and receiving antennas are thus sited is expected to be about three decibels or slightly greater. An alternative explanation is that the receiving antenna will be receiving power from two poorly correlated sources of approximately equal intensity, the effective volume and its image.

The transverse diversity distance S_t for the Cedar Rapids to Sterling path is 9.6λ on the assumption that $\phi = \phi_a = 6$ degrees. Experimentally observed values of envelope correlation as a function of antenna spacing were given in Fig. 20; extrapolation indicates that the correlation is very small for antennas spaced at the computed distance of 9.6λ.

Height-gain observations made early in the 49.8 Mc/s recording program at Sterling showed that the signal intensities as received on a Yagi antenna were not very sensitive to height over a range of heights from about 35 to about 80 feet indicating poor correlation between the Yagi antenna and its image in the ground. The diversity distance S_v for the Cedar Rapids to Sterling path is 11λ as computed for $\psi = \psi_m = 5.2$ degrees. In the distance-dependence tests, height-gain

[34] In these equations certain cosines have been set equal to unity because of the smallness of the angles.

comparisons at Homestead given in Table II for antennas at heights of 40 and 100 feet showed that the daytime signal intensities observed at a height of 100 feet were greater than those at 40 feet by 8½ decibels. For the path length 2,088 kilometers between Cedar Rapids and Homestead, ψ_c will be the limiting angle in determining cone width ψ. By using values for ψ_c from Fig. 51, for an 80 kilometer height, and making approximate allowances for the effects of the heights of the transmitting and receiving antennas, a cone width ψ_c of about 1.1 degrees is determined for this path, corresponding to a diversity distance S_v of about 1,030 feet. The spacing of 200 feet between the antenna and its image for the upper antenna height is substantially less than the computed diversity distance for this path. At night, however, the observed height gain between the 40 and 100-foot heights was 6½ db indicating a somewhat larger cone width ψ_c. This behavior might be anticipated on the basis of the higher observed heights during the night hours and the contributions from meteoric ionization which occur at the greater heights. Similar observations made at shorter distances during the Florida distance dependence tests showed lower height gains than those observed at Homestead, indicating greater effective values of ψ_c. The observed behavior in the experiments discussed above is thus seen to be in good qualitative agreement with the behavior predicted from diversity considerations.

The Significance of the Frequency and Angle-Dependence Results

In the light of the preceding discussion on the role of the antennas it is of interest to consider the extent to which the frequency and angle dependence measurements may be regarded as providing a basis for judging models of the scattering medium having frequency and angle dependence of the kinds discussed earlier. From the theory of Villars and Weisskopf, or from more elementary physical considerations, it is expected that the angle-dependence as expressed by an exponent of $1/\sin \gamma/2$ will vary with frequency and with conditions in the medium. The medium will scatter with a sharper polar diagram as the frequency is raised confining the downcoming waves at the receiving point to a smaller effective cone. Correspondingly the cone angle at the receiver will decrease with an increase in the effective frequency exponent at a fixed frequency. Thus, measurements of frequency dependence using scaled antennas will not accurately represent the frequency dependence characteristics of the scattering mechanism unless the antenna beamwidths are small relative to the beamwidths associated with the scattering mechanism. The beamwidths of the antennas used for the measurements were, in fact, comparable to the natural beamwidths of the scattering mechanism shown for the second beam swinging model and it would be expected that variations in the characteristics of the mechanism with frequency or with time at a given frequency would influence the measured values of n by no more than plus or minus 0.5. A more serious source of difficulty in interpreting the observations results from the existence of meteoric components having varying intensities relative to the scattered signal. In this connection, the relative behavior of the signal intensities at Sterling and at Carysbrook, suggests that for several hours during the afternoon period, the contributions from meteoric ionization are small in comparison with the scattered components. The frequency dependence observations made during this portion of the day are therefore thought to provide a fairly reliable estimate of the frequency dependence of the scattering mechanism. Correspondingly, the observations made during the early morning hours particularly during the winter months can probably be used to provide a reasonably good estimate of an effective frequency dependence of the integrated signal intensities produced by reflections from meteoric ionization for the experimental arrangements. Considering the various uncertainties including experimental errors associated with the observations and the interpretation of the observations it is thought that the effective exponent n representing frequency dependence of the scattering mechanism is being measured to within about twenty per cent when selected data are used.

The interpretation of the angle-dependence observations is similarly beset with difficulties. First, a relatively small systematic error is introduced by the finite beamwidths of the antennas since the scattering angle γ increases on either side of the midpoint in the scattering region. Thus the effective γ would be expected to be somewhat greater than the midpoint value. Secondly, because of experimental difficulties associated with the measurements of pulse signal intensities over the shorter paths used for this experiment, it was not possible to make measurements except during periods of very high signal intensity and consequently only a limited quantity of data was obtained. On the other hand, the data were taken during periods considered to be relatively free from contamination by reflections from meteoric ionization. On the basis of the preceding discussion it is thought that the exponent n associated with the angle dependence of the scattering mechanism at 50 Mc/s was not greater than nine nor less than six, for the particular periods during which the measurements were made.

Part III. Design Considerations for Communication Applications

Introduction

Sufficient experience has been acquired with the propagation mechanism under study to permit an evaluation of some of the communications possibilities. Experience in the Arctic and middle latitudes has provided evidence of the utility of the propagation mechanism for communication purposes. With systems gains comparable to those used on the test paths, or somewhat

greater, and for somewhat lower frequencies, say from 30 to 40 Mc/s, multichannel radio-teletype operation can be realized with a very high degree of reliability. Under these circumstances, radiotelephone communications and transmission of facsimile are also feasible. In the Arctic the known characteristics with respect to magnetic disturbances are of particular value.

Useful Path Lengths

The most useful range of path lengths is from about 1,000 to 2,000 kilometers. Recent experience with the test path between Newfoundland and the Azores has indicated that, subject to the availability of high sites, overlooking the sea for example, path lengths as great as 2,300 kilometers may be used successfully. As discussed earlier in this paper, received signal intensity decreases rapidly with decreasing distance below 1,000 kilometers and for this reason path lengths shorter than about 1,000 kilometers are to be avoided.

Useful Range of Frequencies

The range of frequencies of greatest usefulness is from 25 to 60 Mc/s. Frequencies lower than 25 Mc/s, wherever used, will be subject to and will cause interference to a much greater degree as a result of normal and sporadic ionospheric propagation. The interference will be particularly serious in years of high solar activity, and will be influenced by diurnal, seasonal and geographical factors. Back scatter will be experienced, particularly in middle and low latitudes and in years of high solar activity.

In general, the lower frequencies in the range are less susceptible in high latitudes to the various difficulties described above. The lower frequencies in the range of 25 to 60 Mc/s have other inherent natural advantages. For fixed transmitter power and antenna directivities, use of the lower frequencies will result in greater signal-to-noise ratios, less interference from meteoric effects, and slower fading. Effects of SID's and polar blackouts, although more pronounced on the lower frequencies, will not affect the reliability of communications circuits operating in the lower portion of this range.

It should not be concluded that there is little use for frequencies as high as 50 or 60 Mc/s. In certain seasons, these higher frequencies may be of considerable value. If potential interference from regular-layer propagation and back scatter is to be practically eliminated, the higher frequencies must be used for applications requiring extreme reliability, even at the expense of higher transmitter power.

Bandwidths and Channel Separations

It seems unlikely for some time to come that systems will require bands greater than about 50 kc/s. In many instances substantially smaller bands will suffice. Because of problems associated with slopes of the pass bands in receiving equipment, which may arise during occurrence of very strong signals, it is probably advisable to separate channels about 2 to 3 times the width of the nominally occupied bands. It is also necessary to allow for the effects of sporadic-E propagation, transient meteoric enhancements, and regular ionospheric propagation.

Transmitters and Receivers

In order to take full advantage of the propagational reliability of the mechanism it is important that transmitters of sufficiently high power be used and that the equipment employed at the path terminals be designed to provide a very high degree of reliability.

The transmitters and receivers should be capable of operating in the frequency range 25 to 60 Mc/s. For most applications there is no need to incorporate provisions for continuous "front-panel" frequency changing as large changes in frequency will almost always require careful tuning of new antenna arrangements and need only be provided for within the equipment itself. For some applications, involving low information rates, such as single-channel radio-teletype transmission, transmitter powers of the order of five kilowatts are likely to be found adequate at frequencies of the order of 35 Mc/s, particularly in the Arctic.

In the frequency range 25 to 60 Mc/s external noise will be the limiting factor in communications provided that the receivers have sufficiently low noise figures. A receiver noise figure of two can easily be realized and is adequate.

Multipath Limitations

Various types of multipath propagation have been observed in the experimental program. The most commonly observed multipath effect is produced by reflections from meteoric ionization in the ionospheric volume common to the transmitter and the receiver. Values of maximum multipath delays and corresponding azimuths have been computed from the common volume geometry illustrated in Fig. 50 for the longest and shortest geometrically possible ray paths and are plotted in Figs. 61 and 62. Multipath delays as great as the values derived from Fig. 61 for the shorter paths will be extremely rare since the probability of occurrence of meteor ionization becomes vanishingly small at the points where the tangent planes intersect at meteoric heights. Furthermore, the intensity and duration of received signals will be very low for reflections within the common volume but near the intersections of the tangent planes as a consequence of increased inverse distance attenuation, the decreased obliquity,[24] and the additional directivity discrimination at low angles of elevation resulting from interference between the direct and ground-reflected waves. Observations of such multipath delays were made using pulsed transmission on the 811 kilometer experimental path between Sterling, Va. and Bluffton, S. C. The results summarized

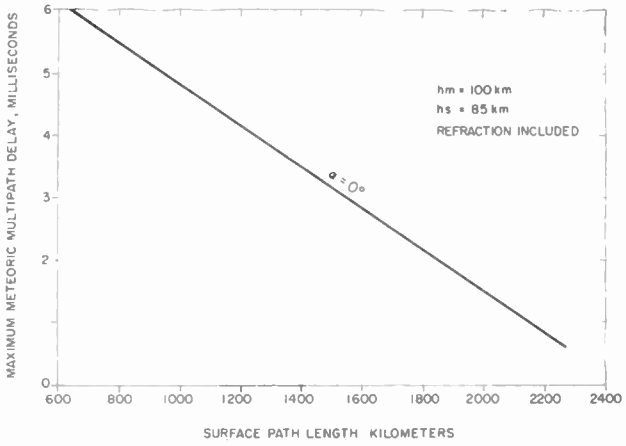

Fig. 61—Maximum meteoric multipath delays for antennas at zero height.

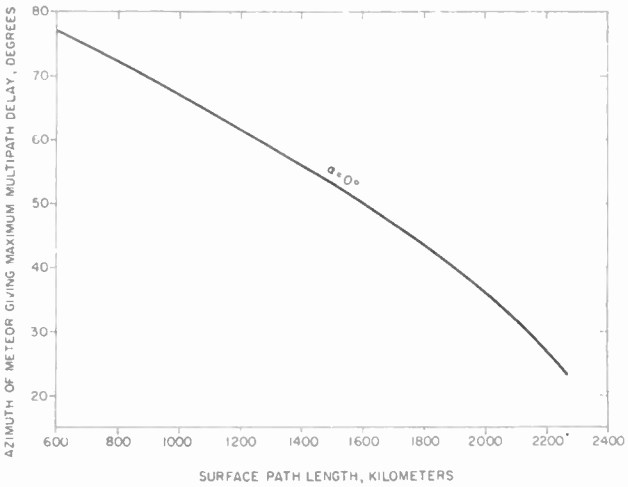

Fig. 62—Azimuth of meteor giving maximum multipath delay for antennas at zero height.

in Fig 63, were obtained from range-time oscillograms of the type shown in Fig. 15.

A second type of multipath effect, associated with sputter, is illustrated in Fig. 35. This type of multipath, characterized by rapid fading is of practical importance as the associated delays may be as much as several milliseconds. It occurs most frequently for paths crossing or near the zone of maximum auroral occurrence, where it may be expected to cause difficulty at times with antennas having typical directivity characteristics. These effects are illustrated by Figs. 35 and 36. Fig. 50 illustrates the common volume geometry associated with this type of multipath as well.

Other possible sources of multipath include off-path reflections from banks of sporadic-E ionization and from ground-scattered energy propagated by $F2$ or E-region reflection for several different types of multipath geometry. The delays associated with multipath arising from back scatter may be as great as 50 milliseconds or more and are potentially capable of seriously limiting the transmission speed. The harmful effects of back scatter may be reduced or eliminated by using antennas designed for suppression of the back lobes.

For transmission by ionospheric scattering, multipath from strong offpath reflections from meteoric ionization is, during its existence, a factor reducing the available radio path bandwidth. The antennas which have been used in the experimental program do not have sufficiently low radiation in the minor lobes, as compared with the main beam, to provide adequate suppression of the off-path meteoric components. Considering the preceding discussion in conjunction with the experimental observations, it seems reasonable to expect that multipath components having delays exceeding half a millisecond will occasionally occur with sufficient intensity to introduce transmission errors on the shorter paths. However, the available radio path bandwidth, as estimated from the reciprocal of the delay, for these shorter paths is greater than 2 kc/s for a large percentage of the time. For the intermediate and longer path lengths the available bandwidths will be

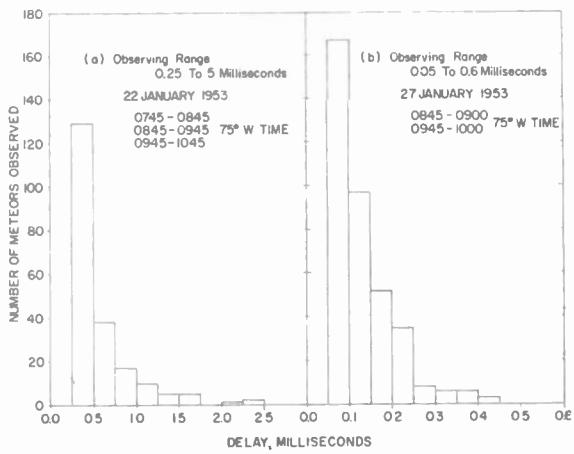

Fig. 63—Distribution of observed meteoric multipath delays observed at Bluffton at 49.7 Mc/s for a transmission path of 811 km from Sterling.

somewhat greater but still largely determined by the minor lobes of the antennas and the reflecting properties of the ground.

With antennas of improved directivity, multipath associated with meteoric ionization will no longer be a problem and the radio path bandwidth will be limited by the antenna beamwidths or the natural beamwidth associated with the scattering process. While the subject of wide-band transmission at vhf by ionospheric scattering has not been extensively analyzed, it is of interest to estimate the inherent bandwidth limitation imposed by the scattering mechanism. Values of a generalized q computed for the Cedar Rapids to Sterling path are presented in Figs. 46 and 47. Multipath delays have been derived from the ray paths associated with the ionospheric midpoint and positions in the common volume corresponding to the half power values of q, assuming $n = 6$ and the use of an omnidirectional transmitting antenna. With these idealizations, the maximum delay is 21 microseconds and is associated with ψ_m. The available path bandwidth for the assumed conditions is 48 kc/s. For practical situations, the effects

of ground reflection will usually be such that the delays associated with ϕ will be greater than those associated with ψ. Assuming sharply beamed antennas ϕ_m is limiting and the delay is 9 microseconds. This corresponds to an available path bandwidth of 110 kc/s. If the transmitting and receiving antenna beamwidths are smaller than bandwidths of the scattering mechanism, still greater bandwidths are in principle available.

Antennas

With the results of the experimental program (Part I) and the discussion of the role of the antennas (Part II), together with the multipath considerations given above, it is possible to establish the characteristics of antenna systems for use in communication applications. For purposes of discussion, Table VI indicates certain desirable characteristics without regard to whether antennas having such characteristics are at present practicable.

TABLE VI
Desirable Antenna Characteristics

Horizontal beamwidth	8 degrees or less
Vertical beamwidth including ground effects	6 degrees or less
Maximum radiation in any minor lobe	At least 40 decibels below radiation in the maximum of the main beam
Radiation efficiency; i.e., ratio of total power radiated to antenna input power	90 per cent or greater
Horizontal orientation of beam	Normally on great-circle bearing between transmitter and receiver
Vertical orientation of beam	85 kilometers above midpoint of great-circle path
Provision for reducing directivity or for varying direction of the beam	For use during periods when scattering is not homogeneous and during periods when scattering from meteoric components will provide higher signal-to-noise ratios
Bandwidth over which characteristics are to be maintained	200 kc/s

Although most of the above set of characteristics are self-explanatory some additional comments are indicated. When a low noise-figure receiver is employed, somewhat lower radiation efficiencies for receiving antennas can be tolerated since the available noise power from galactic sources is much higher than that resulting from internal noise generated in the receiver. For the longer paths, increased vertical directivity is necessary in order to utilize effectively the reduced common scattering volumes. From the common volume point of view, horizontal beamwidths smaller than 8 degrees will not be required for any except the very longest paths. The suggested techniques for varying directivity or for orienting the main beam in directions other than the great circle-bearing have not been tested under operational conditions and a determination of the practical effectiveness of this scheme will require further study and trial. It remains to be seen to what extent antennas having characteristics approaching those envisaged above will find their way into practice.

The use of spaced-antenna receiving diversity is definitely desirable for good communications. From the spaced-antenna observations of envelope correlation between spaced antennas, and from the diversity-distance considerations discussed in Part II, it is concluded that for effective diversity action the component of spacing transverse to the path should not be less than about 10 wavelengths.

The effects of the scattering mechanism with regard to the polarization of the transmitted waves have been considered earlier and it was shown that the scattering losses are somewhat less for horizontal than for vertical polarization. Horizontal polarization is generally to be preferred for additional reasons associated with the reflection characteristics of the ground.[14]

Practical Antenna Siting

A corollary to the observed failure to realize, for a large fraction of the time, antenna gains comparable to the plane-wave gains, is that the additional gain resulting from ground reflection will not be fully realized, even though ideal sites are employed at the transmitter and receiver. The reason for this was discussed in Part II in connection with vertical diversity spacing. Nevertheless there are demonstrable advantages in siting the antennas with respect to a ground surface so that the plane-wave ground-reflection lobe patterns are well formed. In fact, if either antenna is poorly sited, the beams may only partially intersect in the height region where scattering occurs.

For the idealized beam-swinging models discussed in Part II two limiting cases were considered with respect to the transmitting antenna patterns. They were an omnidirectional antenna and an extremely directive antenna. The generalized q-curves representing Case I geometry, in which the effective scattering volume is displaced toward one terminal, are shown in Fig. 46 as a function of α_R. In practice the directivity of the transmitting antenna is intermediate between the two extremes. It is therefore anticipated that slightly greater signal intensities will result if the transmitting and receiving beams are directed toward a point in the scattering stratum slightly displaced in the manner above provided appropriately different directivities are employed at the terminals. While unsymmetrical operation of this kind, employing negligibly increased scattering angles, would represent no disadvantage, it is nevertheless recommended in practice that antenna beams be designed to have their principal lobes directed toward the path midpoint in the ionosphere. The recommended ionospheric height for antenna design and corresponding site selection is 85 kilometers.

Some exceptions to this design recommendation can be made with advantage for paths longer than about 2,200 kilometers. For such extreme path lengths some increase in received signal intensity is likely to be realized with antennas having practical vertical free-space directivities if use is made of heights greater than required to direct the first ground-reflection lobe at the path midpoint in the ionosphere. As the antenna heights increase, ψ_e increases with the increasing depression of the radio horizons. As a consequence the total power radiated into the common volume is increased. Thus, for very long paths greater heights should be used wherever practicable and especially at one terminal if height limitations exist at the other terminal. The design heights indicated for lobe alignment at the path midpoint in the ionosphere should be regarded for paths of extreme length as minimum rather than optimum.

The curves of Fig. 11 show the vertical angle of arrival or departure for various ionospheric midpoint heights as a function of the surface distance between the transmitter and the receiver. They have been found useful in connection with antenna design and siting problems. The values given by these curves have been calculated for elevations near sea level for the assumed condition of no lower atmosphere and for representative radio-wave refraction in mid-latitudes. Some remarks concerning the general applicability of the curves are indicated. First, the refraction corrections decrease with elevation of the terminal above sea level. Secondly, in warm, humid regions, such as many tropical locations, the increase in angle of arrival over that for the case of no lower atmosphere may be about $1\frac{1}{4}$ times the values shown. Thirdly, in polar regions, particularly under winter conditions when the absolute humidity is very low, the increase in angle over that for the case of no lower atmosphere may be only about two-thirds of the values of increase shown. Lastly, the corrections for angles below about one or two degrees may, as a practical matter, be extremely variable, particularly if conditions conducive to superrefraction occur.

In siting an antenna intended to function effectively for small angles of arrival and departure, it is insufficient merely to provide a suitable site on which to perform the construction. Nor is it sufficient simply to have an unobstructed horizon in the desired azimuth for the desired angle of departure or arrival. When the angle of departure or arrival is small, the ground for a considerable distance in front of the antenna plays a critical role in formation of the lobe pattern. The problem of ground-reflection lobes and general requirements for a smooth first Fresnel zone has been given considerable study, particularly with respect to the ground radar siting problem. For the purposes of the following discussion it is assumed that the lowest lobe will be effectively formed when the terrain in front of the antenna is flat and smooth over an area no smaller than the first Fresnel zone. Horizontal polarization only is considered so that lobe formation is not complicated by large variations in the ground-reflection coefficient over the range of angles of interest. Mathematically, the antenna is assumed to be at a point and the ground-reflected wave is assumed to have the same amplitude as the incident wave but to undergo a 180-degree phase change at reflection.

The first Fresnel zone is defined, with the aid of Fig. 64, as the area of ground, assumed smooth and plane, in front of the point antenna A from within which

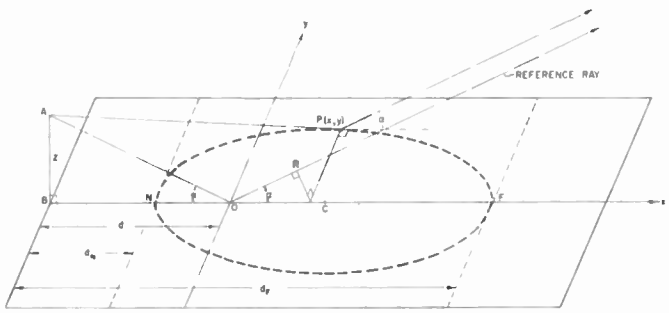

Fig. 64—Geometry of first Fresnel zone.

all secondary wavelets, according to Huygens' principle, contributing to a plane-wave front advancing in the direction of the positive x-axis with an inclination upward of α, differ in phase by 180 degrees or less from a reference ray, obeying strict geometric optics. The origin of the coordinates, O, is situated at the ground-reflection point for the reference ray.

For alignment of the maximum of the first ground-reflection lobe at an angle of elevation α, it is necessary for the point antenna A to be at a height, z, given previously by (43), as follows:

$$z = \frac{\lambda}{4 \sin \alpha},$$

where λ is the wavelength. The distance from the antenna base at B to the geometric ground-reflection point is given by:

$$d = \frac{z}{\tan \alpha}. \tag{44}$$

Now let $P(x, y)$ be a general point obeying the conditions defining the boundary of the first Fresnel zone, so that

$$AP - (AO + OR) = \frac{\lambda}{2}, \tag{45}$$

where R is the point along the reference ray at which the phase comparison is made with the wavelet originating at P.

By using (43) to eliminate λ in (45) and expressing AP, AO, and OR as functions of h, α, and the coordinates x and y, the locus of P is found, after some simplification, to be:

$$\frac{\left(x-\frac{2z}{\tan\alpha}\right)^2}{\frac{8z^2}{\sin^2\alpha}}+\frac{y^2}{8z^2}=1. \tag{46}$$

This is seen to be the standard Cartesian form for an ellipse.

As a practical matter it is of interest to know the distance from the antenna base at B to the near edge of the first zone d_N, to the far edge d_F, and the maximum width w, or the minor axis, of the zone. These distances, increased suitably for the finite dimensions of a practical antenna, determine the extent and location of the ground in front of the antenna which must be flat and free of obstructions for effective lobe formation. From (46) when $y=0$,

$$x=\frac{2z}{\tan\alpha}\left(1\pm\frac{\sqrt{2}}{\cos\alpha}\right), \tag{47}$$

so that,

$$d_N=\frac{z}{\tan\alpha}\left(3-\frac{2\sqrt{2}}{\cos\alpha}\right), \tag{48}$$

$$d_F=\frac{z}{\tan\alpha}\left(3+\frac{2\sqrt{2}}{\cos\alpha}\right), \tag{49}$$

and the maximum width of the zone is:

$$w=4\sqrt{2}z. \tag{50}$$

The effect of the curvature of the earth on the first Fresnel zone will be appreciable only if the angle of arrival or departure, α, is very small. The qualitative result of curvature is to cause the elliptical area to be reduced in size and to be altered into an egg shape elongated with the broad end near the antenna. The quantity d_N is almost unaltered, whereas d is somewhat reduced, and d_F is considerably reduced. The maximum width will be slightly reduced and will occur somewhat nearer the antenna. An additional effect of some practical importance is the reduction in the height, z, of the antenna required for the first lobe maximum to be formed at a specified angle α. For the plane-earth case this height was given by (43).

Curves of z and d have been derived, and are plotted in Figs. 65, 66, and 67 as a function of α for plane earth and for the curved earth, for three fixed values of λ corresponding to frequencies of 30, 40, and 50 Mc/s. Some compensation for the effects of tropospheric refraction has been introduced for curved-earth case. Fig. 68 (next page) gives values of d_F as a function of α for the three sample frequencies for a plane earth according to (49). When α is greater than two or three degrees the values for a curved earth will be smaller by a negligible amount.

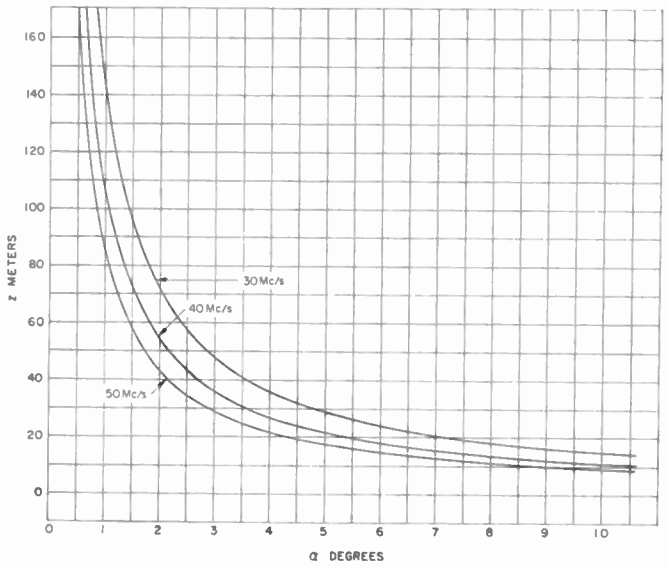

Fig. 65—Antenna heights for aligning first ground-reflection lobe maximum at indicated elevation angle, for horizontal polarization and a plane earth.

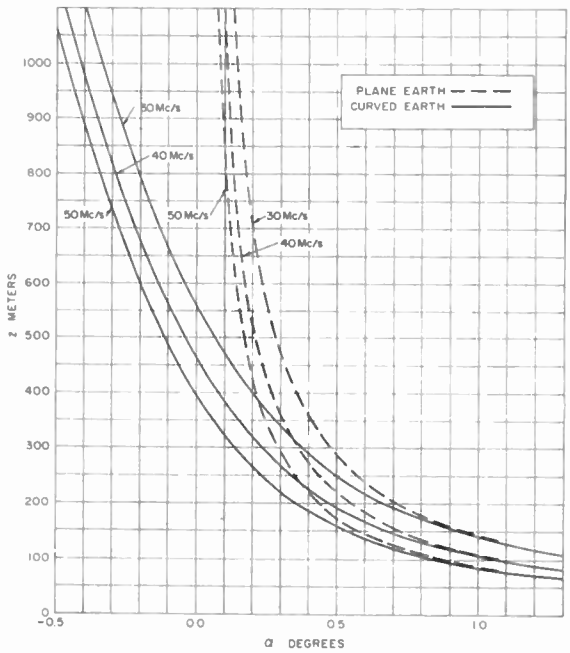

Fig. 66—Antenna heights for aligning first ground-reflection lobe maximum at indicated low elevation angle for horizontal polarization, for plane and curved earth.

When α is less than two or three degrees the curves shown give values of d_F substantially greater than the actual values for a curved earth, and provided they can be satisfied in practice no difficulties can be expected to result from their use.

It is of practical importance to know what sort of departures from the ideal first Fresnel zone may be tolerated. For a well-developed first ground-reflection lobe the entire first zone at least, should be flat, and the horizon from every part of it should subtend less than

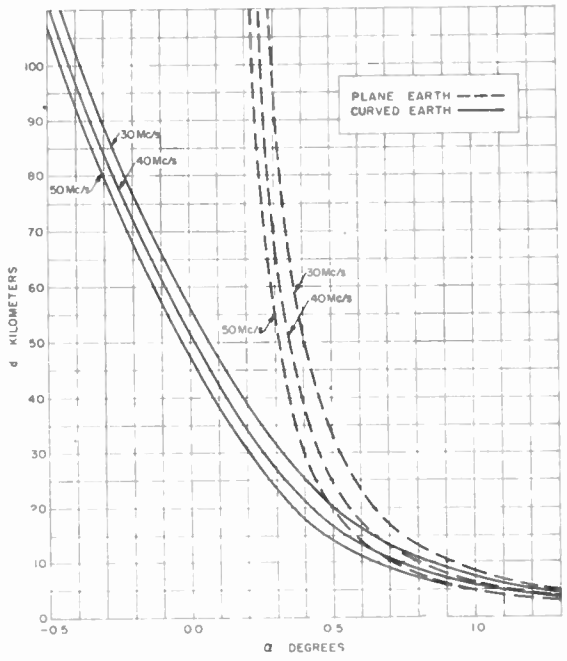

Fig. 67—Distance to ground-reflection point from antenna having first ground-reflection lobe maximum at indicated low elevation angle for horizontal polarization, for plane and curved path.

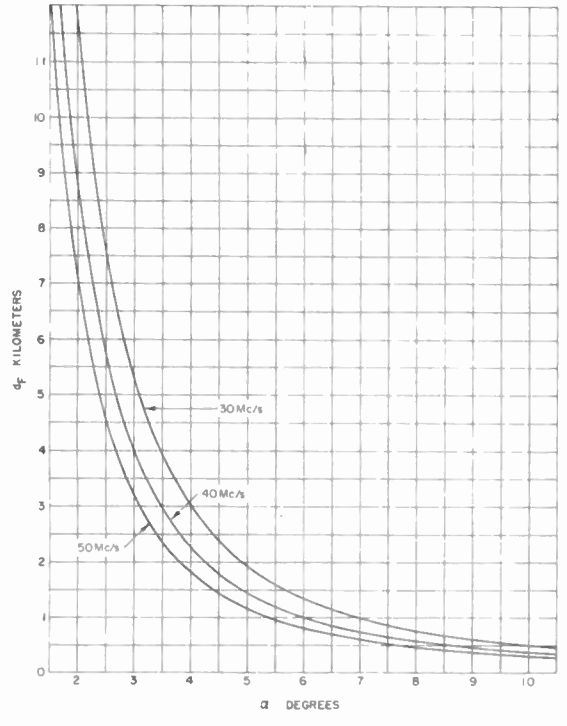

Fig. 68—Distance to far edge of first Fresnel zone from antenna having first ground-reflection lobe maximum at indicated elevation angle for horizontal polarization and plane earth.

the angle α. Norton and Omberg,[35] applying Rayleigh's criterion, state that irregularities in the terrain in the first zone should have a departure from ideal smoothness of not more than one-fourth of the antenna height. As a practical matter, water surfaces make excellent first Fresnel zones, particularly for small values of α.

The ray treatment leading to the results presented above for the curved earth should not be relied upon for values of α less than about 0 degree at which the horizon, for the heights involved, is actually below minus half a degree. For one thing the divergence factor begins to reduce the effectiveness of the ground-reflection in the formation of the lower lobes, though this may be offset by other considerations, as discussed for example by Burrows and Attwood.[36]

Modulation Techniques

In the development of systems utilizing vhf ionospheric propagation it is important that consideration be given to the special behavior characteristics of the received signals in order to realize a system capable of minimizing or eliminating the undesirable transmission effects produced by reflections from meteoric ionization and the fading and multipath characteristics of the normally received signals. Considerations of path geometry and meteor velocities indicate that the difference between the transmitted frequency and the Doppler frequencies should not be greater than about 6 kc/s for the Cedar Rapids to Sterling path at 49.8 Mc/s. This difference in frequency is, for a particular meteoric event, directly proportional to the transmitted frequency.

Estimated System Performance

A considerable body of signal intensity and noise intensity data has been acquired in the experimental program. It is possible, using these data, to estimate the expected reliability of a system employing a typical type of service such as single-channel radioteletype transmission. System reliability estimates are made for several assumed types of service.

Montgomery[37,38] has studied the behavior of several types of modulation for narrow-band transmission of binary-coded messages in the presence of fluctuation noise and has considered the effects of diversity action in the reception of narrow-band frequency-shift transmission. His results will be used for estimating ratios of average signal power to rms noise power required to establish a specified system performance for radiotele-

[35] K. A. Norton and A. C. Omberg, "The maximum range of a radar set," Proc. IRE, vol. 35, pp. 4–24; January, 1947.

[36] C. R. Burrows and S. S. Attwood (Eds.), "Radio Wave Propagation," Academic Press, Inc., New York, N. Y., pp. 80–81, 119–120; 1949.

[37] G. F. Montgomery, "A comparison of amplitude and angle modulation for narrow-band communication of binary-coded messages in fluctuation noise," Proc. IRE, vol. 42, pp. 447–454; February, 1954.

[38] G. F. Montgomery, "Message error in diversity frequency-shift reception," Proc. IRE, vol. 42, pp. 1184–1187; July, 1954.

type transmission. The required ratios of average signal power to rms noise power given by Montgomery for specified error probabilities are based on the use of ideal receivers. These ratios will be increased by three decibels as an allowance for the nonideal receivers used in practice. For the examples illustrating radioteletype operation it will be assumed that a binary error probability of 2×10^{-4}, corresponding approximately to a teletype character error probability of 10^{-3} for synchronous radio-teletype transmission, will provide a satisfactory service.

Fig. 69 presents distributions of the values of the ratios of hourly median signal intensity to rms noise power in a 2 kc/s band observed on three experimental

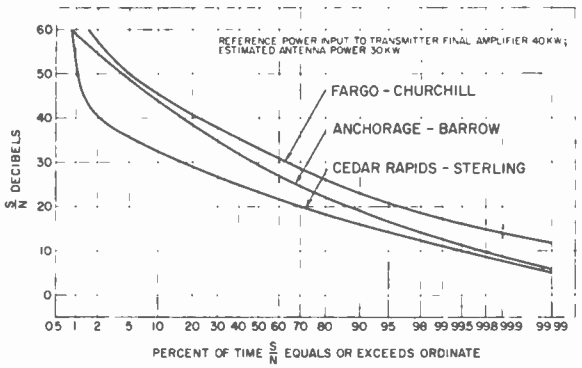

Fig. 69—Cumulative distributions of the ratios of hourly median signal intensity to rms background galactic noise observed at about 50 Mc/s in a 2 kc/s noise band for the year from October, 1951 through Sep ember, 1952.

paths over a 12-month period. Fig. 19 may be used for estimating systems performance at other frequencies. The assumption will be made that the distributions of the ratios of hourly median signal intensities to noise intensities in a 2 kc/s noise band correspond to the actual distributions of the ratios of average signal power to rms noise power in a 2 kc/s band. This assumption is not expected materially to affect the results, as measurements have indicated small differences between the recorded signal intensities and the rms signal power.

For the first example, an estimate is made of the expected reliability for synchronous single-channel frequency-shift radioteletype operation over the Cedar Rapids to Sterling path at 49.8 Mc/s using dual spaced-antenna diversity and suitable dual-filter receivers arranged for elimination of meteor Doppler errors. In this example, the bandwidth of each of the filters is assumed to be 100 cycles per second.

Required ratio of average signal power to rms noise power (Fig. 6 of ref. 37)	+34 db
Allowance for use of nonideal receivers	+ 3 db
Allowance for diversity gain (Fig. 2 of ref. 38)	−14 db
Allowance for bandwidth ratio (2 kc/s to 0.1 kc/s)	−13 db
Required ratio of average signal power to noise power in a 2 kc/s band	+10 db
Expected propagational reliability (Fig. 69)	99.5 per cent.

For the second example, an estimate is made for synchronous four-channel, time-division, radioteletype operation with dual, spaced-antenna diversity at a frequency of 49.7 Mc/s, using the Fargo–Churchill path. Each of the dual filters in the receivers is assumed to have a bandwidth of 400 cycles. Following the procedure used in the preceding example it is found that the required ratio of average signal power to rms noise power in a 2 kc/s band is 16 decibels. From Fig. 9 a value of 99.6 per cent is obtained for the estimated reliability.

Finally, an estimate is made for the expected reliability using narrow-band frequency modulation radiotelephony on the Fargo to Churchill path at 49.7 Mc/s. Dual, spaced-antenna diversity reception is assumed. It is also a value of 14 decibels for the ratio of hourly median signal intensities to rms noise power in a 2 kc/s band is required for satisfactory radiotelephone service. Reference to Fig. 69 gives a value of 99.9 per cent for the estimated propagational reliability.

Some additional comments are in order with respect to the above derived estimates of propagational reliability. As discussed previously, the controlling noise is usually of galactic origin. There are, however, periods when other kinds of noise, such as atmospherics from local thunderstorms or from thunderstorms located within the beam of the receiving antenna and within optical range, precipitation noise, and man-made noise, have to be reckoned with. No allowances have been made for the effects of noise sources other than galactic and the above estimates are probably optimistic by several tenths of a per cent. Outages resulting from the effects of sputter on paths crossing or near the zone of maximum auroral occurrence are estimated to reduce the reliability by no more than half a per cent. Furthermore other sources of outage, such as equipment failures, power failures, and shutdowns for maintenance are likely to be greater than those resulting from insufficient signal-to-noise ratios. Assuming that outages caused by these and related factors do not exceed three per cent, a systems reliability of about 96 per cent or greater should be realized for the types of service considered in the above examples.

Acknowledgment

It is desired to acknowledge the valuable contributions made by our colleagues at the National Bureau of Standards, and in particular the parts played by V. C. Pineo in the experimental program, and K. W. Sullivan in the observational program. The following organizations have made important contributions to this work. The Massachusetts Institute of Technology, the Rand Corporation, the Collins Radio Company, Engineering Experiment Station of North Dakota Agricultural College, E. C. Page Consulting Radio Engineers, and the Department of Defense.

A Message to the Readers

The authors regret that certain basic results of interest and importance are omitted from the above paper as a consequence of revisions and deletions and the withdrawal of a companion paper imposed by policy decisions of the U. S. Government. It is the authors' considered opinion that publication of the paper in its present form is not desirable and it was their expressed request that the paper be withdrawn.—*D. K. Bailey, R. Bateman*

The Editor shares the authors' disappointment regarding the withdrawals and deletions of material from this issue.

The foregoing paper was published in its present revised form upon authorization of the Director of the National Bureau of Standards and over the objections of the authors to the revisions. The Editor took this unusual step because of his firm conviction that withdrawal of this important paper from this issue would be a disservice to the IRE, to the profession, and to the authors themselves.—*The Editor*

On the Scattering of Radio Waves by Turbulent Fluctuations of the Atmosphere*

F. VILLARS† AND V. F. WEISSKOPF†

Summary—**This paper presents a theoretical analysis of the mechanism that enables transmission of vhf-signals over distances of the order of 10^3 km. It is found that turbulent mixing, operating at the lower edge of the *E*-layer ($h = 80$–90 km) produces fluctuations in electron density of sufficient intensity to account for the observed signals. The basic assumptions are the existence of a sufficiently strong gradient of electron density ($dN/dh \gtrsim 10^3$ cm^{-3}/km) and a reasonable level of turbulent activity.**

I. Introduction

A SERIES of experiments by Bailey and collaborators[1] in 1951 established the possibility of transmitting vhf-signals (50 mc per second in their experiment) over distances of the order of 10^3 km. The experiments were carried out after a theoretical estimate of turbulent scattering from the *E*-layer, based on the theory of Booker and Gordon,[2] had given promising results. The results of the experiments established the presence of a permanent signal, with fading characteristics following a Rayleigh distribution. This and the geometry of the experiment (see below) lead to the conclusion that at least the daytime maximum was due to scattering by random fluctuations in the *E*-layer.[3] The complete diurnal variation of the average signal strength suggests the presence of a contribution due to meteoric ionization. Such meteoric effects have recently been investigated theoretically.[4] We shall not discuss them here.

We now proceed to present the evidence of Bailey's experiment in a more quantitative fashion. Fig. 1 describes the geometry of the experiments. We define the scattering volume V as the region of space swept by the emitted beam and seen by the receiver antenna. Every volume element of this region is able to scatter energy from the transmitter into the receiver. Since scattering by random irregularities is incoherent, the total scattered power is proportional to the effective scattering volume. The effective scattering volume is that part of the scattering volume in which the scattering actually takes place. It is the part which contains the scattering particles; for instance, a horizontal layer of a given thickness intercepted by V. This situation lends itself to the introduction of the concept of a scattering cross section per unit volume, defined as follows: Take the energy flux density (Poynting vector) p_0 reaching a volume element dV of V from the transmitter. The total energy flux dP_s scattered out of dV into the solid angle $d\Omega$ (see Fig. 1) is then

$$dP' = p_0 \sigma(\theta) dV d\Omega. \tag{1}$$

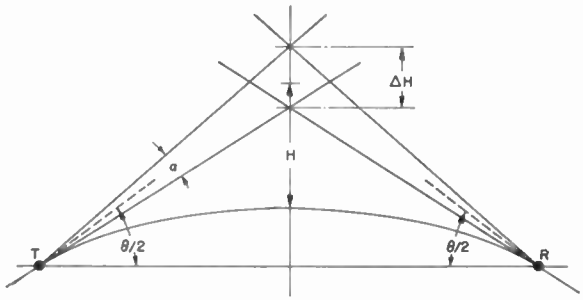

Fig. 1—The geometry in Bailey's experiment. d = distance between transmitter (T) and receiver (R) along the surface of the earth, = 1,245 km. θ = scattering angle = 24 degrees. H = mean height of scattering volume = 80 km. ΔH = vertical extension of scattering volume = 55 km. α = half-power total beamwidth, vertical, = 5 degrees.

Checking dimensions in (1) shows that $\sigma(\theta) dV$ has the dimension of a square of length and $\sigma(\theta)$ that of a reciprocal length. We shall call $\sigma(\theta)$ the differential scattering cross section per unit volume. By writing the expression for dP_s in this form, we have separated out explicitly all the unimportant factors like distance between scatterer and receiver, antenna characteristics, etc., and condensed in $\sigma(\theta)$ all that depends on the physics of the problem.

To extract a cross section from Bailey's data, we define (arbitrarily) an effective scattering volume as a slab of thickness $b = 5$ km at a height of about 80 km. The values for σ thus obtained can easily be converted to other assumptions about the scattering volume. From Fig. 2 (next page) we see that the effective scattering volume is

$$V_{eff} = \frac{Fb}{\sin\theta/2}.$$

The angular element $d\Omega$ is given by

$$\frac{A}{R^2} \cong \frac{4A}{d^2},$$

A being the aperture of the receiving antenna. Since

* Original manuscript received by the IRE, July 25, 1955. The research in this document was supported jointly by the Army, Navy, and Air Force under contract with the Massachusetts Institute of Technology.

† Dept. of Physics and Lincoln Lab., M.I.T., Cambridge, Mass.

[1] D. K. Bailey *et al.* "A new kind of radio propagation at very high frequencies observable over long distances," *Phys. Rev.*, vol. 86, p. 141, April, 1952.

[2] H. G. Booker and E. Gordon, "A theory of radio scattering in the troposphere," PROC. IRE, vol. 38, p. 401; April, 1950.

[3] For an analysis of the fading characteristics see R. A. Silverman and M. Balser, "Statistics of electromagnetic radiation scattered by a turbulent medium," *Phys. Rev.*, vol. 96, p. 560; November, 1954.

[4] V. R. Eshleman and L. A. Manning, "Radio communication by scattering from meteoric ionization," PROC. IRE, vol. 42, p. 530; March, 1954.

p_0F represents the total emitted power P_t, the ratio between emitted and received power is

$$\frac{P_r}{P_t} = \sigma(\theta)\frac{4Ab}{d^2 \sin\theta/2}.$$

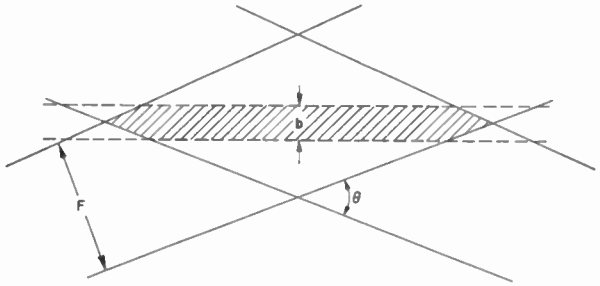

Fig. 2—Definition of the effective scattering volume in Bailey's experiment. b = thickness of layer intercepting the scattering volume. To define a cross section, b is arbitrarily assumed to have a value of 5 km. F = total cross-sectional area of incident beam between half power points. θ = scattering angle. The volume of the shaded region is $V_{eff} = bF/\sin\theta/2$.

In Fig. 3 we plot monthly averages of the cross sections $\sigma(\theta = 24°)$ and display their diurnal variations. The broad maximum around noontime is assumed to be due to turbulence in the E- (or possibly the D-) layer. The cross sections at maximum have average values of about 4×10^{-15} cm^{-1} for summer (June) and 4×10^{-16} cm^{-1} for spring (April).

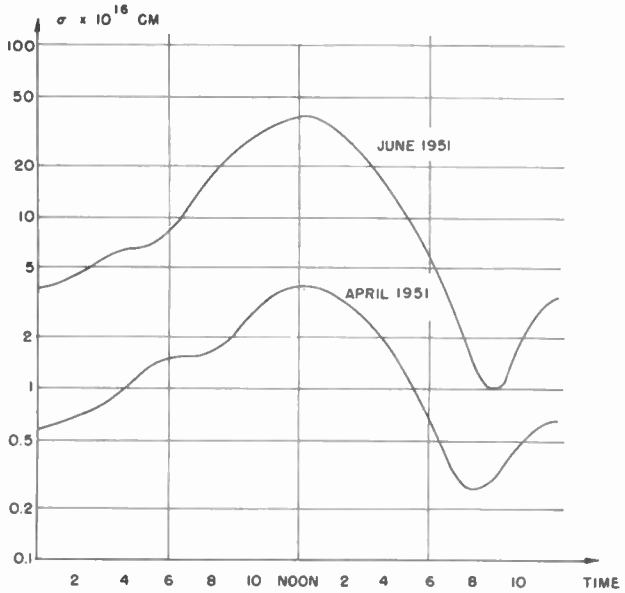

Fig. 3—Diurnal variation of scattering cross section/unit volume in Bailey's experiment. Plotted are monthly averages for April and June, 1951.

II. Scattering of Radiowaves by Random Fluctuations

We ascribe the scattering of the emitted beam to local (and temporary) deviations of the electric polarizability from the average. We assume that the medium carries in the average N free electrons per unit volume and consider the fluctuations $\delta N(x, t)$.

The dielectric susceptibility χ of the medium (defined as dipole moment density/electric field strength: $\chi = P/\epsilon_0 E$) is given by

$$\chi = -\frac{\omega_N^2}{\omega^2}, \tag{2}$$

where ω is the circular frequency $2\pi\nu$ of the incident electromagnetic wave, and ω_N the "plasma" frequency

$$\omega_N^2 = \frac{Ne^2}{m\epsilon_0}, \tag{3}$$

(m being the mass of the electron). Since χ is proportional to N, we have

$$\delta\chi = \chi\frac{\delta N}{N}. \tag{4}$$

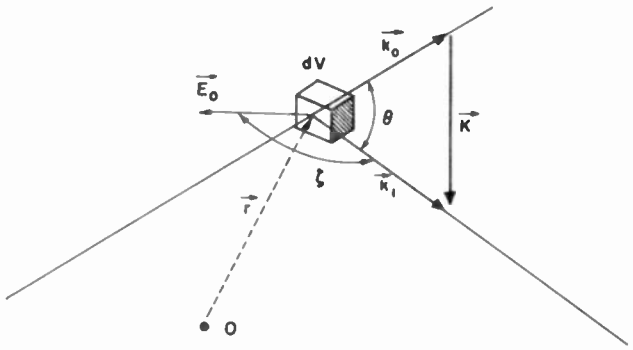

Fig. 4—Geometry underlying (6) for scattered field: k_0 and k_1: Wave vectors of incident and scattered wave, respectively. K = vector difference $\vec{k}_1 - \vec{k}_0$. θ = scattering angle. ζ = angle between E_0 and $\vec{k}_1$. $\zeta = 90$ degrees for horizontal polarization of the incident wave. $\vec{r}$ = position vector of volume element dV.

We shall now estimate the differential cross section for scattering caused by the fluctuations $\delta\chi(x, t)$. The geometry of the experiment allows us to consider the incident beam in the scattering region V as a plane wave

$$\vec{E}_{inc} = \vec{E}_0 e^{i(\omega t - \vec{k}_0 \cdot \vec{x})}.$$

We describe the scattered wave by a wave vector $\vec{k}_1$, forming an angle θ with $\vec{k}_0$. (In the following we shall often simply use k for $\vec{k}$, etc.) k_1 and k_0 have equal magnitude, and their difference

$$\vec{K} = \vec{k}_1 - \vec{k}_0$$

has therefore the magnitude (see Fig. 4 above)

$$K = 2k_0 \sin\frac{\theta}{2}. \tag{5}$$

The amplitude E_s of the scattered field at a distance R from the scattering volume ($R \gg V^{1/3}$) is

$$E_s = \frac{E_0}{4\pi R}\left(\frac{\omega}{c}\right)^2 \left| \int dV\, \delta\chi(r, t) e^{i\vec{K}\cdot\vec{r}} \right| \sin\zeta. \tag{6}$$

In (6), ζ is the angle between E_0 and k_1; an immaterial phase factor has been omitted.

The power scattered into the angular element $d\Omega$ is

$$dP_s = R^2 d\Omega \left| E_s \right|^2 \tag{7}$$

and consequently the average differential cross section per unit volume is

$$\sigma(\theta) = \frac{\overline{dP_s}}{V \left| E_0 \right|^2 d\Omega}.$$

We introduce the Fourier transformed of $\delta\chi$ with respect to the scattering volume V:

$$\delta\chi(k, t) = \int_V dV e^{i\vec{k}\cdot\vec{r}} \delta\chi(r, t) \tag{8}$$

and get from (6) and (7)

$$\sigma = \pi^2 \frac{1}{\lambda^4 V} \sin^2\zeta \, \overline{\left| \delta\chi(K, t) \right|^2} \tag{9}$$

with K defined in (5) and the bar denoting a time average.

With the help of (2), (3), and (4) we can replace $\delta\chi$ by

$$\delta\chi = \frac{\chi}{N}\delta N = -\frac{e^2}{\epsilon_0 mc^2}\left(\frac{c}{\omega}\right)^2 \delta N = -4\pi r_e \left(\frac{c}{\omega}\right)^2 \delta N$$

introducing the well-known "classical electron radius"

$$r_e = \frac{e^2}{4\pi\epsilon_0 mc^2} = 2{\cdot}8 \times 10^{-13} \text{ cm}.$$

We also define the Fourier transformed of the electron number density fluctuation by

$$\delta N(k, t) = \int_V dV e^{iKr} \delta N(r, t) = -\left(\frac{\omega}{c}\right)^2 \frac{1}{4\pi r_e} \delta\chi(k, t)$$

and get then from (9):

$$\sigma(\theta) = r_e^2 \sin^2\zeta \, \frac{1}{V} \overline{\left| \delta N(K, t) \right|^2}. \tag{10}$$

In the next section we discuss the dynamics of turbulence. This will enable us to evaluate the order of magnitude of $\delta N(K)$ in terms of certain models for the medium in which scattering takes place.

III. Turbulence

Turbulent flow arises, as well known, whenever certain stability conditions are violated. The characteristic magnitude in these conditions is the dimensionless Reynolds number Re

$$Re = \frac{\rho v L}{\eta}. \tag{11}$$

In (11) ρ and η stand for density (gr/cm^3) and viscosity of the fluid, L for a characteristic linear dimension and v for the magnitude of velocity change over linear dimensions of order L. The condition for turbulence is then $Re \gg 1$.

The dynamics of turbulence is still poorly understood. The most fruitful results are based on a statistical treatment of the problem.[5] The basic equation underlying this approach is the Nawier-Stokes equation[6] for the velocity field $v(x, t)$:

$$\rho\left(\frac{\partial v}{\partial t} + (v\cdot\nabla)v\right) + \eta\nabla \times (\nabla \times v) + \nabla p = 0. \tag{12}$$

p is the pressure in the medium. We use (12) to derive the energy balance for the liquid enclosed in a volume-element dV. Writing ϵ for the kinetic energy density

$$\epsilon = \tfrac{1}{2}\rho v^2,$$

we derive from (12)

$$\frac{\partial \epsilon}{\partial t} + div(v\epsilon) = -\eta(\nabla \times v)^2 - (v\cdot\nabla p) + \eta \operatorname{div}(v \times (\nabla \times v)). \tag{13}$$

The first term on the right-hand side of (13) gives the viscous energy dissipation inside dV, the second the work done by a pressure gradient, the third the work done by the viscous shear forces on the surface of dV. We shall use (13) to derive, on the basis of purely dimensional arguments, the orders of magnitude of the various terms entering the energy balance.

In a statistical theory of turbulence one deals with the correlation of velocities over a given region of space. To make things simple, we may define an "eddy" of size L and an associated eddy velocity Δv_L as a fluctuation that extends over a region of linear dimension L. Thus, if we call $\langle v\rangle_L$ as the velocity averaged over a spatial region of size L^3, we may define Δv_L as

$$(\Delta v_L)^2 = \langle (v - \langle v\rangle_L)^2 \rangle_L. \tag{14}$$

We are not introducing any directional correlations and hence implicitly assume isotropic conditions. This is not a very good assumption for application to atmospheric problems, but it should be sufficient for a first orientation.

Let us now discuss the energy balance for an eddy of size L. By dimensional arguments, the viscous damping will produce a power loss of order

$$D_L = \eta\left(\frac{\Delta v_L}{L}\right)^2. \tag{15}$$

In a stationary situation, the Δv_L themselves will be time independent in the average. Therefore, power must be fed into an eddy of size L; this is done by the term

$$\operatorname{div}(\epsilon v)$$

of (13) at a rate dimensionally given by

[5] For a comprehensive treatment of the statistical theory of turbulence, see G. K. Batchelor, "The theory of homogeneous turbulence," Cambridge University Press, London, Eng.; 1953. The original ideas are due to A. Kolmogoroff, *Compt. Rend. Acad. Sci.*, (*URSS*), vol. 30, p. 301; 1941; C.f. v. Weizsäcker, *Z. Physik*, vol. 124, p. 614; 1948 and W. Heisenberg, *Z. Physik*, vol. 124, p. 628; 1948.

[6] See for instance O. O. Sommerfeld: "Mechanik der Deformierbaren Medien," Akad. Verl. Ges., Leipzig, Germany; 1946.

$$S_L = \rho \frac{\Delta v_L^3}{L} . \tag{16}$$

This expression is easily understood as follows: The kinetic energy T_L associated with an eddy of size L is: $T_L = \frac{1}{2}\rho(\Delta v_L)^2$. The eddy disintegrates into smaller eddies after a time τ_L, which is of the order of the revolution time: $\tau_L \sim L/\Delta v_L$. Hence the power used up by the eddy is $S_L \sim T_L/\tau_L$. Since the power supply arises from the large-scale dynamics,[7] (16) represents the net rate at which eddies of size $>L$ feed energy into eddies of size $\leqq L$. We notice ratio between (16) and (15) is

$$\frac{S_L}{D_L} = \frac{\rho L \Delta v_L}{\eta} \tag{17}$$

that is, a Reynolds number. We shall call it the Reynolds number Re_L for an eddy of size L. For the largest eddies ($L = L_0$, $v_L = v_0$) one must certainly assume that this number is $\gg 1$. For all values of $L < L_0$, for which S_L/D_L is $\gg 1$, we have negligible viscous damping of the eddies. The power (16) is then transmitted without loss through the whole spectrum of L-values down to a smallest value L_s, where D_L catches up with S_L.

For $L_0 > L > L_s$ we have then a stationary power transfer (16), which must be independent of L, since no energy accumulates in a given L-range. So we find that in this region of eddy sizes, a stationary situation implies

$$\Delta v_L^3/L = \text{const},$$

or, in other words,

$$\Delta v_L \propto L^{1/3}. \tag{18}$$

By this relation, the Reynolds number Re_L (17) is proportional to $L^{4/3}$ and thus decreases with decreasing L. It finally becomes 1 at $L = L_s$. From (15), (16) and (18) we find that

$$\frac{L_0}{L_s} = \left(\frac{\rho v_0 L_0}{\eta}\right)^{3/4} . \tag{19}$$

L_s is the size of the smallest eddies; if smaller ones are formed, they are rapidly destroyed by viscosity.

The most important result for our purpose is given by (18). The magnitude of Δv_L is determined by the initial power supply

$$S_0 = \rho \frac{v_0^3}{L_0} \tag{20}$$

in terms of which we now have

$$\Delta v_L = \left(\frac{S_0 L}{\rho}\right)^{1/3} . \tag{21}$$

[7] We assume that the original power supply (that is, activation of eddies of size $\sim L_0$) is due to large-scale pressure variations, corresponding to the term $(v \cdot \nabla p)$ in (13). But we assume that p has no small scale ($L < L_0$) fluctuations except those induced by the turbulent velocity field itself (see below) and hence plays no role in the transfer mechanism for $L_s < L < L_0$.

IV. Turbulent Density Fluctuations and Turbulent Mixing

We now try to determine the fluctuations δN in the number of electrons per unit volume caused by turbulence in the ionosphere. There are two ways in which turbulence may produce such fluctuations in the number of electrons:

1. Through density fluctuations of the carrier medium.

2. Through turbulent mixing. (This process implies an inhomogeneous average electron density.)

(A) *Density Fluctuations*

Although the gross structure of the pressure is assumed to be externally given, small scale fluctuations of velocity will produce local pressure variations. We may define a Δp_L in a way similar to the definition (14) of Δv_L. A mechanism by which pressure fluctuations arise is illustrated by the well-known Bernouilli theorem

$$p + \tfrac{1}{2}\rho v^2 = \text{const.} \tag{22}$$

Eq. (22) is sufficient to establish the dimensional relationship

$$|\Delta p_L| \cong \rho(\Delta v_L)^2. \tag{23}$$

By the equation of state, the gas will respond to (23) by density fluctuations $\Delta\rho_L$ (of size L):

$$\Delta\rho_L = \gamma \frac{\rho}{p} \Delta p_L \cong \rho \frac{\Delta v_L^2}{v_M^2} . \tag{24}$$

In (24), γ is the adiabatic exponent ($\gamma = 1.4$ for air), and v_M^2 the mean-square molecular velocity:

$$\frac{\rho}{p} = \frac{kT}{m_M} = \frac{1}{3} v_M^2,$$

(m_M being the mean molecular mass).

We may now insert (21) into (24) to get the mean-square density fluctuations of size L:

$$(\Delta\rho_L)^2 = \rho^2 \left(\frac{S_0}{\rho}\right)^{4/3} \frac{L^{4/3}}{v_M^4} . \tag{25}$$

Now for all values $L > L_s$, the fluctuations $\Delta\rho_L$ occur rapidly enough so that no relevant electron diffusion occurs. In that case then the fluctuations of the electron density N follow the fluctuation of the density ρ of the carrier medium:

$$\delta N = \frac{N}{\rho} \delta\rho$$

and consequently, by (25),

$$\Delta N_L^2 = N^2 \left(\frac{S_0}{\rho}\right)^{4/3} \frac{L^{4/3}}{v_M^4} . \tag{26}$$

(B) *Turbulent Mixing*

Whereas in A we assumed an electron density N homogeneous in the average, we are now investigating a

case in which there is an average gradient of N in one direction (height h):

$$N(h) = N_0 + (h - h_0)\left(\frac{dN}{dh}\right) + \cdots . \tag{27}$$

Such a situation for instance occurs at the lower edge of the E-layer, where a large gradient of N accompanies relatively small values of N itself. (See next section.) If a distribution as (27) is embedded in a turbulent carrier medium, electron density fluctuations ΔN_L of size L will be produced by eddies of size L and be of order

$$\Delta N_L \sim \left(\frac{dN}{dh}\right) L. \tag{28}$$

Some comments to this equation are in order:[8]

1. The relation (28) is correct only if the lifetime τ_L of the eddy is short enough so that the fluctuation of the electron density is not wiped out by other effects as, for example, the recombination of electrons and ions. It turns out that the lifetime of the eddies which are relevant for our problem is short enough by a large margin.

2. For a given gradient of N, ΔN_L is independent of the intensity of turbulent excitation provided $L > L_s$.

3. It is obvious that the turbulent mixing process itself tends to smear out any existing electron density gradient. The value of (dN/dh), as calculated for instance in the Chapman theory of layer formation,[9] has to be modified by an amount depending on the degree of turbulent excitation.

Hence, turbulent mixing leads to fluctuations in electron density

$$\left.\begin{aligned} &\Delta N_L^2 \cong \left(\frac{dN}{dh}\right)^2 L^2, \\ &\text{provided} \\ &\left(\frac{\rho \Delta v_L L}{\eta}\right) > 1. \end{aligned}\right\} \tag{29}$$

With these results we may now calculate the scattering cross sections for the two cases. The cross section formula contains the Fourier component $\delta N(K, t)$ of the electron density fluctuation. We must find how this quantity is related to ΔN_L. Using the definitions

$$\delta N(x, t) = \frac{1}{V} \sum_k e^{-i\vec{k}\cdot\vec{x}} \delta N(k, t) \tag{30}$$

and

$$\Delta N_L^2 = \langle N^2 \rangle_L - (\langle N \rangle_L)^2 \tag{31}$$

(in accordance with the definition given for Δv_L in Section III) we find easily that

$$\overline{\Delta N_L^2} = \frac{1}{V^2} \sum_{|k|>2\pi/L}^{\infty} \overline{|\delta N(k, t)|^2} \tag{32}$$

provided that the time averages (barred quantities) satisfy the independence condition

$$\overline{\delta N(k, t) \delta N(-k', t)} = \overline{|\delta N(k, t)|^2} \delta_{k,k'}.$$

From (26) and (29) we see that in both cases ΔN_L^2 are decreasing functions of $K = 2\pi/L$. This indicates that the main contributions to the sum in (26) arise from the lower limit and that the sum is approximately equal to

$$\frac{V}{(2\pi)^3} \int_{k>2\pi/L} d^3k \, \overline{|\delta N(k)|^2} \cong \frac{V}{(2\pi)^3} K^3 \overline{|\delta N(K)|^2}\Big|_{K=2\pi/L}$$

or,

$$\Delta N_L^2 \cong \frac{1}{VL^3} \overline{|\delta N(K)|^2}\Big|_{K=2\pi/L}. \tag{33}$$

With (33) we can evaluate the cross sections given by the general formula (10)

$$\sigma(\theta) = r_e^2 L^3 \overline{\Delta N_L^2} \sin^2 \zeta. \tag{34}$$

Let us insert the values of ΔN_L^2 for the two specific cases which we considered. This leads to the formulas

Case A: Turbulent density fluctuations

$$\sigma_A(\theta) = N^2 r_e^2 \left(\frac{S_0}{\rho}\right)^{4/3} \frac{L^{13/3}}{v_M^4} \sin^2 \zeta. \tag{35}$$

Case B: Turbulent mixing

$$\sigma_B(\theta) = \left(\frac{dN}{dh}\right)^2 r_e^2 L^5 \sin^2 \zeta \tag{36}$$

with $L = \pi/k_0 \sin \theta/2$ for both cases. An alternative way of writing (35) is obtained by substituting the value of S_0/ρ, given by (20),

$$\sigma_A(\theta) = N^2 r_e^2 \left(\frac{v_0}{v_M}\right)^4 \frac{L^{13/3}}{L_0^{4/3}} \sin^2 \zeta. \tag{37}$$

The validity of both expressions (35) and (36) is restricted to values of

$$L > L_s = \frac{L_0}{Re^{3/4}}. \tag{38}$$

V. Physical and Meteorological Conditions in the E-Layer

For an account of the physical theory of layer formation we must refer to the literature.[10] We limit ourselves to recall a few basic facts which shall play an important role in the present analysis.

[8] Similar considerations have been made by Roger M. Gallet, Nat. Bureau of Standards, private communication. Some of the results were published in Internal Publications of a series of lectures given in the Laboratoire National de Radioélectricité, Paris, France; January, 1955).

[9] S. K. Mitra, "The Upper Atmosphere," Asiatic Society Monograph, Series V5; 1952.

[10] See ref. 5, chap. III, sec. 10, pp. 279 ff., and also K. Rawer, "Die Ionosphaere," P. Noordhoff, Groningen, Holland, chap. III, p. 70; 1953.

The lowest well-established layer, the E-layer, builds up from a height of about 80 km, to reach a maximum around 110 km.[11] There are considerable diurnal and seasonal variations. In Table I we shall give sample values of electron density for daytime.

TABLE I

h(km)	N(cm^{-3})	$\frac{dN}{dh}$ (cm^{-3}/km)
80	variable	$\lesssim 5\times10^{3}$ above $h\sim85$ km
90	2×10^{4}	
100	10^{5}	
110	2×10^{5}	

It is well known that below the ionized layers, the temperature decreases with increasing height. The build-up of the ionized layers is accompanied by a temperature inversion, produced by the absorption of solar energy. Such an inversion produces a dynamically stable horizontal stratification which will suppress the onset of turbulence. To understand this in a more quantitative fashion, we must introduce the concept of adiabatic temperature gradient.

$$\left(\frac{dT}{dh}\right)_{Ad} \equiv \Gamma_{Ad} = -\frac{2}{7}\left(\frac{Mg}{R}\right) \cong -10^{0}/km. \qquad (39)$$

(Mg being molecular weight, R ideal gas constant).

Γ_{Ad} gives the rate at which a volume element of air cools down (or warms up) if displaced upwards (or downwards). If Γ is the actual temperature gradient, then by Archimedes' principle the air is dynamically unstable if $\Gamma<\Gamma_{Ad}$, stable if $\Gamma>\Gamma_{Ad}$. In the stable case, the "restoring forces" are proportional to $(\Gamma-\Gamma_{Ad})$. The relevance of these considerations is embodied in Richardson's turbulence criterion:[12]

A "Richardson" number

$$Ri = \frac{g}{T}\left(\frac{dT}{dh} - \Gamma_{Ad}\right) \Big/ \left(\frac{dv_H}{dh}\right)^{2} \qquad (40)$$

is defined in terms of the difference between actual and adiabatic gradient and the horizontal wind shear (v_H is the horizontal wind velocity and $g=10^{3}$ cm sec^{-2}). A thumb rule states turbulence will not occur unless

$$Ri \lesssim 1.$$

In Table II we plot temperature, temperature gradient and density of air as a function of temperature.[13] Actual observations of turbulence in the E- and D-layer region are possible by observing persistent meteor trails.[14] Unfortunately, these observations extend over a considerable range in height (70–110 km) and therefore do not give any evidence of a dependence of turbulent excitation on height in the region of interest. But, nevertheless, they definitely establish the existence of considerable turbulence. Application of Richardson's criterion leads to minimum values of wind shear (dv_H/dh), which increase with height, but only moderately, since the temperature gradients are all quite far from the adiabatic value. Since, in addition, the Reynolds number for a given wind shear decreases with increasing height (due to the decrease of ρ), we expect a decrease of turbulent excitation [for instance, measured in units of (S_0/ρ), (20)] with height.

The most reliable data about electron densities are due to recent rocket ascents.[11] The data are extremely variable, and we can only tabulate orders of magnitudes. The data in Table I are taken from a few measurements of actual electron-density distributions as functions of height, near mid-day (10 am to 1 pm). Characteristic of the experimental curves is the quite sharp lower boundary of the E-layer at 85–90 km. The so-called D-layer occurs at variable height and is occasionally visible only as a slight bulge in the lower part of the E-layer.

TABLE II

ATMOSPHERIC DATA

h(km)	T (°K)	dT/dh (°/km)	ρ(gr/cm^3)
70	218	−2.6	1×10^{-7}
75	209	−1.3	0.46×10^{-7}
80	205	−0.5	2.1×10^{-8}
85	203.6	+0.1	1×10^{-8}
90	206	+0.7	4.1×10^{-9}
95	210	+1.1	1.8×10^{-9}
100	217	+1.4	8.6×10^{-10}
110	233	+1.6	2.1×10^{-10}

VI. Comparison of Theory with Experiment

In this section we shall discuss whether the experimental data for $\sigma(\theta)$ ($\theta=24°$) can be fitted with either formula (35) or (36) for reasonable values of the parameters involved.

In order to explain the observed signal in terms of turbulent scattering, the eddy size L responsible for scattering

$$L = \frac{\lambda}{2\sin\theta/2}$$

(λ being the wave length $2\pi/k_0$ of the beam) must be

[11] See previous references and also: H. Newell, "High Altitude Rocket Research," Academic Press Inc., New York, N. Y., 1953 and J. C. Seddon, "Propagation measurement in the ionosphere with the aid of rockets," *Jour. Geophys. Res.*, vol. 58, p. 323; September, 1953.

[12] H. Lettau, "Atmosphärische Turbulenz," Akad. Verl. Ges., Leipzig, Germany; 1939; W. C. Swinbank and F. L. Richardson, "The criterion of atmospheric turbulence," *Quart. Jour. Roy. Met. Soc.*, vol. 78, p. 420; July, 1952.

[13] These values are given by the Rocket Panel, *Phys. Rev.*, vol. 88, p. 1027; December, 1952. The data refer to a case where oxygen begins to dissociate at $h=80$ km and proceeds uniformly to completion at $h=120$ km. If no dissociation of oxygen is assumed, the temperature raises more sharply above 90 km.

[14] C. deJager, "The spectrum of turbulence in the earth's upper atmosphere," *Mem. Soc Roy. des Sciences*, Liège, vol. 12, p. 223; 1952.

larger than L_S, defined in (19). Since $\lambda = 6m$, $\theta = 24$ degrees, we have

$$L_s > 14.4m. \tag{41}$$

For the discussion of this condition, it is of advantage to rewrite (19) in the form

$$\frac{1}{L_s} = \left(\frac{\rho}{\eta}\right)^{3/4}\left(\frac{v_0^3}{L_0}\right)^{1/4}. \tag{42}$$

The viscosity of air is well known to be $2\times10^{-4}g$ cm^{-1} ·sec^{-1}, independent of density, and ρ can be reasonably well-plotted as a function of h. (See Table II.) We may assume that L_0 is of the order of the scale height (6–8 km) in the E-region. Since there is no basis for the assumption that v_0, the velocity of the macro-eddy, should increase with height (on the contrary!), we infer that L_S increases with height at least as $\rho^{-3/4}$. Using 7 km for L_0, we plot $L_S(h)$ for various values of v_0. The evidence presented in Fig. 5 indicates that $L > L_S$ only below, say, 90 km, if we admit a $v_0 \lesssim 5$ m/sec at this height.[15] We are therefore in favor of an interpretation that locates the effective scattering volume (see Fig. 2) below 90 km.

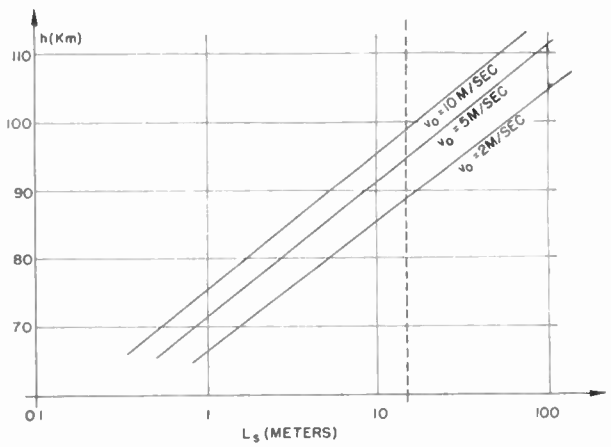

Fig. 5—Illustration of the condition $L > L_s$. Values of L_s, the minimum eddy size, are plotted as functions of height h for various values of the macro-eddy velocity v_0. In Bailey's experiment, $L = 14$ meters, and the condition $L > L_s$ implies $h < 100$ km for $v_0 = 10$ ms, and $h < 90$ km for $v_0 = 2$ ms.

Let us now evaluate the cross section σ_A and σ_B for these tentative data.

[15] We must remember at the macro-eddy L_0, v_0 is probably strongly anisotropic. The construction of (v_0, L_0) is therefore an extrapolation to fictitious isotropic macro-conditions. A useful parameter to describe turbulent excitation is the rate at which kinetic energy is dissipated through turbulence. This rate can be described by a time constant

$$\tau = \frac{1}{2}\left(\frac{v_H}{v_0}\right)^2\left(\frac{L_0}{v_0}\right), \quad v_H \text{ being the (horizontal) wind velocity.}$$

Taking v_H of the order of 50 m/sec, we get

$$\tau \cong 1 \text{ day} \quad \text{for} \quad v_0 = 5 \text{ m/sec}.$$

This looks like a reasonable value; we conclude that v_0 is unlikely to be much more than 5 ms.

In *case A* we have

$$\sigma = N^2 r_e^2 \left(\frac{v_0}{v_m}\right)^4 \frac{L^{13/3}}{L_0^{4/3}},$$

and with our data

$$N \cong 2 \times 10^4 \text{ cm}^{-3}$$

$$v_0 = 5 \times 10^2 \text{ cm sec}^{-1}$$

$$v_m = 4 \times 10^4 \text{ cm sec}^{-1} \; (T \cong 200°K)$$

$$L_0 = 7 \times 10^5 \text{ cm}$$

$$L = 1.4 \times 10^3 \text{ cm},$$

we obtain

$$\sigma \cong 2.4 \times 10^{-18} \text{ cm}^{-1}.$$

This is clearly too small by an order of magnitude (10^3).[16] In order to fit the experimental values with (35), we would have to raise the effective scattering volume to about 100 km *and* at least double the eddy velocity v_0. It appears to us that such a procedure is quite unrealistic and we conclude that the mechanism A is unlikely to produce the observed data.

As for mechanism B, (36) gives, with

$$\frac{dN}{dh} \cong 2 \times 10^3 \text{ cm}^{-3}/\text{km},$$

$$\sigma_B \cong 1.5 \times 10^{-13} \text{ cm}^{-1}.$$

This is of the right order of magnitude. We may recall that the estimate of ΔN_L (28) is likely to be an overestimate of the effect and the above estimate for σ_B is likely to be too high.

We conclude tentatively that the turbulent mixing process, occurring at the lower end of the E-layer, is a mechanism capable of producing a signal of the observed intensity. We feel strongly that this is a very tentative conclusion, which should be subjected to further experimental tests. The most promising line of investigation seems to be a change of wavelength. The cross section is a function of L:

$$\sigma = f(L), \qquad L = \lambda/2 \sin \theta/2.$$

According to (36), $f(L) \propto L^5$ for $L > L_s$, but for $L < L_s$ the theory indicates that $f(L)$ decreases much more rapidly than L^5. Since L_s is in all likelihood not much smaller than 14 m, we expect the signal to disappear completely for a value of L substantially smaller than 14 m. A test of this effect by observations of the wave length and angle dependence of the signal intensity

[16] This result is at variance with the conclusion of our previous paper (F. Villars and V. F. Weisskopf, "The scattering of electromagnetic waves by turbulent atmospheric fluctuations," *Phys. Rev.*, vol. 94, p. 232; April, 1954), where the turbulent power supply was greatly over-estimated. It was assumed that $v_0 \sim 50$ ms; whereas 5 ms would be a more realistic value.

could help to establish the nature of the scattering mechanism and thus give us some insight into a hitherto poorly understood field of ionospheric physics.

Appendix: The Scattering of Radio Waves in the Troposphere

The ideas presented in this paper can also be applied to the scattering of radio waves in the troposphere. The problem here is to explain the transmission beyond the horizon of uhf waves (100 to 10,000 mc) over relatively short distances (100 to 400 miles) so that the scattering volume is at a height only of 7 to 20 km.

The problem of the mechanism which causes this scattering is not yet solved. Turbulent density fluctuations are much too small.[17] It is probable that the humidity of the air and its fluctuations play an important role because of the large refractive index of water vapor. Temperature fluctuations might also be of importance at higher altitudes.

The study of the tropospheric scattering is greatly helped by the direct measurements of the refractive index of the air as a function of height. These measurements have been performed up to heights of 10 km, so that we have evidence as to magnitude and fluctuations of the refractive index directly at the place where the scattering occurs. One can use the results of these measurements as a basis of the calculation of the scattering, and hence one can try to predict the scattering without knowing the actual mechanism which has caused the refractive index and its variations.

The refractometer measurements show that the index of refraction exhibits strong fluctuations in its dependence of height. There are layers in the atmosphere in which the refractive index changes as much as 30 N units (one N unit is 10^{-6}) over 100 m and rates of change of 10^{-2} to 10^{-3} per meter are very common.[18]

Whatever the sources of these fluctuations are, we expect that the turbulent motion of the air will work on the existing gradients of refractivity and will produce smaller and smaller blobs of fluctuations. We expect again that the fluctuations of size L of the refractivity will be given, in analogy to (28), by

$$\Delta n_L \sim \left(\frac{dn}{dh}\right) L. \tag{43}$$

This relation can be used directly for the determination of the scattering cross section. The fluctuation of the susceptibility $\delta\chi$ is connected with the refractivity by $\delta\chi = 2\delta n$. We use the analogs of (33) $(\delta\chi(k)^2 = VL^3(\delta\chi_L)^2$ and get from (9):

$$\sigma = 4\pi^2 \frac{L^5}{\lambda^4} \overline{(dn/dh)^2} = \frac{4\pi^2\lambda}{[2\sin(\theta/2)]^5} \overline{(dn/dh)^2}, \tag{44}$$

where $\overline{(dn/dh)^2}$ is the square of the rate of change of n, averaged over the scattering volume. Let us apply this to a typical tropospheric scattering experiment[19] between two stations at a distance of 360 km with 100 mc radiation. The effective scattering angle in this case is about $\theta = 0.1$ radian. Formula (44) gives $\sigma \sim 10^{-11} m^{-1}$, with $\overline{(dn/dh)^2} \sim 10^{-18} m^{-2}$, which corresponds to an average rate of change for n of 10^{-3} N units per meter. The experimental values are of the same order of magnitude.

Evidently (44) for the cross section of scattering must be considered as very tentative. Similar formulas have been proposed before. Megaw,[20] for example, bases his expression upon the Kolmogoroff intensity spectrum which is proportional to $(L/L_0)^{2/3}$. In this case the fluctuations Δn_L are proportional to the intensity of the eddies, and he gets, instead of (43):

$$\Delta n_L \sim \Delta n_0 (L/L_0)^{2/3} \tag{45}$$

where Δn_0 is the magnitude of the fluctuations of the largest eddies of the size L_0. With (45) we get

$$\sigma = \frac{4\pi^2\lambda^{1/3}}{[2\sin(\theta/2)]^{13/3}} \frac{(\Delta n_0)^2}{L_0^{4/3}} \tag{46}$$

which is essentially Megaw's expression. It gives the right order of magnitude for σ with $\Delta n_0 \sim 10^{-1}$ N-units and $L_0 \sim 100$ m. It differs from (44) by its $\lambda^{1/3}$ dependence. This wavelength dependence agrees better than (44) with the weak λ dependence observed by Herbstreit, Norton, Rice and Schafer[19] at 100 and 1,000 mc. However, it must be said that the physical basis for the assumption (45) is harder to understand than for (43).

Both formulas should be valid only as long as $L = \lambda/2 \sin G/2$ is small compared to the spatial extension L_0 of the primary fluctuations of n. In the above quoted example, $L \sim 30$ m which is rather close to what one would expect to be the order of magnitude of L_0. The observed lack of proportionality with λ might perhaps be explained even on the basis of expression (44), when one takes into account that, for 100 mc, L is already quite close to L_0, a fact which would make the cross section smaller than (44).

[17] *Ibid.*, section c, 2, p. 240.

[18] See Reps. No. 6-01 and 6-02, Elec. Engrg. Res. Lab. of University of Texas; February, 1953. Refractometer Measured Tropospheric Index of Refraction Profiles."

[19] J. W. Herbstreit, K. A. Norton, P. L. Rice, and G. E. Schafer, "Radio wave scattering in tropospheric propagation," 1953 IRE Convention Record, Part 2, "Antennas and Communications," pp. 85–93.

[20] E. C. S. Megaw, "Scattering of electromagnetic waves by atmospheric turbulence," *Nature*, vol. 166, p. 1100; December, 1950.

Aerodynamical Mechanisms Producing Electronic Density Fluctuations in Turbulent Ionized Layers*

R. M. GALLET†

Summary—Various radio effects of the turbulence in the low ionosphere are discussed with a view toward determining the order of magnitude of the turbulence parameters in this region. These effects include vhf scattering, sporadic *E*-layer phenomena, and diffraction patterns in reflection. The required electron density fluctuations $\overline{(\Delta N/N)^2}$ fluctuate around 10^{-4} and the scale of the turbulence l is roughly 100 to 200 meters. The latter quantity measured directly in the troposphere is of about the same order of magnitude.

The underlying purpose of the paper is to study the aerodynamical mechanisms of turbulence. Pressure fluctuations result from the "collisions and extensions between turbulent eddies" in a uniform gas, or from vertical transport in the atmosphere with its varying pressure. It is shown that such pressure fluctuations are too small, by a factor of about 10^{-4}, to produce the observed density fluctuations.

However, the vertical transport mechanism produces two other effects which are independent of the energy of the turbulence and are of the right order of intensity. First, in a nonadiabatic atmosphere the vertical transport of air masses produces fluctuations of temperature. These, in turn, give rise to air density fluctuations, and proportional electron density fluctuations. Second, fluctuations of electron density result directly from transport in the presence of a gradient of electron density. These two effects, for the same uniform turbulence, occur at different levels in an ionospheric layer. They are sufficient to explain the stratification properties of sporadic *E*.

An expression for the scale of turbulence is obtained from the gradients of winds circulating in the low ionosphere. Hence, the properties of sporadic *E* phenomena should be interpreted in terms of meteorological factors (winds, synoptic masses of air, fronts, etc.). It is pointed out that the same transport mechanisms are acting in the troposphere, the gradients of water vapor content playing the role of the gradients of electron density.

Introduction

IN RECENT years the subject of radio propagation by scattering processes has become of great theoretical and practical importance. In the ionosphere the scattering phenomena present a variety of different aspects, such as observations of spread echoes in the *E* and *F* regions, low intensity echoes in the *D* region, ionospheric vhf forward scatter, sporadic *E* phenomena, and diffraction patterns in reflection or transmission, as observed in fading experiments. The basic concept for understanding these phenomena lies in the fluctuations of refractive index from point to point in the propagating medium. In the ionosphere these fluctuations are produced by fluctuations of electronic density. The interpretation of the various radio scattering processes leads to an evaluation of the order of magnitude of the amplitude and effective dimension, or "scale," of the fluctuations.

The electronic density fluctuations are the result of the existing turbulence in the upper atmosphere. It is the purpose of this paper to study the aerodynamical mechanisms producing these fluctuations.

Part I discusses the more important scattering processes in the low ionosphere. An interesting conclusion is that these different aspects lead to the same order of magnitude of the two parameters: amplitude and scale. A comparison with the results of direct measurements of scale in the troposphere is given.

Part II deals with density fluctuations produced in a uniform compressible gas in the presence of a turbulent velocity field. In this case the density fluctuations arise from "collisions" between eddies, and they are obtained in the two limiting cases of isothermal and adiabatic pressure variations. It is concluded that the density fluctuations are several orders of magnitude too small to account for observed effects. Part III outlines two effects of the *vertical transport* of blobs by turbulence in an atmosphere with *vertical gradients*. The nonadiabatic temperature gradient gives rise to temperature fluctuations. The electron density gradient is responsible for direct electronic density fluctuations. Both are numerically of the same order of magnitude and equally important. But their effects occur in different levels, leading to a quantitative explanation of the stratification properties observed in sporadic *E*. Part IV develops an expression for the scale of turbulence, as a function of the gradient of winds. Part V is a summary of the principal conclusions of the paper and indicates some developments of the author which are not given in this paper.

I. Discussion of Various Effects of Turbulence in the Low Ionosphere

VHF Forward Scatter

In their paper of 1952, Bailey *et al.*[1] adapted the Booker-Gordon theory[2] to the ionosphere, and published the first results of experiments with ionospheric vhf forward scatter. They estimated the scale, or effective size, of the scattering blobs to be of the order of 100m, and the mean square fluctuation of the electron density $\overline{(\Delta N/N)^2}$ to be about 10^{-4}. More recent experimental results are presented thoroughly elsewhere in this issue of the Proceedings.[3] In this aspect the total scatter is always small compared to the power contained

* Original manuscript received by the IRE, August 15, 1955; revised manuscript received, August 22, 1955.
† National Bureau of Standards, Boulder, Colo.

in the beam. In other terms, the "optical thickness" of the scattering layer is very small.[1]

In connection with the theory of the scattering, both at vhf and medium frequencies, and for forward and backward scatter, which are discussed in this and the following section, the attention of the author was recently directed by D. K. Bailey to a very remarkable paper by Eckersley in 1932.[4] Many of the present-day results on the polar diagram of scattering, the variation of the wavelength in the medium, etc., were anticipated by at least 20 years. (See[4] pp. 442 and 443.)[2]

Sporadic E

In contrast, ionospheric scattering at frequencies near the critical frequency involves layers of *great optical thickness*, of the order of unity or more, which varies with frequency. In short, there is a semitransparency ranging from opacity near the critical frequency to complete transparency for very high frequencies. Then the *backscatter* varies in complementary fashion from its greatest value near the critical frequency to an extremely low intensity for very high frequencies. These two properties, together with many other detailed results, obtained without further hypotheses, are very similar to the phenomenon described as sporadic E layer.

A comprehensive theory of these conditions needs to take account of the variation of the refractive index μ with frequency. When the frequency decreases towards the local plasma frequency, μ tends to zero. This variation in turn produces two very distinct effects: first, the wavelength $\lambda = 2\pi c/\omega\mu$ and the fluctuation of the dielectric constant $\overline{(\Delta\epsilon/\epsilon)^2}$ inside the medium both tend to infinity as we approach the plasma frequency. [See (3) Part II.] When the wavelength becomes large compared with the dimensions of the "blobs" of turbulence, it modifies both the scattering diagram and the scattered power of the blobs, for a given fluctuation of the dielectric constant. Second, the relative fluctuation of the dielectric constant becomes highly dependent on frequency, near the critical frequency [see (3)]. A true "optical amplification" (see Part II) of the very slight fluctuations of electronic density produced by the turbulence results. Very apparent and important effects are obtained as a function of the frequency and of the parameters of the turbulence. One must also take account of such factors as refraction effects when the frequency is not very high; of true absorption due to the electronic collisions in order to obtain correct expressions of the total attenuation of the main beam for the semitransparency properties; and of the total integrated back scatter for the apparent reflection coefficient of the layer.

The detailed study of these considerations led the author to advance an explanation of the principal properties of sporadic E-layer phenomena, in terms of the effects of the turbulence present in an ionospheric layer only, without recourse to extra sources of ionization. The hypotheses involving extra sources of ionization which have frequently been advanced have never been developed in detail to explain the specific properties of such phenomenon as thin layer, stratifications, reflection coefficient and transparency with respect to frquency, etc.

The above explanation and the essential consequences were reached by the author in 1951 independent of, and at the same time as, the publication of results on very high frequency forward scattering, and published in a short note.[5] This note was well reviewed and favorably received[6],[7] but apparently no further work in this direction has been published. Parts of the author's studies were presented in conferences at the École Normale Superiéure, Paris (1952) and Laboratoire National de Radioélectricité, Paris, December, 1954[8] and at SPIM (French Military Ionospheric Service).

As a consequence of these results for obtaining a satisfactory agreement between the predicted properties and the principal characteristics of the sporadic E phenomena, one can fix the order of magnitude of the two essential parameters of the turbulence affecting the electronic density inside the E region. One finds that these orders of magnitude are somewhat critical, and that the radio properties vary strongly for relatively small variations of the parameters. Specifically, one can account for the sporadic E properties with a "scale" of turbulence l of the order of 100 to 200 meters, and a mean square fluctuation of electronic density $\overline{(\Delta N/N^2)}$ of the order of 10^{-4}.[2],[5]

Comparison

It is very important to note that Bailey *et al.*[1] have arrived at just the same order of magnitude for the two important parameters, scale and mean-square fluctuation, of the turbulence. These values are still considered acceptable. The fact that these two largely different domains of frequency and of geometrical situations require the same values of the parameters is not a coincidence. The same basic phenomenon, the turbulence in roughly the same ionospheric region, is at the root of both.

The recent results indicate that the vhf forward scatter is effective near 75 km in the day time and 90 km at night. Sometimes sporadic E reflections, in the 100–200 km range, are observed simultaneously. On medium frequencies at vertical incidence, we observe only sporadic E reflections, when they are present, although

[1] For these discussions the concept of optical thickness of a semitransparent medium, in contrast to its geometrical thickness, is very useful. It is defined by $\tau = \int k ds$ along the ray path, where k is the energy attenuation coefficient. The attenuation can result from a true absorption, or from the scattering of a part of the energy in all directions or both. Hence, the transmitted power in the main beam is $P = P_0 e^{-\tau}$. This concept is widely used in optics of atmospheres, particularly in astrophysics.

[2] Eckersley's paper (4) anticipated many other results, developed in recent papers on ionospheric propagation, like attenuation theorems, multihop paths and geometrical decrements, divergence and focusing effects, etc. It is unfortunate that this remarkable work had generally escaped attention in recent times.

some reflections occur very rarely in the D region altitudes, with a very low effective reflection coefficient. While details will be not discussed here, it is important to point out that these different levels in two largely different conditions of transmission are not dissimilar. On vhf the refractive index is very nearly unity and the effect depends on the level where the combination

$$\frac{1}{l}\overline{\left(\frac{\Delta N}{N}\right)^2}$$

is maximum, and is independent of the mean electron density. On medium frequency back scatter the effect is highly amplified where the refraction index is minimum, other things being equal. Thus this effect is much more important in the E region where the electron density is between 10 and 100 times greater than in the D region, even when the turbulence is less intense.

Hence, the results in vhf forward scatter and in medium frequency backscatter are complementary. They must be interpreted in *meteorological terms*. They indicate that the combination

$$\frac{1}{l}\overline{\left(\frac{\Delta N}{N}\right)^2}$$

is maximum in the lower levels, and that the turbulence seems to be fairly constant there, with well marked diurnal and seasonal variations. This combination can be discussed in the light of the mechanisms and formulas discussed in Part III and Part IV of this paper. In the E region the turbulence seems to be much more irregular in time and space, with considerable variations of its parameters. Specifically, the "sporadic E clouds" can be interpreted as regions of intense turbulence, analogous to the "fronts" and regions of separation of air masses of different characteristics observed in meteorology. It is the opinion of the author that the observations and statistics of the sporadic E phenomena tell us the nature of the ionospheric E meteorology.

Diffraction Pattern

A third type of information of a different nature is afforded by the study of the diffraction pattern of the waves vertically reflected by the E region, at frequencies smaller than the critical frequency. The level of reflection is a sort of random irregular mirror. The reflected wave has a deformed wave front. The mean spreading of the normal to the front depends on the ratio of the wavelength to the "mean size of ionospheric irregularities." Briggs and Phillips have given a theory of the method of measurement and a more precise statistical meaning of the "mean size" of the irregularities,[9] following the theory developed by Booker, Ratcliffe and Shinn.[10] Their statistical results on many hundreds of observations are reproduced on Fig. 1. The sizes lie between 50 and 400 meters, with a maximum near 200 meters, and a remarkably small dispersion. One can note that the dispersion is greater in conditions of sporadic E reflections and that the most frequent size is slightly smaller ($\sim$150 meters). A good check is furnished by independent measurements on two different frequencies in the ratio 1 to 2 showing no difference in the statistical results. It must be remarked that the size of irregularities during conditions of F reflection is not necessarily representative of the F region, but can characterize a lower layer producing appreciable phase variations along the transmission path.

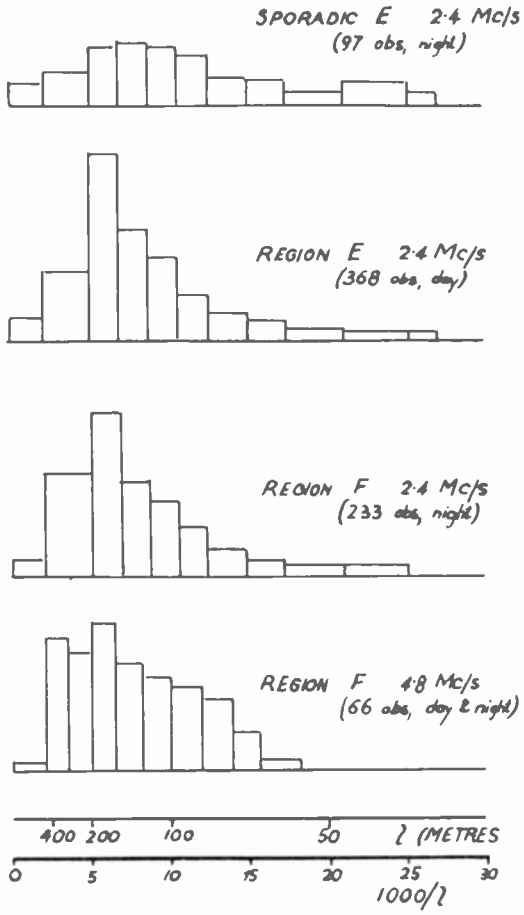

Fig. 1—Reproduced from Briggs and Phillips, *Proc. Phys. Soc.* vol. 63, p. 907; 1950.

Briggs[11] furnishes another very different method of measurement of the spreading of the reflected wave by means of a rapid frequency change experiment. The results are also essentially consistent with the above values.

In a recent theoretical treatment Feinstein[12] has refined the theory of these problems and has given one application to the ground correlation pattern of ionospherically-reflected signals obtained in ionospheric wind investigations. Here also, the best fit corresponds to a "scale" $l \simeq 250$ meters[12] (part II, p. 70).

The diffraction pattern by reflection from the irregular screen does not furnish directly the electronic fluctuation intensity $\overline{(\Delta N/N)^2}$[9],[10] because the phase variation is principally introduced near the reflection level

where the refractive index μ becomes zero and the integral giving the phase variation diverges. The removal of this divergence, which depends on other physical considerations, is a difficult problem. An attempt by Feinstein[12] (part II, p. 70) led to expressions in $\overline{|\Delta N/N|}$ for the spreading caused in the reflection level, at variance with all other expressions in $\overline{(\Delta N/N)^2}$ for the effect on a wave passing through a turbulent layer, i.e., when the frequency is greater than the critical frequency. Certainly this point requires further consideration.

Tropospheric Measurements

Finally, there are also the direct measurements of the scale of turbulence in the troposphere. In their fundamental work, Booker and Gordon[2] (p. 410) accepted provisionally a scale of 10 cm. Soon after, Megaw[13] criticized this value and advocated from his studies a scale of the order of 100 m, and a size of about 10 cm for the smallest effective eddy in the free atmosphere. Recent important series of measurements by Crain, Deam and Gerhardt[14] and Crain, Straiton and Von Rosenberg[15] of the tropospheric index of refraction fluctuations indicate a scale of some meters near the ground but increasing with altitude, and of the order of 100 meters for heights of 300 meters or above in the free atmosphere. Certainly the conditions are largely different in the troposphere and in the upper atmosphere near 100 km. But we have indications that the actual turbulence is a very general meteorological phenomenon with about the same characteristic scale for a wide range of altitudes.[16]

Summary

Hence, a number of very different considerations seem to result in essentially the same values of the two important parameters describing the turbulence affecting the electron density. The "scale" $l \simeq 200$ meters and the "electronic fluctuation intensity" $\overline{(\Delta N/N)^2} \simeq 10^{-4}$.

These parameters, and their variations with altitude, geographical position, and time, diurnal and seasonal, are essentially aerodynamical characteristics of the atmosphere in the D and E regions.

II. Electron Density Fluctuations and Turbulence in a Uniform Gas

Reference Formulas

First, certain useful reference formulas will be established. For the scattering process, the fundamental factor is the fluctuation of the dielectric constant ϵ. Neglecting magnetic field effects we have in an ionized gas

$$\epsilon = 1 - \frac{4\pi e^2 N}{m\omega^2} = 1 - \frac{\omega_p^2}{\omega^2} \tag{1}$$

where N is the number of electrons per cm^3 and ω_p is the local plasma frequency. We obtain immediately

$$\frac{dN}{N} = -\frac{d\epsilon}{1-\epsilon} \tag{2}$$

then

$$\frac{d\epsilon}{\epsilon} = -\frac{dN}{N}\frac{\omega_p^2}{\omega^2 - \omega_p^2}. \tag{3}$$

The power scattered by the slightly inhomogeneous medium is proportional to $\overline{(\Delta\epsilon/\epsilon)^2}$. Hence the effect on electromagnetic waves is *amplified*, compared to the mean square electronic density fluctuation $\overline{(\Delta N/N)^2}$ by the *optical amplification factor*

$$\left(\frac{\omega_p^2}{\omega^2 - \omega_p^2}\right)^2$$

which increases very rapidly when the frequency of the wave tends towards the local plasma frequency[5]. It is this factor which determines the properties of the sporadic E phenomena for frequencies around the critical frequency of the E region. Curiously enough, this aspect has received very little attention, and practically all attention has been devoted to the case of high frequencies $\omega^2 \gg \omega_p^2$ so that (3) becomes the approximation

$$\frac{d\epsilon}{\epsilon} = \frac{dN}{N}\frac{\omega_p^2}{\omega^2}. \tag{4}$$

Now let ρ be the density of the gas, containing n molecules plus ions of mass M per cm^3. When the degree of ionization is a certain constant fraction,

$$\frac{dN}{N} = \frac{d\rho}{\rho}. \tag{5}$$

From the equation of state of gas,

$$\rho = p\frac{M}{kT} \tag{6}$$

so that

$$\frac{d\rho}{\rho} = \frac{dp}{p} - \frac{dT}{T} \tag{7}$$

where k = Boltzmann's constant $= 1.38 \times 10^{-16}$

Fluctuations of Density in a Uniform Gas

The field of turbulence in a compressible gas develops fluctuations of pressure and, in turn, fluctuations of density in the gas. Consider blobs of gas, of a certain dimension l, of volume $v \simeq l^3$, of mass ρv, of mean square turbulent velocity $\overline{u^2}$. It is very reasonable to write that the mean potential energy of the compressions and dilations resulting from the effects of turbulence is equal to the mean kinetic energy E_k

$$E_{pot} = \overline{\left|\int p\,dv\right|} = E_k. \tag{8}$$

This is equivalent to saying that the collisions or separations of blobs, which receive a certain individuality during a time $\tau = l/u$ as a result of the turbulence, produce during this time a mean compression or dilatation

inside the volume such that the mean elastic energy balances the mean kinetic energy $\frac{1}{2}\rho v\overline{u^2}$. Now the compression or dilatation can be adiabatic, that is to say, without heat exchange, through the surface of the blob because of the very low heat conductivity of the gas, or isothermal; i.e. the effect of heat conductivity on the boundary of the blobs is so high that any differences of temperature are cancelled. More generally, because of the conductivity and of the turbulent mixing on the surface by eddies of smaller dimensions, the actual situation is between these two limiting cases, but nearer to the adiabatic case for the big eddies since the heat conductivity of a gas is very small.

a) In the case of isothermal fluctuations, by (7)

$$\frac{d\rho}{\rho} = \frac{dp}{p} \quad \text{and} \quad pv = \frac{\rho v}{M} kT = \text{constant}. \tag{9}$$

Hence, for a small fluctuation Δ_p

$$\int_v p\,dv = -\int_v pv \frac{dp}{p} = -\rho v \frac{kT}{M} \frac{\Delta p}{p}$$

since this mean energy is equal to $\frac{1}{2}\rho v u^2$,

$$\overline{\left|\frac{\Delta p}{p}\right|} = \frac{1}{2} \frac{M}{kT} \overline{u^2}. \tag{10}$$

But the mean square velocity of the molecules of the gas is given by

$$\frac{1}{2} M \overline{U^2} = \frac{3}{2} kT \tag{11}$$

which gives immediately, with (9) and (10),

$$\overline{\left|\frac{\Delta \rho}{\rho}\right|} = \frac{3}{2} \frac{\overline{u^2}}{\overline{U^2}}. \tag{12}$$

b) Turning to the adiabatic case,

$$pv^\gamma = \text{constant} \tag{13}$$

where γ is the ratio of specific heats; $\gamma = \frac{7}{5}$ for diatomic molecules (air). From (13) and the equation of state one obtains the classical adiabatic differentials

$$\frac{dv}{v} = -\frac{1}{\gamma} \frac{dp}{p}; \quad \frac{dT}{T} = -\frac{1-\gamma}{\gamma} \frac{dp}{p}, \tag{14}$$

and from (7)

$$\frac{d\rho}{\rho} = \frac{1}{\gamma} \frac{dp}{p} \tag{15}$$

one now obtains, for a small fluctuation Δp,

$$\int p\,dv = -\int \frac{1}{\gamma} vp \frac{dp}{p} = -\frac{1}{\gamma} \rho v \frac{kT}{M} \frac{\Delta p}{p}, \tag{16}$$

neglecting terms of second order in $\Delta p/p$.

The equality of potential energy (15) and kinetic energy furnishes with (11)

$$\overline{\left|\frac{\Delta p}{p}\right|} = \frac{3}{2} \gamma \frac{\overline{u^2}}{\overline{U^2}} \tag{17}$$

and for the fluctuations of density, by (15)

$$\overline{\left|\frac{\Delta \rho}{\rho}\right|} = \frac{3}{2} \frac{\overline{u^2}}{\overline{U^2}}. \tag{18}$$

One obtains again the same formula as in the isothermal case. However, here there are fluctuations of temperature of the order

$$\overline{\left|\frac{\Delta T}{T}\right|} = \frac{3}{2} (\gamma - 1) \frac{\overline{u^2}}{\overline{U^2}}. \tag{19}$$

It seems that these expressions for the fluctuations of pressure can be obtained by application of the Bernouilli theorem of hydrodynamic continuity $p + \frac{1}{2}\rho v^1 = \text{constant}$. But if one desires to obtain the results of fluctuations of density, pressure, and temperature in the two cases of adiabatic or isothermal fluctuations, the treatment is quite complicated, and one would not have the advantage of a direct insight into the phenomena as in the above discussion.

Clearly the above considerations are applicable to any eddy size in the turbulence, provided that we know the mean square velocity of eddies of size l. It is known from the modern statistical theory of the spectrum of turbulence that in a stationary homogeneous turbulence, and in the limiting case of very great Reynolds number, the principal part of the spectrum (Kolmogoroff spectrum) is such that, if a velocity u_λ is attributed to eddies of "wavelength," in Fourier analysis of velocity field, equal to or smaller than λ, von Weiszacker's relation[17]

$$u_\lambda \propto \lambda^{1/3} \tag{20}$$

results. Under these conditions, which are not as universally satisfied as is usually stated, the above formulas furnish expressions for the spectrum of fluctuations of any size inside the limits of dimensions valid for this part of the spectrum. But very generally the greatest speeds and the bulk of the total energy of turbulence are associated with the biggest eddies which are of the size order of the integral scale.[3]

A more precise theory was given by Batchelor in 1951 for the pressure fluctuations according to the statistical theory of the spectrum. The results are quoted at the end of Batchelor's book[16] and reference *infra*, relation 8.3.21 (p. 182) which is, with our notations

$$\left(\frac{\overline{\Delta p^2}}{p^2}\right)^{1/2} = 3 \times (0.34)^{1/2} \frac{\overline{u^2}}{\overline{U^2}} = 3 \times 0.583 \frac{\overline{u^2}}{\overline{U^2}}, \tag{21}$$

in remarkable agreement with the above simple derivation. This result is derived for an incompressible fluid, however, and consequently is not immediately applicable to *fluctuations of density* and *of temperature* in a gas.

[3] In works on turbulence, integral scale is defined by the integral of the velocity correlation function.

Applications

In the E region the temperature T is near 300°K and U for the air molecules is 460 m/sec^{-1}. It is necessary to obtain $\overline{(\Delta N/N)^2} = \overline{(\Delta\rho/\rho)^2}$ of the order of 10^{-4}. This demands a very large value for the mean turbulent velocity, of the order of 50 m/sec^{-1}. Now the measures of effective random velocities of irregularities in the E region can be obtained by the study of fading. The theory and the order of magnitude were discussed for the first time by Ratcliffe[18]. A discussion of observations on frequencies from 4 mc to 16 kc gave him the order of 1 m/sec^{-1} for u. Not many measurements are available, because observers generally select by inspection the fading curves showing clearly displacements of diffracting patterns by a wind; they reject the cases of preponderant deformation of the diffracting patterns, which require for analysis a much more troublesome computation of autocorrelation functions. It is to be hoped that with more efficient equipment for the reduction of data these measurements will be produced.

In an important work,[19] McNicol has obtained a long series of measurements. His histogram is reproduced as Fig. 2. Clearly the random velocities of irregularities

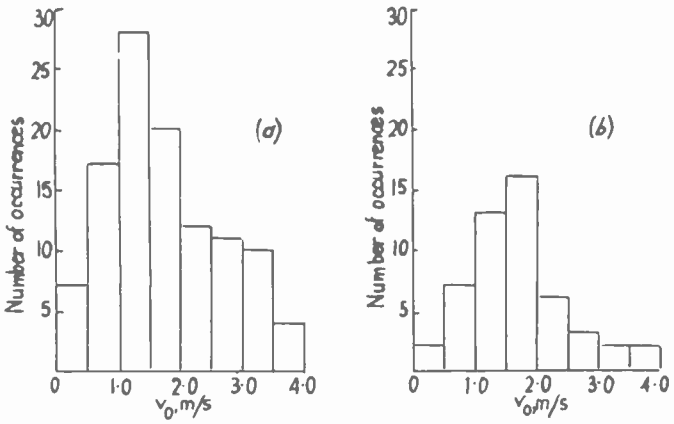

Fig. 2—Reproduced from McNicol, *Jour. I.E.E.*, Part III, vol. 96, p. 517; 1949.

(which were discussed in Part I) are mostly between 1 and 2 m/sec^{-1}. This figure is also reasonable when compared to the order of magnitude of the mean drift in the E region of around 80 m/sec^{-1}.

The density fluctuations expected by this mechanism are then of the order

$$\overline{\left(\frac{\Delta N}{N}\right)^2} = \frac{9}{4}\left(\frac{2^2}{460^2}\right)^2 \cong \frac{1}{8} \times 10^{-8}$$

in *disagreement by a factor* 10^{-4} at least with observations.

In a recent paper Villars and Weisskopf[20] discuss scattering in the E region, in the vhf case. Their work is based on the relation $\Delta\rho/\rho = u^2/\overline{U^2}$. This is their relation (14), which permits them to adopt the Kolmogoroff spectrum for describing the spectrum of electronic density fluctuations and to introduce the energy of the turbulence as the fundamental parameter. But they use in their relation (13a), the value 50 m/sec^{-1} for the turbulence velocity u in place of 1 to 2 meters-sec^{-1} (see Fig. 1). Hence $(\Delta\rho/\rho)^2$ is overestimated at least by a factor of 4.10^5. Therefore their use of the energy of the turbulence as the only parameter relevant for estimating density fluctuations, and the use of a Kolmogoroff spectrum for the description of the electron density fluctuations is unjustified. This error came about through confusion of upper atmosphere wind velocities and turbulence velocities.[4]

One is thus forced to conclude that completely different mechanisms are at work for producing the density fluctuations.

III. Special Mechanisms in an Atmosphere with Vertical Gradients

In Part II the compressions and dilatations of blobs of gas resulting from their random turbulent velocities were considered. Now consider the effects of the transport of these blobs in the actual atmosphere. An eddy is produced, displaced, and disappears by mixing, retaining a certain individuality during a sort of relaxation time $\tau = l/v$. The horizontal components of this transport have no special effect, other than those discussed in Part II. However, the vertical component of the mean square value $u^2/3$ does have special effects, due to the vertical gradients of physical characteristics in the atmosphere. It will be shown that the two special effects arising from the nonadiabatic temperature gradient on the one hand, and the vertical gradient of electron density on the other hand, are of the right order of magnitude and equally important, but that they do not operate on the same level. This property very naturally and also quantitatively explains observed stratification and "thin layer" aspect of sporadic E phenomena.

First, without taking account of the ionization, consider for the masses of air the mean gradients of temperature and pressure. The atmosphere is not isothermal or adiabatic. In the E region above 80 km, the temperature gradient is positive with increasing altitude giving a very stable situation. At any altitude above 50 km, the gradients do not permit thermal convection. The turbulence is imposed by a mechanical cause and not by thermal instability.

When a blob of air is displaced vertically, without exchange of heat with the environment, it adjusts continuously to the pressure of the level, and follows an adiabatic transformation. Let $H = kT/Mg$ be the local scale-height of the atmosphere. In a dry atmosphere in adiabatic equilibrium it is easy to show that

$$\left(\frac{dH}{dh}\right)_{ad} = -\frac{\gamma - 1}{\gamma} \quad \text{and}$$

$$\left(\frac{dT}{dh}\right)_{ad} = -\frac{Mg}{k}\,\frac{\gamma - 1}{\gamma}. \qquad (22)$$

[4] In a new paper, page 1232, this issue, F. Villars and V. F. Weisskopf reject the conclusions of their previous paper (20).

In such an atmosphere the blob of gas is always in equilibrium and at the temperature of the level. Now consider the actual atmosphere with a non-adiabatic gradient dT/dh, positive in the E region. When a mass of air is displaced upward, its temperature decreases adiabatically, whereas the environment has an increasing temperature. This results in fluctuations of temperature and, in turn, fluctuations of density by the relation (7) which becomes

$$\frac{d\rho}{\rho} = -\frac{dT}{T}. \tag{23}$$

The air mass then has a greater density than the mean at this level and by gravity tends to return to its original level. The same effect arises for a downward displacement, the air-mass being relatively too warm and too light. For a displacement Δh the relative difference of temperature is evidently

$$\Delta T = \frac{dT}{dh}\Delta h - \frac{\gamma - 1}{\gamma}\frac{Mg}{k}\Delta h. \tag{24}$$

The mean-square vertical displacement of blobs of size l by the turbulence is of the order of $l^2/3$. Hence

$$|\Delta T| = \frac{l}{\sqrt{3}}\left(\frac{dT}{dh} + \frac{\gamma - 1}{\gamma}\frac{Mg}{k}\right), \tag{25}$$

or

$$\left|\frac{\Delta T}{T}\right| = \left|\frac{\Delta \rho}{\rho}\right| = \frac{1}{\sqrt{3}}\frac{l}{H}\left(\frac{dH}{dh} + \frac{\gamma - 1}{\gamma}\right). \tag{26}$$

Numerical Values

Table I in column two presents the numerical values of interest using the most recent general discussion available on the model of the upper atmosphere.[5] The relevant values of constants are:

$$\frac{\gamma - 1}{\gamma} = \frac{2}{7} = 0.285$$

$$\left(\frac{dT}{dh}\right)_{ad} = -\frac{Mg}{k}\frac{\gamma - 1}{\gamma}$$

$$= -0.990 \times 10^{-4} \text{ (degree cm}^{-1}\text{)}$$

$$\cong -1^\circ \text{ per 100 meters.}$$

From Table I, ΔT is of the order of 1° per 100 meters of vertical transport. And now $\Delta\rho/\rho$ becomes of the order of 10^{-2}. For example at 125 km, about at the maximum of the E layer, one obtains for $l = 200$ meters (see Part I)

$$\overline{\left(\frac{\Delta N}{N}\right)^2} = \overline{\left(\frac{\Delta \rho}{\rho}\right)^2} = \frac{1}{4} \times 10^{-4}.$$

In conjunction with the effect of optical amplification, this transport mechanism gives strong scattering effects *near the level of maximum electronic density* for frequencies slightly greater than the E critical frequency. Another important remark about this mechanism is that a turbulence with uniform scale as a function of altitude furnishes uniform fluctuations $\overline{(\Delta N/N)^2}$. But for a given $\omega(>\omega_c)$ the optical amplification will be maximum at the level of maximum electron density.

TABLE I

h(km)	T (°K)	H(km)	$\frac{dT}{dh}$ (degree/km)	$\frac{dT}{dh}+\frac{\gamma-1}{\gamma}\frac{Mg}{k}$ degree (for 100 meters)
47	271.8	8.07 (max)	0	.99
65	235.0	7.03	−4.0	.59
70	218.0	6.53	−2.4	.75
80	205.0	6.16 (min)	0	.99
90	217.0	6.54	1.8	1.17
100	240.0	7.26	2.5	1.24
110	270.0	8.19	5.2	1.51
120	330.0	10.04	6.0	1.59
125	360.0	10.97	6.0	1.59
130	390.0	11.90	6.0	1.59

Some of the results are shown in Figs. 3, 4, 5 (opposite), and 8, p. 1252. In the next section, a second mechanism which produces a very different situation is considered.

The effect studied here is independent of the velocity of turbulence, that is, of the intensity of the energy, and dependent only on the distance of transport. From the study of turbulence it is known that this distance is of the order of the eddy size. The hierarchy of eddy sizes in the turbulence gives rise to a hierarchy of temperature and density fluctuations proportional to the dimensions of the eddies. Hence, the spectrum of $\overline{(\Delta N/N)^2}$, which is the quantity relevant to scattering problems, is proportional to l^2, a spectrum different from the Kolmogoroff energy spectrum of turbulence.

But the situation must be considered more closely. The above temperature fluctuations can be cancelled in part by exchange of heat. This exchange taking part at the blob boundaries depends on the thermal conductivity and on the mixing by smaller eddies. The mixing time is essentially $\tau = l/v$. For the measured principal ionospheric irregularities we have τ of the order of 100 to 200 seconds. Considering the temperature gradients and the low conductivity of the air, the effect of τ is negligible. But for smaller eddies in the hierarchy, the heat content being proportional to the volume and the losses to the surface, the relative effect becomes important. This requires a more detailed treatment for a study of the spectrum of density fluctuations by this mechanism. There is here a parallelism with the influence of molecular viscosity in the theory of the velocity spectrum for the small eddies. It is the author's purpose here only to point out these interesting aspects, but not to discuss them.

It must also be indicated that in the presence of this transport mechanism the velocity spectrum is certainly

[5] F. L. Whipple, "The Earth as a Planet," G. Kuiper, ed., University of Chicago Press; 1954.

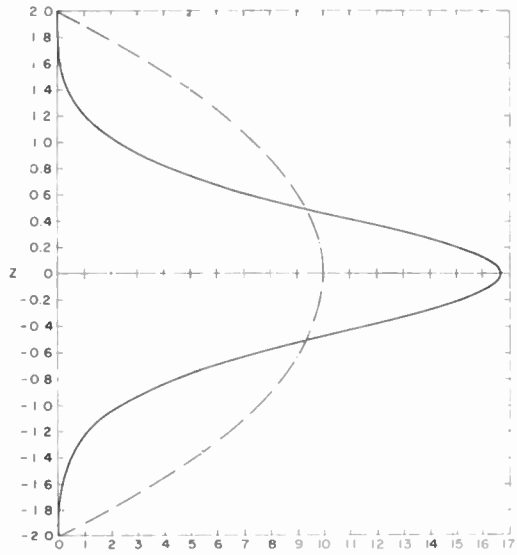

Fig. 3—Local back scatter coefficient for vertical incidence wave inside a parabolic layer when $(\overline{\Delta N/N})^2$ is uniform (temperature fluctuations). Conditions:

$$\frac{4\pi l}{\lambda_c}=10; \qquad \frac{\omega}{\omega_c}=1.11$$

λ_c = wavelength in vacuum corresponding to the critical frequency ω_c.

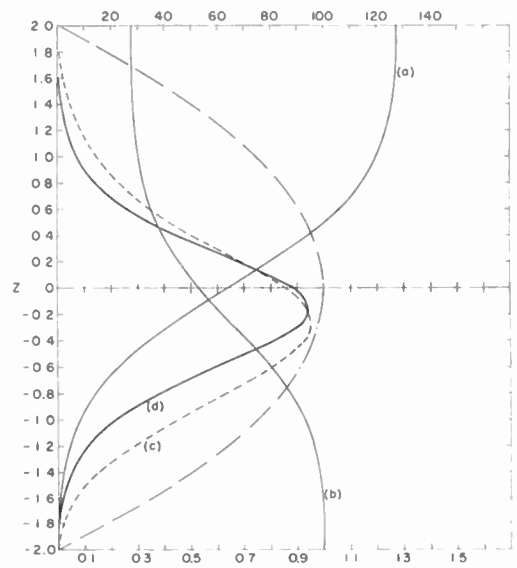

Fig. 4—Same conditions as in Fig. 3; for $\overline{(\Delta N/N)^2}=10^{-4}$. a. Variation as a function of altitude of the optical thickness ($\tau_s=\int a dz$) when the attenuation a is produced by the scattering. b. Corresponding variation of the flux of energy in the incident beam $E=E_0e^{-\tau_s}$. c. Local intensity of the integrated scattering (in all directions). d. Local intensity of the back scatter.

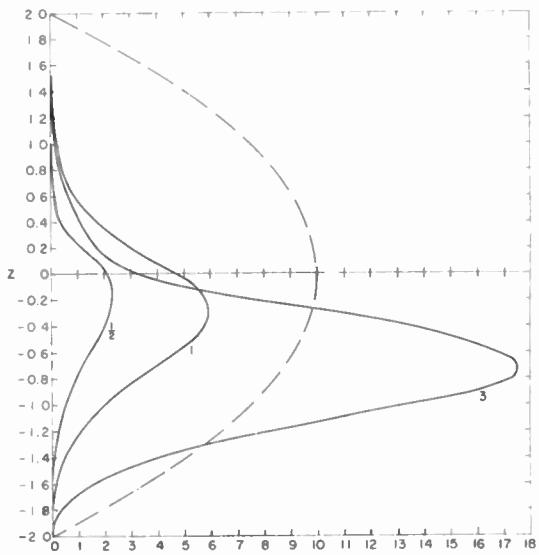

Fig. 5—Same conditions as in Figs. 3 and 4. Comparison of the variation of the local intensity of the back scatter for 3 values of $\overline{(\Delta N/N)}=\frac{1}{2}$, 1 or 3×10^{-4}.

modified, because the inequalities of temperature of the air masses introduce *potential energy*, which does not enter into the usual treatments of turbulence. The density fluctuations in the presence of a gravitational field tend to introduce a field of velocities of their own, expressing the tendency to return to the original level. A vertical acceleration $\Gamma=(\Delta\rho/\rho)g$ acts on the air mass, until this air mass is destroyed by mixing. This tends to give it a mean velocity $u'=\Gamma\tau'$ with $\tau'=l/u'$. So $u'^2=\Gamma l=(\Delta\rho/\rho)gl$; but $\Delta\rho/\rho=\Delta T/T$ which gives

$$u'=\sqrt{gl\frac{\Delta T}{T}}, \tag{27}$$

a formula found by Siedentopf in 1933[21] for the limiting velocity of gas masses in convection. In other words, the introduced potential energy resulting from an atmosphere with vertical gradients will interfere with the kinetic energy of the turbulence. It is believed that this effect is important for the theory of turbulence in stellar atmospheres also.

Finally, the pressure fluctuations, due to vertical transport in the presence of a pressure gradient, which were neglected considering pressure equilibrium at each level, are not completely cancelled during the vertical transport, but are of a second order. It can be proved that the relaxation time for pressure is of the order l/a where a is the sound velocity in the gas, and that the pressure fluctuations are of the order of

$$\frac{\Delta p}{p}\cong\frac{l}{H}\frac{u}{a};$$

but a is of the order of the molecular velocity U, hence:

$$\frac{\Delta p}{p}\cong\frac{l}{H}\frac{u}{U}. \tag{28}$$

Numerically

$$\left(\frac{\Delta p}{p}\right)^2\cong\left(\frac{0.2}{10}\times\frac{2}{460}\right)^2\cong10^{-8}$$

(which is of the same order of magnitude as that in Part II, but by a very different mechanism) when $(\Delta T/T)^2$ is of the order of 10^{-4}. Hence the pressure fluctuations are completely negligible.

In the preceding section electron density fluctuations resulting from air density fluctuations were discussed. Consider now a mechanism having nothing to do with air density fluctuations: the vertical *transport of electrons*. Since the air masses are transported with their electron content, and in the low E region an appreciable electronic density gradient exists, a mass going downward a short distance of the order of l will have a slightly higher density of electrons than the normal mean value at the new level. A mass going upward will have a lower density. This effect is another very important special mechanism producing electronic density fluctuations.[6] If the mean vertical distance of transport is of the order $l/\sqrt{3}$ the fluctuation will be of the order

$$\overline{\left|\frac{\Delta N}{N}\right|} = \frac{l}{\sqrt{3}} \frac{\text{grad } N}{N} \cdot \tag{29}$$

Application

In the E region during the daytime the semi-thickness is of order of 20 km, and $N \simeq 10^5$ cm^{-3}. A rough value of the mean gradient is therefore

$$\overline{\text{grad } N} \cong \frac{10^5}{2 \times 10^4} = 5 \text{ electrons cm}^{-3} \text{ meter}^{-1}.$$

With $l = 200$ m and $N \sim 5.10^4$ in the middle of the lower part of the layer $\overline{(\Delta N/N)^2} = 10^{-4}$. This effect is of the right order of magnitude and is therefore surely important in the ionosphere.

Here there is an important difference compared to the results of Part II. For a homogeneous turbulence (constant scale l as a function of altitude) the electronic fluctuation density is variable with altitude and is maximum where the function grad N/N is maximum. But here also it is an effect independent of the velocity of turbulence, and applying the preceding remarks on the spectrum of these fluctuations, again it does not lead to the Kolmogoroff formula.

However, we must consider the recombination of electrons. The normal mean gradient of electron density results from an equilibrium between production and recombination of electrons. The turbulence, even causing fluctuations of density, changes insignificantly the mass of air above the level of production, and so, does not change the incident flux. The production is modified by the local air density fluctuations. On the other hand, if during the transport of the ionized air mass, essentially during the time $\tau = l/u$, the recombination has enough time to adjust to the normal electronic density of the level, it will also be the same for the production which takes essentially the same time as the recombination, in the state of equilibrium. In this case it will result in a more or less total cancellation of the electron density fluctuations. This *recombination time* for small variations is given by[7]

$$\theta = \frac{1}{2\alpha.N} \cdot \tag{30}$$

If $\theta \gg \tau$, the effect of turbulence is conserved. In contrast, for $\theta \leqq \tau$, the effect of turbulence is diminished. But τ is of the order 100 to 200 seconds. In the low ionosphere α increases by a large factor ($\sim$100) compared to the value in the E layer. Direct measurements of θ in the D layer during eclipses, conducted recently at CRPL, furnish a short time of not more than some minutes. Hence, it is seen that this effect can depend strongly on altitude. The actual variations can be complicated by variations of the scale l and of u, which modify τ, with height. (See Part IV.)

There are strong reasons to believe that the transport effect for electron density gradient produces the stratification of the sporadic E layer observed near the apparent bottom of the E region (near $h'E$). Combined with the maximum of the gradient existing *above* the maximum of E-region electron density, and the effect of temperature fluctuations which is more important at the maximum, the stratification tendency of the E_s region in three levels at least, is explained very naturally on the basis of turbulence extending throughout the E region. The relative importance of these three stratifications depends on the different factors acting on each. The author has used the model of a Chapman layer, fitting the E-layer parameters, with a uniform turbulence of scale l, for developing the theory of the sporadic E effects by a gradient of electronic density. Some of the results are illustrated in Figs. 6 and 7 (opposite). Rocket measurements seem to indicate that the electron density above the maximum of the E region does not diminish as in the Chapman model. However, frequent observations of sporadic E stratification above the maximum are also known.

IV. The Scale of the Turbulence

The most regular cause of the turbulence in the free atmosphere is the wind, or more exactly the stresses produced by the *gradient of the wind*. One can obtain a relation among three quantities: the "scale" (size of the largest eddies where the energy necessary to maintain a permanent turbulence is introduced); the gradient of the wind; and the mean square velocity of the turbulence field. Hence, it is possible to obtain the scale from a knowledge of the winds (experimental or theoretical) and measures of the mean turbulent velocity furnished in certain cases by the study of the fading waves reflected by the E layer.

[6] In their new work, page 1232, this issue, Villars and Weisskopf also consider this effect and retain it as much more important than the fluctuations of the uniform gas. The author reached this conclusion in 1951, and found that this effect together with the effect of the temperature fluctuations give the natural explanation of the E_s stratification. See Gallet (8).

[7] Equation (30) $\Delta t = 1/2\alpha N_m$ was given by the author in 1947 in "Relations entre les phenomenes solaires et geophysiques," International Colloquium of Lyon; September, 1947 (publications of the CNRS-France, 312 pp.) for the discussion of the solar eclipse observed in May, 1947 (see p. 127).

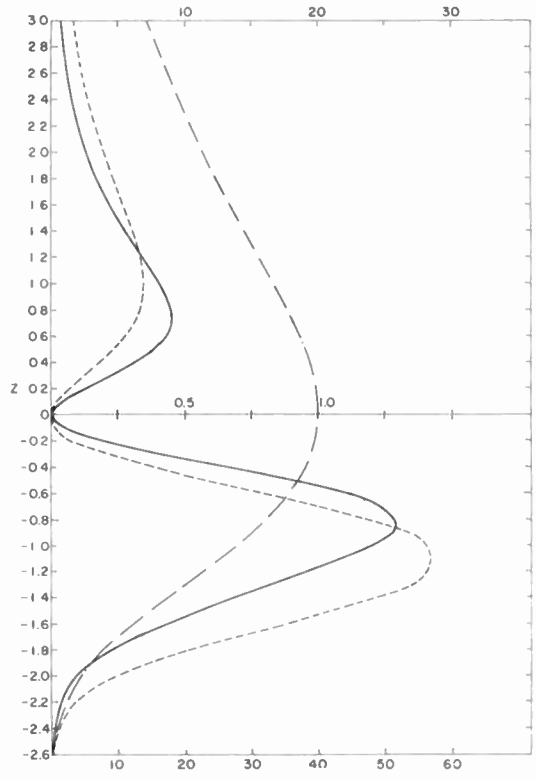

Fig. 6—Electronic transport mechanism (electron gradient effect). —·— Chapman layer model variation of electronic density ($z=h/H$). - - - - Local value of the attenuation coefficient a due to scattering. ——— Local value of the backscatter coefficient. Conditions are as in Fig. 3. Scale of turbulence uniform in all the layer ($l/H=2\times10^{-2}$).

Since we are concerned with order of magnitude only for the size of the observed effective irregularities existing in the E region or below, "scale of turbulence" is used here to mean the size of the largest eddies. More precisely, the notion presented by Batchelor,[16] (p. 103), of "energy containing eddies" with characteristic length l and characteristic velocity, u_l is adopted. This dimension is closely related to the special conditions producing the turbulence and supplying the energy necessary to build up and maintain a steady state. It is furnished by some boundary conditions of motion of the fluid. These largest eddies which play the role of reservoir of energy, give rise to smaller eddies, and so on, until ultimately the mechanical energy is transformed into heat by viscous decay which becomes preponderant for small eddies. This process for eddies of dimensions not too near the largest dimensions is a quasi-universal transformation, very largely independent of the initial conditions, and is described by the theory of statistical equilibrium. The essential result of this theory is the expression of the energy spectrum, with a definite and relatively simple shape in terms of the "wave number" $k=2\pi/\lambda$ in the Fourier analysis of the velocity field.

Now consider the gradients of winds as a special mechanism capable of being the normal cause producing the turbulence in the high atmosphere (and in the troposphere too). These gradients of winds are imposed by the dynamics of the circulation of the atmosphere.

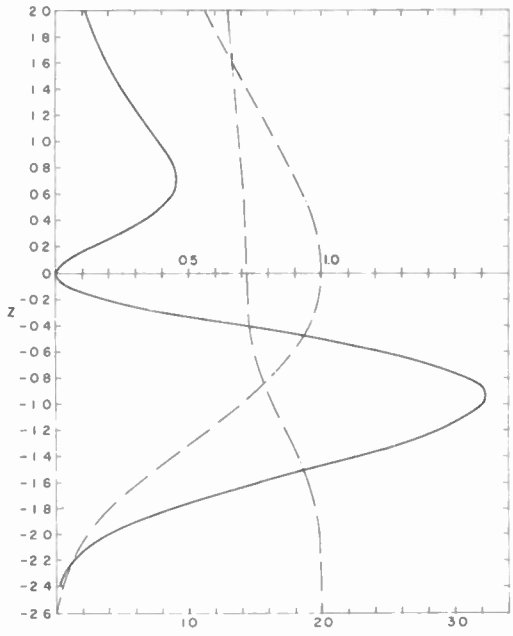

Fig. 7—Electronic transport mechanism (Chapman layer model). Variation of the flux of energy as a function of altitude. Typical result for the local intensity of the back scatter. Conditions as in Figs. 3 and 7. $l/H=2\times10^{-2}$.

There are at least the general circulation around the rotating earth (mean geostrophic wind resulting from temperature and pressure inequalities between the equator and the poles), the tides—solar and lunar (periodic winds with a 12 H period and a velocity amplitude of $\sim$20 m/sec^{-1} in the E region) and certainly some sort of large scale cyclonic circulation. It may be recalled that measurements using radar echoes on meteor trails demonstrate, with some other less precise methods, a vertical gradient of the horizontal wind velocity between 80 and 100 km heights of the order of 5 m/sec^{-1} per km as found by Greenhow in 1952 or 3.6 m/sec^{-1} per km by Elford and Robertson in 1953[23]. (See also footnote[24].)

In the presence of a gradient of wind, the laminar motion is generally unstable and has a tendency to produce "rollers." Perfect rollers are sometimes observed and even filmed with the fog near the ground, and are not uncommon in certain strata of clouds. When the Reynolds number of the flow is great enough, these rollers are also unstable and give rise to irregular turbulence. If the rollers have diameters of order l, they tend to have a rotation velocity

$$v=\frac{l}{2}\,\text{grad}\,V \tag{31}$$

in order to match the differences of velocity of the parcels of air on the boundary with the velocity of the center of the roller. From another point of view, if these rollers are the largest eddies, presenting an organized motion which soon breaks up in very much more irregular motions of smaller eddies, they form the upper limit of eddy sizes described by the statistical theory of turbulence. One interesting property resulting from

this theory, when the Kolmogoroff spectrum can be applied, was presented and used by Von Weizsacker[17]. The mean random velocity between two small masses of air separated by a distance λ, resulting from the random motions of all eddies of size $\leqq\lambda$ between these points is

$$u = A\lambda^{1/3} \tag{32}$$

where A is a constant of proportionality depending on the total kinetic energy of the turbulence. This law extends approximately to the largest eddy size, then breaks down. Hence there are two relations, one giving relative velocities as a result of the tendency to produce somewhat organized motions, the other expressing a certain statistical equilibrium between relative velocities of turbulence. These relative velocities must satisfy approximately the two relations for the largest eddy size l. Hence

$$l \text{ grad } V \cong 2Al^{1/3},$$

or

$$l = \left(\frac{2A}{\text{grad } V}\right)^{3/2}. \tag{33}$$

This law gives the desired relation determining the scale of the turbulence. This simple intuitive derivation needs to be further refined and a precise expression is necessary for the constant A, in order to have a really useful relation. The relation (31) does not determine the scale by itself, but *a posteriori* the above reasoning justifies that v must be of the same order of magnitude as that of the observed mean velocity of turbulence $\bar{u}$, or even a few times greater because of the well-ordered motion. It is finally this relation, obtained by a very rough picture, which is the root of the scale determination. As a check with $l\simeq 200$ m/sec^{-1} and grad $V\simeq 5$ meter sec^{-1} per km, (*mean* vertical gradient only. At each instant the local gradients can be very much greater), (31) furnishes $\bar{u}\simeq 0.5$ m/sec^{-1}, which is somewhat small but satisfactory.

A more exact treatment, using the spectrum of the turbulence will now be presented. For the limiting case of very great Reynolds number, which is about the case for the winds observed in the E region, the principal part of the spectrum expressed in the Kolmogoroff form is:

$$F(k) = \left(\frac{8}{9}K\right)^{2/3}\epsilon^{2/3}k^{-5/3} \tag{34}$$

between two limits $k_0 = 2\pi/l$ and k_s = wave number related to the small eddy size, where the decay of energy by molecular viscosity becomes preponderant. The spectrum $F(k)$ is such that the total kinetic energy per unit of volume (erg cm^{-3}) contained in the field of turbulence velocity is given by the product

$$\rho E_{\text{Kin}} = \rho \times \int_0^\infty F(k)dk \quad (\rho = \text{fluid density}) \tag{35}$$

over the complete range of wave numbers.

In (34) ϵ is the dissipation energy (per unit of volume, of time and of density), which is given by

$$\epsilon = 2\nu\int_0^\infty k^2F(k)dk. \tag{36}$$

$$\nu = \frac{\mu}{\rho} = \text{kinematic viscosity.}$$

k is a universal constant characteristic of this equilibrium spectrum, and of the order of 1 (about 0.45 from measurements of Proudman in 1951.)

The shape of the spectrum is valid approximately until $k_0 = 2\pi/l$, and falls rapidly for smaller wave numbers. k_0 characterizes the biggest eddies and determines the expression for the total energy. Integrating the spectrum (31) between k_0 and ∞:

$$E_{\text{Kin}} = \frac{3}{2}\left(\frac{8}{9}K\right)^{2/3}\epsilon^{2/3}k_0^{-2/3}. \tag{37}$$

This permits one to estimate ϵ from E and k_0 (which can be measured more directly), when the conditions of the Kolmogoroff spectrum of velocities are fulfilled.

Let:

$$E_{\text{Kin}} = \tfrac{1}{2}\overline{u^2} \tag{38}$$

which defines a mean square velocity of the turbulence field. This is about the observed velocity of biggest eddies or irregularities (in ionosphere about 1 to 3 meter sec^{-1}. See Part II). Then (37) is equivalent to saying

$$\epsilon = \left(\frac{8}{9}K\right)^{-1}\frac{2\pi}{3^{3/2}}\frac{\overline{u^3}}{l}. \tag{39}$$

Here Von Weiszacker's expression (32), used before in the particular case of the greatest eddies, is verified, but the relation is general because the flow of the dissipation energy ϵ, through the entire range of wave numbers k, is constant.

Now it is reasonable to assume that the total kinetic energy stored in the turbulence field built up and maintained by the wind shears, is proportional to the energy of the *relative* velocities introduced in the medium by the gradients of winds over distances of the order of the largest eddies created. It permits one to write:

$$\tfrac{1}{2}\overline{u^2} = (\alpha l \text{ grad } V)^2, \tag{40}$$

α being the constant of proportionality. α can be large because there is a continuous supply of energy building progressively the field of turbulent velocities.

From (37), (38) and (40),

$$l = \frac{3^{3/4}}{2\pi^{1/2}}\left(\frac{8}{9}K\right)^{1/2}\frac{\epsilon^{1/2}}{(\text{grad } V)^{3/2}}\frac{1}{\alpha^{3/2}}. \tag{41}$$

This is a more precise form of (33), relating the important parameters of the spectrum ϵ, $l = 2\pi/k_0$ with grad V.

Using (39) for eliminating ϵ in (41) the relation

$$l = \frac{1}{\alpha} \frac{\bar{u}}{\text{grad } V} \tag{42}$$

results which verifies the homogeneity in (41). This relation is almost trivial, but is equivalent to (31), which is thus justified *a posteriori*. (42) can be obtained on purely dimensional grounds.

Equation (41) can be verified by other works. In a paper on the turbulence produced by the Keplerian differential rotation in a gaseous solar envelope, S. Chandrasekhar and D. Ter Haar[25] study the scale of turbulence. They do not state (41) explicitly but if one combines their expressions A, 9; A, 16; A. 17; A, 20 one obtains

$$l = \frac{2\pi}{(4\zeta)^{3/4}} \, 3^{3/4} \left(\frac{8}{9} K\right)^{1/2} \epsilon^{1/2} \frac{1}{|\text{grad } V|^{3/2}}$$

where grad V is the velocity gradient in the Keplerian differential rotation, and ζ is a factor of order unity introduced in A, 5. The identity with (41) is obvious. The relation (42) or (31) has already been verified.

The author desires to indicate here that the values of a vertical grad V of the observed order of 3–5 m sec^{-1} per km, are well explained by *tidal winds*. It is impossible to enter here into a detailed discussion; we shall only indicate roughly the main points. Except near nodal altitudes, the tidal wind has a tendency to increase exponentially with altitude according to[8]

$$V = V_0 e^{h/2H} \quad \text{where} \quad H = \frac{kT}{Mg}. \tag{43}$$

The reason is to be found in a tendency to have a constant kinetic energy of the horizontal wind flow at any altitude. One deduces a gradient of the order of

$$\frac{dV}{dh} = \frac{1}{2H} V_0 e^{h/2H}. \tag{44}$$

For a reference level at 100 km the observed tidal winds are of the order 20 to 50 m sec^{-1}[24]. With $H \simeq 7$ km one obtains a grad V of 1.4 to 3 m sec^{-1} per km, which fits the observations correctly.

V. Conclusions

In Part I many different observations related to "irregularities" of the electron density in the E region or below were discussed. It is remarkable, and fortunate, that these largely different methods agree for the order of magnitude of the parameters $\overline{(\Delta N/N)^2} \simeq 10^{-4}$ and $l \simeq 100$ to 200 meters.

Part II discussed the fluctuations resulting from the compressions and dilatations of blobs of gas in uniform gas in turbulence. These effects are only of the order $(u^2/\bar{U}^2)^2 \simeq 10^{-8}$ for $\overline{(\Delta N/N)^2}$, and cannot explain the observations.

The explanation would appear to reside in the special *mechanisms of transport* by turbulence in an atmosphere in a gravitational field, with pressure and density decreasing with altitude. The fluctuations of pressure due to this transport are negligible (and furnish at most $\overline{(\Delta N/N)^2} \simeq 10^{-8}$). The fluctuations of *temperature* produced in an atmosphere with nonadiabatic temperature gradient, cause fluctuations of density of air and proportional fluctuations of electronic density of the order $\overline{(\Delta N/N)^2} \simeq 10^{-4}$. When the turbulence is uniform in altitude this effect is uniform inside all the layer, but the radio scattering effect is amplified by the variation of refraction index and has a maximum intensity near the maximum of the layer (see examples on Figs. 3, 4, and 5).

The transport of air-masses containing ionization produces also fluctuations of electron density proportional to the *gradient of the vertical electron distribution*

$$\overline{\left(\frac{\Delta N}{N}\right)^2}_{\text{grad}} \cong \frac{1}{3} l^2 \left(\frac{\text{grad } N}{N}\right)^2.$$

The gradients are of the order given by a Chapman model of the layers and in this case one obtains the following expression

$$\overline{\left(\frac{\Delta N}{N}\right)^2}_{\text{grad}} = \frac{1}{4 \times 3} \left(\frac{l}{H}\right)^2 (e^{-h/H} - 1)^2 \cong 10^{-4}, \tag{45}$$

with h measured from the level of maximum electron density. The gradient is zero at this level and maximum at points about one scale height above and below the density maximum. Radio scattering effect is also maximum near these two levels, taking account of refractive index influence. (See examples on Figs. 6 and 7.)

These two different effects resulting from *transport mechanisms* by turbulence explain very naturally, with a uniform turbulence, at least 3 levels of scattering effects (stratifications, observed in E_s). A detailed study of thin layer aspect, distances between stratifications, and transparency and reflection coefficients against frequency (Fig. 8, next page), reproduces observed characteristics of sporadic E fairly well, and will be published.

The transport mechanisms furnish $\overline{(\Delta N/N)^2}$ as a function of the scale l, or more generally of the blob dimension, and not directly as a function of the intensity of the turbulence measured by the agitation velocity u. Secondary effects can modify the results in terms of the ratio of the "recombination time" compared to the relaxation time of the turbulence. The spectrum of the electronic density fluctuations, which must be different from the spectrum of the turbulence velocities, has been discussed briefly.

Part IV gave an attempt to obtain theoretically the scale of the turbulence l, based on limiting conditions imposed by gradients of winds and application of the Kolmogoroff spectrum.

In the course of the work many observations of air motions were reviewed and used, and many numerical checks to the formulas were given. For lack of space the

[25] M. V. Wilkes, "Oscillations of the Earth's Atmosphere," Cambridge Univ. Press, Cambridge, Eng., p. 31 (eqs. 33, 34); 1949.

author wishes merely to indicate that this aerodynamical theory is to be developed in two directions. It is sure that electromagnetic forces are acting on the ionosphere, especially in periods of perturbation by magnetic storms and auroras. The electric fields produce displacements of ions and electrons, and can be another cause of turbulence, particularly in the F region. It is the opinion of the author that so called "spread F echoes" and the sometimes very strong F scattering may be interpreted in detail in this way, and that the auroral sporadic E is also in great part due to a turbulence of electric nature rather than to extra corpuscular ionization.

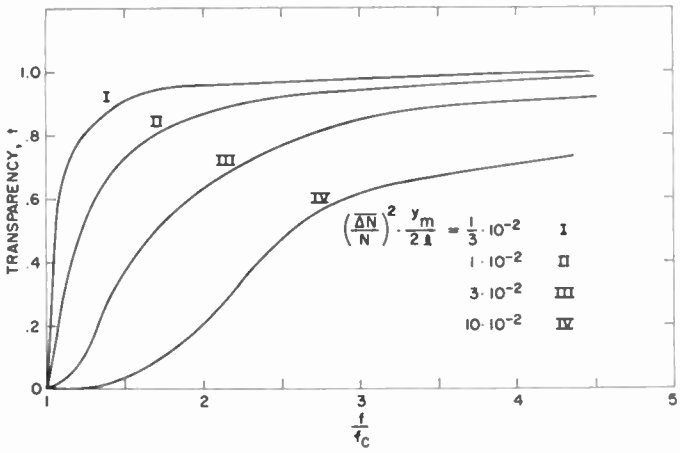

Fig. 8—Occultation properties of Sporadic *E* Transparency (in energy) for a wave of frequency f traversing vertically a scattering parabolic layer of semithickness y_m, of critical frequency f_c. Uniform turbulence (only temperature fluctuations): 4 different values of the determining parameter.

Of great interest also is the effect of the earth's magnetic field on the displacements of electrons and ions by turbulence. An *anisotropy* of the electronic blobs results, which are elongated horizontally at the magnetic equator and vertically in high latitudes. This anisotropy will certainly play a role in the explanation of the latitude variations of sporadic E aspects.

In conclusion, the author wishes to point out also that the same transport mechanisms, producing fluctuations of temperature and of water vapor content proportional to the gradient of this quantity, are at work *in the troposphere*. These two mechanisms act somewhat independently and are certainly of great importance in causing tropospheric scattering. However, we have restricted this discussion to electronic density fluctuations only.

Acknowledgment

The author expresses his sincere thanks to E. K. Smith and K. Bowles for their invaluable aid and patience during preparation of this paper for publication. To K. A. Norton, T. N. Gautier and D. K. Bailey he is grateful for help in the presentation of this work. Without the criticisms and encouragements of all them, the paper could not have been published.

Bibliography

1. Bailey, D. K., Bateman, R., Berkner, L. V., Booker, H. G., Montgomery, G. F., Purcell, E. M., Salisbury, W. W., Weisner, J. B., "A New Kind of Radio Propagation at Very High-frequencies Observable over Long Distances," *Physics Review*, vol. 86 (1952) pp. 141–145.
2. Booker, H. G., and Gordon, W. E., "A Theory of Radio Scattering in the Ionosphere." PROCEEDINGS OF THE IRE, Vol. 38 (April, 1950) pp. 401–412.
3. Bailey, D. K., Bateman, R., and Kirby, R. C., "Radio Transmission at VHF by Scattering and Other Processes in the Lower Ionosphere." PROCEEDINGS OF THE IRE, Vol. 43 (October, 1955—this issue).
4. Eckersley, T. L., "Studies in Radio Transmission." *Journal of the Institute of Electrical Engineers*, Vol. 71 (September, 1932) pp. 405–459.
5. Gallet, R. M., "On the Nature of the Sporadic E Layer and the Turbulence in the Upper Atmosphere," *Comptes Rendus Academie Science*, Paris, Vol. 233 (1951) pp. 1649–1950.
6. Morgan, M. C., "Radio Progress During 1952," PROCEEDINGS OF THE IRE, Vol. 41 (April, 1953) p. 502, 505.
7. Ratcliffe, J. A., "Irregularities and Movements in the Ionosphere," Proceedings of the Cambridge Conference on Physics of the Ionosphere (September, 1954). Published by the Physical Society, London, 1955.
8. Gallet, R. M., "Applications of Scattering Theories by Turbulence to the Ionosphere," *Lab. Nat. Radioelectricite*, Paris (December, 1954). In French. In publication, in Proceedings of Conference of the Propagation Study Group.
9. Briggs, B. H., and Phillips, "A Study of the Horizontal Irregularities of the Ionosphere," *Proceedings of the Physical Society*, Vol. B 63 (1950) pp. 907–923.
10. Booker, H. G., Ratcliffe, J. A., Shinn, D. H., "Diffraction from an Irregular Screen With Applications to Ionospheric Problems." *Philosophical Transactions of the Royal Society*, London, Vol. 242 (1950) pp. 579–609.
11. Briggs, B. H., "Investigation of Certain Properties of the Ionosphere by Means of a Rapid Frequency-Change Experiment." *Proceedings of the Physical Society*, Vol. B 64 (1954) pp. 255–274.
12. Feinstein, J., "Some Stochastic Problems in Wave Propagation," *Transactions of the IRE*, Vol. AP-2; Part I (January, 1954) pp. 23–30. Part II (April, 1954) pp. 64–70.
13. Megaw, E. C., "Scattering of Electromagnetic Waves by Atmospheric Turbulence." *Nature*, Vol. 166 (1950) pp. 1100–1104; see also "Waves and Fluctuations." *Proceedings of the Institute of Electrical Engineers*, England, Part III, Vol. 100 (1953) pp. 1–8.
14. Crain, C. M., Deam, A. P., Gerhardt, J. R., "Measurements of Tropospheric Index of Refraction Fluctuations and Profiles." PROCEEDINGS OF THE IRE, Vol. 41 (February, 1953) pp. 284–290.
15. Crain, C. M., Straiton, A. W., Von Rosenberg, C. E., "Statistical Survey of Atmospheric Index of Refraction Variation." *Transactions of the IRE*, Vol. AP-1 (October, 1953) p. 43.
16. Batchelor, G. K., "The Theory of Homogeneous Turbulence." Cambridge, Cambridge University Press, 1953; p. 124.
17. Von Weizsacker, G. F., *Problems of Cosmical Aerodynamics*, Paris, 1949; p. 158. Proceedings of the Symposium (Central Air Doc. Office 1951); also, Von Karman, T., pp. 129–148.
18. Ratcliffe, J. A., "Diffraction from the Ionosphere and the Fading of Radio Waves." *Nature*, Vol. 162 (1948) pp. 9–11.
19. McNicol, R. W., "The Fading of Radio Waves of Medium and High Frequencies." *Journal of the Institute of Electrical Engineers* (England) Part III, Vol. 96 (1949) pp. 517–524.
20. Villars, F., Weiskopf, V. F., "The Scattering of Electromagnetic Waves by Turbulent Atmospheric Fluctuations," *Physics Review*, Vol. 94 (1954) pp. 232–240.
21. Siedentopf, *Astronom. Nachrichten*, Vol. 247 (1933) p. 297.
22. Greenhow, J. S., *Journal of Atmospheric and Terrestrial Physics*, Vol. 2 (1952) pp. 282–291.
23. Elford, W. G., Robertson, D. S., *Journal of Atmospheric and Terrestrial Physics*, Vol. 4 (1953) p. 284.
24. a) Briggs, B. H., Spencer, M., "Horizontal Movements in the Ionosphere," Reports on Progress in Physics, Vol. 17 (1954) pp. 245–280.
    b) Brasefield, C. J., *Journal of Geophysical Research*, Vol. 59 (1954) pp. 233–237.
    c) Toman, K., *Journal of Geophysical Research*, Vol. 60 (1955) p. 59.
25. Chandraseckhar, S., Ter Haar, D., "The Scale of Turbulence in a Differentially Rotating Gaseous Medium." *Astrophysical Journal*, Vol. 111 (1950) pp. 187–190. Appendix to a paper by D. Ter Haar.

Some Remarks on Scattering from Eddies*

RICHARD A. SILVERMAN†, MEMBER, IRE

Summary—**The gaussian character of electromagnetic radiation scattered from turbulent atmosphere fluctuations is shown to follow from the Central Limit Theorem, even when the scattering is from only one macro-eddy and there is coupling between eddy motions of different sizes. It is suggested that including the effects of eddy coupling may increase the calculated average scattered power enough to give agreement with experiment.**

RECENTLY Villars and Weisskopf have begun the task of investigating in detail the scattering of electromagnetic radiation from turbulent fluctuations in the ionosphere.[1,2] They have proposed two models to account for the fluctuations of electron density that produce scattering: density fluctuations associated with the pressure fluctuations in the turbulent medium (the latter being calculated just as by Heisenberg),[3] and turbulent mixing operating in the region of large electron density gradient at the lower edge of the E-layer. In this note we give a simple demonstration of the fact that the first of these models leads to the scattering of incident monochromatic radiation as Gaussian noise. If the scattering volume contains a large number of macro-eddies, then the demonstration is a trivial consequence of the Central Limit Theorem, since contributions to the scattered field coming from the different macro-eddies are independent. However, even if the scattering is from only one macro-eddy, the scattered field is Gaussian by a more sophisticated application of the Central Limit Theorem. A proof which is in substance the same as that given below has already appeared in a paper by the author and M. Balser.[4] The present proof is more rigorous, and can be given a simple physical interpretation. Moreover, it goes through even when we remove the restriction that eddy motions of different sizes be independent.

We expand the deviation of the dielectric constant from its average value in Fourier series in a box with volume just that of a macro-eddy:

$$\Delta\epsilon(\vec{r}, t) = \sum_k \Delta\epsilon_k{}^t \exp(-i\vec{k}\cdot\vec{r}).$$

Then, if $\vec{K}$ is the difference between the incident and scattered wave vectors, the scattered field is proportional to $\Delta\epsilon_K{}^t$, which is in turn proportional to $p_K{}^t$, the corresponding Fourier coefficient of the random pressure field.[1] Thus, if the incident field has time dependence exp $(i\omega_0 t)$, the scattered field (apart from multiplicative constants) is just

$$p_K{}^t \exp(i\omega_0 t),$$

with real part

$$A(t)\cos\omega_0 t + B(t)\sin\omega_0 t,$$

where we have written

$$A(t) = \mathrm{Re}\,(p_K{}^t),$$
$$-B(t) = \mathrm{Im}\,(p_K{}^t).$$

Villars and Weisskopf have shown (following Heisenberg) that

$$p_K{}^t \sim \sum_k (\vec{K}\cdot\vec{v}_k{}^t)(\vec{K}\cdot\vec{v}_{K-k}{}^t), \tag{1}$$

where the $\vec{v}_k{}^t$ are Fourier coefficients of the turbulent velocity field. Eq. (1) arises from the nonlinear term of the Navier-Stokes equation. Writing

$$\vec{v}_k{}^t = \vec{R}_k{}^t + i\vec{I}_k{}^t,$$

and taking real and imaginary parts, we can write (1) as two real equations

$$A(t) = 2\sum_k{}' [(\vec{K}\cdot\vec{R}_k)(\vec{K}\cdot\vec{R}_{K-k}) - (\vec{K}\cdot\vec{I}_k)(\vec{K}\cdot\vec{I}_{K-k})],$$
$$-B(t) = 2\sum_k{}' [(\vec{K}\cdot\vec{R}_k)(\vec{K}\cdot\vec{I}_{K-k}) + (\vec{K}\cdot\vec{I}_k)(\vec{K}\cdot\vec{R}_{K-k})], \tag{1a}$$

where the prime on the summations prevents the occurrence of duplicated terms. (For simplicity of notation we have suppressed the superscript t).

The simultaneous presence of eddies of a wide variety of sizes is a basic feature of the von Weizsäcker-Heisenberg theory of turbulence, the starting point for the work of Villars and Weisskopf. Although the incident monochromatic radiation is scattered only by pressure fluctuations of size $2\pi/K$, (1) shows that eddies of every size contribute to the pressure fluctuations of size $2\pi/K$, and hence to the scattered field. The summands of (1) and (1a) are incremental pressure fluctuations, and are the counterpart of the *scattering blobs* of more naive models. It is to these increments that we apply the Central Limit Theorem.

It is usually assumed that the coefficients $\vec{v}_k$ belonging to different wave numbers are independent.[1-4] This assumption is certainly justified if the eddy sizes are

* Original manuscript received by the IRE, August 5, 1955.

† Formerly Dept. of Elec. Engrg., Mass. Inst. Tech., Cambridge, Mass.; now Inst. Math. Sci., Div. Electromagnetic Res., New York Univ., New York, N. Y.

[1] F. Villars and V. F. Weisskopf, "The scattering of electromagnetic waves by turbulent atmosphere fluctuations," *Phys. Rev.*, vol. 94, pp. 232–240; April, 1954.

[2] F. Villars and V. F. Weisskopf, "On the scattering of radio waves by turbulent fluctuations in the E-layer of the ionosphere," p. 1232, this issue.

[3] W. Heisenberg, "Zur statistichen Theorie der Turbulenz," *Z. Physik*, vol. 124, pp. 628–657; 1948.

[4] R. A. Silverman and M. Balser, "Statistics of electromagnetic radiation scattered by a turbulent medium," *Phys. Rev.*, vol. 96, pp. 560–563; November, 1954.

widely different. Indeed, it is just the fact that the smaller eddies have *forgotten* the much larger eddies they have come from that allows statistical reasoning to be applied to turbulence in the first place. However, the motions of eddies whose sizes are nearly the same must be coupled, as Chandrasekhar has emphasized.[5] Otherwise turbulence could not occur, since energy could not be transferred from the larger to the smaller eddies. Lacking any experimental or theoretical information about the coupling between eddies of nearly like sizes, we provide for coupling by making the following quite reasonable assumption: If the N incremental pressure fluctuations are suitably ordered, say as

$$X_1, X_2, \cdots, X_N$$

then we can separate them into n *independent* aggregates,[6] namely

$$(X_1, \cdots, X_{r_1}), (X_{s_1}, \cdots, X_{r_2}), \cdots, (X_{s_{n-2}}, \cdots, X_{r_{n-1}}), (X_{s_{n-1}}, \cdots X_N) \quad (2)$$

by the removal of $(n-1)d$ terms; i.e., by setting

$$s_i - r_i = d + 1, \qquad 1 \leqq i \leqq n - 1.$$

For the large Reynolds numbers of the ionosphere and troposphere, the extent of coupling is certainly small compared to the ratio between the sizes of the largest and smallest eddies; i.e., $d \ll N$. It can then be shown[7] that the sum of the terms (2) is approximately Gaussian, and that a negligible fraction of the variance of the sum is sacrificed by deleting the $(n-1)d$ terms, provided that $1 \ll n \ll N/d$.

Complete incoherence of all N incremental pressure fluctuations produces an average scattered power of order N, whereas N/d groups of coherent fluctuations may be expected to produce an average scattered power of order $d^2(N/d) = dN > N$. Since the average scattered power calculated by Villars and Weisskopf on the assumption of independent $\vec{v}_k$ is much too small, an understanding of the physics of eddy coupling is now needed more than ever.

The $2n$-variate distribution of

$$A(t_1), B(t_1), \cdots, A(t_n), B(t_n)$$

for any n instants of time can be shown to be approximately multi-dimensional Gaussian by using appropriate generalizations of the dependent Central Limit Theorem of Hoeffding and Robbins.[7] We can now give an alternate derivation of (15) of reference 4, the correlated bivariate envelope distribution, by making the following substitutions in a familiar formula of Rice:[8]

$$R_1^2 = \xi, \quad R_2^2 = \eta, \quad \psi_0 = \sigma_0, \quad \mu_{13} = \sigma_\tau, \quad \mu_{14} = 0.$$

The narrow-band character of the scattered signal is, of course, a consequence of the fact that the time scale of turbulent motions is very large compared to a period of the incident radiation.

The author is indebted to Dr. E. J. Akutowicz for suggesting the use of the Hoeffding-Robbins form of the Central Limit Theorem, and for his careful reading of this note in manuscript.

[5] S. Chandrasekhar, "A theory of turbulence," *Proc. Roy. Soc. A*, vol. 229, pp. 1–19; April, 1955.

[6] I.e., such that any two terms belonging to different aggregates are independent.

[7] W. Hoeffding and H. Robbins, "The central limit theorem for dependent random variables," *Duke Math. Jour.*, vol. 15, pp. 773–780; September, 1948.

[8] S. O. Rice, "Mathematical analysis of random noise," p. 216 of N. Wax's collection, "Selected papers on noise and stochastic processes," Dover Publications, New York, N. Y.; 1954. The formula referred to is eq. (3-7-13).

Investigations of Scattering and Multipath Properties of Ionospheric Propagation at Radio Frequencies Exceeding the MUF*

W. G. ABEL†, ASSOCIATE MEMBER, IRE, J. T. DEBETTENCOURT†, MEMBER, IRE, J. H. CHISHOLM†, AND J. F. ROCHE†, MEMBER, IRE

Summary[1]—Some results are given of studies of ionospheric forward scatter propagation at frequencies exceeding normal muf in the high hf and low vhf range with the view of investigating potential point-to-point communications. Approximately 13,000 hours of data were analyzed from measurements conducted since late 1951, on several frequencies and paths, predominantly 1,000 to 1,100 miles in length, in mid-latitudes. Signal level characteristics are presented in summary form and discussed.

Most of the work was conducted at 49.6 mc on the 1,066 mile Cedar Rapids, Ia. to Round Hill, Mass. path. Nominal 30 kw transmitters and large rhombic transmitting antennas were employed. The median received signal levels were relatively weak, of the order of 100 db below free space values. Fading during short periods in the absence of meteoric or sporadic *E* enhancements was found to be Rayleigh distributed. For longer periods, of the order of an hour, the fading was essentially Gaussian, although meteoric and sporadic *E* enhancements often changed the slope of the fading distribution curves at higher signal levels. The normalized median levels were generally lower and the diurnal variations less marked than those reported by CRPL for the shorter Cedar Rapids to Sterling path (773 miles). Seasonally, the median levels were higher in winter and summer and lower in spring and fall. There was an indication of lower levels with decreasing sunspot activity. The vertically-polarized component of the received signal was some 6 db (median) lower than the horizontally polarized component, when using the 2,000-foot horizontal rhombic transmitting antenna. Studies in 1952 of off-path signal levels and measurements of cosmic noise are described. The rms velocity of scatterers averaged over a winter day was found to be 6 to 7 mc, using autocorrelation analysis.

Effective heights of scattering were found to be 84 to 94 km, for December, 1954, using two-way 49.6 mc pulse transmissions over a short path (387 miles); daytime heights were lower than nighttime values. Recent one-way pulse transmission tests at the same frequency on a longer path (1,066 miles) are described. Observations of ionospheric, meteoric, sporadic *E*, and tropospheric modes are discussed.

The received power, when using the same 2,000-foot rhombic transmitting antenna on 49.6 and 27.8 mc, was found to vary inversely with the frequency most probably to the third or fourth power, the exponent decreasing with increasing 49.6 mc signal level.

Additional measurements at 22.9 mc are described for the Alpine, N. J.-to-Goose Bay, Labrador path (1,059 miles) conducted for about a half-year in 1953. Observations at 21.6 mc are reported for signals received at Limestone, Me. from transmissions at Cincinnati (997 miles); signal level data and two-stage space diversity results for the three-day period of observation in November, 1952 are described.

I. INTRODUCTION

THE STUDY of vhf ionospheric transmission over distances up to approximately 1,100 miles commenced with the prediction that such fields should be observed, based on the Booker-Gordon theory of turbulent scatter radio transmission [1, 2], and experimental verification in January, 1951.[2] The first experiments involved high-power 49.8 mc transmissions from the Collins Radio Company station at Cedar Rapids, Ia., and reception at the National Bureau of Standards (CRPL) field station at Sterling, Va. 773 miles away. 1,000-foot horizontal transmitting and receiving rhombic antennas were employed.

The Lincoln Laboratory research program was initiated in order to determine the potential application of the new transmission phenomena to point-to-point communication. Emphasis of the research was placed on circuits of the longer variety, i.e., 1,000 miles or greater. Of initial concern were the fading characteristics of the received signal, including instantaneous, diurnal, and seasonal variations. Knowledge was also desired of the parameters which would shed light on the propagation mechanism and, simultaneously, would assist those concerned with communication circuit design. These parameters include signal level distributions, effective height of the scattering region, the various transmission modes, the effect of polarization, angular spread of scattered power, frequency and distance dependence of the signal level, external noise level, and multipath delays.

With these objectives in mind, further transmissions from Cedar Rapids were desired, and the Collins Radio Company, as a sub-contractor of M.I.T., has continued to enlarge and operate the Cedar Rapids (Konigsmark) stations since the first tests. The transmission facilities were expanded to provide transmissions at various frequencies and with antennas beamed in various directions. The received signal characteristics have been measured by CRPL at its field station in Sterling and, since December, 1951, by Lincoln Laboratory at Round Hill. The continued operation of the Cedar Rapids transmission facility has enabled additional measurements to be made by numerous other interested groups, in-

* Original manuscript received by the IRE, June 24, 1955; revised edition received July 15, 1955; second revised edition received August 1, 1955.

† Lincoln Lab., M.I.T., Lexington, Mass.

[1] The research reported in this paper was made possible through support extended the Massachusetts Institute of Technology (Research Laboratory of Electronics) initially by the U. S. Department of State, International Information Administration; additional support was extended by the Army Signal Corps, the Navy Department (Office of Naval Research) and the Air Force under Signal Corps contract. Further support was extended to the Lincoln Laboratory by the Army, Navy and Air Force under Air Force contract.

[2] Excellent summaries of results of the extensive CRPL program were presented by D. K. Bailey at the Eleventh General Assembly of URSI at The Hague in August, 1954 [8] and at the Physical Society Conference on the Physics of the Ionosphere at Cambridge in September, 1954 [9].

cluding Cornell University, the Radio Physics Laboratories (Ottawa), the F.C.C., radio amateurs, the Bell Telephone Laboratories, R.C.A. (Riverhead), and Air Force Cambridge Research Center.

The early work on 49.8 mc transmissions required time sharing of the radiation directed toward Sterling and Round Hill. Transmissions on a second frequency of 49.6 mc commenced early in 1952. The 49.8 mc frequency was then used primarily for tests by CRPL and the 49.6 mc frequency for tests by Lincoln Laboratory.

Theory indicated that the lower the frequency the greater the received power, all other parameters of the transmission equation remaining constant [2]. Existence of high-power hf transmissions beamed toward Europe from the VOA station at Cincinnati, Ohio afforded an early opportunity for exploratory measurements of signal level characteristics at times when the transmission frequencies exceeded muf for the Cincinnati to Round Hill path. Recordings were made of signals received simultaneously at 15, 17 and 21 mc, on half-wave dipoles.

The signals received on such frequencies were much stronger than those being received from Cedar Rapids on 49.6 mc, upon normalizing the transmission equation parameters. The results were not considered sufficiently precise to determine the exact frequency dependence law because accurate knowledge of the hf transmitting antenna systems was not available and different ionospheric paths were involved.

The potential utility of frequencies much lower than 50 mc toward the region just above muf was attractive. Some short tests were next made on the Cincinnati 21.6 mc transmissions beamed toward Europe. But, a receiving site in Maine was chosen because it was more nearly on beam and the distance approximately 1,000 miles.

At about the same time, high-power transmissions were begun at a frequency near 22.9 mc over a path from Alpine, N.J., to Goose Bay, Labrador. At the latter site, measurements were made over an extended period of signals received on a large 45-degree corner reflector antenna.

Frequency dependence data in the hf-vhf spectrum were desired for the circuits on which the bulk of vhf signal level measurements had been made, namely, Cedar Rapids-to-Sterling and Cedar Rapids-to-Round Hill. A frequency near 27.8 mc was assigned and transmissions were shared between the two paths. At Round Hill, 27.8 mc signal levels were compared with those at 49.6 mc; the two frequencies were transmitted from Cedar Rapids simultaneously on the 2,000 foot rhombic antenna.

In an attempt to determine effective heights of the scattering region and to measure multipath delays, two-way pulse transmission tests were conducted in cooperation with CRPL over the Round Hill-to-Sterling path (387 miles). Later, one-way pulse transmission measurements were made over the Round Hill-to-Cedar Rapids path.

Over 13,000 hours of data have been analyzed on the various frequencies and circuits. In Section II, results are reported of the measurements of signal level characteristics, including instantaneous, diurnal, seasonal, and annual variations. Measurements of external (cosmic) noise for one full year (1952) are given. Polarization and angle dependence studies for shorter periods are described. Also included are the preliminary results of the two-way pulse transmission measurements and of the more recent one-way pulse measurements. The average value of rms particle velocity as determined from several measurements during one day is reported.

In Section III are described the results of the measurements at 27.8 mc including comparison with 49.6 mc signal levels. 22.9 mc signal level characteristics are described in Section IV for the Alpine-to-Goose Bay path (1,059 miles) and for the Alpine-to-Round Hill path (161 miles). Results of signal level recordings at 21.6 mc over the Cincinnati-to-Limestone path (997 miles) are contained in Section V.

The results of the various experiments enumerated above are briefly summarized in Section VI. These results, coupled with those obtained by others, notably CRPL,[2] have materially contributed to knowledge of the new phenomenon and its utilization for reliable point-to-point communications.

II. 49.6 MC Transmissions

Scope of the Program

By far the bulk of results of research to be given in this report concerns transmissions from Cedar Rapids directed toward Round Hill at 49.6 mc. Approximately, 8,300 hours of signal level data have been analyzed since measurements began in December, 1951. Operations were conducted on a 24-hour day, 7-days-per-week basis until the end of January, 1953. During 1953, special modulation tests as well as frequency and space diversity tests were carried out, with no regular signal level measurements being made. In January, 1954, routine level recordings were begun again, but on a 40-hours-per-week basis, continuing until August of that year when hurricanes "Carol" and "Edna" severely damaged the receiving installations at Round Hill. Recordings were resumed in late November. From the reception data, the short- and long-period fading characteristics were determined.

During January, 1952, the switching schedule of the 49.8 mc Cedar Rapids transmissions, alternately directed toward Round Hill and Sterling, permitted some observations of off-path scattering. Some early measurements of cross-polarization were attempted in the spring of 1952 using highly directive antennas and, late in 1954, further measurements were made using less directive antennas. In the winter of 1952, auto-correlation analysis of signal fading yielded values of scattering particle velocity. A technique using oscillographic scatter plots was conceived [3], and investigated for space diversity measurements in June, 1953.[3]

[3] A similar technique was independently investigated by G. Sugar of CRPL for obtaining correlation coefficients between two random variables.

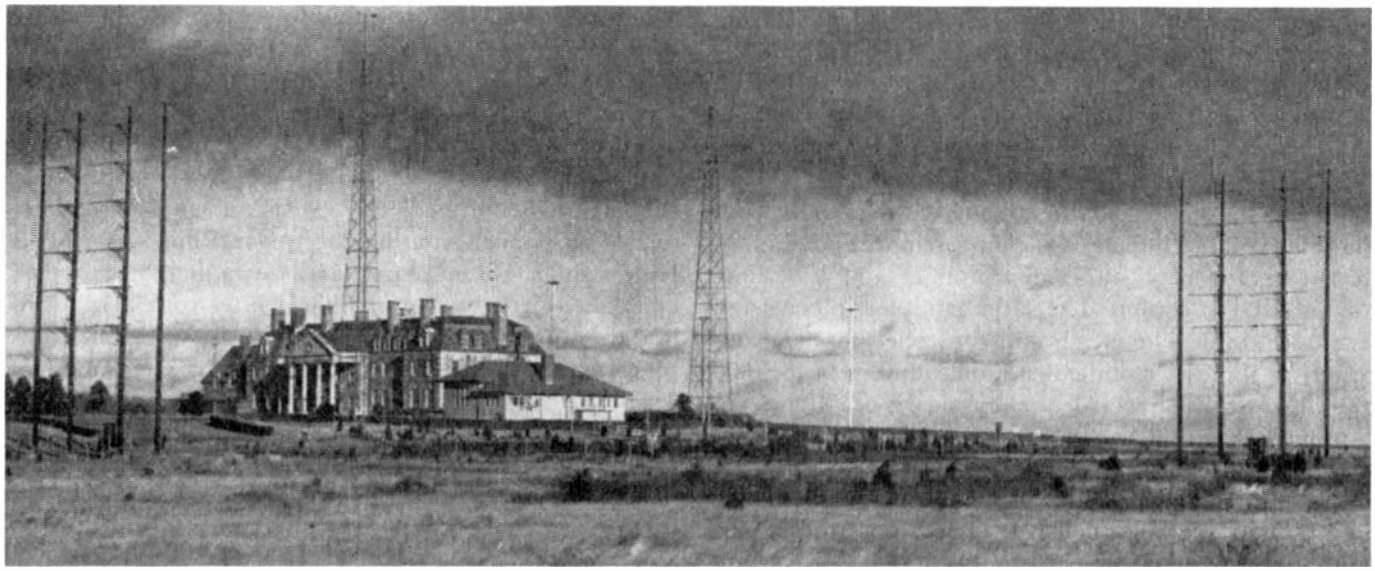

Fig. 1—Round Hill (S. Dartmouth, Mass.) 49.8 mc receiving terminal, December 1951. The above view shows the original horizontally-polarized broadside arrays.

Cosmic noise levels recorded at Round Hill in 1952 were analyzed for magnitude and statistical trends.

In November and December, 1954, two-way pulse transmission tests were initiated between Round Hill and Sterling (387 miles) in an attempt to determine effective transmission height of the ionospheric scattering and multipath delays. In May, 1955, one-way pulse transmissions on a longer path, Round Hill to Cedar Rapids (1,066 miles), were started.

The studies and significant results are described in the following sections.

Experimental Systems for Measuring Signal Level Characteristics

Geometrical parameters of various propagation paths utilizing sites at Cedar Rapids, Sterling, and Round Hill are given in Table I, below.

The original receiving installation at Round Hill is shown in the photograph above taken in December, 1951. Each of the two horizontally-polarized arrays consisted of 12 full-wave, broad-band tubular elements, arranged in four interconnected groups of triplets, and disposed in front of a grid reflecting screen. Parallel feed lines were replaced subsequently by coaxial lines to provide higher electrical and mechanical stability. The measured gain was 13 db (HWSH),[4] the major lobe maximum being at 4 degrees elevation and directed toward Cedar Rapids. The arrays were separated 250 feet laterally and 250 feet longitudinally with respect to the great circle path to Cedar Rapids. Receiving-recording equipment was housed in the small building

[4] The abbreviation (HWSH) is used throughout to indicate the gain of an antenna relative to that of a "half-wave dipole at the same height," and having the same polarization, as the antenna being described.

TABLE I

GEOMETRICAL PARAMETERS OF PROPAGATION PATHS

Transmitter						
Location	Cedar Rapids		Alpine		Cincinnati	Round Hill
Latitude (° N.)	41.91		40.96		39.08	41.54
Longitude (° W.)	91.67		73.92		84.50	70.94
Receiver						
Location	Round Hill	Sterling	Goose Bay	Round Hill	Limestone	Sterling
Latitude (° N.)	41.54	38.99	73.92	41.54	46.95	38.99
Longitude (° W.)	70.94	77.47	60.43	70.93	67.88	77.47
Path Length (stat. mi.)	1,056	773	1,059	161	997	387
Bearings (degrees)						
Of receiver, at transmitter	84.4	100.4	31.9	74.5	51.6	245.0
Of transmitter, at receiver	278.3	289.7	221.8	256.5	243.0	60.8
Vertical Angles (degrees) of arrival or departure, including typical tropospheric refraction; 85 km effective height assumed.	2.2	5.2	2.2	33.0	2.8	13.9
Frequencies (Mcps)	49.6 49.8 27.8	49.8 27.8	22.9	22.9	21.7	49.6

between the radio towers of the early broadcast station WAMF. The large building in the back ground was the summer residence of the late Colonel E. H. R. Green.

The original receiving equipment consisted of a special cascode converter connected to a modified BC-794E receiver which was used as first and second IF stages, the local oscillators being crystal-controlled. The avc voltage indicated signal strength and was recorded by use of a stable dc amplifier and Esterline-Angus chart recorder. The later equipment consisted of a more stable 49.6 mc crystal-controlled cascode converter, a slightly modified Hammarlund type SP-600 crystal-controlled receiver for double IF amplifiers, an improved dc amplifier and an Esterline-Angus chart recorder. Signal level distributions were measured by Gates Radio Company signal level totalizers, the Esterline-Angus recordings being used for monitoring purposes. The Gates totalizers were first modified mechanically (modified Gates) to permit more accurate reading of the counters during sampling periods as short as one minute. The totalizing devices were further improved (Gates-Atomic) to give higher frequency response by changing the Gates amplifier circuitry and replacing the mechanical counters by Atomic Instrument Glow Transfer decade counters.

The transmitting site, originally near the Collins Radio Company hangar at the Cedar Rapids airport, was moved in early 1952 to a location at nearby Konigsmark. The first high power source was an AN/FRT-6 transmitter, modified to operate on 49.8 mc. A second similarly-modified transmitter was supplied later for 49.6 mc transmissions. These modified transmitters were operated at a nominal 50 kw dc power input to the final amplifiers, with about 25 to 30 kw rf input to the antennas.

The transmitting antenna layout in use in October, 1952 at Konigsmark consisted of five directive antennas. Of these, the 2,000-foot horizontal rhombic and shorter vertical half-rhombic antennas were used for 49.6 mc transmissions toward Round Hill; the other antennas were used in tests by CRPL. By July, 1953, the vertical half-rhombic antenna was dismantled and the 2,000-foot rhombic antenna was modified to permit 27.8 as well as 49.6 mc transmissions. The latter antenna had a measured gain of 19.5 db (HWSH), with the major lobe maximum at 3 degrees elevation angle, (49.6 mc). Electrically, it is the longest rhombic antenna used in the experiments, 50 wavelengths on a side.

Signal Level Characteristics Including Instantaneous, Diurnal, Seasonal, and Annual Variations

Most of the signal level measurements were made on cw transmissions, and a nominal receiver IF bandwidth of 3 kc was employed. Data used initially were the calibrated Esterline-Angus recordings, the total signal content on the record being scaled for hourly median values. The records were similar in appearance to those described previously.[2] The distribution curves, from which the median, upper, and lower decile values were determined, were obtained from the modified Gates or improved Gates-Atomic totalizer.

The Booker-Gordon scattering theory [1, 2] and the more recent one of Villars and Weisskopf [4] lead to the conclusion that the short-term fading should have a Rayleigh distribution [3, 5]. Measurements were made to test this conclusion, on the Cedar Rapids-to-Round Hill path in December, 1953, the fading distribution being measured by the modified Gates totalizers. One-minute samples gave consistent results, when the samples were free of strong enhancements due to meteoric or sporadic-*E* reflections. Typical results of several runs are given in the literature [5] and show the *instantaneous fading* to have a Rayleigh distribution.

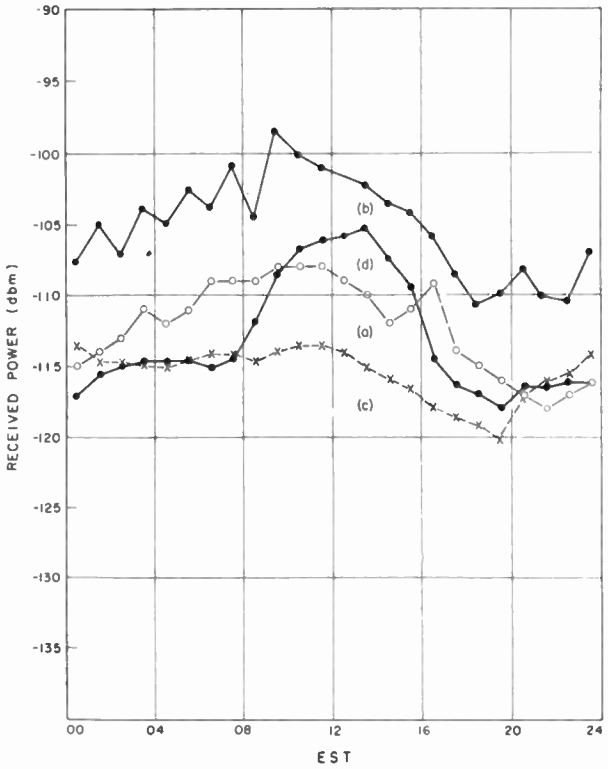

Fig. 2—Diurnal variation of hourly median signal level, 49.6 mc, in 1952, on Cedar Rapids-to-Round Hill path, for the months of April (a), June (b), September (c), and December (d).

The *diurnal variation* of the hourly median signal level shows a maximum in midday, and a minimum in the evening. Curves depicting this variation are shown in Fig. 2[5] for April, June, September, and December, in 1952. Maximum levels are seen to be generally higher in winter and summer than in spring and fall. The diurnal variation on the Cedar Rapids-to-Round Hill path also appears to be less marked than on the shorter Cedar Rapids-to-Sterling path [8].

[5] Signal levels are given in decibels relative to 1 milliwatt (dbm). A signal level of −120 dbm corresponds to a level of 110 db below the "specular-reflection received power, P_s." The power, P_s, is defined as that which would be received assuming a perfectly reflecting layer at 85 km height, perfect earth reflection, typical tropospheric refraction, and appropriate antenna gain functions.

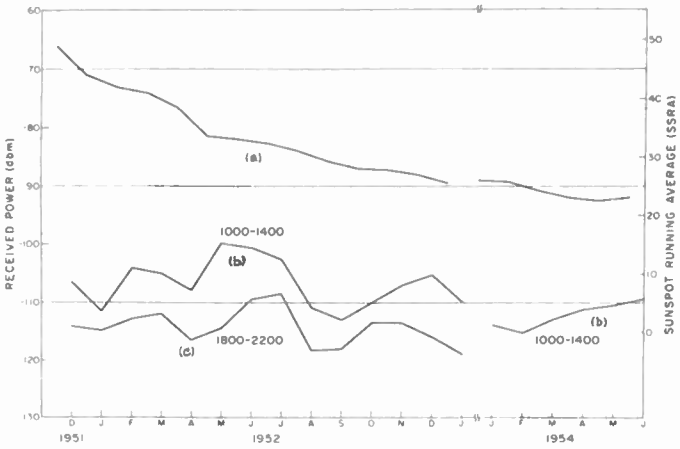

Fig. 3—Seasonal variation of hourly median signal level, (b) 1000–1400 EST and (c) 1500–2200 EST, 49.6 mc, on Cedar Rapids-to-Round Hill path, for December, 1951 to January, 1953 and January to June, 1954, together with running average of sunspot numbers, SSRA, in curve (a).

The *seasonal trend* of hourly median signal levels is also shown in Fig. 3. Shown plotted are the median values of the level for each month, for the periods of the maximum (1000–1400 EST) and minimum (1800–2200 EST) signal level, over the 26-month interval of December, 1951 through January, 1953, and for the period of maximum signal only for the months of January through June, 1954. The sunspot running average (SSRA) is also shown for the same months. These curves again show that median signal levels reach a maximum during the winter and summer months and a minimum during the fall and spring months. Comparison of median levels for 1952 with those for the same months during 1954 shows also a *yearly variation* which appears to depend on sunspot activity, lower signal levels occurring during the time of low sunspot numbers.

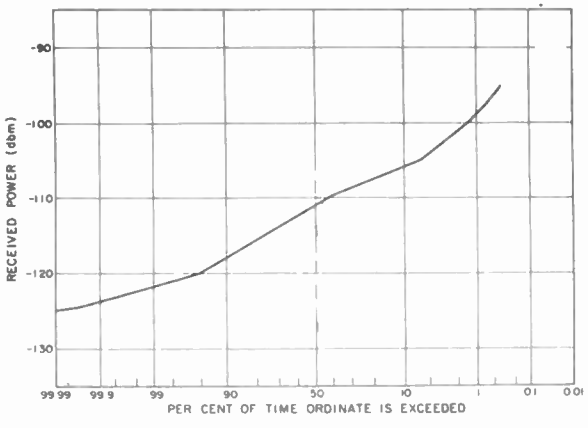

Fig. 4—Distribution of signal levels obtained on 49.6 mc over the Cedar Rapids-to-Round Hill path, 1502–1530 EST, July 23, 1954, obtained using time-totalizing equipment.

Distributions of signal fading with the half-hour or hour were also determined, using the improved time-totalizing equipment. A sample distribution of signal levels taken on July 23, 1954, from 1502 until 1530 EST, is given in Fig. 4. This curve, plotted on normal probability paper, shows the percentage of time each level is exceeded. Distributions of signal levels are essentially Gaussian for such periods, though they often show the effects of high noise and sporadic E propagation.

External Noise Measurements

HF and vhf transmissions were interrupted for a period of approximately two minutes every half-hour to permit measurement of the external noise level at the receiving site. For the most part, received noise is considered to be of cosmic origin though, infrequently at hf, atmospheric noise was also received. At times, too, high local noise raised the recorded level of both received noise and signal. High levels of local and atmospheric noise can be separated from cosmic noise.

From the noise levels measured during each hour of a given month, the average value of noise level was obtained. These average values, as determined for each month of 1952, are plotted as dots in Fig. 5. The solid curve is the median of the monthly average values. The 0600 peak coincides with the location of discrete noise sources in Taurus and that at 1700 with similar but weaker sources near Ophiuchus, when taking into account the declination of the area swept out on the celestial sphere by the antenna beam.

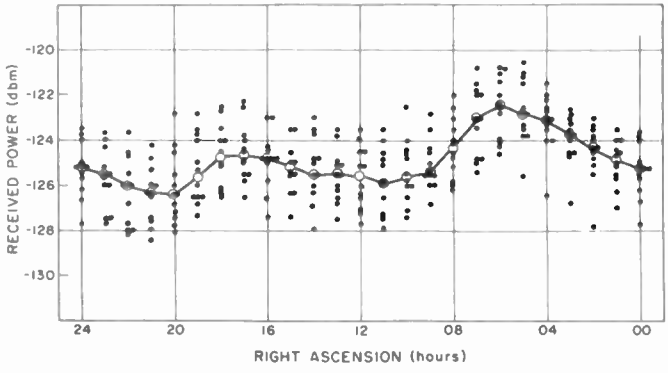

Fig. 5—Hourly median values of noise level recorded at Round Hill on 49.6 mc vs right ascension for the months January through December, 1952, together with the hourly median values for the year.

Cross-Polarization Studies

Late in 1954, two identical 5-element Yagi antennas, one polarized horizontally and the other vertically, were constructed and set up at Round Hill in order to measure the cross-polarized components of signals from Cedar Rapids. The antennas were located 90 feet above ground to provide a maximum of the first lobe at approximately 3 degrees elevation. Spacing between the two antennas was 32 feet normal to the great circle path to Cedar Rapids. Measured gains were 8 db (HWSH) for the horizontal Yagi and 7.5 db (HWSH) for the vertical Yagi. Receiving equipment comprised a dual-channel crystal-controlled converter, two Hammarlund SP-600 receivers, dc amplifiers, and Esterline-Angus chart recorders. The two receivers were modified to accommodate a common crystal-controlled local oscillator. Their IF sections were also adjusted to have the same center frequency and band-pass characteristics at 200, 400, and 700 cycles bandwidth. During these studies, a bandwidth of 700 cycles was used.

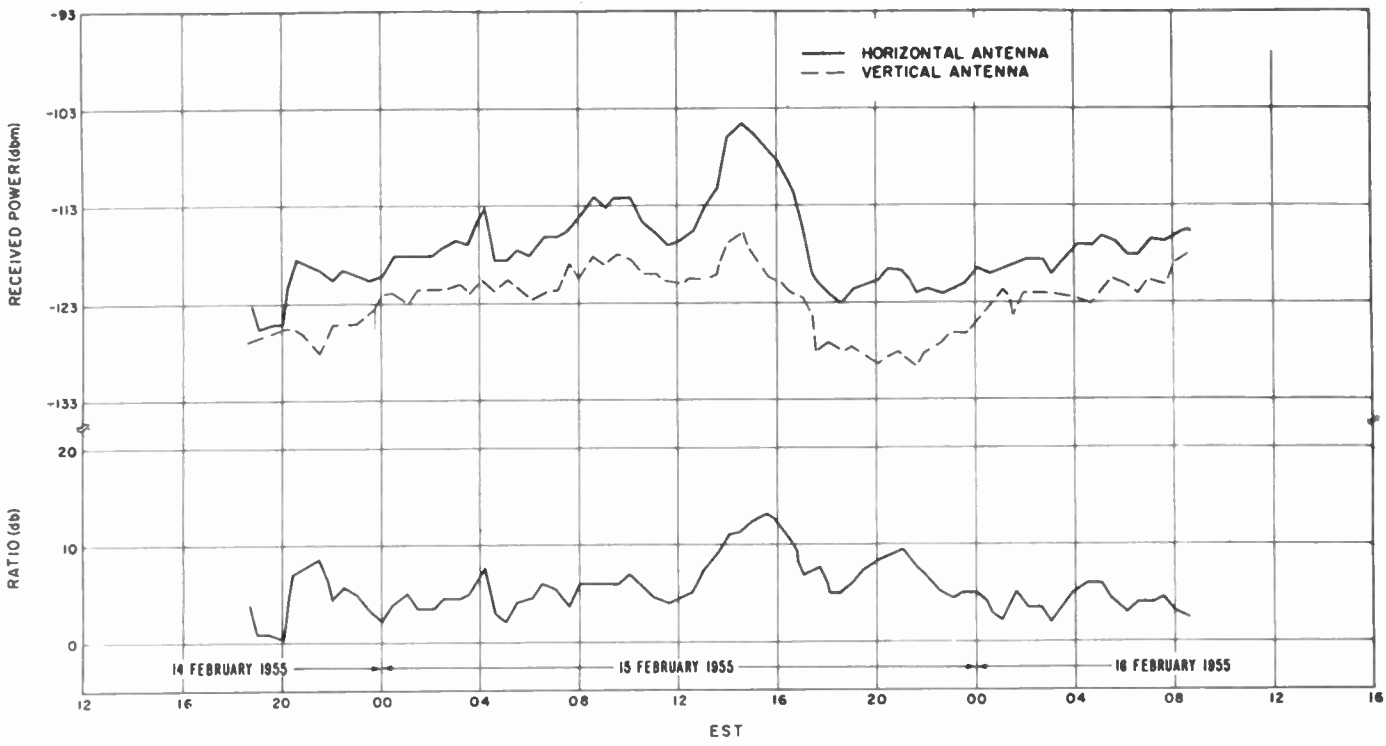

Fig. 6—Hourly median values of signal levels received on cross-polarized Yagi antennas at Round Hill of 49.6 mc transmissions from Cedar Rapids, and the ratio of the horizontally-polarized to the vertically-polarized hourly median levels, February 14 to 17, 1955.

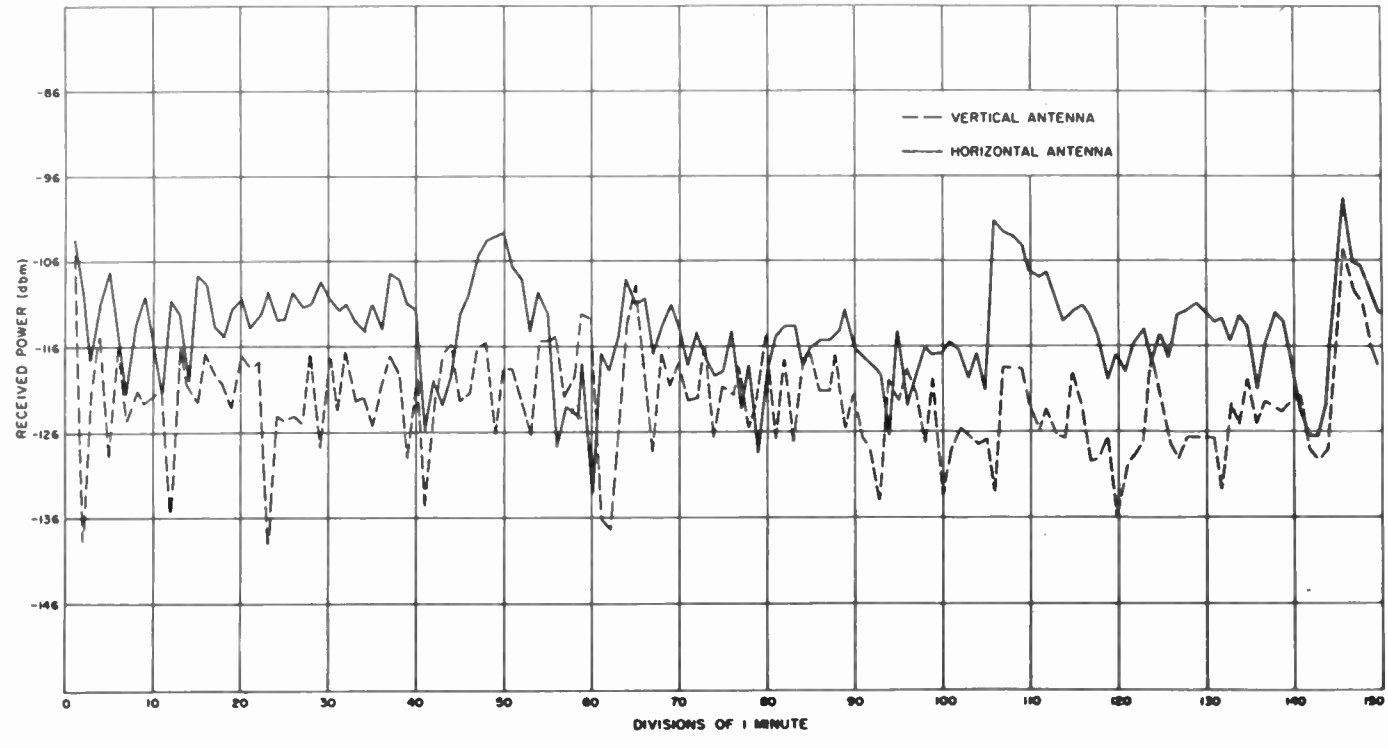

Fig. 7—Variation of instantaneous values of signal levels received on cross-polarized Yagi antennas at Round Hill of 49.6 mc transmissions from Cedar Rapids during a one-minute period.

Measurements were ordinarily made over a continuous 48-hour period once each week. Median values of signal level obtained with each of the two cross-polarized Yagi antennas, during half-hour intervals, are given in Fig. 6 for the period February 14 to 17. The ratio of the horizontal to vertical levels is also shown. The figure further shows that, in general, median values of the cross-polarized components of signal varied together and that, on an average, the ratio of the two levels was some 6 db. During periods of high signal level, the ratio tended to be higher than during periods of low signal level.

To determine the correlation of the amplitudes of the fading signals received on the two antennas, data were obtained using Brush fast-speed recorders at a chart speed of 25 mm. Fig. 7 shows the variation of instan-

taneous signal levels during a period of about one minute. The correlation is apparently poor and the computed correlation coeff cient is less than 0.1.

The low correlation found between these instantaneous values of signals indicated the possibility of polarization diversity but the results of these tests are not considered completely conclusive. It is felt that simultaneous transmission with horizontally- and vertically-polarized broad-beam antennas such as Yagis and reception with the same type of antennas is required for more conclusive evidence.

Off-Path Study at 49.8 MC

During January, 1952, when transmissions from Cedar Rapids on 49.8 mc were beamed during alternate half-hour periods toward Sterling and toward Round Hill, recordings of resulting signal level were made continuously at Round Hill. It was desired to determine whether the measurements of received power together with a knowledge of relative antenna characteristics would suffice to ascertain the origin of the signals received at Round Hill when the transmissions at Cedar Rapids were directed toward Sterling.

The basic geometry of the propagation paths is given in Table I. Additionally, the midpoint of the Cedar Rapids-to-Sterling path is 622 miles from Round Hill. At Cedar Rapids, the bearing of Round Hill is 16 degrees more northerly than that of Sterling. At Round Hill, the bearing of the Cedar Rapids-to-Sterling midpoint is 10.1 degrees more southerly than that of Cedar Rapids.

Data were obtained for the period January 1 to 16, 1952. The diurnal variations of hourly median signal levels are shown in the curves of Fig. 8. The levels recorded at Round Hill are given in curves (b) and (c), the former when transmissions are beamed from Cedar Rapids toward Round Hill, and the latter for transmissions beamed toward Sterling. Curve (a) shows the levels recorded at Sterling when transmissions are beamed toward that site.[6]

Comparisons of the levels in the curves of Fig. 8 will be based upon an effective height of 85 km of the scattering region and typical tropospheric refraction. At Cedar Rapids, the 2,000-foot rhombic antenna directed toward Round Hill had a measured on-beam gain (G_1) of 18 db (HWSH), at the 2.2 degree reference vertical angle. The 1,000-foot horizontal rhombic antenna had a measured on-beam gain (G_2) of 15 db (HWSH), at the 5.2 degree reference vertical angle; a similar antenna was employed for reception at Sterling, with similar gain (G_3). At Round Hill, the West Broadside receiving array had a measured gain (G_4) of 11 db (HWSH), at a reference 2.2-degree vertical angle.

We shall make the simplifying assumption that received power varies directly as the product of transmitting and receiving antenna gains, and inversely as the square of transmission distance. Comparing the "direct path" signals in curves (a) and (b), the antenna gain product appropriate to curve (a) is G_2G_3 or 30 db (HWSH), while that for curve (b) is G_1G_4 or 29 db (HWSH). Allowing for the different transmission distances (2.8 db), then the levels of curve (a) should be higher than those of curve (b) by about 4 db. It is seen that curve (b) is lower than curve (a), but the ratio varies diurnally, being about 14 to 15 db in the midday strong signal periods, and about 2 to 4 db during the periods of weak signals. Particularly during strong signal periods, when antenna gains are more nearly realized [8], the simplifying assumption for explaining the relative levels is inadequate. In weak signal periods, plane wave antenna gains are not realized [8], and the amount of the deterioration is unknown here. It appears that an adequate explanation must consider angular scattering effects and the relation of dissimilar antenna beams to the scattering polar diagram of the scattering medium.[3]

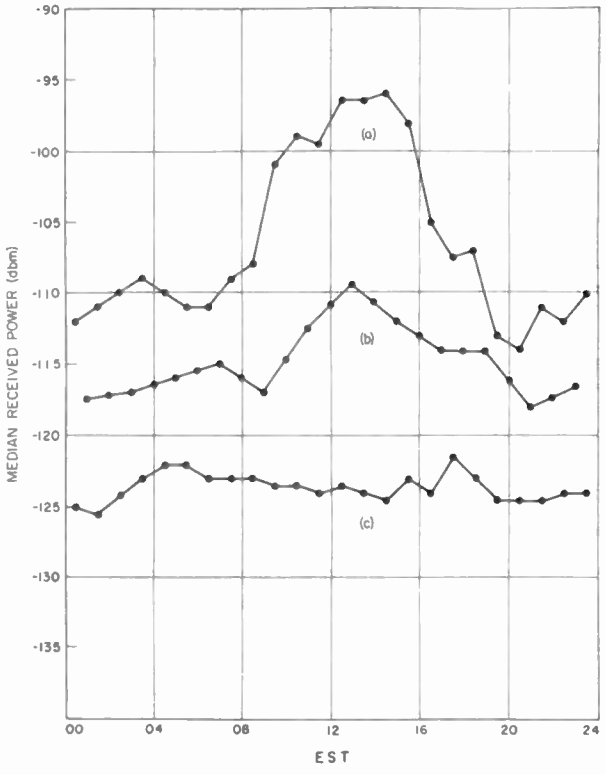

Fig. 8—Comparison of direct and off-path signal levels (half-hour median values, 49.8 mc, January 1 to 16, 1952). Curves (a) and (b) are direct path levels recorded at Sterling and Round Hill respectively. Curve (c) is the off-path level recorded at Round Hill when transmissions are directed toward Sterling, with Cedar Rapids transmitting.

The "off-path" levels in curve (c) are weaker and exhibit much less diurnal variation than those of the "direct-path" levels in curve (b). One might be tempted to speculate that curve (c) is due to propagation other than direct from Cedar Rapids due to off-beam radiation from the transmitting antenna. Estimates of the effective power and polarization radiated are suspect

[6] Curve (a) was based upon tabulated data supplied by R. C. Kirby of CRPL whose assistance is acknowledged. The CRPL data were given in terms of open-circuit antenna voltage; these values were then converted into received power.

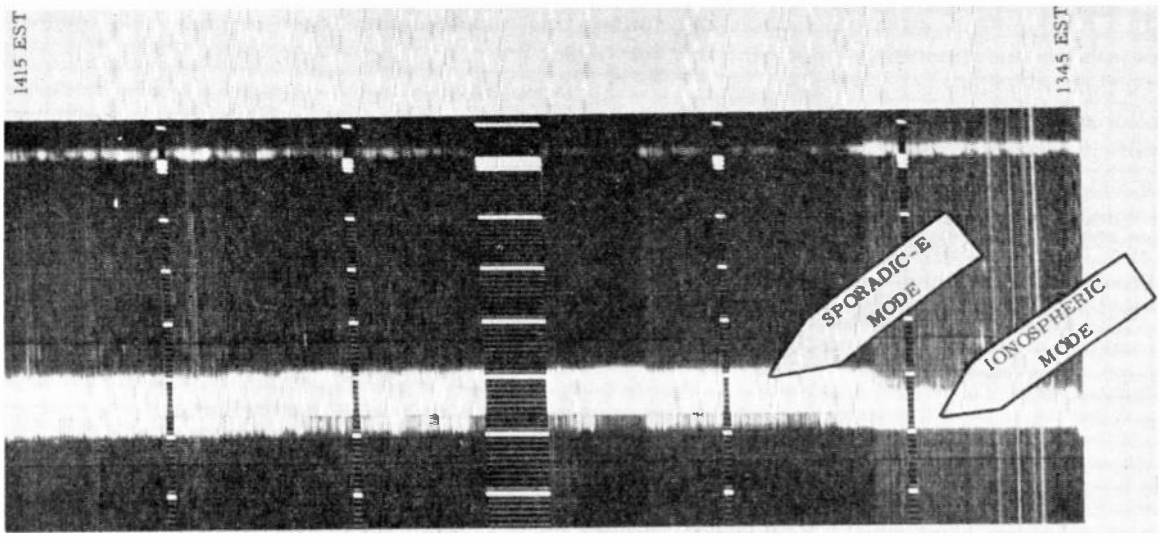

Fig. 9—Photograph of Round Hill signals on 49.6 mc recorded at Cedar Rapids on intensity modulated sweep, 1345–1415 EST June 10, 1955.

for radiation so far off-beam in the region of the rhombic side-lobes. If the level in curve (c) were due to scattering at the Cedar Rapids-to-Sterling midpoint, the value of receiving antenna gain to use for the Round Hill antenna is likewise subject to error, since the vertical angle is so low and radiation would be arriving so far off in azimuth. For these reasons and others such as aforementioned pertaining to the direct-path signal comparisons, a suitable explanation for the observed levels in curve (c) is not completely understood and further studies are desired.

It is believed that more suitable off-path measurements can be made now that the high-power pulse transmitter is available. Pulse transmission techniques will assist identification and measurements of intensity of the propagation modes.

Pulse Transmission Experiments

To obtain measurements of effective "scattering" layer heights and of multipath delays, and to determine the several transmission modes, two-way pulse transmissions were made over a short path (Round Hill-to-Sterling) and one-way pulse transmissions, over a long path (Round Hill-to-Cedar Rapids). The geometry of these paths is given in Table I.

The pulse transmitter at Round Hill, used for transmissions toward both Sterling and Cedar Rapids, has a nominal peak power of 500 kw at $8\frac{1}{3}$ per cent duty cycle. For these tests, however, the peak power output was approximately 300 kw, using a repetition frequency of 50 pulses per second and pulse widths of 20 to 100 μsec.

For the two-way tests, two small horizontal rhombic antennas at a height of 20 feet were used at Round Hill, one for transmission (11.4 db gain HWSH, vertical lobe at 14 degrees) and the other for reception (12.2 db gain HWSH, vertical lobe at 13 degrees). Similar antennas were used by CRPL at Sterling. At Round Hill, a small Yagi at a higher height was also employed, at times, to enhance the observed tropospheric pulse signals.

The receiving, timing, and recording equipment, used at Round Hill for the two-way test and at Cedar Rapids for the one-way tests, are identical. The pulse receivers were developed for the Laboratory by Collins Radio Company. The timing and indicating equipment consisted of a Western Electric Company 100 kc crystal oscillator, a modified Navy type UJ-1 Loran timer-indicator, and a special oscilloscope for displaying the received pulse signals on an intensity-modulated trace. The received pulses were photographed on continuously moving 35 mm film.

Two-way pulse transmission tests were made during December, 1954.[7] Tropospheric, ionospheric "scatter," and meteoric modes were identified. Effective ionospheric "scatter" heights were found to be 84–88 km during the daytime and 89–94 km during the night. An abrupt decrease in height was noted between 0500 and 0800 EST.[8]

One-way pulse transmissions, Round Hill to Cedar Rapids, were commenced in late May, 1955. During the day, a 20 microsecond pulse width and 100 kc receiver band pass were used; during the night, a 100 μsec pulse width and 10 kc bandpass.

Ordinarily, a steady signal component is received via an ionospheric "scatter" mode, and intermittent signals via reflections from ionized meteor trails. The latter usually have a duration of only a few seconds, though, at times, they may last for as long as a minute or so. No tropospheric mode was identified. On several occasions, during both day and night, signals were received via a third mode believed due to sporadic E reflection. Fig. 9 is an enlargement of a photographic recording

[7] The cooperation of CRPL and especially of V. C. Pineo in this two-way pulse test is gratefully acknowledged.

[8] A much more detailed report of the two-way pulse tests and results is in preparation.

made at Cedar Rapids of the received pulse signals showing the three propagation modes. The oscilloscope sweep, shown vertically in the figure, was 800 μsec long. The transmitted pulse was 40 μsec wide.

Up to 1351 EST, only one steady weak trace (ionospheric mode) was present. At about this time, however, a much stronger signal (several thousand μv, 50 ohms) having a delay of 30 to 40 μsec with respect to the first arriving pulse appeared and continued for almost half an hour. Inspection of 27.8 mc records, Cedar Rapids-to-Round Hill, showed the presence of strong sporadic *E* during the time of the very strong pulse signals on 49.6 mc. Assuming a height of 110 km for sporadic *E*, the equivalent scattering height of the ionospheric mode is computed to be approximately 85 km.

The trace at the top of the figure is a spurious signal produced by leakage from the sweep generator counter chain. The two thin horizontal lines bracketing the pulse signals mark a pulse gate used in signal intensity recording. Weakening of background noise and of the ionospheric pulse is due to the avc action of the receiver during the presence of the strong sporadic *E* signal.

The simultaneous existence of the strong sporadic *E* and the weaker ionospheric "scatter" modes suggests that the relative delay between these two modes, as determined from one-way pulse transmission measurements, may be used to obtain effective ionospheric "scatter" height. Additionally, for useful transmission bandwidth, the observed relative delay indicates reduction in bandwidth over that when either mode is present.

Auto-correlation Studies—Determination of Velocity of Scattering Particles[9]

Auto-correlation studies were made in 1952 on the 49.6 mc signals received at Round Hill from Cedar Rapids. It was the object of the studies to obtain some of the statistical properties of the signal and some information on the parameters of scattering.

The signal amplitudes were recorded on magnetic tape, analysis being performed with various correlators, such as the MIT Digital Electronic Correlator and the MIT Servomechanisms Mechanical Correlator (using Brush paper tape recordings). The details of the devices as used are given elsewhere [3].

Four-minute data samples were taken at five different times from 1100 to 1600 EST on December 4, 1952, and an auto-correlation function was obtained for each data sample. From the five individual auto-correlation curves an average auto-correlation function was obtained for the five-hour period. By matching several possible theoretical auto-correlation curves to the average experimental curve, the average rms velocity of the scattering particles was determined to be between 6 and 7 meters per second for this five-hour period.

[9] This work was based upon a doctoral research by A. J. Lephakis, E.E. Department, M.I.T., 1953.

Space-Diversity Correlation Coefficients from Oscillographic Scatter Plots

A knowledge of the correlation between the fading of signals received on spaced antennas is desirable for application in the design of communication systems using diversity, and for obtaining information on useful sizes of antenna apertures.

A technique was employed which is simple to use for indicating approximately the order of correlation between two randomly-fading voltages such as the avc voltages from the two receivers connected to two space-diversity antennas [3]. More accurate results can be obtained by more lengthy analytical procedures, or by using more complicted correlator devices.

Licklider and Dzendolet [10] have shown how to use an oscilloscope to obtain a scatter plot to determine what, if any, correlation exists between two sets of random functions.[10] One varying voltage is applied to the *X* axis and the other to the *Y* axis deflection plates. The spot moves about under the influence of both voltages. A group of dots appears if the spot intensity beam is pulse modulated at the desired rate. A camera using time exposure is used to photograph the scatter diagram of the dots, each dot representing a sample.

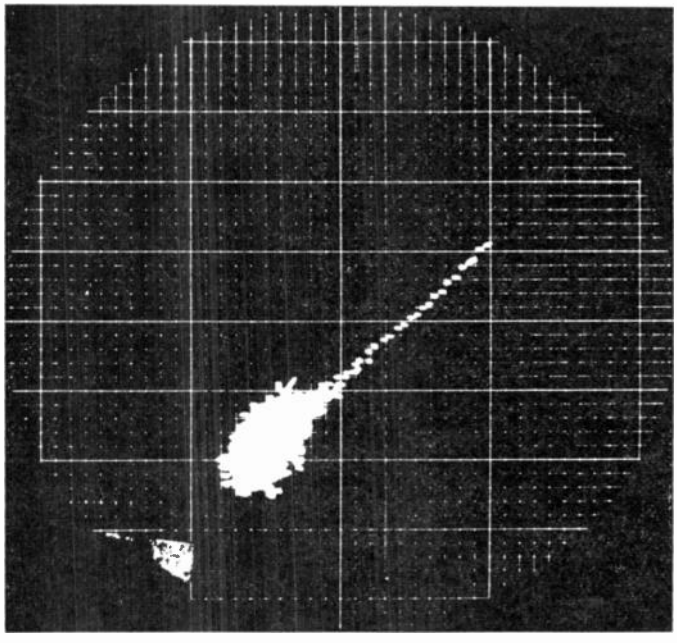

Fig. 10—Typical amplitude scatter plot using spaced antennas—49.6 mc, Round Hill broadside arrays, June 9, 1953.

An example of the scatter plots obtained is shown in the photograph of Fig. 10, and pertains to measurements on the two Round Hill broadside arrays. The photograph was obtained on June 9, 1953, at midday, for 49.6 signals from Cedar Rapids. The sampling rate was 10/s (200 μsec sampling pulse width) and the exposure was 5 minutes, giving about 3,000 dots. Twin-channel, crystal-controlled receivers were employed,

[10] G. Sugar, *loc. cit.*

each channel connected to one broadside array. Over-all adjustments were made such that if the antenna voltages were perfectly correlated, a line of dots at 45 degrees to the axis would be obtained. If the voltages on the scope axes are normally distributed, an elliptical dot outline is obtained, the major axis of which is tilted at 45 degrees and the axial ratio of which determines the correlation coefficient [3].

In the photograph, a "tad-pole" shape of dots is noted. The "tail" is believed due to a meteoric enhancement lasting 2.7 seconds, the two antenna voltages being very highly correlated. In the "body," the average signal-to-noise ratio was about 15 db. The contour of the dots was approximately elliptical and gave an estimated correlation coefficient of 0.6.

There are sources of error such that the technique cannot be used for high accuracy. One source of error is that of assuming the voltages on the antennas are normally distributed when their fading may be Rayleigh distributed. Another source is that the oscilloscope voltages are not linearly proportional to rf signal amplitude, but this can be overcome by replotting the photographic figure. The results will, however, give a rough picture of signal correlation behavior. When the "ellipses" are very thin, the correlation is high; when they are "fat" the correlation is poor.

III. 27.8 Mc Transmissions

Description of Tests and Equipment

Transmissions on 27.8 mc from Cedar Rapids-to-Round Hill were begun in late May, 1953 on a time sharing basis, with transmissions from Cedar Rapids to Sterling on the same frequency. However, data taken prior to November, 1953, were not considered reliable because of the unknown and changing character of radiation from the Cedar Rapids antenna system, and are disregarded.

The geometry of the Cedar Rapids-to-Round Hill circuit for 27.8 mc is given in Table I.

The transmitter at Cedar Rapids was a Collins type 734-A fm transmitter modified for operation at 27.8 mc. The antenna was the single-wire horizontal rhombic used for 49.6 mc transmissions. This antenna was diplexed to permit simultaneous transmission on the two frequencies. The measured gain of the antenna at 27.8 mc was 15.4 db (HWSH), at 6 degrees elevation. At 2.3 degrees, the gain was down about 2 db.

After June, 1954, receiving equipment at Round Hill consisted of a 27.8 mc converter, Hallicrafter SX-73 receiver as IF, a dc amplifier, and an Esterline-Angus chart recorder. Prior to that time, the SX-73 receiver was used without a converter. The antenna was a five-element horizontal Yagi located at a height of 122 feet. The gain of this antenna was measured as 8.5 db (HWSH) at 3.5 degrees elevation. At 2.3 degrees, the gain was approximately 8 db. The calibrated avc output of the receiver was recorded as a measure of signal level variations. After installation of the converter in late June, time totalizing equipment, consisting of a Gates Radio Company amplifier and mechanical counter, was used to obtain signal level distributions. This equipment recorded, essentially, the percentage of time each of ten preset signal levels was exceeded.

Signal Level Characteristics

The fading characteristics of the signals received at Round Hill on 27.8 mc are similar to those on 49.6 mc. Median values of signal level were obtained for each hour for the months of November, 1953 through June, 1954 from Esterline-Angus recordings. The variations of the median values exceeding 10 per cent, 50 per cent and 90 per cent of the time were also determined.

Distributions of the signal levels recorded during half-hour periods were determined from time-totalizing data. Resulting curves showed distribution to be essentially Gaussian, with sporadic E and meteoric propagation increasing the curve slope at higher signal levels.

The levels of signals exceeding 10 per cent, 50 per cent and 90 per cent of the time were obtained for the months July through December, 1954, except for the month of November, for which no reliable data were available.

Distributions of the hourly median levels for the midday period (1000–1400) were determined for the months November, 1953 through December, 1954, except for November, 1954. The distributions of these median values tend to be Gaussian, though at times sporadic E propagation increased the slope of the curves at the higher signal levels.

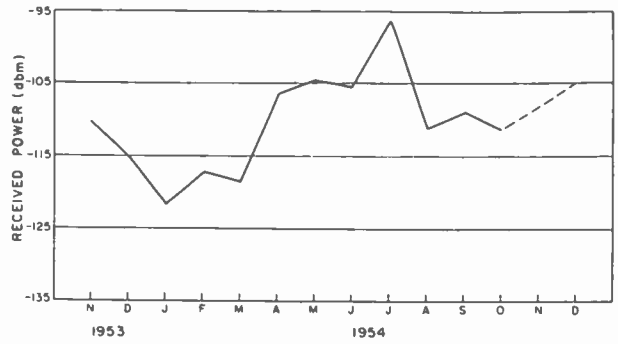

Fig. 11—Seasonal variation of hourly median signal levels, 1000–1400 EST, 27.8 mc, on Cedar Rapids-to-Round Hill path, for November, 1953 to December, 1954.

The seasonal trend of midday median values of received signal level is given in Fig. 11. Generally, this curve shows that signals on this frequency are higher in the winter and summer months, and lower in the spring and fall, as was previously observed for 49.6 mc.

A more detailed account of results obtained on this frequency is given elsewhere [3].

Comparison of 27.8 Mcps with 49.6 Mcps Levels for Constant Aperture Transmitting Antenna

Simultaneous recordings of signal levels on 27.8 and 49.6 mc were made in February and March, 1955 on a two-day (48 hours) per week basis, using broad beam

(Yagi) antennas at about the same height. Useful data were obtained for about 10 days. The half-hour median values of signal level were scaled for each frequency. The received powers were normalized, taking into account the transmission line losses at the transmitter and at the receiver, and the transmitter power levels for the two frequencies.

The ratios of normalized received power (ratio of power received at 27.8 mc to that at 49.6 mc) were determined and 361 points plotted as a histogram and on probability paper. It was at once evident that the exponent of frequency is not constant. Assuming P_R varies as f^{-n} where f is the frequency, it was found that values of the exponent n were normally distributed, and that the most probable value is between 3 and 4.[11]

The ratios of received power (in db) on 27.8 mc to those on 49.6 mc were plotted vs the power received on 49.6 mc. The results are shown in the scatter plot of Fig. 12. It is seen the ratios (in db), and thus the exponent n, decrease relative to the 49.6 mc level.

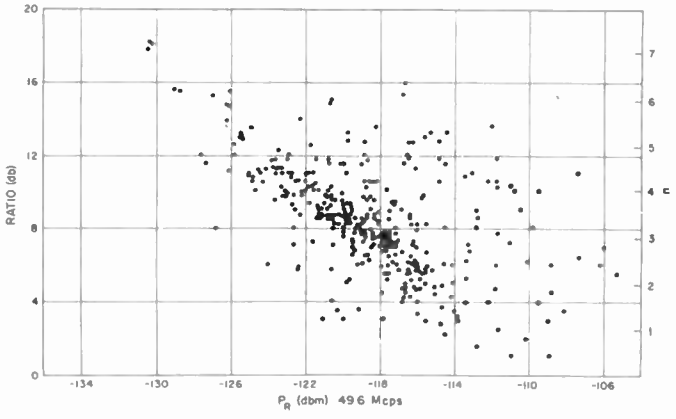

Fig. 12—Scatter diagram of the ratio of received power on 27.8 mc to received power on 49.6 mc plotted vs 49.6 mc received power. The quantity n is the frequency exponent where $P_R \propto f^{-n}$.

The correlation coefficient of the points in Fig. 12 was computed to be about 0.6, indicating reasonably good correlation of power ratio (or n) with the 49.6 mc signal levels.

IV. 22.9 Mc Transmissions

Description of Tests and Equipment

With earlier theoretical and experimental indications of the advantages of using frequencies lower than 50 mc for increased signal-to-noise ratio, it was decided to set up a circuit from Alpine, New Jersey, to Goose Bay, Labrador, for operation at frequencies below 30 mc. Transmissions over this circuit were begun on a frequency of 22.9 mc in November, 1952 and continued through September, 1953. Initially, operation was scheduled for 8 hours per day, 5 days per week. From February until September, 1953, a 24-hour-day schedule was added twice per month.

In June, 1953, radiations from Alpine directed toward Goose Bay were detected off-path at Round Hill, when transmitting from the Yagi antenna array. Later, special tests were conducted to determine the mode of propagation for this shorter path.

The geometries of the Alpine-to-Goose Bay and Alpine-to-Round Hill paths are given in Table I.

The transmitter, a modified commercial fm transmitter, was operated at a nominal average power of 8 kw into the antenna. For signal level recordings, a cw signal was transmitted; however, for several modulation tests, the signal was frequency modulated using narrow deviations. From November, 1952 until June of the following year, the transmitting antenna was a horizontal rhombic having a measured gain of 11 db (HWSH), with the maximum of the first lobe at 8 degrees elevation. Because of the low gain of this antenna at low angles, a dual stacked 5-element Yagi antenna was installed at a height of 240 feet above ground on an existing 400-foot tower at Alpine, and used from June until the end of the program. The gain of this antenna was measured at 6 db (HWSH) at 2.2 degrees elevation.

The receiving antenna at Goose Bay, a 45-degree horizontal corner reflector with four colinear half-wave dipoles, was located at the edge of a 100-foot cliff overlooking a broad plain. The computed gain of this antenna was 20 db (HWSH) at approximately 4 degrees elevation. The receiving equipment included a dual complement of a Hammarlund SP-600 receiver, dc amplifier, and an Esterline-Angus chart recorder. The amplified avc output of the receiver was recorded as a measure of signal level.

Signal Level Characteristics

From the Esterline-Angus charts, the hourly median values of signal and noise level were obtained for each day. From these values, the median signal levels exceeding 10 per cent, 50 per cent and 90 per cent of the hour were determined for each month. Variations of median signal and noise level for the months November, 1952 through September, 1953 were then obtained [3]. Because only two days of 24-hour data were obtained each month, it was not possible to determine the complete diurnal characteristics of the signal with any degree of assurance. The available data indicated a maximum level near midday and a low level in the early evening. The presence of sporadic E propagation, especially during the summer months, often caused departure from this general trend. At times, during the winter, regular F layer transmissions also occurred for short periods of some days.

Distribution of median signal levels for the midday period (1000–1400), as obtained for each month, was found to be essentially Gaussian, though, at times,

[11] These values are lower than those obtained by CRPL and reported by Bailey.[8] The CRPL values for n, between 5 and 6, apply to a comparison of 49.8 and 24.3 mc (roughly the same frequency range), for an Alaskan circuit, in June, 1953. More important perhaps is that the CRPL results are based upon constant directivity antennas (i.e., scaled T and R rhombics), whereas results reported here were obtained using the same rhombic transmitting antenna (approximately constant aperture) at two frequencies.

sporadic E propagation changed the slope at the high signal levels [3].

As a brief summary, the seasonal trend of median signal levels for the midday period is given in Fig. 13. Even though a complete year of data was not taken, this curve shows that maximum signal levels tend to occur during summer and winter months, and minimum signals, during the fall and spring.

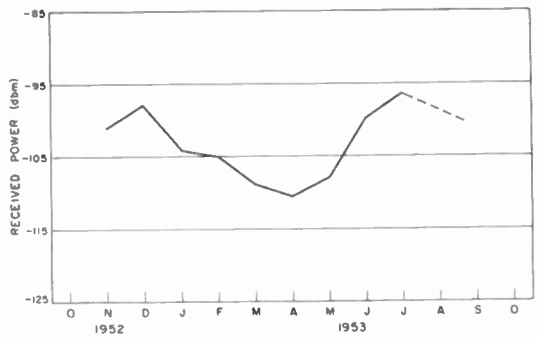

Fig. 13—Seasonal variation of hourly median signal levels, 1000–1400 EST, 22.9 mc on Alpine-to-Goose Bay path, for November, 1952 to September, 1953.

Tone and voice modulation using very narrow band fm (deviations up to ± 5 kc) were transmitted from Alpine on several occasions and tape recordings were made at Goose Bay. However, because of the high level of man-made noise at Goose Bay, it was not possible to evaluate the quality of the received modulation, which was generally low, in terms of circuit parameters alone.

Measurements to Determine Transmission Mode (ionospheric or tropospheric) Alpine-to-Round Hill

When recordings were first made of the Alpine signals received off-path at Round Hill, the question arose as to whether the signals were propagated via the troposphere or ionosphere. Ionospheric modes which were thought plausible (excluding meteors) were those associated with hf ground backscatter at, and beyond, skip distance from Alpine.

Upon termination of the transmissions toward Goose Bay in September, 1953, the dual-stacked 5-element horizontal Yagi antenna at Alpine was turned and beamed toward Round Hill. At Round Hill, signals were received simultaneously on a 5-element horizontal Yagi antenna directed on-path toward Alpine, and on a 3-element horizontal Yagi antenna directed seaward 180 degrees to the direction of Alpine. Both antennas were located approximately 90 feet above the reflecting plane. The forward gain of the 3-element Yagi over the back lobe of the 5-element was approximately 10 db [3].

Because of the greater gain of the seaward antenna (3-element Yagi) in a direction toward Europe, it was expected that, if signals were arriving at Round Hill as energy backscattered from the Atlantic Ocean, the signals received on the seaward antenna would be stronger than those received on the on-path antenna. Recordings of signals received on the two antennas were made over a period of several weeks, and, while there was some variation in the ratio of the two signal levels, at no time did levels recorded on the seaward antenna equal or exceed those received on the on-path antenna. From this it was concluded that the 22.9 mc signals received at Round Hill from Alpine were not due to backscatter ionospherically propagated. Median levels of signals received on the two antennas during the period June 28 to 30, 1954, and the ratio of the two levels, are shown in Fig. 14.

Also, height-gain measurements made at Round Hill, and at the path mid-point (details are described elsewhere [3]), produced height-gain curves typical of signals scattered tropospherically beyond the ratio horizon.

From the results of these two experiments, it was concluded that the transmission mode of the 22.9 mc propagation from Alpine to Round Hill was tropospheric and not ionospheric.

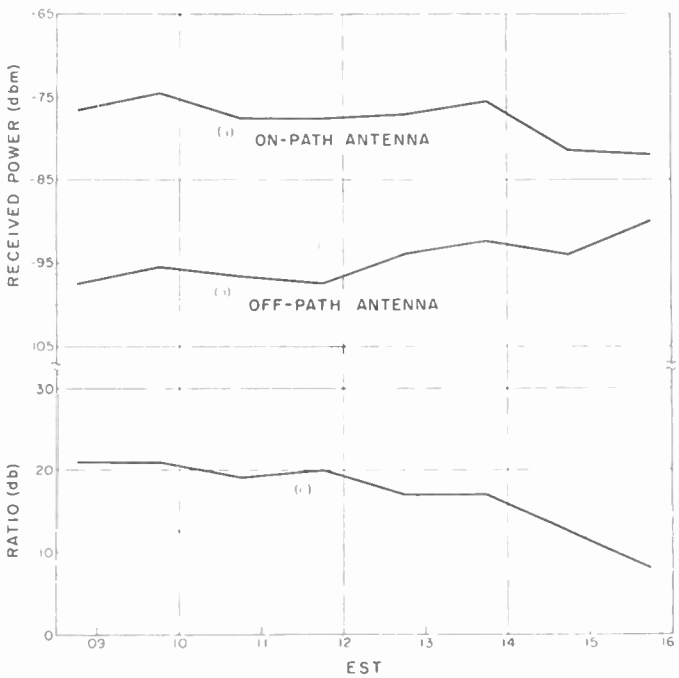

Fig. 14—Signal levels recorded at Round Hill (a) with on-path antenna and (b) with off-path antenna, and (c) their ratio; 22.9 mc transmissions from Alpine, June 28 to 30, 1954.

V. 21.6 Mc Transmissions

Description of Tests and Equipment

It was decided to test hf propagation with regular am transmissions plus diversity reception over a relatively long path, of the order of 1,000 miles, at frequencies believed to be near and above muf. In November, 1952, a temporary site was set up near Limestone, Me. to record transmissions from the Voice of America station WLWO at Cincinnati on 21.6 mc. The receiving site was only 4 degrees south of the great circle path along which the transmissions were beamed. Recordings were made only over a period of a few days. The results of this brief test are included here.

The geometrical parameters of the Cincinnati-to-Limestone path are given in Table I.

The transmitter was normally operated at an estimated average power of 50 kw into the antenna. The antenna, a multiwire horizontal rhombic, had a com-

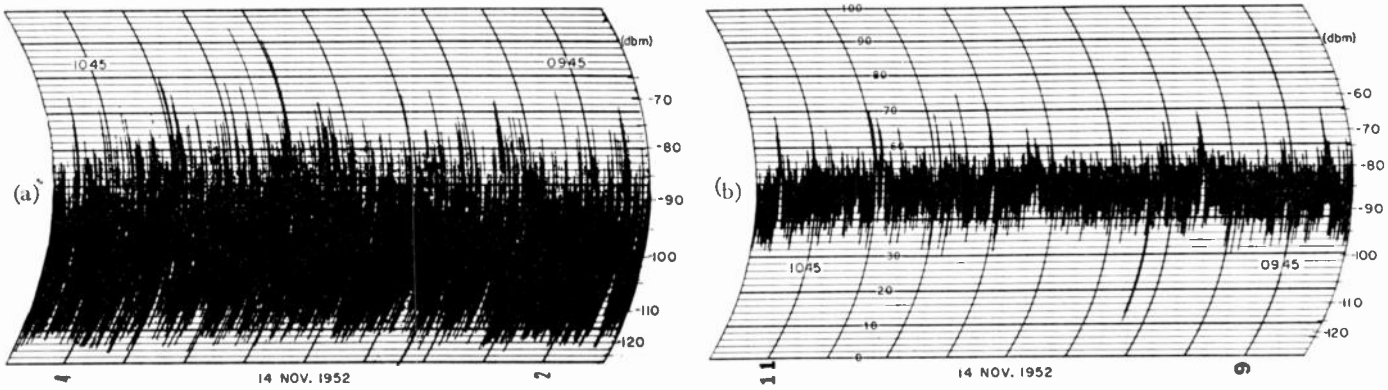

Fig. 15—Photographs of sections of an Esterline-Angus chart showing (a) 21.6 mc signals received at Limestone on a single Yagi antenna and (b) 21.6 mc signals received at the same time using two Yagi antennas in space diversity.

puted gain of 14 db (HWSH) at 4 degrees elevation. The horizontal beamwidth 6 db down from the maximum of the lobe was 16 degrees. In the direction of Limestone, and at 2.8 degrees elevation, the gain of the antenna was estimated to be 11 db.

The receiving equipment comprised two Hallicrafter SX-73 receivers, dc amplifiers, Esterline-Angus chart recorders, Brush fast-speed recorders, and two types of diversity equipment. The antennas were 5-element horizontal Yagis, located at a height of 90 feet and separated by 1,000 feet along a line normal to the Cincinnati-to-Limestone path. In addition to recording signals, the level of noise was measured at irregular intervals by tuning slightly off-frequency to a clear channel.

Signal Level and Diversity Characteristics

During the three days[12] over which recordings were made, median signal levels averaged some 30 db above the received noise. The character of the received signals is shown in a section of the Esterline-Angus chart given in Fig. 15(a). (Time of day is indicated at the top of the chart, calibration of the signal level in db above one milliwatt.) Signal levels received on the common detector diversity system during the same time interval are shown in Fig. 15(b). Inspection shows that during this time, signal levels received on the diversity setup were about 10 db greater than those received on the single antenna. Also, the fading range of signals received on the single antenna was about 20 db greater than those received on the diversity system.

Median signal levels were scaled from the recordings during the three-day period, together with a comparison of levels received on a single antenna with those received on the diversity system [3]. On an average, diversity seems to have given about 6 to 7 db improvement in the median signal level over that on a single antenna.

Demodulated audio signals from the output of the single antenna were often unintelligible during periods of low average signal level or during deep fades. During such times, the audio signals from the diversity system were quite intelligible, even though their quality was somewhat low.

VI. Discussion and Summary

Most of the work herein concerns work at frequencies of about 50 mc or less, and on circuits which are relatively long, of the order of 1,000 miles or more. As such, this work, coupled with that of others, notably CRPL, should present a fair picture of the present state of the art of vhf ionospheric forward scatter propagation.

The signal level chart data which were scaled, and the signal level distributions which were obtained from totalizers, have included effects of such mechanisms as sporadic E and meteoric reflections in the total signal analysis. These additional transmission modes put "kinks" into the distribution curves, usually Gaussian for periods of an hour or more, or Rayleigh for short periods of the order of a minute in the absence of such modes.

For paths approximately 1,000 miles long, the hourly median signal levels are higher in midday than at night, with evidence of a minimum in early evening. Maximum signal levels are higher in winter and summer than in spring and fall. Lower signal levels are encountered in periods of lower sunspot activity (see Section II).

At frequencies near 50 mc, signal levels on the 1,066 mile Cedar Rapids-to-Round Hill circuit are much weaker than those on the shorter (773 mile) Cedar Rapids-to-Sterling path, particularly in midday. The difference is much less marked in periods of low signal.

External noise at 50 mc is higher than receiver noise in receivers of low noise figure design. Neglecting man-made noise effects and interference due to efficient sporadic E transmission, external noise is presumed to be cosmic in origin. At lower frequencies, 21 to 27 mc, regular ionosphere-layer transmission is also encountered and gives rise to increased noise levels.

For transmissions on a horizontal 2,000-foot rhombic antenna at 49.6 mc, the hourly median values of the horizontal and vertical components of the received signal vary in similar fashion, the vertical component being several db weaker; the instantaneous fading of the two components is poorly correlated.

[12] The efforts of G. L. Mellen, of Lincoln Laboratory, in assembling equipment and conducting the tests under somewhat adverse conditions, and his assistance in preparing this section are gratefully acknowledged by the authors.

When radiations at 49.8 mc were directed from Cedar Rapids to Sterling, the "off-path" signals received at Round Hill were considerably weaker than those received when the radiation was directed toward Round Hill. The "off-path" signal varied very little throughout the day compared with the larger diurnal variation of the "direct-path" signals. The characteristics of "off-path" signals do not appear amenable to simple interpretation.

Effective heights of ionospheric scattering, determined by two-way pulse transmission measurements in cooperation with CRPL on the Round Hill-to-Sterling path, were lower than usual E layer heights. The average values for daytime in December, 1954 are lower than nighttime values; the daytime values were 84 to 88 km, the nighttime values running 89 to 94 km. Tropospheric, ionospheric, and meteoric modes were evident. On a longer path (1,066 miles), no tropospheric mode appeared but during sporadic E enhancement, the weaker "scatter" mode continued at a lower effective height. Meteoric reflections were not observed at shorter transmission times than the "scatter" mode and frequently occurred later.

Auto-correlation measurements and analysis at 49.6 mc gave a daytime (December, 1952) average rms scattering particle velocity of 6 to 7 m/sec.

When using the same large horizontal antenna (2,000-foot rhombic) simultaneously at 27.8 and 49.6 mc on the Cedar Rapids-to-Round Hill path and broad beam (Yagi) antennas for reception the frequency exponent for received power varied between 1 and 7, the most probable value lying between 3 and 4. The exponent decreased with the level of the 49.6 mc signal, the correlation coeff cient being about 0.6.

The use of still lower frequencies on 22.9 mc (Alpine to Goose Bay) and 21.6 mc (Cincinnati to Limestone) revealed signals whose fading was quite similar to that at the higher frequencies. Effects of sporadic E and regular layer transmission were more prevalent.

It is concluded that for 1,000 mile point-to-point communication, the frequency range of 20 to 50 mc can be usefully employed, and that the transmission takes place via ionospheric scattering at effective heights ranging from 84 to 94 km. Equipment must be designed to handle the wide dynamic range of received power due to meteoric and sporadic E enhancements. At shorter distances, 350 miles or so, where the tropospheric mode is evident, the differential time delay caused in this mode further limits useful bandwidth even when meteoric or sporadic E transmission is not evident.

High power, of the order of 10 kw, is required and high gain antennas are needed to give adequate signal-to-noise ratios. High antenna directivity is desirable for reducing multipath [3]. Design preferably should be based upon an effective height of about 90 km.

With increasing sunspot activity and higher muf approaching, the use of the higher frequencies in the 20 to 50 mc range is recommended to reduce interference and noise effects due to regular layer propagation.

VII. Acknowledgment

The research reported herein was conducted under the immediate supervision of Professors W. H. Radford and J. B. Wiesner. Special akcnowledgment is due to them for their leadership, encouragement, and assistance in the direction of the work.

It is obvious that the results of our work have been obtained through the effort of several organizations and many individuals, and not every contribution can be acknowledged in detail. We gratefully acknowledge the assistance of colleagues in Lincoln Laboratory for substantial help, and for assistance rendered by individuals and organizations in the sponsoring agencies, and at the National Bureau of Standards (Central Radio Propagation Laboratory), by the Federal Communication Commission, Research and Development Board, Collins Radio Company, E. C. Page Consulting Radio Engineers, Cornell University, and the Radio Physics Laboratory (Ottawa).

Bibliography

[1] Booker, H. G., and Gordon, W. E., "A Theory of Radio Scattering in the Troposphere," Proc. IRE, vol. 38 (April 1950), pp. 401–412.
[2] Bailey, D. K., *et al.*, "A New Kind of Radio Propagation at Very High Frequencies Observable Over Long Distances," *Phys. Rev.*, vol. 86, No. 2 (April, 1952), pp. 141–145.
[3] Abel, W. G., de Bettencourt, J. T., Roche, J. F., and Chisholm, J. H., Lincoln Laboratory Technical Report in preparation.
[4] Villars, F., and Weisskopf, V. F., "The Scattering of Electromagnetic Waves by Turbulent Atmospheric Fluctuations," *Phys. Rev.*, vol. 94 (April 15, 1954), pp. 232–240.
[5] Silverman, R. A., and Balser, M., "Statistics of Electromagnetic Radiation Scattered by a Turbulent Medium," *Phys. Rev.*, vol. 96 (November 1, 1954), pp. 560–563.
[6] de Bettencourt, J. T., and Klemperer, H., "The Beacon Technique as Applied to Oblique Incidence Ionospheric Propagation" Proc. IRE, vol. 38 (January 1950), pp. 791–792 (abstract).
[7] Chisholm, J. H., de Bettencourt, J. T., Roche, J. F., and Portmann, P. A., "Investigations of Angular Scattering and Multipath Properties of Tropospheric Propagation of Short Radio Waves Beyond the Horizon," submitted to Proc. IRE for publication.
[8] Bailey, D. K., paper on VHF Ionospheric Forward Scattering. An account of this paper and discussion appears in "Report to the National Research Council USA National Committee on the Eleventh General Assembly of URSI at The Hague, Netherlands, August 23 to September 3, 1954," pp. 3–43 through 3–58.
[9] Bailey, D. K., "Scattering at Oblique Incidence from Ionospheric Irregularities." A summary of this talk, prepared by J. A. Ratcliffe, appears in "Report of the Physical Society Conference on 'The Physics of the Ionosphere' held at the Cavendish Laboratory, Cambridge, September, 1954," published by *Phys. Soc.* (1955), pp. 99–100.
[10] Licklider, J. C. R., and Dzendolet, E., "Oscillographic Scatterplots Illustrating Various Degrees of Correlation," *Science*, vol. 107 (January, 1948), pp. 121–124.

UHF Long-Range Communication Systems*

G. L. MELLEN†, W. E. MORROW†, JR., ASSOCIATE, IRE, A. J. POTÉ†, SENIOR MEMBER, IRE, W. H. RADFORD†, FELLOW, IRE, AND J. B. WIESNER†, FELLOW, IRE

Summary—**Recent discoveries about long-range propagation of uhf radio waves, together with careful utilization of high-powered transmitters and large antennas, have made possible reliable multichannel point-tc-point uhf radio communication systems which operate over distances of 200 miles or more beyond the horizon. Measurements by various investigators have shown that transmission losses on such paths have median values of the order of 80 db below free-space levels. A program of investigation at Lincoln Laboratory, MIT, has yielded detailed propagation data necessary for the design of long-distance multichannel uhf radio communication circuits. This has also led to the design of specialized equipment for this application. These circuits employ antennas having transmitting and receiving gains of 25–40 db; high-power FM transmitters of up to 10-kw output; sensitive FM receivers having low-noise input circuits, and excellent selectivity; and space-diversity reception. A procedure for system design is outlined.**

I. Introduction

RECENT discoveries that vhf, uhf, and shf signals are propagated to distances well beyond the horizon with losses much less than are predicted by diffraction theory and with high reliability have made possible the design of reliable point-to-point communication systems to operate over distances of two hundred miles or more beyond the horizon. Systems have been operated at frequencies from 300 to 5,000 mcps. These systems employ high-gain antennas, high-power transmitters and space-diversity reception. The cost of such equipment is justified in many applications because the need for intermediate repeater stations is obviated.

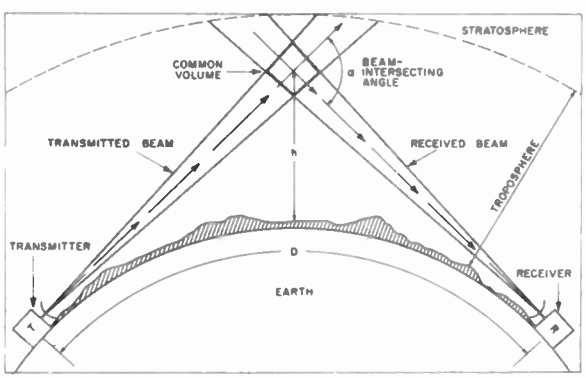

Fig. 1—Path geometry of a scatter uhf circuit.

Fig. 1 shows, in exaggerated form, the path geometry of a typical system. By a mechanism which as yet is not fully understood, a minute portion of the transmitted energy reaches the receiving antenna through scattering and reflections from inhomogeneities in the troposphere. Even though path losses of 60 to 80 db in excess of free space are incurred in this process, the received signals are much larger than would be expected from earth-diffraction effects alone.

This paper reviews those aspects of "scatter" propagation that are important in the design of a communication system (Section II); the next section discusses the design features of equipment suitable for beyond-the-horizon uhf circuits including antenna systems, modulation techniques, and transmitting and receiving equipment; Section IV examines methods of system design. Choice of frequency, site selection, and calculation of circuit reliability are discussed.

II. Propagation Characteristics

A. General

Until recently, the use of uhf communication circuits was limited to line-of-sight distances. Observations made during World War II with high-power radar sets had demonstrated, however, that occasionally uhf signals were propagated well beyond the horizon with losses only slightly greater than free space. These cases were attributed to conditions of ducting or superrefraction in the troposphere. After the war, various researchers began to explore this field of uhf and shf beyond-the-horizon propagation. A series of propagation measurements showed that signals well in excess of levels calculated from diffraction theory were transmitted well beyond the horizon, not just occasionally, but consistently.[1] During the same period, extensive measurements were also made by research workers at NBS,[2] Collins Radio Co.,[3] BTL,[4] and in England.[5]

These measurements demonstrated that the attenuation of beyond-the-horizon uhf signals (hereafter referred to as "scatter signals") was much less than that predicted by diffraction theory. Various theories have been proposed to account for this propagation; they differ considerably, but in general the propagation is attributed to minute perturbations in the electrical properties of

* Original manuscript received by the IRE, August 3, 1955. The research in this document was supported jointly by the Army, Navy, and Air Force under contract with MIT.

† Lincoln Lab., Mass. Inst. Tech., Lexington, Mass.

[1] T.I.D. Report 2.4.5., "Summary of tropospheric Propagation measurements and the development of empirical propagation charts," Federal Communications Commission (27989); October 20, 1948.

[2] J. W. Herbstreit, K. A. Norton, D. L. Rice, and G. E. Schafer, "Radio-wave scattering in tropospheric propagation," 1953 IRE CONVENTION RECORD, NBS Report 2459 of April 15, 1953.

[3] L. H. Gerks, "Propagation at 412 mc from a high-powered transmitter," PROC. IRE, vol. 39, pp. 1374–1382; November, 1951.

[4] K. Bullington, "Radio propagation variations at vhf and uhf," PROC. IRE, vol. 38, pp. 27–32; January, 1950.

[5] E. C. S. Megaw, "The scattering of short radio waves by tropospheric turbulence," *Nature*, vol. 166, pp. 1100–1104; December, 1950.

the troposphere. Measurements have shown that variations in the dielectric constant of the air are present due to turbulence and stratification. Calculations show that these variations are sufficient to produce the observed signals. Further details of these theories are given in papers by Gordon and Booker,[6] and by Carroll.[7]

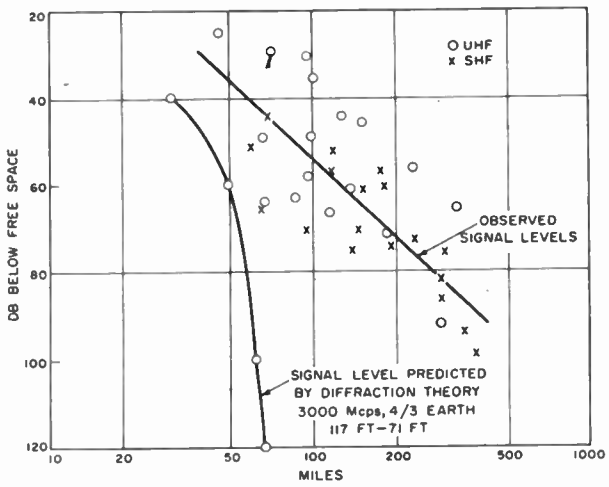

Fig. 2—Median signal levels in 300- to 4,000-mc band.

B. *Median Loss below Free Space vs Distance*

The results of many uhf measurements at various distances beyond the horizon have been collected by Bullington of BTL.[8] Fig. 2, above, based on his paper, shows various measurements of the loss in excess of free space as a function of distance. Dispersion of the data is probably due to variations in path geometry and differing climatological conditions for the cases plotted. It is interesting to note that the loss below free space is not markedly frequency-dependent. Accurate data are not yet available on frequency dependence, but it is probable that, with moderate gain antennas (<30 db), less than 6 db difference in loss exists between 300 and 3,000 mcps. The median loss is most accurately known in the 100- to 200-mile region because of the numerous measurements made at these distances. The median loss at distances of 300 miles and beyond is in some doubt and Lincoln Laboratory is now making measurements at these greater distances.

C. *Variations in the Path Loss*

Path loss variations may conveniently be divided into two components: (1) fluctuations in the short-term (10 minutes to one hour) median loss with season of the year, time of day, and weather; and (2) rapid fading at rates of 1 to 10 cps. The characteristics of this rapid fading depend on many factors, the most important of which is carrier frequency.

It has been observed that the lower percentile values of the received signal level vary in a random fashion about the monthly median values. In general, the received signals are stronger in the warmer seasons of the year. The diurnal variations follow no consistent patterns. Circuits over paths of different climatological conditions have significantly different characteristics. One striking phenomenon, quite prevalent in the warmer seasons, is the occurrence of "trapping" conditions which produce signals approaching free-space levels. Under these circumstances, the behavior of the signal is entirely different from that usually observed; the rapid fading characteristic of scatter propagation disappears except for effects caused by aircraft.

Because of the random nature of the median signals, the path loss is best characterized statistically. Good data are available on the variations in the median signals at distances up to 200 miles beyond the horizon. In obtaining propagation data, the smallest practicable antennas (10λ aperture or less) should be used. Larger antennas fail to achieve their free-space gains under weak-signal conditions due to lack of phase coherence across the surface of the antenna. Because of this, signals received by large-aperture antennas show a tendency toward greater variation in level than signals from small antennas.

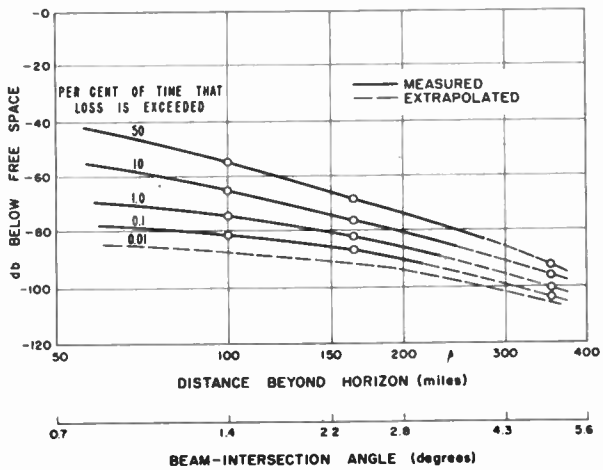

Fig. 3—Short-term median propagation losses for scatter uhf paths.

Accurate knowledge of the short-term median loss and its variation with distance is of extreme importance in the design of "scatter" systems. Variation in short-term median loss is one of the principal factors that establish the percentage reliability to be expected with a particular circuit design. Data from measurements by Gerks, by Bullington, and by groups at Lincoln Laboratory have been combined in Fig. 3, above, in a form that permits determining, for various distances, the loss below free space which must be overcome to achieve specified reliability.

[6] W. E. Gordon and H. G. Booker, "A theory of radio scattering in the troposphere," PROC. IRE, vol. 38, pp. 401–412; April, 1950.

[7] T. J. Carroll and R. M. Ring, "Normal Tropospheric Propagation of Short Radio Waves Well Beyond the Horizon," Lincoln Lab. Technical Report; not generally available.

[8] K. Bullington, "Radio transmission beyond the horizon in the 40 to 4,000 mc band," PROC. IRE, vol. 41, pp. 132–135; January, 1953.

Adequate information on the rapid fading characteristics of scatter signals is available from high-speed recordings made at this Laboratory. The rapid fading of such signals is also attributed to fluctuations in the dielectric constant of the troposphere. Fig. 4 shows typical rapid fading at approximately 400 mcps over a 180-mile path. Analysis of such data indicates that the amplitude of the signal is Rayleigh-distributed and of the form

$$P(x) = \frac{2x}{\overline{(x^2)}} \exp\left[-x^2/\overline{x^2}\right], \qquad (1)$$

where $P(x)$ = probability density of value x, and $\overline{x_2}$ = 2nd moment of the distribution.

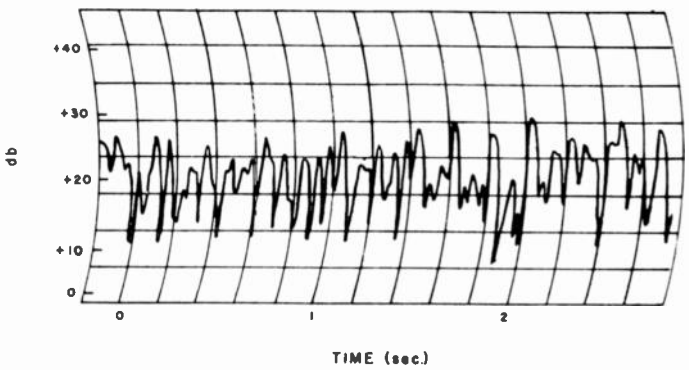

Fig. 4—Rapid variations in signals received over a scatter circuit.

Fig. 20 in Section III, *D* shows a plot of a more useful form of this type of distribution in which the signal levels relative to the median are plotted as functions of the percentage of time that the level is exceeded. This curve was obtained by integrating the probability density:

$$(\text{Probability of } x \text{ or greater}) = \int_x^\infty P(x)dx. \qquad (2)$$

It should be noted that the rapid fading distributions vary appreciably. For instance, when trapping occurs, there may be no appreciable fading. Even though there is relatively little fading due to propagation, rather large variations may be introduced by aircraft flying through the antenna beams. For design purposes, however, it is reasonably safe to assume that the rapid fading is Rayleigh-distributed. Details of diversity techniques for reducing the effects of these rapid variations are described in Section III, *D*.

D. Space Coherence of Received Signals

The space coherence of received signals is of great importance in scatter circuits; on it, two aspects of circuit design depend: the maximum realizable antenna gains, and the spacing between antennas required for successful space-diversity reception.

The term "space coherence" is used here to describe the degree of amplitude and phase correlation of received signals at different points on an equiphase surface (i.e., a surface normal to the average direction of arrival of an electromagnetic wave). With a point source, the equiphase surfaces are concentric spheres centered on the source. If, however, the source is distributed, the amplitudes and phases will not be equal at separated locations. In scatter circuits, the source illuminating the receiving antenna can be considered to be distributed over the common volume in the troposphere determined by the transmitting and receiving antenna beams. In addition, the amplitude and phase relationships fluctuate because of variations in the refractive index of the troposphere. It is not possible to correct for these variations.

In typical cases of scatter transmissions over paths as long as 200 miles, it has been found that lack of space correlations can seriously impair the gain of a large antenna (e.g., 730λ). The effects appear to be most marked during weak-signal periods. It has been found that antenna gain is realized to within 1 or 2 db if the free space gain does not exceed 30 db (see Section III, A, below). However, antennas with considerably more gain may be desirable to reduce the multipath effects described in the next section.

It has been determined experimentally that satisfactory space-diversity reception can be achieved with antenna separations of 25 wavelengths or more, normal to the path. In practice, antennas have usually been spaced at 100 wavelengths or more to insure good space-diversity action. Measurements by the National Bureau of Standards at Boulder, Colorado, indicate that for antennas spaced along the path approximately five times the separation is required as for antennas aligned normal to the path.[9]

E. Dispersion and Multipath Effects

Another manifestation of a fluctuating distributed source is the imperfect correlation of amplitudes and phases of signals transmitted on different frequencies. This effect is of considerable importance because it limits the maximum information bandwidth that may be transmitted by a specific modulation technique.

It is possible to divide dispersion and multipath effects into two classes, those due to atmospheric disturbances alone, and those due to aircraft. According to measurements made at Lincoln Laboratory at frequencies of 400, 3,670, and 5,050 mcps employing antennas having several degrees beamwidth, the medium itself (without aircraft) introduces time delays much smaller than 1.0 microsecond, at distances of about 200 miles. These studies indicate that under favorable conditions, modulation bandwidths of several megacycles can be achieved. The results of pulse tests at 3,670 mcps with 0.6-degree antenna beams by Chisholm of Lincoln Laboratory indicate that dispersive effects of

[9] A. P. Barsis, J. W. Herbstreit, and K. O. Hornberg, "Cheyenne mountain tropospheric propagation experiments," NBS Circular 554, January 3, 1955.

no more than the order of 0.1 to 0.2 microseconds occur in the absence of aircraft reflections. These results are supported by theory. Gordon[10] and Booker and de Bettencourt[11] estimated that at distances of 200 miles beyond the horizon the bandwidth capabilities should be approximately 4 to 6 mc.

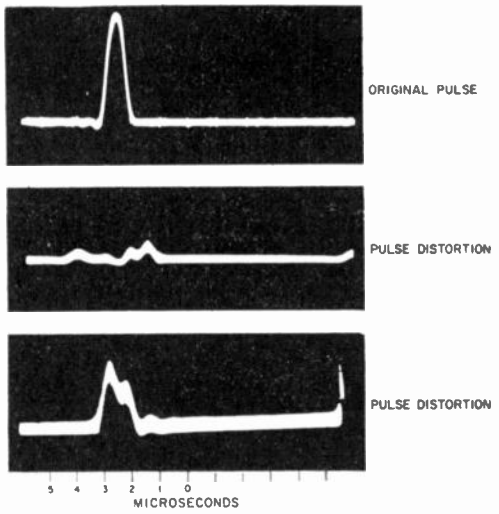

Fig. 5—Pulse distortion caused by reflections from aircraft.

Severe multipath effects can be caused by aircraft flying in or near the antenna beams. Fig. 5 shows pulse distortion observed during transmission over a 180-mile circuit at 400 mc using 6-degree antenna beams. Fig. 9 shows that delays of up to 1.5 microseconds can be expected from aircraft located 3.0 degrees off path in such a system. It is obvious that aircraft flying slightly outside the 6-degree 3 db beamwidth of the antennas could produce the observed delays. The equation in Fig. 9 shows that the multipath delay is proportional to the square of the off-beam angle from which the delayed signals are received. Therefore, a very effective method of reducing this type of multipath is to reduce the antenna beamwidth.

F. Polarization Effects

Accurate data on polarization characteristics of scatter propagation are not available at this time. However, it can be said that no measurable differences in transmission loss are observed between horizontal and vertical polarization. Measurements have been made at 400 mc to determine if there are any appreciable differences in the fading characteristics between vertically, horizontally, and circularly polarized signals. No significant differences were observed in signal levels of fading distributions. Measurements at 3,670 mcps indicate that the plane of polarization is generally preserved in transmission. Approximately 90 per cent of the received energy is in the plane of polarization of the transmitting antenna.

[10] W. E. Gordon, "Radio scattering in the troposphere," PROC. IRE, vol. 43, pp. 23–28; January, 1955.
[11] H. G. Booker, J. T. de Bettencourt, "Theory of radio transmission by tropospheric scattering using very narrow beams," PROC. IRE, vol. 43, p. 281; March, 1955.

III. ANTENNAS AND EQUIPMENT

In order to overcome the large transmission losses encountered on beyond-the-horizon radio circuits, it is necessary to use high-gain antennas, powerful transmitters, and sensitive receivers.

A. Antennas

Among the factors which affect the choice of antennas for a particular application are: (1) required gain; (2) signaling bandwidth (considered jointly with the length of the circuit); (3) gain degradation effects; (4) siting and environmental requirements; and (5) cost.

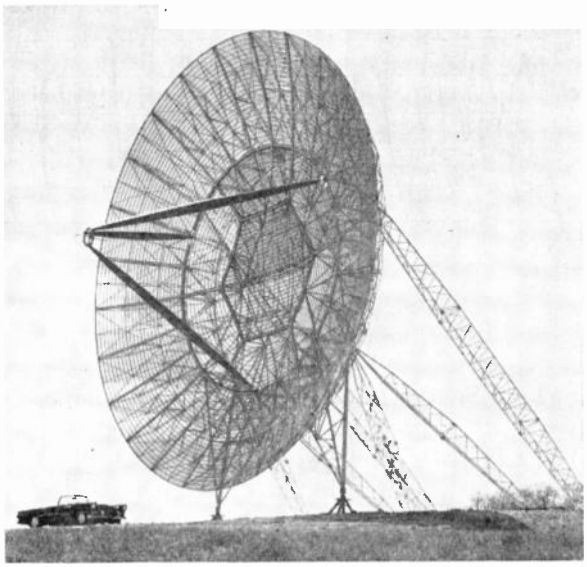

Fig. 6—60-foot-diameter paraboloidal antenna.

Most of the antennas now in use on experimental and operational circuits are simple center-fed, circular paraboloids of revolution. Fig. 6 shows a paraboloid sixty feet in diameter and weighing about 6,000 pounds, and Fig. 7 (next page) shows a similar 28-foot-diameter antenna weighing ca. 1,600 pounds. These antennas are fabricated of welded aluminum tubing and expanded aluminum mesh and are designed to withstand winds of 100 miles per hour when coated with one inch of ice. Fig. 7 also shows a typical mounting which permits raising the dish above nearby obstructions and allows a limited adjustment in azimuth to correct for surveying or construction errors.

In siting antennas it is necessary to avoid foreground obstructions such as trees, buildings, or other high objects. Height gain is realized until the bottom of the antenna is approximately 20 wavelengths above the ground. Horizon obstruction not exceeding 0.1 degree above the horizontal does not significantly increase the path loss.

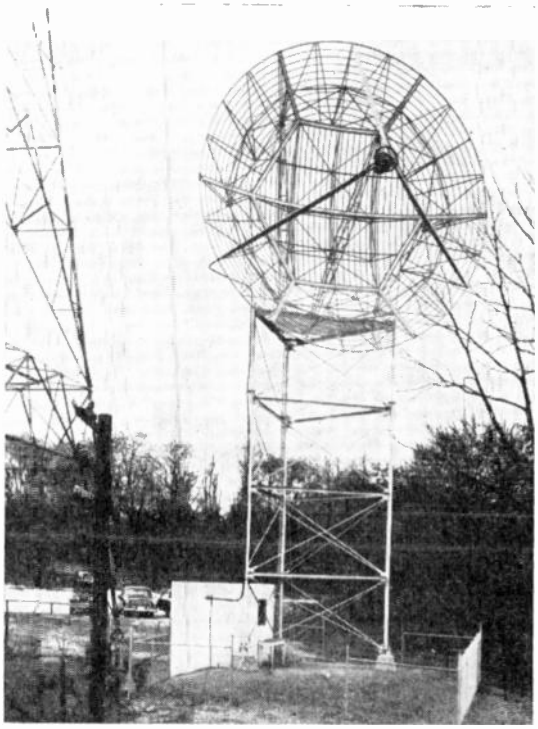

Fig. 7—28-foot paraboloidal antenna and mount.

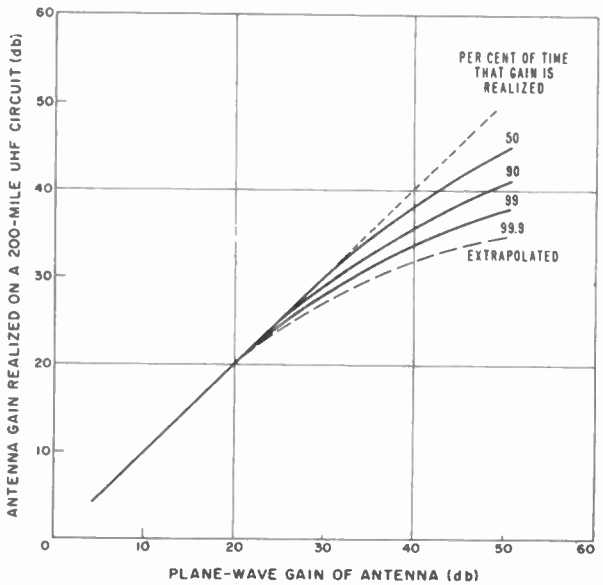

Fig. 8—Antenna gain realized on long-range uhf circuit.

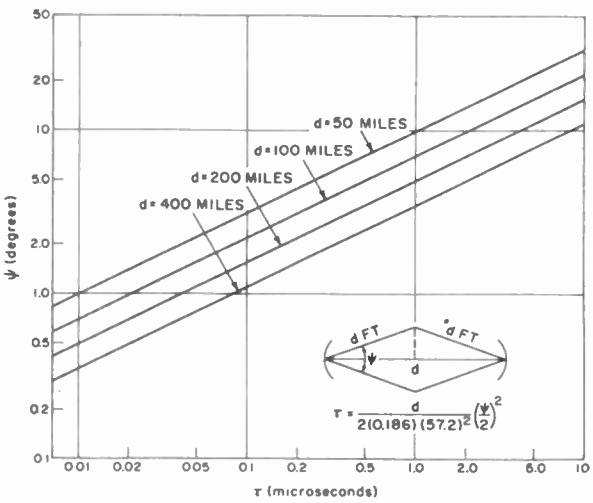

Fig. 9—Multipath delay as a function of distance and antenna beamwidth.

As previously indicated, the full gain of large-aperture antennas is not realized at all times. Fig. 8 shows this variation as a function of the antenna aperture in wavelengths.

The longest significant multipath delay establishes the maximum signaling bandwidth. This matter is discussed in a companion paper.[12] The other source of serious multipath in scatter circuits is reflections from aircraft flying near the transmission path. Fig. 9 shows the time delay incurred as a function of beamwidth caused by a reflecting object at the midpoint of the path and at the half-power points of the antenna beams.

The antenna feed systems and transmission lines used in the Lincoln Laboratory scatter systems are conventional. At the lower frequencies in the uhf band dipole feeds and coaxial transmission lines are used. At higher frequencies, horn feeds and waveguide are more satisfactory.

Since the antenna systems are large and costly, it is desirable to diplex antennas for simultaneous transmission and reception. Diplexing is rather difficult owing to the very large difference in levels of transmitted and received signals, which may approach 200 db in some cases. For satisfactory diplexing, it is necessary to attenuate signals emanating from the transmitter at the receiver frequency to a level less than the minimum detectable signal. With care, spurious output from the transmitter on frequencies removed from the carrier by a few per cent or more can be held to 100 or 150 db below carrier level. Thus, for satisfactory diplexing it is usually necessary to provide additional attenuation of 50 to 100 db. It is also necessary to isolate the receiver input from the transmitter to prevent overloading.

Satisfactory diplexing has been accomplished using (1) A crossed polarization antenna feed together with separate transmitting and receiving lines. (From 20 to 50 db of isolation can be obtained in this way. Additional filtering is usually required at the receiver input.) (2) A common feed and transmission line system, together with branching filters connecting to transmitter and receiver.

A filter diplexing scheme which has been employed successully is shown in Fig. 10 (next page). Filtering is done by multiple stubs attached to the transmission lines. This system has advantages in that no special antenna feed is required; a single transmission line or wave-

[12] J. H. Chisholm, P. A. Portmann, J. T. deBettencourt, and J. F. Roche, "Investigations of angular scattering and multipath properties of tropospheric propagation of short radio waves beyond the horizon," p. 1317, this issue.

guide is used; and voltages and currents in each element do not exceed those in the matched transmission line. However, filter elements in the transmitter line are required; also, it has only discrete stop and pass rather than band-pass characteristics. The stubs may have either open or short circuit terminations. Assuming the former, the stub lengths are adjusted to be approximately an even integral number of quarter-wavelengths at the desired pass frequency and an odd integral number of wavelengths at the desired stop frequency. The length of the stub turns out to be approximately a quarter-wavelength at the difference between the transmitter and receiver frequencies.

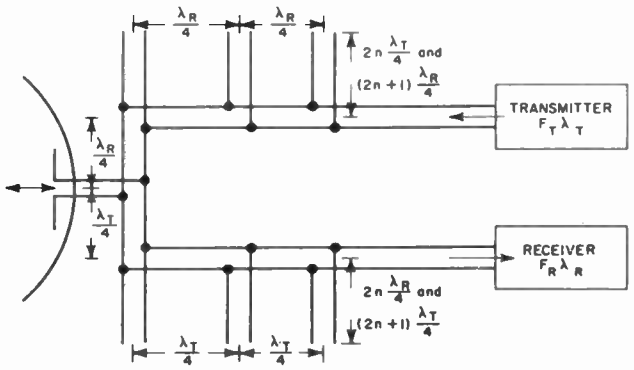

Fig. 10—Long stub filter diplexer.

B. Multiplexing and Modulation Techniques

In scatter systems, it is important to take advantage of the most efficient multiplexing and modulation techniques. Frequently, multichannel operation is required, using either time-division or frequency-division multiplexing techniques. Normally, single-sideband frequency division is employed because of the minimal bandwidth requirements of this technique, the simplicity and reliability of the equipment, and its compatibility with the present telephone plant.[13]

Any of the well-known modulation techniques might be used.[14] Obviously, techniques requiring excessive bandwidth or having relatively poor performance against noise are undesirable. All things considered—including propagation effects and equipment problems—the techniques of frequency modulation[15] and single-sideband modulation appear to be the most satisfactory.

Although frequency modulation does not make most efficient use of bandwidth, and has marked threshold effects, it does have characteristics which in a properly designed system are particularly advantageous for scatter applications—notably relative freedom from distortion, and insensitivity to rapid fading so long as received signals exceed the threshold level. When FM is used, it appears desirable to restrict the modulation index to 2 or 3 to enable a reasonable compromise between the conflicting requirements for good FM signal-to-noise improvement and low threshold sensitivity.[16] Through 6 db per octave pre-emphasis of the higher modulating frequencies, it is possible substantially to equalize the signal-to-noise ratios in the several channels in a multiplexed system (see Fig. 11).

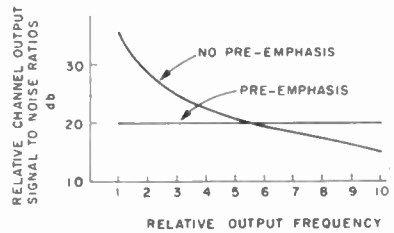

Fig. 11—Effect of pre-emphasis on channel signal-to-noise ratios in a multichannel FM system.

Single-sideband modulation,[17] although not presently employed in scatter systems, has several features which make its use attractive: the minimal use of bandwidth (6 to 8 times less than FM), tolerance of considerable dispersion in the transmission medium, no threshold effects, and a considerably lower average power requirement compared to FM (see Fig. 12). On the other hand, single-sideband equipment requires high-linearity power amplifiers and extremely good frequency stability.

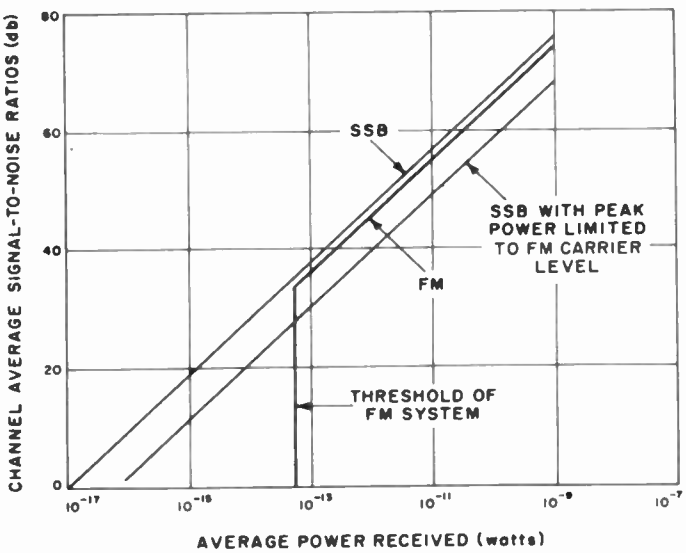

Fig. 12—Relative performance of 100 channel SSB and FM systems.

C. Transmitters

Typical FM transmitters now employed in scatter systems are quite conventional in conception. Transmitter powers range from 100 watts to 10 kw.

[13] H. S. Black, "Modulation theory," D. Van Nostrand Co., New York, pp. 68–69; 1953.
[14] V. D. London, "Theoretical analysis of various systems of multiplex transmission," *RCA Rev.*, vol. 9; June and September, 1948.
[15] A. A. Roetken, K. D. Smith, and R. W. Friis, "The TD-2 microwave radio relay system," *Bell Sys. Tech. Jour.*, vol. 30, pp. 1041; October, 1951.
[16] H. S. Black, *op. cit.*, p. 225.
[17] *Ibid.*, p. 169.

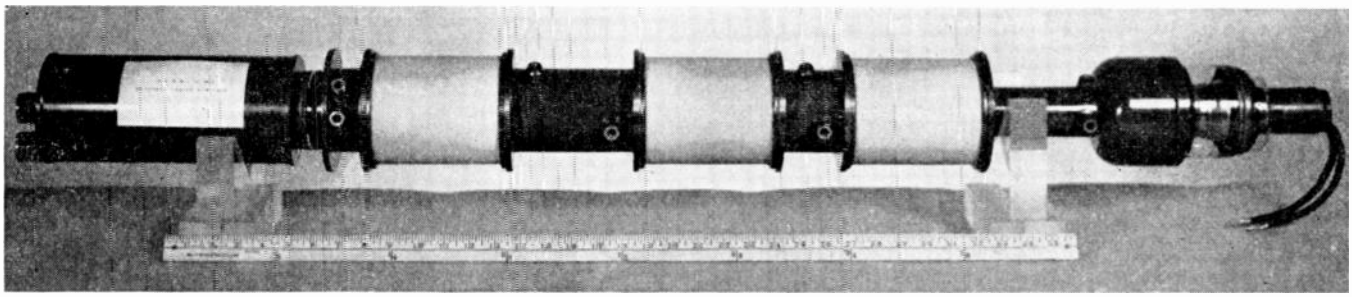

Fig. 13—10 kw-375-600 mcps-external cavity klystron.

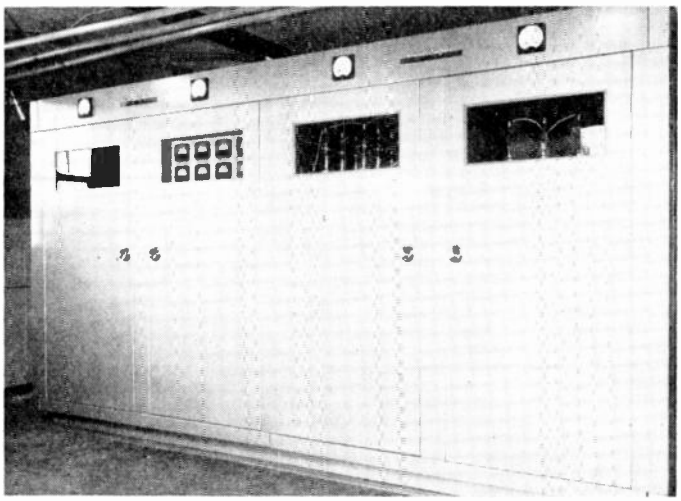

Fig. 14—400-mc 10-kw klystron amplifier.

A phase[18] or frequency modulator[19] is employed to drive a series of low-level triode or tetrode frequency-multiplier stages which increase the frequency deviation to the desired value. The power level in the final frequency multiplier stages is increased to the level required to drive the power amplifier, which may employ either a tetrode or a klystron.

The power amplifiers employing uhf tetrodes are also conventional in design. Ordinarily, coaxial resonator circuits are used with these tubes. At the present time, high-power tetrode power amplifiers are limited to frequencies less than 1,000 mcps.[20]

Klystron power amplifiers have been used more extensively than tetrodes in scatter systems because of such features as high-power gain, ease of application, and long life.[21] External-cavity klystrons have proved particularly useful because they permit wide tuning ranges with a single tube. Fig. 13 shows a 10-kw external cavity tube capable of operation from 375 to 600 mcps. Integral-cavity klystrons thus far have had somewhat limited tuning ranges, although it may be possible to extend the tuning range.

[18] J. R. Day, "Serrasoid f-m modulator," *Electronics*, vol. 21, p. 72; October, 1948.
[19] F. E. Terman, "Radio Engineering," McGraw-Hill Book Co., New York, p. 493; 1947.
[20] L. L. Koros, "High-power uhf-TV uses grid-control tube," *Electronics*, vol. 28, pp. 130; April, 1955.
[21] D. H. Preist, C. E. Murdock, and J. J. Woerner, "High-power klystrons at uhf," PROC. IRE, vol. 41, pp. 20–25; January, 1953.

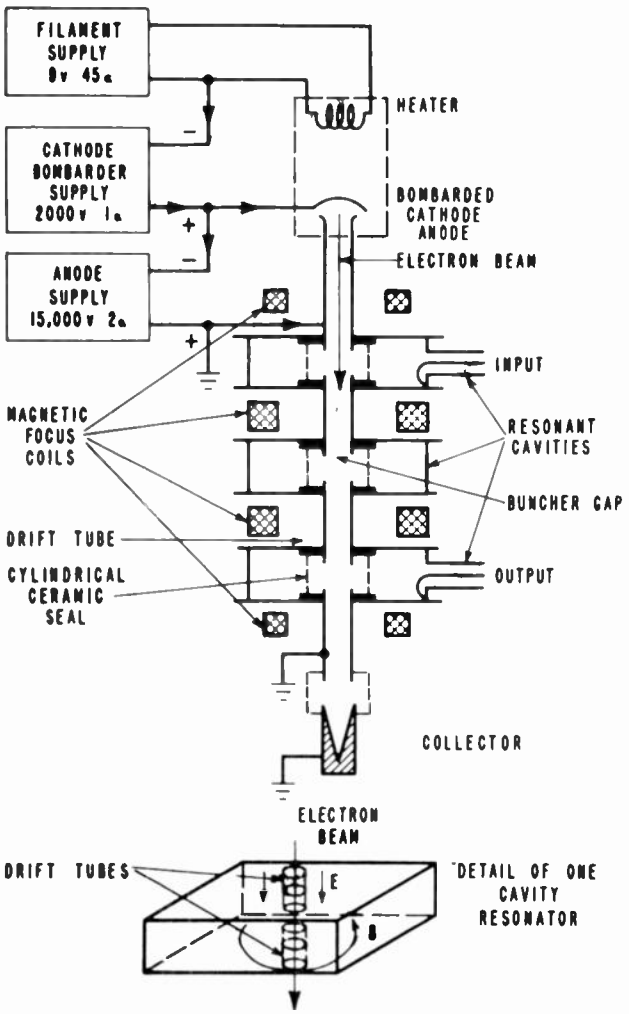

Fig. 15—Arrangement of external cavity klystron with its cavities, focus magnets, and power supplies.

Fig. 14 shows a view of a 400-mcps 10-kw klystron amplifier that employs an external-cavity klystron. Fig. 15 shows the arrangement of the tube with its cavities and magnetic circuits. The electron gun forms a 15-kv beam of about two amperes which passes in succession through three cavity resonators and then into a water-cooled collector. The input power is coupled into the first cavity. Output power is extracted from the bunched beam by the third resonator. Such an amplifier has a power gain of 30 to 40 db and thus requires a driving power of only 1 to 10 watts. The ac power requirement of the amplifier is about 40 kw, giving an over-all

efficiency of about 25 per cent. A coaxial output line of $1\frac{5}{8}$ or $3\frac{1}{8}$ inch diameter is used for frequencies up to 1,000 mcps. Above 1,000 mcps, waveguide is desirable because of its low loss and high power handling capability.

D. Receivers

The large path loss of scatter circuits makes it imperative that the receivers be designed for extreme sensitivity; consequently, low-noise input stages and a high degree of selectivity are employed.

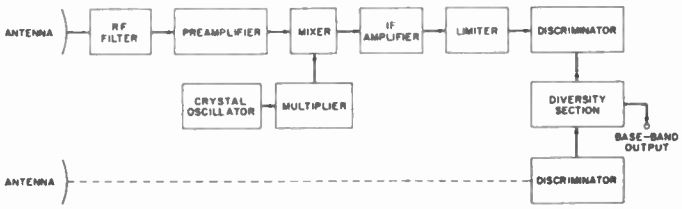

Fig. 16—Diversity uhf FM receiver.

A block diagram for a typical FM receiver for scatter circuits is shown in Fig. 16 above. A preselector filter is used to reduce the image and other spurious responses to a satisfactory level. This filter consists of several quarter-wave coaxial resonators coupled in cascade and adjusted to have a Q of 100 to 400. By proper design, the insertion losses of the filters can be kept to less than 1 db. At the lower uhf frequencies, a low-noise vacuum-tube preamplifier is used to improve the noise figure of the receiver. Fig. 17 shows that below about 900 mc, considerable improvement in the receiver noise figure can be achieved with a preamplifier. These preamplifiers typically use grounded-grid circuits employing closely-spaced planar triodes such as the Western Electric Co. 416B. Above 900 or 1,000 mcps, it is possible to achieve noise figures of approximately 8 db by using special crystal diode mixer designs.

The local oscillator signal is generated by a quartz crystal oscillator operating between 10 and 50 mc followed by a chain of frequency multipliers. In the design of the frequency multiplier filtering circuits, care must be taken to reduce the local oscillator spurious outputs to an absolute minimum.

The center frequency of the IF amplifier is usually between 10 and 60 mc. The lower frequencies are used where narrow IF bandwidths are required. The bandwidth of this amplifier is designed to accommodate all the significant components of the FM signals with a minimum of phase and amplitude distortion. The IF bandwidth should be kept to a minimum so the receiver has as low a threshold signal level as possible.

The design of the limiter discriminator section in equipment used to date is based on the work of Arguimbau and Granlund at the Research Laboratory of Electronics, MIT.[22] These design features include wide

[22] J. Granlund, "Interference in frequency-modulation reception," Tech. Rep. No. 42, MIT Res. Lab. of Electronics; January 20, 1949.

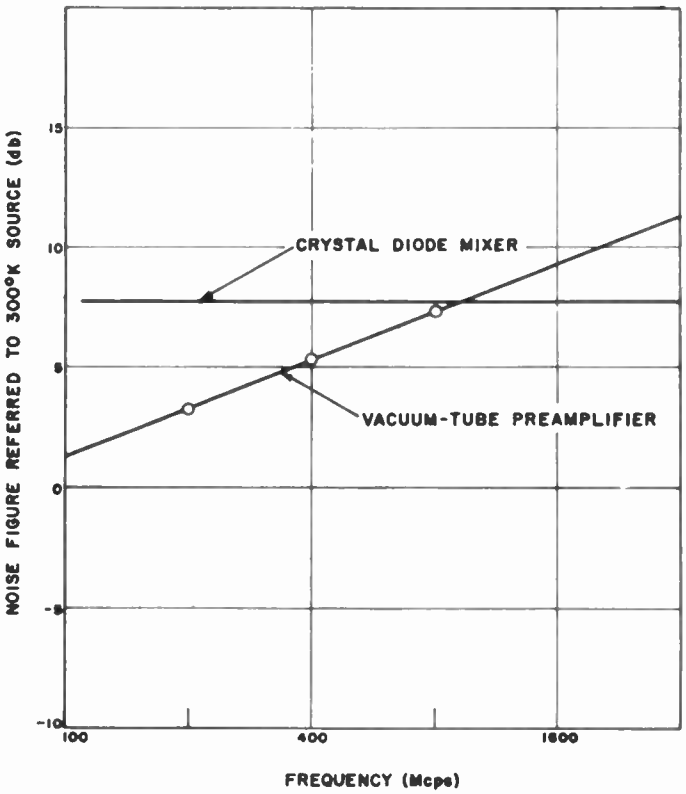

Fig. 17—Noise figure of typical vacuum tube and crystal front ends.

band high-speed limiters and wide-band high linearity discriminators. Receivers embodying these features have superior performance under multipath conditions.

E. Diversity Techniques

Space-diversity reception can be employed to reduce the effects of rapid fading. This technique capitalizes on the fact that, when the signal has faded to a low value on one antenna, it is highly probable that a stronger signal will be received on another antenna located at a sufficient distance. Diversity reception can therefore significantly improve the over-all gain of a system. The distribution of signal strength during a fading signal period is characterized most conservatively by the Rayleigh distribution shown in Fig. 18 (next page). A high performance circuit (i.e., one whose received signal strength exceeds the minimum necessary for acceptable communications more than 99 per cent of the time) requires 20 db more system gain than is needed to overcome the median path loss.

Signals received on widely separated frequencies or at widely separated times also are characterized by a lack of correlation of fading. However, diversity systems capitalizing on these effects have not been used because of the extra frequency spectrum required, and because of the time delays inherent with time diversity. Independently of the means by which the separate signals are obtained, either of two selecting techniques are employed, (1) switching diversity; or (2) combination diversity.

When switching diversity is employed, the quality of the signals from each of the receiving systems are compared, and the best one is selected. Fig. 19 shows a block diagram of such a system. The switching may be carried out either before limiting in the IF section or after demodulation in the output amplifier section. Switching before limiting is preferable because the switching transients generated are small compared with the transients generated when switching is done after demodulation.

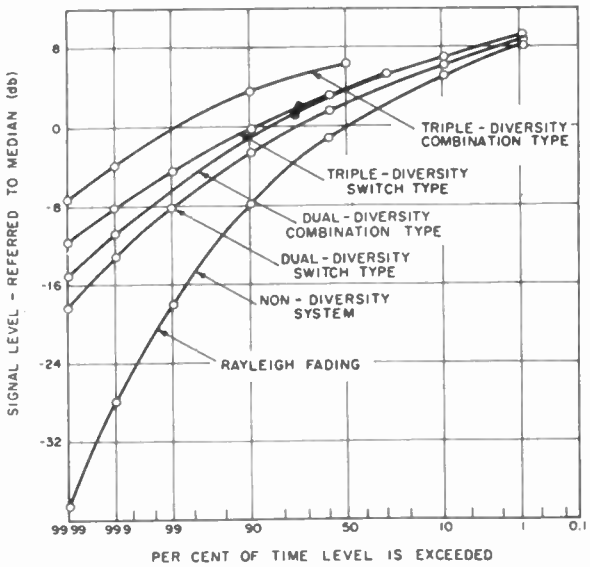

Fig. 18—Signal-level distribution vs order of diversity.

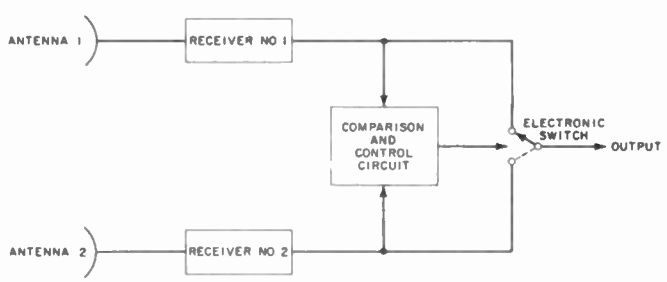

Fig. 19—Receiver switching diversity.

Fig. 18 illustrates the advantage achieved by switching diversity. The following relation is used for the case of Rayleigh-distributed fading:

$$f = 1 - \left\{1 - \exp\left[-x^2/\overline{x^2}\right]\right\}^n, \qquad (3)$$

where

f = fraction of time that the signal level after switching exceeds level x,
x = the level,
$\overline{x^2}$ = the second moment of the Rayleigh distribution,
n = number of receivers employed.

In most FM diversity systems, the comparison of the quality of the signals is based on the output noise from the individual receivers. Because this noise provides a direct measure of the quality of the received signals, this arrangement is preferred to a comparison of the avc voltages which are sensitive to variations in the gain of the amplifier and the noise figures of the receiving tubes.

With switching diversity, the poorer signals are totally rejected in favor of the best. It has been pointed out by Kahn[23] and others that, by proper combination of *all* the signals received in a diversity system, a better output signal-to-noise ratio is obtained than that of any single receiver. This improvement is possible because the noise components are random in character and add in an rms fashion, while the signals add linearly. The improvement in instantaneous output signal-to-noise ratio compared to the best single receiver output is

$$\frac{(S/N)_{\text{combined}}}{(S/N)_{\text{best single receiver}}} = \frac{\sqrt{(S_1/N_1)^2 + (S_2/N_2)^2 + (S_3/N_3)^2}}{S/N_{\max}}. \qquad (4)$$

The maximum advantage occurs when all receiver outputs have the same signal-to-noise ratio, and is equal to 3 db for dual diversity, 4.8 db for triple diversity, 6 db for quadruple diversity, etc. Fig. 18 shows the advantage that may be achieved with dual and triple combiner diversity over the switching types, assuming Rayleigh-distributed signals. To the obvious advantage of combination diversity for the reduction of fading, there is the added merit that such a system introduces no switching transients.

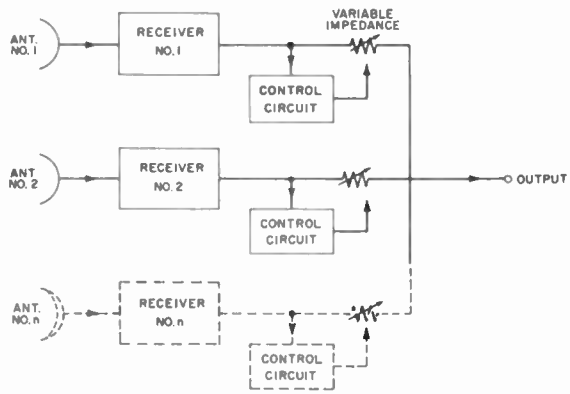

Fig. 20—Signal combination diversity.

Fig. 20 shows the block diagram of a diversity-combining system that has been used successfully. The combining is accomplished by paralleling the outputs of the several receivers, the output impedances of which vary in proportion to the noise-power output of each receiver. Thus, a receiver with a poor signal-to-noise ratio (and, hence, a high output noise level) will have a very high output impedance which will prevent the noise from appearing in the output.[24]

[23] L. R. Kahn, "Ratio squarer," PROC. IRE, vol. 42, p. 1704; November, 1954.

[24] For further discussion see companion paper by C. L. Mack, "Diversity reception in uhf long-range communications," p. 1281, this issue.

IV. System Analysis and Design

With specific requirements for a communications system—distance, capacity, reliability—the designer must choose among various engineering solutions. While it is recognized that cost is an important consideration, the procedures for arriving at the optimum design costwise are rather involved and are dependent on local conditions; consequently the discussion in this section will be restricted to the problems of circuit design.

A. Choice of Frequency

The operating frequency is among the first parameters that should be established for a long-range uhf communication system. Among the factors that bear on the choice of frequency are variation of path loss with frequency, equipment availability, and possible frequency allocations.

The propagation loss of a scatter circuit can be separated into two components: the free-space loss and the beyond-the-horizon loss. Available data indicate that the scatter loss is not strongly dependent on frequency. At shf frequencies (>5,000 mcps), the scattering of electromagnetic waves by rain and absorption of the energy by water vapor introduces additional loss which is frequency-sensitive.

The free-space loss can be expressed as:[25]

$$\text{loss db} = 36.6 \text{ db} + 20 \log_{10} fd \text{ (for isotropic antennas)}$$

where f is in megacycles per second and d is in statute miles. This expression indicates that the loss between isotropic antennas in free space increases as the square of the frequency. This occurs because the effective cross section of an isotropic receiving antenna decreases inversely as the square of the frequency. If antennas of the same aperture are used at different frequencies, the net loss will *decrease* with the square of the frequency ratio up to the frequency at which the antennas fail to achieve their plane-wave gains. In summary, where antenna sizes are limited, higher frequencies are preferred; where the minimum net transmission loss is desired (circuits designed for maximum distance), the use of lower frequencies with very large antennas is indicated.

B. Siting

An advantage of scatter circuits at uhf is that the terminals need not be within line of sight of each other. The sites may, in fact, be separated by several hundreds of miles.

Nevertheless, care must be exercised in siting the antennas. They should be so located that a clear view of the horizon exists and that there are no nearby obstructions such as trees or buildings. It is important that obstructions at the horizon be no greater than a small fraction of a degree above the horizontal. In addition, antennas should not be aimed at intense sources of electrical noise. Ideally, antennas should be high enough to maintain a first Fresnel clearance 25 or more wavelengths between foreground objects and line of sight.

For diversity reception, the receiving antennas should be spaced at least 25 and preferably 100 wavelengths normal to the path. Fig. 21 shows a typical space-diversity antenna arrangement. (It is possible to use a single tower with the antennas spaced vertically with spacings of 25 wavelengths or more; however, failure of a single tower will disable the circuit.)

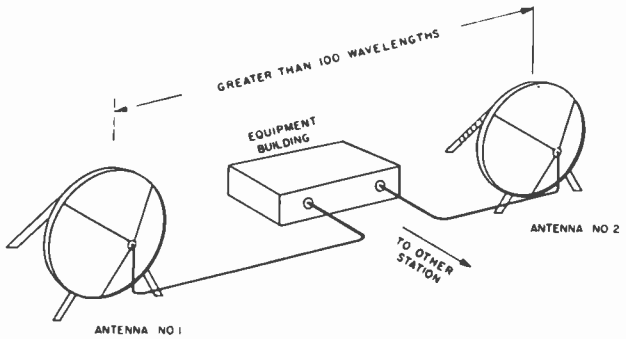

Fig. 21—Typical dual-diversity antenna arrangement.

Before making a final choice of exact antenna locations it is essential to plot a path profile. A profile (plotted for 4/3 earth radius) for a typical path appears in Fig. 22 (next page). Exact prediction of components of path loss caused by horizon obstructions is difficult owing to sparseness of pertinent experimental data. However, it is suggested that useful estimates of the effects of obstruction or antenna elevation can be obtained from Fig. 3. First it is necessary to determine an appropriate value for the beam intersection angle. In the case of an obstruction, the angle between the horizontal and the radio horizon should be added to the "obstruction-free" beam intersection angle; with an elevated antenna the angle should be subtracted.

C. System Reliability

In the discussion that follows, "system reliability" will be defined as the ratio of total usable circuit time to total elapsed time. Thus, with a system reliability of 0.999, outages totaling about 8 hours per year can be expected. It is likely, of course, that the individual outages will be rather short in duration. The outages can be divided into two classes: (1) those due to propagation, and (2) those due to equipment failure. This section is concerned with calculations of the expected circuit failures due to propagation alone. The next section will discuss some of the techniques that can be used to insure high equipment reliability.

Calculations of circuit outage due to propagation require the following information: (1) path distance; (2) elevation of radio horizon above horizontal at each terminal; (3) frequency; (4) transmitter power output; (5) transmitting and receiving antenna gains;

[25] Federal Telephone and Radio Corp., "Reference data for radio engineers," 3rd Ed., American Book—Knickerbocker Press, New York, pp. 434–436; 1949.

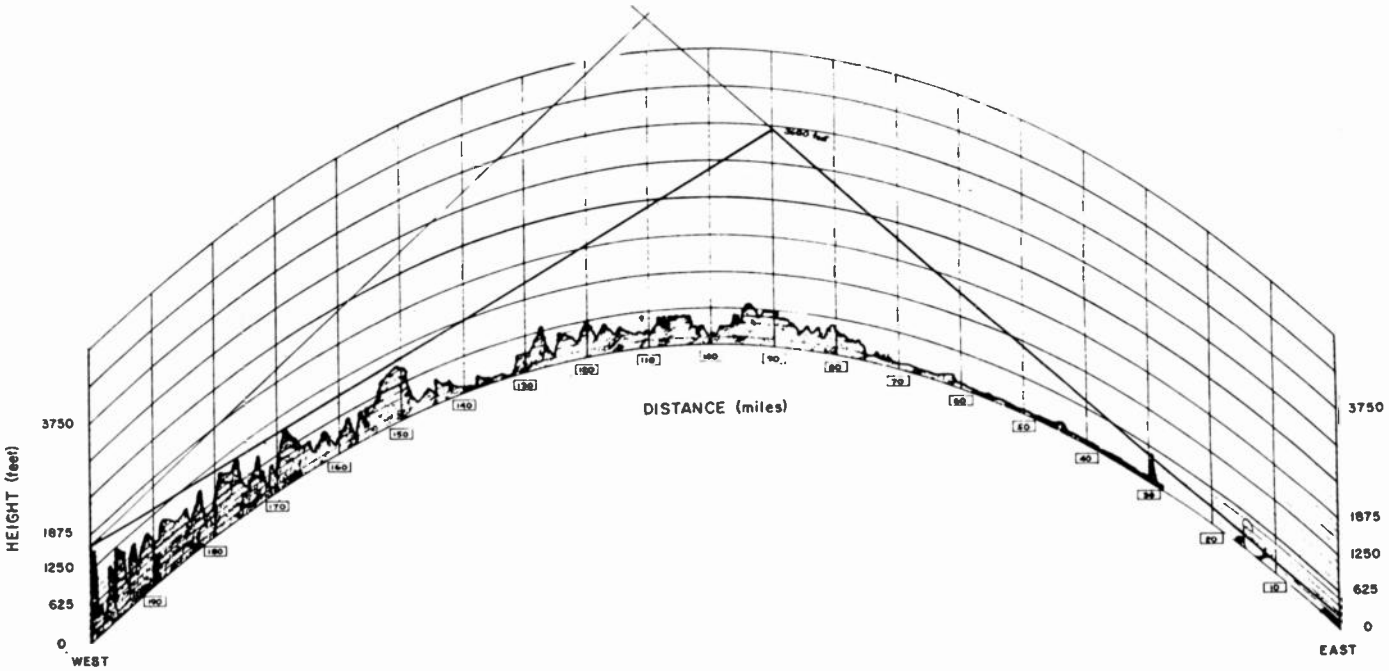

Fig. 22—Typical earth profile plot.

(6) transmission line losses; (7) diplexing filter and preselector losses; (8) receiver noise figure; (9) order and type of diversity reception used; (10) type of modulation; (11) number of channels; (12) minimum acceptable channel output signal-to-noise ratios; (13) acceptable short-term reliability.

Using the above data, the long-term reliability of a circuit may be determined with the aid of the charts given in Figs. 3 and 18. Obviously the results will be no more accurate than the propagation data. At the present time, results accurate to perhaps ± 5 db are available for paths up to 200 miles. Beyond 200 miles, the uncertainty increases due to lack of accurate propagation data, until at 400 miles it may be as great as ± 10 db. The required reliability is established by the circuit user. In order to equal average telephone toll circuit performance, long-term reliabilities of greater than 99.9 per cent are necessary. In some cases, lower reliability may be acceptable.

The design calculations for a scatter system are fundamentally those of a line-of-sight system with allowance made for the additional loss due to propagation beyond the line of sight.

In a line-of-sight system, received power is given by

$$P_R = \frac{P_T G_T A_R}{4\pi D^2} = \frac{P_T G_T G_R}{(4\pi)^2 D^2}(\lambda)^2 = \frac{P_T G_T G_R c^2}{(4\pi)^2 D^2 f^2}, \qquad (5)$$

where P_T = transmitted power in watts, P_R = received power in watts, D = distance between terminals in meters, G_T = gain of transmitting antenna over isotropic, G_R = gain of receiving antenna over isotropic, A_R = intercept area of receiving antenna in square meters, λ = wavelength in meters, f = frequency in cycles per second, and c = velocity of light meters per second. A second relation can be established which gives the approximate channel output signal-to-noise ratio as a function of the received signal power. This function varies with the modulation technique; however, a linear relation can be established for single-sideband and for FM systems operating above the threshold:

$$(S/N)_{\text{rms}} \text{ channel output} = \frac{P_R \cdot G_{FM}}{NKT^\circ \cdot B \cdot (10\sqrt{\eta})}, \qquad (6)$$

where P_R is the peak or cw received power, N is the receiver noise figure, G_{FM} is the FM improvement factor (= 1.0 for SSB) [$\simeq$(deviation ratio)^2 for FM], K is Boltzmann's constant, B is the bandwidth of one channel in cps (3,000 cps in the case of telephone circuits), η is the number of channels, and $T = 300$ degrees K.

The factor $(10\sqrt{\eta})$ is used to approximate the loading allowance for multichannel telephone systems. This relation is based on telephone-plant experience, and takes into account the peaked nature of voice signals. (It is assumed that only 25 per cent of the channels are active at any instant.)

Eqs. (5) and (6) yield a relation between the channel output signal-to-noise ratios and the other parameters:

$$S/N_{\text{rms}} \text{ at channel output} = \frac{P_T \cdot G_T \cdot G_{FM} \cdot G_R \cdot c^2}{(4\pi)^2 D^2 \cdot N \cdot K \cdot T \cdot B(10\sqrt{n}) f^2}. \qquad (7)$$

In order to apply (7) to scatter systems, it is necessary to introduce additional terms to account for the beyond-the-horizon loss. As mentioned above, the propagation loss varies about a median value. This variation can be divided into fast-fading and long-term changes in the median loss below free space.

A modification for fast fading and for the benefits of diversity reception can be made by means of the data of Fig. 20. This graph shows the extra margin required for arbitrary short-term reliabilities (assuming Rayleigh fading) for the different diversity systems. For voice operation, adequate performance can be achieved with 99 per cent short-term reliability. When the fast-fading correction is introduced into (7), one obtains

$$\text{channel output signal-to-noise ratio exceeded 99 per cent of time} = \frac{P_T G_T G_R G_{FM} c^2}{(4\pi)^2 D^2 N \cdot B \cdot KT^3 (10\sqrt{\eta}) f^2} \times \kappa, \qquad (8)$$

where

$$\kappa = \frac{\text{signal level exceeded 99 per cent of time}}{\text{median signal level}}$$

(short-term fading correction).

The ratio of (8) to the minimum acceptable signal-to-noise ratio is the margin of the system over free space:

$$M \cong \frac{P_T G_T G_R G_{FM} c^2}{(4\pi)^2 D^2 N \cdot B \cdot KT (10\sqrt{\eta}) f^2 (S_0/N_0)} \times \kappa, \qquad (9)$$

where

$(S_0/N_0 =$ minimum acceptable channel output signal-to-noise ratio.

For an assumed transmitter power this gives the system margin available to compensate for the scatter-propagation loss.

The long-term reliability of the system may now be determined by reference to Fig. 3. This graph shows the loss below free space that is exceeded for different percentages of time. Using the path length (in miles) and the margin factor M (in db) from (9), it is possible to determine the per cent outage time that can be expected over extended periods.

The use of (9) can be greatly facilitated by expressing the factors in decibels.

$$M_{db} = 120 + 10\log_{10} P_T + 10\log_{10} G_T + 10\log_{10} G_R + 20\log_{10}\delta - 10\log_{10}\kappa - 20\log_{10} D - \log_{10} N - 5\log_{10}\eta - 20\log_{10} f - 10\log_{10} S_0/N_0, \qquad (10)$$

where the constant (120) includes K, T, channel bandwidth, and numerous conversion factors, G_T and G_R are the appropriate antenna gains reduced by the losses in transmission lines and diplexers, and those due to excessive antenna aperture (see Fig. 8), $\delta =$ FM deviation ratio, $D =$ distance in statute miles, and $f =$ frequency in megacycles per second.

The minimum acceptable average channel output signal-to-noise ratio is dependent upon the specified circuit quality. Quite often this minimum is set by the threshold point of the FM system. For FM systems having 50 to 100 voice channels and deviation ratios of 2.0, the average channel signal-to-noise ratio will be about 22 db (see Fig. 12). Due to the peaked nature of the voice signals, the peak signal-to-noise ratio will be around 32 db. If compandors are used on each voice channel, an additional improvement of at least 15 db can be achieved.

An example of the use of (10) in estimating the reliability of a typical long-range scatter system is given below.

10-kw transmitter output (referred to 1 w)	+40 db
28-foot paraboloidal transmitting antenna at 1,000 mcps	+36 db
transmission-line, diplexer, and antenna-aperture losses	−2 db
28-foot paraboloidal receiving antenna at 1,000 mcps	+36 db
same losses as transmitting antenna	−2 db
FM gain for deviation ratio of 2.0	+6 db
Proportionality constant	+120 db
Short-term fading allowance assuming dual combiner diversity and 99 per cent short-term reliability	−6 db
150-mile path distance	−44 db
Receiver noise figure	−8 db
50 telephone channels	−8 db
Frequency 1,000 mcps	−60 db
Minimum acceptable channel signal-to-noise ratio	−22 db
M db = Margin above free space:	+86 db
Long-term reliability at 150 miles (see Fig. 3)	99.9 per cent

D. Equipment Reliability

On the basis of present knowledge and recent experience it is now possible to design uhf scatter communication circuits which will have a very high degree of reliability. Our experience has shown that over-all system reliability tends to be governed by equipment reliability rather than by propagation difficulties.

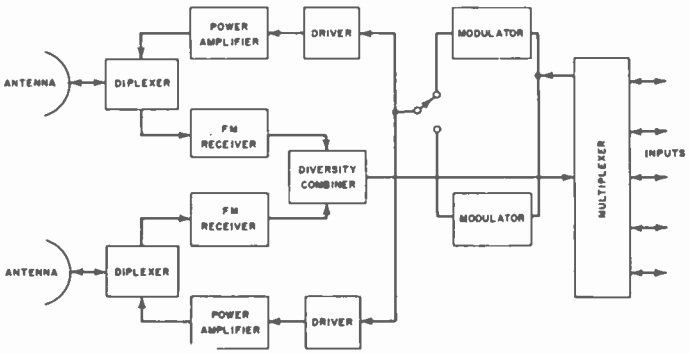

Fig. 23—Scatter uhf terminal.

It is common practice to employ spare equipment to achieve an increase in equipment reliability. In theory two sets of equipment each of 99 per cent reliability could together achieve a reliability of 99.99 per cent. However, the usual method of employing a set of standby spare equipment often fails to achieve this desired improvement because of the problems of automatically detecting a failure and rapidly performing the necessary switching operations. The switching problem is particularly difficult where high-power levels are involved.

A more desirable sparing technique is one that employs both regular and spare equipments simultaneously in a fashion such that the failure of either one would not

materially affect the operation of the circuit. This technique has the further advantage that the two systems can be tied together at various points to achieve an even higher reliability.

Fig. 23 (previous page) shows an arrangement of equipment for a beyond-the-horizon system in which the paralleling sparing technique is employed. The single sideband multiplex equipment is not spared since it normally has considerably greater reliability than other units. The baseband signals from the multiplexer drive two modulator units. Unfortunately, it is not possible to parallel the modulator units when frequency modulation is used and a switching arrangement is required at the modulator outputs. The operating modulator output is used to drive two power amplifiers. The amplifier outputs feed two antennas which are separated for space diversity reception. This technique is feasible because the fine lobe structure of the radiation pattern resulting from the two separated antennas is not preserved in beyond-the-horizon propagation. The receiving terminal employs space diversity reception with separate receivers and diversity combining units. The combined outputs of the various sections of the receiving system are fed to the multiplexer. With this arrangement, it is possible to maintain uninterrupted operation even though several sections of the system may fail. For instance, operation is possible with the loss of one transmitter, exciter, modulator, antenna, and receiver.

Diversity Reception in UHF Long-Range Communications*

C. L. MACK†

Summary—**Several diversity techniques employed in uhf beyond-the-horizon systems are discussed. Field experience is evaluated in terms of equipment reliability, flexibility and performance.**

A nonswitching parallel combiner has become the standard military diversity circuit for uhf long-range receivers. The circuit is described and analyzed.

Introduction

ONE OF THE characteristic properties of long-range UHF communication circuits is a random, time-variant circuit loss. The nature of this randomly varying loss is illustrated by Figs. 1 and 2 in which the distribution of hourly median signal levels throughout a year can be seen to cover a range of sixty decibels in the region of interest, while the distribution within the hour (rapid fading distribution) can extend over a 36-decibel range from the 99.9 per cent value.

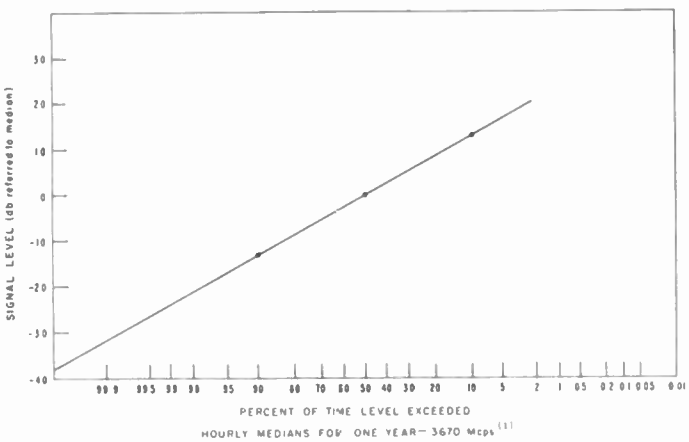

Fig. 1

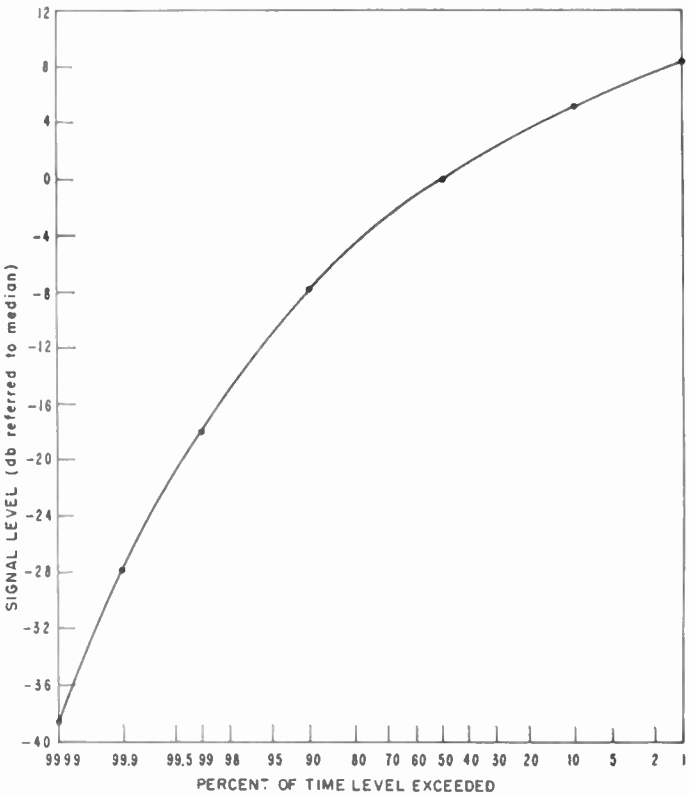

Fig. 2—Short-term Rayleigh distribution.

* Original manuscript received by the IRE, August 8, 1955. The research in this document was supported jointly by the Army, Navy, and Air Force under contract with the Massachusetts Institute of Technology.

† Lincoln Laboratory, Mass. Inst. Tech., Lexington, Mass.

The latter curve indicates that a circuit providing a median rf signal-to-noise ratio of 10 decibels can be totally inoperative for a total of 4 minutes out of an hour. A diversity system reduces the effect of random fading by employing two or more communication circuits in which the individual fading is independent or uncorrelated, and by providing a means of extracting the best signal from the group. A variety of criteria have been employed in combining the signals from the various circuits. The simplest basis on which selection can be made is merely to select that channel which has the best signal-to-noise ratio. The probability of finding low rf levels on all of the antennas at the same time becomes vanishingly small as the probability of finding a low level on one antenna becomes small. This can easily be assessed quantitatively in the case of a Rayleigh distribution in the following manner.

The fraction of the time during which a signal is equal to or less than some value x is given by

$$f(x) = \int_0^x \frac{2x_1}{\bar{x}^2} e^{-x_1^2/\bar{x}^2} dx_1 = 1 - e^{-x^2/\bar{x}^2}, \quad 0 \leqq x < \infty, \quad (1)$$

for the normalized Rayleigh distribution, where $\bar{x}^2 =$ 2nd moment of the distribution

For n uncorrelated signal levels, the fraction of time during which all n signals are simultaneously below the level x is

$$f^n(x) = (1 - e^{-x^2/\bar{x}^2})^n, \quad (2)$$

where n is the order of diversity.

Plotting x in decibels referred to the median value, and $(1-f^n(x))$ in per cent, generates the solid curves in Fig. 3. Starting with a log normal distribution and repeating the steps in (1) and (2) results in the dashed curves shown in Fig. 3. A discussion of the distributions obtained experimentally over a specific path can be found in another paper included in this issue.[1]

These results were based on the assumption that the correlation between the signal levels is negligible. This condition is relatively easy to satisfy (at least in space diversity). The correlation coefficients between two antennas with a vertical separation of 22 wavelengths ranges from less than 0.1 to a maximum of 0.34 as measured on paths as short as 72 miles.

These coefficients are measured when fading conditions exist; the nonfading correlation coefficient is necessarily unity. For a correlation coefficient of 0.34, the error in the curves of Fig. 3 is at most 5 per cent. Experiments relating correlation coefficient, geometry and median signal level are in progress.

Diversity Techniques

The separable parameters which could theoretically be exploited to produce a diversity system include:

1. Path Geometry
2. Frequency
3. Time
4. Polarization

1. Diversification of path geometry (spaced antennas) is the only technique that has been utilized extensively in uhf long-range circuits.

2. The short-term signal strength correlation between different frequencies on the same path has not been studied comprehensively, but data obtained by Von Beyer[2] on frequency selective fading indicate a fairly rapid loss of correlation with dropping signal level, indicating that frequency diversity can be accomplished within a quite reasonable spectrum. The frequency allocator may look askance at the notion since he must find twice as many frequencies in a crowded spectrum to assign to such a circuit, but there are many areas of the world in which this presents no insurmountable problem.

3. Time diversity is only attractive in digital systems such as radio teletype, therefore no use has been made of this technique in uhf systems to date.

4. Data taken on existing circuits show substantial correlation between vertically and horizontally polarized signal strengths even at low levels. Diversity applications therefore look unpromising.

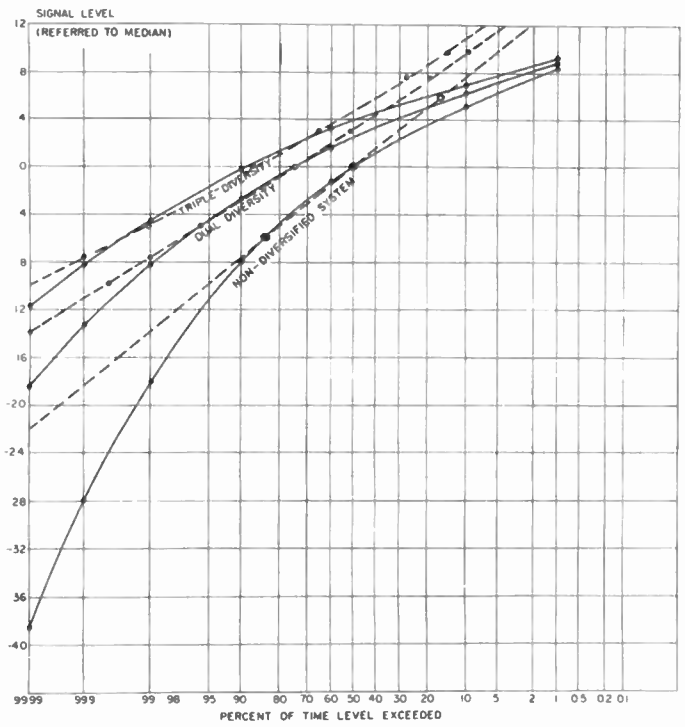

Fig. 3—Signal level distribution vs order of diversity.

Space Diversity Reception

Since information concerning the instantaneous path loss is only available at the receiving terminal, space

[1] J. H. Chisholm, P. A. Portmann, J. T. de Bettencourt, and J. R. Roche, "Investigations of angular scattering and multipath properties of tropospheric propagation of short radio waves beyond the horizon," Proc. IRE, p. 1317; this issue.

[2] Hans Von Beyer, Chief Engineer, Systems Engineering Group, RCAF, Ottawa, Canada. Private communication.

diversity usually involves the use of suitably separated receiving antennas providing two or more geometrically distinct paths. To provide a basis for selection of the best path, one must measure the instantaneous path loss.

The usual criterion for quality in a modulated received signal is the signal-to-noise ratio after demodulation. In a frequency modulation system operating above the threshold, the signal level in the baseband is a function of the deviation and is invariant with rf signal level. The comparison of signal-to-noise ratio between receivers is therefore a function of the noise power alone. Measurement of the IF signal in the receiver is not an accurate criterion of the signal-to-noise ratio, since the gains of the various amplifier stages will drift with time. Furthermore, a change in receiver noise figure is often not reflected in a change in the IF signal level or magnitude of the avc voltage. For this reason, the criterion for quality of received signal employed in the systems described in this paper is the noise power present in the baseband. In the diversity switches themselves, the modulating signals are rejected by a high-pass filter and the remaining noise spectrum above the intelligence band integrated and measured. This technique is readily applicable to frequency modulated systems, where the available baseband noise spectrum is several times greater than the usable modulation spectrum. In a simple AM system, however, the signal is a function of the rf level being received and the noise is generally constant (at the frequencies under consideration). However, fast acting automatic gain control circuits are normally employed which, at least for the demodulated signal, restore the condition existing in FM receivers, viz., a baseband signal which has very nearly the same level at the output of each receiver, but a noise which varies inversely with the RF signal level. The out-of-band noise is then extracted after the automatic gain controlled stages but ahead of the selective intermediate frequency stages which are designed to pass only the modulation spectrum.

The question yet to be answered concerns the minimum bandwidth of the noise spectrum which can be used for this purpose. In FM systems this is hardly a problem, but in AM systems any additional spectrum required by the noise control circuit means greater "guard bands" between frequency assignments. In anticipation of the crowded conditions in the "tropospheric communications spectrum" this question is receiving careful attention.

The space diversity techniques reported on here can be grouped as follows:

1. Antenna switching
2. Receiver switching
3. Signal Combination

Antenna Switching

The first diversity scheme employed on a uhf long-range circuit was of the antenna switching type shown in Fig. 4(a). This scheme employs only one receiver whose baseband noise (exclusive of the modulation band) is monitored by a decision element controlling the plate supply to each of two front ends. Spaced antennas are connected to the fron tends and their outputs, when chosen, are fed to the IF amplifier, limiter, discriminator, and baseband amplifier. When the quality of the signal received on one antenna falls below a preset threshold, the switch turns off its corresponding front end and energizes the other. Depending upon the relationship between the threshold and the median signal level at the time, it is more or less probable that the second antenna is receiving a signal which is above threshold. If, however, this signal is also unacceptable, the switch contrives to select alternate antennas until the threshold is again exceeded. The speed with which this function can be performed is ordinarily limited only by the receiver's speed of response and was normally adjusted to approximately 60 microseconds for a receiver with a modulation bandwidth of 25 kilocycles.

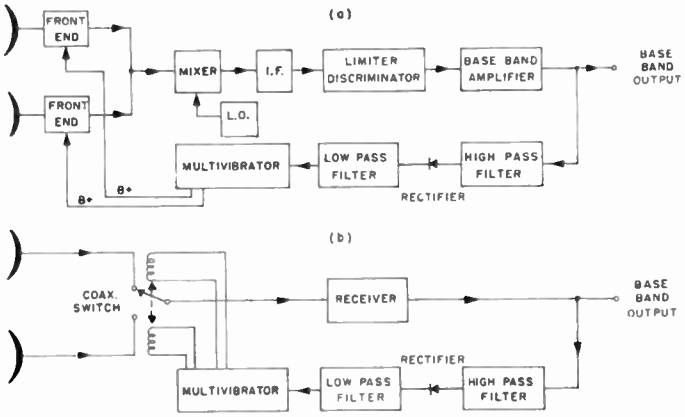

Fig. 4—Antenna switching.

Sometimes switching speed is not of prime importance (e.g., a single voice circuit). In this case very simple rf relays may be employed. Figure 4(b) shows an antenna switching system which utilizes electromechanical relays. A dual diversity switch of this type having a time constant of less than a millisecond and less than one-half decibel insertion loss at 2,000 mc has been bench tested. Excellent coaxial relays are in production which make it possible to increase the number of antennas participating in such a scheme to four or six with comparable speed and performance.

The advantage gained by a diversity system depends, to a certain extent, on the modulation technique employed. In bandwidth exchange systems such as pulse modulation and frequency modulation, the quality of received signals is generally totally acceptable above a sharp threshold level, and essentially useless below threshold. In such systems if the switching threshold is set to correspond to the receiver threshold, the gain in usable communication time afforded by antenna switching diversity is equal to that of the more elaborate schemes to be described. In AM systems, other forms of diversity provide more usable communication

time. The disadvantages of antenna switching are difficult to compute. The most serious is that the scheme will make no attempt to take advantage of a better signal-to-noise on an inactive antenna until the threshold has been reached on the active antenna, a shortcoming which is aggravated by the increased likelihood of better signals on alternate antennas as the active antenna level fades below the median signal level. Another is the time wasted in sequential search for a suprathreshold signal, whereas a more knowledgeable system, e.g., receiver switching, would immediately select the best available signal without random search. A disadvantage of importance in high reliability circuits is the "Achilles heel" imposed by the use of a single receiver, a failure of which interrupts the circuit until spare equipment can be activated or the original repaired.

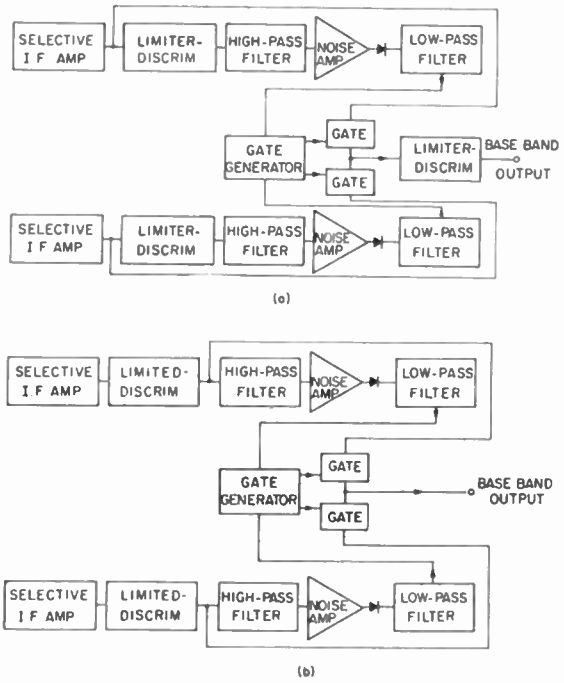

Fig. 5—Receiver switching. (a) IF switching, (b) audio switching.

Receiver Switching

Two forms of receiver switching have been employed and they are illustrated in Fig. 5. In system (a), the IF output of the receiver having the higher signal-to-noise ratio is switched into a common detector; in (b) the baseband output of the favored receiver is switched on the output line. As in the previous system, the out-of-band noise is rectified, integrated and measured to provide an evaluation of the signal quality. In the IF switching system additional demodulators must be provided with each receiver for this purpose. The statistics governing the net RF signal level enjoyed in such a system are illustrated by the curves in Fig. 3.

Receiver baseband switching is plagued with a variety of technical problems concerning the transients produced at the instant of switching. (1) Changes in gain of the baseband amplifiers or drift in the slope of the discriminators will cause sharp transients when the outputs are switched. (2) Abrupt changes in the dc levels of the gate tubes at the instant of switching cause pulse type transients. (3) Drift in dc gating levels causes overlapping, which, in baseband switching, gives rise to abrupt 6 db changes in level during the switching period.

Switching the IF of FM receivers, however, makes possible a significant improvement in this respect. The limiters and discriminators of the receivers have already been designed to overcome multipath distortion and thus have extremely large bandwidths. The problems represented by (1) and (3) are thereby diminished. The DC transient is much more easily eliminated by making use of the circuit shown in Fig. 6. The gate tubes are switched complementarily into a common load along the linear portion of the i_p vs e_{g^3} curve of the 6AS6. A difference in gain of 10 db can be obtained in this region and is quite sufficient to provide switching in an FM receiver. This is true because of the capture properties of the demodulator and the fact that the "on" signal is always higher or at least equal to the "off" signal. In this arrangement the current through the load is held constant during the switching operation, the only change being in the tube "modulating" it.

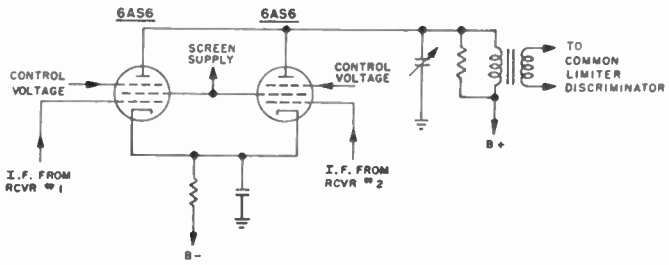

Fig. 6—Gate circuit. IF switching.

Such switches are free of switching transients as long as the frequency stability of the transmitter and local oscillator is adequate. This precaution is necessitated by the fact that a drift in the intermediate frequency is reflected in a DC bias of the discriminator. As the switching takes place, this bias will begin to fall toward the center and then will snap back to the value dictated by the offset IF. The result is a spike whose amplitude, compared with a fully modulated signal, is approximately the ratio of the offset frequency to the peak deviation of the system. In at least one instance the effects of frequency stability have been minimized by advancing the rate at which the newly selected signal is switched in, striking a compromise between dc and frequency offset transients.

Sensitivities of the order of 0.25 db and over-all speeds greater than 100 kc are readily obtained but are never used in practice because such a switch is at the mercy of noise spikes that occur in increasing numbers near the threshold of the receiver. Such spikes cause the switch to "chatter" at the crossover point, more than negating the advantages of the increased speed and

sensitivity. Operational systems are usually designed with a sensitivity of one decibel (differential) and a noise sampling time constant of from 2 to 5 milliseconds. The time constant of the actual switching operation is ordinarily ten microseconds or less—depending upon the intermediate frequency employed.

Signal Combination Diversity

The schemes discussed to this point are characterized by total rejection of alternate signals in favor of one particular signal being received at a given instant of time. It has been pointed out by Kahn[3] that this is a wasteful procedure. If one undertakes to combine all of the signals received in a diversity system, the net signal-to-noise ratio afforded by suitable post-detection combination is better than that of the best individual signal.

Explicitly, optimum combination provides

$$P = \sum_{i=1}^{n} p_i, \tag{3}$$

where P = combined output signal/noise power ratio, p_i = output signal-to-noise power ratio of receiver i, and n = order of diversity employed.

Eq. (3) is proved in theorem form in a letter by D. G. Brennan.[4] The reason such enhancement of signal/noise occurs is best seen by a comparison of equations (3) and (4) of Brennan's note.

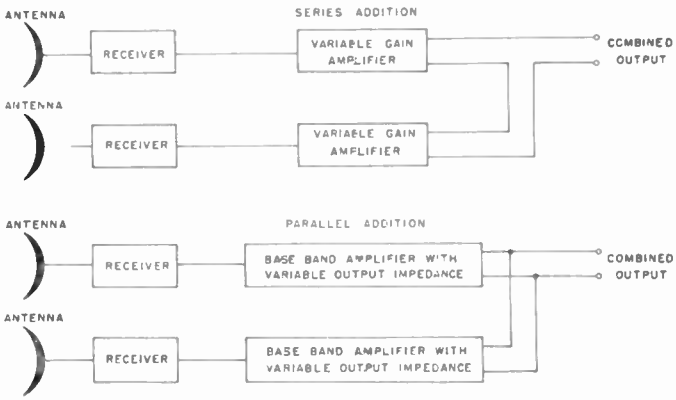

Fig. 7—Signal combination schemes.

Kahn accomplishes optimum signal combination by the "series addition" technique illustrated in Fig. 7. The gains of the output amplifiers are varied in accordance with the received signal levels and their outputs are added in series. Unfortunately, the agc amplifiers must have a large dynamic range and a highly linear transfer function throughout the range in order to meet the requirements of multichannel uhf systems. Furthermore, due to the fluctuations in combined output level, a high performance agc amplifier must be employed between the combined output terminals and the channeling equipment.

The technique developed by Lincoln Laboratory avoids the distortion and regulation problems of series addition by combining the output currents of several receivers instead of the output voltages. As illustrated in Fig. 7, the baseband amplifiers are provided with variable output impedances and are connected to a common load. It will be seen in the following analysis that the output level does not fluctuate, no specialized common equipment is required, and the linearity with which combination is effected is of a very high order.

Fig. 8 is the equivalent circuit of an "n-order" diversity system in which the receiver outputs are connected in parallel, where e_i = instantaneous output voltage of receiver #i, R_i = output impedance of receiver #i, and e_0 = output voltage of the n-order combiner. Let

$$e_i = s_i(t) + n_i(t), \tag{4}$$

where $s_i(t)$ is the signal voltage component of the output of receiver #i and $n_i(t)$ is the noise voltage component of the output of receiver #i.

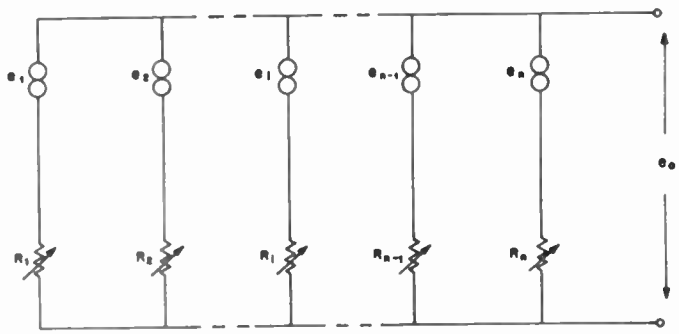

Fig. 8

In an FM receiver, $s_i(t)$ depends exclusively on the frequency variation of the transmitted carrier and can therefore be expected to be identical in the output of each receiver (within reasonable limits). In an AM receiver, a good deal of trouble is taken with automatic gain control circuits to achieve the same result. Consequently, it is reasonable to write

$$e_i = s(t) + n_i(t). \tag{5}$$

The analysis of the circuit illustrated in Fig. 8 can be conceptually separated into two parts: (1) that pertaining to the coherent demodulated signals, and (2) that pertaining to the random noise components of the individual receiver outputs.

Signal Response

Keeping in mind that the instantaneous signal voltages, $s(t)$, are equal in amplitude and phase, it is seen that no signal current flows in any of the branches of the circuit in Fig. 8. The signal component of the output voltage, e_0, is therefore completely independent of the various values taken on by the R_i's and is, in fact, just

[3] L. Kahn, "Ratio squarer," Proc. IRE, vol. 42, p. 1704; November, 1954.

[4] D. G. Brennan, "On the maximum signal-to-noise ratio realizable from several noisy signals," p. 1530; this issue.

equal to $s(t)$. There is therefore no output level regulation problem to be anticipated when this form of diversity combiner is employed. Of course, the imposition of a passive load at the output terminals whose impedance is comparable to the net shunt impedance of the R_i's, would lead to severe output fluctuation as the R_i's were caused to vary. However, it will be seen that the provision of a load impedance which is at all times very large compared to the net shunt impedance of the generators is no problem up to several megacycles of bandwidth of $s(t)$.

Noise Response

Since the signal output is unaffected by the parallel combination illustrated in Fig. 8, and since the rms noise voltages in the various generator outputs are expected to rise and fall with the RF signal levels being received, it is reasonable to expect that it is the resultant *noise* component of the output signal e_0 that we shall attempt to minimize by varying receiver output impedances R_i.

The least arduous method of deriving the proper impedance function is to make use of the "optimizing" coefficient contained in Brennan's general theorem.[4] The optimum performance indicated in (3) will be realized if a_i is made equal to $\sqrt{\overline{s_i^2}}/\overline{n_i^2}$, where

$$e_0(t) = \sum a_i s_i(t) + \sum a_i n_i(t). \tag{6}$$

A close look at Fig. 8 reveals that the amount of noise contributed to e_0 by each noise source, n_i, will depend upon (1) the series impedance of the source, and (2) the load impedance represented by the parallel combination of the other R_i's in the circuit. Explicitly,

$$e_0 = s(t) + \sum_{i=1}^{n} c_i n_i(t), \tag{7}$$

where

$$c_i = \frac{\text{shunt impedance}}{\text{series impedance} + \text{shunt impedance}}.$$

The shunt impedance involved in c_i can be written

$$\frac{1}{\sum_{j\neq i}^{n} 1/R_j} = \frac{\prod_{j\neq i}^{n} R_j}{\sum_{k\neq i}^{n} \prod_{j\neq i, j\neq k}^{n} R_j}, \tag{8}$$

which gives

$$c_i = \frac{\dfrac{\prod_{j\neq i}^{n} R_j}{\sum_{k\neq i}^{n} \prod_{j\neq i, j\neq k}^{n} R_j}}{R_i + \dfrac{\prod_{j\neq i}^{n} R_j}{\sum_{k\neq i}^{n} \prod_{j\neq i, j\neq k}^{n} R_j}}, \tag{9}$$

or

$$c_i = \frac{\prod_{j\neq i}^{n} R_j}{R_i \sum_{k\neq i}^{n} \prod_{j\neq i, j\neq k}^{n} R_j + \prod_{j\neq i}^{n} R_j}. \tag{10}$$

The denominator in (10) can be condensed as follows:

$$R_i \sum_{k\neq i}^{n} \prod_{j\neq i, j\neq k}^{n} R_j + \prod_{j\neq i}^{n} R_j = \sum_{k\neq i}^{n} \prod_{j\neq k}^{n} R_j + \prod_{j\neq i}^{n} R_j = \sum_{k=1}^{n} \prod_{j\neq k}^{n} R_j. \tag{11}$$

Thus, from (10) and (11),

$$c_i = \frac{\prod_{j\neq i}^{n} R_j}{\sum_{k=1}^{n} \prod_{j\neq k}^{n} R_j} = \frac{1}{\sum_{j=1}^{n} \frac{R_i}{R_j}} = \frac{1}{R_i \sum_{j=1}^{n} 1/R_j}, \tag{12}$$

but $\sum_{j=1}^{n} 1/R_j$, being independent of i, will appear in all c_i and can be treated as a scale factor, $1/c_0$. Thus,

$$c_i = \frac{c_0}{R_i}. \tag{13}$$

To provide optimum combination, this expression must be identical with

$$a_i = \sqrt{\overline{s_i^2}}/\overline{n_i^2}, \tag{14}$$

except for a possible scale factor.

Let $\sqrt{\overline{s_i^2}} = \sqrt{\overline{s^2}} = a_0$, a constant. Then,

$$c_i = \frac{c_0}{R_i} = \frac{a_0}{\overline{n_i^2}}, \tag{15}$$

or

$$R_i = \frac{c_0}{a_0} \overline{n_i^2}, \tag{16}$$

which is the proper relationship between R_i and $\overline{n_i^2}$ to yield maximum net signal-to-noise ratio as given by (3).

Eq. (16) is usually written

$$R_i = \frac{R_0}{\overline{n_0^2}} \overline{n_i^2}, \tag{17}$$

where R_0 = minimum value of receiver output impedance, and $\overline{n_0^2}$ = minimum value taken on by rms noise (generally the modulator noise, local oscillator noise, incidental FM, etc.).

The output impedance of the receiver is thus made to increase in direct proportion to noise power in its demodulated output. An intuitive feeling for the scheme is afforded by appealing to the notion of minimizing net noise power transferred to combined output terminals.

A worth-while analogy exists between a combiner of this sort and an antenna. If the area of the antenna is doubled, the received signal (and thus the demodulated

signal-to-noise ratio) is increased 3 db. This will hold true as long as the RF is spatially correlated over the area of the antenna. When the antenna has grown so large that spatial correlation of the received RF no longer extends over its dimensions, the point of diminishing returns is reached. On the other hand, the spatial correlation of the much lower frequency base band signal still obtains and can be used in a combiner to provide an enhancement of the net signal-to-noise ratio. Indeed the improvement in signal-to-noise ratio obtained when the individual signal-to-noise ratios are very nearly the same is 3 db for dual combination, 4.8 db for triple combination, etc. The statistical improvement of net signal-to-noise ratio compared to the *best* individual signal-to-noise ratio is shown in Fig. 9

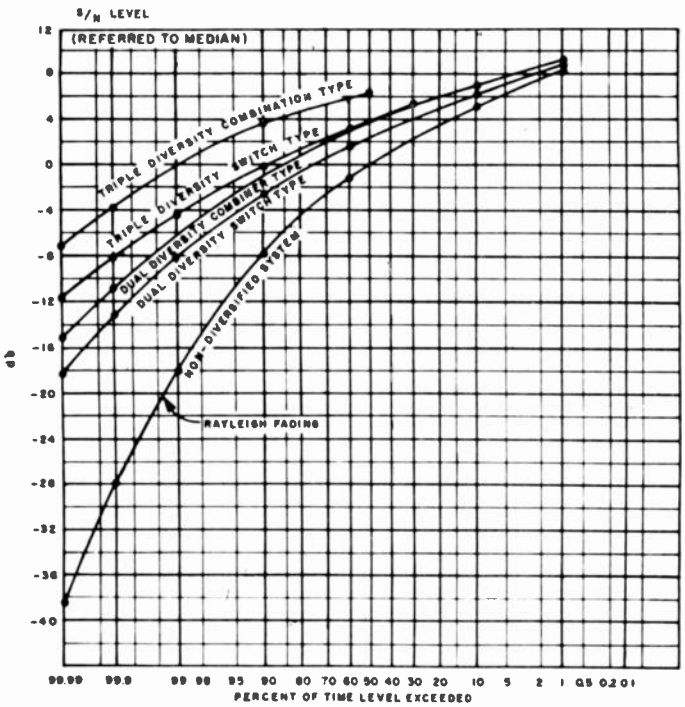

Fig. 9—s/n distribution vs order of diversity.

for the dual and triple diversity cases. The combiner curves were obtained by graphical integration based on (3). It can be seen that when the signals are quite low, and therefore when any obtainable improvement is highly desirable, the improvement approaches the maximum predictable from (3). In this sense, then, the addition of another receiving antenna; i.e., the doubling of the available receiving antenna area, provides virtually the same gain in net signal-to-noise ratio as would have been the case in a coherent RF field.

Common Cathode Combiner

One of the many ways in which the output impedance of an amplifier can be varied electronically is shown in Fig. 10. The baseband voltage is applied to the grid of a cathode follower whose bias is controlled by the integrated out-of-band noise. As the noise level rises in the baseband, the out-of-band noise will cause a gradual biasing of the cathode follower with attendant rise in the output impedance seen by e_g. The impedance looking in at the terminals AB can never exceed R_k, but we shall see that this does not materially affect the performance of the combining circuit.

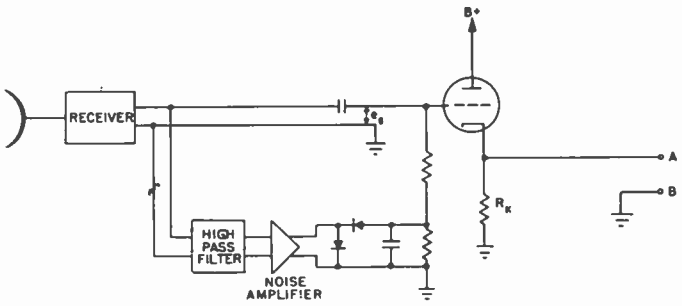

Fig. 10

The most elegant form of the parallel combiner employed to date was suggested by Day and Gruber.[5] Each receiver employs a cathode follower output to which the integrated noise is applied as a bias voltage. The cathode is returned to a large negative voltage and the outputs are connected together without blocking condensers. The technique of returning the cathode to a negative voltage through a large resistor is known as cathode stabilization. It is generally employed to stabilize the gain of a tube by providing a large amount of dc feedback around it. If tube aging or the effect of other components in the circuit tend to change the cathode current of the tube, the large change in cathode bias quickly restores the original current. Since the transconductance of a tube depends, more than anything else, on this one parameter (assuming mechanical stability), the gain of an amplifier and the output impedance of a cathode follower are thereby held constant.

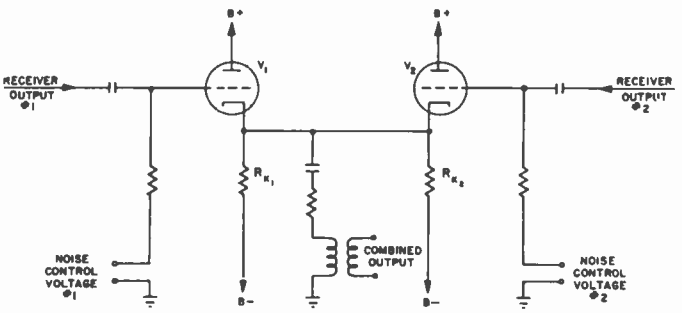

Fig. 11

A dual diversity arrangement is shown in Fig. 11. Since there is no dc isolation between the two cathodes, the *total* plate current $i_{p_1}+i_{p_2}$ will be essentially equal to $B-/R_k'$ where R_k' is the resistance of R_{k_1} and R_{k_2} in parallel. This will remain true no matter what values are taken on by the individual bias voltages (noise control voltages). Consequently, the net output impedance of V_1 and V_2 in parallel is a constant, although their individual output impedances may vary over a considerable range. The analysis of the circuit is again simplified by treating the signal case independent of the noise case.

[5] J. Day and P. Gruber, Radio Engrg. Labs., Long Island City, N. Y. Private communication.

Signal Response

The three major design aims in regard to signal behavior are, (1) Flat frequency response at all times, (2) No fluctuation in signal output as bias voltages vary, (3) Distortion less than one-tenth per cent under all conditions.

It is highly desirable that the design aims be met under conditions of signal imbalance from one receiver to the other. This imbalance can take the form of differences in amplitude or in phase; however, for the bandwidths treated to date, amplitude imbalance only is anticipated. A certain amount of tolerance to this imbalance will eliminate the need for automatic level regulators which would increase the complexity (and therefore the vulnerability) of a combiner system.

When there is no imbalance; i.e., when the signal inputs to V_1 and V_2 in Fig. 11 are identical, the entire system can be treated as a single cathode follower output stage whose transconductance is approximately twice the zero grid bias transconductance of one side. When one tube is in the process of being cut off due to an increase in the noise level of its output, it would at first appear that distortion may result. That this is not the case can be seen in the "black-box" experiment of Fig. 12.

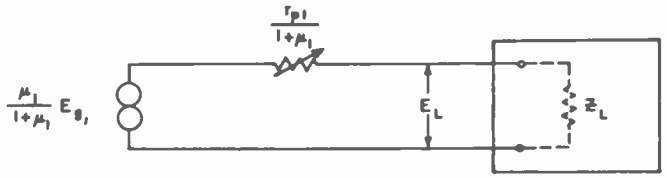

Fig. 12

The equivalent circuit of the tube being cut off is represented as a voltage generator and a series resistance looking into the load presented by the common cathode circuit of Fig. 11. As the transconductance of V_1 is reduced, that of V_2 is actually increased from an already high value and the voltage in the load, E_L, remains the same even though the series resistance of Fig. 12 is increased to that of complete cutoff. Consequently, Z_L is infinite to all intents and purposes, and the cathode follower, V_1, never enters the nonlinear portion of its operating characteristic. Another way of looking at it is to note that the initial ac voltage between the grid and cathode of V_1 will not increase as V_1 is cut off. Thus, even though it is biased into a very nonlinear portion of the curve, negligible distortion will be generated in its output. With an imbalance in the signal levels driving the two cathode followers, the situation illustrated in Fig. 12 is altered somewhat. Defining the ratio of grid drive on tube V_1 to that on V_2 as ρ, where ρ is not equal to unity, it is seen that the semi-static operating point previously enjoyed is now moving at the baseband frequency over a range given by

$$|\Delta e| \doteq |(\rho - 1)e_{g_1}|. \tag{18}$$

This variation in position of the operating point will be on an increasingly nonlinear portion of the curve as the tube is biased off. On the other hand, the magnitude of the series resistance in Fig. 12, $r_p/1+\mu_1$, will have increased, while the magnitude of Z_L for this "unbucked" portion of the voltage will be very low (of the order of 100 ohms since the plate current denied V_1 now flows in V_2 raising its transconductance to something of the order of 10^{-2} mho). The resulting voltage division permits a rather generous imbalance in receiver output (>5 per cent) before distortion exceeds 0.1 per cent.

Frequency response enjoyed is that of a single cathode follower of 20,000 micromhos net transconductance feeding a passive load of several thousand ohms.

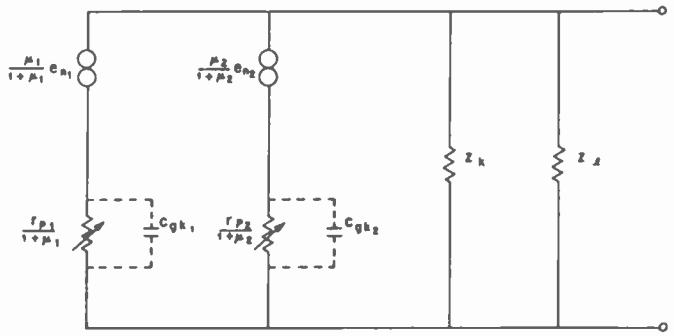

Fig. 13

Noise Response

As in the discussion pertaining to Fig. 8, the "noise generators" can be separated into a pair of independent voltage sources attached to a common load through voltage dividers. The circuit shown in Fig. 13 is the equivalent circuit for the noise inputs, where e_{n_1} and e_{n_2} are the noise voltage outputs of receivers #1 and #2 respectively which are applied to the grids of their output cathode followers. It is seen that the noise from receiver #1 that appears in the output can be written

$$\left(\text{assuming } Z_k, Z_l \gg \frac{1}{g_{m_1} + g_{m_2}}\right)$$

as

$$e_{n_1 \text{ load}} = \frac{\dfrac{r_{p_2}}{1+\mu_2}}{\dfrac{r_{p_1}}{1+\mu_1} + \dfrac{r_{p_2}}{1+\mu_2}} \cdot \frac{\mu_1}{1+\mu_1} e_{n_1}, \tag{19}$$

neglecting distributed capacitance for the time being.

Considering the attenuation of e_{n_1} as it becomes significantly greater than e_{n_2}, we can simplify (19) by writing

$$\frac{r_{p_2}}{1+\mu_2} \doteq \frac{1}{g_{m_2}}.$$

Then,

$$e_{n_1 \text{ load}} = \frac{e_{n_1}}{1 + \dfrac{g_{m_2}}{g_{m_1}} + \dfrac{1}{\mu_1}}, \tag{20}$$

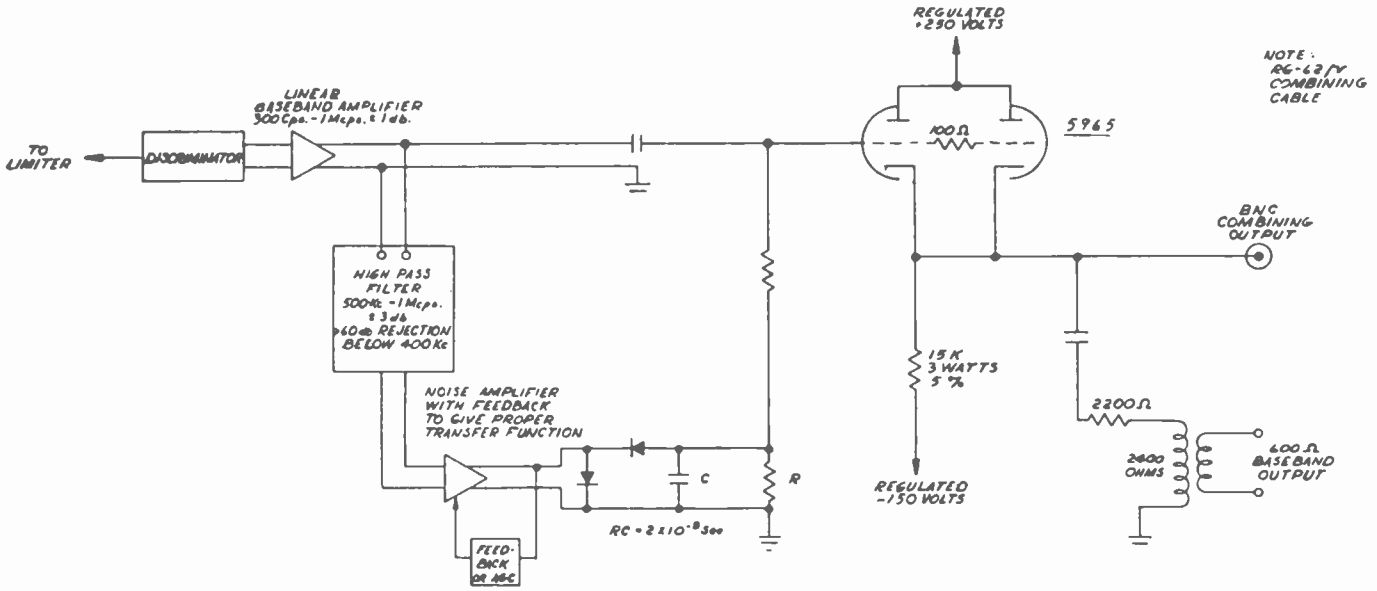

Fig. 14

which provides attenuation well in excess of 80 decibels for low and medium frequencies.

As the modulation spectrum extends well above 100 kilocycles, however, the grid-cathode capacitance sets an upper limit to the value of the series impedance. The maximum achievable attenuation then depends entirely on the maximum transconductance of the tube supplying the shunt impedance of the voltage divider. Since grid-cathode capacitance does not increase in proportion to the transconductance of various tube types, high g_m tubes such as the 6299 can be expected to extend the operating range of combination diversity into the video region.

Standard Combiner Element

The principal advantages of parallel combining diversity are:

1. The net signal-to-noise ratio is better than that afforded by switching diversity.
2. There are no switching transients.
3. There is no "black box" into which the outputs of several receivers are fed and the best extracted electronically. This avoids the "sudden death" of switching diversity in which the failure of one component in a common element denies the use of several receivers and antennas until a complicated change-over to a spare switch is completed. Receiver fail-safe provisions in combiner diversity involve simple "relay" removal of common cathode lead without further adjustment.
4. Since no equipment other than receivers with specialized baseband amplifiers is required, identical receivers can be designed, constructed, and warehoused for issue in connection with systems of any order of diversity (indeed with no diversity at all) without depot adjustment or field modification. No specialized switching "panels" must be inventoried in anticipation of changing field requirements with attendant waste and shortages.

In view of the considerations above, and since the transfer function of the noise amplifier-output tube combination must be designed specifically for each tube type in order to provide optimum diversity combination, it has been necessary to standardize the tube and circuit employed in the combiner output element. This "Standard Combiner Element" is shown in Fig. 14. A high μ dual triode of ruggedized design and intended for 10,000 hour operation is used. Both sections are strapped together for the following reasons:

1. The transfer functions of the two sections are averaged, thus making the circuit less sensitive to variability in tube characteristics.
2. A larger margin of plate current capacity is afforded. That this is necessary can be seen in the case of triple diversity when two of the three received levels go into a simultaneous fade. One element is now required to conduct three times its normal plate current.
3. The total transconductance of the tubes is doubled, allowing a smaller passive load impedance and so a smaller voltage stepdown in the output transformer.

The type 5965 is used because of its superior construction, high transconductance, large plate current capability, and design protection against change in characteristics after long periods of complete cutoff. (This can occur if an antenna or transmission line failure is undetected for a period of time or is deliberately effected during maintenance procedures.)

Performance Data

Frequency Range: 300 cps to 500 kcps (with appropriate noise filter).

Output Level: +10 dbm maximum.

Distortion: Less than 0.1 per cent.

Speed of Response: 2 milliseconds.

Order of Diversity: Up to but not exceeding 3.

Tolerable Baseband Unbalance: 5 per cent.

Factors Affecting Spacing of Radio Terminals in a UHF Link*

I. H. GERKS†, SENIOR MEMBER, IRE

Summary—**Measurements made by Central Radio Propagation Laboratory and others have established the feasibility of producing uhf fields at long distances which are sufficiently strong and consistent to be usable for communication purposes. This paper assembles the results of several investigators of the field strength-distance relation and shows that these results are in reasonable agreement in a range of about 75 to 250 miles. Statistical variations from the median due to fading are discussed. Graphical means are developed to facilitate the determination of the signal-to-noise ratio at the receiver for various ranges of distance, antenna gain, frequency, transmitter power, bandwidth, and receiver noise figure. Diversity systems are explored briefly. Estimates are made of the effect of the medium upon the antenna gain and the maximum bandwidth.**

Introduction

NUMEROUS studies have shown that the field strength well beyond the horizon and in the frequency range from about 100 mc to about 4,000 mc varies only slowly with distance. When the field strength is referred to the free-space field strength, the loss is on the order of 0.1 db per mile and is largely independent of frequency. Furthermore, the effect of the terrain beyond the horizon is negligible, and high antennas are not required except to the extent that obstacles in the antenna beam at close range should be avoided so as to reduce absorption and scattering. This leads one to suppose that it should be possible to establish practical communication systems in this frequency range with terminal spacings of several hundred miles. The object of this paper is to develop simple means for predicting the performance of such systems and to emphasize certain precautions.

Relation between Median Field Strength and Distance

In this section, an effort is made to deduce a reasonably accurate relation between the median tropospheric field strength and distance by consolidating the results published by various authors. As previously indicated, this relation is believed to be largely independent of frequency. Consequently, it has been deemed permissible to consolidate results of measurements covering a rather wide frequency range without any sort of adjustment. Low antennas are to be assumed. Where antenna heights were given in published results, data were adjusted for antenna heights of 10 and 40 feet at the two terminals.

Data from four sources were employed. The corresponding curves are shown in Fig. 1. The CRPL results[1] are based on measurements made on a Colorado-Kansas path at frequencies of 100 mc, 192.5 mc, and 1,046 mc. The transmitting antenna was located on a mountain at an elevation of about 3,000 feet above the plain, whereas the receiving antenna height was on the order of 40 feet. The Bell Telephone Laboratories results[2] are based on measurements made principally over land in the New York-New England area and covering generally the frequency range from 300 mc to 4,000 mc. No correction was made for antenna height because of the large variation of this parameter in the tests included in the survey. The Megaw results[3] are based on measurements made over the North Sea at 3,000 mc. The antenna heights were not reported. The Collins Radio Company results[4] are based on measurements made at 412 mc over Iowa terrain with 10-ft. and 40-ft. antenna heights. Agreement of the four curves is surprisingly good to a distance of 200 miles. Beyond this, measurements are scantier and curves probably less reliable.

Since there was no entirely logical basis on which to combine the results to obtain the over-all median field strength, it was arbitrarily decided that the same weight would be assigned to each of the four sets of data and that arithmetic mean of ordinates in Fig. 1 (next page) would be used to derive a combined median field strength. Result is shown by the solid curve in Fig. 2 (next page). It was found that this curve could be approximated by a straight line in range beyond 100 miles with an error no greater than 1.5 db. This linear relation between scattering loss (field strength in db relative to free space) and distance, correspondingly to 0.117 db per mile, has been used in constructing nomogram appearing in this paper. This relation may be written

$$L_{sc} = 57 + 0.12(d - 100) \text{ db} \quad (d > 100) \qquad (1)$$

Time and Space Variations from the Median

In establishing a point-to-point link in which a high degree of reliability is required, allowance must be made for fading of the received signal. Two types of fading may be distinguished. One is the fast type associated with multipath propagation. This signal may be assumed to have an amplitude which is Rayleigh distributed over periods which are so short that the tropospheric conditions change very little. The other is the slow fading which results from major changes in tropospheric conditions, such as variations in the

* Original manuscript received by the IRE, June 20, 1955. Paper presented at Spring, 1954, meeting of URSI, Washington, D. C.

† Collins Radio Co., Cedar Rapids Div., Cedar Rapids, Iowa.

[1] A. P. Barsis, B. R. Bean, J. W. Herbstreit, K. O. Hornberg, and K. A. Norton, "Propagation of Radio Waves over Land at 1,046 Mc," NBS Rep. 2494; May 1, 1953.

[2] K. Bullington, "Radio propagation beyond the horizon in the 40-to-4,000-mc band," PROC. IRE, vol. 41, pp. 132–135; January, 1953.

[3] E. C. S. Megaw, "Scattering of short radio waves by atmospheric turbulence," *Nature*, vol. 166, p. 1100; December, 1950.

[4] I. H. Gerks, "Propagation at 412 megacycles from a high-power transmitter," PROC. IRE, vol. 39, pp. 1374–1382; November, 1951.

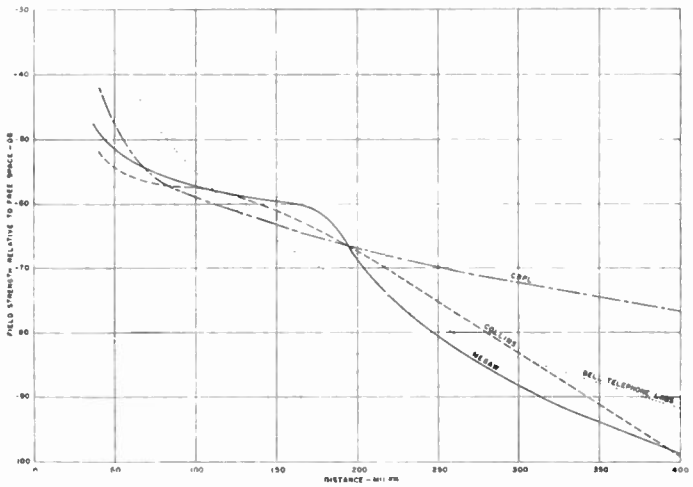

Fig. 1—Median field strength relative to free space as a function of distance according to four sources. Frequency range, 100 to 4,000 mc. Antenna heights less than 100 feet.

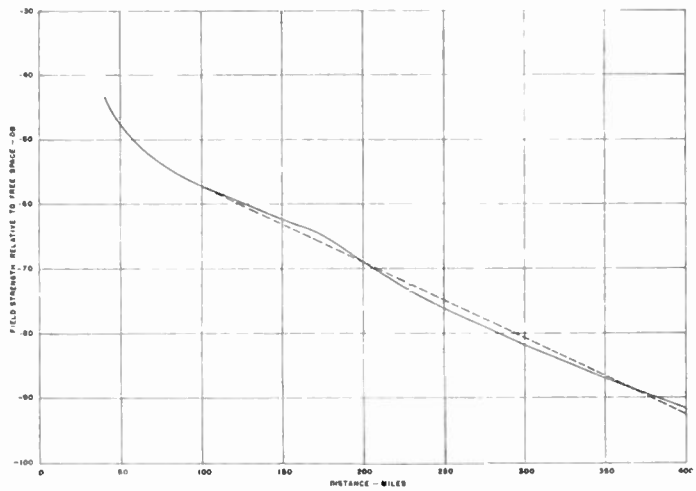

Fig. 2—Median field strength relative to free space as a function of distance—average of results according to four sources. Frequency range, 100 to 4,000 mc. Antenna heights less than 100 feet. Solid line=experimental curve; broken line=empirical linear approximation.

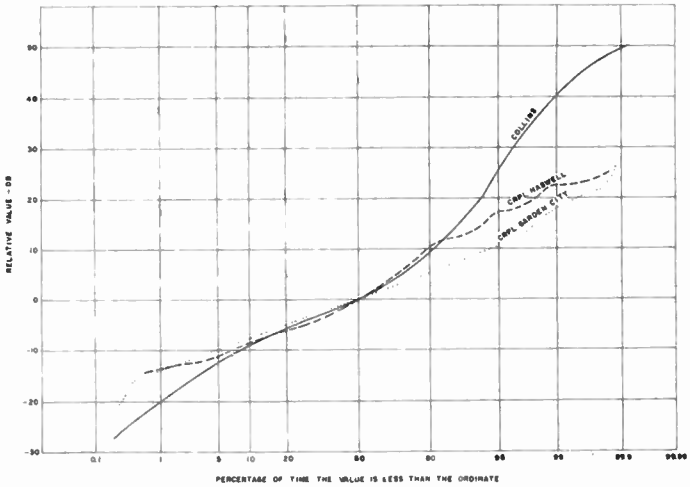

Fig. 3—Distribution of hourly medians for three paths. Solid line =Collins Radio Co., Cedar Rapids to Waukon, Iowa, 98 miles, 412 mc, May to August. Broken line=CRPL, Cheyenne Mountain to Haswell, Colorado, 97 miles, 1,046 mc, all year. Dotted line=CRPL, Cheyenne Mountain, Colorado to Garden City, Kansas, 227 miles, 1,046 mc, all year.

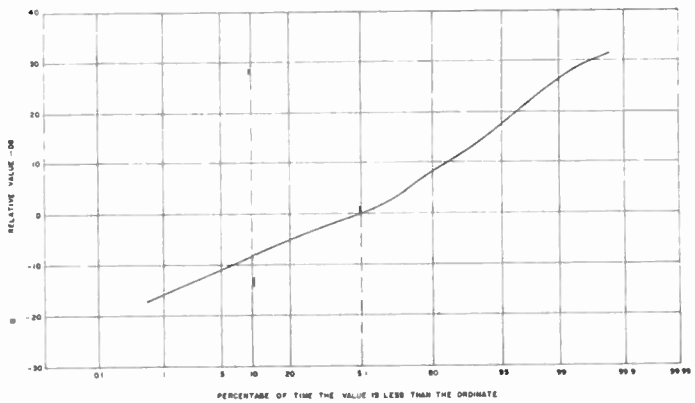

Fig. 4—Distribution of hourly medians averaged for the three paths of Fig. 3.

average refractive index gradient. The latter type of fading may be analyzed by plotting the distribution of hourly medians, as in Fig. 3. The CRPL results were again taken from Barsis, *et al.*[1] It is seen that the distribution in this case is approximately log normal except for the hump produced at one end of the Collins curve by the rather high incidence of super-refraction. The curves of Fig. 3 were combined by averaging the ordinates and the results plotted as a single curve in Fig. 4. We see from this that one may expect the signal to fade more than 8 db below the median level 10 per cent and more than 16 db 1 per cent of the time.

The slow fading cannot be significantly reduced by receiving space diversity, though K. A. Norton has reported instances in which the hourly median signals of spaced antennas were not perfectly correlated. On the other hand, the reliability of a circuit as it is affected by fast fading can often be greatly improved by the use of spaced antennas at the receiving terminal. Though conclusive information is not available regarding the required spacing of the receiving antennas, theoretical and experimental results indicate that a spacing transverse to the propagation path of 20 to 50 wavelengths causes received signals to be poorly correlated on long paths.

From the work of W. E. Gordon,[5] we obtain a formula

$$D = K\frac{R\lambda}{d} \tag{2}$$

for the maximum useful diameter of the antenna, where D is aperture diameter, R effective earth radius, λ wavelength, d path length, and K a constant having a value on the order of 1.5. If we arbitrarily assume that an antenna spacing of twice the value given by (2) is adequate for space diversity, we have for the required spacing

$$S = 3\frac{R\lambda}{d}. \tag{3}$$

[5] W. E. Gordon, "Radio scattering in the troposphere," PROC. IRE, vol. 43, pp. 23–28; January, 1955.

It should be noted that the required spacing decreases with increasing path length. For a path length of 100 miles, gives a spacing of about 160 wavelengths.

The cumulative Rayleigh distribution, which may be assumed to represent the probability that the instantaneous signal exceeds some value E, is given by

$$P(E) = \exp\left(\frac{-E^2}{E_0^2}\right), \tag{4}$$

where E_0 represents the long-time rms value. From (4), we deduce that the median value of the signal is 1.6 db below the rms value, that the signal fades 8.2 db or more below the median value 10 per cent of the time, 18.4 db or more below the median 1 per cent of the time, and so forth.

If we assume completely uncorrelated fading on two spaced receiving antennas and if the receiver is arranged so as to respond only to the stronger of the two signals, then we achieve the results shown in Table I.

TABLE I

Depth of fade below median, db	Percentage time with no diversity	Percentage time with dual diversity
2.9	30	9
4.9	20	4
8.2	10	1
11.3	5	0.25
15.4	2	0.04
18.4	1	0.01

It is beyond the scope of this paper to discuss the statistical relation between the received signal level and the antenna location relative to irregularities on the surface. On fixed, point-to-point links, it is nearly always possible to pick a favorable antenna location, either by choosing a natural terrain prominence or by erecting a tower of sufficient height so that no allowance need be made for a loss relative to the over-all median level. Experience has indicated that the propagation path should be clear of obstacles at short distances and that the skyline should have the least possible elevation angle above the horizontal. If the skyline elevation is more than a few tenths of a degree, then Norton's angular distance concept[6] should be employed to determine an equivalent distance correction, given essentially by

$$\Delta d = 92\Delta\theta, \tag{5}$$

where Δd is the distance in miles to be added to the path length and $\Delta\theta$ is the elevation of the skyline above the horizontal plane in degrees.

Median Transmission Loss

The median basic transmission loss as a function of path length and frequency may be determined by combining the scattering loss taken from Fig. 2 with the free-space loss. The free-space loss is given by

$$L_{FS} = 20 \log (4\pi d/\lambda). \tag{6}$$

The basic transmission loss as a function of distance and for several values of frequency is shown in Fig. 5.

In order to obtain the actual transmission loss, we must subtract the combined antenna gain from the basic transmission loss. It is assumed that any incidental transmission-line losses are accounted for in the antenna gain values. We must now recognize that high-gain antennas employed on long scatter links may fail to yield their calculated plane-wave gains. It is assumed that all or most of the experimental results forming the basis for Fig. 2 were obtained with relatively low-gain antennas, so that the antenna-to-medium coupling losses may be considered negligible. However, where very large apertures and long paths are encountered, it is necessary to allow for such coupling losses.

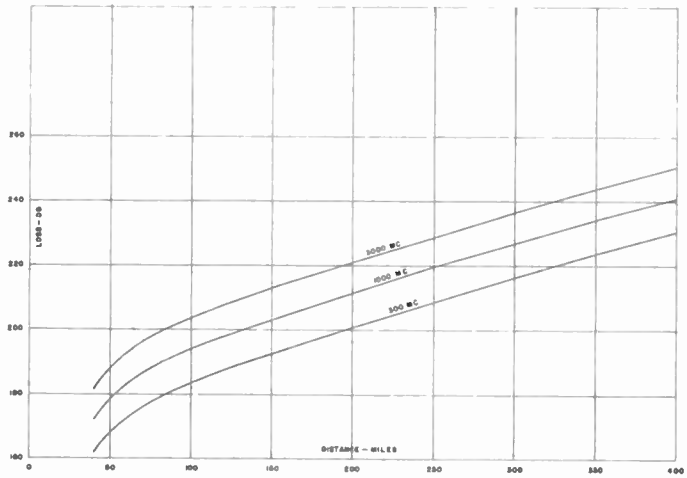

Fig. 5—Median basic transmission loss as a function of distance and frequency. Results are based on Fig. 2.

Though experimental data on this subject are still very meager, we may adopt the theoretical methods of Booker and deBettencourt[7] in forming an estimate of the magnitude of the coupling loss. They derive the following formulas for the ratio of the received available power to that obtained under free space conditions when identical antennas are used on the two ends of the link. For very narrow-band antennas ($\alpha < \alpha_e$):

$$\frac{P_R}{P_F} = \frac{2d\alpha^3}{(\theta_0 + \alpha/2)^5} S_P, \tag{7}$$

and for broad-beam antennas ($\alpha \gg \alpha_e$),

$$\frac{P_R}{P_F} = 0.86 \frac{R^2}{d} S_P; \tag{8}$$

where d is the path length, R is the effective earth radius, α is the half-power antenna beam angle, α_e is the scattering angle taken as $2/3\ d/R$, θ_0 is d/R, and S_P is the

[6] K. A. Norton, "Angular distance in tropospheric propagation," paper presented at 11th General Assembly of URSI, August, 1954; to be published.

[7] H. G. Booker and J. T. de Bettencourt, "Theory of radio transmission by tropospheric scattering using very narrow beams," paper presented at the 11th General Assembly of URSI, August 1954, Proc. IRE, vol. 13, pp. 281–290; March, 1955.

scattering parameter. Combining (7) and (8), we obtain for the antenna-to-median coupling loss for the link:

$$\Delta G = 10 \log 1.45 \left[\frac{(1 + \alpha/3\alpha_c)^5}{(\alpha/\alpha_c)^3}\right]. \qquad (9)$$

Eq. (9) is plotted in Fig. 6, the curve drawn arbitrarily near its lower end to indicate zero loss for $\alpha/\alpha_c = 10$.

In order to facilitate application of these results, they have been reduced to the form of nomograms. Fig. 7 may be used to determine the basic transmission loss as a function of distance and frequency. The actual transmission loss may also be found if the effective antenna gain is known. Fig. 8 (next page) may be used to determine the effective antenna gain for a link when the diameter of a circular aperture, the frequency, and the path length are given. In the preparation of Fig. 8 a 10-db illumination taper and an illumination factor of

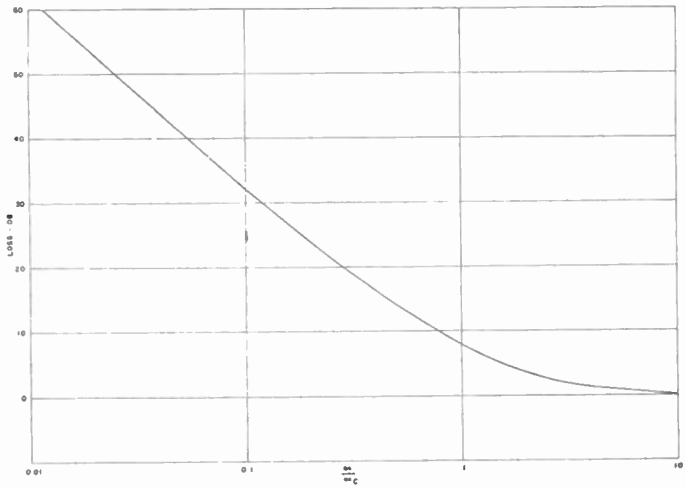

Fig. 6—Estimated antenna-to-medium coupling loss for two similar antennas as a function of antenna beam angle and scattering angle. α=antenna beam angle, α_c=scattering angle=$2/3\ d/R$, d=path length, R=effective earth radius (assumed 8,000 km).

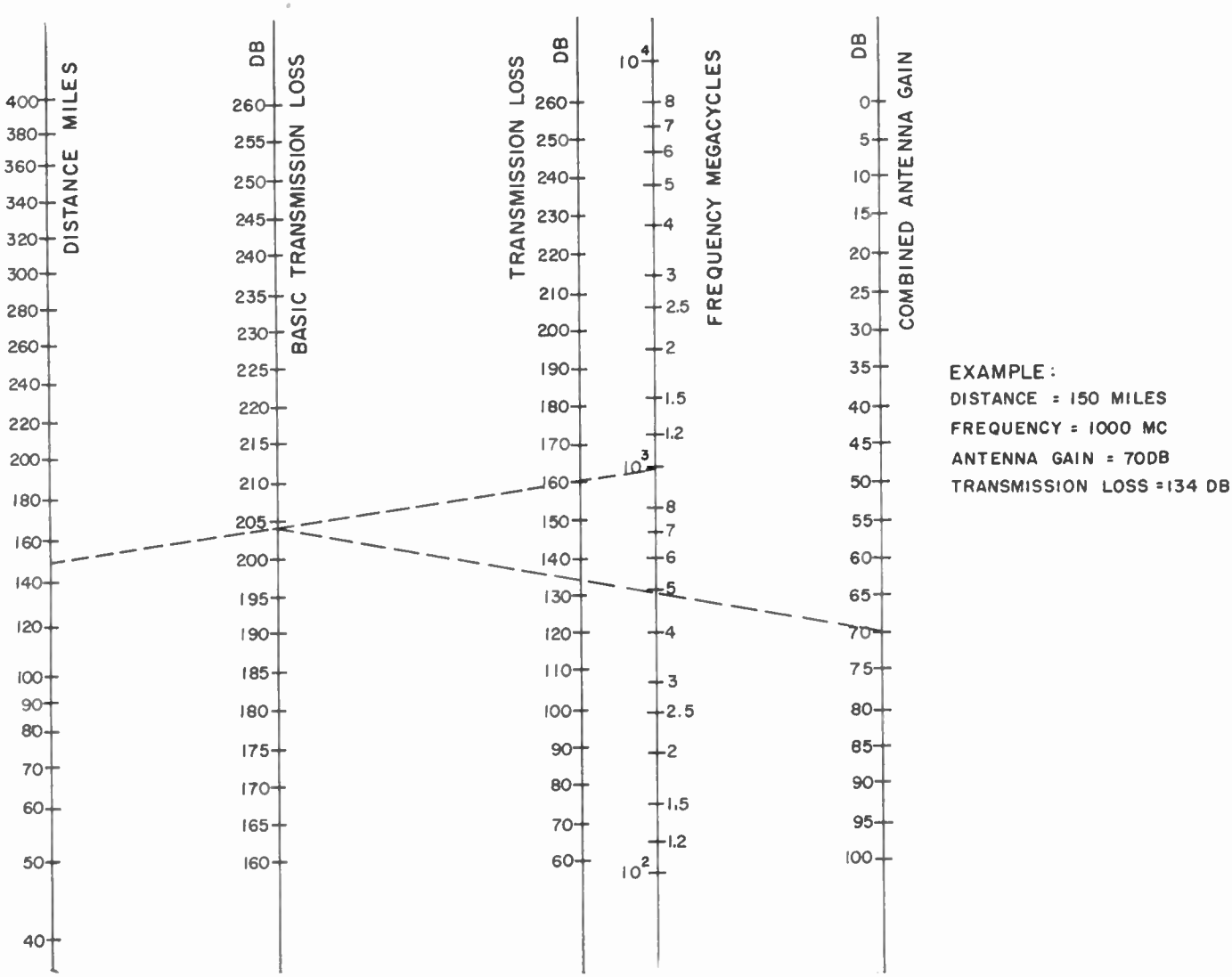

Fig. 7—Nomogram for use in determining transmission loss as a function of path length, frequency, and antenna gain.

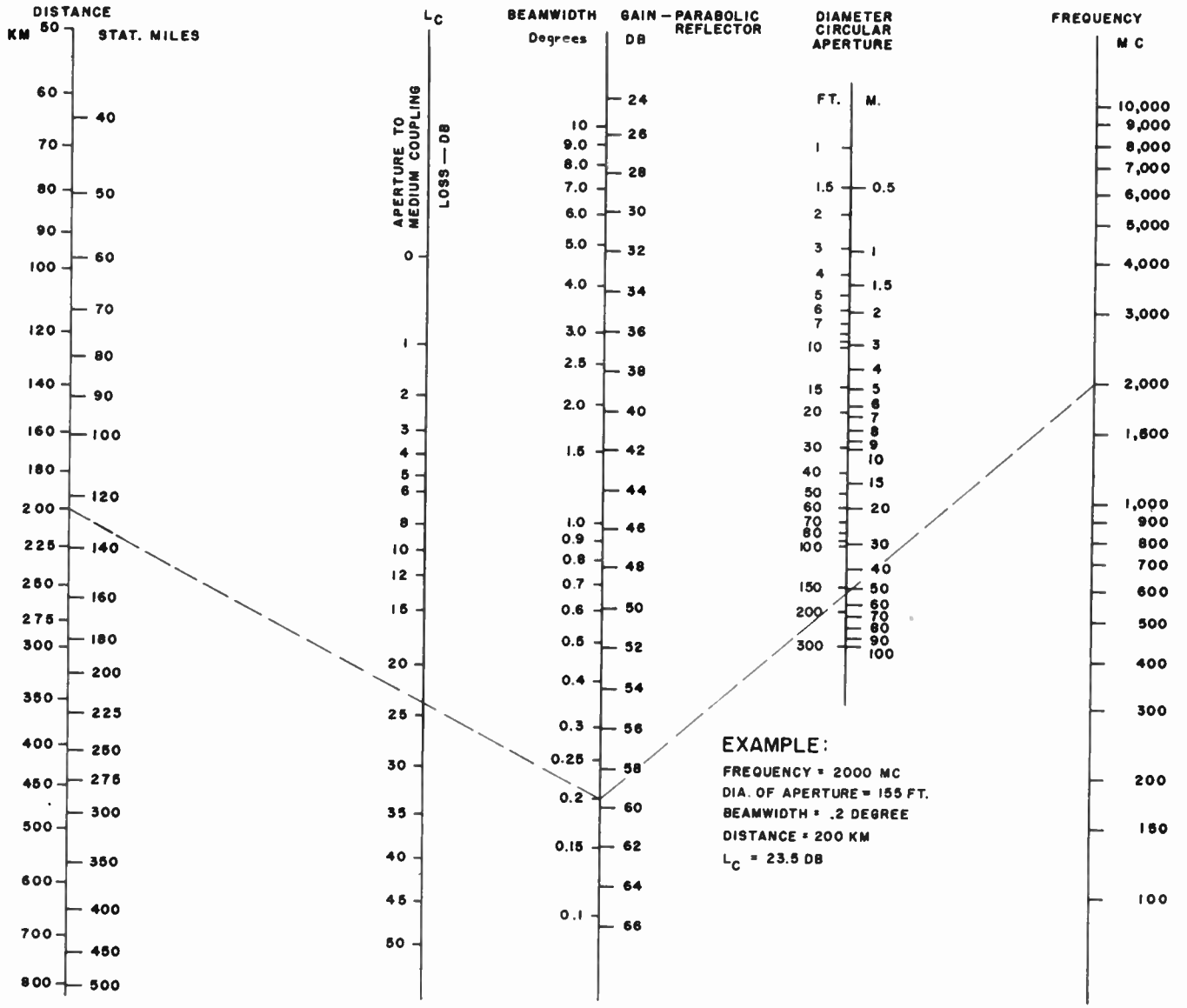

Fig. 8—Nomogram for use in estimating the antenna-to-medium coupling loss as a function of path length, frequency, and antenna diameter.

0.75 were assumed. The appropriate formulas are:

$$\alpha = 70\lambda/D \text{ Degrees} \tag{10}$$

$$G = 10 \log (36{,}000/\alpha^2). \tag{11}$$

Maximum Allowable Transmission Loss

Under the conditions considered in the paper, the external noise may generally be neglected. Then the received signal power is given by

$$P_R = (S/N)(NF)(KTB), \tag{12}$$

where S/N is signal-to-noise power ratio at receiver input, NF receiver noise figure, K Boltzman's constant, T absolute temperature, and B bandwidth. This is plotted in Fig. 9 for a S/N ratio of 1, a temperature of 288° K, and for several values of noise figure. Maxi-

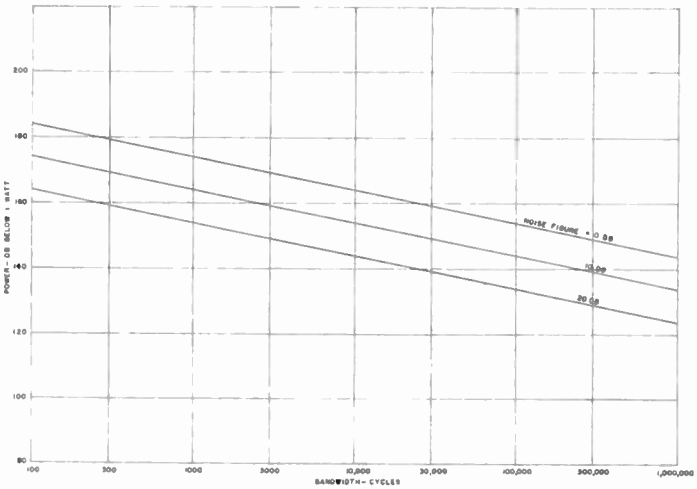

Fig. 9—Receiver noise level as a function of bandwidth and noise figure.

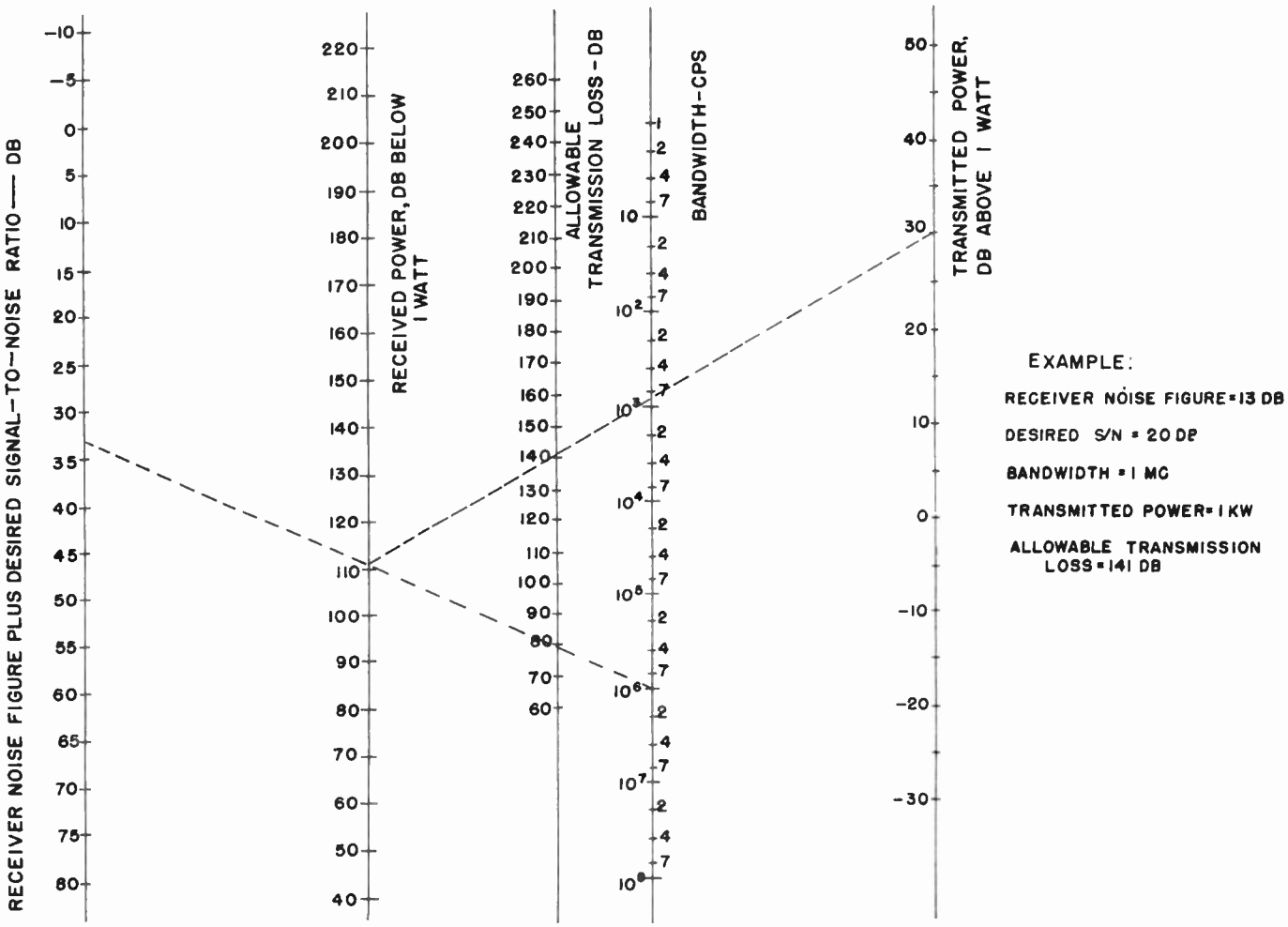

Fig. 10—Nomogram for use in determining the maximum allowable transmission loss as a function of receiver noise figure, signal-to-noise ratio, bandwidth, and transmitted power.

mum allowable transmission loss is

$$\begin{aligned} L_{\max} &= 10 \log P_T/P_R \\ &= 10 \log P_T - 10 \log (S/N) - 10 \log (NF) \\ &\quad - 10 \log B + 204. \end{aligned} \tag{13}$$

For convenience of application, this relation has been represented by a nomogram, which is shown in Fig. 10 (above).

Maximum Allowable Bandwidth

In tropospheric scatter propagation, the received power is the resultant of power scattered from all parts of a volume which is common to the transmitting and receiving antenna beams. Booker and deBettencourt[7] define the bandwidth of the medium as the reciprocal of the differential propagation time on the shortest and the longest paths through such a common volume. This definition is based on a calculation of the length of the received pulse when an ideal impulse (or pulse of extremely short duration) is transmitted. This length is, of course, equal to the differential propagation time mentioned above. The Fourier transform applied to the transmitted and received pulses indicates that an indefinitely large transmitted bandwidth results in a bandwidth at the receiver equal to the reciprocal of the differential propagation time.

Booker and deBettencourt[7] give bandwidth formulas both for very narrow and for broad antenna beams:

$$B_1 = \frac{4cR}{\alpha d^2(1 + \alpha R/d)} \quad (\alpha \ll \alpha_c); \tag{14}$$

$$B_2 = \frac{4.7cR^2}{d^3} \quad (\alpha \gg \alpha_c); \tag{15}$$

where c is the velocity of propagation and the other parameters are as defined after (7) and (8). Eq. (14) may also be written

$$B_1 = \frac{6cR^2}{(\alpha/\alpha_c)d^3(1 + 2/3\,\alpha/\alpha_c)} \quad (\alpha \ll \alpha_c). \tag{16}$$

We see that the bandwidth is given by

$$B = \frac{cR^2}{d^3} F(\alpha/\alpha_c), \tag{17}$$

where

$$F(\alpha/\alpha_c) = \frac{6}{\alpha/\alpha_c(1 + 2/3\ \alpha/\alpha_c)} \quad (\alpha \ll \alpha_c)$$

or

$$F(\alpha/\alpha_c) = 4.7 \qquad (\alpha \gg \alpha_c). \tag{18}$$

The function F is plotted in Fig. 11 where α = antenna beam angle, α_c = scattering angle = $2/3\ d/R$, d = path length, R = effective earth radius, and $B = cR^2/d^3F(\alpha/\alpha_c)$. The section of this curve representing the transition between the two asymptotes must be drawn in arbitrarily and may vary somewhat with personal judgment.

By using (17) and Fig. 11, we may now prepare a nomogram to facilitate estimation of the bandwidth of the medium. This is shown in Fig. 12. In the preparation of this nomogram, R has been taken as 8,000 km or about 5,000 miles, so that (17) becomes

$$B_{mc} = \frac{4.6}{(d/100)^3} \qquad F(\alpha/\alpha_c). \tag{19}$$

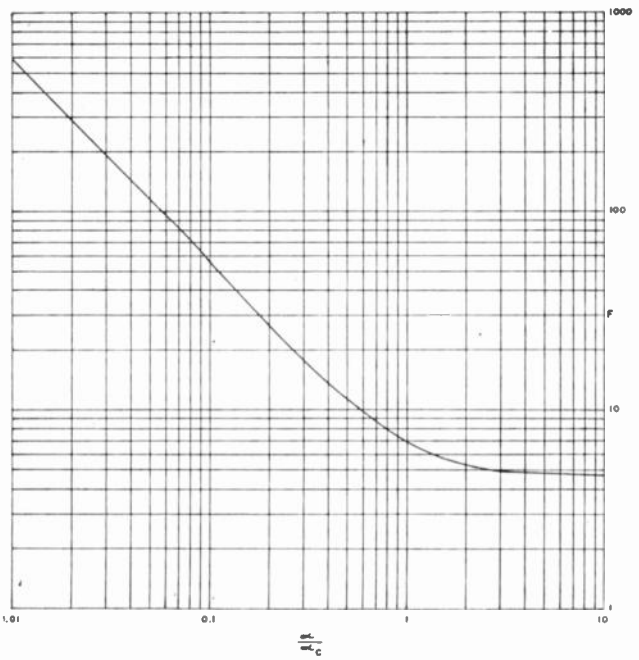

Fig. 11—Plot of the function F used in determining estimated maximum allowable bandwidth for a link with two similar antennas as a function of antenna beam angle and scattering angle.

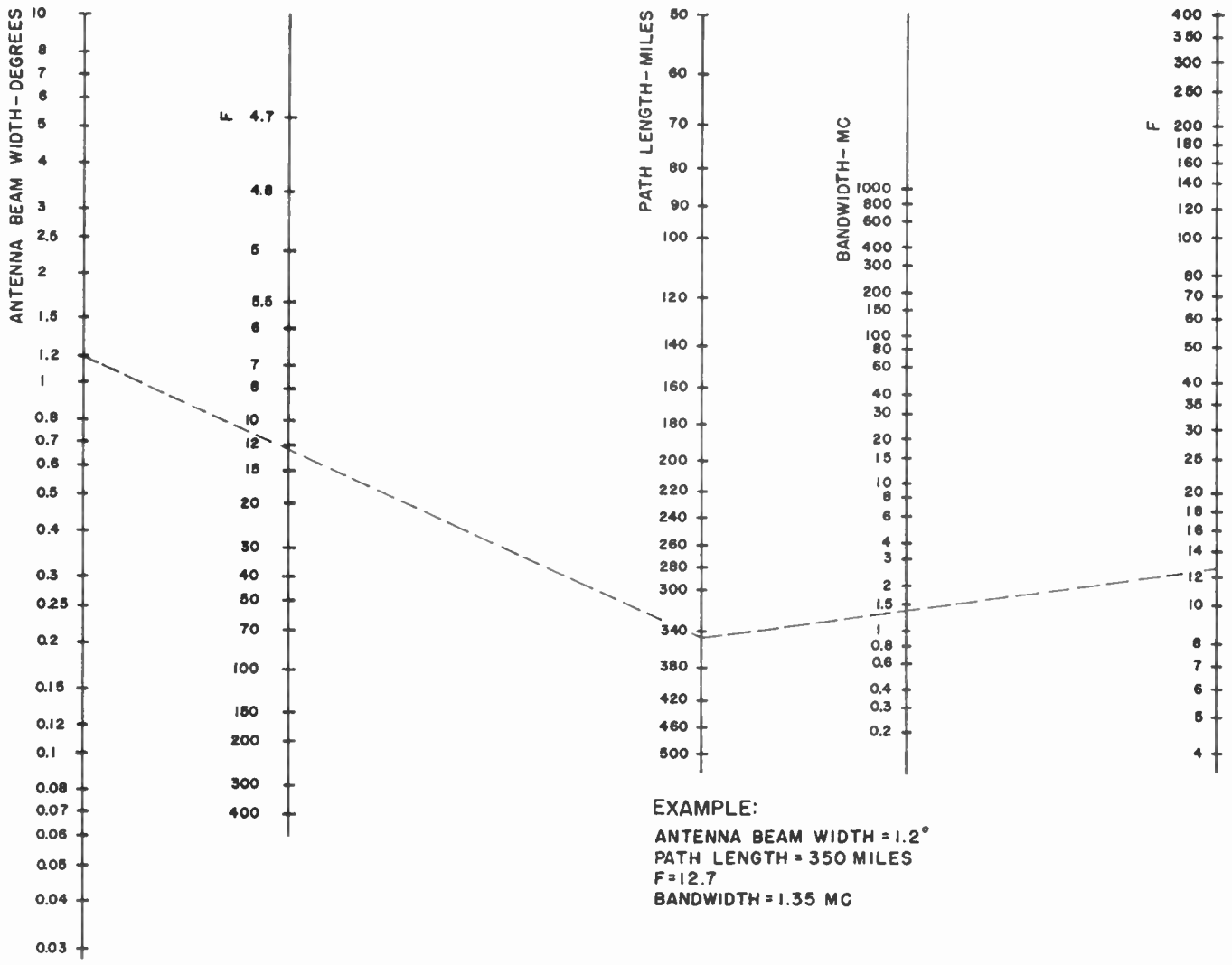

Fig. 12—Nomogram for use in estimating the maximum allowable bandwidth as a function of antenna beam angle and path length.

Conclusions

A combination of the results of various propagation measurements in the uhf and upper vhf range yields the conclusion that the median field strength is approximately 57 db below the free-space value at 100 miles and that a further loss of about 0.12 db per mile occurs at increasing distances. An allowance of 8 to 16 db must be made for slow fading, depending upon the degree of reliability desired. With dual space diversity at the receiving station, a further allowance of about 3 to 8 db must be made for Rayleigh type fading, and somewhat more than twice this allowance must be made without diversity. When high-gain antennas are employed, account must also be taken of the failure to realize the plane wave gain. This loss increases with increasing path length and antenna gain. It may be estimated with the aid of Fig. 8. Since scatter propagation involves multipath effects, there is a limitation also on the bandwidth which may be employed. This may be estimated with the aid of Fig. 12. The bandwidth decreases with increasing distance, and it increases with increasing antenna gain.

These results indicate generally large values of available bandwidth. It is apparent also that the frequencies in a frequency diversity system may have to be widely spaced in order to produce the desired incoherence.

The methods presented in this paper should facilitate many of the steps involved in the design of long tropospheric communication links. The analysis must be considered tentative, however, since some of the effects which are known to exist have not yet been subjected to extensive experimental study, and since variations from median conditions in individual cases cannot be accurately predicted.

Demonstration of Bandwidth Capabilities of Beyond-Horizon Tropospheric Radio Propagation*

W. H. TIDD†, SENIOR MEMBER, IRE

Summary—**Tropospheric radio transmission beyond the horizon is characterized by rapid and selective fading, which suggests a possible limitation on the useful bandwidth. The tests discussed were made to explore the bandwidth capabilities of this medium.**

Bell Telephone Laboratories conducted these tests in cooperation with the M.I.T. Lincoln Laboratory on a 188-mile path at 5,050 mc with a power of 300w and 28-foot paraboloidal antennas.

Two types of tests were made. First a 12-voice-channel multiplex system for intermodulation crosstalk. IF band was 1.3 mc. Then television tests were made with a deviation of ±4 mc and IF bandwidth of 30 mc. No significant impairment in system quality could be attributed to distortion in transmission medium in either test.

Introduction

TROPOSPHERIC transmission beyond the horizon has opened up many new radio possibilities. The principal application seems to be for point-to-point communication services at distances of 150–200 miles or more.

This type of transmission is characterized by rapid and selective fading, which suggests a possible limitation on the useful bandwidth. Radar pulse tests made about 5 years ago by Bell Telephone Laboratories at 3,700 mc showed that one-microsecond pulses were not substantially widened after transmission over distances up to 285 miles. From these tests it was postulated that bandwidths of several megacycles might be available.

A more convincing test required large antennas and a high power cw transmitter that could be modulated. Suitable equipment became available in late 1953 and wideband tests have been carried out by Bell Telephone Laboratories in cooperation with Lincoln Laboratory of Massachusetts Institute of Technology. These tests were made on a 188-statute-mile path between the Bell Telephone Laboratories' site at Holmdel, New Jersey, and the M.I.T. Round Hill field station at South Dartmouth, Massachusetts. A map of this area is shown in Fig. 1, and a profile of this path is shown in Fig. 2 (next page). Noted that horizontal beams from transmitting and receiving antennas intersect at an elevation of about 4,400 feet under standard atmospheric conditions.

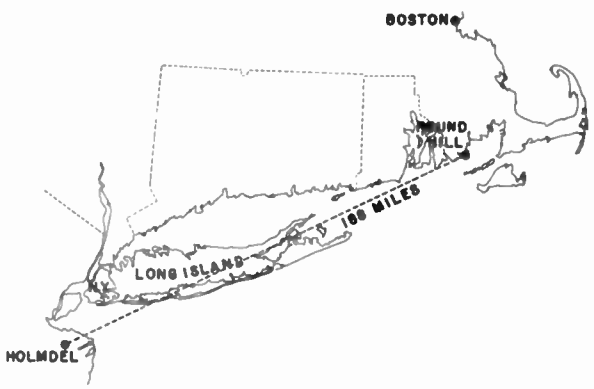

Fig. 1—Radio path.

* Original manuscript received by the IRE, July 14, 1955. This program was undertaken as part of contract AF-18(600)-572 with the U. S. Air Force, Air Res. and Dev. Command.

† Bell Telephone Labs., Inc., New York, N.Y.

The transmitter used an experimental klystron developed by Sperry to provide a power output of about 300 watts at 5,050 mc. Outside of the power amplifier, the basic radio components were from the conventional TD-2 radio relay equipment which is used in the Bell System nation-wide microwave network. Twenty-eight-foot parabolic antennas were used at both ends of the path. The receiver had a bandwidth capability of up to 30 megacycles and a noise figure of 9 db. A simplified block diagram is shown in Fig. 3.

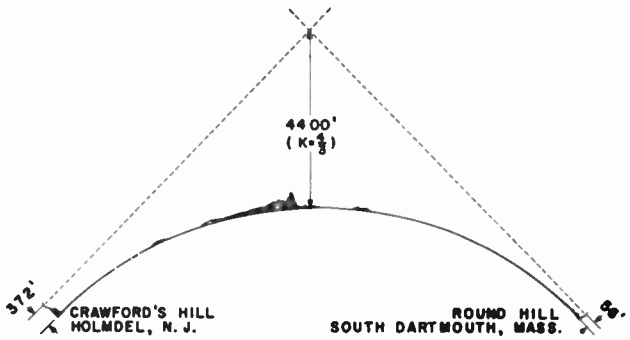

Fig. 2—Profile.

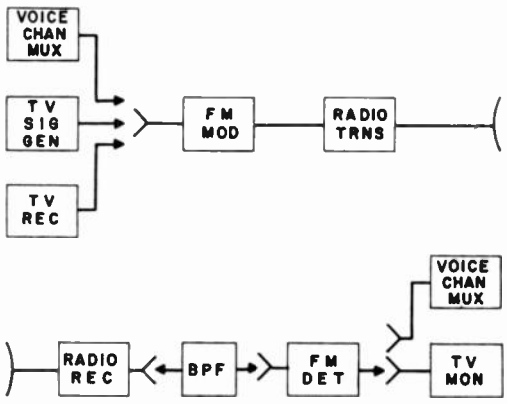

Fig. 3—Block diagram.

Two types of tests have been made to determine the distortion caused by selective fading. First, a 12-voice-channel multiplex system was tested for inter-channel crosstalk. In this case a 1.3 megacycle filter was inserted in the receiver IF to improve its performance. When this test showed that the distortion caused by selective fading was negligible for this bandwidth, a second test using a much wider band was proposed. Since television transmission is known to require a wide band, television tests were made using both a window pattern and television pictures. In this case also no significant impairment in system quality could be attributed to distortion in the transmission medium. This test circuit does not have adequate signal to noise margin to provide commercial reliability with the present transmitter power and antennas. Provision of a satisfactory signal to-noise ratio seems to be the major problem with this type of transmission, in that there appears to be no inherent bandwidth limitation up to several megacycles.

Multichannel Tests

The multiplex equipment was set up to simulate a 12-channel system for most of the tests. Four channels of a Western Electric Type O carrier telephone terminal were used occupying the frequency space from 40 to 56 kc. Most of the observations were made in channels 3 and 4, 40–44 and 44–48 kc. The range 0 to 36 kc was loaded with random noise simulating 9 channels with average talkers. The 44-kc carrier for channels 3 and 4 was equivalent to the loading of two more average talkers. Thus observations were made on the top channel of a system equivalent to a 12-channel system with 11 active channels.

Two sets of tests were made, the first with the transmitting and receiving equipment operating back to back at Holmdel, N. J., and second with the terminals separated by the 188-mile radio path.

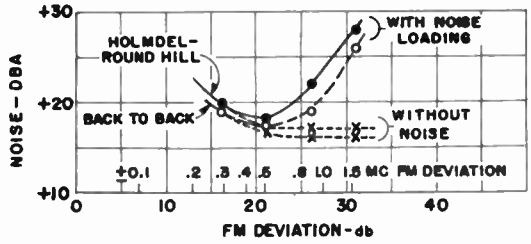

Fig. 4—Multiplex tests—intermodulation data. Received signal—50 dbm.

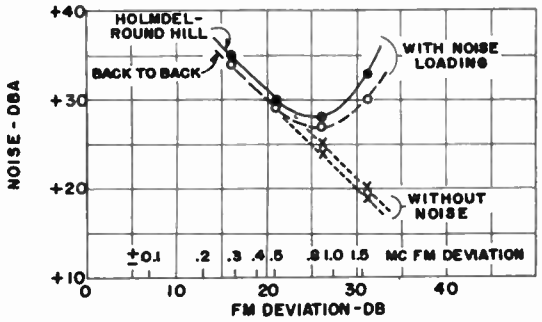

Fig. 5—Multiplex tests—intermodulation data. Received signal—75 dbm.

The results of some of these observations are shown on Figs. 4 and 5. The ordinates of these two graphs are noise measured in Channel 4 at the receiving end of the system. The units are dba at a −9 db transmission level, the usual Bell System units. The abscissas are FM deviations expressed as 20 log (frequency deviation /44 kc). Data for two levels of received radio carrier, −50 dbm and −75 dbm are plotted. In each case data are plotted for noise loading off and noise loading on. Observations were made this way to make certain any intermodulation present was observed even though the noise was varying considerably with the received radio carrier levels. It will be noted that the curves of channel noise without noise loading follow the usual law for FM systems, decreasing uniformly as the deviation is increased, at least until the asymptotic noise level for the terminal equipment is reached.

When noise loading is added no increase is noticed until the FM deviation approaches ±0.5 mc. This deviation effectively occupies that portion of the intermediate frequency band which has reasonably uniform delay. Beyond this deviation intermodulation products increase rapidly. The curves for the long path are almost exactly parallel to those for the back-to-back tests, indicating that the radio transmission has not added any observable intermodulation. The 1-db displacement between the curves for these two test conditions are attributed to tube aging or slightly poorer alignment after transportation.

Several other sets of tests of the same general type were made, observing at different received carrier levels and using other carrier channels. In no case was there any increase in intermodulation which could be attributed to the transmission medium.

Broadband Tests

For the broadband tests, the system was modified by removing the 1.3 megacycle band filter from the receiver. The bandwidth becomes of the order of 30 megacycles. The tests were made with a window test signal generator which produces a white rectangle on a dark background. Standard television synchronizing and blanking signals were supplied. The test pattern being received was examined on a television monitor with triggered synchronization. The window test pattern was used because any delayed multipath transmission should be visible in the uniform field at the right of the vertical edges of the pattern. A few transmissions were made of television pictures to demonstrate picture quality.

The system levels were adjusted so that the FM system was deviated plus and minus 4 megacycles. This requires a bandwidth somewhat in excess of 8 megacycles. When the pictures were transmitted the fine structure required bandwidths of the order of 12 to 16 megacycles.

Test Pictures

Still pictures and motion pictures were taken of the television monitor screen at Round Hill when the received signal levels permitted. With median carrier to noise ratios of from 18 to 24 db, excellent television vision picture quality was observed with only occasional fades into noise. The window pattern was observed to have sharp edges with no evidence of delay distortion. With lower median signal levels the fades occurred more frequently and occasionally caused excessive noise and a loss of synchronization.

Three still photographs of the television monitor screen are shown in Figs. 6, 7 and 8. The window pattern taken at a carrier to noise (C/N) ratio of approximately 15 db shows no evidence of delayed transmissions. The window pattern taken when the C/N ratio was approximately 6 db shows noise mottle and uneven edges, which are attributed to the disturbance of the triggered synchronizing circuits used in the monitor.

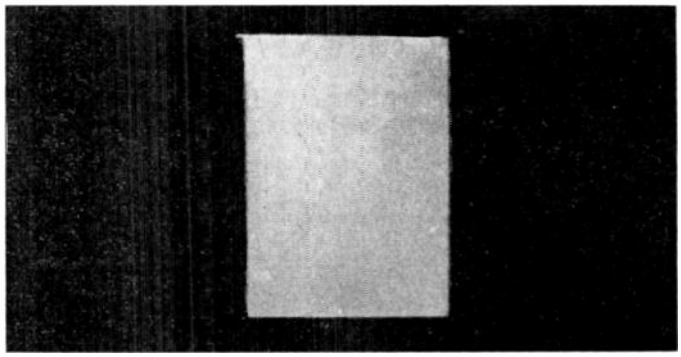

Fig. 6—Window pattern—C/N ratio approximately 15 db.

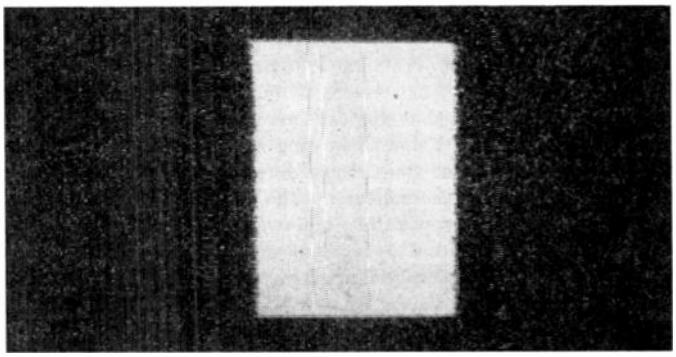

Fig. 7—Window pattern—C/N ratio approximately 6 db.

Fig. 8—Television picture—C/N ratio approximately 20 db.

The television picture was taken when the C/N ratio was approximately 20 db.

Conclusion

It was concluded that bandwidths capable of transmitting television pictures are available on beyond-horizon uhf and shf circuits, provided high transmitter power and narrow beam antennas are used.

Acknowledgment

The assistance of K. Bullington, Bell Telephone Laboratories, Inc., and J. A. Chisholm and P. A. Portmann, Lincoln Laboratory, in planning these tests, and the assistance of many on the staffs of both organizations in executing the test program, is gratefully acknowledged.

Characteristics of Tropospheric Scattered Fields*

L. G. TROLESE†, SENIOR MEMBER, IRE

Summary—**Experimental results obtained with transmissions at wavelengths of 3.2, 9.3, and 24 cms over a 46.3-mile path are presented. With low terminal heights the scattered field was dominant on this path. Tests with a narrow beam antenna indicate that the scattered field arrives at the receiver spread over an appreciable angle. This angle is some five to seven times as large as the Booker-Gordon theory predicts on the assumption that the scale of turbulence is large compared to the wavelength. Loss in ability to receive power in proportion to antenna gain was encountered for antennas with aperture diameters greater than about 20 wavelengths. This loss occurs for aperture sizes considerably smaller than the Booker-Gordon theory predicts.**

The speed of fading of the scattered field signal increases almost linearly with frequency. This agrees fairly well with the concept (due to Ratcliffe[1] and applied to tropospheric scattering by Booker and Gordon[2]) that fading is due to beating between various scattered field components whose frequencies differ by a fractional Doppler shift due to motion of the scatterers. The speed of fading always increases, during the day, with time of day and does not correlate with mean upper wind speed. This increase with time of day is probably connected with the repetitive diurnal meteorological cycle prevalent in Arizona.

Introduction

In 1950 Booker and Gordon[2] published their theory of tropospheric scattering which sought to explain the occurrence, in the absence of super-refraction, of fluctuating fields at a distance far beyond the horizon which are much stronger than standard diffraction theory predicts. In later papers, Gordon,[3] and Booker and deBettencourt[4] derived various approximate formulas based on this theory which can be applied to specific cases. The object of this paper is to compare the experimental results obtained on a 46.3 mile path in the Arizona desert with the predictions of the Booker-Gordon theory.[5]

Experimental Setup

A profile of the path used is shown in Fig. 1. The terrain deviates from a spherical surface by no more than 80 feet and deviations of this magnitude are not near the two terminals. Towers equipped with elevators at each terminal permitted antenna heights to be varied from 4 to 195 feet above the surface. Transmissions at wavelengths of 3.2, 9.3 and 24 cms were used in the tests with peak pulse transmitter powers of 25, 30 and 50 kw respectively.

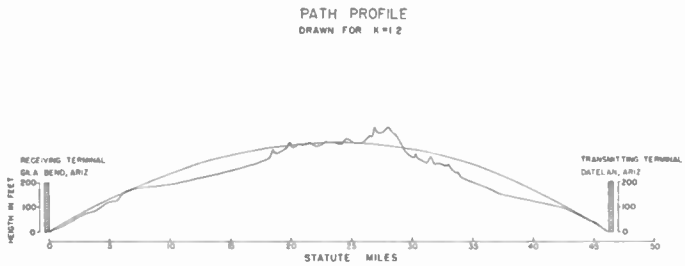

Fig. 1—Profile of path drawn for $k=1.2$.

The tests were made during the winter season when a definite repetitive diurnal meteorological cycle is prevalent. For a very large portion of the time, the daytime atmosphere is well mixed and nearly standard. After sundown, a ground-based radiation inversion quickly sets in and increases in height and intensity during the night. Shortly after sunrise, heating of the ground causes mixing in the lower atmosphere which rapidly dissipates the nocturnal inversion. Consequently, radio transmissions show no evidence of super-refractive effects during the daytime, but microwave transmissions to distances beyond the horizon are enhanced during the nighttime.

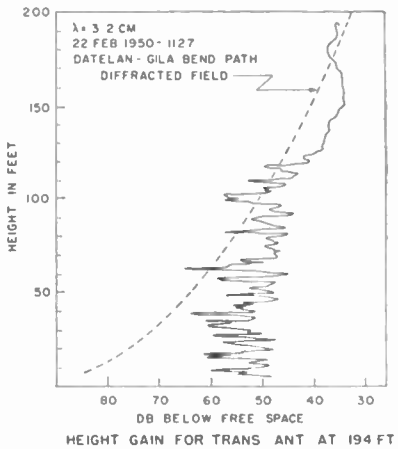

Fig. 2—Measured receiver height gain curve with transmitting antenna at 194 feet.

Height Gain Measurements

Fig. 2 shows a typical height-gain curve made during the daytime with transmission at a wavelength of 3.2 cm and a transmitting antenna height of 194 feet. When the receiving terminal is above 130 feet the received sig-

* Reprinted from IRE Transactions, Vol. AP-3, pp. 117–122; July, 1955.

† Formerly at U. S. Navy Electronics Lab., San Diego, Calif. Now at Smyth Research Associates, San Diego, Calif.

[1] J. A. Ratcliffe, "Diffraction from the ionosphere and the fadings of radio waves," *Nature*, vol. 163, pp. 9–11; July, 1948.

[2] H. G. Booker and W. E. Gordon, "A theory of radio scattering," Proc. IRE, vol. 38, pp. 401–412; April, 1950.

[3] W. E. Gordon, "Radio scattering in the troposphere," Proc. IRE, vol. 43, pp. 23–28; January, 1955.

[4] H. G. Booker and J. T. deBettencourt, "Theory of radio transmission by tropospheric scattering using very narrow beams," Proc. IRE, vol. 43, pp. 281–290; March, 1955.

[5] These experimental results were presented in part at the meetings of the International Scientific Radio Union at Zurich, Switzerland, by J. B. Smyth, in August, 1950. Also, presented at the Dedication Meetings, National Bureau of Standards, Boulder, Colo., September, 1954.

nal is steady and is near the value calculated for diffracted field (dashed line). As the receiving antenna is lowered below 130 feet the signal begins to fluctuate rapidly with time and shows little variation of average received field with height. Fig. 3 shows a height gain curve measured with the transmitting antenna at a height of 4 feet; in this case the average received field is independent of height of the receiving antenna and very much stronger than the calculated diffracted field. Thus, with terminals low, the received field fluctuates rapidly with time, exhibits little or no height-gain, and is very much stronger than the diffracted field value. These three characteristics of the signal lead to the conclusion that scattered field is dominant in this situation.

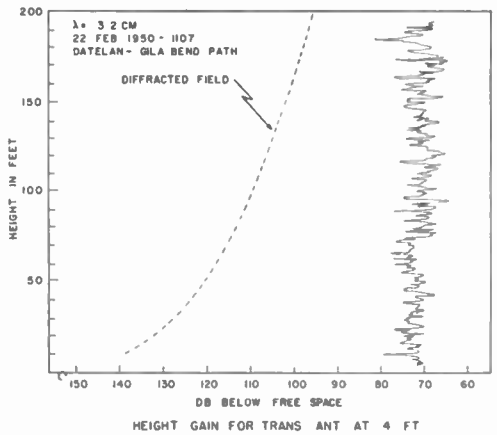

Fig. 3—Measured receiver height gain curve with transmitting antenna at 4 feet.

The Effect of Variation of Antenna Beamwidth

A series of tests were made during the daytime in which the power received with different size antenna apertures was compared using transmissions at 3.2 cm wavelength. Arrangements were made to use either a 1-foot or a 4-foot diameter paraboloid antenna at each terminal. At a wavelength of 3.2 cms the 1-foot antenna has a diameter of 9 wavelengths with a beamwidth of 7 degrees and the 4-foot antenna a diameter of 38 wavelengths with a beamwidth of 1.75 degrees. The tests were made by recording the received power for a period of 1 minute with each antenna and comparing the average of the 1-minute records. The results shown in Table I are the average of the power ratios obtained in some 10 to 15 such comparisons over a period of 10 days. The first line of the table shows the result of comparing a large and small receiving antenna aperture while using a broad-beam transmitting antenna. The ratio of received power amounted to 6 db in contrast to 12 db which would be expected under free space conditions. When both terminals were elevated from 4 feet to 194 feet, into the diffracted field domain, the same comparison yielded values close to 12 db. The second line of the table shows the result of a similar comparison except that the measurement was made with a large aperture transmitting antenna, and consequently the transmitted power was confined so as to illuminate a smaller volume. In this case, the comparison of the two receiving apertures resulted in a power ratio of 7.9 db, a value somewhat closer to the ratio of the plane wave gains of the two antennas. If the ratio of received power as measured as the transmitting aperture, rather than the receiving aperture, is changed from 9 to 38 wavelengths, comparable results are obtained as shown in lines 3 and 4 of the table. A comparison made by simultaneously changing antenna aperture size at both transmitting and receiving terminals gave a measured received power ratio of 14.8 db in contrast to a value of 24 db which would be expected under free space conditions. This is shown in the last line of the table.

TABLE I

Variation of Received Power with Antenna Aperture Size

Transmitting Antenna Diameter	Receiving Antenna Diameter	Measured Ratio of Received Power	Ratio of Plane Wave Gains
9λ	38λ / 9λ	6.0 db	12 db
38λ	38λ / 9λ	7.9 db	12 db
38λ / 9λ	9λ	5.0 db	12 db
38λ / 9λ	38λ	7.1 db	12 db
38λ / 9λ	38λ / 9λ	14.8 db	24 db

λ = 3.2 cm; Antenna Height 4 Feet; 46.3 Mile Path.

Since the measurements indicate that an antenna with a 1.75 degree beam fails to absorb power proportional to its gain when receiving scattered fields, one would expect that as the antenna is rotated, the received power would not fall off in accordance with the polar diagram of the antenna. The results of rotating the 4-foot receiving antenna with a 1.75-degree beam in the horizontal plane are shown by Fig. 4 (next page) and in the vertical plane by Fig. 5 (next page). These measurements were made using a 1-foot transmitting antenna with a 7-degree beam. The left-hand diagrams show the points obtained when the measurements were made with the diffracted field dominant, and the right-hand diagrams are for measurements in the scattered field. In both cases the scattered field points tend to be spread in angle outside the beam of the antenna.

Gordon and Booker and deBettencourt have concluded that presently available measurements of atmospheric turbulence indicate the scale of turbulence, l, is very large compared to microwave wavelengths. With the additional assumption that the angle between the

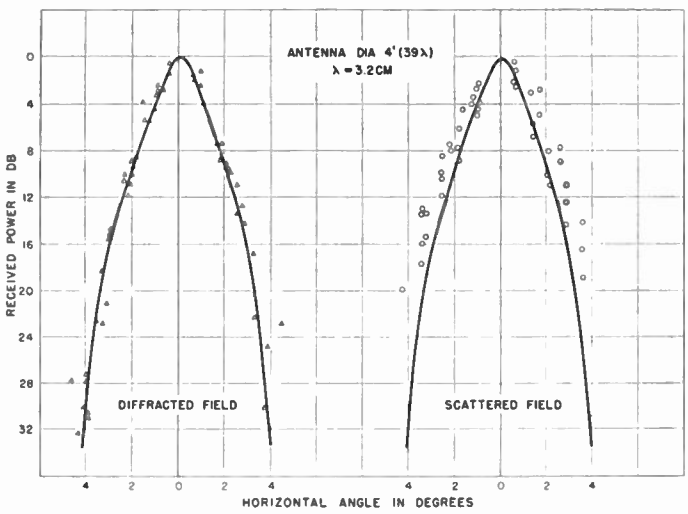

Fig. 4—Effect of rotating receiving antenna in horizontal plane.

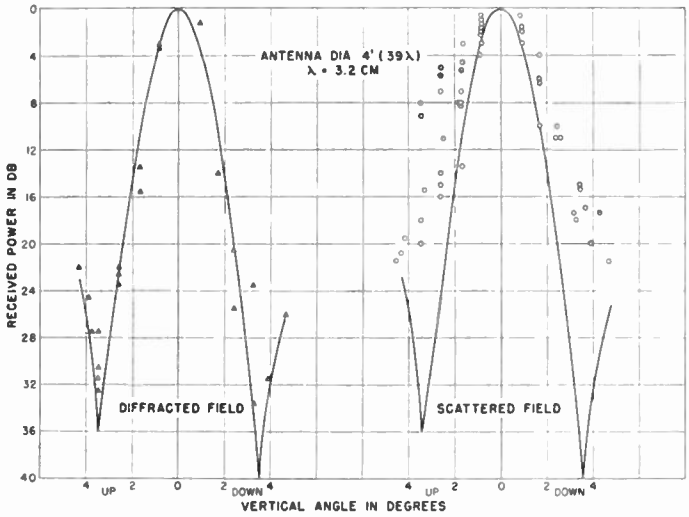

Fig. 5—Effect of rotating receiving antenna in vertical plane.

direction of incidence and the direction of scattering, θ, is small compared to one radian, Gordon derived, from the basic Booker-Gordon scattering formula, the following expressions for the horizontal angle α_c and the vertical angle θ_1, over which scattered radiation is spread at the receiver:

$$\alpha_c = 2/3\theta_0 = 2/3\frac{d}{R}, \tag{1}$$

$$\theta_1 = 1.19\theta_0 = 1.19\frac{d}{R}, \tag{2}$$

where θ_0 is the minimum value of θ imposed by the earth's curvature, d is the distance between transmitting and receiving antennas and R is the radius of the earth modified to account for refraction by a standard atmosphere. These formulas are valid provided,

$$\frac{\lambda}{2\pi l} \ll \theta \ll 1. \tag{3}$$

The horizontal angle α_c is the limiting angle and for the 46.3-mile path over which the tests were made the calaulated value of α_c is 0.35 degrees.

Booker and deBettencourt concluded that the antenna beamwidth must be appreciably smaller than α_c for the spread to be clearly visible in the direction of scattered wave, but a beamwidth five times the computed value of α_c is narrow enough in this case to show the effect.

A comparison between experiment and the theory can also be made by fitting data obtained with several antenna apertures on a chart such as that of Fig. 6, which was used by Booker and deBettencourt to illustrate the effect of antenna beamwidth on received power. This graph is based on their two equations

$$\frac{P_R}{P_F} = 0.86\frac{R^2}{d}S_p \quad \text{for} \quad \alpha \gg \alpha_c \tag{4}$$

$$\frac{P_R}{P_F} = \frac{2d\alpha^3}{(\theta_0 + \alpha/2)^5}S_p \quad \text{for} \quad \alpha \ll \alpha_c, \tag{5}$$

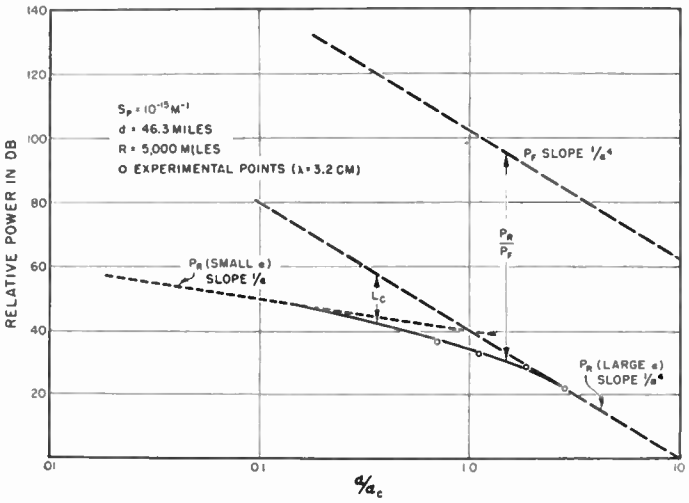

Fig. 6—Received power as a function of α/α_c.

where P_R is received power, P_F is received power in free space, α is antenna beamwidth (assuming identical transmitting and receiving antennas), and S_p is the scattering parameter of the atmosphere given by

$$S_p = \frac{1}{2\pi l}\left(\frac{\overline{\Delta\epsilon}}{\epsilon}\right)^2,$$

where $\overline{(\Delta\epsilon/\epsilon)^2}$ is the mean-square deviation of the dielectric constant from the mean. These two equations are valid provided the conditions of (3) are met. For α large compared to α_c, the antennas function as if in free space and P_R and P_F both vary as $1/\alpha^4$, P_R/P_F is independent of beamwidth and (4) applies. When α is small compared to α_c, P_R/P_F varies as α^3 according to (5) and consequently P_R is proportional to $1/\alpha$. The chart of Fig. 6 has been drawn for the 46.3-mile path, assuming a value of S_p equal to 10^{-15} meter^{-1}. The quantity labeled Lc on the graph which increases as the ratio α/α_c decreases, has been termed the "aperture-

medium coupling loss" by Booker and deBettencourt.[6] Experimentally determined values of Lc are available from measurements made in Arizona. Using 3.2-cm transmissions, measurements were made of received power as the transmitter and receiver were simultaneously shifted from 4-foot to 1-foot, $2\frac{1}{2}$-foot to 1-foot, and $1\frac{1}{2}$- to 1-foot diameter antennas. Or in terms of beamwidth received power was measured as α was changed successively from $1\frac{3}{4}$ to 7, 2.8 to 7, and 4.6 to 7 degrees. Changing antenna diameter from 1 to $1\frac{1}{2}$ feet or α from 7 to 4.6 degrees resulted in a power change of 6.9 db as compared to 7.0 db which would be expected under free space conditions. Thus, it is apparent that Lc must be zero for $\alpha=7$ degrees and the value of received power measured with this beamwidth should lie on the dashed line with slope $1/\alpha^4$ valid for large α. Consequently, the measured values of P_R should be placed on the graph so as to form a smooth transition between the dashed lines having slopes $1/\alpha$ and $1/\alpha^4$, with the value for $\alpha=7$ degrees on the latter line. The experimental values placed in this fashion are shown as circles on the graph, and this fixes α_c as equal to 2.5 degrees. This value is 7 times larger than the value of 0.35 degrees computed from Gordon's formula (1).

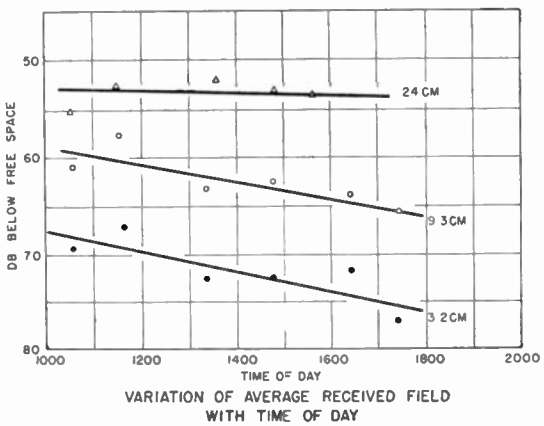

Fig. 7—Variation of received field with time of day.

Variation of Received Field with Wavelength

The measured variation of average received field strength with time of day is shown in Fig. 7 for wavelengths of 3.2, 9.3 and 24 cms. These measurements were made with transmitting and receiving antennas 4 feet in diameter located 4 feet above the ground. The received power decreases somewhat with time of day, with the decrease greatest for the shortest wavelength. However, this variation with time of day is not large. The variation of the ratio P_R/P_F with wavelength is more pronounced, as shown in Fig. 8. The variation with wavelength is slightly less in the morning than in the afternoon. The 4-foot diameter antennas used at a wavelength of 24 cms have a beamwidth of 14 degrees so that formula (4) valid for large α should apply. Assuming $S_p=10^{-15}$ meter^{-1} the computed value using this formula is shown as point (1) on Fig. 8, which is about 8 db below the measured values. If S_p were assumed equal to 10^{-14} meter^{-1} the computed value of P_R/P_F for 24 cm would be shifted by 10 db and the agreement would be better. For 4-foot antennas at 3.2 cms the beamwidth is 1.75 degrees, some five times the computed value for α_c of 0.35 degree, and one would expect on the basis of the theory that the formula for large α would be applicable. However, this would predict no dependence of P_R/P_F on wavelength. If α_c is assumed to be 2.5 degrees and $S_p=10^{-15}$ M^{-1} and a value of P_R/P_F for 3.2 cms is determined from Fig. 6, point (2) on Fig. 8 is obtained which is in agreement with the data for this wavelength. But then the value for 24 cms is 8 db off and it would appear that this experimental data shows more wavelength dependence than allowed for by the Booker-Gordon theory.

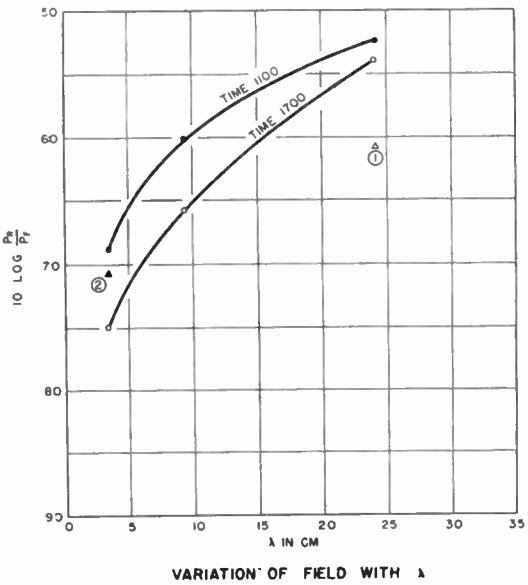

Fig. 8—Variation of received field with wavelength.

Fluctuating Characteristics

The scattered fields fluctuate rapidly with time as shown in the sample records of Fig. 9 (next page), which were made with Brush recorders at 3.2, 9.3, and 24 cm transmissions and quite obviously the character of the fluctuations are a function of wavelength. Booker and Gordon utilized a concept by Ratcliffe[1] to explain the fluctuations. Ratcliffe defined a quantity, S, the speed of fading by

$$S=\frac{\overline{|U_\tau|}}{\tau\overline{E}}, \tag{6}$$

where E is the signal amplitude, U_τ is the difference between successive values of E taken at intervals τ

[6] This loss sometimes has been referred to incorrectly as a "loss of antenna gain." Gain, as defined usually, is a constant for a given antenna (e.g. S. Silver, "Microwave Antenna Theory and Design," M.I.T. Radiation Lab. Ser., McGraw-Hill Book Co., Inc., New York, N. Y., vol. 12, p. 3; 1949).

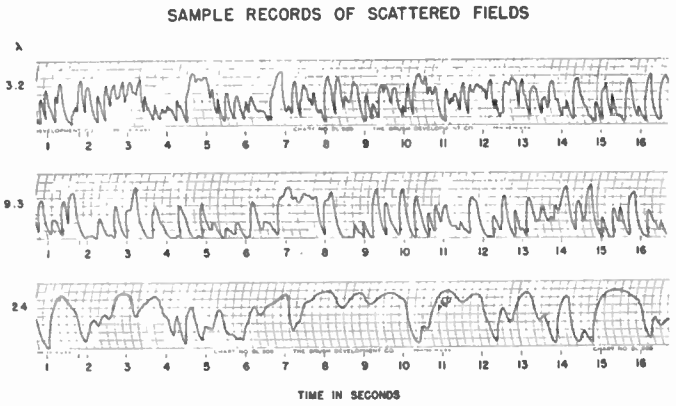

Fig. 9—Typical records of scattered field signals for three wavelengths.

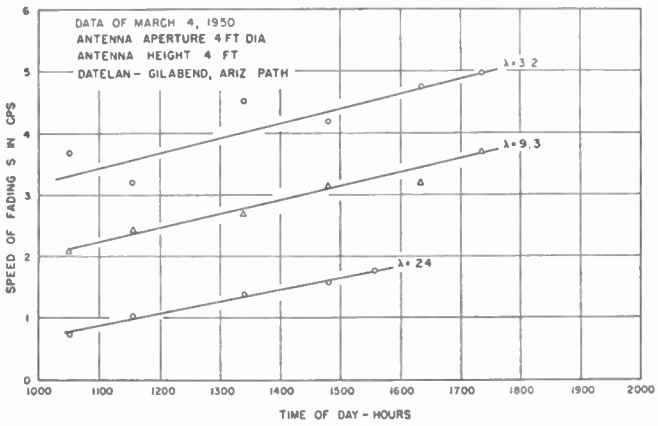

Fig. 11—Variation of speed of fading with time of day.

seconds apart, with τ sufficiently small so that E does not vary greatly in one interval. He has shown that the speed of fading can be related to a fractional Doppler shift in frequency due to effective speed of the scatterers, V, by the following relation

$$S = \frac{2Vf \sin \theta/2}{C}, \qquad (7)$$

where f is the radio frequency, C the velocity of light and θ is the angle between the direction of incidence and the direction of scattering. Thus the speed of fading should vary directly as the radio frequency. Using (6), the speed of fading was calculated for a number of cases at three frequencies (or wavelengths of 3.2, 9.3 and 24 cms). Fig. 10 is a typical sample of the results which

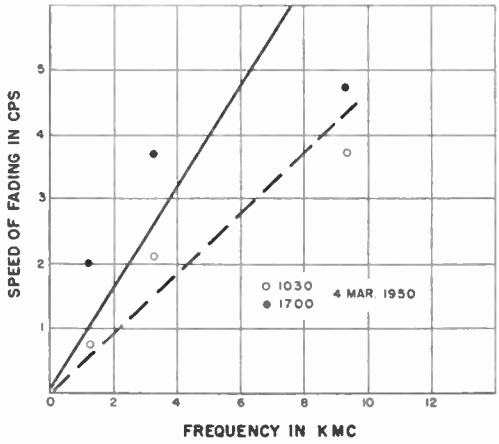

Fig. 10—Variation of speed of fading with frequency.

were obtained. The points obtained from data taken at 10:30 in the morning fit fairly well on a straight line but the afternoon points are a poorer fit to (7). Data taken simultaneously at more than three frequencies would be desirable to determine if the speed of fading follows formula (7) or some other relationship.

Fig. 11 shows a plot of the variation of speed of fading with time of day. For all three wavelengths the speed of fading increases slowly with time of day. Earlier than 10:00 in the morning or later than 6:00 in the evening the presence of the radiation inversion causes the refracted field component to swamp out the scattered field. This gradual increase of speed of fading was consistently observed every time scattered field recordings were made. This would seem to indicate that fading is not due to the fact that scatterers drift with

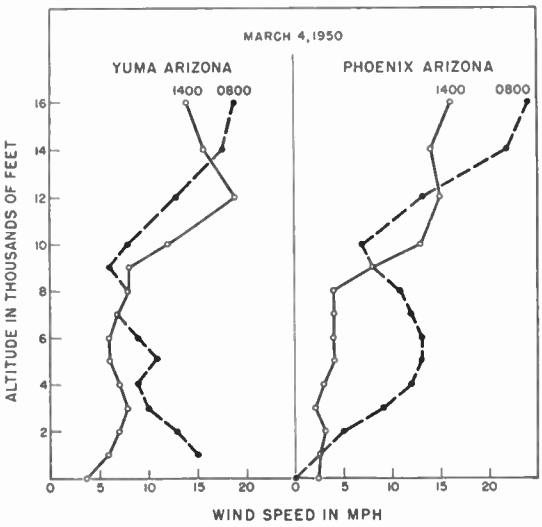

Fig. 12—Wind speed as a function of altitude.

the mean wind. Fig. 12 shows profiles of wind speed aloft for the same day that the data of Fig. 11 was taken. Two sets of wind data are shown, one taken at Yuma, Arizona, 100 miles west of the propagation path, and the second taken at Phoenix, Arizona, 100 miles northeast of the path. Below 7,000 feet the wind speed is greater at 0800 than at 1400. With antenna beamwidth of $1\frac{3}{4}$ degrees and a pathlength of 46.3 miles, the important scattering volume should lie below 4,000 or 5,000 feet altitude, so it is apparent that the trend in upper wind is opposite to the trend in speed of fading. It appears more likely that the increase of speed of fading during the day is connected with the diurnal meteorological cycle. The nocturnal radiation inversion is dissipated in the morning by heating of the ground and a turbulent layer is propagated upward as the day

progresses and ground heating is intensified. Consequently the velocity V in formula (7) is probably an effective velocity due to the upward motion of the turbulence during the day.

Conclusions

Scattered fields measured on a 46.3-mile path in Arizona with low terminal heights arrive at the receiving antenna spread over an appreciable angle. This angle is some 5 to 7 times as large as the angle computed using an approximate formula derived by Gordon based on the assumption that the scale of turbulence is large compared to the wavelength. Appreciable aperture to medium coupling loss occurs for antennas with beamwidth considerably larger than this computed angle.

The ratio of received power to power received in free space measured at wavelengths of 3.2, 9.3 and 24 cms shows a greater wavelength dependence than predicted by the Booker-Gordon theory.

The speed of fading measured at wavelengths of 3.2, 9.3 and 24 cms increases with increasing frequency or decreasing wavelength. The increase of speed of fading with frequency follows fairly well the linear relationship inherent in Booker and Gordon's equation based on Ratcliffe's concept. The speed of fading on this path always increases during the day and does not correlate with mean upper wind speed. This increase with time of day is probably connected with the diurnal meteorological cycle.

Acknowledgment

The author is indebted to W. C. Hoffman, C. A. Potter, and J. B. Smyth for many helpful discussions; and to E. L. Culler and M. D. Rocco who assisted with the computations.

Results of Propagation Tests at 505 mc and 4,090 mc on Beyond-Horizon Paths*

K. BULLINGTON†, SENIOR MEMBER, IRE, W. J. INKSTER‡, AND A. L. DURKEE†, VOTING ASSOCIATE, IRE

Summary—**This paper gives the results of some radio propagation tests which were made on two beyond-horizon paths in Newfoundland. During these tests simultaneous transmissions at 505 mc and 4,090 mc over a 150-nautical mile path were measured for a full year, and transmission at 505 mc over a 255 mile path was measured for a period of 5 months. Both of these paths were partly over land and partly over water. Long term median signal levels and fading statistics for the two paths are given, as well as the results of some measurements of the improvement obtained from space diversity reception and the gain realized from large (28 foot) antennas on the 150-mile path. The test results provide further evidence of the feasibility of using uhf beyond-horizon links in communication systems.**

Introduction

THIS PAPER presents the results of some radio propagation tests which were made on two beyond-horizon paths in Newfoundland during the period from October, 1953 to October, 1954. In these tests continuous measurements of radio transmission were made on a 150-nautical mile path for a full year, using frequencies of 505 mc and 4,090 mc. In addition, measurements were made at 505 mc on a 255-nautical mile path for a period of 5 months. The work was done for the U. S. Air Force and the main objective was to obtain long-term propagation data on which estimates of the performance of beyond-horizon communication links could be based. The Air Force, Bell Telephone Co. of Canada, and Bell Telephone Laboratories collaborated in planning and carrying out the test program.

The tests consisted mainly in transmitting unmodulated carriers and making continuous graphical records of the signals received. This paper gives the results of an analysis of these records to determine long term median signal levels and the characteristics of the variations about the median levels. Also included in the test program were measurements of the improvement obtained from space diversity reception and the gain realized from large (28 foot) antennas on the 150-mile path. The results of these supplementary tests are also discussed in this report.

Summary of Results

These tests, covering a period of a full year, have provided further evidence of the feasibility of using uhf beyond-horizon links for communication systems. The long-term median signal levels at the 505 mc test frequency were found to be very close to the expected values on both the 150- and 255-nautical mile paths. The fading statistics also were in good agreement with expectations. At no time during the year of testing was there a failure to record the 505 mc signal on the 150-mile path because of poor propagation conditions. At 4,090 mc there were occasional propagation outages. The equipment employed did not provide as much transmission margin at 4,090 mc as at 505 mc and, in addition, the average path loss at 4,090 mc turned out to be about 14 db greater than had been anticipated.

The principal results of the tests are summarized in the following paragraphs:

1. The long term median signal level at 505 mc on the 150-nautical mile path was 67 db below the free space value, or 3 db higher than the value predicted from previous experience on other beyond-horizon paths. When the distance was increased from 150 miles to 255 miles, the reduction in median signal level referred to free space amounted to about 12 db, which is within 2 db of the predicted value.
2. The long-term median signal level at 4,090 mc on the 150-mile path was 84 db below the free-space value, or about 14 db below expectations. It appears that part of this discrepancy can be attributed to a reduction in the effective gain of 28-foot dishes on the beyond-horizon path as compared with the gain obtained on line-of-sight paths at 4,000 mc.
3. There was a pronounced seasonal variation in average signal level at both frequencies on the 150-mile path, the signals being considerably higher in the summer and fall than in the winter and spring. The difference between the highest and lowest monthly medians was 19.5 db at 505 mc and 13 db at 4,090 mc.
4. There was evidence of a small diurnal variation in average signal level and signal variability. The average signal levels were several db higher for the hours between midnight and noon than for the hours between noon and midnight, and the variability was a little less in the afternoon than it was around midnight and in the early morning. Both effects were more noticeable in the summer than in the winter.
5. There was a marked similarity in the slow variations of hourly median signal levels at 505 mc and 4,090 mc on the 150-mile path. Also, the slow variations of the 505 mc signals received simultaneously on the 150- and 255-mile paths were generally similar.

* Original manuscript received by the IRE, August 12, 1954.
† Bell Telephone Labs., Inc., New York, N.Y.
‡ Bell Telephone Co. of Canada, Montreal, Canada.

6. The depth of fading within the hour, as defined by the ratio of the signal levels exceeded for 50 per cent and 99 per cent of the hour, was largely independent of the median signal level for the hour.
7. The signals received at both frequencies on the beyond-horizon path were characterized by a practically continuous rapid fading superimposed on much slower variations in average signal level. Over short intervals of time the instantaneous signal amplitudes were found to have approximately a Rayleigh distribution. An investigation of the duration of individual rapid fades at 505 mc showed that in a typical hour there were 32 such fades exceeding 15 db in depth. Of these, only one lasted longer than 3 seconds.
8. Space diversity reception was found to be effective in reducing the range of the fast fading, although it did not materially affect the slow variations. On the average, the signal level exceeded for 99 per cent of the time was approximately 10 db higher for the dual diversity combination than for a single antenna. This result indicated that substantially the full theoretical diversity improvement was obtained with the antenna separation of 200 feet which was used in the tests.
9. A comparison of distribution curves of instantaneous signal levels taken simultaneously on the 28-foot dish and a small reference dish, together with a comparison of hourly medians on the two antennas, indicated that at 4,090 mc the average effective gain of the large dish over the small one was 2 to 4.5 db less than the value expected for line-of-sight paths.
10. There was a marked tendency for the hourly median signal levels to be depressed during snowstorms and enhanced when there was fog over the path. The magnitude of these effects was of the order of 6 to 10 db. There was also some evidence of signal depression during rainfall, but the effect was less pronounced than for snowfall.

Test Circuits

Transmission Paths

The paths on which the propagation tests were made are indicated on the map of Fig. 1. The shorter path extended from St. Anthony to Gander, a distance of about 150 nautical miles. This path was over water except for about 35 miles at the Gander end. The test sites provided good foreground clearance in the transmitting and receiving directions.

As indicated in Fig. 1, measurements were also made on a path from St. Anthony to Harbour Main during the latter part of the test program. This path was about 255 nautical miles long, partly over land and partly over water. The elevation of the land was less than 1,000 feet at all points on the path. The tests on this path were confined largely to the 505 mc frequency because the transmitter power and antenna gains at 4,090 mc were not sufficient to provide a satisfactory signal at Harbour Main for recording.

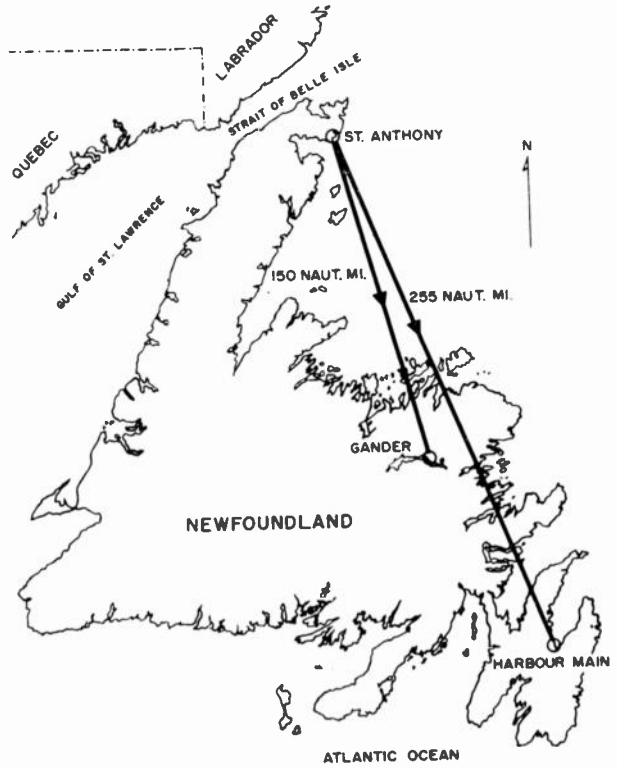

Fig. 1—Map showing test paths.

Antennas

The antennas used on the test circuits were of the parabolic reflector type. On the 150-mile path reflectors 28 feet in diameter were employed. A single antenna was provided at the St. Anthony transmitting site, with a dual feed arrangement to permit simultaneous transmission at 505 mc and 4,090 mc. The polarization was horizontal at 4,090 mc and vertical at 505 mc. Two similar antennas were used at the Gander receiving site, arranged for space diversity tests at both frequencies. These antennas were located about 200 feet apart on a line at right angles to the direction of reception. In all cases the 28-foot antennas were supported so that their lower edges were about 3 feet above ground. At St. Anthony the terrain in the immediate foreground dropped sharply to sea level, while at Gander the foreground was reasonably flat for the first several miles.

In order to make tests on the 255-mile path the transmitting antenna at St. Anthony was turned toward Harbour Main. When this was done the average 505 mc signal level dropped 17 db at Gander but it still was high enough for recording. At Harbour Main the signal was received from St. Anthony on a $5\frac{1}{2}$-foot antenna which had about 14 db less gain than the 28-foot receiving antenna at Gander.

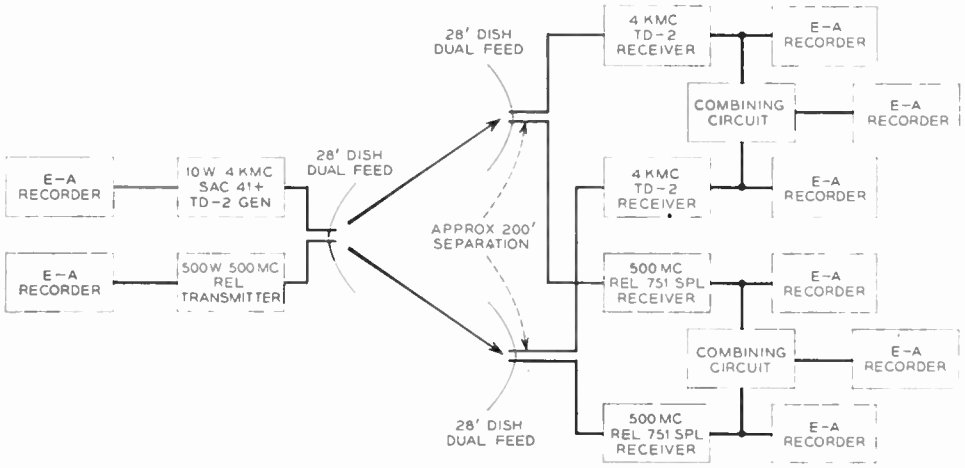

Fig. 2—Test facilities, 150-mile path.

The transmitting and receiving antennas were connected to the equipment by means of WR229 waveguides at 4,090 mc, and by $1\frac{5}{8}$-inch Styroflex cable at 505 mc. The waveguide and cable runs were pressurized.

Equipment

The radio transmitters and receivers for the tests were built by Radio Engineering Laboratories (REL). The 505 mc equipment was of REL design throughout, while the 4,090 mc equipment made considerable use of components that were developed for the TD-2 relay system. The transmitters had power outputs of 500 watts at 505 mc and 10 watts at 4,090 mc. The latter output was obtained by means of a power amplifier built around a Sperry SAC41 klystron. Throughout the tests continuous records were made of the power outputs of all transmitters, and the received signal data were corrected for any significant variations in transmitter power.

The radio receivers were calibrated at frequent intervals by means of signal generators so that they measured the magnitude of the signal power delivered by the receiving antennas. Narrow band IF amplifiers were incorporated in the receivers in order to obtain as high a signal-to-noise ratio as practicable in the recording circuits. These bandwidths were 20 kc and 100 kc in the 505 mc and 4,090 mc receivers, respectively. The necessary frequency stability in the receivers, as well as in the transmitters, was obtained by the use of temperature controlled crystals. Although the tests consisted mainly in recording unmodulated carrier transmissions, provision was made in the equipment for transmitting speech over the circuits by frequency modulation of the radio carriers.

The rectified outputs of the receivers were recorded graphically by means of Esterline-Angus recorders. Compressor-amplifiers, in which the output voltage was proportional to the logarithm of the input voltage, were inserted ahead of the recording point in the receivers, so that a recording characteristic substantially linear in db over a 40 to 50 db range of inputs was obtained. In addition to recording individual receiver outputs recorders were also connected to the diversity receiver pairs so that a record was obtained of the stronger of the two output signals of each pair. These records provided data for evaluating the improvement obtained from diversity reception. The time constant of the recording circuits was about $\frac{1}{2}$ second, and the chart speed normally was 3 inches per hour. Provision was made for increasing the speed to 3 inches per minute when greater resolution in the record was desired.

Primary power for operating the equipment was obtained from an existing plant at St. Anthony, and from 30 kw diesel engine-alternators at the other test sites. Voltage regulators were employed at all locations to minimize the effects of line voltage fluctuations on transmitter power output and receiver characteristics.

The test facilities as described above for the 150-mile path are shown in the diagram of Fig. 2. The main features of the arrangements on the 150- and 255-mile paths are summarized in Table I.

TABLE I

PROPAGATION TEST FACILITIES

Path	Frequency	Transmitting Power	Antenna Size		Diversity Receiving Antenna Spacing
			Transmitting	Receiving	
150 miles	505 mc	500 w	28 feet	28 feet	200 feet hor.
	4,090	10	28 feet	28 feet	200 feet hor.
255 miles	505	500	28 feet	5.5	Single ant.

TEST RESULTS

The Esterline-Angus records obtained on these beyond-horizon paths showed practically continuous rapid fading. This fast fading, characterized by periods of the order of seconds, was superimposed on much slower changes in average signal level. The records obtained at 505 mc and 4,090 mc were generally similar in these respects.

The normal chart speed of 3 inches per hour was satisfactory for recording the long term signal variations

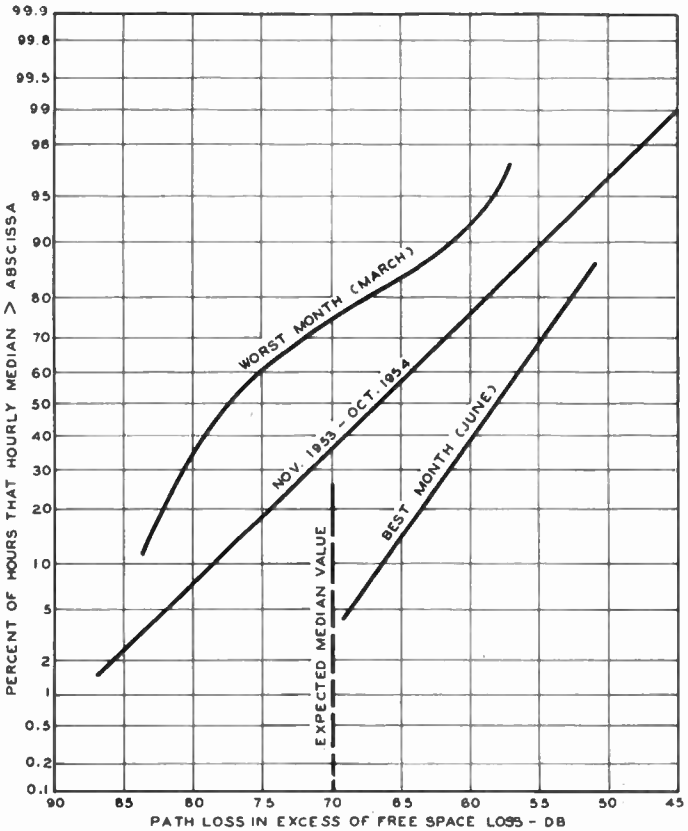

Fig. 3—Distribution of 505 mc hourly medians path loss.

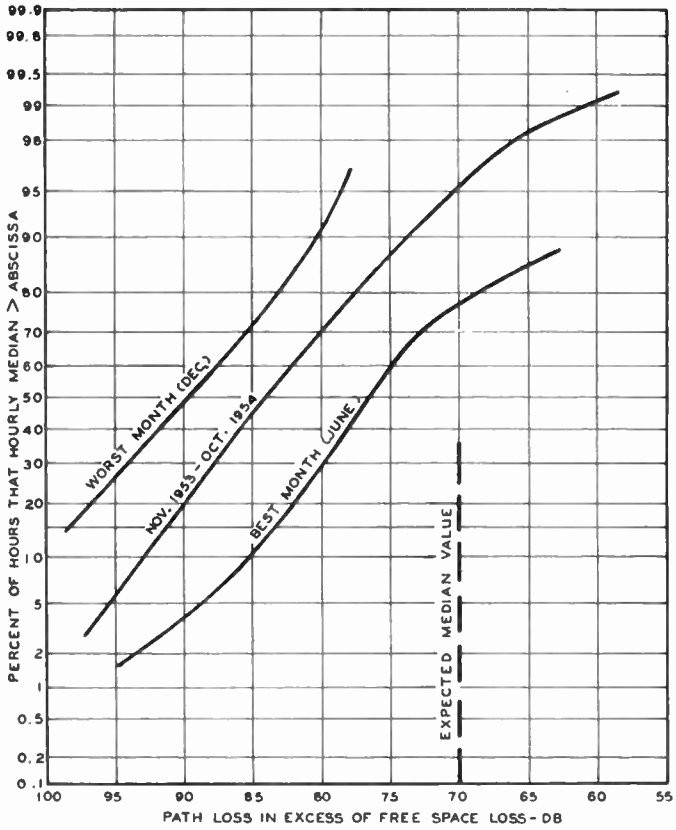

Fig. 4—Distribution of 4,090 mc hourly median path loss.

but, of course, was too slow to resolve the fast fades. To determine the nature of the fast fading the signals were recorded from time to time with a chart speed of 3 inches per minute. In addition, test runs were made with a Level Distribution Recorder (LDR). This is a device which automatically samples the signal level at intervals of one second and stores the information in a set of counters. The LDR was capable of following signal variations as rapid as 60 cps, whereas the graphic recording circuits averaged out any variations exceeding a few cycles per second.

The analysis of the Esterline-Angus Records to determine long term variations consisted in estimating the signal levels exceeded for 50 per cent and 99 per cent of each hour. The 50 per cent (median) value indicated the average condition and the 99 per cent (percentile) value the low signal condition for the hour. The ratio of the median to the percentile was taken as a measure of the depth of fading within the hour. Distribution curves showing how the instantaneous signal levels varied for selected short intervals were obtained from the high speed (3 inches per minute) Esterline-Angus charts and from the LDR data.

Range of Hourly Medians

Over the period of a year there was a wide variation in hourly median signal levels. This is indicated in Figs. 3 and 4 which show cumulative distribution curves of the hourly medians for 505 mc and 4,090 mc on the 150-mile path for the whole year and for the best and worst months. The scale of abscissas in these figures gives measured path loss in db referred to the value that would be expected for free space transmission. The results can be represented reasonably well by log-normal distributions, with standard deviations of about 9 db and 7.5 db for 505 mc and 4,090 mc, respectively.

From previous experience on other beyond-horizon paths it was expected that the long term median loss on the 150-mile path at both frequencies would be about 70 db greater than the free space values.[1] It will be seen from Figs. 3 and 4 that the measured medians were 67 db and 84 db at 505 mc and 4,090 mc, respectively. Thus, at 505 mc the median loss was 3 db less than the expected value while at 4,090 mc it was about 14 db greater than anticipated. The computed loss at 4,090 mc was based on the assumption that the 28-foot dishes would have the same gain (about 46 db) on the 150-mile beyond-horizon path that they show on shorter line-of-sight paths. However, antenna comparison tests which are described in another section of this paper indicate that the average gain at 4,090 mc fell several db short of the expected value, and part of the discrepancy between predicted and measured path losses can be attributed to this factor.

The path loss data for Figs. 3 and 4 were obtained by comparing measured values of received signal power

[1] K. Bullington, "Radio transmission beyond-the-horizon in the 40–4,000 mc band," PROC. IRE, vol. 41, pp. 132–135; January, 1953.

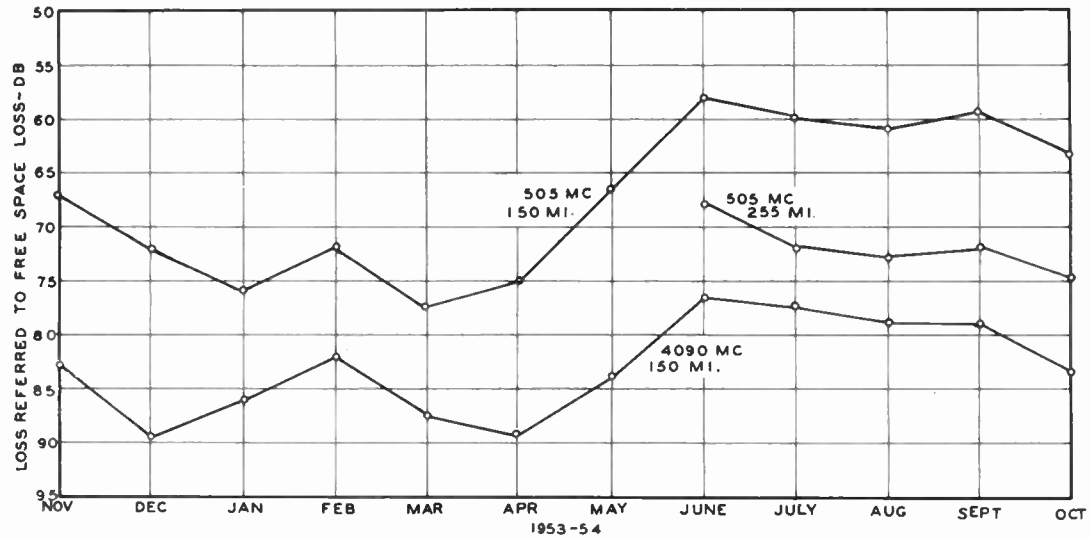

Fig. 5—Monthly medians of hourly medians of path loss.

with the values that would be expected for free-space transmission. The latter were calculated in the manner shown in Table II.

TABLE II

RECEIVED SIGNAL POWER FOR FREE SPACE TRANSMISSION

1. Frequency—mc	505	4,090	505
2. Distance—nautical miles	150	150	255
3. Free space loss (isotrop. ants.)—db	135	153	140
4. Transmitting antenna gain—db	31	46	31
5. Receiving antenna gain—db	31	46	16
6. Transmission line losses—db	1	2	2
7. Net path loss—db	74	63	95
8. Transmitting power—dbw	27	10	27
9. Received signal power—dbw	−47	−53	−68

Seasonal Variation

The wide range of hourly median signal levels experienced over the year naturally raises the questions as to how the medians were distributed in time. It is of particular interest to know when the low signal periods occurred and how long they lasted. One important effect was the change in average signal level with season. This effect is illustrated in Fig. 5 which shows monthly medians of the hourly medians of path loss. There is a marked seasonal variation at both frequencies, the average signal levels being considerably higher in the summer and fall than in the winter and spring. The difference between the highest and lowest monthly medians was 19.5 db at 505 mc and 13 db at 4,090 mc. The highest signal levels occurred in June for both frequencies, while December and April were the low months for 4,090 mc and March the low month for 505 mc.

Monthly medians for 505 mc transmission on the 255-mile path are also plotted in Fig. 5 for June through October. It can be seen that the median loss of this path, referred to free space, was about 12 db greater than that for the 150-mile path over the same period of time. An empirical rule which has been derived from data taken on other beyond-horizon paths says that the excess loss over free space for paths 50–300 miles long increases about 18 db when the distance is doubled. On this basis, an increase in path length from 150 to 255 miles would be expected to increase the loss referred to free space by 13.8 db, which is in reasonably good agreement with the 12 db of Fig. 5.

The 505 mc signal on the 150-mile circuit was always far enough above the noise level so that satisfactory hourly median values could be estimated during low signal periods. On the other hand, the signal was sometimes so high as to be outside the recording range, with the result that maximum hourly medians could not be estimated for several of the months. The lowest hourly median signal level observed was 93 db below the free space value, and it occurred in January. The highest hourly median and the month in which it occurred cannot be specified exactly for the reason just given, but it is known to have been at least 57 db higher than the January minimum.

Diurnal Variation

There was some evidence of a systematic change in average signal level with time of day, but this effect was comparatively small. In general, the average signal levels were several db higher for the hours between midnight and noon than for the hours between noon and midnight. The effect was somewhat more pronounced in the summer than in the winter. The range of variation of the hourly medians was a little less in the afternoon than it was around midnight and in the early morning. Here again, the effect was more noticeable in the summer than in the winter.

Number and Duration of Slow Fades

In order to show how the low values of hourly median signal levels were distributed in time, the lengths of individual periods during which the hourly medians were more than 5, 10 and 15 db below the median for the

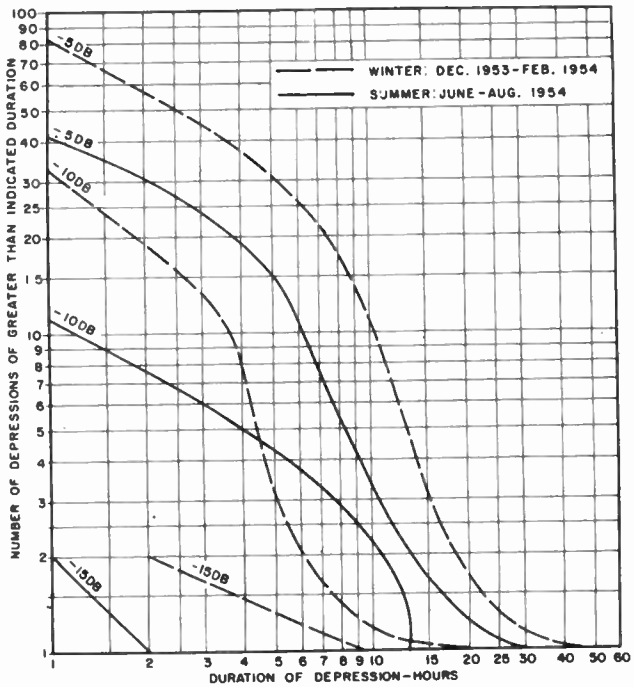

Fig. 6—Number of slow fades vs duration—505 mc.

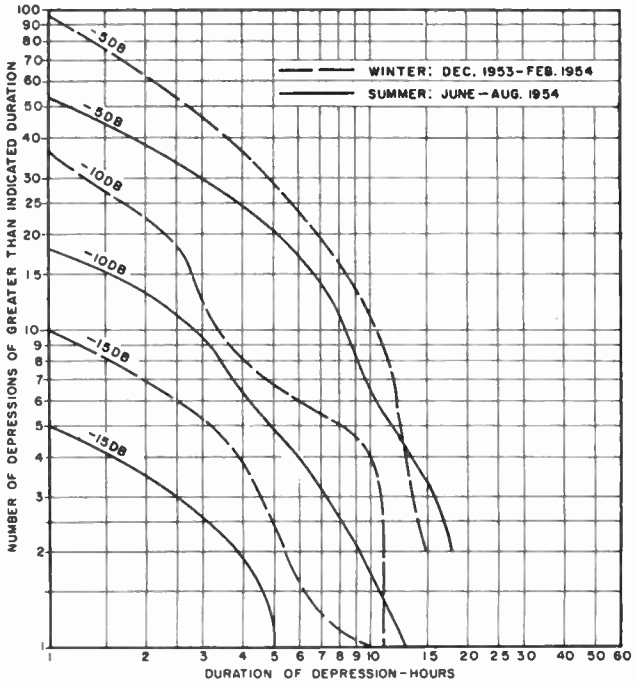

Fig. 7—Number of slow fades vs duration—4,090 mc.

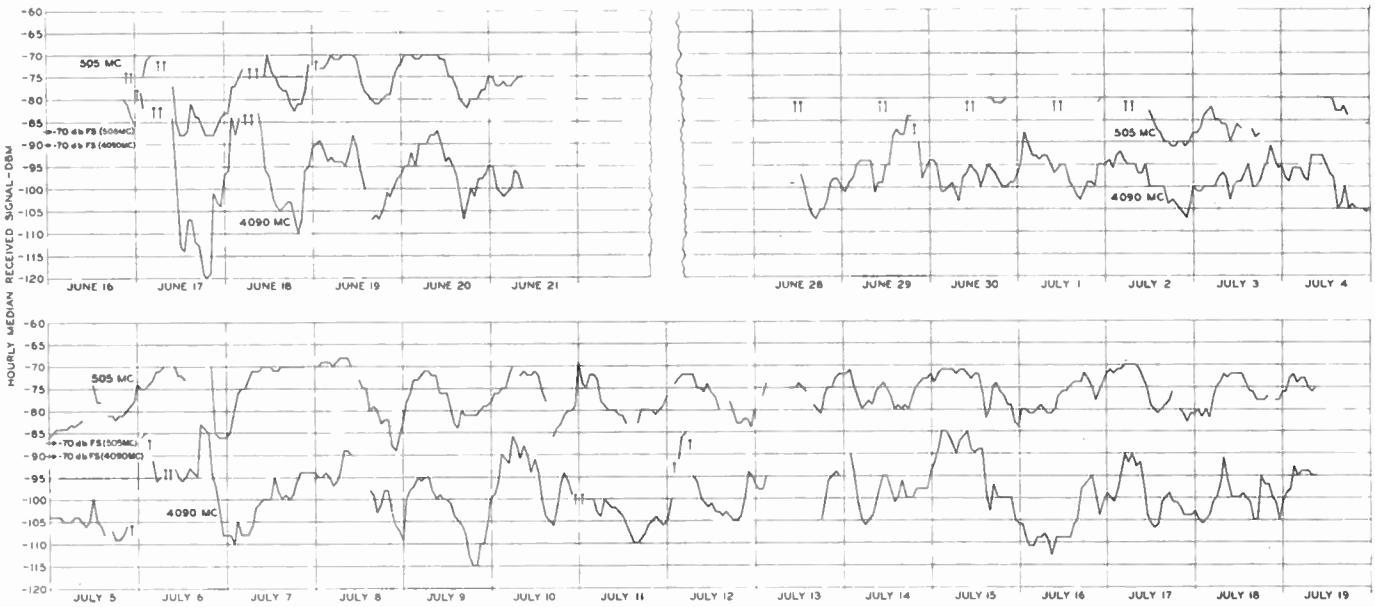

Fig. 8—Comparison of 505 mc and 4,090 mc hourly median received signals.

month were tabulated. The results are shown by the distribution curves of Fig. 6 for 505 mc and Fig. 7 for 4,090 mc. Separate curves are plotted for the summer and winter seasons. It will be noted that in all cases the depressions were more numerous and of longer average duration in the winter than in the summer. Comparing the two frequencies, it will be seen that depressions of 15 db or more were considerably more numerous at 4,090 mc than at 505 mc. The longest single depression of 15 decibels or more was 10 hours in both cases.

Comparison of 505 mc and 4,090 mc Signals on 150-Mile Path

Throughout the tests there was a marked similarity in the slow changes in average signal level at 505 mc and 4,090 mc on the 150-mile path. This is illustrated by Fig. 8 which is an hour-by-hour plot of the median signal levels at the two frequencies for a period of a month during the summer. While the two traces are not alike in detail, it is apparent that the major, large amplitude variations are generally similar and occur at about the

same time. These major variations are slow enough so that the change in median signal level from hour to hour is usually a gradual one. The magnitude of these variations was somewhat greater at 4,090 mc than at 505 mc for the period covered in Fig. 8. There was also a marked similarity in the long term variations of the 505 mc signals received simultaneously on the 150- and 255-mile paths.

Hourly Fading Depth

Ratio of signal levels exceeded for 50 and 99 per cent of each hour is called hourly fading depth. This quantity is a measure of within-the-hour variability resulting from fast fading, and is convenient for evaluating effects of fast fading over long periods of time.

It was found that the magnitude of the fast fading, as indicated by hourly fading depth, showed no significant variation with time of day and very little with season. Fig. 9 gives distribution curves of hourly fading depth at 505 mc for three summer and three winter months. The median value of the fading depth was about 16 db in the summer as compared with 14 db in the winter, and the maximum values recorded were 29 db and 25 db for summer and winter, respectively.

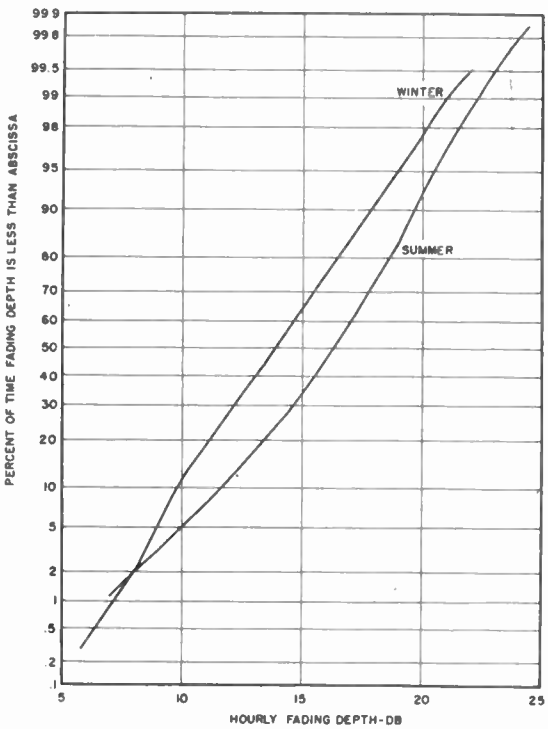

Fig. 9—Distribution of hourly fading depth—505 mc.

Mass plots of hourly fading depth versus hourly median signal level are shown in Fig. 10 for the months of March (low average signal level) and August (high average signal level). There is some indication in these plots that the smallest values of fading depth tend to occur when the median signal level is very high, but for the normal range of signal levels there is no significant relationship between fading depth and median level. The apparent tendency for the fading depth to decrease at low levels (March data) is probably due to the difficulty in reading the percentile values which were near the noise level of the receiver.

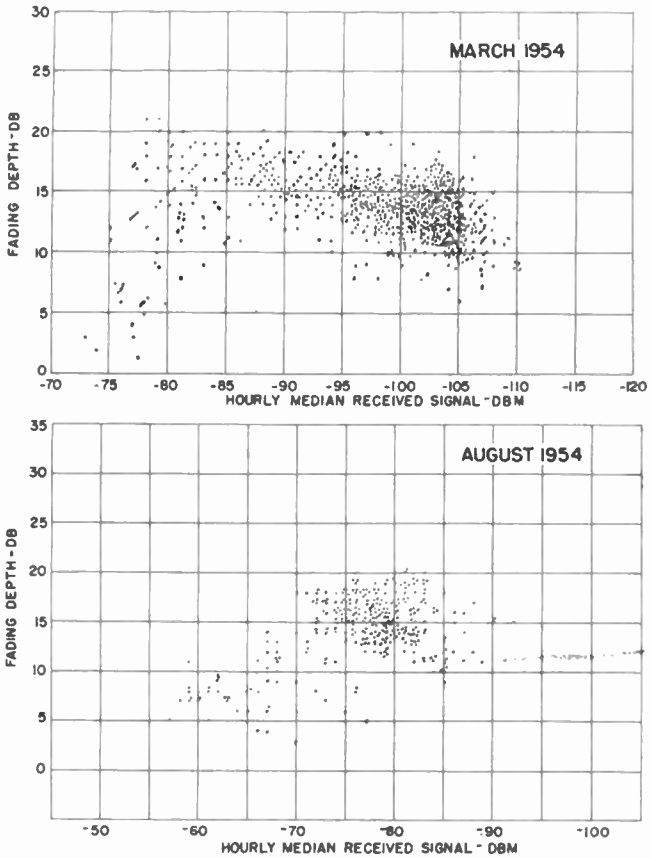

Fig. 10—Hourly fading depth vs hourly median signal level—505 mc.

Fast Fading

Statistical information on the fast fading over short intervals was obtained by means of the Level Distribution Recorder. Test runs about 15 minutes in length were made with the LDR, and the data accumulated from the individual runs were used to plot the distribution curves of instantaneous signal amplitude shown in Figs. 11 and 12 (next page). Signal levels for each curve are expressed in db referred to the median level for period during which run was made. In this way the effects of any long term variations have been removed so that the curves show only the fast fading variations.

It was expected that the instantaneous signal amplitudes over short periods of time would have a Rayleigh distribution. Accordingly, the distribution curves of Figs. 11 and 12 are plotted on a scale of ordinates which makes the Rayleigh distribution a straight line, as indicated in the figures. It can be seen that some of the individual runs depart considerably from the Rayleigh form. However, the group as a whole is pretty well centered about the Rayleigh line at both 505 mc and 4,090 mc. It is possible that systematic departures from the Rayleigh curve in the low percentage region may

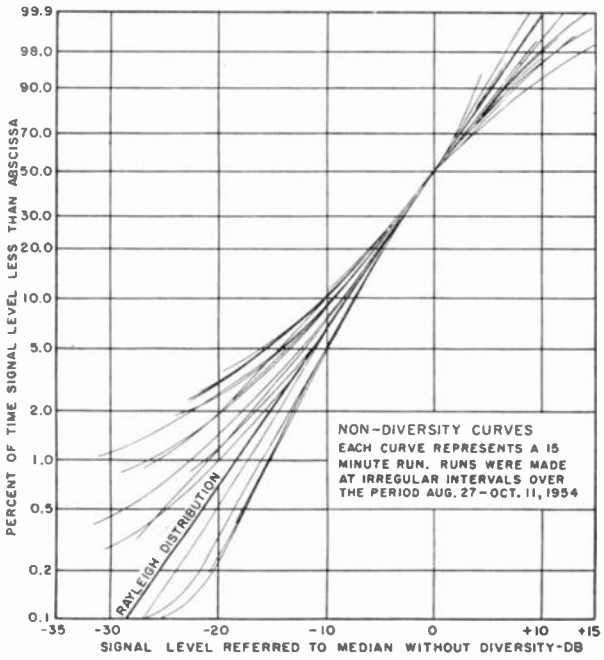

Fig. 11—Distributions of instantaneous signal level—505 mc.

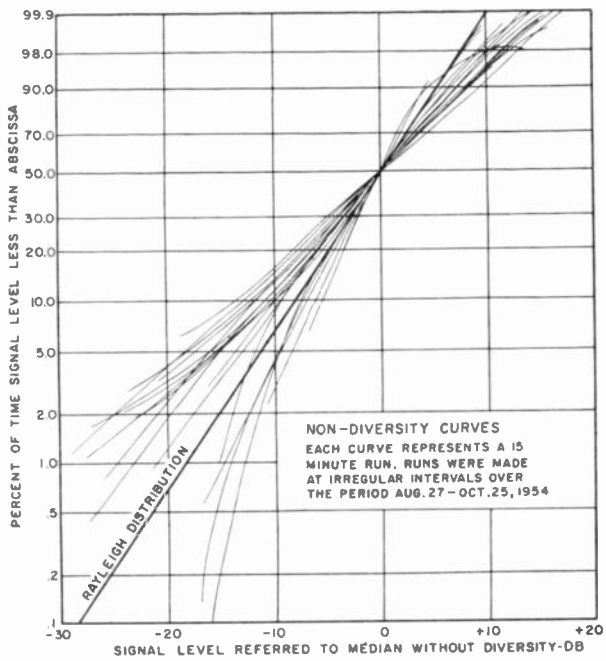

Fig. 12—Distributions of instantaneous signal level—4,090 mc.

have been introduced by instrumentation difficulties rather than by propagation effects.

In order to complete the picture the instantaneous level distribution data just discussed need to be supplemented by information as to how often fades of a given depth are likely to occur and how long they may last. Information of this kind, obtained from the high speed Esterline-Angus records, is shown in Fig. 13 for the 505 mc circuit. At 4,090 mc the fast fading was roughly 8 times faster than it was at 505 mc, and it appeared that the recorder could not follow all of the rapid variations.

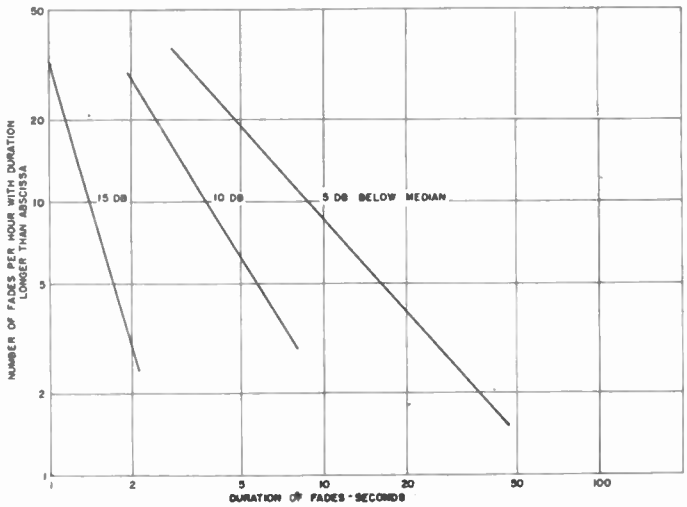

Fig. 13—Number vs duration of fast fades—505 mc.

The three curves in Fig. 13 give the number of fades per hour which were more than 5, 10 and 15 db below the hourly median level and lasted longer than the time intervals shown on the abscissa scale. These data indicate that in a typical hour there would be some 32 fades exceeding 15 db in depth and lasting longer than 1 second. Of these, only one would last longer than 3 seconds. Similarly, there would be about 90 fades exceeding 10 db in depth and 1 second in duration, only one of which would be longer than about 15 seconds.

Diversity Advantage

When the fast fading discussed in the preceding section is superimposed on low median signal levels, the signal minima can drop down into the noise unless the circuit in question has ample transmission margin. The margin required can be reduced considerably by the use of diversity reception. Diversity does not materially affect the long term signal variations, but it is effective in reducing the range of the superimposed rapid variations.

The advantage gained from space diversity reception over extended periods is shown by a comparison of the signal levels exceeded for 99 per cent of each hour with and without diversity. As indicated previously, these percentile values are a good indication of fast fading depth within the hour. Fig. 14 (next page) shows a distribution curve of differences (in db) of hourly percentiles for a single receiver and a diversity pair at 505 mc over a period of three summer months. The curve shows that the percentile signal levels with diversity were 4 to 16 db higher than those without diversity. The median value of the difference was 10.3 db. If two Rayleigh distributions of signal amplitude are combined, assuming the variations to be uncorrelated, it is found that the value exceeded for 99 per cent of the time on the combined curve is approximately 10 db higher than the 99 per cent value on the single curve. Comparing this result with the 10.3 db median difference in Fig. 14, it is concluded that the 200-foot antenna separation in the

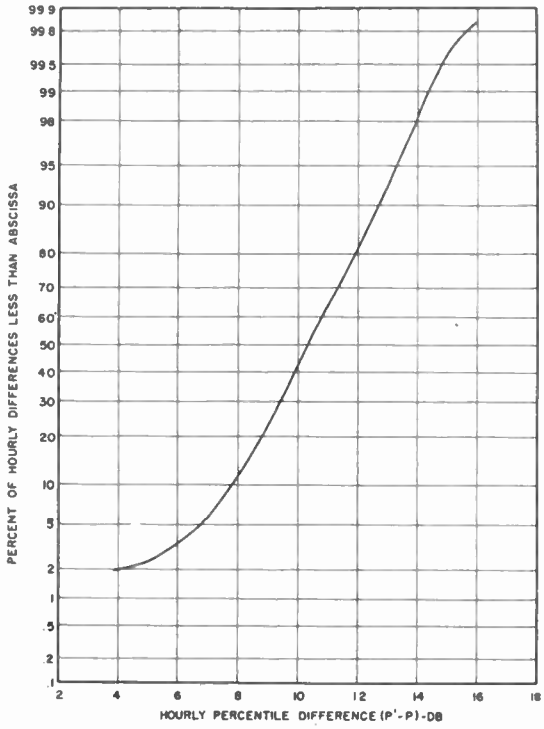

Fig. 14—Distribution of differences of hourly percentile signal levels with and without diversity—505 mc.

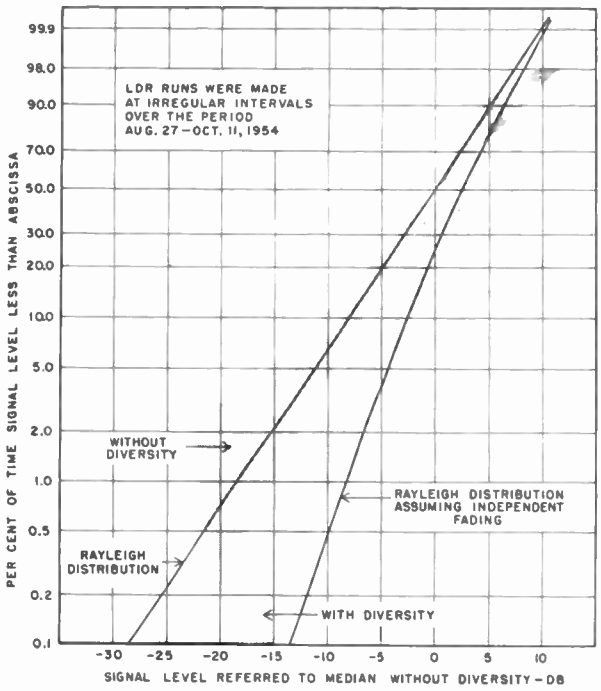

Fig. 15—Distribution of instantaneous signal levels with and without diversity—505 mc.

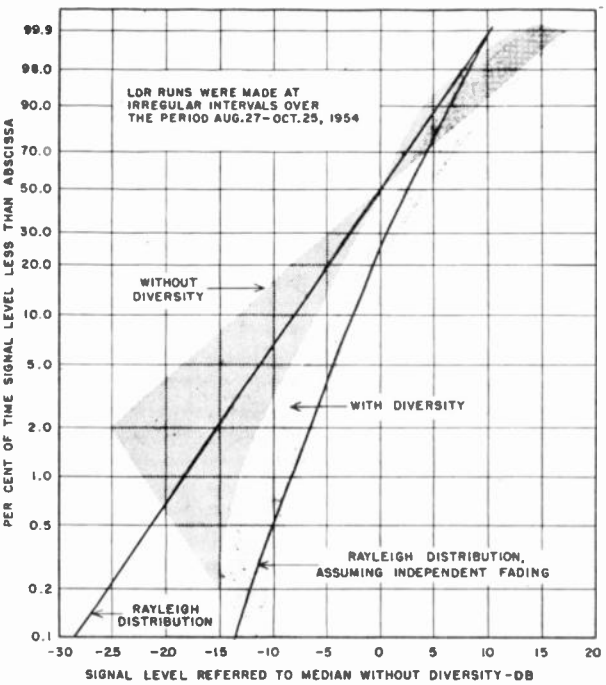

Fig. 16—Distribution of instantaneous signal levels with and without diversity—4,090 mc.

tests was enough to provide essentially independent fading of the two signal outputs and to obtain the maximum diversity improvement.

The diversity improvement was also evaluated by comparing distributions of instantaneous signal levels for short intervals with and without diversity. This was done by recording alternately the output of a single receiver and the output of the diversity pair, using the LDR. Figs. 15 and 16 show the results of these tests at 505 mc and 4,090 mc. The signal levels are given in db referred to the median level without diversity in order to take out the effects of slow changes in the median level from one LDR run to another. The distributions with and without diversity fall into two groups as indicated by the shaded areas. The two heavy lines are shown for reference and represent a single Rayleigh distribution and two combined on a random basis. There is considerable spread within the groups of LDR runs, but the average separation of the two groups is approximately the same as the separation of the two reference lines. This is further evidence that substantially the full theoretical diversity improvement was obtained at both frequencies with the 200-foot antenna separation employed in the tests.

Antenna Gain Comparisons

During the tests an attempt was made to determine whether the 28-foot dish had the same gain on the 150-mile beyond-horizon path that it has on line-of-sight paths. The procedure consisted in comparing the signal received on the 28-foot dish with that received on a small reference dish, the theory being that any reductions in gain due to incoherence of the wave front would be greater for the large antenna than for the small one. At 505 mc the reference dish was 66 inches in diameter, and at 4,090 mc it was 57 inches. The gains of these dishes were taken as 17 db and 33 db at 505 mc and 4,090 mc, respectively, which values correspond to 65 per cent of the computed area gains. On the same basis the gain of the 28-foot dish at 505 mc was taken as 31 db. At 4,090 mc this dish had a measured gain of 46 db

on a line-of-sight path. On the basis of these figures the expected median differences in signal output during the comparison tests were 14 db at 505 mc and 13 db at 4,090 mc.

Distributions of instantaneous signal levels for the large and small antennas were obtained by recording for one minute intervals on the two antennas alternately, using the LDR. From each complete LDR run, lasting about ½ hour, the median value of the difference in signal outputs was determined. Distribution curves of these median differences for a large number of runs were computed and plotted in Fig. 17. It can be seen that the differences varied over a considerable range.

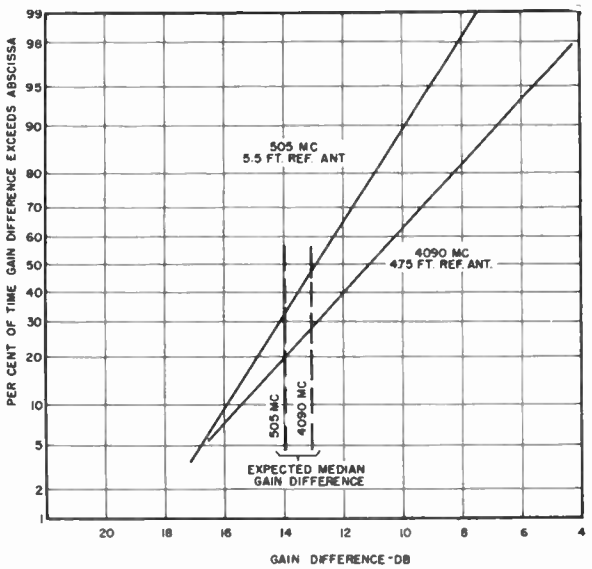

Fig. 17—Antenna gain comparisons.

The median value of the 505 mc distribution is 13 db, which is only 1 db less than the expected median difference of 14 db. At 4,090 mc the median of the distribution of Fig. 17 is about 11 db, or 2 db less than the 13 db difference expected at this frequency.

The comparison of instantaneous signal levels described above was supplemented by observations of hourly median signal levels on the 28-foot dish and the reference dishes. For a total of some 650 hours of data the median value of the differences in hourly medians was 13 db at 505 mc, which is in agreement with the LDR results shown in Fig. 17. At 4,090 mc the median value of the differences was about 8.5 db. or 2.5 db less than the value from the LDR data. There appeared to be no definite trend of antenna gain difference with median signal level for those periods in which the signal output of the small reference dish was high enough to be unaffected by noise.

The above results are summarized in Table III in the following column.

It is concluded from these comparisons that there was a significant reduction in average gain of the 28-foot dish at 4,090 mc of the order of 2–4.5 db. It is believed that the apparent 1 db reduction at 505 mc may be an indication that the assumption of 65 per cent for the effective area of the 28-foot dish at this frequency was too high. The line-of-sight gain measurement of 46 db at 4,090 mc, which is about 5 db down from area gain, indicates that a value somewhat less than 65 per cent for the effective area at 505 mc might be more realistic.

In the above comparisons, differences in transmission line losses have been taken into account. However, since the two antennas could not be located at exactly the same spot, systematic errors due to slightly different foreground conditions may have had a small effect on the results.

TABLE III

ANTENNA GAIN COMPARISONS ON 150-NAUTICAL MILE PATH

	505 mc	4,090 mc
Gain of 28-foot dish (L-S path)	31 db*	46 db†
Gain of reference dishes	17* (5.5′)	33* (4.75′)
Expected difference (L-S path)	14 db	13 db
Median measured difference		
Instantaneous signal levels	13	11
Hourly median signal levels	13	8.5
Gain reduction	1 db	2–4.5 db

* Computed values (65 per cent of area gain).
† Measured value.

Weather Effects

It seemed likely that the long term variations of signal level were connected in some way with local weather conditions. Detailed information on atmospheric conditions over the transmission path would of course be required in order to establish any close correlations between propagation variations and weather phenomena. Lacking such detailed information, an investigation was made to see whether any significant relationships could be found between large scale transmission variations and the weather data recorded at the Gander airport.

It has been shown (Fig. 5) that the average signal levels were considerably higher in the summer than in the winter. Inasmuch as temperature and absolute humidity are higher in summer, it was not surprising that monthly median signal levels were found to be reasonably well correlated with monthly average temperature and dew point at Gander. However, attempts to correlate these variables on an hour-by-hour or day-by-day basis were considerably less successful. Data on wind velocity and barometric pressure also were examined, but there appeared to be no systematic relationship between hourly, daily or monthly averages of these quantities and the corresponding median signal levels.

Fairly early in the tests it was observed that the signal levels seemed to be depressed during snowstorms and, on the other hand, often were enhanced in foggy weather. In order to isolate these effects, the 505 mc data for November through April have been sorted out and separate distribution curves have been plotted for

these special conditions. Curve 3 on Fig. 18 shows a distribution of all the hourly median signal levels for the six month period. Curve 2 is a distribution of hourly medians for only those hours when snowfall was reported at Gander, and curve 4 is a distribution for the hours when fog was reported. From the 50 per cent points on these curves it will be seen that the median value of signal level reduction during hours of snowfall was about 4 db, as compared with all hours, and the increase for the hours when fog was present was about 6 db.[2]

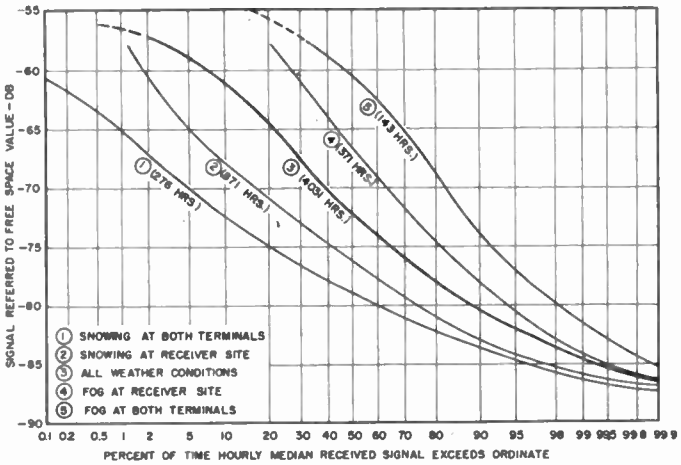

Fig. 18—Distributions of 505 mc hourly median signal levels with and without snow and fog.

These effects are even more striking when observations at the St. Anthony end of the path are included. Curves 1 and 5 on Fig. 18 show distributions for the hours when snow and fog, respectively, were observed at both ends of the path. Compared with curve 3 for all hours, the degradation with snow in this case is about 6.5 db and the enhancement accompanying fog is about 12 db.

Discussion of Results

In order to predict the performance of a radio relay system, either line-of-sight or beyond-horizon, information is needed regarding the long-term median path losses and the characteristics of the fading to be expected. The median loss on line-of-sight paths with good clearance (e.g., first Fresnel zone) can be counted on to be within a few db of the free space value; hence it can be determined in advance with considerable accuracy for any given path. For estimating the performance of line-of-sight systems, therefore, the principal need is for statistics on fading appropriate to the locations involved.

In contrast to the line-of-sight case, the prediction of long-term median signal levels on beyond-horizon paths is subject to considerable uncertainty. The loss on such paths may be 60 to 80 db greater than the free-space loss, and at present it can only be predicted on the basis of previous experience on other paths. The spread of the available data is such that predictions based on the median may be in error by as much as ± 15 db. The average path loss at 505 mc on the St. Anthony-Gander path was within 3 db of the value predicted from the median of the available data, but at 4,090 mc the loss was greater than expected. Part of this discrepancy has been attributed to failure to realize the full theoretical gain of the 28-foot antenna at 4,090 mc, but it is possible that in addition there is a frequency dependence factor in beyond-horizon propagation not previously observed experimentally.

The fading on the Newfoundland test path at both 505 mc and 4,090 mc was similar to that experienced on other beyond-horizon paths. The slow variations were approximately normally distributed (in db) with standard deviations in the range 7–9 db. The superimposed fast fading had approximately a Rayleigh distribution. These results were completely in line with expectations.

While most of the testing was done with single frequency transmission, speech was transmitted over the circuits from time to time. The speech transmission was consistently good at 505 mc, but at 4,090 mc it was subject to occasional bursts of noise as a result of the smaller fading margin on this circuit. Signals simulating a 5-channel multiplex system also were transmitted successfully over the 505 mc circuit. From these observations and the results of multichannel tests on other long paths, it is concluded that no inherent limitations on the transmission of several dozen multiplexed voice channels are likely to be encountered on beyond-horizon links.

[2] It is not intended to imply that these results establish snow and fog as the direct cause of the observed effects.

Investigations of Angular Scattering and Multipath Properties of Tropospheric Propagation of Short Radio Waves Beyond the Horizon*

J. H. CHISHOLM†, P. A. PORTMANN†, MEMBER, IRE, J. T. DEBETTENCOURT†, ASSOCIATE, IRE, J. F. ROCHE†, MEMBER, IRE

Summary—Experiments designed to investigate the potential communications capacity of uhf and shf tropospheric propagation beyond the radio horizon were conducted by the MIT Lincoln Laboratory on circuits of from 161 to 188 miles in length along the coastal regions of the northeastern United States. Some of these tests were made in cooperation with the Bell Telephone Laboratories and the late Major E. H. Armstrong. A study of the following aspects of tropospheric propagation was considered necessary in order to gain a better understanding of the factors involved in design of communications systems:

1. The extent of useful communication bandwidths.
2. Variation of uhf and shf median signal levels over a full seasonal cycle.
3. The range and rates of fading.
4. The effective gain of highly directional antenna systems.
5. The effect of multipath propagation on modulated signals.
6. The polarization properties of scattered fields.
7. The angular dependence of scattered fields.

Such experiments made from 1953 to 1955 have confirmed the utility of tropospheric circuits for wide-band communication systems and have provided information useful in the evaluation of tropospheric propagation mechanisms.

Introduction

A PROBLEM often confronting radio system designers is that of obtaining reliable point-to-point radio communications with adequate bandwidth capacity over paths from one hundred to four hundred miles in length where intervening relay stations are not feasible. It is well known that radio frequencies at which waves are propagated by ionospheric and ground-wave modes are not particularly suitable in a number of geographical areas for communications over such path lengths because of the variability of ionospheric conditions, the earth's conductivity, and the contributions of external noise. In order to explore the possibility of using the higher radio frequencies for these purposes, the Lincoln Laboratory of MIT made early detailed studies of the research of tropospheric propagation of radio waves well beyond the horizon which had been conducted over the past decade. These studies, completed in 1952, indicated that short radio waves propagated well beyond the horizon by the troposphere would probably provide a feasible means of achieving reliable point-to-point communications over distances of one hundred to three hundred miles provided that sufficient transmitter power and highly directive diversity antenna systems were employed and that serious multipath distortion was not encountered.

During the last ten years numerous experimental observations have been made of radio waves propagated well beyond the horizon from high powered transmitters operating at frequencies from 40 to 10,000 mcps.[1–6] The field intensities observed at distances from 100 to 500 miles beyond the horizon (50 to 100 db below free space) are many orders of magnitude greater than those computed from the conventional theory of waves diffracted around a spherical earth.

Reports of the results of early vhf measurements, and the more recent measurements utilizing high-powered uhf and shf transmitters had indicated that signal levels were relatively independent of frequency and that median levels, obtained under a wide variety of geographical and climatic conditions, showed that these weak fields seemed to be present at all times.

A study of the early experimental results indicated a need for further research to provide the following information necessary for the design of communication systems:

1. The extent of useful communication bandwidth.
2. Distortion of modulation by multipath contributions to the received signal.
3. A detailed analysis of the lower percentile values of signal level over a complete seasonal cycle.
4. The range and rate of fading over short periods of time.
5. The effective gains of highly directive antenna systems.
6. The appropriate spatial arrangement of diversity antennas.

* Original manuscript received by the IRE, July 13, 1955. The research in this paper was supported jointly by the Army, Navy and Air Force under contract with Mass. Inst. Tech. The original signal level measurements program was enlarged by the Lincoln Lab. as a subcontractor to the Western Electric Co. under contract No. AF 18(600)-572 (Western Electric Contract X-213).

† Staff Members, Mass. Inst. of Tech. Lincoln Laboratory, Lexington, Massachusetts.

[1] G. W. Pickard and H. T. Stetson, "Comparison of tropospheric reception," *Jour. Atmos. Terr. Phys.*, vol. 1, pp. 32–36; January, 1950.
[2] K. Bullington, "Radio propagation variations at vhf and uhf," PROC. IRE, vol. 38, pp. 27–32; January, 1950.
[3] M. Katzin, R. W. Bauchman, and W. Binnian, "3- and 9-cm propagation in low ocean ducts," PROC. IRE, vol. 35, pp. 891–905; September, 1947.
[4] M. D. Rocco and J. B. Smyth, "Diffraction of high-frequency radio waves around the earth," PROC. IRE, vol. 37, pp. 1195–1203; October, 1949.
[5] I. H. Gerks, "Propagation at 412 megacycles from a high-power transmitter," PROC. IRE, vol. 39, pp. 1374–1382; November, 1951.
[6] E. C. S. Megaw, "The scattering of electromagnetic waves by atmospheric turbulence," *Nature*, vol. 166, pp. 1100–1104; Dec., 1950.

This paper describes the results of an experimental program designed to investigate the potential communications capacity of uhf and shf radio waves propagated well beyond the horizon, to provide experimental data suitable for evaluating the utility of various theoretical models of tropospheric propagation mechanisms, and to provide data suitable for predicting the performance of communications systems. Experimental systems employing high-powered uhf and shf transmitters and highly directive antennas were operated from March, 1953 to March, 1955 over paths of from 161 to 188 miles in length and located in the coastal region of northeastern United States.

Theoretical Models Related to the Design of the Experimental Systems

A theoretical explanation of the presence of weakly propagated short radio waves well beyond the horizon, in the absence of superrefractive conditions, was advanced by Booker and Gordon[7] in July, 1949. They attributed these weak fields to the effect of scattering from irregularities in the radio index of refraction caused by atmospheric turbulence. This model of atmospheric turbulence was developed further in a subsequent paper.[8] The important parameters in this theory were (1) the mean-square deviation of the dielectric constant of the atmosphere, (2) the appropriate scale size of the atmospheric irregularities, (3) radio wavelength, (4) the volume common to both transmitting and receiving antenna radiation patterns, and (5) the angular direction between the normal to the incident wave front and the receiver for each elementary common scattering volume. An evaluation of the universal application of theories of scattering of radio waves by atmospheric turbulence, for computation of expected radio fields strength, depends upon a knowledge of the fluctuations of the radio index of refraction in the troposphere as a function of season, altitude, and geographical location. Later measurements of the radio index of refraction of the troposphere utilizing an airborne radio refractometer[9] have indicated that the sizes of the fluctuations of the radio index of refraction in the lower troposphere for temperate geographical regions were large in terms of centimeter radio wave lengths. The general implications of these measurements were that the scattering of short radio waves by the large irregularities in the radio index of refraction in the troposphere would be constrained largely to angles of a few degrees to the normal of the incident wave front. Consideration of the possible angular variation of vertical and horizontal angles of arrival caused by the refractive bending of centimeter waves by the troposphere indicated that deviations of the ray paths probably would not exceed a few tenths of a degree in the horizontal plane[10] under all but extreme conditions. Larger angular variations in the vertical plane[11,12] would be expected because of the tendency of the troposphere to be horizontally stratified under meteorological conditions conducive to nonstandard vertical gradients of the radio index of refraction. For these reasons, it was difficult to evaluate the effect of nonstandard vertical gradients of the refractive index upon the narrow beams of large highly directive antennas directed along a path several hundred miles in length. However, the confinement of radiation pattern of the transmitting antennas and reception pattern of the receiving antenna to very small vertical angles, for a scattering model of the troposphere, was considered desirable in order to reduce multipath contributions. Computation of the path delays on a basis of ray geometry indicated that the differential multipath delays of the contributions of the elementary scatterers (neglecting angular dependence of scattered power) are increased more rapidly with variation of elevation angle than with variation of horizontal angle for paths well beyond horizon under standard refractive conditions.

An alternative theory to turbulent scattering was advanced by Feinstein[13] and Carroll[14] to explain the radio fields propagated well beyond the horizon based on these authors' interpretation of a theoretical study by Bremmer.[15] Although different in concept it would appear that multipath contributions from elementary partial reflections postulated in this theory would be comparable with the scattering model. A more recent development by Carroll and Ring[16] in terms of mode solutions could not be interpreted easily in terms of the reduction of multipath contributions by the use of directive antenna systems on a simple geometric ray basis.

The magnitude of the frequency dependence and of the potential multipath contributions, as computed from various theoretical models utilizing idealized parameters, was uncertain for purposes of experimental design. However, the experimental observations by Katzin,[17] Megaw,[18] and Bullington[19] indicated that the

[7] H. G. Booker and W. E. Gordon, "An Elementary Theory of Scattering in the Troposphere," NEL Symposium on Tropospheric Wave Propagation, July 25–29, 1949; Naval Electronics Laboratory Report 173.

[8] H. G. Booker and W. E. Gordon, "A theory of radio scattering in the troposphere," Proc. IRE, vol. 38, pp. 401–412; April, 1950.

[9] C. M. Crain, "Directly recorded tropospheric refractive index fluctuations and profiles," Trans. IRE, vol. AP-2, pp. 79–83; August, 1952.

[10] A. W. Straiton and J. R. Gerhardt, "Results of horizontal microwave angle-of-arrival measurements," Proc. IRE, vol. 36, pp. 916–922; July, 1948.

[11] W. M. Sharpless, "Measurements of angle-of-arrival of microwaves," Proc. IRE, vol. 34, pp. 837–845; November, 1946.

[12] A. B. Crawford and W. M. Sharpless, "Further observations of the angle-of-arrival of microwaves," Proc. IRE, vol. 34, pp. 845–848; November, 1946.

[13] J. Feinstein, "Tropospheric propagation beyond the horizon," *Jour. Appl. Phys.*, pp. 1292–1293; October, 1951.

[14] T. J. Carroll, "Internal reflection in the troposphere and propagation beyond the horizon," Trans. IRE, PGAP, vol. 2, pp. 9–27; March, 1952.

[15] H. Bremmer, "The propagation of electromagnetic waves through a stratified medium and its WKB approximations for oblique incidence," *Physica*, vol. XV, pp. 594–608; August, 1949.

[16] T. J. Carroll and R. M. Ring, "Normal tropospheric propagation of short radio waves well beyond the horizon," MIT Lincoln Lab. Tech. Rep. No. 38; February 12, 1954.

[17] Katzin, *et al.*, *op. cit.*

[18] Megaw, *op. cit.*

[19] K. Bullington, "Radio transmission beyond the horizon in the 40 to 4,000 mc band," Proc. IRE, vol. 41, pp. 132–135; Jan., 1953.

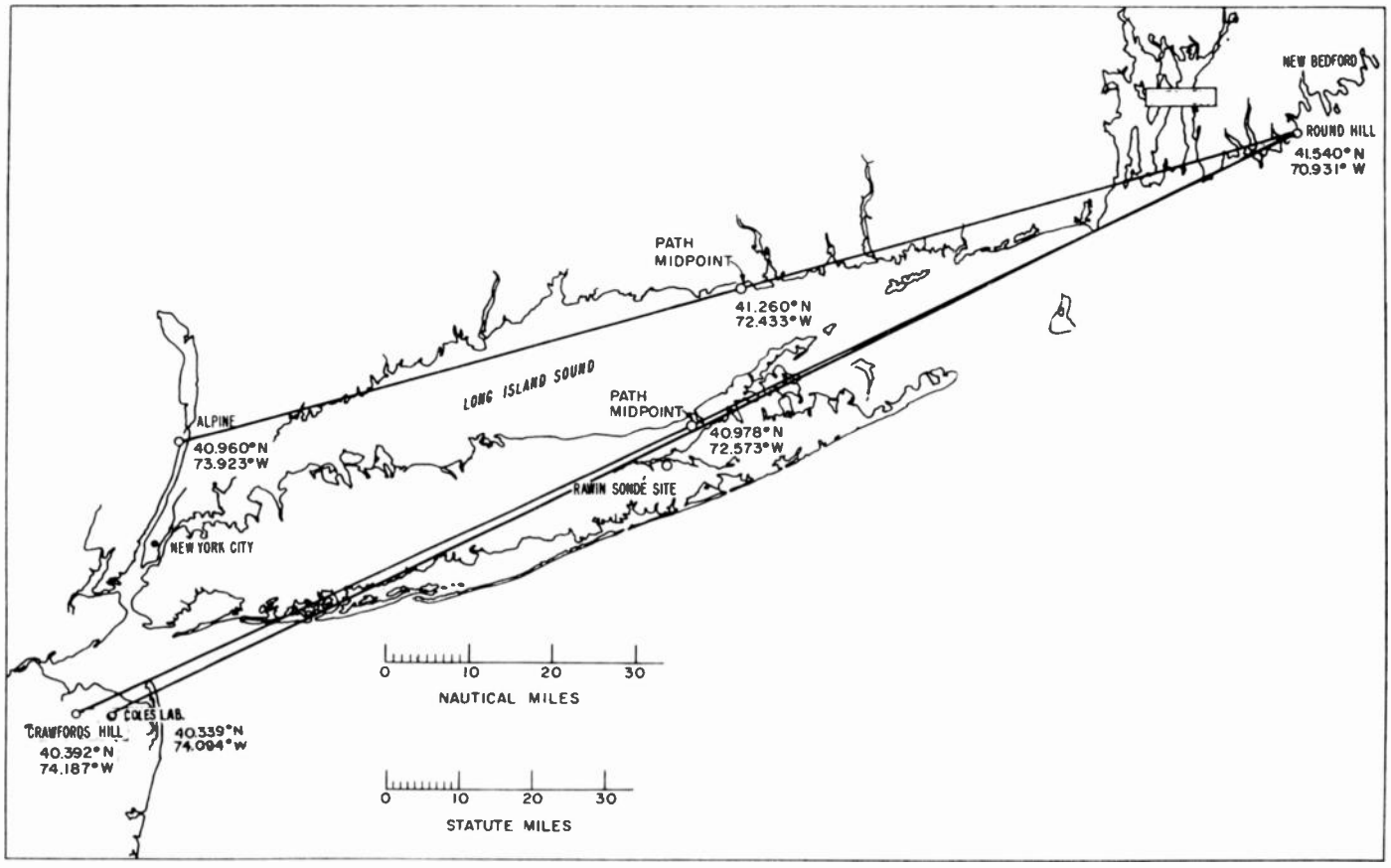

Fig. 1—Map showing experimental uhf and shf paths.

signal levels of microwaves propagated well beyond the horizon during summer periods were comparable with the measurements at vhf and uhf. Experimental measurements by Smyth[20] of the correlation of the amplitude of scattered signals at 3,300 mcps, received over a short nonoptical path as a function of horizontal and vertical spacing of small antennas, indicated that the coefficient of correlation was reduced to a small fraction of unity for spacings normal to the path in the range 10 to 35 wavelengths horizontally and in the range 10 to 20 wavelengths vertically. These data indicated that the effective gain of large antennas (10 to 100 λ in diameter) in scattered fields would not increase linearly with increasing size of the antenna aperture as compared with gains measured under plane wave conditions. For frequencies in the range of 400 mcps ($\lambda = 2.46$ feet) the effective gains of paraboloidal antennas of 15 to 30 feet in diameter over scatter paths could be expected to approach those obtained under plane wave conditions. The angular half-power beamwidths in the 400 mcps range, for the above aperture sizes, are approximately 12 to 6 degrees respectively. Antenna systems with these beamwidths could accept multipath contributions delayed by as much as 1 to 5 μsec over a 200-mile path as computed by ray geometry and depending upon the angular scattering function chosen for each elementary volume enclosed in the large volume common to both transmitting and receiving antennas. At 4,000 mcps, antennas of these sizes might be expected to exhibit some reduction in effective gains over a 200-mile path as compared with plane wave gain values. However, multipath contributions as computed in a similar manner should be reduced to delays of 0.2 to 0.5 μsec.

[20] J. B. Smyth, "Signal Fluctuation and Scattering," NEL symposium on Tropospheric Wave Propagation; July 25–29, 1949; Naval Electronics Lab. Rep. 173.

UHF Experiments

Modulation Tests Conducted over Alpine–Round Hill Path

An experimental program designed to make a preliminary investigation of the communication capacity at uhf over a 161-mile tropospheric path between Alpine, New Jersey, and the MIT Round Hill Field Station located at South Dartmouth, Massachusetts, was conducted in the early spring and summer of 1953 in cooperation with the late Major E. H. Armstrong. This path, shown in Fig. 1, is a composite land-sea path principally along the southern coast of New England.

The transmitting antenna at Alpine was a 16-foot diameter paraboloid mounted on a 100-foot tower. The center of the antenna was 610 feet above sea level. The profile of the foreground on a bearing toward Round Hill shows that the radio horizon extends to the low lying land-sea area at a distance of approximately 30 miles. At Round Hill, several antennas of different sizes

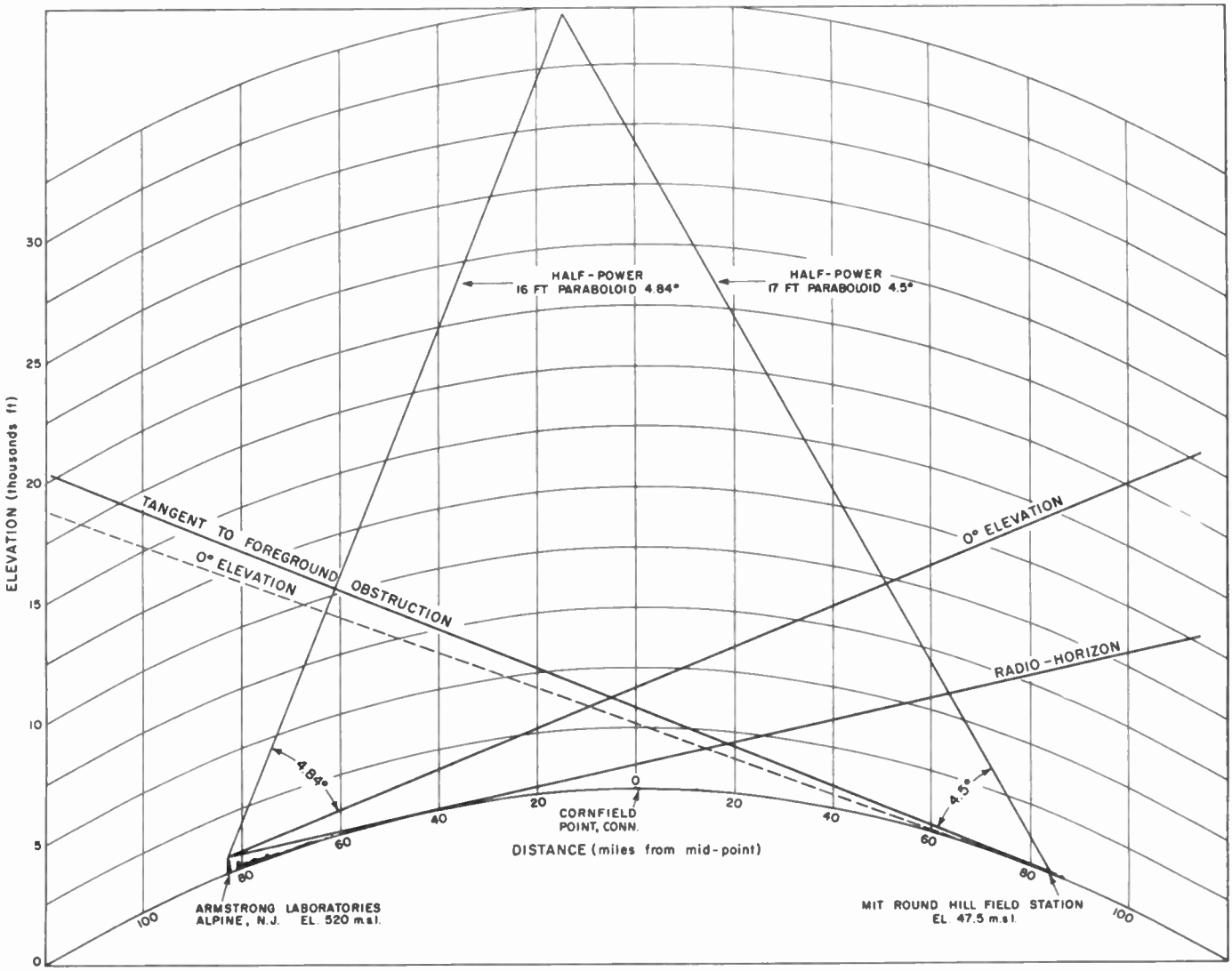

Fig. 2—Path profile and path geometry of the initial uhf experimental system showing the intersection of half-power beam angles of the 17-foot paraboloid at Round Hill and 16-foot paraboloid at Alpine.

were mounted on a hill overlooking the sea with their centers at an elevation of 56.5 feet above sea level. A narrow peninsula extending into the sea, at a distance of one mile from the antennas, forms an angular obstruction of 0.2 degree in the direction of Alpine. Fig. 2 shows a full-path profile and the path geometry for the half-power beamwidths of the free-space patterns of the 16-foot and 17-foot antennas.

The uhf transmitter at Alpine consisted of a crystal controlled 13-kw CW Resnatron power amplifier. A Serasoid phase modulator was used to provide high quality frequency modulation. The 16-foot diameter transmitting antenna had a computed gain of 23.7 db above an isotropic radiator. The antenna was connected to the transmitter with a rigid coaxial line having a measured attenuation of 1.0 db.

The receiving antennas at Round Hill consisted of a 28-foot diameter, a 17-foot diameter paraboloid, and a corner-reflector, having gains of 28.6 db, 24.3 db, and 12.0 db, respectively, above an isotropic radiator. Two crystal-controlled FM communications receivers, having bandwidths of 30 kcps, were modified to operate with common local oscillators. These receivers employed triple conversion and were equipped with auxiliary 455 kcps AGC amplifiers to operate high-speed signal level recording equipment.

A series of preliminary narrow band frequency modulation experiments were undertaken on the Alpine to Round Hill circuit in March, 1953. The median signal levels observed on the 17- and 28-foot antennas during this period ranged from 20 to 40 db above the level required to produce 20-db noise quieting (−110 dbm) of these receivers when equipped with a low noise rf amplifier. Audio tones of 1,000, 2,000 and 4,000 cps, with a deviation of ±9 kcps, were used in these initial tests.

The output of the receiver audio amplifier was observed on an oscilloscope and qualitative visual, as well as aural, monitoring indicated that the audio tones were reproduced without apparent distortion except during the deeper fades. A close observation of the fading signal level recorded on a high speed Sanborn recorder indicated that distortion during fades could be attributed only to those below the limiting threshold of the receiver. On the larger antenna systems, the fading of the

signal below the noise threshold was very infrequent. FM voice transmissions over this circuit utilizing ±9 kcps deviation were comparable in quality and intelligibility to that expected from this type of receiver under conventional "line-of-sight" operations.

Several observations of a similar nature were made using corner reflectors and, with exception of more frequent fades below limiting threshold of receivers, no degradation in quality or intelligibility was detected. These initial experiments were sufficiently encouraging to indicate that wider bandwidths might be tolerated.

In April, 1953, arrangements were made by Major E. H. Armstrong to provide wide-band high-quality music over the Alpine transmitter utilizing ±75 kcps deviation. Reception of these transmissions, on the larger antennas, utilizing a receiver with a bandwidth of 200 kcps was considered uniformly good by a number of observers experienced in assessing high quality audio reproduction. Several magnetic tape recordings were made of these transmissions. Similar recordings made with the corner reflector were also of good quality although interspersed with more frequent noise bursts caused by fading of signal below receiver threshold.

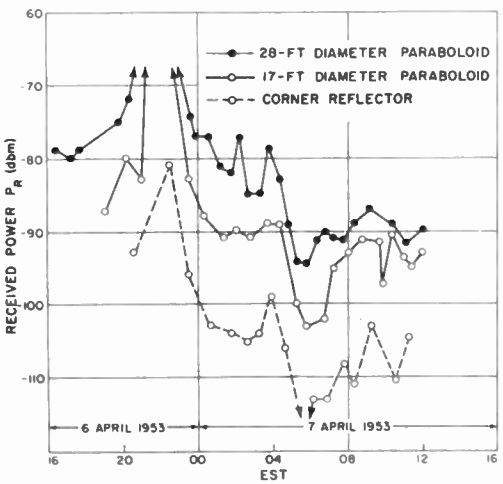

Fig. 3—Comparison of median values of signal level received at Round Hill on 28-foot and 17-foot diameter paraboloids and a corner reflector of transmissions from 16-foot paraboloid antenna at Alpine, N. J., at 425 mcps.

An early test comparison of the signal levels received utilizing antennas with different sizes of aperture was conducted from 1600, April 6, 1953, to 1200, April 7, 1953. The median signal levels recorded continuously, during this period, on one receiver using the 28-foot antenna, are shown in Fig. 3. A second receiver was alternately switched from the 17-foot antenna to a corner reflector for a 15-minute period during each hour. Some caution should be exercised in taking the differences of the decibel levels literally from the lines connecting the medians obtained from the various antennas over noncoincident periods of time. The difference in signal level between each of the antennas appears to be consistent with the difference in computed plane wave gain values of each of the antennas.

Measurement of Phase Variation and Amplitude Correlation of Signals Observed on Two Spaced Antennas

The dual-receiver system employing common local oscillators was utilized to observe the correlation between signals received on two identical corner reflectors as function of horizontal spacing along a line normal to the Alpine bearing. The 455 kcps IF signals of each receiver were displayed as vertical and horizontal deflections on an oscilloscope.

Qualitative observations and motion pictures were made of the resulting elliptical patterns as the antennas were spaced from 2 feet to 50 feet and later to 75 feet and 100 feet. It appeared from a number of oscilloscope observations that the degree of correlation for each spacing had gross variations over hourly periods of time. Several instances of good correlation for several minutes at distances of 100 feet were observed for signal levels near 40 db below free space. For lower signal level values, trend to less correlation of amplitudes and large variations of phase was marked for spacings over 50 feet.

Signal Level Distributions on 385.5 and 399.5 Mcps

A duplex uhf circuit was established by the Lincoln Laboratory, in cooperation with the U. S. Army Signal Corps, between Round Hill and the Coles Signal Laboratory, Red Bank, N. J., a distance of 184 miles. This system employed 5 kw CW klystron amplifiers operating at frequencies 385.5 and 399.5 mcps. Twenty-eight foot diameter paraboloidal antennas, having gains of 28 db above an isotropic radiator, were employed for both transmission and reception.

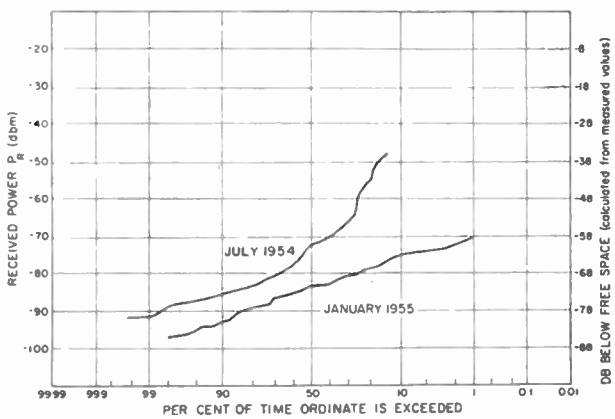

Fig. 4—Cumulative distribution of median values of signal level received over a 184-mile path between Round Hill and Coles Signal Laboratory on 28-foot antennas at frequencies 399.5 mcps and 385.5 mcps (cases: July, 1954—240, January, 1955—130)

Signal levels were recorded from July, 1954, to February, 1955, on a five day per week schedule with the exception of November and December of 1954. During this period the circuits were out of operation due to hurricane damage. The seasonal variation of the monthly median values of received power ranged from a high of −73 dbm in July to a low of −84 dbm in January. Cumulative distributions of the median values of signal level are shown in Fig. 4 for the months of July, 1954 and January, 1955. The data for July is based on

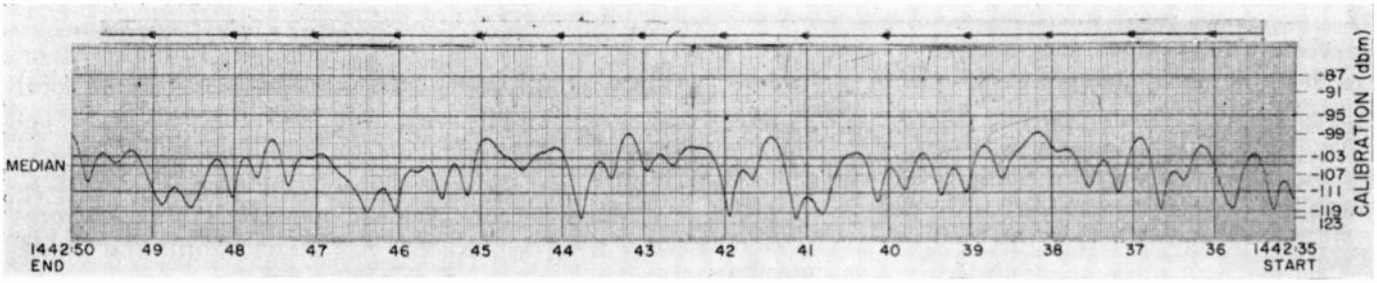

Fig. 5—A 15-second sample of a record of the signal received over a 184-mile path at uhf.

successive 15 minute median values recorded at Round Hill on a frequency of 399.5 mcps. The data for January is based on hourly median values of signal level recorded at the Coles Signal Laboratory at a frequency of 385.5 mcps. The range of variation of the medians for the July data, from the 50 per cent to the 90 per cent values, is 13 db, while in the case of the January data the range for the same percentile values is only 10 db.

A recorded sample of signal levels is shown in Fig. 5 to illustrate the type of fading encountered on these circuits under typical conditions. Fading rates, defined as half of the average number of median crossings per unit time, are approximately 1.5 cps for this sample.

SHF Experiments

Experimental Facilities

The use of microwaves for long range point-to-point communications was believed potentially advantageous because of the availability of wide communications bandwidths and of the relative ease of achieving large plane-wave gains with antennas of moderate physical dimensions. Tests were conducted in cooperation with the Bell Telephone Laboratory over a 188-mile path from Crawfords Hill, New Jersey, to Round Hill, Massachusetts, shown on the map in Fig. 1, during the period May, 1953, to April, 1955.

The transmitting antennas at Crawfords Hill consisted of a 28-foot diameter and a 5-foot diameter paraboloidal reflector. The elevation of the center of these antennas was 389 feet above sea level. The profile of the foreground on a bearing toward Round Hill indicated that the radio horizon extended approximately 28 miles to the low-lying land areas of Long Island. A similar pair of 28-foot and 5-foot diameter receiving antennas were mounted on a hill overlooking the sea at Round Hill. The elevation of the centers of each of the antennas was 56.5 feet above sea level. A narrow peninsula extending into the sea at a distance of 1.1 miles formed an angular obstruction of 0.15 degree in the direction of Crawfords Hill.

The measured horizontal pattern (*E*-plane) of the 28-foot diameter antennas at 3,670 mcps and 5,050 mcps is shown in Fig. 6. The measured gain of the 28-foot antennas at 3,670 mcps was 47.5 db above an isotropic radiator and 51.3 db at 5,050 mcps. The antenna reflector was mounted on a turntable to permit rotation in azimuth. Elevation of the beams of the large antenna system over a few degrees was accomplished by vertical movement of the horn feeds. A full path profile and the path geometry of the 28-foot antenna systems is shown in Fig. 7 (facing page) for elevations of 0.0 and 1.2 degrees.

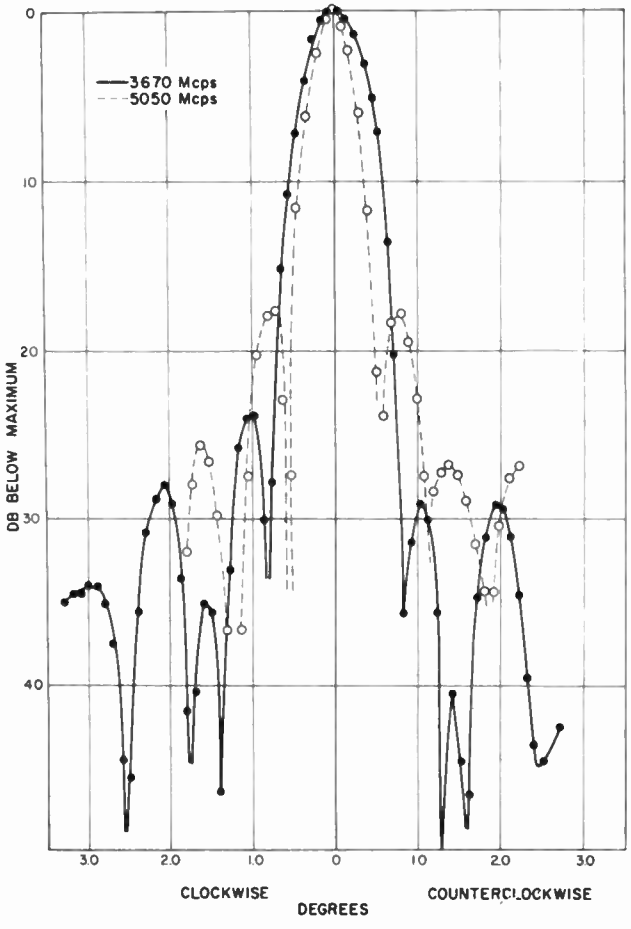

Fig. 6—Measured patterns of 28-foot antenna in horizontal plane at 3,670 mcps and 5,050 mcps using horizontal polarization.

A block diagram of equipment employed in 3,670 mcps pulse measurements is shown in Fig. 8 (page 1324). The transmitting system at Crawfords Hill consisted of a Navy radar modified to operate with a crystal controlled pulse repetition frequency of 500 cps. This unit has a fixed pulse length of 1.5 μsec and operates with a

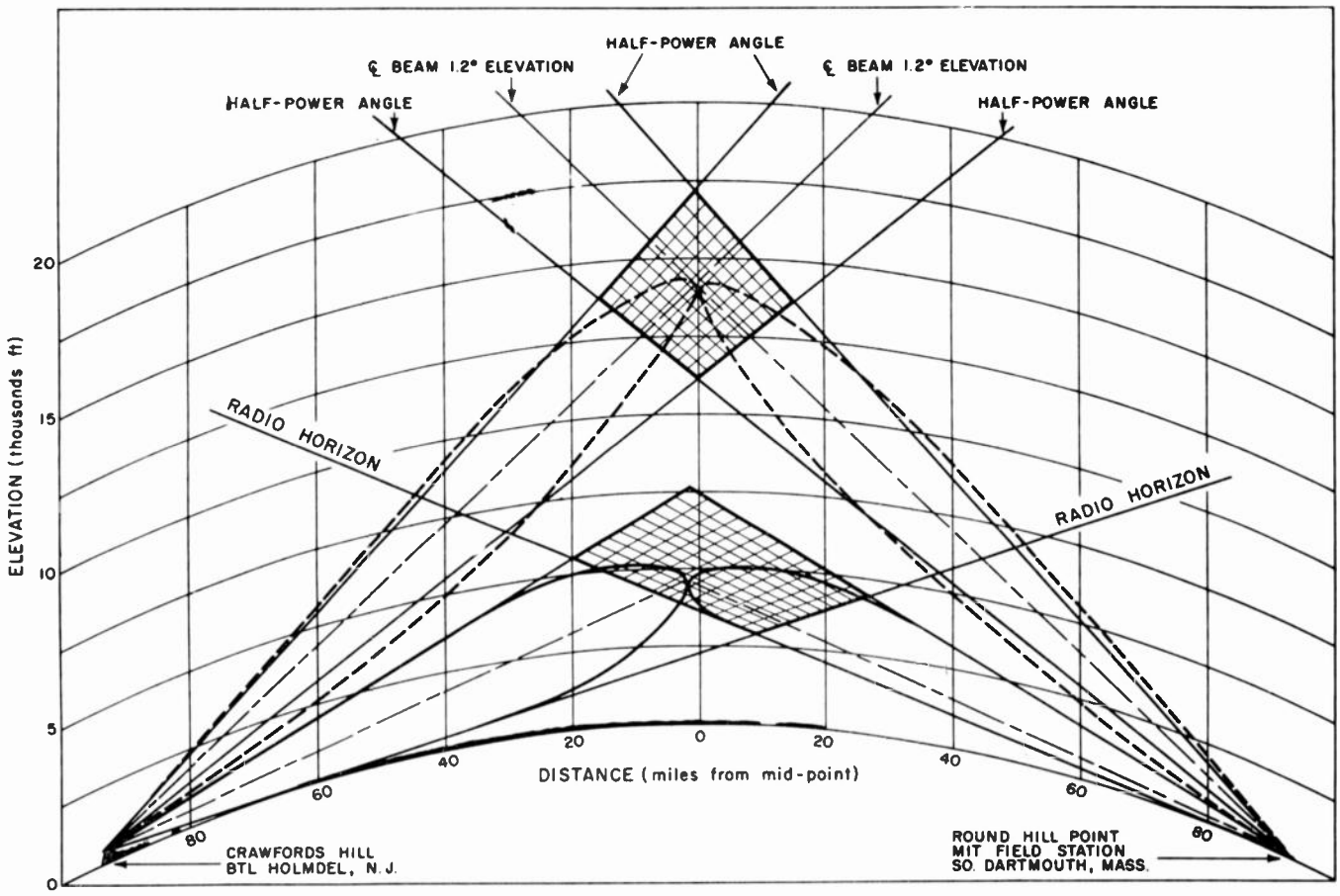

Fig. 7—Path profile and path geometry of the shf experimental system showing half-power beam angles of 28-foot antennas at 3,670 mcps. Constant power contours are shown for antenna beam elevations of 0.0 and 1.2 degrees.

duty cycle of 0.00075. The magnetron used in the transmitter delivered a peak pulse power of 400 kw or an average power of 300 watts for this duty cycle. The transmitter trigger is derived from a frequency divider controlled by a high stability 100 kcps quartz-crystal oscillator. The transmitter was connected to the antenna feed horn by a waveguide transmission line approximately 50 feet in length having a measured attenuation of 0.5 db.

The receiving equipment at Round Hill, shown in the block diagram of Fig. 8, consisted of two pulse receivers operated with a common local oscillator, an Esterline-Angus Recorder, a Sanborn Model 60 high-speed dual-channel recorder, signal-level distribution recorders, and a photographic oscilloscope. The 3,670 mcps pulse receivers were designed to provide two distinct means of observing the received pulses, namely, to record the signal level on a logarithmic scale and to record the pulse shape accurately. In order to achieve the latter, a bandwidth of 3 mcps was chosen (approximately three times the optimum radar bandwidth for a 1.5 μsec pulse). An experimental measurement of the transmitted pulse shape, as compared on the receiver versus a wide band rf envelope detector, indicated that only a minor improvement in pulse reproduction would result from further extension of the bandwidth with a consequent decrease in receiver recording sensitivity. A time constant of 4 milliseconds was chosen for the agc detector to provide a rapid response to fading frequencies of 0–40 cps. This time constant was sufficiently long that the receiver functions as a fixed gain linear receiver during the period of the pulse. The agc circuit of the receiver was designed to produce an output voltage very nearly proportional to the logarithm of the peak amplitudes of the pulses occurring at the 2-millisecond intervals. Experimental measurements of the amplitude response of the receiver were made utilizing a diode modulator to vary the amplitude of the pulse signals at rates from 1–40 cps. The output agc voltage obtained on a Sanborn recorder indicated that reliable reproduction of fast fading was obtained over this spectrum of fading frequencies. Other than the agc design, these pulse receivers were conventional single conversion units employing a balanced crystal mixer, a 60-mcps IF amplifier, a video detector, and a video amplifier.

Synchronization for the oscillographic presentation of successive received pulses was obtained from a highly stable 100-kcps crystal oscillator and a frequency divider similar to that which is employed to generate the transmitter trigger.

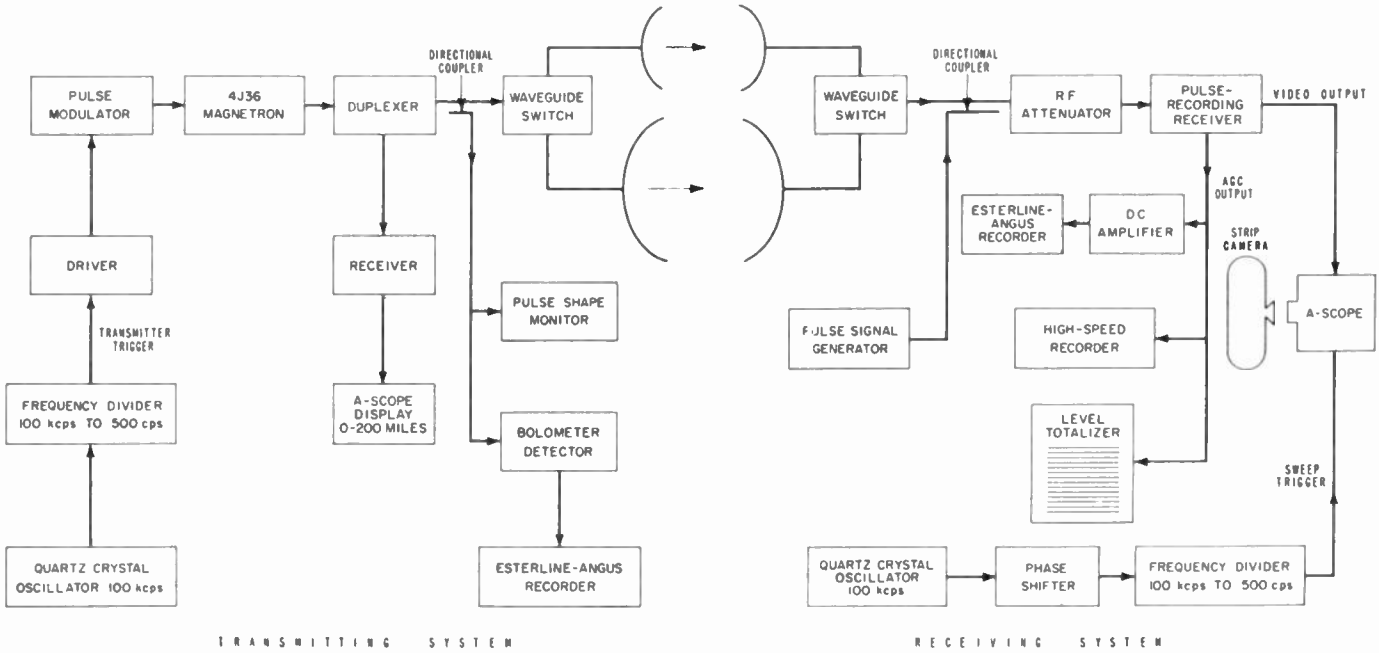

Fig. 8—Block diagram of transmitting and receiving system used in experimental 3,670 mcps pulse system.

Investigation of the Angular Scattering Properties of the Troposphere Utilizing Narrow Beams

Experiments designed to investigate the scattering properties of the troposphere, at 3,670 mcps, were made periodically throughout the recording program. The angular relations of the antenna beams, for two angular positions in the vertical plane over the Crawfords Hill to Round Hill path, are shown in Fig. 7. This figure presents a simplified ray treatment of the path geometry for standard refractive conditions.

A study of related propagation experiments, reported by other investigators, implied that antenna beamwidths of less than one degree would be required to resolve the contributions of various portions of the troposphere to the signals received beyond the horizon. The two 28-foot diameter antennas employed for these tests had a half-power beamwidth of 0.65 degree in azimuth (E-plane) and of 0.70 degree in elevation.

The interpretation of results in the angular explorations of radio waves scattered by the troposphere, utilizing narrow antenna beams, requires careful consideration of the effect of the finite width of the beams, the effect of surface reflections in the foregrounds of the antennas, and the refractive effects of variable gradients in the radio index of refraction. Under standard refractive conditions, surface reflections from the foreground of the antennas produce a periodic interference pattern in the vertical plane[21] when the antenna is pointed in a horizontal direction. This interference effect would become progressively less prominent as the antenna is elevated, and as the illumination of the foreground is reduced to a small fraction of the maximum intensity at the center of the beam. The magnitude of surface reflections producing the interference pattern depends upon the effective reflection coefficient of the surface, and, for centimeter waves, this reflection coefficient is determined largely by surface roughness rather than the electrical constants of the reflecting surface. Reflection coefficients near unity, for small grazing angles over sea and terrain surfaces comparable to the foreground of the Crawfords Hill antenna, can be expected for this frequency. An evaluation of the influence of foreground reflections at Round Hill is complicated by the obstruction described previously. Under these conditions, a complex interference pattern caused by multiple diffraction and reflection paths, would be expected in the diffraction zone of the obstruction. The net effect, when surface reflections contribute to the formation of a pronounced lobe structure, is an enhancement of the power radiated per unit solid angle for angles just above the horizon. The angular positions and the definition of the maxima and minima in the lobe structure may be expected to be altered by variations in the gradients of refractive index, and, for antennas sited over the sea, by changes in tidal conditions.

In view of these factors, the power contours shown in Fig. 7 are intended to represent a rough average of the power radiated per unit solid angle by the numerous maxima in the vertical pattern of the antenna. For beam alignment at an elevation angle of 1.2 degrees, the free space pattern of the antenna can be considered a good representation of the actual power pattern since the illumination of the foreground is reduced 20 db or more.

In the horizontal plane, the free space patterns of the antennas can be considered to be a reasonably accurate representation of the angular intensities of radiation

[21] D. E. Kerr, "Propagation of Short Radio Waves," McGraw-Hill Book Co., Inc., New York, N. Y., ch. II, sec 2; 1951.

since the character of reflecting foreground does not change appreciably for horizontal rotations of a few degrees.

A precise survey was made at each site in order to orient the antennas on the true great circle bearings. This was done by means of astronomical observations of the position of Polaris with appropriate orbital corrections, together with measurements of the mechanical and electrical alignment of the antennas utilizing nearby test sites. The measurements indicated that over-all angular accuracy of entire system was 0.1 degree or better.

Observations of scattered signals were made in the summer and winter periods of 1953 and 1954, by simultaneous rotation, and elevation, of the transmitting and receiving antennas of the type shown in Fig. 9. A typical

Fig. 9—Photograph of 28-foot and 5-foot diameter antennas used in the shf experimental system.

plot of the median value of signals received as a function of the 0.1 degree increments of the azimuthal position of the two antennas, with the beams oriented vertically along the horizontal, is shown in Fig. 10. The multiplied

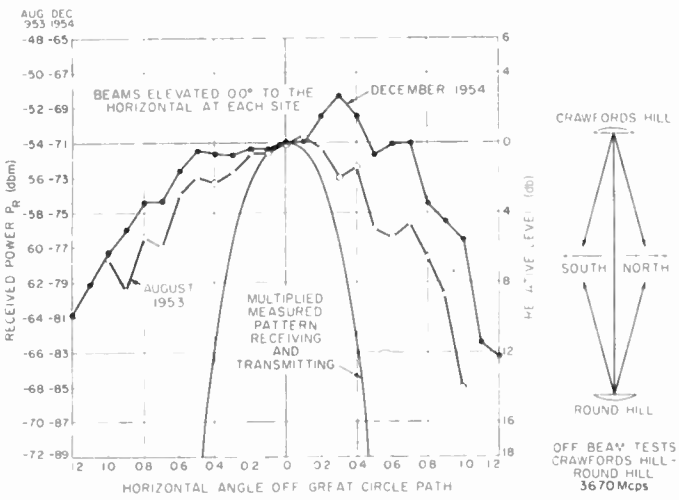

Fig. 10—Variation in received power at Round Hill on 28-foot antenna of transmissions from Crawfords Hill, N. J., with simultaneous azimuthal rotation of the transmitting and the receiving antenna.

free space patterns of the transmitting and receiving antennas, assuming simultaneous rotation about parallel axes, are plotted in this figure for reference. In each of the tests, the median signal level observed when the antennas are oriented on the great circle bearings were normalized to zero db. The medians observed for these summer and winter tests were −54 and −71 dbm respectively.

It is interesting to compare the results plotted in Fig. 10 with the results obtained from an experiment, conducted under the same summertime signal level conditions, with the transmitting antenna fixed on the great circle path, and rotating the receiving antenna only. Fig. 11 shows the median levels as a function of receiving antenna orientation, together with the summertime data obtained with both antennas rotated. The pattern obtained for the receiving antenna at a nearby test site is shown for comparison.

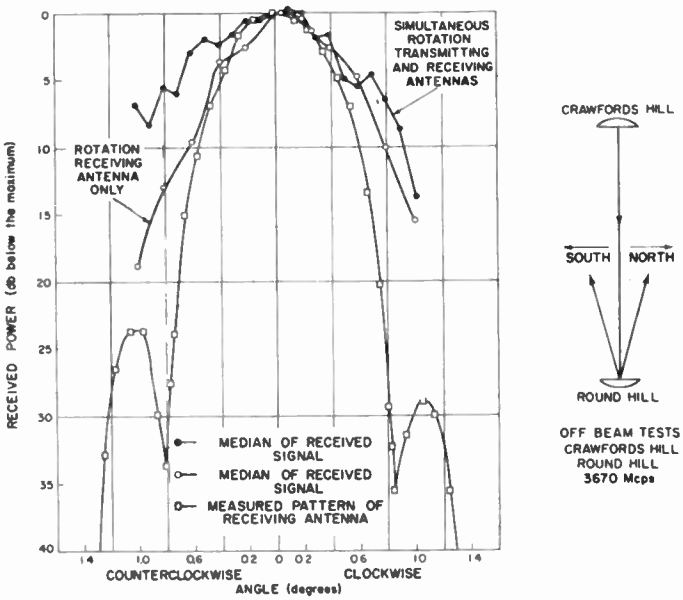

Fig. 11—Comparison of the received power for azimuthal rotation of the receiving antenna only with the received power obtained for simultaneous rotation of both antennas.

These data show a reduction in signal level when the receiving antenna is rotated away from the region strongly illuminated by the transmitting antenna. With the receiving antenna oriented toward a strongly illuminated region off the path, as is the case for the simultaneous rotation of the antenna beams, a much less pronounced reduction in signal level is observed for the same angular movement.

A series of complementary tests were made in which the beams were elevated and depressed from the normal horizontal position. In the first of this series of tests, the receiving antenna was maintained in the horizontal position and the transmitting antenna was shifted from one degree below horizontal to 0.4 degree above. At the transmitter site, the radio horizon is 0.3 degree below the horizontal. During the test period the median signal levels were −72 dbm when the antenna was oriented in the normal horizontal positions. A curve of the median signal levels observed at Round Hill as a function of the vertical angular position of the transmitting antenna is

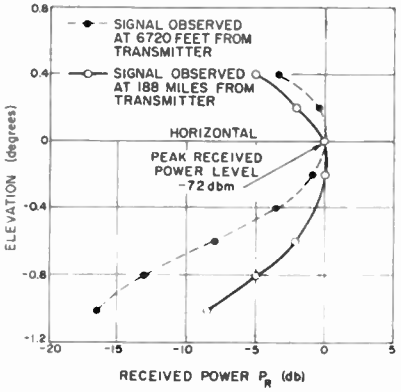

Fig. 12—Variation in received power when the 28-foot receiving antenna is fixed and the beam of the 28-foot transmitting antenna is varied in elevation.

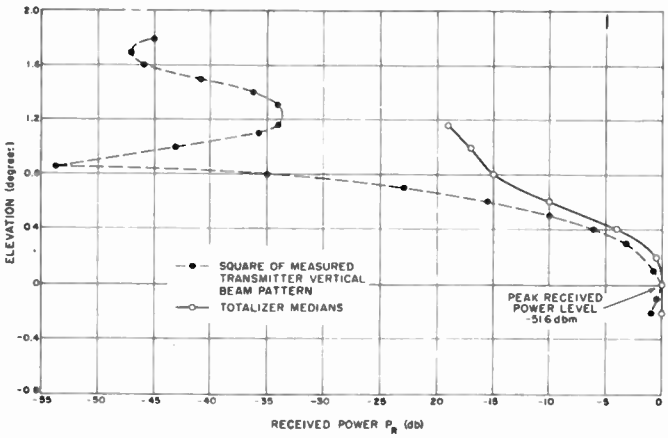

Fig. 13—Variation in received power when both 28-foot antennas are elevated simultaneously. The square of the measured transmitting antenna pattern is shown for comparison.

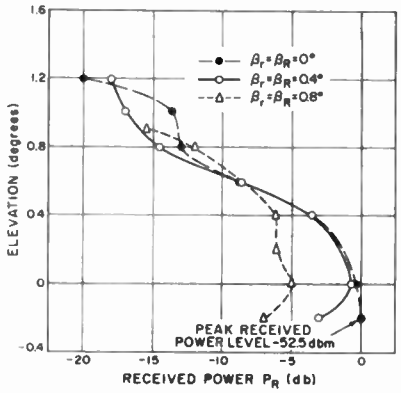

Fig. 14—Variation in received power for simultaneous elevation of the antennas at fixed azimuthal angles of the transmitting antenna (β_T) and the receiving antenna (β_R).

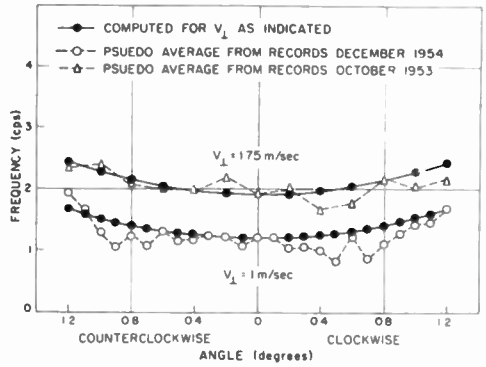

Fig. 15—Variations in fading rate with simultaneous rotation in azimuth of the 28-foot antennas.

shown in Fig. 12. A curve showing the variation of signal level as a function of vertical angular position, measured with a nearby test antenna at the same height as the transmitting antenna, is shown for reference. It is evident that a very small increase in signal level is obtained by depressing the transmitting antenna to the radio horizon.

A second experiment, in which both transmitting and receiving antennas were elevated and depressed simultaneously, was made during a period for which the median signal level was −52 dbm. The median levels observed at Round Hill together with the multiplied vertical patterns of the transmitting and receiving antennas are shown in Fig. 13. A comparison of this experiment with the previous one indicates that the signal level decreases with vertical angle at comparable rates in the two experiments.

The effects of simultaneous elevation of the two antennas at several azimuthal positions were observed in a series of three experiments during which the signal level under normal operating conditions was −53 dbm. Received signals were observed as a function of elevation angle of the two antennas for azimuthal positions of 0.0, 0.4, and 0.8 degrees, and are shown in Fig. 14.

Analysis of Fading Rates as a Function of the Angle of Scatter

In conjunction with the experimental measurements of signal levels received as a function of angular movement of the antenna systems, observations were made of the fading and of the shapes of the received pulses displayed on a synchronized 5-μsec time base of an oscilloscope. These observations did not indicate any substantial increase in pulse deterioration for the extreme off-path angular positions. Although a knowledge of the amplitude vs frequency spectrum of all components of the fading frequencies is probably required to describe the fading phenomena completely, a pseudo-average fading rate for each sample was obtained by counting the crossing of the median signal level by the recorder trace. Arbitrarily defining each two successive crossings in opposite directions as a cycle, the average fading frequency was determined graphically and tabulated for each angular position. Plots of the values of these rates for horizontal angular movement of the antenna system with a fixed angular elevation of zero degrees are shown in Fig. 15 for data obtained in early October, 1953. A similar plot of the rates for a period of weaker signal levels in December, 1954 is shown in the same figure. A trend toward increasing frequency of fading for the extreme horizontal angular positions is indicated for both experiments. A similar analysis was made for horizontal

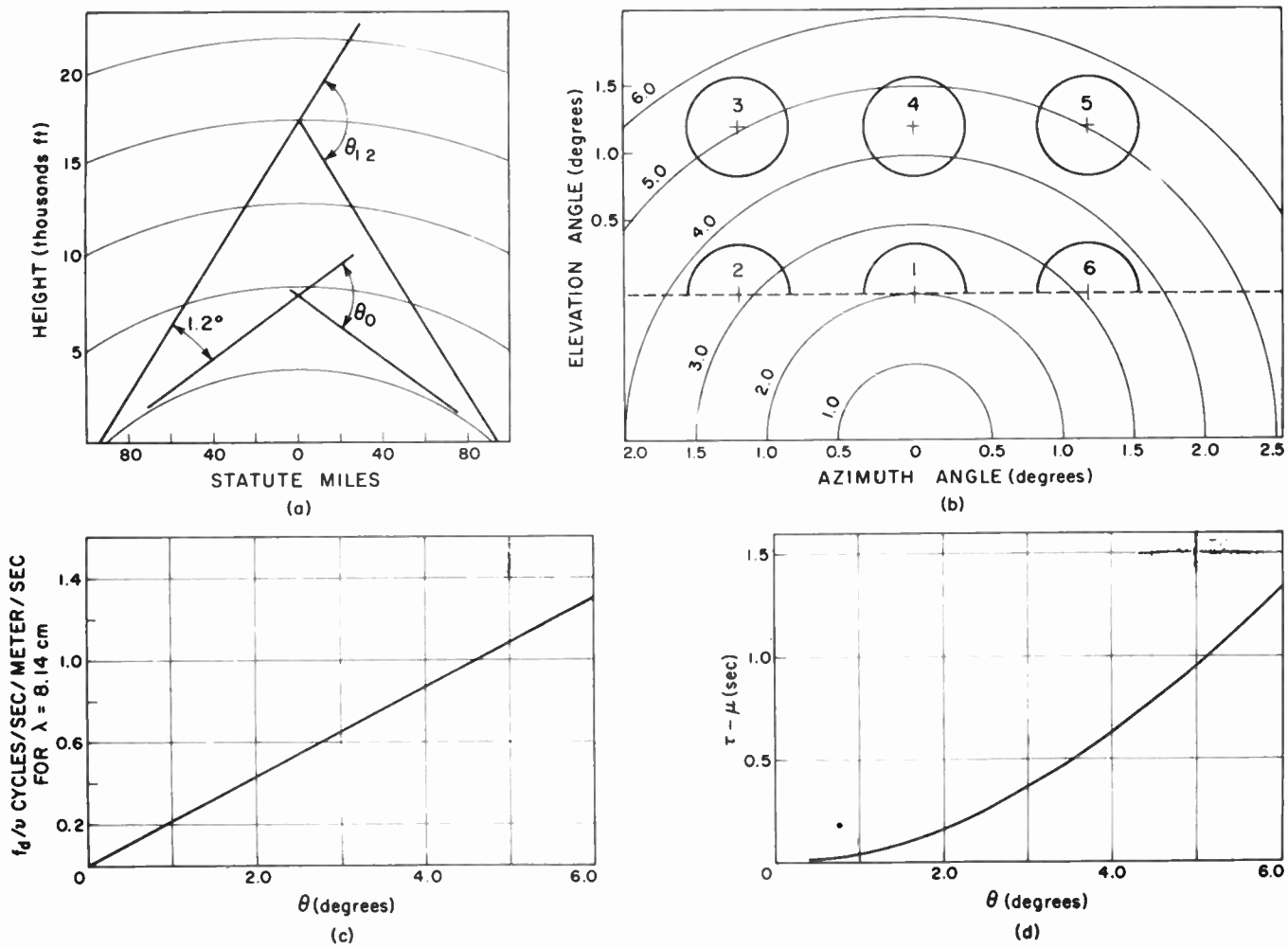

Fig. 16—A graph of the angular relations of ray paths for the 188-mile experimental path including curves for computing path delay (τ) and fading rate (f_d).

beam rotations with the antennas elevated to 0.5 degree. The trend toward increasing fading rates is less discernible for these elevated positions. There was also little evidence of a marked variation in the rapidity of fading as a function of the simultaneous elevation of the antennas. A convenient graphical method of computing the angular relations of ray paths and multipath time delays for the 188 mile experimental path is shown in Fig. 16. Assuming a 4/3 earth's radius to account for standard refractive conditions, ray paths of the maxima of the antenna patterns are shown in Fig. 16(a) as straight lines intersecting at the mid-path for horizontal alignment and for an angular elevation of 1.2 degrees of the antenna systems. The acute angle (θ) formed by these intersections represents the angular direction of the receiving antenna with reference to the wave normal of the transmitted wavefront upon its arrival at the mid-path. The regions of the troposphere influencing the results of these angular explorations can be considered to range from 4,900 to 15,000 feet in altitude under standard refractive conditions. The angle θ is simply twice the angle of elevation of the beam maximum with reference to an imaginary path along a straight line connecting the antennas and passing through the interior of the earth. A representation of the contours of constant angle (θ) is plotted on an imaginary plane normal to this connecting line at the midpoint of the path [Fig. 16(b)]. Since the off-path angles are small, the effective earth's curvature is neglected in the direction normal to the path. The vertical and azimuthal angular positions of the intersections of the beam maxima for 0.0 degree azimuth and 0.0 degree elevation [position 1 in Fig. 16(b)] and the extremities of angular movement used in these experiments in both azimuth and elevation (positions 2, 3, 4, 5, 6) are shown on this mid-path plane. An angular scale for antenna rotation, as measured relative to the true bearings at each antenna location, is shown at the bottom of the figure. A similar angular scale for vertical elevation is shown adjacent to the diagram. Intersections of the half-power beamwidths of the antenna systems are shown as circles for the elevated positions and as semicircles for 0.0 degree elevation. The relative time delay can be computed for each ray path from the transmitting antenna to an assumed scattering source in the mid-path plane and thence to the receiving antenna with reference to an imaginary free space path along the line connecting the antenna locations. Assuming primary scattering only, it can be

shown that the time delay relative to the imaginary free space path can be computed by a simple formula valid for small angles:

$$\tau = \frac{L\theta^2}{8c} \times 10^6 \text{ microseconds},$$

where L = path length in miles, θ = acute angle between intersecting ray paths at the mid-point in radians for each assumed scattering source, and c = velocity of radio waves in miles/second.

The maximum differential time delay for the ray path intersections of the half-power beamwidths (or any other arbitrary power points) can be computed by determining graphically from Fig. 16(d) the maximum and minimum values of θ appropriate to the heavy line outlining the area formed by the intersections of the half power beamwidths on the mid-path plane:

$$\Delta\tau = \frac{L}{c}\left[\frac{\theta^2_{\max} - \theta^2_{\min}}{8}\right] \times 10^6 \text{ microseconds}.$$

$\Delta\tau$ can be computed graphically from the curve of τ versus θ plotted in Fig. 16(d). The maximum differential delay computed in this manner for the on-path orientations of the antennas is approximately 0.14 μsec and 0.4–0.5 μsec for the extreme angular positions. The latter values appear too large compared with experimental observations of 1.5 μsec pulses. However, an examination of values of received signal levels as a function of angular position indicates that a rapid decrease in signal level occurs over the finite width of the beams of the antennas for these extreme angular positions and that the outboard portions of the beam are not equally productive of multipath contributions. This interpretation also implies that the angular scattering function of the troposphere is probably more directive than it appears on the plots of signal level versus angular rotation of the experimental data in the preceding figures.

An approximate formulation for maximum fading frequency caused by the Doppler effect of scattering sources in motion can be obtained by the differentiation of the path delay relations with respect to time and considering only velocity components lying in the vertical mid-plane and normal to the path. It can be shown geometrically that motion of reflecting or scattering sources produces a maximum Doppler shift in frequency at the mid-path when the direction of the motion is normal to and directed either toward or away from the imaginary free space path connecting the antenna positions. If $V_\perp$ is this component of velocity of the scattering sources in the mid-path plane normal to path L, then

$$\frac{dP}{dt} = 2V_\perp \sin\frac{\theta}{2}$$

$$= 2V_\perp\left[\frac{\theta}{2} - \frac{\theta^3}{48} + \cdots\right]$$

$$\cong V_\perp\theta.$$

P = path lengths in meters

$V_\perp$ = velocity in meters/second

θ = radians

λ = wavelength in meters.

For a given wavelength, the Doppler shift in frequency is

$$f_d \cong \frac{V_\perp\theta}{\lambda} \text{ cycles/second}.$$

The difference or beat frequency for two ray paths assuming possible opposite directions of the velocity component $V_\perp$ for the scattering sources associated with each of the two paths is then:

$$\Delta f = \frac{V_\perp}{\lambda}(\theta_{\max} + \theta_{\min}) \text{cycles/second}.$$

The maximum beat frequency occurs for ray paths where θ is in the vicinity of the maximum and where there may be scattering sources with equal but opposite velocity components ($V_\perp$). Under these conditions,

$$\Delta f = \frac{2V_\perp\theta_{\max}}{\lambda}.$$

These expressions are the fading rate only for two elementary scattered waves differing slightly in frequency. The amplitude of the fading signals as recorded can be interpreted as the logarithm of a rectified envelope of a group of waves resulting from the superposition of a spectrum of waves slightly different in frequency arriving over a multiplicity of paths. For the simple case of two components of equal magnitude and slightly differing frequencies the envelope of the group is cyclic with a period $t = 1/\Delta f$ seconds. A graph of the Doppler shift in frequency relative to the imaginary free space path for 1 meter per second velocity ($V_\perp$) as a function of the angle (θ) is shown in Fig. 16(c).

Plots of the fading rates as a function of horizontal angular position, determined experimentally, are shown in Fig. 15, together with the curves obtained from the above simple ray formula. A value of $V_\perp$ was chosen to fit the experimental fading data on the on-path antenna positions and then extended by computations from the graph in Fig. 16(c) to each horizontal position of the antennas off the great circle path. Although the values of $V_\perp$ are appropriate for ray paths where θ is near the maximum, there is a good agreement with the variation of fading rates for the off-path positions. Computations in a similar manner for horizontal rotation of the antennas when elevated 0.5 degree indicate that the increases in fading rates should be less for the elevated positions off-path. The experimental data obtained for the elevated positions were in general agreement with these computations.

Photographic Studies of Short Pulses under Various Propagation Conditions and Combination of Antenna Apertures

Periodically during the operation of the 3,670 mcps system, high-speed photographs of successive received pulses were obtained in order to determine the distortion introduced by the propagation medium. This series of pictures was obtained by displaying the received pulse on an oscilloscope having a sweep time of approximately 5 microseconds, and utilizing a P-15 tube with a very short persistence phosphor. The 5-microsecond time base of the oscilloscope was synchronized by a timing pulse at precise 2,000 microsecond intervals derived from the 100-kcps crystal-controlled frequency divider. Since the transmitted pulse repetition frequency was controlled in a similar manner, the received pulses could be positioned in the short sweep by a phase-shifter in the output of the crystal oscillator. The relative frequency stability between the crystal oscillators was sufficient to maintain the received pulses in the 5-microsecond sweep without adjustment for periods of 15 to 20 minutes. This technique made the synchronization of the time base of the oscilloscope independent of the time of arrival of the pulses and provided a means of observing possible variations in relative time of arrival of successive pulses.

Tests of the transmitter and the pulse receiver made in the laboratory indicated that the relative over-all timing error for successive pulses was less than 0.1 microsecond. Pulse photographs were obtained with a photographic recording camera operated at film speeds of 10,800 inches per minute. The combination of film motion and oscilloscope sweep provides a series of successive traces at the 500 cps pulse repetition frequency, which are distinguishable one from another, but do overlap to some extent. Since the agc time constant (4 milliseconds) was sufficiently long no appreciable distortion of the pulse shape is caused by the agc system during the time duration of the pulse. The saturable-core reactor used in the modulator of the transmitter provides a pulse shape which has a steep leading edge and a rounded sloping trailing edge.

A sequence of motion picture photographs taken at 64 frames per second on September 10, 1953, during median signal levels of −50 dbm, is shown in Fig. 17. This sequence was selected to illustrate the typical pulse breakup occurring during the infrequent deep fades. It is interesting to note that the break in the center of the pulse is not accompanied by extreme broadening or smearing but is more suggestive of frequency selective fading conditions. A careful study of the 1-microsecond marker reference positioned on the leading edge of the pulse suggests a barely perceptible shift in time of arrival. Similarly, an interpolation between the marker on the rear portion of the 1.5 microsecond pulse and the succeeding 1 microsecond marker on the base line indicates an approximate 0.1 microsecond elongation of the trailing edge of the pulse during this fade. The time duration of the breakup of the pulse is approximately $\frac{1}{8}$ of a second. This sequence is typical of deeper fades but represents conditions occurring only for a small percentage of the fades.

Observations were made of pulse distortion obtained with various combinations of antenna apertures. Typical sequences of successive pulses obtained for the weaker signal levels during the winter periods are shown in Fig. 18 (next page). Sequence 1 shows successive pulses obtained with 28-foot diameter transmitting and receiving antennas for median signal levels of −62 dbm. With this antenna combination, pulse breakup during the infrequent deep fades were similar to those shown in the motion picture sequence of Fig. 17 for summertime conditions.

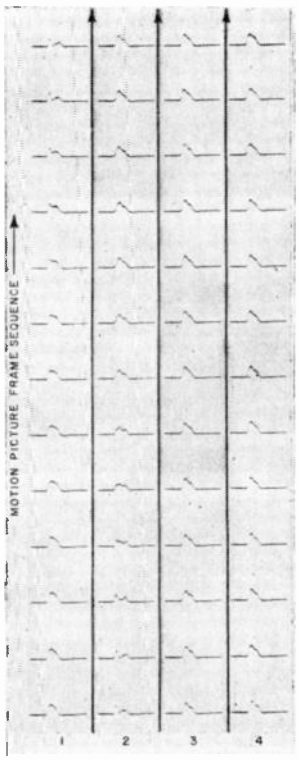

Fig. 17—Motion picture sequence of received pulses at 3,670 mcps during a deep fade. The sequences begin at the bottom of column 1 and end at the top of column 4.

Sequence 2 was obtained, using a 5-foot diameter transmitting antenna and a 28-foot diameter receiving antenna, a few minutes after Sequence 1. There is some evidence of increased distortion of the received pulse for a less directive transmitting antenna.

Sequence 3 was obtained several days later utilizing 5-foot diameter transmitting and receiving antennas under relatively high signal level conditions for the winter period. The pulse distortion appears slightly greater than for the pulses in Sequence 2.

Sequence 4 was obtained during a deep fade on the same antenna combination utilized in Sequence 2. Under these conditions considerable distortion and some elongation of the pulses is evident.

Sequence 5 shows the pulse shapes obtained for the same 5-5 antenna combination during a fade. This sequence shows the pronounced distortion and evidence of multipath delays of several tenths of a microsecond.

It appears from this data that the use of antennas with narrow beamwidths reduces the distortion of the pulse over scatter paths. The improvement in pulse shape is believed to result from the reduced illumination by the highly directive transmitting antenna of the off-path regions of the troposphere capable of scattering (or reflecting) radio waves with increasing time delays with reference to the on-path contributions. Some further reduction of delayed multipath contributions is accomplished by the use of highly directive receiving antenna. This combined effect of increasing antenna directivity may well serve to broaden the intrinsic bandwidth of the tropospheric medium although the effective gain of large antennas on these paths may not increase linearly with the area of the large apertures.

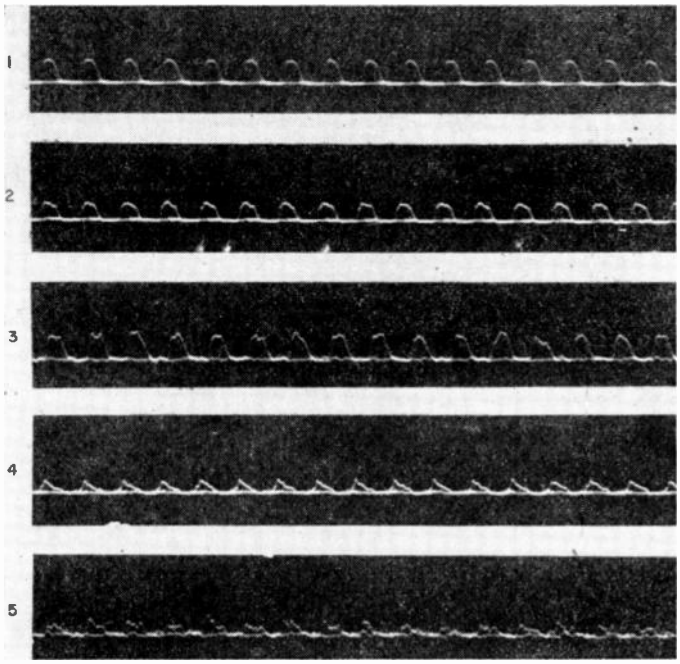

Fig. 18—Sequences of successive pulses received over the 188-mile path during winter periods: (1) Pulse shapes obtained for 28-foot transmitting and receiving antennas, (2) pulse shape obtained for 5-foot transmitting antenna and 28-foot receiving antenna, (3) pulse shape obtained for 5-foot transmitting and receiving antennas, (4) effect of a deep fade on the pulse shape for the 5-foot and 28-foot antenna combination, (5) effect of a deep fade on the 5-foot transmitting and receiving antenna.

Comparison of Horizontally and Vertically Polarized Components of Signals Received at 3,670 Mcps

The regularly scheduled recording program for the 3,670 mcps system utilized horizontally polarized antennas exclusively. In order to investigate the effects of the propagation medium on the polarization of signals received over the Crawfords Hill–Round Hill path, several experiments utilizing combinations of horizontal and vertical polarization were conducted.

Preliminary measurements were made of the cross-polarized components of the 28-foot diameter antennas from local test sites. Signals received on a small horn antenna rotated 90 degrees with respect to polarization of the horn feed of the large paraboloid were reduced 29 db or more from the signals received on the small horn antenna when aligned on the same polarization as the feed of the large antenna. Further measurements indicated that the patterns were approximately the same for each polarization.

Polarization studies were conducted on the Crawfords Hill–Round Hill path on December 8, 1953. The median value of the signal level during this period was −60 dbm and is near the median value for the month of December. The transmissions at Crawfords Hill were switched from horizontal to vertical polarization at alternate 15 minute periods with reception at Round Hill on horizontal polarization. When the transmitting antenna was cross-polarized with respect to the receiving antenna, the signal was barely recordable. A study of the signal level records indicated that the signal level received on a horizontally-polarized antenna over the scatter path from a vertically-polarized transmitting antenna was from 12 to 20 db below the signal levels recorded during the alternate periods of operation with the same polarization. These results indicate that some depolarization may be caused by the troposphere.

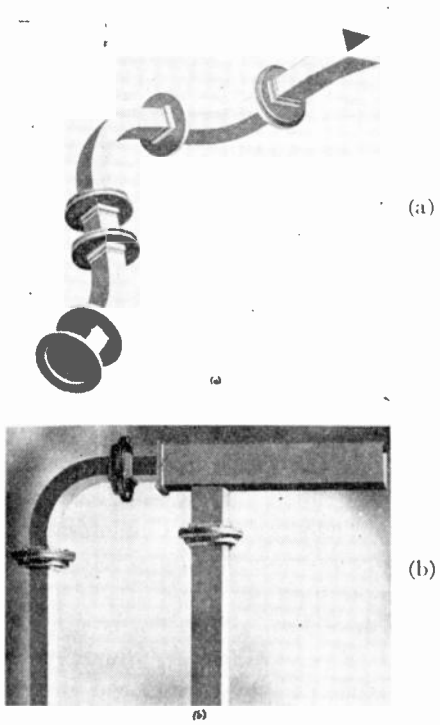

Fig. 19—(a) Photograph of transmitting feed for 45-degree polarization. (b) Photograph of feed for simultaneous reception of horizontal and vertical components of polarization.

Because of the interest in the potential application of polarization diversity to large directive antenna systems and in the polarization of radio waves propagated well beyond the horizon by the troposphere, antenna feeds were designed to enable a study of the fading of horizontally and vertically polarized signals trans-

mitted simultaneously. An antenna feed was utilized at Crawfords Hill to radiate approximately equal horizontally- and vertically-polarized components by use of a 45-degree orientation of the feed as shown in Fig. 19(a) (previous page). Horizontal and vertical components were received separately and simultaneously on two receivers at Round Hill utilizing an experimental feed as shown in Fig. 19(b). The signal levels for each receiver were recorded on separate Sanborn records utilizing the normal logarithmic compression of signal levels. Successive points obtained at 0.1 second intervals from the records were converted to a plot of signal intensity versus time for each receiver. Because of different line losses, separate scales were chosen to adjust the levels recorded on each receiver. A 15-second sequence of plots of two signal level intensities vs time typical of these records are shown in Fig. 20. These curves indicate near-synchronous fading for each polarization. Correlation

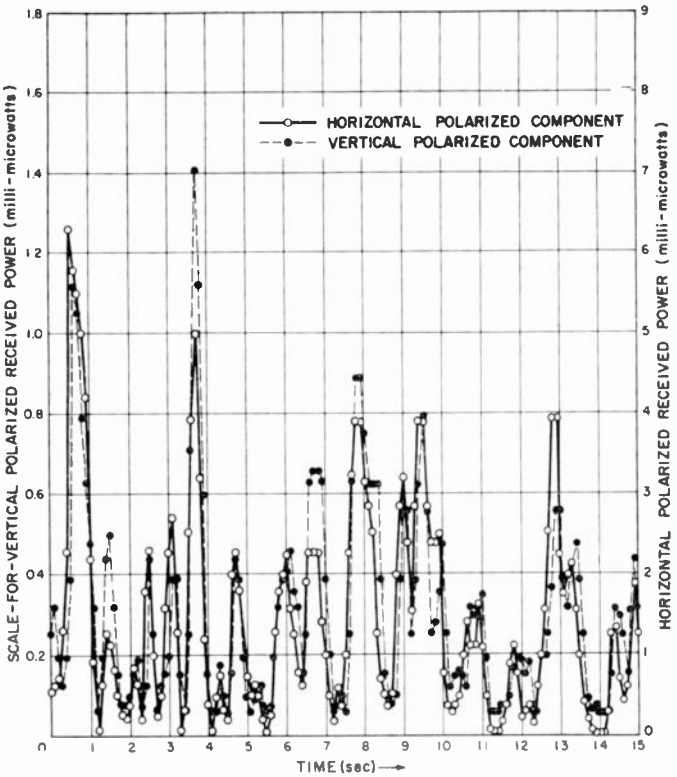

Fig. 20—A 15-second sample of the signals received simultaneously for each polarization component.

coefficient, computed for the points in this sequence on an equivalent voltage basis, is 0.6. The results of these tests indicate that the use of polarization diversity would not provide a high degree of protection against simultaneous fading for highly directive antennas.

Effective Gains of Various Antenna Combinations

Experiments designed to investigate the effective system gain of various sizes of antenna apertures at 3,670 mcps over the 188-mile circuit were conducted in 1954. The planned antenna system consisted of 5, 17, and 28-foot diameter paraboloidal antennas at each terminal. Destruction of the first of two experimental 17-foot diameter antennas located at Round Hill by Hurricane Carol prevented the use of the intermediate sizes of antenna apertures. The experimental measurements described are confined to combinations of the 5-foot and 28-foot diameter antennas. For brevity, the antenna combinations are denoted by hyphenated numbers of the antenna diameters with the transmitting antenna diameter appearing first.

The first of this series of measurements of comparative signal levels received on antennas of different sizes of apertures was conducted October 1 to 22, 1954, utilizing alternate half-hour transmissions from the 28-foot diameter and 5-foot diameter antennas at Crawfords Hill. Only the 5-foot diameter antenna was used for reception at Round Hill because of the hurricane damage to the 28-foot antenna. A distribution of the differences in decibels between the signal levels for each antenna combination was obtained by comparing the median of the half-hourly recordings on 5-5 with the mean of the prior and subsequent medians of the half-hour periods recorded on 28-5. This curve, shown in Fig. 21, indicates that for 90 per cent of the cases the median level received on 28-5 exceeds the median of 5-5 by 7 db. The corresponding values for 50 per cent and 10 per cent of the cases are 10.3 and 16.2 db respectively. The difference in the gain products of the 28-5 and 5-5 antenna combinations computed from the gains for each antenna measured under plane-wave conditions from local test sites is 13.8 db. Those differences greater than the value computed from plane-wave measurement may be attributed, in part, to time variations of the signal level from one half-hourly period to the next.

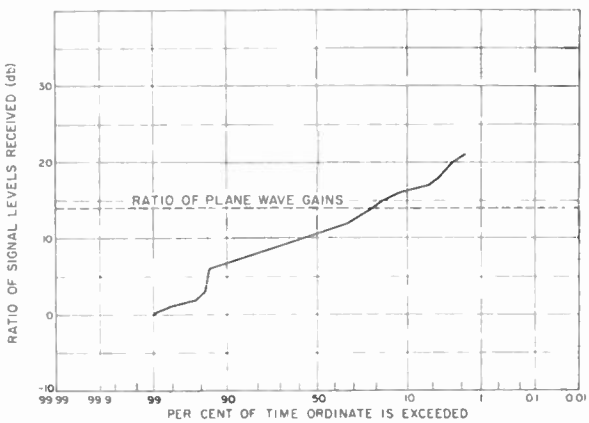

Fig. 21—Distributions of differences of median values received on a 5-foot antenna of alternate transmissions from a 28-foot and 5-foot antenna during October, 1954 at 3,670 mcps (109 cases).

Replacement of the 28-foot antenna at Round Hill in late October, 1954 permitted simultaneous reception on the 28-foot and 5-foot antennas of transmissions from the 28-foot antenna at Crawfords Hill for the period November 1, 1954 to January 30, 1955. Because of the seasonal decrease in signal level only a few hours of

usable recordings could be obtained on the 5-5 combination during this period. It should be emphasized that the distributions obtained from the data for this period are believed to be more reliable because of the simultaneous reception and the absence of the influence of hour-to-hour variations of signal level. The difference in the gain product of the 28-28 and 28-5 combinations for plane-wave conditions was 18.2 db. The distributions of the differences in the hourly median values of signal level received simultaneously on the 28-foot and 5-foot antennas at Round Hill of transmissions from the 28-foot antenna at Crawfords Hill are shown for each monthly period in Fig. 22. The variation of the

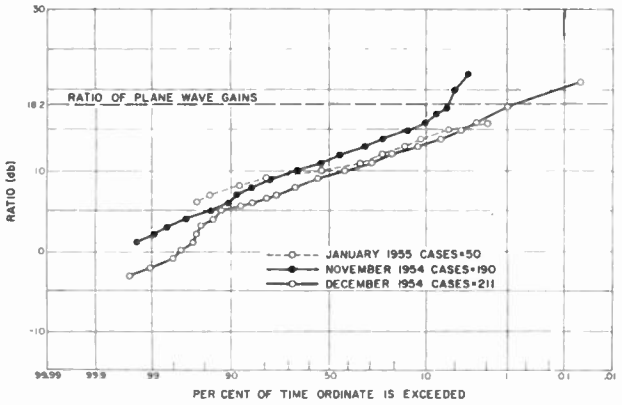

Fig. 22—Distribution of differences of hourly median values received simultaneously on 28-foot and 5-foot antennas of transmissions from 28-foot antenna at 3,670 mcps.

differences for these winter months appear similar. A comparison of the effective gains of the 28-28 with the 28-5 combination, for differences exceeded 10, 50, and 90 per cent of the time, is shown in Table I.

TABLE I
EFFECTIVE GAINS OF ANTENNA SYSTEMS OVER THE 188-MILE SCATTER CIRCUIT

Month	Measured differences in signal level exceeded for indicated percentage of time			Differences of gain products from plane wave measurements of the 28-28 and 28-5 combinations
	90%	50%	10%	
November	6.6 db	11.5 db	16.2 db	18.2 db
December	5.4 db	9.4 db	13.4 db	18.2 db
January	7.5 db	10.1 db	14.3 db	18.2 db

Observed Signal Levels

The design of communication systems employing tropospheric scatter requires detailed information of the seasonal and diurnal variations of median signal levels and of the range of fading encountered under the diurnal and seasonal changes of the median signal levels. During the period from July, 1953 to April, 1955 recordings were made over the Crawfords Hill to Round Hill circuit on 3,670 mcps by means of signal level distribution recorders ("totalizers"). Distributions of 3,200 hourly samples were obtained under a wide variety of meteorological conditions, and for representative periods throughout the year.

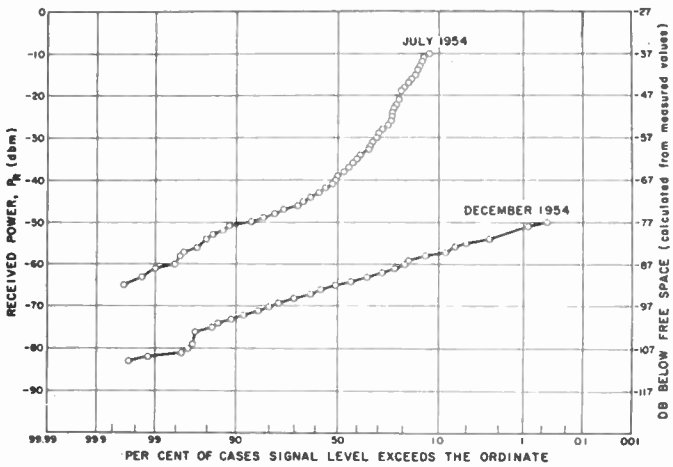

Fig. 23—Cumulative distributions of hourly median values of signal level received on a 28-foot antenna at Round Hill of 3,670 mcps transmission from a 28-foot antenna at Crawfords Hill, N. J., for the months of July and December, 1954.

A cumulative distribution of the incidence of medians exceeding a given signal level for the months of July, 1954 and December, 1954 are shown in Fig. 23. The median value, as determined from these cumulative distributions of the incidence of medians, for each month throughout the recording period, has been used to plot the seasonal trend shown in Fig. 24. Good agreement is obtained for the corresponding months observed during successive years.

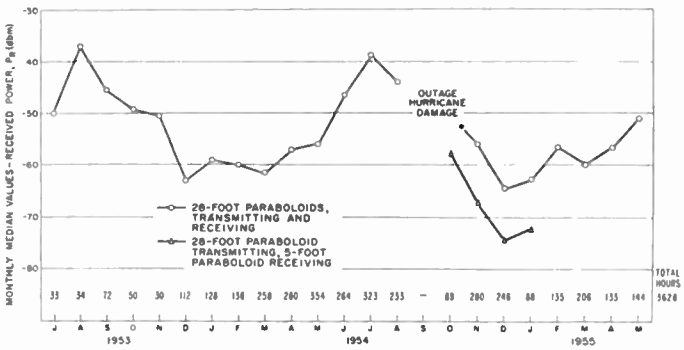

Fig. 24—Seasonal variation of monthly median of the hourly median values of signal level received at Round Hill for the period July, 1953 through May, 1955 at 3,670 mcps.

An accumulation of the level distributions for the period from June, 1954, to December, 1954, have been analyzed for diurnal variations. The median values, together with the values exceeded 10 per cent and 90 per cent of the time, are plotted for each hour of the day [Fig. 25 (next page)]. No discernible diurnal trend is found for the 90 per cent and median values. The 10 per cent value, however, shows a marked increase during the hours of darkness. Similar plots of diurnal variations for monthly periods during the winter show an absence of diurnal variation of the 10 per cent levels; those for the summer months, however, invariably show this diurnal trend.

Fading range was determined from over 500 samples of hourly signal level distributions selected at random,

from the hourly samples whose median values were less than the yearly median. The fading range for each sample was determined in terms of the standard deviation of the distribution. A class interval of median signal level was chosen and each sample was assigned to one of the intervals. Distributions of the standard deviations were made for the samples in each class interval. The median values of these distributions was 5.5 db for all 5-db class intervals of signal levels from −55 to −70 dbm.

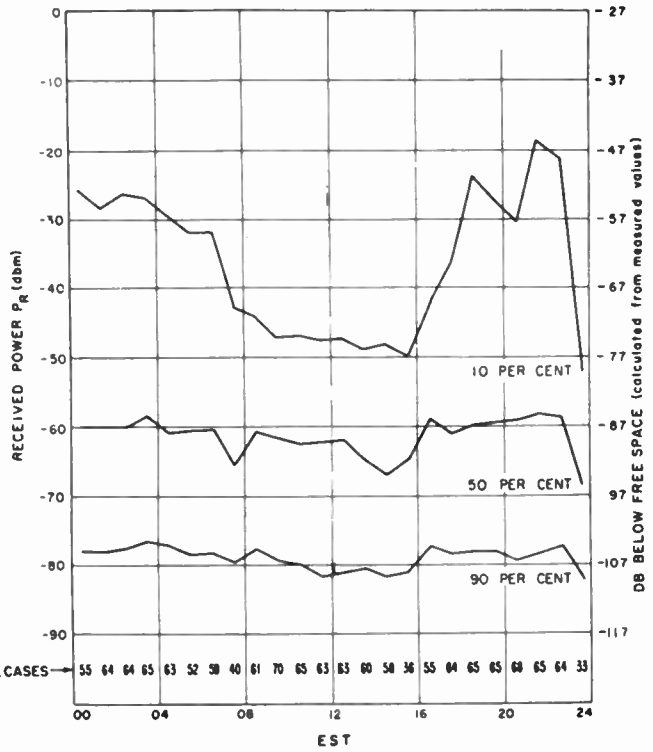

Fig. 25—Diurnal variation of signal level exceeded 10, 50, and 90 per cent of the time received on 28-foot antenna at Round Hill of 3,670 mcps transmission from Crawfords Hill, N. J., for the period June, 1954–December (865 hours).

A study of the signal level distribution as a function of sampling time was made to determine possible changes in the character of the distribution curve. The distributions for sampling periods of 15 seconds, one minute, 4 minutes and 16 minutes are shown in Fig. 26 (next page). The solid curve in each figure is a Rayleigh distribution whose median coincides with the observed median value. The observed distributions for the 15 second and 1 minute sample agree fairly well with the Rayleigh curve. The 4 minute sample shows a clear departure from the Rayleigh curve but is not quite normally distributed. The 16-minute sample shows a good fit with a normal distribution. This trend from the Rayleigh distribution to the normal distribution as the sampling period is increased in time has been observed repeatedly. A sample of a fast speed record illustrating typical fading for the 3,670 mcps signals is shown in Fig. 27 (next page).

Modulation Tests at 5,050 Mcps

In order to make preliminary modulation tests at shf, a 400-watt FM transmitter was designed and constructed to operate at 5,050 mcps. The crystal oscillator and low frequency multipliers for this unit were modified components from a Bell System TD-2 radio relay system. The transmitter was frequency modulated by means of a 70 mcps signal obtained from a Western Electric FM terminal. A separate waveguide and antenna feed system was used to excite the 28-foot diameter antennas. The measured pattern of these antennas for this frequency is shown in Fig. 6. The measured gain of the 28-foot antenna was 51.3 db above an isotropic radiator and the waveguide line loss was 0.9 db.

Modulation experiments were conducted over the Crawfords Hill–Round Hill path during the period November, 1953, to August, 1954, in cooperation with the Bell Telephone Laboratories utilizing voice multiplex terminals from the Bell System TD-2 radio relay equipment. The initial tests utilized a simulated 12-channel (0–56 kcps base band) system and a frequency deviation of the shf carrier of ±500 kcps. The receiver employed for these tests was modified TD-2 equipment and had an IF bandwidth of 1.3 megacycles and a noise figure of 9 db. The voice transmissions made during these tests over the path indicated negligible intermodulation or distortion except for the infrequent fades below the limiting threshold of receiver.

The encouraging results of these early tests suggested a more ambitious experiment utilizing wider bandwidths. In August, 1954, a series of experiments were attempted utilizing standard video modulation techniques. For these tests, the 1.3 mcps filter, used in the receiver for the multiplex tests was removed to provide a bandwidth of 30 mcps. A rectangular "window" test pattern was transmitted with a frequency deviation of ±4 mcps over the circuit without evidence of distortion from multipath delays. These first video tests were followed by transmissions of a live program over the circuit. The picture quality obtained in these tests was good as long as the received signal level was sufficient to maintain synchronization of the picture.

Photographs of the results of the video tests and a description of the methods used to simulate and test the 12 voice channel multiplex system are contained in a paper in this issue by W. H. Tidd.[22]

Comparison of UHF and SHF Data

Assumption of a frequency dependence, based upon signal levels observed relative to the values computed from plane-wave antenna gains in free space, may not be proper under conditions where an angular spectrum of scattered waves is incident upon antennas large in

[22] W. H. Tidd, "Demonstration of bandwidth capabilities of beyond horizon tropospheric radio propagation," p. 1297, this issue.

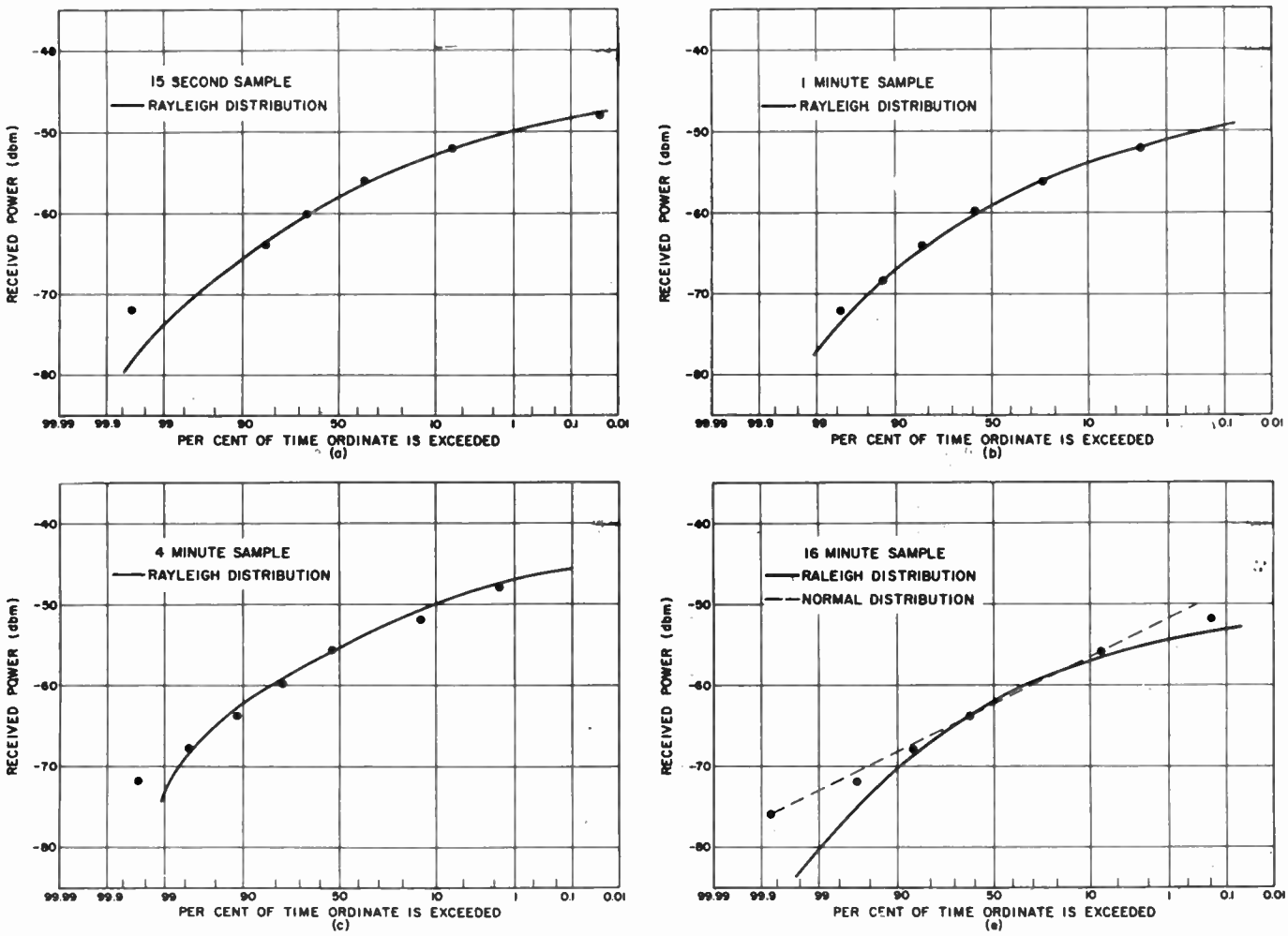

Fig. 26—Distribution of signal level received on a 28-foot dish of Round Hill of 3,670 mcps transmissions from Crawfords for short sampling periods. (a) 15 second sampling period, (b) 1 minute sampling period, (c) 4 minute sampling period, (d) 16 minute sampling period.

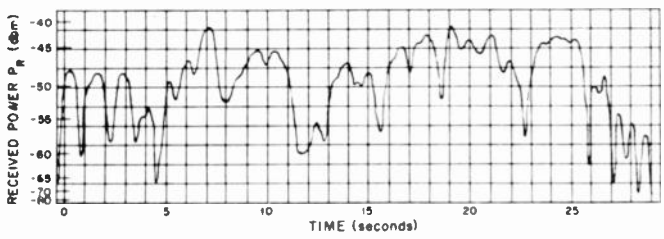

Fig. 27—Sample of fast speed recording of signal received at Round Hill at 3,670 mcps under typical summertime conditions.

terms of wavelength. It is suggested that the ratio of P_r/P_t for experimental measurements of tropospheric scattering, as determined from the power (P_r) actually delivered to the receiver from the receiving antenna system and the power delivered by the transmitting antenna (P_t), is a more suitable method of comparing systems operating at different frequencies and with different sizes of apertures. This method is applicable only for comparisons based upon recorded data for specific path lengths, frequencies, and antenna sizes.

An analysis of the 385.5 mcps and 399.5 mcps signal levels recorded over a path 181 miles in length from Round Hill to the U. S. Army Signal Corps, Coles

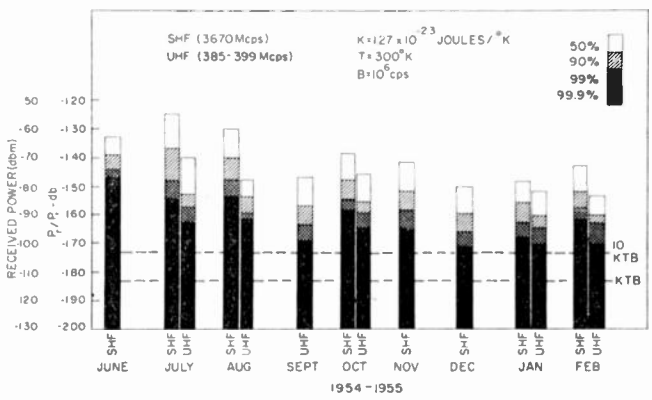

Fig. 28—Comparison of seasonal variations of signal level received over uhf and shf experimental systems.

Signal Laboratory and the data obtained on the 3,670 mcps Round Hill–Crawfords Hill path, 188 miles in length, is shown in Fig. 28. Both systems utilized 28-foot diameter antennas for transmission and reception. The diameters of the antenna are 11 wavelengths and 104 wavelengths at uhf and shf respectively. The monthly distribution curves obtained from the recorded data were normalized to the same transmitted

power of 10 kw. This data, presented in terms of the ratio of received power to transmitted power, does not involve any speculation on theoretical models. It is interesting to note that on an equal aperture and equal power basis, the received monthly medians of signal level for shf exceeds the similar uhf signal levels by 15 db during July. The apparent seasonal decrease of shf levels for the winter period is 26 db, while apparent uhf seasonal decrease is 14 db (assuming the February data as the lowest value since data in December was not available). The ratio of P_r/P_t is nearly the same for both frequencies under these wintertime conditions.

For free space conditions, in the absence of scattering, P_r(shf) should be approximately 19 decibels greater than P_r(uhf) for these particular frequencies and system parameters. This analysis suggests that any frequency dependence for scattered signals, under summertime conditions, is a matter of a few decibels at most since the indicated difference of the levels for the July medians for these two frequencies are 15 db compared to the 19 db expected. The near disappearance of this difference during the weaker wintertime conditions is less amenable to simple interpretation. The increased angular spread of the 3,670 mcps scattered signals described previously in the shf experiments, for data obtained in December, 1954, when compared to the August data would imply that the effective gain of the 28-foot diameter antennas at 3,670 mcps would be decreased to a greater degree than for the same antenna operating at uhf. Until measurements at uhf are made over scatter paths with antennas of directivity equal to those used at shf, some frequency dependence under wintertime conditions may be considered plausible.

Conclusion

The results of these experimental measurements have shown that reliable communications with useful bandwidths can be achieved at uhf and shf over paths at 150 to 200 miles in length utilizing radio waves scattered by the troposphere provided that several kilowatts of power and highly directional antenna systems are utilized. The angular measurements of pulse signals scattered by the troposphere indicate that the mechanism of scattering is highly directive and that the multipath delays are less serious than indicated by earlier versions of scatter models.

Theoretical multipath delays and bandwidth computations by Booker and deBettencourt[23] are in general agreement with the experimental results based upon their model of atmospheric turbulence.

The narrow beamwidth of 28-foot diameter antennas at shf provides some reduction of multipath contributions over the 188 mile path but also exhibit reduced gain effectiveness in the winter periods. Comparisons of the uhf and shf data indicate that a spectrum, several thousands megacycles wide, is potentially useful for communications over tropospheric scatter paths.

Acknowledgment

This research program was conducted under the supervision of Professor W. H. Radford and Professor J. B. Wiesner of Lincoln Laboratory, whose early suggestion of the communication possibility made this program possible. The contributions of numerous individuals were responsible for the design, construction, and installation of these experimental systems. The authors wish to gratefully acknowledge the efforts of other members of the Lincoln Laboratory as well as the members of the U. S. Army Signal Corps, Navy and Air Force Liaison Offices at the Lincoln Laboratory and members of the following organizations: Air Force Cambridge Research Center, Coles Signal Laboratory, Armstrong Laboratories, Bell Telephone Laboratories, and Stavid Engineering, Inc. The authors are also indebted to Dr. H. G. Booker, consultant to Lincoln Laboratory, and Dr. T. J. Carroll and Dr. R. M. Ring for stimulating discussions on tropospheric theories and interpretation of experimental results.

[23] H. G. Booker and J. T. deBettencourt, "Theory of radio transmission by tropospheric scattering using very narrow beams," Proc. IRE, vol. 43, pp. 281–290; March, 1955.

Some Tropospheric Scatter Propagation Measurements Near the Radio Horizon*

H. B. JANES†, MEMBER, IRE, AND P. I. WELLS†, ASSOCIATE, IRE

Summary—Measurements of small variations in 100 mc field intensity within and just beyond the radio horizon are reported. The measured fields are assumed to be the resultant of two field components, one having a constant amplitude and the other being a rapidly-fading scattered component. The fading range of the resultant field intensity over a 10-minute period is used to determine K. Here, K is the ratio in decibels of the root-mean-square amplitude of the scattered component to the amplitude of the constant vector. Curves showing the measured median values of basic transmission loss, fading rate, and K plotted vs hour of the day are included for three of the Cheyenne Mountain transmission paths. Diurnal variation of these quantities is also discussed. The average basic transmission loss of the scattered component, L_{bs}, can be found if K and the resultant basic transmission loss, L_{bm}, are known. Median values of L_{bs} and L_{bm} are plotted vs the angular path distance, θ. Measurement of the correlation of the resultant field strengths received on two horizontally-spaced antennas within the radio horizon is reported. When the spacing was varied from $\frac{1}{2}$ to 20 wavelengths and the correlation compared to other characteristics of the field, the correlation was found to be as much a function of L_{bs} and fading rate as it was of antenna spacing.

Introduction

SINCE the advent of the Booker-Gordon theory of atmospheric scattering it has become very convenient to consider received vhf and uhf fields as consisting essentially of two components.[1] One has a slowly-varying amplitude and results from some mechanism such as ground-wave propagation within the horizon or diffraction accompanied by ducting in propagation beyond the horizon. Another component has a rapidly-fluctuating amplitude and results from atmospheric scattering. In the case of transmissions at large angular distances[1] beyond the radio horizon, the steady component is attenuated to such an extent that the scattered component predominates and the resultant amplitude is very nearly Rayleigh-distributed. In general, the ratio of scattered component to steady component decreases with decreasing angular path distance until, for line-of-sight paths (i.e., for negative angular distances), the received field is relatively constant and the scattered component is usually not detectable with ordinary recording equipment.

In order to extend our basic knowledge of the scattering mechanism and to evaluate the effect of scattering in certain practical applications involving line-of-sight transmission, a series of scattered field strength measurements have been conducted within and just beyond the radio horizon. These measurements were made on a frequency of 100 mc, using the special gain-stable receiver and differential voltage recorder described below.

The transmission paths used in the measurements extended from the summit of Cheyenne Mountain near Colorado Springs to three of the Cheyenne Mountain Project receiving sites in eastern Colorado. These facilities have been described in detail previously.[2] The sites are located at Kendrick, Karval, and Haswell in eastern Colorado. The Kendrick site is 49.3 miles from the Cheyenne Mountain summit transmitter site and is well within the radio horizon. The Karval site is at a distance of 70.2 miles and just within the radio horizon. Haswell, at a distance of 96.6 miles, is in the diffraction region. Simple half-wave dipole antennas located approximately nineteen feet above ground were used at all three receiving sites. Both the transmitting and receiving antennas had rather broad beams.[2] Hence, for each of the transmission paths, the parameters of the scattering integral were determined almost entirely by the scattering elements themselves.

The recordings at Kendrick were made during the periods August 17 to 21, and August 24 to 27, 1953. Those at Karval were made one year later during the period August 16 to 29, 1954. Those at Haswell were made during August 18 and 19, 1954. It will be noted that the only period during which simultaneous recordings were made at two sites was during August 18 to 19, 1954. At Karval, however, simultaneous measurements were made using two adjacent antennas with variable spacing in order to study the correlation of the fading as a function of antenna spacing.

Description of the Recording Equipment and Data

The receiving and recording equipment used in these measurements has been described in detail previously.[2] Briefly, it consists of the gain-stable receiver Type GS-2 developed at the National Bureau of Standards, and a differential voltage recorder. Two special output circuits have been installed in the GS-2 receiver. The output of one of these is proportional to the long-time-constant average output voltage of the detector which, in turn, is proportional to the average field strength. The time constant employed was of the order of 5 minutes. The output voltage of this circuit is recorded on a clock-driven chart. The other output circuit is ahead of the long-time-constant filter and provides a voltage pro-

* Original manuscript received by the IRE, August 1, 1955; revised manuscript received August 8, 1955.

† Central Radio Propagation Lab., National Bureau of Standards, Boulder, Colorado.

[1] K. A. Norton, P. L. Rice, and L. E. Vogler, "The use of angular distance in estimating the transmission loss and fading range for propagation through a turbulent atmosphere over irregular terrain," p. 1488, this issue.

[2] A. P. Barsis, J. W. Herbstreit, and K. O. Hornberg, "Cheyenne Mountain Tropospheric Propagation Experiments," NBS Circular 554; December, 1954.

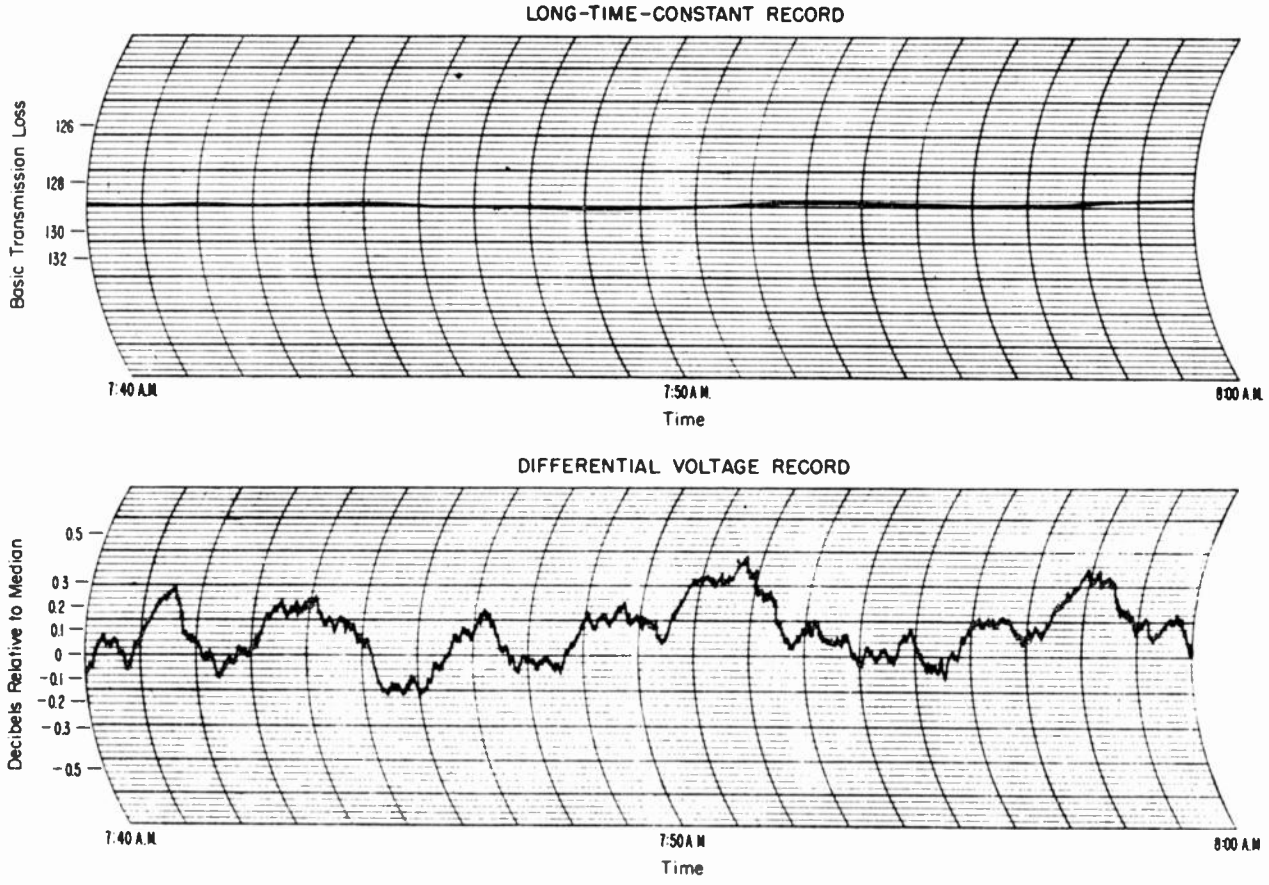

Fig. 1—Sample long-time-constant and differential amplifier recordings. (Cheyenne Mountain—Kendrick Path, 100 mc, August 20, 1953.)

portional to the instantaneous field strength. The differential voltage recorder amplifies and records on another clock-driven chart the difference between these two output voltages. In the discussion that follows, these recordings are referred to as the long-time-constant data, and the short-time-constant or differential amplifier data, respectively.

The data presented in this paper were recorded at chart speeds of $\frac{3}{4}$ inch per minute at Kendrick and Karval and $1\frac{1}{2}$ inch per minute at Haswell. To insure synchronization of the long- and short-time-constant recordings, simultaneous time markings were placed on the two charts every minute by means of chronographs actuated by a common timer. Fig. 1 shows a representative sample of both the long-time-constant and the differential amplifier recordings at Kendrick. This illustrates the very greatly expanded scale on the differential amplifier chart. Since the voltage calibration of the differential amplifier is constant, the corresponding calibration in terms of instantaneous field strength in decibels relative to the average field strength is variable, and depends upon the average level recorded on the long-time-constant chart.

Analysis of the Data

As was stated previously, the hypothesis on which the analysis of these measurements was based is that the received field consists of a constant component and a scattered component. The purpose of the analysis was to determine the relative magnitude of these two components in terms of K, where K is the ratio in decibels of the root-mean-square amplitude of the scattered component to the amplitude of the constant component. The procedure was to determine from the distribution of instantaneous field intensity levels (or, more specifically, from the fading range) the corresponding value of K. Fading range is defined as the ratio in decibels of the amplitudes exceeded 10 per cent and 90 per cent of the time interval being analyzed. Two functional relationships between fading range and K were used. For the data recorded beyond the radio horizon at Haswell, the curve of fading range vs K given on Fig. 6 in the paper by Norton, Vogler, Mansfield and Short[3] was applicable, since the scattered component was considered to have a Rayleigh-distributed amplitude and random phase relative to the constant component. At both Kendrick and Karval, however, a different interpretation was needed. Here the constant component is actually the resultant of the constant components of the direct and ground-reflected waves while the scattered component is the resultant of the scattered vectors associated with these two waves. Furthermore, it has been shown[4] that within

[3] K. A. Norton, L. E. Vogler, W. V. Mansfield, and P. J. Short, "The probability distribution of the amplitude of a constant vector plus a Rayleigh distributed vector," p. 1354, this issue.

[4] A. D. Wheelon and R. B. Muchmore, "Line-of-sight propagation phenomena, II. Scattered components," p. 1450, this issue.

the radio horizon, the amplitude of the scattered vector is normally distributed and its phase relative to the constant component is always $\pm\pi/2$. The path-length difference between the direct and ground-reflected rays is very small for both paths (6.5 degrees at Kendrick and 16.7 degrees at Karval) and the reflection coefficient is close to unity. Thus the resultant constant vector is very nearly normal to both the direct and ground-reflected vectors and so is either in phase or 180 degrees out of phase relative to the resultant scattered vector. Under these circumstances it can be shown[3] that the relationship between fading range and K is given approximately by:

$$R(0.1) - R(0.9) = 22.2628k + 12.1880k^3 \qquad (1)$$

where $R(0.1)-R(0.9)$ is the fading range and $K = 20 \log_{10} k$. This relation was used to obtain K from the fading ranges measured at Kendrick and Karval.

The fading ranges measured at Haswell were all less than 3 decibels. From Fig. 6 of reference 3, it will be seen that this corresponds to a value of $R(0.5)$ less than 0.1 decibel, where $R(0.5)$ is the median resultant amplitude expressed in decibels relative to the constant component. Thus at this site, the constant component has very nearly the same amplitude as the resultant field strength. Under the assumptions made above, the same is true for the Kendrick and Karval data. The long-time-constant recording can to a very close approximation be considered to represent the constant component as well as the average value of the resultant. The differential amplifier record shows variations in the instantaneous amplitude of the resultant. If a steady level is maintained on the long-time-constant chart, the fading rate and fading range of the resultant field can be determined directly from the differential amplifier record.

The data were divided into 10-minute intervals for analysis. This time interval was long enough to include a large number of fades in the rapidly-varying component but short enough to prevent the slowly-varying (*constant*) component from undergoing appreciable changes in magnitude during the interval. The short-time-constant recording was analyzed to determine for each such 10-minute period the distribution of instantaneous field intensities. From this distribution the fading range and corresponding value of K were determined. The fading rate N, defined as the number of times per minute that the field strength trace level crosses the median level with a positive slope, was also computed for each period.[5] The long-time-constant charts were used to determine a quantity which, strictly speaking, should be called the median of the averaged resultant amplitude. However, to a very good approximation, it is equal to the median of the instantaneous resultant amplitudes, and is expressed in terms of the median basic transmission loss, L_{bm}.

The medians of all of the 10-minute values of the three quantities, L_{bm}, K, and N were determined for each hour of the day. These median values are shown plotted vs time of day in Fig. 2 (next page). On the Haswell graph, the dashed lines cross periods during which no data were recorded. The number of periods on which each curve is based is shown in the figure. Note that these curves are based on statistically small samples and therefore should not be read too literally. They are presented only to illustrate some rather persistent diurnal trends in the data.

The two 3-day recording periods at Kendrick are plotted separately because there is quite a marked difference in the character of the fields measured during the two periods. During August 24–27, there is a wider diurnal variation in L_{bm} than during the previous period, although in both periods it follows the familiar pattern of weaker fields during the day than during the night. A more striking difference appears in the variation of K and N. During the August 17–21 period there is no distinct diurnal pattern in K, and the over-all median value would appear to be about -33 decibels. During August 24–27 in the late morning hours there is a definite build-up in K; i.e., in the scattered component of the received field. Only at the peak does K reach -33 decibels. The over-all median value is about -38 decibels. The diurnal pattern in the plots of N is similar for both periods. There is a substantial increase in fading rate during the afternoon hours at about the same time that the basic transmission loss is also at a maximum. However, it should be noted that the fading rate during the first period was much lower than during the second. The over-all median value of N was slightly greater than 1 fade per minute for the first period and approximately three times that much during the second period.

The diurnal variation of the three parameters at Karval more closely resembles the second period at Kendrick. However, a direct comparison should not be made since the Kendrick and Karval recording periods are separated by one year. It is interesting to compare the diurnal variation of K at Karval with the diurnal variation of within-the-hour fading range measured at this site during August, 1952.[6] In that instance there was a decrease in fading range during the daylight hours; i.e., the reverse of the diurnal pattern of K shown in Fig. 2. However, the previous fading range data were based on hourly distributions of instantaneous field intensities instead of 10-minute distributions as in the present analysis. Thus, slow but relatively large fades which usually occur during the night were included in the distributions. This accounts for the larger fading range during the night. It has been pointed out that the diurnal pattern might be completely inverted if fading range were measured over a smaller increment of time so as to eliminate these slow fades.[5] Fig. 2 indicates that

[5] K. A. Norton, P. L. Rice, H. B. Janes, and A. P. Barsis, "The rate of fading in propagation through a turbulent atmosphere," p. 1341, this issue.

[6] H. B. Janes, "An analysis of within-the-hour fading in 100- to 1,000-mc transmissions," *Journal of Research of the NBS*, vol. 54, pp. 231–250; April, 1955. (See Fig. 9.)

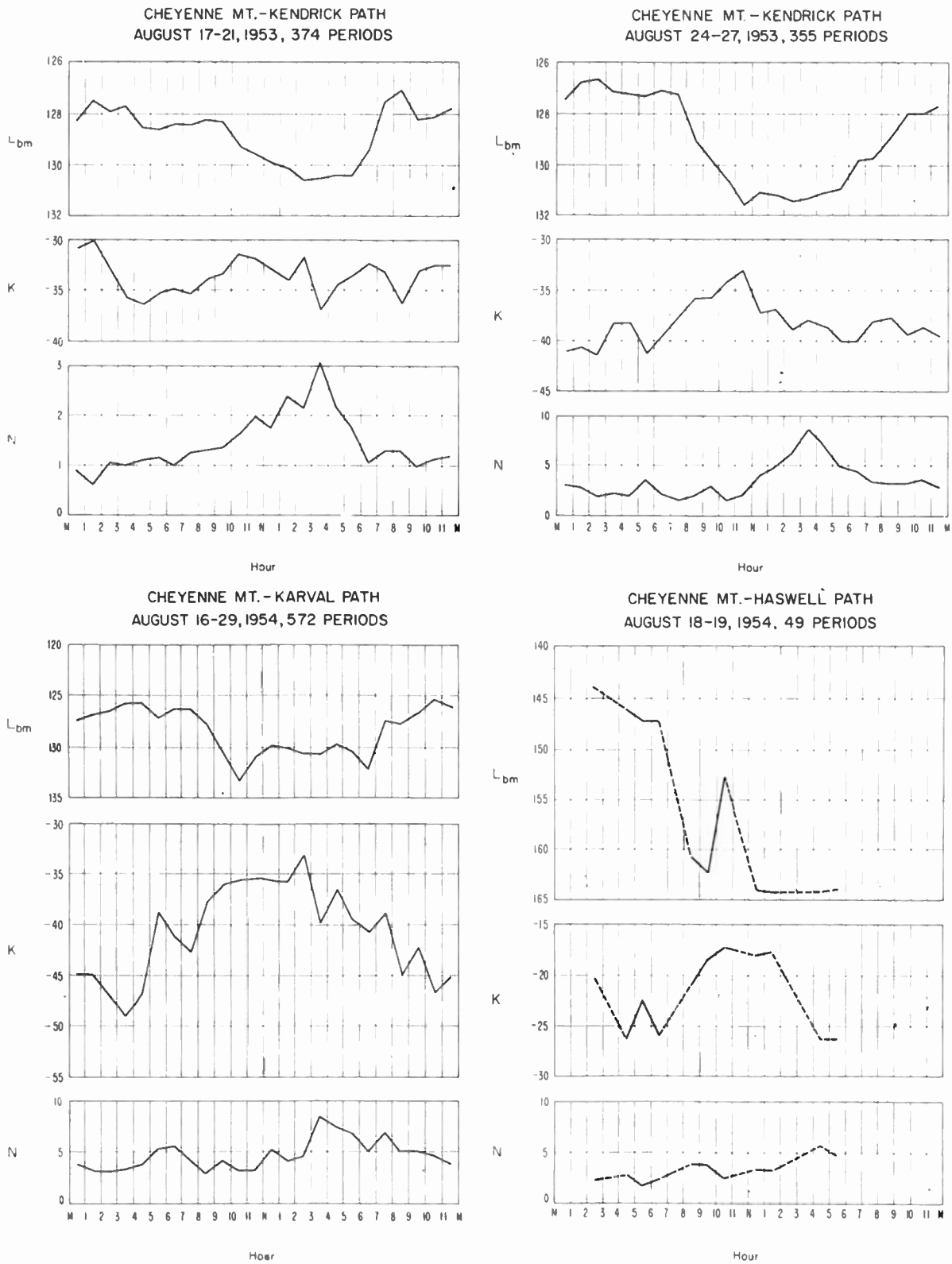

Fig. 2—Median values of L_{bm}, K, and N vs time of day. (Based on analysis of 10-minute recording periods.)

this is apparently the case. Of course, in the present analysis the slow fading was eliminated by the choice of the 10-minute increment and by the properties of the recording equipment. It will be recalled that the slow fading does not show up on the differential recorder (from which K is obtained).

If K and L_{bm} are known, the average basic transmission loss for the scattered component, L_{bas}, can be determined by use of the relation

$$L_{bas} = L_{bm} + R(0.5) - K. \qquad (2)$$

This equation follows from the definitions of the several

terms. As was pointed out previously, $R(0.5)$ may be neglected for the small values of K measured at Haswell and is essentially equal to zero at Kendrick and Karval. Thus an estimate of the 10-minute value of L_{bas} can be obtained simply by subtracting K from corresponding value of L_{bm}. This has been done in Fig. 3, in which median values of L_{bm} and L_{bas}, as measured at each site, are plotted as functions of angular path distance, θ.

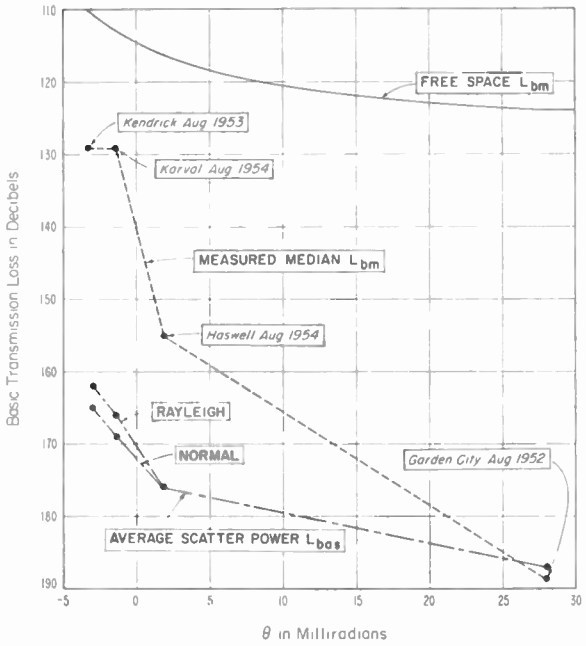

Fig. 3—Variation of total and scattered power with angular distance.

There is some experimental evidence[7] that at Kendrick (and therefore probably at Karval also) neither the assumption of an *in-phase* scattered vector nor of a Rayleigh-distributed scattered vector adequately describes the situation. However, these two approaches may be expected to represent the extreme situations. To illustrate the difference in results obtained using these two assumptions, two values of L_{bas} are shown for Kendrick and Karval in Fig. 3. The lower points are based on the same assumption used in obtaining the K values shown in Fig. 2. The upper points are based on the assumption of a Rayleigh-distributed scattered component.

Although not strictly within the scope of this paper, points are also shown for the 225-mile path from Cheyenne Mountain to Garden City, Kansas. The latter points are based on data recorded during August, 1952. Here, the L_{bm} shown is the median of 294 hourly medians measured during all 24 hours of the day. The instantaneous values of the received field strength were very nearly Rayleigh-distributed, indicating that K is very large. In this case $R(0.5) = K - 1.59$, and the average scatter power was obtained by subtracting 1.59 decibels from the median value.

[7] J. W. Herbstreit and M. C. Thompson, Jr., "Measurements of the phase of radio waves received over transmission paths with electrical lengths varying as a result of atmospheric turbulence," p. 1391, this issue.

Of interest from the standpoints of theory and application is the correlation of the field strength fluctuations received on two spaced antennas. A brief measurement of the cross-correlation of levels received at 100 mc on two antennas was made at Karval on August 24, 1954. Both antennas were approximately nineteen feet above the ground. The spacing of the antennas was varied along a line normal to the propagation path, starting with $\frac{1}{2}$ wavelength and extending to 20 wavelengths. Recordings of approximately eight minutes' duration were made at fourteen different spacings, and the entire group of measurements extended over the period 4 to 7 P.M.

The results of the measurements were somewhat surprising in that the correlation coefficient did not decrease steadily with increasing spacing as had been expected. Instead, it apparently varied more as a function of time than of spacing. That this is the case is verified by comparing the correlation coefficient with the characteristics of the fields recorded by each antenna. In Fig. 4, the correlation coefficient, fading rate, and L_{bas} are plotted as functions of antenna spacing. It would appear that the correlation coefficient is closely related to N and L_{bas}. For example, the high cross-correlation at a spacing of eleven wavelengths coincides with a decided decrease in fading rate and in L_{bas}.

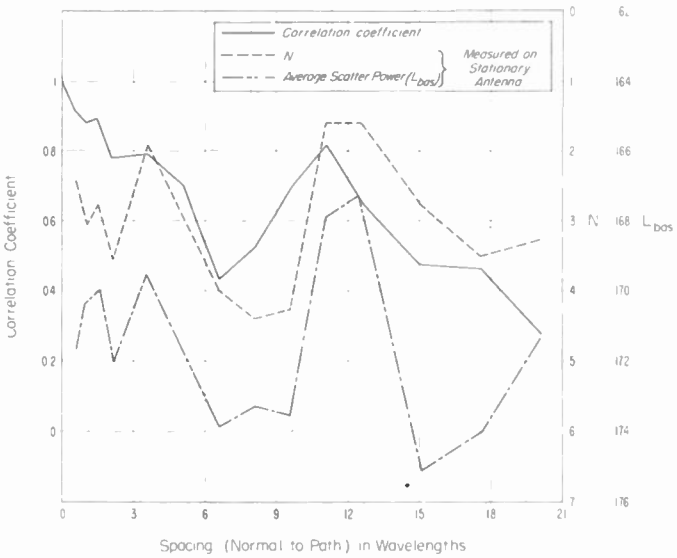

Fig. 4—Correlation coefficient vs antenna spacing compared to other characteristics of received field. (Cheyenne Mountain—Karval Path, 100 mc, August 24, 1954.)

The structure of the atmosphere was apparently undergoing significant changes during the measurement period, as evidenced by the variations in N and L_{bas}. This suggests the advisability of making such measurements during periods when atmospheric conditions can be expected to remain stable, as during the early afternoon, for example. Alternatively, measurements could be made at a number of spacings simultaneously or a large number of runs could be made and the results treated statistically.

The Rate of Fading in Propagation through a Turbulent Atmosphere*

K. A. NORTON†, FELLOW, IRE, P. L. RICE†, MEMBER, IRE, H. B. JANES†, MEMBER, IRE, AND A. P. BARSIS†, MEMBER, IRE

Summary—**Fading rate is defined to be the number of times per minute that the envelope of the received field crosses its median level with a positive slope. This definition of fading rate is equally useful for ionospheric or tropospheric propagation studies. Furthermore, it may be used with equal facility on short transmission paths where the ground wave component of the received field predominates and on the longer transmission paths where the scattered component of the received field predominates. It is shown that this definition of fading rate provides a quantity which is numerically related to the parameters of the propagation medium under certain conditions which are normally satisfied in either ionospheric or tropospheric propagation studies. The pertinent parameters of the propagation medium in beyond-the-horizon transmission are the location and shape of the scattering volume and the turbulent and drift velocities of the scatterers. An extensive discussion is given of the shape of the tropospheric scattering volume for beyond-the-horizon transmission. An analysis is then given of some fading rate data obtained in the National Bureau of Standards tropospheric propagation program in the 92 to 1046 mc range of frequencies on transmission paths 70, 97, 226, and 394 miles in length. Finally an analysis is given for within-the-horizon propagation. In this case it is advantageous to define fading rate as the number of times per minute that the phase of the received field crosses its median level with a positive slope.**

I. Definition of Fading Rate

THE FIELD received in propagation between two points will vary with time as a result of variations in the propagation medium. Since these variations in field are still present when the radiated power from the transmitting antenna is constant, it is evident that the instantaneous transmission loss for the path is actually varying. It is convenient to classify these changes into long term and short term variations. The long term variations are caused by slowly varying changes in the propagation medium, such as changes in ionospheric absorption or changes in the intensity of turbulence in the troposphere. The short term variations, on the other hand, are attributed to phase interference among simultaneously occurring modes of propagation. Thus we may consider the received field to be made up of a number of components which arrive at the receiving antenna after traversing various paths with lengths varying at random in time over such a range that the component path length differences may sometimes be as much as several wavelengths. The interference between these components is considered to be the sole cause of the fading with which we will be concerned in this paper. In fact, it will be convenient to define "short term" as that maximum length of time within which the fading is primarily due to phase interference and a negligible component of the variance in transmission loss is due to other causes. In a companion paper[1] dealing with the statistical distribution of the amplitudes of this short term fading, it is pointed out that this maximum length of time decreases in general with increasing radio frequency and may be as much as several hours or may be even less than a minute.

Fig. 1 (next page) shows transmission loss variations and our definition of fading rate for several tropospheric propagation paths ranging in length from 70.2 to 226.5 miles and for both negative and positive angular distances; i.e., for transmission paths within and beyond the radio horizon. We will make use of several general mathematical relations obtained by Rice[2,3] in order to relate our definition of fading rate to the power spectrum $w(f)$ of the received fading envelope and to the parameters of the propagation medium. Thus Rice[2] has derived an expression for the expected number $N(r)$ of positive crossings of a specified envelope level r in a unit period of time:

$$N(r) = \left[\frac{b_2}{4\pi b_0}\right]^{1/2} p(r) \tag{1}$$

where

$$b_0 = \int_0^\infty w(f)df \tag{2}$$

$$b_2 = (2\pi)^2 \int_0^\infty (f - f_0)^2 w(f)df \tag{3}$$

$$p(r) = \frac{2r}{k} F(2r/k^2) \exp\left[-(1 - r)^2/k^2\right] \tag{4}$$

$$F(x) = \frac{1}{\pi} \exp(-x) \int_0^\pi \exp(x\cos\phi)d\phi = \exp(-x)J_0(ix). \tag{5}$$

In the above f_0 denotes the carrier frequency. The function $p(r)$ denotes the probability density of the envelope at the level r. The power spectrum of the received fading envelope $w(f)$ will be discussed later. The above relations (1), (2), and (3) apply in general to fading spectra such that $w(f)$ is symmetrical with respect to f_0. The particular relations (4) and (5), however, may

* Original manuscript received by the IRE, August 12, 1955.
† Central Radio Propagation Laboratory, National Bureau of Standards, Boulder, Colo.

[1] K. A. Norton, L. E. Vogler, W. V. Mansfield, and P. J. Short, "The probability distribution of the amplitude of a constant vector plus a Rayleigh distributed vector," p. 1354, this issue

[2] S. O. Rice, "Statistical properties of a sine wave plus random noise," *Bell Sys. Tech. Jour.*, vol. 27, pp. 109–157; January, 1948. Also published as Bell Telephone System monograph B-1589. See eq. (4.8) on page 125.

[3] S. O. Rice, "Statistical fluctuations of radio field strength far beyond the horizon," PROC. IRE, vol. 41, pp. 274–281; February, 1953.

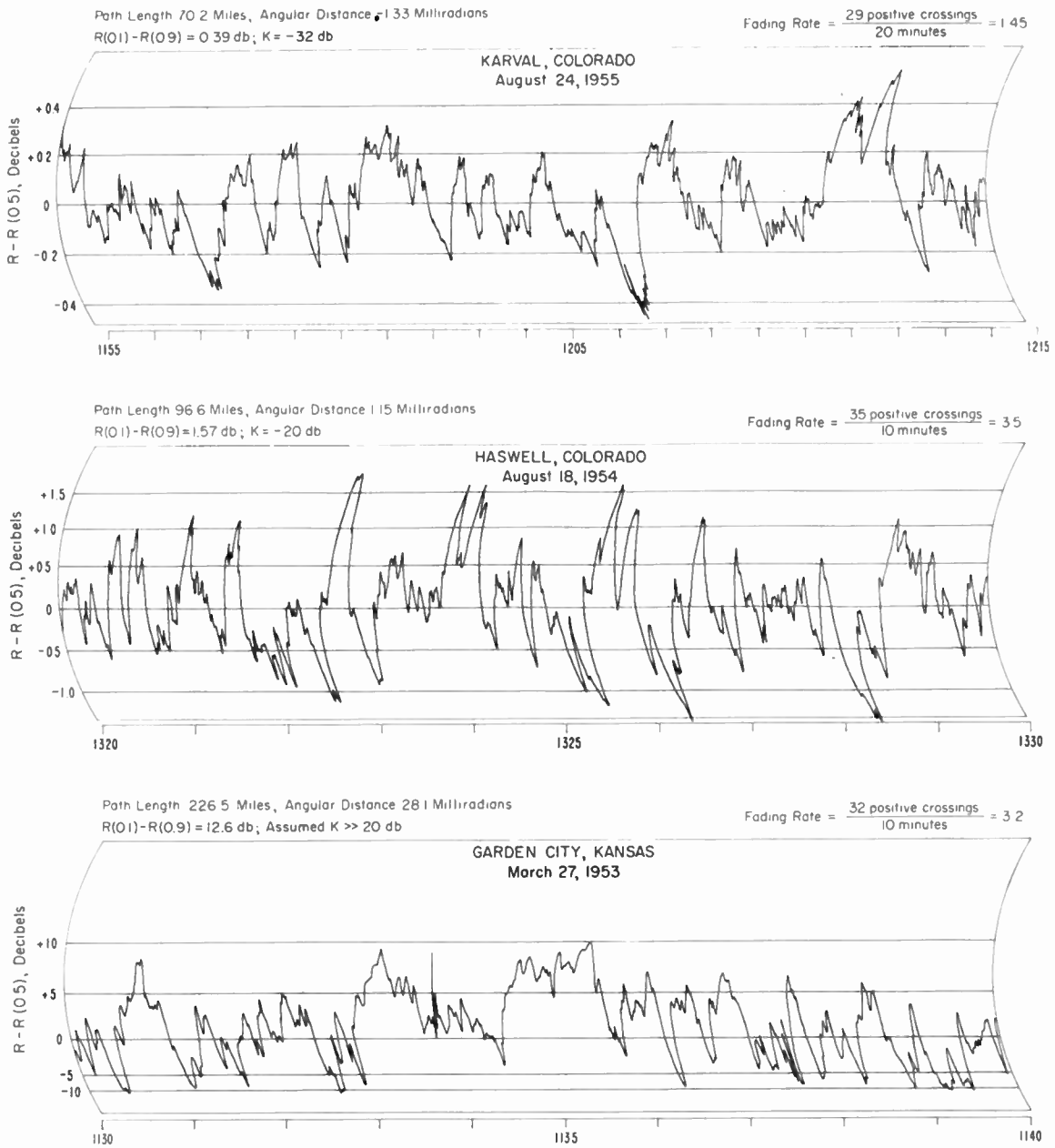

Fig. 1—Chart samples for 100 mc transmissions from Cheyenne Mountain.

be used only when the received field may be considered to be the sum of a constant vector, the ground wave for example, and a Rayleigh distributed vector. As used in a companion paper[1] $R \equiv 20 \log_{10} r$ denotes the amplitude of the resultant received field expressed in decibels above the amplitude of the constant component, while $K \equiv 20 \log_{10} k$ denotes the root-mean-square amplitude of the scattered Rayleigh distributed vector, expressed in decibels above the amplitude of the constant component.

Fig. 2 (facing page) gives probability distribution function $p(r)$ as a function of $R - R(0.5)$, the level, expressed relative to median level, of fading signal envelope and with K as a parameter. Also in Fig. 2 are two measured distributions of the number of positive crossings as a function of envelope level for two of the data samples on Fig. 1. These measured data were normalized so that $p[r(0.5)]$ has theoretical value shown on Fig. 3, opposite. Measurements shown in lower dashed curve in Fig. 2 were obtained at a small angular distance where a strong steady component was present. If we define fading range to be the difference, $R(0.1) - R(0.9)$, in levels which are exceeded by the envelope 10 per cent and 90 per cent of the time, respectively, then use may be made of the relation between fading range and K shown on Fig. 6 of reference 1 to estimate the level K of the root-mean-square amplitude of the Rayleigh distributed component above the level of the steady component. For the Haswell sample of data, $R(0.1) - R(0.9) = 1.57$ decibels, and reference to Fig. 6 of reference 1 indicates that $K = -20$ decibels. We see on Fig. 2 that the Haswell fading rate data agree reasonably well with the

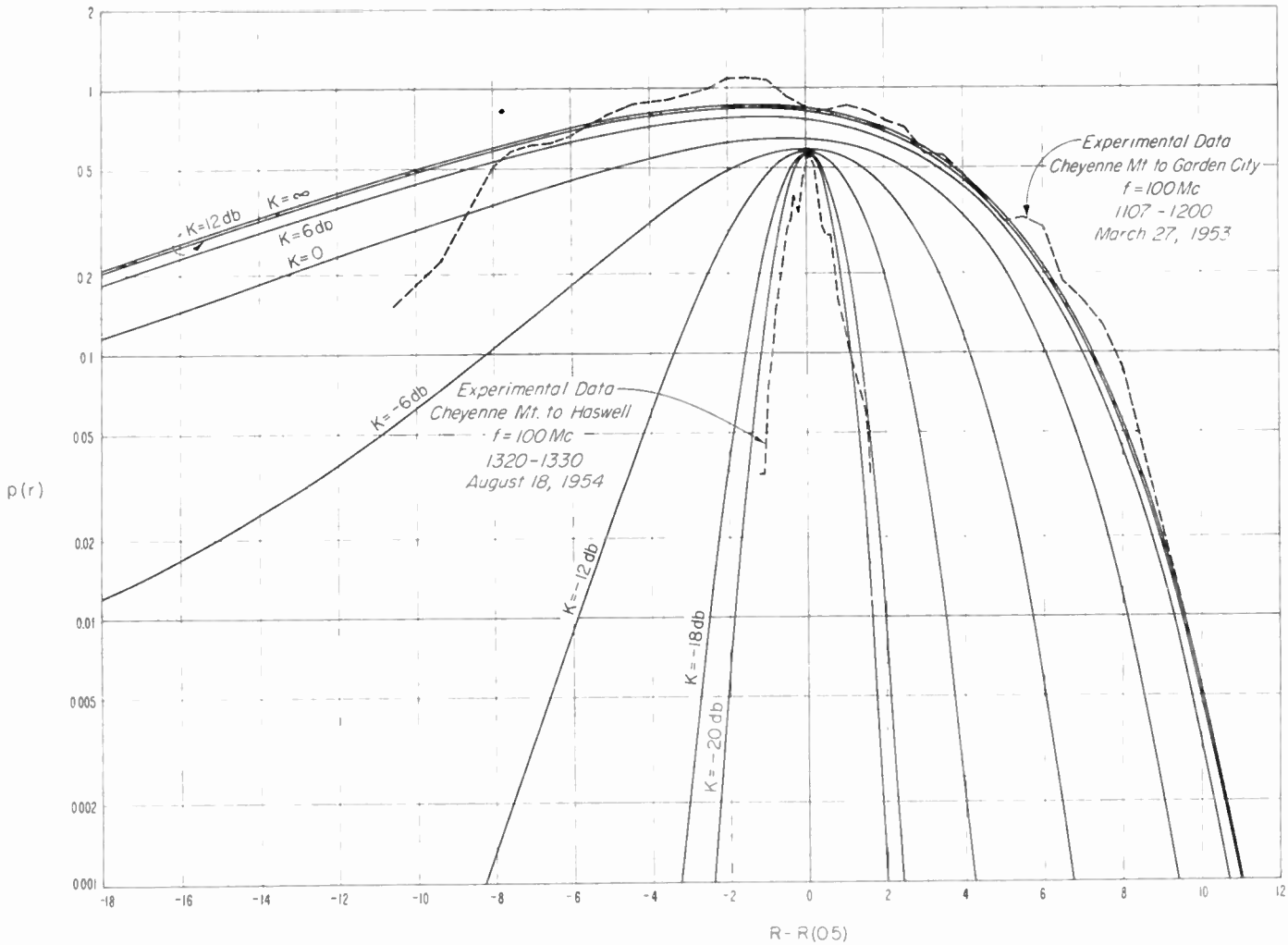

Fig. 2—Graph of probability distribution function $p(r)$.

theoretical fading rate curve for $K = -20$ decibels. The measurements shown in the upper part of Fig. 2 were made on the sample of data obtained near noon between 11:07 and 12:00, March 27, 1953 on 100 mc on the Cheyenne Mountain transmission path with an angular distance $\theta = 28.1$ milliradians. At this large angular distance one would expect agreement with the theoretical distribution[4] corresponding to $K = +\infty$, and it is evident on Fig. 2 that there is fair agreement in this sample down to a level about 8 decibels below the median level.

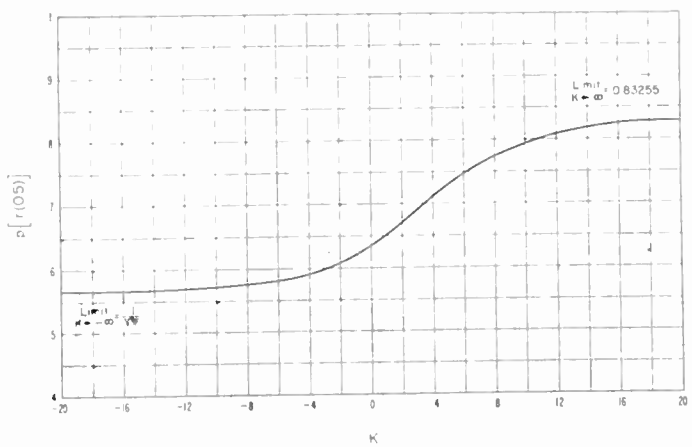

Fig. 3—Graph of $p[r(0.5)]$ as a function of K.

It should be clear from the results shown on Fig. 2 that a convenient definition of the fading rate for a given sample of fading data is the number of times per minute that the envelope of the received field crosses its median level with a positive slope. Thus, fading rate may be designated by $N[r(0.5)]$. Fig. 3 gives $p[r(0.5)]$ as a function of K. Note that this definition is equally useful regardless of the amount of steady component present in the received field. The periods of time over

[4] Note that the observed fading range for this particular period of observation was 12.6 decibels rather than the 13.4 decibels expected for Rayleigh distributed fields; this difference could be attributed to the presence of a steady component (with an amplitude only 2.3 decibels below the median level of the resultant field—see Fig. 6 in reference 1) or could be attributed to a statistical sampling fluctuation. Since the calculated value of the diffracted component is far below the observed median level and since steady components from elevated layers are not often observed at Garden City, we think it more likely that this observed 0.8 decibel departure from the fading range expected for Rayleigh distributed fields arises from a sampling fluctuation.

which such determinations of $N[r(0.5)]$ may be made should be long enough to include many crossings of the median and yet short enough so variations in received field may be attributed primarily to phase interference.

Rice has shown[3] for his particular model[5] of the tropospheric scattering volume, which applies to the case of propagation by forward scattering beyond the radio horizon, that the power spectrum of the received fading field may be expressed:

$$w(f) \sim \exp\left[-(f - f_0)^2/2\sigma_a^2\right] \tag{6}$$

where

$$\sigma_a^2 = \frac{1}{\lambda^2}\left\{\left[2u \sin(\theta_c/2)\right]^2 + \left[V_n\theta_w\right]^2\right\}. \tag{7}$$

In deriving (7) Rice assumed that the scatterers are moving at random, with a three-dimensional Maxwellian distribution of velocities, in much the same way as do the molecules of a gas. The mean-square value of the fluctuations of velocity of the scatterers about their drift velocity, V, is $3u^2$; V_n denotes the component of the drift velocity normal to the great circle plane through the transmission path terminals. The angle θ_c is the scattering angle corresponding to the "center" of the scattering volume, while $(\sqrt{3}\theta_w)$ measures the effective angular width of the scattering volume. λ is the wavelength of the radio waves. Rice assumed that the transmitting antenna was at a sufficiently large distance from the scattering volume so that plane waves would be incident on it, and in this case $\theta_w = (w_c/2\sqrt{3}d_2)$ where w_c is the effective width of the scattering volume and d_2 is its distance from the receiving antenna. If we let d_1 denote the distance of the scattering volume from the transmitting antenna, the generalized expression for θ_w is:

$$\theta_w = \frac{w_c}{2\sqrt{3}}\left(\frac{1}{d_1} + \frac{1}{d_2}\right). \tag{8}$$

Note that the above approaches Rice's formula when d_1 is sufficiently large.

An estimate of θ_w may be obtained experimentally by measuring the correlation of the envelopes of the fields received on the receiving antenna and on an antenna at a distance w normal to the great circle plane which passes through the transmission path terminals. Thus Rice[3] has shown that the expected correlation coefficient for the signals on the spaced antennas for his assumed model of the tropospheric scattering volume is approximately equal to

$$\rho \cong \exp\left[-\left(\frac{2\pi w}{\lambda}\right)^2\left(\frac{\theta_w}{2\sqrt{3}}\right)^2\right]. \tag{9}$$

When (6) is introduced into (2) and (3) and these resulting values introduced into (1), we obtain finally the following simple expression relating the observed fading rate to σ_a in the case of beyond-the-horizon propagation:

$$V[r(0.5)] = \sqrt{\pi}\sigma_a p[r(0.5)]. \tag{10}$$

The Scattering Volume

In order to make further progress in the analysis of fading rate data obtained in beyond-the-horizon propagation, it is necessary to estimate the angular width $(\sqrt{3}\theta_w)$ of the scattering volume and to determine the location of its "center" so that θ_c may be estimated. The starting point of our present investigation is the description of this scattering volume as given in a recent paper.[6] We will consider first the shape of this scattering volume for isotropic antennas and without any allowance for the ground reflection lobes of either the transmitting or receiving antennas, and an approximate allowance for the effects of these lobes will be introduced later. In the frequency range, 92 to 1,046 mc, of our present application, the transmission loss for the scattered field relative to that expected in free space is observed to be approximately independent of the radio frequency,[7,8] and this implies[9] that the scattering cross section in this range of frequencies is approximately proportional to $(\alpha+\beta)^{-4}$ where $\alpha+\beta$ denotes the scattering angle. Thus, in this frequency range, the Booker-Gordon model of tropospheric scattering[10,11] should be applicable. This model is based on the assumption that an isotropic exponential correlation function describes the refractive index variations in the troposphere:

$$C(R) = C(0) \exp(-R/l_0), \tag{11}$$

where R denotes distance between two points in scattering volume, l_0 is scale length representative of Booker-Gordon model, and $C(0)$ denotes mean-square departure $\langle(\Delta n)^2\rangle$ of refractive index from mean value. There is evidence[12] that those turbulent "blobs," which have scales[13] in the range of magnitudes responsible for the

[5] This model is also applicable to scattering from a turbulent ionosphere. The spherical shape of the scattering volume assumed in Rice's model does not correspond well with its actual shape—see following section below for a description of the shape of the tropospheric scattering volume—but the influence of this shape is only of secondary importance in our present application.

[6] Readers not interested in this detailed discussion of the shape of the scattering volume may go directly to the next section.

[7] J. W. Herbstreit, K. A. Norton, P. L. Rice, and G. E. Schafer, "Radio wave scattering in tropospheric propagation," 1953 IRE Convention Record, Part 2, "Antennas and Communication," pp. 85–93.

[8] K. A. Norton, P. L. Rice, and L. E. Vogler, "The use of angular distance in estimating transmission loss and fading range for propagation through a turbulent atmosphere over irregular terrain," p. 1488, this issue.

[9] Harold Staras, "Scattering of electromagnetic energy in a randomly inhomogeneous atmosphere," *Jour. Appl. Phys.*, vol. 23, p. 1152; October, 1952.

[10] W. E. Gordon, "Radio scattering in the troposphere," Proc. IRE, vol. 43, pp. 23–28; January, 1955.

[11] A. D. Wheelon, "Note on scatter propagation with a modified exponential correlation function," p. 1381, this issue.

[12] Harold Staras, "Forward scattering of radio waves by anisotropic turbulence," p. 1374, this issue.

[13] F. Villars and V. F. Weisskopf, "On the scattering of radio waves by turbulent fluctuations in the atmosphere," p. 1232, this issue.

forward scattering in the 92- to 1046-mc band, are anisotropic. Since the magnitude of this anisotropy is not large nor quantitatively well determined, it will be neglected in our present discussion. Thus we will assume that the scattering cross section may be represented by

$$\sigma(\alpha+\beta)=\frac{2C(0)\sin^2\chi}{\pi l_0(\alpha+\beta)^4}\cdot f[(l_0/\lambda)\cdot(\alpha+\beta)]. \quad (12)$$

In the above $\sin^2\chi$ allows for the small effects of polarization on the scattered power and may be set equal to one especially in our present application which involves only horizontal polarization. It has been shown[7] that $f[(l_0/\lambda)\cdot(\alpha+\beta)]$ may be set equal to unity in evaluating the transmission loss provided the wavelength $\lambda<5l_0\theta$,[14] where θ is the angular distance; i.e., the minimum value, $(\alpha_0+\beta_0)$, which the scattering angle, $\alpha+\beta$, may have within the entire scattering volume. Since l_0 is of the order of 70 meters,[15,16] $\theta>0.025$ radian, and $\lambda<3.25$ meters for the fading rate analyses of Section III, it appears that the use of (12) with $f[(l_0/\lambda)\cdot(\alpha+\beta)]\cdot\sin^2\chi=1$ should give correct order of magnitude results for the shape of the scattering volume in our present application. In this case the scattered power relative to that expected in free space will be equal to

$$I=4d^2\int_V\frac{\sigma dv}{R_0^2R^2}=\left(\frac{8d^2}{\pi}\right)\cdot\int_V\frac{C(0)\,dw\,dh\,dx}{l_0(R_0R)^2(\alpha+\beta)^4}. \quad (13)$$

A factor 4 is included in this integral to allow effects of ground reflection for ease of high transmitting and receiving antennas. Fig. 4 represents a cross-section view of the scattering volume, determined by the great circle plane passing through transmitting and receiving antennas. Co-ordinate w measures distance normal to great circle plane of differential volume elements dv. Later we shall divide the integral into four components I_1', I_1'', I_2', and I_2'' (see Fig. 4). We assume $[C(0)/l_0]=4h_0B/h^3\cong B/(h-h_0/2)^2$; i.e., decreases approximately, at low heights, in inverse proportion to the square of height $(h-h_0/2)$ above ground.[8] If we set $(\alpha+\beta)=d\sqrt{w^2+h^2}/(RR_0)$ and approximate R_0 by (d_1-x_1) and R by (d_2+x_1), we obtain

$$I_1'+I_1''=\frac{32h_0B}{\pi d^2}\cdot\int_0^{d_1}\int_{h_{1m}}^{\infty}\int_{-\infty}^{+\infty}\frac{(d_1-x_1)^2(d_2+x_1)^2dx_1dhdw}{h^3(w^2+h^2)^2}, \quad (14)$$

where $h_{1m}=\beta_0(d_2+x_1)$,

$$I_2'+I_2''=\frac{32h_0B}{\pi d^2}\cdot\int_0^{d_2}\int_{h_{2m}}^{\infty}\int_{-\infty}^{+\infty}\frac{(d_1+x_2)^2(d_2-x_2)^2dx_2dhdw}{h^3(w^2+h^2)^2}, \quad (15)$$

where $h_{2m}=\alpha_0(d_1+x_2)$.

Because of the approximations introduced in the above, the integrations with respect to x_1 and x_2 were carried only to d_1 and d_2, respectively. This seems reasonable from a physical standpoint since a negligible contribution would be expected from that portion of the atmosphere behind the antennas. Furthermore, when these limits of integration are adopted for the case where $[C(0)/l_0]$ is assumed independent of height and the h^3 term therefore removed from the integrands, we obtain by integrating (14) and (15) and adding:

$$I_0=\frac{2d}{3\theta^2}\left[\frac{C(0)}{l_0}\right] \quad \begin{array}{l}\text{(For } [C(0)/l_0] \text{ constant through-}\\ \text{out the scattering volume).}\end{array} \quad (16)$$

In the limiting case of small θ, which is the only case of interest in tropospheric propagation, the above expression is equal to an exact evaluation[7] of (13) obtained by integrating with respect to α, β, and ϕ over all of the space above the horizon planes of the transmitting and receiving antennas. Thus it appears that the use of d_1 and d_2 as limits of integration in (14) and (15) happens to compensate exactly, when θ is small, for the approximations involved in setting $R_0\cong d_1-x_1$ and $R\cong(d_2+x_1)$.

When the h^3 factor is retained in the integrands of (14) and (15), we obtain

$$I_1'+I_1''=\frac{16B}{5\theta^4d}\cdot A(s), \quad (17)$$

$$I_2'+I_2''=\frac{16B}{5\theta^4d}\cdot A(1/s), \quad (18)$$

where the asymmetry factor $s=(\alpha_0/\beta_0)$ and

$$A(s)=(s+1)^3\left[s\log_e\left(\frac{s+1}{s}\right)+\frac{1}{2s}-1\right]. \quad (19)$$

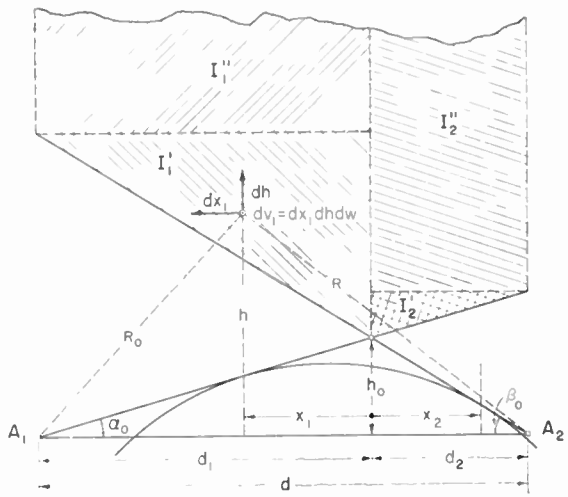

Fig. 4—The scattering volume in the great circle plane.

[14] When $\lambda=5l_0\theta$ the theoretical transmission loss by scattering is one decibel more than that predicted by setting $f[(l_0/\lambda)\cdot(\alpha+\beta)]=1$ and approaches this latter value in the limit for much smaller values of λ (see references 7 and 8).

[15] C. E. von Rosenberg, C. M. Crain, and A. W. Straiton, "Atmospheric refractive-index fluctuations as recorded by an airborne microwave refractometer," Univ. of Texas EERL Report No. 6-01; February 6, 1953.

[16] George Birnbaum, H. E. Bussey, and R. R. Larson, "The microwave measurement of variations in atmospheric refractive index," TRANS. IRE, vol. AP-3, pp. 74–78; August, 1952.

Thus

$$I=\frac{16B}{5\theta^4 d}\left[A(s)+A(1/s)\right] \quad (\text{For } |C(0)/l_0|=4h_0B/h^3). \quad (20)$$

The above equation gives the total power scattered to the receiver relative to that expected for propagation through free space over the same distance and allows for a systematic decrease of $[C(0)/l_0]$ with height. It should be noted that the limits of integration on the above integral provide no useful information as to the shape of the "effective" scattering volume. It will be convenient now to define the "effective" scattering volume as that volume described below which scatters, with $[C(0)/l_0]$ constant, just half of the total power scattered to the receiving antenna. Reference to (13) indicates that the decay in the magnitude of the integrand is then controlled largely by the increase in $(\alpha+\beta)$ within the scattering volume relative to its minimum value $(\alpha_0+\beta_0)$. This indicates that a good estimate of the shape of the "effective" scattering volume as defined above is the locus of constant $(\alpha+\beta)=c\theta$ where c is a constant which we will proceed to demonstrate is equal to 2.44. We see by Fig. 5 that the locus of $(\alpha+\beta)=c\theta$ in the great circle plane is the arc of a circle which passes through the antennas A_1 and A_2 and through a point A_3 at a height approximately $(c-1)h_0$ above the cross-over of radio horizons. Outside of the great circle plane the locus of $(\alpha+\beta)=c\theta$ is the surface generated by this circular arc when it is rotated about the chord A_1A_2.

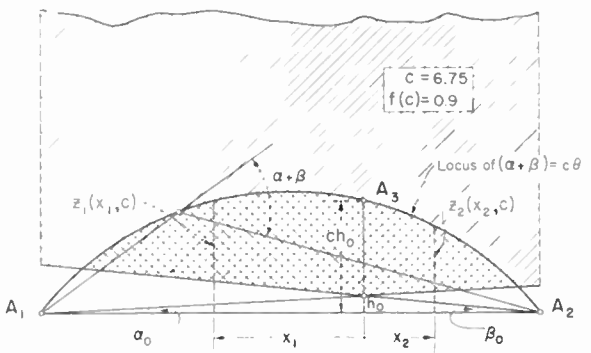

Fig. 5—Scattering volume containing 90 per cent of total power.

We may now integrate (14) and (15), with $[C(0)/l_0]$, assumed to be constant, out to limits determined by the circular arc; thus in (14) the limits on w are $\pm\sqrt{z_1^2-h^2}$ where $z_1=RR_0c\theta/d\cong c\theta/d(d_1-x_1)(d_2+x_1)$. The details of the integration are not interesting; when carried out we obtain

$$I_{0c}=\frac{2d}{3\theta^2}\left[\frac{C(0)}{l_0}\right]f(c), \quad (21)$$

where

$$f(c)=\left[\frac{2}{\pi}\cos^{-1}(1/c)+\frac{2}{\pi c^2}\sqrt{c^2-1}+\frac{12}{\pi c^2}\sin^{-1}(1/c)\right.$$
$$\left.-(6/c^2)+\frac{8}{\pi c^3}\log_e\left(c+\sqrt{c^2-1}\right)\right]. \quad (22)$$

Comparing (16) and (21) we see that $f(c)$ is the fraction of the power scattered (with $[C(0)/l_0]$ constant throughout the scattering volume) from that portion of the scattering volume for which $\theta\leqq(\alpha+\beta)\leqq c\theta$. Fig. 6 gives

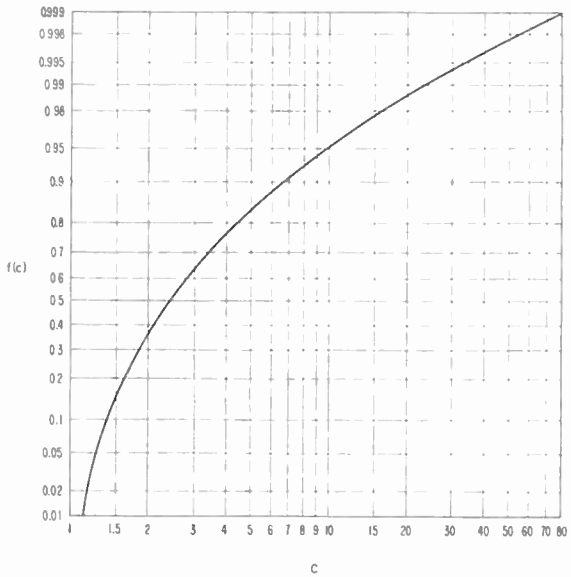

Fig. 6—Fraction of power scattered for $(\alpha+\beta)<c\theta$ for an assumed scattering cross section proportional to $(\alpha+\beta)^{-4}$ and otherwise independent of height.

$f(c)$ as a function of c and we see that the half-power point corresponds to $c=2.44$, while 90 per cent of the power is scattered from the volume within which $(\alpha+\beta)\leqq 6.75\theta$. As c approaches infinity $f(c)$ approaches 1 and I_{0c} approaches I_0 as would be expected. Fig. 7 (facing page shows actual shape of "effective" scattering volume as defined above for one of Cheyenne Mountain paths. Height and distance scales are the same on this diagram, and we see that the "effective" scattering volume is quite long. This diagram also illustrates the location of the "effective center" of scattering, which will be discussed below, as well as the scattering angle, θ_c, and width, w_c, of the "effective" scattering volume at the center of scattering.

When $[C(0)/l_0]$ varies with height as in (14) and (15), the volume described by $(\alpha+\beta)\leqq 2.44\theta$ will scatter somewhat more than half of the power. However, this variation in height will affect the shape of the "effective" scattering volume primarily in the vertical dimension while its length and width will be only slightly smaller. Consider now the location of the "effective center" of scattering; it is clear that this will lie in the great circle plane through the transmitting and receiving antennas, and we will, somewhat arbitrarily, define its x- and h-co-ordinates as those values of x_c and h_c for which the integrand of the scattering volume I is a maximum after integration with respect to the other two variables. Thus to determine x_c integrate (14) with respect to w

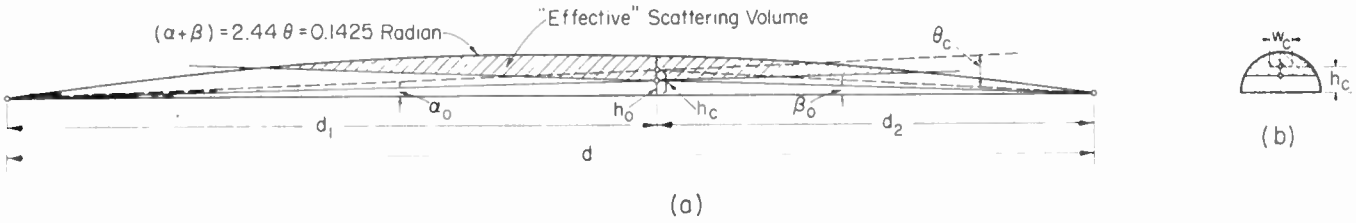

Fig. 7—Effective scattering volume for Cheyenne Mountain-Anthony path drawn to scale.

and h; the resulting integrand is a function of x_1 only, and is a maximum when $x_1=0$. Thus $x_c=0$ and, as might have been anticipated, the "effective center" of scattering will lie on a line directly above the crossover of the radio horizons.

The determination of the height, h_c, of the "effective center" of scattering is somehwat more complicated. If (14) and (15) are integrated first with respect to w and then with respect to x_1 and x_2, respectively, we obtain the following expressions for I_1', I_1'', I_2', and I_2'' with the integrand expressed in terms of the variable $y=(h/h_0)$:

$$I_1' = \frac{16B(1+s)^3}{\theta^4 ds}\int_1^{((1+s)/s)} \frac{(y-1)}{y^6} \cdot\left[1+(1-s)(y-1)+\frac{(1-s)^2}{3}(y-1)^2-\frac{2s}{3}(y-1)^2 -\frac{s}{2}(1-s)(y-1)^3+\frac{s^2}{5}(y-1)^4\right]dy \quad (23)$$

$$I_2' = \frac{16B(1+s)^3}{\theta^4 ds}\int_1^{(1+s)} \frac{(y-1)}{sy^6} \cdot\left[1+\frac{(s-1)}{s}(y-1)+\frac{(s-1)^2}{3s^2}(y-1)^2-\frac{2}{3s}(y-1)^2 -\frac{(s-1)}{2s^2}(y-1)^3+\frac{1}{5s^2}(y-1)^4\right]dy \quad (24)$$

$$I_1'' = \frac{16B(1+s)^3}{\theta^4 ds}\int_{((1+s)/s)}^{\infty}\left[\frac{1}{3}+\frac{1}{6s}+\frac{1}{30s^2}\right]\frac{dy}{sy^6} \quad (25)$$

$$I_2'' = \frac{16B(1+s)^3}{\theta^4 ds}\int_{(1+s)}^{\infty}\left[\frac{1}{3}+\frac{s}{6}+\frac{s^2}{30}\right]\frac{dy}{y^6}. \quad (26)$$

When the above integrands are added appropriately—see Fig. 4; i.e., at low heights $f_1'(y)+f_2'(y)$, at intermediate heights $f_1'(y)+f_2''(y)$, and at high heights $f_1''(y)+f_2''(y)$—and plotted versus y, they represent power density vs height above the crossover of radio horizons neglecting the effects of ground reflection on the transmitting and receiving antenna radiation patterns. If we let h_{te} and h_{re} denote the effective heights[8] of the transmitting and receiving antennas above the ground with h_{te} at the A_1 or α_0 end of the transmission path, then an approximate allowance for ground reflection may be made by multiplying the sums of the appropriate integrands $[f_1(y)+f_2(y)]$ above by the usual expressions:[8]

$$g_t g_r = 16\sin^2\left[\frac{2\pi h_{te}\alpha_0}{\lambda}(y-1)\right] \cdot\sin^2\left[\frac{2\pi h_{re}\beta_0}{\lambda}(y-1)\right]. \quad (27)$$

The above is shown on Fig. 8 (next page) for one of the Cheyenne Mountain paths. Height, h_c, of the "effective center" of scattering is taken to be the height at which the product $g_t g_r$ times the sum of the above integrands reaches a maximum. Since (h_{te}/λ) was very large for this path, the corresponding sine-squared term in (27) oscillated too rapidly to be plotted, and it was consequently replaced by its mean value (1/2).

Finally, the effective width of the scattering volume may be obtained from (14) or (15) by noting that the half power points at the height, h_c, of the "effective center" of scattering are separated by a width, w_c, defined by

$$\int_{-0.5w_c}^{+0.5w_c}\frac{dw}{(w^2+h_c^2)^2}=\frac{1}{2}\int_{-\infty}^{+\infty}\frac{dw}{(w^2+h_c^2)^2}=\frac{\pi}{4h_c^3}. \quad (28)$$

The above relation is satisfied for

$$w_c \cong 0.8832 h_c. \quad (29)$$

From Fig. 7 we obtain, when we note that θ_c is small,

$$\theta_c = h_c\left(\frac{1}{d_1}+\frac{1}{d_2}\right). \quad (30)$$

Finally, when (29) is substituted in (8), we find that

$$\theta_w = 0.2550\theta_c \quad (31)$$

III. Analysis of Fading Rates Observed Far Beyond the Radio Horizon ($K>20$ db)

The fading rate data described in this section were all obtained at angular distances, θ, greater than 28 milliradians, and it seems likely that scattering alone was the predominant mode of propagation.[8] In this case $p[r(0.5)]=0.83255$. Consequently our formula for fading rate in the scattering region ($K>20$ db) may be written:[17]

$$N[r(0.5)]\cong 0.2952 f_{mc}\theta_c\sqrt{u^2+0.0650V_n^2}$$

(fades per minute), (32)

[17] Eq. (32) may be used for beyond-the-horizon propagation with $K<20$ db simply by reducing the coefficient of (32) by the factor $(p[r(0.5)]/0.83255)$ which may be determined from Fig. 3.

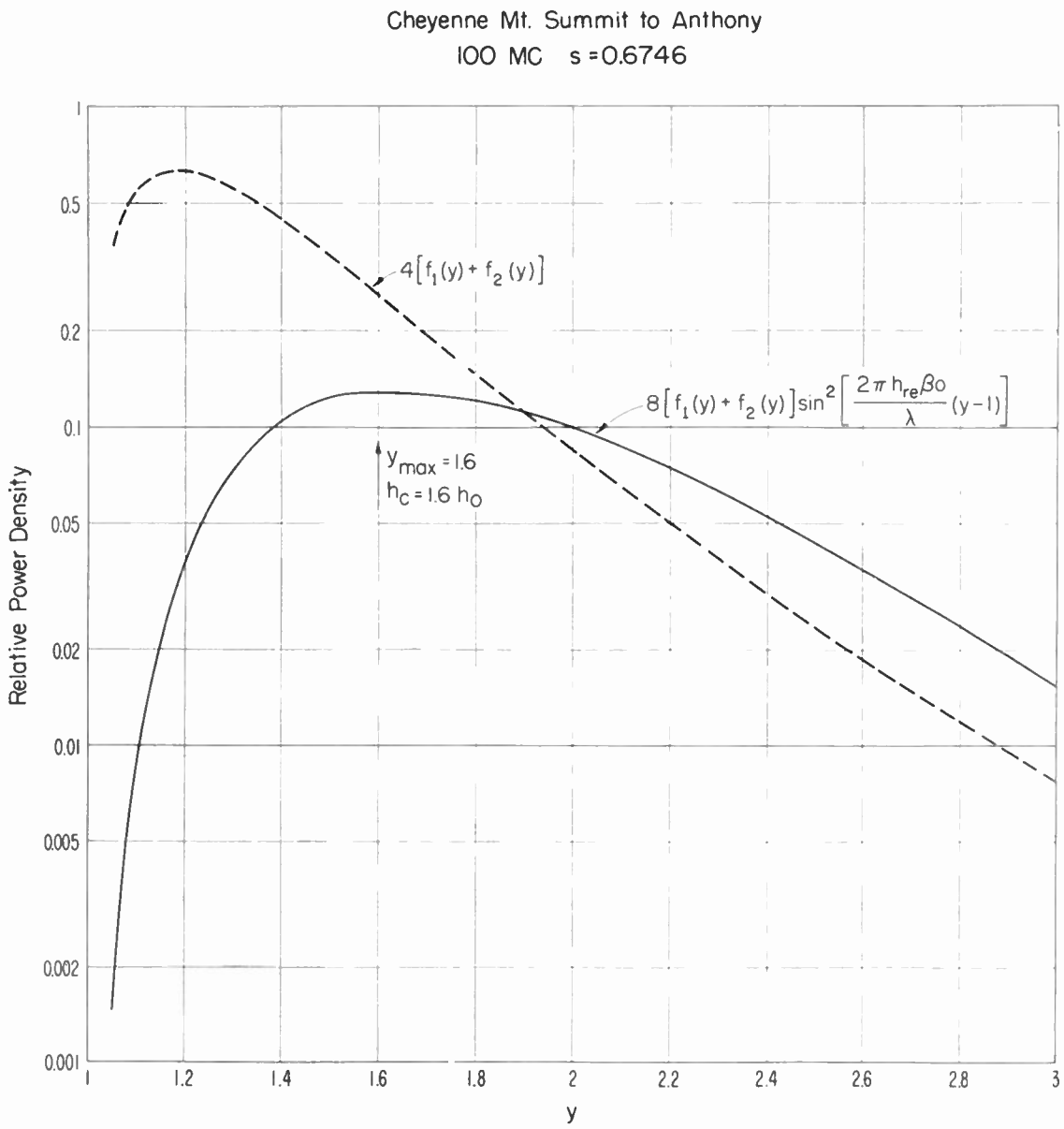

Fig. 8—Graph of scattered power density as a function of height (Cheyenne Mountain Summit to Anthony; 100 mc; $s=0.675$).

where f_{mc} is the frequency in megacycles per second, u is the rms component turbulent velocity of the scatterers in meters per second, and V^n is the component of the drift velocity normal to the great circle plane in meters per second.

The Tropospheric Propagation Research Section of the National Bureau of Standards has conducted a long term measurements program on frequencies in the 100- to 1000-mc range over paths extending eastward from the Front Range of the Rocky Mountains into the Colorado and Kansas plains. Several receiving stations were established at distances far beyond the transmitting antenna's radio horizon in order to investigate the character of long-distance tropospheric wave propagation. Transmitting and receiving facilities have been described in a National Bureau of Standards Circular.[18]

[18] A. P. Barsis, J. W. Herbstreit, and K. O. Hornberg, "Cheyenne Mountain tropospheric propagation experiments," NBS Circular 554; January, 1955.

This also contains a detailed description of the methods employed in data collection and analysis.

Due to the lengthy process of counting fading rates, only two relatively short periods of time have been selected for a fading rate study. For August 16, 1952, data obtained at Anthony, Kans. (approximately 400 miles from the transmitter sites), have been analyzed. August 16, 1952 was characterized by exceptionally high fields in the morning hours which corresponded to low fading rates. During the times for which the high fields were observed meteorological soundings for Lowry Air Force Base and Dodge City Weather Bureau Office show an extended elevated layer combined with a strong super refractive ground-based layer. These conditions had disappeared by mid-afternoon, when the fading rates increased markedly. Selection of August 16, 1952, therefore, represents somewhat exaggerated contrasts, which, however, are not unusual for summer

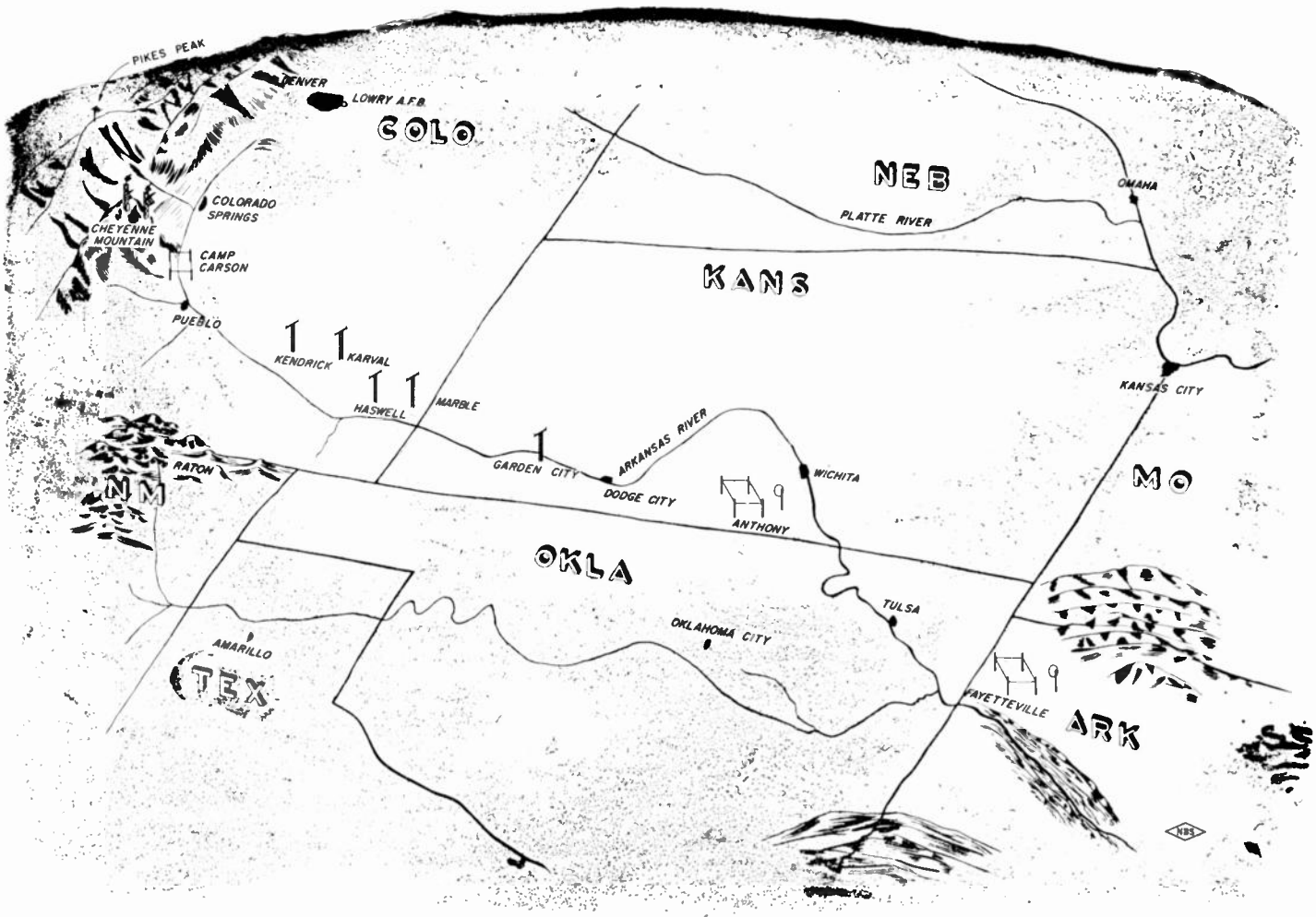

Fig. 9—Pictorial view of Cheyenne Mountain transmission paths.

months. The following frequencies were used: 100 mc (transmitted during alternate hours from Cheyenne Mountain Summit and from Pikes Peak), and 192.8 mc and 1,046 mc (both transmitted from Cheyenne Mountain Summit only).

For the period February 24–25, 1953, data obtained at Garden City as well as at Anthony have been analyzed. The February dates were selected at random, and with the emphasis on availability of reliable data. It is believed that the days chosen represent average winter conditions over the path. The Garden City receiving site is at approximately 225 miles from the transmitters. During the second period 100 mc was used during alternate two-hour periods from Cheyenne Summit and Camp Carson, 192.8 mc and 1,046 mc were transmitted from Cheyenne Mountain Summit, and 92 and 210.4 mc from the Cheyenne Mountain "Base" site. All frequencies were recorded at Garden City, while during the February period only data on 100 mc were obtained at Anthony. A pictorial view of the path with all transmitting and receiving sites is shown on Fig. 9.

The NBS Circular quoted[18] contains complete data on the antennas used. All transmissions were continuous wave and horizontally polarized. Both the transmitting and the receiving antenna beam widths are large in comparison with angular dimensions of the effective scattering volume so that antenna directivity is not an important factor in the analysis of the fading rate data.

All data were recorded on graphic milliammeter charts at a speed of 1.5 inches per minute, except the 1,046 mc frequency at Anthony where the chart speed was 6 inches per minute.

For purpose of this study fading rate was defined as outlined above, and illustrated on Fig. 1. Basic period of analysis for which median values were obtained is five minutes. Fig. 10 (next page) shows additional chart samples on several frequencies which illustrate character of the field received at Garden City. The numerous spikes which are evident on the 92-mc record are undoubtedly caused by reflections from meteor trails and were ignored in our fading rate analysis. Fading rates obtained for individual five-minute periods were averaged over each hour of record.

Fig. 11, p. 1351, shows average fading rates plotted vs hour of day for one of the recording periods. It is evident that there is good correlation between average hourly fading rates on various frequencies, even if the paths are not quite identical. Compare the 1,046-mc fading rates

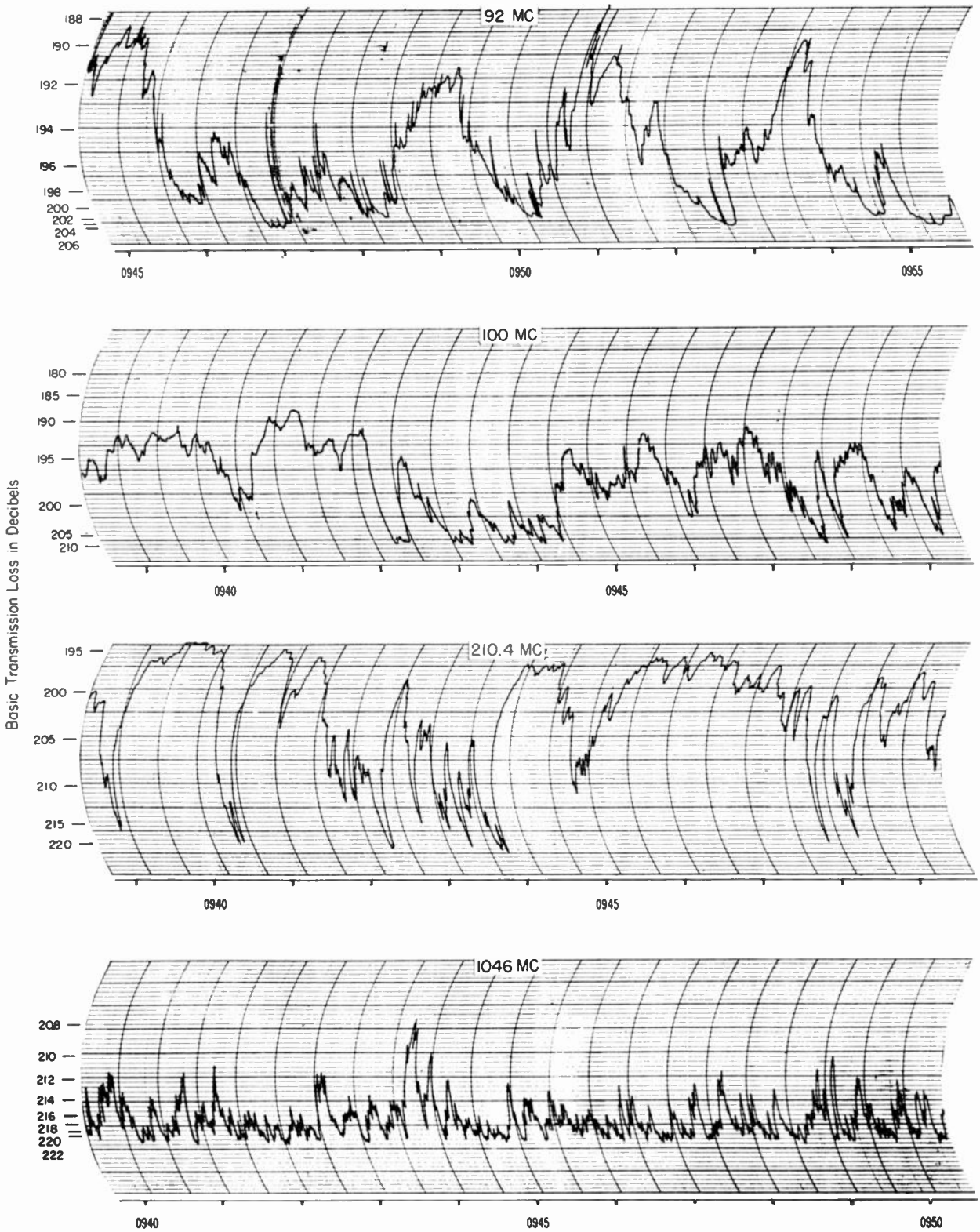

Fig. 10—Chart samples of transmissions received at Garden City (March 8, 1953).

(from Cheyenne Mountain Summit) with the 210.4-mc rates (from Cheyenne Mountain Base), and with the 100-mc rates from Camp Carson. The following diurnal trends are also easily seen: high fading rates in the afternoon when a high degree of atmospheric turbulence is present, and low fading rates in the morning hours when there is a good possibility of stratification in the atmosphere.

Inspection of Fig. 11 (next page) suggests average fading rates are roughly proportional to frequency. This does not apply in all cases, however. Especially in the comparison of the 1,046-mc data with data on the other

frequencies the ratios of fading rates are less than the corresponding frequency ratios. In this case the paths are identical as far as the locations of the transmitting and receiving antennas are concerned, but the effective antenna heights will produce different lobe elevations on the various frequencies investigated.

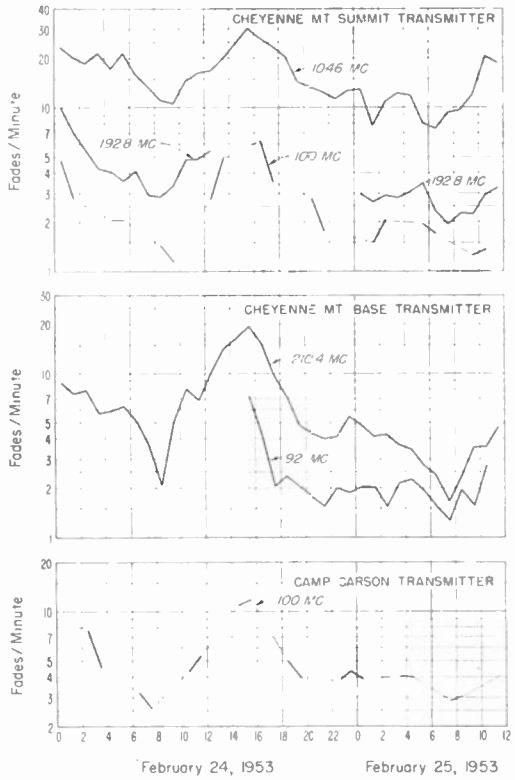

Fig. 11—Diurnal variations of average fading rates.

Table I below shows pertinent parameters for the paths under consideration. Here the heights h_0 and h_c have been designated as h_{0s} and h_s, respectively, and are given in feet above mean sea level.

Eq. (32) above shows that the fading rate is proportional to the scattering angle, the frequency, and the root-sum-square of the turbulent wind velocity u and a fraction of the steady cross-drift velocity V_n. In the actual evaluation of the measured data it has been found more practical to use the height of the scattering center h_s above mean sea level than the scattering angle. This height h_s may be readily computed from the path parameters, and meteorological observations provide wind data for these heights.

Fig. 12 (next page) shows average fading rates for February recording period plotted vs h_s. Fading rate data have been normalized to 100 mc by multiplication by $100/f_{mc}$. The data were divided into four time blocks. The symbol location indicates the average fading rate for each time block, and the "wings" denote the standard deviation.

This representation suggests that (except for the 1200–1800 time block) fading rate data increase with increasing height of the scattering center up to a certain point, and then decrease again. The 1200–1800 time block also shows a substantially greater variance of fading rates than the others. If the fading rate is taken as primarily a function of wind velocity at the elevation at the scattering center, the distribution of velocities with height inferred from Fig. 12 are in accordance with general meteorological observations which place maximum wind velocities in the 30–40,000-foot range.

Wind records at elevations up to 70,000 feet are in general available from Weather Bureau Stations. For the Cheyenne Mountain Paths observations at Dodge City, Kansas, are applicable. Unfortunately, the Dodge City data did not extend to sufficiently great heights for the February recording period. An attempt was made to substitute data from Lowry Air Force Base (near Denver), but they are hardly applicable to the path, and very little correlation with fading rates was obtained.

For the August 16, 1952, data correlation with wind speeds at Dodge City was more successful. Fig. 13, p. 1353, is a plot of wind speed at height of scattering center vs average fading rate during the hours adjacent to the wind observations. The upper portion shows total wind regardless of direction, and the lower portion shows the steady cross-drift component V_n versus fad-

TABLE I

Frequency; mc	Transmitter	Receiver	Distance; miles	θ milli-radians	θ_c milli-radians	Feet above mean sea level		$s=\alpha_0/\beta_0$
						h_{os} crossover of radio horizons	h_s scattering center	
92	Cheyenne Mt. Base	Garden City	226.6	31.7	53.0	7,670	13,760	0.6615
100	Cheyenne Mt. Summit	Garden City	226.5	28.1	50.5	6,490	12,330	0.4699
100	Camp Carson	Garden City	223.6	37.8	94.5	9,230	25,780	0.8067
100	Cheyenne Mt. Summit	Anthony	393.5	58.5	93.7	15,000	32,560	0.6746
100	Camp Carson	Anthony	390.7	68.0	136.0	19,610	54,570	0.8941
100	Pikes Peak	Anthony	404.1	50.9	84.1	11,800	27,680	0.5176
192.8	Cheyenne Mt. Summit	Garden City	226.5	28.0	50.4	6,460	12,270	0.4646
192.8	Cheyenne Mt. Summit	Anthony	393.5	58.4	89.4	14,940	30,400	0.6721
210.4	Cheyenne Mt. Base	Garden City	226.6	31.7	50.7	7,650	13,090	0.6558
1,046	Cheyenne Mt. Summit	Garden City	226.5	28.8	47.5	6,620	11,460	0.4592
1,046	Cheyenne Mt. Summit	Anthony	393.5	59.8	87.9	15,490	29,460	0.6563

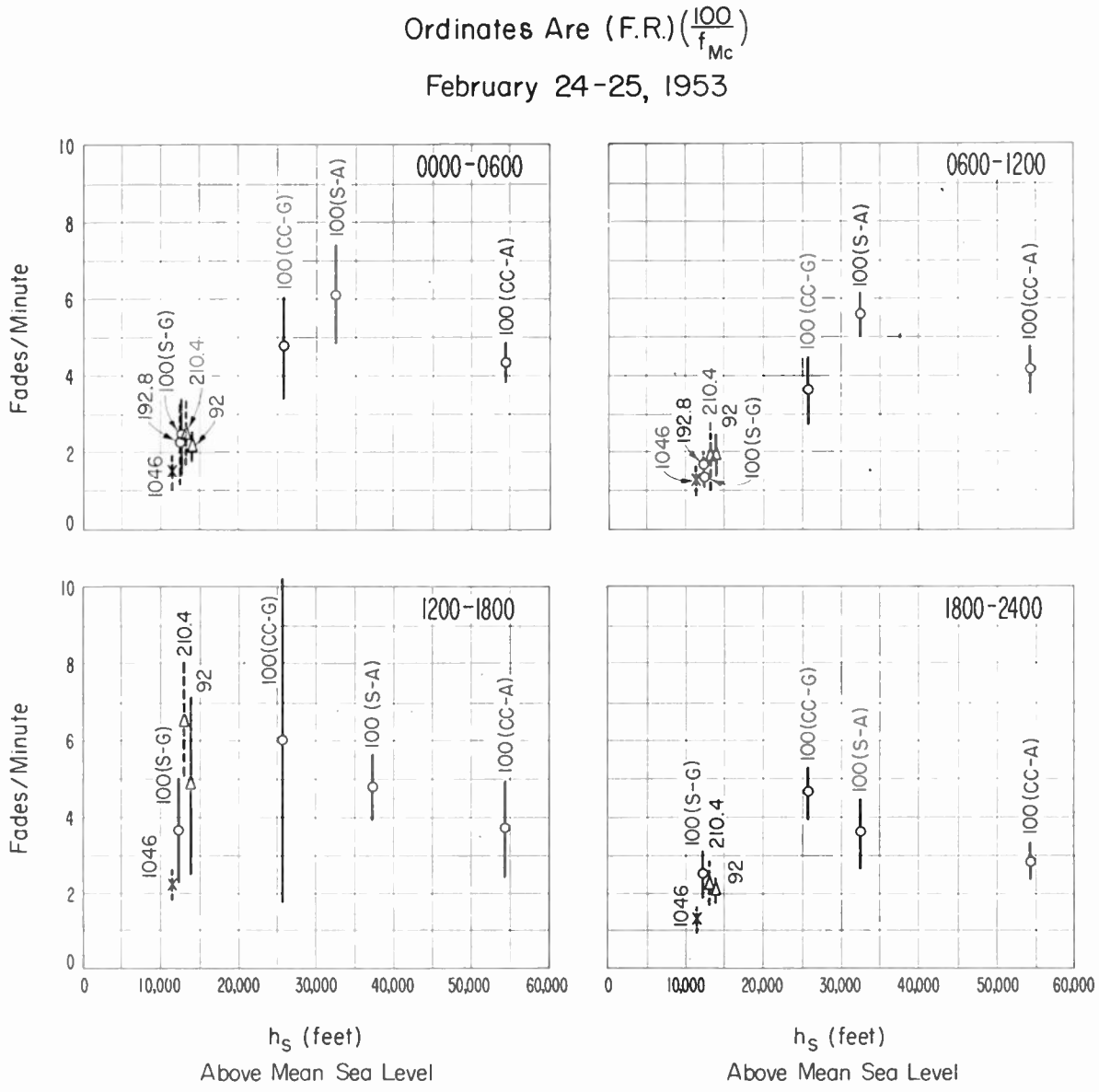

Fig. 12—Average fading rates vs height of effective scattering center [Ordinates are (F.R.)(100/f_{mc}); February 24–25, 1953].

ing rate. The correlation coefficient between fading rates and wind velocity was not significantly larger for the normal component: 0.85 as compared to 0.76 for the total wind velocity. Since the principal contribution from (32) is seen to be the turbulent velocity it seems possible that this turbulent velocity is a function of total wind speed, thus explaining the comparatively high correlation with total wind velocity. Many more independent observations would be required before any definitive conclusions can be reached, however, since the observed correlations are only just barely significantly different from zero at the five per cent level for our small samples of 8 independent observations.

IV. Fading Rates on Short Line-of-Sight Transmission Paths

On line-of-sight transmission paths the amplitude and the phase of the received radio waves vary with time as a result of atmospheric inhomogeneities which drift across the path with a velocity V_n normal to it. Elsewhere in this issue Wheelon and Muchmore[19] have demonstrated theoretically and Herbstreit and Thompson[20] have confirmed experimentally that the phase on short line-of-sight paths free from the effects of ground reflection tends to vary in direct proportion to the magnitudes of the atmospheric inhomogeneities, while the variance of the amplitudes of the received waves is only a second order effect. Thus it becomes more convenient to study the rate of fading of the phase rather than of the amplitude on these line-of-sight paths.

[19] A. D. Wheelon and R. B. Muchmore, "Line-of-sight propagation phenomena, II. Scattered components," p. 1450, this issue.

[20] J. W. Herbstreit and M. C. Thompson, Jr., "Measurements of the phase of radio waves received over transmission paths with electrical lengths varying as a result of atmospheric turbulence," p. 1391, this issue.

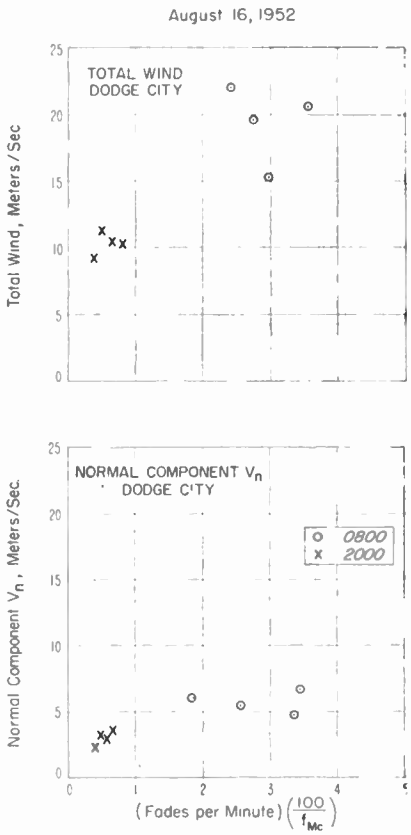

Fig. 13—Wind velocity at height of effective scattering center vs average fading rate (August 16, 1952).

We may assume that the phase is normally distributed about its mean and the appropriate value of $p[r(0.5)] = (2\pi)^{-1/2}$, where now $r(0.5)$ denotes the median value of the varying phase. Muchmore and Wheelon[21] have derived expressions for the power spectrum of the phase for three different assumptions regarding the form of the correlation function describing the atmospheric turbulence: (1) the exponential, (2) Gaussian, and (3) generalized Cauchy form.

When the formula for the power spectrum corresponding to the exponential correlation function is substituted in (3) of Section I, the resulting integral is infinite, and we are unable to obtain an expression for fading rate. This situation is a reflection of the well known[21] misbehavior of the exponential correlation function for small values of its argument.

When the formula for the power spectrum corresponding to the Gaussian form is substituted in (2) and (3), and the resulting values of b_0 and b_2 substituted in (1), we obtain

$$N[r(0.5)] = V_n/2\pi l_0. \tag{33}$$

In the above l_0 is a scale factor for the turbulence representative of the Gaussian form of the correlation function. Note that the fading rate is now independent of the radio frequency. Eq. (33) has a simple physical explanation. Thus it indicates that one fade will occur, on the average, during the time required for an inhomogeneity of length $2\pi l_0$ to drift across the transmission path. It should be noted that the fading power spectrum was derived on the assumption that the entire air mass, with the inhomogeneities embedded in it, moves across the path with the velocity V. A more realistic model would involve movements of various portions of the air mass with different velocities. It seems likely that predicted fading rates for a given average wind velocity would be larger for the latter model.

Using the generalized Cauchy form the integrals (2) and (3) may be evaluated[22] and we obtain for the fading rate,

$$N[r(0.5)] = \sqrt{3}\,\frac{V_n}{2\pi l_0}\cdot \tag{34}$$

The above differs from (33) only by the constant factor $\sqrt{3}$, and this undoubtedly arises simply from the different magnitudes of l_0 in the Gaussian and generalized Cauchy correlation functions.

No detailed use of the above formulas has yet been made, but data of the type reported by Herbstreit and Thompson[20] agree qualitatively in their lack of frequency dependence with (33) and (34). Preliminary estimates of fading rates from measured values of V_n and l_0 are of the order of one-tenth of the measured fading rates. These preliminary estimates cannot be considered conclusive, however, because the measured wind velocities were substantially different on the two ends of the path. It does appear that a theoretical model of atmospheric turbulence which allowed explicitly for varying wind velocities along the path and for a continuous spectrum of turbulence would indicate systematically larger fading rates than (33) or (34). This would be more in accordance with our preliminary observations.

One of the difficulties with fading rate analyses of phase data arises from the trends present in the measured phase. These trends arise from the presence of very large scale atmospheric inhomogeneities which move slowly across the path. These trends are simply the low-frequency components of the power spectrum of the phase variations. When these low-frequency components have a large amplitude they systematically reduce the fading rate as we have defined it in terms of positive crossings of the median level. It seems possible that a better definition of fading rates for phase data might involve the number of maxima, since such a definition would eliminate the analysis difficulty arising from trends and should be applicable to the continuous spectrum of turbulence characteristic of the atmosphere.[13]

[21] R. B. Muchmore and A. D. Wheelon, "Line-of-sight propagation phenomena—I. Ray treatment," p. 1437, this issue.

[22] A. D. Wheelon and John T. Robacker, "Table of Integrals Involving Bessel Functions," Ramo-Wooldridge Corporation, Los Angeles, California; 1954; see formula No. 4.301 on page 70.

The Probability Distribution of the Amplitude of a Constant Vector Plus a Rayleigh-Distributed Vector*

K. A. NORTON†, FELLOW, IRE, L. E. VOGLER†, W. V. MANSFIELD†, AND P. J. SHORT†

Summary—**Formulas, tables, and graphs are given for the probability distribution of the instantaneous resultant amplitude of the sum of a constant vector and a Rayleigh-distributed vector. It is emphasized that two distributions are required to describe a Rayleigh-distributed vector: the distribution of its amplitude and the distribution of its phase. A summary is presented of physical conditions which must be satisfied for a given phenomenon to exhibit statistical properties of a Rayleigh-distributed vector. References are made to ways in which these distributions may be used to describe random variables occurring in ionospheric, tropospheric, and irregular terrain propagation problems. Finally, a discussion is given of amplitude and phase distributions of two other random vectors encountered in tropospheric propagation studies.**

The Rayleigh-Distributed Vector[1,2]

IN THIS SECTION we will define the requirements which must be satisfied for a random vector to be Rayleigh-distributed. These requirements are somewhat less restrictive than those under which Lord Rayleigh derived his distribution, and no pretense is made that the essentially heuristic arguments given to make them seem reasonable are rigorous. Thus we will determine the probability distributions of the intensity and of the phase of the resultant electric vector obtained by adding together, with random relative phase, a large number of component vectors with unequal amplitudes E_1, E_2, and so forth up to E_n, as shown in Fig. 1. If following four requirements are satisfied: (1) $\sum_{i=1}^{n} E_i^2$ has constant value k^2, (2) $E_i^2 \ll k^2$ for $i = 1$ to n, (3) phase of each component vector E_i is a random variable, and, moreover, all values of its phase between 0 and 2π are equally likely, and (4) n is sufficiently large, then reasons will be given for believing:

1. The amplitude of the resultant vector E_s is a random variable and its probability distribution is determined (arbitrarily closely) by the Rayleigh distribution:

$$P(E_s > z) = \exp(-z^2/k^2). \tag{1}$$

2. The phase θ' of the resultant vector E_s is a random variable, and, in fact, all values of its phase between 0 and 2π are equally likely:

$$P(\theta' > \theta) = 1 - \frac{\theta}{2\pi}. \tag{2}$$

3. The amplitude E_s and phase θ' of the resultant vector E_s are independent random variables.

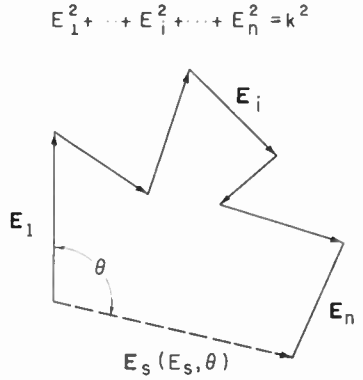

Fig. 1—The sum of vectors E_i with random relative phase is a vector E_s with Rayleigh-distributed amplitude and phase.

We will call any vector described by the above three characteristics a Rayleigh-distributed vector since Lord Rayleigh did show that the above conclusions follow under the following more restrictive requirements: (1) the amplitudes of the component vectors are equal, (2) each has a random phase which lies, with equal likelihood, anywhere within the range from 0 to 2π, and (3) n is a sufficiently large integer. Note that our requirement (1) $\sum_{i=1}^{n} E_i^2 =$ constant implies that the individual component amplitudes may actually be variable in magnitude or that n may also be variable. It appears likely that this weaker requirement (1) is adequate to define a Rayleigh distribution when we note that a Rayleigh-distributed vector is completely specified by this single constant k which is, in effect, a measure of its average power. Our requirement (2) $E_i^2 \ll k^2$ for $i = 1$ to n implies that the individual components need not have equal amplitudes as was postulated in Lord Rayleigh's proof. The sufficiency of this latter requirement is suggested by two facts: the distribution of the amplitude of the resultant of a constant vector plus a Rayleigh-distributed vector approaches the Rayleigh-amplitude distribution arbitrarily closely as the amplitude of the constant vector becomes very small relative to the rms amplitude of the added Rayleigh vector as is demonstrated in the next section; and the phase of the

* Original manuscript received by the IRE, August 8, 1955.
† Central Radio Propagation Lab., National Bureau of Standards, Boulder, Colo.

[1] P. M. Woodward, "Probability and information theory with applications to radar," McGraw-Hill Book Co., Inc., New York, N. Y., pp. 20–21; 1953. This reference gives a brief and concise account of the origin and meaning of the Rayleigh distribution. For the historical development see reference 2.

[2] Lord Rayleigh, (a) "On the resultant of a large number of vibrations of the same pitch and of arbitrary phase," *Phil. Mag.*, vol. 10, pp. 73–78; August, 1880; and vol. 27, pp. 460–469; June, 1889. (b) "Theory of Sound," 2nd ed., par. 42a; MacMillan & Co., Ltd., London; 1896. Same edition republished by Dover Publications, Inc.; 1945. (c) "On the problem of random vibrations and of random flights in 1, 2, or 3 dimensions," *Scientific Papers*, Cambridge Univ. Press, Cambridge, Eng., vol. 1, p. 491; 1899. (d) *Phil. Mag.*, vol. 37, pp. 321–347; April, 1919.

resultant of a constant vector plus a Rayleigh-distributed vector approaches the uniform Rayleigh distribution of phase as the amplitude of the constant vector becomes very small relative to the amplitude of the added Rayleigh vector, as was demonstrated in a paper by Norton, Shultz, and Yarbrough.[3]

It is easy to show for a Rayleigh-distributed vector that the mean-square value of its amplitude $\langle E_s^2 \rangle = k^2$. Furthermore, if we let p_a' denote the instantaneous power available from a resistance, ρ, across which the envelope voltage E_s appears, then p_a' will be proportional to E_s^2/ρ and the probability that the instantaneous available power will be greater than p_a is given by the Rayleigh distribution of power:

$$P(p_a' > p_a) = \exp(-p_a/\langle p_a \rangle). \tag{3}$$

It is of interest to note that the instantaneous radio frequency voltage $v = E_s \cos(\omega t + \theta')$ associated with the Rayleigh-distributed vector E_s having the amplitude and phase distributions (1) and (2), respectively, is normally distributed with a mean value of zero and a standard deviation $k/\sqrt{2}$:

$$P(v > x) = \frac{1}{\sqrt{2\pi}} \int_{(x\sqrt{2}/k)}^{\infty} \exp(-y^2/2)dy. \tag{4}$$

It has already been mentioned that a complete specification of a Rayleigh-distributed vector can be made in terms of a single parameter which is, in effect, a measure of its average power. This single parameter might be k, the rms value of E_s, which is exceeded by 36.8 per cent of all of the values which E_s may have, or it could be the rms value of v which is equal to $k/\sqrt{2}$. It could also be defined in terms of a value exceeded for some specified percentage of the time; for example, the median amplitude is equal to $0.8326k$.

It should be noted that the vector sum of two or more independent Rayleigh-distributed vectors is also a Rayleigh-distributed vector. The mean power available from the sum of several independent Rayleigh-distributed vectors is equal to the sum of the mean powers available from each of them. This latter conclusion has important applications in assessing the joint radio interference arising from several independent sources, each characterized by a Rayleigh-distributed vector.

We will now consider in a little more detail some of the above conditions necessary for a Rayleigh distribution. Fig. 2 shows the result of reducing the number n of component vectors. The particular graph paper on which these cumulative distributions are shown has been designed in such a way that the distribution of the amplitude E_s of a Rayleigh-distributed vector will be represented by a straight line with a 45-degree slope. A transmission loss scale is shown on Fig. 2 for convenience in determining the range of fading expected in scatter communication. The distributions shown here are for n unit vectors added with random relative phase.

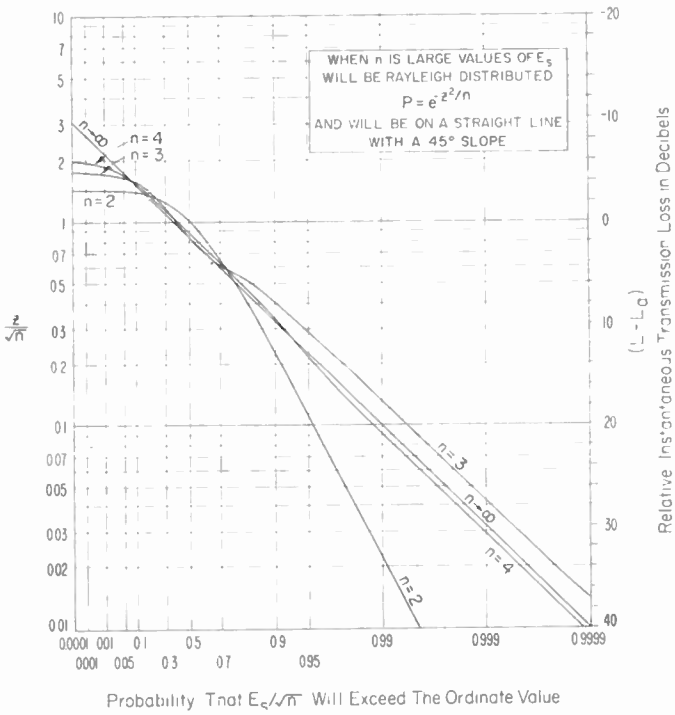

Fig. 2—The distribution of the resultant of n unit vectors with random relative phase.

Thus, the root-sum-square value in each case is equal to $\sqrt{n}$. The ordinate on Fig. 2 gives z divided by this root-sum-square value. The rms value of E_s is also equal to $\sqrt{n}$. The maximum amplitude of the resultant of n unit vectors will occur when they are all in phase and is thus simply equal to n. The rapid approach to a Rayleigh distribution as n increases is clearly shown by the curves for $n = 2$, 3, and 4. The distribution for $n = 2$ was obtained from the relation:

$$P(E_s > z) = \frac{1}{\pi} \arccos\left(\frac{z^2 - 2}{2}\right), \tag{5}$$

and for $n = 3$ by numerical methods which involve the addition, with a uniformly distributed relative phase, of a unit vector to vectors with the particular amplitudes E_s obtained from (5) for equally spaced values of P; the curve for $n = 4$ was then obtained in a similar way. In a recent paper Greenwood and Durand[4] have given tables of this distribution, including the 5 and 1 per cent levels, for all integral values of n from 6 to 24; these results provide a convenient means for determining how large n must be for a given maximum departure from the Rayleigh distribution throughout a given range of probabilities. It appears evident from Fig. 2 that departure from Rayleigh distribution for large n

[3] K. A. Norton, E. L. Shultz, and H. Yarbrough, "The probability distribution of the phase of the resultant vector sum of a constant vector plus a Rayleigh-distributed vector," *Jour. Appl. Phys.*, vol. 23, pp. 137–141; January, 1952. Note that the k in this reference is a power ratio rather than a voltage ratio and that the formulas and graphs give the distribution of $|\phi|$.

[4] J. A. Greenwood and D. Durand, "The distribution of length and components of the sum of n random unit vectors," *Ann. Math. Stat.*, vol. 26, pp. 233–246; June, 1955.

is greatest, when expressed in decibels, when P is quite small. From Greenwood and Durand's Table 2 we find departure from a Rayleigh distribution at $P=0.01$ is 0.52 db at $n=6$, 0.32 db at $n=10$, and 0.12 db at $n=24$; for larger values of P departures are even smaller.

Consider next the requirement that $\sum_{i=1}^{n} E_i^2 \equiv k^2$ must be constant. In order to gain an appreciation of the physical significance of this requirement, it will be useful to consider an idealized model of a propagation problem for which this condition would be satisfied. Let us assume that the radio waves received over a transmission path arrive at the receiving antenna as a result of reflection from a large number of dielectric spheres, each with a refractive index differing in absolute value by the constant ΔN from that of the medium in which they are located. Assume next that these spheres are moving at random over distances sufficiently large, in the interval of time chosen for examining the statistical distributions, that the waves reflected from each of them arrives with random relative phase at the receiving antenna. If we let E_i denote the received vector component corresponding to the waves reflected from the ith sphere, then $\sum_{i=1}^{n} E_i^2$ will be practically a constant provided a constant number n of these moving spheres are always within the scattering volume; i.e., the common volume defined by the crossed beams of the transmitting and receiving antennas. It should be clear in this example that k^2 will not be exactly constant in practice over long periods of time since both n and ΔN would be expected to vary with time. Thus we may expect the observed amplitudes E_a to be Rayleigh-distributed only over the short periods of time for which k is relatively constant. In other words, we may view the received power as a stochastic process in which we have an instantaneous power $p_a = p \cdot \delta$ composed of a slowly varying component p and a rapidly varying component δ. We then assume δ to be that component of the fading which is due only to phase interference and that p varies slowly as a function of other longer-term variations in propagation conditions. Experience has shown, both for ionospheric and tropospheric waves, that this maximum period of time, for which the Rayleigh distribution provides an adequate representation of the received fields, will decrease with increasing radio frequency as a result of the greater variability of the transmission loss at the higher frequencies; i.e., the greater variance of p. In some cases this maximum period of time may be several hours, while in other cases it may be less than a minute. Fortunately, the rate of fading arising from phase interference is directly proportional to the radio frequency so that approximately the same number of phase interference fades will occur at all radio frequencies in those periods of time for which the Rayleigh distribution provides an adequate description of the fading. Observations have shown that the slowly varying component p is log normally distributed, and thus we find in practice that observed distributions of the power available from the receiving antenna will vary from Rayleigh to log-normal as the sampling period is increased from a very small to a very large value. The expected distribution of the product $p \cdot \delta$ over long periods of time, with p log normally distributed, has been studied by G. McCrossen at the Central Radio Propagation Laboratory as a function of the standard deviation of log p, and these results are available for limited distribution to interested research workers.

The above example referred to a situation in which the transmitting and receiving antennas were fixed and the variations in δ were attributed to phase interference between the waves arriving from the moving reflecting spheres. Alternatively the spheres might be considered to be fixed in space and either the transmitting or receiving antenna moved. This alternate situation is often encountered in studying effects on radio propagation of irregularities in terrain. An example of such application has been given by one of the authors.[5]

The Vector Sum of a Constant Vector and a Rayleigh-Distributed Vector

In this section we will consider the effect of modifying the requirement that $E_i^2 \ll k^2$ for $i=0$ to n. Thus we will assume that zeroth component is a reference vector of unit amplitude and will let the Rayleigh-distributed vector sum of remaining components have an rms amplitude k. This is shown in Fig. 3 (next page). The need for an analysis of this vector combination arises frequently in radio propagation studies. For example, when the length of a radio transmission path is quite short, the received waves may be represented by a constant vector which is called the ground wave; as the transmission path is lengthened additional ionospheric or tropospheric waves are present at the receiving antenna, and these may often be represented by Rayleigh-distributed vectors. This type of analysis was used in a paper[6] by one of the authors for describing statistically the combination of a ground wave and a tropospheric wave and by Vandivere[7] for an explanation of the variations in the path transmission loss for a combined ground wave and ionospheric wave.

If we let r denote the resultant instantaneous amplitude of the sum of the reference vector and the Rayleigh-distributed vector, then an equation for the probability distribution of r derived by Rice[8] may be expressed as follows using the above notation:

[5] K. A. Norton, "Propagation over rough terrain," Report of Symposium on Tropospheric Wave Propagation, U. S. Navy Elec. Lab., San Diego, Calif., pp. 101–105; July, 1949.

[6] K. A. Norton, "Propagation in the FM Broadcast Band," "Advances in Electronics," Academic Press, Inc., New York, N. Y., vol. 1, pp. 406–408; 1948.

[7] E. F. Vandivere, "Some notes on probability functions and distributions," Appendix to report of FCC Committee III in preparation for the Clear Channel Hearing, Docket 6741; 1946.

[8] S. O. Rice, "Mathematical analysis of random noise," *Bell Sys. Tech. Jour.*, vol. 23, pp. 282–332, 1944; and vol. 24, pp. 46–156, 1954; also published as Bell Telephone Monograph B-1589, and has been included in "Selected Papers on Noise and Stochastic Processes," N. Wax, Ed., Dover Publications, New York, N. Y.; 1954. (See Fig. 7 and the equation at the bottom of p. 103 in the journal, p. 109 in the monograph, and p. 241 in the book.)

$$P(r' > r) = \frac{2}{k^2}\int_r^\infty r \exp\left[-(1+r^2)/k^2\right] I_0(2r/k^2)\,dr, \quad (6)$$

where

$$I_0(x) = J_0(ix) = \frac{1}{\pi}\int_0^\pi \exp(x\cos\phi)\,d\phi. \quad (7)$$

Rice[8] gave several approximate formulas for calculating the value of $P(r'>r)$, together with a graph of these distributions with k as a parameter. The primary purpose of the present paper is to give formulas, tables, and graphs of $P(r'>r)$ as a function of r and also r as a function of $P(r'>r)$ with k as a parameter with somewhat greater accuracy and for a greater range of probabilities than may presently be found in the literature. [Note that phase ϕ of the resultant of a constant vector plus a Rayleigh-distributed vector (see Fig. 3) is uniformly distributed between 0 and 2π only in the limit when k is very large; formulas, tables, and graphs of the distribution of $|\phi|$ are given as a function of k^2 in a paper by Norton, Shultz, and Yarbrough.[3]]

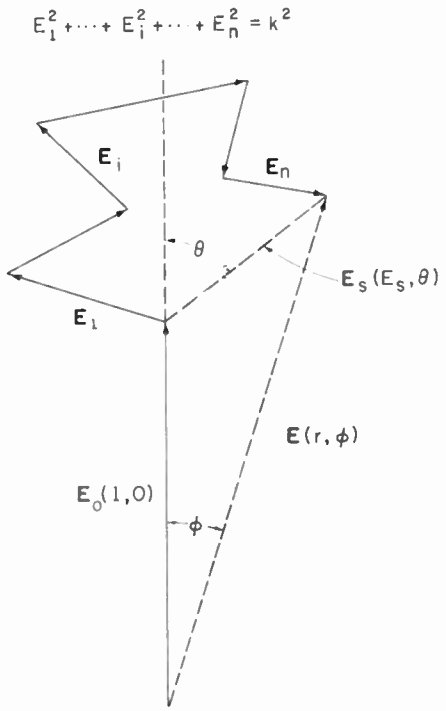

Fig. 3—The sum of a constant unit vector E_0 and a Rayleigh-distributed vector E_s is the vector E with an amplitude distribution which is the subject of this paper.

No attempt has been made to show that any of the series expansions developed in this paper for the probabilities or percentage points for the distributions are convergent, but it is later shown that the various expressions give the same numerical values in their overlapping ranges of utility.

Consider first the case where k is very small; i.e., the case of a large constant vector added to a Rayleigh-distributed vector with a small rms value. If we introduce the asymptotic expansion for I_0 in (6) and then expand the resulting expression in ascending powers of $(r-1)$, the result may be integrated term by term to obtain the following:

$$P(r'>r) = \frac{1}{\sqrt{2\pi}}\int_y^\infty \exp(-x^2/2)\,dx + \frac{k}{4\sqrt{\pi}}\exp(-y^2/2)\cdot\left[1+\frac{k^2}{16}+\frac{9k^4}{512}-\frac{k}{4\sqrt{2}}\left(1+\frac{9k^2}{32}+\frac{75k^4}{512}\right)y^3 + \frac{k^2}{16}\left(1+\frac{9k^2}{16}\right)y^2 - \frac{5k^3}{128\sqrt{2}}\left(1+\frac{7k^2}{8}\right)y_3 + \frac{7k^4}{512}\left(1+\frac{135k^2}{112}\right)y^4 - \frac{21k^5}{2048\sqrt{2}}y^5\right]. \quad (8)$$

In the above $y=\sqrt{2}(r-1)/k$ and in the derivation of (8) terms of order k^7 and higher have been omitted. Eq. (8) is an extension (with higher order terms) of a formula of Rice.[8]

When k is sufficiently small, we see by the first term in (8) that r' is approximately normally distributed about unity with a standard deviation of $k/\sqrt{2}$. This is shown graphically on Fig. 4 by the straight line labelled $K=-\infty$, together with the distributions of $(r-1)/k$ for other values of K as obtained by the methods discussed later in this paper. In the remainder of this paper capital letters will be used to denote the decibel equivalents of the corresponding quantities designated with lower-case type. Thus $K\equiv 20\log_{10}k$ and $R=20\log_{10}r$. Rice[8] presented graphically the results of his evaluation of (6) in essentially the same form as our Fig. 4.

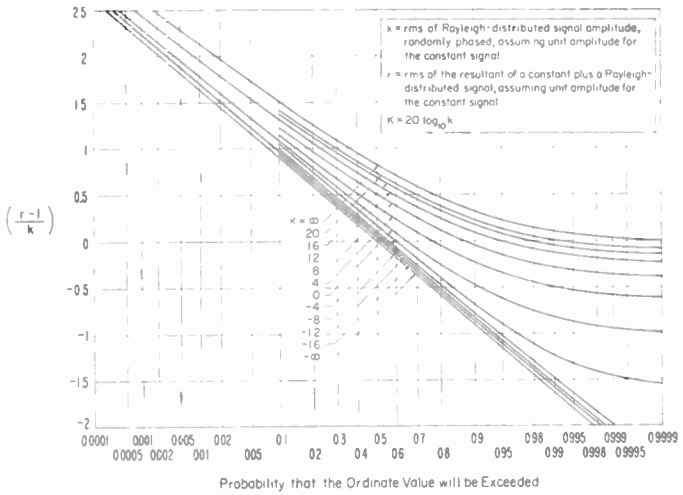

Fig. 4—The distribution of $[(r-1)/k]$; the power in the random component is K decibels relative to the power in the constant component.

It is often useful to have explicit expressions for particular probability levels, and these may be obtained as follows. Let $P(r'>r)=f(y)$ and expand this function in a Taylor's series thus:

$$P(r' > r) = f(y_0+\Delta y) = f(y_0) + \Delta y f'(y_0) + \frac{(\Delta y)^2}{2}f''(y_0) + \frac{(\Delta y)^3}{6}f'''(y_0) + \cdots, \quad (9)$$

where y_0 denotes the value of y corresponding to the given probability level $P(r'>r)$ for the limiting case as k approaches zero. The values of y_0 may thus be found in a table of the normal probability function. For example, $y_0=1.281552$ for $P(r'>r)=0.1$, $y_0=0$ for $P(r'>r)=0.5$ and $y_0=-1.281552$ for $P(r'>r)=0.9$. If we set $\Delta y=a_1k+a_2k^2+\cdots+a_5k^5$ in (9) we obtain a polynomial in k which may be solved for the a_i in order by assuming the coefficients of the various higher powers of k equal to zero. The following equation illustrates the method for determining a_i; for this case, it is only necessary to retain the first derivative in (9):

$$P(r'>r)=\frac{1}{\sqrt{2\pi}}\int_{y_0}^{\infty}\exp(-x^2/2)dx+\frac{k}{4\sqrt{\pi}}\exp(-y_0^2/2)-\frac{\Delta y}{\sqrt{2\pi}}\exp(-y_0^2/2)+\text{terms of higher order in } k. \quad (10)$$

The first two terms in (10) represent $f(y_0)$ and the third term represents $\Delta y f'(y_0)$.

Since, by definition of y_0, the first term on the right in (10) is just equal to $P(r'>r)$, we find that the sum of the second and third terms must be equal to zero; thus $\Delta y\equiv a_1k=k\sqrt{2}/4$ so that $a_1=\sqrt{2}/4$. In this way we obtained the following expression which gives directly, when k is small, the level r corresponding to the probability $P(r'>r)$:

$$r=1+\frac{k}{\sqrt{2}}(y_0+\Delta y)=1+\frac{ky_0}{\sqrt{2}}+\frac{k^2}{4}-\frac{k^3y_0}{8\sqrt{2}}-\frac{k^4}{96}+\frac{k^4y_0^2}{24}+\frac{3k^5y_0}{128\sqrt{2}}-\frac{k^5y_0^3}{32\sqrt{2}}+\frac{7k^6}{1920}-\frac{17k^6y_0^2}{960}+\frac{k^6y_0^4}{80}. \quad (11)$$

When k is sufficiently small (11) may be expressed in decibels directly:

$$R=8.68589\left[\frac{ky_0}{\sqrt{2}}+\frac{k^2}{4}-\frac{k^2y_0^2}{4}-\frac{3k^3y_0}{8\sqrt{2}}+\frac{k^3y_0^3}{6\sqrt{2}}-\frac{k^4}{24}\right]. \quad (12)$$

The following special cases are of particular interest:

$$R(0.1)=7.8711k-1.3949k^2-0.7971k^3 \quad (13)$$

$$R(0.9)=-7.8711k-1.3949k^2+0.7971k^3 \quad (14)$$

$$R(0.5)=2.1715k^2-0.3619k^4 \quad (15)$$

$$R(0.1)-R(0.9)=15.7422k-1.5942k^3. \quad (16)$$

Terms of order k^4 and higher have not been included in the above logarithmic expressions except for $R(0.5)$ since greater accuracy can be obtained, whenever these higher order terms would be required, by first calculating r by (11) and then taking the logarithm.

We may now turn to a consideration of formulas which are useful when k is large; i.e., the case of a small constant vector added to a large Rayleigh-distributed vector. If we use the series expansion for I_0 in (6) and integrate the resulting expression term by term we obtain:

$$P(r'>r)=\exp\left[-(1+r^2)/k^2\right]\sum_{n=0}^{\infty}\sum_{m=0}^{n}\frac{(r/k)^{2(n-m)}}{n!(n-m)!k^{2n}}. \quad (17)$$

By expanding the above double series and recombining the terms, it can be expressed in the following form:

$$P(r'>r)=\exp\left[-(1+r^2)/k^2\right]\sum_{m=0}^{\infty}A_mr^{2m} \quad (18)$$

where

$$A_m=\frac{1}{m!k^{2m}}\sum_{n=m}^{\infty}\frac{1}{n!k^{2n}}. \quad (19)$$

Finally the above may be further simplified to:

$$P(r'>r)=\exp(-r^2/k^2)\left[1+\sum_{m=1}^{\infty}B_m(r/k)^{2m}\right], \quad (20)$$

where

$$B_m=\frac{1}{m!}\left[1-\exp(-1/k^2)\sum_{n=0}^{m-1}\frac{1}{n!k^{2n}}\right]. \quad (21)$$

The above is in a very useful form for numerical calculation since the successive values of B are easily determined from their predecessors. Thus $B_1=1-\exp(-1/k^2)$, $B_2=\frac{1}{2}[B_1-1/k^2\exp(-1/k^2)]$, $B_3=\frac{1}{3}[B_2-1/4k^4\exp(-1/k^2)]$, etc. When (20) was used for calculations of the percentage points of the distribution, a rough estimate of the correct value of r was made and then Newton's method was used for rapidly converging on a value of r with the desired number of significant figures. If we let $P(r'>r)$ denote the given value of the probability for which an estimate of r is required, N denote the number of terms in the series required to provide the desired accuracy, and r_q denote the q^{th} estimate using Newton's method, we obtain:

$$(r_{q+1}/k)^2=(r_q/k)^2-\frac{1+\sum_{m=1}^{N}B_m(r_q/k)^{2m}-P(r'>r)\exp(r_q^2/k^2)}{\sum_{m=1}^{N}mB_m(r_q/k)^{2m-2}-P(r'>r)\exp(r_q^2/k^2)}. \quad (22)$$

Using a procedure similar to that for determining (11) but applying it now to series expansion (17), the following series has been obtained, useful for calculating r as a function of k and $P(r'>r)$ when k is large:

$$r^2=k^2x_0\left[1+\frac{1}{k^2}+\frac{1}{2k^4}\left(1-\frac{x_0}{2}\right)+\frac{1}{6k^6}\left(1-\frac{5x_0}{2}+\frac{2x_0^2}{3}\right)+\frac{1}{24k^8}\left(1-\frac{17x_0}{2}+\frac{49x_0^2}{6}-\frac{33x_0^3}{24}\right)+\cdots\right], \quad (23)$$

where $x_0=-\log_e[P(r'>r)]$. It is also convenient to express (23) in decibels:

$$R=K+10\log_{10}x_0+\frac{4.3429}{k^2}\left[1-\frac{x_0}{4k^2}-\cdots\right] \quad (24)$$

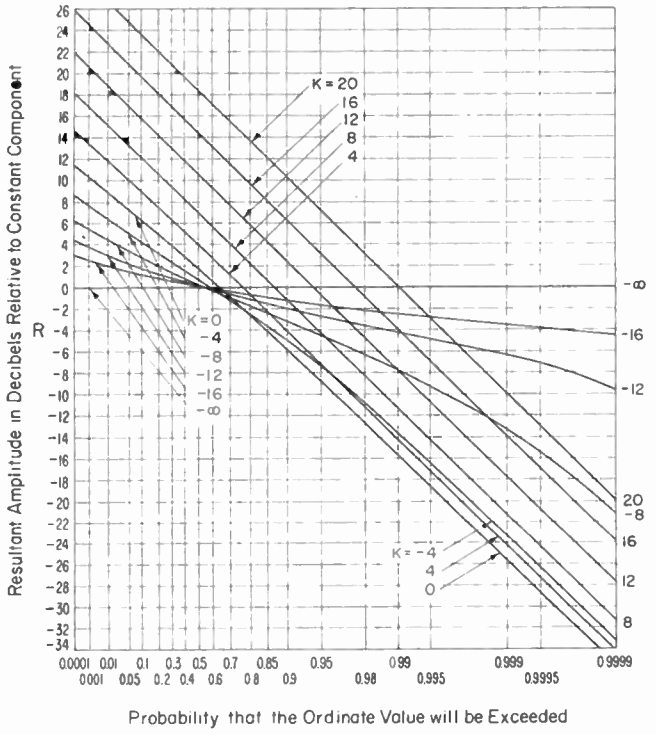

Fig. 5—The distribution of the amplitude of a constant vector plus a Rayleigh-distributed vector; the power in the random component is K decibels relative to the power in the constant component.

$$R(0.1) = K + 3.6222 + \frac{4.3429}{k^2} - \frac{2.5000}{k^4} + \cdots \quad (25)$$

$$R(0.5) = K - 1.5918 + \frac{4.3429}{k^2} - \frac{0.7525}{k^4} - \cdots \quad (26)$$

$$R(0.9) = K - 9.7733 + \frac{4.3429}{k^2} - \frac{0.1144}{k^4} - \cdots \quad (27)$$

$$[R(0.1) - R(0.9)] = 13.3955 - \frac{2.3856}{k^4} + \cdots . \quad (28)$$

Terms of order higher than $(1/k)^4$ have not been included in (24) to (28) since greater accuracy can be obtained, whenever these higher order terms would be required, by first calculating r^2 by (23) and then taking the logarithm.

Table I, on page 1360, gives $R \equiv 20 \log_{10} r$ for several values of $P(r'>r)$ with K parameter. Values in the table were obtained by (11) when $K<0$, and by (23) when $K>0$, except that the values designated by an asterisk (*) were obtained by (20). When used in overlapping regions of utility (11), (20), and (23) gave the same results for $R(P)$ out to the fourth figure beyond the decimal point. Thus, in each column of the table, (20) was used to check those values obtained by (11) or (23) which are adjacent to the values indicated by an asterisk (*). Most of the values given in Table I were computed to five figures beyond the decimal point and rounded off to four.

Fig. 4 gives the distribution of $(r-1)/k$ for several values of K on normal probability paper and illustrates

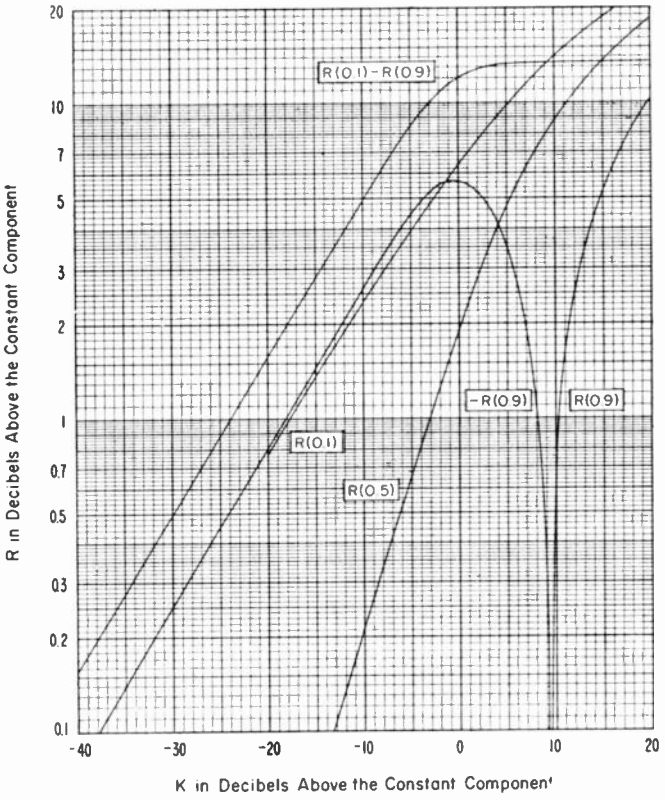

Fig. 6—Parameters of the distribution of the amplitude of a constant vector plus a Rayleigh-distributed vector; the power in the random component is K decibels relative to the power in the constant component.

the fact that the distribution of r becomes approximately normal as K approaches $-\infty$. Fig. 5 gives the distribution of R for several values of K on graph paper so designed that the distribution of the amplitude of a Rayleigh-distributed vector expressed in decibels will be represented by a straight line with a 45-degree slope. It should be noted that the distribution of R approaches this Rayleigh distribution as K approaches $+\infty$.

It is convenient to define the fading range of a received radio wave to be the ratio of the amplitudes of the waves exceeded for 10 per cent and 90 per cent of a period of time which is sufficiently short so that appreciable changes in k do not occur; in some cases this period of time might be as much as an hour, while in other cases it may be less than a minute. Fig. 6 gives the fading range $R(0.1)-R(0.9)$ together with the values of $R(0.1)$, $R(0.5)$, and $R(0.9)$ as a function of K.

The Vector Sum of a Constant Vector Plus Vectors with Normally Distributed Amplitudes

In two papers appearing in this issue Wheelon and Muchmore[9] have demonstrated theoretically and Herbstreit and Thompson[10] have confirmed experimentally

[9] A. D. Wheelon and R. B. Muchmore, "Line-of-sight propagation phenomena, II. Scattered components," p. 1450, this issue. See the discussion accompanying (2.20).

[10] J. W. Herbstreit and M. C. Thompson, Jr., "Measurements of the phase of radio waves received over transmission paths with electrical lengths varying as a result of atmospheric turbulence," p. 1391, this issue.

TABLE I—THE RESULTANT AMPLITUDE $R(P)$ IN DECIBELS VS P AND K FOR A CONSTANT VECTOR PLUS A RAYLEIGH DISTRIBUTED VECTOR (The mean power in the random vector is K decibels relative to the power in the constant component)

K \ P	0.0001	0.0002	0.0005	0.001	0.002	0.005	0.01	0.02
−40	0.2257	0.2150	0.2000	0.1880	0.1752	0.1570	0.1419	0.1254
−35	0.3976	0.3789	0.3528	0.3318	0.3094	0.2775	0.2511	0.2221
−30	0.6958	0.6636	0.6186	0.5823	0.5437	0.4884	0.4425	0.3920
−25	1.2035	1.1496	1.0738	1.0124	0.9470	0.8529	0.7745	0.6880
−20	2.0431	1.9560	1.8328	1.7327	1.6254	1.4703	1.3401	1.1955
−18	2.5063	2.4021	2.2548	2.1346	2.0056	1.8183	1.6607	1.4851
−16	3.0582	2.9351	2.7604	2.6177	2.4639	2.2399	2.0506	1.8390
−14	3.7091*	3.5653*	3.3606*	3.1928*	3.0115*	2.7464*	2.5214*	2.2688*
−12	4.4682*	4.3022*	4.0654*	3.8705*	3.6593*	3.3492*	3.0847*	2.7863*
−10	5.3424*	5.1535*	4.8830*	4.6598*	4.4170*	4.0589*	3.7520*	3.4038*
−8	6.3361*	6.1242*	5.8198*	5.5676*	5.2925*	4.8847*	4.5334*	4.1329*
−6	7.4510*	7.2164	6.8787*	6.5980*	6.2908*	5.8334*	5.4373*	4.9832*
−4	8.6844*	8.4288*	8.0596*	7.7518*	7.4138*	6.9085*	6.4689*	5.9624*
−2	10.0318*	9.7570*	9.3590*	9.0263*	8.6599*	8.1103*	7.6301*	7.0742*
0	11.4856*	11.1939*	10.7708*	10.4159*	10.0245*	9.4355*	8.9190*	8.3192*
2	13.0362*	12.7304*	12.2858*	11.9125*	11.5000*	10.8778*	10.3309*	9.6942*
4	14.6734*	14.3562*	13.8945*	13.5065*	13.0772*	12.4289*	11.8583*	11.1931*
6	16.3869*	16.0610*	15.5866*	15.1875*	14.7460*	14.0789*	13.4915*	12.8068*
8	18.1666*	17.8345*	17.3513*	16.9450*	16.4953*	15.8161*	15.2184*	14.5218*
10	20.0023*	19.6665*	19.1779*	18.7671*	18.3127*	17.6266	17.0229*	16.3205*
12	21.8840*	21.5462*	21.0546*	20.6414	20.1845*	19.4947	18.8882	18.1823*
14	23.8017*	23.4628	22.9697	22.5554	22.0972	21.4057	20.7978	20.0905
16	25.7460*	25.4066	24.9129	24.4980	24.0392	23.3470	22.7385	22.0305
18	27.7092*	27.3696	26.8755	26.4604	26.0013	25.3088	24.7001	23.9918
20	29.6852*	29.3455	28.8513	28.4361	27.9769	27.2842	26.6754	25.9670

K \ P	0.05	0.1	0.2	0.5	0.8	0.9	0.95	0.98
−40	0.1006	0.0786	0.0518	0.0002	−0.0516	−0.0788	−0.1014	−0.1268
−35	0.1785	0.1359	0.0921	0.0007	−0.0917	−0.1404	−0.1808	−0.2265
−30	0.3158	0.2475	0.1640	0.0022	−0.1628	−0.2503	−0.3232	−0.4060
−25	0.5565	0.4381	0.2924	0.0069	−0.2884	−0.4469	−0.5799	−0.7322
−20	0.9741	0.7725	0.5220	0.0217	−0.5092	−0.8001	−1.0479	−1.3355
−18	1.2189	0.9675	0.6583	0.0343	−0.6379	−1.0110	−1.3317	−1.7073
−16	1.5116	1.2101	0.8303	0.0543	−0.7976	−1.2783	−1.6963	−2.1920
−14	1.8755*	1.5106	1.0472	0.0859	−0.9943	−1.6169	−2.1667	−2.8297
−12	2.3187*	1.8811	1.3202	0.1356	−1.2342	−2.0452	−2.7763	−3.6787*
−10	2.8544*	2.3354	1.6631	0.2136	−1.5212	−2.5839*	−3.5681*	−4.8236*
−8	3.4956*	2.8882*	2.0920	0.3354	−1.8533	−3.2507*	−4.5933*	−6.3817*
−6	4.2554*	3.5548*	2.6252*	0.5241	−2.2133*	−4.0473*	−5.8818*	−8.4491*
−4	5.1445*	4.3496*	3.2829*	0.8130*	−2.5480*	−4.8971*	−7.3086*	−10.7055*
−2	6.1709*	5.2856*	4.0853*	1.2490*	−2.7280*	−5.5384*	−8.3788*	−12.2200*
0	7.3393*	6.3726*	5.0524*	1.8944*	−2.5527*	−5.6323*	−8.6609*	−12.6457*
2	8.6504*	7.6169*	6.2007*	2.8081*	−1.9064*	−5.1993*	−8.1924*	−12.2190*
4	10.1014*	9.0195*	7.5376*	4.0058*	−0.8327*	−4.0674*	−7.1818*	−11.2215*
6	11.6834*	10.5713*	9.0512*	5.4480*	0.5591*	−2.6906*	−5.8126*	−9.8566*
8	13.3801*	12.2516*	10.7119	7.0767	2.1674	−1.0879*	−4.2126	−8.2582
10	15.1689*	14.0324*	12.4837	8.8348	3.9175	0.6595*	−2.4657	−6.5118
12	17.0266	15.8863*	14.3338	10.6792	5.7589	2.5000*	−0.6256	−4.6720
14	18.9330	17.7911*	16.2369	12.5799	7.6583	4.3995	1.2734	−2.7730
16	20.8721	19.7287*	18.1747	14.5169	9.5948	6.3358	3.2097	−0.8368
18	22.8330	21.6904	20.1351	16.4769	11.5546	8.2956	5.1694	1.1229
20	24.8081	23.6653	22.1100	18.4516	13.5292	10.2702	7.1440	3.0975

K \ P	0.99	0.995	0.998	0.999	0.9995	0.9998	0.9999
−40	−0.1438	−0.1594	−0.1784	−0.1917	−0.2043	−0.2200	−0.2312
−35	−0.2572	−0.2853	−0.3194	−0.3435	−0.3663	−0.3948	−0.4153
−30	−0.4616	−0.5129	−0.5754	−0.6195	−0.6614	−0.7138	−0.7516
−25	−0.8352	−0.9305	−1.0475	−1.1305	−1.2096	−1.3092	−1.3813
−20	−1.5327	−1.7172	−1.9461	−2.1103	−2.2683	−2.4694	−2.6163
−18	−1.9671	−2.2118	−2.5177	−2.7389	−2.9532	−3.2278*	−3.4301*
−16	−2.5388	−2.8688	−3.2859*	−3.5909*	−3.8890*	−4.2757*	−4.5639*
−14	−3.3013*	−3.7563*	−4.3412*	−4.7760*	−5.2074*	−5.7763*	−6.2035*
−12	−4.3359*	−4.9832*	−5.8367*	−6.4883*	−7.1506*	−8.0509*	−8.7567*
−10	−5.7697*	−6.7316*	−8.0522*	−9.1060*	−10.2248*	−11.8333*	−12.9142*
−8	−7.8064*	−9.3032*	−11.4979*	−13.3510*	−15.4376*	−18.5400*	−21.1370*
−6	−10.5731*	−12.8953*	−16.0274*	−19.0233*	−21.8850*	−25.7680*	−28.7447*
−4	−13.4416*	−16.2887*	−20.1592*	−23.2154*	−26.0831*	−30.3797*	−33.0950*
−2	−15.1768*	−18.1583*	−22.1189*	−25.1288*	−28.1261*	−32.1323*	−35.1176*
0	−15.6568*	−18.6674*	−22.6467*	−25.6571*	−28.6674*	−32.6468*	−35.6572*
2	−15.2446*	−18.2625*	−22.2463*	−25.2583*	−28.2693	−32.2513	−35.2616
4	−14.2515*	−17.2716*	−21.2569*	−24.2691*	−27.2810*	−31.2606	−34.2709
6	−12.8881	−15.9085*	−19.8946	−22.9069*	−25.9184	−29.8984	−32.9087
8	−11.2902	−14.3113	−18.2971	−21.3096	−24.3209	−28.3010	−31.3113
10	−9.5440	−12.5652	−16.5511	−19.5636	−22.5749	−26.5550	−29.5653
12	−7.7042	−10.7254	−14.7113	−17.7238	−20.7352	−24.7153	−27.7256
14	−5.8053	−8.8265	−12.8125	−15.8249	−18.8363	−22.8164	−25.8267
16	−3.8691	−6.8903	−10.8763	−13.8887	−16.9001	−20.8802	−23.8905
18	−1.9094	−4.9306	−8.9165	−11.9290	−14.9404	−18.9204	−21.9307
20	0.0652	−2.9560	−6.9419	−9.9544	−12.9658	−16.9458	−19.9561

that tropospherically scattered waves on sufficiently short line-of-sight propagation paths tend to arrive at the receiving antenna very nearly in phase-quadrature with the direct wave. This limiting case may be illustrated by Fig. 3 if we consider that each elementary vector, E_i, has a phase $\theta = \pm(\pi/2)$, and then E_s will also have the phase $\theta = \pm(\pi/2)$. In this case E_s has a normally distributed amplitude:[11]

$$P(E_s > z) = \frac{1}{\sqrt{2\pi k^2}} \int_z^\infty \exp(-z^2/2k^2)dz, \qquad (29)$$

where, as before, $k^2 = \sum_{i=1}^n E_i^2 = \langle E_s^2 \rangle$ and is a measure of the average power in the scattered wave relative to that of the constant vector. In our present application the scattered wave power is always quite small relative to the direct wave power so that $k^2 \ll 1$. We are interested in the distribution of the amplitude, $r = \sqrt{1+z^2}$, and of the phase, $\phi = \tan^{-1} z$, of the resultant vector $E(r, \phi)$. Since z is normally distributed, it is clear that r will not be normally distributed. We will derive expressions for the mean, standard deviation, median, and fading range of r:

$$\langle r \rangle = \frac{1}{\sqrt{2\pi k^2}} \int_{-\infty}^{+\infty} \sqrt{1+z^2} \exp(-z^2/2k^2)dz$$

$$= 1 + \frac{k^2}{2} - \frac{3k^4}{8} + \frac{15k^6}{16} - \cdots \qquad (30)$$

$$\langle r^2 \rangle = \frac{1}{\sqrt{2\pi k^2}} \int_{-\infty}^{+\infty} (1+z^2) \exp(-z^2/2k^2)dz = 1 + k^2 \qquad (31)$$

$$\sigma_r^2 = \langle r^2 \rangle - (\langle r \rangle)^2 = \frac{k^4}{2}(1 - 3k^2 + \cdots) \qquad (32)$$

$$r(P) = \sqrt{1 + z^2(P)} \qquad (33)$$

$$P = \frac{2}{\sqrt{2\pi k^2}} \int_{z(P)}^\infty \exp(-z^2/2k^2)dz. \qquad (34)$$

In the above P denotes the probability that the resultant r will exceed $r(P)$. Since k is small, it is convenient to express $R(P)$ in decibels:

$$R(0.5) = 10 \log_{10} [1 + (0.67449k)^2]$$

$$= 1.9758k^2 - 0.4494k^4 + \cdots \qquad (35)$$

$$R(0.1) = 11.7500k^2 - 15.8951k^4 \qquad (36)$$

$$R(0.9) = 0.0686k^2 - 0.0005k^4 \qquad (37)$$

$$R(0.1) - R(0.9) = 11.6814k^2 - 15.8946k^4. \qquad (38)$$

When the above are compared with (13), (14), (15), and (16), we see that the variations of the amplitude of the resultant are of second order in k in the above phase-quadrature model rather than a first order effect as in the Rayleigh scattering model.

Under certain circumstances, we may expect the scattered vector components to be in phase with the constant vector. Consider, for example, propagation over a short line-of-sight propagation path involving ground reflection. When the antenna height is low or is otherwise adjusted so that the ground-reflected wave is nearly in phase opposition and is comparable in magnitude to the direct wave, the resultant received wave will be nearly in phase-quadrature with the direct wave and thus nearly in phase (or 180 degrees out-of-phase) with the scattered components. In this limiting case the variance of the resultant amplitude will be equal to the variance of the scattered field, and the phase of the resultant will be independent of the scattering. From the standpoint of the statistician this is the trivial case of adding 1 to a normally distributed random variable with zero mean. Both the mean and median values of the resultant amplitude are then equal to 1, and we obtain:

$$R(0.1) = 11.1314k - 7.1327k^2 + 6.0940k^3 \qquad (39)$$

$$R(0.9) = -11.1314k - 7.1327k^2 - 6.0940k^3 \qquad (40)$$

$$R(0.1) - R(0.9) = 22.2628k + 12.1880k^3. \qquad (41)$$

Table II provides a summary of the approximate interrelations of the variances of amplitudes and phases in the above three limiting cases which provide upper and lower bounds to the values expected on line-of-sight propagation paths.

TABLE II

Approximate Interrelations Between the Variances of the Phase and Amplitude of the Resultant for Three Limiting Distributions Encountered in Scatter Type Propagation

(The scattered power is assumed to be small relative to that of the direct wave, *i.e.*, $k^2 \ll 1$.)

Scattered Waves Rayleigh Distributed	Scattered Waves in Phase-Quadrature ($\pm\pi/2$)	Scattered Waves with Phase 0 or π
$\sigma_r^2 = \frac{k^2}{2}$*	$\sigma_r^2 = \frac{k^4}{2}$	$\sigma_r^2 = k^2$
$\sigma_\phi^2 = \frac{k^2}{2}$†	$\sigma_\phi^2 = k^2$	$\sigma_\phi^2 = 0$
$\sigma_\phi^2 = \sigma_r^2$	$\sigma_\phi^2 = \sigma_r\sqrt{2}$	

* First term of (8).
† See reference 3.

On actual propagation paths the observations[10] indicate that none of the above models are applicable since the scattered field components apparently have phases which are neither uniformly distributed nor constant. A really adequate treatment of the experimental data must await the development of propagation theories capable of predicting joint phase and intensity distributions of the scattered fields. Meanwhile the above three models should provide useful upper and lower bounds for within-line-of-sight propagation phenomena.

Acknowledgment

This paper has been considerably improved as a result of comments made on an earlier version by members of the NBS Applied Mathematics Division.

Rayleigh, *loc. cit.*, 2(a).

Trans-Horizon Microwave Propagation over Hilly Terrain*

YOSHITAKA KURIHARA†, ASSOCIATE, IRE

Summary—**By introducing three path parameters into the geometry of scattered signal transmission, the spherical earth formulas of W. E. Gordon[1] were extended to the nonspherical earth case. This paper describes the result of analysis. The nonspherical earth formulas were applied to the prediction of the signal power and characteristics of tropospheric scattered fields on the hilly 93-mile path between Ithaca and Wethersfield-Springs, N. Y., and on the 119-mile path between Ithaca and Buffalo, N. Y. The transmission experiments over these two paths were conducted at Cornell University, at frequencies of 2,780 mc and 9,150 mc. The results of the experiments are presented together with the predictions in this paper.**

Introduction

THE SCATTERING theory of Booker and Gordon[2] gives a good explanation for the phenomenon of the unusually high fields encountered in radio-wave propagation well beyond the horizon. In his further work,[1] Gordon gave detailed numerical estimates of the received signal power and characteristics of tropospheric scattered fields such as diversity distances for spaced receivers, maximum useful antenna size, height above which antenna output becomes nearly constant, fading rate, and frequency diversity bandwidth. All these works are based on the geometry of a smooth spherical earth, and give the prediction of first-order approximation for the nonspherical earth transmission of the scattered signal.

In order to take into account the effect of peculiarities of the transmission path on the scattered fields, three path parameters are introduced into the geometrical analysis of the scattered fields. Most of the spherical earth formulas are generalized simply by deriving correction factors for the nonspherical earth case with the aid of these parameters. Some formulas are, however, derived in a manner which departs somewhat from Gordon's treatment. Details of the derivation of the general formulas are not presented in this paper, but will be found in another paper[3] of the author.

Path Parameters

With the aid of Fig. 1, three path parameters are defined as follows:

$$\delta \equiv \frac{r_2}{d} \text{ (Index of symmetry)},$$

$$h \equiv \frac{H_0}{h_0} \text{ (Index of height)},$$

$$e \equiv \frac{H}{H_0} \text{ (Index of elevation)}.$$

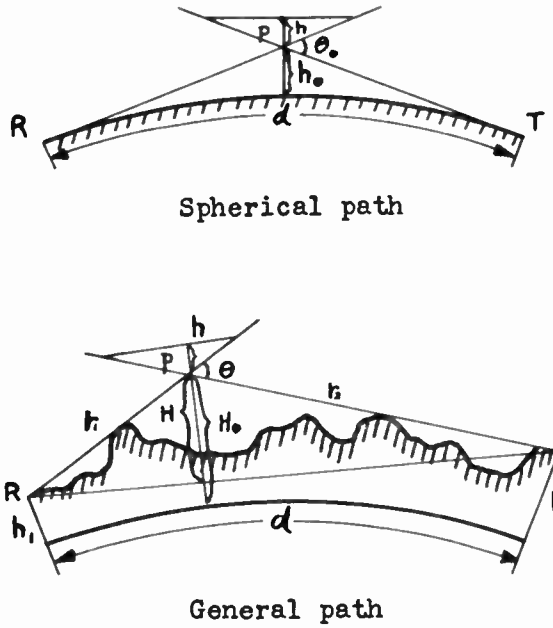

Fig. 1—Geometrical relation of path profile.

As named above, δ is a measure of symmetry of the transmission path, h is simply the height above sea level of the intersection P measured in units of h_0, and e is a measure of flatness or steepness of the path. Although these parameters are easily obtainable from the path profile, they are more accurately determined by the following formulas:

$$\delta = \frac{4 + \gamma_1 \dfrac{d}{h_0} + \dfrac{h_1 - h_2}{h_0}}{8 + (\gamma_1 + \gamma_2)\dfrac{d}{h_0}}$$

$$h = 4(1-\delta)^2 + \gamma_1(1-\delta)\frac{d}{h_0} + \frac{h_1}{h_0}$$

$$e = \frac{\delta(1-\delta)\left\{8 + (\gamma_1 + \gamma_2)\dfrac{d}{h_0}\right\}}{4(1-\delta)^2 + \gamma_1(1-\delta)\dfrac{d}{h_0} + \dfrac{h_1}{h_0}}.$$

* Original manuscript received by the IRE, July 5, 1955. Research sponsored by the Rome Air Development Center under contract AF 30(602)-682. Presented at the Dedication Scientific Meeting, Boulder Laboratories, N.B.S., Boulder, Colorado.

† Radio Research Laboratories, Tokyo. Engaged in research at Cornell University, July, 1953 to September, 1954.

[1] W. E. Gordon, "The Scattering of Radio Waves by Turbulence in the Troposphere," Elec. Engrg. Rep. EE 163, Cornell University; 1953.

[2] H. G. Booker and W. E. Gordon, "A theory of radio scattering in the troposphere," PROC. IRE, vol. 38, pp. 401–412; April, 1950.

[3] Y. Kurihara, "Trans-horizon Radiowave Propagation over a Nonspherical Earth," Elec. Engrg. Rep. EE 229, Cornell University, 1954.

where most of geometrical factors are shown in Fig. 1 except γ_1 and γ_2. γ_1 and γ_2 are the elevation angles of the local horizon at R and T respectively, of which signs are positive if the local horizon is higher than the spherical earth horizon and negative if the former is lower than the latter.

Nonspherical Earth Formulas

Scattered Power

For the correlation function expression $(-r/l)$, large scatterers and off-beam scattering, the scattered power P relative to the free space power P_{FS} at a distant receiver is

$$\frac{P}{P_{FS}} = (A \cdot B \cdot C)\left[\frac{2.45ca^4}{sd}\right], \tag{1}$$

where

$$A = \{4\delta(1-\delta)\}^2$$

$$B = h^{-4}$$

$$C = \frac{1}{0.0074(e-1)^5} \cdot \left\{(e+3)\ln e + \frac{3}{2} + \frac{3}{2e} - \frac{1}{6e^2} - \frac{17}{6}e\right\},$$

c is a constant associated with the scattering intensity, a is the modified radius of the earth, r is the separation between points in the scatterer, l is the scale of turbulence and s is $2\pi l$.

For the spherical earth path, the correction factor $(A \cdot B \cdot C)$ reduces to unity, leaving the bracketed term alone in the formula. The same argument applies for the succeeding formulas.

Diversity Distances

Horizontal correlation distance normal to the path is given by

$$D_H = \frac{4(1-\delta)}{e \cdot h}\left[\frac{a\lambda}{1.3d}\right] \tag{2}$$

and vertical correlation distance is given by

$$D_V = \frac{2(1-\delta)}{\eta \cdot h}\left[\frac{a\lambda}{d}\right], \tag{3}$$

where λ is the wave-length and η is a function of e, of which curve is given in Fig. 2.

Maximum Useful Antenna Size

According to Dr. Gordon, the maximum useful antenna size is defined by that size of antenna the beam of which is just filled by the scattering volume. The beam angle of this antenna is the size of the source divided by its distance from the antenna. The aperture width is, by the usual antenna formula, the wavelength divided by the beam angle. This results in a value of aperture width which is twice the correlation distance.

Examination of (2) and (3) discloses that the value of D_H is not necessarily about the same with D_V. This fact leads to a conclusion that the maximum useful antenna size may be more closely determined by describing antenna aperture in horizontal and vertical directions. For the antenna with the aperture of circular cross section, however, a single value D given by the following formula might be convenient:

$$D \equiv \tfrac{1}{2}(2D_H + 2D_V) = D_H + D_V. \tag{4}$$

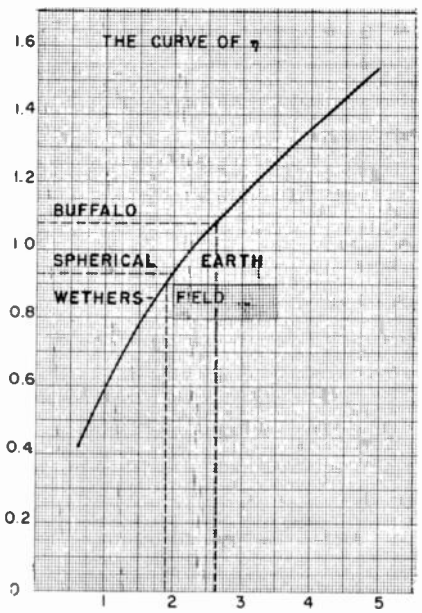

Fig. 2—Curve of η.

A Practical Limitation on Antenna Height

A practical limitation on antenna height H_V is defined by the correlation distance of an antenna relative to the ground, in other words, by the correlation distance between an antenna placed above ground and its image. This is a measure of the antenna height above which the antenna output becomes essentially constant. H_V is given by the formula

$$H_V = \frac{2(1-\delta)}{\eta \cdot h}\left[\frac{2a\lambda}{d}\right]. \tag{5}$$

Fading Rates

The spherical earth formulas of fading rates derived by Gordon are extended to the nonspherical earth case simply by interpreting the correlation distances in his formulas as general ones given in this paper. One of the formulas,

$$D_H\tau_0\{(2\bar{u}_h\tau_0)^2 + D_H^2\}^{-1/2}, \tag{6}$$

was used for the prediction of fading rates at the transmission experiments. In (6), $\bar{u}_h$ is the mean drift velocity of the scatterer across the path in the horizontal direc-

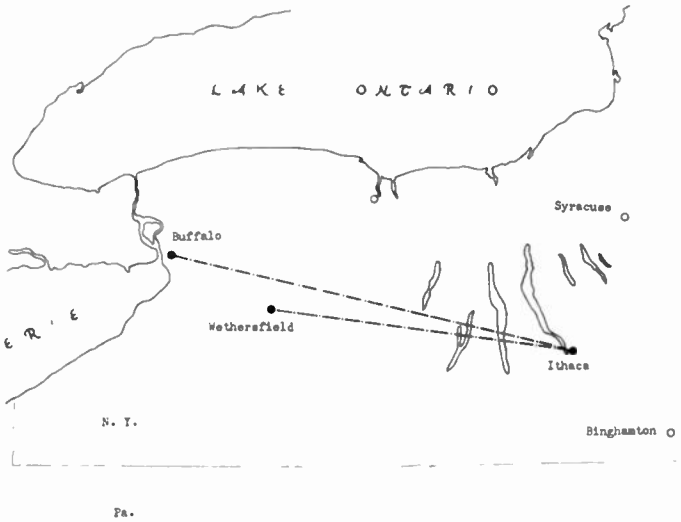

Fig. 3—Trans-horizon microwave transmission paths.

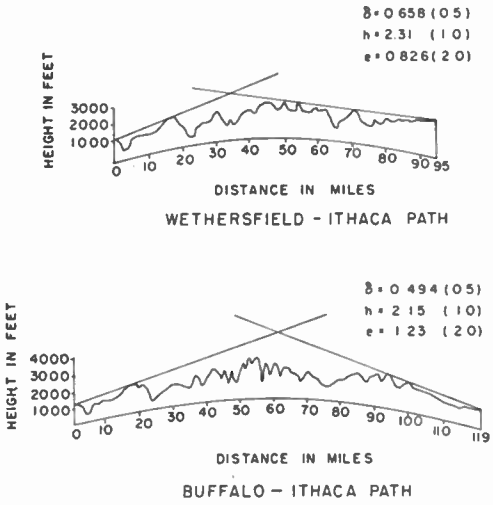

Fig. 4—Profiles of the transmission paths.

tion, τ_0 is $s/\sqrt{\overline{u'^2}}$ for small scattering angle and $\sqrt{\overline{u'^2}}$ is rms value of isotropic turbulent velocity of the scatterer.

Frequency Bandwidth

The frequency bandwidth of the transmission path, over which correlation of the fading of carrier frequencies is expected, is given by

$$B = \frac{12\delta(1-\delta)}{\eta \cdot h^2(\eta + e)}\left[\frac{25}{d^3}\right] \qquad (7)$$

in megacycles for d in hundreds of miles.

Transmission Experiments

For the purpose of investigating the characteristics of the scattered fields, a program of microwave transmission experiments was conducted at Cornell University from the beginning of 1954. The locations of the receiving site, Ithaca, and of the transmitting sites, Wethersfield-Springs (labeled as Wethersfield for simplicity) and Buffalo, N.Y., are indicated in Fig. 3. The profiles of these two paths are shown in Fig. 4. Three path parameters are indicated at each profile, where the figures in the parentheses are those of the spherical earth.

The transmitters and receivers used in the experiments are essentially the components of Radio Set AN/MPN-1. The transmitted signals are impulsed 2,780-mc and 9,150-mc microwaves. For simplicity, these waves will be labeled as S- and X-band respectively. The average transmitted powers are 50 watts on the S-band and 18 watts on the X-band.

The experiment was carried out first on the Wethersfield-Ithaca path by the end of July, 1954. Then the whole setup of the transmitter was moved to the transmitting site at Buffalo, and the experiment was continued.

Observations and Results

Signal Power

Examples of signal as recorded on Esterline-Angus recorders are shown in Fig. 5 (next page). The first, third, fifth and seventh tapes, counting from the top, are of the X-band signal, and rest S-band. Eastern Standard Time is marked on the top of the tapes for every half hour with increasing time reading from right to left and from top to bottom. The tape speed is one foot per hour.

A general trend of signal is seen from the tapes, that the signal level increases early in the morning, stays high around noon, and decreases in the afternoon. This trend, the diurnal variation of signal level, is common to the S- and X-band signals, though the variation of the X-band signal is generally larger than that of the S-band.

Hourly median levels were obtained from the time totalizing recorder. These are shown in Figs. 6 and 7 on page 1366.

The S-band signal is indicated by solid lines and the X-band signal is by broken lines. The scale on the left side is for the S-band signal and the scale on the right is for the X-band. These signal levels are given in the received signal levels minus the antenna gains and the transmitter power levels, thus allowing direct comparison of the measured values with the prediction. The predicted signal levels are -200 db and -210 db for the S- and X-band respectively on the Wethersfield-Ithaca path, and -209 db and -219 db on the Buffalo-Ithaca path. These were computed by (1), assuming $s = 100$ meters and $c = 6\times10^{-6}$ meter^2 which corresponds to strong scatterers. The X-band signal levels are slided upward by 10 db, allowing the deviation of the measured system difference between the S- and X-band signal levels from the prediction to be read directly as the difference of levels between solid and broken lines.

Most of the data show fairly close accordance with the prediction in regard to the system difference, though

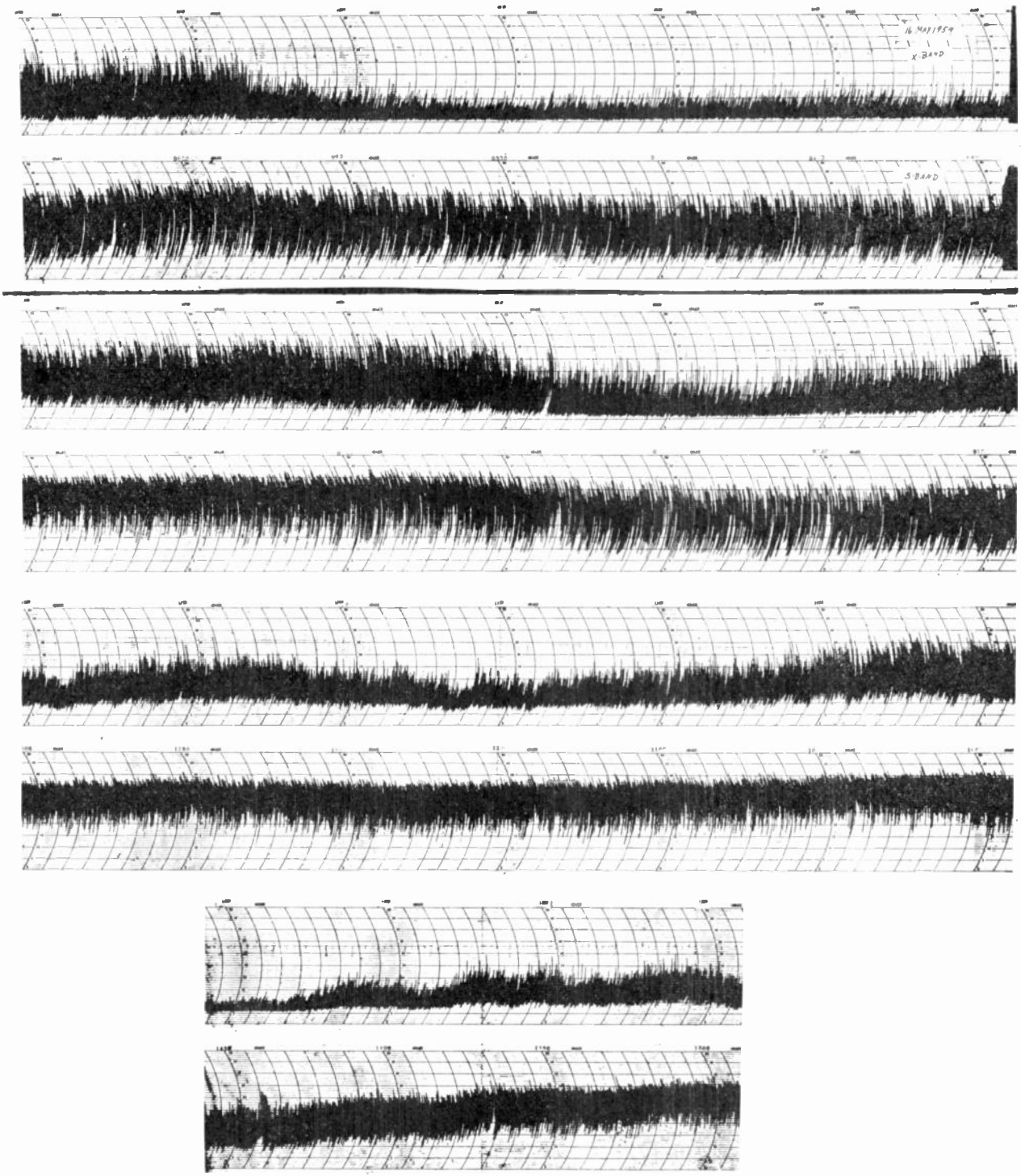

Fig. 5—E.A. recording (May 16, 0400–1430).

the variation of the X-band signal level is generally larger than those of the S-band as pointed out before. Large system differences were observed, for example, every night from June 12 to 15. In those cases, reduced amplitude of fading, relative to its median value, was frequently observed on the Esterline-Angus recorder on the S-band, but not so much on the X-band.

Although no specific data were taken for the purpose of correlating scattered signal with meteorological conditions, some relations of them were observed. According to observation, strong signals were usually accompanied by hot and calm weather and weak signals by cold and windy weather. For instance, a sudden drop of signal level observed around 1400 EST on June 7 was accompanied by a rapid change of the weather from warm to cold and windy.

The S-band signal level reached and exceeded the predicted level around the end of July at the Wethersfield-

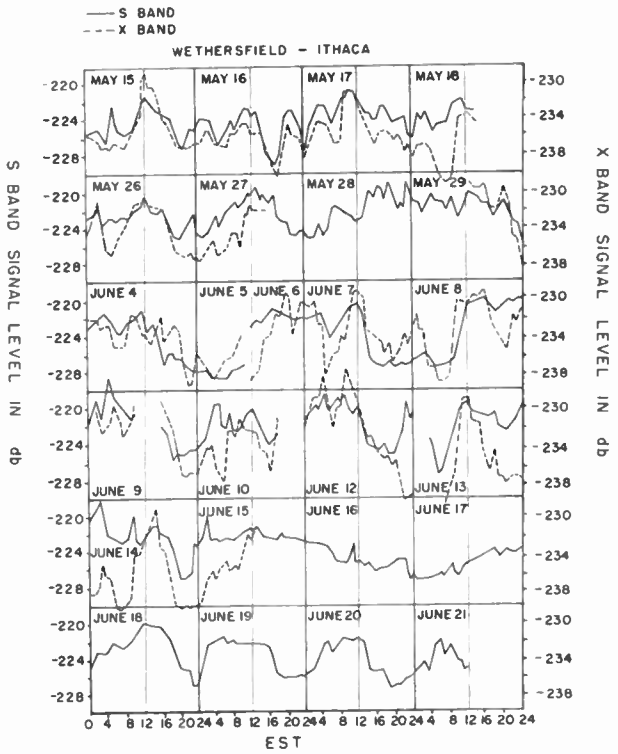

Fig. 6—Variation of hourly median level of scattered signal (Wethersfield-Ithaca Path).

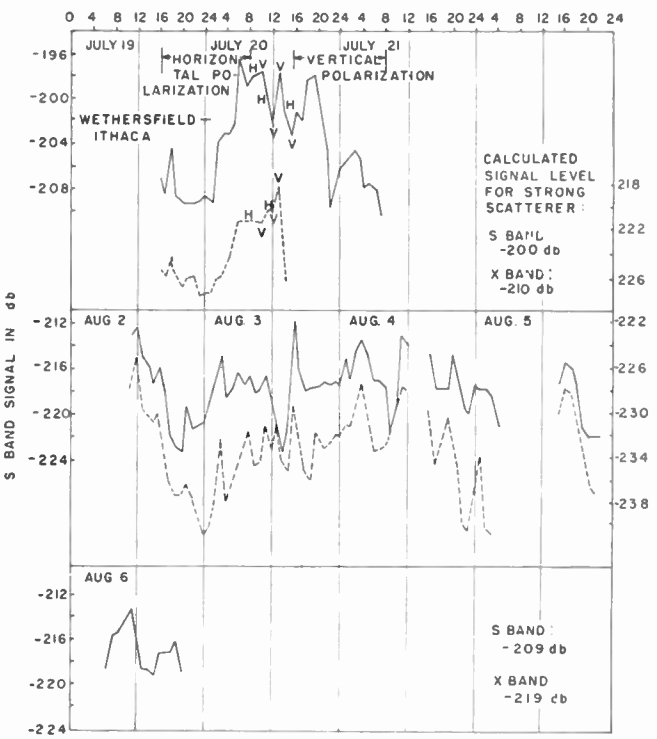

Fig. 7—Variation of hourly median level of scattered signal (Wethersfield- and Buffalo-Ithaca Path).

Ithaca test, though the X-band signal level remained some 8 db lower than the predicted level. During the Buffalo-Ithaca test both signal levels stayed fairly high, that is, few db below the predicted level at their maxima. The period of these tests corresponds to the time when the heat from the sun reaches its maximum, and then the strongest scatterers are most likely to be formed. Although no reliable data were obtained during the coldest season, it might be deduced from the available data and observations that the seasonal variation of the median level of the scattered signal exceeds 20 db.

Correlation of Field Strengths Received on Spaced Antennas

Horizontal and vertical correlations of the field strengths received on spaced antennas were obtained in the following way. Outputs from a pair of 4-foot paraboloid antennas were recorded simultaneously on a Brush recorder for about two minutes at the tape speed of one inch per second. The process was repeated for various spacings of the antennas. An example of closely correlated S-band signals of horizontally spaced antennas are shown in Fig. 8. Correlation coefficients were computed from the tapes by taking 100 sampling points for an interval of about five seconds at each step of antenna spacing. The results of computation are shown in Fig. 9 (next page) where the spacing of the antennas is given in wavelength so that both the S- and X-band are plotted in the same scale.

Predicted values of horizontal and vertical correlation distances D_H and D_V, computed by (2) and (3), are pointed out by arrows.

In the Wethersfield-Ithaca test, the measurements resulted in larger horizontal and smaller vertical correlation distances than the predicted values. A possible reason for this discrepancy is the different accuracy of antenna alignment between the horizontal and vertical setups. Care was paid for this matter in the Buffalo-Ithaca test, which resulted in better accordance of the measurement and prediction. The ratio of the vertical correlation distances of the Wethersfield-Ithaca path to Buffalo-Ithaca path is about 1.1 against 1.0 of the prediction, while that of the horizontal correlation distances is about 1.7 against 1.24.

Maximum Useful Antenna Size

Gains of a 6- and 10-foot paraboloid antenna over a 4-foot paraboloid antenna were measured on the

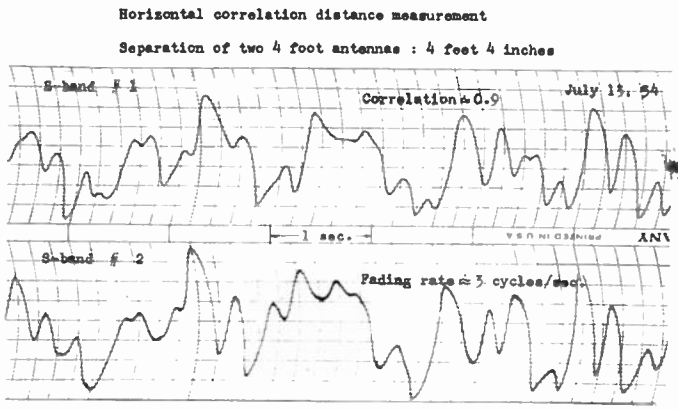

Fig. 8—Example of closely correlated signals as recorded on Brush recording tape.

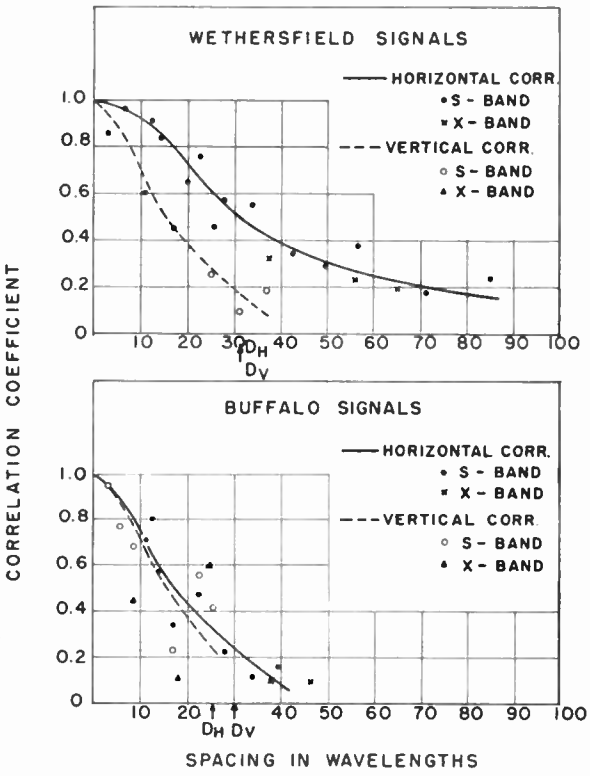

Fig. 9—Correlation of field strength received on spaced antennas at Ithaca, N. Y.

Wethersfield- and Buffalo-Ithaca paths, and were compared with the plane wave gain differences. The results are tabulated in Tables I and II.

TABLE I

	S-Band	
	Difference between 4- and 6-foot antennas	Difference between 4- and 10-foot antennas
Plane wave gain difference	3 db	8 db
Wethersfield signal	3 db	8 db
Buffalo signal	3 db	8 db

TABLE II

	X-Band	
Plane wave gain difference	6.0 db	10.5 db
Wethersfield signal	5.5 db	8.0 db
Buffalo signal	3.0 db	4.5 db

Predicted sizes as computed by (4) are 22 feet of the S-band and 6.6 feet of the X-band for the Wethersfield-Ithaca path, and 20 feet of the S-band and 6 feet of the X-band for the Buffalo-Ithaca path.

In the S-band measurements, no deviation of antenna gain from the plane wave gain was observed, as shown in Table I. In the X-band measurements, however, significant amount of deviation was observed. With the Wethersfield signal, the deviation tends to appear at 6-foot antenna and becomes definite at 10-foot antenna measurement. This is more conspicuous in the

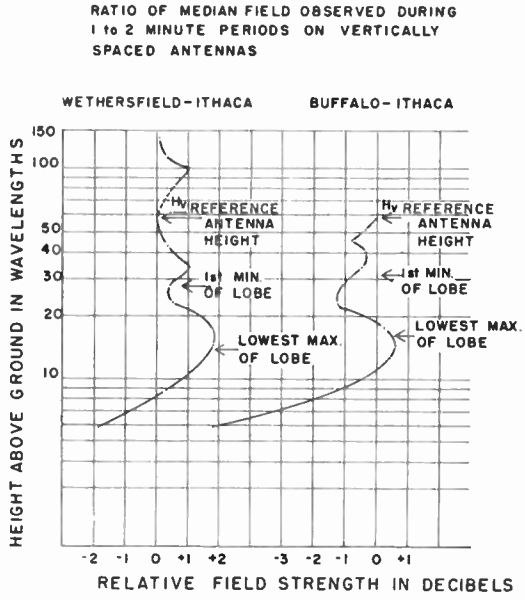

Fig. 10—Height gain observations (S band).

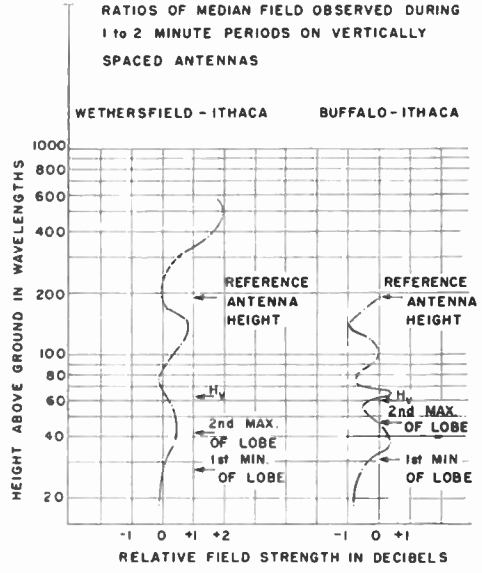

Fig. 11—Height gain observations (X band).

measurement with the Buffalo signal. With the aid of the knowledge of correlation distance, the maximum useful antenna size would be estimated by measurement as a value close to 6 feet between 6 and 10 feet for the Wethersfield-Ithaca path, and a value close to 6 feet between 4 and 6 feet for the Buffalo-Ithaca path.

Height Gain

Two 4-foot paraboloid antennas were used in the measurements. One is for recording of the signal power at various heights and the other is for reference. The results of the measurements are plotted in Figs. 10 and 11, where the height of the reference antenna, the height of the antenna lobe structure, and the predicted value of the practical limitation on antenna height H_V as computed by (5) are indicated by arrows.

Clear lowest lobe structures are seen on the S-band recording but not on the X-band. This may be attributed to the fact that the minimum antenna height is limited by the size of the antenna. Around and above the height H_V, the lobe structure becomes irregular and the amplitude of the height gain variation stays in the order of one db, which is comparable with the error of measurement.

Fading Rates

An example of the signal fluctuation as recorded on the Brush tape is shown in Fig. 12. Signals were sampled for about one minute every one and half or three hours at the tape speed of one inch per second.

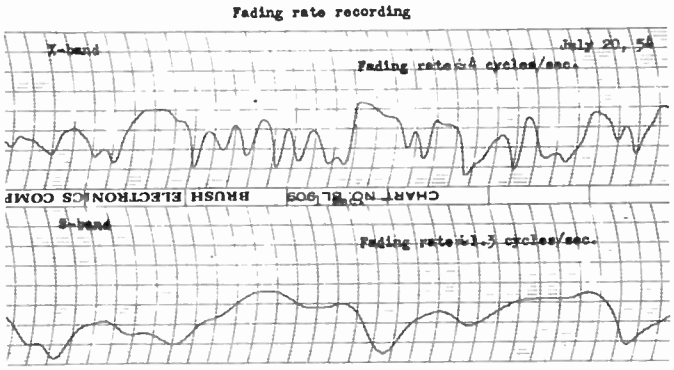

Fig. 12—Example of fading signals as recorded on Brush recording tape.

Rather coarse values of average fading rates were obtained by dividing number of significant peaks of signal fluctuation by corresponding time interval. Minor variations were discarded in counting number of peaks. Data obtained this way are shown in Fig. 13.

Predicted fading rates as computed by (6), assuming a root-mean-square turbulent velocity of 2 meters per second and a scale of turbulence of 16 meters, are shown in Table III below.

TABLE III

	Wethersfield-Ithaca path	Buffalo-Ithaca path
Drift velocity of scatterer	1–10 meters/second	1–10 meters/second
S-band	0.6–6 cycles/second	0.7–7 cps
X-band	2–20 cycles/second	2.5–25 cps

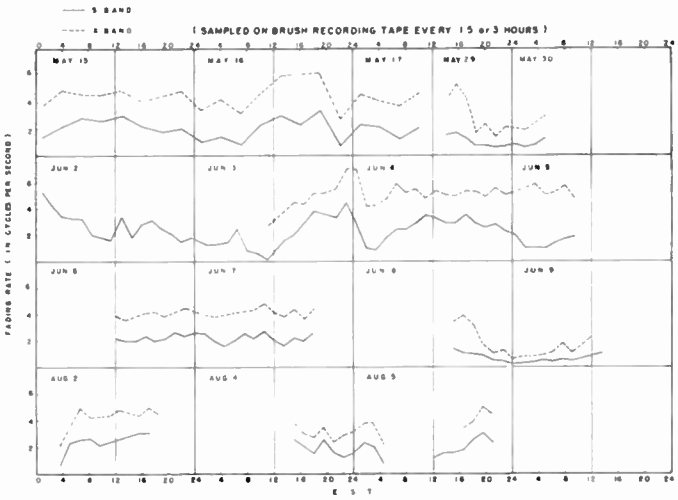

Fig. 13—Variation of fading rate.

ACKNOWLEDGMENT

The author wishes to express his appreciation to Dr. W. E. Gordon for his guidance, and to Messers N. H. Bryant, S. M. Colbert and L. D. Arons of Cornell University for their help. His further gratitude is due to the staff of the Cornell Radio Astronomy Laboratory for their able assistance in carrying out this study.

VHF Tropospheric Overwater Measurements Far Beyond the Radio Horizon*

L. A. AMES†, P. NEWMAN†, SENIOR MEMBER, IRE, AND T. F. ROGERS†, MEMBER, IRE

Summary—**Using a high-power radar-type transmitter near Boston, Massachusetts, point-to-point measurements have been made at a frequency of 220 mcps on 200- and 400-statute-mile overwater paths extending along the east coast. Comparisons are made with similar data available for overland paths. Correlations between the shorter path field-strength data and sea echo back-scatter near the transmitter site are indicated. Airborne field-strength measurements have also been made out across the North Atlantic Ocean to a distance in excess of 400 miles; the variation of field strength with distance is graphically displayed by this technique.**

INTRODUCTION

DURING THE past several years it has been clearly established that vhf-uhf tropospheric field strengths deep within the diffraction region are consistently much higher than smooth earth diffraction theory predicts for a homogeneous atmosphere. This paper reports on that part of the Air Force Cambridge Research Center's propagation research program which concerns itself particularly with overwater vhf point-to-point and airborne field-strength measurements at distances far beyond the radio horizon.

The amount of quantitative information available concerning such overwater tropospheric propagation is very small. The work of Katzin, Bauchman, and Binnian[1] in the Caribbean Sea and of Megaw[2] in the North Sea did not include the measurement of point-to-point field-strength variations with time; Robbins[3] reported measurements on a 130-mile southern path obtained during one season only.

It seems desirable, therefore, to establish median signal strength levels under both summer and winter conditions, to ascertain the statistical departures from these median values, to correlate such signal levels with the local radio-meteorological situation to the extent possible, and to determine the dependence of the median signal level upon the path length.

Certain of these results have been reported earlier before the International Scientific Radio Union[4] and at the Boulder Dedication Meeting of the National Bureau of Standards Laboratories.[5] The present paper is an abbreviated version of an AF Cambridge Research Center report bearing the same title.

EQUIPMENT

The transmitter, located on the coast south of Boston near Scituate, Massachusetts, is a 220-mcps experimental radar which radiates a peak power of about one megawatt during a 50-microsecond pulse interval; the pulse repetition rate is 60 cps. This power is radiated from a large 70-foot × 30-foot dipole array having a half-power beam width of 4 degrees in azimuth and 8 degrees in elevation. It has a measured gain of 27 decibels. The array is located at the water's edge, is 77 feet above mean sea level and is capable of being electrically rotated through a 60-degree azimuth angle by adjusting the phase relationships of various dipoles in the array.

Several receiving antennas were used on the ground at different times. All were of the Yagi type and had gains of between 13 and 18 db above isotropic. The airborne antenna was a 10-element single-bay Yagi which, when properly matched, yields a gain of about 13 db above isotropic.

An AN/APR-4 intercept receiver was modified for use as a field strength recorder: the rf bandwidth was reduced to 500 kilocycles, a low noise 220-mcps preamplifier added, and the dynamic range increased to 60 db, which could be further extended by a 100-db variable step attenuator. The receiver output was fed to a pulse peak reading circuit and thence to an Esterline Angus strip chart recording meter. This combination of receiver, peak reader and E.A. metering circuit had a sensitivity of better than 135 dbw.

POINT-TO-POINT MEASUREMENTS

Most measurements reported here were obtained on a 200-statute-mile overwater path between Scituate, Massachusetts, and Seal Harbor on Mt. Desert Island, Maine; see Fig. 1 (next page). Additional data were obtained on a 400-statute-mile path, the major portion of which is also overwater, from Scituate to Chincoteague, Virginia. In both cases, the receiving antenna was elevated some 20 feet above the immediate terrain and was located within 300 feet of the shoreline.

In order to obtain a warm-cold weather comparison of signal strength, measurements were made on the

* Original manuscript received by the IRE, July 5, 1955.
† Air Force Cambridge Research Center, Cambridge, Mass.
[1] M. Katzin, R. W. Bauchman, and W. Binnian, "3 and 9 cm propagation in low ocean ducts," PROC. IRE, vol. 35, pp. 891–905; September, 1947.
[2] E. C. S. Megaw, "Scattering of electromagnetic waves by atmospheric turbulence," *Nature*, vol. 166, pp. 1100–1105; December, 1950.
[3] R. L. Robbins, "Measurement of path loss between Miami and Key West at 3675 mcps," TRANS. IRE, vol. AP-1, pp. 5–8; July, 1953.
[4] P. Newman, L. A. Ames, and T. F. Rogers, "VHF field strength measurements far beyond the radio horizon," Joint URSI—IRE and Amer. Geophys. Union Meeting, Washington, D. C.; May, 1954.
[5] T. F. Rogers, "VHF propagation beyond the horizon," Dedication Scientific Meetings, National Bureau of Standards, Boulder (Colorado) Laboratories; September, 1954.

200-mile path during August of 1953 and January of 1954, since information from other sources indicated that data gathered during these two months would probably be representative of the annual extremes in

Fig. 1—Map showing propagation paths. Solid lines are point-to-point paths; dotted line indicates airborne course.

signal variation. Fig. 2 summarizes the data recorded during the summer and winter periods. Median values have been estimated from E.A. chart records for every valid 15-minute interval; this figure, therefore, represents some 800 such individual median values. This method of obtaining signal level medians introduces some error and, including other possible measurement error sources, it seems reasonable to assign an overall accuracy estimate of ±2 db to these final graphed values.

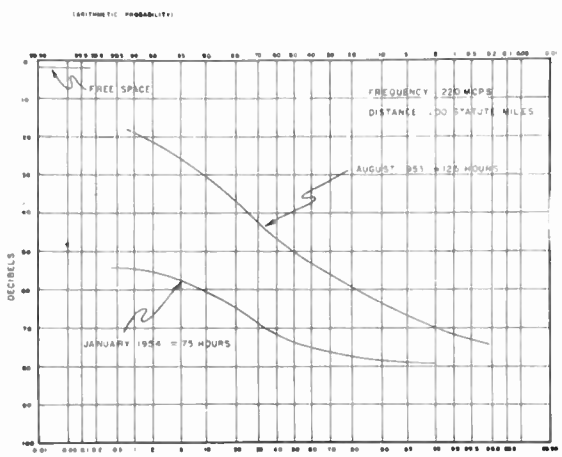

Fig. 2—Field strength distribution for 200 mile overwater path.

Assuming, for the distance and antenna beamwidths utilized, that there is no appreciable departure from the antenna plane-wave gain values, the summer median signal level is seen to be 48 db below free space—the winter value, 73 db. This indicates a year-round median value of some 61 ±2 db below free space. This is a somewhat lower median loss than the overland values reported recently by Rice and Daniel[6] on 100 mcps; i.e., 66–68 db below free space for comparable antenna heights, and by Barsis, Bean, Herbstreit, Hornberg and Norton[7] on 1,046 mcps—65 db below free space at 225 miles with a transmitting antenna height of about 3,000 feet above the foreground. The summer to winter median variation of 24 db is a large one compared with certain other similar results. For instance, the NBS group[7] reports a summer/winter median ratio of 13 db; the 93-mc–150-mile data of Wickizer and Braaten[8] indicates 15 db. However, if all of our summer data hours known to be markedly influenced by super-refraction (see below) are cast out and the remaining, more "normal," hours then analyzed, the resulting summertime median is 5 db lower and a summer/winter median ratio of 19 db obtains.

Of particular note is the high signal level reached for short periods of time during the summer: while the graphed values approach to within 17 db of free space for 1 per cent of the time, study of the E.A. charts indicates that for some shorter time periods the receiver was saturating for very high signal levels and it would not be surprising to find signal levels very close to free space occurring upon occasion.

During the interval that field strength recordings were being made at Seal Harbor, photographs of the sea echo observed on the radar A-scope were taken every few minutes. It is to be expected that the extent of the sea echo return would bear some relationship to the lower atmosphere refractive index conditions prevailing along at least the initial portion of the path, and the studies of Wickizer and Braaten[9] and of Pickard and Stetson[10] have indicated some long-term correlation between beyond-the-horizon field strengths and refractive index values.

Fig. 3 (next page) graphs both time variation of signal received at Seal Harbor and that of maximum distance of sea echo during summer period. It can be seen that extreme super-refraction or elevated layer propagation conditions prevailed during many successive hours during August 7 and 8, with echoes being returned from distances between 120 and 220 statute miles. These times correspond well to the intervals of maximum-received signal strength, as might be expected.

[6] P. L. Rice and F. T. Daniel, "Radio transmission loss vs distance and antenna height at 100 mc," TRANS. IRE, vol. AP-3, pp. 59–62; April, 1955.

[7] A. P. Barsis, B. R. Bean, J. W. Herbstreit, K. O. Hornberg, and K. A. Norton, "Propagation of Radio Waves Over Land at 1,046 mc," N.B.S. Rep. 2494; May 1, 1953.

[8] G. S. Wickizer and A. M. Braaten, "Field strengths recorded on adjacent FM channels at 93 mc over distances from 40 to 150 miles," PROC. IRE, vol. 40, pp. 1694–1699; December, 1952.

[9] G. S. Wickizer and A. M. Braaten, "Propagation studies on 45.1, 474 and 2,800 megacycles within and beyond the horizon," PROC. IRE, vol. 35, pp. 670–679; July, 1947.

[10] G. W. Pickard and H. T. Stetson, "Comparison of tropospheric reception of 44.1 mc, and at 92.1 mc, over the 167-mile path, Alpine, New Jersey to Needham, Massachusetts, 1947–1948," *Jour. Atmos. Terr. Phys.*, vol. 1, pp. 32–36; January, 1950.

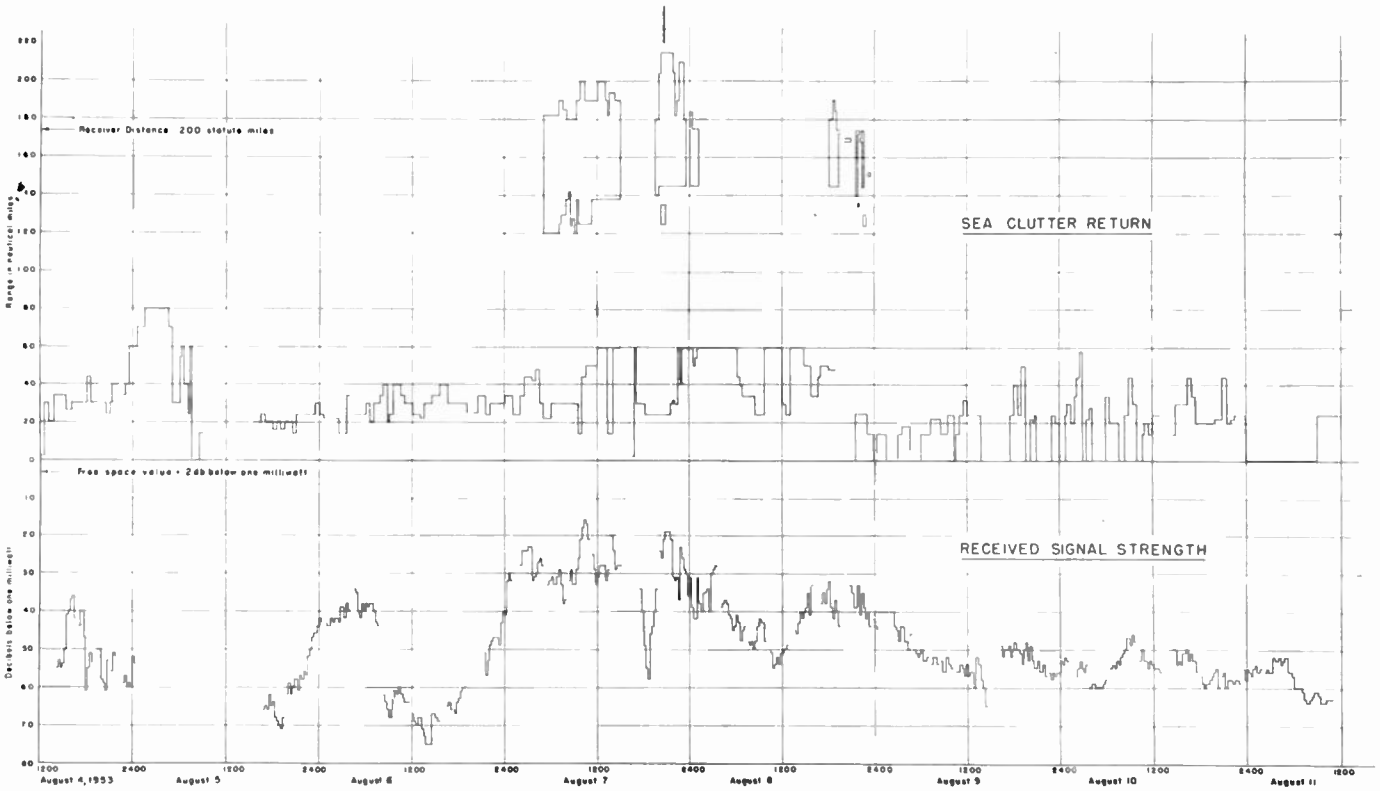

Fig. 3—Comparison of received signal level and sea clutter return on 200-mile path during the entire summer measurement program.

An hour-to-hour comparison, however, does not indicate any apparent correlation. If a gross comparison is made between the average sea clutter extent during the two measurement periods, it is found that there is a summer-winter ratio of about 1.4; it was previously noted that the summer median signal was 24 db over the winter median.

During the summer measurement period of August 9–10, fog conditions were reported all along the New England coast northward from Boston to Eastport, Maine. The fog was reported as particularly heavy during August 10, when a visibility of less than $\frac{1}{4}$ mile was recorded in Boston. There is no obvious large-scale influence exerted by such fog conditions on the signal level: at other periods field strength values both appreciably lower and higher were measured.

Several times during the summer period measurements were conducted in an attempt to determine whether or not the transmitting radiation pattern was broadened. The transmitting antenna was stepped across a total of 8 degrees in 1-degree increments, and the median signal level estimated from the E.A. record for each of the one-minute periods during which the transmitting antenna was fixed in direction. Because of the large field-strength variations which take place in a minute's time, the individual median values necessarily showed some scatter and the pattern obtained during a single run exhibited some distortion. Admittedly, such distortions could be evidence of some true short-term variation in the pattern; upon averaging several runs, however, it was found that the original 4-degree half-power horizontal beamwidth was very closely maintained. Booker and de Bettencourt[11] suggest that any beam-swinging experiment conducted to measure the off-path scattering should involve simultaneously changing both the transmitting and receiving antennas in order that the spatial volume common to the two antennas not be radically altered. In our case it was not believed necessary to swing the receiving antenna, since it has such a relatively broad horizontal pattern compared with the 4-degree transmitting beam. From the scatter theory calculations made by Gordon,[12] it is estimated that the scattering angle at 200 miles should be about 1.5 degrees, and, therefore, probably incapable of resolution by a 4-degree beam; our measurements, therefore, are not in disagreement with this scattering theory prediction.

Measurements of the short-time fading rate of the received signal—really a measurement of the average zero-crossing rate in the fading rate spectrum—results in a value of about one-to-three cycles per minute. It is interesting to note that this fading rate was observed to change during the beam-swinging experiments. As the transmitting antenna was turned away from the great circle heading of the receiving point, the fading rate invariably increased; when the beam was so swung that the received power was down about 6 db, the fade rate was approximately doubled.

[11] H. G. Booker and J. T. de Bettencourt, "Theory of radio transmission by tropospheric scattering using very narrow beams," PROC. IRE, vol. 43, pp. 281–290; March, 1955.
[12] W. E. Gordon, "Radio scattering in the troposphere," PROC. IRE, vol. 43, pp. 23–28; January, 1955.

During August, 1954, a total of 40 data hours were gathered on a 400-statute-mile path extending over southern Massachusetts, Rhode Island, and the Atlantic Ocean. Receiving point was on the Virginia coast near Chincoteague (see Fig. 1). Of 400 miles approximately 320 are over water. The median signal level was measured to be 98 db below free space; i.e., a further decrease of 50 decibels from the 200-mile path summer median and 38 db below the indicated 200-mile path yearly median. This signal level is appreciably lower than might have been expected from extrapolation of the 200-mile overwater path data at the attenuation rate indicated by our overwater airborne measurements (see below). Two reasons may be advanced for this: (1) The sample of received signal level was a relatively short one and cannot be expected to be representative of a longer time summer median; the 15-minute median signal level estimates varied over a range of about 50 db during the measurement period and (2) in contrast to the 200-mile overwater path, the transmitter views a horizon angle of very nearly one degree when directed toward Chincoteague. Measurements (as yet unpublished) by our co-workers indicate that at an increased horizon angle of one degree, a signal level reduction of 8–10 db from the zero angle case is to be expected.

Airborne Measurements

Mounting of ten-element 220-mcps Yagi antenna in tail section of an AF C-54 (DC-4) aircraft, and the installation therein of essentially the same equipment used in the ground measurements, enabled airborne records of tropospheric field strength to be obtained.

During the winter of 1953–54 several flights were made out over the North Atlantic on a general course directed toward Sable Island (Fig. 1). This course enabled the aircraft to conduct measurements entirely over water, remaining reasonably close to land to provide a terminal navigation check point over island.

On most of the flights, as the aircraft flew away from the transmitting site keeping its antenna pointed toward Scituate, the transmitting antenna pattern was swung back and forth about the aircraft course at a regular rate. This procedure ensured that a true sample of the emitted narrow-beam energy was always received by the aircraft even if winds aloft caused a drift away from the initial heading; also, the reception of a periodic signal in this manner made possible its ready identification in the presence of interference. The antenna sweep rate was adjusted so that the length of time during which the beam was directed at the aircraft was sufficient for the receiving and recording equipment to reach essentially steady state.

The flights were made at several altitudes between 500 and 15,000 feet, all out to distances of 500 statute miles. In every case, regardless of altitude, signals were received out to 400 miles. There is some indication that signals were received to greater distances at the higher altitudes, thereby indicating some height-gain, but the evidence is not conclusive inasmuch as day-to-day changes in signal level are sufficient to mask any comparable variation with altitude.

Fig. 4 is representative of the results obtained. Initially, the received signal is seen to vary considerably from point-to-point; here the aircraft is flying through the direct ray-sea reflected ray lobe structure as modified by the transmitting pattern and, because of the beam-swinging measurement technique, the "sampling" interval is commensurate with the lobe interval. As the radio horizon is approached (about 150 statute miles at the aircraft altitude of 10,000 feet) the diffraction zone is entered. Diffraction field strengths are then recorded out to about 180 miles, where the transition to the extra-diffraction propagation mode is abruptly made. Recordings are continued thereafter out to 500 miles, although the signal-to-noise ratio generally became too small to measure accurately in the 400–450 mile region.

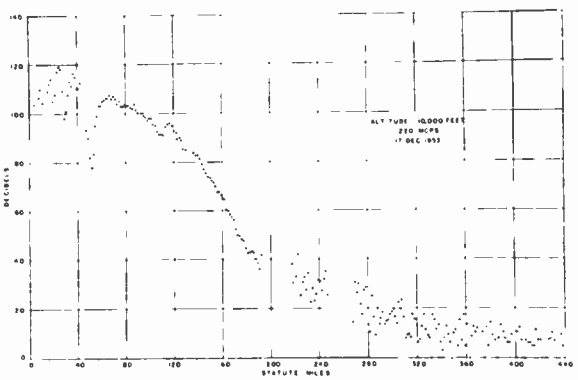

Fig. 4—Wintertime overwater field strengths recorded in an aircraft at 10,000 feet.

In Fig. 4 all valid data points are graphed. Blank spaces correspond to transmitter down time or to periods in which either the aircraft position was not known with sufficient accuracy or during which it was "dog-legging" back to its proper course. Points on the baseline are times at which a signal should have been received but was not. Because of rather severe experimental difficulties, we believe absolute accuracy of these measurements is known only within ± 5 db; relative accuracy within any one run is probably maintained within ± 2 db. At 200 miles, 0 decibel on the ordinate; i.e., receiver noise level, is close to 90 db below free space.

Fig. 5 (next page) offers for comparison a 500-foot flight over essentially the same path with same equipment and during the same winter season. Again, signal level is sufficient to provide good data out to somewhat beyond 400 miles. Two flights were made at 500 feet on successive days, and on this basis a field strength attenuation rate of some 0.13 db per statute mile for low antenna heights was deduced; these low-altitude flight results were presented in more detail in a recent publication,[13] in which both the distance and frequency dependence of this attenuation are discussed.

[13] T. F. Rogers, "VHF field strength far beyond the radio horizon," Proc. IRE, vol. 43, p. 623; May, 1955.

While some indication of the changed nature of the field strength at different distances is given in Fig. 4, a more graphic indication is presented in Fig. 6. On one flight low wind velocities and careful navigation permitted "searchlighting" the aircraft with the transmitting antenna: the aircraft flew essentially straight out along this great circle radiation path heading for a distance of 1,000 miles, and recordings were made on a

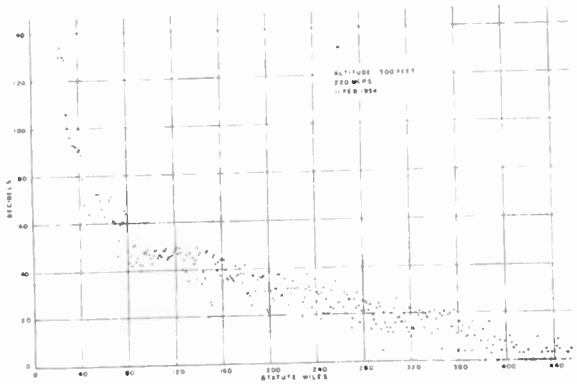

Fig. 5—Overwater measurements at an aircraft altitude of 500 feet.

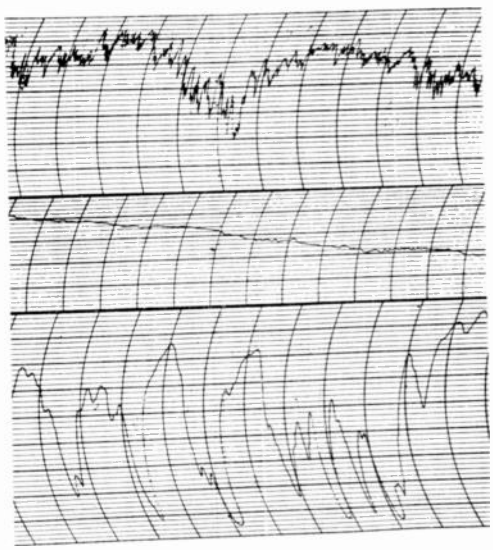

Fig. 6—Comparison of airborne-measured fading rates and intensities. Top chart sample: within line of sight. Middle chart: diffraction region. Bottom chart: extra-diffraction region.

continuous basis. In Fig. 6, three sections of the E.A. chart are reproduced. In each section of chart the relative amplitude and time scale are the same: each large vertical division represents a field strength change of about 3 db and the total time in each case is about 2 to 3 minutes. The top section is a portion of the chart representative of the field strength variation within line of sight; the large lobe structure is readily apparent with the usual small scintillation type of fading superimposed upon it. The center chart section is a sample of the field strength near the radio horizon; i.e., in the diffraction region; now the rate of decay is readily apparent and the fading has essentially disappeared. In the lower section the extra-diffraction, or scatter, region is being flown through. Now the decay rate is masked by the intense short-time variations; of particular note is that, compared with the line-of-sight short-time variations, these intense fluctuations take place at a much slower rate. The fading rate observed in the air compares closely with that observed on the ground; i.e., one to three fades per minute.

Conclusions

Several conclusions may be drawn from these experiments. For a temperate zone overwater propagation path at 220 mcps and 200 miles, the median signal level is probably at least as high as on comparable overland smooth-earth paths. As might be expected, the signal level variation is very large during the summer months when super-refractive and elevated layer conditions are prevalent; the seasonal median level change appears to be greater than that observed by others on overland paths.

There is a good correlation between the seasonal median received signal levels and the refractive index of the lowest few hundred feet of the troposphere near the transmitting terminal as indicated by the extent of sea return. No correlation has been found on any short time basis, except for the highest summertime signal levels associated with abnormal refractive index gradients. Heavy fog along the path exerts no obvious influence on the signal level. The measurements show that any off-path scattering must be confined to an angle less than 4 degrees at 200 miles, a not unexpected result from the viewpoint of the turbulent scattering theory.

Airborne overwater measurements of the distance-attenuation law during the winter season indicate a total loss of some 13 db/100 statute miles at heights of a few hundred feet. The evidence for any large height gain between 500 and 15,000 feet is inconclusive. The field-strength variations measured in the air within the extra-diffraction region show an intense minute-to-minute variation of 10–20 db.

Further airborne measurements on both overwater and overland paths with more sensitive equipment are required to give additional insight into seasonal variations, height-gain, attenuation beyond 400 miles, and the influence of terrain. A program of such measurements is now in progress.

Acknowledgment

The authors wish to express their appreciation to many co-workers who assisted both in making the ground and airborne measurements and in the data reduction. Particular mention should be made of the contributions of J. Frazier, R. Barrett, E. Bosma, T. Wilson, Lt. H. Chapman, and Margaret Hill, all of the Propagation Laboratory, AFCRC. Personnel of the Antenna Laboratory designed and constructed both the ground and airborne Yagi antenna arrays. The success of the airborne measurements has been, to a great extent, due to the competent navigation and piloting, provided by the C-54 Air Force military crew.

Forward Scattering of Radio Waves by Anisotropic Turbulence*

HAROLD STARAS†, SENIOR MEMBER, IRE

Summary—This paper extends the theory of tropospheric scatter by deriving the appropriate formulas for the important radio system parameters under the assumption that the turbulence is anisotropic; i.e., that the scale of turbulence in the horizontal dimension is different from the scale of turbulence in the vertical dimension. The frequency dependence of the scattered radiation is the same for anisotropic large-scale turbulence as for isotropic. Furthermore, those radio systems parameters which depend only on the rate of decrease of scattered energy with elevation angle (such as the vertical correlation function and height gain) remain unchanged under the assumption of anisotropy while those parameters which depend on the energy coming out of the great circle plane (such as the horizontal correlation function) can be influenced quite substantially by anisotropy. Several other parameters such as the longitudinal correlation function, bandwidth of the medium and effective antenna gain may also be influenced by anisotropy but generally to a lesser extent. A comparison is made between our theory and some recent NBS data—indicating that anisotropy does exist.

I. Basic Formulation

IN A RECENT paper,[1] Gordon has expressed the received scattered power measured relative to free space as

$$\frac{P}{P_{FS}} = Kd^2 \int \frac{\sigma(\theta, \chi)}{R_0^2 R^2}\, dv$$

where $\sigma(\theta, \chi)$ is the scattering cross section per unit volume and the other parameters are defined in Fig. 1.

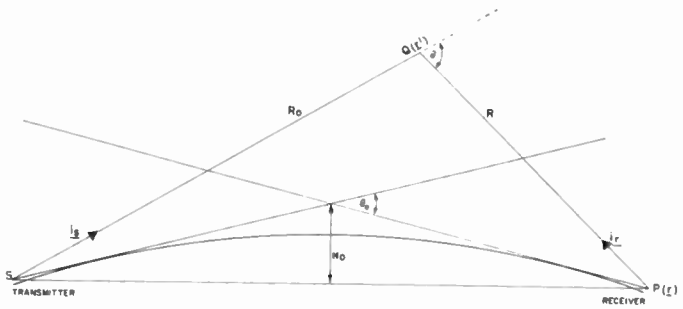

Fig. 1—The path geometry of a typical scatter circuit.

If we express the current in the load due to the scattered radiation relative to the rms current which would exist if the antennas were in free space, we obtain[2]

$$I = \frac{\sqrt{2}\, d\beta^2}{4\pi} e^{j\omega t} \int \frac{\epsilon_1(r', t)}{\epsilon_0} [f_0(\Omega_0) \cdot f(\Omega)] \frac{e^{-j\beta(R_0' + R')}}{R_0' R'}\, dr'. \quad (1)$$

In (1), $f_0(\Omega_0)$ is the normalized antenna voltage pattern of the transmitting antenna. It is a vector in the direction of the electric vector generated by the transmitting antenna and is a function of the spherical angles θ_0, ϕ_0 measured from the transmitter. It is to be noted that no restriction to conical beams is intended. The function $f(\Omega)$ plays the same role for the receiving antenna. ϵ_0 is the average dielectric constant of the medium, ϵ_1 represents the random variation in the dielectric constant and $\beta = 2\pi/\lambda$. Eq. (1) is the starting point for the development of the statistical parameters of the scattered signal. It is to be noted that f_0 and f have maximum values of unity along the antenna beam axes.

II. The Average Scattered Power

The average scattered power is, of course, given by

$$\langle \mathrm{II}^* \rangle = \frac{d^2\beta^4}{8\pi^2} \iint \left\langle \frac{\epsilon_1(r, t)}{\epsilon_0} \frac{\epsilon_1(r', t)}{\epsilon_0} \right\rangle (f_0 \cdot f)(f_0', f') \times \frac{e^{j\beta(R_0 - R_0' + R - R')}}{R_0 R R_0' R'}\, dr dr'. \quad (2)$$

Now

$$\left\langle \frac{\epsilon_1(r, t)}{\epsilon_0} \frac{\epsilon_1(r', t)}{\epsilon_0} \right\rangle = N(r - r')$$

is the space correlation function of ϵ_1. $N(r - r')$ is a function which has the property that $N \to 0$ for $|r - r'| > l$ (l is referred to as the scale of turbulence). Because of this property, the major contribution to the double volume integral in (2) occurs when r and r' are within a distance l of each other. All antenna patterns are sufficiently broad at the distances considered in this paper that we may consider $f_0 \cdot f$ at the point r to be approximately equal to $f_0' \cdot f'$ at the point r'. Also $R_0 \cong R_0'$ and $R \cong R'$. Eq. (2) may therefore be written

$$\langle |I|^2 \rangle = \frac{d^2\beta^4}{8\pi^2} \iint N(r - r') \frac{(f_0 \cdot f)^2}{R_0^2 R^2} e^{j\beta(R_0 - R' + R - R')} dr dr'.$$

Again since major contribution to above integral comes when $r = r'$, we assume that wave may be considered plane over such a region. We, therefore, write

$$e^{j\beta R_0} \cong e^{j\beta i_s \cdot r} \qquad e^{-j\beta R_0'} \cong e^{-j\beta i_s \cdot r'}$$
$$e^{j\beta R} \cong e^{j\beta i_r \cdot r} \qquad e^{-j\beta R'} \cong e^{-j\beta i_r \cdot r'}.$$

In the above, i_s is the unit vector from S to Q and i_r is the unit vector from P to Q (see Fig. 1). The above integral may, therefore, be written

$$\iint N(r - r') \frac{(f_0 \cdot f)^2}{R_0^2 R^2} e^{j\beta(i_s + i_r) \cdot (r - r')} dr dr'.$$

* Original manuscript received by the IRE, July 22, 1955. Based on a thesis submitted by the author to the Graduate Faculty, University of Maryland, in partial fulfillment of the requirements for the Ph.D. degree (1955).

† Engineering Products Div., RCA, Camden, N.J.

[1] W. E. Gordon, "Radio scattering in the troposphere," PROC. IRE, vol. 43, pp. 23–28; January, 1955.

[2] H. Staras, "A Mathematical Study of Beyond the Horizon Scatter Propagation." Ph.D. dissertation on which this paper is based. See Section I in particular.

From Fig. 2 we see that $\beta(i_s+i_r)=\Gamma$ has a magnitude, $\Gamma=2\beta\sin\theta/2\cong\beta\theta$ (θ being the scattering angle) because $|i_s+i_r|=\sqrt{2(1-\cos\theta)}=2\sin\theta/2$.

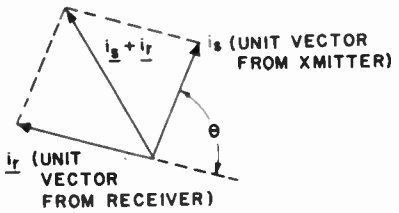

Fig. 2—Evaluating the scattering law dependence on angle and frequency.

We now keep r fixed and introduce $\rho=r-r'$ and since $N(\rho)$ goes to zero in a length l much smaller than a linear dimension of the volume of integration, we can formally extend the integration of ρ over all of space. The average scattered power becomes

$$\langle|I|^2\rangle=\frac{d^2\beta^4}{8\pi^2}\int\frac{(f_0\cdot f)^2}{R_0^2R^2}\left\{\int N(\rho)e^{iv\cdot\rho}d\rho\right\}dr. \qquad (3)$$

The inner integral over ρ is a function of r because Γ, being a function of the scattering angle θ is a function of r.

We will at this point refer to the inner integral as the scattering coefficient and denote it by $S(\theta)$. From (3) we note that

$$\langle|I|^2\rangle\sim\beta^4\int\frac{(f_0\cdot f)^2}{R_0^2R^2}S(\theta)dr.$$

($\sim$ means proportional to)

A fair amount of experimental evidence exists[3,4] that the average scattered power is quite insensitive to frequency changes from 50 mc to 2,000 mc, approximately. This suggests very strongly that we take $S(\theta)\sim(\beta\theta)^{-4}$, at least for θ not too close to zero. It may be of interest to note that if the auto-correlation function of atmospheric turbulence were given by

$$N(r-r')=\exp\{-|r-r'|/l\}$$

then $S(\theta)\sim|1+(\beta l\theta)^2|^{-2}\cong(\beta l\theta)^{-4}$ for $l/\lambda\gg1$ (i.e., large scale turbulence). In the remainder of this paper, we will consider $S(\theta)$ to be of that form which makes the average scattered power independent of frequency.

III. The Correlation Functions

Associated with the "scatter" mechanism of signal transmission are other important circuit parameters which are required to be known if one is to intelligently design a reliable communication system utilizing "scatter" propagation. We have up to the present discussed the basic formulation for the average scattered signal as a function of distance and frequency. We will now discuss the basic formulation for spaced antenna correlation functions, the bandwidth of the medium, the height-gain function and the effective antenna gain on a scatter circuit, all under the general assumption that the turbulence may be anisotropic.

Space Correlation of the Received Signals

Consider the signal arriving at two nearby locations, labeled 1 and 2. Then

$$I_1\sim\int\frac{\epsilon_1(r,t)}{\epsilon_0}(f_0\cdot f)\frac{e^{j\beta(R_0+R_1)}}{R_0R_1}dr$$

$$I_2\sim\int\frac{\epsilon_1(r',t)}{\epsilon_0}(f_0'\cdot f')\frac{e^{j\beta(R_0'+R_2')}}{R_0'R_2'}dr'$$

where R_0, R_0', R_1, and R_2' are shown in Fig. 3. The correlation between I_1 and I_2, $\rho(I_1,I_2)$ is proportional to $\langle I_1,I_2^*\rangle$ which is given by

$$\langle I_1I_2^*\rangle\sim\int\int N(r-r')\frac{(f_0\cdot f)^2}{R_0^2R^2}e^{j\beta(R_0-R_0'+R_0-R_2')}drdr'.$$

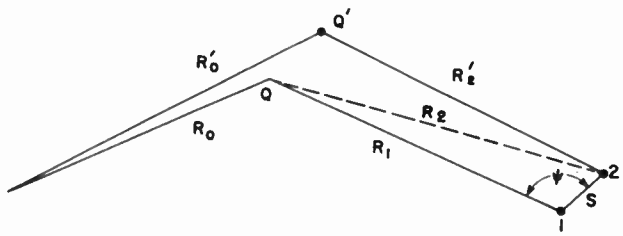

Fig. 3—The geometry for evaluating the space correlation functions.

From Fig. 3, we have

$$R_2=(R_1^2+s^2-2R_1s\cos\psi)^{1/2}\cong R_1-s\cos\psi\text{ for }s\ll R_1.$$

Therefore,

$$\langle I_1I_2^*\rangle\sim\int\frac{(f_0\cdot f)^2}{R_0^2R^2}S(\theta)e^{j\beta s\cos\psi}dr$$

The correlation between the envelope of the received signals[2] is given by

$$|\rho(I_1,I_2)|^2\sim\left|\int\frac{(f_0\cdot f)^2}{R_0^2R^2}S(\theta)e^{j\beta s\cos\psi}dr\right|^2. \qquad (4)$$

Frequency Correlation of the Received Signal

Consider two signals arriving via tropospheric scattering at a receiving antenna. Let one signal be coming at a frequency f_1 (propagation constant $=\beta_1$) and the second signal be coming at a frequency f_2 (propagation constant $=\beta_2=\beta_1+\Delta\beta$).

$$I_1\sim\int\frac{\epsilon_1(r,t)}{\epsilon_0}(f_0\cdot f)\frac{e^{j\beta_1(R_0+R)}}{R_0R}dr$$

$$I_2\sim\int\frac{\epsilon_1(r',t)}{\epsilon_0}(f_0'\cdot f')\frac{e^{j\beta_2(R_0'+R')}}{R_0'R'}dr'.$$

[3] K. Bullington, "Radio transmission beyond the horizon in the 40- to 4,000-mc band," PROC. IRE, vol. 41, pp. 132–135; January, 1953.

[4] J. W. Herbstreit, K. A. Norton, P. L. Rice, and G. E. Schafer, "Radio scattering in tropospheric propagation," 1953 IRE CONVENTION RECORD, Part 2, "Antennas and Communications," pp. 85–93.

The correlation between the two signals is $\sim\langle I_1, I_2^*\rangle$ where

$$\langle I_1 I_2^*\rangle \sim \iint \frac{N(r-r')}{R_0^2 R^2}(f_0\cdot f)^2 e^{j\beta_2(R_0-R_0'+R-R)'-j\Delta\beta(R_0+R)}dr dr'$$

$$\sim \int \frac{(f_0\cdot f)^2}{R_0^2R^2}S(\theta)e^{-j\Delta\beta(R_0+R)}dr.$$

Again, the correlation between the envelopes is given by

$$|\rho_f(I_1, I_2)|^2 \sim \left|\int \frac{(f_0\cdot f)^2}{R_0^2R^2}S(\theta)e^{j\Delta\beta(R_0+R)}\,dr\right|^2. \qquad (5)$$

We now proceed with the explicit evaluation of the parameters developed previously.

IV. The Scattering Coefficient Assuming Anisotropy

Before evaluating the various radio systems parameters, it is necessary to define a co-ordinate system with respect to which the point of the scattering volume is measured and then evaluate the scattering angle, θ, and the scattering coefficient, $S(\theta)$, in terms of our co-ordinates. We begin by defining an x, y, z Cartesian co-ordinate system centered at the intersection of the horizon planes from transmitter and receiver (see Fig. 1). A distance H_0 below this origin, we consider a Cartesian x, y, h co-ordinate system, where $h=z+H_0$. The scattering angle, θ, is then given by (see Fig. 4)

$$\theta = \theta_1 + \theta_2 \cong \sqrt{x^2+h^2}\left(\frac{1}{R_0}+\frac{1}{R}\right) \cong \frac{d\sqrt{x^2+h^2}}{R_0R}.$$

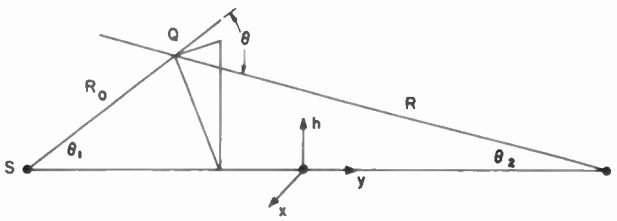

Fig. 4—As a function of the Cartesian co-ordinates x, y, h.

We next evaluate $S(\theta)$, which has been defined as [see (3)]

$$S(\theta) = \iiint_{-\infty}^{\infty} N(r-r')e^{i\Gamma\cdot(r-r')}dr'. \qquad (6)$$

We will consider the autocorrelation function of atmospheric turbulence, $N(r-r')$, to be of the form

$$N(r-r') = N\left(\frac{x-x'}{l_0}, \frac{y-y'}{l_0}, \frac{z-z'}{l_v}\right).$$

We are thus assuming that the scale of turbulence in the horizontal dimension is different from that in the vertical dimension. Letting

$$\xi = \frac{x-x'}{l_0}, \qquad \eta = \frac{y-y'}{l_0}, \qquad \zeta = \frac{z-z'}{l_v}$$

(6) can be written

$$S(\theta) = l_0^2 l_v \iiint_{-\infty}^{\infty} N(\rho)e^{iq\cdot\rho}d\rho, \qquad (7)$$

where ρ has components ξ, η, ζ and q has components $\Gamma_x l_0$, $\Gamma_y l_0$, $\Gamma_z l_v$. We next make the assumption that $N(\rho)=N(0)e^{-|\rho|}$; i.e., that the constant correlation surfaces are ellipsoids of revolution, and average scattered power is independent of frequency. This was discussed in Section II. We then obtain for $S(\theta)$ the expression

$$S(\theta) \cong \frac{8\pi l_0^2 l_v N(0)}{q^4},$$

where $q=|q| = l_0(\Gamma_x^2+\Gamma_y^2+r^2\Gamma_z^2)^{1/2}$ and $r=l_v/l_0$. The above expression for $S(\theta)$ is valid only for large scale turbulence; i.e., $(\beta l\theta)^2 \gg 1$ where l is the smaller of l_0 and l_v. This condition is apparently satisfied for all cases of interest on practical scatter circuits. We next evaluate the components of Γ. Fig. 5(a) shows the direction of the vector Γ which lies in the SQP plane which is rotated through an angle ϕ with respect to the great circle plane between the source S and the receiver P. The vectors i_s and i_r are unit radial vectors from S and P respectively. Fig. 5(b) shows the SQP plane only and defines a vector direction σ which appears vertical on the diagram but is not vertical in our scattering volume since the plane SQP is rotated through an angle ϕ with respect to the vertical plane. From considerations of geometry, $\Gamma_z=\Gamma\cos\alpha\cos\phi$, where $|\alpha| = |\theta_1-\theta_2|/2$ and $\cos\phi = h/(x^2+h^2)^{1/2}$. Since θ_1 and θ_2 are small quantities over the important part of the volume of integration, $|\theta_1-\theta_2|/2$ is particularly

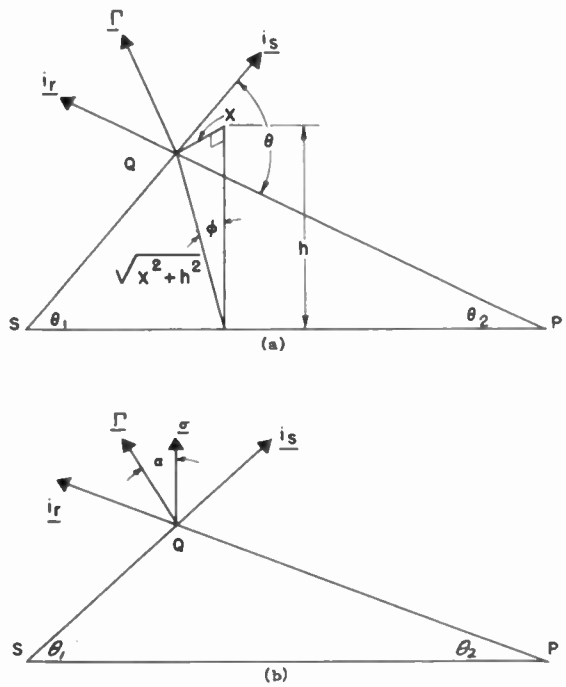

Fig. 5—Evaluating the scattering coefficient for anisotropic turbulence.

so. In the important transverse midplane between S and P, $\theta_1-\theta_2=0$. We may therefore take $\cos\alpha=1$ with a high degree of accuracy. Thus

$$\Gamma_z^2=\frac{\Gamma^2h^2}{x^2+h^2} \quad \text{and} \quad \Gamma_x^2+\Gamma_y^2=\frac{\Gamma^2x^2}{x^2+h^2}.$$

Finally, since

$$\Gamma^2\cong\beta^2\theta^2\cong\frac{\beta^2d^2}{R_0^2R^2}(x^2+h^2),$$

we may write

$$S(\theta)\cong\frac{8\pi rR_0^4R^4N(0)}{l_0\beta^4d^4}(x^2+r^2h^2)^{-2}.$$

The fundamental difference between the scattering coefficient for anisotropic turbulence as compared to isotropic turbulence as it is understood to date is that for isotropic turbulence we consider $r=l_v/l_0$ to be unity. The implication of r not equal to unity on various parameters of scattered radiation will be discussed next.

V. Evaluating the Radio Systems Parameters

The Average Scattered Power

From (3), and $S(\theta)$ as just derived, we obtain for the average scattered power measured relative to free space the following expression:

$$\langle I^2\rangle=\frac{r}{\pi l_0d^2}\int\int\int\frac{N(0)R_0^2R^2}{(x^2+r^2h^2)^2}(f_0\cdot f)^2dxdhdy. \quad (8)$$

The limits of integration are, of course, determined by the V-shaped region of integration. That part of the integrand given by $(x^2+r^2h^2)^{-2}$ comes from scattering angle law and decays fairly rapidly from its maximum value at $x=0$, $h=H_0$. If the antenna beams are more than about 2° wide, $(f_0\cdot f)$ is fairly constant over the important scattering volume determined by $(x^2+r^2h^2)^{-2}$. The dimensions of this volume are at most several miles on a side so that $R_0\cong R\cong d/2$ over the entire scattering volume. In what follows, we will take $f_0\cdot f$ as unity over the scattering volume (see last sentence of Section I). If, however, very narrow beams were used (less than 1°, say), then $f_0\cdot f$ could be less than unity over some part of the significant scattering volume. The average scattered power measured relative to free space would then be lower than for wider beam antennas. This phenomenon is referred to as antenna gain degradation or antenna-to-medium coupling loss. Taking $R_0\cong R\cong d/2$, integration over y is quite simple. The length of the volume is a function of height and from Figs. 1 and 4, we have $h=H_0+(\theta_0/2)y$. Therefore, the length of the volume is given by $(4/\theta_0)(h-H_0)=(4a/d)(h-H_0)$ where a is the radius of a 4/3 earth. Eq. (8) becomes

$$\langle I^2\rangle=\frac{rad}{4\pi l_0}\int_{H_0}^{\infty}\int_{-\infty}^{\infty}\frac{N(0)(h-H_0)}{(x^2+r^2h^2)^2}dxdh. \quad (9)$$

In the author's Ph.D. dissertation, many of the important radio systems parameters were evaluated assuming that $N(0)$ was constant throughout the atmosphere.[2] However, this assumption leads to the conclusion that the average scattered signal decays as $1/d$ relative to free space. This result is apparently not consistent with experimental data[2,5] which suggests a $1/d^5$ dependence relative to free space. To accommodate this data we may assume with Gordon[1,6] that in the important scattering regions, $N(0)$ decays with height as $1/h_e^2$ where $h_e=h-H_0/2$ is height above the earth. When substituted in (9), we obtain

$$\langle I^2\rangle\sim\int_{H_0}^{\infty}\int_{-\infty}^{\infty}\frac{(h-H_0)}{(x^2+r^2h^2)^2\left(h-\frac{H_0}{2}\right)^2}dxdh.$$

When evaluated, we do get a $1/d^5$ dependence. The degree of anisotropy measured by $r=l_v/l_0$ enters only as a multiplicative factor. Therefore, the frequency and distance dependence of the scattered radiation is not influenced by the assumption of anisotropy. We now evaluate the other important statistical parameters.

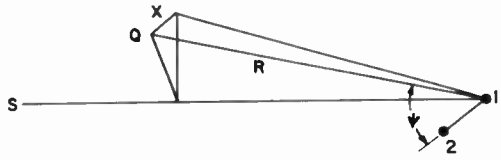

Fig. 6—Cos ψ for normal-to-path correlation.

Normal-to-Path Correlation

To evaluate any space correlation functions, we use (4) and evaluate cos ψ in our co-ordinate system terms, other functions already having been evaluated. In Fig. 6 we see, for normal-to-the-path correlation, $\cos\psi\cong 2x/d$. Our correlation function, thus, becomes

$$\rho_\perp(q)=\int_{H_0}^{\infty}\int_{-\infty}^{\infty}\frac{(h-H_0)e^{iqx}}{(x^2+r^2h^2)^2\left(h-\frac{H_0}{2}\right)^2}dxdh. \quad (10)$$

where $q=2\beta s/d$. It should be recalled that the normalized correlation function is given by $|\rho_\perp(q)/\rho_\perp(9)|^2$. We will, therefore, always neglect multiplicative constants. Integrating over x yields

$$\rho_\perp(q)=\int_{H_0}^{\infty}\frac{(h-H_0)e^{-qrh}}{\left(h-\frac{H_0}{2}\right)^2}\left(\frac{1}{h^3}+\frac{qr}{h^2}\right)dh.$$

This integral can be evaluated by separating the integrand into partial fractions, for example,

$$\frac{(h-H_0)}{h^3\left(h-\frac{H_0}{2}\right)^2}=\frac{16}{H_0^4}\left\{\frac{2H_0}{h-H_0/2}-\frac{1}{4}\frac{H_0^2}{(h-H_0/2)^2}-\frac{2H_0}{h}-\frac{3H_0^2}{4h^2}-\frac{H_0^3}{4h^3}\right\}.$$

[5] T. F. Rogers, "VHF field strength far beyond the radio horizon," Proc. IRE, vol. 43, p. 623; May, 1955.

[6] W. E. Gordon, "The Scattering of Radio Waves by Turbulence in the Troposphere," Res. Rep. EE 163, School of Elec. Engrg., Cornell Univ., Ithaca, N. Y.; September 15, 1953.

After such a separation, we integrate term by term. The final result is

$$-[4+2\Phi+(\Phi/2)^2]e^{-\Phi/2}E_i(-\Phi/2)$$
$$+[4-(\Phi/2)^2]E_i(-\Phi)-e^{-\Phi}\left(\frac{11}{4}+\frac{3\Phi}{4}\right), \qquad (11)$$

where $\Phi=r\beta sd/2a$. This function normalized to unity for $s=0$ and squared is plotted in Fig. 7. The correlation

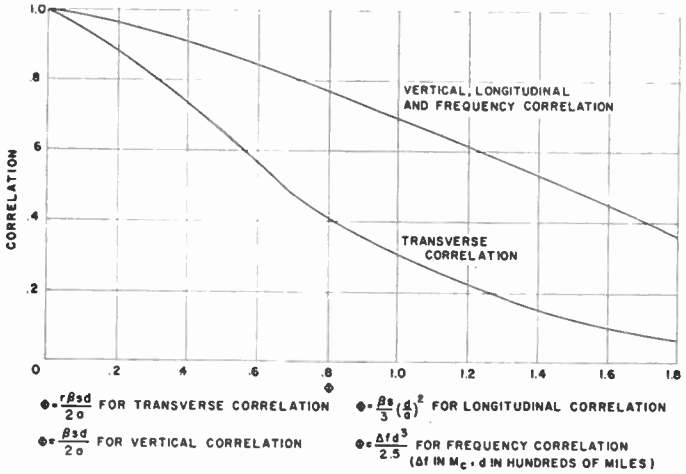

Fig. 7—Theoretical correlation functions.

drops to a low value when Φ becomes 0.8. This means that the separation between antennas necessary to achieve diversity action is given by

$$\frac{s}{\lambda}=\frac{0.8a}{\pi rd}\cong 0.3\frac{a}{rd}.$$

One should note that the diversity separation is inversely proportional to distance and the degree of anisotropy (i.e., to $r=l_v/l_0$). Fig. 8 shows a comparison of our theory with National Bureau of Standards[7] data.

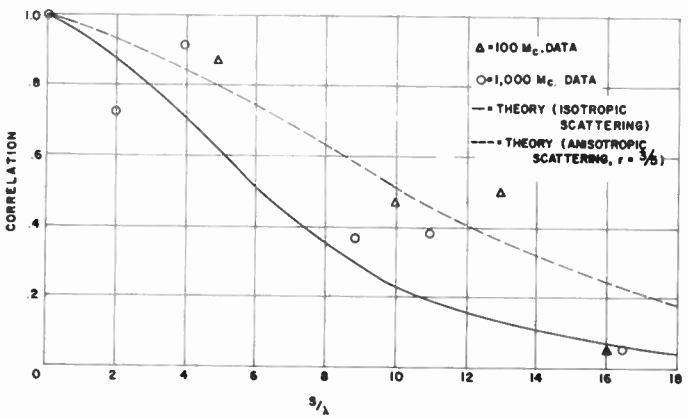

Fig. 8—Normal-to-path correlation, theory and data.

The solid theoretical curve (assuming isotropic scattering) seems to lie below the bulk of the data. If r were taken as 3/5, one obtains the dashed theoretical curve.

[7] A. P. Barsis, J. W. Herbstreit, and K. O. Hornberg, "The Cheyenne Mountain Tropospheric Propagation Experiments," NBS Circular, 554, Washington, D. C.; December, 1954.

These radio data suggest that anisotropy does exist, the degree of anisotropy being given by $r\cong 3/5$.

Vertically Separated Antennas

For this case, cos ψ of (4) becomes (see Fig. 9) $\cos\psi=h/R\cong 2h/d$.

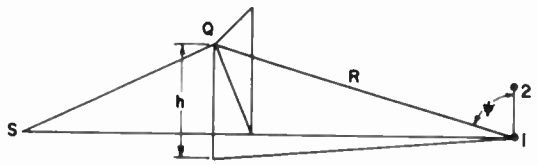

Fig. 9—Cos ψ for vertical correlation.

The vertical correlation function, therefore, becomes

$$\rho_v=\int_{H_0}^{\infty}\int_{-\infty}^{\infty}\frac{(h-H_0)e^{iqh}}{(x^2+r^2h^2)^2(h-H_0/2)^2}dxdh$$

where, as before, $q=2\beta s/d$. Integrating over x, we obtain (we can neglect multiplicative constants)

$$\rho_v=\int_{H_0}^{\infty}\frac{(h-H_0)e^{iqh}}{h^3(h-H_0/2)^2}dh. \qquad (12)$$

The most prominent feature of (12) is that the vertical correlation function is independent of r. Thus, the vertical correlation function will not be influenced by anisotropy. Eq. (12) was evaluated by the same procedure as discussed earlier. The final result is

$$\mathcal{E}_i\left(\frac{qH_0}{2}\right)e^{j(qH_0/2)}(8-jqH_0)$$
$$+\mathcal{E}_i(qH_0)\left(-8-j3qH_0+\frac{q^2H_0^2}{2}\right)$$
$$-e^{jqH_0}\left(5.5+j\frac{qH_0}{2}\right) \qquad (13)$$

where $\mathcal{E}_i(X)=\int_X^{\infty}\frac{e^{jx}}{x}dx$.

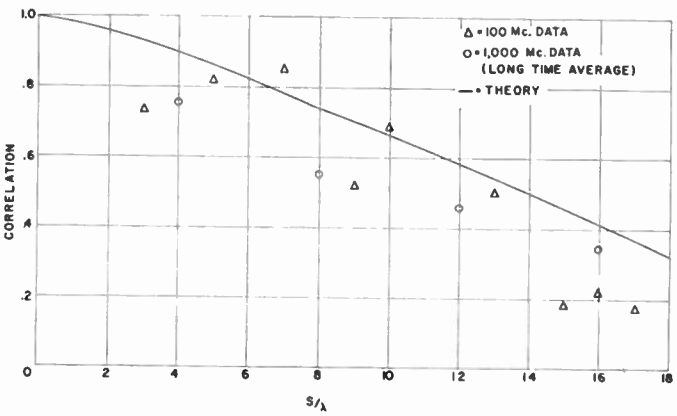

Fig. 10—Vertical correlation, theory and data.

The absolute square of this function is also plotted in Fig. 7. A comparison of our theory with NBS's data is shown in Fig. 10. We see that the theoretical curve lies at the upper end of the data points. In a previous report, where $N(0)$ was assumed not to decrease with

height, the theoretical curve lay below the data points.[2] This suggests that the NBS data on vertical correlation can best be interpreted with the assumption that $N(0)$ decays less rapidly than $1/h_e^2$ with height. As a matter of fact, a $1/h_e$ dependence of $N(0)$ explains the NBS data on the decay of signal strength with distance.

Longitudinally Separated Antennas

In this case, (see Fig. 11)

$$\cos\psi \cong 1 - \frac{\sin^2\psi}{2} = 1 - \frac{x^2+h^2}{2R^2}.$$

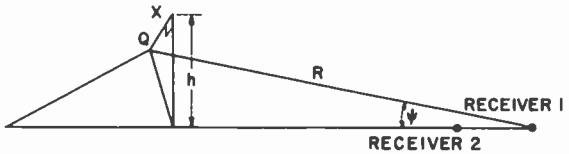

Fig. 11—Cos ψ for longitudinal correlation.

The longitudinal correlation function is then

$$\rho_L = \int_{H_0}^{\infty}\int_{-\infty}^{\infty} \frac{(h-H_0)e^{-jb^2(x^2+h^2)}}{(x^2+r^2h^2)^2(h-H_0/2)^2}\,dxdh, \quad (14)$$

where $b^2 = 2\beta s/d^2$ since $R \cong d/2$. Before evaluating the above integral, the following should be recognized. The width of the scattering volume (i.e., that value of $|x|$ which reduces the integrand to about its half-power point as compared to $x=0$) depends on rh. The case of isotropic scattering, corresponding to $r=$ unity, involves a width such that the variation of the incoming energy with h is the controlling factor; that is to say, that value of b^2 which reduces the correlation function due to the integration over h to a low value will hardly affect the correlation due to the integration over x. This phenomenon is discussed quite fully elsewhere.[2] Mathematically, the above means that b^2x^2 is a small quantity over the important part of the region of integration. If $r = l_v/l_0$ is less than unity, then the effective width of the volume is even less and b^2x^2 is an even smaller quantity than before over the important part of the scattering volume. It is very likely that if anisotropy does exist that r would be less than unity. It is expected then that in (14), we can neglect the term $e^{-jb^2x^2}$ leaving us with (after integration over x)

$$\rho_L = \int_{H_0}^{\infty} \frac{(h-H_0)e^{-jb^2h}}{h^3(h-H_0/2)^2}\,dh. \quad (15)$$

It is to be emphasized that the above is valid only for $r \leqq 1$. If r gets to be larger than unity, then the effective width of the volume will increase and the energy coming outside of the great circle plane may become more important than the energy coming in over the great circle plane in determining the longitudinal correlation function. The appropriate formula for this case has been evaluated in another report.[2] But since it is unlikely that r is greater than unity, we will restrict our consideration to (15). One more approximation is still possible. It is to be noted that the lower limit of integration is H_0. A graphical analysis of the amplitude of the integrand[6] shows that the integrand is zero at $h=H_0$, then rises rapidly to its maximum value and drops to its half-power point at $h \cong 3H_0/2$ and to less than its quarter power point at $h \cong 2H_0$. If in the phase term, h^2 is expanded as a Taylor series in the neighborhood of a point in the middle of effective scattering volume, e.g., $h=(5/4)H_0$, we get

$$h^2 = \frac{25}{16}H_0^2 + \frac{10}{4}H_0\left(h-\frac{5}{4}H_0\right) + \left(h-\frac{5}{4}H_0\right)^2.$$

The ratio of the quadratic term to the linear term in $h-(5/4)H_0$ is $(h-1.25H_0)/2.5H_0$. This ratio is at most 1/10 between half-power points, at most 3/10 between quarter power points. It would thus appear that the quadratic term in $h-(5/4)H_0$ is negligible over the important region of integration. Longitudinal correlation is then given by

$$\rho_L = e^{j(25/16)b^2H_0^2}\int_{H_0}^{\infty} \frac{(h-H_0)e^{-j2.5b^2H_0h}}{h^3(h-H_0/2)^2}\,dh. \quad (16)$$

Since we are interested in the absolute square of the above expression, we see that longitudinal correlation is analogous to vertical correlation with $q = 2.5b^2H_0 \cong 1.25(\beta s/a$ as it was in vertical correlation. In particular, we can use Fig. 7 with

$$\Phi \cong \frac{\beta s}{3}\left(\frac{d}{a}\right)^2$$

for longitudinal correlation. The longitudinal separation at which correlation drops to a low value is then given by $s/\lambda = 3/4(a/d)^2$. When compared to the lower limit estimate of the longitudinal correlation distance obtained,[2] this estimate is approximately six times as large. (This is apparently due to the fact that in reference 2, $N(0)$ was assumed constant rather than decreasing with height.)

Frequency Correlation

For this case the phase term in the correlation function is of the form $\Delta\beta(R_0+R)$. Using the Fresnel approximations for R_0 and R, we obtain

$$R_0 = [(d/2+y)^2 + x^2 + h^2]^{1/2} \cong d/2 + y + \frac{1}{2}\frac{x^2+h^2}{d/2+y}$$

$$R = [(d/2-y)^2 + x^2 + h^2]^{1/2} \cong d/2 - y + \frac{1}{2}\frac{x^2+h^2}{d/2-y}$$

$$R_0 + R \cong d + (2/d)(x^2+h^2).$$

Our frequency correlation function becomes

$$\rho(\Delta\beta) = \int_{H_0}^{\infty}\int_{-\infty}^{\infty} \frac{(h-H_0)e^{j(2\Delta\beta/d)(x^2+h^2)}}{(x^2+r^2h^2)^2(h-H_0/2)^2}\,dxdh.$$

By precisely the same reasoning as used in the case of longitudinal correlation, we arrive at the conclusion that again we can use Fig. 7 with

$$\Phi \cong \frac{\Delta\beta d^3}{2a^2} \cong \frac{\Delta f d^3}{2.5},$$

where in the last expression Δf is the bandwidth in mc and d is distance in hundreds of miles. We see, therefore, that the bandwidth can be taken as

$$\Delta f = \frac{4}{d^3}.$$

This is a factor of four larger than the lower limit estimate[2] derived previously and is again due to the different assumption concerning the behavior of $N(0)$.

It should be emphasized, as already stated in the first paragraph of Section V, that all the radio system parameters are being evaluated under the assumption that the antenna beams are broader than the effective cone of arrival of the scattered energy which is approximately $1/2^0$ per hundred miles of path length. If on a 200 or 300 mile circuit, one used very narrow beams of $1/2^0$ or so, then all our estimates would have to be modified by inserting the functional form of $(f_0 \cdot f)$ in all the previous integrals. In particular, there would occur not only the antenna gain degradation phenomenon already referred to, but also the bandwidth of the medium as well as all the correlation distances would be increased. An experimental verification of a wide bandwidth on a 188 mile path is presented in another paper[8] in this issue. A mathematical estimate of the lower limit of the bandwidth for the conditions described by Tidd was made by utilizing (5) of this paper, considering $S(\theta)$ constant and assuming a Gaussian form for $(f_0 \cdot f)$. The result is that a lower limit of the effective bandwidth is about 5.5 mc. A further word of caution is necessary in that bandwidth as defined here is a measure of the frequency separation between signal components whose correlation is approximately 0.5. But no one has as yet analyzed the detailed implication of a 0.5 correlation on different types of modulation systems. A more detailed discussion from a physical standpoint of antenna gain degradation and bandwidth utilizing narrow beam antennas has been given.[9]

Height-Gain

We have up to the present essentially neglected the effect of reflections from the earth. The approximation inherent in this neglect of earth reflections is considered quite satisfactory in that no very pronounced height-gain effects have been noticed.[3] To investigate the possible systematic, even though small, height-gain effect due to ground reflections we need merely to replace our antenna patterns $f_0(\Omega_0)$ and $f(\Omega)$ by $f_0(\Omega_0)\,H(\Omega_0)$ and $f(\Omega)\,H(\Omega)$, where $H(\Omega)$ is the height-gain function over a smooth earth. If we take $H(\Omega)$ to be the height-gain function over a plane earth for horizontal polarization, we have approximately $H = \sin(\beta h' \psi)$, where h' = antenna height above the earth while ψ can be interpreted as the angle above the horizon plane. When substituted in our basic equation for $\langle I^2 \rangle$, we have

$$\langle I^2 \rangle \sim \int_{H_0}^{\infty} \int_{-\infty}^{\infty} \frac{(h - H_0)\sin^2[q(h - H_0)]}{(x^2 + r^2h^2)^2(h - H_0/2)^2}\,dx\,dh$$
$$\sim \int_{H_0}^{\infty} \frac{(h - H_0)\sin^2[q(h - H_0)]}{h^3(h - H_0/2)^2}\,dh,$$

where $q = 2\beta h'/d$. We evaluate the above integral by recognizing that

$$\sin^2[q(h - H_0)] \sim 1 - \cos[2q(h - H_0)]$$
$$= 1 - \cos 2qH_0 \cos 2qh - \sin 2qH_0 \sin 2qh$$

When substituted into the above expression for $\langle I^2 \rangle$, we obtain the result (see discussion on vertical correlation)

$$\langle I^2 \rangle \sim 1 - \cos\left(\frac{\beta h' d}{a}\right)\left[\text{Re } \rho_v\left(\frac{\beta h' d}{a}\right)\right]$$
$$- \sin\left(\frac{\beta h' d}{a}\right)\left[\text{Imag } \rho_v\left(\frac{\beta h' d}{a}\right)\right],$$

where ρ_v is the normalized vertical correlation function already developed. A graphical presentation of this height-gain effect is shown in Fig. 12.

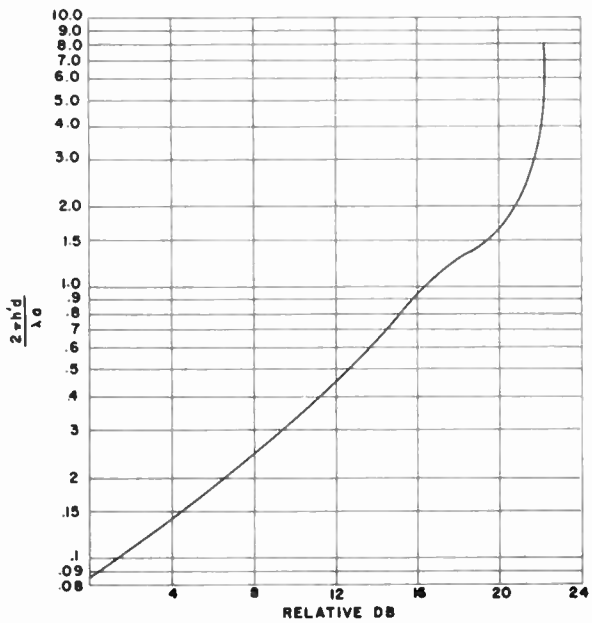

Fig. 12—Theoretical height-gain function for scatter propagation.

Similar procedure to obtain height-gain function was used in Herbstreit's, *et al.* paper, but their expression did not allow for variation of $N(0)$ with height.

ACKNOWLEDGMENT

Grateful acknowledgment is extended to K. A. Norton, CRPL; M. Katzin, NRL; and R. F. Drenick, RCA, for the many helpful suggestions and for the encouragement received by the author while completing the work in this paper.

[8] W. H. Tidd, "Demonstration of bandwidth capabilities of beyond-horizon tropospheric radio propagation," p. 1297, this issue.

[9] H. G. Booker and J. T. de Bettencourt, "Theory of radio transmission by tropospheric scattering using very narrow beams," PROC. IRE, vol. 43, p. 281–290; March, 1955.

Note on Scatter Propagation with a Modified Exponential Correlation*

A. D. WHEELON†

Summary—A phenomenological exponential space correlation of dielectric fluctuations is normally used to predict scatter field strengths beyond the horizon. This paper introduces a modified exponential model which includes effects of the smallest blob cutoff in the turbulent spectrum and rectifies the correlation's cusp at the origin. It is found that the present agreement of troposphere scatter experiments with the exponential function does not depend on this cusp. It is suggested that frequency-dependent tropospheric fields recently measured below 25 cm may indicate the influence of the correlation's fine structure. The same model is then applied to the ionosphere, where the extended range VHF scatter wavelengths just straddle the smallest blob size (~3 m) in the *E* layer. The turbulence fine structure is most important for this propagation and gives a qualitative explanation of the curious dualism in frequency scaling laws observed at opposite ends of the VHF band. Satisfactory variation of signal strength with scattering angle is also predicted by this model. It is shown that scatter measurements can provide valuable estimates of the atmosphere's fine structure at various heights.

IN A RECENT paper,[1] limitations of the usual exponential space correlation of dielectric fluctuations in the atmosphere were pointed up in connection with angle-of-arrival calculations on optical paths. The basic problem there is the finite slope of this function at the origin. A modified exponential correlation was subsequently devised which corrected this situation.

It is interesting to consider the predictions which the new correlation function makes for both the tropospheric and ionospheric forward-scatter propagation modes. In particular, it should help to clarify T. J. Carroll's contention that agreement of tropospheric scatter experiments with the exponential correlation only is due solely to its cusp-like behavior near the origin, and therefore constitutes an argument against scatter theory. In the ionospheric experiments, a number of curious scaling laws remain to be explained. It is just possible that our new correlation can predict such variations. The present note gives a preliminary evaluation of the effects which the correlation's small argument behavior has for scatter propagation.

To circumvent the cusp for line-of-sight problems, a modified exponential correlation was introduced to bring the curve into the origin with zero slope.[2] The proposed function

$$C(R) = \left(1 - \frac{l_s}{l_0}\right)^{-1} \left\{e^{-|R|/l_0} - \frac{l_s}{l_0} e^{-|R|/l_s}\right\} \qquad (1)$$

contains a second term which represents, in some sense, the natural cutoff imposed by atmospheric viscosity on the eddy decay system. The correlation introduced in this way is frankly phenomenological, although detailed investigations of the turbulence dynamics indicate that (1) describes the physics quite well. The micrometeorological scale l_s[3] is identified with the smallest "blob" size in the progressive turbulence decay scheme proposed by Villars and Weisskopf[4] to explain these same scatter experiments. In the troposphere l_s is probably of the order of centimeters; while in the *E*-layer of the ionosphere, it is several meters.

The scattering cross section[5] is found by solving Maxwell's equations in a region characterized by the dielectric constant $\epsilon = \epsilon_0 + \Delta\epsilon$, with the $\Delta\epsilon$'s correlated in space by (1). The asymptotic form of scattered field gives

$$\sigma = \frac{\pi^2}{\lambda^4}\overline{\left|\frac{\Delta\epsilon}{\epsilon_0}\right|^2} \int_V d^3R e^{i\vec{q}\cdot\vec{R}} C(R). \qquad (2)$$

The scattering volume V is usually enormous compared with the range of $C(R)$, so that we may write the volume integral in spherical coordinates and run the variables over all space. Integrating over the sphere gives

$$\sigma = \frac{4\pi^3}{\lambda^4 q}\overline{\left|\frac{\Delta\epsilon}{\epsilon_0}\right|^2} \int_0^\infty dR R \sin(qR) C(R), \qquad (3)$$

where $q = (4\pi/\lambda)\sin(\theta/2)$ and θ is the scattering angle. It is now a simple matter to introduce (1) and perform the remaining integral. Since l_0 is always much greater than the wavelength λ, one may make the usual approximation for small θ and find a negative correction to the familiar exponential result.[5]

$$\sigma = \frac{\overline{\left|\frac{\Delta\epsilon}{\epsilon_0}\right|^2}}{2\pi l_0 \theta^4} \left\{1 - \frac{\left(\frac{2\pi l_s \theta}{\lambda}\right)^4}{\left[1 + \left(\frac{2\pi l_s \theta}{\lambda}\right)^2\right]^2}\right\}. \qquad (4)$$

This correction varies from zero to unity as product $2\pi l_s\theta/\lambda$ goes from zero to infinity. If product is very small,

$$\sigma = \frac{1}{2\pi l_0}\overline{\left|\frac{\Delta\epsilon}{\epsilon_0}\right|^2} \cdot \frac{1}{\theta^4}, \qquad l_s < \frac{\lambda}{2\pi\theta}. \qquad (5)$$

When l_s is substantially greater than the wavelength, however,

* Original manuscript received by the IRE, August 5, 1955.
† Ramo-Wooldridge Corp., Los Angeles, Calif.
[1] R. B. Muchmore and A. D. Wheelon, "Line-of-sight propagation phenomena—I. Ray treatment," p. 1437, this issue.
[2] E. Levin and M. Weisfeld (private communication) have shown that one can remove all odd derivations at the origin without introducing new constants, other than l_s. Terms past those in (1) are incredibly small, however, so that we shall work here with this simple form.
[3] Some workers refer to the geometric mean $\sqrt{l_0 l_s}$ as microscale.
[4] F. Villars and V. F. Weisskopf, "The scattering of electromagnetic waves by turbulent atmosphere fluctuations," *Phys. Rev.*, vol. 94, pp. 232–240; April 15, 1954.
[5] H. G. Booker and W. E. Gordon, "A theory of radio scattering in the troposphere," PROC. IRE, vol. 38, pp. 401–412; April, 1950.

$$\sigma = \frac{1}{4\pi^3 l_0 l_s^3}\overline{\left|\frac{\Delta\epsilon}{\epsilon_0}\right|^2}\cdot\frac{\lambda^2}{\theta^6}, \qquad l_s > \frac{\lambda}{2\pi\theta}. \tag{6}$$

These two results form the basis for our subsequent discussions of tropospheric and ionospheric forward-scatter propagation.

Troposphere

In the troposphere, dielectric fluctuations are due to turbulent concentrations of water vapor and temperature-density variations. The microscale for *dry* air density variations is approximately one millimeter.[4] The microscale of moist air fluctuations, however, is not known so surely. Since humidity fluctuations undoubtedly play a major role, we should see what predictions both (5) and (6) make. Integrating over the typical scattering volume,[6] one finds for the scattered-to-free field power ratios

$$\frac{P_s}{P_F} = \frac{1}{4}\frac{a^2}{dl_0}\overline{\left|\frac{\Delta\epsilon}{\epsilon_0}\right|^2}, \qquad l_s < \frac{\lambda}{2\pi\theta} \tag{7}$$

and

$$\frac{P_s'}{P_F} = \frac{1}{16\pi^2}\frac{a^4\lambda^2}{d^3 l_s^2}\overline{\left|\frac{\Delta\epsilon}{\epsilon_0}\right|^2} \qquad l_s > \frac{\lambda}{2\pi\theta}. \tag{8}$$

The scattering angle θ is essentially the transmission distance d over 4/3 the earth's radius a and is approximately 1/10 for the pertinent experiments.[7]

With reasonable values of the scattering parameters,[8] one finds about -70 db from both expressions. The new result (8) depends more strongly on range d, in partial agreement with experiments which indicate a d^{-5} law.[9] Gordon[6] has shown that this range variation may be imparted to (7) by assuming that the quotient

$$\frac{1}{l_0}\overline{\left|\frac{\Delta\epsilon}{\epsilon_0}\right|^2}$$

decreases with altitude as h^{-2}; so that we do not have a real argument for abandoning (7) in favor of (8). Furthermore, the frequency dependence of (8) is unsatisfactory, since the experimental evidence indicates that the scattered-to-free field power ratio is frequency insensitive from 100 to 2,000 mc.[7,10] The alternative is to assume that the *moist* air's l_s is less than $\lambda/2\pi\theta \simeq 25$ cm, which is certainly consistent with our estimates of the dry air microscale. The experiments of Trolese[11] at 24, 9.3, and 3.2 cm in the Arizona desert, however, indicate a power separation of 10 db between the frequencies. Such results are in substantial agreement with the λ^2 dependence of (8) and indicate that l_s is probably of the order of 10 cm. Since the cross sections frequency dependence permits putting bounds on microscale, it would be valuable to extend the present frequency range of simultaneous scatter experiments.

It is interesting that the body of the correlation function and not its behavior near the origin is significant for propagation experiments. The agreement of the ordinary exponential correlation alone with scatter experiments is held by Carroll to be an argument against scatter theory, since its finite slope at the origin is physically unsatisfactory. We have just seen, however, that the correction term which was introduced in (1) to remedy this situation plays no effective role in tropospheric scatter with $l_s < \lambda$. The cusp, therefore, has nothing to do with the current tropospheric scatter experiments, and is an esthetic point that remains to be resolved by turbulence theory alone. Until such a resolution is effected, the adjusted correlation (1) may be used as a reasonable representation of the way the viscosity cutoff of any theory may rectify this situation.

Ionosphere

Extended range vhf propagation has been identified with turbulence scattering in the E-region (height $\sim$90 km) of the ionosphere.[12] These transmissions have been made in the frequency range, 30 to 110 mc. Villars and Weisskopf early estimated the microscale of this turbulence as $l_s \simeq 2.5$ m.[4] The microscale is thus likely to split wavelength range used in experiments, so that possibility exists for observing both cross sections, (5) and (6). Different frequency scaling laws at frequency range's two ends seem to have been observed experimentally and our interest is thus sharpened.

The mean-square dielectric fluctuation which appears in (2) is identified with turbulent motion of the ionized electrons in the E-layer. If the electron density is denoted by N, we have

$$\overline{\left|\frac{\Delta\epsilon}{\epsilon_0}\right|^2} = \left|\frac{\lambda}{\lambda_c}\right|^4\overline{\left|\frac{\Delta N}{N}\right|^2},$$

where λ_c is the critical or plasma wavelength of the E-region (i.e., $\omega_c = 1.5$ mc). The experimental results are expressed in terms of the scattered-to-transmitted power ratio, which is given in terms of the cross section and standard geometry[11] by

$$\frac{P_s}{P_t} = 4\sigma\frac{Ab}{D^2\sin(\theta/2)}, \tag{9}$$

where b is the scattering layer's thickness, A the equivalent aperture of the receiving antenna, D is nearly the surface transmission distance and the other symbols have their previous meaning. We may substitute our two cross-section results here to obtain:

[6] W. E. Gordon, "Radio scattering in the troposphere," Proc. IRE, vol. 43, pp. 23–28; January, 1955.

[7] NBS Rep. No. 3520, "Survey of CRPL Research in Tropospheric Propagation," January 1, 1955.

[8] I.e., $l_0 = 100$ m, $d = 300$ km, $\overline{|\Delta\epsilon/\epsilon_0|^2} = 10^{-12}$ and $\lambda/l_s \simeq 1/3$.

[9] T. F. Rogers, "Vhf field strength far beyond the radio horizon," Proc. IRE, vol. 43, p. 623; May, 1955.

[10] K. Bullington, "Radio transmission beyond the horizon in the 40- to 4,000-mc band," Proc. IRE, vol. 41, pp. 132–135; January, 1953.

[11] L. G. Trolese, "Characteristics of tropospheric scattered fields," p. 1300, this issue.

[12] D. K. Bailey, R. Bateman, L. V. Berkner, H. G. Booker, G. F. Montgomery, E. M. Purcell, W. W. Salisbury, and J. B. Wiesner, "A new kind of radio propagation at very high frequencies observable over long distances," *Phys. Rev.*, vol. 86, pp. 141–145; April 15, 1952

$$\frac{P_s}{P_t} = \frac{4Ab}{\pi l_0 \lambda_c^4} \overline{\left|\frac{\Delta N}{N}\right|^2} \frac{\lambda^4}{D^2\theta^5}, \qquad l_s < \frac{\lambda}{2\pi\theta} \tag{10}$$

and

$$\frac{P_s'}{P_t} = \frac{2Ab}{\pi^3 l_0 l_s^2 \lambda_c^4} \overline{\left|\frac{\Delta N}{N}\right|^2} \frac{\lambda^6}{D^2\theta^7}, \qquad l_s > \frac{\lambda}{2\pi\theta}. \tag{11}$$

This second result is rather milder in its λ and θ dependence than the corresponding expression (53) first derived by Villars and Weisskopf. Their form would appear to disagree, however, with frequency scaling laws.[13] The initial experiments of Bailey, *et al.*[12] on 50 mc used the numerical values: $A = 3\ 10^6$ cm^2, $b = 5\ 10^5$ cm, $\theta = 24$ degrees, $D = 1{,}250$ km, $\lambda = 6$ m, $\lambda_c = 200$ m, and $l_0 = 5\ 10^5$ cm. With $\left|\Delta N/N\right|^2 = 10^{-5}$ and $l_s = 3$ m, one computes $1/2\ 10^{-18}$ from both (10) and (11), which should be compared with the measured value of $0.3\ 10^{-18}$. The agreement is probably not significant, since there are several adjustable parameters in both results. The ratio

$$\frac{P_s}{P_s'} = \frac{2\pi^2\theta^2 l_s^2}{\lambda^2},$$

however, contains only one unknown and is very near unity for the accepted values of l_s. The two results are thus in substantial agreement as to power-level predictions. To learn more about the transmission, we must study the distance and frequency dependence of the received signals.

In a continuing series of experiments, Bailey, Bateman, and Kirby have investigated the variation of signal strength with scattering angle.[13] They found that the received-to-transmitted power ratios at 50 mc vary about as the inverse eighth power of the scattering angle θ. If we were to choose between (10) and (11), we would be inclined to regard the new result (11) as most appropriate at 50 mc. Using $\theta = 0.42$ and $\lambda = 6$ m, this indicates that the E-layer microscale is somewhat greater than two meters. It would be interesting to examine the angular relation at longer wavelengths, to see if a transition to form (10) is observed.

A second series of experiments was undertaken to determine the frequency dependence of the scattered signals.[13] Using the Sterling-to-Cedar Rapids path ($D = 1{,}243$ km), three frequencies were transmitted simultaneously at 107.8 mc, 49.8 mc, and 27.78 mc. With scaled (rhombic) antenna apertures and heights, Bailey *et al.* found that the ratio of scattered powers, $P_s(108)/P_s(50)$ varies about as the eighth power of the corresponding wavelengths, with the exponent representing the mean of values running from 4 to 12. The ratio $P_s(50)/P_s(28)$, however, seems to vary as the fifth (5.0 to 5.5) power of the wavelengths. A similar experiment in Alaska on 48.87 and 24.325 mc over a 1,156 km path favors an exponent of 4.5 to 5.0. Such variation in scaling laws over this small frequency range is hard to understand in terms of single classical formula (10).

It does seem possible to explain these curious results by using the complete correlation of (1). Since the microscale now cuts across the frequency range employed, it is altogether reasonable that the results (10) and (11) apply to different ends of the frequency range. From the variation with scattering angle, we have already seen that 50 mc transmission is likely to be described by the new formula (11). At 108 mc, the wavelength is halved, so that it too must be characterized by (11). We should therefore expect the scattered powers at these two frequencies to stand in the ratio,

$$\frac{P_s(108)}{P_s(50)} = \left(\frac{\lambda_{108}}{\lambda_{50}}\right)^6; \tag{12}$$

a result quite close to the mean exponent of eight indicated by experiment. Variability of this exponent may be ascribed to variations in microscale l_s caused by changing turbulent conditions in the E-region.

If a transition between the two cases does occur, it is likely to come between 28 and 50 mc. If the 30-mc power is given by (10), the appropriate power ratio should vary with wavelength as,

$$\frac{P_s(50)}{P_s(28)} = 2\left(\frac{\lambda_{50}}{2\pi\theta l_s}\right)^2\left(\frac{\lambda_{50}}{\lambda_{28}}\right)^4. \tag{13}$$

This result is quite close to the 4.5 to 5.5 variation observed, since the coefficient $2(\lambda/2\pi\theta l_s)^2$ is nearly unity. It would thus seem that 28-mc propagation is described by (10), which in turn allows us to place an upper bound on the microscale l_s. When we combine this observation with the previous lower bound, we find that the E-layer microscale probably satisfies

$$2m < l_s < 4m. \tag{14}$$

These limits are certainly consistent with the careful analysis of this parameter recently made by Villars and Weisskopf.

Our principal result here then is the important role which the microscale *may* play in determining vhf transmission in the ionosphere. It seems that l_s may just divide the vhf region, so that two transmission expressions are appropriate at opposite ends of the band. The observation of just such a dualism in the experimental data indicates that we may be on the verge of a satisfactory interpretation of the distance and frequency dependence of this important propagation mode.[14]

Acknowledgment

I should like to thank K. A. Norton and D. K. Bailey of the Central Radio Propagation Laboratory, National Bureau of Standards, Boulder Colo., for invaluable discussion of these matters.

[13] D. K. Bailey, R. Bateman, and R. C. Kirby, "Radio transmission at vhf by scattering and other processes in the lower ionosphere," p. 1181, this issue.

[14] Using the genuine turbulence theory of dielectric fluctuations developed in reference 4, one is able to reproduce the mean experimental exponent exactly with the choice $l_s = 3$ m. This work will be reported in a later publication.

Propagation of Short Radio Waves in a Normally Stratified Troposphere*

T. J. CARROLL†, MEMBER, IRE, AND R. M. RING†

Summary—Experiments of the past decade give stronger fields well beyond the horizon than are calculated by the 4/3 airless earth approximation. Post-war work on the theory of the WKB approximation for wave propagation in slowly varying inhomogeneous media, and the peculiar results for eigenvalues of the bilinear refractive index profile offer valuable clues in the search for an oversight in conventional propagation theory. If the absolute value as well as the gradient of the refractive index at the earth's surface be specified, with a refractive index profile which tapers to vacuum at some arbitrarily large height, then allowed modes of the wave equation permit the field to be calculated within, just beyond, and well beyond the horizon, in agreement with many vhf and microwave experiments. Modes thus calculated are supported by ordinary coherent molecular scattering in normal air dielectric layer. At times, superrefraction and macroscopic turbulence are additional mechanisms for propagation deep into the shadow of the earth bulge.

Motivating Considerations

THE CHIEF experimental features of observed fields in the deep shadow of the earth bulge seem to be less attenuation with distance, larger absolute value, and less height gain than were expected on the basis of well established methods for calculating diffraction of radio waves around a smooth airless spherical earth, even when the radius of the earth is changed to a "4/3 effective" value to allow for refraction in the lower troposphere. The earth bulge is definitely not as great an impediment to propagation of fields deep into the shadow as conventional calculations had indicated. Most attempts to understand these observations on fields well beyond the horizon have started with the idea that some additional property of the atmosphere (such as turbulence) or deviations from the smooth spherical profile might be the cause of the discrepancy between experiment and theory. The present calculation tries to see how far the observations can be understood merely from a more careful calculation of the effect of the earth's normal layer of tropospheric air as a stratified inhomogeneous medium tapering to vacuum at great heights, keeping the idealizations of a nonturbulent troposphere and a perfectly reflecting spherical earth. The effect of the almost linear decrease of index of refraction in the troposphere is usually taken to be entirely equivalent to replacing the earth radius by a suitably enlarged "4/3 effective" radius, and treating the calculation from that point on as if the earth were airless. It is believed by us that this calculation is only an approximate way of taking account of the refractive effects of the earth's tropospheric envelope, which breaks down for calculation of weak fields deep in the shadow of the earth bulge, when the internal reflection effects of the layer become also important. Refractive but not reflective effects of the air layer are allowed for by the effective radius notion, although both effects should be present in any exact calculation. "Bodies reflect and refract light by one and the same power, variously exercised in various circumstances" (Newton's Optics (1704), Book II, Prop. 9). All reflective and refractive effects of a material medium for electromagnetic waves are the results of coherent scattering of the waves by elements of the medium acting as secondary sources when they are stimulated by an external wave. The scattered waves add to the primary wave with definite phase relations, and thus give rise to the changed speed of the total wave in a homogeneous medium with index of refraction n. In contrast, the combination of fields in random phase from several sources should be called "incoherent scattering," to distinguish it from the coherent type giving rise to the index of refraction of air in Maxwell's equations. The index of refraction appearing in Maxwell's equations for a material medium is a reminder of the coherent scattering contributed by the elements of the medium. Although the term "scattering" is rarely explicitly mentioned in the following calculation, the whole procedure amounts to a more complete calculation of the effect of a coherently scattering air layer on the propagation of radio waves, particularly beyond the horizon.

Some Steps in the Historical Development

Limitation to the Effective Earth Radius Notion

The effective earth radius notion is deduced from ray theory arguments valid above the horizon, but its extension to regions well beyond the horizon where rays cannot be traced in a normal atmosphere surely needs proof. The Eckersley and Millington treatment of the late 1930's suffered from the approximate Liouville-Rayleigh-Gans-Jeffreys-Wentzel-Kramers-Brillouin methods employed to solve the wave equation and the misbehavior of their assumed index of refraction profile at great heights, where it approached the value 3/4 instead of unity appropriate to a vacuum with no dielectric or ionization present. Bremmer,[1] Schelkunoff,[2] and

* Original manuscript received by the IRE, July 11, 1955. The research in this document was supported jointly by the Army, Navy, and Air Force under contract with MIT.

† MIT, Lincoln Lab., Lexington, Mass.

[1] H. Bremmer, "The propagation of electromagnetic waves through a stratified medium and its WKB approximations for oblique incidence," *Physic*, vol. 15, pp. 594–608; August, 1949.

[2] S. A. Schelkunoff, Remarks concerning wave propagation in stratified media; "Theory of electromagnetic waves," Interscience Publishers, Inc. (N. Y., pp. 181–192; 1951, or *Comm. Pure Appl. Math.*, vol. 4, pp. 117–128; June, 1951. See also, "Solution of linear and slightly nonlinear differential equations," *Quart. Appl. Math.*, vol. 3, pp. 348–355; October, 1945.

Rydbeck[3] all emphasized in their writings after the war that the WKB method for a slowly varying medium involves the neglect of the partial reflections which are inevitably generated when a wave passes through any but a strictly homogeneous medium. The scattering coefficient per unit thickness of a stratified medium may be deduced as Bremmer does and used to estimate roughly the magnitude of first-order corrections to the WKB method.

Neglect of the Absolute Value of the Surface Index in Conventional Theory

When the question of the absolute value of the index is mentioned at all, the 4/3 fictitious earth is imagined to be surrounded by a homogeneous atmosphere filling all space with the same index as that near the surface of the real earth. The real atmosphere manifestly does not fill up all space homogeneously, but thins out roughly exponentially with height and the index decreases by about e^{-1} for each 7.5 km increase of height. A homogeneous air layer containing the same amount of dielectric as the actual troposphere would be 7.5 km thick and would not fill all space. The customary definition of "standard radio atmosphere" as one in which the index decreases at the rate of $39(10)^{-6}$ km^{-1} unfortunately does not define an atmosphere, since the excess of absolute value of the index over unity, which specifies the effect of the medium as compared with empty space, is not even specified. Taken literally the "standard radio atmosphere," imagined to continue to heights more than 10 km, would imply the existence of indices less than one and even ultimately less than zero! It is precisely this absolute value of the index n as compared with the vacuum value unity which was shown in the last decade by Pickard and Stetson[4] to have such a surprisingly high correlation with measured tropospheric fields well beyond the horizon.

In analogous problems in wave mechanics in atomic physics, the potential energy function between two interacting particles enters the Schrödinger wave equation in the same way as does the square of the index of refraction in the electromagnetic wave equation. Most well-known problems in the wave mechanics of two interacting elementary particles require the specification of the whole potential energy curve at all particle distances, and results usually depend both on the depth and the slope of the side of the potential well. Ignoring the depth of a potential well; i.e., the absolute value of the potential energy relative to infinite particle separation, and specifying only the potential gradient over a certain interparticle distance range, is permissible only for a particle in a closed orbit such as a closed elliptical Bohr orbit, where only the force (potential gradient) between the particles need be specified at points on the orbit. For the general wave mechanical problem, when the particle is not confined to an orbit, the potential energy must be specified for all interparticle distances, including very large separations. Just as Bohr orbits are approximations to the exact wave mechanical solution, so also are the direct and reflected rays above the horizon approximations to the exact electromagnetic wave solution, and the ray approximation requires only specification of index gradient or refracting power of inhomogeneous medium. Electromagnetic propagation beyond horizon, however, can only be described by wave equation without ray approximations, and therefore, conventional theory must be regarded as incomplete because of failure to specify absolute value of index at great heights to which most of the energy escapes after air layer has abstracted a very small but not negligible fraction for useful propagation into the shadow region.

Neglect of the depth of a potential well and specification only of the slope of the potential curve over a limited range of distances precludes any wave mechanical solution in which escape of the particle to infinity is permitted. Similarly, exclusive concern with index gradient and complete neglect of the absolute value of the index is a kind of ray-type thinking inappropriate beyond the horizon where wave language undefiled by ray approximations must be used from the beginning.

The consequences of ignoring the absolute value of the index of refraction in tropospheric propagation can be instructively compared with the discrepancies which could be imagined to develop if spectroscopists should suddenly start forgetfully to compare uncorrected wavelengths measured in laboratory air to the wavelengths calculated for electrons moving around nuclei *in vacuo*. In an unevacuated spectroscope, of course, the air is homogeneous, and the correction from air to vacuum wavelengths is simple. In the radio case, however, the atmospheric dielectric layer as an "optical instrument" for guiding radio feebly around the earth bulge introduces the problem of inhomogeneous medium propagation at the beginning. Radio waves propagate with a different phase velocity through the air in which antennas are immersed than they do in the vacuum outside the earth into which the radiation ultimately escapes. Proper calculation of the effect of the gravitationally produced inhomogeneity of the earth's air envelope is the central problem underlying this approach to propagation well beyond the horizon.

Behavior of Eigenvalues of Infinitely Thick Surface Ducts for the Bilinear Model of the Refractive Index Profile

Considerable theoretical work is described in Chapter 2 of MIT Radiation Laboratory Series, vol. 13,[5] on the

[3] O. E. H. Rydbeck, "On the propagation of radio waves," *Trans. Chalmers Inst. Tech.* (Gothenberg, Sweden), no. 34, 1944.

[4] G. W. Pickard and H. T. Stetson, "Comparison of tropospheric reception," *Jour. Atmos. Terres. Phys.*, vol. 1, pp. 32–36; January, 1950.

[5] D. E. Kerr, ed., "The Propagation of Short Radio Waves," MIT Rad. Lab. Ser., McGraw-Hill Book Co., Inc., New York, vol. 13, pp. 140–170, 1951.

eigenvalues and eigenfunctions appropriate for radio wave propagation in surface ducts describable by a bilinear modified index profile. The eigenvalues are investigated extensively there for the case of a layer thickness approaching infinity. It was regarded as a distressing situation that these limiting eigenvalues did not go over into those for an airless earth specified by a linear modified refractive index. Since it is these airless earth eigenvalues which disagree with experiment, we wondered whether this disagreement of the limiting bilinear values should be regarded as not distressing after all. The bilinear model can meet the logical objection to a linear model, because it has two parameters, which may be taken as the slope and the total amount of the air dielectric which modifies the index profile from the airless earth value. This hunch has turned out correct, and the complication of the bilinear model as compared with the linear is to be welcomed rather than deplored in connection with the puzzling discrepancy between experiment and theory mentioned earlier.

Bilinear Model Modes Contrasted with Airless Earth Modes

Allowed Modes and Mode Sums

The vertical Hertz vector ψ excited by a vertical Hertzian dipole transmitting antenna at height Z_0 has a value at a point of height Z and horizontal distance X as measured along the earth's surface which may be expressed as a sum of normal modes as follows, assuming time variation of the form exp $(+i\omega t)$ at every point:

$$\psi = \frac{2\sqrt{\pi}}{L\sqrt{X}} \exp\left[-i(kLX + \pi/4)\right] \cdot \sum_m \exp\left(iA_m X\right) U_m(Z_0) U_m(Z). \tag{1}$$

The components of the electric and magnetic fields may be obtained by differentiation from this Hertz vector or polarization potential. The heights Z are expressed in true earth natural units $H \equiv (\lambda^2 a/8\pi^2)^{1/3}$, where a is the geometrical earth radius and λ is the vacuum wavelength. The horizontal distance X is measured in the natural unit of length $L \equiv 2(\lambda a^2/8\pi)^{1/3}$. $k \equiv 2\pi/\lambda$. The horizontal distance is assumed large compared to the antenna heights in (1) but small compared to the earth radius. The height gain functions U_m are normalized solutions to the differential equation

$$\frac{d^2U_m}{dZ^2} + (Y + A_m)U_m = 0, \tag{2}$$

in which A_m are a set of complex numbers which allow the solutions to satisfy the boundary conditions of the problem which are:

1. $U_m = 0$ when $Z = 0$, for the case of a perfectly reflecting earth;
2. U_m shall behave like an outgoing wave in vacuum at great heights.

The function $Y(Z)$ appearing in (2) is proportional to what is sometimes called the excess modified refractive index, a terminology which we shall avoid, because of the importance of distinguishing between that part of Y which expresses the effect of earth geometry on the propagation without any effects of inhomogeneous air, and that part which depends on the presence of the inhomogeneous dielectric layer to which we shall idealize the troposphere.

$$Y(Z) = Z + \left\{\frac{a}{H}(n - 1)\right\} \tag{3}$$

For $n = 1$ (airless earth), Y becomes simply $Y = Z$, and the effect on the wave functions defined by (2) is solely that of earth curvature. The second term of (3) in curly brackets expresses the effect on the wave function of the layer of inhomogeneous air with index of refraction n a function of height only, in addition to the effect of earth curvature represented by the first term.

Airless Earth Modes

For the airless earth case, the wave functions U_m are proportional to $h_2(Z + A_m)$, where h_2 is the modified Hankel function of order 1/3 as defined in MIT Radiation Laboratory Series, vol. 13.[5] The eigenvalues A_m, complex numbers specifying the attenuation rate and phase velocity corrections for allowed modes, are determined, from condition 2, as roots of the equation

$$h_2(A_m) = 0. \tag{4}$$

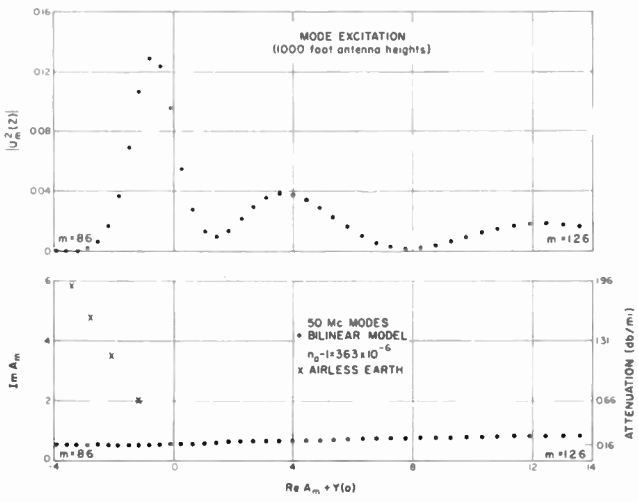

Fig. 1

These roots lie on the 120-degree ray in the complex A-plane and are shown by crosses on bottom part of Fig. 1, above. They are infinite in number, and the numbering is usually arbitrarily done in order of increasing imaginary parts. For distances X larger than the sum of the horizon distances of the terminal heights (Z_0, Z), only the mode of lowest attenuation (smallest imaginary part) contributes appreciably to the sum

(1), although at shorter ranges within the horizon many more modes must be computed if mode sum (1) is used to compute the fields rather than the vastly simpler though approximate direct and reflected ray methods.

Bilinear Model Modes for Standard Refraction

We assume surface index $n_0-1=363(10)^{-6}$, and imagine for simplicity that the gradient is constant with the so-called standard value of $-39(10)^{-6}$ km^{-1}, until the height 9.3 km is reached, where the air density will be zero and the index of refraction unity, which we suppose to be maintained at all "airless" levels higher than this. (In natural units, this height of the top of the air layer is denoted by g. For 50 mc, $g=65.3$; for 3,000 mc, $g=1{,}000$.) In natural units, below $Z=g$, the index profile is assumed to be linear:

$$n-1=(g-Z)(1-s^3)H/a. \tag{5}$$

For the standard index gradient and the natural units used s^3 has the numerical value $\frac{3}{4}$ because the small quantity $1/a$, geometrical earth curvature, has been introduced as a convenient unit in which to express the small quantity $n-1$, which is sometimes called the refractivity of the air at any height, or half the electric susceptibility. The linearly stratified layer of air (5) alters Y for $Z<g$ to

$$Y(Z)=s^3(Z-g)+g \tag{6a}$$

$$Y(0)=g(1-s)^3=\frac{(n_0-1)}{H/a}. \tag{6b}$$

$Y(0)$ at the surface thus has the physical significance of the surface refractivity expressed in the natural units of the earth curvature, H/a. Eq. (6a) together with $Y=Z$ for $Z>g$ describes a bilinear continuous function, which through (2) specifies the effect of a finite linearly graded transition layer of air on the propagation of radio waves around a curved earth. The resulting modes are termed transitional because for $s^3=3/4$ (standard refraction), there are no real eigenvalues giving trapped unattenuated modes as with super-refractive ducts, but modes are nevertheless supported which are less strongly attenuated with distance (less leakage) than are the well-known airless earth modes already described.

The Hertz vector and its first derivative must be continuous at $Z=g$, in order that all components of the fields be continuous at the vacuum air interface, and no charge or current layers at the interface be allowed to be present in the solution. This requires that U_m for $Z<g$ must be taken to be a linear combination of *both* of the linearly independent modified Hankel functions of order 1/3 appropriate to the air layer

$$U_m(Z)=P_m h_1(s(Z-g)+s^{-2}(A_m+g)) + Q_m h_2(s(Z-g)+s^{-2}(A_m+g)). \tag{7}$$

The coefficients P_m and Q_m are fixed by the requirement of continuity of the Hertz vector and its first derivative with the solution above the air layer, $U_m=K_m h_2(Z+A_m)$, K_m being a normalizing constant. The eigenvalues A_m of the allowed modes are determined by the transcendental equation which results when it is required that $U=0$ for $Z=0$ in (7), corresponding to the boundary condition 1 of perfectly reflecting earth. The complex eigenvalues A_m satisfying (7) and (1) are numbers which make the two terms on the right-hand side of (7) equal in magnitude and opposite in phase for $Z=0$. For a 50-mc frequency, and a linearly stratified layer of air with $n_0-1=363(10)^{-6}$, forty-one of the eigenvalues computed from the transcendental (7) are shown by the solid points at the bottom of Fig. 1, with mode numbers $m=86$ to 126 inclusive. Both (4) and (7) for $U_m(0)=0$, being transcendental equations, have infinitely many solutions A_m. Fortunately not all the infinitely many modes are equally important in contributing appreciable terms to the mode sum for an actual situation where the Hertzian transmitting dipole height Z_0 is specified as well as the height Z of the receiving point a horizontal distance X away. The parameters s and g specify the index gradient and thickness of the linearly graded coherently scattering air layer, which should be imagined physically to be a continuous distribution of secondary sources scattering radiation coherently under the influence of the primary dipole source singularity at height Z_0. The eigenvalues defined by (4) or (7) with $U_m(0)=0$, together with the associated eigenfunctions, form a complete set of eigenfunctions in terms of which the field radiated by any transmitter may be expanded. There is no air layer of secondary scattering sources present in (4) which defines only modes suitable to an airless earth, but the effect of the air layer is specifically included in the eigenvalues specified by (7) with $U_m(0)=0$. The scheme chosen for numbering the roots of a transcendental equation is more or less arbitrary, but the numbering chosen for the bilinear model modes is such that m counts the number of oscillations in the absolute value of the associated wave function in the air layer. The oscillatory character of U_m results from the superposition of h_1 and h_2 functions in (7), which in empty space represent downcoming and upgoing waves.

At the top of Fig. 1 is shown the product of the absolute values of the wave functions for 1,000 foot terminal heights, for the same group of modes whose eigenvalues are shown below, mode numbers $m=86$ to 126 inclusive. To the left of mode 86 the modes are negligibly excited because of the depth loss effect, i.e., strong cancellation of the two terms of (7) for the specified terminal heights as well as for $Z=0$. Modes to the right of $m=126$ make decreasing contributions at large distances because of decreasing normalizing factor K_m and the increase of the imaginary part of the eigenvalue with increasing m. The eigenvalues at the bottom of Fig. 1 do have a shallow minimum in their imaginary parts around $m=92$. The modes on Fig. 1 which con-

tribute most to the field expressed as a sum of modes according to (1) are those which are close to the mode of minimum attenuation. The real parts of A_m delay the phase by just the amount to be expected in ray-type propagation through a medium of index n_0 and wavelength λ/n_0. Thus phase velocity as determined by the real parts of the eigenvalues is a reliable guide to calculation for particular terminal heights, rather than the arbitrary mode number, which happens to be quite large for the important modes of the bilinear model. The similarity of the db/mile attenuation rates and the absolute value of the field contributed by the mode of minimum attenuation at 50 mc, as well as at frequencies one and two orders of magnitude higher, was the first indication of the importance of the usually neglected term $Ph_1(Z)$ in the wave function. Mode $m=95$ on Fig. 1 can be more physically described as the mode of maximum contribution. All the important modes in the mode sum have phase delay approximately characteristic of the reduced phase velocity in the surface air layer containing the terminals.

Bilinear Model Mode Sums

The full power of the mode sum to represent the field vs distance curve at other distances within the horizon and just beyond, as well as far beyond, is shown on Fig. 2. The points represent the amplitude of the resultant field computed at various distances according to (1) as the partial sums of 30, 35 and 40 of the modes shown on Fig. 1, for terminal heights of 1,000 feet. The curve computed for conventional direct and reflected ray theory is shown by a broken line within the horizon. Beyond the horizon, the single mode diffracted field over a 4/3 airless earth is indicated by the dashed lines. The mode sum curve agrees well with ray theory within the horizon, giving a minimum at the right range corresponding to the first null of the Lloyd's mirror interference pattern above the horizon, and a maximum above free space at the range of the lowest lobe maximum predicted by ray theory. The mode sum follows airless 4/3 earth theory for about 40 miles beyond the horizon, but then follows more nearly the rate of attenuation characteristic of the bilinear modes with the air layer fully considered. Beyond 500 miles the rapid decrease of the mode sum curve is to be associated with the limitations of our bilinear model, the neglect of air above 9.3 km. At such ranges all of the secondary scattering air lies below the horizon lines of one or both terminals, so that further increase of distance will increase the exponential part of the attenuation in the propagation path from transmitter via secondary scatterers in the air to receiver along a "stretched string path." Also shown on Fig. 2 is the mode of maximum contribution ($m=95$). In the region well beyond the horizon this line both as to absolute value and slope follows reasonably well the general course of the mode sum curve, without the oscillations of the latter. This contrasts with the clear inadequacy of the airless 4/3 earth calculation well beyond the horizon. Similar calculations with these same modes for antenna heights of 500 and 30 feet go well beyond average observations of the last ten years on stations out to about 350 miles.

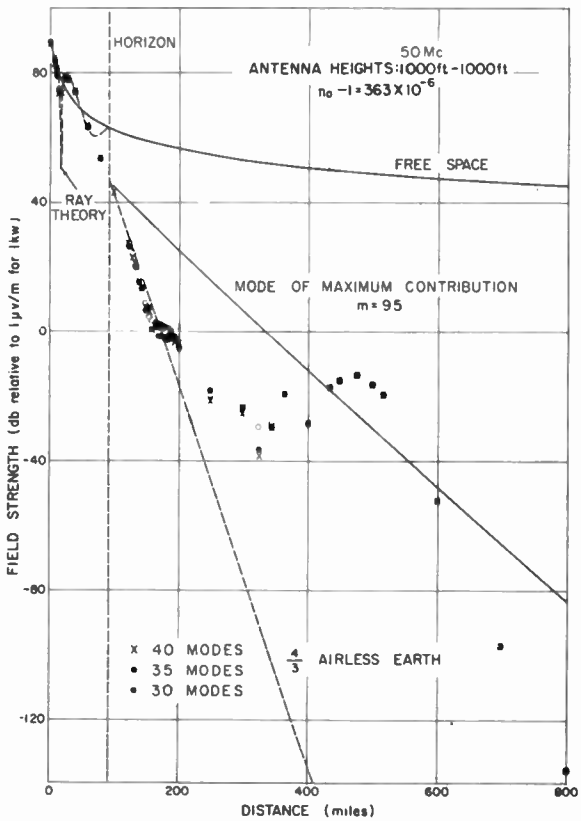

Fig. 2

Fig. 3 (page 1389) shows results of calculations on bilinear model for same atmosphere for 3,000 mc ($\lambda=10$ cm). Solid points are Megaw's experimental points, first shown at the Zurich General Assembly of URSI in 1950.[6] The crosses give the sum of fields contributed by 80 modes near that of maximum contribution or minimum attenuation. While the convergence of the 80-mode sum appears not so good at this frequency as the 40 mode sums used on Fig. 2 for 50 mc, enough modes have been used to get good agreement with (1) the first lobe within the horizon, (2) the rapid attenuation just beyond, in approximate agreement with 4/3 airless earth curves, and (3) the much more slowly attenuating fields in the deep shadow, where the airless earth field is hopelessly too small in absolute value, and too rapidly attenuated with distance.

[6] E. C. S. Megaw, "The scattering of electromagnetic waves by atmospheric turbulence," *Nature*, vol. 166, pp. 1100–1104; December 30, 1950. See also: "Waves and fluctuations," *Proc. IEE, Part III*, pp. 1–8; January, 1953.

Curvilinear and Trilinear Models

The inset of Fig. 3 shows several other profiles for which modes have been calculated for comparison with Megaw's data. For the inverse square-linear model, the

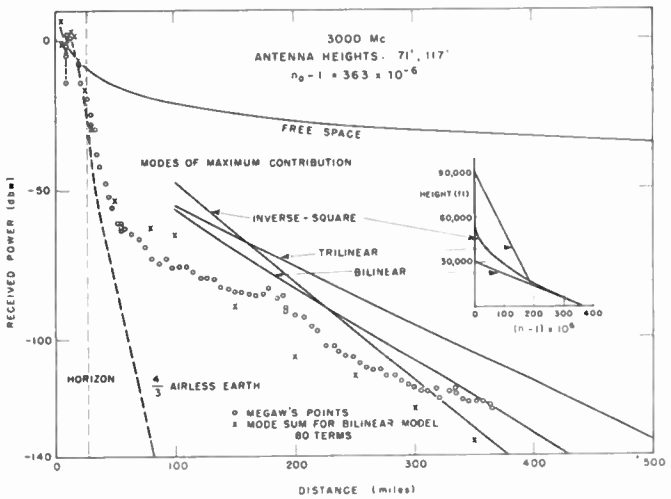

Fig. 3

index is represented by a monotonically decreasing curve with the same surface index and gradient used for the bilinear model and a zero gradient at 60,000 feet, above which vacuum propagation is assumed as before. Although this model also neglects all air above 60,000 feet, the absolute value and slope of the mode of maximum contribution agree well as to order of magnitude with Megaw's points. Another model used has been the trilinear, in which a different slope for the index profile has been assumed between 15,000 and 90,000 feet, chosen to have the correct total amount of air dielectric (represented by the area under the profile). The slope and the absolute value of the field contributed by the mode of maximum contribution are somewhat closer to Megaw's points than our bilinear and curvilinear models which contain less air dielectric. The agreement of the mode of maximum contribution of the curvilinear profile with Megaw's observations appears to dispose of the repeated objection which has been raised in the last decade against piecewise linear refractive index profiles on the ground that discontinuities of first derivatives of the index profiles at the points produce spurious effects. The inverse square-linear model is a two-piece analytic one in which the second derivative of the index profile changes at the level where the waves emerge into vacuum. Here, we repeat, the careful matching of solutions assures continuity of all components of the fields, so that no charge or current distributions are permitted to collect on the bounding surface. Physically the height of the "break" in a two-piece analytic profile $Y(Z)$ should be thought of as a height above which no air is considered, so that it is allowable to use only one of the two solutions of the differential equation for U_m to represent the outgoing waves above the air and the transmitter. Within the air layer, both solutions must be used to get eigenfunctions representing the primary field and the field coherently scattered by the perfectly reflecting earth and the air layer. Failure to use a two-piece analytic model for the eigenvalue problem with the twin complications of earth curvature and an air layer, with the air absent in the upper portion, makes it impossible to apply rigorously the Sommerfeld outgoing radiation condition at any height. Careless but conventional use of the Sommerfeld radiation condition to neglect one of the two independent solutions of the second-order differential equation (2) in inhomogeneous air leads to unwitting neglect of the internal reflection effect of the air layer, and the 4/3 earth dogma, regardless of how much air dielectric is assumed to compose the index profile.

Conclusion

Assume the conventional but logically defective "linear gradient" troposphere to be amended by specifying the absolute value as well as the standard gradient of refractive index at the surface, with a constant or monotonically decreasing gradient with increasing height, tapering to vacuum at some large height. Then the allowed modal solutions, more accurately computed than by WKB methods, show a remarkable similarity to long puzzling experimental observations of weak, slowly attenuating fields in the deep shadow region. These same modes also allow the field to be calculated within and just beyond the horizon, in agreement both with experimental facts and conventional calculations. The physical basis of these transitional modes supported by the normal air layer is just the coherent scattering by the polarizable air constituting the troposphere. The slight inhomogeneity built into the air by gravitational effects thus acts to support radio wave propagation in a way neglected by conventional airless 4/3 earth theory, which allows only for the refractive effect of the air layer and neglects the internal reflections. Of course, at times abnormal stratification of the troposphere can produce fields as large as the inverse distance value of free space. Also effects of macroscopic turbulence must be added in, when and where it is present in sufficient intensity to exceed the normal fields supported by coherent scattering in an idealized nonturbulent, nonsuperrefracting, dielectric air layer.

Literature

The preceding synopsis was prepared for and orally summarized at the eleventh general assembly of the International Scientific Radio Union at The Hague, August 28, 1954. More complete detail will be published soon. In the meantime, the interested reader may be directed to a number of places in the literature although some of them may be comparatively inaccessible and others are only abstracts. References to most experi-

mental literature on the subject may be found in the sections on tropospheric propagation of the PROCEEDINGS OF THE IRE annual progress reviews for the years 1947–1953.[7–13] Additional short reviews of the facts and theories are available.[14,15] The earliest applications of the theory of first order corrections to the WKB method to the explanation of tropospheric propagation well beyond the horizon were by Feinstein[16] and one of the present authors.[17] Conflicting views which developed over the applicability of these approximate correction methods are indicated in mimeographed vols. 3 and 4 (1952) of the TRANSACTIONS OF THE PROFESSIONAL GROUP ON ANTENNAS AND PROPAGATION. A number of abstracts by one or both of the present authors are published.[18] Some bilinear model results for 50-mc additional to this paper are also to be found.[19] Some details of the calculation for the linearly tapered atmosphere are given in an unpublished report,[20] and for the curvilinearly tapered atmosphere.[21,22]

Since the preparation and submission of this paper, a three-part paper[23] by Northover has been published which reaches again the conventional conclusion that omnipresent observed fields in the "radio twilight" region well beyond the horizon cannot be explained as an effect of modes propagated in the tapered air dielectric layer, in seeming contradiction to the conclusion above. Part I offers a proof of the "effective earth radius" modes as valid even well beyond the horizon, based on the assumption that the atmospheric index profile falls off with height according to a single analytic function, even at great heights where the usual outgoing radiation condition is applied in defining the eigenvalues just as in the airless earth case. Only in a homogeneous medium of constant index can progressive waves be recognized, the outgoing radiation condition strictly applied, or the wavelength of the radiation precisely defined. Our calculations for finite layers apply to index profiles with linear or curvilinear taper to vacuum at some large height. The index profile is therefore a two-piece analytic function, one piece representing the air layer, where a linear combination of both solutions of the wave equation is used, and the other piece representing the constant index for empty space above the air where only the outgoing solution is used. We do not maintain that the real atmosphere is limited in height, of course, but only that no mathematical method has yet been invented for dealing accurately with the eigenvalue problem for propagation around a curved earth surmounted by an inhomogeneous air layer extending to infinitely great height. The calculations above indicate that our neglect of a very small amount of air sufficiently high in the atmosphere is unimportant in understanding observed "radio twilight" fields, but allows us to use the conventional outgoing radiation condition correctly. Most of Parts II and III of Northover's paper, we believe, can ultimately be regarded as confirmation and some extension of our calculations, if only they be reinterpreted as the effect of the coherent scattering by the air molecules throughout the volume of the air layer. In optical theory of propagation through a slab, the waves which appear to come from the boundaries fundamentally arise from the superposition of secondary scattered waves from all the molecules of the slab. The term "radio twilight" has recently[24] been suggested as a terminology accurately descriptive of tropospheric propagation in the deep shadow region, and seems to have won some acceptance at the recent symposium on "Normal Mode Theory" at Navy Electronics Laboratory, San Diego, July 1955.

[7] "Radio progress during 1947," PROC. IRE, vol. 36, pp. 531–534; April, 1948, especially references (277), (281), (290).

[8] "Radio progress during 1948," PROC. IRE, vol. 37, pp. 308–310; March, 1949, especially references (475), (498), (513).

[9] "Radio progress during 1949," PROC. IRE, vol. 38, pp. 386–388; April, 1950, especially references (748), (753), (760).

[10] "Radio progress during 1950," PROC. IRE, vol. 39, pp. 391–393, April, 1951, especially references (945), (946), (949), (951), (958), (968).

[11] "Radio progress during 1951," PROC. IRE, vol. 40, pp. 424–426; April, 1952, especially references (509), (510), (511), (516).

[12] "Radio progress during 1952," PROC. IRE, vol. 41, pp. 497–500; April, 1953, especially references (960), (961–965).

[13] "Radio progress during 1953," PROC. IRE, vol. 42, pp. 709–710; April, 1954, especially references (56–61), (66), (67).

[14] T. J. Carroll, "Tropospheric propagation well beyond the horizon—A Review," in Supplement to the *Proc. Conf. Radio Meteorology*, published by Bureau of Engineering Research, University of Texas, Austin, Texas, pp. I (1–7); 1954.

[15] T. J. Carroll, "Overcoming the line-of-sight shibboleth with the air and high power," 1954, *Convention Record of the IRE*, Part I, pp. 121–125. Also in PROC. IRE (Australia), vol. 16, pp. 107–112; April, 1955.

[16] J. Feinstein, "Tropospheric propagation beyond the horizon," *Jour. Appl. Phys.*, vol. 22, pp. 1292–1293; October, 1951. Also TRANS. IRE, vol. AP-2, pp. 2–8; March, 1952; and vol. 4, pp. 2–13, December, 1952.

[17] T. J. Carroll, "Internal reflection in the troposphere and propagation beyond the horizon," TRANS. IRE, vol. AP-2, pp. 9–27; March, 1952. Also. TRANS. IRE, vol. AP-3, pp. 84–100; August, 1952, and vol. 4, p. 19; December, 1952 (abstract only). Texts available from author.

[18] Abstracts on the subject of this paper: *Phys. Rev.*, vol. 85, p. 732; February, 1952; *Phys. Rev.*, vol. 86, p. 614; May, 1952; *Phys. Rev.*, vol. 91, p. 458; July, 1953; *Phys. Rev.*, vol. 95, p. 623; July, 1954; *Bull. Am. Met. Soc.*, vol. 34, p. 325; September. 1953.

[19] T. J. Carroll and R. M. Ring, "Important modes in the troposphere treated as a linearly graded layer of dielectric"; *Proc. Conf. Radio Meteorology*, published by the Bureau of Engineering Research, University of Texas, Austin, Texas, pp. 1–6; 1953.

[20] T. J. Carroll and R. M. Ring, "Normal tropospheric propagation of short radio waves well beyond the horizon," MIT Lincoln Lab. Technical Report (not generally available).

[21] R. M. Ring, "The Complex Eigenvalue Problem for Radio Waves in a Curvilinear Tapered Atmosphere," Brown University Doctoral Thesis, May, 1954 (unpublished).

[22] B. Friedman and B. Lippman, "Higher-order modes in tropospheric propagation," Abstract of paper at Washington URSI-IRE meeting, Washington, D. C.; May 6, 1954.

[23] F. H. Northover, "Long Distance VHF Fields," *Can. Jour. Physics*, 33, Part I, pp. 241–256, May 1955; Part II, pp. 316–346, June 1955; Part III, pp. 347–349, June 1955.

[24] T. J. Carroll and R. M. Ring, "Radio and Optical Twilight and Modes," Paper presented at URSI Michigan Symposium June 1955. To be published in TRANS. IRE PGAP Supplement to Vol. 3 (Abstract only).

Measurements of the Phase of Radio Waves Received over Transmission Paths with Electrical Lengths Varying as a Result of Atmospheric Turbulence*

J. W. HERBSTREIT†, SENIOR MEMBER, IRE, AND M. C. THOMPSON†, SENIOR MEMBER, IRE

Summary—**A system for the measurement of the variations in electrical lengths of radio propagation paths is described. The observed path-length instabilities are considered to be caused by the same atmospheric turbulence responsible for the existence of very high frequency and ultra high frequency fields far beyond the radio horizon. Results obtained on 172.8 mc and 1,046 mc along 3½-, 10-, and 60-mile paths are reported. It is pointed out that measurements of this type provide a powerful tool for the study of the size and intensity of the refractivity variations of the atmosphere giving rise to the observed phenomenon.**

Introduction

THE STABILITY of the phase of a wave propagated through the inhomogeneous atmosphere is important in considerations of the ultimate accuracy of radio direction-finding systems. The spatial and temporal variations of the refractive index of the atmosphere[1-3] are now considered to explain the existence far beyond the radio horizon of useful vhf and uhf signal strengths. The magnitude and the spatial distribution of these inhomogeneities have been the subjects of both ground and airborne measurement by a number of investigators.[4,5] Their results have been shown to provide a basis for the explanation, at least in a qualitative manner, of the transmission loss observations made over long propagation paths.[6,7] The subject of this paper is the measurement of the effect of these inhomogeneities on the stability of the electrical path length (phase of arrival relative to the transmitted phase) of electromagnetic waves as they pass through the lower regions of the atmosphere. Theoretical aspects of the electrical path length stability have been treated in several papers.[8-10]

The NBS phase measurement system has been operated over three areas in the vicinity of Colorado Springs, Colorado:

1. Cheyenne Mountain to Fort Carson, approximately 3½ miles.
2. Pikes Peak to Garden of the Gods, approximately 10 miles.
3. Pikes Peak to Kendrick, approximately 60 miles.

Paths are their profiles are shown in Fig. 1, p. 1392.

Instrumentation has been developed to measure (1) the variations in the phase difference of the waves at the two ends of a single path and (2) simultaneously the variations in the phase difference between the waves arriving over the first path and those arriving over an adjacent path. In addition, instrumentation reported previously[1] has been developed to measure the very small changes in the amplitude of the received field which occur within the radio horizon. The use of these two types of instrumentation is expected to make possible the evaluation of the parameters important in the interpretation of scatter-type propagation mechanisms particularly when used in conjunction with microwave refractometers and other meteorological equipment under a variety of atmospheric turbulence conditions.

Description of Phase Measurement System

The system for measurement of phase variations along a single path is shown in Fig. 2, on the next page. One transmitter on a nominal frequency of 1,046 mc is located at each terminal of the path and the frequencies are held to approximately two parts in 10^9 over a period of several hours. The frequencies of these transmitters, T_1 and T_2 are so chosen that their difference is an audio frequency in the range of 2 to 9 kc. At each terminal a

* Original manuscript received by the IRE, August 1, 1955. The research reported in this paper has been sponsored in part by the Air Force Cambridge Research Center, Air Research and Development Command.

† Centeral Radio Propagation Laboratory, National Bureau of Standards, Boulder, Colorado.

[1] A. P. Barsis, J. W. Herbstreit, and K. O. Hornberg, "Cheyenne Mountain Tropospheric Propagation Experiments," Nat. Bur. Standards Circular 554; January 3, 1955.

[2] H. G. Booker and W. E. Gordon, "A theory of radio scattering in the troposphere," PROC. IRE, vol. 38, pp. 401–412; April, 1950.

[3] H. Staras, "Scattering of electromagnetic energy in a randomly inhomogeneous atmosphere," *Jour. Appl. Phys.*, vol. 23, pp. 1152–1156; October, 1952.

[4] C. E. von Rosenberg, C. M. Crain, and A. W. Straiton, "Atmospheric Refractive-Index Fluctuations as Recorded by an Airborne Microwave Refractometer," paper presented at URSI Spring Meeting, Washington, D. C.; also Electrical Engineering Research Laboratory, University of Texas, Report 6-01; 1953.

[5] H. E. Bussey and G. Birnbaum, "Measurement of variations in atmospheric refractive index with an airborne microwave refractometer," *Nat. Bur. Standards Jour. Res.*, vol. 51, pp. 171–178; October, 1953.

[6] J. W. Herbstreit, K. A. Norton, P. L. Rice, and G. E. Schafer, "Radio wave scattering in tropospheric propagation," 1953 IRE CONVENTION RECORD, Part 2, pp. 85–93.

[7] W. E. Gordon, "Radio scattering in the troposphere," PROC. IRE, vol. 43, pp. 23–28; January, 1955.

[8] P. G. Bergman, "Propagation of radiation in a medium with random inhomogeneities," *Phys. Rev.*, vol. 70, pp. 486–492; October, 1946.

[9] V. A. Krasilnikov, "The effect of the coefficient of refraction in the atmosphere upon the propagation of ultrashort radio waves," *Izvest. Akad. Nauk*, USSR, *Ser. Geografich. Geofiz.*, vol. 13, pp. 33–57; 1949.

[10] R. B. Muchmore and A. D. Wheelon, "Direct ray line-of-sight propagation phenomena," p. 1437, this issue. A. D. Wheelon and R. B. Muchmore, "Scattered field line-of-sight propagation phenomena," p. 1450, this issue. A. D. Wheelon, "Near-field corrections to line-of-sight propagation," p. 1459, this issue.

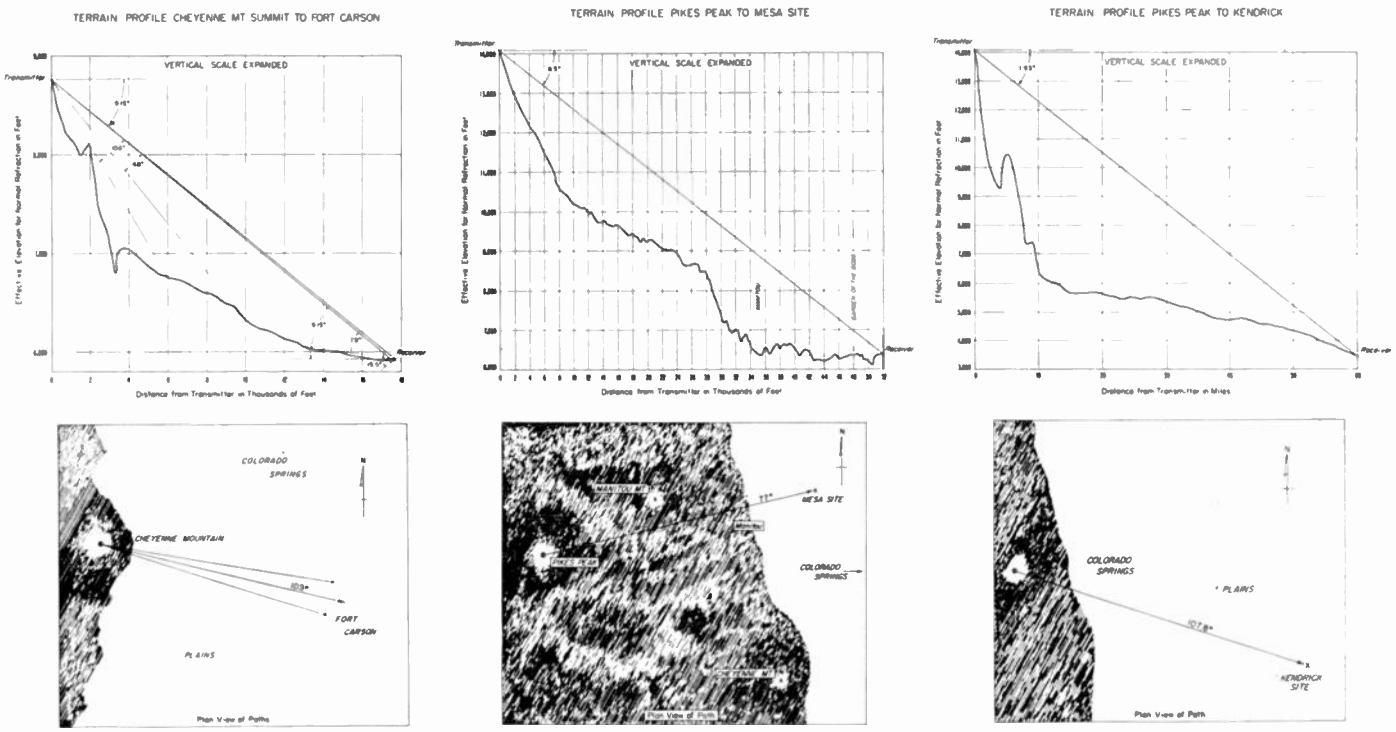

Fig. 1—Terrain profiles and plan views of propagation paths studied.

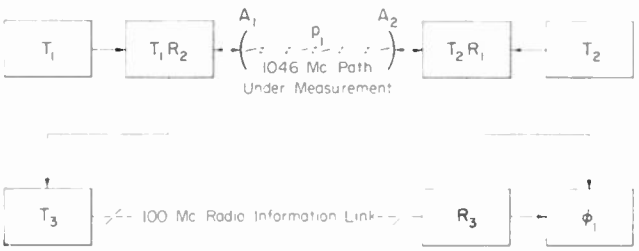

Fig. 2—Single-path measurement system.

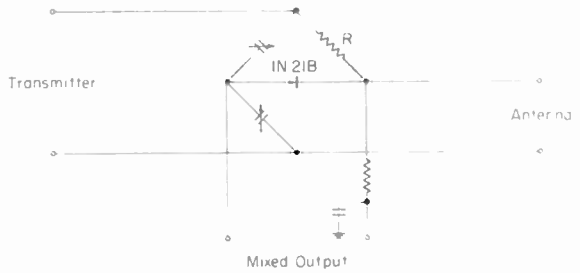

Fig. 3—Duplexer-mixer schematic.

directional antenna is used together with a duplexing system such that each antenna simultaneously transmits one frequency and receives the other; the duplexer-crystal-mixer combinations are designated T_1R_2 and T_2R_1. These mixers are adaptations of coaxial bridge type directional couplers arranged with the antenna as one leg of an almost-balanced bridge, the crystal mixer being in the null portion of the circuit when observed from the transmitter, and in the high sensitivity portion when observed from the antenna. Thus, only a very small portion of the high-level local transmitter energy appears across the mixer, a much larger portion being transmitted by the antenna; simultaneously a large portion of the energy received by the same antenna from the distant transmitter appears across the mixer. The circuit is illustrated in Fig. 3. A coaxial tuning stub is used as one capacitive arm of the bridge and also provides a dc return for the mixer.

The variations in the relative phase of the two audio signals appearing at the output of the two mixers, one at each end of the path, are equal to twice the variations in the electrical length of the path. In order to make the phase comparison, the audio signal appearing at T_1R_2 is transmitted as a modulating signal on a 100-mc FM auxiliary transmitter to the other end of the path where it is received by a 100-mc auxiliary receiver and compared in phase by means of a recording electronic phase meter with the audio signal detected in duplexer mixer T_2R_1.

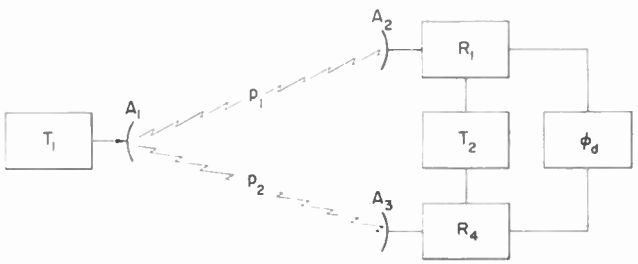

Fig. 4—Path-difference measurement system.

In the two-path measurements illustrated in Fig. 4, the wave from the single transmitting system, T_1, is received on each of two receiving systems R_1 and R_4, some miles distant from T_1. The two heterodyne receivers

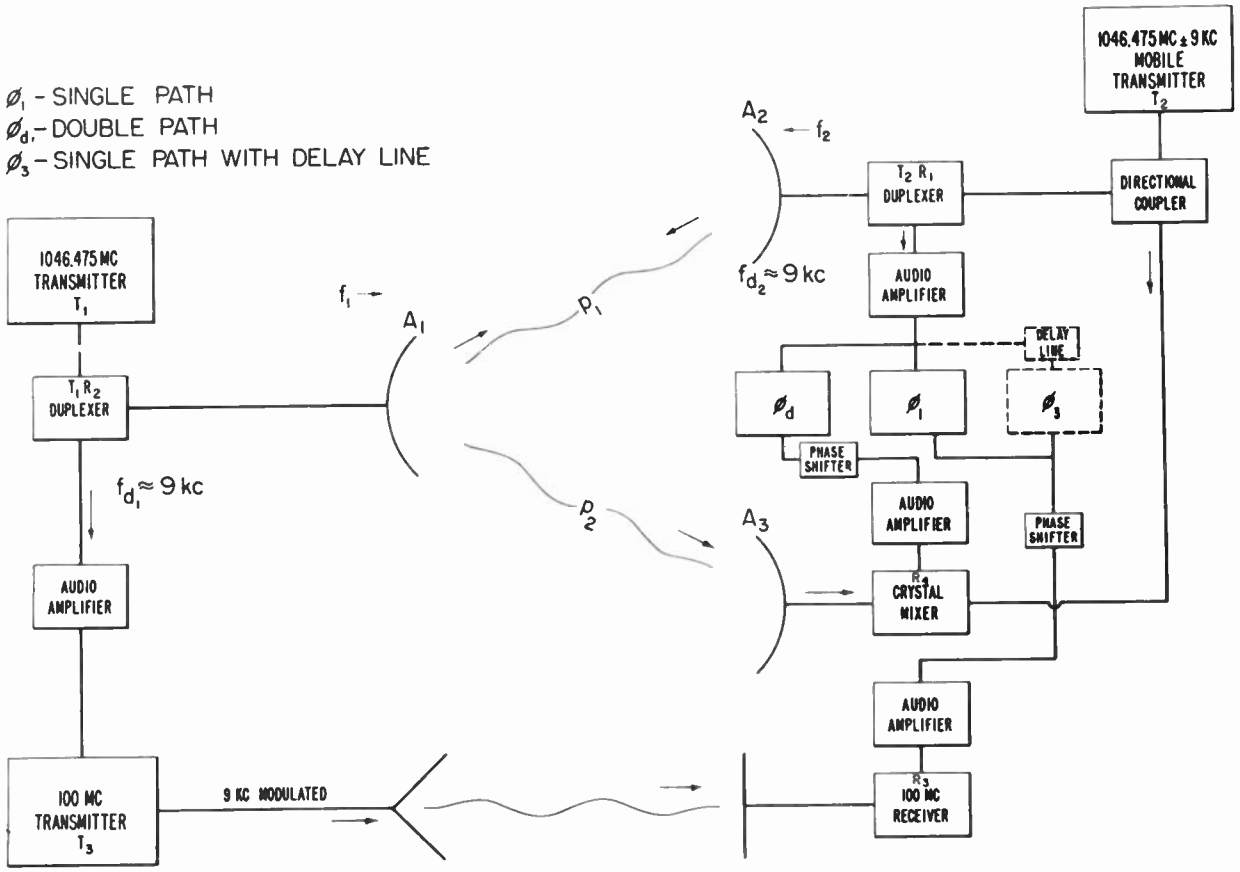

Fig. 5—Cheyenne Mountain 1,046-mc phase measurement system.

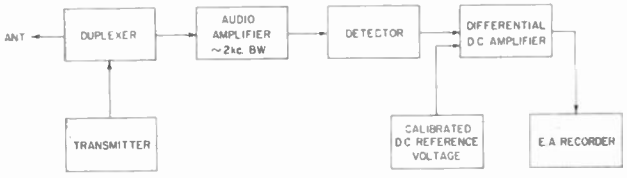

Fig. 6—System for recording variations in signal amplitude.

consisting of crystal mixers and audio amplifiers employ a common local oscillator which is actually the same transmitter, T_2, used in the single path measurements. The phases of the audio signals from receivers R_1 and R_4 are compared in a separate electronic recording phase meter to record the variations in the difference in effective electrical path length of the two paths p_1 and p_2.

A block diagram of the complete system which integrates the two types of phase measurement (single-path and two-path) is shown in Fig. 5 above. Analysis of system performance is given in the Appendix. Fig. 6, above, shows auxiliary equipment used to measure small changes in signal amplitude. The instrumentation has been undergoing continuous development to eliminate various sources of phase instability, the most serious of which has been the temperature instability of the transmission lines originally employed between the two spaced receiving antennas at the Fort Carson receiving site. Much of this phase instability in this earlier system was eliminated by burying the transmission lines under approximately one foot of earth. The system has more recently been operated on the Pikes Peak to the Garden of the Gods site using three simultaneously operated single path systems at 1,046 mc, which essentially eliminates all transmission lines.

In order to study the effect of frequency on the effective electrical path-length difference an almost identical two-path system is in operation at 172.8 mc using equipment previously developed by E. Florman to determine the velocity of radio waves.[11] In addition, the University of Texas has operated a path-difference system at 9,375 mc for short periods on closely adjacent paths in conjunction with the NBS 172.8 and 1,046 mc measurements.[12]

Results of Measurements

The data taken to date consist of the following measurements:

1. Phase variation of radio waves over single paths.
2. Variations in phase-difference between waves arriving over different paths on frequencies of 172.8 mc and 1,046 mc. Phase difference measurements

[11] E. Florman, "A measurement of the velocity of propagation of vhf radio waves at the surface of the earth," *Nat. Bur. Standards Jour. Res.*, vol. 54, pp. 335–345; June, 1955.

[12] A. P. Deam and B. M. Fannin, "Phase-difference variations in 9,350 mc radio signals arriving at spaced antennas," p. 1402, this issue.

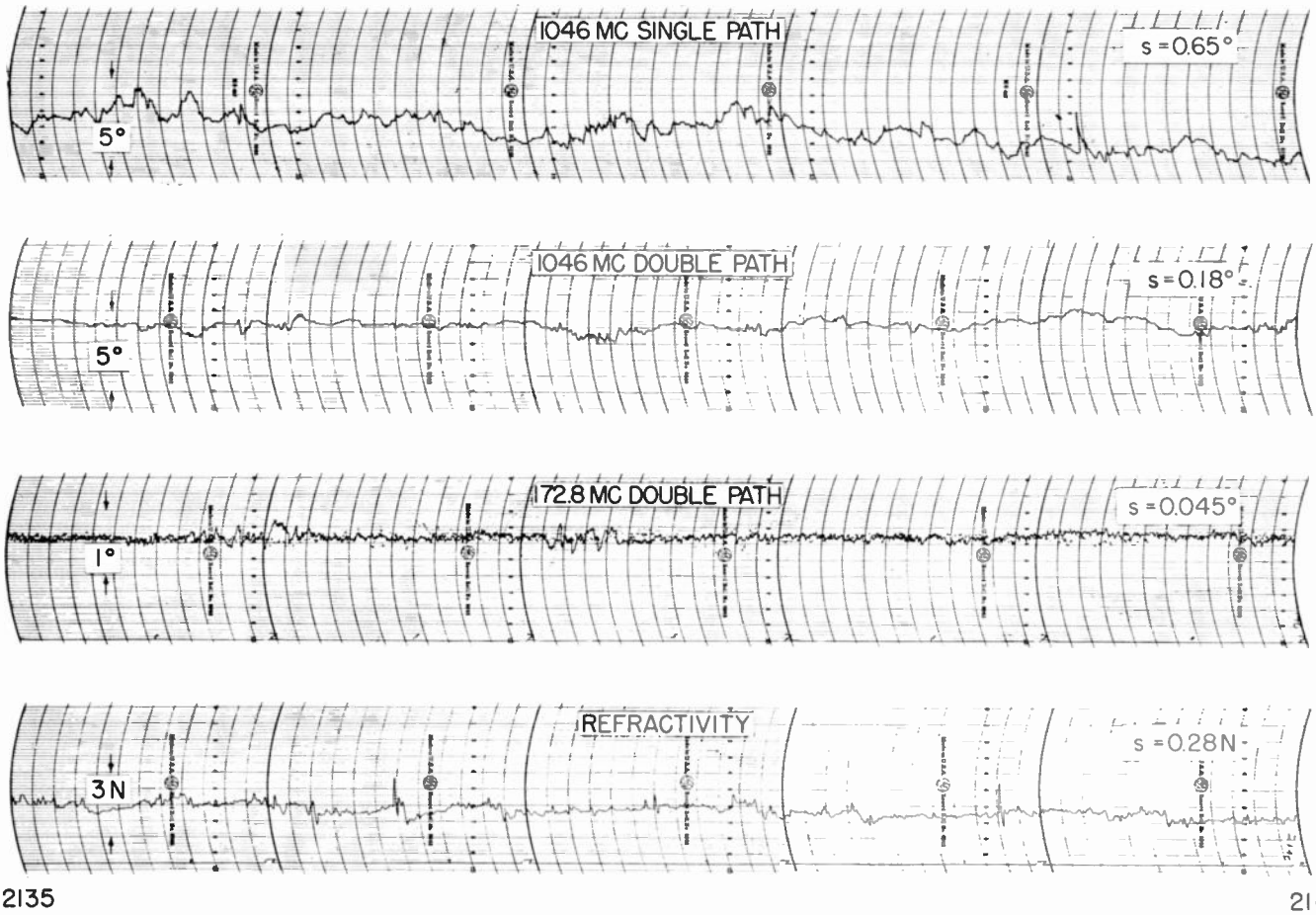

Fig. 7—Sample phase and refractometer recordings taken on Cheyenne Mountain to Fort Carson Path, 2,135–2,140 MST, March 15, 1955. Antenna spacing of 500 feet for double path measurements.

on 9,350 mc were made by the University of Texas on the Cheyenne Mountain–Fort Carson and Pikes Peak–Garden of the Gods paths and are reported in a separate paper appearing in this issue.[12]

3. Refractive index fluctuations approximately 20 feet above ground level at each end of the paths.
4. Amplitude variations of radio waves propagated over a single path.
5. Wind velocity, temperature, relative humidity, and barometric pressure at both ends of the paths.
6. Color photographs taken from each end of the paths looking toward the opposite end to record the existence of any visible atmospheric phenomena such as clouds, dust, etc.

To illustrate the general character of the data obtained, short samples of four kinds of records (phase and refractometer) taken simultaneously are shown in Fig. 7, above. Simultaneous phase and amplitude records appear in Fig. 8 for Pikes Peak–Garden of the Gods paths.

Fig. 9 shows distributions of samples of phase variations over paths $3\frac{1}{2}$, 10 and 60 miles long.

Fig. 10 gives phase difference measurements as a function of frequency for a short sample of data taken from a period when 9,375 mc data were being recorded simultaneously with those on frequencies of 172.8 and 1,046 mc; the 9,375 mc data were taken by the University of Texas. The standard deviation of phase differences, s_d, was obtained for each of six two-minute sampling periods mentioned above. At the time these data were taken, the antenna spacing on all three frequencies was nominally 500 feet. It is evident that s_d was observed on this occasion to be very nearly directly proportional to the radio frequency in accordance with current theoretical predictions.[8–10]

Fig. 11, on page 1396, shows correlation coefficient for one of the two-minute sampling periods as a function of relative time displacements of the two records being compared. Going from south to north, the 1,046 mc, 172.8 mc, and 9,375 mc antenna systems were located on the baseline in that order, with approximately 50 feet separation between centers. The average wind speed was approximately 7 feet per second and essentially normal to the path. For the 50-foot system spacings, time delays of about 7 seconds in the correlation coefficients would be expected provided the atmospheric in homogeneities which caused the changes in phase difference were moving with the average velocity of the wind. It is seen in Fig. 11 that the time delays corresponding to maximum correlation are of the correct sign, but their magnitudes are not in agreement with the above hypothesis.

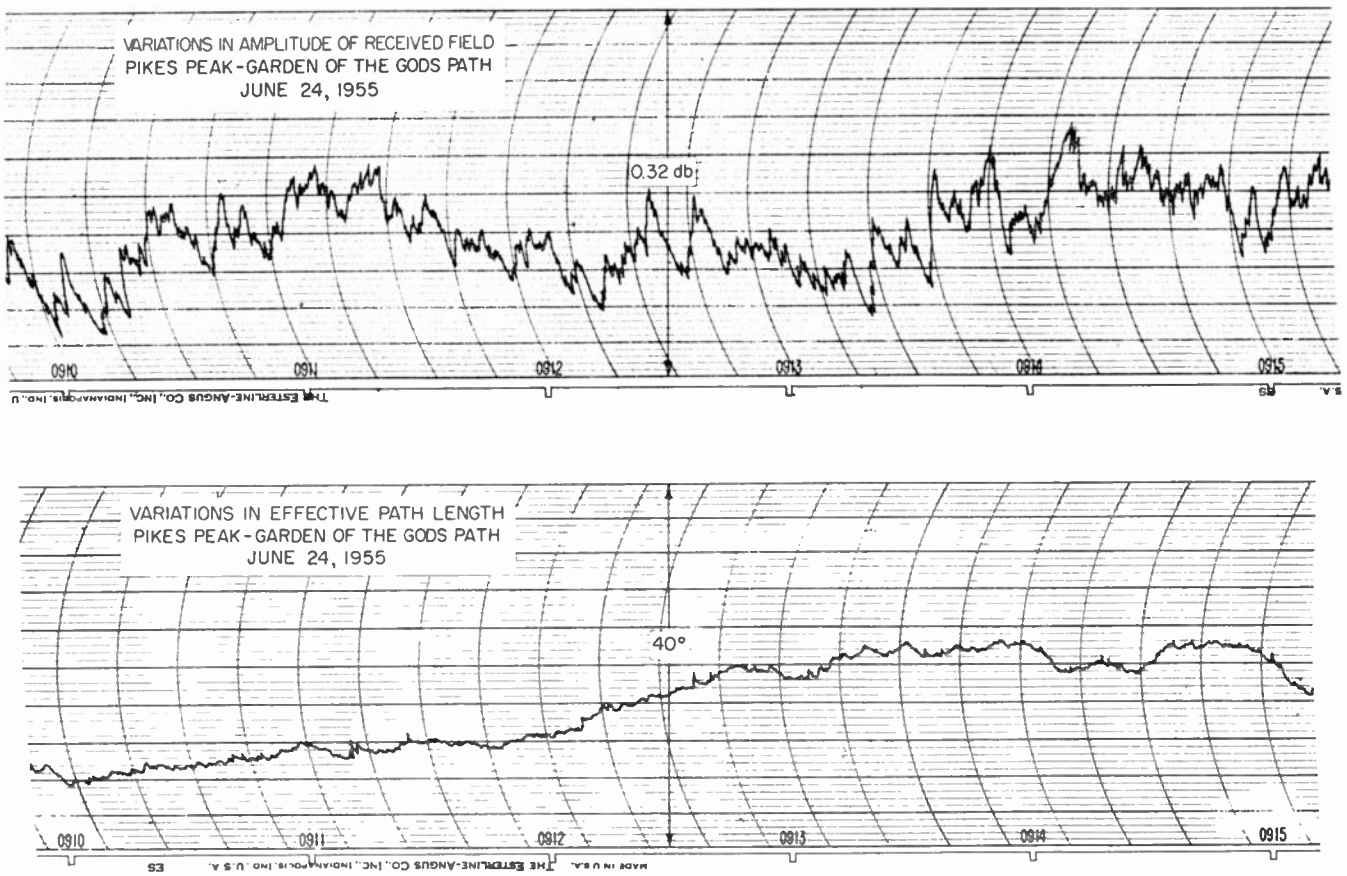

Fig. 8—1,046-mc amplitude and phase variations as recorded Pikes Peak–Garden of the Gods path, 0910–0915 MST, June 24, 1955.

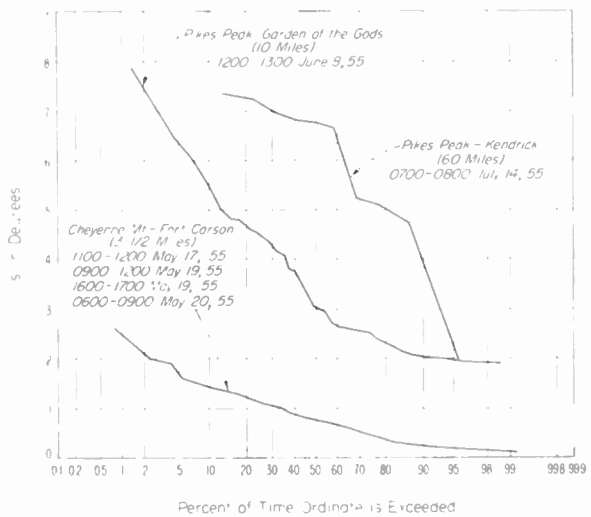

Fig. 9—Sample distributions of the standard deviation s of 1,046-mc electrical path length changes observed in 5-minute sampling periods.

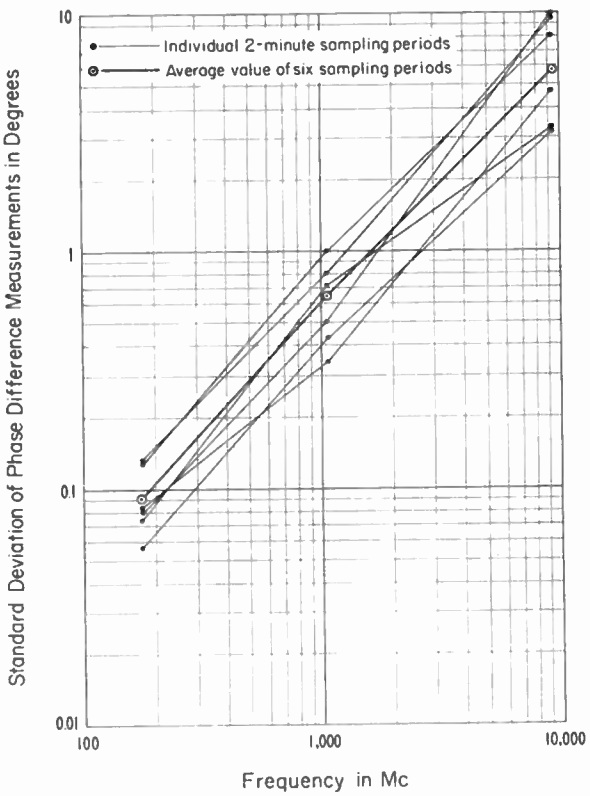

Fig. 10—Standard deviations of phase difference vs radio frequency, Cheyenne Mountain–Fort Carson path, 1504–1521 MST, March 18, 1955. Antenna spacing 500 feet.

Discussion of Results

The variations in phase and amplitude of radio fields propagated through the atmosphere are considered to result from the inhomogeneous nature of the atmosphere. A number of theoretical treatments of the effects of this inhomogeneity have been advanced. However, a considerable number of questions have been raised

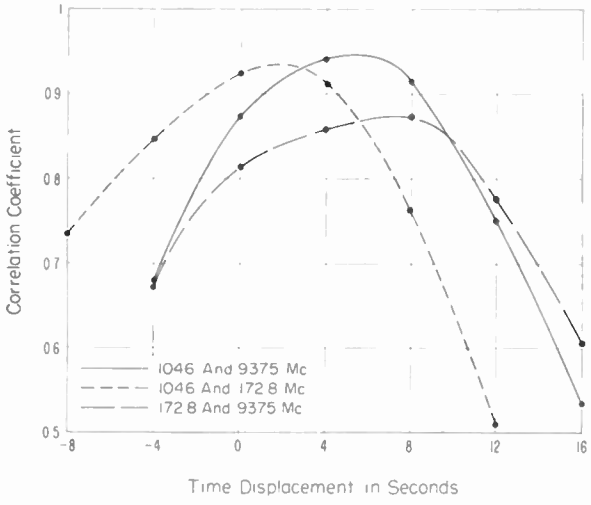

Fig. 11—Correlation coefficient of instantaneous phase difference vs time displacement, Cheyenne Mountain to Fort Carson path, 1516–1518 MST, March 18, 1955.

concerning the validity of these theories. The simultaneous measurement of the small changes in the phase and the amplitude of radio fields propagated through the atmosphere provides a means of studying the applicability of the various theories and a basis for their improvement.

One hour of phase, amplitude and meteorological data taken with the NBS measurement system has been selected for intensive study. The hour chosen was 0440–0540, June 24, 1954, which was taken as a period when a maximum amount of information was being recorded, and when all equipment was performing at high efficiency. A digest of the recorded data is shown in Fig. 12, below. Values of phase, phase difference, signal amplitude, refractivity, temperature, humidity, wind speed, and wind direction are given. The plots of phase, phase difference, and amplitude were made from data points spaced 40 seconds apart and no attempt has been

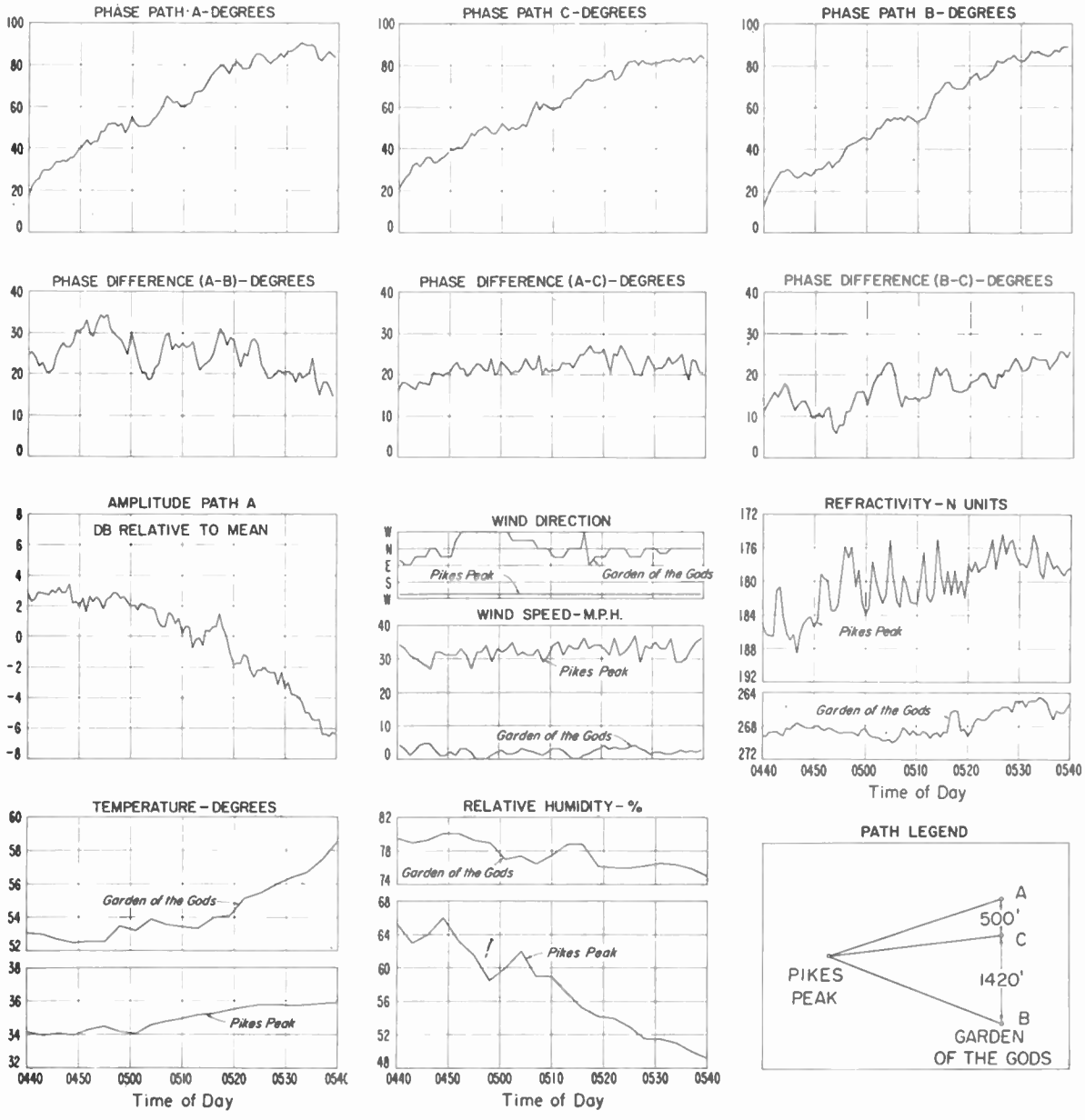

Fig. 12—Digest of measurements, 1,046-mc Pikes Peak–Garden of the Gods, 0440–0450 MST, June 24, 1955.

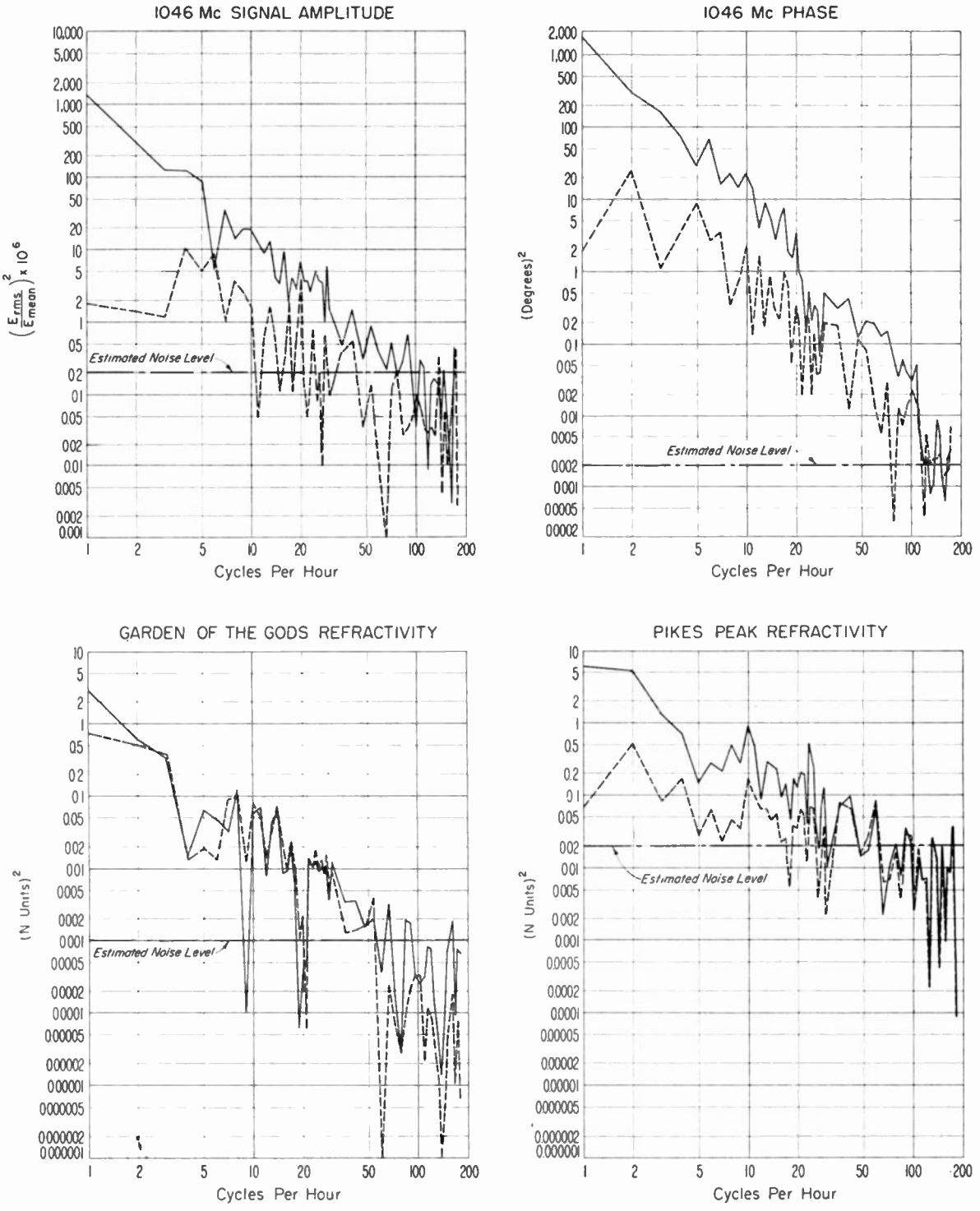

Fig. 13—Fourier spectra of measurements Pikes Peak–Garden of the Gods path, 0440-0450 MST, June 24, 1955. ——— Original data, broken line, parabolic trend removed.

made to include the small scale variability which is contained in the original recordings. One of the indicated properties of these data is a large scale change of phase which occurs almost identically on each of the single paths over the period of an hour. This is considered to result from large changes in the refractive index occurring over the entire path. However, superimposed on these large changes are more rapid fluctuations in effective path length which, to a greater or lesser degree, occur simultaneously on each path. The degree to which they do occur simultaneously may be expressed in terms of a correlation coefficient.

Fourier Spectrum Analyses of Data

The spectra of the intensities of both the phase and the amplitude variations of the received field as well as of the refractivity have been investigated using data points taken every ten seconds in terms of 60-point Fourier analyses. Intensities are plotted in Fig. 13, above, for components up to 180 cycles per hour both for

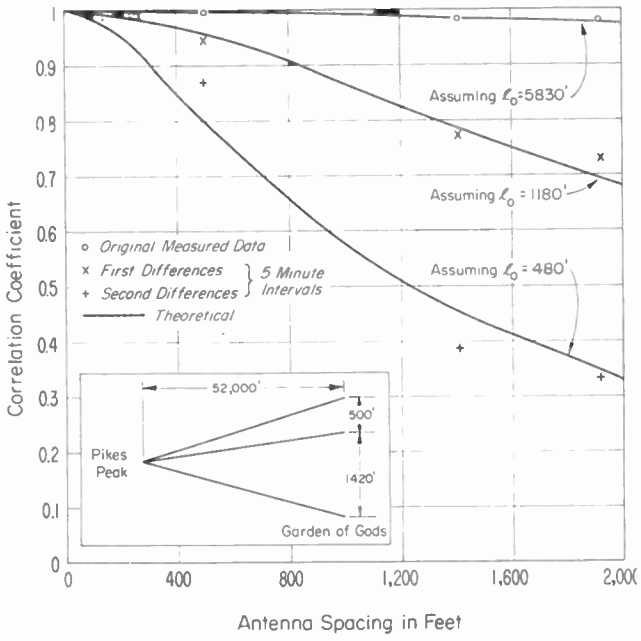

Fig. 14—Correlation Coefficient of Phase Measurements vs antenna spacing 1,046-mc Pikes Peak–Garden of the Gods path, 0440–0540 MST, June 24, 1955.

the original data as recorded and for the same data with a parabolic trend removed. The ordinates were determined by taking the sum of the squares of the two Fourier coefficients for each frequency. It may be observed that the intensity spectra with the parabolic trends removed have the low-frequency components, representing the large slow changes within the hour, reduced considerably in amplitude. Although the spectra are calculated up to 180 cycles per hour, it is clear that little reliance should be placed on ordinate values indicating intensities below the estimated noise level of the measuring instruments.

Phase Correlation on Spaced Antennas

Fig. 14 illustrates the correlation of the phase observations between adjacent paths as a function of antenna separation at the Garden of the Gods site for three methods of handling the data. The expression used to determine the correlation coefficients r_{12} of the data samples is as follows:

$$r_{12} = \frac{s_1^2 + s_2^2 - s_d^2}{2s_1s_2}, \tag{1}$$

where s_1^2 and s_2^2 are variances of the phase measured on paths 1 and 2, respectively, while s_d^2 is the variance of the differences of these two phases. Included on this figure are theoretical[13] curves of phase correlation vs antenna spacing[10] assuming the space correlation of refractivity of the atmosphere to have the form $\rho_N = \exp(-|r|/l_0)$, where r is distance and l_0 is a characteristic scale length. This is the same form of refractivity space correlation function assumed by Booker and Gordon in their original work on tropospheric scatter.[2] It may be seen that the original data, which contain the large scale phase changes occurring within the hour, are very well correlated over all paths and appear to fit the theoretical curve assuming a characteristic scale length of 5,830 feet. The intermediate data on this figure were determined by using the variate difference method[14] using first differences between observed data spaced five minutes apart. This has the property of reducing the effect of the long term variations occurring over the hour. The lower curve was determined by using the second differences also taken five minutes apart, which further reduces the effects of the long term variations occurring over the hour. As would be expected, shorter and shorter characteristic scale lengths are indicated for each of the three sets of points.

Field Amplitude Variability

Wheelon and Muchmore[10] have presented an atmospheric model which considers the received field within the Fresnel zone of the scatterers to consist of a constant direct field plus a normally distributed field component in phase-quadrature. The component in phase-quadrature is considered to result from reradiation from the displacement currents induced in the dielectric inhomogeneities along the direct path. On the basis of this model, the following relationship is obtained between the phase and amplitude fluctuations of the resultant field:[15]

$$\sigma_{\phi_d}^2 \cong \sqrt{2}\sigma_r \text{ (radians}^2\text{)} \tag{2}$$

where $\sigma_{\phi_d}^2$ is the variance of the phase deviations and σ_r is the square root of the variance of the amplitude fluctuations of the field divided by its mean amplitude.

A second theoretical model is considered in an attempt to explain the variations in the amplitude of the received field. It assumes that the received field is the vector sum of a constant direct field and small Rayleigh scattered components[15] arriving from off-beam heterogeneities in the medium. In this case the variability of the phase of the resultant field relative to that of the constant component may be calculated from the results given by Norton, Shultz, and Yarbrough.[16] When the scattered component is sufficiently small, the phase, ϕ_s, of the resultant is approximately normally distributed about zero with a standard deviation given by

[13] Assuming an atmospheric refractive index correlation of the form $\rho_{12} = \exp(-|r|/l_0)$, the following expression is obtained in reference 10 for the correlation of phase variations between fields received by two spaced antennas over paths having one common end-point:

$$\rho_{12} = \frac{\pi}{2}\left[K_0\left(\frac{S}{l_0}\right)L_{-1}\left(\frac{S}{l_0}\right) + L_0\left(\frac{S}{l_0}\right)K_{-1}\left(\frac{S}{l_0}\right)\right] - K_0\left(\frac{S}{l_0}\right),$$

in which S is antenna separation and is assumed small compared with the path lengths, l_0 is the characteristic scale length of refractive index, K denotes modified Bessel functions of the second kind, and L the modified Struve functions.

[14] G. Tintner, "The Variate Difference Method," Principia Press, Inc., Bloomington, Indiana; 1940.

[15] K. A. Norton, L. E. Vogler, W. V. Mansfield, and P. J. Short, "The probability distribution of the amplitude of a constant vector plus a Rayleigh distributed vector," p. 1354, this issue.

[16] K. A. Norton, E. L. Shultz, and H. Yarbrough, "The probability distribution of the phase of the resultant vector sum of a constant vector plus a Rayleigh distributed vector," *Jour. Appl. Phys.*, vol. 23, pp. 137–141; January, 1952.

TABLE I

COMPARISON OF OBSERVED AND CALCULATED PHASE VARIATIONS BASED ON TWO MODELS OF CONSTANT PLUS SCATTERED FIELDS

	Pikes Peak–Garden of the Gods, 0440–0540 MST, June 24, 1955			Pikes Peak–Kendrick 0710–0800 MST, July 14, 1955		
	Root-Mean-Square Deviation in Degrees					
	Observed	Calculated		Observed	Calculated	
		Quadrature	Rayleigh		Quadrature	Rayleigh
Original data	19.95	12.3	1.87	8.99	15.7	3.02
First differences (5-minute interval)	4.92	7.07	.618	9.50	16.3	3.28
Second differences (5-minute interval)	2.83	6.14	.465	—	—	—

$$\sigma_{\phi_s}^2 \cong \frac{k^2}{2} \cong \sigma_r^2 \quad \text{(radians}^2\text{)} \tag{3}$$

In the above, k is the root-mean-square amplitude of the Rayleigh distributed component relative to that of the constant component as in reference 14,[17] and is related, as shown above, to the variance, σ_r^2, of the amplitude fluctuations.

Table I, above, presents the standard deviations of the phase as measured directly and as calculated for both of the above models from the amplitude measurements made simultaneously. The data for the Pikes Peak–Garden of the Gods path are shown for three methods of data reduction: (1) the observed data with long-term variations included, (2) determined from first differences (variate difference method), and (3) determined from second differences. Data for the Pikes Peak–Kendrick path are also shown for methods of data reduction (1) and (2) above. It may be seen that the root-mean-square phase variations calculated from the amplitude variations on the basis of the phase-quadrature model[15] are somewhat greater than those observed except for the original Pikes Peak–Garden of the Gods data, and those calculated on the basis of the Rayleigh scattering model are all much too small. The fact that the original Pikes Peak–Garden of the Gods observations fall outside of the two models may be explained on the basis that there are large scale changes in refractivity of the atmosphere which effect the phase of the constant component, but do not influence the amplitude of the received field. The fact that the remaining values for the two models bracket the observed data and the further fact that the shorter path data show a tendency to agree better with the phase-quadrature model indicates the qualitative utility of these models.

CONCLUSION

A system of measuring the variability of the effective length of the electrical path has been developed by the National Bureau of Standards. This system measures simultaneously (1) the variations in the effective electrical length of a single propagation path, (2) the difference in effective electrical lengths of propagation paths from a common transmitter to each of two spaced receiving antennas, and (3) the very small amplitude variations. These three sets of simultaneous measurements have provided valuable data for the study of the nature of the refractivity variations of the atmosphere.

Wheelon and Muchmore[10] have derived theoretical expressions for the mean square value of the phase variations of the direct wave which contain as parameters the frequency, the mean path length, a mean scale of turbulence and the mean square variation of the refractivity along the path. Expressions have also been derived,[10] depending principally upon the scale of turbulence, for the correlation of the effective electrical path lengths expected on two neighboring propagation paths. These theoretical derivations are based on various models of the turbulent atmosphere designed to explain scatter-type tropospheric propagation.

Scatter of energy from variations in the refractivity of the atmosphere also give rise to variations in the amplitude of the received field. These amplitude variations are considered in terms of a direct wave with a scattered field superimposed. Observed phase variations on relatively short paths are greater than would be predicted from observed amplitude variations on the basis of the above hypothesis assuming a Rayleigh scattered field. The observed phase variations are smaller, however, than similar predictions based on phase-quadrature scattering. In addition, use of the variate-difference method revealed that the variance of phase was larger than would be expected on the basis of inhomogeneities along the path. This is explained by the existence of large scale changes in refractive index which affect the phase without causing changes in amplitude of the received field.

Thus, simultaneous measurements of the variability of electrical path lengths and received field amplitudes provide a means for studying the applicability of these assumed models of the atmosphere and provide a radio measure of their parameters.

[17] In reference 16, k was a power ratio and thus equal to the square of the k used above and in reference 15. Reference 16 gives the distribution of $|\phi|$ and the values from this reference should be used when k is not small or for extreme values of the probability even when k is small.

Appendix

The system for the measurement of the variations in the electrical path length essentially measures the variations in the time of propagation over the path. Variations in the time of propagation may be considered in terms of variations in the phase of arrival of the signal propagated with respect to a reference signal which has adequately stable phase characteristics. In the single-path system, signals are transmitted from both ends of the path. These same signals are also used as the phase reference signals after the time taken to traverse the path. This requires, in order to be able to measure the variations in transit time over the path, that the signal sources must have, over the transit time period, phase fluctuations which are small compared to the variations in phase of arrival introduced by the inhomogeneities of the propagation medium along the path. Since the signals are propagated in opposite directions, the transit times in the two directions, even for the same time of arrival, could conceivably be different particularly if changes in the medium occur nonuniformly along the path during the period of transit. There is a further complication introduced by the fact that the phase information for propagation in one of the directions must be transmitted to the point of phase comparison which requires an additional period of time.

The operation of the phase measurement system may be explained in the following manner: A signal of angular frequency ω_2 leaves transmitter T_2 at one end of the path and is propagated along this path toward the duplexer-mixer T_1R_2. After being in transit for the time interval Δt_1 this signal arrives at the opposite end of the path where it is received with the phase $\omega_2(1+3)\Delta t_1$ and is heterodyned with the signal of frequency $\omega_1(3)$ being transmitted from that end. The notation $\omega_2(1+3)$ indicates the frequency of transmitter T_2 at time $(t-\Delta t_1-\Delta t_3)$ while $\omega_1(3)$ denotes the frequency of T_1 at time $(t-\Delta t_3)$; t is the time of phase measurement, and Δt_3 is the time required for the mixed signal to be transmitted over the 100-mc link. The value of the difference frequency at T_1R_2 is $[\omega_2(1+3)-\omega_1(3)]$. Similarly, a signal of angular frequency ω_1 leaves transmitter T_1 and traverses a path towards duplexer-mixer T_2R_1 where it arrives at some time Δt_2 later with the phase $\omega_1(2)\Delta t_2$ and is heterodyned with a signal from the local transmitter T_2, having an angular frequency of $\omega_2(0)$ at this time. The value of the difference frequency at T_2R_1 is $[\omega_2(0)-\omega_1(2)]$.

In general, since the structure of the atmosphere between the two sites is undergoing continuous change, the transit times for the signals travelling in opposite directions will not be equal to each other even when the signals are transmitted simultaneously from the opposite ends of the path. This difference in the transit times has been indicated above by using Δt_1 and Δt_2.

The actual measurement consists of obtaining the difference in phase between the two difference frequency signals just described. Since the system requires that the difference frequency signal generated at T_1R_2 be returned to the other end of the path for comparison, this signal experiences the additional delay Δt_3 which is the time required for its transmission over the 100-mc link. Thus, the signals responsible for the final phase comparison are those which were transmitted earlier by the interval $\Delta t_1+\Delta t_3$ for the signal from transmitter T_2 and by Δt_2 for the signal from the transmitter T_1.

The results of the above discussion may be summarized in the following equation:

$$\begin{aligned}\phi_1 &= \omega_2(1+3)(t-\Delta t_1-\Delta t_3)-\omega_1(3)(t-\Delta t_3)\\ &\quad -[\omega_2(0)t-\omega_1(2)(t-\Delta t_2)]\\ &= [\omega_2(1+3)-\omega_2(0)]t-\omega_1(2)\Delta t_2-\omega_2(1+3)\Delta t_1\\ &\quad +[\omega_1(3)-\omega_2(1+3)]\Delta t_3+[\omega_1(2)-\omega_1(3)]t, \quad (3)\end{aligned}$$

in which ϕ_1 is the instantaneous phase difference between the two difference frequency signals measured at the location of transmitter T_2 at reference time t; $\omega_2(0)$ is the angular frequency of transmitter T_2 at time t; $\omega_2(1+3)$ is the corresponding value of ω_2 at time $t-\Delta t_1-\Delta t_3$; $\omega_1(2)$ is the angular frequency of transmitter T_1 at time $t-\Delta t_2$; and Δt_2 is the transit time for a signal arriving at T_2R_1 (from T_1) at time t.

From (3) it may be seen that in the case where $[\omega_1(3)-\omega_2(1+3)]\ll\omega_2$, the effect on ϕ_1 of variations in Δt_3 may be neglected. This equation also illustrates the way in which the frequency stabilities of the transmitters T_1 and T_2 directly influence the relation between the measurements and the propagation path behavior. In the system used for these measurements between Cheyenne Mountain and Fort Carson, $\Delta t_1\approx\Delta t_2\approx\Delta t_3\approx 20\mu s$, $\omega_2\approx\omega_1\approx 2\pi\times 10^9$ radians per second. Under these conditions, $[\omega_2(1+3)-\omega_2(0)]t$ will introduce an error of 0.14 degrees as a result of the interval $\Delta t_1+\Delta t_3$ when the stability of the frequency ω_2 is of the order of one part per 100 million. Since the interval $\Delta t_2-\Delta t_3$ may be made essentially zero, the term of $[\omega_1(2)-\omega_1(3)]t$ will introduce negligible error. Thus, the utility of the system is limited fundamentally by the "noise spectrum" of the frequency of transmitter T_2.

If the frequency drifts $[\omega_2(1+3)-\omega_2(0)]t$ and $[\omega_1(2)-\omega_1(3)]t$ are made sufficiently small, (3) becomes:

$$\phi_1 = -\omega_1(2)\Delta t_2-\omega_2(1+3)\Delta t_1, \quad (4)$$

and the measured ϕ_1 will be a function of the propagation path during the two intervals Δt_2 and Δt_1, which do not coincide in time. A first-order correction may be made by inserting an additional time delay in the signal generated in duplexer-mixer T_2R_1 equal to the delay involved in the transmission over the 100-mc link (Δt_3). By introducing such a delay, an expression for ϕ_1 is obtained similar to (4) but in which the two transit times are essentially concurrent. This delay also has the effect of decreasing the importance of the frequency stability of transmitter T_2, but increases proportion-

ately the influence of the frequency stability of transmitter T_1. Preliminary experiments using such a delay line failed to show any significant differences in the measurements. However, due to equipment limitations simultaneous measurements of both delayed and undelayed signals were not made and it is felt that the preliminary tests are, therefore, inconclusive.

The development of an expression for the phase difference ϕ_d, over two paths of the same physical length is much simpler since the signals travel along both paths simultaneously. Thus

$$\begin{aligned}\phi_d &= \omega_1(2)(t - \Delta t_2) - \omega_1(4)(t - \Delta t_4) \\ &= [\omega_1(2) - \omega_1(4)]t + \omega_1(4)\Delta t_4 - \omega_1(2)\Delta t_2, \qquad (5)\end{aligned}$$

where $\omega_1(2)$ is the transmitted frequency at time $t-\Delta t_2$, $\omega_1(4)$ is the transmitted frequency at time $t-\Delta t_4$, and Δt_2 and Δt_4 are the transit times over paths p_1 and p_2 respectively. In this case it should be noted that there is only a very small second-order dependence on transmitter frequency stability to the extent that Δt_2 differs from Δt_4.

Acknowledgment

The work reported here was a group endeavor of the Tropospheric Propagation Research Section, Boulder Laboratories, National Bureau of Standards, and involved the assistance of a large number of individuals. In particular, we would like to acknowledge the contributions of several groups working under the direction of the following persons: Charles F. Peterson, transmitter operations; A. F. Barghausen, recording operations; Walter E. Johnson, Robert W. Hubbard, and Paul I. Wells, special instrumentation; Harris B. Janes, radio analysis; Bradford R. Bean, meteorological analysis; Albrecht P. Barsis, special analysis, and K. O. Hornberg, project coordinator.

Phase-Difference Variations in 9,350-Megacycle Radio Signals Arriving at Spaced Antennas*

A. P. DEAM†, MEMBER, IRE, AND B. M. FANNIN†, MEMBER, IRE

Summary—**The phase difference between 9,350 megacycle-per-second radio signals received from a common transmitter at two horizontally spaced antennas was measured by the Electrical Engineering Research Laboratory of the University of Texas during March, 1955. The transmitter was located on Cheyenne Mountain in Colorado and the site of the receiver was at Fort Carson, 3.5 miles distant. The elevation angle of the transmitter as seen from the receivers was 9 degrees. This paper presents and discusses the results of these measurements.**

Introduction

PERSONNEL from the Electrical Engineering Research Laboratory at the University of Texas have made measurements of the relative phase difference, as a function of time, between two radio signals propagated over different paths. These tests were performed at a frequency of 9,350 megacycles with the emission from the transmitter a continuous wave. A profile and plan of the propagation path is included as

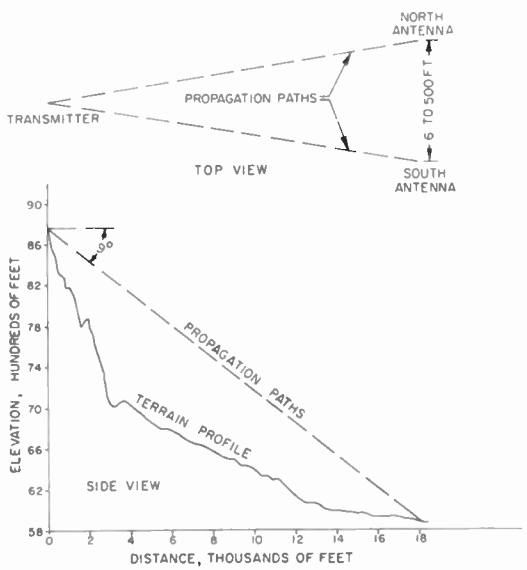

Fig. 1—Propagation paths geometry.

Fig. 1 and shows that the baseline between the two receiving antennas was variable between the limits of 6 and 500 feet. All the measurements reported herein were made on or between March 5 and 18, 1955, at a site near Colorado Springs, Colorado.

* Original manuscript received by the IRE, July 18, 1955. The research reported in this paper has been sponsored by the AF Cambridge Res. Center, Air Res. and Dev. Command, under Contract AF 19(604)-494; and the St. Louis Ordnance District, under Contract DA 23-072-ORD-763.

† Electrical Engrg Res. Lab., University of Texas, Austin, Texas.

Discussion of Measuring Technique

Equipment

A detailed description of the equipment is thought unnecessary since the methods employed are conventional. The signals received at the two antennas are conveyed through waveguide to the midpoint of the baseline where they are added together after one of them has passed through a rotating phase shifter. The envelope of the resultant radio-frequency signal is essentially that of a fully rectified sine wave, the time position of the nulls being related directly to the relative phase existing between the signals at the two antennas and to the rotation of the phase shifter.

Two triggers, one developed at the envelope minima and the other from the line voltage to which the rotary phase shifter is synchronized, are applied to two halves of an Eccles-Jordan circuit. This produces an approximately rectangular voltage pulse whose average value is proportional to relative phase.

The phase information is recorded on an Esterline-Angus recording milliammeter, the rate of writing phase changes being limited primarily by this instrument.

Accuracy of the Measurements

Of the several factors that contributed to the inaccuracy of the measurements, thermal expansion of the waveguide is believed to have been the largest single source of error. In order to reduce this error the waveguide was wrapped in glass wool and inserted into new galvanized downspout. Tests were run with each arm of the waveguide run out 81 feet, folded, and returned to the center where a common signal was fed into both ends. These tests of the over-all receiving system stability revealed that the indicated phase difference still possessed a slow drift on occasions but none of the rapidly varying character of the actual phase data. Although enough data on the measurement errors were not obtained to permit a definite number to be assigned to their magnitude, the above mentioned tests and the good correlation of the phase data with those recorded at a different frequency reported later strongly indicate that errors contributed only a minor portion of the recorded data.

Discussion of Data

Rms of Phase Difference vs Antenna Separation

Plots of the rms values of the phase difference vs antenna separation, for those occasions when a series of

spacings were employed in succession, are presented in Fig. 2. The rms of the phase difference increases as the antenna separation is increased, with the rate of increase with separation becoming less as the spacing becomes greater. That the points in general do not define very smooth curves is not surprising in view of the extreme variability of the weather conditions encountered.

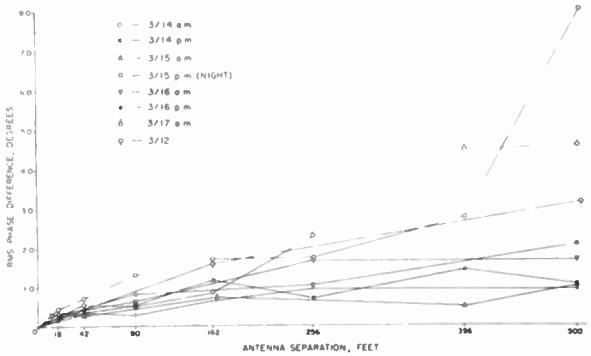

Fig. 2—Rms phase difference vs antenna spacing.

It was the rule rather than the exception for conditions to change decidedly in the approximately three hours required to obtain data for all seven separations. For example, the data for 500 feet separation on the morning of March 14 was obtained under very calm conditions while an hour and a half later mean winds of 23 mph were encountered. The same general wind conditions prevailed on the morning of March 17. On the morning of March 17 the sky condition changed from clear to completely overcast (with some snow falling) to clear again by noon, but by 3:20 P.M. it was heavily overcast again and snowing heavily.

Distribution of Rms Values of Phase Difference at Several Antenna Spacings

In order that the reader may be given an over-all picture of the general magnitude of the phase variations, Fig. 3 has been included. These distributions were

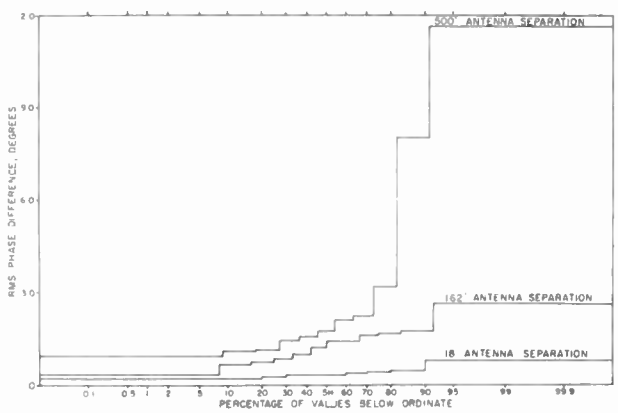

Fig. 3—Time-space distribution of rms phase difference.

prepared in the following manner. A day's recording was divided into three periods—morning, afternoon, and evening—and the measurements averaged over each of these periods. This average value was then considered a bit of data. After compiling all data, for various days, at a particular spacing, a distribution was plotted of the various rms values calculated.

No particular trend is to be inferred in these plots because of the limited amount of data; they are included in the effort to present the over-all data picture.

Phase Difference Spectra

As the antenna separation is increased the rms value of the phase difference increases, and a larger portion of the "power" is contained in the lower frequencies. This character is illustrated by the normalized spectra of the phase difference presented in Fig. 4. In order to

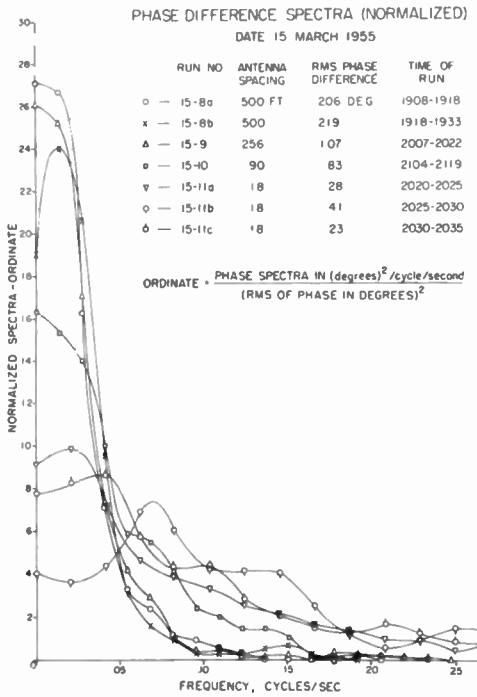

Fig. 4—Phase difference spectra (normalized).

show more clearly the relative portion of the "power" contained in different frequencies all of the spectra were normalized by dividing by the mean square of the phase difference, thus making the area under all of the curves unity. The fact that the spectra in general do not show a smooth trend as the antenna spacing is varied again points up the extremely variable nature of the propagation conditions encountered.

Amplitude vs Phase

On occasions the phase difference data possessed variations of over a quarter of a radian (with a mean period of about a minute). If the field is visualized as being composed of a relatively small, randomly-phased field superimposed upon a larger constant field, then a variation in signal amplitude of several decibels would be predicted on the basis of phase fluctuations of the above magnitude. However, the signal amplitude fluc-

tuations were always unmeasurably small, the uncertainty in the measuring system stability being about ±0.1 decibel. Thus it is evident that any physical concept that leads to a randomly-phased perturbation of the field distribution is incorrect.

Correlation between 9,350 Mc and 1,040 Mc Phase Differences

Measurements on 1,040 megacycle-per-second made over the same path by the National Bureau of Standards are reported in a companion paper appearing in this same issue.[1]

On the assumption that the phase of the field at a point is approximately equal to the integral of the reciprocal of the phase velocity along the ray path of geometrical optics through the point, which is generally believed to be valid for the range and wavelengths employed in these tests, the phase difference at each instance would be expected to be directly proportional to the frequency for a given pair of propagation paths. The cross-correlation function for 15-minute sections of 9,350 mc and 1,040 mc phase difference data recorded simultaneously, taken under similar environments, have been computed. In both cases the receiving antenna separation was 500 feet and the range the same, but the 1,040 mc receiving antennas were displaced 98 feet to the south of those in the 9,350 mc set-up. The afternoon of March 18, when the data were obtained, was bright and warm with a few small patches of snow still remaining in protected areas from the two inches which blanketed the ground earlier in the day. Thus relatively large phase differences were expected and observed.

The cross-correlation was found to be −0.88 for these two data. This serves as a satisfactory check on the validity of both the measuring techniques. The fact that the correlation is negative merely indicates the two groups picked opposite receiving antennas as the reference for phase differences. The wind that afternoon was from the south with a mean velocity of 3.0 mph at a recording anemometer located 11 feet above the ground near the center of the receiving baseline. The time required for a point moving at the measured mean wind speed to travel the 98 feet offset of the antennas for the two frequencies is approximately 22 seconds, which, although it does not compare well with the computed time lag for best correlation of 8 seconds, is in the right direction.

The rms values of the phase differences for this period were 12.6 degrees and 1.09 degrees for the 9,350 mc and 1,040 mc data, respectively. These values are moderately close to being in the same ratio as the frequencies.

Later Data

Measurements of the same nature have been conducted again during the first part of June, 1955, at which time more emphasis was placed on improving the accuracy of the phase measurements. In these tests the range was approximately 10 miles, the elevation angle involved again being about 9 degrees. The analysis of these later data is not complete, but the following general conclusions have been reached.

1. All the recordings at 500 feet were averaged for each period of measurements (March and June) and it was found that the June average was approximately 3.5 times the March average. It is felt that this increase was due in large part to increased water vapor content of the atmosphere as well as to the increased range.
2. No marked difference was noted in the phase difference spectra obtained for the two measuring periods.
3. Phase difference recordings made by the National Bureau of Standards in June 1955 at 1,046 mcps have been cross correlated with simultaneous phase recordings at 9,350 mcps by the University of Texas group. Antenna spacings were 500 feet in all cases, and coefficients ranging in value from approximately −0.60 to −0.88 have been obtained for eight samples. The majority of the samples were approximately 15 minutes in length with none less than 10 minutes.
4. The relative amplitude of the signal appearing at one of the antennas was again monitored in the June measurements but again primary emphasis was placed on phase difference measurements and no attempt was made in the interim period to increase the sensitivity of the equipment to amplitude variations. However it may be said, although no extensive program of analysis has been undertaken, that the amplitude variations were generally confined to a range of ±0.2 db about a mean.

[1] J. W. Herbstreit and M. C. Thompson, Jr., "Measurements of the phase of signals received over transmission paths with electrical lengths varying as a result of atmospheric turbulence," p. 1391, this issue.

Survey of Airborne Microwave Refractometer Measurements*

C. M. CRAIN†, SENIOR MEMBER, IRE

Summary—**This paper presents a summary of airborne refractive index measurements which have been made at many locations in the United States both over land and off the east and west coasts, by several organizations. Included are the results of studies of the mean vertical structure of the index of refraction of the atmosphere as a function of such factors as location, season, horizontal distance, and time. Included also are the results of measurements of the fine detail variations of refractive index about its mean value at several locations for altitudes up to 20,000 feet mean sea level.**

Introduction

SINCE THE development of the University of Texas airborne microwave refractometer[1–4] a great amount of data has been gathered on the index of refraction structure of the atmosphere. Most of these data have been obtained by the Propagation Unit of the Wright Air Development Center and the Propagation Section of the Air Force Cambridge Research Center using various versions of the University of Texas refractometer. Types of measurements made fall into two general categories: (1) index of refraction change with altitude and (2) index of refraction variations about the mean value at various altitudes.

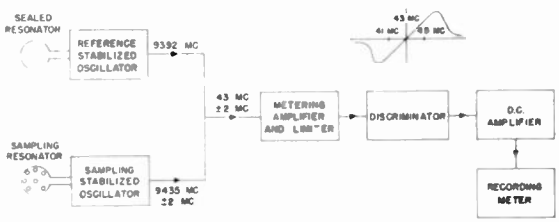

Fig. 1—Block diagram of the University of Texas refractometer.

Previous to the development of the airborne refractometer no data were available on the small scale variations of the index of refraction of the atmosphere and the measurements of index of refraction profiles made with such devices as the radiosonde and the airborne psychrograph in many cases provided insufficient detail for propagation studies due to the relative long time constants associated with the equipment.

A considerable amount of the data obtained with the refractometer has been previously reported in detail.[5–10] The material presented here, therefore, includes only a general survey of the refractive index profile measurements previously reported and is primarily concerned with more recent measurements of small scale variations of index of refraction using refractometers especially designed for this purpose.

A summary of the refractometer data which have been obtained and organizations which have made the measurements is included at the end of this paper.

Discussion of University of Texas Refractometers

Profile Refractometer

The airborne microwave refractometer, as previously reported, is a device for recording continuously the index of refraction of the medium in which a cavity resonator associated with the instrument is located. Fig. 1 shows in block form the arrangement used. The stabilized oscillators are of basic type originally described by Pound[11] and incorporated modification suggested by Tuller *et al.*[12] Frequencies of klystron oscillators are very closely controlled by frequency of associated cavity resonators. Short time stabilities of the order of 10^{-8} or better are obtainable with suitable design and long time stabilities are determined essentially by changes in cavity resonator frequencies. For refractometers intended for profile measurements, the cavity resonators are built of treated invar with a

* Original manuscript received by the IRE, July 18, 1955. This research has been supported by Wright Air Dev. Center, Wright-Patterson AF Base, Contracts AF 18(600)-113 and AF 33(616)-2423; AF Cambridge Res. Center, Contract AF 19(604)-494; and Office of Naval Research, Contract Nonr 375(01).

† Electrical Engrg. Res. Lab., University of Texas, Austin, Texas.

[1] C. M. Crain and A. P. Deam, "An airborne microwave refractometer," *Rev. Sci. Instr.*, vol. 23, pp. 149–151; April, 1952.

[2] D. Metcalf, "Engineering Report on Type II (Light Weight-Battery Operable) Refractometer," EERL Rep. No. 5-03, University of Texas; 1954.

[3] C. M. Crain, "Interim Engineering Report on the Type III (Sensitive Scale Fluctuation) Refractometer," EERL Rep. No. 5-04, University of Texas; 1954.

[4] C. M. Crain, "Engineering Report on the Type IV Microwave Refractometer," EERL Rep. No. 5-05, University of Texas; 1954.

[5] C. M. Crain and J. R. Gerhardt, "Some preliminary studies of the rapid variations in the index of refraction of atmospheric air at microwave frequencies," *Bull. Amer. Met. Soc.*, vol. 31, pp. 330–335; November, 1950.

[6] C. M. Crain, A. P. Deam, and J. R. Gerhardt, "Measurement of tropospheric index of refraction fluctuations and profiles," PROC. IRE, vol. 41, pp. 284–290; February, 1953.

[7] C. M. Crain and J. R. Gerhardt, "Measurements of the parameters involved in the theory of radio scattering in the troposphere," PROC. IRE, vol. 40, pp. 50–54; January, 1952.

[8] C. M. Crain, J. R. Gerhardt, and C. E. Williams, "A preliminary survey of tropospheric refractive index measurements for U. S. interior and coastal regions," TRANS. IRE, vol. AP-2, pp. 15–22; January, 1954.

[9] C. M. Crain and V. E. Moyer, "Refractometer Measured Tropospheric Index of Refraction Profiles, Volumes I, II, III and IV," EERL Reps. Nos. 6-02, 6-03, 6-06, and 6-09, University of Texas; 1953–1955.

[10] H. E. Bussey and G. Birnbaum, "Measurement of variations in atmospheric refractive index with an airborne microwave refractometer," *Jour. Res. Nat. Bur. Stand.*, vol. 51, pp. 171–178; October, 1953. A discussion of measurements made with another type of refractometer.

[11] R. V. Pound, "Frequency stabilization of microwave oscillators," PROC. IRE, vol. 35, pp. 1405–1415; December, 1947.

[12] W. G. Fuller, W. C. Galloway, and F. P. Zaffarano, "Recent developments in frequency stabilization of microwave oscillators," PROC. IRE, vol. 36, pp. 794–799; June, 1949.

temperature compensating end plate. Cavities having resonant frequency variations of the order of 2 parts in 10^7 or less per degree Centigrade can be fabricated with reasonable effort. By using such cavity resonators, the change in frequency of each of the approximately 9,400 mc oscillators can be made a function essentially of the changes in index of refraction of the gas in the associated cavity resonator.

Since the instrument operates on the beat frequency principle, it can be easily and precisely calibrated using conventional frequency measuring equipment. A change of index of refraction of one N unit [$N=(n-1)10^6$, where n is the index of refraction of the air in a cavity resonator operating at 9,400 megacycles] will change the resonant frequency of the resonator 9,400 cycles.

In the case of profile refractometers, one cavity resonator is evacuated and sealed and the other is placed external to the aircraft in a place suitable for sampling the air. Therefore, the beat frequency between the two oscillators changes proportionally to the change in index of refraction of the atmospheric air in the sampling resonator. This beat frequency can thus be applied to a conventional amplifier, limiter, and discriminator and a dc output obtained whose magnitude is a direct function of the index of refraction of the atmospheric air being sampled. This voltage is then applied to a recording meter through an appropriate differential amplifier. By building a discriminator having a linear range of about 4 megacycles a useful linear range of 400 N units is easily obtained. Normally it is desirable to record on scales having a range of 50 to 100 N units to obtain more detail in measurements. By applying in calibrated steps a small compensating voltage in grid circuit of amplifier driving recording meter, one can record on a 50 or 100 N unit scale over a 400 N unit range.

Sensitive Scale Refractometer for Measuring Microvariations in Refractive Index

Due to the widespread interest which has been focused in recent years on the beyond-the-horizon radio field intensity and the need for knowledge on the nature of small variations in the index of refraction of the atmosphere which might cause a considerable increase in beyond-the-horizon radio signals, the basic profile measuring refractometer described above was modified to measure such variations. The block diagram of the sensitive scale refractometers which have been developed for the Propagation Unit of the Wright Air Development Center is the same as shown in Fig. 1 except that a metering amplifier-discriminator having a center frequency of 10.7 megacycles and a linear bandwidth of about 200 kilocycles, and cavity resonators having this difference in resonant frequency have been used. In addition, the reference cavity resonator is not sealed, and provision is made to modify its resonant frequency slightly by means of a small screw inserted into the resonator through one end plate. With these modifications, scales of 1 to 20 N units (full-scale deflection of an Esterline-Angus milliammeter) have been used. A separate output has been provided from the metering amplifier and has been used to drive a photographic recorder having scales from 0.17 to 1.67 N units per inch deflection and film speeds from 1 to 6 inches per second. The time constant of the recording meter which WADC has used is about 0.008 second. As the stabilized oscillators and metering amplifiers have time constants of the order of a few microseconds, the only time constant of importance (excluding the recording meter) associated with the University of Texas refractometer is the time required to flush the air through the sampling resonator, which should be approximately the time to travel, say, no more than 10 lengths of the cavity resonator through the air. Thus, using a recording meter of 0.008 second time constant and rates of plane travel of near 250 feet per second, one would expect to resolve index "discontinuities" over a minimum distance of about 2 feet. Changes of several N units have been observed over distances of this order at altitudes of a few thousand feet.

The principal problem which has been encountered in obtaining meaningful values of these minimum resolvable fluctuations is that of separating the true atmospheric variations from those produced by the sampling method and by electrical noise. A flight made with the sampling cavity resonator closed to the free passage of air indicated a peak to peak "noise level" of about 0.04 N unit which is some four times as large as the peak to peak variations occurring in intervals of seconds under the same conditions in the laboratory.

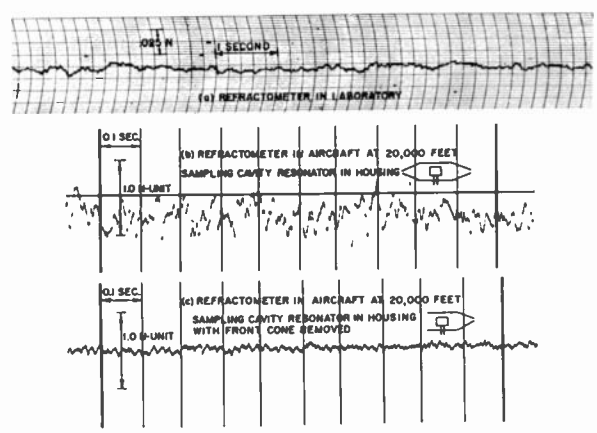

Fig. 2—Samples of data obtained with the sensitive-scale refractometer showing the effect of the method of sampling.

Fig. 2 shows examples of this problem. The data shown were obtained on the second University of Texas sensitive scale refractometer which was developed for the WADC Propagation Unit. Data (a) were obtained in the laboratory on a Brush recorder and showed short time changes near 0.01 N unit. Data (b) were obtained with the same instrument at 20,000 feet over Camp Carson, Colorado. In this case the sampling cavity resonator was enclosed in a housing, as indicated in Fig. 2. Curve (c) was obtained at the same altitude with the front cone of the housing removed. Removing

both cones produced a spurious fluctuation level in between the extremes shown in (b) and (c). The problem remains of reducing what all tests to date indicate are index variations created by turbulence in the housing and/or cavity resonator itself to a lower value. The rms value of the spurious variations as shown in Fig. 2(c) is about 0.04 N units; however, as these variations seem to be higher in frequency than the index variations of comparable size, it is possible to satisfactorily extract real index of refraction variations of this order or less from the data by smoothing the high-frequency variations in the analysis.

Summary of Index of Refraction Profile Data

A major portion of the index of refraction profiles which have been measured with University of Texas refractometers since 1951 have been reported elsewhere.[5–9] These include measurements made in Ohio, Colorado, and elsewhere by the WADC Propagation Unit, and measurements made off various parts of the east and west coasts of the United States by the Cambridge Air Force Research Center and the Electrical Engineering Research Laboratory. The examples of profiles shown here have been chosen in an attempt to illustrate the wide range of type of profiles encountered under various conditions. All profiles shown are simply a replot of the data obtained. No correction has been made for small temperature effects on the resonant frequency of both resonators or small pressure effects on the sealed reference resonator.

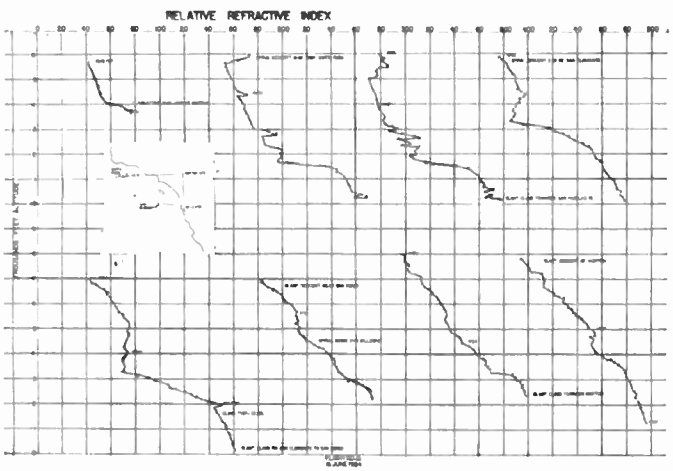

Fig. 3—Index of refraction profiles obtained off the coast of Southern California, June 16, 1954.

Fig. 3 shows profiles obtained off the coast of Southern California on June 16, 1954. Perhaps the most interesting feature apparent in this series of profiles is the considerable change in the structure of the profile with geographical positions. The profile obtained at Santa Rosa shows a commonly observed strong inversion (40 N units over 200 feet in this case) associated with the stratus layer off the west coast, whereas at San Clemente and San Diego the "layer" was some 1,200 feet thick and the index of refraction decreases were some 60 and 80 N units respectively.

Fig. 4 (next page) shows profiles obtained July 22, over Southwest Ohio and Fig. 5 (next page) shows profiles over same area on July 24, 1952. All profiles illustrated were plotted by taking points at 100-foot increments of altitude off continuously recorded data. Fig. 4 shows an example of how rapidly index structure of atmosphere may vary locally with time. Fig. 5 is typical of the large layers common over the Ohio area in summer months. Fig. 6 (p. 1409), which was plotted from data obtained off the coast of Washington state, is an example of how profiles can vary over short distances. Note how super-refracting and substandard layers present at 75 miles from the coast gradually merge with distance from the coast and are almost nonexistent in the last profile, obtained somewhere between 100–150 miles from the coast.

Fig. 7 (p. 1409) shows one of the most regular sets of profiles that has been observed of the several thousand which have been obtained. Even here deviations of 5–10 N units in 200 foot height intervals are observed. These profiles were obtained on November 13, 1952, off the Long Island coast.

Index of Refraction Fluctuation Data

In 1953 a report[13] was made of the analysis of some 1,200 samples of index of refraction fluctuations up to 15,000 feet mean sea level. Most of these samples were obtained from data taken previously for determining index of refraction profiles, and, hence, the sensitivity (full scale deflections of 50 to 80 N units were used) of the recording was much less than optimum for fluctuation analysis. This placed a lower limit on the size of rms variations which could be resolved from the data of somewhere near 0.1 N in most cases. Also, since the data were recorded on a meter for which the response was down 30 per cent at 0.8 cycle per second, higher frequency components present were recorded with reduced amplitude. The spectral characteristics of the data obtained, however, indicated that the 0.8 cycle per second response was fairly satisfactory for obtaining the rms intensity of the variations as the power spectrums obtained from the data always decreased with frequency at a rate much greater than the square of the recording meter response. The measurements made later with a higher speed and wider response recorder indicate this conclusion was apparently correct; however, even though higher frequency components may be normally negligible as far as their contribution to total rms value of fluctuations is concerned their rms value is important, as shown later, in determining such a parameter as $(\Delta n)^2/l$ (l being a scale of turbulence) which is of current interest in scattering theory.

[13] C. M. Crain, A. W. Straiton, and C. E. Von Rosenberg, "A statistical survey of atmospheric index of refraction variation," Trans. IRE, vol. AP-1, pp. 43–46; October, 1953.

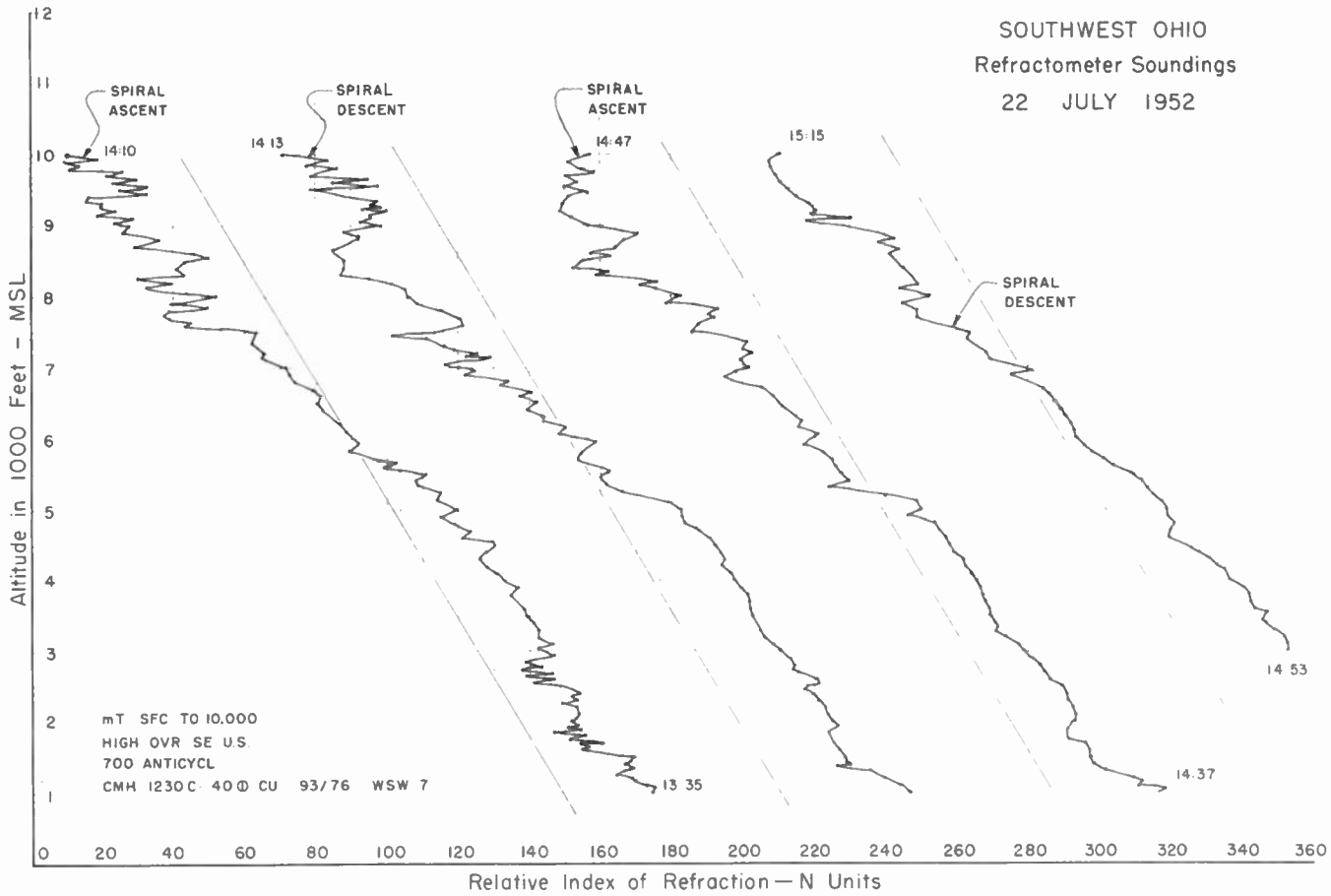

Fig. 4—Index of refraction profiles obtained over Southwestern Ohio on July 22, 1952

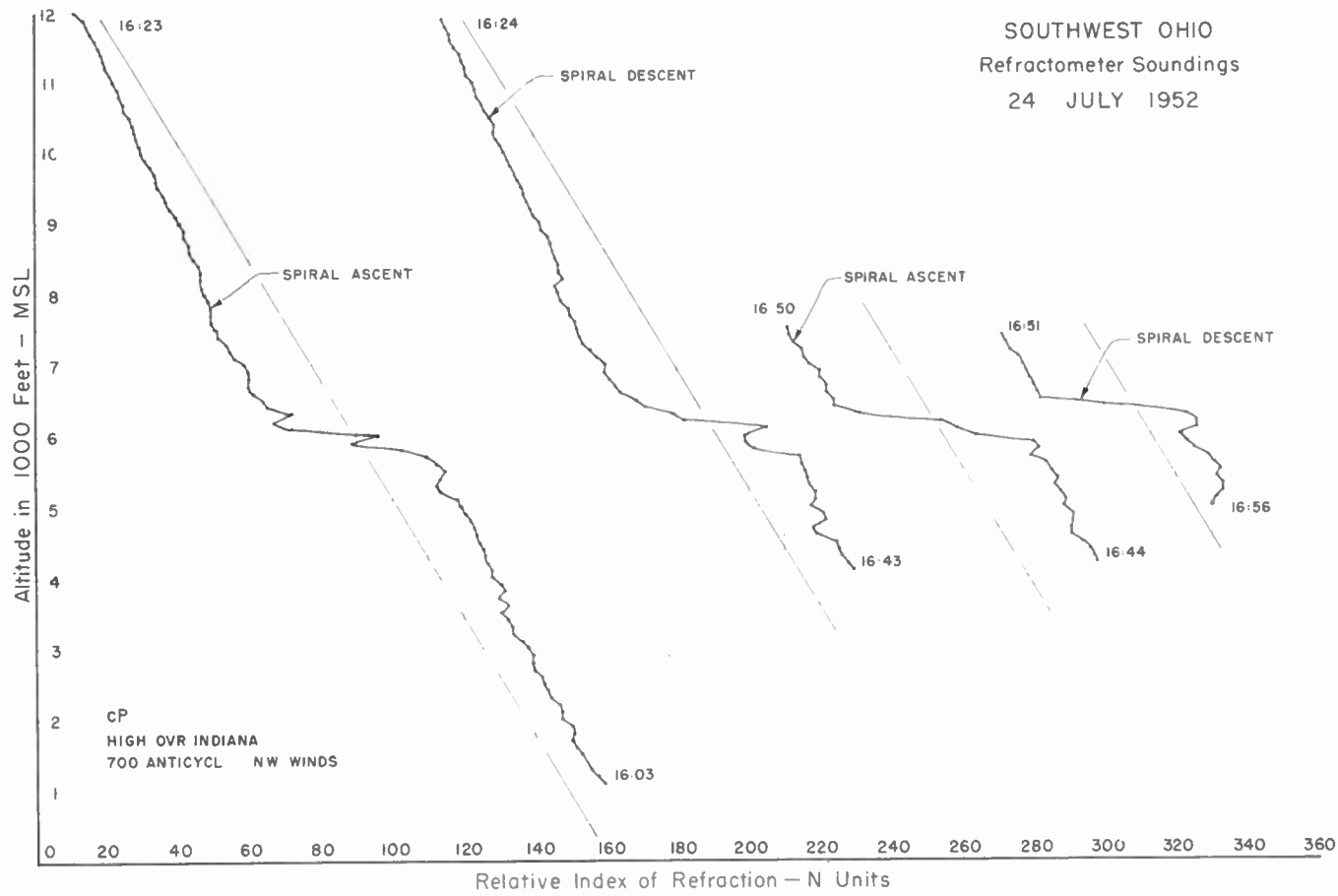

Fig. 5—Index of refraction profiles obtained over Southwestern Ohio on July 24, 1952.

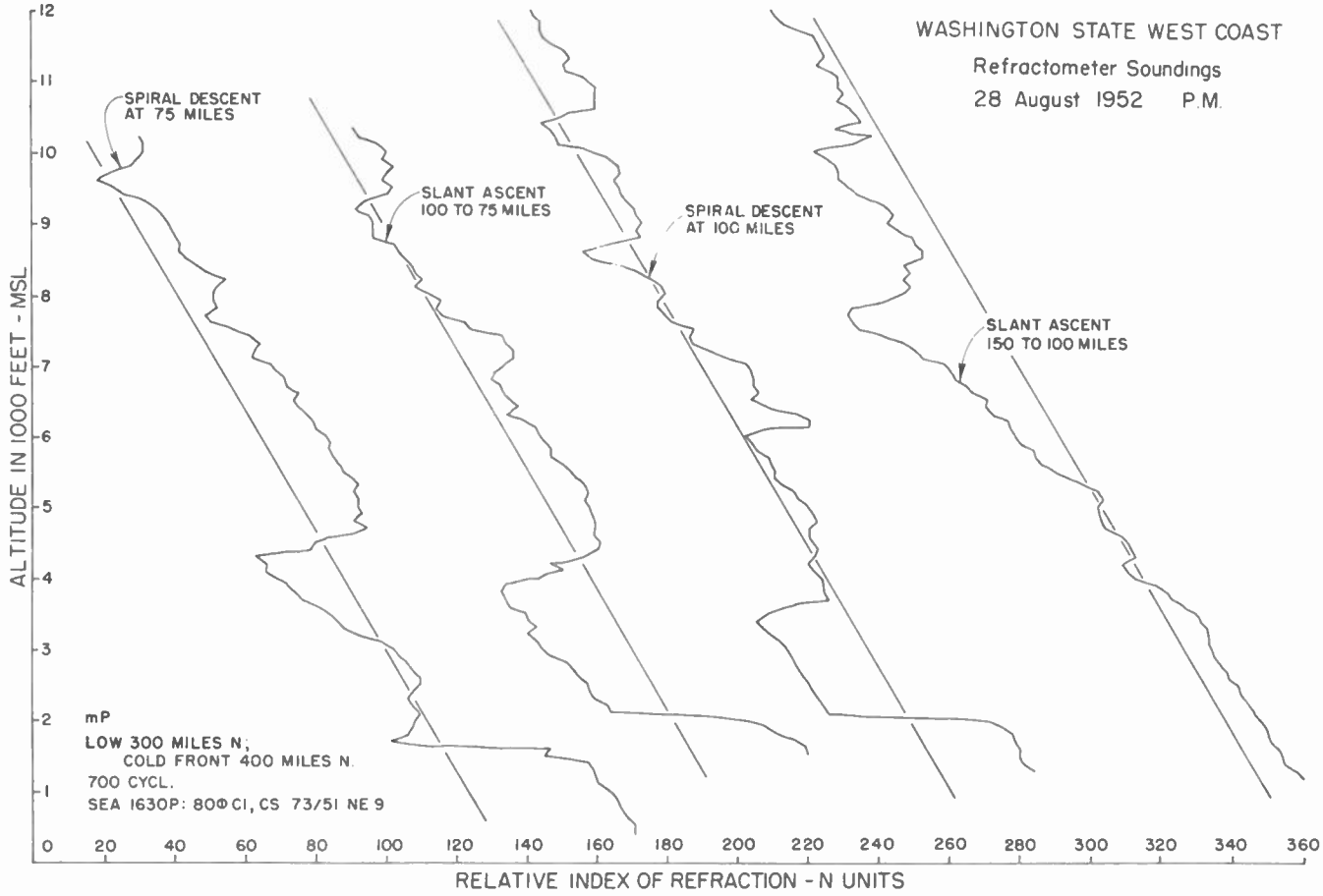

Fig. 6—Index of refraction profiles obtained off the coast of Washington state on August 28, 1952.

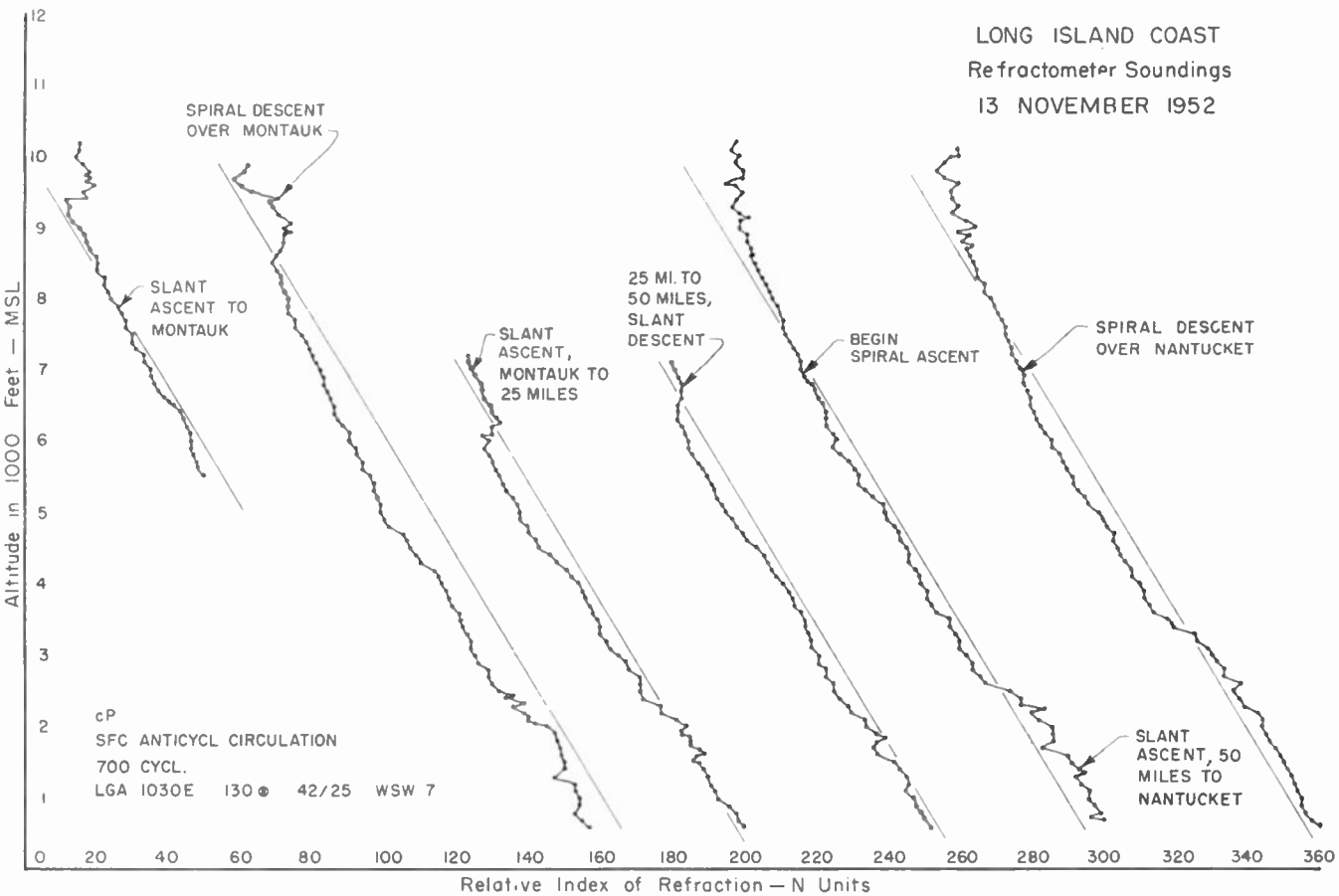

Fig. 7—Index of refraction profiles obtained off the Long Island Coast on November 13, 1952.

The combination of low meter sensitivity and a drop in meter response at such a low frequency resulted in it not being possible to resolve average values of $\Delta n^2/l$ any smaller than about 10^{-15} per meter in the previous analysis.

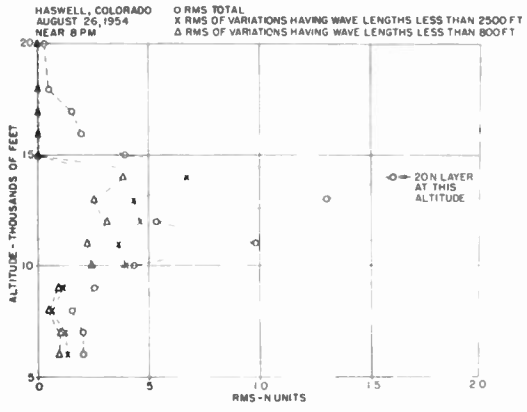

Fig. 8—Rms variations in index of refraction over Haswell, Colorado, on August 26, 1954.

Using the instruments described in the second section of this paper it has been found possible to resolve values of $\Delta n^2/l$ of the order of 4×10^{-18} per meter. Improvements in the sampling technique used could lower this value to perhaps 10^{-18} or better (assuming a scale of 100 meters and a resolution of 0.03 N unit peak to peak).

During August, 1954, and March, 1955, the Propagation Section of the Wright Air Development Center made a series of measurements in the vicinity of Colorado Springs, Hartman, and Haswell, Colorado. The data obtained in August have been analyzed to determine the rms intensity of the variations and their spectral distributions. Fig. 8 shows the altitude vs rms intensity curve obtained on one of the flights. This figure

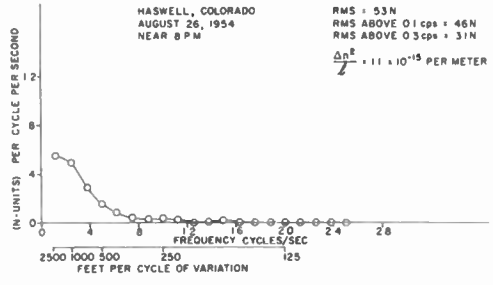

Fig. 9—Typical spectral distribution of the index of refraction variations.

shows the commonly observed large values of rms associated with the over-land elevated layers and the also commonly observed extremely small values of rms at altitudes above the layer. The values for rms of variations having wavelengths less than 2,500 feet and less than 800 feet were obtained from the spectral density plot for the given set of data. For example, the spectral density plot for the data at 12,000 feet in Fig. 8 is shown in Fig. 9. The area under the curve for frequencies greater than 0.1 cycle per second gives the square of the rms intensity of the variations having wavelengths of 2,500 feet or less (based on a plane speed of 250 feet/second), and the area under the curve for frequencies greater than 0.3/cycle per second gives the $(\text{rms})^2$ of variations having wavelengths of 800 feet or less. These calculations were made for all data in order to remove from the total rms value the contribution of long period variations and hence, to obtain an rms value of the variations for distances of importance insofar as scattering of radio waves is concerned. In addition, the method employed for the measurements (i.e., using a slowly flushing reference cavity resonator) prevented indications of variations which occurred with periods greater than several tens of seconds from necessarily having true meaning. Variations of this type were simultaneously recorded by a profile refractometer which employed a sealed reference cavity resonator. Fig. 10

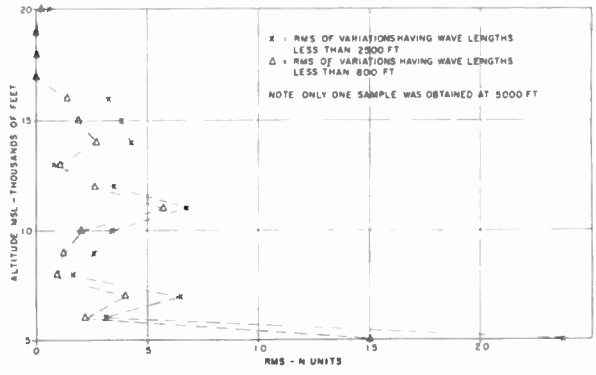

Fig. 10—Average of rms variations in index of refraction for six flights over Southeastern Colorado in August, 1954.

shows the average values of rms obtained at the various altitudes up to 20,000 feet for the six flights. The values shown at 17, 18, and 19 thousand feet were plotted as zero as the fluctuations for the six flights made were so low their rms value could not be accurately ascertained (in the order of less than 0.04 N unit).

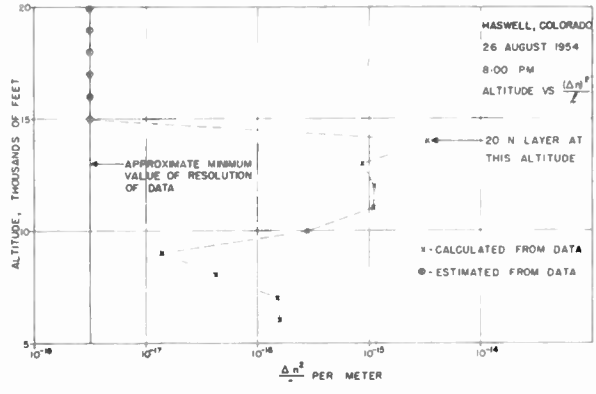

Fig. 11—Variations of $\Delta n^2/l$ with altitude for flight over Haswell, Colorado, on August 26, 1954 (See Fig. 8).

Fig. 11 shows the variation of $\Delta n^2/l$ with altitude for the same flight for which the rms intensity of variations shown in Fig. 8 were plotted. The values of $\Delta n^2/l$ were obtained by numerically integrating the spectral density plots using 0.1 cycle per second intervals.

The values for $(\Delta n)^2/l$ were obtained by applying the following relationship:

$$\frac{(\Delta n)^2}{l} \approx \Sigma\left[\frac{(\Delta n_1)^2}{l_1} + \frac{(\Delta n_2)^2}{l_2} + \frac{(\Delta n_3)^2}{l_3} + \cdots + \frac{(\Delta n_n)^2}{l_n}\right],$$

where $l_1, l_2, \cdots, l_n$ are the lengths in meters corresponding to the centers of the 0.1 cycle/second intervals (obtained in each case by dividing the plane speed by the center frequency of the appropriate frequency interval) and $(\Delta n_1)^2, (\Delta n_2)^2, \cdots, (\Delta n_n)^2$ are the areas in square N units under the power spectrum curve in the various 0.1 cycle/second intervals. For the curve shown in Fig. 9 the value of $(\Delta n)^2/l$ obtained was 1.1×10^{-15} per meter with one half of the total value being contributed by components having frequencies greater than 0.5 cycle per second and one quarter of the value contributed by components having frequencies greater than 1.0 cycle per second. Inspection of Fig. 9 indicates that the contribution of the frequencies above 1.0 cycle per second to the total rms value of the data is negligible. This indicates, as stated previously, the importance of higher frequency components, which normally contribute little to the total rms value of the data, in determining the value of the parameter $(\Delta n)^2/l$.

The numerical integration method was used instead of simply dividing the square of the rms of the data by the distance over which the autocorrelation function of the data dropped to $1/e$ due to the fact that the normalized autocorrelation function rarely could be represented in the simple form, e^{-x}/l_0, where l_0 is so-called scale of turbulence and x correlation distance.

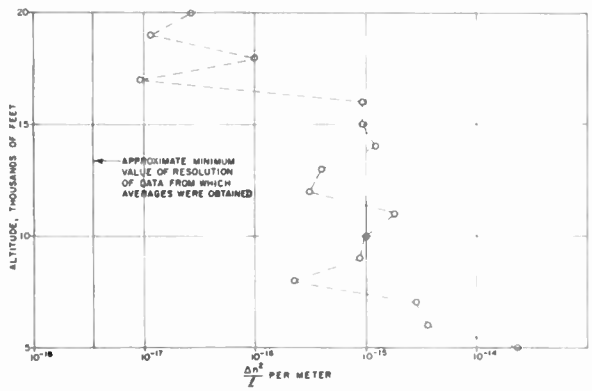

Fig. 12—Average of $\Delta n^2/l$ values obtained on six flights over Southeastern Colorado in August, 1954.

Fig. 12 shows the average of the parameter, $\Delta n^2/l$, for the six flights. It should be emphasized here that the values shown should be considered as representing maximum values due to the fact that at some altitude the values used were the values considered to be the minimum of resolution of the data. Then, too, any extraneous factors tending to give irregularities in data would tend to give larger values of $\Delta n^2/l$ than are real; however, instrument stability was such that for the order considered here this effect is thought negligible.

One of the more interesting features observed on the fluctuation data as mentioned previously is the existence of rather sharp gradients. Unfortunately the resolution in the developed film was too poor to permit reproducing here; however, a critical analysis of the film revealed many instances where changes of 2 N units and sometimes greater were recorded over distances of 5 feet or less. Inasmuch as this was the order of the resolution obtainable with the recorder as used for the measurement (one inch per second writing speed) the actual gradients could have been even sharper. Later measurements made by the WADC Propagation Unit off the Florida Coast in April 1955 using faster recorder writing speeds have indicated numerous changes of some 5 N units in some 2 feet, again the approximate limit of resolution. Additional studies will be made of the nature of these gradients; this will involve decreasing the time constant of the recording meter by using a suitable galvanometer. This will reduce the time constant of the instrument to a value determined simply by the flushing time of the sampling cavity resonator itself.

Summary of Refractometer Data Accumulated

The following list gives in general summary the airborne refractometer data which has been obtained by various activities since 1951:

1. New Jersey Coastline, April, 1951, EERL, University of Texas.
2. Southwestern Ohio, June, 1951, Propagation Unit, WADC.
3. California Coast, October, 1951, EERL, University of Texas.
4. Southwestern Ohio and nearby region, since July, 1952, Propagation Unit, WADC.
5. Coast of Washington state, August and September, 1952, Propagation Sec., AFCRC and EERL.
6. Chesapeake Bay, Maryland, August 19, 1952, CRPL, National Bureau of Standards.[10]
7. Coast of Central California, October, 1952, AFCRC and EERL.
8. Coast of New Jersey and Long Island, November and December, 1952, AFCRC and EERL.
9. Vicinity of Cambridge, Massachusetts, since August, 1953, AFCRC.
10. Alaska, August, 1953 to June, 1954, WADC.
11. Florida Coast at various times since 1954, WADC.
12. Southeastern Colorado, February, 1954, WADC.
13. Southern California, April, May and June, 1954, AFCRC, WADC, EERL.
14. Florida Coast since August, 1954, AFMTC.
15. Southeastern California, August, 1954, WADC.
16. California Coast since Sept., 1954, USNAMTC.
17. California Coast, July to December, 1954, AFCRC and EERL.
18. Florida Coast, January and February, 1955, AFCRC.
19. Southeastern Colorado, March, 1955, WADC.
20. Southeastern Colorado, April and May, 1955, AFCRC.
21. Small amounts of data in Texas, Montana and elsewhere by the various above activities.

Amplitude, Scale, and Spectrum of Refractive Index Inhomogeneities in the First 125 Meters of the Atmosphere*

GEORGE BIRNBAUM†, MEMBER, IRE, AND H. E. BUSSEY†

Summary—**An extensive series of observations was obtained with two refractometers and meteorological equipment installed on various levels of a 128-meter tower at the Brookhaven National Laboratory, Long Island, New York. One of the refractometers was equipped with a multiple cavity unit for the study of correlation between two positions in the horizontal direction. The errors arising from the exposure of the cavity to the atmosphere and its ventilation were investigated.**

The amplitude of the refractive index variations could be correlated with various meteorological conditions. From the experimentally determined cross-correlation coefficient, and assuming that its variation with distance is given by the exponential (Taylor) form, scales in the neighborhood of 60 meters were obtained. A crude analysis of the data indicated that the intensity of the refractive index inhomogeneities varied, on the average, as the 1.6 power of their size.

Introduction

THE DISCOVERY that inhomogeneities in the refractive index of the atmosphere are important in scattering radio waves created the pressing need for a detailed knowledge of the refractive index structure of the atmosphere, particularly with regard to the amplitude and extent of these inhomogeneities. With the development of recording microwave refractometers the direct measurement of the variations in atmospheric refractive index became possible, and naturally the first measurements of this kind were made near the ground.[1–4] Progress in this direction had hardly begun when the emphasis was shifted to studies of index variations in the troposphere with airborne refractometers. However, observations from high towers are important in leading to an understanding of the refractive index structure of the atmosphere, and in supplementing the observations from aircraft. The limitations of aircraft installation have not thus far allowed the use of spaced cavity resonators for correlation studies and the more direct determination of scale.

This paper reports the results of an extensive series of observations made with two refractometers and meteorological equipment installed on various levels of a 128-meter tower at the Brookhaven National Laboratory, Long Island, New York.[5] One of the refractometers was equipped with a multiple cavity unit for the study of correlation in index variations between two positions (in the horizontal direction) separated by a short distance. The two refractometers, each located on different tower levels, were used to investigate correlation in index variations over large distances. The data were subjected to detailed analysis, in particular to obtain information on the extent and amplitude of the index inhomogeneities, to determine the spectrum, and to compare the index variations with various meteorological factors. Included in the paper is a discussion of the errors arising from the flow of the atmosphere through the cavity.

The Microwave Refractometer

The refractometer measures by a sweep frequency technique very small frequency differences between two cavity resonators.[6] In the present case, these were about 3 cm long and 5 cm in diameter inside, and operated in the cylindrical TE_{011} mode at a frequency of about 9,000 mc. To permit the flow of the atmosphere through the cavities, circumferential slots were cut in its end plates. Although about 30 per cent of the areas of each end plate was removed, the decrease in the original loaded Q of about 10,000 was quite small. Wind tunnel tests indicated that the air speed through the cavity was about 0.2 that of the external air speed. To record the small variations from the mean refractive index, a dc amplifier was connected to the output of the refractometer. The response time of the equipment was limited

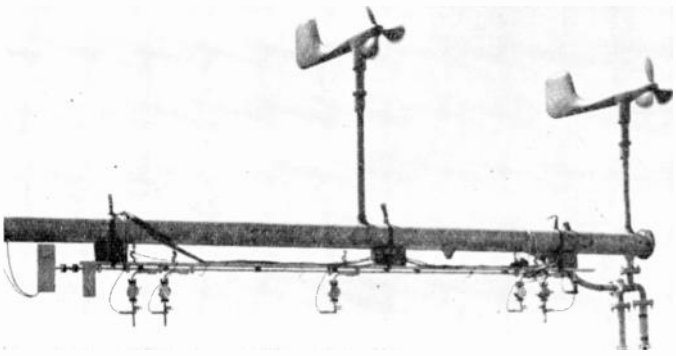

Fig. 1–Multiple cavity unit on boom at 125-meter height.

* Original manuscript received by the IRE, July 21, 1955.
† National Bureau of Standards, Boulder, Colorado.
[1] C. M. Crain and J. R. Gerhardt, "Some preliminary studies of the rapid variation in index of refraction of atmospheric air at microwave frequencies," *Bull. Am. Meteorol. Soc.*, vol. 31, pp. 330–335; November, 1950.
[2] G. Birnbaum, "Fluctuations in the refractive index of the atmosphere at microwave frequencies," *Phys. Rev.*, vol. 82, pp. 110–111; April, 1951.
[3] C. M. Crain and J. R. Gerhardt, "Measurements of the parameters involved in the theory of radio scattering in the troposphere," PROC. IRE, vol. 40, pp. 50–54; January, 1952.
[4] G. Birnbaum, H. E. Bussey, and R. R. Larson, "The microwave measurement of variations in atmospheric refractive index," TRANS. IRE, vol. AP-3, pp. 74–78; August, 1952.
[5] A brief and preliminary account of this investigation is given in ref. 4.
[6] G. Birnbaum, "A recording microwave refractometer," *Rev. Sci. Instr.*, vol. 21, pp. 169–176; February, 1950.

to about 0.1 second by the recording milliammeter (the air in the cavity was changed in a period much less than this by the lowest wind speeds encountered).

With the cavities sealed off the noise level of the equipment was such that the indicated index variation was rarely greater than an amplitude of 0.05 N units.[7] The long time stability of the equipment depends for the most part on the sensitivity of the cavity and klystron frequencies to changes in temperature. For this reason rather massive invar cavities were used; the cavities were chromium plated and the klystron and its housing were enclosed in a metal can painted white to reflect radiation. These means achieved a stability such that for the meteorological conditions usually encountered and with the cavities sealed off the indicated change was no greater than 0.2N over several minutes.

The Multiple Cavity Unit

When an open and a closed cavity are compared, the refractometer output current is directly proportional to the variations in index Δn_1 from the mean value. When two open cavities are compared, this current is proportional to the difference in index variations between positions 1 and 2 $(\Delta n_1 - \Delta n_2)$. These quantities are sufficient to determine a correlation coefficient ρ from the equation

$$\rho = 1 - \overline{(\Delta n_1 - \Delta n_2)^2}/2\overline{\Delta n_1^2}, \qquad (1)$$

which is obtained from a well-known theorem in statistics with the condition that $\overline{\Delta n_1^2} = \overline{\Delta n_2^2}$. This condition can normally be expected to hold in a relatively homogeneous atmosphere, at least for small distances, at a fixed height. It is clear that ρ is a function of the distance of separation between the cavities, approaching the value 1 for sufficiently small distances and decreasing for increasing distances.

The multiple cavity unit (Fig. 1) used here had been developed for a previous investigation (to obtain $(\Delta n_1 - \Delta n_2)$ for several cavity separations for the purpose of estimating the scale).[2,8] The klystron is connected to a long section of waveguide containing directional couplers to which are attached the cavities and crystal detectors. The crystal outputs are brought to a switch so that any two cavities could be selected for frequency comparison. As only one pair of amplifiers were used, Δn_1 was not obtained concurrently with $(\Delta n_1 - \Delta n_2)$, but it was easy to determine whether $\overline{\Delta n_1^2}$ was sufficiently constant during interest interval by switching between open-closed and open-open pairs of cavities.

It may be noted that the measurement of index difference fluctuations automatically discriminates against those fluctuations which have an effective wavelength significantly greater than the spacing between the cavities. Thus the problems involved with the analysis of data having a time-varying mean value are reduced.

In the present work only the pair of open cavities separated by the greatest distance, 2.3 meters, was employed as the usefulness of the cavity pairs separated by the smaller distances was limited by the response of the recording milliammeter and the wind speed. Consider, for example, the cavities separated by only 0.2 meter. As indicated previously, this system discriminates against those fluctuations which have wavelength components significantly greater than 0.2 meter and responds to components less than this. However, for a wind speed of 10 mph or 4.6 m/sec a component whose wavelength is about 2 meters, or whose frequency is 2 cps, will be decreased by the factor 0.7 by the recorder whose response time is roughly 0.1 second. Shorter wavelengths are damped even more. Thus, the components to which the 0.2 meter cavity pair responds are damped by the recorder. To make measurements at small separations it is merely necessary to use a faster recorder, or at very small separations both a faster recorder and a faster klystron sweep rate, as was done in the aircraft refractometer observations.[9]

Errors Associated with Cavity Ventilation

In terms of changes of temperature ΔT(°C) and vapor pressure Δe(mb) from the mean values, the change of refractive index Δn from the mean is given by

$$\Delta n\, 10^6 = -1.4\Delta T + 4.2\Delta e, \qquad (2)$$

which is obtained from the equation for the refractive index of air,[10] using the mean values of the temperature, vapor pressure, and barometric pressure that existed during the investigation. It is clear that the values of ΔT and Δe associated with a given packet of air can be changed by the cavity, and that in turn the condition of the cavity can be changed by the air. This may give rise to the following errors in the determination of refractive index variations.

Change in ΔT of an Air Sample During Its Passage through the Cavity

The air on entering the cavity tends to assume its temperature and in doing so the amplitude of ΔT is reduced. To determine quantitatively this effect a large duct was constructed through which air could be drawn with a powerful fan. The cavity was first heated to some temperature higher than that of the air and then the fan was started; the pertinent temperatures were measured as a function of time by thermocouples and recording milliammeters. For the cavities used in the present experiment (Fig. 1) it was found that for a

[7] The N-unit is defined by $N = (n-1)10^6$, where n is the refractive index.

[8] A similar system employing temperature elements is described in detail by J. R. Gerhardt, C. M. Crain, and H. W. Smith, "Fluctuations of atmospheric temperature as a measure of the scale and intensity of turbulence near the earth's surface," *Jour. Meteorol.*, vol. 9, pp. 299–310; October, 1952.

[9] H. E. Bussey and G. Birnbaum, "Measurement of variations in atmospheric refractive index with an airborne microwave refractometer," *N.B.S. Jour. Res.*, vol. 51, pp. 171–178; October, 1953.

[10] E. K. Smith and S. Weintraub, "The constants in the equation for atmospheric refractive index at radio frequencies," Proc. IRE, vol. 41, pp. 1035–1037; August, 1953.

wind speed of 10 mph ΔT was reduced by 30 per cent, and at 30 mph this reduction amounted to about 15 per cent. As may be expected, these figures were found to vary with the construction of the cavity and the degree to which it was opened to the atmosphere, nevertheless they may be taken as representative of magnitude of error. As long as Δe plays the significant role in determining Δn, however, this error is not significant.

Change in Cavity Frequency Due to Thermal Expansion

Originally an attempt was made to deal with the problem of thermally stabilizing the cavities by trying to have the open and closed cavities expand at the same rate, and accordingly both cavities were constructed from a common block of brass. Such a dual cavity unit was used in the present work with one of the refractometers. While it proved to be satisfactory, probably because the atmospheric temperature was quite uniform, tests showed that the desired equalization was not achieved unless ventilating holes were drilled through the part of the metal block around the closed cavity. Even so, better thermal stability was achieved by making individual cavities from invar. Those used here were found to expand[11] at an indicated rate of 2 to 3 N units per °C and to have a thermal time constant for a wind speed of 10 mph of the order of 4 minutes.

Changes in cavity temperature and hence frequency may arise from changes in air temperature and from changes in wind speed when the cavities are exposed to the sun. From the solar insolation constant and the known rate of heat transfer from the cavity to a wind stream of 10 mph, for example, it was calculated that the cavity could at most be about 1° C warmer than the air (at 3 mph wind speed the cavity would be 2° C warmer). This situation does not result in a false Δn when the wind is steady, or its fluctuation period is short compared with the thermal time constant of the cavity. On the other hand, a sustained or slow change in wind speed could cause a long-time drift in the indicated value of Δn. It is clear that similar considerations apply to the effect of changes in air temperature on the cavity temperature. For the meteorological conditions usually encountered the equipment drift over several minutes was no greater than 0.2 N units.

Change in Δe Due to Adsorption of Vapor on the Walls of the Cavity

Since it is well known that water vapor is strongly adsorbed by various surfaces, some measurements were made to determine the rate and amount of water vapor that was removed from moist air by the cavity walls. Although this work was not done with a moving air stream the results obtained indicated adsorption and desorption effects are not significant in altering the concentration of vapor in air flowing through the cavity.

Change in Cavity Frequency Due to Water Condensation

Although the electric field is extremely small everywhere on the walls of a cavity operating in the TE_{011} mode, it rapidly increases away from the walls, and consequently it is interesting to calculate the effect on the cavity frequency of a thin, uniformly condensed layer of water. By applying the formula of first-order perturbation theory we found that the change in frequency varied as the cube of the layer thickness, and that, for example, for a 3 cm wavelength cavity with a layer of water 0.03 mm thick the fractional change in frequency was 10^{-6} or 1 N unit. It is seen then that condensation and evaporation of water, which might occur under a saturated vapor condition, may have a significant influence on the frequency of the cavity.

Experimental Arrangement

Observations during the day and night from August 24 to August 29, 1951, were made with refractometers and meteorological equipment installed on two levels of a 128-meter tower at the Brookhaven National Laboratory. The terrain in all directions from this site is level and unobstructed; its general location is shown in Fig. 2. The tower[12] has platforms for working space and has counter-balanced booms about 6 meters long at 8 heights ranging from 3 to 125 meters.

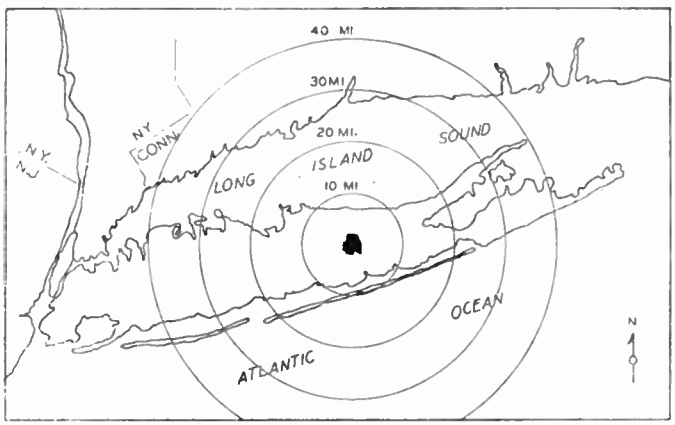

Fig. 2—General location of Brookhaven National Laboratory.

The multiple cavity unit was mounted on the boom at 125 meters. The dual cavity unit (one cavity open, the other closed) was mounted on the boom at 11 meters during the first few days and then at 108 meters for the rest of the time. The cavities were ventilated by the motion of the atmosphere, consequently the booms were oriented so that the axes of the cavities were parallel to the direction of the wind. Originally we planned to place the cavities on the platforms since this was the most convenient arrangement. However, tests of the turbulence generated by the wind on passing through

[11] In our later work (see ref. 9), the thermal expansion coefficient was considerably reduced by using a special heat treatment for invar invented by B. S. Lement, B. L. Averbach, and M. Cohen, and described in "The dimensional behaviour of invar," *Trans. Am. Soc. Metals*, vol. 42, pp. 1072–1097; 1950.

[12] A description of the tower and the meteorological equipment it carries is given in a paper by N. R. Beers, "Stack meteorology and atmospheric disposal of radioactive waste," *Nucleonics*, vol. 4, pp. 28–38; April, 1949.

the tower indicated that this location was definitely not suited for the studies at hand.

In order to compare index variations with those of temperature and wind speed, bead thermistors[13] were mounted close to the open cavities. A bridge-type circuit was employed to measure the electrical resistance of the thermistor elements, the resistance being a measure of air temperature if the thermistor was unheated or a measure of wind speed if the thermistor was electrically heated. The outputs of the bridges were recorded by Esterline Angus milliammeters. In still air the time constant of the thermistor was roughly 0.5 second and became smaller in moving air. Timing markers were transmitted to all the recording milliammeters so that the recorded data could be synchronized for correlation analysis.

During the course of this investigation the temperature ranged from 19 to 28° C, and the vapor pressure for the most part fell within the limits 16 to 24 mb. Winds with speeds from 3 to 16 mph were encountered and from directions which indicated that the air reaching the site had over-water and in other instances over-land trajectories. The weather generally was fair with little or no cloudiness.

Discussion of Results

Table I on page 1416 gives the weather conditions associated with the eleven pairs of runs that were studied, and Table II on page 1417 summarizes the results of a detailed analysis of the data. Several runs were not suitable for the present analysis either because they were of an exploratory nature or else because of power failure or trouble with the apparatus. In what follows we will first discuss the nature of the index variations, the correlation of the index variations with various meteorological parameters, and then deal with those aspects of the data of interest in radio scattering.

A striking feature of the refractive index data was the variability in the character of the fluctuations indicating the nonuniform nature of the atmospheric turbulence encountered. In view of this it was not surprising that a spectral resolution of the data (Table II, columns 1, 2, and 3) indicated that the medium and short wavelength components were not present all the time and in addition that each of the components were present different percentages of the time. It was necessary for the purpose of analysis to divide certain records into smooth and strongly fluctuating portions (runs 8 and 10).

Correlation of Refractive Index Fluctuations with Various Meteorological Factors

Temperature Variation (Column 7): Except for runs 1 and 2 the temperature variation was usually less than 0.2° C, and hence from (1) it is apparent that the index variations were due mainly to variations in vapor pressure. Even so it was noticed in scanning the records that variations in temperature usually showed correlation with variations in index. The temperature variations were greater at 11 meters than at 125 meters (runs 1 to 5), but the index variations showed no obvious trend with height.

Wind Speed Variation (Column 5): In almost all cases there was no obvious correlation of index with wind speed variations.

Vapor Pressure and Wind Direction (Columns 3 and 4): During runs 1 to 5 and 11 the wind trajectory was mainly from over land, and the vapor pressure at 125 meters was approximately 17 mb. For these conditions ΔN rms (Table II, columns 1, 2, and 3) tended to be smaller than in the case of over-water trajectories, except for runs 2 and 11. These runs taken in the morning show larger amplitudes which were probably associated with the break-up of the nocturnal temperature inversion with the solar heating. During runs 6 through 10 the wind came from over the ocean and the vapor pressure was greater than 20 mb. These runs showed a tendency toward larger index variations than those considered above where the air mass was drier. Exceptions are furnished by runs 6 and 10, both of which were associated with nocturnal temperature inversions. It is not to be inferred from these results that the amplitude of ΔN is necessarily directly dependent on the vapor pressure, more likely it is dependent on the character of the air masses.

Vertical Temperature Gradient (Column 2): was determined by thermal elements located at various levels on the tower. As might be expected, there was definite correlation between temperature gradient and amplitude of index variation. A positive gradient, an inversion, which occurs at night and represents a stable condition of the atmosphere with regard to vertical transport always made ΔN small (Table II, columns 1, 2, and 3). The largest negative gradients, which occurred during runs 1, 2, 11 of the over-land air mass group and run 8 of the over-water group, were associated with the largest index fluctuations. An exception to this is run 10 which is discussed below.

In run 10 the inversion extended to a heightbetween 108 and 125 meters, and the negative gradient above the inversion was very great, 1° C per 100 feet. The index variations at 108 meters in the stable air were small. The index variations at 125 meters were rather small except for periods of one or two minutes at three different times during the run. During these periods the temperature increased by a few tenths of a degree, the refractive index increased by 4 N approximately, probably due to the approach of the wavelike top of the inversion surface, and index fluctuations became large and rapid. This situation was quite different from runs 3 and 6 where fluctuations at 125 meters were quite small.

Data Analysis

Spectrum of Refractive Index Inhomogeneities: The atmosphere may be regarded as an assembly of air parcels whose refractive index values differ from one another

[13] Manufactured by the Western Electric Co., Type No. D-176980

TABLE I

Run Identity No. Date (in Aug. 1951) Time (est)	1	2		3	4		5	6	7
		Meteorological Conditions at Refractometer							
	Surface Weather, Clouds, Temp. (°C), Rel. Humidity, Wind	Ht. of Instrument Meters	Vertical Temp. Gradient at Instrument °C per 100 ft	Vapor Pressure mb	Wind Direction, Speed (mph) Land or Water Trajectory		Variation in Wind Speed mph Over 1 to 2 Min Intervals	Temp. °C	Variation in Temp. °C Over 1 to 2 Minutes
1 24th 1449–1545	Fair, 0.4 cloud 24°, 60 per cent NNE, 2 mph, changes to SE in sea breeze	125 11	−0.5 −3.0	16.7 22.8	45° land	4.6 4.0	— 3	20.4 22.6	0.4 1.3
2 25th 0930–1001	Partly cloudy, 0.6 cld 24°, 60 per cent, NNE, 8 mph	125 11	−0.4 −1.2	16.0 —	30° land	14.1 10.0	2 3.5	19.0 —	0.3 0.5
3 26th 1837–1930	Fair, 0.1 cld 19°, 84 per cent SW-1	125 11	0.0 (a) +2.0	16.8 16.9	245° land	13.5 4.5	0.1 1.5	19.0 18.4	0.05 —
4 26th 2133–2226	Clear, and fog 13°, 95 per cent Calm	125 11	+0.5 +6.0	15.8 16.8	250° land	13.9 3.0	0.1 0.4	19.3 16.2	0.02 0.25
5 27th 0840–0918	Fair, 0.1 cld 22°, 84 per cent WNW-2	125 11	−0.3 −1.0	18.3 20.1	300° land	2.5 2.0	1.5 1.5	22.1 22.9	0.1 0.4
6 27th 2000–2019	Fair, haze, 0.3 cld 26°, 65 per cent SW-3	125 108	−0.25 (b) −0.25	22.6 —	160° water	16 16	0.2 0.3	21.1 21.3	0.05 0.02
7 28th 1036–1054	Fair, haze, 0.2 cld 26°, 65 per cent S-3	125 108	−0.25 −0.25	21.6 —	130° water	7 7	1.5 —	23.5 23.6	0.15 0.15
8 28th 1352–1418	Clear, haze 27°, 70 per cent S-5	125 108	−0.3 −0.3	20.9 —	90° water	12 12	1.7 1.5	24.4 24.0	0.1 0.2
9 28th 1519–1535	Clear, haze 26°, 60 per cent SSW-5	125 108	−0.25 −0.25	20.1 —	150° water	11 13	2 1.5	23.7 24.0	0.05 0.1
10 28th 1931–2005	Clear, haze 19°, 90 per cent SSW-1	125 108	−1.0 (a) 0.0	24.5 —	140° water	10 10	0.4 0.2	21.1 21.5	0.05 0.0
11 29th 0930–0947	Clear, haze 26°, 71 per cent NNW-1	125 108	−0.5 −0.5	17.5 —	295° land	3.4 4.5	0.6 0.9	23.0 23.4	0.15 0.1

(a) Inversion up to 108 meters; (b) Inversion up to 92 meters.

and in general from the mean value. Within any large parcel there may be smaller parcels of smaller index variations and so on. The refractive index amplitude of a parcel was taken as the peak positive or negative deviation from the local mean, and the size as the interval between consecutive intersections of the record with the local mean multiplied by the mean wind speed. The analysis was restricted to three parcel sizes, which were chosen to represent the large, medium, and small sizes in a given run. The sizes admitted in any category covered a range of about 2 to 1. A rough estimate was made of the percentage of time that parcels of various sizes appeared to be present. The large parcel-size estimates were obtained from smoothed curves which represent a visually obtained 15-second moving average of the original data. The information regarding the smaller sizes was obtained by carefully scanning the original data. An independent observer checked some of this work and obtained amplitude values which agreed within 50 per cent with the present work. It is thought results of this analysis, given in columns 1, 2, and 3, may be roughly related to Fourier amplitudes and wavelengths.

To see whether the spectrum of parcel sizes tended to follow some law, the amplitude multiplied by the fraction of time present was squared to obtain the mean intensity, and these for each run were plotted versus size on logarithmic paper. Four runs were omitted from this analysis: run 3 at 11 meters because the index fluctuations were extremely small and hence the amplitude estimates subject to large error; run 4 at 11 meters because the only two points obtained were too close together in wavelength; and run 10 at both levels because of an unusual inversion condition. Of the 18 runs considered, 13 had slopes of 1.4 to 1.75, three had slopes of

TABLE II

Run No.	Height	1 Parcel Amplitude as a Function of Parcel Size: Large Parcel Size Region, Present 100 Per Cent of Time		2 Parcel Amplitude as a Function of Parcel Size: Medium Parcel Size Region, Present 75 Per Cent of Time		3 Parcel Amplitude as a Function of Parcel Size: Small Parcel Size Region, Present 50 Per Cent of Time		4 Amplitude of ΔN: Open vs Closed	5 Amplitude of ΔN: 2 Open Cavities 2.3m Apart	6 Correlation Coefficient for a Separation of 2.3m	7 Scale of Turbulence Estimated from Pairs of Cavities (Taylor Model)	8 Correlation Coefficient of ΔN at the Two Heights	9 Scale (Vertical) from Correlation of 108- and 125-Meter Data (Taylor Model)
1	125*m*	150*m*	1.1 N	12*m*	0.42 N	4.5*m*	0.1 N	0.6 N	0.07 N	0.995		0.13	
	11	75	2.7	12	0.66	4.5	0.4						
2	125	380	3.4	92	0.13	11.5	0.4	1.5	0.3	0.98	114*m*	0.25	
	11	460	1.4	70	0.13	6	0.14						
3	125	275	0.85	15	0.13	(a)		0.5	0.07	0.99		—	
	11	75	0.24	15	0.45	3	0.23						
4	125	185	0.7	92	0.33	9.3	0.1					0.3	
	11	21	0.85	10	0.37								
5	125	21	1.4	7	0.64	2.1	0.24	4.2 1.5[e]	1.0 0.6[e]	0.97 0.92[e]	73 27[e]	0.18	
	11	21	1.7	5	0.06	1.4	0.14						
6	125	430	0.4	55	0.23	11	0.08	0.36	0.12	0.94	41	0.26	12*m*
	108	430	0.28	75	0.17	13	0.14						
7	125	185	1.8	12	0.95	3.8	0.17	1.7	0.17	0.995		0.86	92
	108	185	1.5	18	0.65	5.4	0.56						
8	125	305	5.5	45 45	0.7 (S) 4.2 (F)	9.2 9.2	0.28 2.3	9.3	3.7	0.92	27	0.67	27
	108	305	5.5	45 45	0.14 (S) 4.2 (F)	9.2 9.2	0.65 2.4						
9	125	305	3.7	28	1.8	5.5	0.62	1.3	0.77	0.82	13	0.61	34
	108	230	3.4	28	1.7	5.5	0.37						
10	125	275	3.0	15 15	0.21 (S) 1.0 (F)	9.2 9.2	0.07 0.54	2.8	0.28	0.995		0.26	*
	108	415	0.92	15	0.28	6.9	0.30						
11	125	115	8.0	15	2.4	3.1	0.60					0.82	85
	108	115	6.6	15	3.0	3.1	0.20						

(a) Small amplitude obscured by noise of 0.05N; (S) Smooth portion of run; (F) Fluctuating portion of run; [e] After end of run; * Inversion separates two levels.

about 1.1 and two had slopes of about 2.3 for the dependence of log $\Delta N^2(S)$ on log S, where S is the size. To give an idea of the uncertainty of these slopes, standard deviations were estimated by the usual statistical method assuming error in only one variable, log $\Delta N^2(S)$. Of these standard deviations ten were approximately 0.1 to 0.3, five were approximately 0.4 to 0.7, two were greater than 1 and that for run 3 was indeterminate since only two points determined the line.

Average eighteen slopes was 1.6 which gives an empirical relation between parcel intensity and parcel size

$$\Delta N^2(S) \propto S^{1.6}. \quad (3)$$

This result is interesting in that functional dependence $S^{1.6}$ resembles, although perhaps fortuitously, the equilibrium spectrum of the Kolmogoroff theory of turbulence,[14,15] which predicts that the density of mean square fluctuations of velocity varies as the 5/3 power of wavelength. In view of these results, it is planned to obtain power density spectra by usual statistical methods. A Fourier analysis made on 4 runs tended to confirm the slopes obtained by the parcel size analysis.

[14] See G. K. Batchelor, "The Theory of Homogeneous Turbulence," Cambridge University Press, Cambridge, Eng., p. 122; 1953.
[15] E. C. S. Megaw, "Interpretation of stellar scintillation," *Quart. J. Roy. Meteor. Soc.*, vol. 80, pp. 248–251; April, 1954.

Results of Multiple Cavity Unit and Scale of Turbulence: The amplitudes obtained with the open-closed cavity pair and the two open cavities spaced 2.3 meters apart are given in columns 4 and 5. The correlation coefficients calculated from these data by (1) are given in column 6. These are all high indicating that the variation in index is well correlated over a distance of 2.3 meters, and sizes of most of the most intense index eddies or parcels are considerably larger than this distance.

It has been customary to characterize the entire range of eddy sizes by a single parameter, a mean size called the scale. This can be calculated provided the correlation coefficient has been obtained as a function of distance.[16] However, to calculate the scale from just a single value of the correlation coefficient it is necessary to assume a functional form for its variation with distance. Because of its simplicity, the exponential form $\exp -(r/l)$, where r is the separation and l the scale, introduced by Taylor to describe isotropic and homogeneous turbulence has often been used. Using this correlation function, we calculated the scales given in column 7, except where the correlation was too close to unity. It was felt that in these cases the results could be subject to especially large error.

Cross-Correlation Coefficient: The cross-correlation coefficient between simultaneous variations in index at positions 1 and 2 is defined by

$$\rho = \overline{\Delta N_1 \Delta N_2} / (\overline{\Delta N_1^2})^{1/2} (\overline{\Delta N_2^2})^{1/2} \qquad (4)$$

which may be easily transformed to (1). The correlation in index variation between two heights (see column 8) was calculated by (4) from points separated 15 seconds apart, obtained from the smoothed curves described previously. Where the refractometers were separated by about 114 meters the correlation was quite low. On the other hand when the refractometers were at 108 meters and 125 meters the correlation was high except when an inversion extended to 95 meters or more as in runs 6 and 10. As before, a scale can be obtained from the correlation coefficient and the separation (17 meters), provided the functional form of the coefficient is known. Using Taylor's function, with the aforementioned reservations, we obtained the scales shown in column 9, which are to be compared with the scales of column 7. In general, very close agreement between these results should not be expected because of the roughness of the analysis and the uncertain validity of the correlation function, and because one scale is for a horizontal direction and the other for the vertical direction. There is, nevertheless, some measure of agreement between the scales of columns 7 and 9. Furthermore, the scales of roughly 60 meters obtained here appear to be in general agreement with those derived from aircraft observations, and stellar scintillations.

Autocorrelation Coefficient: An autocorrelation analysis was made on the index data of run 8 at 125 meters from points spaced 1 second apart. Fig. 3 is a plot of the autocorrelation coefficient as a function of the time lag. The oscillatory component so evident in the figure was also noticed in a visual inspection of the data, and represented a wavelike spatial distribution of refractive index. The initial portion of the correlation coefficient can be approximated by an exponential and lends some support to the use of the Taylor correlation function for the short wavelength end of the spectrum. The scale deduced from the exponential portion of the coefficient has the value 58 meters. This is appreciably longer than that obtained from the vertical cross-correlation coefficient for run 8 and may possibly indicate the nonisotropic nature of the turbulence.

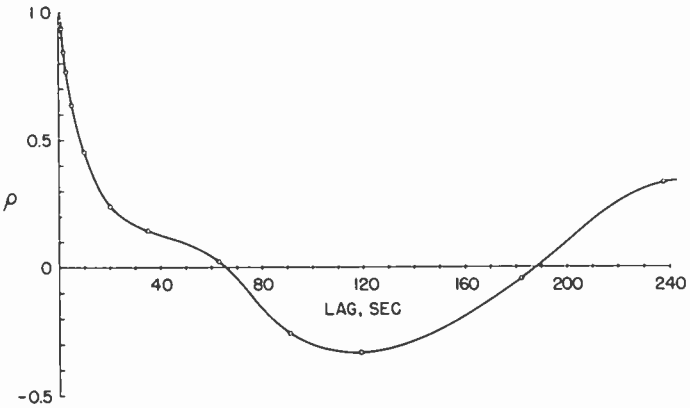

Fig. 3—Autocorrelation coefficient as a function of time lag, run 10 at 125 meters.

Conclusions

From the experimentally determined cross-correlation coefficient, and *assuming* the variation with distance is given by the (Taylor) exponential form, scales in the neighborhood of 60 meters were obtained: this result seems to generally agree with values reported from aircraft observations and stellar scintillations.

It was found from a crude analysis of 18 different runs that, on the average, the parcel intensity was proportional to the 1.6 power of the parcel size.

It was also found that the character of the refractive index fluctuations changed erratically with time, but that the rms amplitude of these fluctuations was somewhat correlated with various meteorological factors.

A detailed investigation of the errors arising from ventilation of the cavity and its exposure to the atmosphere indicated that these are (or had been made) sufficiently small so that the refractometer accurately measures variations in atmospheric refractive index. With simultaneous measurement of temperature fast variations of water vapor density can be determined.

Acknowledgment

We wish to thank R. R. Larson for his assistance with the experimental work, and the members of the meteorological group at the Brookhaven National Laboratory for their generous cooperation. We also wish to express our appreciation for the interest and encouragement of H. Lyons and K. A. Norton.

[16] O. G. Sutton, "Micrometeorology," McGraw-Hill Book Co., Inc., New York, N. Y., p. 93; 1953.

Some Applications of the Monthly Median Refractivity Gradient in Tropospheric Propagation*

B. R. BEAN† AND F. M. MEANEY‡

Summary—**A consistent correlation has been found between the monthly median values of 100mc transmission loss and an atmospheric parameter ΔN which is determined from standard radiosonde observations. ΔN is defined as the difference between the refractivity at the earth's surface and at one kilometer above the earth's surface. ΔN is determined from the midpoint of the propagation path and is taken to represent an effective gradient of the refractive index. It is found to yield correlation coefficients with transmission loss of about 0.7 even in the far scattering region. This correlation is also used to derive estimates of the annual, geographic, and terrain variances of the transmission loss. Six-year average values of ΔN are presented for the United States and can be used as an aid in the prediction of the annual cycle of 100 mc transmission loss. The possibility of using surface observations of N for times of day other than the radiosonde observation hours is examined and found to be encouraging. One of the major conclusions is that the observed dependence of transmission loss upon ΔN is five times greater than that indicated by standard propagation theory.**

Introduction

FOR SEVERAL years the National Bureau of Standards has sponsored the monitoring of vhf field strengths by various institutions throughout the United States, as well as maintaining its own vhf-uhf monitoring program with the transmitters located on Cheyenne Mountain, Colo. This monitoring program, a portion of which is shown pictorially in Fig. 1, was designed to cover a wide range of distances, terrain features, and climate. Used in this study are some 680 station-months of radio data from 25 independent transmission paths. Detailed information for the paths used in this study is given in Table I.

It is the objective of this paper to demonstrate that a consistent correlation exists between the gradient of the radio refractivity[1] of the atmosphere in the first kilometer above the earth's surface and the transmission loss[2] when both variables are taken on a monthly median basis. The correlations will be used to derive estimates of the annual, geographic and terrain variances of 100 mc transmission loss. It will also be indicated how the correlations may be used to predict an annual cycle of transmission loss from long term averages of the refractivity gradient.

* Original manuscript received by the IRE, August 1, 1955. Portions of this paper were presented at the Conference on Radio-Meteorology, Univ. of Texas, Austin, Tex., November 9–12, 1953, and the Dedication and Scientific Meetings of the National Bureau of Standards, Boulder Laboratories, Boulder, Colo., September 8–14, 1954.

† Central Radio Propagation Lab., National Bureau of Standards, Boulder, Colo.

‡ Formerly of Central Radio Propagation Lab., National Bureau of Standards, Boulder, Colo.

[1] E. K. Smith, Jr. and S. Weintraub, "The constants in the equation for atmospheric refractive index at radio frequencies," PROC. IRE, vol. 41, pp. 1035–1037; August, 1953.

[2] K. A. Norton, "Transmission loss in radio propagation," PROC. IRE, vol. 41, pp. 146–152; January, 1953.

Correlation of ΔN and Transmission Loss

The radio refractivity of the atmosphere,[1] N, is given with an uncertainty which is negligible in our present investigation by the relationship:

$$N = (n - 1) \times 10^6 = \frac{77.6}{T}\left(p + \frac{4810 e_s RH}{T}\right)$$

where

n = refractive index of the atmosphere
p = atmospheric pressure in millibars
T = temperature in degrees Kelvin
e_s = saturation vapor pressure in millibars for the temperature, T, and
RH = relative humidity.

Although the atmosphere's refractivity frequently varies with height in a complex manner, we shall attempt to describe those characteristics of this complicated distribution which are pertinent to our radio propagation applications by means of ΔN, which is the simple difference between the value of the refractivity at the earth's surface and at one kilometer above the earth's surface. ΔN is always determined for the midpoint of the propagation path under study. The monthly median values of ΔN are negative. The experimental results presented in this paper may be used directly in those theories of propagation based on the assumption of a constant refractivity gradient. This is illustrated in Fig. 2, p. 1421, where the transmission loss calculated from smooth-earth diffraction theory[3] is plotted vs ΔN and effective earth's radius factor, k, throughout the normal range of both ΔN and k. Fig. 2 is designed to show two things: (1) from theory one can expect the transmission loss to vary with ΔN, and (2) transmission loss is expected to be nearly a linear function of ΔN while a curvilinear function of k. Thus, although ΔN and k are functionally related, it is simpler to use ΔN rather than k in order to apply linear regression analysis. Although this theory[3] does indicate an approximately linear dependence of transmission loss with ΔN, we will see later that the observed changes with ΔN are some five times as great.

Fig. 3 presents a comparative plot of the observed monthly median transmission loss, L_{b0}, for the hours of radiosonde observation (0300 and 1500 GMT) and

[3] K. A. Norton, P. L. Rice, and L. E. Vogler, "The use of angular distance in estimating transmission loss and fading range for propagation through a turbulent atmosphere over irregular terrain," p. 1488, this issue.

Fig. 1—National Bureau of Standards 100 mc radio climatological program.

TABLE I

INFORMATION RELATIVE TO RADIO PATHS UTILIZED IN THIS STUDY

Station Number	Call Letters	Transmitter Location	Receiver* Location	Frequency (Mc)	Distance (Miles)	θ Milli-radians
1	KXYZ	Houston, Tex.	Austin, Tex.[a]	96.5	147.8	20.30
2	KPRC	Houston, Tex.	Austin, Tex.[a]	102.9	147.8	23.80
3	KIXL	Dallas, Tex.	Austin, Tex.[a]	104.5	175.9	32.30
4	KWKH	Shreveport, La.	Austin, Tex.[a]	94.5	277.0	47.40
5	KLTI	Longview, Tex.	Austin, Tex.[a]	105.9	227.2	40.40
6	WFAA	Dallas, Tex.	Austin, Tex.[a]	97.9	174.2	32.50
7	WMBI	Chicago, Ill.	Urbana, Ill.[b]	95.5	126.0	16.10
8	WCSI	Columbus, Ind.	Urbana, Ill.[b]	93.7	136.9	19.50
9	KXOK	St. Louis, Mo.	Urbana, Ill.[b]	93.7	146.6	19.34
10	WHKC	Columbus, Ohio	Hudson, Ohio[c]	98.7	125.0	19.25
11	WCOL	Columbus, Ohio	Hudson, Ohio[c]	92.3	121.2	20.10
12	WJAS	Pittsburgh, Pa.	State College, Pa.[d]	99.7	117.1	30.44
13	WEST	Easton, Pa.	State College, Pa.[d]	107.9	139.3	36.70
14	WTOP	Washington, D. C.	State College, Pa.[d]	96.3	136.8	61.90
15	KFSD	San Diego, Calif.	Santa Anna, Calif.[e]	94.1	84.6	29.00
16	KFOR	Lincoln, Neb.	Grand Island, Neb.[e]	102.9	93.2	14.60
17	WCAC	Anderson, S. C.	Powder Springs, Ga.[e]	101.1	127.5	19.80
18	KDKA	Pittsburgh, Pa.	Hudson, Ohio[c]	92.9	96.7	12.20
19	WTIC	Hartford, Conn.	Millis, Mass.[e]	96.5	80.6	16.30
20	NBS-CRPL	Cheyenne Mt., Colo.	Kendrick, Colo.[f]	100	49.3	−3.18
21	NBS-CRPL	Cheyenne Mt., Colo.	Karval, Colo.[f]	100	70.2	−1.33
22	NBS-CRPL	Cheyenne Mt., Colo.	Haswell, Colo.[f]	100	96.6	1.805
23	NBS-CRPL	Cheyenne Mt., Colo.	Garden City, Kan.[f]	100	226.5	28.12
24	NBS-CRPL	Cheyenne Mt., Colo.	Marble Colo.[f]	100	141.0	9.28
25	WIP-FM	Philadelphia, Pa.	Laurel, Md.[e]	93.3	104.1	12.04

* Recording Agency:
[a] University of Texas
[b] University of Illinois
[c] United Broadcasting Company
[d] University of Pennsylvania
[e] Federal Communications Commission
[f] National Bureau of Standards.

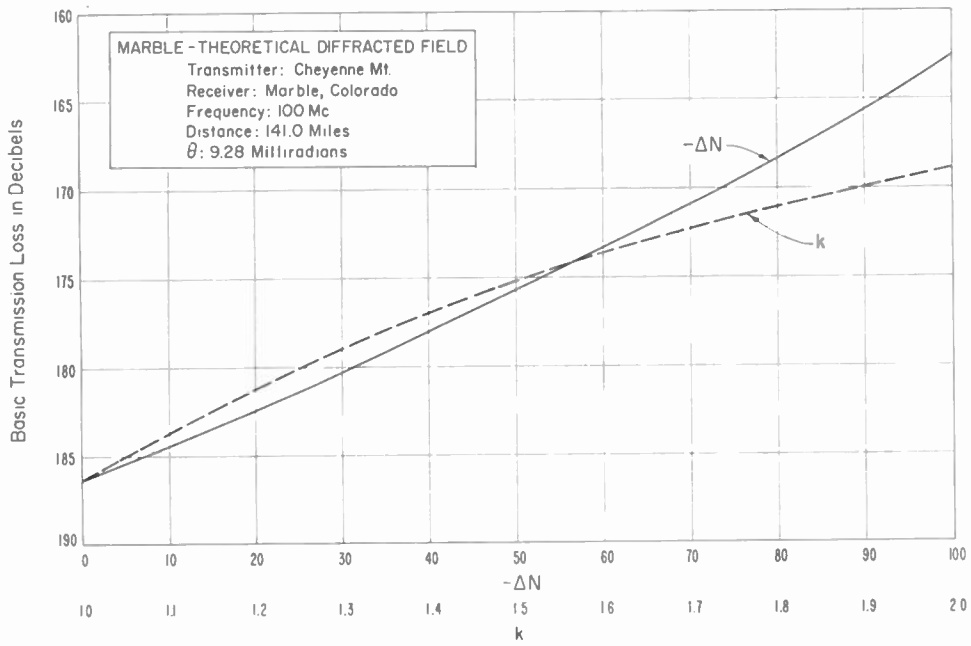

Fig. 2—Transmission loss calculated from diffraction theory vs effective earth's radius factor k, and the refractivity gradient, ΔN.

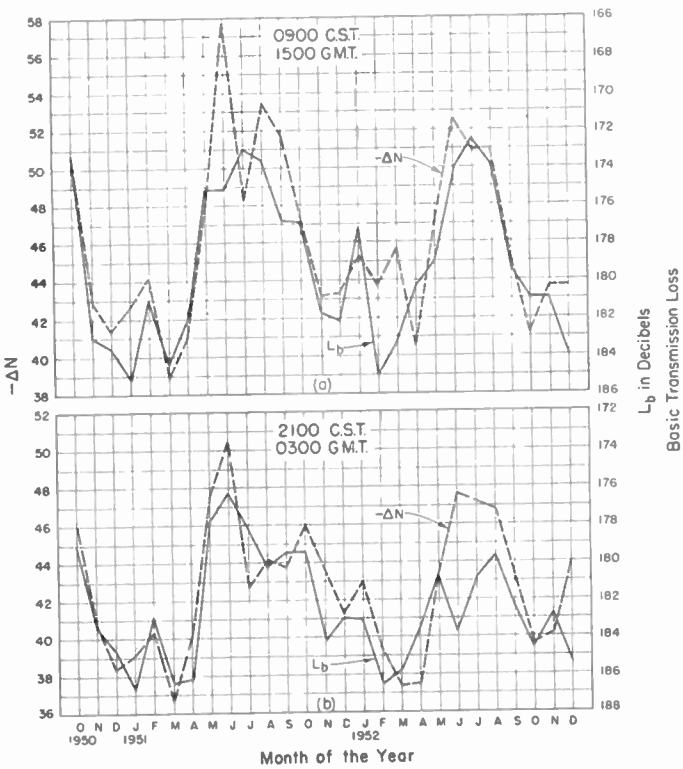

Fig. 3—Comparison of the monthly median basic transmission loss and refractivity gradient for KIXL-FM. Dallas, Tex., recorded at Austin, Tex.

the monthly median value of ΔN calculated for the mid-point of the propagation path of KIXL-FM (175 miles) for the period October, 1950 through December, 1952. The data for this path were recorded by the University of Texas and were selected for graphical presentation because they form the longest and most continuous record available. It can be seen that the transmission loss and ΔN display the same general annual cycle for both times of day. A regression line[4] of transmission loss on ΔN, of the form $L_{b0}=a+b\Delta N$, was then determined for each of these two observing periods. The resulting equation for the 1500 GMT regression line is $L_{b0}=212.74+0.727\ \Delta N$ (remembering that monthly median values of ΔN are negative) and is in close agreement with the 0300 GMT regression line $L_{b0}=211.57+0.691\ \Delta N$. Plots of the observed points and the regression line showed no systematic correlation between L_b and ΔN other than linear. Therefore, this regression equation gives us a method of estimating the monthly median transmission loss from observed values of ΔN.

Similar regression lines were obtained for each of the radio paths of Fig. 1. Table II, on page 1422, presents means and standard deviations of both transmission loss and ΔN for both times of radiosonde observation. Also in Table II are the correlation coefficients, slopes, and intercepts of the regression lines as derived for each time of radiosonde observation. By the application of a statistical test, the "sign" test,[5] using the 5 per cent significance level, the correlation coefficients, intercepts, and slopes of the regression lines for the 0300 and 1500 GMT data may be shown not to display any consistent difference. Therefore, for the sake of convenience, these data were combined at each station. The Cheyenne Mountain recording paths (paths No. 20–24) do not have over eight months' observation at any one time of radiosonde observation; hence only the combined 0300–1500 data are presented in Table II. The average cor-

[4] G. W. Snedecor, "Statistical Methods," Iowa State College Press, Ames, Ia., 4th ed., pp. 108–113.

[5] For a detailed illustration of this statistical test, see W. J. Dixon and F. J. Massey, "Introduction to Statistical Analysis," McGraw-Hill Book Co., Inc., New York, N. Y., pp. 247–254; 1951.

TABLE II

DATA USED IN DETERMINING THE REGRESSION LINES

Station Numbers*	n	$\overline{L_{bo}}$	$s_{L_{bo}}$	$\overline{\Delta N}$	$s_{\Delta N}$	r	b	a
0300 Observation								
1	19	171.51	2.93	44.94	3.09	0.694	0.659	201.11
2	21	172.34	2.37	46.99	4.94	0.566	0.271	185.09
3	28	181.86	3.34	42.94	4.01	0.830	0.691	211.51
4	17	192.42	2.52	47.78	3.62	0.619	0.430	212.97
5	15	190.48	2.00	47.31	3.02	0.484	0.321	205.65
6	10	185.72	2.91	45.64	5.48	0.729	0.386	203.36
7	14	172.66	3.23	43.38	5.79	0.548	0.305	185.91
8	24	178.90	3.73	45.40	6.01	0.624	0.388	196.52
9	21	173.46	3.94	42.87	6.06	0.574	0.374	189.49
10	19	169.21	4.68	43.42	5.61	0.647	0.541	192.69
11	19	167.53	3.71	43.42	5.60	0.510	0.338	182.19
12	18	172.87	3.62	40.53	5.22	0.840	0.582	196.46
13	11	177.42	2.24	41.98	5.44	0.883	0.364	192.68
14	17	180.58	3.78	42.12	7.20	0.914	0.479	200.76
15	21	153.25	6.72	57.87	12.78	0.922	0.485	181.31
16	17	169.59	3.63	42.02	5.06	0.768	0.549	192.68
17	17	170.97	4.33	46.75	5.81	0.475	0.354	187.53
18	8	172.21	4.56	40.71	5.40	0.911	0.770	203.54
19	13	162.29	2.27	43.40	9.39	0.792	0.191	170.60
25	19	153.21	5.80	45.92	8.25	0.730	0.513	176.77
1500 Observation								
1	19	170.78	1.99	49.09	4.43	0.531	0.240	182.54
2	21	173.15	3.08	51.31	6.01	0.627	0.319	189.51
3	28	179.05	4.14	46.27	4.66	0.816	0.726	212.67
4	17	190.27	3.20	49.59	4.41	0.812	0.588	219.41
5	15	187.72	3.48	50.28	3.94	0.814	0.719	223.88
6†								
7	14	170.64	3.91	41.91	4.09	0.866	0.828	205.36
8	24	178.02	4.21	43.98	4.60	0.831	0.762	211.54
9	22	172.12	3.78	43.18	5.63	0.669	0.449	191.52
10	19	170.54	4.40	42.28	4.84	0.601	0.546	193.63
11	19	168.65	3.32	42.28	4.84	0.481	0.330	182.60
12	18	173.34	3.41	39.31	5.02	0.822	0.557	195.22
13	12	177.87	2.76	41.01	4.92	0.875	0.490	197.98
14	17	180.02	3.69	40.04	6.24	0.902	0.534	201.39
15†								
16†								
17†								
18	8	174.83	3.36	38.26	4.54	0.668	0.492	193.67
19†								
25	19	150.43	4.01	8.35	7.08	0.675	0.382	166.61
Combined 0300–1500 Observations								
1	38	171.15	2.50	47.01	4.32	0.568	0.329	186.62
2	42	172.75	2.75	49.15	5.89	0.498	0.233	184.19
3	56	180.46	4.00	44.60	4.63	0.844	0.729	212.95
4	34	191.34	3.04	48.68	4.08	0.750	0.558	218.50
5	30	189.10	3.12	48.79	3.76	0.759	0.629	219.78
6	10	185.72	2.91	45.64	5.48	0.729	0.386	203.36
7	28	171.65	3.67	42.65	4.98	0.595	0.438	190.33
8	48	178.46	3.96	44.69	5.41	0.685	0.502	200.90
9	43	172.77	3.88	43.03	5.78	0.615	0.413	190.54
10	38	169.87	4.53	42.85	5.20	0.631	0.551	193.47
11	38	168.09	3.52	42.85	5.20	0.505	0.342	182.76
12	36	173.11	3.46	39.92	5.09	0.832	0.567	195.75
13	23	177.65	2.47	41.47	5.08	0.870	0.424	195.23
14	34	180.30	3.68	41.08	6.72	0.881	0.483	200.15
15	21	153.25	6.72	57.87	12.78	0.922	0.485	181.31
16	17	169.59	3.63	42.02	5.06	0.768	0.550	192.68
17	17	170.97	4.33	46.75	5.81	0.475	0.354	187.53
18	16	173.52	4.10	39.49	4.99	0.829	0.681	203.42
19	13	162.29	2.27	43.40	9.39	0.792	0.191	170.60
20	12	133.58	1.30	37.04	4.25	0.0815	0.0248	134.50
21	14	134.11	1.48	36.88	4.18	0.581	0.206	141.72
22	14	152.82	2.20	37.16	4.17	0.802	0.423	168.54
23	16	193.13	4.97	39.59	5.97	0.603	0.501	212.96
24	4	151.65	15.72	40.45	9.62	0.979	1.598	216.29
25	38	151.82	5.12	44.13	7.80	0.725	0.476	172.82

* Station numbers correspond to path numbers given in Table I

n—Number of months of observations

$\overline{L_{bo}}$—Mean value of the observed transmission loss

$s_{L_{bo}}$—Standard deviation of the observed transmission loss $= [\sum_1^n (L_{bo} - \overline{L_{bo}})^2/(n-1)]^{1/2}$

$\overline{\Delta N}$—Mean value of the observed ΔN

$s_{\Delta N}$—Standard deviation of the observed ΔN's (defined like $s_{L_{bo}}$)

r—Correlation coefficient of L_{bo} and ΔN

b—Slope of the regression line (db change per unit change in ΔN)

a—Intercept on the L_{bo} axis of the regression line.

† No observation.

relation coefficient[6] for all the data is 0.722; consequently the fraction $(0.722)^2$ or 52 per cent of the variance of transmission loss over a given path can be accounted for, on the average, by variation in ΔN for the path.[7] Until such time as radiosonde observations become generally available for a larger number of times during the day, it will be difficult to use the techniques discussed in this paper for predicting the diurnal cycle of radio transmission loss as a function of ΔN, although this is known to be comparable[8] in magnitude to the annual cycle of transmission loss due to ΔN.

To account to a first approximation for the systematic effects of such characteristics of the radio transmission path as its length, the antenna heights and roughness of terrain, the slopes of the regression line as well as the error[9] in determining the slopes were plotted in Fig. 4 against the angular distance θ.[3] The angular distance θ is defined as the angle between the lines drawn from the transmitting and receiving antennas to their respective radio horizons in the great circle plane containing the antennas and for the radio standard atmosphere. This angle θ is taken to be negative for receiving locations within the radio horizon of the transmitting antenna, zero on the radio horizon, and positive beyond the radio horizon. Fig. 4 presents the slopes of the regression lines (i.e., db change per unit change in ΔN) vs the angle θ determined for the actual terrain of each propagation path. Also plotted on Fig. 4 is a theoretical curve[3] for atmospheres with constant refractivity gradient over a smooth spherical earth. Since only one out of twenty points lies on or below the theoretical curve, this theory is evidently not consistent with these data.

As will be seen in the last section, we will need to be able to estimate values of b for any value of θ without actually going thorugh the correlation process. This is most easily done by fitting a curve to the observed values of b in Fig. 4. One such curve that immediately suggests itself is to multiply the theoretical curve of Fig. 4 by a constant. Least squares was employed to determine the constant by which the theoretical curve should be multiplied in order to best fit the observed slopes. This constant was 5.09. This value of this constant appears to the authors to indicate that the assumption of a linear refractive index profile for the calculation of transmission loss is not an adequate representation of the actual profile. If, however, the theory were based on the physically more realistic exponential profile (such as $n = n_0 \exp(-kh)$ where n is the refractive index at the height h, n_0 is the surface value of n, and k an empirically determined constant), then one might expect the calculated variation in transmission loss to be greater for a given change in ΔN.

An interesting point arose in the original fitting of the theoretical curve to the observed data. At that time there were no radio paths in the region 8 to 12 milliradians of θ and consequently the dependence of b upon θ was not clear. A recording site was established at a θ value of about 9 milliradians to investigate this very point. This station, called Marble, was established in the Cheyenne Mountain program, and data were obtained in February and August of 1954. The high value of b observed at Marble was instrumental in affecting the choice of fitting the theoretical curve multiplied by a constant to the observed data.

Correlation of Surface Refractivity and Transmission Loss

One might wonder at this point if the preceding correlations might also be derived for other hours throughout the day. Since standard radiosonde observations are taken only twice a day, and both observations are during periods of transition from daytime to nighttime conditions, the diurnal cycle of ΔN is not clearly defined. Therefore, correlations involving the diurnal cycle of transmission loss vs the diurnal cycle of ΔN are difficult, if not impossible, to make. To extend our study to the diurnal cycle of transmission loss, one might ask if the surface values of refractivity yield as good a correlation coefficient with L_b as those obtained using ΔN. Early work by Pickard and Stetson[10] and later work by Randall[11] have shown marked correlation between functions of the surface refractivity and transmission loss for a single radio path.

Three propagation paths were selected to study this question: Cheyenne Mountain to Haswell, Colo., and Garden City, Kans. (Paths 22 and 23); and KIXL-FM Dallas, Tex., to Austin, Tex. (Path 3). One of the cardinal reasons for selecting these particular propagation paths is the propinquity of Air Force radiosonde stations which take observations four times a day rather than twice a day. Radiosonde observation points used for following correlations are: Lowry Air Force Base at Denver, Colo., for Cheyenne Mountain propagation paths, and Carswell Air Force Base, Ft. Worth, Tex., for KIXL-FM propagation path. In Table III (next page) correlations between monthly median values of ΔN and transmission loss are tabulated together with correlations of monthly median values of surface refractivity, N_S, with transmission loss. Sample sizes in Table III are the same as appear in Table II.

With but two exceptions (the 1400 observations at Haswell and Garden City), the correlation coefficients of L_b and N_S are comparable with or greater than those

[6] Snedecor, *op. cit.*, pp. 151–155.
[7] *Ibid.*, pp. 185–186.
[8] P. L. Rice and F. T. Daniel, "Radio transmission loss vs distance and antenna height at 100 mc," Trans. IRE, vol. AP-3, pp. 59–62; April, 1955.
[9] The error in determining the slope of the regression line was obtained by multiplying the standard error based on the assumption of independent observations (see reference 4, p. 119) by a factor designed to remove, to a first approximation, the effects of serial correlation within the ΔN and L_b data as well as the cross-correlation between the AM and PM data.
[10] G. W. Pickard and H. T. Stetson, "A study of tropospheric reception at 42.8 mc and meteorological conditions," Proc. IRE, vol. 35, pp. 1445–1450; December, 1947.
[11] D. L. Randall, "A study of the meteorological effects on radio propagation at 96.3 mc between Richmond, Virginia, and Washington, D. C.," *Bull. Amer. Met. Soc.*, vol. 35, pp. 56–59; February, 1954.

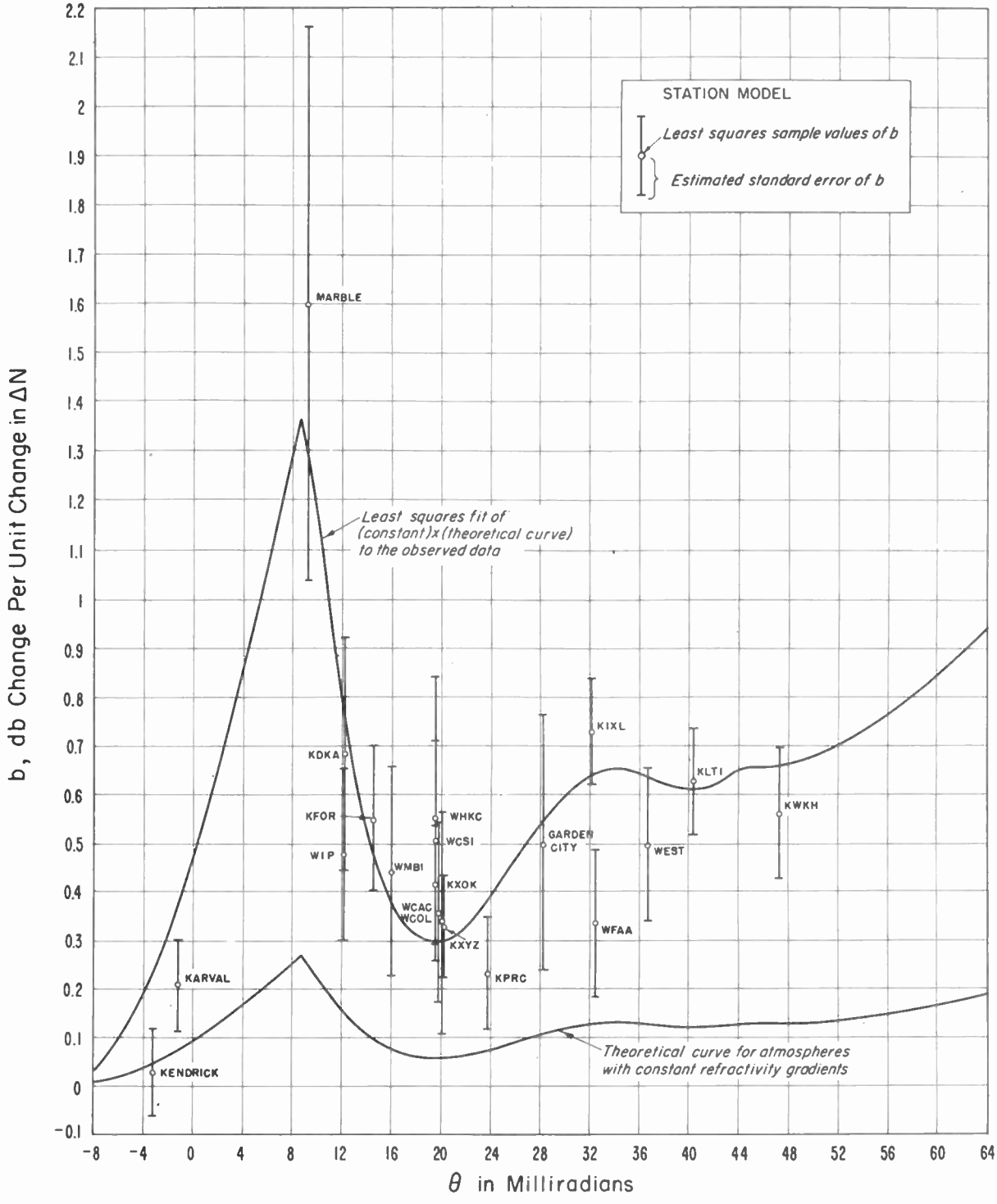

Fig. 4—Slope b of the regression line, $L_b = b\Delta + Na$, vs the angle θ.

TABLE III.—Comparison of Correlations Between Transmission Loss and ΔN or N_S

Time (MST)*		Haswell s_{N_s} or $s_{\Delta N}$	r	s_{Lb}	Garden City s_{N_s} or $s_{\Delta N}$	r	s_{Lb}	KIXL-FM s_{N_s} or $s_{\Delta N}$	r
0200	N_s 3.00	9.46	0.525	5.55	7.97	0.875	5.70	19.56	0.918
	ΔN 3.00	3.44	0.486	5.55	2.88	0.884	5.70	5.82	0.848
0800	N_s 3.29	10.36	0.112	5.46	8.30	0.874	4.15	20.42	0.893
	ΔN 3.29	5.12	0.221	5.46	4.20	0.886	4.15	7.49	0.835
1400	N_s 2.27	7.22	0.007	5.48	5.79	0.593	2.09	18.43	0.819
	ΔN 2.27	2.11	0.599	5.48	2.16	−0.585	2.09	6.06	0.338
2000	N_s 2.19	8.59	0.009	4.26	7.28	0.645	3.36	18.43	0.873
	ΔN 2.19	2.71	0.039	4.26	2.31	0.635	3.36	5.00	0.566

* The local times for the KIXL-FM propagation path are in CST; therefore, one hour should be added to the times listed to obtain local time on the KIXL-FM path.

of L_b and ΔN. Considering only the correlation coefficients, one could conclude that N_S was as good a predictor of the transmission loss as ΔN. A strong point in favor of the surface observations is that they are available from many places for each hour of the day, while radiosonde observations are taken at relatively few observation points a maximum of four times per day. However, before choosing between N_S and ΔN as predictors one should also compare the geographic and diurnal variations of the dependence of L_b on N_S and ΔN as well as the applicability of N_S and ΔN to present propagation theory.

To study the geographic variation of the dependence of L_b on N_S requires correlations from many geographically diverse propagation paths. Such correlations have not been calculated at this writing.

It has already been pointed out that the correlation of L_b and ΔN has direct application in those theories of propagation which assume a constant refractivity gradient. The surface values can also be fitted into these constant gradient propagation theories at least in so far as the surface values of refractivity are correlated with the values of ΔN. Table IV presents such correlations for each time of observation at Lowry Air Force Base, Denver, Colo., and Carswell Air Force Base, Ft. Worth, Tex. With the exception of the 1400 observations all of the correlations are at least 0.8. This is somewhat as one would expect, since the correlation coefficients of transmission loss on N_S and ΔN given in Table III differ the most for the 1400 observations, indicating that for that time N_S and ΔN are less correlated than during other observational periods. These correlations indicate one means of using the surface values of refractivity in those propagation theories that postulate a constant gradient of refractivity.

TABLE IV

CORRELATION OF MONTHLY MEAN VALUES OF N_S AND ΔN FOR LOWRY AFB AND CARSWELL AFB

Time (MST)*	Lowry AFB			Carswell AFB		
	Number of Observations	Slope of Regression Line	Correlation Coefficient	Number of Observations	Slope of Regression Line	Correlation Coefficient
0200	19	0.337	0.926	25	0.254	0.854
0800	19	0.486	0.973	25	0.338	0.920
1400	19	0.0443	0.152	25	0.215	0.653
2000	19	0.289	0.916	25	0.215	0.792

* The local times for the KIXL-FM propagation path are in CST; therefore, one hour should be added to the times listed to obtain local time on the KIXL-FM path.

In conclusion, then, the comparisons presented above indicate that the correlations of transmission loss with surface values of refractivity appear to be, in all respects examined, as reliable as the correlations with ΔN. The most obvious factor in favor of the surface observations is that they are available throughout the day and are therefore more applicable to studies involving the diurnal cycle of transmission loss.

Estimation of the Annual, Geographic, and Terrain Variances of 100 Mc Transmission Loss

For the purpose of this analysis it seems reasonable to assume that the departure of the observed transmission loss in decibels, L_{b0}, from the predicted value, L_{bp}, is composed of the following components:

$$L_{b0} - L_{bp} = A + G + T + E, \tag{1}$$

where

L_{b0} = the observed monthly median transmission loss
L_{bp} = the predicted value of transmission loss
A = a component due to the annual variations of the atmosphere
G = a component due to the geographic variations of the atmosphere
T = a component due to terrain effects
E = errors in observation.

The predicted value, L_{bp}, given on Fig. 5, (p. 1426) is derived from prediction curves presented in an unpublished version of reference three. It is the authors' understanding that the prediction curve plotted in Fig. 5 is based on assumptions similar to those presented in reference three. Since the newer prediction curves were not available to the authors at the time of writing, the older curve was necessarily employed in this study. However, the correlations presented in this paper will be of even more practical use to the radio engineer with a prediction method which has a smaller root-mean-square deviation of observed monthly median transmission loss from prediction. This will be discussed more fully in the next section. The authors have not seen a quantitative evaluation of such deviations for reference 3, but the more refined techniques of analysis used there would imply a more favorable root-mean-square value than in the prediction from Fig. 5. These prediction curves are designed to be applied on an all-year basis for any location in the United States, and consequently do not take into account geographic or annual variations of transmission loss due to the atmosphere.

Examining the individual terms of (1), we assume that each term is composed of a component attributable to ΔN and a component which is independent of ΔN. Accordingly, the terms on the right-hand side of (1) become:

$$A = A_s + A_r,$$
$$G = G_s + G_r,$$
$$T = T_s + T_r,$$

and

$$E = E_s + E_r,$$

where the subscript s denotes a component attributable to ΔN, while the subscript r denotes a component independent of ΔN. A_s and G_s are, by virtue of the observed regression of L_b and ΔN, linear functions of ΔN. How-

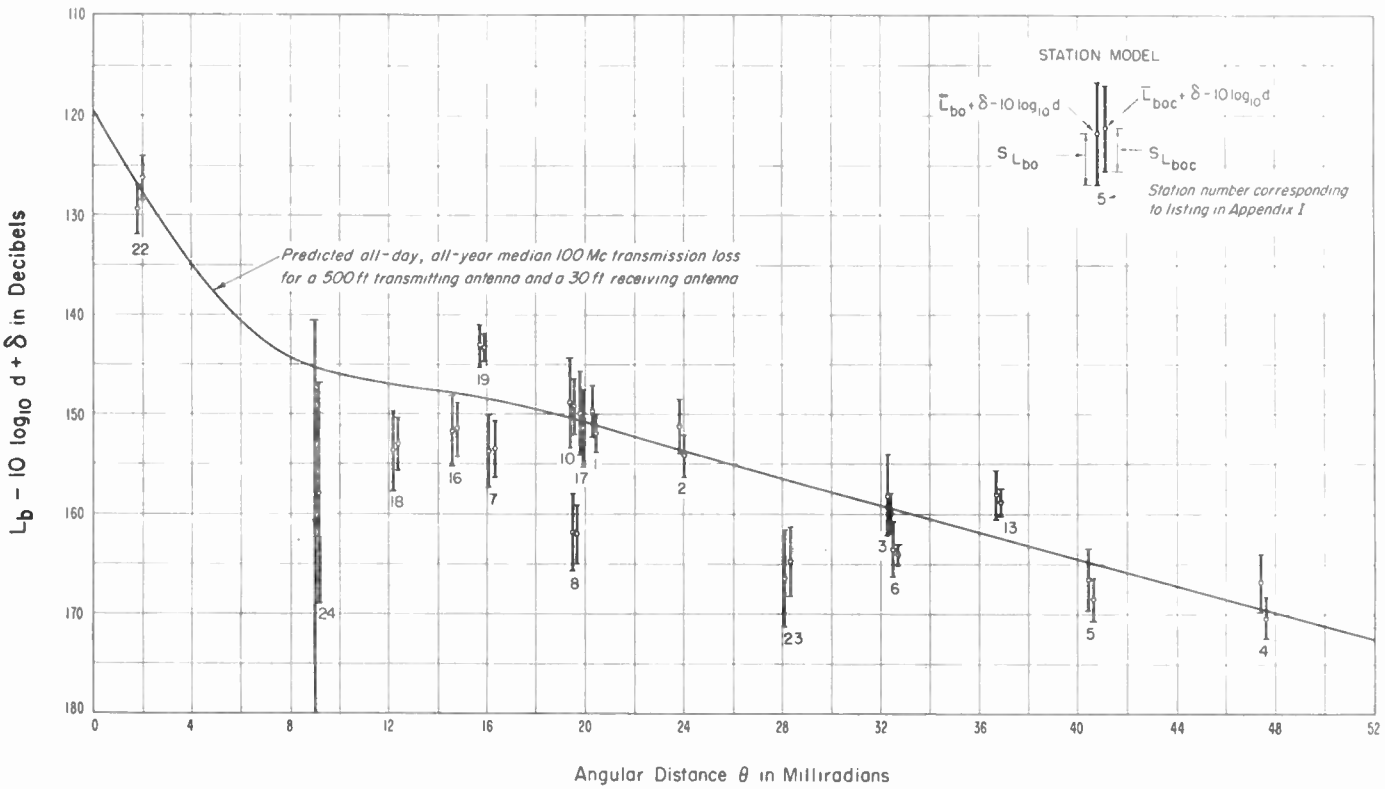

Fig. 5—Comparison of observed transmission loss, L_{bo}, and refractivity corrected transmission loss L_{boc}, to the predicted 100 mc median basic transmission loss where $L_{boc}=L_{bo}-b_\theta\,(\Delta N_A+44.65)$.

ever, T_s and E_s are assumed to be zero, and in the case of E_r we have two independent sources of error, namely observational errors at a station, E_{r1}, and observational errors between stations, E_{r2}. We may restate (1) as:

$$L_{b0}-L_{bp}=A_s+A_r+G_s+G_r+T_r+E_{r1}+E_{r2}. \quad (2)$$

The variance over the entire country and for a long period of time of the quantities, $L_{b0}-L_{bp}$, is given by:

$$\sigma^2(L_{b0}-L_{bp})=\sigma_{As}^2+\sigma_{Ar}^2+\sigma_{Gs}^2+\sigma_{Gr}^2+\sigma_{Tr}^2+\sigma_{Er1}^2+\sigma_{Er2}^2 +2(\rho_{AsGs}\sigma_{As}\sigma_{Gs}+\rho_{AsAr}\sigma_{As}\sigma_{Ar}+\cdots +\rho_{Er1Er2}\sigma_{Er1}\sigma_{Er2}), \quad (3)$$

where the ρ's are the pertinent correlation coefficients.

The terms in parentheses involve correlation between variables that are considered to be independent and the terms are therefore taken to be equal to zero.[12] Eq. (3) now reduces to:

$$\sigma^2(L_{b0}-L_{bp})=\sigma_{As}^2+\sigma_{Ar}^2+\sigma_{Gs}^2+\sigma_{Gr}^2+\sigma_{Tr}^2+\sigma_{Er1}^2+\sigma_{Er2}^2. \quad (4)$$

In order to evaluate the above variances, we must first consider how we may account for annual and geographic variations of observed transmission loss. Since changes in transmission loss appear to a first approximation to be linearly related to changes in ΔN, we may obtain the refractivity corrected transmission loss, L_{bpc}, for a particular month of the year and geographical area by adding to the predicted transmission loss, L_{bp}, a refractivity correction term:

$$L_{bpc}=L_{bp}+b(\Delta N+44.65), \quad (5)$$

where b is slope of regression line (db change per unit change of ΔN) for each propagation path. The term in parentheses is departure of monthly median value of ΔN from an average value, $\overline{\Delta N}=-44.65$, determined for all stations and all months of our sample

$$\left[\text{i.e., } \overline{\Delta N}=\frac{1}{k}\sum_{i=1}^{k}\overline{\Delta N_i}\right.$$

$$\left.\text{where the } i\text{th station has a mean of } \overline{\Delta N}_i\right].$$

The notation, L_{bpc}, will be used hereafter to designate that refractivity correction term has been added to predicted transmission loss. Conversely, L_{b0c}, shall indicate that correction term has been subtracted from observed monthly median transmission loss:

$$L_{b0c}=L_{b0}-b(\Delta N+44.65). \quad (6)$$

Consider now Fig. 5, where we have plotted the all-day, all-year predicted 100-mc transmission loss from reference 8. The ordinate of Fig. 5 is the predicted median basic transmission loss, L_{bp}, minus 10 $\log_{10}d$ where d is the propagation path distance in miles. This means that for a given value of θ there are different values of L_{bp} corresponding to different propagation path distances. Also plotted on Fig. 5 are $\bar{L}_{b0}+\delta-10\log_{10}d$, σ_{Lb0}, $\bar{L}_{b0c}+\delta-10\log_{10}d$, and σ_{Lb0c}, where δ is a constant which allows for the difference in the actual antenna

[12] The term $2\rho_{AsGs}\sigma_{As}\sigma_{Gs}$ is zero since the predictable geographic component, G_s, for each station is, by definition, the mean of the annual cycle.

heights on the particular path involved and the 500, 30-foot antenna heights assumed in the prediction curves.[8] The $\overline{L}_{b0}+\delta-10\log_{10}d$ data are plotted on the value of θ for each station while the $\overline{L}_{b0c}+\delta-10\log_{10}d$ data are displaced to the right of the actual θ for each station. We shall make use of Fig. 5 to illustrate the tack used in estimating the annual, geographic, and terrain variances. We note two things about the data plotted on Fig. 5: (a) The values of $\overline{L}_{b0c}+\delta-10\log_{10}d$ generally lie nearer the predicted value than do the values of $\overline{L}_{b0}+\delta-10\log_{10}d$, thus indicating an appreciable component of variance σ_{Gs}^2 due to predictable geographic variations; and (b) the values of σ_{Lb0c} are generally smaller than those of σ_{Lb0}, thereby indicating an appreciable component of variance σ_{As}^2 due to predictable annual variations.

It would be desirable to have a random sample of all possible propagation paths in the United States as a basis for predicting transmission loss variations. The actual data do not form such a sample. The following analysis of transmission loss variations into components attributable to identified sources is therefore strictly applicable only to the particular paths used and approximate country-wide values only in so far as these paths are representative of the country as a whole.

The prediction curve was adjusted to our sample mean ΔN of -44.65 from the country-wide mean of -42.25, using the sample mean slope of 0.52 db/ΔN to give a constant correction of $+1.17$ db.

Another deficiency of the data which affects the analysis and results is the variation in the number of months for which data are available from the various stations; in particular, the data are not available for all months of the same year or of a period of full years. (The shortest period is two months; the longest 28 months.) However, it seems least objectionable to base the estimates made below of σ_{As}^2, σ_{Gs}^2, and other between-station components of variance on equal weighting of stations.

The following analysis does not include the detailed, rather involved, derivation of the appropriate sample estimates for the component variances; the final formulas are given in Table V, while their derivation is in the hands of the authors.

TABLE V

EVALUATION OF THE COMPONENT VARIANCES OF (4)

Row	Population Variance	Estimated By	Value
1	$\sigma_\epsilon^2=\sigma_{Ar}^2+\sigma_{Er_1}^2$	$s_\epsilon^2=\dfrac{1}{\sum_{i=1}^{k}(n_i-2)}\sum_{i=1}^{k}(n_i-1)(s_{Yi}^2-b_i^2s_{\Delta Ni}^2)$ where $s_{Yi}^2=\dfrac{1}{n_i-1}\sum_{i=1}^{ni}(Y_{ij}-\overline{Y}_i)^2$, $s_{\Delta Ni}^2=\dfrac{1}{n_i-1}\sum_{j=1}^{ni}(\Delta N_{ij}-\overline{\Delta N_i})^2$	(2.80 db)²
2	σ_{As}^2	$s_{As}^2=\dfrac{1}{k}\sum_{i=1}^{k}\dfrac{n_i-1}{n_i}b_i^2s_{\Delta Ni}^2-s_\epsilon^2\dfrac{1}{k}\sum_{i=1}^{k}\dfrac{1}{n_i}$	(3.91 db)²
3	σ_{Gs}^2	$s_{Gs}^2=\dfrac{1}{k}\sum_{i=1}^{k}b_i^2(\overline{\Delta N_i}-\overline{\Delta N})^2-\dfrac{1}{k}s_\epsilon^2\sum_{i=1}^{k}\dfrac{(\overline{\Delta N_i}-\overline{\Delta N})^2}{(n_i-1)s_{\Delta Ni}^2}$	(1.96 db)²
4	$\sigma_\lambda^2=\sigma_{Gr}^2+\sigma_{Tr}^2+\sigma_{Er2}^2$	$s_\lambda^2=\dfrac{1}{k}\sum_{i=1}^{k}(\overline{Y}_i-\overline{Y})^2-s_\epsilon^2\dfrac{k-1}{k^2}\sum_{i=1}^{k}\dfrac{1}{n_i}-s_{Gs}^2$ where $\overline{Y}=\dfrac{1}{k}\sum_{i=1}^{k}\overline{Y}_i=\dfrac{1}{k}\sum_{i=1}^{k}\dfrac{1}{n_i}\sum_{i=1}^{ni}Y_{ij}$	(5.25 db)²
5	σ_{Er1}^2	Assumed	(1 db)²
6	σ_{Er2}^2	Assumed	(2 db)²
7	σ_{Ar}^2	$s_{Ar}^2=s_\epsilon^2-\sigma_{Er1}^2$	(2.61 db)²
8	σ_{Gr}^2	$s_{Gr}^2=\dfrac{s_{Ar}^2}{s_{As}^2}s_{Gs}^2$	(1.31 db)²
9	σ_{Tr}^2	$s_{Tr}^2=s_\lambda^2-s_{Gr}^2-\sigma_{Er2}^2$	(4.68 db)²
10	σ_Y^2	$s_Y^2=s_\lambda^2+s_{Gs}^2+s_{As}^2+s_\epsilon^2$	(7.39 db)²

There are seven components of variance in (4), assumed independent, but, from the data on L_b, alone, we can estimate only two independent components or groups of components because there are only two classifications of the data—between stations, and within stations. From the first classification we can estimate $\sigma_{Gs}^2+\sigma_{Gr}^2+\sigma_{Tr}^2+\sigma_{Er2}^2$, and from the second we can estimate $\sigma_{As}^2+\sigma_{Ar}^2+\sigma_{Er1}^2$. However, there are also data on the correlated variable ΔN, which enables us to estimate σ_{Gs}^2 and σ_{As}^2.

We may write an alternative expression for (2) for a particular propagation path i, and during a particular month j, based on the regression equation of L_b on ΔN:

$$Y_{ij} \equiv L_{b0ij} - L_{bpi} = \alpha_i + \beta_i \Delta N_{ij} + e_{ij}$$
$$i = 1, 2, \cdots, k; \quad j = 1, 2, \cdots, n_i, \tag{7}$$

where the subscripts refer to the jth month of data on the ith propagation path, α_i and β_i are the intercept and slope of the population regression line for the ith propagation path, and e_{ij} represents the month-to-month random variations at the ith station. In the calculations we will approximate α_i and β_i with the values a_i and b_i calculated from the sample data.

Eq. (6) may be rewritten as:

$$Y_{ij}=\alpha_i+\beta_i\overline{\Delta N}+\beta_i(\overline{\Delta N}_i-\overline{\Delta N})+\beta_i(\Delta N_{ij}-\overline{\Delta N}_i)+e_{ij}, \tag{8}$$

where the quantity ΔN is the mean value over all stations, all stations being weighted equally, and is equal to -44.65, $\overline{\Delta N}_i$ is determined by

$$\overline{\Delta N}_i = \frac{1}{n_i}\sum_{j=1}^{n_i} \Delta N_{ij} \tag{9}$$

and

$$\alpha_i + \beta_i\overline{\Delta N} = G_{ri} + T_{ri} + E_{r2}, \tag{10}$$

$$\beta_i(\overline{\Delta N}_i - \overline{\Delta N}) = G_{si}, \tag{11}$$

$$\beta_i(\Delta N_{ij} - \overline{\Delta N}_i) = A_{sij} \tag{12}$$

$$e_{ij} = A_{rij} + E_{r1ij}. \tag{13}$$

Returning to the evaluation of the components of variance of (4) but referring to the formulation (8), we can evaluate from the data the four terms on the right of the equation

$$\sigma_Y^2 = \sigma_\lambda^2 + \sigma_{Gs}^2 + \sigma_{As}^2 + \sigma_e^2, \tag{14}$$

where for any station i, $\lambda_i=\alpha_i+\beta_i\Delta N$, and

$$\sigma_\lambda^2 = \sigma_{Gr}^2 + \sigma_{Tr}^2 + \sigma_{Er2}^2, \quad \sigma_e^2 = \sigma_{Ar}^2 + \sigma_{Er1}^2. \tag{15}$$

The values to be obtained for the right-hand terms of (14) will be denoted by s_λ^2, s_{Gs}^2, s_{As}^2, and s_e^2 because they are estimates from sample data of the corresponding population parameters and are subject to considerable error due to sampling fluctuations, aside from difficulties in the assumed mathematical model. Likewise other derived estimates which follow are designated by s^2 rather than σ^2 since they depend indirectly on sample data. By assuming the values of σ_{Er1}^2 and σ_{Er2}^2 we may find an estimate s_{Ar}^2 of σ_{Ar}^2 and of the combination $s_{Gr}^2+s_{Tr}^2$ from (15). By further assuming that

$$\frac{\sigma_{Gr}}{\sigma_{Gs}} = \frac{\sigma_{Ar}}{\sigma_{As}} \tag{16}$$

we can evaluate s_{Gr}^2 as

$$s_{Gr}^2 = \frac{s_{Ar}^2}{s_{As}^2} s_{Gs}^2. \tag{17}$$

Then

$$s_T^2 = s_\lambda^2 - s_{Gr}^2 - \sigma_{Er2}^2. \tag{18}$$

With this general outline we shall pass on to Table V where the specific equations for the four estimates of the variance components in (14) and the calculated or assumed values for all of the components are given. It may be noted that both s_{As}^2 and s_{Gs}^2 have correction terms involving s_e^2 to account for the effect of sampling fluctuations in the station values of b_i; these correction terms are relatively small.

The values assumed for σ_{Er1}^2 and σ_{Er2}^2 seem reasonable in the light of present radio recording equipment and techniques.

The propagation paths used in this section are those for which the prediction curves are strictly applicable, i.e., propagation paths that are either entirely within the radio horizon of the transmitter (paths 20 and 21) or subject to knife-edge diffraction (paths 12, 14, 15, 19, and 22) have been omitted.

If any of the cross-product terms in (3) are not zero, then our estimate of the terrain variance would contain the added terms and our value of (4.68 db)² would be incorrect, either too large or too small depending on the signs of the correlation coefficients in (3).

The many numerical assumptions of our analysis and the possible inapplicability of our assumed statistical model render the results of this section quite tentative. In addition it is difficult to determine the probable errors associated with each of the estimated variances. The results are, therefore, presented as no more than a possible representation of the component variances of transmission loss.

The Use of the Refractivity Gradient to Improve the VHF Prediction Process

The useful application of the observed regression lines of transmission loss of ΔN for improving the National Bureau of Standards vhf prediction process is limited by one outstanding factor: the variance of the observed values of transmission loss from predicted, $s_Y^2=(7.39\text{ db})^2$, is large with respect to the total effect of ΔN, $s_{As}^2+s_{Gs}^2=(4.49\text{ db})^2$. This is presumably due to the terrain effects, $s_{Tr}^2=(4.68\text{ db})^2$, possibly attributable to knife-edge diffraction as well as other effects that are not sufficiently well understood to be included in the prediction curves at the present time.

The fact that the geographical variance due to ΔN is small may be explained by considering the geographical distribution of our sources of transmission loss (Fig. 1) as used in the analysis of variance. With the exception of the Cheyenne Mountain data, which constitute less than 4 per cent of our sample, the data are distributed about a line running roughly from Austin, Tex., to Albany, N. Y. By considering the climatic maps of ΔN (Figs. 6 through 9, pp. 1430–1431) we see that our transmission loss data are distributed along rather than across the contours of ΔN. Consequently, we would expect the geographic variation of our sample to be smaller than if our sample had been distributed more evenly across the United States.

If the prediction process were perfect, that is, if the long-term station means of L_{b0} were identical with the predicted values, then we could expect a reduction in the variance of L_{b0}, through knowledge of the monthly values of ΔN, by a factor of $(1-r^2)$ or about 52 per cent rather than the 35 per cent reduction

$$\left(\frac{s_{A_s}^2 + s_{G_s}^2}{s_Y^2}\right)$$

of the previous section. However, the present correlations between L_{b0} and ΔN will become more useful as new methods are devised for reducing the variance of mean transmission loss from the predicted value.

However, if the engineer has either estimated from the prediction curve or measured a monthly mean level of transmission loss then he may use the slope of the adjusted curve, b_θ, from Fig. 4 and the six-year average values of ΔN, ΔN_A, obtained from Figs. 6 through 9, to estimate his expected value of transmission loss, L_{be}, from the expression

$$L_{be} = L_{bp} + b_\theta(\Delta N_A + 42.25), \qquad (19)$$

where the value of 42.25 was estimated as the average ΔN for the United States, determined from the climatic data presented in Figs. 6–9.

The usefulness of (19) to the engineer is dependent upon the degree to which ΔN_A is correlated with the month-to-month variations of L_{b0}. The correlations between these variables have been investigated and are presented in Table VI.

These correlation coefficients are surprisingly high considering that the ΔN data are six-year averages and the L_{b0} data are for individual months generally not in the six-year period. One can infer from these correlation coefficients that the year to year variations of L_b and ΔN for any given month are relatively small compared to the within year variation. The value of b_θ obtained from Fig. 4 will not be significantly different from what one would have obtained using the slopes derived from the six-year averages, ΔN_A, rather than the individual monthly values.

The use of this equation would of course not account for all variation in L_{b0} due to ΔN even if the parameters of the equation were determined without error, since the future monthly median values of ΔN and L_{b0} will deviate randomly from ΔN_A and the corresponding value of L_{be} given by the above equation.

The present study was made for frequencies around 100 mc. Although one might not expect such a study to be particularly useful at higher frequencies, preliminary investigation has shown correlations of the same magnitude as above, even at 1,000 mc, in some cases. In order to improve the correlations at these higher frequencies, it may be necessary to use a more complex presentation of the refractivity profile. Some improvement in the correlation at these higher frequencies might be obtained simply by using a smaller height increment above the ground in determining ΔN.

TABLE VI

CORRELATION COEFFICIENTS OF L_{be} VS ΔN_A

Station Number	$r_{L_{be}\Delta N_A}$
1	0.613
2	0.607
3	0.867
4	0.800
5	0.784
6	0.927
7	0.639
8	0.776
9	0.617
10	0.646
11	0.592
12	0.790
13	0.841
14	0.870
15	0.214
16	0.644
17	0.377
18	0.740
19	0.741
20	0.278
21	0.336
22	0.500
23	0.771
24	0.960
25	0.681

ACKNOWLEDGMENT

The authors would like to acknowledge the assistance of W. V. Mansfield and R. L. Abbott for aiding in the rather laborious calculations involved in this study. Particular acknowledgment should be given K. A. Norton, whose suggestions pertinent to the analysis of variance have considerably broadened the original conclusions of the paper, and E. L. Crow for his careful and critical appraisal of the analysis and manuscript.

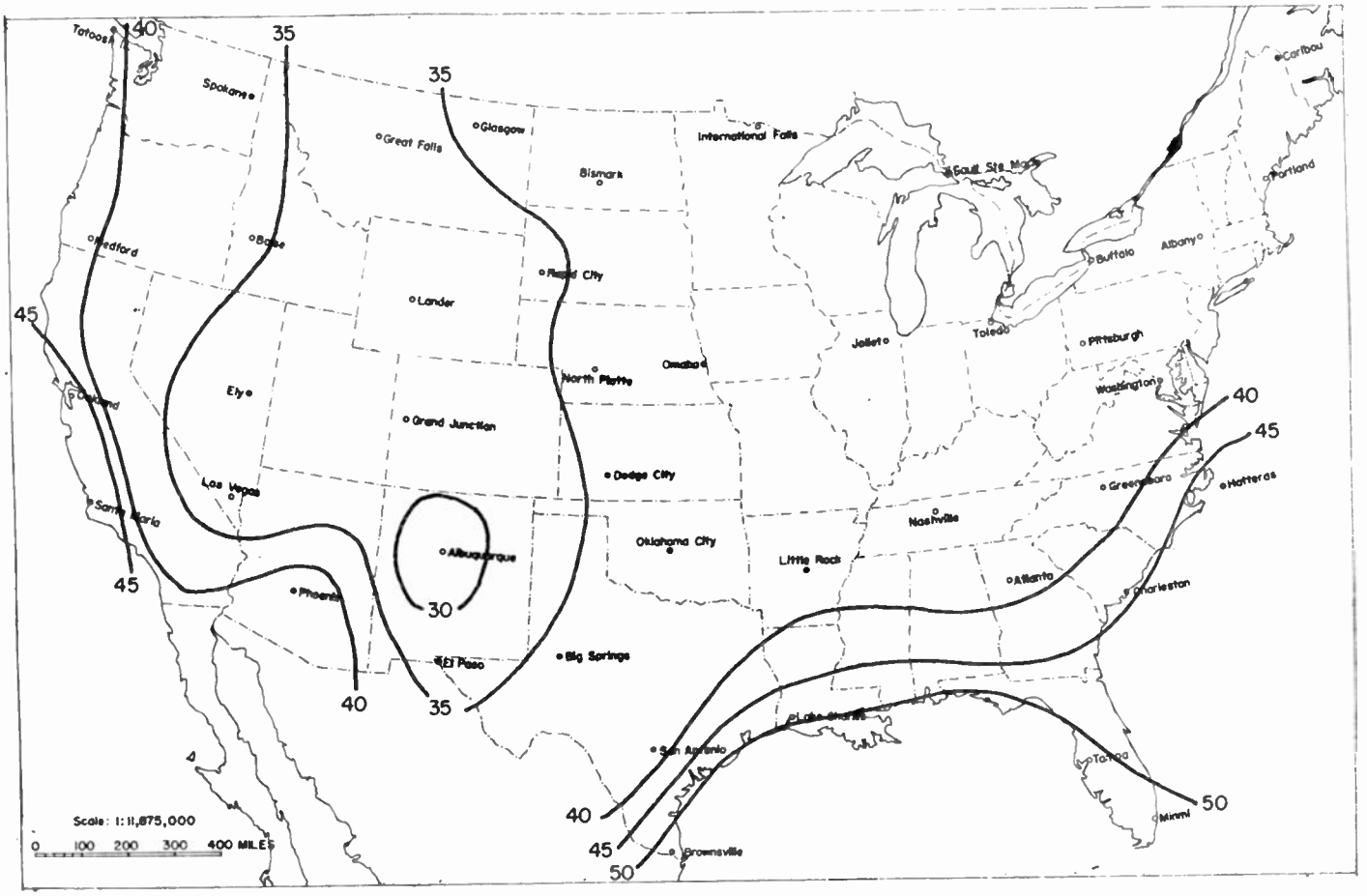

Fig. 6—Six-year average of monthly median values of $-\Delta N$ taken from the surface to one kilometer above the surface in February (0300 GMT–2200 EST).

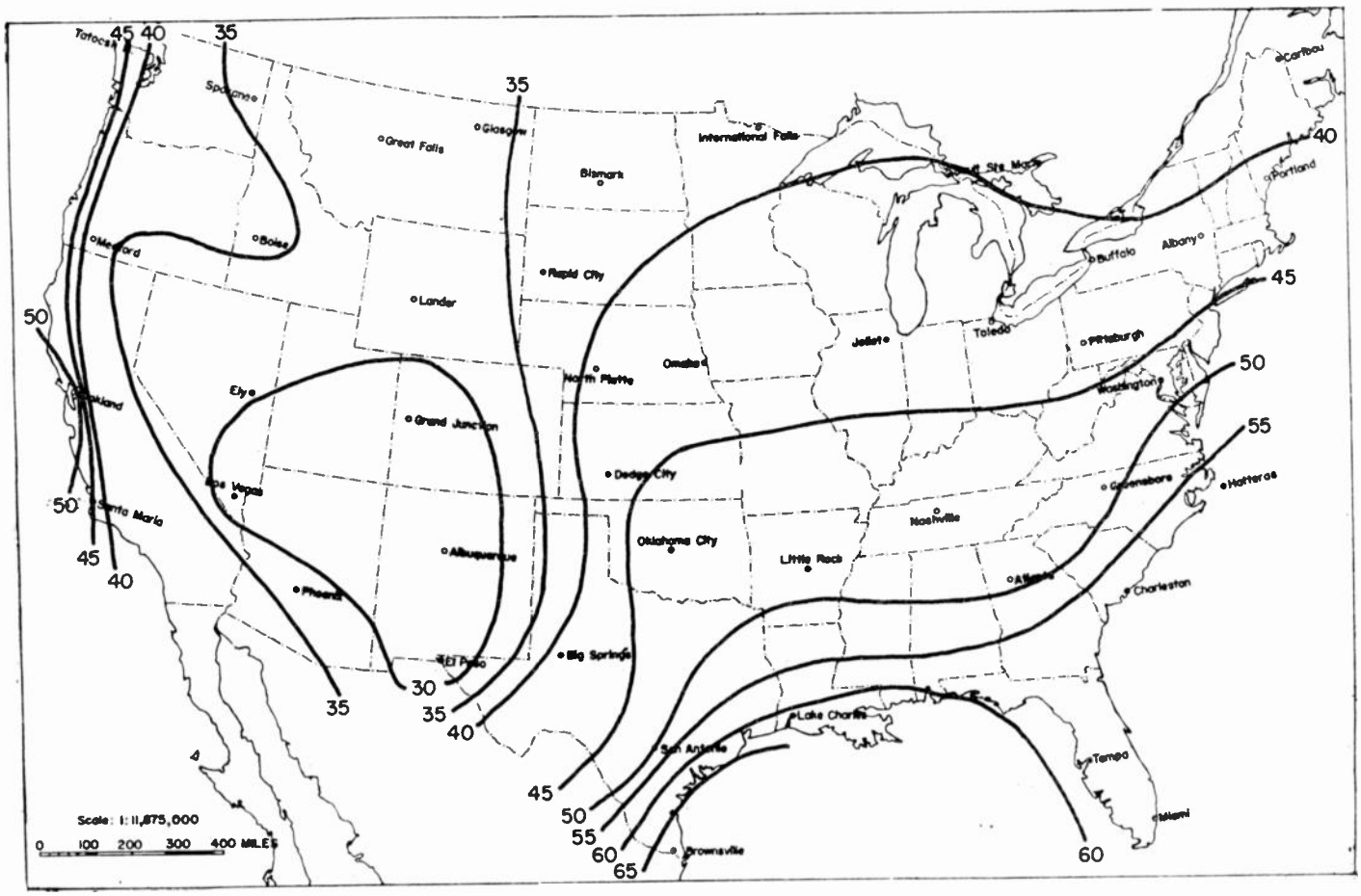

Fig. 7—Six-year average of monthly median values of $-\Delta N$ taken from the surface to one kilometer above the surface in May (0300 GMT–2200 EST).

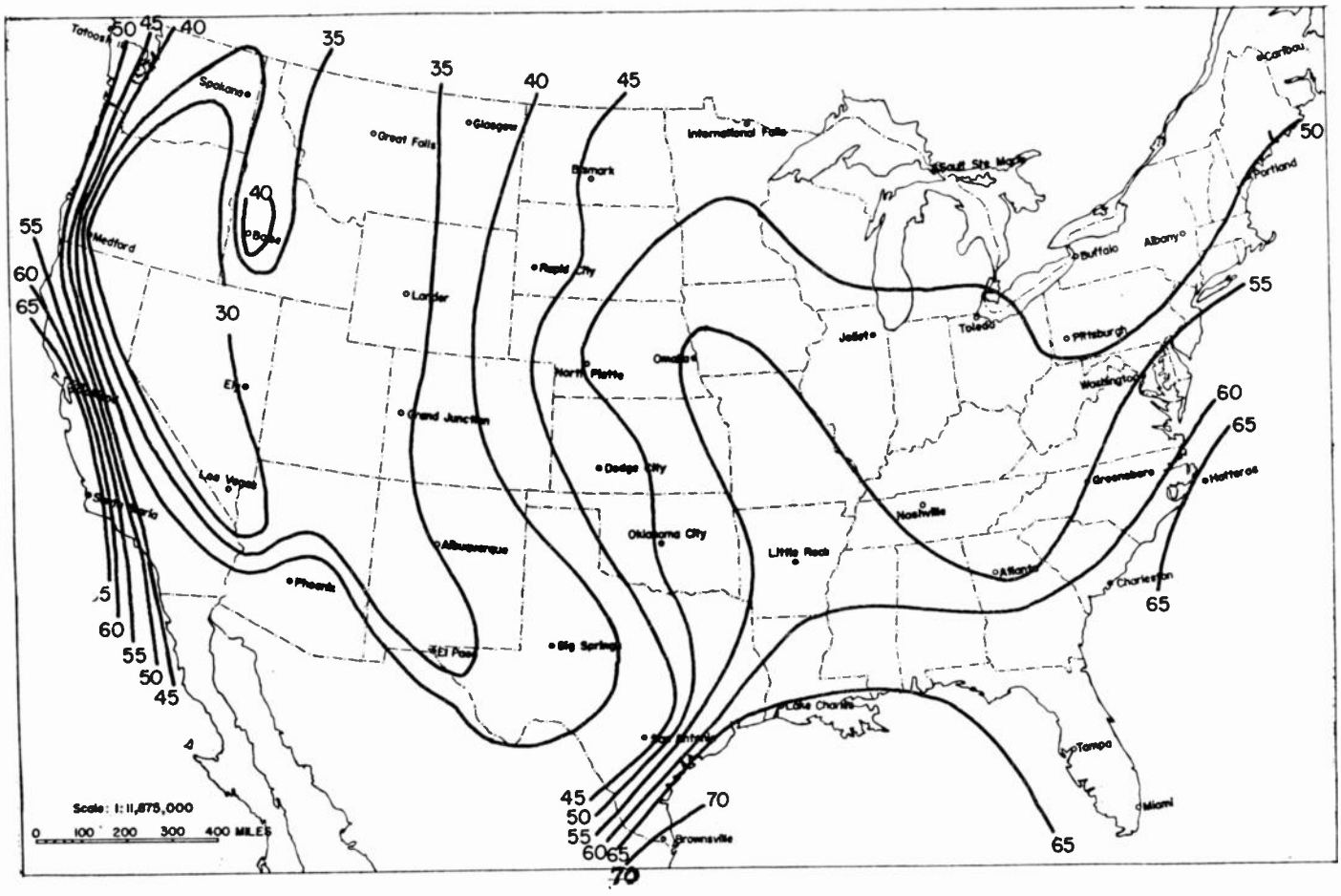

Fig. 8—Six-year average of monthly median values of $-\Delta N$ taken from the surface to one kilometer above the surface in August (0300 GMT–2200 EST).

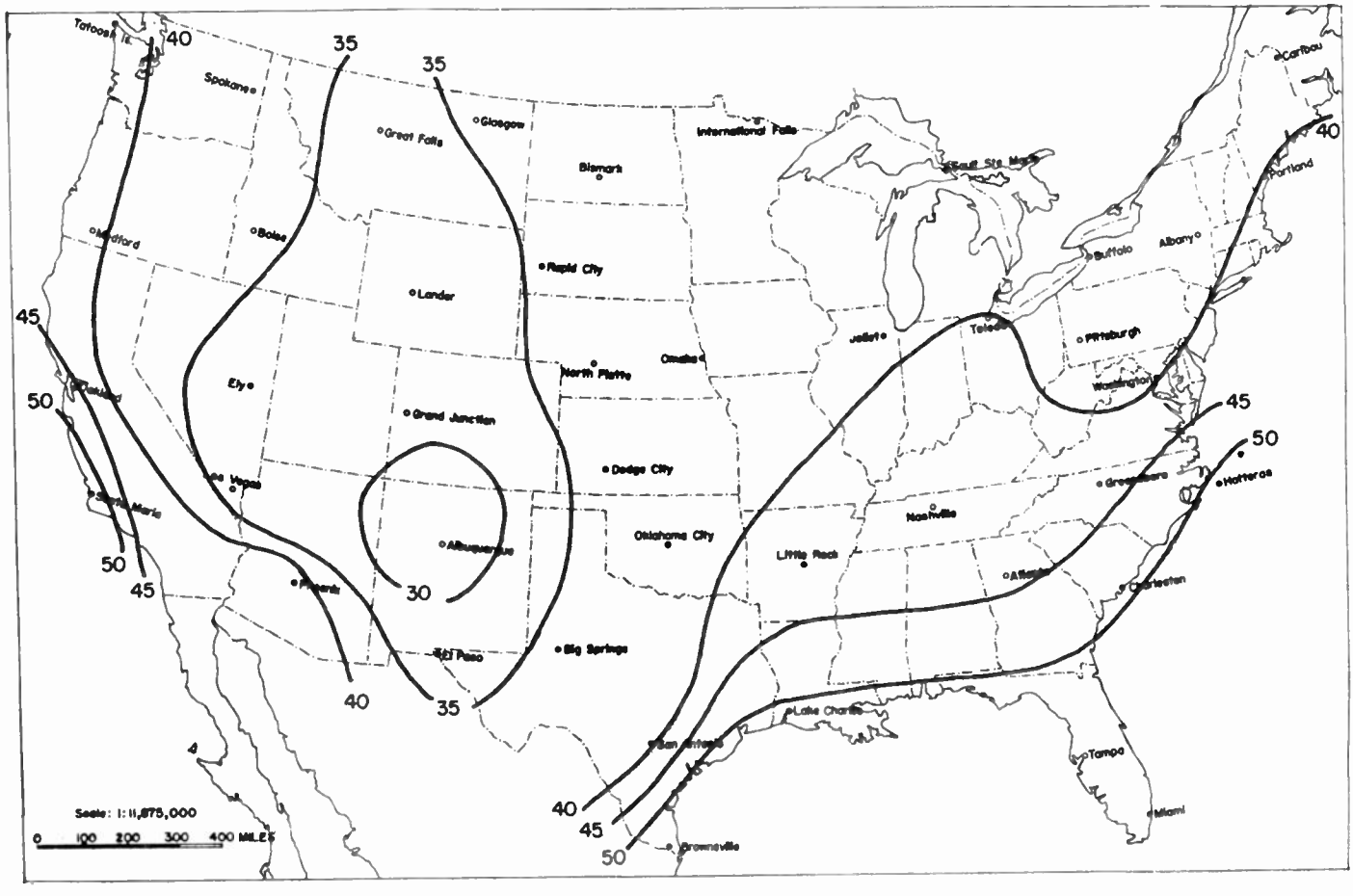

Fig. 9—Six-year average of monthly median values of $-\Delta N$ taken from the surface to one kilometer above the surface in November (0300 GMT–2200 EST).

Some Fading Characteristics of Regular VHF Ionospheric Propagation*

G. R. SUGAR†, MEMBER, IRE

Summary—Some short-term fading characteristics of a type of ionospheric propagation first described by Bailey, *et al.*[1] are presented and discussed. Continuous wave transmissions from Cedar Rapids, Iowa, on 49.8 mc were received at Sterling, Virginia, on either rhombic or Yagi antennas directed toward the transmitter. The second detector output of a linear receiver was used to provide a voltage proportional to the envelope of the received signal. This fluctuating voltage was recorded, edited, and then analyzed to determine the probability distribution and autocorrelation function of the signal envelope. The correlation of the envelopes of signals received on spaced antennas was similarly determined for antennas spaced both normal and parallel to the transmission path.

Introduction

EARLY IN 1951 a new type of weak regular ionospheric radio propagation was observed at the National Bureau of Standards when continuous wave 49.8 megacycle transmissions from Cedar Rapids, Iowa, were received at Sterling, Virginia. These transmissions, over a distance of 1,243 kilometers, were unusual in that the frequency used was much higher than those usually reflected by the ionosphere and that the diurnal variation of the received voltage was small relative to that of signals received by conventional high-frequency ionospheric propagation. An announcement of the discovery of this type of propagation and a description of some of its significant characteristics has already been published by Bailey *et al.*[1]

It is the purpose of this paper to present the results of further investigations of some of the short-time fading characteristics of signals propagated in the above manner. These results are of interest since they may be useful in relating the observed propagation characteristics to the various propagation mechanisms which have been proposed. This paper, however, is intended to be a description of experiments and observations and not a proposal of a propagation mechanism.

The body of the paper is divided into six sections. In the first section the experimental facilities are briefly described, and in the second section some general characteristics of the received signals are discussed. The third and fourth sections give the details and results of measurements of signal envelope probability distributions and autocorrelation functions. The fifth section describes measurements of the correlation of signals received on spaced antennas. In the sixth section the validity of the experimental results is briefly discussed.

* Original manuscript received by the IRE, July 11, 1955.

† National Bureau of Standards, Washington 25, D. C.

[1] D. K. Bailey, R. Bateman, L. V. Berkner, H. G. Booker, G. F. Montgomery, E. M. Purcell, W. W. Salisbury, and J. B. Wiesner, "A new kind of radio propagation at very high frequencies observable over long distances," *Phys. Rev.*, vol. 86, pp. 141–145; April, 1952.

Experimental Facilities

Continuous-wave 49.8 megacycle transmissions from Cedar Rapids were directed toward the ionospheric region 100 kilometers above the ground midpoint of the Cedar Rapids—Sterling great circle path. The transmitter power output was approximately 30 kilowatts and the transmitting antenna was a horizontal rhombic antenna with a nominal plane-wave power gain of 60 relative to a half-wave dipole at the same height above ground. The half-power beam widths of the main lobe were 6 degrees in the horizontal plane and 5 degrees in the vertical plane.

The transmissions were received at Sterling either with a similar rhombic antenna or with one or more horizontal Yagi antennas directed toward the same ionospheric region as the transmitting antenna. The Yagi antennas had a nominal plane-wave power gain of 7.6 relative to a half-wave dipole at the same height above ground. The corresponding main-lobe half-power beam widths were 65 degrees and 6.5 degrees in the horizontal and vertical planes respectively.

The second detector outputs of linear receivers were used to provide voltages proportional to the envelopes of the received signals. These fluctuating voltages were recorded using either a direct writing oscillograph or a magnetic-tape data recorder. The nominal receiver bandwidths were 3 kilocycles and both recording instruments had a voltage vs frequency response approximately constant from dc to 100 cps. The data were recorded in ten minute samples and after editing were analyzed to determine the signal envelope characteristics.

Description of Received Signals

The received voltage can be considered to consist of the sum of two independent components, a signal voltage and a noise voltage. The signal voltage may be further separated into the sum of two components, received voltages which result directly from the scattering of transmitted energy by columns of meteoric ionization and a received voltage which appears to be independent of transient meteoric phenomena. The relative proportions of these two signal components vary with time and it is not always possible to distinguish between them. The meteor-independent or "persistent" component is the one which appears to be of ionospheric origin and is the component discussed in this paper. The noise, that part of the received voltage which is independent of the transmitted carrier, is important since it may mask weak signal voltages. Extraneous

phenomena, such as sporadic-*E* propagation, may also mask the desired signal, and data taken when they were present has been rejected.

Before proceeding to the discussion of the short-time fading characteristics it is useful to examine the diurnal variation of the received signal. Fig. 1[1] shows the monthly

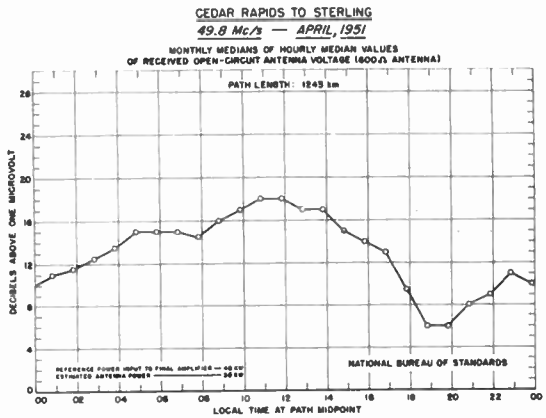

Fig. 1—Median received signal, April, 1951.

medians of the hourly median received signal for April, 1951. The significant diurnal characteristics shown here are the noon maximum, the secondary maximum at 0600 and the minimum near 1900. As indicated by Bailey this typical daily variation of received signal can be synthesized as the sum of two components, a solar term and a meteoric term, which vary as shown in Fig. 2. The solar influence would produce the midday maximum and the meteoric term would account for

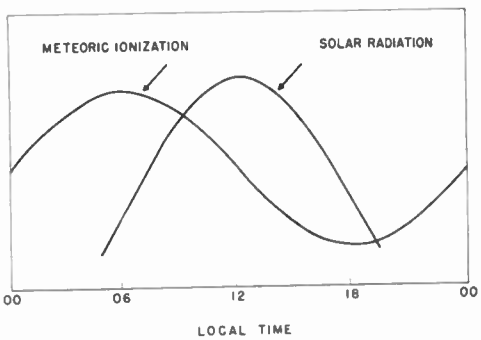

Fig. 2—Diurnal variation of solar radiation and meteoric ionization.

the early morning secondary maximum and evening minimum. This signal synthesis suggests that four times of day should be considered in examining data for diurnal variations, the above three times, and midnight, the time of minimum solar influence.

Oscillograms of the received signal envelope, appear in Figs. 3 and 4, and Figs. 5 and 6 (next page). In each the ordinate scale indicates received open-circuit antenna voltage in microvolts. Fig. 3 shows signal at 1230, a time when the persistent component is large relative to the meteoric component. The only indications of meteoric activity are the occasional slight irregularities superposed on the slow fluctuation of the persistent component. Fig. 4 was made at 2030 when the persistent component was weak but also when the meteoric activity was low. Here the large sudden enhancement of the signal by meteoric ionization is clearly visible in the first and third lines and smaller meteoric effects are also visible. It should be observed here that the signal, though weak, is greater than the noise level throughout most of the interval. The increased width of the trace here is an indication of a lower signal to noise ratio than in the previous oscillogram. In Fig. 5, made at 0030, the meteoric activity has increased and it now becomes difficult to separate the persistent and meteoric components. The same situation prevails in Fig. 6, made at 0530. In both of these, however, there are parts of the data which appear to have characteristics similar to those seen in the 1230 data (Fig. 3). In the editing it is these parts which are assumed to represent the persistent component. They would be analyzed and the remainder of the data would be rejected. The amount of data rejected per ten-minute sample varied from 1 per cent to 80 per cent with an average of 23 per cent rejected.

The Envelope Probability Distribution

The data were analyzed after editing by scaling from oscillograms the envelope voltages at one-second intervals. For each of four times of day, several ten-minute samples were scaled separately and the tabulated values combined when it appeared that the mean value of the signal had not changed significantly from one sample to the next. The probability distributions of the four sets of data are shown in Figs. 7 and 8 (next page).

Each probability distribution is shown in three ways. The histogram on the left indicates the distribution of the data. The points on the center and right graphs show the cumulative distribution of the data and are plotted on co-ordinates such that Gaussian and Rayleigh distributions would be straight lines on the center and right graphs respectively. In the center graph the straight line indicates the Gaussian distribution having the same mean and standard deviation as the experimental data. In the right graph the straight line indicates the Rayleigh distribution having the same median as the experimental data.

In each of the four cases shown it appears that the data is better represented by the Rayleigh distribution than by the Gaussian distribution. Other data, not presented here, tends to favor the use of the Rayleigh distribution. For example, in other observations the normalized standard deviation of the signal envelope approaches the constant value expected for a Rayleigh distribution.

The Envelope Autocorrelation Function

The second characteristic to be discussed is the autocorrelation function of the signal envelope. If $R(t)$ represents the signal envelope as a function of time then the

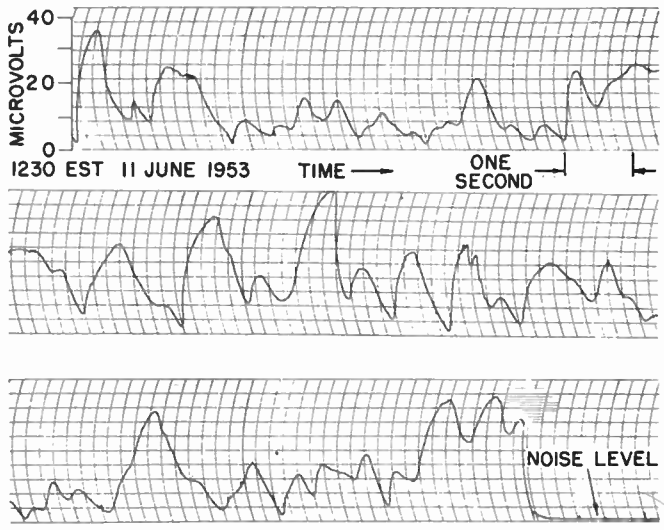

Fig. 3—Oscillogram of signal envelope; 1230 EST, June 11, 1953.

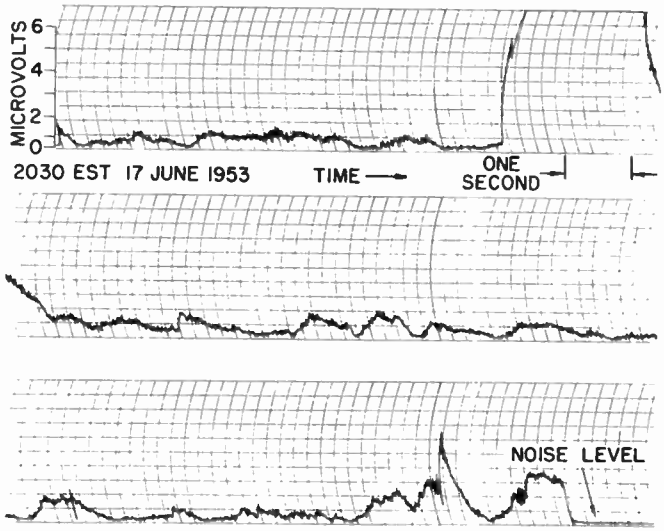

Fig. 4—Oscillogram of signal envelope; 2030 EST, June 17, 1953.

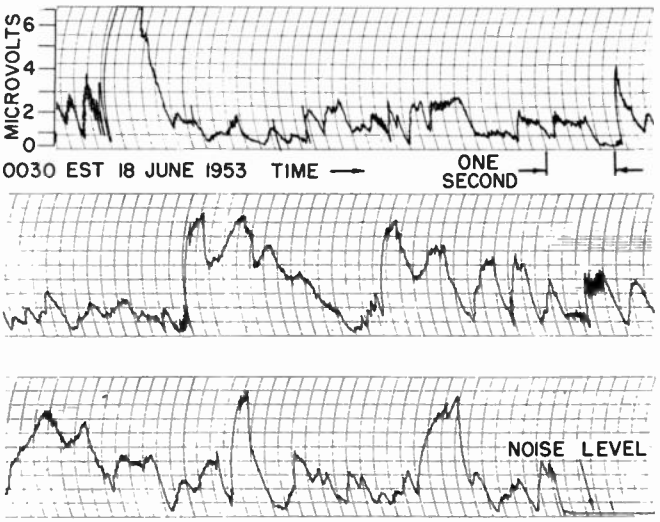

Fig. 5—Oscillogram of signal envelope; 0030 EST, June 18, 1953.

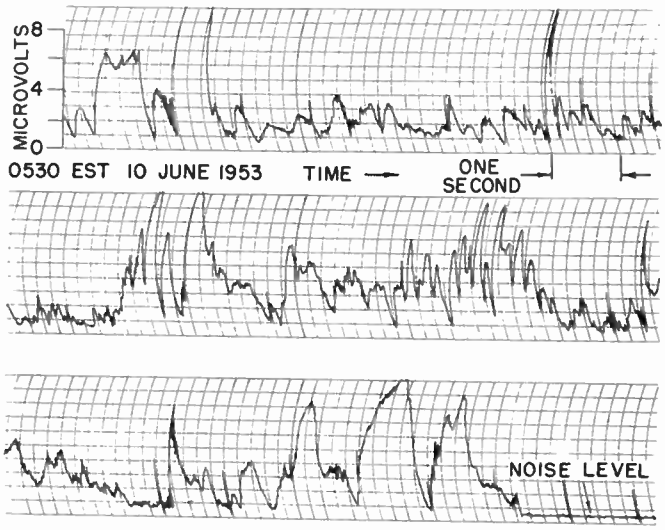

Fig. 6—Oscillogram of signal envelope; 0530 EST, June 10, 1953.

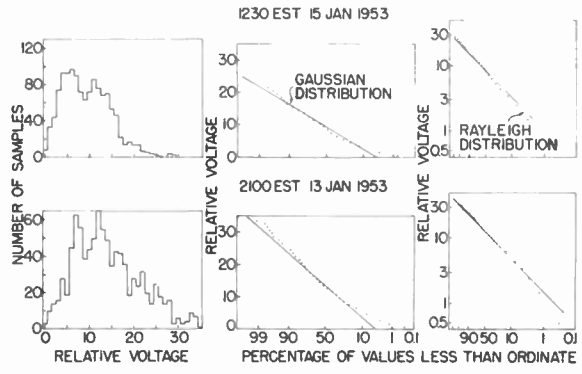

Fig. 7—Probability distributions of envelope of persistent component; 1230 EST, January 15, 1953, and 2100 EST, January 13, 1953.

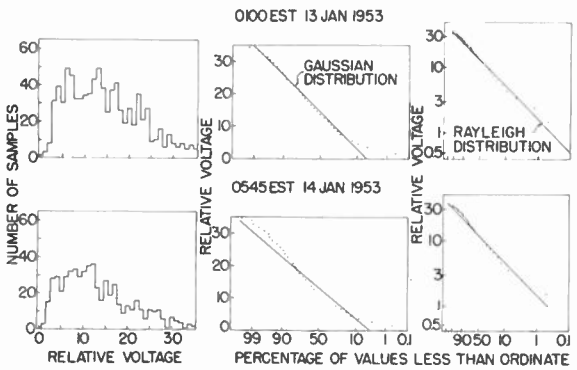

Fig. 8—Probability distributions of envelope of persistent component; 0100 EST, January 13, 1953 and 0545 EST, January 14, 1953.

autocorrelation function $\phi(\tau)$ can be defined as

$$\phi(\tau) = \frac{\langle R(t) \cdot R(t+\tau) \rangle - \langle R(t) \rangle^2}{\langle R(t)^2 \rangle - \langle R(t) \rangle^2}.$$

where $\langle R(t) \rangle$ indicates the average value of $R(t)$ for a given data sample.

When defined in this manner $\phi(\tau)$ is just the coefficient of correlation between pairs of signal envelope samples spaced a time τ apart and is thus an indication of the rate of signal fading. The power spectrum of the signal envelope is related to the autocorrelation function through a Fourier transformation and thus, in principle,

the power spectrum can be computed from the autocorrelation function.

Autocorrelations were determined for several 10-minute data samples obtained at each of four times of day. These were obtained by electronic analog computation from the edited data recorded on magnetic tape. The median autocorrelations of the samples are shown in Fig. 9. The differences between the autocorrelations of two independent 10-minute samples taken simultaneously were sometimes as great as the maximum differences between the curves of Fig. 9.

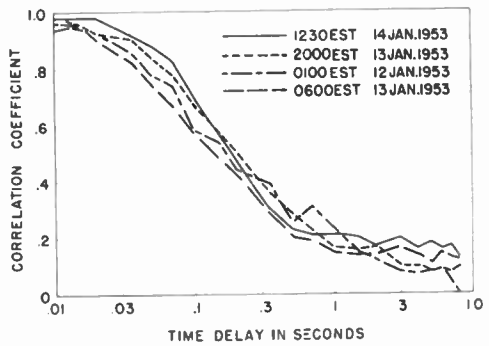

Fig. 9—Autocorrelation functions of envelope of persistent component.

An attempt was made to fit various one-parameter functions to the median observed autocorrelation. The best fit was obtained with the function

$$\phi(\tau) = \frac{1}{1 + 5|\tau|},$$

shown in Fig. 10(a). The power spectrum associated with this function is shown in Fig. 10(b). This spectrum is likely to be a poor representation of the experimental data in the region below one cycle per second. In the region above one cycle per second, however, it is considered likely to be a satisfactory representation of the envelope power spectrum. Here it shows that the most probable fading rate is below a few cycles per second. This result is consistent with the data shown in the oscillogram in Fig. 3.

The Space Correlation Function

The coefficient of correlation between the envelopes of signals received on spaced antennas was determined in the following manner. Three Yagi antennas were arranged at the vertices of a right triangle with one leg along the Cedar Rapids—Sterling great circle. The envelopes of the signals received on each of the three antennas were recorded simultaneously. These recorded voltages were later compared in pairs to obtain the desired correlation coefficients. After recording for 10 minutes at one pair of antenna spacings the antennas were moved and data taken for another pair of spacings. The total time required to obtain data for six pairs of spacings was approximately 90 minutes.

Measurements were made at many times of day during several days in January and April, 1953. The six pairs of antenna spacings used most frequently were from 1.25λ across the path and 2.5λ along the path to 6.25λ across the path and 20λ along the path, where λ is the wavelength. Occasional measurements were made at 6.25λ across the path and 30λ or 40λ along the path. Spacings of 28.2λ, 40λ, and 68.2λ along the path were

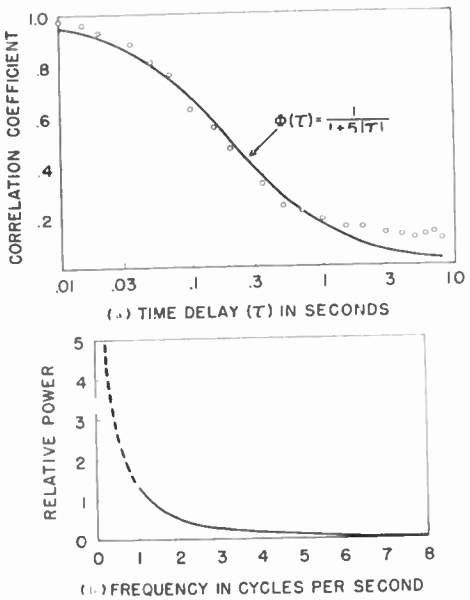

Fig. 10—(*Top*) Autocorrelation function empirically fitted to medians of observed values, (*Bottom*) Power spectrum computed for $\phi(\tau) = 1/(1+5|\tau|)$.

used one day at a time when unusually strong noontime signals were being received. The accuracy of the analysis was such that an error of ±0.1 in the correlation coefficient might occur as a result of errors in the analog computation process. The variations between successive measurements at the same antenna spacing were usually relatively large and no diurnal trend could be detected. The data are therefore presented in Fig. 11 (next page) with the medians of all observations indicated. Each point represents the correlation coefficient determined from a ten-minute data sample. The number of measurements at a given distance varied from 2 to 24. It is seen that the envelope correlation coefficient falls to 0.5 at 3.5 wavelengths antenna spacing for separations normal to the transmission path and at 40 wavelengths antenna spacing for separations along the transmission path.

Discussion

The experimental results may be summarized as follows. We assume that there are two propagation mechanisms, one the direct scattering of transmitted energy by columns of meteoric ionization, and a second mechanism, not directly related to the first, producing the persistent component of signal. The recorded data are

edited to remove all obvious occurrences of the first kind of propagation and the characteristics of the remaining data are determined. It is found that the envelope distribution approximates the Rayleigh distribution,[2] that the median autocorrelation is as given by the points in Fig. 10(a), and that the median spaced-antenna correlations are as given in Fig. 11. No diurnal variation of any of these characteristics was detected. However, random errors in the analysis and the relatively small amount of data analyzed would prevent the detection of moderate diurnal variations.

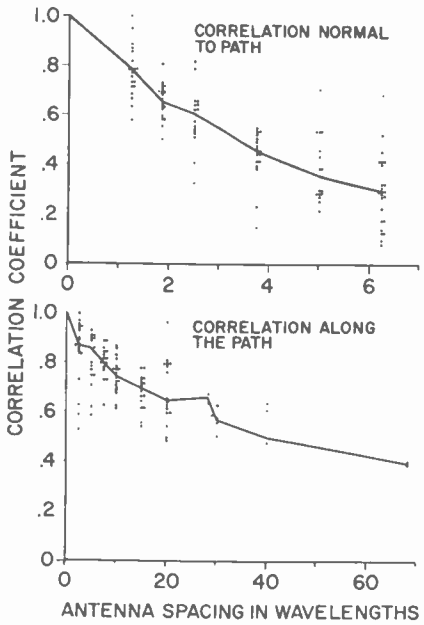

Fig. 11—Observed values and medians of space correlation.

In relating the results obtained to the experimental facilities and techniques we consider separately the results of (1) measurements made during the middle of the day when the persistent component of signal was strong relative to the meteoric component, and (2) measurements made at other times when the persistent component of signal was not strong relative to the meteoric component.

In the first category the two components of signal were easily distinguished and separated, and only a small amount of data was discarded in the editing process. Therefore, it appears likely that these results are essentially the same as those which might be obtained if there were no meteoric component of signal.

In the second category, the persistent component of signal was not strong relative to the meteoric component and the two components were not always easily distinguished and separated. Often a large amount of data was discarded in the editing process. Although results in this category may represent various combinations of persistent and meteoric components varying from nearly all persistent component to nearly all meteoric component no significant difference was found between these and results representing primarily the persistent component. This absence of diurnal variations, where they would normally be expected, can be interpreted in several ways. For example, it might be concluded that a persistent component was always present and properly separated from the meteoric component and that its characteristics as measured in this experiment do not vary diurnally. Alternatively it might be concluded that even if the propagation mechanism varied diurnally the experimental conditions were such as to minimize and obscure any variation in the observed characteristics.

This ambiguity in interpretation has not yet been resolved. However, progress has been made in computing the space correlation to be expected for a given experimental arrangement. These calculations, based on results obtained by Staras[3] in a study of tropospheric scattering, indicate that the observed correlations were strongly influenced if not controlled by the extreme directivity of the transmitting antenna rather than the propagation mechanism.

Acknowledgment

The author wishes to acknowledge the assistance of his colleagues at the National Bureau of Standards in performing the measurements and evaluating the results.

[2] This result is consistent with the early measurements by Bailey *et al.* (reference 1) of Cedar Rapids to Sterling 49.8 megacycle transmissions. The more recent measurements of Silverman and Balser over a different transmission path and using other measuring techniques appear to be consistent with the above conclusion. They report that for 49.6 megacycle Cedar Rapids to South Dartmouth, Massachusetts, transmissions the distribution of the signal envelope fits a Rayleigh distribution very closely (R. A. Silverman and M. Balser, "Statistics of electromagnetic radiation scattered by turbulent motion," *Phys. Rev.*, vol. 96, pp. 560–563; November, 1954).

[3] H. Staras, "The Statistics of Scattered Radiation," presented at National Bureau of Standards, Boulder, Colorado; September 9 1954.

Line-of-Sight Propagation Phenomena—I. Ray Treatment*

R. B. MUCHMORE†, SENIOR MEMBER, IRE AND A. D. WHEELON†

Summary—**The effect of variations in index of refraction on line-of-sight propagation of electromagnetic waves in the troposphere is investigated using, in this paper, a ray theory approach. Mean-square variations in phase delay and phase correlation between two paths are calculated. It is shown that these quantities are relatively insensitive to the form of space correlation function assumed for the index of refraction. The mean-square phase is proportional to $\overline{\Delta N^2} l_0$ where l_0 is scale length and $\overline{\Delta N^2}$ the mean-square variation in index of refraction, whereas in beyond line-of-sight propagation the received power is proportional to $\overline{\Delta N^2}/l_0$.**

Variations in angle of arrival are also calculated and it is shown that here the assumed space correlation of index of refraction is critical in determining the angle of arrival characteristics. It is shown, however, that a certain portion of the angle-of-arrival spectrum is insensitive to the choice.

Introduction

THIS PAPER and the following one[1] summarize the first results of an investigation initiated to answer the simple question: "With what precision can one propagate microwave electromagnetic energy along a line-of-sight path in the real atmosphere." Such a question arises naturally if one asks for the ultimate accuracy of radio location measurements or ultra-high speed communication techniques. One can imagine a variety of scattering and phase shifting mechanisms which might operate in the atmosphere to produce angle of arrival problems, multipath propagation modes, signal phase scintillation, and broadening of received energy patterns.

Considerable attention has recently been focused on the atmosphere in connection with beyond-line-of-sight (scatter) communication systems. A theory of turbulence scattering has been proposed[2,3] to account for observed propagation anomalies and a thoroughgoing examination of the atmosphere variations initiated. In addition to the usual meteorological disturbances (snow, rain, clouds, and dust), an atmospheric fine structure extended from the very surface of the earth to ionospheric heights has thereby been uncovered. This structure is measured as time and space varying concentrations of index of refraction in the troposphere and free electron densities in the ionosphere.

The present study exploits phenomenological models for turbulence and precipitation scattering which have been fitted to such experiments. Effects of turbulence and clouds are computed from estimated departures of the index of refraction from its median values. In general, no attempt has been made to determine the effects of signal attenuation nor is any attention paid to ducting produced by uniform horizontal layers. The essential output of the following calculation is: (1) rms phase error and phase correlation for adjacent paths, and the corresponding scintillation spectra, and (2) angle of arrival correlations and spectra. No account is taken in this paper of the stratified nature of the atmosphere; only deviations from the mean are considered. This study indicates two points rather clearly: (1) the atmosphere can be a limiting factor in very accurate radio location schemes, and (2) attendant phase variations simply a real distortion limit for ultra-high speed communication systems.

The troposphere is in continuous turbulent motion, and is therefore neither uniformly stratified nor homogenously mixed. At a given instant there are both horizontal and vertical fluctuations in the temperature, pressure, and humidity about their respective means. One may think of these micrometeorological disturbances as a turbulent boundary layer phenomenon associated with motion of the winds over the earth's rough surface or wind shears in the atmosphere itself. A detailed eddy decay scheme has been suggested which imagines these large scale wind-produced clusters to subdivide until their size and energy are eventually absorbed in molecular friction.[4] We shall base our development on a purely phenomenological description of these tropospheric variations.

The statistical properties of the troposphere's dielectric constant, and hence its index of refraction, are given in terms of the rms dielectric fluctuation and normalized space correlation function

$$\overline{\Delta\epsilon^*(r_1)\Delta\epsilon(r_2)} = \overline{|\Delta\epsilon|^2} C(\vec{r}_{12}). \tag{1}$$

Here r_{12} is the vector distance between points (1) and (2), and $\Delta\epsilon$ is the variation of the dielectric constant about its mean. This function defines the cross correlation $C(\vec{r}_{12})$ between simultaneous records of dielectric

* Original manuscript received by the IRE, July 18, 1955.

† Guided Missile Res. Div., Ramo-Wooldridge Corp., Los Angeles 45, Calif.

[1] A. D. Wheelon and R. B. Muchmore, "Line-of-sight propagation phenomena—II, the scattered wave," p. 1450, this issue.

[2] H. G. Booker and W. E. Gordon, "A theory of radio scattering in the troposphere," PROC. IRE, vol. 38, pp. 401–412; April, 1950.

[3] C. L. Pekeris, "Wave theoretical interpretation of propagation of 10-centimeter and 3-centimeter waves in low-level ocean ducts," PROC. IRE, vol. 35, p. 453; May, 1947.

[4] F. Villars and V. F. Weisskopf, "The scattering of electromagnetic waves by turbulent atmosphere fluctuations," *Phys. Rev.*, vol. 94, p. 232; 1954. They have given a fuller theory of turbulence scattering based on the Navier-Stokes equation. Their paper also contains references to the basic work of Heisenberg, Batchelor, and others. A revised version of this paper is given on p. 1232, this issue.

constant taken at two points a distance r apart. The atmosphere is assumed to be isotropic and homogenous, so that $C(\vec{r})$ is a function neither of the direction nor the end points of $\vec{r}$. Limited tests[5-7] tend to support the exponential correlation

$$C(\vec{r}_{12}) = \exp\left[-\frac{|r_{12}|}{l_0}\right], \tag{2}$$

where l_0 is a measure of the scale of the turbulence. Further measurements indicate that isotropic assumption is not strictly true; scale length l_0 differs in both horizontal and vertical directions. Direct measurement[8] has also shown this scale increases with altitude. Variations in measurement with location and time of day are such that it was not considered worthwhile to attempt to correct for these variations in scale length.

The correlation function of (2) has the disadvantage that it describes a physical process without finite mean square derivatives. The cusp at the origin implies that the function $\Delta\epsilon(x, y, z)$ is discontinuous everywhere—at least on a microscale. It is similar in communications technique to the output (time) function from a simple low-pass RC filter with white noise applied. Such a function also lacks finite mean-square derivatives and hence is strictly a nonphysical function. It is, nevertheless, very useful in analysis because of its very simple properties. To answer the possible objection that the process described by (2) is not meaningful, two other correlation functions have been carried along through most of the calculations. These are the Gaussian form

$$C_g(\vec{r}_{12}) = \exp\left[-\frac{|r_{12}|^2}{l_0^2}\right] \tag{2a}$$

and the generalized Cauchy form

$$C_c(\vec{r}_{12}) = \frac{1}{\left[1+\frac{|r_{12}|^2}{l_0^2}\right]^2}. \tag{2b}$$

These same forms were used by Staras[9] in investigating beyond line-of-sight scatter propagation. Both (2a) and (2b) describe processes having derivatives of all orders. Neither of the alternate forms for $C(r)$ [(2a) and (2b)] is really the most suitable substitution for (2). Experiment seems to show that for the whole measured range of r, (2) is a good fit to the data. The fact that (2) applies strictly only to a process having no finite mean-square derivatives means that the experimental data have had insufficient fine detail.[10] A better function for a phenomenological theory might be

$$C(r) = (1 - l_s/l_0)^{-1}\left[\exp\left(-\frac{|r|}{l_0}\right) - \frac{l_s}{l_0}\exp\left(-\frac{|r|}{l_s}\right)\right]. \tag{2c}$$

This has another disposable constant l_s (presumably $l_s \ll l_0$). No data are available now to enable one to set this constant for the troposphere so this form has not been carried through the calculations. The results are, of course, directly obtained from those for (2) .

Phase Shift

Rms Phase Shift

To estimate the phase shift suffered by a wave traversing the atmosphere, we first use a simple ray picture. Imagine a light ray traversing an inhomogeneous medium such as described in the introduction. We assume that $\Delta\epsilon$ is very small ($\Delta\epsilon/\epsilon_0 \cong 10^{-6}$ in a typical case). In traversing this medium, the ray undergoes a series of random phase delays as it encounters first more dense and then less dense "blobs" of air. It is also bent continually one way and then another so that its path is a sinuous twisted line.

The lengthening caused by this ray bending is of second order in $\Delta\epsilon/\epsilon_0$, however, so that the net phase delay is simply the sum of the phase delays introduced by the variable medium along the path. The phase delay α produced at wavelength λ by $\Delta\epsilon$ can be written

$$\alpha = \frac{\pi}{\lambda}\int_0^L dl\,\frac{\Delta\epsilon(l)}{\epsilon_0}, \tag{3}$$

which is merely the sum of all phase perturbations along the ray of length L.[11] The mean value of α vanishes identically, since $\Delta\epsilon = 0$ so that we turn immediately to the mean square.

$$\overline{\alpha^2} = \frac{\pi^2}{\lambda^2}\int_0^L dl_1\int_0^L dl_2\,\frac{\overline{\Delta\epsilon^*(l_1)\Delta\epsilon(l_2)}}{\epsilon_0^*\epsilon_0}. \tag{4}$$

The integrand is just $|\Delta\epsilon/\epsilon|^2 C(l_1 - l_2)$ by our definition (1) so that one has, for the exponential correlation (2),

[5] J. R. Gerhardt, C. M. Crain, and H. W. Smith, "Fluctuations of atmosphere temperature as a measure of the scale and intensity of turbulence near the earth's surface," *Jour. Met.*, vol. 9, p. 299; 1952.

[6] G. Birnbaum, "Fluctuations in the refractive index of the atmosphere at microwave frequencies," *Phys. Rev.*, vol. 82, p. 110; 1951.

[7] H. W. Liepmann, J. Laufer, and K. Liepmann, "On the Spectrum of Isotropic Turbulence," NACA TN2473; November, 1951.

[8] C. M. Crain, A. W. Straiton and C. E. von Rosenberg, "A statistical survey of atmospheric index-of-refraction variation," TRANS. IRE, vol. AP-1, pp. 43–46; October, 1953.

[9] C. L. Staras, "Scattering at electromagnetic energy in a randomly inhomogeneous atmosphere," *Jour. Appl. Phys.*, vol. 23, p. 1152; October, 1952. One other form used by Staras has been omitted by us since it is an inadmissible functional form for a correlation (it implies negative power spectral densities).

[10] Ref. 7 describes some wind-tunnel experiments on turbulence in which care was taken to examine this fine detail and the existence of derivatives to several orders verified.

[11] It is readily shown that (3) is consistent with the first term of a WKB solution for a wave propagating in one dimension through a randomly stratified medium. The usual conditions for validity for ray theory are that the index of refraction change by very small amounts in one wavelength and that the rays do not change relative spacing by too much in one wavelength. See D. E. Kerr, "Propagation of Short Radio Waves," M.I.T. Rad. Lab. Series, McGraw-Hill Book Co., Inc., New York, N. Y., vol. 13; 1951. The validity of the results obtained in this paper will be more carefully examined in the following paper.

See Appendix for effect of a finite size receiving antenna.

$$\overline{\alpha^2} = \frac{\pi^2 \overline{\left|\frac{\Delta\epsilon}{\epsilon}\right|^2}}{\lambda^2} \int_0^L dl_1 \int_0^L dl_2 \exp\left[-|l_1 - l_2|/l_0\right],$$

$$\cong \frac{8\pi^2 l_0 L \overline{\Delta N^2} \cdot 10^{-12}}{\lambda^2} \tag{5}$$

for $L/l_0 \gg 1$. Here $\Delta N = \frac{1}{2}\Delta\epsilon \cdot 10^6$ has been used where ΔN is measured in N units in the usual notation.[8] Mean-square phase shifts for other spatial correlations

$$\overline{\alpha_g^2} = \frac{\pi^{5/2} l_0 L \overline{\Delta N^2} \cdot 10^{-12}}{\lambda^2} \tag{5a}$$

$$\overline{\alpha_c^2} = \frac{\pi^3 l_0 L \overline{\Delta N^2} \cdot 10^{-12}}{2\lambda^2} \tag{5b}$$

again with $(L/l_0) \gg 1$. Note that these are all of the same form and within a factor of 1.3 of one another. In contrast with the results for beyond line-of-sight scatter propagation,[9] the correlation function $C(r)$ makes very little difference here. Another interesting point is that $\overline{\alpha^2}$ depends on the product $l_0\overline{\Delta N^2}$ while for long distance scatter propagation the far field depends[2,9] on $\overline{\Delta N^2}/l_0$ when $l_0 \gg \lambda$. [As will be shown in (37), mean-square deviation of angle of arrival also depends on $\overline{\Delta N^2}/l_0$.] Thus possibility is open for two independent measurements to give l_0 and $\overline{\Delta N^2}$ directly from propagation data.

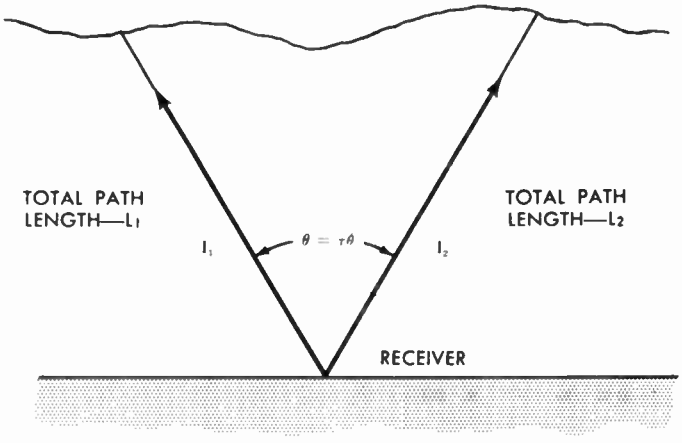

Fig. 1—Geometry of rotating line-of-sight.

Phase Correlations and Spectra

In this section the correlation between the phase deviations along two separated line-of-sight paths is calculated. Two configurations have been chosen; one (Fig. 1) has two paths with one end point in common. The other (Fig. 2) places the two paths parallel but displaced laterally. Measurements on paths like those of Fig. 1 are described by Herbstreit, *et al.*[12]

[12] J. W. Herbstreit and M. C. Thompson, Jr., "Measurements of the phase of signals received over transmission paths with electrical lengths varying as a result of atmospheric turbulence," p. 1391, this issue.
A. P. Deam and B. M. Fannin, "Phase difference variations in 9,350 megacycle radio signals arriving at spaced antennas," p. 1402, this issue.

To anticipate the results, one finds that the phase correlation between two such paths depends only upon the spacing and the scale length. To a fair approximation, it is also true that the particular one used in (2) makes little difference in the results. As a consequence, measurement of the phase correlation for various spacings affords a direct measure of the scale length l_0, independent of ΔN.

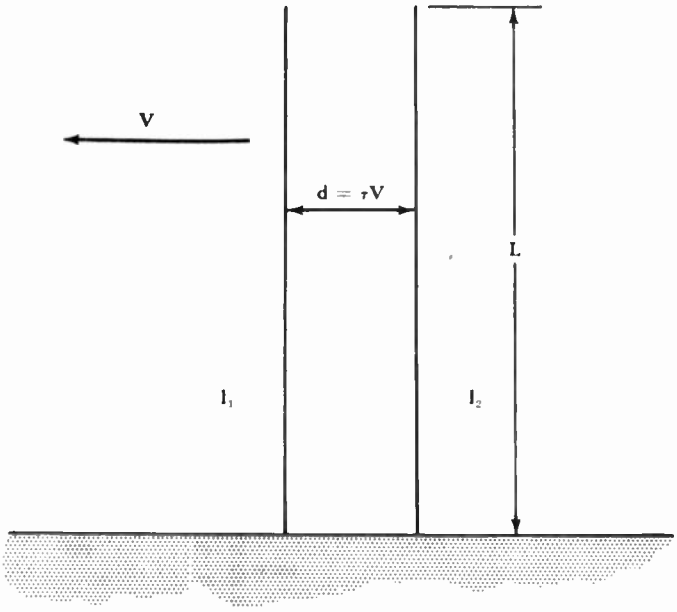

Fig. 2—Geometry for line-of-sight moving parallel to itself.

Another reason for calculating these correlations is that in radar or communication system design, it is nearly always necessary to know not only the rms noise to be expected but its spectrum as well. To determine a time spectrum for phase, a time spectrum for the turbulence must be known. Consider a mass of turbulent air moving with an average velocity v. Take a set of coordinates moving with the mass (i.e., at speed v); measurements of fluctuations in this system will give data from which the time spectrum can be calculated. Unfortunately, such data are not available and in their absence an approximate treatment must be used. In the following we shall calculate the time spectrum produced by a line-of-sight moving through a turbulent air mass containing variations which are not changing in time relative to one another. This is equivalent to assuming that the line of sight moves through a characteristic length l_0 in a time short compared to the time of significant change in the turbulence pattern. That this procedure will yield useful results is suggested by the experiments of Straiton and Smith.[13]

The two-path correlation becomes directly the time auto correlation by noting that a rotating line-of-sight

[13] A. W. Straiton and H. W. Smith, "Progress of microwave radio scintillations at wind speed on an overwater path," PROC. IRE, vol. 38, p. 825; July, 1950.

sweeps through an angle $\theta=\dot{\theta}\tau$, or a parallel line-of-sight moves a distance $d=v\tau$, in time τ where $\dot{\theta}$ is angular rate of rotation of the line-of-sight or v is its lateral velocity relative to the air mass.

Consider the example of Fig. 1 first. Defining α as before, one can write

$$\overline{\alpha(t)\alpha(t+\tau)}=\frac{\pi^2}{\lambda^2}\int_0^{L_1}dl_1\int_0^{L_2}dl_2\frac{\overline{\Delta\epsilon^*(x_1,\,y_1)\Delta\epsilon(x_2,\,y_2)}}{|\epsilon^2|}, \quad (6)$$

where the first integral is taken along path l_1 at time t, and the second along line l_2 at τ seconds later. Using (2) and measuring distance along line-of-sight from origin, (6) can be written for exponential correlation

$$\overline{\alpha(t)\alpha(t+\tau)}=\frac{4\pi^2\overline{\Delta N^2}\cdot 10^{-12}}{\lambda^2}\int_0^{L_1}dl_1\int_0^{L_2}dl_2 \cdot\exp\left(-\frac{1}{l_0}\sqrt{l_1^2+l_2^2-2l_1l_2\cos\theta}\right). \quad (7)$$

It is convenient to assume that $L_1\cong L_2$, (i.e., that the path is long compared to any changes in length), so that (7) can be changed to polar coordinates and the radial integral performed

$$\overline{\alpha(t)\alpha(t+\tau)}=\frac{8\pi^2\overline{\Delta N^2}\cdot 10^{-12}l_0^2}{\lambda^2}\int_0^{\pi/4}d\phi\left\{\frac{1}{1-\sin 2\phi\cos\theta}-\frac{L\exp\left[-\dfrac{L\sqrt{1-\sin 2\phi\cos\theta}}{l_0\cos\phi}\right]}{l_0\cos\phi\sqrt{1-\sin 2\phi\cos\theta}}-\frac{\exp\left[-\dfrac{L\sqrt{1\sin 2\phi\cos\theta}}{l_0\cos\phi}\right]}{1-\sin 2\phi\cos\theta}\right\}. \quad (8)$$

The first term is readily integrated again. If $L/l_0\gg 1$, the last two terms make significant contributions only for $\theta\ll\pi/2$ and $\phi\cong\pi/4$. One may put

$$\sin 2\phi\cong 1-\frac{\left(2\phi-\frac{\pi}{2}\right)^2}{2}, \quad \cos\phi\cong\frac{1}{\sqrt{2}}, \quad (9)$$

and with the substitution

$$\phi=\sqrt{\frac{1-\cos\theta}{2\cos\theta}}\sqrt{y^2-1}+\frac{\pi}{4}, \quad (10)$$

the second term in (8) becomes

$$\int_0^{\pi/4}d\phi\frac{L\exp\left[-\dfrac{L\sqrt{1-\sin 2\phi\cos\theta}}{l_0\cos\phi}\right]}{l_0\cos\phi\sqrt{1-\sin 2\phi\cos\theta}}\cong\frac{L}{l_0\sqrt{\cos\theta}}\int_1^Y dy\frac{\exp\left[-\dfrac{Ly\sqrt{2(1-\cos\theta)}}{l_0}\right]}{\sqrt{y^2-1}} \quad (11)$$

where

$$Y=\sqrt{\frac{\pi^2\cos\theta}{8(1-\cos\theta)}+1}. \quad (12)$$

When $L/l_0\gg 1$ and $\theta\ll\pi/2$, one can put $Y=\infty$ with small error. The integral thus becomes

$$\frac{L}{l_0}\int_1^\infty dy\frac{\exp\left[-\dfrac{|\theta|Ly}{l_0}\right]}{\sqrt{y^2-1}}=\frac{L}{l_0}K_0\left(\frac{|\theta|L}{l_0}\right), \quad (13)$$

where K_0 is the modified Bessel function of the second kind. The last term can be treated in a similar fashion.

$$\begin{aligned}&\frac{1}{|\theta|}\int_1^\infty dy\frac{\exp\left[-\dfrac{|\theta|Ly}{l_0}\right]}{y\sqrt{y^2-1}}\\&=\frac{1}{|\theta|}\int_{|\theta|L/l_0}^\infty d\eta\int_1^\infty dy\frac{\exp(-\eta y)}{\sqrt{y^2-1}}\\&=-\frac{\pi}{2|\theta|}+\frac{\pi L}{2l_0}\left[K_0\left(\frac{|\theta|L}{l_0}\right)L_{-1}\left(\frac{|\theta|L}{l_0}\right)+K_1\left(\frac{|\theta|L}{l_0}\right)L_0\left(\frac{|\theta|L}{l_0}\right)\right]. \quad (14)\end{aligned}$$

L_μ denotes the modified Struve function. Combining all of these results, one finds:

$$\overline{\alpha(t)\alpha(t+\tau)}=\frac{8\pi^2l_0\overline{\Delta N^2}\cdot 10^{-12}}{\lambda^2}\left(\frac{L}{l_0}\right)\left\{\frac{\pi}{2}\cdot\left[K_0\left(\frac{|\theta|L}{l_0}\right)L_{-1}\left(\frac{|\theta|L}{l_0}\right)+K_{-1}\left(\frac{|\theta|L}{l_0}\right)L_0\left(\frac{|\theta|L}{l_0}\right)\right]-K_0\left(\frac{|\theta|L}{l_0}\right)\right\}, \quad (15)$$

where $\theta=\dot{\theta}\tau$. When $\theta=0$, (15) reduces to (5).

The spectrum may be found by taking the cosine transform of (15)[14]

$$W(f)=\int_{-\infty}^{\infty}d\tau\cos(2\pi f\tau)\overline{\alpha(t)\alpha(t+\tau)}. \quad (16)$$

Upon substituting (15) into (16), the second term may be integrated directly. The first term is simplified by using the identity

$$\frac{1}{z}\left[1-\frac{2}{\pi}\int_z^\infty K_0(x)dx\right]=K_0(z)L_{-1}(z)+K_{-1}(z)L_0(z).$$

The integral to be evaluated can then be written

$$\frac{2l_0}{L\dot{\theta}}\int_0^\infty du\frac{\cos\omega_1 u}{u}\left[1-\frac{2}{\pi}\int_u^\infty K_0(x)dx\right], \quad (17)$$

where $\omega_1=2\omega fl_0/L\dot{\theta}$. Eq. (17) may be integrated once by parts to give

[14] $W(f)$ is defined such that $\overline{\alpha^2}=\int_{-\infty}^{\infty}W(f)df$.

$$\frac{4l_0\pi}{\theta L}\int_0^\infty du K_0(u)\int_{\omega_1 u}^\infty dt\,\frac{\cos t}{t}. \tag{18}$$

By changing the variable in the second integral to $y=t/\omega_1 u$, the order of integration may be reversed and the remaining integration performed directly. The complete result is

$$W(f)=\frac{8\pi^3\cdot 10^{-12}\overline{\Delta N^2}l_0^2}{\lambda^2\theta}\cdot\left[\log\frac{1+\sqrt{1+\omega_1^2}}{|\omega_1|}-\frac{1}{\sqrt{1+\omega_1^2}}\right]. \tag{19}$$

With similar approximations, phase correlations and spectra for the other space correlations may be found. One has for the Gaussian correlation (2a)

$$\overline{\alpha_g(t)\alpha_g(t+\tau)}=\frac{2\pi^3 l_0 L\overline{\Delta N^2}\cdot 10^{-12}}{\lambda^2}\left(\frac{l_0}{L|\theta|}\right)\operatorname{erf}\left(\frac{L|\theta|}{l_0}\right) \tag{15a}$$

and for the Cauchy model (2b):

$$\overline{\alpha_c(t)\alpha_c(t+\tau)}=\frac{2\pi^3 l_0 L\overline{\Delta N^2}\cdot 10^{-12}}{\lambda^2}\frac{1}{\sqrt{1+\frac{L^2\theta^2}{l_0^2}}}, \tag{15b}$$

the corresponding spectra become

$$W_g(f)=-\frac{4\pi^3 l_0^2\overline{\Delta N^2}\cdot 10^{-12}}{\lambda^2\theta}Ei\left(-\frac{\omega_1^2}{4}\right) \tag{19a}$$

and

$$W_c(f)=\frac{4\pi^3 l_0^2\overline{\Delta N^2}\cdot 10^{-12}}{\lambda^2\theta}K_0(|\omega_1|) \tag{19b}$$

where $-Ei(-x)$ is the exponential integral function.

The three-phase correlations are plotted together on Fig. 3 (next page) (normalized to unity at $\theta=0$). By changing the definition of l_0, which is completely arbitrary, the three curves could be made to agree quite well over their whole range. Thus, the form assumed for the correlation of $\Delta\epsilon$ evidently is not critical here any more than in the mean-square calculation.

The three power spectra are plotted in Fig. 4 (next page) and it is evident a change of scale would make them agree quite well. (Curves plotted were normalized such that all have the form $\log 2/\omega_1$ for $\omega_1\to 0$.)

If the line-of-sight moves parallel to itself instead of rotating about one end point, the distance between two reference points becomes:

$$r_{12}=\sqrt{(l_2-l_1)^2+d^2}. \tag{20}$$

The initial line-of-sight is denoted by l_1, and that τ seconds later by l_2. The space interval between the two points l_1 and l_2 is $d=v\tau$ where v is the velocity of the path (see Fig. 2).

The autocorrelation of the phase shift is computed as in (6)

$$\begin{aligned}\overline{\alpha(t)\alpha(t+\tau)}&=\frac{4\pi^2\overline{\Delta N^2}\cdot 10^{-12}}{\lambda^2}\int_0^L dl_1\int_0^L dl_2\cdot\exp\left[-\frac{\sqrt{(l_2-l_1)^2+d^2}}{l_0}\right]\\&=\frac{8\pi^2\overline{\Delta N^2}\cdot 10^{-12}}{\lambda^2}\int_0^L dx(L-x)\cdot\exp\left[-\frac{\sqrt{x^2+d^2}}{l_0}\right].\end{aligned} \tag{21}$$

The change of variable $y^2=1+(x^2/d^2)$ gives:

$$\begin{aligned}&\overline{\alpha(t)\alpha(t+\tau)}\\&=\frac{8\pi^2 l_0^2\overline{\Delta N^2}\cdot 10^{-12}}{\lambda^2}\left\{\frac{|d|L}{l_0^2}\int_1^{\sqrt{1+L^2/d^2}}dy\,\frac{y\exp\left(-\frac{|d|y}{l_0}\right)}{\sqrt{y^2-1}}\right.\\&\left.-\frac{|d|^2}{l_0^2}\int_1^{\sqrt{1+L^2/d^2}}dy\,y\exp\left(-\frac{|d|y}{l_0}\right)\right\}.\end{aligned} \tag{22}$$

If $L/d\gg 1$, the upper limit may be relaxed to infinity with small error and the second term neglected in comparison with the first. The integration may then be performed analytically.

$$\overline{\alpha(t)\alpha(t+\tau)}=\frac{8\pi^2 l_0 L\overline{\Delta N^2}\cdot 10^{-12}}{\lambda^2}\frac{|d|}{l_0}K_1\left(\frac{|d|}{l_0}\right), \tag{23}$$

where K_1 is the modified Bessel function of the second kind. One may verify that this expression reduces to (5) when $d=0$. The cosine transform of (23) yields the power spectrum,

$$W(f)=\frac{8\pi^3 l_0^2 L\overline{\Delta N^2}\cdot 10^{-12}}{\lambda^2 v}\frac{1}{(1+\omega_2^2)^{3/2}} \tag{24}$$

with $\omega_2=2\pi f l_0/v$.

The corresponding Gaussian and Cauchy cases are

$$\overline{\alpha_g(t)\alpha_g(t+\tau)}=\frac{4\pi^{5/2} l_0 L\overline{\Delta N^2}\cdot 10^{-12}}{\lambda^2}\exp\left[-\left(\frac{d}{l_0}\right)^2\right] \tag{23a}$$

$$\overline{\alpha_c(t)\alpha_c(t+\tau)}=\frac{2\pi^3 l_0 L\overline{\Delta N^2}\cdot 10^{-12}}{\lambda^2}\frac{1}{\left[1+\left(\frac{d}{l_0}\right)^2\right]^{3/2}} \tag{23b}$$

for the phase correlations and

$$W_g(f)=\frac{4\pi^3 l_0 L\overline{\Delta N^2}\cdot 10^{-2}}{\lambda^2 v}\exp\left[-\frac{\omega_2^2}{4}\right] \tag{24a}$$

$$W_c(f)=\frac{4\pi^3 l_0 L\Delta N^2\cdot 10^{-12}}{\lambda^2 v}|\omega_2|K_1(|\omega_2|) \tag{24b}$$

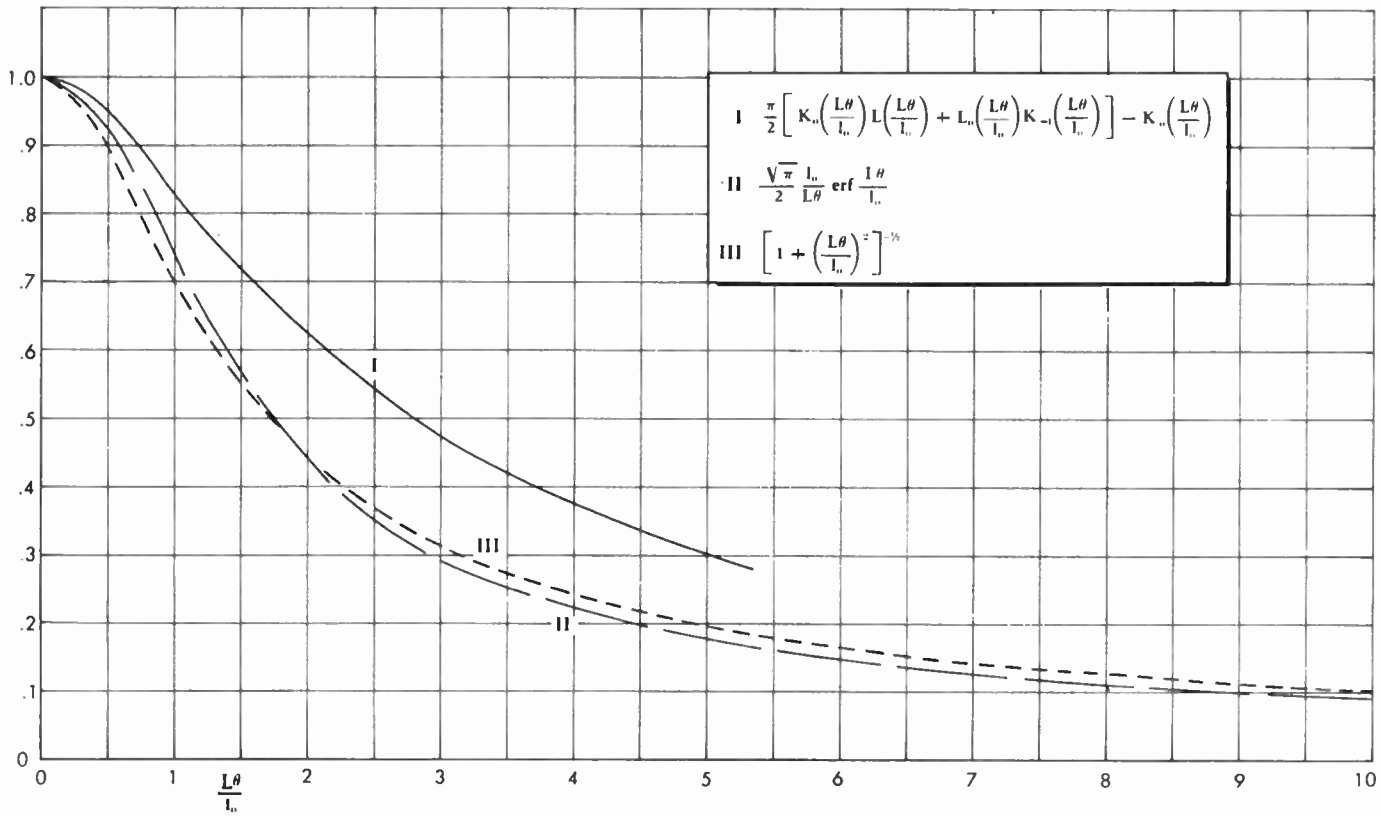

Fig. 3—Phase correlation for rotated line-of-sight.

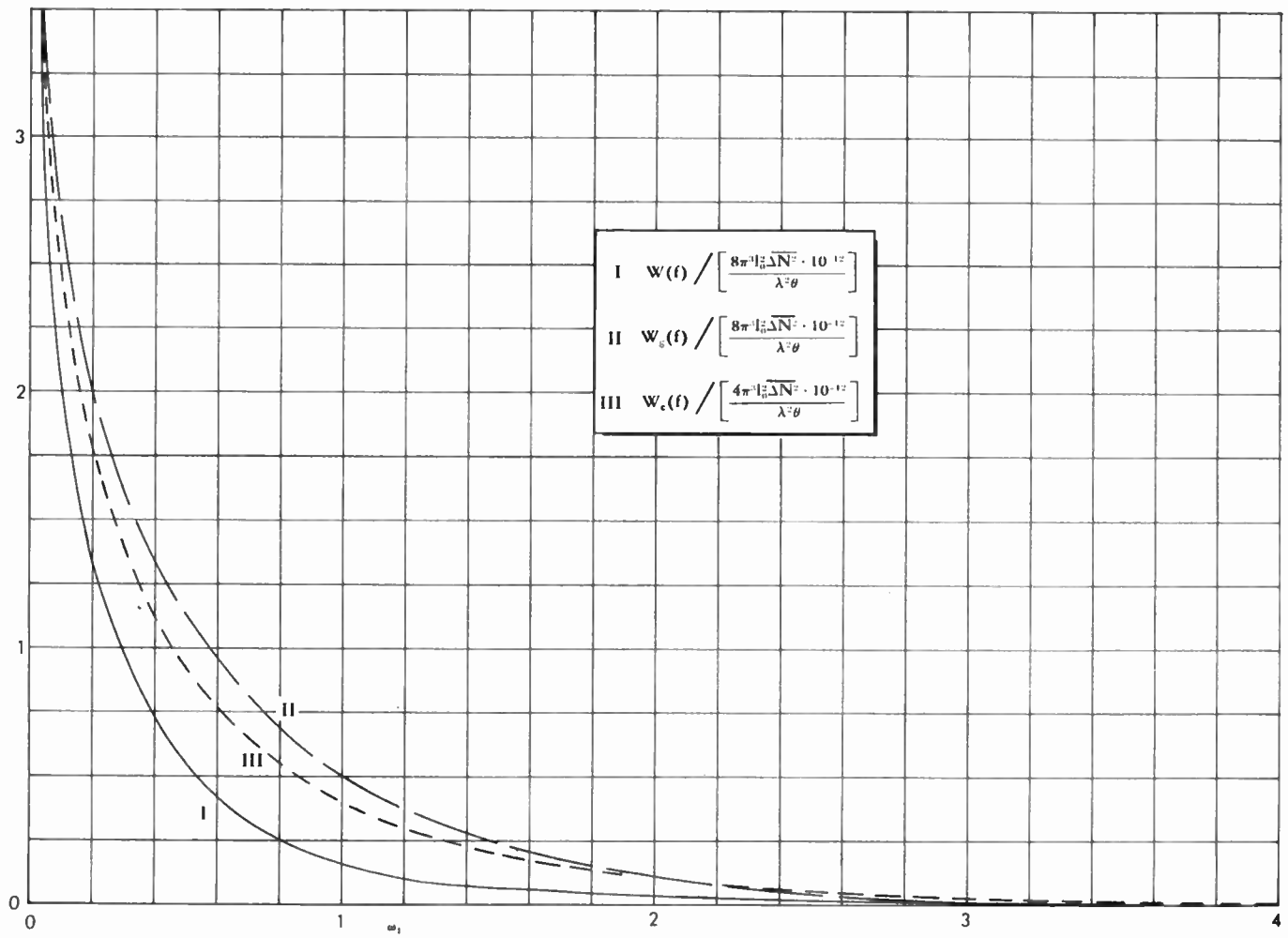

Fig. 4—Power spectra of phase for rotating line-of-sight.

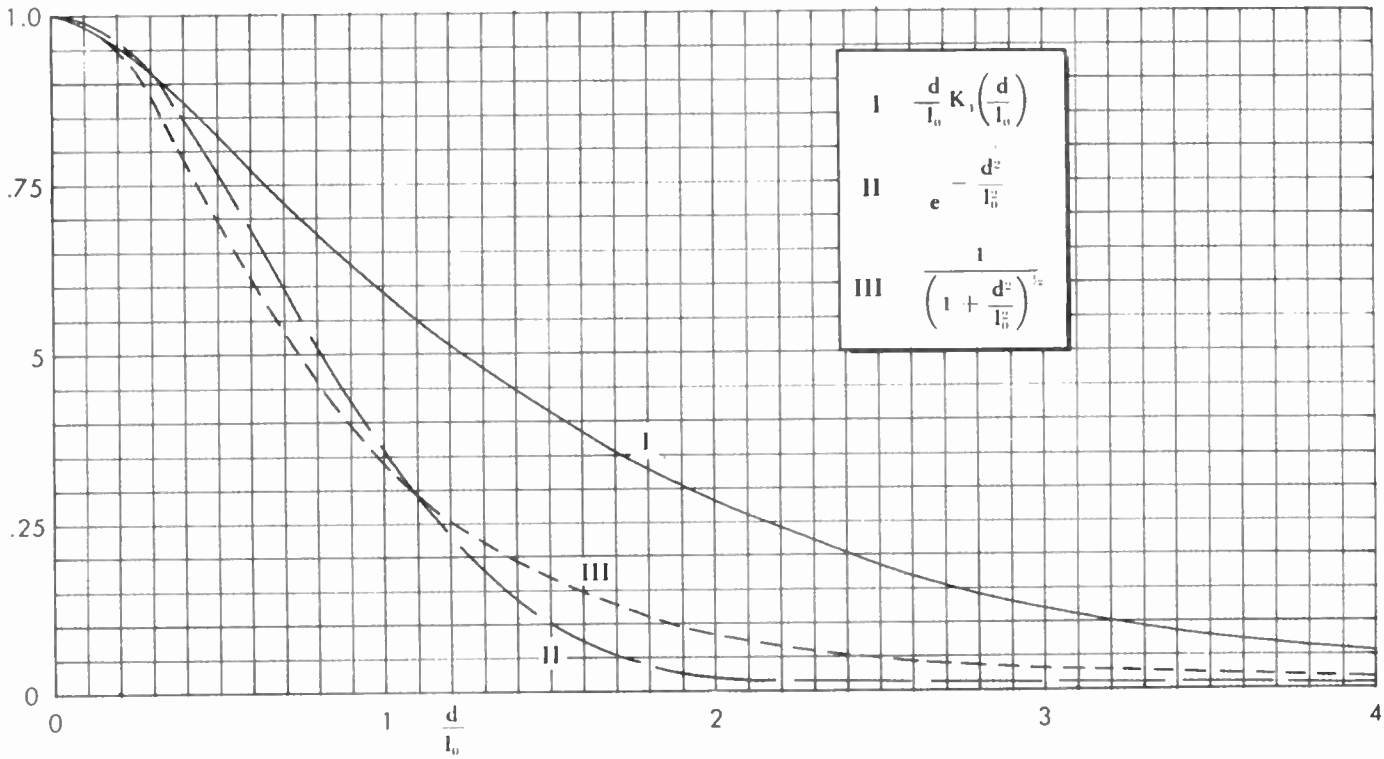

Fig. 5—Phase correlation for two parallel lines-of-sight.

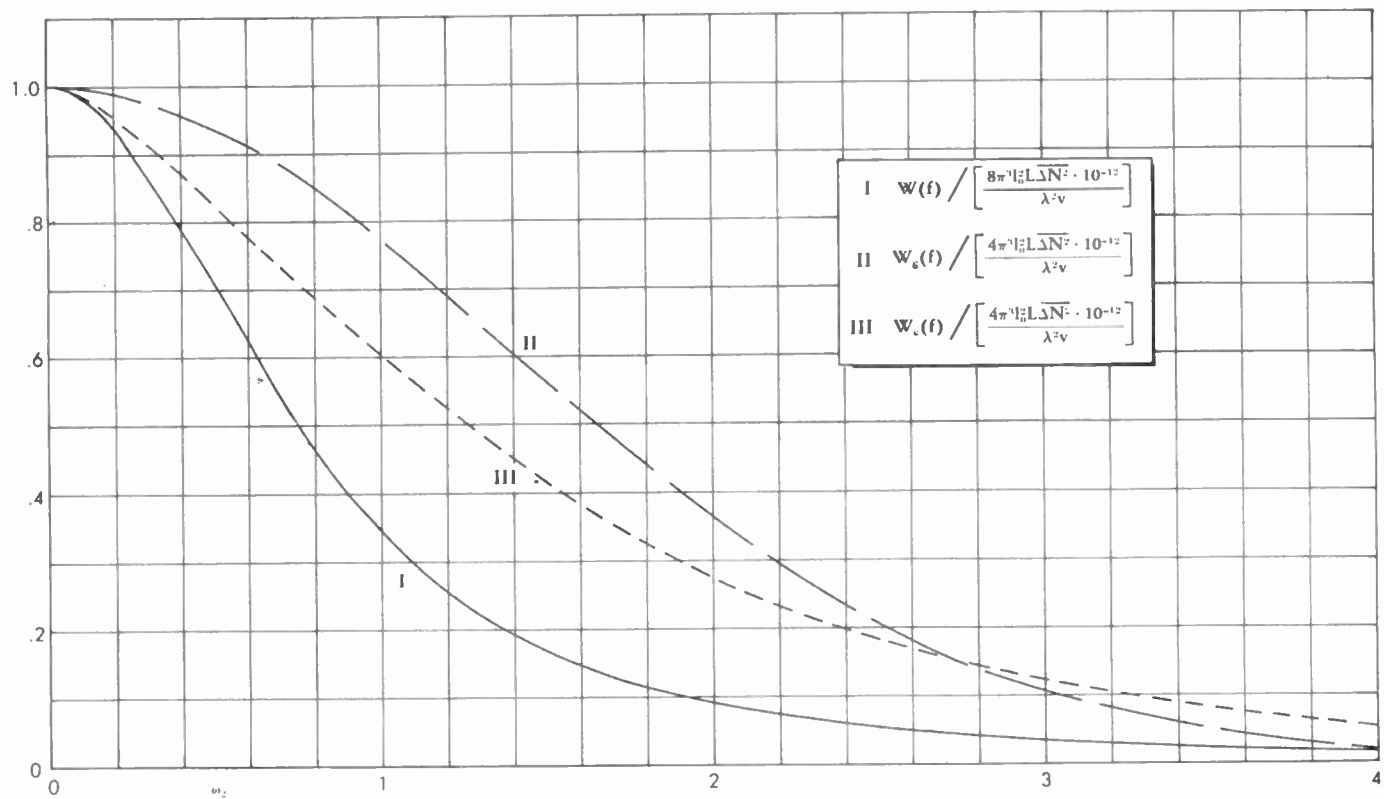

Fig. 6—Power spectra for phase for parallel lines-of-sight.

for the spectra. The correlations are plotted in Fig. 5 and the power spectra in Fig. 6. Just as for the rms values and rotating LOS correlations and spectra it is apparent that (within the limits again of a suitable redefinition of l_0) there is little dependence on the form assumed for space correlation of dielectric constant.

Angle of Arrival Fluctuations

In addition to phase delay suffered in traversing the troposphere, a ray will exhibit a random variation in

angle of arrival at the receiver. This effect is analogous to the angular scintillations of star images[15] and is produced by gradients in the index of refraction at right angles to the ray path. The equation governing propagation of a ray through a variable medium according to Fermat's principle is,[11]

$$\frac{d}{dl}(n\vec{t}) - \vec{\nabla} n = 0, \tag{25}$$

where $\vec{t}$ is a unit vector along the ray, l is the distance along the ray, and n is the index of refraction. Eq. (25) can be rearranged to read,

$$\frac{d\vec{t}}{dl} = \vec{\nabla}[\log n] - \vec{t}\,(\vec{t}\cdot\vec{\nabla}[\log n].) \tag{26}$$

To evaluate these operations, introduce the decompositions:

$$n = n_0 + N_1 \quad \text{and} \quad \vec{t} = \vec{t_0} + \vec{q}, \tag{27}$$

where $\vec{t_0}$ is the initial value of $\vec{t}$, n_0 is the mean index of refraction (and is very nearly equal to unity) and N_1 is the variable part of n.[16] To first order in q and N_1 (which must be very small), (26) can be written,

$$\frac{d\vec{q}}{dl} = \vec{\nabla} N_1 - \vec{t_0}\frac{\partial N_1}{\partial l}, \tag{28}$$

$d\vec{q}/dl$ defines the angle (and direction) of ray displacement. Eq. (28) gives this angle in terms of the gradient normal to the path. Integrating over the whole path gives the total angular deflection.

Instead of calculating rms values separately first, we go now directly to the autocorrelations since the mean squares are directly obtained from the correlations at zero lag.

For a line-of-sight moving parallel to itself, the ray deviations are:

$$\phi_x = \int_0^L dz \frac{\partial N_1}{\partial x}, \tag{29}$$

and

$$\phi_y = \int_0^L dz \frac{\partial N_1}{\partial y} \tag{30}$$

so that the corresponding autocorrelations become

$$\overline{\phi(t)\phi_x(t+\tau)} = \int_0^L dz_1 \int_0^L dz_2 \overline{\frac{\partial N_1}{\partial x}\bigg|_1 \frac{\partial N_1}{\partial x}\bigg|_2}, \tag{31}$$

and

$$\overline{\phi_y(t)\phi_y(t+\tau)} = \int_0^L dz_1 \int_0^L dz_2 \overline{\frac{\partial N_1}{\partial y}\bigg|_1 \frac{\partial N_1}{\partial y}\bigg|_2}. \tag{32}$$

[15] S. Chandrasekhar, "A statistical basis for the theory of stellar scintillation," *Monthly Notices, Roy. Astr. Soc.*, vol. 112, p. 475; 1952. See also H. W. Liepmann, "Reflection and Diffusion of a Light Ray Passing Through a Boundary Layer," Douglas Aircraft Co., Inc., Rep. SM-14397; May 16, 1952, for a discussion of a similar phenomenon.

[16] In terms of N units, $N_1 = \Delta N \cdot 10^{-6}$.

One can average the gradients in (31) and (32) as[15]

$$\overline{\frac{\partial N_1}{\partial u}\bigg|_1 \frac{\partial N_1}{\partial u}\bigg|_2} = \overline{N_1^2}\left[\frac{\xi^2}{r_{12}}\left(\frac{dC^2}{dr_{12}^2} - \frac{1}{r_{12}}\frac{dC}{dr_{12}}\right) + \frac{1}{r_{12}}\frac{dC}{dr_{12}}\right], \tag{33}$$

where $u = x$ or y, and $\xi = x_2 - x_1$ or $y_2 - y_1$ respectively. In rectangular coordinates, r_{12} is given by

$$r_{12} = \sqrt{(x_2 - x_1)^2 + (y_2 - y_1)^2 + (z_2 - z_1)^2}. \tag{34}$$

Using (33) and (34) in (31) one finds

$$\overline{\phi_x(t)\phi_y(t+\tau)} = \frac{2L\overline{\Delta N^2}\cdot 10^{-12}}{l_0}\left[K_0\left(\frac{|d|}{l_0}\right) - \frac{|d|}{l_0}K_1\left(\frac{|d|}{l_0}\right)\right] \tag{35}$$

when using (2) for $C(r)$. The alternate forms are

$$\overline{\phi_{xg}(t)\phi_{xg}(t+\tau)} = \frac{2\sqrt{\pi}L\overline{\Delta N^2}\cdot 10^{-12}}{l_0}\left(1 - \frac{2d^2}{l_0^2}\right)\cdot\exp\left(-\frac{d^2}{l_0^2}\right) \tag{35a}$$

and

$$\overline{\phi_{xc}(t)\phi_{xc}(t+\tau)} = \frac{3\pi L\overline{\Delta N^2}\cdot 10^{-12}}{2l_0}\cdot\frac{\left(1 - \frac{4d^2}{l_0^2}\right)}{\left(1 + \frac{d^2}{l_0^2}\right)^{7/2}}. \tag{35b}$$

Note that as $d \to 0$, (35) gives $\overline{\phi_x^2} \to \infty$. This is simply a consequence of our choice for the correlation function made in (2). Unfortunately, (2) describes a (Markov) process which has no derivatives. This can be corrected by using any of the alternate forms of (2a, b or c) with (c) being perhaps preferred eventually when l_s has been evaluated. Curves of the three correlations are plotted in Fig. 7 (next page). The same normalization for all curves has been used in order to show the variation in zero intercept (mean-square value).

The infinite mean square of (35) need not disturb one unduly, since a spectrum can still be found from (35) by taking its cosine transform. The spectrum $W_x(f)$ obtained from the cosine transform of (35) is

$$W_x(f) = \frac{\pi L\overline{\Delta N^2}\cdot 10^{-12}}{v}\frac{\omega_2^2}{(1+\omega_2^2)^{3/2}}, \tag{36}$$

with ω_2 defined as in (24). This spectrum is meaningful, except as the frequency $f \to \infty$. The behavior at large f is such that $\int_{-\infty}^{\infty} df W(f)$ diverges, yet the density at low frequencies is correct.

Different choices for $C(r_{12})$ produce, of course, different answers. In particular, the spectra derived from

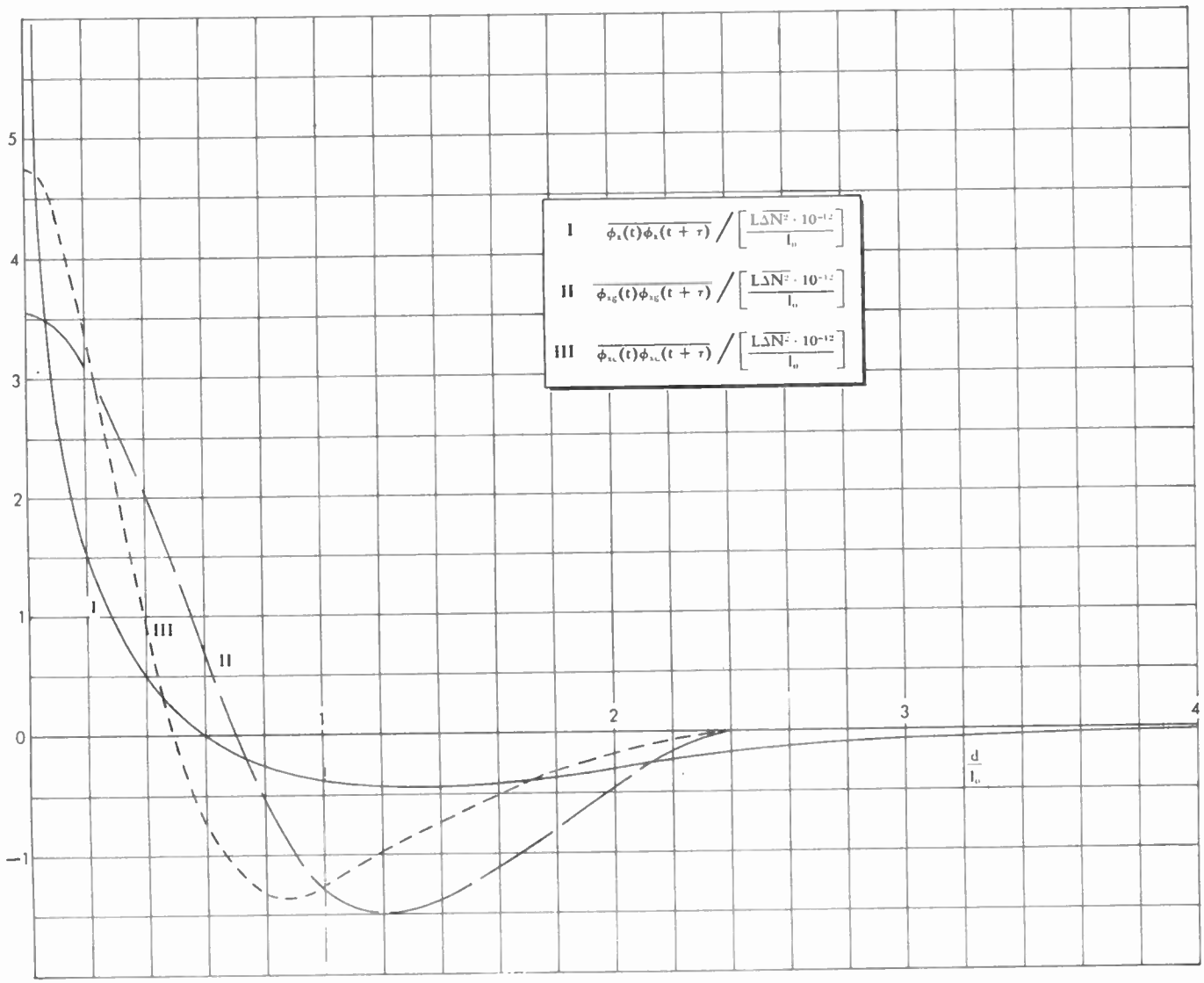

Fig. 7—Angle of arrival correlations for parallel lines-of-sight (x-coordinate).

(35a) and (35b) are

$$W_{xg}(f) = \frac{\pi L\overline{\Delta N^2}\cdot 10^{-12}}{v}\,\omega_2^2 \exp\left(-\frac{\omega_2^2}{4}\right) \qquad (36a)$$

$$W_{xc}(f) = \frac{\pi L\overline{\Delta N^2}\cdot 10^{-12}}{v}\,|\omega_2|^3 K_1(|\omega_2|). \qquad (36b)$$

These spectra have a finite integral. The mean-square errors derived from the spectra [or from (35a) and (35b) at $d=0$] are

$$\overline{\phi_{xg}^2} = \frac{2\sqrt{\pi}L\overline{\Delta N^2}\cdot 10^{-12}}{l_0} \qquad (37a)$$

$$\overline{\phi_{xc}^2} = \frac{3\pi L\overline{\Delta N^2}\cdot 10^{-12}}{2l_0}. \qquad (37b)$$

While these finite mean-square values are more reasonable physically than the infinite result from (35), the experimental data available to the authors show a better fit to the form of (2) than to (2a) or (2b). It can be easily demonstrated that still other choices for $C(r)$ can give $\overline{\phi_x^2}$ values widely differing from (37). For instance, use of (2c) will give a mean-square value dependent on l_s. Obviously, the choice of spatial correlation is critical in deriving the mean-square angular deviations.

A quantity less sensitive to the function chosen is the spectral density of ϕ at zero frequency. Note that the spectrum amplitude near $\omega_2=0$ does not depend on l_0. The spectra for ϕ on the alternate choices above are plotted in Fig. 8 (next page) along with $W_x(f)$ from (36). Note that all are the same in the low-frequency region. Any physical measurement will, in some way, filter out some of the high-frequency components of any spectra, particularly in the case of $W_x(f)$, and thus the measured results will be sensitive to the form of space correlation or not, depending on the degree of filtering. If heavy filtering is done, any choice above is adequate; otherwise more experimental data are needed.

Thus far, only one component of ϕ has been calculated. The results for the other component are

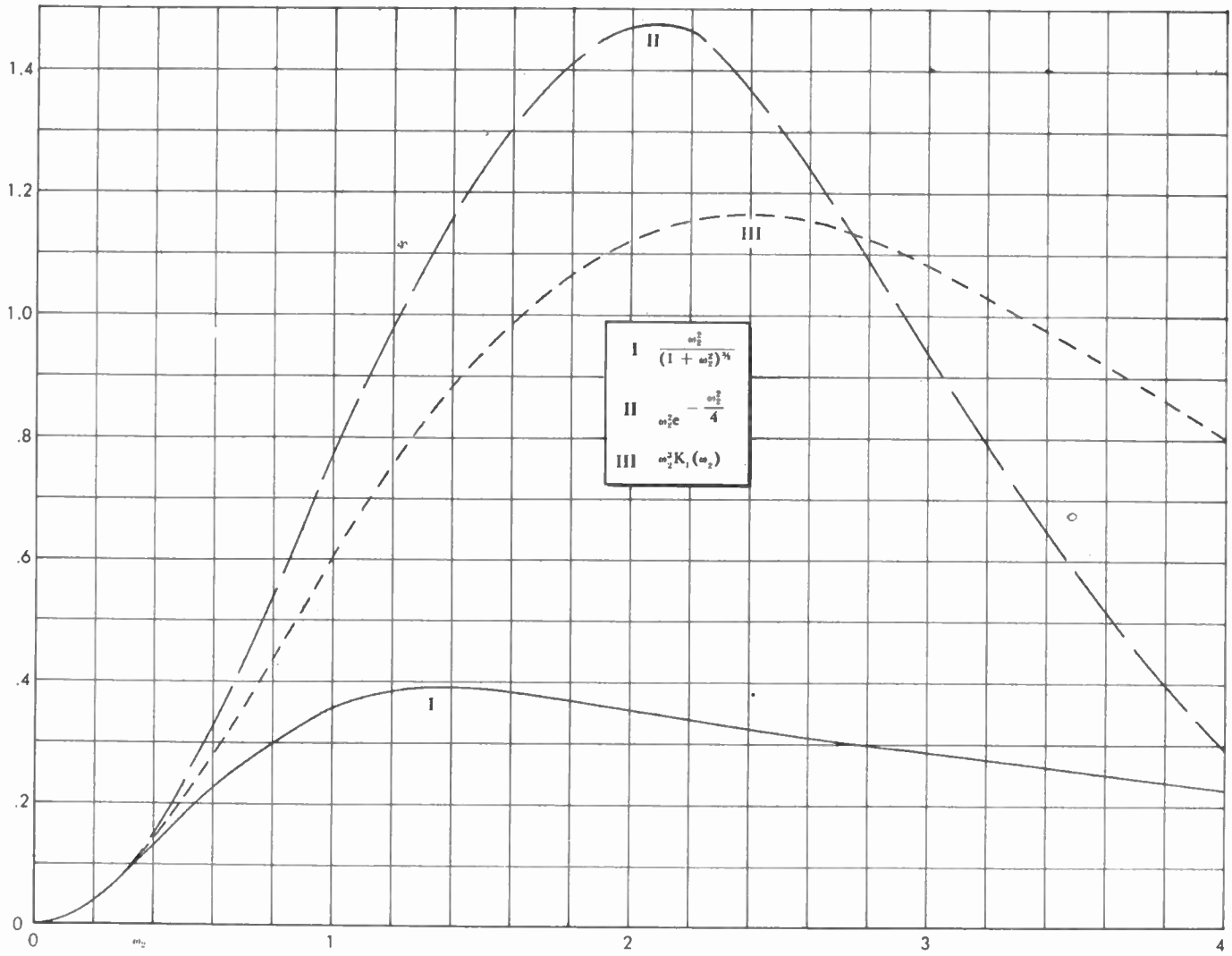

Fig. 8—Power spectra for angle of arrival (x-component) for parallel lines-of-sight.

$$\overline{\phi_y(l)\phi_y(l+\tau)} = \frac{2L\overline{\Delta N^2}\cdot 10^{-12}}{l_0} K_0\left(\frac{|d|}{l_0}\right) \tag{38}$$

$$\overline{\phi_{yy}(l)\phi_{yy}(l+\tau)} = \frac{2\sqrt{\pi}L\overline{\Delta N^2}\cdot 10^{-12}}{l_0} \exp\left(-\frac{d^2}{{l_0}^2}\right) \tag{38a}$$

$$\overline{\phi_{yc}(l)\phi_{yc}(l+\tau)} = \frac{3\pi L\overline{\Delta N^2}\cdot 10^{-12}}{2l_0} \frac{1}{\left(1+\frac{d^2}{{l_0}^2}\right)^{5/2}}, \tag{38b}$$

with corresponding spectral densities as follows:

$$W_y(f) = \frac{2\pi L\overline{\Delta N^2}\cdot 10^{-12}}{v} \frac{1}{(1+\omega_2^2)^{1/2}} \tag{39}$$

$$W_{yy}(f) = \frac{2\pi L\overline{\Delta N^2}\cdot 10^{-12}}{v} \exp\left(-\frac{\omega_2^2}{4}\right) \tag{39a}$$

$$W_{yc}(f) = \frac{2\pi L\overline{\Delta N^2}\cdot 10^{-12}}{v} \cdot \left[\tfrac{1}{2}\omega_2^2 K_0(|\omega_2|) + |\omega_2| K_1(|\omega_2|)\right]. \tag{39b}$$

The remarks above concerning mean-square values and low-frequency spectral densities apply equally well for the y component. The spectra of (39) are plotted in Fig. 9, facing page.

It is easily shown[15] that $\overline{\phi_x\phi_y}=0$ and thus one can write

$$\overline{\phi^2} + \overline{\phi_x{}^2} + \overline{\phi_y{}^2} = \overline{2\phi_x{}^2} = \overline{2\phi_y{}^2}$$

for the total angular deviation of the ray.

Let us return now to the rotating line-of-sight problem. Using cylindrical coordinates (with the z-axis normal to the page, see Fig. 1), the orthogonal components of angle deviation obtained from (28) are:

$$\phi_z = \int_0^L dl \frac{\partial N_1}{\partial z} \tag{40}$$

$$\phi_\theta = \int_0^L dl \frac{1}{l} \frac{\partial N_1}{\partial \theta}. \tag{41}$$

The autocorrelations of these two functions are thus:

$$\overline{\phi_z(l)\phi_z(l+\tau)} = \int_0^L dl_1 \int_0^L dl_2 \overline{\left.\frac{\partial N}{\partial z}\right|_1 \left.\frac{N}{\partial z}\right|_2} \tag{42}$$

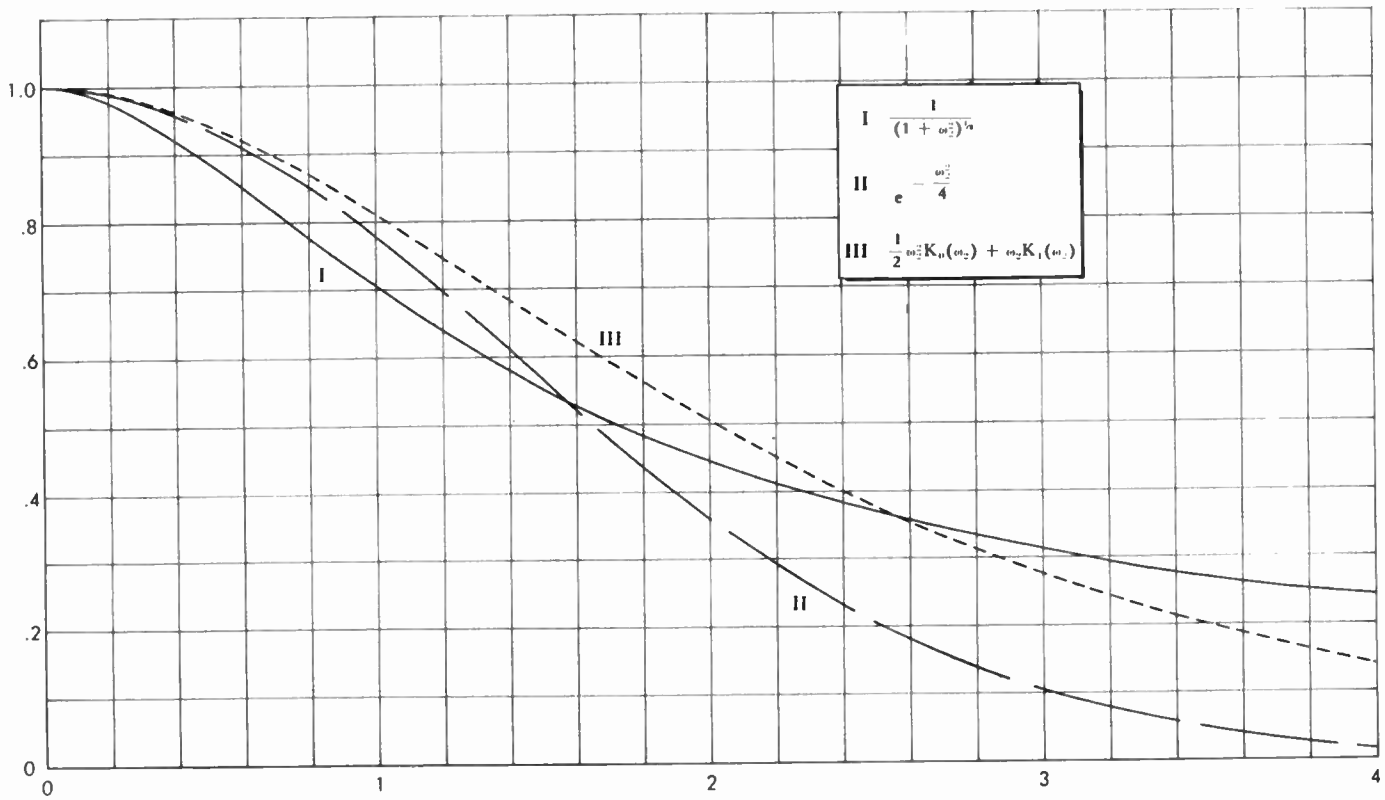

Fig. 9—Power spectra for angle of arrival (y component) for parallel lines-of-sight.

$$\overline{\phi_\theta(t)\phi_\theta(t+\tau)} = \int_0^L dl_1 \int_0^L dl_2 \frac{1}{l_1 l_2} \overline{\frac{\partial N}{\partial \theta}\Big|_1 \frac{\partial N}{\partial \theta}\Big|_2}. \quad (43)$$

In cylindrical coordinates, the distance between two general points (1) and (2) is

$$r_{12} = [l_1^2 + l_2^2 - 2l_1 l_2 \cos(\theta_2 - \theta_1) + (z_2 - z_1)^2]^{1/2}. \quad (44)$$

The gradient correlations in (42) and (43) can be found in terms of derivatives (in cylindrical coordinates) of $C(r_{12})$ as before. Using (2) one has for (42),

$$\overline{\phi_z(t)\phi_z(t+\tau)} = \frac{\overline{N_1^2}}{l_0} \int_0^L dl_1 \int_0^L dl_2 \frac{\exp\left\{-\dfrac{[l_1^2 + l_2^2 - 2l_1 l_2 \cos\theta]^{1/2}}{l_0}\right\}}{[l_1^2 + l_2^2 - 2l_1 l_2 \cos\theta]^{1/2}}. \quad (45)$$

The methods used in integrating (7) may be applied here to yield

$$\overline{\phi_z(t)\phi_z(t+\tau)} = \pi\overline{\Delta N^2}\cdot 10^{-12} \cdot \frac{L}{l_0}\left[K_0(\mu)L_{-1}(\mu) + K_{-1}(\mu)L_0(\mu)\right] \quad (46)$$

with

$$\mu = \frac{L|\theta|}{l_c}$$

the spectrum of this component is

$$W_z(f) = \frac{2\pi\overline{\Delta N^2}\cdot 10^{-12}}{\dot{\theta}} \log \frac{1 + \sqrt{1 + \omega_1^2}}{|\omega_1|}. \quad (47)$$

The orthogonal component ϕ_θ, has autocorrelation and spectrum

$$\overline{\phi_\theta(t)\phi_\theta(t+\tau)} = \frac{2L\overline{\Delta N^2}\cdot 10^{-12}}{l_0} K_0(|\mu|) \quad (48)$$

$$W_\theta(f) = \frac{2\pi^2\overline{\Delta N^2}\cdot 10^{-12}}{\dot{\theta}} \frac{1}{(1 + \omega_2^2)^{1/2}}. \quad (49)$$

The previous remarks made concerning angular deviations apply here also. The mean squares computed from (46) and (48) are infinite and the spectra of (47) and (49) have divergent integrals over an infinite range. The spectra are correct, however, in the vicinity of zero frequency (they do not depend on l_0 in this region) and some filtering in the measuring (or tracking) process will make the results insensitive to the assumed space correlation. The alternate forms are not given since they contribute nothing new.

Probability Density of Phase and Angle-of-Arrival

The phase angles are given (3) as the sum of an infinite number of infinitesimal random quantities. The central limit theorem[17] in probability may be invoked to

[17] H. Cramer, "Mathematical Methods of Statistics." Princeton University Press, Princeton, N. J.; 1946.

show that α will have a normal distribution over an infinite range, with $\overline{\alpha^2}$ given by one of (5), (5a) or (5b). Because phase is ordinarily considered modulo 2π, we must modify the distribution of α accordingly. Writing the normal density with mean-zero and mean-square α^2 in terms of a variable β with $\beta = \alpha \bmod |\pi|$, one has for the probability density of β,

$$p(\beta) = \sum_{n=-\infty}^{\infty} \frac{1}{\sqrt{2\pi\overline{\alpha^2}}} \exp\left[-\frac{(\beta - n\pi)^2}{2\overline{\alpha^2}}\right]; \quad |\beta| < \pi$$

$$= \frac{1}{2\pi}\Theta_3\left(\frac{\beta}{2\pi}, \frac{i\alpha^2}{2\pi}\right); \quad |\beta| < \pi \quad (50)$$

where Θ_3 is a theta function and $i = \sqrt{-1}$. When[18] $[\alpha^2]^{1/2} \ll 2\pi$, (50) reduces to

$$p(\beta) = \frac{1}{\sqrt{2\pi\overline{\alpha^2}}} \exp\left(-\frac{\beta^2}{2\overline{\alpha^2}}\right), \quad (51)$$

where now $\alpha = \beta$.

Angles of arrival are distributed normally by the central limit theorem with mean squares as given previously.

Numerical Estimates and Applications

Some estimates have been made for the parameters which appear in the foregoing expressions. Microwave refractometer flights[8] indicate that ΔN varies between $\frac{1}{2}$ and 1 N units from several hundred to fifteen thousand feet. This altitude range includes most of the tropospheric region in which refractive fluctuations affect propagation. The correlation length l_0 has a ground level value of 20 feet and increases rapidly to an asymptotic value of one or two hundred feet. Since the precise values of l_0 and ΔN vary with both geographic location and time, we shall choose the convenient averages: $\Delta N = \frac{1}{2}$ and $l_0 = 200$ feet. We take $\lambda = 1$ foot and the line-of-sight transmission path length L to be 20,000 feet. The values of L and λ used here are appropriate to the experiments described by Herbstreit.[12]

Substituting the above parameters into (5), we find at 1,000 mc,

$$\alpha_{\text{rms}} = 8.9 \times 10^{-2} \cong 10^{-1} \text{ rad.}$$

This error represents approximately 6° rms thereby posing a genuine problem for systems requiring very high phase stability over the transmission path.

The spectrum of such phase fluctuations is of considerable interest also. Since the characteristic turbulent self-motions (and hence Doppler shifts) are known only in terms of the qualitative picture of eddy degeneration,[4] we have computed spectra for a moving line-of-sight. Consider a rotating path, the spectrum of which is given in Fig. 4. A measure of spectral width is given by $2\pi f l_0/L\dot{\theta} = 1$. If one assumes that the line-of-sight is rotating so as to track an aircraft flying 1,000 fps at an altitude of 20,000 feet (overhead), $\dot{\theta}$ is approximately 0.05 radians per second. Using this with the parameters above, the effective width is approximately 0.8 cps.

A somewhat different model is obtained by considering the spectrum for a line-of-sight moving parallel to itself with speed v through a stationary turbulence configuration, see (4). A measurement of bandwidth is $2\pi f l_0 v = 1$. With $v = 20$ feet per second and $l_0 = 200$ feet, an effective (noise) bandwidth $B = 0.016$ cps is produced. Very near the ground one has $l_0 = 20$ feet so that $B \cong 0.16$ cps.

We have also investigated the angle-of-arrival fluctuations which a ray experiences. The correlation of (2) produces an infinite rms deviation because of its cusp-like behavior at the origin. Other correlations produce

$$\phi_{\text{grms}} \cong 1.3 \times 10^{-2} \text{ milliradians}$$

$$\phi_{\text{crms}} \cong 1.5 \times 10^{-2} \text{ milliradians.}$$

Here the example of the rotating line-of-sight has been used and the two orthogonal components have been combined to give

$$\phi_{\text{rms}} = \sqrt{\overline{\phi_z^2} + \overline{\phi_\theta^2}}.$$

The spectrum widths for deviation of the rays is the same as that for the phase variations if the measures above are used. The foregoing applications have all been to a homogeneous turbulent air mass on the tacit assumption that it is clear (optically) air. It is quite interesting to apply the above results to clouds.

Index of refraction data for clouds are notably sparse. From meteorological measurements and aircraft gust load experience, however, it is known that the interiors of cloud formations are very turbulent and contain relatively large index fluctuations. Extensive circulation and mixing is known to take place within clouds in addition to over-all movement and structural rearrangements.[19,20] Both directional and turbulent currents of very dense water vapor suggests a "tighter" correlation than that found in free air. Records of refractometer flights[21,22] through clouds substantiate this, and indicate that the scale of turbulence is probably of the order 10 to 20 feet. These same records suggest that rms excursions of the index of refraction may be as large as 10 or 20 N units.

To illustrate the foregoing results we shall assume $l_0 = 20$ feet, $L = 5{,}000$ feet, $\lambda = 1.0$ foot, and $[\Delta N^2]^{1/2} = 10$. The rms phase deviation is

$$\alpha_{\text{rms}} = 3 \times 10^{-2}$$

[18] In this paper (and the following), α must be small for the results to be valid.

[19] J. S. Malkus and C. Ronne, Wood's Hole Oceanographic Institution, Ref. No. 54-18; March, 1954.

[20] J. S. Malkus and C. Ronne, Wood's Hole Oceanographic Institution, Ref. No. 55-5; January, 1954.

[21] C. M. Crain, A. P. Deam, and J. R. Gerhardt, "Measurement of tropospheric index-of-refraction fluctuations and profiles," PROC. IRE, vol. 41, pp. 284–190; February, 1953.

[22] G. Birnbaum and H. Bussey, "Measurement of variations in atmospheric refractive index with an airborne refractometer," *NBS Jour. Res.*, vol. 51, p. 171; October, 1953.

Clouds thus constitute an important source of phase deviation for any propagation process.

Appendix

In all of the foregoing, we have imagined the line-of-sight signals to be detected by point receivers. Actual measurements, however, are made with reflectors of finite aperture. One naturally inquires if an extended collector does not smooth out the phase irregularities in the wave front. This effect may be evaluated with the techniques already employed.

Assume a paraboloid of revolution with a collector at the focus. The total field measured at the focus is the sum of all rays reflected to it by the dish. Each of the parallel rays crossing the focal plane is correlated with its neighbor according to the ray separation. The total signal may be represented as the average of all rays collected by the reflector of area A as

$$E_T e^{i\mu+i\phi} = \frac{1}{A}\int dA E_0 e^{i\mu+i\alpha(x,y)} \tag{52}$$

where E_T is total field[23] of phase ϕ and E_0 is the incident field strength of phase α. The integral is over the aperture (taken to be in the x, y plane).

[23] μ is the constant phase delay $2S\cdot 2\pi/\lambda$ for all rays, where S is the focal length.

We assume both α and ϕ to be small and expand the exponentials to get

$$\phi \cong \frac{1}{A}\int dA\alpha(x, y). \tag{53}$$

The mean value of ϕ is zero since $\bar{\alpha}=0$. The mean square can be written in terms of the phase correlation ρ between adjacent (unreflected) rays as

$$\overline{\phi^2} \cong \frac{1}{A^2}\int dA \int dA'\overline{\alpha^2}\rho(|r-r'|), \tag{54}$$

where $|r-r'|$ is the distance between integration area elements dA and dA'.

For mathematical simplicity the Gaussian form for $C(r)$, (2a), will be chosen. This yields

$$\rho = \exp\left(-\frac{|r-r'|^2}{l_0^2}\right)$$

and one obtains from (54)

$$\overline{\phi^2} \cong \overline{\alpha^2}\left(1-\frac{R^2}{l_0^2}+\cdots\right) \tag{55}$$

where R is the radius of the circular aperture. As long as $R \ll l_0$, which will ordinarily be the case, one has $\overline{\phi^2}\cong\overline{\alpha^2}$[2] and the corrections for the dish may be ignored.

Line-of-Sight Propagation Phenomena—II. Scattered Components*

A. D. WHEELON† AND R. B. MUCHMORE†, SENIOR MEMBER, IRE

Summary—**The foregoing[1] investigation of line-of-sight propagation through a turbulent atmosphere is continued and enlarged. Generalizations of the ray calculation to include scattering contributions by off-axis blobs are given. It is found that the previous expressions for rms phase errors are substantially maintained. The dependence of these fluctuations on receiving antenna beamwidth is adduced. These techniques are then applied to estimate phase scintillation for transmission through a rainstorm. Meteorological data are used to relate such errors to rainfall intensity and infer scintillation frequency spectra. Numerical values for these effects are given for representative atmospheric conditions.**

I. Introduction

THE RAY approach to phase scintillation on line-of-sight paths needs to be extended in several ways. The receiving antenna characteristics find no room in such an analysis and we should like to investigate their effect. The previous approximation is really a one-dimensional description in that it considers a stack of horizontally uniform laminas, each with turbulent fluctuations of its dielectric constant. Actually, we know that the turbulent structure is composed of blobs with more or less equal correlation in all directions. Only in so far as the reciever is in the Fresnel (or near) field of a blob can one really regard the blobs as uniform layers.

For wide-beam antennas and for long path lengths, we should expect the blob scattering mechanism to project energy from off-axis volume elements into the receiver. The path difference surplus of these kinked paths over the optical line-of-sight path imply phase shifts which must be added according to the strength of their scattered amplitudes. These problems can be studied by means of a complete field theoretic treatment of the scattering.[2] We shall stop short of this difficult treatment and exploit the now familiar scattering cross-section approximation.[3] The results so obtained are substantially correct and offer a relatively elementary intuitive approach. Unfortunately, the approximations are such that one cannot estimate phase correlations over adjacent paths. These and subsequent restrictions are removed in the fuller analysis.

To discuss multipath phase variations, consider the scattering diagram of Fig. 1 where the wave transmitted at T falls on a turbulent region. The receiver is at the origin, (0). Let x denote the path difference between the scattered (kinked) path and that which lies along the

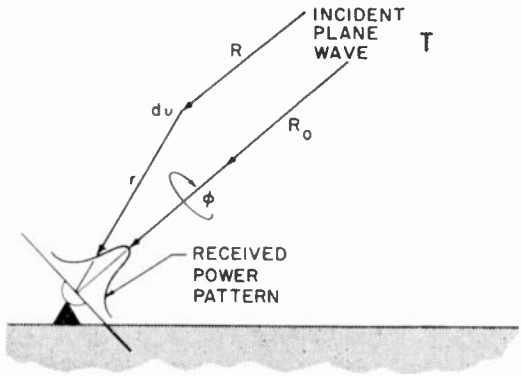

Fig. 1—Multipath propagation by scattering.

axis of symmetry. If $E(x)$ is the amplitude of the wave so-scattered, one may examine the vector voltage combination of $E(x)$ and the primary signal E_0 in Fig. 2 to

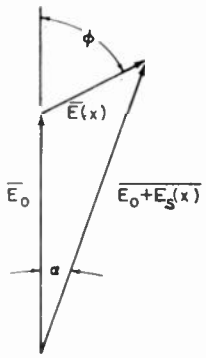

Fig. 2—Vector voltage diagram for superposition of multipath signal.

find that the total phase shift is just the integral over-all path differences of the out-of-phase projection of E_s divided by E_0.

$$\alpha = \int_0^\infty dx \, \frac{E_s}{E_0} \sin\left(\frac{2\pi x}{\lambda}\right). \tag{1}$$

The mean-phase $\bar{\alpha}$ vanishes, since $E_s(x)$ is proportional to $\Delta\epsilon$ in the first Born (single-scattering) approximation and $\overline{\Delta\epsilon} = 0$. The mean-square average is

$$\overline{\alpha^2} = \int_0^\infty dx \int_0^\infty dy \, \frac{\overline{E_s(x)E_s(y)}}{E_0^2} \sin\left(\frac{2\pi x}{\lambda}\right) \sin\left(\frac{2\pi y}{\lambda}\right). \tag{2}$$

* Original manuscript received by the IRE, July 18, 1955.
† Ramo-Wooldridge Corp., Los Angeles 45, Calif.
[1] R. B. Muchmore and A. D. Wheelon, "Line-of-sight propagation phenomena—I. Direct ray," p. 1437, this issue.
[2] A. D. Wheelon, "Near field corrections to line-of-sight propagation," URSI Electromagnetic Wave Symposium, Univ. of Michigan; 1955 and p. 1459, this issue.
[3] H. G. Booker and W. E. Gordon, "A theory of radio scattering in the troposphere," PROC. IRE, vol. 38, pp. 401–412; April, 1950.

The essential assumption for the present development,

$$\overline{E_s(x)E_s(y)} = \overline{E_s^2(x)}\delta(x - y), \tag{3}$$

implies that wave components arriving with path differences greater than one wave length are uncorrelated. This is precisely the assumption made in the scattering theory of Booker and Gordon[2] so that their results fit naturally into the present discussion. Eq. (3) is amply valid for rainfall scattering since the average drop size is several orders of magnitude smaller than the wavelength when using microwaves. If (3) be true, the mean-square-phase error is given by

$$\overline{\alpha^2} = \int_0^\infty dx \sin^2\left(\frac{2\pi x}{\lambda}\right)\overline{\left|\frac{E_s(x)}{E_0}\right|^2}. \tag{4}$$

When $\overline{E_s^2(x)}$ is a slowly varying function of x, one may put $\sin^2(2\pi x/\lambda) \simeq 1/2$ and the total phase is then just one-half the ratio of the total received scattered power to the direct power.[4]

The next problem in reducing (4) is to determine that fraction of power which is scattered to the receiver with path difference x. The differential scattered power received from dv at $\vec{r}$ is given terms of the power incident on that volume element, P_{inc}, and the scattering cross-section σ per unit volume per unit solid angle.

$$dP_s = \sigma \frac{A\cos\theta}{r^2} P_{inc} dv. \tag{5}$$

Here A is the antenna aperture and the spherical coordinates are identified in Fig. 1. The power density P_{inc} incident on dv at a distance ρ from an isotropic transmitter is just P_{tr}/ρ^2. The power which would be received through a vacuum along the direct line (R) connecting transmitter and receiver is $P_{tr} = A/R^2$, so that the ratio of (5) to this "direct power" is independent of the receiver aperture.

$$\frac{dP_s}{P_{tr}} = \left[\frac{R}{\rho}\right]^2 \frac{\sigma\cos\theta}{r^2} dv.$$

The total scattered power ratio is the integral of this expression over all volume included in the receiving antenna's beamwidth.[5]

$$\frac{P_s}{P_{tr}} = \int_V dv \frac{\sigma}{r^2}\cos\theta\left[\frac{R}{\rho}\right]^2. \tag{6}$$

[4] One could derive this result directly, of course, by adding the uncorrelated signals from all volume elements ($dv > l_0^3$) in the beam. Each component signal satisfies the conditions of the central limit theorem and the sum is Gaussian. The in- and out-of-phase components are also Gaussian with standard deviation of $1/\sqrt{2}$ times the total standard deviation which gives the factor 1/2 as above.

[5] The receiver's gain re-enters the problem at this point. To account for the exact lobing patterns of the transmitter and receiver, one may replace the simple cut-off volume V by two antenna pattern functions $[f(\vec{\psi})]^2$ and $[g(\vec{\theta})]^2$ in the integral and run the volume integral over all space. We shall not use this refinement in view of our other approximations.

The fraction of scattered energy arriving with path difference between x and $x+dx$ is:

$$\frac{P_s(x)}{P_{tr}} = \int_V dv \frac{\sigma}{r^2}\cos\theta\delta[x - (r + \rho - r)]\left[\frac{R}{\rho}\right]^2, \tag{7}$$

where $\delta(t)$ is the Dirac delta function. This result forms the basis for our present development. When the transmitter is very far from the receiver and turbulent air mass, the incident wave is essentially plane and one may write (7) in terms of the coordinates of Fig. 1 as:

$$\frac{P_s(x)}{P_{tr}} = \int_V dv \frac{\sigma}{r^2}\cos\theta\delta[x - r(1 - \cos\theta)]. \tag{7a}$$

Eq. (7) may be combined with (4) to give the total phase error,

$$\overline{\alpha^2} = \int_0^\infty dx \sin^2\left(\frac{2\pi x}{\lambda}\right)\int_v dv \frac{\sigma}{r^2} \cdot\cos\theta\,\delta[x - (r + \rho - r)]. \tag{8}$$

Replacing the phase factor by 1/2, we have

$$\overline{\alpha^2} = 1/2\int dv \frac{\sigma}{r^2}\cos\theta, \tag{9}$$

which is just one-half the total scattered-to-direct power ratio (as before).

We shall always assume that the incident wave is plane, corresponding to an infinitely distant source (i.e. $R \simeq \rho$). Gordon has discussed the case in which the blobs stand close to the receiver as well as the transmitter and reader is referred to his results.[6]

The utilization of the scattering cross section in the foregoing calls for a word of caution. Firstly, a cross section is always calculated for points distant from the scattering target and employs asymptotic expansions for the outgoing waves. In the case of line-of-sight propagation, however, all blobs along the path contribute to the scintillation—including those which stand just on top of the receiver. A second problem lies in another approximation of the cross section theory. It is assumed[2,3] in deriving σ that variations in path difference are small compared to a wavelength for volume elements close enough together that $\Delta\epsilon$ is significantly correlated between these elements. This again restricts the theory to a consideration of scatterers which are a long distance from both transmitter and receiver.

II. Turbulence Scattering

The statistical properties of the dielectric fluctuations are defined by:

$$\overline{\Delta\epsilon(r_1)\Delta\epsilon(r_2)} = \overline{\Delta\epsilon^2}\zeta(|\vec{r_1} - \vec{r_2}|). \tag{10}$$

[6] W. E. Gordon, "Investigation of air-to-air and air-to-ground electromagnetic propagation," Res. Rep. EE163,15, Cornell University, Ithaca, N. Y.; September, 1953.

Beginning with the wave equation in a medium with dielectric constant $\epsilon_0+\Delta\epsilon(r)$, Booker and Gordon[3] have shown that the scattering cross section σ per unit volume per unit solid angle per unit incident power density is given in terms of the asymptotic form of the scattered component of the total field by[7]

$$\sigma=\frac{r^2}{V}\overline{\left|\frac{E_s(r)}{E_0}\right|^2}=\frac{k^4}{16\pi^2}\overline{\left|\frac{\Delta\epsilon}{\epsilon_0}\right|^2}\int_V d^3R e^{i\vec{q}\cdot\vec{R}}C(R)\sin^2(\xi). \quad (11)$$

This result follows from assumptions of single scattering and distant scattering volumes.[2] One may write the above integral in terms of $\vec{q}$ centered spherical coordinates.

$$\sigma=\frac{k^4}{16\pi^2}\overline{\left|\frac{\Delta\epsilon}{\epsilon_0}\right|^2}\int_0^\infty dRR^2\int_0^\pi d\theta\sin\theta\int_0^{2\pi}d\phi C(R)e^{iqR\cos\theta},$$

$$=\frac{k^4}{4\pi q}\cdot\overline{\left|\frac{\Delta\epsilon^2}{\epsilon_0}\right|^2}\int_0^\infty dRR\sin(qR)C(R). \quad (12)$$

The radial limits have been relaxed to infinity since $C(R)$ decreases very rapidly for large R. The magnitude of the difference vector is $q=2k\sin\theta/2$, with θ the angle between $\vec{K}_{inc}$ and $\vec{K}_{sc}$. The last step in evaluating (12) is a simple integration in each of the following cases:

A. $C(R)=e^{-|R|l_0/l_0}$

$$\sigma=\frac{\frac{1}{\lambda}\left(\frac{2\pi l_0}{\lambda}\right)^3\overline{\left|\frac{\Delta\epsilon}{\epsilon_0}\right|^2}}{\left[1+4\left(\frac{2\pi l_0}{\lambda}\right)^2\sin^2\left(\frac{\theta}{2}\right)\right]^2}. \quad (13)$$

B. $C(R)=e^{-R^2/l_0l_0}$

$$\sigma=\frac{\sqrt{\pi}}{8\lambda}\left(\frac{2\pi l_0}{\lambda}\right)^3\overline{\left|\frac{\Delta\epsilon}{\epsilon_0}\right|^2}\exp\left[-\left(\frac{2\pi l_0}{\lambda}\right)^2\sin^2\left(\frac{\theta}{2}\right)\right]. \quad (14)$$

C. $C(R)=[1+R^2/l_0^2]^{-2}$

$$\sigma=\frac{\pi}{8\lambda}\cdot\left(\frac{2\pi l_0}{\lambda}\right)^3\overline{\left|\frac{\Delta\epsilon}{\epsilon_0}\right|^2}\exp\left[-2\left(\frac{2\pi l_0}{\lambda}\right)\sin\left(\frac{\theta}{2}\right)\right]. \quad (15)$$

These are the same results obtained, in whole or in part, by Booker and Gordon,[3] Gordon,[4] and Staras,[8] and are repeated here for reference.

Since $l_0\gg\lambda$ for microwavelengths, each of these results represents a strong concentration of scattered energy in the forward direction. This is precisely what one expects from the extremely weak equivalent lens represented by the large blobs, since very little refraction takes place; and, therefore, almost all of the scattered field must go straight ahead. Let us denote the principal scattering cone angle $\lambda/2\pi l_0$ by γ. Either γ or the receiving antenna's beamwidth β is a critical parameter in scattering problems, depending on their relative magnitudes.

We turn now to the problem of estimating the mean-square-phase error given by (8). The simplest calculation is that for an incident plane wave. If the receiving antenna has a half angle β and looks through uniform turbulence (i.e., l_0, $\overline{\Delta\epsilon^2}$ constant throughout the medium) for a distance L, we have for the exponentially correlated model (13):

$$\overline{\alpha^2}=\frac{1}{2}\int_0^L drr^2\int_0^\beta d\theta\sin\theta\cdot\int_0^{2\pi}d\phi\frac{\frac{\cos\theta}{r^2}\cdot\frac{1}{\lambda}\left(\frac{2\pi l_0}{\lambda}\right)^3\overline{\left|\frac{\Delta\epsilon}{\epsilon_0}\right|^2}}{\left[1+4\left(\frac{2\pi l_0}{\lambda}\right)^2\sin^2\left(\frac{\theta}{2}\right)\right]^2}$$

$$=\overline{\left|\frac{\Delta\epsilon}{\epsilon_0}\right|^2}\pi^2\frac{Ll_0}{\lambda^2}\cdot\frac{1}{1+\frac{\gamma^2}{\beta^2}}. \quad (16)$$

If $\gamma=\lambda/2\pi l_0\ll\beta$, we regain the ray theory result of our paper I,[1] but for a factor of two whose significance will be shown later. In the case $\gamma\ll\beta$, the limitation of the scattering cone overrides the acceptance pattern of the receiver by defining an effective scattering volume. If, on the other hand, $\gamma>\beta$, we find

$$\overline{\alpha^2}\cong 4\pi^4\frac{Ll_0^3}{\lambda^4}\cdot\beta^2\overline{\left|\frac{\Delta\epsilon}{\epsilon_0}\right|^2}, \quad (17)$$

which depends explicitly on the antenna characteristics. The effective scattering volume is thus defined by the smaller of the scattering and beamwidth angles. The other correlations give results in essential agreement with these statements.

$$\overline{\alpha_G^2}=\frac{\sqrt{\pi}}{2}\pi^2\frac{Ll_0}{\lambda^2}\overline{\left|\frac{\Delta\epsilon}{\epsilon_0}\right|^2}[1-e^{-\beta^2/4\gamma^2}] \quad (18)$$

$$\overline{\alpha_G^2}=\frac{\pi}{4}\pi^2\frac{Ll_0}{\lambda^2}\overline{\left|\frac{\Delta\epsilon}{\epsilon_0}\right|^2}[1-e^{-\beta/\gamma}(1+\beta/\gamma)]. \quad (19)$$

Each of these phase errors also disagrees with the corresponding calculations of paper I by a factor $\frac{1}{2}$.

It has tacitly been assumed above that $L\gg 2\pi l_0^2/\lambda$ is the criterion that the receiver be in the Fraunhofer (far) zone of the scattering blobs. Only in this case are the approximations inherent in the scattering cross-section derivation valid. If the opposite is true; i.e., if $L<2\pi l_0^2/\lambda$, a different treatment is needed. Now the receiver is in the Fresnel zone of the scatterers and sees

[7] The notation is as follows: r = distance to scattering volume, V = total scattering volume, $k=2\pi/\lambda$, $\vec{q}=\vec{K}_{inc}-\vec{K}_{sc}$ with $\vec{K}_{inc}$ and $\vec{K}_{sc}$ the incident and scattered field propagation respectively. ξ is the angle between the incident electric field vector and K_{sc} (and is close to $\pi/2$ for line-of-sight problems).

[8] H. Staras, "Scattering of electromagnetic energy in a randomly inhomogeneous atmosphere," *Jour. Appl. Phys.*, vol. 23, p. 1152; 1952.

coming toward it not spherical waves from individual scattering elements but plane waves, all going in the same direction as the original wave.

The scattered power in each wave must be calculated differently. The total amount of scattered power per unit incident power density is obtained by integrating σ over 4π solid angle. Taking the Gaussian example, case B,

$$\int \sigma d\Omega = \frac{\sqrt{\pi}}{8\lambda}\left(\frac{2\pi l_0}{\lambda}\right)^3 \overline{\left|\frac{\Delta\epsilon}{\epsilon_0}\right|^2} \int_0^{2\pi} d\phi \int_0^{\pi} d\theta \sin\theta \cdot \exp\left[-\left(\frac{2\pi l_0}{\lambda}\right)^2 \sin^2\frac{\theta}{2}\right]$$

$$= \frac{\pi^{5/2} l_0}{\lambda^2} \overline{\left|\frac{\Delta\epsilon}{\epsilon_0}\right|^2} (1 - e^{-2\pi^2 l_0^2/\lambda^2})$$

$$\cong \frac{\pi^{5/2} l_0}{\lambda^2} \overline{\left|\frac{\Delta\epsilon}{\epsilon_0}\right|^2} \tag{20}$$

where the last assumes $2\pi l_0/\lambda \gg 1$.

The phase of the scattered field relative to the unperturbed field (see Fig. 2) is now more definitely known. Only those scatterers directly in line between transmitter and receiver are effective. The scattered field arises from the induced dipole moment.[3] This dipole moment is produced, not by oscillating charge, but by oscillating displacement current. The scattered field is in phase with the displacement current $\partial D/\partial t$ which is obviously in quadrature with the applied field E. Since no bent paths (with their attendant extra delay) are effective here, the scattered field phase must be either plus or minus $\pi/2$ with respect to E_0. Thus:

$$\alpha = \frac{E_s}{E_0} \tag{21}$$

for E_s small and

$$\overline{\alpha^2} = \frac{\overline{E_s^2}}{E_0^2} = \frac{P_s}{P_0}. \tag{22}$$

The total scattered power divided by P_0 is obtained by integrating (20) along the line-of-sight, which gives:

$$\overline{\alpha^2} = \frac{\pi^{5/2} l_0}{\lambda^2} \overline{\left|\frac{\Delta\epsilon}{\epsilon_0}\right|^2} \int_0^L ds = \frac{\pi^{5/2} l_0 L}{\lambda^2} \overline{\left|\frac{\Delta\epsilon}{\epsilon_0}\right|^2} \tag{23}$$

in agreement with the WKB solution used in paper I. Note that this is twice the result obtained from (13) by letting $\beta/\gamma \gg 1$. Parallel results can be obtained for cases A and C. The factor of two is readily explained. When only plane waves from directly along the line of sight are added, there is no possibility for phase shifts of other than exactly $\pm\pi/2$. If the off-axis scatterers can be counted (when $L \gg 2\pi l_0^2/\lambda$), the phase of E_s with respect to E_0 can take any value. In the limit, half the scattered power has phase in quadrature with E_0 and half is in-phase. Only the portion which is in quadrature has an effect on α and hence (9) contains a factor of $\frac{1}{2}$ and (22) does not.

One very interesting feature of the above is that the parameters enter in the same way in both expressions for $\overline{\alpha^2}$ (near and far zones). The phase shift expressions of paper I then are strictly accurate when $L \ll 2\pi l_0^2/\lambda$ but are very nearly correct at any range where single scattering theory applies.

Another result of the $\pi/2$ phase relation between E_s and E_0 for short paths is that phase shift appears as a first-order effect in the parameter $|E_s/E_0|_1$ while amplitude variation is second order. Thus, one should look for phase fluctuations on short paths instead of amplitude variations when attempting to investigate the properties of the medium. Only when $L \gg 2\pi l_0^2/\lambda$ will amplitude fluctuations begin to show.

The angular distribution of incoming scattered power about the receiver axis may be obtained directly from (6). In terms of our antenna-fixed spherical coordinates:

$$\frac{P_s}{P_{tr}} = \int_0^L dr \int_0^{2\pi} d\phi \int_0^{\beta} d\theta \sin\theta \cos\theta \left(\frac{R}{\rho}\right)^2 \sigma(\theta), \tag{24}$$

and the angular distribution of receiver power is just the integrand of the solid angle $d\Omega = d\theta d\phi \sin\theta$; i.e.

$$\frac{1}{P_{tr}} \frac{dP}{d\Omega} = L\left(\frac{R}{\rho}\right)^2 \sigma(\theta) \cos\theta. \tag{25}$$

This interpretation of the scattering cross section as the received pattern function has been exploited by Booker, Ratcliff, and Shinn[9] and others. We may use this angle weighting function to calculate an equivalent rms angle-of-arrival fluctuation ($R \simeq \rho$)

$$\overline{\delta\theta^2} = \int_0^{2\pi} d\phi \int_0^{\beta} d\theta \sin\theta [L\sigma(\theta) \cos\theta]\theta^2. \tag{26}$$

With the Gaussian cross section (14), we find:

$$\overline{\delta\theta^2} \cong \sqrt{\pi} \overline{\left|\frac{\Delta\epsilon^2}{\epsilon_0}\right|} \frac{L}{l_0} \tag{27}$$

with the assumption that $2\pi l_0/\lambda \gg 1$. This shows that again the result of paper I, while strictly correct only in limited circumstances, is qualitatively correct over a much wider range of parameter values.[10]

The probability densities for phase and angle of arrival were given in paper I and these results still apply. The method of solution of paper I predicts no variation of amplitude at all (in the Fresnel, or near, region). The

[9] H. G. Booker, V. A. Ratcliff, and D. H. Shinn, *Phil. Trans.* (*A*), vol. 262, p. 579; 1950.

[10] Eq. (27) should be compared with paper I.

work just presented shows how the amplitude variations appear.

From Fig. 2, the total amplitude is

$$E_T = \sqrt{E_0^2 + E_s^2} \cong E_0\left(1 + \frac{E_s^2}{2E_0^2}\right). \tag{28}$$

Thus E_T has no variation to first order, and to second order has the density function of E_s^2. Since E_s will be normal, as previously stated, one has the density of the variable part of E_T, $\Delta E_1/E_0$,

$$p\left(\frac{\Delta E_1}{E_0}\right) = \frac{1}{2\sqrt{\pi \frac{\Delta E_1}{E_0}\sigma}} e^{-\Delta E/E_0\sigma}, \tag{29}$$

where $\sigma^2 = \overline{|E_s|^2}$. In the Fraunhofer zone, $\Delta E/E_0$ becomes normal.

III. Rainfall

The theory of multipath transmission through singly scattering media developed in Section II may be exploited to discuss rain-produced scintillation errors as a radar beam traverses a precipitation area. The drops will be idealized as small dielectric spheres; signal perturbations arise from classical Rayleigh scattering. Since the drops are now small compared with the wavelength, one may expect the multipath signal summation (8) to provide an accurate description. The concept of scattering cross section for a given point is now defined quite well and the path difference power density is valid even for large scattering angles. When such results are combined with appropriate meteorological data, the theory predicts the rms phase error for propagation through an arbitrary raincloud. Combining this approach with backscattered signal scintillation measurements, one can predict a frequency spectra for the received power.

Static Multipath Effects

Our description begins with an expression for the scattering by the single droplet illustrated in Fig. 3.

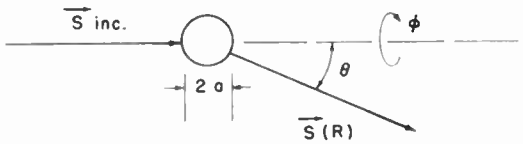

Fig. 3—Scattering of a plane wave by a spherical drop.

Since the raindrops are considered spherical, one may compute the angular distribution of scattered-to-incident power exactly by electromagnetic theory.[11,12] We shall see presently that most raindrops are less than 2 millimeters in diameter so that one may pass directly to the Rayleigh limit ($2\pi a/\lambda \ll 1$) in the microwave region.

$$\left|\frac{E_s(R)}{E_0}\right|^2 = \frac{\lambda^2}{4\pi^2 R^2}\left|\frac{\epsilon - 1}{\epsilon + 2}\right|^2\left(\frac{2\pi a}{\lambda}\right)^4 \cdot [\sin^2(\phi) + \cos^2(\theta)\cos^2(\phi)], \tag{30}$$

represents reradiation by the drop as an electric dipole. The scattering cross section per drop per unit solid angle is this ratio times $4\pi R^2$.

To compute the scattering cross section per unit volume which appears in the multipath density (8), one must estimate the number of drops per unit volume in each radius interval (da). Rigby and Marshall have fitted the exponential function (31) to meteorological experiments.[13]

$$\frac{dN}{dadv} = c\exp -\left[\frac{2a}{b}\right]\frac{\text{drops}}{(cm)(cm)^3}. \tag{31}$$

Their normalization constant c is roughly 0.08 and the "drop scale size parameter" b is given in terms of the rainfall rate R (measured in millimeters per hour), by

$$b = \frac{R^{0.21}}{41}(cm). \tag{32}$$

Table I correlates R and b with familiar precipitation intensities.

TABLE I
Rainfall Rate Versus Drop Scale Size

Rain Type	R	b
Drizzle	0.25 mm/hour	0.018 cm
Light rain	1.00 mm/hour	0.024 cm
Moderate rain	4.00 mm/hour	0.033 cm
Heavy rain	10.00 mm/hour	0.040 cm
Very heavy rain	16.00 mm/hour	0.044 cm
Very heavy rain	20.00 mm/hour	0.046 cm
Very heavy rain	25.00 mm/hour	0.048 cm
Very heavy rain	30.00 mm/hour	0.050 cm
Very heavy rain	50.00 mm/hour	0.055 cm
Very heavy rain	100.00 mm/hour	0.064 cm
Very heavy rain	150.00 mm/hour	0.070 cm

Expression (8) for the static multipath power distribution may now be computed by combining (30) and (31) and averaging over-all drop sizes.

$$\frac{P_s(x)}{P_{tr}} = \int_0^\infty dac^{-2a/b}\int_{R1}^{R_2} dr\int_0^\beta d\theta\sin\theta \cdot \int_0^{2\pi} d\phi 4\pi a^2\left|\frac{\epsilon - 1}{\epsilon + 2}\right|^2\left(\frac{2\pi a}{\lambda}\right)^4 \cdot [\sin^2(\phi) + \cos^2(\theta)\cos^2(\phi)] \cdot \delta(x - r(1 - \cos\theta)]\cos\theta. \tag{33}$$

[11] D. E. Kerr, "Propagation of Short Radio Waves," M.I.T. Rad. Lab. Series, McGraw-Hill Book Co., New York, N. Y., vol. 13, p. 445; 1951.

[12] J. A. Stratton, "Electromagnetic Theory," McGraw-Hill Book Co., Inc., New York, N. Y., p. 563; 1941.

[13] E. C. Rigby and J. S. Marshall, "Modification of Rain with Distance Fallen," Scientific Rep. MW-3, MacDonald Phys. Lab., McGill University, Montreal, Canada; January, 1952.

The spherical coordinate system of Fig. 4 has been used to write out the beam-limited volume integral. With (33), one computes the mean-square-phase error in a sinusoidal voltage received at the origin as:

$$\overline{\alpha^2} \simeq 9b^3\left(\frac{2\pi b}{\lambda}\right)^4 \cdot \int_0^\beta d\theta \sin\theta[1+\cos^2(\theta)] \cdot \left|\frac{\epsilon-1}{\epsilon+2}\right|^2 \cos\theta \left\{\frac{R_2-R_1}{\cos(\theta)} - \frac{\sin\left[\frac{4\pi R_2}{\lambda}(\operatorname{Sec}\theta-1)\right]}{4\pi/\lambda} + \frac{\sin\left[\frac{4\pi R_1}{\lambda}(\operatorname{Sec}\theta-1)\right]}{4\pi/\lambda}\right\}. \quad (34)$$

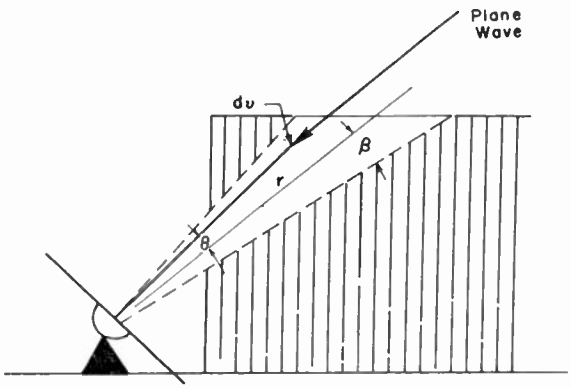

Fig. 4—Coordinates for scattering by rainfall.

The trigonometric terms may be ignored in comparison with the viewing thickness (R_2-R_1), which is again tantamount to replacing the $\sin^2(2\pi x/\lambda)$ factor in (8) by $\frac{1}{2}$.

$$\overline{\alpha^2} \simeq 9b^3\left(\frac{2\pi b}{\lambda}\right)^4\left|\frac{\epsilon-1}{\epsilon+2}\right|^2 (R_2-R_1)\mathfrak{Z}(\beta). \quad (35)$$

$\mathfrak{Z}$ denotes a beam shape factor,

$$\mathfrak{Z}(\beta) = \int_0^\beta d\theta \sin(\theta)\,[1+\cos^2(\theta)] \simeq \beta^2 \text{ for } \beta \ll 1. \quad (36)$$

The result indicates that α_{rms} varies about as the seven-tenths power of the rainfall rate and directly with the square root of the transmission depth. The persistance of the antenna beamwidth β underscores the fact that the scatterers are now small compared with a wavelength and therefore do not provide an "overriding beamwidth" (given for turbulence by $\gamma=\lambda/2\pi l_0$).

To give numerical estimates for (35), we note that the dielectric constant of water varies from $\epsilon=78.5-i$ 12.3 at $\lambda=10$ cm to $34.2-i$ 35.9 at $\lambda=1.24$ cm for $t=18$ degrees C.[14] The corresponding values of $|\epsilon-1/\epsilon+2|^2$ range from 0.9286 to 0.9206, with an average value of 0.925. In Fig. 5, we plot $2/3(R_2-R_1)$ for various wavelengths (λ) and rainfall rates (R). From these curves we read for $\lambda=30$ cm and $R=100$ mm per hour (a very heavy rain)

$$\overline{\alpha^2} \simeq 8\cdot 10^{-9}(m^{-1})\beta^2(R_2-R_1). \quad (37)$$

A typical antenna beam $\beta=4$ degrees and raindepth, $R_2-R_1=3{,}000$ meters gives:

$$\alpha_{\text{rms}} \simeq 2\cdot 10^{-2} \text{ radians}. \quad (37a)$$

This error is an order of magnitude smaller than the corresponding effect of tropospheric turbulence derived in paper I. The sensitivity of (35) to (R_2-R_1) and the rainfall rate R, however, encourage one to estimate local meteorological conditions with some care before attempting precision measurements with small wavelengths.

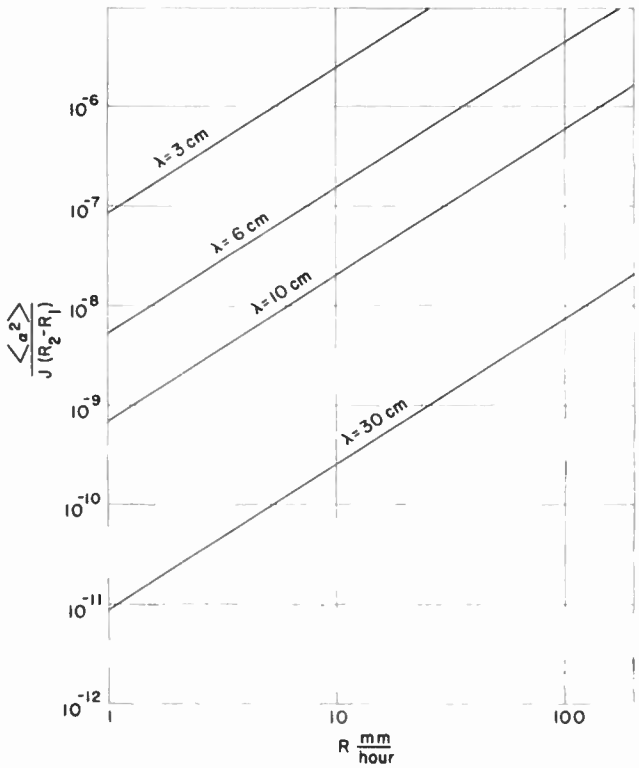

Fig. 5—Rms phase error for scattering by rainfall.

An angular distribution of power about the receiving antenna's pointing direction may be extracted from the total scattered power as before.

$$\frac{1}{P_0}\frac{dP_s}{d\Omega} = \frac{2\pi(6)!}{2^7} c\left(\frac{2\pi b}{\lambda}\right)^4 b^3(R_2-R_1) \cdot [1+\cos^2(\theta)]\left|\frac{\epsilon-1}{\epsilon+2}\right|^2. \quad (38)$$

The corresponding mean-square angle-of-arrival is given by

[14] Kerr, *op. cit.*, p. 610.

$$\overline{\delta\theta^2} = \int_0^{2\pi} d\phi \int_0^{\pi} d\theta \sin\theta(\theta^2)(1+\cos^2\theta)c(R_2 - R_1) \cdots$$

$$= 110c\left(\frac{2\pi b}{\lambda}\right)^4 b^3(R_2 - R_1)\beta^4\left|\frac{\epsilon-1}{\epsilon+2}\right|^2 \cdot \qquad (39)$$

Scintillation Spectra

We should now like to supplement the rms phase error with the frequency spectrum for such phase scintillations. The anomolous signal is compounded from the scatterings by thousands of raindrops in the beam. Time variations of the phase error may be regarded as the composition of Doppler frequency shifts from the individual droplets moving relative to one another in changing order. We may anticipate the magnitude of these frequencies from the Doppler relation: $\Delta f \simeq u/c\ f_0$. For relative drop speeds of one meter per second and $f_0 = 5{,}000$ mc, $\Delta f = 16$ cps, and such a scintillation is evidently of some importance in precision measurements.

We first resolve all drop velocities along the pointing (z) direction of the antenna, as shown in Fig. 6. If the

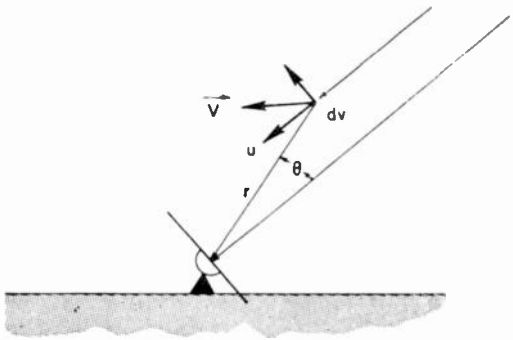

Fig. 6—Drop velocity resolution for Doppler shift analysis.

incident plane wave meets a drop at dv with speed u and reradiates at an angle θ to the incident beam, the net frequency change during the scattering process is $\Delta f = f_0 u/c(1-\cos\theta)$. With the analytical device introduced in (7), one may show that the ratio of the scattered-to-incident power with path difference between x and $x+dx$ and signal frequency between f and $f+df$ is given by:

$$\frac{Q(x,f)}{P_0} = \int_0^{\infty} da N(a) \int_0^{\infty} du P(u\,|\,a) \int \frac{'dv}{r^2}\sigma(a;r,\theta)$$

$$\cdot\delta[x - r(1-\cos\theta]\cos\theta$$

$$\cdot\delta\left[f - f_0 - f_0\frac{u}{c}(1-\cos\theta)\right]. \qquad (40)$$

$P(u|a)$ denotes the conditional probability distribution for a drop with radius a having a velocity component u parallel to the antenna axis. We do not know this density *a priori*, but shall see presently how one may infer it from other propagation experiments.

The integrations of (40) may be performed with relative ease if one assumes $P(u|\alpha)$ to be independent[15] of drop size (a). The scintillation frequencies are given by excursions from the carrier frequency f_0, so that the frequency spectrum is a function of $\nu = f - f_0$. Inserting the appropriate forms for $N(a)$ and σ from (31) and (30) respectively, one finds:

$$\frac{Q(x,\nu)}{P_0}$$

$$= \int_0^{\infty} du P(u) \int_0^{\infty} dace^{-2a/b} \int_0^{\beta} d\theta \sin(\theta) \int_{R1}^{R2} dr \int_0^{2\pi} d\phi$$

$$\cdot\left\{4\pi a^2\left|\frac{\epsilon-1}{\epsilon+2}\right|^2\left(\frac{2\pi a}{\lambda}\right)^4\right.$$

$$\left.\cdot[\sin^2(\phi)+\cos^2(\phi)\cos^2(\theta)]\right\}\cos\theta.$$

$$\cdot\delta[x - r(1-\cos\theta)]\delta\left[\nu - f_0\frac{u}{c}(1-\cos(\theta)\right]. \qquad (41)$$

If one uses this expression to compute the phase error, power spectrum for α^2 emerges without further effort.

$$\overline{\alpha^2(\nu)} = \int_0^{\infty} dx \sin^2\left(\frac{2\pi x}{\lambda}\right)\frac{Q(x,\nu)}{P_0}$$

$$= \frac{\pi}{2}(R_2 - R_1)g(\lambda)\frac{c}{f_0}$$

$$\cdot\int_0^{\beta} d\theta \frac{\sin(\theta)}{1-\cos(\theta)}[1+\cos^2(\theta)]\cos\theta.$$

$$\cdot P\left[\frac{c\cdot\nu}{f_0(1-\cos(\theta)}\right]. \qquad (42)$$

Since the velocity distribution's argument $c/f(1-\cos\theta)^{-1}$ is large for the small values of $(1-\cos\theta)$ inherent in a narrow beam, the net effect is to relegate most of the scintillation power to small frequencies. $g(\lambda)$ denotes a wavelength-dependent term arising from the drop radius averaged cross section.

$$g(\lambda) = \int_0^{\infty} da(ce^{-2a/b})4\pi a^2\left|\frac{\epsilon-1}{\epsilon+2}\right|^2\left(\frac{2\pi a}{\lambda}\right)^4$$

$$\simeq \frac{1}{2}b^3\left(\frac{2\pi b}{\lambda}\right)^4. \qquad (43)$$

To determine the function $P(z)$, we shall make use of experimental data for spectral analysis of precipitation echoes. Fig. 7 (opposite) exhibits backscattering process for a moving drop. A plane wave sent out by antenna θ radians off-axis enjoys a frequency shift $u/c\cos\theta$~both on reception and reradiation. The appropriate variation of (40) for the backscattered amplitudes is

[15] Such an assumption is probably warranted if relative drop motion is due to local gusts and turbulent conditions in rainfall area.

$$\frac{R(x,\nu)}{P_0} = \int_0^\infty daN(a) \int_0^\infty duP(u \mid a) \int' \frac{dv}{r^2} \sigma_{B.Sc.}(a) \cos^2\theta \cdot \delta[x - r(1-\cos\theta)]\delta\left[\nu - 2f_0 \frac{u}{c}\cos\theta\right]. \quad (44)$$

An amplitude scintillation spectrum may be deduced from this form by integrating over (x) and substituting the appropriate backscattering cross section from (30).

$$\overline{B^2(\nu)} = P_0 \int_0^\infty daN(a) 4\pi a^2 \left|\frac{\epsilon - 1}{\epsilon + 2}\right|^2 \left(\frac{2\pi a}{\lambda}\right)^4 \int_0^\infty duP(u) \cdot \int_0^\beta d\theta \sin\theta \int_{R_1}^{R_2} dr \int_0^{2\pi} d\phi \int_0^\infty dx \cdot \delta[x - r(1-\cos\theta)]\cos^2\theta\delta\left[\nu - 2f_0\frac{u}{c}\cos\theta\right]$$

$$= P_0 g(\lambda)\pi(R_2 - R_1)\frac{c}{f_0}\int_0^\beta d\theta \sin(\theta) \cdot P\left[\frac{c\nu}{2f_0\cos(\theta)}\right]\cos^2\theta. \quad (45)$$

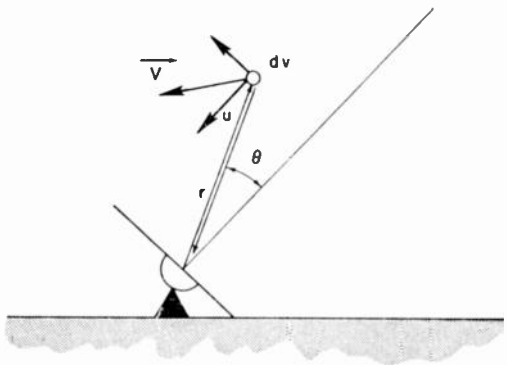

Fig. 7—Echo process for moving drop.

The spectrum normalized to unity at $\nu = 0$ is simply,

$$G(\nu) = \frac{\int_0^\beta d\theta \sin(\theta) P\left[\frac{c\nu}{2f_0\cos(\theta)}\right]\cos^2\theta}{P(0)[1-\cos\beta]}. \quad (45a)$$

The small (<4 degree) values assumed for β permit one to replace $\cos\theta$ by unity and thus extract $P(z)$ from within the integrand.

$$P\left[\frac{2c}{2f_0}\right] \simeq P[0]G(\nu). \quad (46)$$

This important relation permits one to infer the velocity distribution of raindrops from the experimental[16] echo fluctuation spectra $G(\nu)$. In Fig. 8 we reproduce the measurements of Goldstein and others[17] for $\lambda = 9.2$ cm, as measured on three occasions. These curves give just the normalized (Doppler) frequency power density of the backscattered amplitudes, $G(\nu)$.

Our integral expression (42) for the phase error may now be combined with (45a) and (46) to yield:

$$\overline{\alpha^2(\nu)} = \frac{\pi}{2}(R_2 - R_1)g(\lambda)\frac{c}{f_0}P(0)\int_0^\beta \frac{d\theta \sin\theta}{1-\cos\theta}\cos\theta \cdot [1\cos^2\theta]G\left[\frac{2\nu}{1-\cos\theta}\right]. \quad (47)$$

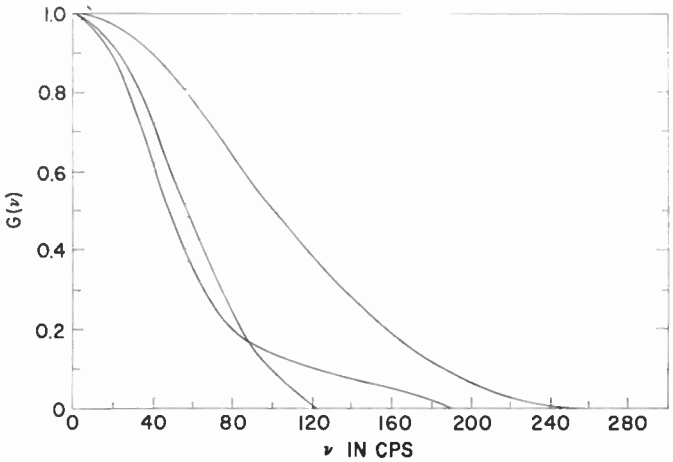

Fig. 8—Power frequency spectrum of the fluctuations of precipitation echo on 9.2 cm as measured on three occasions.

The remaining integration has been performed numerically using the values for $G(\nu)$ given by Fig. 8. In Fig. 9, we plot the normalized[18] spectrum for several beamwidths (β). These curves emphasize the concentration of power at low frequencies.

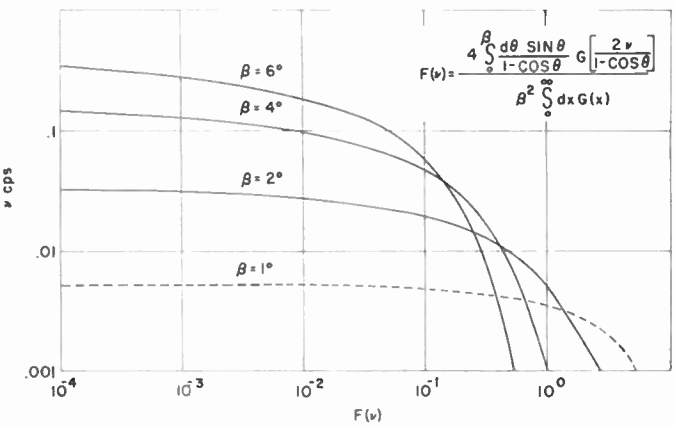

Fig. 9—Phase-error spectra for rainfall scattering.

One may also compute a phase angle spectrum by considering an ensemble of drops falling through stagnant air under gravity. The viscous drag force predicts greater fall speeds for heavy drops than for light ones. Small spheres $(a < 0.008$ cm) obey Stoke's law for steady-state terminal velocity. Very large drops are relatively unstable and tend to break up into smaller ones during long descents. The intermediate region is of some interest for this study, in view of the drop scale

[16] Note that (46) is independent of the beamwidth (β) used in these experiments.

[17] Kerr, *op. cit.*, p. 576.

[18] Normalized so that $\int_0^\infty d\nu \overline{\alpha^2}(\nu) = 1$.

sizes listed in Table I. Gunn and Kinzer[19] have measured the terminal velocities of drops with diameters in the range $0.01 < D. < 0.68$ cm. Their results may be summarized by an approximate formula,

$$v(\alpha) = v[1 - e^{-\Lambda a}], \tag{48}$$

with $v = 1{,}020$ m per sec and $\Lambda = 5.04$ cm^{-1}. The conditional probability density for the distribution of velocities with fixed radius (α) may be given explicit form in terms of (48).

$$P(u \mid \alpha) = \delta[\vec{u} - \vec{k} \cdot v(a)]. \tag{49}$$

If the angle between the local vertical (i.e., k) and the antenna's pointing is denoted by γ,

$$\begin{aligned}\overline{\alpha^2(\nu)} &= \int_0^\infty dx \sin^2\left(\frac{2\pi x}{\lambda}\right) \int_0^\infty daN(a) \\ &\cdot \int_0^\infty du\delta[u \sec \gamma - v(a)] \\ &\cdot \int_0^\beta d\theta \sin\theta \int_{R_1}^{R_2} dr \int_0^{2\pi} d\phi\sigma(\theta, \phi; a) \\ &\cdot \delta[x - r(1 - \cos\theta)] \cos\theta\delta\left[\nu - f_0 \frac{u}{c}(1 - \cos\theta)\right] \\ &\simeq 4\pi^2(0.08)(R_2 - R_1)\frac{c}{f_0}\left|\frac{\epsilon - 1}{\epsilon + 2}\right|^2 \\ &\cdot \int_0^\infty daa^2 \left(\frac{2\pi a}{\lambda}\right)^4 \frac{e^{-(2a/b)}}{v(a)}.\end{aligned} \tag{50}$$

The scintillation frequency (ν) persists in the (drop-size) integration condition,

$$v(a) > \frac{c\nu}{f_0} \frac{\sec\gamma}{1 - \cos\beta}. \tag{51}$$

If the curve-fitted function (48) is inserted, the (origin-normalized) phase spectrum becomes:

$$F(\nu) = \frac{\int_\xi^\infty da \dfrac{a^6 e^{-(2a/b)}}{1 - e^{-\Lambda a}}}{\int_0^\infty da \dfrac{a^6 e^{-(2a/b)}}{1 - e^{-\Lambda a}}}, \tag{52}$$

with

$$\xi = \frac{1}{\Lambda} \ln\left|1 - \frac{\nu c}{K f_0} \cdot \frac{\sec\gamma}{(1 - \cos\beta)}\right|. \tag{52a}$$

It is clear from this form that all frequencies greater than

$$\nu_{\max} = \frac{K}{c} f_0 \cos\gamma (1 - \cos\beta)$$

are eliminated in (52). We may estimate this cut-off by assuming: $f_0 = 5{,}000$ mc, $\cos\gamma = 0.4$, $\beta = 4$ degrees, $K = 10^3$ m per sec, so that $\nu_{\max} = 16$ cps. The quotient (52) was computed numerically for moderately heavy rain, $R = 4$ mm per hour and is displayed in Fig. 10 for the range $0.01 < \nu < 16$ cps. It would be very valuable to perform a controlled experiment measuring line-of-sight and echo scintillations simultaneously within the same rainstorm. Such a test could criticize the result (45a) and perhaps give information on the mixture of turbulent and free-fall drop motion within rainstorms.

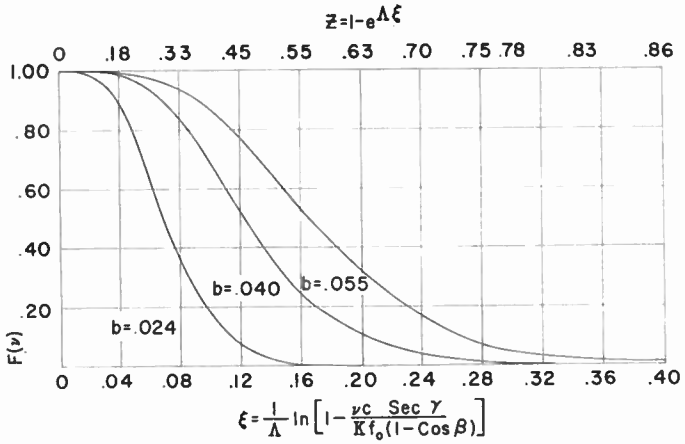

Fig. 10—Phase-error spectra for scattering by freely falling drops.

Ray Bending in Rainstorms

In addition to scattering off-axis energy into the antenna, a rainstorm will act as a prism and bend rays passing through it. If the drop sizes are small compared with the wavelength of the incident radiation, the equivalent index of refraction for a collection of perfect dielectric spheres is:

$$\eta = 1 + 2\pi a^3 N_a. \tag{53}$$

Where a is the sphere radius and N_a the number of spheres per unit volume, one may use (31) to average this expression over all drop sizes.

$$\bar{\eta} \simeq 1 + 0.2b^4 \tag{54}$$

For a heavy rain $R = 10$ mm per hour, and $b = 0.04$, so that

$$\bar{\eta} \simeq 1 + \tfrac{1}{2}10^{-6}. \tag{55}$$

The bending at entrance and exit of a ray passing through such a region can be computed with standard techniques.

When the drop spacing is small compared with the wavelength, one must exploit a detailed picture of the scattering processes. H. C. Corben[20] has performed such an analysis and concludes that the essential factors in (54) are preserved. He finds that multiple scattering may be disregarded for most applications.

[19] R. Gunn and G. D. Kinzer, "The terminal velocity of fall for water droplets in standard air," *Jour. of Meteorology*, vol. 6, p. 243; August, 1949. Their experiments were performed under 760 mm pressure, with a temperature of 20 degrees C. and relative humidity of 50 per cent.

[20] Private communication, August, 1954.

Near-Field Corrections to Line-of-Sight Propagation*

A. D. WHEELON†

Summary—**This study considers the line-of-sight propagation of electromagnetic waves in a turbulent medium. Interest here centers on the received signal's phase stability. The field equation describing propagation through a region characterized by random dielectric fluctuations is first developed. Solutions of this equation which represent the scattered field are derived with ordinary perturbation theory. These solutions are next used to calculate the rms phase error for an arbitrary path in the troposphere. This approach includes both a three dimensional and near-field description for the multipath, scattered amplitudes; thereby overcoming the limitations of previous treatments. The phase correlation between signals received on two parallel transmission paths is derived last to illustrate the role of overlapping antennae beams.**

I. Introduction

SCIENTISTS and engineers alike have displayed considerable interest in the recent success of microwave communication links operating well beyond the horizon. The propagation mechanism is presumably a scattering from turbulent fluctuations of the troposphere's dielectric constant.[1,2] As do all natural phenomena, however, this scattering presents both opportunities and limitations. I shall focus this study on the restrictions which such fluctuations impose on ordinary line-of-sight propagation.

The reality of troposphere scatter forces are to abandon the usual idealization of line-of-sight propagation to vacuum transmission. One must now anticipate that both phase and angle-of-arrival scintillations will arise from random variations of the atmosphere's dielectric constant. Such effects are evidently of prime importance when one asks for the ultimate accuracy of radio location schemes and high speed communication systems. The phase fluctuations on a single tropospheric path were first estimated using a rectilinear transmission (i.e., geometrical optics) approximation,[3]

$$\langle \alpha^2 \rangle \simeq \pi^2 \langle \Delta\epsilon^2 \rangle \frac{L l_0}{\lambda^2}, \qquad (1)$$

where $\langle \Delta\epsilon^2 \rangle$ is the mean square excursion of the dielectric constant from unity, l_0 is the turbulence scale length, L denotes the transmission distance and λ is the incident radiation's wavelength. The contributions of multipath signals scattered by off line-of-sight turbulence structures can only be calculated with a full three dimensional description of the scattered field. This extension was made in a second study[4] using the cross section approximation. This latter approach relies on asymptotic expansions for the outgoing waves and is valid only when one measures the field at great distances from the scattering centers—as in scatter communication.

Line-of-sight propagation, however, is influenced by all turbulent "blobs" on the path, including those just next to the receiving antenna. The following development removes the distant field restriction by providing a field description valid throughout the transmission volume. Calculations of phase error and phase correlation are based on an expansion of the total field in powers of the dielectric fluctuations; corresponding to treating single, double, triple, etc. scattering as successive approximations. The incident field is assumed to be a simple plane wave and the received signal is to be measured with a moderately well defined antenna pattern. Using principally the single scattering approximation, analytic expressions are then derived for the signal stability on an arbitrary path.

We shall frequently wish to facilitate and illustrate our calculations with typical turbulence parameters. Direct measurements of the troposphere's dielectric excursions with an airborne microwave refractometer[5] give several parts in 10^6. The associated scale length seems to vary between one and five hundred feet. For continuing reference, we shall choose $l_0 = 200$ feet and $\langle \Delta\epsilon^2 \rangle = 10^{-12}$, quite arbitrarily. Herbstreit and Thompson have described a series of most interesting experiments which were established to measure line-of-sight signal variations directly.[6] The path length in these experiments is almost 20,000 feet and the principal transmitter frequency 1,000 mc. We shall use these values in concert with the above to provide theoretical estimates for the rms phase errors on a single path and the phase correlation between parallel paths.

II. The Propagation Equation

One may represent the troposphere's electromagnetic properties by a single phenomenological parameter—its dielectric constant. We shall therefore concentrate

* Original manuscript received by the IRE, July 7, 1955. Presented at the URSI "Symposium on Electromagnetic Wave Theory," University of Michigan, Ann Arbor, Mich.; June, 1955. To be published in TRANS. IRE, vol. AP-3, reprinted by special request of the sponsors of this issue.

† Ramo-Wooldridge Corp., Los Angeles 45, Calif.

[1] H. G. Booker and W. E. Gordon, "A theory of radio scattering in the troposphere," PROC. IRE, vol. 41, p. 401; April, 1950.

[2] F. Villars and V. F. Weisskopf, "The scattering of electromagnetic waves by turbulent atmospheric fluctuations," *Phys. Rev.*, vol. 94, p. 232; April, 1955.

[3] R. B. Muchmore and A. D. Wheelon, "Line-of-sight propagation phenomenon, I. Ray treatment," p. 1437, this issue.

[4] A. D. Wheelon and R. B. Muchmore, "Line-of-sight propagation phenomenon, II. Scattered component," p. 1450, this issue.

[5] C. M. Crain, A. W. Straiton, and C. E. vonRosenberg, "A statistical survey of atmospheric index-of-refraction variation," TRANS. IRE, vol. AP-1, p. 43; October, 1953.

[6] J. W. Herbstreit and M. C. Thompson, "Measurements of the phase of signals received over transmission paths with their electrical lengths varying as a result of atmospheric turbulence," p. 1391, this issue.

our first effort on developing the field equations which describe propagation through a dielectric medium. Let us decompose the time and space varying dielectric constant into its mean (unit Gaussian) value and a stochastic function to describe turbulent fluctuations of the medium.

$$\epsilon(\bar{r}, t) = 1 + \Delta\epsilon(\bar{r}, t). \tag{2}$$

The anticipated deviations from plane wave, phase stable transmission arise from the random variation $\Delta\epsilon \cong 10^{-6}$.

The starting point for any realistic description of electromagnetic propagation is Maxwell's equations. We shall consider these relations in a region characterized by unit permeability and the dielectric constant (2). In the lower atmosphere permanent charge and current densities are both sensibly absent, so that

$$\overline{\nabla} \times \overline{H} = \frac{1}{c} \frac{\partial \overline{D}}{\partial t} \tag{3}$$

$$\overline{\nabla} \times \overline{E} = -\frac{1}{c} \frac{\partial \overline{B}}{\partial t} \tag{4}$$

$$\overline{\nabla} \cdot \overline{B} = 0 \qquad \overline{\nabla} \cdot \overline{D} = 0, \tag{5}$$

where,

$$\overline{B} = \overline{H} \quad \text{and} \quad \overline{D} = \epsilon \overline{E}. \tag{6}$$

The magnetic field may be eliminated in this system to yield:

$$\nabla^2 \overline{E} - \frac{1}{c^2} \frac{\partial^2}{\partial t^2} (\epsilon \overline{E}) = \overline{\nabla}(\overline{\nabla} \cdot \overline{E}). \tag{7}$$

Time derivatives here operate principally on $\overline{E}$, since the atmospheric fluctuations represented by $\Delta\epsilon$ are considered very active if they rearrange themselves in a fraction of a second. If we denote the propagation constant by $K = \omega/c = 2\pi/\lambda$, the resulting equation is

$$[\nabla^2 + K^2(1 + \Delta\epsilon)]\overline{E} = \overline{\nabla}(\overline{\nabla} \cdot \overline{E}). \tag{8}$$

We recognize the anomalous refraction effect in $K^2\Delta\epsilon$. The phase scintillations produced in a plane wave by this term have been investigated previously.[3] This same term's ability to scatter energy completely out of the primary (plane) wave implies that volume elements which do not lie directly on the rectilinear path can also contribute to the received signal's stability. Our interest will center on this latter problem. Before we can proceed, however, we must provide a brief interpretation for the divergence term $\overline{\nabla}(\overline{\nabla} \cdot \overline{E})$ in (8). If we combine (6) and (7), one finds,

$$\overline{\nabla} \cdot \overline{E} = -\frac{1}{\epsilon} \overline{E} \cdot \overline{\nabla}\epsilon \tag{9}$$

so that the gradient of this expression becomes:

$$\overline{\nabla}(\overline{\nabla} \cdot \overline{E}) = \frac{\overline{\nabla}\epsilon}{\epsilon}\left(\overline{E} \cdot \frac{\overline{\nabla}\epsilon}{\epsilon}\right) - \frac{1}{\epsilon}(\overline{E} \cdot \overline{\nabla})\overline{\nabla}\epsilon$$

$$- \frac{1}{\epsilon}(\overline{\nabla}\epsilon \cdot \overline{\nabla})\overline{E} - \frac{1}{\epsilon}\overline{\nabla}\epsilon \times (\overline{\nabla} \times \overline{E}).$$

Since each of these terms is already of order $\Delta\epsilon$, one may replace $\overline{E}$ with the incident plane wave $\overline{E}_0 = E_0 \bar{j} e^{iKz}$.

$$\overline{\nabla}(\overline{\nabla} \cdot \overline{E}) \simeq E_0 e^{iKz} \cdot \left\{ \bar{k} \frac{1}{\epsilon} \frac{\partial \epsilon}{\partial y} iK + \frac{1}{\epsilon^2} \frac{\partial \epsilon}{\partial y} \overline{\nabla}\epsilon + \frac{1}{\epsilon} \frac{\partial}{\partial z} \overline{\nabla}\epsilon \right\}.$$

Squares and derivatives of $\overline{\nabla}\epsilon$ may usually be neglected in comparison with the normal gradient.

$$\overline{\nabla}(\overline{\nabla} \cdot \overline{E}) \simeq \bar{k} E_0 e^{iKz} \cdot iK \frac{1}{\epsilon} \frac{\partial \epsilon}{\partial y}. \tag{10}$$

This vector is directed along the incident field's propagation path, so that its composition with the primary wave distorts the phase front. This is simply equivalent to bending the incident beam, and its dependence on the normal gradient of ϵ provides contact with a similar result of geometrical optics. We must now contrast (10) with the anomalous refractive term in (8). The ratio of their magnitudes is $R = 2\pi\lambda/\Delta\epsilon \cdot \partial\epsilon/\partial y$, so that one may disregard the divergence term in (8) unless $\Delta\epsilon$ changes by its rms value in one wave length. Correlations of the major turbulence-sponsored dielectric excursions over hundreds of meters[7] ensure that this is quite a good assumption for radio frequencies. The central result of our discussion is familiar linear propagation equation

$$[\nabla^2 + K^2(1 + \Delta\epsilon)]\overline{E} = 0. \tag{11}$$

III. Solution for the Scattered Field

We shall now turn our attention to solving the propagation equation (11) for the scattered field. This task is complicated by the appearance of the stochastic variable $\Delta\epsilon$. We shall proceed as though this were an ordinary function of position, taking ensemble averages only at the end to recover the solution's statistical properties. We shall assume that the $\Delta\epsilon$ represent a Gaussian process with zero mean. The ensemble average of the product of n such variables may thus be expressed in terms of the space correlation function and mean square dielectric fluctuation alone.

$$\langle \Delta\epsilon \rangle = 0$$

$$\langle \Delta\epsilon(r_1)\Delta\epsilon(r_2) \rangle = \langle \Delta\epsilon^2 \rangle C(r_1 - r_2)$$

$$\langle \Delta\epsilon(r_1)\Delta\epsilon(r_2)\Delta\epsilon(r_3) \rangle = 0$$

$$\langle \Delta\epsilon(r_1)\Delta\epsilon(r_2)\Delta\epsilon(r_3)\Delta\epsilon(r_4) \rangle = \langle \Delta\epsilon^2 \rangle^2 \cdot [C(r_1 - r_2)C(r_3 - r_4) + C(r_1 - r_3)C(r_2 - r_4) + C(r_1 - r_4)C(r_2 - r_3)]$$

$$\cdots \text{ etc.} \tag{12}$$

We shall frequently wish to illustrate our results with

[7] Detailed descriptions of turbulent structures indicate that an entire spectrum of blob sizes is present, each with its characteristic dielectric excursion ($\Delta\epsilon \cong l^{2/3}$). This corresponds to an eddy decay scheme in which the initiating turbulent blobs subdivide until frictional forces just absorb their energy (see ref. 2). Although this lowest state has a scale size of the order of millimeters and is thus comparable with a wavelength, its intensity is sufficiently reduced to make it a small effect.

concrete examples. To provide a consistent basis for comparison, we chose the Gaussian model:

$$C(R) = e^{-R^2/l_0^2} \tag{13}$$

to represent the atmosphere's turbulent aspects. The "blob coupling constant" $\langle \Delta\epsilon^2 \rangle$ is a number like 10^{-12}, and provides a convenient expansion parameter.

Iterative Solution

To solve our fundamental field equation (11), we shall first adopt the philosophy of the quantum mechanical Born approximation. Its basic idea is to remove the term $K^2\Delta\epsilon$ to the right-hand side and use plane wave ($\Delta\epsilon = 0$) solutions to initiate an iterative solution. The result is a power series expansion in $\Delta\epsilon$; the zero order term which is simply the incident wave. The term linear in $\Delta\epsilon$ describes single scattering; the quadratic, double scattering, and so on. We first recognize that the solution of (11) characterizes the *total* field E_T.

$$[\nabla^2 + K^2]\overline{E}_T = -K^2\Delta\epsilon\overline{E}_T. \tag{14}$$

This equation may be inverted directly by introducing Green's function and the homogeneous solution added to give:

$$\overline{E}_T(R) = \overline{E}_0(R) + K^2 \int_V d^3r G(R, r)\Delta\epsilon(r)\overline{E}_T(r), \tag{15}$$

where the integration region V includes all volume elements which contribute to the scatter. We separate the total electric field into the incident plane wave E_0 and a scattered component E_s. The integral term in (15) evidently describes this scattered field. In the first approximation, E_T in the integrand is adequately given by the incident field, so that if ζ denotes the angle between E_0 and the scattering direction, the amplitude of E_s is simply:

$$E_s(R) = K^2 \int_V d^3r G(R, r)\Delta\epsilon(r)E_0(r) \sin\zeta + 0(\Delta\epsilon^2). \tag{16}$$

The Green's function appropriate to our problem satisfies,

$$[\nabla^2 + K^2]G(R, r) = -\delta(R - r) \tag{17}$$

and the outgoing wave condition of Sommerfeld, $\lim_{r\to\infty}[\partial/\partial r - iK]G(R, r) = 0$. Explicit and transform representations for $G(R, r)$ are:

$$G(R, r) = \frac{1}{4\pi} \frac{e^{iK|\overline{R-r}|}}{|\overline{R-r}|} \tag{18}$$

and

$$G(R, r) = \frac{-1}{(2\pi)^3} \int d^3p \cdot \frac{e^{i\bar{p}\cdot(\overline{R-r})}}{K^2 - p^2 + i\epsilon} \tag{19}$$

respectively. The second form incorporates a small imaginary term which directs one round the denominator's poles so as to represent outgoing waves.

1. *The Cross Section Approximation.* When one measures the field only at very great distance from the scattering volume V, one may employ the cross section approximation. This approach exploits an asymptotic expansion for the Green's function in (16) and is particularly well suited to "scatter propagation" calculations, in which the common beam transmission volume V is midway between the sender and receiver.[1] If we denote the incident and scattered propagation vectors by $\overline{K}_0$ and $\overline{K}_1$ respectively, it follows that

$$G(R, r) = \frac{e^{iKR}}{R} \cdot e^{-i\overline{K}_1\cdot\bar{r}} + 0(1/R^2). \tag{20}$$

If the incident plane wave is written $\overline{E}_0 = \overline{E}_0 e^{i\overline{K}_0\cdot\bar{r}}$, one may compute the total power scattered to R with the aid of (16) as,

$$|E_s(R)|^2 = \frac{|E_0|^2}{R^2} \cdot \frac{K^4}{16\pi^2} \int_V d^3r_1 \int_V d^3r_2 e^{i\bar{q}\cdot(\overline{r_1-r_2})}\Delta\epsilon(r_1)\Delta\epsilon(r_2) \cdot \sin(\zeta_1)\sin(\xi_2), \tag{21}$$

where $\bar{q} = \overline{K_1 - K_0}$ and $|\overline{K}_1| = |\overline{K}_0| = K = 2\pi/\lambda$. This solution depends on the random $\Delta\epsilon$, so that one must yet average both sides on their ensemble. If one uses the second of relations (12) and a simple change of variable, the customary expression for the scattering cross section per unit volume, per unit solid angle emerges.

$$\sigma = \frac{R^2}{V}\left\langle \left| \frac{E_s(R)}{E_0} \right|^2 \right\rangle = \frac{K^4}{16\pi^2}\langle \Delta\epsilon^2 \rangle \cdot \int d^3\rho e^{i\bar{q}\cdot\bar{\rho}} C(\rho) \sin^2(\zeta). \tag{22}$$

Cross section corresponding to Gaussian model (13) is

$$\sigma = \frac{\sqrt{\pi}}{8\lambda}\langle \Delta\epsilon^2 \rangle \sin^2(\zeta) \left(\frac{2\pi l_0}{\lambda}\right)^3 \cdot \exp - \left(\frac{2\pi l_0}{\lambda}\right)^2 \sin^2(\theta/2), \tag{23}$$

where θ is the angle included between $\overline{K}_0$ and $\overline{K}_1$. Since $l_0 \gg \lambda$ at radio frequencies, the scattered power is concentrated very strongly in the forward direction; the cone of "significant energy" having a half opening of $\lambda/2\pi l_0$ radians.

The scattering cross section finds several important applications. For instance, one may now compute the ratio of scattered to direct powers for line-of-sight propagation as

$$\frac{P_s(R)}{P_0} \simeq \int' dv \frac{\sigma}{r^2}, \tag{24}$$

where the primed volume integration restricts that process to the receiving antenna's acceptance pattern. A conical antenna with half angle $\beta \ll 1$, looking through L meters of uniform turbulence described by (23) measures

$$\frac{P_s(R)}{P_0} = \sqrt{\pi}\pi^2\langle\Delta\epsilon^2\rangle \frac{Ll_0}{\lambda^2} \operatorname{Sin}^2(\xi)\left[1 - e^{-(\pi l_0\beta/\lambda)^2}\right]. \quad (24')$$

Such estimations are always marred by the restriction that one measures this power only at great distances from all centers. It may seem paradoxical that we treat the scattered field with such care, while using a simple angular cutoff (β) for the antenna patterns. The far field of an antenna is reached long before that of the two-hundred-foot blob (lenses), so that we worry first about the transmission medium. Studies of receiver-to-medium coupling effects are deferred to a later publication.

2. *Symmetrical Theory.* We shall now turn to a fuller description of the scattered field. The power received at $\overline{R}$ may be computed without resorting to an asymptotic expansion for $G(R, r)$. In fact, one has only to square (16) and average directly over the $\Delta\epsilon$.

$$\left\langle \frac{P_s(R)}{P_0} \right\rangle = K^4\langle\Delta\epsilon^2\rangle \int_V d^3r_1 \int_V d^3r_2 G^*(R, r_1)G(R, r_2) \cdot e^{i\overline{K}_0\cdot(\overline{r_2}-\overline{r_1})} C(|\overline{r_1 - r_2}|) \sin(\zeta_1)\sin(\zeta_2). \quad (25)$$

The correlation function now knits the two volume integrations together on an equal footing and thereby retains the manifest symmetry of the problem. The cross section approach averages the power scattered from a region of order l_0^3 about a particular point and then sums the contributions of all such points in the beam. Our new casting provides a satisfactory description of the singly-scattered field at all points in space. While its formal and conceptual advantages are evident, the computational hazards have increased correspondingly. We shall postpone an exemplary calculation until we discuss phase fluctuations of the received signal—a quantity of considerably more interest.

Multiple scattering corrections to the field may be derived by pursuing the iteration procedure outlined above. This process is now complicated, since volume elements which do not lie in the receiver's beam may take part in the first $n-1$ scatterings. Strictly speaking, one should run the iterated volume integrals over all space for which $\langle\Delta\epsilon^2\rangle$ exists. The vigorous concentration of scattered energy in the forward direction described by our cross section (23) assures us that such scattering combinations are not likely to be important. The doubly-scattered wave correction to (25) may be written out with the help of (12).

$$\left\langle \frac{P_s(R)}{P_0} \right\rangle = K^4\langle\Delta\epsilon^2\rangle \int d^3r_1 \int d^3r_2 G^*(R, r_1)G(R, r_2) \cdot e^{i\overline{K}_0\cdot(\overline{r_2}-\overline{r_1})} C(r_1r_2) + [K^4\langle\Delta\epsilon^2\rangle]^2 \int_V d^3r_1 \int_V d^3r_2 \int d^3r_3 \cdot \int d^3r_4 G^*(R, r_1)G(R, r_2) \cdot G^*(r_1r_3)G(r_2r_4)e^{i\overline{K}_0\cdot(\overline{r_4}-\overline{r_3})} \cdot [C(r_1r_2)C(r_3r_4) + C(r_1r_3)C(r_2r_4) + C(r_1r_4)C(r_2r_3)]. \quad (26)$$

The second-order term here is exceedingly small compared with the first; so that one is led to regard first-order perturbation theory as a sufficient tool. Actually the series is an asymptotic one, in the sense that it converges for the first L/l_0 terms and then begins to diverge. The utility of such representations for actual calculations is well known,[8] so that we shall not labor the point here.

IV. Line-of-Sight Phase Stability

A quantity of central interest for line-of-sight transmission is the rms phase error. We shall imagine a plane wave to fall on a region of turbulent dielectric, as shown in Fig. 1. An elementary approach to the calculation

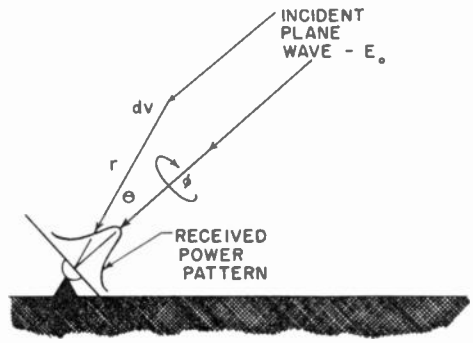

Fig. 1—Multipath propagation via single scattering.

of phase stability is to consider only the energy which is propagated along the antenna's axis.[3,9] The Laplacian operator in (11) may then be specialized to a single direction (s) and the WKB approximation[6] applied to give:

$$E(L) \simeq E(0) \frac{e^{iK\int_0^L ds(1+\Delta\epsilon)^{1/2}}}{(1+\Delta\epsilon)^{1/4}} \cdot \quad (27)$$

The random phase fluctuations are recognized in this exponential form and correspond to alternate accelerations and retardations of the incident wave in traversing the stack of turbulent laminae. One now squares and averages this quantity over the $\Delta\epsilon$ with (12).

$$\langle\alpha^2\rangle = \frac{\pi^2\langle\Delta\epsilon^2\rangle}{\lambda^2} \int_0^L ds_1 \int_0^L ds_2 C(|s_1 - s_2|). \quad (28)$$

With the Gaussian correlation (13), this becomes,

$$\langle\alpha^2\rangle = \sqrt{\pi}\pi^2\langle\Delta\epsilon^2\rangle \frac{L\cdot l_0}{\lambda^2}, \quad (29)$$

[8] P. M. Morse and H. Feshbach, "Methods of Theoretical Physics," McGraw Hill Book Co., Inc., New York, N. Y., vol. I, p. 434; 1953.

[9] P. G. Bergmann, "Propagation of radiation in a medium with random inhomogeneities," *Phys. Rev.*, vol. 70, p. 486; October, 1946.

although one should note that the result here is relatively insensitive to the actual correlation function employed.[3]

The scattered field also contributes to the phase stability of the received signal. Off-axis turbulent blobs project a portion of their scattered energy into the receiving antenna. The greater propagation distances associated with these "kinked" paths implies phase delays for each such contribution. Their composition with the direct signal is illustrated by the vector voltage diagram of Fig. 2. The corresponding phase error is given by the ratio of the scattered field's out-of-phase component to the primary signal E_0.

$$\alpha \simeq \frac{1}{|E_0|} \operatorname{Im}(E_s(R)). \tag{30}$$

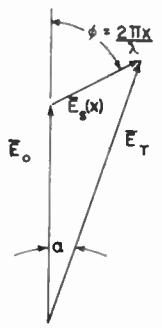

Fig. 2—Vector voltage diagram for superposition of multipath signals, x is the path difference.

One may now substitute the first-order approximation (16) for E_s and introduce the usual incident plane wave.

$$\alpha \simeq \frac{K^2}{4\pi} \int_V d^3r \frac{\Delta\epsilon(r)}{|\bar{R}-\bar{r}|} \sin\left[K|\bar{R}-\bar{r}| + \bar{K}_0'\bar{r}\right]. \tag{31}$$

To evaluate this expression, we choose the origin to coincide with the receiving antenna ($\bar{R}=0$) and erect a system of spherical coordinates on the antenna's axis, as in Fig. 1.

$$\alpha \simeq \frac{K^2}{4\pi} \int_0^L dr r \int_0^\beta d\theta \sin\theta \cdot \int_0^{2\pi} d\phi \Delta\epsilon(r) \sin\left[Kr(1-\cos\theta)\right]. \tag{32}$$

Here L is the transmission distance and β denotes the half-angle of the reception beam.

The mean value of α vanishes identically, since $\langle\Delta\epsilon\rangle = 0$. Its mean square fluctuation survives and is given by a six-fold integral,

$$\langle\alpha^2\rangle = \frac{K^4}{16\pi^2}\langle\Delta\epsilon^2\rangle \int_0^L dr_1 r_1 \int_0^\beta d\theta_1 \sin\theta_1 \int_0^{2\pi} d\phi_1 \int_0^L dr_2 r_2 \cdot \int_0^\beta d\theta_2 \sin\theta_2 \int_0^{2\pi} d\phi_2 \sin\left[Kr_1(1-\cos\theta_1)\right] \cdot \sin\left[Kr_2(1-\cos\theta_2)\right] C(R_{12}). \tag{33}$$

R_{12} is the scalar distance between the two volume elements (1) and (2).

$$R_{12}^2 = r_1^2 + r_2^2 - 2r_1r_2\left[\cos\theta_1\cos\theta_2 + \sin\theta_1\sin\theta_2\cos(\phi_1-\phi_2)\right]. \tag{34}$$

We shall assume a good directional receiver $\beta \ll 1$, so that small angle approximations may be used in (33) and (34). If one sets $r_1 = l_0 x$ and $r_2 = l_0 y$, with $M = L/l_0$ and $p = \pi l_0/\lambda$, it follows that

$$\langle\alpha^2\rangle = \frac{p^4}{\pi^2}\langle\Delta\epsilon^2\rangle \int_0^M dx x \int_0^M dy y \int_0^\beta d\theta_1\theta_1 \int_0^\beta d\theta_2\theta_2 \int_0^{2\pi} d\phi_1 \cdot \int_0^{2\pi} d\phi_2 \sin(px\theta_1^2)\sin(py\theta_2^2) e^{-(x-y)^2} \cdot e^{-xy[\theta_1^2+\theta_2^2-2\theta_1\theta_1\cos(\phi_1-\phi_2)]}. \tag{35}$$

This integral is a formidable one and a Monte Carlo machine sampling procedure immediately suggests itself. Automatic digital computation is made extremely difficult, however, by the very rapid oscillations of the phase (sine) terms and encourage one to attempt the integrations by analytical devices.

We shall evaluate the multiple integral (35) in several interesting limits. The pertinent quantities are βM and βp. The first describes the ratio of the beam's largest (conical) radius to the scale size, and is essentially a measure of the number of blobs in the receiving beam. We found in (23) that $1/p = \lambda/\pi l_0 \simeq \gamma$ represents the cone angle of significant scattered energy from a single blob. Those blobs which project a measurable amount of energy into the receiver must therefore lie within a beam of half angle γ. The effective receiver cone is then the lesser of these angles, so that $p\beta$ must be considered carefully.

1. $\beta M < 1$

When this condition obtains, one may replace the entire second exponential in (35) by unity and perform the angular integrations analytically.

$$\langle\alpha^2\rangle = 4p^2\langle\Delta\epsilon^2\rangle \int_0^M dx \int_0^M dy e^{-(x-y)^2} \cdot \sin^2\left(\frac{px\beta^2}{2}\right)\sin^2\left(\frac{py\beta^2}{2}\right). \tag{36}$$

In the usual physical situation, the scattering beam is much smaller than the receiver's beam ($p\beta > 1$), so that p and not β should appear in the answer. The trigonometric terms in (36) each oscillate very rapidly ($p\beta > 1/M\beta$) with average values of 1/2. The resulting integrations give the rectilinear result,

$$\langle\alpha^2\rangle = \sqrt{\pi} M p^2 \langle\Delta\epsilon^2\rangle = \sqrt{\pi}\pi^2 \frac{Ll_0}{\lambda^2}\langle\Delta\epsilon^2\rangle. \tag{37}$$

To understand this coincidence physically, we note that the greatest conical radius seen by the receiver is less than one scale length, so that the beam sees only small

sections of whole blobs. This sequence of turbulent "plugs" appears as a stack of almost uniform turbulent laminae to the receiver and the problem is substantially one dimensional. Bremmer's derivation[10] of the first WKB approximation from a continuous single transmission (forward scattering in one dimension) picture provides the necessary contact between the two methods of calculation.

The opposite limit, $p\beta=\beta/\gamma<1$ can be evaluated directly by using small argument expansion for the sine terms. This corresponds physically to being always in the near field of *both* the blobs and antenna. Close to the receiver, however, one cannot use a simple (β) cutoff for the antenna pattern, so that we shall omit this case.

(2) $\beta M>1$

The more difficult problem occurs when the receiver sees several blobs across the width of the beam. This is the situation in the Cheyenne Mountain experiments[6] for which $\beta M\simeq 10$. Scintillation then arises from a genuine three-dimensional scattering mechanism and the angular coordinates in the second exponential of (35) cannot be ignored. The azimuthal integrations may be performed to give $4\pi^2 I_0(2xy\theta_1\theta_2)$, which in turn we approximate by its asymptotic form. (The rather more accurate interpolation formula, $i_0(u)=e^u/\sqrt{1+2\pi u}$ is not required here since the factor $xy\theta_1\theta_2$ handles the singularity at the origin.)

$$\langle\alpha^2\rangle \simeq \frac{2p^4}{\sqrt{\pi}}\langle\Delta\epsilon^2\rangle\int_0^M dx\int_0^M dy\int_0^\beta d\theta_1 \cdot\int_0^\beta d\theta_2\sqrt{xy\theta_1\theta_2}\,e^{-(x-y)^2} \cdot\sin\left[px\theta_1^2\right]\sin\left[py\theta_2^2\right]e^{-xy(\theta_1-\theta_2)^2}. \tag{38}$$

The principle contribution to the x, y integrals comes from the diagonal $x=y$. We introduce a factor $\sqrt{\pi}$ to account for the effective cross span of this ridge,[11]

$$\langle\alpha^2\rangle \simeq p^4\langle\Delta\epsilon^2\rangle\int_0^M dx x\int_0^\beta d\theta_1\int_0^\beta d\theta_2\sqrt{\theta_1\theta_2}\,e^{-x^2(\theta_1-\theta_2)^2} \cdot\left\{\cos\left[px(\theta_1-\theta_2)(\theta_1+\theta_2)\right] - \cos\left[px(\theta_1^2+\theta_2^2)\right]\right\}. \tag{39}$$

The experimentally observed increase of phase scintillation with distance leads one to expect $\langle\alpha^2\rangle$ to vary about as M. The x integral must thus depend on running over the large range (M), and not on gathering contribution from small x. When x is large, however, the exponential term is very small unless θ_1 and θ_2 are nearly equal. We may estimate this coalescence directly by rotating the coordinates $\pi/4$ radians: $u=\theta_1-\theta_2$ and $v=\theta_1+\theta_2$.

$$\langle\alpha^2\rangle \simeq \frac{p^4}{2}\langle\Delta\epsilon^2\rangle\int_0^M dx x\int_0^\beta du\int_u^{2\beta-u} dv\sqrt{v^2-u^2}\,e^{-x^2u^2} \cdot\left[\cos(pxuv) - \cos\left(px\frac{u^2+v^2}{2}\right)\right]. \tag{40}$$

For large x, the principle contribution to the u integral comes from small values, so that one may eliminate u from the v limits, square root, and second cosine. With the condition $\beta M>1$ one may now relax β to infinity in the u integration to find,

$$\langle\alpha^2\rangle \simeq \frac{p^4}{2}\langle\Delta\epsilon^2\rangle\int_0^M dx x\int_0^{2\beta} dv v\int_0^\infty du e^{-x^2u^2} \cdot\left[\cos(pxuv) - \cos\left(\frac{pxv^2}{2}\right)\right]. \tag{40'}$$

The second cosine oscillates rapidly and gives zero integral, if $p\beta^2 M\gg 1$. The remaining integrations give

$$\langle\alpha^2\rangle = \tfrac{1}{2}p^2M\sqrt{\pi}\,(1-e^{-p^2\beta^2})\langle\Delta\epsilon^2\rangle, \tag{41}$$

which is exactly the result predicted by cross section theory.[4] In the limit $p\beta>1$, it differs from the rectilinear result (30) only by a factor 1/2.

When the scattering angle $\gamma=1/p$ is greater than the beamwidth, one derives the β-dependent result,

$$\langle\alpha^2\rangle = \frac{\sqrt{\pi}}{2}\cdot\pi^4\,\frac{Ll_0^3}{\lambda^4}\beta^4\langle\Delta\epsilon^2\rangle. \tag{42}$$

This stronger dependence on the frequency is of considerable importance for high resolution antennae or small turbulence scale lengths. Other inequalities amongst the transmission parameters may be evaluated from (35) by similar integration techniques.

The approach given here has the advantage of providing an accurate near-field description. Since blobs which stand close both to the axis and receiver have small path differences and large scattered amplitudes, their phase effect is undoubtedly quite large. Previous treatments[4] of this problem based on the cross section approximation suffer in this critical region. For line-of-sight propagation, the added computational burden of our symmetric formulation seems fully justified. The sufficiency of first-order perturbation theory is argued for by the discussion of (26).

V. Phase Correlation

The use of two-spaced antennae to observe the same transmitter has proven a powerful tool in tropospheric investigations.[6] The phase correlation between two antennae, spaced D meters apart normal to the transmission path, depends only on the ratio D/l_0. If both the single path phase error and phase correlation between two adjacent paths are measured simultaneously, one can determine the two phenomenological scattering parameters l_0 and $\langle\Delta\epsilon^2\rangle$ at once.

[10] H. Bremmer, "The W.K.B. Approximation as the First Term of a Geometrical-optical Series," paper in "Theory of Electromagnetic Waves," Interscience Publishers, New York, N. Y., p. 105; 1951.

[11] Using the formula

$$\int_0^M dx\int_0^M dy f(x,y)e^{-(x-y)^2}\simeq\sqrt{\pi}\int_0^M dx f(x,x)\quad\text{for}\quad M\gg 1.$$

To provide a theoretical estimate of this correlation, one may go to several levels of sophistication. The simplest is that employed in reference (3) to discuss two parallel, rectilinear paths. From Fig. 3 and (28),

$$\langle \alpha_1 \alpha_2 \rangle = \frac{\pi^2}{\lambda^2} \langle \Delta\epsilon^2 \rangle \int_0^L ds_1 \int_0^L ds_2 C(\sqrt{(s_1 - s_2)^2 + D^2}); \quad (43)$$

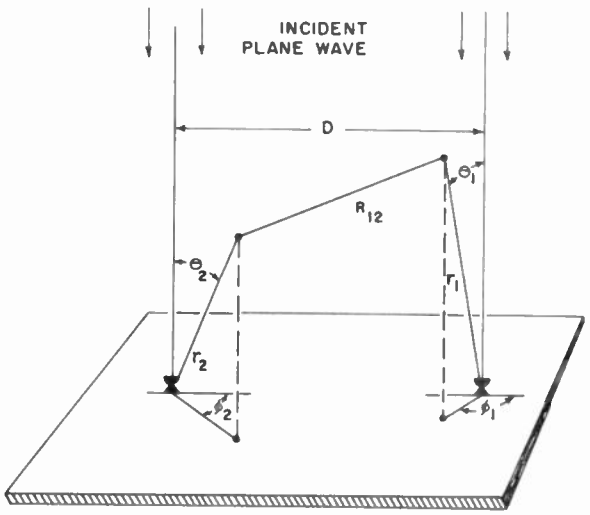

Fig. 3.—Coordinates for calculation of phase correlation between parallel transmission paths.

so that with the turbulence model of (13),

$$\rho_{12} = \frac{\langle \alpha_1 \alpha_2 \rangle}{\langle \alpha^2 \rangle} = e^{-D^2/l_0^2}. \quad (44)$$

The normalized phase correlation is thus a rapidly decreasing function of D/l_0. Such a treatment necessarily neglects the overlapping region of the two receiver's (diverging) antenna patterns; an effect which should tend to increase the correlation (44). A short investigation shows that the cross section approach precludes such a calculation by its very assumptions, so that we must immediately use the symmetrical theory.

One may properly include these common volume elements by simply averaging the product of two disjoint α's. If we establish a system of spherical coordinates on each receiver's pointing direction, one has from (32):

$$\langle \alpha_1 \alpha_2 \rangle = \frac{K^4}{16\pi^2} \langle \Delta\epsilon^2 \rangle \int_0^L dr_1 r_1 \int_0^\beta d\theta_1 \sin\theta_1 \int_0^{2\pi} d\phi_1 \cdot \int_0^L dr_2 r_2 \int_0^\beta d\theta_2 \sin\theta_2 \int_0^{2\pi} d\phi_2 \cdot \sin\left[K r_1 (1 - \cos\theta_1)\right] \cdot \sin\left[K r_2 (1 - \cos\theta_2)\right] e^{-R_{12}^2/l_0^2}. \quad (45)$$

The distance between typical volume elements in beam (1) and (2) is now a rather complicated function of all the variables.

$$R_{12}^2 = D^2 + r_1^2 + r_2^2 - 2r_1 r_2[\cos\theta_1 \cos\theta_2 + \sin\theta_1 \sin\theta_2 \cos(\phi_1 - \phi_2)] - 2D[r_1 \sin\theta_1 \cos\phi_1 - r_2 \sin\theta_2 \cos\phi_2]. \quad (46)$$

The role of the overlapping conical antenna beams may be inferred from this form. The essential competition is between terms which are (at most) of order $(L\beta)^2$ and those of order $L\beta D$. If both are much less than l_0^2, the rectilinear result (44) is rightly regained. If $2L\beta$ is less than D, the two beams do not overlap and one expects few corrections to (44). It is only when both beams see common scattering volumes ($q = D/l_0 < 2M\beta$) that a significant modification should arise. These conditions are represented mathematically by keeping the first and/or second square brackets in (46).

We again assume $\beta \ll 1$ and proceed with the evaluation of (46) according to the value of βM, utilizing the abbreviations introduced after (34). We shall actually calculate the phase correlation $\rho_{12} = \langle \alpha_1 \alpha_2 \rangle / \langle \alpha^2 \rangle$ as a function of $q = D/l_0$, by dividing with the appropriate mean square value from Section IV.

1. $\beta M < 1$

For small beamwidths, one may replace the factor of $r_1 r_2$ by unity in (46) and perform the azimuthal integrations directly. We focus our efforts on values of $p\beta > 1/\beta M$, so that with (37):

$$\rho_{12} = \frac{4p^2 e^{-q^2}}{\pi^2 \sqrt{\pi}\, M} \int_0^M dx x \int_0^M dy y \int_0^\beta d\theta_1 \theta_1 \int_0^\beta d\theta_2 \theta_2 e^{-(x-y)^2} \cdot \sin(p x \theta_1^2) \sin(p y \theta_2^2) I_0[2qx\theta_1] I_0[2qy\theta_2]. \quad (47)$$

Quite a large range of receiver spacings is covered by $q < 1/\beta M$, for which small argument expansion may be used for the Bessel functions and the integrals performed analytically. To first order in q^2,

$$\rho_{12} = \left[1 - q^2 \frac{2M}{p} \sin(pM\beta^2)\right] e^{-q^2}. \quad (48)$$

Since $\beta M < 1$ and $p\beta \gg 1$, M/p is less than unity and the calculated correction to (44) is small. This is in agreement with our previous arguments, since here $q > \beta M$. Larger values of q are quite rare, so that we proceed directly to the next limit.

2. $\beta M > 1$

When $\beta M > 1$, we may encompass a rather large range of q, while satisfying the condition for overlapping beams, $\beta M > q$. Both exponential terms in (46) must now be retained and the first azimuthal integration can be performed immediately.

$$\mu = \int_0^{2\pi} d\phi_1 \int_0^{2\pi} d\phi_2 e^{-2xy\theta_1\theta_2\cos(\phi_1 - \phi_2) - 2qx\theta_1\cos\phi_1 + 2qy\theta_2\cos\phi_2}$$

$$= 2\pi \int_0^{2\pi} d\phi_1 e^{-2qx\theta_1\cos\phi_1} I_0[2y\theta_2\sqrt{x^2\theta_1^2 - 2qx\theta_1\cos\phi_1 + q^2}].$$

One may safely resort to the I_0 function's asymptotic form and invoke the inequality $\beta M > q$ to expand the troublesome square root. The second integral can thus be done to give

$$\mu = \frac{2\pi^2}{\sqrt{\pi x y \theta_1 \theta_2}} e^{2xy\theta_1\theta_2} I_0[2q(x\theta_1 + y\theta_2)], \qquad (49)$$

which is independent of the order of integration employed. When this result is substituted into (45), the form is that for the mean-square phase shift, except for two new factors: e^{-q^2} and $I_0[2q(x\theta_1+y\theta_2)]$. We proceed to collapse the $x-y$ integration as before and rotate the θ_i coordinates by $\pi/4$. With the approximations used in Section IV and $p\beta > 1$,

$$\rho_{12} = \frac{p^2}{M\sqrt{\pi}} e^{-q^2} \int_0^M dx\, x \int_0^{2\beta} dv\, v \cdot I_0[2qxv] \int_0^{\beta} du e^{-x^2\theta^2} \cos(pxuv). \qquad (50)$$

When x is large, the β limit of the u integration may be sent to infinity.

$$\rho_{12} \simeq \frac{1}{2}\frac{p^2}{M} e^{-q^2} \int_0^M dx \int_0^{2\beta} dv v I_0[2qxv] e^{-p^2v^2/4}.$$

The v integral may now be done analytically if one recalls that $p\beta > 1$, which allows 2β to be relaxed to infinity if $p > M$.

$$\rho_{12} \simeq \frac{e^{-q^2}}{M} \int_0^M dx e^{(4q^2/p^2)x^2}. \qquad (51)$$

When q is less than one and $M < p$, one may expand the exponential to find,

$$\rho_{12} \simeq 1 - q^2\left(1 - \frac{4}{3}\frac{M^2}{p^2}\right) + 0(q^4). \qquad (52)$$

Overlapping antennae patterns are thus seen to enhance the phase correlation over that which would be calculated for parallel, disjoint paths. The result is independent of β, since the scattering cone again serves as the effective beamwidth.

When q is greater than one, the integration of (51) needs be performed numerically. Setting $x = Mz$ brings out the essential dependence on $2M/p$. Upper and lower bounds for the correlation are given by:

$$e^{-q^2} \leqq \rho_{12} = e^{-q^2} \int_0^1 dz e^{z^2q^2(2M/p)^2} \leqq e^{-q^2[1-(2M/p)^2]}, \qquad (53)$$

and provide a very good estimate if $2M/p$ is small. When this ratio is one-sixth, the geometrical optics result (44) is verified to within ten per cent over most of the range on q. The integration scheme which leads to (51) breaks down when $2M/p$ reaches one and a new approach is required. The possible combinations of transmission parameters are too numerous to be dealt with exhaustively here. We content ourselves with having studied those cases which correspond to the propagation measurements mentioned at the outset. Further work should probably be directed toward correlation functions other than (13), so as to test the sensitivity of this broader theory to the assumed properties of the turbulence structure.

Acknowledgment

The author wishes to thank R. B. Muchmore, who has given generously both time and thoughtful discussion to this continuing study. G. Culler has played a most valuable role in checking and computing the several lengthy analytical results.

Obstacle Gain Measurements Over Pikes Peak at 60 to 1,046 Mc*

R. S. KIRBY†, MEMBER, IRE, H. T. DOUGHERTY†, ASSOCIATE MEMBER, IRE, AND P. L. McQUATE†

Summary—**Radio transmission loss measurements made over four propagation paths approximately 100 miles in length show the effect of a large mountain obstacle on vhf and uhf ground-to-ground propagation. Recordings of transmission loss were obtained at four sites as a function of receiving antenna height and by mobile measurements along a route normal to the propagation path.**

Measurements for propagation directly over Pikes Peak exhibit the well defined lobing associated with four ray-path diffraction theory. Theoretical approximations based on the Fresnel-Kirchhoff scalar knife-edge diffraction theory predict values of transmission loss and lobe structures which are in good agreement with those observed.

Measurements for propagation to the east and west of Pikes Peak are characterized by lower fields at all frequencies and large fading ranges.

Introduction

MANY INSTANCES of signal enhancement by a large opaque obstacle in a propagation path have been reported in the literature.[1–9] Usually such an obstacle consists of a mountain or a high ridge which lies between the points of transmission and reception. The Fresnel-Kirchhoff approximate theory of diffraction has been employed in some of these instances to provide numerical results which compare favorably with observations when possible ground reflections between obstacle and terminals are taken into account.

It is the purpose of this paper to present the results of a series of transmission loss measurements made over a high mountain obstacle at frequencies from 60 to 1,046 mc. This series of measurements has been made possible by support from the Signal Corps Engineering Laboratories at Ft. Monmouth, New Jersey. Measurements were made on several paths of approximately 100 miles in length, one of which passed directly over Pikes Peak at an elevation of 14,109 feet above sea level. In order to investigate the effect of ground reflections, continuous measurements were made while the receiving antennas were raised from 24 feet to 100 feet above the ground.

When transmission was directly over the summit of Pikes Peak the signals were much higher than they were when the propagation paths passed on either side of the peak. Very little fading was observed in this location and pronounced lobing was evident indicating the presence of strong ground reflections. Values of transmission loss calculated for a knife-edge in place of Pikes Peak and accounting for ground reflections give results which compare very closely to the observed values both in the value of transmission loss and the position of the lobes.

Theoretical Obstacle Gain

When an opaque obstacle of finite extent is placed between the terminal points in a propagation path so that it obscures one end from the other, radio energy arrives at the receiving point by diffraction around and over the edges of the obstacle. This is explained by application of Huygens' principle in which each elementary area of a wave front represents a new source of waves which radiate energy into the area behind the obstacle. The summation of all these elementary contributions is given by the Fresnel integrals as a function of the parameter, v, which depends on frequency and the geometry of the diffraction path. A derivation of the scalar Fresnel-Kirchhoff theory of diffraction directed particularly to radio engineers is presented in the Summary Technical Report of the NDRC Committee.[10]

* Original manuscript received by the IRE, July 11, 1955.

† Central Radio Propagation Laboratory, National Bureau of Standards, Boulder, Colorado.

[1] J. C. Schelleng, C. R. Burrows, and E. B. Ferrell, "Ultra short-wave propagation," PROC. IRE, vol. 21, pp. 427–463; March, 1933.

[2] H. Selvidge, "Diffraction measurements at ultra-high frequencies," PROC. IRE, vol. 29, pp. 10–16; January, 1941.

[3] C. M. Jansky and S. L. Bailey, "Effects of Hills and Trees as Obstructions to Radio Propagation," Report prepared for the National Defense Research Committee; November, 1943.

[4] K. A. Norton and R. S. Kirby, "A Theory of the Effect of Irregularities in Terrain on Radio Propagation at Frequencies Above 300 mc," attached as an appendix to a statement presented by K. A. Norton at the September 20, 1948, Television Hearing before the Federal Communications Commission relative to the comparative coverage to be expected from television broadcasting stations operating in the 50 to 1,000 mc range.

[5] K. A. Norton, M. Schulkin, and R. S. Kirby, "Ground Wave Propagation Over Irregular Terrain at Frequencies Above 50 mc," Reference C to the report of the Ad Hoc Committee of the Federal Communications Commission for the evaluation of the radio propagation factors concerning the television and frequency modulatiom broadcasting services in the frequency range between 50 and 250 mc, June 6, 1949.

[6] J. H. Chisholm, "Measurements of Microwave Diffraction Over Trees," Record of the Symposium of Tropospheric Wave Propagation held at the U. S. Naval Electronics Laboratory, San Diego, California, July 25–29, 1949.

[7] S. Matsuo, "The Method of Calculating VHF Field Intensity and Research on Its Variations," Report of the Electrical Communications Laboratory 621.30.001.6(047.3), Ministry of Telecommunications, Tokyo, Japan; August, 1950.

[8] F. H. Dickson, J. J. Egli, J. W. Herbstreit, and G. S. Wickizer, "Large reductions of vhf transmission loss and fading by the presence of a mountain obstacle in beyond line-of-sight paths," PROC. IRE, vol. 41, pp. 967–969; August, 1953.

[9] T. Kono, Y. Uesugi, M. Hirai, S. Niwa and H. Irie, "Measurement of field intensity of vhf radio waves behind Mt. Fugi," *Jour. Radio Res. Labs.*, vol. 1, pp. 1–16 (Ministry of Postal Services, Tokyo, Japan); June, 1954.

[10] Summary Technical Report of the Committee on Propagation, NDRC, vol. 3, "The Propagation of Radio Waves Through the Standard Atmosphere," Columbia University Press; 1946. This material is also available in the Consolidated Summary Technical Report of the Committee on Propagation of NDRC, "Radio Wave Propagation," by C. R. Burrows and S. S. Attwood, Academic Press, New York; 1949.

The calculations of expected transmission loss over a knife-edge obstacle show that under proper conditions the loss with an obstacle in the propagation path is considerably less than it would be if the obstacle were not there. Fig. 1 shows the results of such a calculation for propagation at 100 mc over a 4/3 earth. A hypothetical case is assumed in which the two terminals of the path are elevated 100 feet above the spherical earth and separated by first 50 miles and then by 150 miles. A knife-edge obstacle is assumed to be located in the center of the path and its height is varied from 0 to 40,000 feet. There are four possible ray paths which can be considered separately and summed up in proper relative phase and amplitude to arrive at the total. It is possible for the energy associated with all four ray paths to arrive almost exactly in phase for certain heights of the obstacle so as to produce a minimum transmission loss. In Fig. 1 the first such obstacle height is about 2,500 feet for the 50-mile propagation path and about 10,000 feet for the 150-mile path. The difference between the values for transmission loss with and without the obstacle, the obstacle gain, is about 24 db for the 50-mile path and 80 db for the 150-mile path.

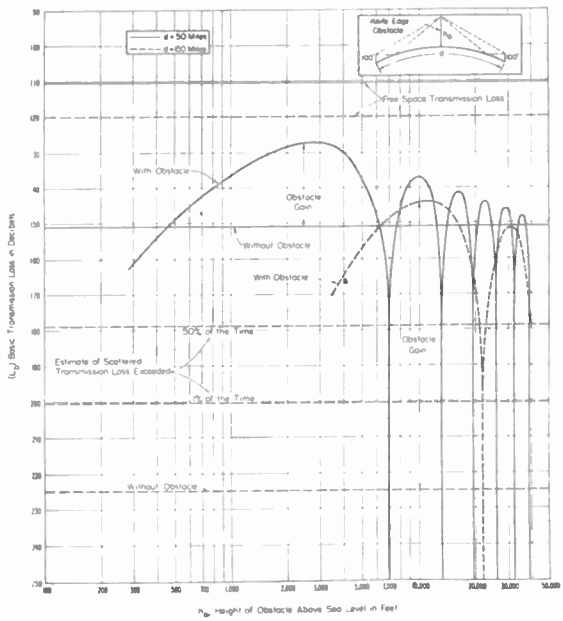

Fig. 1—Theoretical obstacle gains at 100 mc assuming four-ray knife-edge diffraction theory. Transmitting receiving antenna heights each 100 feet above the surface.

Obstacle Gain Measurements

In June of 1953 a series of preliminary transmission loss measurements was made at selected points along Rt. U.S. 50 in the Pueblo-Canon City area of Colorado. The measurements were of the aural transmission from a Denver TV station, KFEL-TV at 59.75 mc. Fig. 2 is a map of the Pikes Peak region showing the location of Pueblo, Canon City, the TV transmitting site on Lookout Mountain and the topography of the intervening terrain.

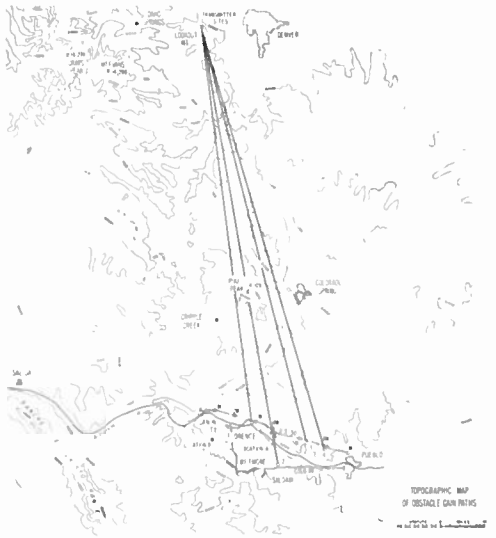

Fig. 2—Topographic map of obstacle gain paths.

The location of the receiving sites for the preliminary measurements are identified in Fig. 2 as locations $1M$ through $7M$ and locations A and B located approximately 100 miles from the transmitter. Fig. 3 is a presentation of the recording charts for two-minute recordings of basic transmission loss[11] made at locations $1M$ through $7M$ with a receiving antenna height of 30 feet.

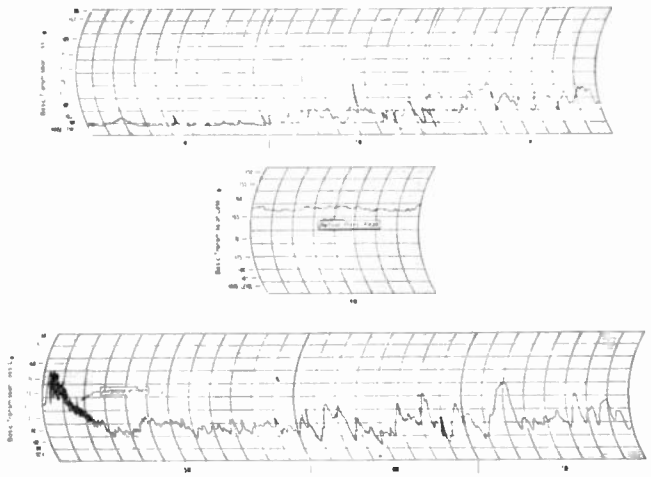

Fig. 3—Chart records of KFEL-TV, 59.75 mc, made along route U. S. 50 at five-mile intervals with an antenna height of thirty feet. Data taken for two minutes at each location, June 4, 1953.

With the exception of location $4M$, for which propagation was very nearly directly over the summit of Pikes Peak as shown on Fig. 2, the recordings exhibit high values of basic transmission loss and severe fading with time. It can be seen that the effect of Pikes Peak is to produce a smaller value of basic transmission loss at location $4M$ as well as a marked reduction in fading with time which is in agreement with the observations of Norton and Kirby.[4] Median values of basic transmis-

[11] K. A. Norton, "Transmission loss in radio propagation," PROC. IRE, vol. 44, pp. 146–152; January, 1953.

sion loss noted are given in Table I below. A decrease in basic transmission loss of 18.9 db at location $4M$ under the average of the other six locations is apparent. Unfortunately, due to an error in maps, the location $4M$ was not exactly behind the peak but was some 4,000 feet eastward. Later when measurements were made directly behind the peak and for the same antenna height the observed basic transmission loss was found to be another 10 db less; i.e., a decrease of about 29 db under the average of the other six locations.

TABLE I

Location	1 M	2 M	3 M	4 M	5 M	6 M	7 M
L_b	192.4	184.3	178.8	162.9	179.5	178.8	177.1

Fig. 4 is a representation of the recording chart for longer time measurements made at locations A and B at a receiver antenna height of 30 feet. Location A, for which propagation is approximately over Pikes Peak, corresponds to location $4M$ and is characterized by the lower basic transmission loss and negligible fading. The recording chart for location B, for which the propagation path lies far west of Pikes Peak, exhibits the characteristics associated with locations $1M$ through $3M$ and $5M$ through $7M$, namely, increased basic transmission loss and pronounced fading.

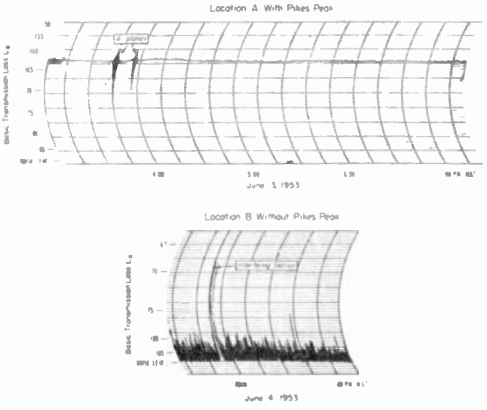

Fig. 4—Slow speed recordings made at 59.75 mc at 96 miles with and without Pikes Peak in the path.

In October and November of 1954 a more detailed series of measurements was made. For these measurements a portable, hydraulic, 100-foot, telescoping mast was employed for reception at four frequencies in the range 59.75 to 1,046 mc. The telescoping mast and mobile recording trailer housing the receiving equipment are shown in Fig. 5. Also clearly visible is Pikes Peak in the center of the photograph approximately 40 miles to the north. The transmitting sources for this series of measurements were the KBTV (191.75 mc) and KFEL-TV (59.75 mc) transmitting antennas located on Lookout Mountain and the National Bureau of Standards portable transmitters operating at 100 mc and 1,046 mc. The NBS portable transmitter installations and antennas are shown in Fig. 6 at their location

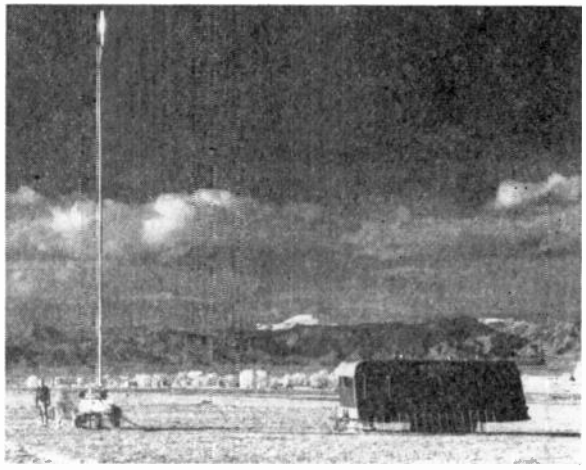

Fig. 5—NBS mobile recording installation in Pueblo-Canon City area. Pikes Peak is in the center of the photograph forty miles distant.

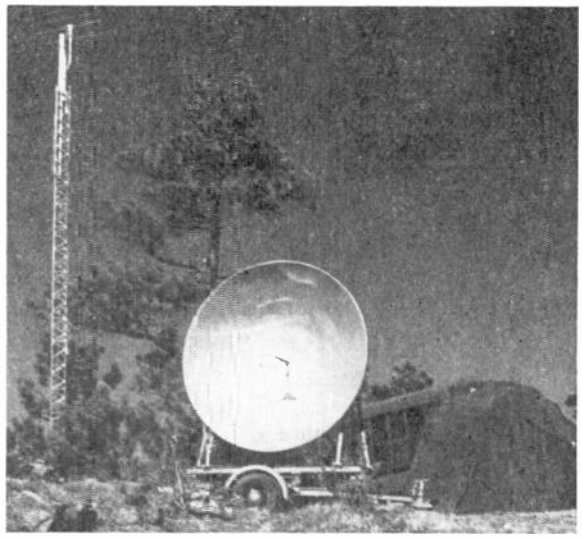

Fig. 6—NBS portable 100 mc and 1046 mc transmitting installation on Lookout Mountain.

on Lookout Mountain. The 1,046 mc antenna is a ten-foot parabolic reflector and the 100 mc antenna is a five-element Yagi array mounted on a thirty-foot mast. Nearby this location, but not shown in the photograph, are the two Denver television transmitting antennas of KFEL-TV and KBTV-TV. The heights above sea level to the center of radiation, total power radiated, antenna gain, and latitude and longitude co-ordinates are given in Table II.

TABLE II

	KFEL-TV 59.75 mc	NBS 100 mc	KBTV-TV 191.75 mc	NBS 1046 mc
Elevation to center of radiation	7421 feet	7340 feet	7615 feet	7320 feet
Power delivered to antenna	8.5 kw	1 kw	11.66 kw	20 watts
Antenna gain relative to an isotropic antenna	9.86 db	8.46 db	12.97 db	25.6 db
Latitude	39°43'59"N	39°43'43.5"N	39°43'46"N	39°43'43.5"N
Longitude	105°14'11"W	105°14'19.3"W	105°14'08"W	105°14'19.3"W

Power available at the receiving antenna was obtained by observing the power available at the receiver terminals and adding to that the power lost in the transmission line to the receiver. Transmission loss in decibels is then defined as 10 $\log_{10}$ (power radiated/power available). The receiving antennas in all cases were half-wave dipoles, with a gain of 2.15 db over an isotropic antenna. Assuming that both the transmitting and receiving antenna gains are realized, the basic transmission loss, or the transmission loss for a system employing isotropic antennas for both transmitting and receiving, can be expressed in decibels as follows:

$$L_b = P_r + G_t + G_r - P_a$$

where

P_r = 10 log (power radiated relative to one watt),
G_t = transmitting antenna gain in db,
G_r = receiving antenna gain in db,
P_a = power available at the receiving antenna.

This is the value used in calibrating all records and in tabulating all the data in this paper.

Measurements

The transmission loss measurements made directly over Pikes Peak and observed at site 2 will be considered first. The variation in observed transmission loss with height of the receiving antenna for each of the four

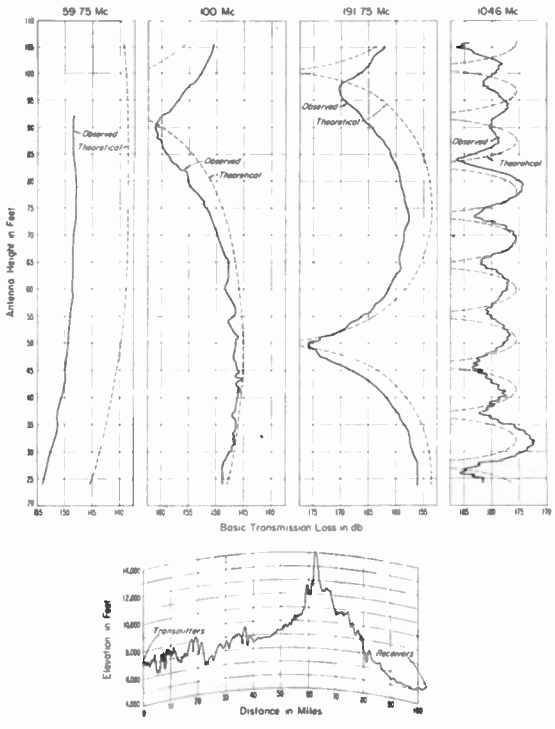

Fig. 7—Variation of transmission loss with receiving antenna height for a 100-mile propagation path obstructed by Pikes Peak.

frequencies is shown in Fig. 7. The profile of the propagation path is shown at the bottom of Fig. 7. Very pronounced lobing is evident at all frequencies observed. At 59.75 mc only a part of the first lobe could be observed at heights up to 92 feet, which is as high as the mast could be raised with the heavy 59.75 mc antenna and transmission line on it. At 100 mc the entire first lobe and part of the second lobe are observed; at 191.75 mc the first, second, and part of the third lobe are observed; and at 1,046 mc a total of nine distinct lobes are observed in going from 24 feet to 105 feet.

Numerical determinations of the expected values of transmission loss as a function of the height of the receiving antennas were made based on Fresnel-Kirchhoff scalar diffraction theory. For the purpose of numerical computation certain simplifications of the profile were made which were more tractable mathematically but which approximate the actual profile near the receiving antennas very closely. Pikes Peak is treated as a knife edge at the same height as the peak and of infinite extent in the horizontal direction normal to the path of propagation; this is justified by the fact that the width of the first Fresnel zone at Pikes Peak for the transmission path from the transmitter to the receiver is only 2,800 feet for the lowest frequency, 59.75 mc, and correspondingly smaller for the higher frequencies. The maximum deviation of Pikes Peak from a knife edge within the first Fresnel zone at 59.75 mc is about 700 feet. A plane reflecting surface is fitted to the terrain in front of the receiver out to a distance which includes the first Fresnel zone for the lowest frequency and the highest receiving antenna height. This plane represents a first-order regression curve fit to the actual terrain and is assumed to have a reflection coefficient of minus one. From the profile, no plausible locations for reflections can be determined to exist on the transmitter end of the path due to the extreme roughness of the mountainous terrain involved, and it is assumed that reflected wave components are negligible on this end of the path.

The theoretical values of expected transmission loss determined from this simplified geometry are shown plotted as dotted lines on Fig. 7. The positions of the lobes calculated for all frequencies correspond very closely to those observed. The values of transmission loss are in agreement within a few decibels with the exception of the measurements of KFEL-TV at 59.75 mc where the lack of agreement is on the order of ten decibels. One possible explanation for this lack of agreement in this case may be in the fact that the KFEL-TV transmitter is located on the north slope of Lookout Mountain, and the line-of-sight from the antenna to Pikes Peak very nearly grazes the top of Lookout Mountain. One might be inclined to add something of the order of an additional six decibels to the theoretical values of transmission loss on this account, but this was not done as it is felt that there is insufficient theoretical procedure to numerically evaluate the effect of Lookout Mountain.

Another way of treating the problem of diffraction is to calculate the expected transmission loss in propa-

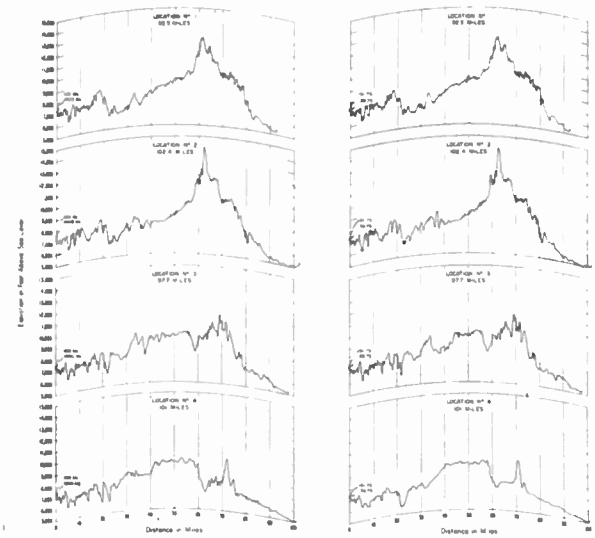

Fig. 8—Profiles of propagation paths from Lookout Mountain transmitters to receiving locations in Pueblo-Canon City area. Correction made for refraction in a standard atmosphere by assuming a 4/3's earth radius.

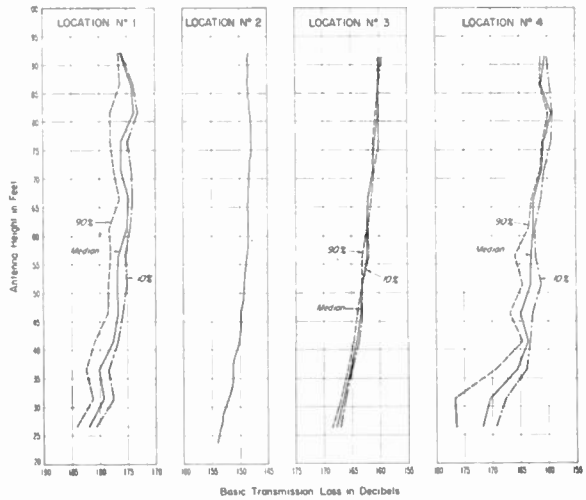

Fig. 9—Observed variation with antenna height at 59.75 mc for different receiving locations. For sites 1, 3, and 4 the distribution of transmission loss with time for five-foot intervals of height is indicated in terms of the percentage of time the observed values were less than the abscissa.

gation over a parabolic cylinder. In a recent paper, S. O. Rice[12] has considered this problem and has shown that the resulting fields are very similar to those obtained for knife-edge theory in the limiting case when the radius of curvature of the cylinder approaches zero, and agree with the Bremmer-van der Pol smooth-earth diffraction fields when the radius of curvature of the parabolic cylinder is equal to that of the earth. The application of the Bremmer-van der Pol smooth-earth theory to obstacle gain calculations has been treated by Norton and Rice.[13] Items 57, 58, 59, and 127 of Table II in this reference list the results of this application to site 3 for KFEL-TV (59.75 megacycles) and KBTV (191.75 megacycles).

Measurements were made at three additional sites in which the paths of propagation do not pass over Pikes Peak. These sites are numbered 1, 3, and 4 on the map in Fig. 2. The profiles of these propagation paths are shown in Fig. 8. The profiles from the NBS transmitters are slightly different from those for the television transmitters. None of the three sets of profile paths which do not pass over Pikes Peak represent a knife-edge obstructed path when the normal earth's atmosphere with a lapse rate of 39.2 N units of refractivity per kilometer is present. It might be possible with greater lapse rates, and consequently less effective earth's curvature, for some paths to act like knife-edge obstructed paths.

Fig. 9 shows the observations made for the 59.75 mc transmissions at all four sites. The recordings for sites 1, 3, and 4 have been resolved into three points on the distribution of all values for each five-foot interval of height. The observed values of basic transmission loss were less than the value indicated by each curve for the percentage of time shown for each five-foot interval. This gives a measure of the fading associated with these paths. At site 3 no appreciable fading was apparent. There is a strong suspicion that the lack of fading on the day of these measurements is not always characteristic inasmuch as the preliminary measurements shown for location 5M on Fig. 2, which were obtained very close to the location 3 for the 100-foot tower measurements showed a considerable amount of fading to be present at the earlier date.

Figs. 10 and 11 (next page) show similar sets of measurements obtained at four sites for 100 mc and 191.75 mc respectively. No measurements were obtained at 1,046 mc at sites 1, 3, and 4, although in each case an effort was made to record it. Apparently, the values of basic transmission loss at these sites exceeded 190 db, which is the highest value the 1,046 mc system was capable of measuring. A comparison of the values of basic transmission loss at all four sites for 59.75 mc, 100 mc and 191.75 mc is shown in Table III of minimum value of the medians of transmission loss, L_{bm}, for five-foot intervals for each site and the minimum value observed at site 3.

TABLE III

Minimum Value of L_{bm} in Decibels

	Site 1 L_{bm}	Site 2 L_b	Site 3 L_{bm}	Site 4 L_{bm}
KFEL-TV 59.75 mc	173.5	148.0	159.7	158.1
NBS 100 mc	167.8	145.3	166.0	176.6
KBTV-TV 191.75 mc	179.0	155.9	177.5	177.1

The differences between the values observed at sites 1, 3, and 4 and the values observed over Pikes Peak at site 2 are shown in Table IV on the following page.

[12] S. O. Rice, "Diffraction of plane radio waves by a parabolic cylinder," *Bell Sys. Tech. Jour.*, vol. 33, pp. 417–504; March, 1954.
[13] K. A. Norton, P. L. Rice and L. E. Vogler, "The use of angular distance in estimating the median transmission loss and fading range for propagation through a turbulent atmosphere over irregular terrain," p. 1489, this issue.

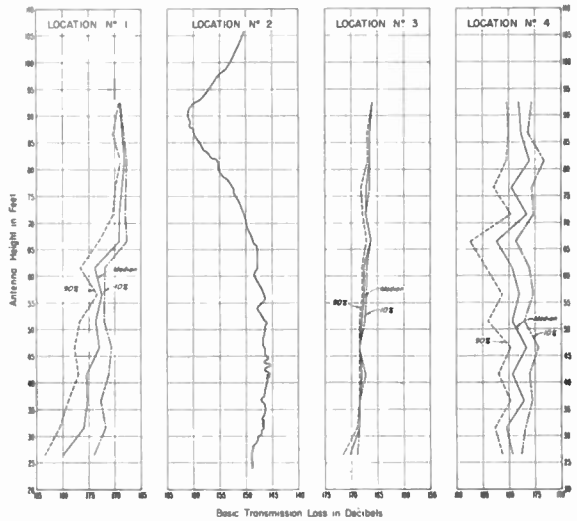

Fig. 10—Observed variation with antenna height at 100 mc for different receiving locations. For sites 1, 3 and 4 the distribution of transmission loss with time for five-foot intervals of height is indicated in terms of the percentage of time the observed values were less than the abscissa.

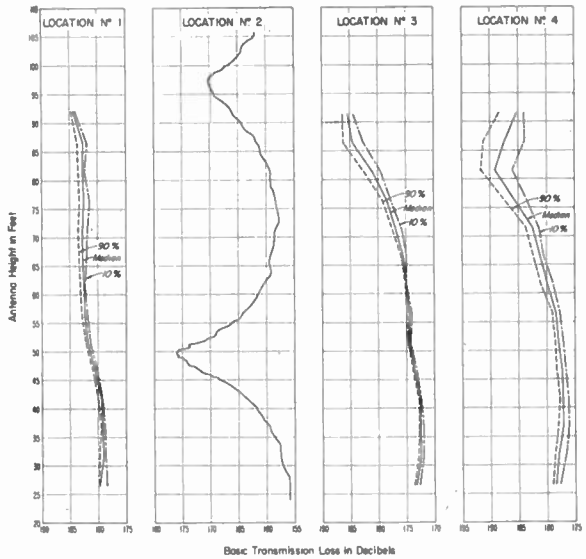

Fig. 11—Observed variation with antenna height at 191.75 mc for different receiving locations. For sites 1, 3 and 4 the distribution of transmission loss with time for five-foot intervals of height is indicated in terms of the percentage of time the observed values were less than the abscissa.

These numbers can be considered in a sense a measure of the observed obstacle gain.

It seems quite probable in view of some of the differences in observed values of transmission loss at 59.75 mc measured in June, 1953, and then again in October and November, 1954, that there is a strong possibility that the meteorological conditions were not the same.

TABLE IV

	Site 1	Site 3	Site 4
KFEL-TV 59.75 mc	25.5 db	11.7 db	10.1 db
NBS 100 mc	22.5 db	20.7 db	31.3 db
KBTV-TV 191.75 mc	23.1 db	21.6 db	21.2 db

The propagation paths were not the same for both sets of measurements but in some cases they were very close to each other. This effect was noted during a height run at 100 mc on site 1. While the antenna was being raised the signals faded considerably and the values of transmission loss were generally high. As the antenna reached its full height the fading diminished and the values of transmission loss were smaller. This is the case shown in Fig. 10. Upon lowering the antenna back to 24 feet the fading and median value of observed transmission loss did not change appreciably from the value observed at the full height. This clearly showed that the propagation characteristics along the path had undergone change during the two-hour period of raising and lowering the antenna. This situation points up the desirability of taking measurements both directly behind the obstacle and on the other paths for considerably longer periods of time.

Conclusion

Large obstacles which act like single knife-edges in ground-to-ground propagation paths can effectively reduce both the transmission loss and the fading under what they would be without the obstacle. Pronounced interference type lobing occurs due to waves arriving at the receiving locations with more than one ray path. Numerical results closely approaching observed values of transmission loss have been obtained using Fresnel-Kirchhoff scalar diffraction theory.

The measurements reported herein do not cover extensive periods of time, and some variations in propagation characteristics have been noted during the course of the measurements. It appears desirable to continue investigations of obstacle-gain phenomena in particular with the following objectives in mind: (1) To obtain long-time continuous measurements behind the obstacle to see what effect variations in the meteorological conditions may have, (2) To make comparative measurements over long-time periods for the non-knife-edge propagation paths simultaneously with the first objective, and (3) To make measurements over propagation paths where discrete reflections would be possible on both sides of the obstacle so that four ray-path interference phenomena can be investigated.

The Role of Meteors in Extended-Range VHF Propagation*

O. G. VILLARD, JR.†, SENIOR MEMBER, IRE, V. R. ESHLEMAN†, ASSOCIATE MEMBER, IRE, L. A. MANNING†, SENIOR MEMBER, IRE, AND A. M. PETERSON†

Summary—**The main factors influencing the propagation of continuous radio signals by reflection from meteoric ionization trails are reviewed and summarized. A procedure is given for calculating the system parameters required to maintain the signal received over a given path above the cosmic background noise level for 95 per cent of the time. It is pointed out that the variation of signal level with frequency and path length measured for certain "ionospheric forward scatter" circuits, agrees well with calculations based on the assumption that the propagation is entirely by scattering from meteor ion trails. It is suggested that ionospheric scatter is predominantly meteoric at night in the lower latitudes. To the extent that this is true, the minimum performance level of existing circuits could be improved by use of antennas designed to maximize the meteoric component of the signal. Present designs actually tend to discriminate against meteors.**

INTRODUCTION

IONIZATION columns formed by the passage of meteoric particles through the *E*-region of the ionosphere are capable of reflecting or scattering radio waves obliquely over distances up to 2,200 km. The particles are very numerous and the columns efficient reflectors. By proper choice of system parameters, meteor reflections at a remote receiver may be made so frequent that they overlap, thereby providing an essentially continuous signal which is available at all times of day.[1,2] Assuming moderate transmitter power, this mode of propagation is effective in the frequency range from 6 to 75 megacycles over distances from 400 to 1,500 km. The range can be extended up to 2,000 km by careful antenna design. At the lower frequencies, it can be extended down to zero by use of sufficient power.

The continuous signal provided by meteor reflections is weak and subject to rapid fluctuations, but it is reliable and it is not interrupted by magnetic disturbances.

One of the purposes of this paper is to summarize the main factors which must be taken into account in designing a communication circuit utilizing this mode of propagation. A second purpose is to outline a procedure for estimating the circuit parameters required to maintain the signal received over a given path above the cosmic noise background level for 95 per cent of the time. The third purpose is to discuss the relationship between meteor-reflection propagation and "ionospheric forward scatter."

METEOR REFLECTIONS WITH TRANSMITTER AND RECEIVER AT SAME LOCATION (RADAR CASE)

Meteoric particles of sufficient size create ionization columns in the height interval between 80 and 120 km. The speeds at which the particles strike the earth's atmosphere vary between limits of 11 and 73 km/second. Those particles which evaporate before striking the earth follow straight paths and decelerate a negligible amount. Ionization is released in the form of a column, initially very small, which rapidly expands owing to diffusion. The ionized atoms are evaporated meteoric material; relatively few air atoms are ionized. To a first approximation, the maximum electron density created per unit length of trail is dependent only on the mass of the particle and the cosine of the zenith angle of its path.[3]

Order-of-magnitude estimates of relationships between particle number, particle mass, visual magnitude, particle size, and line density of ionization produced, are listed in Table I. Particles of mass as small as 10^{-5}

TABLE I

SPORADIC METEORS: ORDER-OF-MAGNITUDE ESTIMATES OF THEIR MASS, BRIGHTNESS, SIZE, NUMBER AND THE ELECTRON LINE DENSITY IN THEIR TRAILS

	Mass (grams)	Visual Magnitude	Radius	Number of this mass or greater swept up by the earth each day	Electron line density (electrons per meter of trail length)
Particles pass through the atmosphere and fall to the ground	— 10^{4}	— −12.5	— 8 cm	— 10	— —
Particles totally disintegrated in the upper atmosphere	10^{3}	−10.0	4 cm	10^{3}	—
	10^{2}	− 7.5	2 cm	10^{3}	—
	10	− 5.0	0.8 cm	10^{4}	10^{16}
	1	− 2.5	0.4 cm	10^{5}	10^{17}
	10^{-1}	0.0	0.2 cm	10^{6}	10^{18}
	10^{-2}	2.5	0.08 cm	10^{7}	10^{15}
	10^{-3}	5.0	0.04 cm	10^{8}	10^{14}
Approximate limit of radar measurements →	10^{-4}	7.5	0.02 cm	10^{9}	10^{13}
	10^{-5}	10.0	0.008 cm	10^{10}	10^{12}
?	10^{-6}	12.5	40 microns	?	?
	10^{-7}	15.0	20 microns		
	10^{-8}	17.5	8 microns		
Micro-meteorites (Particles float down unchanged by atmospheric collisions)	10^{-9}	20.0	4 microns	total for this group estimated as high as 10^{20}	practically none
	10^{-10}	22.5	2 microns		
	10^{-11}	25.0	0.8 micron		
	10^{-12}	27.5	0.4 micron		
Particles removed from the solar system by radiation pressure	10^{-13} —	30 —	0.2 micron —	— —	— —

* Original manuscript received by the IRE, July 14, 1955. The research in this paper was supported jointly by the Army, Navy, and Air Force under contract with Stanford University. The paper was presented in preliminary form at the IRE National Convention, New York City, 1955.

† Radio Propagation Lab., Stanford University, Stanford, Calif.

[1] O. G. Villard, Jr., A. M. Peterson, L. A. Manning, and V. R. Eshleman, "Extended-range radio transmission by oblique reflection from meteoric ionization," *Jour. Geophys. Res.*, vol. 58, pp. 83–93; March, 1953.

[2] D. W. R. McKinley, "Dependence of integrated duration of meteor echoes on wavelength and sensitivity," *Canadian Jour. Phys.*, vol. 32, pp. 450–467; July, 1954.

[3] T. R. Kaiser, "Radio echo studies of meteor ionization," Res. Rev., *Phil. Mag. Supp.*, vol. 2, pp. 495–544; October, 1953.

grams are believed to produce radio-reflecting columns detectable with radar equipment of moderate power. The number of smaller particles is very great. For example, it is estimated that on the average at least 10^{10} particles of mass greater than 10^{-5} grams are swept up by the earth each day.

What this means in terms of radar echoes may be surmised from the following. If a radar illuminated the entire sky above a vertical angle of 30 degrees, the area in the 100-km height region from which echoes can be received is roughly 10^5 square kilometers. Through this region will pass some 20 of these particles per second, of which about five per cent will produce trails so oriented as to be detectable. Thus the radar should receive about one echo per second from particles weighing 10^{-5} grams or more.

Very small particles (10^{-9} to 10^{-12} grams) radiate away the heat generated by molecular collisions so rapidly that no ionization is produced. These are the "micrometeorites," which float down through the atmosphere unharmed.[4] Estimates of the number and mass of micrometeorites indicate that there may be several thousand times as many particles in the intermediate mass range from 10^{-6} to 10^{-8} grams, than would be expected from an extrapolation of the measured mass distribution of the larger meteors. The exact mass of the smallest particles which can still produce ionization is not yet known.

If the line density of ionization generated by a meteor is 10^{14} electrons/meter or less (that is, if the meteor is of the 5th visual magnitude, or smaller), the electrons in the trail can be considered to be independent scatterers which do not disturb a passing radio wave-front irrespective of its frequency. These columns are known as "underdense." On the other hand, if the line density exceeds 10^{14} electrons/meter of trail length, the column will behave in a manner roughly analogous to a metallic reflector; i.e., the incident wave will be turned back at the point where the column density N exceeds the critical value of $f^2/81$, where N is the number of electrons/m^3 and f is the radio frequency in cps. Such columns are called "overdense."

The most important type of reflection from meteor ion columns is the specular, obtained when the trail becomes perpendicular to the line of sight. This gives rise to the familiar meteor "burst." Another type of "reflection" consists of energy diffracted from the head of a meteor column during its formation. This is a weak signal detectable both before and after the trail reaches the perpendicular reflection point.

Owing to a Doppler shift resulting from the motion of the meteor, this diffracted signal when combined with reference voltage from the transmitter gives rise to a characteristic beat note, or "whistle." Diffracted energy contributes a negligible amount to the total propagated by meteor trails.

Specular reflections from underdense columns show a rapid rise to peak amplitude, followed by an exponential decay [see Fig. 1(a)]. In the absence of wind distortion of the trails, reflections from overdense columns attain a maximum amplitude which remains nearly constant for a relatively long period, finally falling rapidly to zero, as in Fig. 1(b). A large percentage of the trails which endure for a time interval longer than a second or so are distorted by nonuniform upper-atmosphere winds, so that reflection may be obtained simultaneously from two or more separated portions of the trail which are undergoing a displacement relative to each other. The result is a fluctuation in amplitude of total echo, as shown in Fig. 1(c). The majority of overdense echoes will fade.

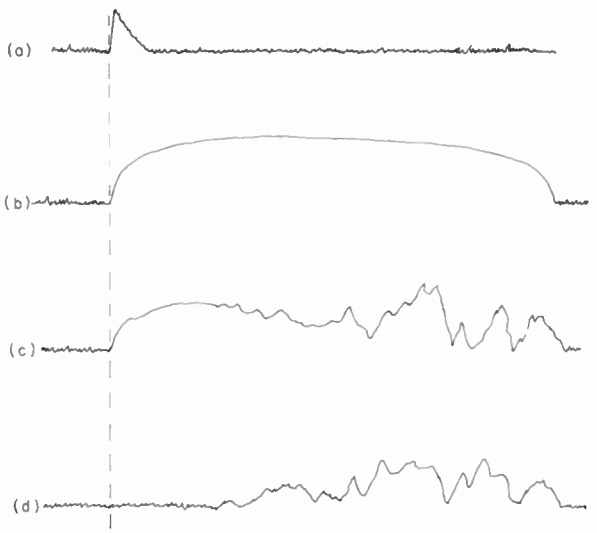

Fig. 1—Typical signal-strength versus time plots of radio reflections from meteor ionization trails. (a) Specular reflection, underdense trail. (b) Specular reflection, overdense trail. Wind distortion absent. (c) Specular reflection, overdense trail. Wind distortion present. (d) Nonspecular reflection, overdense trail. Wind distortion present.

Specular reflections from underdense columns [Fig. 1(a)] are highly directional; the column orientation must satisfy the perpendicular requirement in order for this type to be seen at all. Thus two radar stations separated by a few miles may not necessarily see the same underdense meteors. On the other hand, diffraction echoes (Doppler whistlers) are much less aspect-sensitive; such whistles may be heard when the column is quite far from the perpendicular reflection point. Similarly, wind-distorted columns are less aspect-sensitive. In Figs. 1(a), (b), and (c), the columns crossed the perpendicular reflection point at the beginning of the echo—hence the rapid rise in signal strength. The wind distorted column of Fig. 1(c), however, is much less aspect-sensitive, and might produce a reflection such as that of Fig. 1(d) at a distant station so located that the perpendicular reflection requirement was not initially satisfied.

[4] F. L. Whipple, "The theory of micrometeorites," *Proc. Nat. Acad. Sci.*, Part I, vol. 36, pp. 687–695, 1950; Part II, vol. 37, pp. 19–30; 1951.

Echoes such as those of Fig. 1(b) through (d) are of relatively infrequent occurrence in comparison with those of Fig. 1(a). Since we are concerned in this paper with the continuous signal which can be propagated by means of meteor reflections, echoes from overdense trails will be given no further consideration. When such echoes occur, they will greatly enhance the received signal strength; when they are absent, continuous transmission will depend on the background of overlapping echoes from the underdense trails.

The efficiency of meteor echoes as radar reflectors is illustrated by the fact that a particle of mass 10^{-3} grams will produce a column whose echoing power, expressed in terms of radar cross section, is about 2 square kilometers. (This assumes a radio frequency of 20 megacycles and a slant range of 250 kilometers.)

The peak power amplitude of the echoes from the underdense trails varies as $(\lambda/R)^3 P_T q^2$, where λ is the radio wavelength, R the range to the trail, P_T the transmitted power, and q the line density of electrons in the column at the reflection point. Since meteor echoes are most useful for communication at wavelengths and at times of day when transmission by regular layers is not possible, cosmic noise generally determines the strength of the minimum signal which can be detected. Cosmic noise power varies approximately as $\lambda^{2.3}$ in a receiver connected to a broad beam antenna.[5] Thus the ratio of the peak echo power to the cosmic noise power varies as $\lambda^{0.7} R^{-3} P_T q^2$. As shown in Table I, the number of trails having line densities greater than q is proportional to $1/q$. It follows that the number of underdense echoes detected above a cosmic noise background level is proportional to $\lambda^{0.35} R^{-3/2} P_T^{1/2}$. The decay time constant of the exponential echoes from the underdense trails is proportional to λ^2.

To propagate a continuous signal by means of underdone trails, it is necessary that the received reflections be so numerous and long-enduring that they overlap. It can be seen from the foregoing considerations that the number and duration of meteor echoes is maximized by choosing long wavelengths and high power. Lengthening the wavelength will increase the time constant of the echoes, and will increase the number of echoes having amplitudes sufficient to make them detectable in the presence of a cosmic noise background. Increasing power at a fixed frequency increases the total number of echoes which are detected.

Since echo occurrences are to a first approximation random events, the meteor-propagated signal will be available 95 per cent of the time if on the average there are three echoes present at a time. That is, when the product of number of echoes per unit time and echo duration equals 3 or more, the meteor-propagated signal will be virtually continuous.

Having chosen power and frequency, the designer's next task is to maximize the probability of detecting an echo by suitable antenna design. Only about five per cent of all the meteoric particles striking the atmosphere at a given time will satisfy the perpendicular-reflection requirement and so be detectable. Furthermore, the reflection-producing trails are not distributed over the sky at random. For example, an important consideration is the lack of such trails directly above a radar set.

Several factors contribute to this circumstance. In the first place, to satisfy the perpendicular-reflection requirement in this situation, the meteor must be traveling virtually horizontally. It happens that the total ionization produced by a given meteoric particle is to a first approximation proportional only to the particle's mass. This is because virtually every atom becomes ionized as it boils off. Particles traveling nearly vertically burn out quickly, and release their ionization in a column relatively short in length. Those traveling nearly horizontally will, in general, produce very long trails in which the line density of ionization is low. If the line density becomes too small, the column may not be detectable at all.

A second equally-important factor is the relative thinness of that region of the atmosphere in which meteors ionize. Thus downcoming meteors, grouped together with a certain density in space, will produce more columns per unit area of atmospheric layer when arriving vertically, than when arriving nearly horizontally; see Fig. 2.

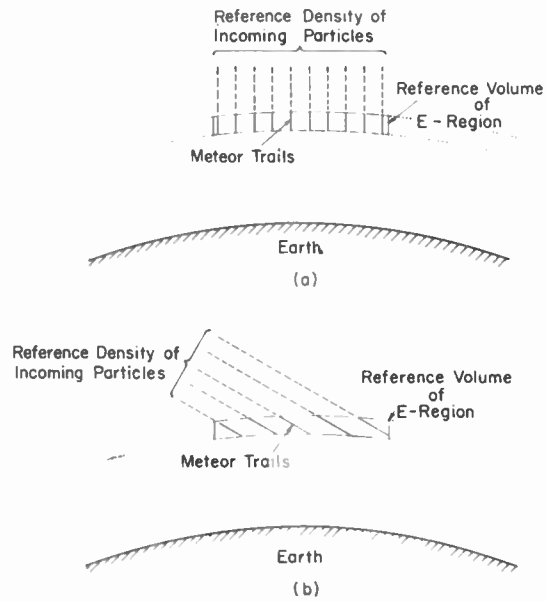

Fig. 2—Illustrating number of trails produced in a thin ionospheric layer by a given concentration of meteors (a) vertically disposed, and (b) nearly horizontally disposed.

Taking these factors into account, it is possible to arrive at a representation of the volume density of trails suitably oriented to produce specular reflections, as a function of plan position in the E-region above a radar as in Fig. 3(a) (next page). It is assumed here that meteors are randomly oriented with respect to earth. If

[5] H. V. Cottony and J. R. Johler, "Cosmic radio noise intensities in the vhf band," Proc. IRE, vol. 40, pp. 1053–1060; September, 1952.

density of such trails in any element of volume in the layer in which they occur is plotted as a function of angle above the horizon at radar site, the results are as shown in Fig. 3(b). The maximum density is seen to occur at an angle of 45 degrees. If a radar having a narrow beam of fixed width were to survey the number of echoes received as a function of elevation angle, the maximum would occur at a vertical angle of roughly 5 degrees; see the solid curve of Fig. 3(c). This is because the beam encompasses a progressively larger area in the 100-km height region as its elevation angle decreases. At very low elevations earth curvature and increasing slant range of the echoes limit number detectable.

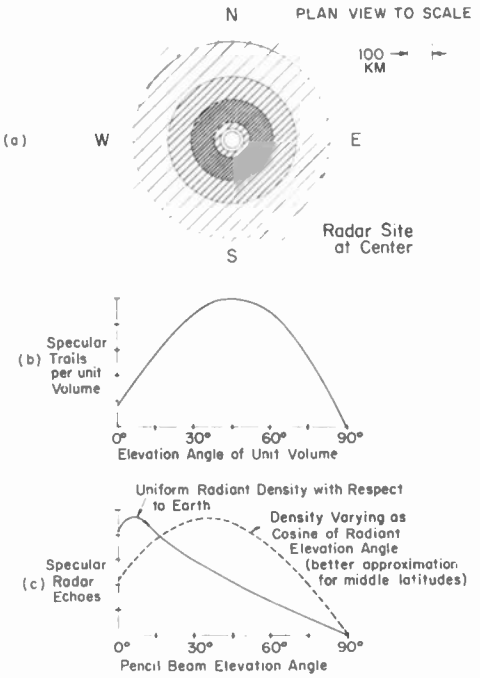

Fig. 3—(a) Representation of the relative number of meteor trails properly oriented to produce specular reflections, as a function of position in the *E*-region of the ionosphere above a radar site. (Meteors are assumed to be randomly distributed relative to the earth.) (b) Number of such trails in a unit volume, plotted as a function of angular elevation of that volume. (c) Number of echoes detected by a pencil-beam radar, as a function of beam elevation angle, for two assumed radiant distributions.

The solid curve of Fig. 3(c) will be considerably changed for a distribution of meteor radiants which is not random with respect to the earth. (The "radiant" is the point in the sky from which the meteor appears to emanate.) At moderate latitudes, most of the meteor radiants are low in the sky. Assuming a distribution of radiants that varies as the cosine of the elevation angle above the horizon, the radar would then obtain a maximum number of echoes by elevating its beam to about 35 degrees, as shown in the dotted curve of Fig. 3(c).

Meteoric particles fall into two general classifications: "sporadic" and "shower" meteors. The latter are believed to be remnants of comets' tails—particles which travel at the same speed through space, along parallel tracks. Meteor showers occur relatively infrequently, and hence are of no great practical significance in radio propagation by meteoric reflections. It is known that the orbits of the larger sporadic meteors are concentrated in the plane of the ecliptic.[6,7] Very little is known, as yet, about the orbits of the smaller radar meteors. Both shower and sporadic meteors are members of the solar system.

If sporadic meteors were distributed randomly with respect to the sun, consideration will confirm that the number of particles scooped up, and the average velocity at which the particles are moving with respect to the earth, will be a function of the time of day, the season, and the geographical location of the observer. In June and December, an observer at the equator would observe the greatest number of meteoric collisions in the early morning hours, for at that time the line representing the earth's track in space points directly overhead. The situation for December is illustrated in Fig. 4. During the evening hours, only meteors having sufficient velocities to enable them to catch up with the earth will be observed. On the other hand, an observer at the pole would not observe any daily change in numbers. An observer at moderate latitude in either hemisphere will find the largest number of meteors entering the atmosphere in the morning diurnally, and in autumn seasonally. The smallest number will enter in the evening diurnally, and in the spring seasonally.

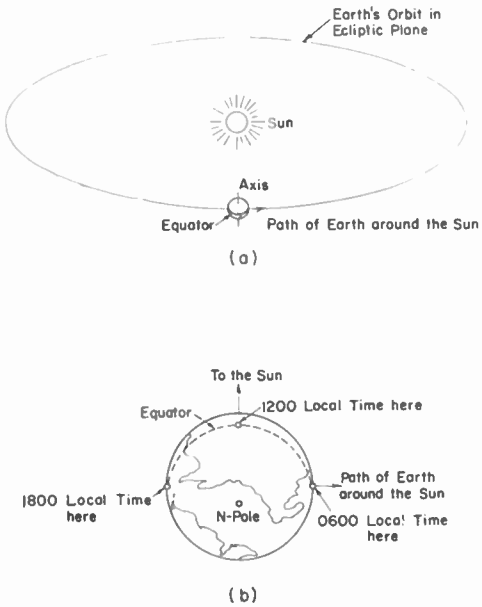

Fig. 4—Relationship between earth and sun in December. (a) Illustrates the ecliptic plane; (b) illustrates, for various times of day, the position of an observer at the equator with respect to the direction of the earth's track in space.

There will also be an accompanying change in the average *direction* from which the meteoric particles come. For example, the equatorial observer will find,

[6] F. L. Whipple, "Photographic meteor orbits and their distribution in space," *Astro. Jour.*, vol. 59, pp. 201–217; July, 1954.
[7] A. C. B. Lovell, "Meteor Astronomy," Oxford University Press, New York, N. Y., Ch. 6; 1954.

at noon, that more meteors are coming out of the western than out of the eastern part of the sky. (This is a consequence of the earth's motion, and is analogous to the way in which vertically-falling raindrops appear to be slanted when viewed from a moving vehicle.) Because of this fact, the equatorial observer will wish to direct his radar beam to the east in order to obtain the greatest number of perpendicular reflections.

The effect of average direction of arrival on number of echoes received, is illustrated in Fig. 5(a). This figure is a representation of the relative number of radar echoes received within a short time interval when a radar beam elevated at 45 degrees is aimed successively at the various azimuthal directions. A random distribution of meteors relative to the sun is assumed, and the radar is located at 37.5 degrees N latitude. At any given time and location, then, there will be a preferred azimuthal direction (in addition to the preferred vertical angle) in which the greatest number of meteor echoes can be detected. The highest radar echo rate will be obtained when transmitter and receiver beams both illuminate this portion of the sky only.

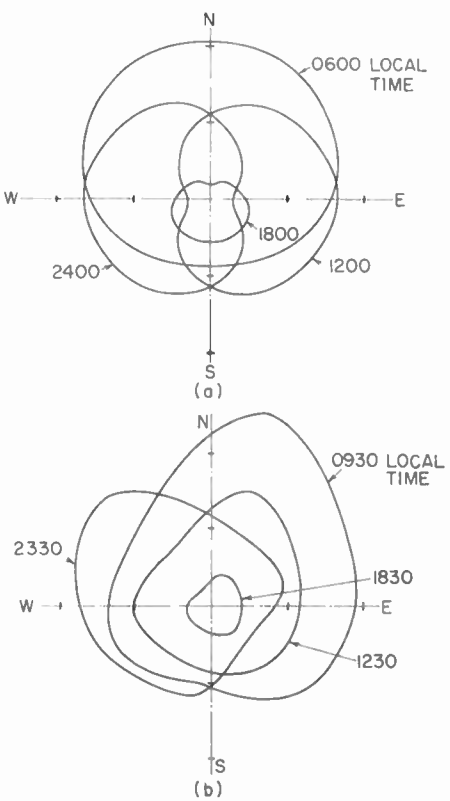

Fig. 5—(a) Relative number of meteor echoes detectable by a narrow-beam radar, as a function of azimuth. Deduced on the following assumptions: (1) meteors randomly distributed with respect to the sun, (2) a location at 37.5 degrees north latitude, and (3) the month of June. Beam elevation 45 degrees. (b) Plot similar to (a) made with a radar at Stanford University.

The reality of this azimuthal variation of the preferred direction for obtaining meteor echoes is illustrated by the experimental data of Fig. 5(b), which shows plots of echo number vs direction taken with an actual radar. Both the daily variation in total number of echoes detected, and the variation in azimuth from which the echoes are received, are apparent. When the experimental curves for the various times of day are compared with the corresponding theoretical ones, a net displacement toward the north direction will be seen. This is a consequence of the fact that meteors are not distributed entirely at random relative to the sun; the northward shift is evidence that the meteoric material is concentrated to an appreciable extent in the plane of the ecliptic.

Because of the diurnal changes in the rate and direction of arrival of meteor echoes, plots such as those of Fig. 3(a) must be modified to take into account the actual distribution of meteoric radiants. An example of these effects is shown in Fig. 6 for the early morning hours and a station at middle northern latitudes.

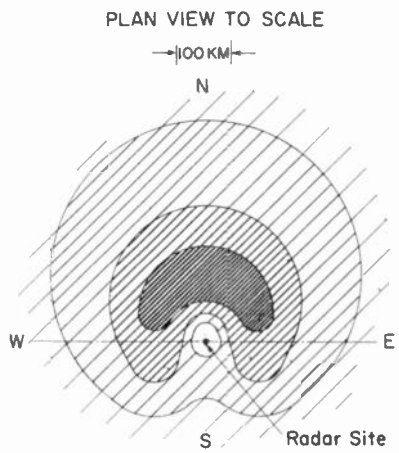

Fig. 6—Plot similar to Fig. 3(a), but taking into account the actual distribution of meteor radiants. This is typical of the situation at middle northern latitudes in the early morning hours.

By the use of a frequency in the lower high-frequency band, sufficiently high power, and antenna beams directed at that portion of the sky from which the greatest number of echoes are received, the number and duration of radar echoes can be raised to the point at which overlapping occurs. If the echoes overlap sufficiently, a signal will be present for all but a very small fraction of the time. Thus continuous communication by meteoric reflection can be maintained over very short paths, if desired.

Meteor Reflections with Transmitter and Receiver at Separate Locations

When transmitter and receiver are separated by fairly large distances, an additional factor controlling reflection duration and amplitude comes into play. The geometry is shown in Fig. 7 (next page). For any trail orientation, the reflection duration increases in proportion to the square of the secant of the forward-scattering angle, ϕ. For meteor trails located within a plane through the transmitter and receiver, Fig. 7(a), the amplitude increase is proportional to the secant

of the forward-scattering angle. For meteors lying perpendicular to this plane, Fig. 7(b), there is no amplitude increase.

The above expectations might be termed first approximations, since it is very difficult to calculate exactly the forward-reflection characteristics of meteor trails for all geometrical situations. Recent machine-computation studies have shown that the amplitude and duration of signals forward-scattered from underdense trails is well represented by the above factors.

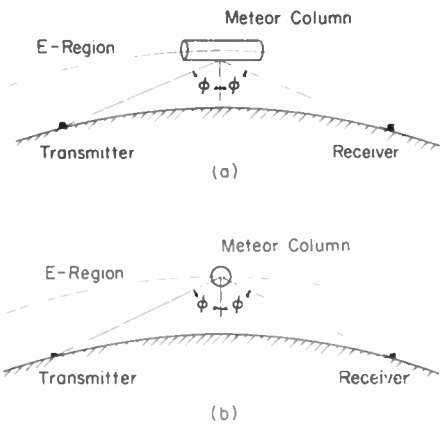

Fig. 7—Geometry of oblique meteor reflections. (a) Column within a plane passing through transmitter and receiver. Echo duration proportional to $\sec^2 \phi$. Echo amplitude proportional to $\sec \phi$. (b) Column perpendicular to that plane. Echo duration proportional to $\sec^2 \phi$. Echo amplitude independent of ϕ.

However, it was also found that the amplitude of the signals forward-scattered from overdense trails is much greater than had previously been expected. Full details are given in a companion paper in this issue.[8] It is interesting that forward-reflection geometry does not change the general shape of the different types of meteor reflections shown in Fig. 1. The main effect of forward-reflections is simply to stretch out the time axis.

Once again assuming meteors to be randomly distributed with respect to the earth, a plot analogous to that of Fig. 3(a) may be constructed for separated transmitter and receiver. The results are shown in Fig. 8(a). This again is a representation of those areas of the sky at a height of 100 km in which the largest number of suitably-oriented trails will be found. To maximize the continuous component of the received signal, however, echo duration is as important as echo number, and when the detection probability of Fig. 8(a) is multiplied by the $\sec^2 \phi$ factor, the contour plot of Fig. 8(b) is obtained. Note the "hole" in the vicinity of the midpoint between the stations, resulting from the absence of horizontally-disposed trails.

The next step is to take the average meteor radiant distribution into account, as in Fig. 6. Here the geographical location and orientation of the oblique path is obviously important. If the path is east-west, in the middle latitudes of the northern hemisphere, it will be found that the situation is similar to that illustrated in Fig. 8(c) for the early morning hours, with the peak on the northern side of the path changing somewhat in amplitude and position throughout the day.

It is interesting that if transmitter and receiver of a radar system are separated, the *number* of echoes received is not very greatly changed. In particular if the separation is roughly 1,000 km, and narrow beam antennas are used which illuminate roughly 10^5 square kilometers of the commonly-accessible area at the center of the path, it turns out that the same meteoric particles of 10^{-5} grams or larger which produced one echo per second at back reflection can still produce about one-third of a reflection per second in the forward-reflection case, on the average. These latter reflections will, however, be considerably longer-enduring, owing to the duration increase for oblique geometry.

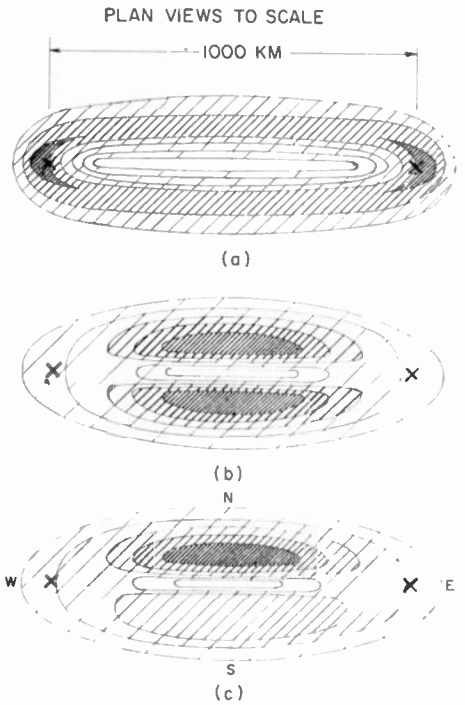

Fig. 8—(a) Plot analogous to Fig. 3(a), for separated transmitter and receiver, X's mark transmitter, receiver locations. (b) Same as (a), but with the number of trails per unit volume multiplied by the duration-increase factor ($\sec^2 \phi$) appropriate to that volume. (Gives a measure of the contribution of each portion of the E-region to the continuous signal.) (c) Same as (b), but taking the actual radiant distribution into account in the manner of Fig. 6. Valid for an east-west path in the northern hemisphere during the early-morning hours.

Estimating the Received Signal Level

To estimate the integrated signal level over a path of given length, the theoretical development given in an earlier paper by Eshleman and Manning[9] may be used. In particular, for a given path length, a plot of the probability of detection p' times $\sec^2 \phi$ as a function of position in the 100-km height region is needed. Such a

[8] G. H. Keitel, "Certain mode solutions of forward scattering by meteor trails," p. 1481, this issue.

[9] V. R. Eshleman and L. A. Manning, "Radio communication by scattering from meteoric ionization," PROC. IRE, vol. 42, pp. 530–536; March, 1954.

plot—for a 1,000-km path—is shown in Fig. 5 of that paper. [It is analogous to Fig. 8(b) of this paper.] By a straightforward extension of the theoretical development of that paper, it may be shown that $P_{0.95}$, the power level above which the signal exists 95 per cent of the time, is given by the following expression:

$$P_{0.95} = 0.3 \times 10^{-33} P_R \lambda^7 D^{-3} \cdot \left[\int_{A_h} (p' \sec^2 \phi)(G_R G_T)^{1/2} dA_h \right]^2, \quad (1)$$

where MKS units are used throughout and

P_T = transmitter power,
G_R, G_T = power gain of the receiving and transmitting antennas expressed as a function of position in A_h,
$(p' \sec^2 \phi)$ = probability-duration factor, from contour plot,
$2D$ = path length,
A_h = area of ionosphere at the 100-km level illuminated by the antenna beams, and
λ = wavelength.

In this expression, $p' \sec^2 \phi$, G_R and G_T are all functions of position in the area A_h. It was assumed in the derivation that the number of meteors striking the ionosphere per square meter per second having a line density of q electrons per meter or greater, is proportional to $160/q$. This is based on best available experimental evidence.

If it is assumed that narrow beams having power gains of 25 to 30 db are used at the transmitter and the receiver, a useful simplification of this equation can be carried out. Over the small area in A_h illuminated by such beams, $p' \sec^2 \phi$ will be essentially a constant. If it is assumed that both beams illuminate exactly the same volume, then $G = 16(\Delta\theta)^{-2}$, where $\Delta\theta$ is the antenna beam width in radians. For this situation $A_h = \pi R^2 (\Delta\theta)^2 \sec \phi / 4$, so that

$$P_{0.95} = 0.5 \times 10^{-26} P_T \lambda^7 (p' \sec^2 \phi)^2 \sec^3 \phi. \quad (2)$$

From this equation, it is seen that the power level of the continuous signal propagated by meteors should vary as the 7th power of the wavelength, and as the 7th power of the secant of the forward-scattering angle.

The accuracy of these two equations is limited by incomplete knowledge of meteor rate and radiants, particularly for the smaller meteors. However, while these uncertainties may affect the estimates of the numerical constants given, it is not expected that they would have a large effect upon the predicted variation of $P_{0.95}$ with path and system parameters. Because of the diurnal variation of echo rate, it is estimated that $P_{0.95}$ will vary about 5 db to either side of the value given in these equations, being higher during the early morning hours and lower during the evening hours.

When the high-gain antennas are directed toward areas of the h-plane which are favorable for meteor propagation, a conservative estimate of p' would be about 0.02. As an example, assume $\lambda = 10_m$, $P_T = 10^3$ watts, and path distance = 1,000 km. Then, from the second equation, the power level exceeded 95 per cent of the time can be found to be about 5×10^{-16} watts.

If cosmic noise is assumed to be the limiting factor in reception, and the same idealized beams are employed with $\lambda = 10_m$, a receiver bandwidth of 100 cps, $p' = 0.02$, and a path distance of 1,000 km, it follows that only 120 watts of transmitted power would theoretically be required to maintain a meteor signal above the cosmic noise level for 95 per cent of the time.

It should be emphasized that the numerical results in this and the preceding example were obtained by assuming that neither antenna illuminates a meteor trail which is not also illuminated with comparable gain by the other antenna. This may not be easy to achieve in practice. In addition, it was assumed in the second example that cosmic noise is the only factor limiting the reception of weak signals. In many situations, this level may be set by man-made noise or interference. It should also be remembered that cosmic noise sources are not uniformly distributed, so that the noise level will depend on the time of day and upon antenna directivity factors. It is estimated that there may be a factor of 10 db or more between practical circuits and the theoretically-ideal situation, so that several kilowatts of transmitted power would probably be required in practice to obtain signal indicated in second example.

Comparison of the Theoretical Characteristics of Continuous Meteor Propagation with Measured Signals

Measurements of the signal propagated by meteors over paths of the order of 1,000 km in length have been made by the authors at Stanford University at frequencies near 20 mc.[1] The measured signal strength checks well with the value predicted from (1), using reasonable estimates for the antenna gain factors.[9]

Extensive ionospheric forward-scatter tests have been conducted by workers at the National Bureau of Standards.[10,11] At the present time, the exact nature of this scattering is not well understood. The original hypothesis, on the basis of which the experiment was first attempted, held that wind motions and turbulence in the E-region of the ionosphere would produce more or less isotropic inhomogeneities of electron density capable of scattering the expected signal. Later experimental work at low latitudes using high-power pulsed equipment suggests that one or more weakly-reflecting "layers" are effective in propagating the energy, particularly during the day time. Large numbers of meteor reflections are found on such records, and it is not clear

[10] D. K. Bailey, R. Bateman, L. V. Berkner, H. G. Brooker, G. F. Montgomery, E. M. Purcell, W. W. Salisbury, and J. B. Wiesner, "A new kind of radio propagation at very high frequencies observable over long distances," *Phys. Rev.*, vol. 86, pp. 141–145; April, 1952.

[11] D. K. Bailey, Technical Session on Forward Scattering, XI General Assembly of URSI, The Hague, August 23–September 2 1954, as reported in Ionospheric Research, Thayer School of Engineering, Dartmouth College, Hanover, N. H., December 1, 1954.

what proportion of a continuous-wave signal would be propagated by meteoric reflections, and what by the layers themselves. It is known that the forward-scatter is stronger at all times at high latitudes, but no satisfactory explanation for this effect is as yet available.

From measurements of ionospheric forward-scatter made near 24 and 48 mc, D. K. Bailey of the NBS group has reported[11] that the most likely exponent for the wavelength dependence of the median received power is 7. From measurements near 50 and 100 mc, the most likely exponent for the wavelength dependence is 9. (As actually given by Bailey, the wavelength dependence per unit antenna aperture was 5 for the 24–48 mc tests, and 7 for the 50–100 mc tests. These values have been adjusted for scaled antennas, so that direct comparison can be made with the above equations for meteoric propagation.) It is interesting that the first-order meteor theory predicts the same law of variation of median-received power with wavelength as was actually measured at 24 and 48 mc.

At frequencies above about 75 mc, however, various second-order effects[12] decrease the amplitude and duration of meteor echoes more than indicated in (1) and (2). Taking these effects into account, the expected value of the meteoric wavelength-dependence exponent in the 50 to 100-mc region would be between 7.5 and 9, again in reasonable agreement with the 50–100 mc tests conducted by the NBS group.

On the basis of some preliminary measurements of the distance dependence at 50 mc for relatively long distances, Bailey reported that the received power may vary as $R^{-2}\sec^{9}\phi$, or approximately as $\sec^{7}\phi$. The meteor theory also predicts the same distance (or angle) dependence of the signal.

If this agreement between observed results and predictions based on the meteoric explanation were to persist down to very small values of ϕ (that is to very small distances), a means for assessing the relative contribution of meteors and turbulent scattering to the forward-propagated signal comes to mind. Back-reflections from layers or turbulent scattering should be strongest when the antenna is pointed directly overhead; there is no reason to expect any other vertical angle dependence. Back reflections from meteoric echoes, however, will be most numerous at some beam elevation angle below 45 degrees. Thus far, the attempts which have been made to detect scatter echoes coming from above a radar site have been without success. Strong meteoric reflections coming back from the lower angles, however, are familiar to many workers. As mentioned earlier, continuous signals back-scattered from meteors may be obtained by proper choice of power, frequency, and antenna directivity.[13]

Meteor showers have little effect on the continuous signal propagated by meteors. It is now known that visible showers contain relatively few small meteors. During a shower, then, a marked increase in the number of individual large meteor bursts will be observed, but the continuous background signals will be little affected.

It is worth observing that individual meteor bursts over an oblique path vary in power amplitude somewhere between $\lambda^{3}\sec^{-3}\phi$ and $\lambda^{3}\sec^{-1}\phi$, while the median signal level varies as $\lambda^{7}\sec^{7}\phi$. Therefore, at high frequencies and over short paths, records of continuous-propagation signal strength should appear "spikier" than would be the case if low frequencies or long paths had been utilized.

The known diurnal variations of back-scatter echo rate for the larger meteoric particles do not agree with the diurnal variations of ionospheric forward-scatter signal level recorded at 50 mc. However, some recent experimental evidence suggests that the daily variation in meteor echo rate over a forward-reflection path does in fact correlate reasonably well with the median forward-scatter signal level propagated over another forward-scatter path.[14] The median signal level is usually maximum near noon, while the echo rate measured over the above-mentioned oblique path was maximum near 10 A.M.

An interesting possibility offered in explanation of this remaining discrepancy is that the background excitation level of the gas in the *E*-layer may affect the probability of ionization by the smaller meteoric particles. It has recently been reported by Bowles[15] that the meteoric echo rate in the vicinity of College, Alaska increases during auroral displays. If this effect results from an increase in the general ionization level at the time of the auroral display, it may also be that the noontime density of ionization in the *E*-region can perceptibly increase the total ionization produced by each meteoric particle, thus increasing the number of small meteor echoes detectable. Such a mechanism could result in a noontime maximum of signal propagated via meteors.

Improvement of Ionospheric Scatter Circuits

In the existing very high frequency ionospheric scatter circuits, antennas of high gain are directed to an area over the path midpoint. As can be seen in Fig. 8, this is exactly the area where the meteoric contribution is minimum. It is interesting that the received signal nevertheless has many characteristics which can be explained by assuming that all the energy is propagated by meteoric ionization.

[12] V. R. Eshleman, "The effect of radar wavelength on meteor echo rate," TRANS. IRE, vol. AP-1, pp. 37–42; October, 1953.

[13] V. R. Eshleman, P. B. Gallagher, and A. M. Peterson, "Continuous radar echoes from meteor ionization trails," PROC. IRE, vol. 43, p. 489; April, 1955.

[14] P. A. Forsyth and E. L. Vogan, "Forward-scattering of radio waves by meteor trails," *Canadian Jour. Phys.*, vol. 33, pp. 176–188; May, 1955.

[15] K. L. Bowles, "VHF auroral and meteor echoes including simultaneous observations," presented at the joint URSI-IRE meeting in Washington, D. C.; May 4, 1954.

Taking all available evidence into account, the authors believe that ionospheric scatter is primarily meteoric at low latitudes and at times of day when the signal is weak. To the extent that this is true, it should be possible to improve the minimum performance of ionospheric scatter circuits by designing antennas in such a way as to favor the meteoric component of the signal.

Proper antenna design requires knowledge of meteor rate and radiant distributions as well as knowledge of the geography of the path. It has already been indicated [see Fig. 8(c)] that in the case of an east-west transmission located north of the tropic of Cancer, the antenna beams should intersect in a region of the ionosphere which is north of the path midpoint, for maximum meteoric signal.

Such antenna considerations suggest a definitive test for the relative contributions of meteoric and other types of scatter, since the "ionospheric forward scatter" component should suffer a large reduction when high-gain beams are directed away from the great-circle direction. Any contribution due to partial or total reflection from horizontal layers would suffer an even greater reduction when the beams are turned to one side of the direct path.

Conclusions

Signal transmission by overlapping reflection from meteoric ionization trails may be regarded as a practical means for communicating over moderate distances.

At a frequency of thirty megacycles, a power of one kilowatt should be ample to maintain a relatively narrow-band transmission such as single-channel teletype over distances of the order of 800 miles. The only unusual requirements are high-gain antennas of suitable-design, and a low-noise receiving location. The signal will be available at all hours of day, independent of variations in the regular layers, or of ionospheric storminess. The spectrum-saving possibilities of this technique are obvious, as are the advantages of being able to use one frequency and one antenna system at all times. Considerably less power will be required at lower frequencies; considerably more at higher.

In view of the agreement between the predicted behavior of meteorically-propagated signals and the observed characteristics of "ionospheric forward scatter" propagation, it is suggested that "ionospheric scatter" is primarily meteoric at low latitudes, and at night. To the extent this is true, it should be possible to improve minimum performance of such circuits by redesign of antenna systems to favor the meteoric component.

Certain Mode Solutions of Forward Scattering by Meteor Trails*

G. H. KEITEL†, MEMBER, IRE

Summary—**Scattering of a plane wave normally incident on a meteor trail which has a Gaussian radial distribution of ionization is investigated for various line densities by the wave-matching technique. Solutions were obtained by numerical integration methods with the aid of the SWAC, a high-speed digital computer. For a column of low line density, 10^{13} electrons per meter, scatter in the back direction checks very closely the results of approximate analyses made by previous workers. In the case of a low-line-density column having a diameter comparable to a wavelength, scatter in all other directions for both transverse and parallel electric vector polarization of the incident wave checks simple theory based on the summation of scattering by individual electrons. The energy back-scattered by a trail of high line density, 10^{17} electrons per meter, is found to be nearly equal to the energy which would be back-scattered from an equivalent metal cylinder, thus checking previous approximate calculations. The equivalent metal cylinder is also found to be a good approximation to the actual ion column for scattering in other directions, but only in the case of parallel polarization of the incident wave. The results further show that echoes from high-line-density trails in directions other than the back direction may be appreciably higher than would be anticipated. This would tend to confirm certain recent experimental observations of forward scattering from meteor trails.**

* Original manuscript received by the IRE, July 7, 1955. The work described in this paper was partially supported by Air Force Cambridge Research Center, Air Research and Development Command, under contract No. AF 19(604)-1031. This material was originally presented in the author's Dissertation submitted to Stanford University in partial fulfillment of the requirements for the degree of Doctor of Philosophy. The author held a National Science Foundation Predoctoral Fellowship during the period of this research, 1954–1955. The computations were performed on the SWAC at Numerical Analysis Research, University of California at Los Angeles, which is supported by contracts from the Office of Naval Research and the Office of Ordnance Research.

† Radio Propagation Laboratory, Stanford University, California. Now at Cavendish Laboratory, Cambridge, England.

Introduction

WHEN METEORIC particles pass through the upper atmosphere, they create long, narrow columns of ionization which scatter hf and vhf radio waves. Until a few years ago, both theoretical and experimental studies of radio reflections from such trails were made for the situation in which the transmitter and receiver are at the same location.[1] However, the forward scattering properties of meteor trails are

[1] T. R. Kaiser, "Radio echo studies of meteor ionization," *Res. Rev. Phil. Mag. Suppl.*, vol. 2, pp. 495–544; October, 1953.

now being investigated experimentally,[2–4] and exact theoretical studies of forward scattering are beginning.

It is the purpose here to describe a method used to obtain exact solutions for scattering by a Gaussian column of ionization illuminated by a normally-incident plane wave, and to compare scattering in the back direction with approximate results found by previous workers. Forward scattering from the columns is also investigated, and computation results are qualitatively related to experimentally-observed characteristics of signals forward-scattered by meteor trails.

Theoretical Considerations

Theory of Scattering

Ionization in a meteor trail is described in terms of the number of electrons per unit length of the trail (the line density), and a function describing the radial distribution of ionization at a given point along the trail. It is a good approximation to consider the line density along a particular column to be constant. The effect of the electrons within a column on a passing radio wave is taken into account by determining the reduced dielectric constant for any portion of the trail from the equations of motion of the electrons.[5]

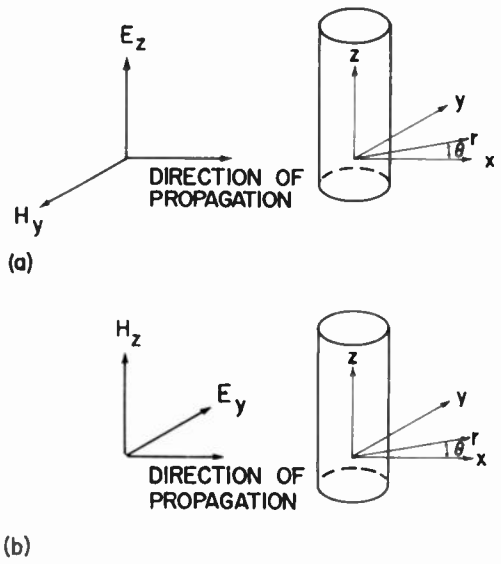

Fig. 1—Geometry for plane waves normally incident on column of ionization. Orientation of field components for: (a) parallel electric polarization, and (b) transverse electric polarization.

Consider the cylindrical coordinates shown in Fig. 1. Let the column axis coincide with the z-axis. The present investigation deals with a plane wave of arbitrary polarization normally-incident on the column from the negative x-direction ($\theta = 180$ degrees). Such a wave may be resolved into two plane waves with the polarizations shown in Fig. 1(a) and Fig. 1(b), each of which can be treated separately. The time factor is $\exp(-i\omega t)$ and the units are MKS. The complex relative dielectric constant is denoted here by $\epsilon(r)$, where r is distance from the column axis. The wave-matching treatment used by Herlofson,[6] Feinstein,[7] and Eshleman[8] provides equations which describe the electromagnetic fields scattered by such a column of ionization.

For a unit-amplitude plane wave with the polarization shown in Fig. 1(a), (the parallel electric vector case), the electric field has a z-component only. The electric field within the column of ionization is

$$E_{z\,\mathrm{int}} = \sum_{n=0}^{\infty} b_n P_n(r) \cos(n\theta), \tag{1}$$

where function $P_n(r)$ satisfies differential equation

$$\frac{d^2P_n}{dr^2} + \frac{1}{r}\left[\frac{dP_n}{dr}\right] + \left[k^2\epsilon(r) - \left(\frac{n}{r}\right)^2\right]P_n = 0; \tag{2}$$

k is the wave number and the b_n are constants. Expansions similar to (1) are used for electric field of incident wave in terms of Bessel functions of argument kr, and of scattered wave in terms of Hankel functions of the first kind of argument kr. Plane-wave scattering coefficient for parallel polarization $\rho_\parallel(\theta)$ is defined as[8]

$$\rho_\parallel(\theta) = \sqrt{\frac{\pi k R_0}{2}}\left[\frac{\text{scattered electric field strength at distance } R_0 \text{ from column}}{\text{incident electric field strength at the column}}\right],$$

where R_0 is distance to receiver and $kR_0 \gg 1$. Satisfying boundary conditions at matching radius, $\rho_\parallel(\theta)$ is

$$\rho_\parallel(\theta) = \sum_{n=0}^{\infty} A_n \cos(n\theta), \tag{3}$$

where

$$A_n = -\tau_n\left[\frac{J_n(kr_a)P_n'(r_a) - kJ_n'(kr_a)P_n(r_a)}{H_n^{(1)}(kr_a)P_n'(r_a) - kH_n^{(1)\prime}(kr_a)P_n(r_a)}\right]. \tag{4}$$

τ_n = Neumann factor

$= 1,\ n = 0$

$= 2,\ n \neq 0$

and r_a is the radius at which the incident and scattered waves are matched to the fields within the column. The matching radius r_a is either chosen as the outer limit of the ionization, or as the radius at which the ionization density is essentially zero. The scattering coefficient $\rho_\parallel(\theta)$ reduces to the reflection coefficient derived by previous workers[6–8] for the case of back reflection, $\theta = 180$

[2] P. A. Forsyth and E. L. Vogan, "Forward-scattering of radio waves by meteor trails," *Can. Jour. Phys.*, vol. 33, pp. 176–188; May, 1955.

[3] D. W. R. McKinley, "Dependence of integrated duration of meteor echoes on wavelength and sensitivity," *Can. Jour. Phys.*, vol. 32, pp. 450–467; July, 1954.

[4] O. G. Villard, Jr., A. M. Peterson, L. A. Manning, and V. R. Eshleman, "Extended-range radio transmission by oblique reflection from meteoric ionization," *Jour. Geophys. Res.*, vol. 58, pp. 83–93; March, 1953.

[5] J. A. Stratton, "Electromagnetic Theory," McGraw-Hill Book Co., Inc., New York, N. Y., p. 326; 1941.

[6] N. Herlofson, "Plasma resonance in ionospheric irregularities," *Arkiv för Fysik*, vol. 3, pp. 247–297; 1951.

[7] J. Feinstein, "The interpretation of radar echoes from meteor trails," *Jour. Geophys. Res.*, vol. 56, pp. 37–51; March, 1951.

[8] V. R. Eshleman, "The mechanism of radio reflection from meteoric ionization," Tech. Rept. 49, Electronics Research Lab., Stanford Univ., California; 1952.

degrees. For compactness of notation, $\rho_{\parallel}(\theta)$ will be referred to as the "parallel scattering coefficient."

Similarly for a unit-amplitude plane wave with the polarization as shown in Fig. 1(b), (the transverse electric vector case), the magnetic field has a z-component only. The magnetic field within column of ionization is

$$H_{z\,\mathrm{int}} = \sum_{n=0}^{\infty} d_n T_n(r) \cos(n\theta), \tag{5}$$

where $T_n(r)$ satisfies the differential equation

$$\frac{d^2T_n}{dr^2} + \left[\frac{1}{r} - \frac{1}{\epsilon(r)}\frac{d\epsilon(r)}{dr}\right]\frac{dT_n}{dr} + \left[k^2\epsilon(r) - \left(\frac{n}{r}\right)^2\right]T_n = 0, \tag{6}$$

and the d_n are constants determined by the boundary conditions at the matching radius.

The plane-wave scattering coefficient for transverse polarization $\rho_{\perp}(\theta)$ is

$$\rho_{\perp}(\theta) = \sum_{n=0}^{\infty} B_n \cos(n\theta), \tag{7}$$

where

$$B_n = \tau_n\left[\frac{k\epsilon(r_a)J_n'(kr_a)T_n(r_a) - J_n(kr_a)T_n'(r_a)}{k\epsilon(r_a)H_n^{(1)\prime}(kr_a)T_n(r_a) - H_n^{(1)}(kr_a)T_n'(r_a)}\right], \tag{8}$$

and $\epsilon(r_a)$ is the complex relative dielectric constant found by approaching the matching radius from the interior. The term "transverse scattering coefficient" will be used to indicate $\rho_{\perp}(\theta)$.

Numerical Integration Method

Solutions of the differential equations (2) and (6) were obtained by numerical methods with the aid of SWAC (National Bureau of Standards Western Automatic Computer) at the University of California at Los Angeles. Tabulated or analytic solutions for these equations exist only for the simple case of a column of ionization with a constant radial distribution. Milne's three-point technique[9] formed the basis of the numerical integration method used. The program for the SWAC was so set up that the integration step size was halved or doubled whenever necessary or possible. This resulted in a considerable saving in computation time.

If collisional losses are neglected, (6) will have a singular point where $\epsilon(r) = 0$, at the so-called critical radius. However, by considering a small collisional loss in the column, the singular point is moved slightly off the real r-axis, making it possible to integrate along this axis with little trouble.

Radial Distribution of Ionization

Most meteor trails are believed to have a radial ionization distribution which may be described by a Gaussian function of the distance from the column axis.[1] Thus ratio of volume ionization density at any point to density at column axis, is equal to $\exp\left[-(r/r_0)^2\right]$, where r_0 is that radius at which ionization volume density is 37 per cent of the value on axis. This radial distribution results by normal diffusion from a column having a very small initial diameter. In all subsequent discussion, Gaussian distribution is assumed.

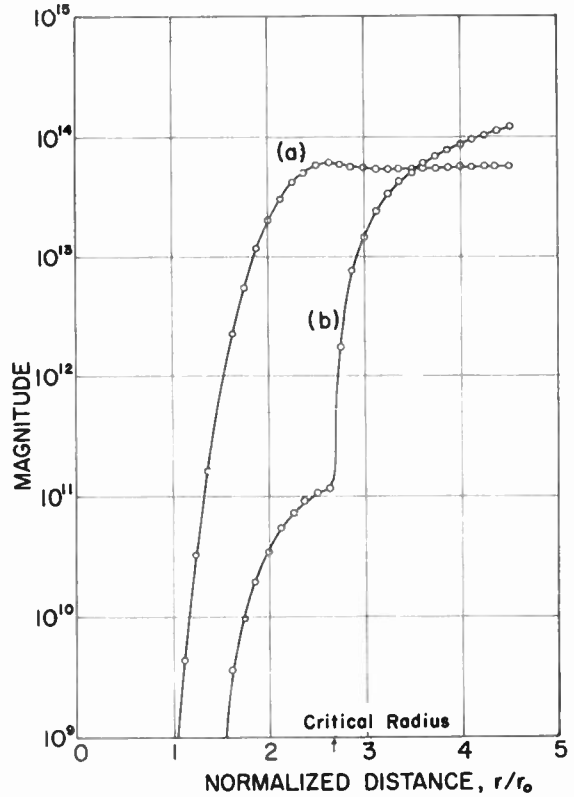

Fig. 2—Typical curve of the numerically-integrated function for transverse electric polarization. (a) Real part. (b) Imaginary part. 10^{17} electrons per meter, $kr_0 = 1.0$, $\nu/\omega = 10^{-4}$.

A typical plot of the function described by (6) is in Fig. 2 above. This plot was obtained by numerical integration assuming reasonable values for line density, losses, and column size. The rapid increase in the imaginary part of the function in the region near the critical radius checks approximate calculations made by Kaiser and Closs[10] and Herlofson.[6] They have shown by the theory of complex variables that the imaginary part of the function $T_n(r)$ must suffer a jump if losses are considered only in the immediate neighborhood of the critical radius. In this region, during the machine computation, the integration step size became very small in order to maintain accuracy of the integrated function.

Discussion

The difficulty of obtaining a rigorous solution for scattering by a column of ionization in which the ionization density is a function of the distance from the column axis has caused previous workers to make vari-

[9] W. E. Milne, "Numerical Solution of Differential Equations," John Wiley and Sons, Inc., New York, N. Y., pp. 64–66; 1953.

[10] T. R. Kaiser and R. L. Closs, "Theory of radio reflections from meteor trails; I," *Phil. Mag.*, vol. 43, pp. 1–32; January, 1952.

ous approximations. Electron scatter analysis consists of summing the fields independently scattered by individual electrons. It assumes that the incident wave is not appreciably modified by the column of ionization. This analysis has been applied to back scatter from trails of low line density.[6–8,10] For columns of line densities greater than about 10^{14} electrons per meter, the electron scatter assumptions are no longer tenable, and the metallic-reflection approximation has been used. Here the columns are assumed to reflect in the same manner as metal cylinders of the appropriate radius.[6–8,10] The accuracy and regions of validity of these approximations have never been checked by comparison with exact solutions for back scatter by the actual column of ionization. And only one attempt has been made on the basis of electron scatter analysis to predict forward scattering by a meteor trail of low line density.[8]

In this work, scattering coefficients were calculated for Gaussian columns of two-line densities for both parallel and transverse electric polarization. First, a low-density column, 10^{13} electrons per meter, was picked to verify electron scatter type of analysis. Second, a high-density column, 10^{17} electrons per meter, was studied to verify metallic-reflection approximation.

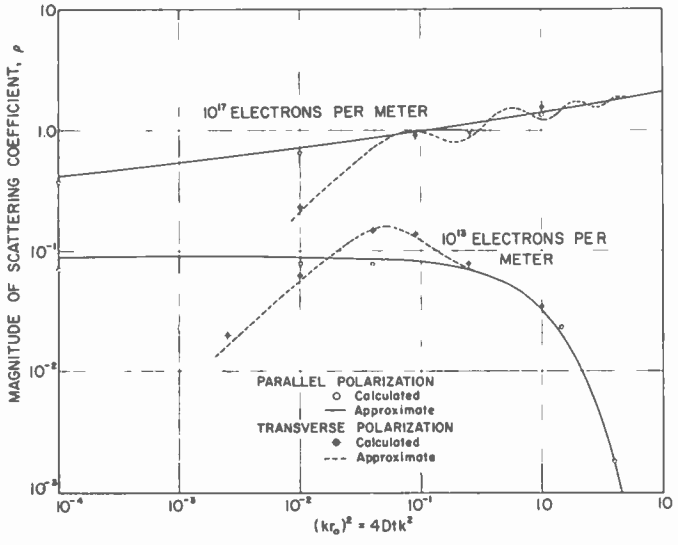

Fig. 3—Comparison of exact scattering coefficients for the back direction and approximate reflection coefficients found by Kaiser and Closs[10] and Eshleman[8] for the Gaussian column.

Scattering Coefficients for Back Direction

The parallel and transverse scattering coefficients for the back direction are plotted in Fig. 3, above, for comparison with results obtained by Kaiser and Closs[10] and Eshleman.[8] The agreement is very good. Calculated parallel scattering coefficient for the low-density column shows a decrease with increasing wavelength, as seems reasonable in view of the fact that the metallic-reflection approximation for high-density trails also decreases with increasing wavelength. This decrease is probably due to multiple scattering effects in the small column.

The calculated transverse scattering coefficients for the back direction for 10^{13} electrons per meter verify the plasma resonance peak calculated by Kaiser and Closs[10] on the basis of an approximate numerical solution of the dipole mode, $n=1$. Preliminary calculations for a trail density of 10^{15} electrons per meter seem to show some plasma resonance—a ratio of transverse to parallel scattering coefficients of the order of 1.5. This is contrary to the expectation of Kaiser and Closs that there should be no plasma resonance for line densities greater than approximately 10^{14} electrons per meter.

Multiple resonant dipole modes have been claimed for the Gaussian column. Makinson and Slade[11] examined a small Gaussian column and approximated the Gaussian function by a stepped distribution function. They found a resonant mode for each step in the distribution. They claim that some of these resonant modes will be observable when the steps become infinitely small and in the limit the stepped distribution approaches a smooth distribution. This claim is not substantiated by the present work.

Forward Scatter Results

Scattering coefficients for directions other than the backward one are also of practical importance. The polar diagrams, Figs. 4–7 (facing page), show magnitude of scattering coefficients $\rho_{\parallel}(\theta)$ and $\rho_{\perp}(\theta)$ as functions of scattering angle θ. Because of the symmetry of scattering coefficient series (3) and (7) about the 0–180 degree line, only one-half of the polar diagram is shown. The plane wave is incident from 180-degree direction.

The parallel scattering coefficient of a low-density column, 10^{13} electrons per meter (see Fig. 4), shows that a column small compared with a wavelength scatters the incident wave equally at all scattering angles. As the column increases in size compared with a wavelength, the back scatter decreases and the forward scatter builds up to a maximum. Eshleman[8] has derived by electron scatter analysis the reflection coefficient for forward scattering from a column whose size is comparable to a wavelength. His results compare very well with results obtained by the exact method. For example, electron scatter analysis predicts a maximum of 0.08852 in the $\theta=0$ degrees direction as compared with the calculated value of 0.08846.

Similarly, transverse scattering coefficients for same line density, 10^{13} electrons per meter (see Fig. 5), exhibit characteristic dipole pattern with a null at $\theta=90$ degrees. For $kr_0=1.0$, these results check Eshleman's[8] result for forward scattering. Because of plasma resonance, electron scatter analysis is not applicable to any smaller size trail at this particular line density and for this polarization of incident wave. The effect of plasma resonance is observable at all scattering angles.

The parallel scattering coefficient for a high-density trail, 10^{17} electrons per meter (Fig. 6), shows the growth of the so-called geometrical optics "shadow term" as the trail expands. The polar diagram of the transverse scattering coefficient for this trail (Fig. 7), shows a much more complex variation as the trail grows in size.

[11] R. E. B. Makinson and D. M. Slade, "Dipole resonant modes of an ionized gas column," *Aust. Jour. Phys.*, vol. 7, pp. 268–278; June, 1954.

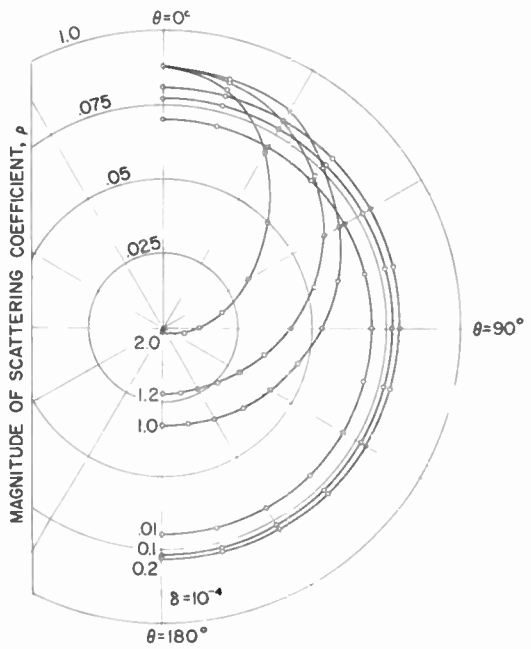

Fig. 4—Polar diagrams of the parallel electric polarization scattering coefficients for the Gaussian column, 10^{13} electrons per meter, kr_0 indicated on curves.

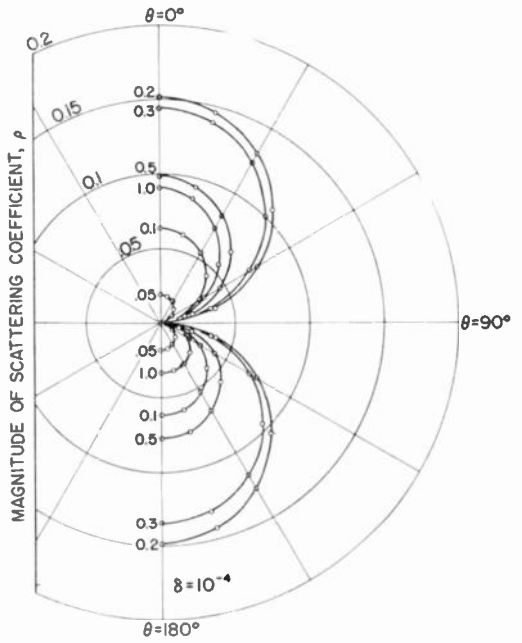

Fig. 5—Polar diagrams of the transverse electric polarization scattering coefficients for the Gaussian column, 10^{13} electrons per meter, kr_0 indicated on curves.

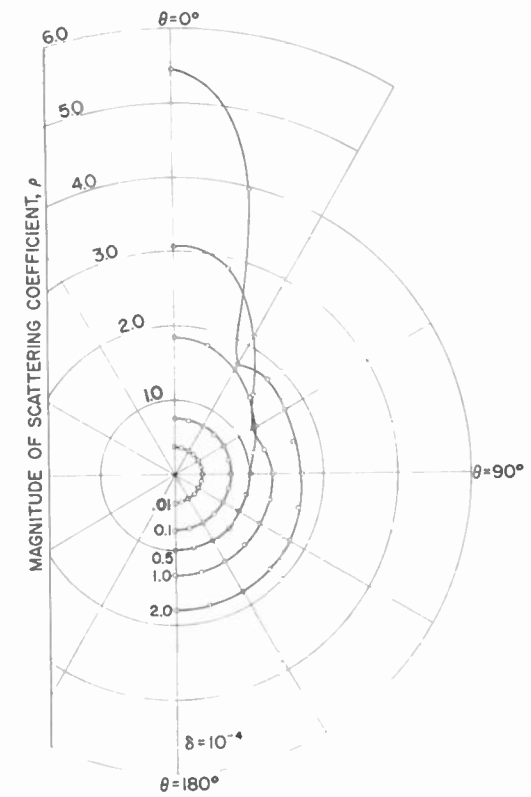

Fig. 6—Polar diagrams of the parallel electric polarization scattering coefficients for the Gaussian column, 10^{17} electrons per meter, kr_0 indicated on curves.

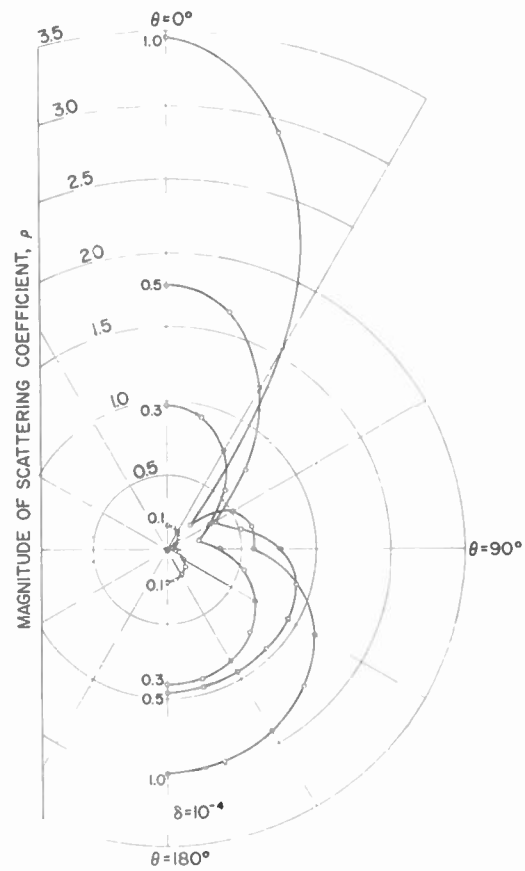

Fig. 7—Polar diagrams of the transverse electric polarization scattering coefficients for the Gaussian column, 10^{17} electrons per meter, kr_0 indicated on curves.

For a Gaussian radial distribution, the time variation of the complex relative dielectric constant is related to r_0 by[10]

$$r_0^2 = 4\,Dt,$$

where D is the diffusion constant and t is the time measured from the instant of formation of the trail.

In Figs. 8 and 9 (next page) are the calculated parallel and transverse scattering coefficients, respectively, for various angles as functions of $(kr_0)^2$. Increased duration (time being proportional to r_0^2) as a function of the scattering angle for low-density trails predicted by Eshleman[8] is verified here. The high-density trail

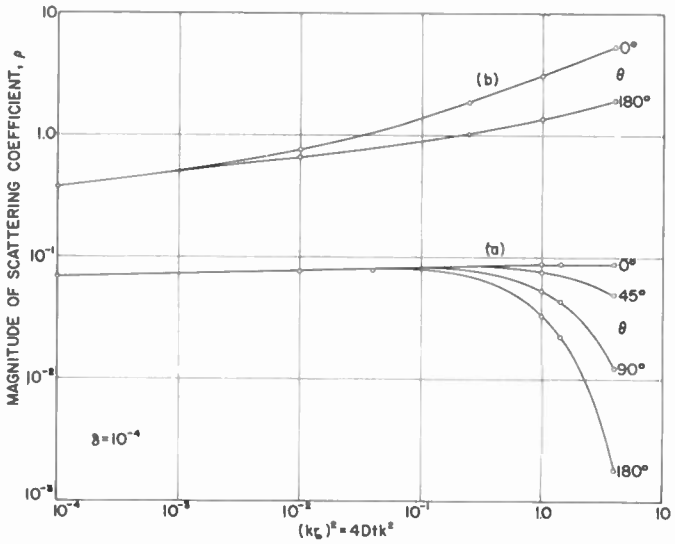

Fig. 8—Parallel electric polarization scattering coefficients for a Gaussian column as a function of $(kr_0)^2$ for various scattering angles. (a) 10^{13} electrons per meter. (b) 10^{17} electrons per meter.

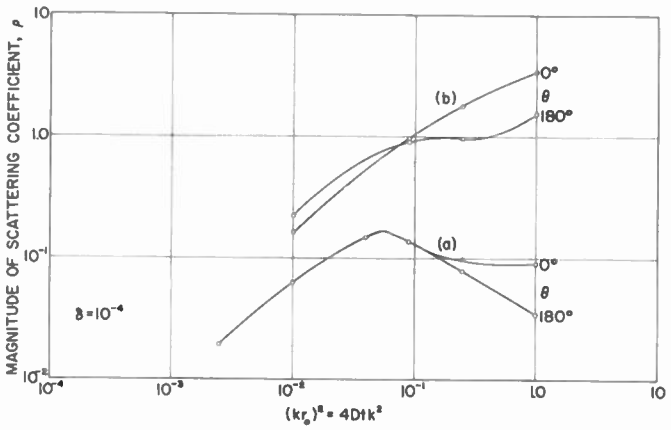

Fig. 9—Transverse electric polarization scattering coefficients for a Gaussian column as a function of $(kr_0)^2$ for various scattering angles. (a) 10^{13} electrons per meter. (b) 10^{17} electrons per meter.

shows a large increase in the forward-scattered signal over the backward-scattered signal as the trail expands. It was not feasible to carry these computations far enough to determine the total duration of the echoes from the high-density trail.

The polar diagrams of scattering coefficients were examined for several column sizes and loss ratios, where the loss ratio δ is ν/ω and ν is the collisional frequency, for line densities of 10^{13} and 10^{17} electrons per meter and for both polarizations. The changes due to increasing the loss ratio from 10^{-4} to 10^{-2} were insignificant. The per cent reduction in the scattering coefficient for an increase to $\delta = 1.0$ was approximately the same at all angles. For the radio frequencies ordinarily used to observe meteor trails, and for the commonly-accepted collisional frequency[12] for the height region of 80 to 120 km ($\nu = 3 \times 10^5$ sec^{-1}), the loss ratio is of the order of 10^{-2} and the scattering coefficients are almost independent of losses.

Metallic Reflection Approximation

Various authors[6-8,10] have used a metal cylinder of the appropriate radius as an approximation to the high-density Gaussian column for scattering in the backward direction. Perhaps the most refined analysis of this type is that of Manning,[13] who used a ray-theory treatment to estimate the refractive effects of the ionization exterior to the point of maximum penetration of the ray scattered back to the transmitter. He shows how to determine the radius of a metal cylinder which will give the same back scatter as the actual ion column.

As part of the present investigation, scattering-coefficient polar diagrams for a high-density Gaussian column of ionization (10^{17} electrons per meter; $kr_0 = 1.0$; and $\nu/\omega = 10^{-4}$) were determined. For this column, the critical radius is $kr = 2.65$, and Manning's radius for the equivalent metal cylinder is $kr = 2.47$. Similar diagrams for metal cylinders of critical and equivalent radii for parallel polarization and of critical radius for transverse polarization were also determined and the results compared with the Gaussian column. It is found that a metal cylinder of Manning's equivalent radius forward scatters in almost exactly the same manner as the Gaussian column for parallel polarization, although the derivation is based on back reflection only.

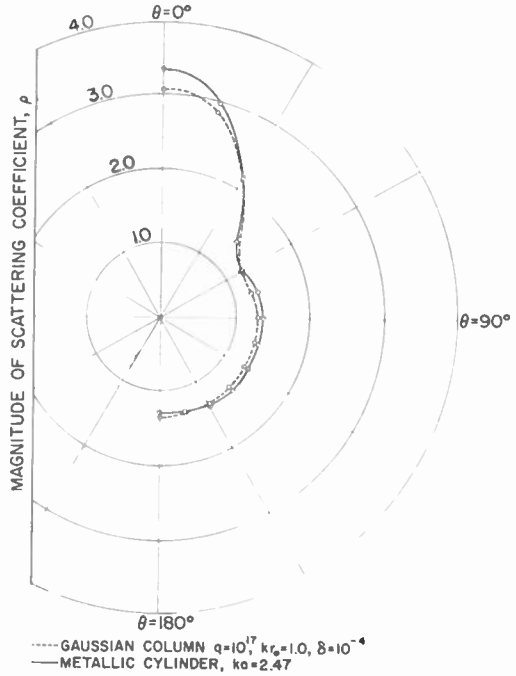

Fig. 10—Comparison of scattering coefficients of a Gaussian column of ionization and of a metal cylinder with radius equal to Manning's equivalent radius,[13] for parallel electric polarization.

This is shown in Fig. 10. The only serious deviation is found at the very small scattering angles. The over-all correspondence is slightly better than for a metal cylinder of critical radius.

For transverse polarization, Manning's ray theory analysis is not applicable unless the trail is very large. Therefore comparison is made only between scattering

[12] T. R. Kaiser, *op. cit.*, p. 499.
[13] L. A. Manning, "The strength of meteoric echoes from dense columns," *Jour. Atmos. Terr. Phys.*, vol. 4, pp. 219–225; 1953.

by a metal cylinder of critical radius, and the actual column of ionization. The scattering coefficient polar diagrams are shown in Fig. 11. It is seen here that the general character of the polar diagrams is very different and the agreement for most angles is very poor.

The good agreement for parallel polarization and the poor agreement for transverse polarization may be explained qualitatively on physical grounds. For parallel polarization, the currents on the metal cylinder are constrained to flow axially, in the same direction as the notion of the electrons which constitute a radiating current in the case of the column of ionization. However, for transverse polarization, the currents on the metal cylinder must flow circumferentially, while the electrons in the actual column may move circumferentially and radially. Thus one could not expect much similarity between the scattering coefficient polar diagrams for transverse polarization.

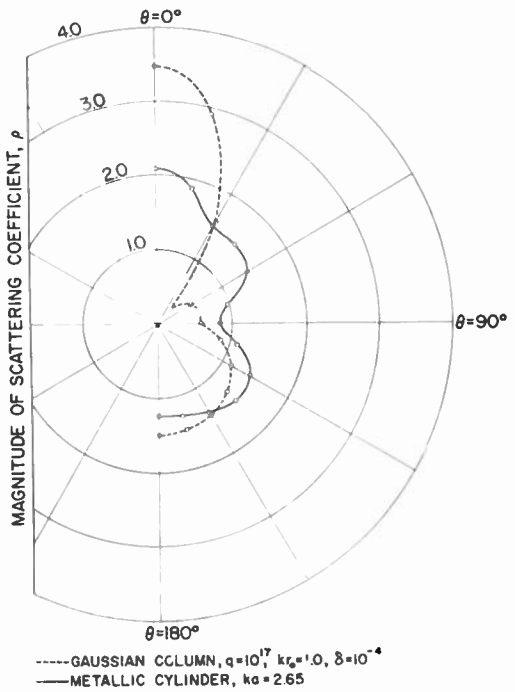

Fig. 11—Comparison of scattering coefficients of a Gaussian column of ionization and of a metal cylinder with radius equal to the critical radius of the column, for transverse electric polarization.

Conclusions

The approximate treatments of scattering by a Gaussian column by previous workers were found to compare very well with the exact solutions for backward scattering. The approximate solution for forward scattering by a low-density column checked very closely with the exact solution. The relationship between echo duration and forward scattering angle was verified for the low-density trail. Although it had not been suggested as an approximation for forward scattering, the metal cylinder was found to scatter almost identically to the actual high-density column for parallel polarization, but not for transverse polarization. The computations for the high-density trail could not be carried far enough to determine the variation of the echo duration with the scattering angle.

As they expand, high-density trails exhibit increased scattering for forward directions as compared with backward direction. Except for very small forward angles, this increased scattering coefficient means forward-scattered signal from meteor trails may be much larger than expected on basis of previous theory. Although there are fewer high-density trails, this greater peak echo amplitude will make these trails more important than previously assumed. Thus, the number of large-amplitude echoes would be expected to be greater than when the same columns are viewed at back reflection, and would tend to confirm experimental results of Forsyth and Vogan[2] where observed relation between echo rate and echo amplitude for forward scatter were compared with relation expected on basis of back-scatter measurements. A larger percentage of strong forward-scattered echoes was found.

The numerical integration program devised for the SWAC, although specifically applied here to a Gaussian column of ionization, is of general applicability and may be used in the study of scattering by any cylindrically-symmetric distribution of ionization. Other distributions, described by exponentials or even by a differential equation, could be treated with equal facility. However, because of rapid increase in computation time per mode for increasing ionization density, it is not feasible in the Gaussian distribution case to consider line densities greater than about 10^{17} electrons per meter. The large number of modes required for large columns also limits the size to $kr_0 = 4.0$ and smaller.

The parallel and transverse scattering coefficients were derived above on the assumption of plane waves normally incident on the column of ionization. The equations for scattering of a plane wave obliquely incident on a column with a constant radial distribution of ionization have been derived by Wait.[14] He found that the scattered field contains transverse-electric components for a transverse-magnetic incident wave, due to coupling between the two modes at the surface of the homogeneous cylinder. A solution for the fields scattered at oblique incidence by a column in which the ionization density is a function of the distance from the column axis, is more difficult to obtain. There are coupling terms between the transverse-electric and transverse-magnetic waves throughout the column which arise due to the gradient of the relative dielectric constant. Thus the general oblique-incidence case requires the simultaneous numerical solution for both waves. The same physical situation which gives rise to plasma resonance for the transverse-electric case treated above, also occurs in the oblique-incidence transverse-magnetic case.

Acknowledgment

The assistance, during this research, of Drs. V. R. Eshleman, R. A. Helliwell, L. A. Manning, A. M. Peterson, and O. G. Villard, Jr., Radio Propagation Laboratory of Stanford University, is gratefully acknowledged.

[14] J. R. Wait, "Scattering of a plane wave from a circular dielectric cylinder at oblique incidence," *Can. Jour. Phys.*, vol. 33, pp. 189–195; May, 1955.

The Use of Angular Distance in Estimating Transmission Loss and Fading Range for Propagation through a Turbulent Atmosphere over Irregular Terrain*

K. A. NORTON†, FELLOW, IRE, P. L. RICE†, MEMBER, IRE, AND L. E. VOGLER†

Summary—A discussion is given of the transmission loss expected in free space with various types of antennas, followed by a description of theoretical prediction curves for the transmission loss expected in tropospheric propagation on over-land paths.

The Bremmer-van der Pol theory of diffraction and the Booker-Gordon and Weisskopf-Villars theories of tropospheric forward scattering are then developed in terms of angular distance as a parameter. Angular distance is the angle in the great circle plane between the radio horizon rays from the transmitting and receiving antennas. It is shown that this parameter replaces, to a first order of approximation, both the transmission path length and the antenna heights. Angular distance is shown to be useful for predicting the short term within-the-hour fading range as well as the median transmission loss. Illustrations are presented of the theoretical dependence of transmission loss on the angular distance, transmission path length, antenna height, radio frequency, and a parameter ΔN which is a measure of the vertical gradient of atmospheric refractive index. Most of the long-term variations of the scattered field intensities with time, as well as the climatological variations, are attributed to changes in ΔN.

A new theory of obstacle gain is developed, and it is shown that this is particularly useful for explaining some of the unusually strong fields which have been observed just beyond the horizon in over-land propagation.

The diffraction and scattering theories are compared with extensive data on radio transmission loss involving 136,000 hourly median values recorded over 122 propagation paths at frequencies between 66 and 1,046 megacycles. Estimates of the Booker-Gordon scattering parameter $[\overline{(\Delta n/n)^2}/l_0]$ and of the Weisskopf-Villars scattering parameter $\{[\overline{(dn/dh)^2}]-[\overline{(dn/dh)}]^2\}$, determined from our median ratio data and normalized to a height of one kilometer above the surface, are considered to be correlated with the gradient of refractivity, ΔN. The radio data indicate that the magnitude of the scattering cross section decreases in inverse proportion to the radio frequency in the range we have studied. This provides strong evidence in favor of the Weisskopf-Villars tropospheric forward scattering theory presented elsewhere in this issue of the Proceedings.

Theoretical curves of the average value of the path antenna gain to be expected in tropospheric forward scatter propagation are presented as a function of the angular distance, the asymmetry factor, and the free space gains of the transmitting and receiving antennas.

I. INTRODUCTION

THE PRIMARY purpose of this paper is to provide comparatively simple formulas sutiable for estimating the median transmission loss and the fading range for transmission paths extending beyond the radio horizon. An examination of experimental transmission loss data obtained during the past 20 years will establish the fact that the formula for propagation around a smooth sphere with a radius equal to 4/3 that of the earth[1,2] indicates in some cases far too weak fields, and thus far too much transmission loss at points beyond the radio horizon either because the terrain is rugged to the extent that obstacle gain is present[3,4,5] or because of energy reflected or scattered by a turbulent atmosphere.[6,7,8,9,10] A history of recent developments in tropospheric transmission beyond the horizon is given by Bullington[11] in a paper appearing in this issue.

The theoretical formulas presented in this paper have been developed around the assumption that two modes of propagation are present in beyond-the-horizon transmission: the diffracted mode and the tropospheric-forward-scatter mode. We denote by K the ratio, expressed in decibels, of the mean power in the scattered mode to that in the diffracted mode. K increases rapidly with increasing distance beyond the horizon. The fading range increases from zero for very small values of K to

* Original manuscript received by the IRE, August 29, 1955. This paper was originally presented with the title "The Role of Angular Distance in Tropospheric Radio Wave Propagation" at the West Coast Annual Meeting of the IRE at San Francisco in August, 1953, and was later presented in a series of papers to the Eleventh General Assembly of the International Scientific Radio Union (URSI) at The Hague in August, 1954. Section VIII on Obstacle Gain in the Diffraction Region was presented at the joint meeting of URSI and IRE in Washington, D. C. in May, 1955.

† Central Radio Propagation Laboratory, National Bureau of Standards, Boulder, Colo.

[1] H. Bremmer, "Terrestrial Radio Waves," Elsevier Publishing Co., Inc., New York, N. Y.; 1949.

[2] K. A. Norton, "The calculation of ground-wave field intensity over a finitely conducting spherical earth," PROC. IRE, vol. 29, pp. 623–639; December, 1941.

[3] K. Bullington, "Radio propagation at frequencies above 30 megacycles," PROC. IRE, vol. 35, pp. 1122–1136; October, 1947.

[4] S. Matsuo, "The method of calculating vhf field intensity and research on its variation," Rep. Electr. Commun. Lab. 621.39.001 (947.3) Ministry of Telecommunications, Tokyo, Japan; August, 1950.

[5] F. H. Dickson, J. J. Egli, J. W. Herbstreit, and G. S. Wickizer, "Large reductions of vhf transmission loss and fading by the presence of a mountain obstacle in beyond-line-of-sight paths," PROC. IRE, vol. 41, pp. 967–969; August, 1953. See also the discussion of this paper by J. H. Crysdale, PROC. IRE, vol. 43, p. 627; May, 1955.

[6] C. R. Englund, A. B. Crawford, and W. W. Mumford, "Ultra-short-wave transmission and atmospheric irregularities," Bell. Sys. Tech. Jour., vol. 17, pp. 489–519; October, 1938.

[7] K. A. Norton, "A theory of tropospheric wave propagation," presented before the Federal Communications Commission at the Hearing in the Matter of Aural Broadcasting on Frequencies Above 25,000 Kilocycles; March 18, 1940.

[8] Report of the Federal Communications Commission Ad Hoc Committee for the Evaluation of the Radio Propagation Factors Concerning the Television and Frequency Modulation Broadcasting Services in the Frequency Range Between 50 and 250 mc; May, 1949.

[9] K. A. Norton, "Propagation in the FM Broadcast Band," "Advances in Electronics," Academic Press, Inc., New York, N. Y., vol. 1, pp. 406–408; 1948.

[10] K. Bullington, "Radio transmission beyond the horizon in the 40- to 4,000-mc band," PROC. IRE, UHF Issue, vol. 41, pp. 132–135; January, 1953. This paper gives a good summary of data available up to that time.

[11] K. Bullington, "Characteristics of beyond-the-horizon radio transmission," p. 1175, this issue.

that expected for a Rayleigh distribution when K is large; i.e., when all of the signal power reaches the receiving antenna by the scattered mode of propagation.

The geometrical parameter used in the theoretical prediction formula is the angular distance, θ, which is defined to be the angle in the great circle plane between the radio horizon rays from the transmitting and receiving antennas. When the distance and the angular distance are both fixed, it is shown that the shape of that portion of the earth which establishes the radio horizons still may have a very large influence[12] on the intensity of the diffracted mode but a much smaller influence on the intensity of the scattered mode. The simple model adopted in this paper for describing the electromagnetically important geometrical parameters of the terrain is described in Section III.

The advantages of the concept of "transmission loss," L, in describing the characteristics of radio wave propagation have been discussed in recent papers by one of the authors.[13,14] A brief review of this concept together with a few new definitions will be presented here.

L is defined to be the ratio, expressed in decibels, of the power, p_r, available for radiation from the transmitting antenna to the power, p_a, available from the receiving antenna:

$$L \equiv 10 \log_{10} (p_r/p_a). \tag{1}$$

It may be shown that the transmission loss in free space, L_f, may be calculated for a given transmission path and associated transmitting and receiving antennas by means of the formula.

$$L_f = 20 \log_{10} (4\pi d/\lambda) - G_p, \tag{2}$$

where (d/λ) denotes the path length expressed in wavelengths, and G_p (expressed in decibels) denotes the "path antenna gain"; i.e., the combined "effective" gain (expressed in decibels) of the transmitting and receiving antennas relative to that of isotropic antennas. Note that this effective antenna gain for the path is generally somewhat less than the sum of the actual limiting gains, G_t and G_r, of these antennas when they are located sufficiently far apart in free space and appropriately oriented with respect to each other:

$$G_p \leqq G_t + G_r. \tag{3}$$

An example illustrating when $G_p = G_t + G_r$ is the case of propagation in free space or over a plane surface between half-wave horizontal antennas separated by a distance $d \gg \lambda$ and oriented normal to the plane of incidence.

It is convenient to express the results of propagation measurements and theoretical calculations in terms of the "basic transmission loss" expected if isotropic transmitting and receiving antennas were used. This basic transmission loss, L_b, may be determined from a measured transmission loss, L, by adding the path antenna gain:

$$L_b \equiv L + G_p. \tag{4}$$

When this path antenna gain is not known, an estimate of L_b may be made by assuming that the free space gains of the transmitting and receiving antennas are realized; this estimated value of basic transmission loss will, of course, always be a little too large.

Since the results of many propagation studies made in the past have been expressed in terms of the field strength, E, expressed in decibels above one microvolt per meter for one kilowatt effective power radiated from a half-wave dipole, it is desirable to be able to compute L_b from E:

$$L_b = 139.367 + 20 \log_{10} f_{mc} - E. \tag{5}$$

In most determinations of E from measured data it has been implicitly assumed that the free space antenna gains were realized; i.e., that $G_p = G_t + G_r$, and thus the values of L_b determined by (5) from such values of E will generally be a little too large, not only in the region near the transmitter[14] where the directivity of the transmitting antenna in the direction of the receiver may not have been a maximum when the measurements of E were made, but also in the distant scattering region where a wide angular range of propagation paths is involved.[15] For propagation paths involving forward scattering, G_p varies with time and may be considered to be a random normally-distributed variable.

II. Transmission Loss in Free Space

It is of interest to illustrate the magnitude of the transmission loss to be expected in free space; i.e., that component of the total transmission loss which is independent of the effects of the earth and the atmosphere.

Fig. 1 (next page) gives basic transmission loss in free space as function of frequency in megacycles, with the distance in miles as a parameter. The equation for the free space basic transmission loss in this case is simply:

$$L_{bf} = 36.58 + 20 \log_{10} d + 20 \log_{10} f_{mc} \tag{6}$$

where d is the distance in miles between the isotropic antennas, and f_{mc} is the radio frequency in megacycles. The losses given by (6) and shown on Fig. 1 are more or less typical of a mobile broadcast type of service in which essentially non-directional antennas are used at both terminals of the transmission path. With half-wave dipoles at each end of the path, subtract $G_p = 2.15 + 2.15 = 4.3$ decibels from the values of L_{bf} given by (6)

[12] This is the phenomenon of obstacle gain which was found in theory to exceed 120 decibels on some of the transmission paths studied.

[13] K. A. Norton, "Transmission loss in radio propagation," Proc. IRE, vol. 41, pp. 146–152; January, 1953.

[14] K. A. Norton, "Transmission loss of space waves propagated over irregular terrain," Trans. IRE, vol. AP-3, pp. 152–166; August, 1952.

[15] J. W. Herbstreit, K. A. Norton, P. L. Rice, and G. E. Schafer, "Radio Wave Scattering in Tropospheric Propagation," 1953 IRE Convention Record, Part 2, "Antennas and Communication," pp. 85–93.

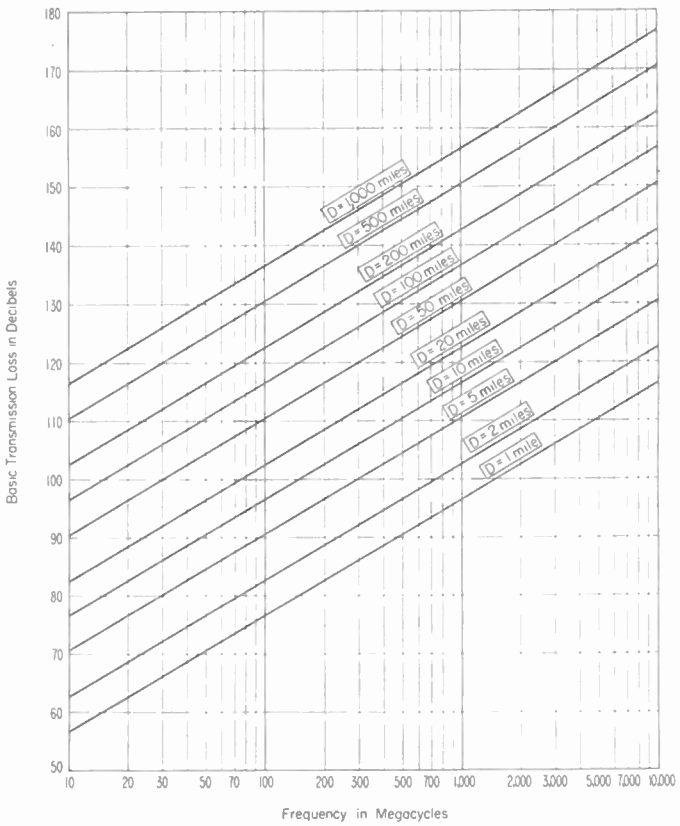

Fig. 1—Basic transmission loss in free space, i.e., with isotropic antennas at both terminals.

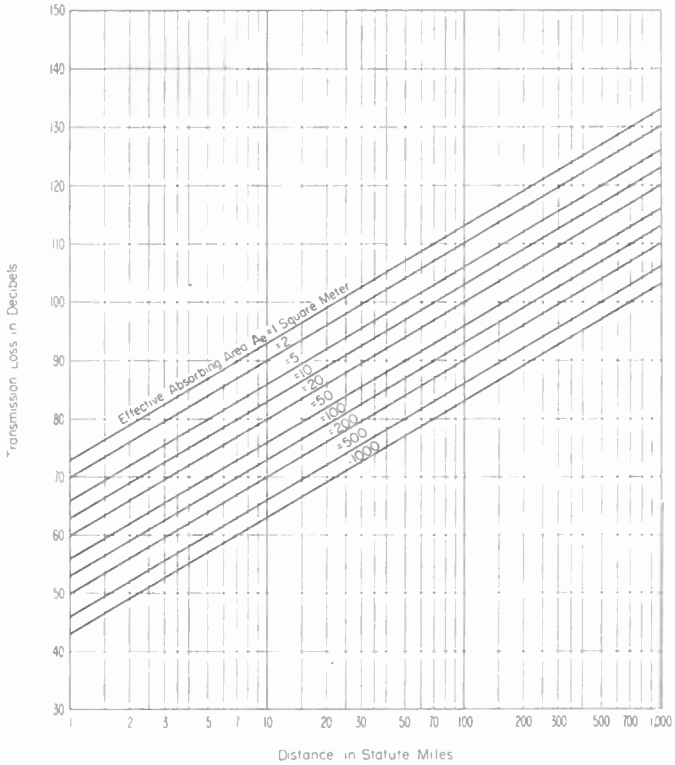

Fig. 2—Transmission loss in free space with a half-wave dipole at one terminal and an antenna with an effective absorbing area A_e square meters at the other terminal. (For $f_{mc} > 100/\sqrt{A_e}$.)

and on Fig. 1 in order to obtain estimates of the expected transmission loss L_f. Note that the losses increase rapidly with increasing frequency because of the decreasing absorbing area of the receiving antenna. This indicates the desirability, in general, of keeping this kind of service at the lowest available frequencies.

Fig. 2 gives the expected transmission loss in free space for a type of broadcast service in which a half-wave dipole antenna (nondirectional in the equatorial plane) is used at one terminal while a directional array with an effective absorbing area of A_e square meters is used at the other terminal. Such an array has a gain relative to an isotropic antenna given by[16]

$$G = 10 \log_{10} (4\pi A_e/\lambda^2)$$
$$= 10 \log_{10} A_e + 20 \log_{10} f_{mc} - 38.54 \quad (7)$$
$$(\text{For } f_{mc} > 100/\sqrt{A_e}),$$

and the free-space transmission loss may be expressed

$$L_f = 72.97 + 20 \log_{10} d - 10 \log_{10} A_e \quad (8)$$
$$(\text{For } f_{mc} > 100/\sqrt{A_e}).$$

Note that the free space transmission loss in this case is independent of the frequency. In this case again, because of the additional loss arising from the effects of irregular terrain[14] which usually increases somewhat with increasing frequency, it is generally desirable to keep this kind of broadcasting service at the lowest available frequencies.

Finally, Fig. 3 gives the expected transmission loss in free space for a point-to-point type of service in which high gain (and thus highly directional) antennas may be used at both terminals of the transmission path. The equation for the free space transmission loss in this case becomes:

$$L_f = 113.67 + 20 \log_{10} d - 20 \log_{10} f_{mc} - 20 \log_{10} A_e \quad (9)$$
$$(\text{For } f_{mc} > 100/\sqrt{A_e}).$$

For services of this type it is clear that the highest frequencies free from the effects of atmospheric absorption are likely to be the most efficient.

We see on Fig. 3 that the expected transmission loss is shown equal to zero at the shorter distances and higher frequencies. It should be noted, however, that a transmission loss of zero implies that the power available from the receiving antenna is equal to that radiated from the transmitting antenna and this is, of course, impossible. This difficulty arises from the fact that the gain $G = 10 \log_{10} (4\pi A_e/\lambda^2)$ assumed in these calculations will not be fully realized at these higher frequencies and shorter distances. This phenomenon is one which deserves further study. In particular, it would appear that there should be an optimum size of antenna for a given frequency and distance range.

As was described in more detail elsewhere,[13,17] the

[16] J. C. Slater, "Microwave Transmissions," chapter VI, McGraw-Hill Book Co., Inc., New York, N. Y., and London, England; 1942.

[17] W. Q. Crichlow, D. F. Smith, R. N. Morton and W. R. Corliss, "World-wide radio noise levels expected in the frequency band from 10 kilocycles to 100 megacycles," NBS Circular 557, Aug. 25, 1955.

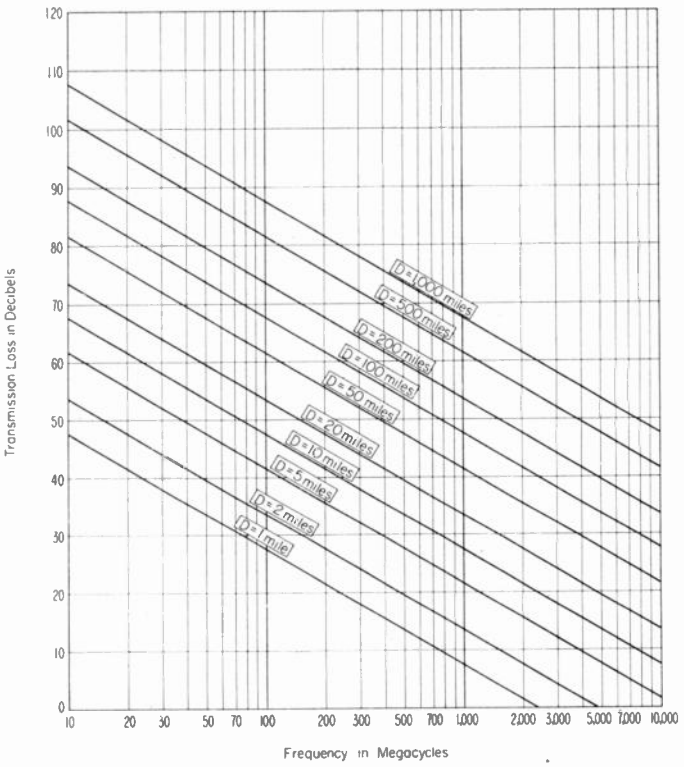

Fig. 3—Transmission loss in free space for antennas with 200 square meters effective absorbing area at both terminals.

determination of an optimum frequency for any particular type of radio service requires, in addition to transmission loss information, that appropriate allowance be made for the effects of atmospheric, galactic, and receiver noise on the minimum received signal power required for satisfactory service, as well as for the transmitter powers realizable in the various frequency bands. All of the values of transmission loss shown in Figs. 1, 2, and 3 are for transmission in free space. To determine the transmission loss expected for an actual path, it is necessary to add the additional transmission loss expected for the actual path relative to these free space values, together with any additional loss in path antenna gain due to scattering.[15] The assessment of these additional losses on beyond-the-horizon paths is the primary purpose of this paper.

The next section describes, in some detail, the geometrical parameters required to define the essential features of a long-distance propagation path.

III. The Geometrical Parameters Describing the Transmission Path

In this paper two important assumptions are made in order to define a model of the terrain which is amenable to theoretical treatment: that consideration need be given only to the terrain along the great circle path; and that this terrain along the great circle path may be described adequately by replacing it by four circular arcs which are tangent to the radio horizon rays from the transmitting and receiving antennas at the same two points that these horizon rays are tangent to the earth. These four circular arcs are described in detail later.

The justification for the first of the above assumptions was discussed for the case of propagation within the radio horizon in a recent paper by one of the authors;[14] in beyond-the-horizon transmission there is a further justification for this assumption in that the formulas for the diffraction loss over a sphere and over a parabolic cylinder—with axis normal to the great circle plane and with the same radius of curvature in the great circle plane as that of the sphere—have exactly the same exponential term deep in the shadow region even though the curvatures of these two models are far different in the plane normal to the path.[18] Basically the justification for considering only the terrain along the great circle path arises from the principle of stationary phase. Assumption above was made in order to provide a simple modified smooth earth model for which diffraction and scattering calculations can readily be made.

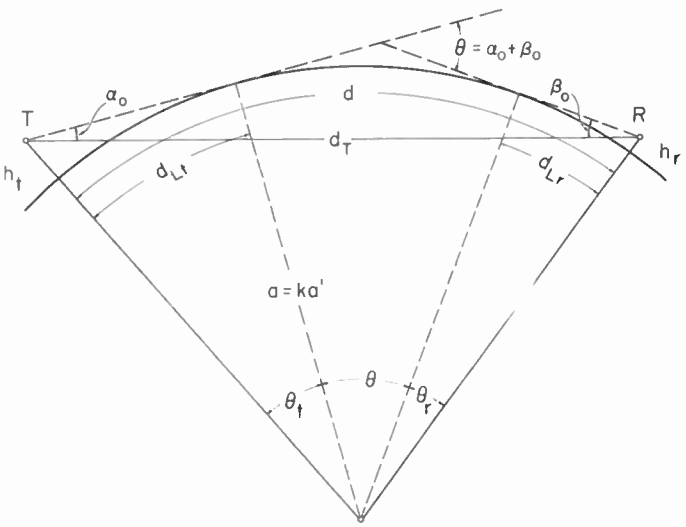

Fig. 4—Geometry for determining the angular distance, θ, in propagation over a smooth sphere.

Fig. 4 illustrates the geometry for propagation over a smooth sphere. The angular distance, θ, is defined to be the angle in the great circle between the horizon rays from the transmitting and receiving antennas as determined for a radio standard atmosphere; i.e., with an effective radius of the earth 4/3 of its actual value. The angular distance is positive for receiving antennas below the horizon ray from the transmitting antenna, is equal to zero for receiving antennas on this horizon ray, and is negative for receiving antennas above this horizon ray.

The factor, k, is the ratio of the effective to the actual radius of the earth and allows only for the systematic effects of a linear gradient of refractive index of the atmosphere. This gradient is usually negative and is

[18] S. O. Rice, "Diffraction of plane radio waves by a parabolic cylinder," *Bell Sys. Tech. Jour.*, vol. 33, pp. 417–504; March, 1954; also Bell Telephone System Monograph 2278.

measured in a companion paper by Bean and Meaney[19] by the change ΔN in the scaled up refractivity between the surface and a height of one kilometer above the surface. The scaled up refractivity is given by $N \equiv (n-1)\cdot 10^6$ where n denotes the refractive index of the atmosphere. The factor, k, is given by:

$$(1/k) = 1 + a'(dn/dh) = 1 + 0.006373\Delta N, \qquad (10)$$

and we see that $\Delta N = -39.23$ for $k = 4/3$. The paper by Bean and Meaney[19] provides the expected monthly median values of ΔN for the United States in the form of isopleths for several months of the year.

The actual radius of the earth, a', is taken to be 3,960 miles so that $ka' = 5{,}280$ miles for a radio standard atmosphere for which $k = 4/3$. Although it is possible to compute different values of θ for different values of k (corresponding to different linear gradients of refractive index), this has, in general, not been found to be a useful method of analysis. Instead, a single value of θ is computed for each propagation path assuming $k = 4/3$, and then separate allowance is made for linear gradients of refractivity other than that corresponding to $k = 4/3$.

We see by Fig. 4 that the formula for θ over a smooth spherical earth is simply:

$$\theta = \frac{d - d_{Lt} - d_{Lr}}{ka'} \text{ radians} \qquad (11)$$

where the distances d_{Lt} and d_{Lr}, to the radio horizons of the transmitting and receiving antennas may be determined by:

$$d_{Lt} \cong \sqrt{2ka'h_t} \qquad (12)$$

$$d_{Lr} \cong \sqrt{2ka'h_r}. \qquad (13)$$

Since tropospheric propagation usually involves distances, d, much less than 1,000 miles, negligible error will be made by assuming $\sin(\theta/2) = (\theta/2)$ and $d = d_T$; e.g., over a smooth earth of radius $ka' = 5{,}280$ miles with $h_t = h_r = 0$, $\theta = (d/ka') = 0.2$ radian for $d = 1{,}056$ miles and $\sin(\theta/2) = 0.0998$ which differs from $(\theta/2)$ by much less than 1 per cent even for such an extreme case. Although it will usually be more convenient to illustrate the terrain paths by using a height scale much expanded relative to that used for distance, the reader should bear in mind that the actual angles involved are always very small. Since these angles are small, it will often be convenient to express the angular distance, θ_{mr}, in milliradians; for the transmission paths so far studied the largest value of $\theta_{mr} = 108$ milliradians.

The principal advantage of the use of θ in propagation analyses arises, however, in applications to propagation over irregular terrain. Fig. 5 illustrates the geometry for determining over irregular terrain the location of the horizon of an antenna in the great circle plane.[14] Let h denote the height above sea level of the terrain along the great circle path at a distance, x, from the antenna for which the horizon is to be determined and plot $(h - x^2/2ka')$ as a function of x on linear graph paper.[20] A straight line from the transmitting antenna at a height, h_{ts}, above sea level will be tangent to this terrain plot at the horizon. Although both horizons can be determined from a single graph, as illustrated on Fig. 5 with the receiving antenna height at $(h_{rs} - d^2/2ka')$, it is often more convenient to determine the locations of the two horizons by means of two separate graphs with x measured first from the transmitting antenna and then from the receiving antenna. It should be clear from the above discussion that the location of the actual radio horizon will depend upon the linear gradient of refractive index characteristic of the transmission path; however, the geometrical parameters are all defined in terms of a standard atmosphere throughout this paper.

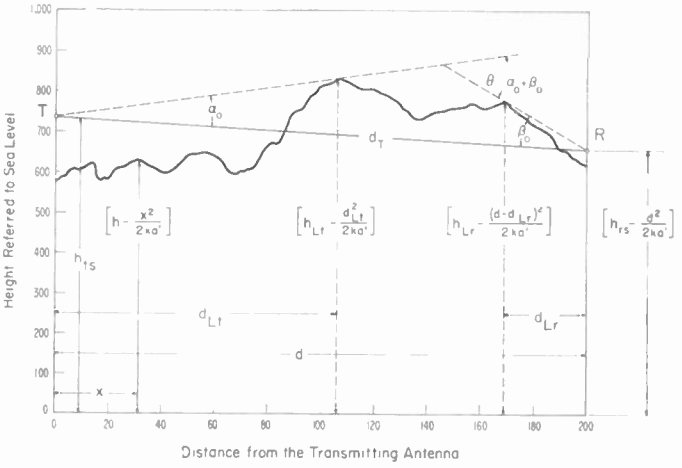

Fig. 5—Method of determining the great circle plane profile used for calculating the geometrical parameters in propagation over irregular terrain.

If now we let h_{Lt} and h_{Lr} denote the heights of the terrain above sea level at the respective horizons of the transmitting and receiving antennas, then the following formulas may be used to calculate α_0 and β_0 and thus the angular distance $\theta \equiv \alpha_0 + \beta_0$:

$$\alpha_0 = \frac{\left(h_{Lt} - \frac{d_{Lt}^2}{2ka'} - h_{ts}\right)}{d_{Lt}} + \frac{\left(h_{ts} - h_{rs} + \frac{d^2}{2ka'}\right)}{d} \qquad (14)$$

$$\beta_0 = \frac{\left(h_{Lr} - \frac{d_{Lr}^2}{2ka'} - h_{rs}\right)}{d_{Lr}} + \frac{\left(h_{rs} - h_{ts} + \frac{d^2}{2ka'}\right)}{d}. \qquad (15)$$

The derivation of the above expression for α_0 should be clear from Fig. 5, and the derivation for β_0 may be obtained simply by interchanging the t and r subscripts.

[19] B. R. Bean and F. M. Meaney, "Some applications of the monthly median refractivity gradient in tropospheric propagation," p. 1419, this issue.

[20] The scales in Fig. 5 show height in feet and distance in miles, but in the formulas height and distance are in the same units. When h is expressed in feet, x in miles, and the calculations are confined to a standard atmosphere so that $ka' = 5{,}280$ miles, the quantity to be plotted is simply $(h - x^2/2)$.

Fig. 6 shows geometry involved in fitting four circular arcs of effective radii, $k_{te}a'$, $k_{re}a'$, k_ta', k_ra' to the terrain.

If we require that the two circular arcs in the middle of the path merge smoothly and also require that they be tangent to the horizon rays at the horizons of the antennas, we find that:

$$k_ta' = \frac{1}{\alpha_1}\left(\frac{d\beta_0}{\theta} - d_{Lt}\right)$$

$$\cong \frac{(d - d_{Lt} - d_{Lr})}{\theta} \cdot \frac{\left(d\,\frac{\beta_0}{\theta} - d_{Lt}\right)}{\left(d\,\frac{\alpha_0}{\theta} - d_{Lr}\right)}, \qquad (16)$$

$$k_ra' = \frac{1}{\beta_1}\left(\frac{d\alpha_0}{\theta} - d_{Lr}\right)$$

$$\cong \frac{(d - d_{Lt} - d_{Lr})}{\theta} \cdot \frac{\left(d\,\frac{\alpha_0}{\theta} - d_{Lr}\right)}{\left(d\,\frac{\beta_0}{\theta} - d_{Lt}\right)}. \qquad (17)$$

$$\alpha_1 = \theta \cdot \frac{\left(d\,\frac{\alpha_0}{\theta} - d_{Lr}\right)}{(d - d_{Lt} - d_{Lr})}, \qquad (18)$$

$$\beta_1 = \theta \cdot \frac{\left(d\,\frac{\beta_0}{\theta} - d_{Lt}\right)}{(d - d_{Lt} - d_{Lr})}. \qquad (19)$$

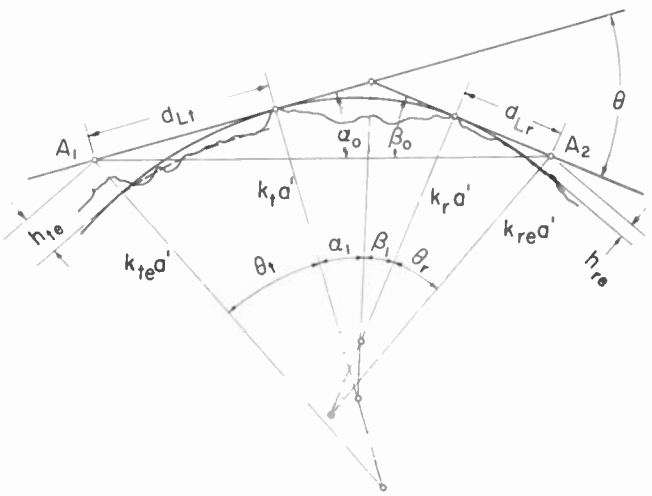

Fig. 6—Smooth earth model illustrating how the four different effective earth's radius factors k_{te}, k_{re}, k_t, and k_r are defined. Note that the transmitting antenna is defined to have a height h_{te} above the dashed curve which is a linear least squares fit to the heights above sea level of the central eight-tenths of the terrain between the transmitting antenna and its radio horizon.

The radii of curvature $k_{te}a'$ and $k_{re}a'$ are determined, as may be seen on Fig. 6, by requiring that the corresponding circular arcs be tangent to the horizon rays at the horizons of the transmitting and receiving antennas, respectively, and that they also pass through specified points immediately below these antennas. These specified points are at heights $(h_{ts} - h_{te})$ and $(h_{rs} - h_{re})$ above sea level where h_{te} and h_{re} are the "effective" heights of these two antennas above the irregular terrain surface. When these two conditions are satisfied, we find the following approximate expressions for the radii of curvature of the circular arcs at the two ends of the transmission path:

$$k_{te}a' \cong \frac{d_{Lt}^2}{2h_{te}} \qquad (20)^{21}$$

$$k_{re}a' \cong \frac{d_{Lr}^2}{2h_{re}}. \qquad (21)$$

The proper determination of the effective heights, h_{te} and h_{re}, presents a difficult problem which we do not yet claim to have solved adequately. Thus, in some cases these effective heights have been considered to be the actual structural heights of the centers of radiation of the antennas above the local terrain; this was the case, for example, for all of the receiving antennas on the transmission paths studied in this paper. In those cases where the transmitting antenna site is especially selected so as to be high above the surrounding terrain, its effective height, h_{te}, was determined either as (a) the height above a curve fit to a part—usually the central eight-tenths—of the terrain between the antenna and its radio horizon, as illustrated by the dashed curved line on Fig. 6; or (b) the height above the average terrain 2 to 10 miles from the antenna along the transmission path; or (c) the height above the average of all of the surrounding terrain 2 to 10 miles from the antenna. In view of these rather arbitrary definitions, it is fortunate, as will become evident later that the need for accurate determinations of these effective heights is largely eliminated by using angular distance as the principal parameter in our transmission loss formulas. It is of interest to note that k_t and k_r are both equal to zero when the transmitting and receiving antenna have a common horizon, since $d = d_{Lt} + d_{Lr}$ for such a case; for these cases the knife-edge diffraction formula should be applicable, since a parabolic cylinder with a radius of curvature equal to zero is just a knife edge.[18]

In summary, then, the engineer wishing to estimate the median transmission loss for a particular propagation path of length, d, would proceed as follows to determine the remaining pertinent geometrical parameters. The distances, d_{Lt} and d_{Lr}, to the radio horizons of the two antennas are determined by plotting the antenna heights and the terrain heights above sea level in the manner illustrated on Fig. 5. Such a terrain plot also serves, however, to determine h_{Lt} and h_{Lr}. When these two additional parameters of the terrain are known, it is possible to calculate, using the above for-

[21] An exact solution for $k_{te}a'$ may be obtained by solving the transcendental equation $\sec\theta_t = (1 + h_{te}/k_{te}a')$ where $\theta_t = (d_{Lt}/k_{te}a')$; the value given by the approximate expression (20) will be in error by less than 1 per cent when the resulting value of θ_t is less than 0.15 radian.

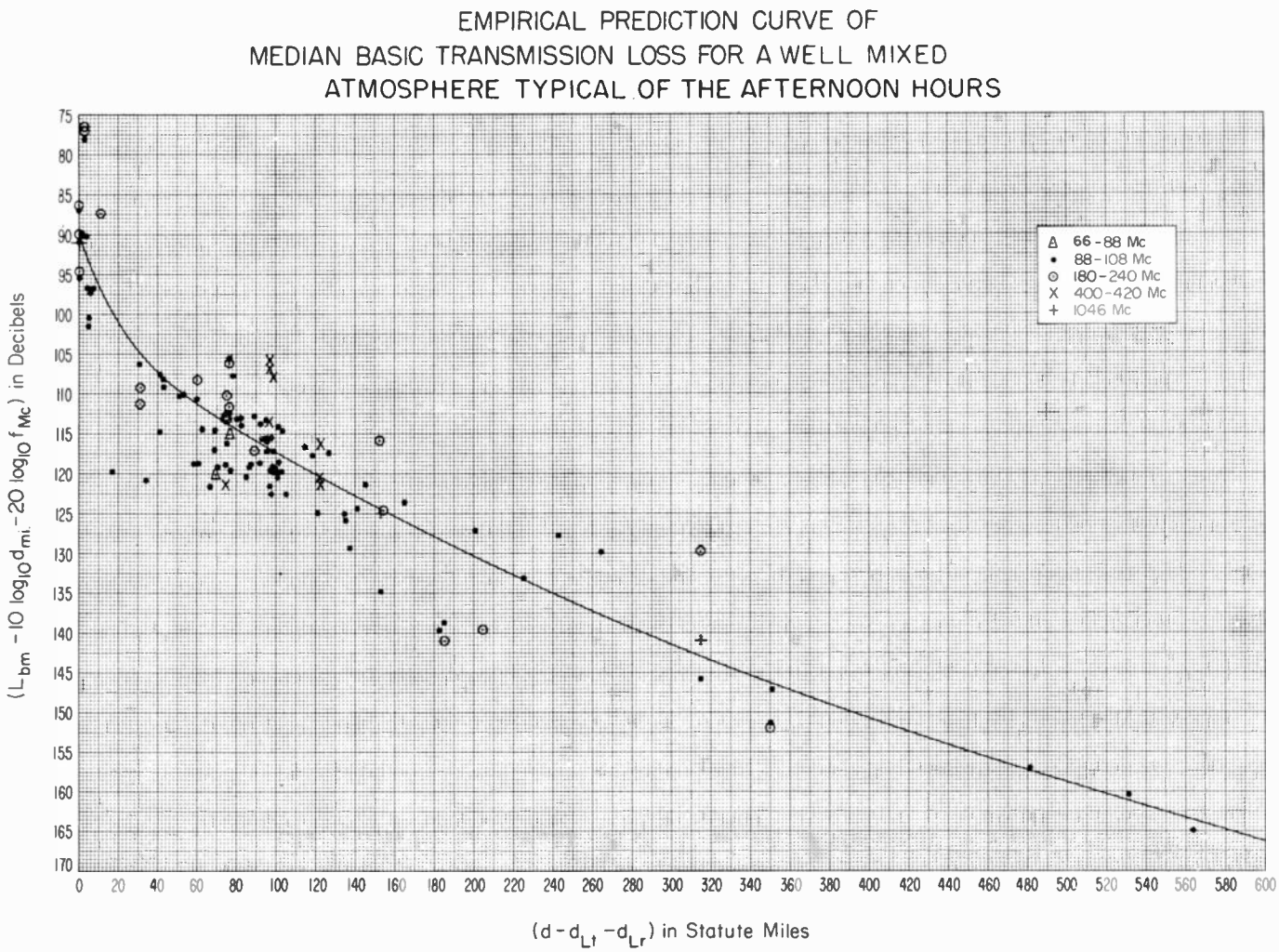

Fig. 7—Empirical prediction curve of modified median basic transmission loss for a standard atmosphere. To determine median basic transmission loss L_{bm} add $10 \log_{10} d_{mi} + 20 \log_{10} f_{mc}$ to the ordinate value read from the curve.

mulas, the values of α_0, β_0, θ, k_t, k_r, α_1, and β_1. Rough estimates of h_{te} and h_{re} may now be made and k_{te} and k_{re} then calculated. These are all of the geometrical parameters required for use in the theoretical formulas for the diffracted and scattered fields.

This completes the discussion of the geometrical parameters defining our terrain models, and we may proceed to the development of our transmission loss formulas.

IV. An Empirical Curve for Predicting Transmission Loss and a Description of the Radio Data

In this section an empirical curve is presented which appears to be useful for correlating our radio data on over-land transmission paths. It is important to emphasize that this curve will be useful only in the restricted range of frequencies, distances and antenna heights covered by the data from which it was derived. Appendix IV gives some of the details of the 122 transmission paths involved. The frequencey ranged from 66 to 1,046 megacycles, the distance ranged from 44.9 to 628.1 statute miles, the angular distance ranged from 0.9 to 107.8 milliradians, the lower of the two terminal antenna heights ranged from 8 to 123 feet above the local terrain, while the higher of the two terminal antenna heights ranged from 40 to 7,800 feet above the terrain. An attempt was made to use data only for the times of day—1 P.M. to 6 P.M.—when great departures of refractive index profiles from a linear gradient are least likely in order to avoid the frequent occurrence of ducting and layer conditions. Estimates of the mean values of ΔN for the periods of time covered by our measurements are listed in Appendix IV and range from -36.6 to -53.3, the average value being -42.8, and thus a somewhat larger gradient than for a standard atmosphere. The above choice of data tends to yield the maximum values of transmission loss likely to be encountered in practice and are thus on the safe side for engineering purposes. It also yields data which are easier to interpret theoretically.

Fig. 7 gives our empirical transmission loss prediction curve for a well mixed atmosphere typical of the afternoon hours. The theoretical discussion in Appendices I and II indicates that the basic transmission loss in beyond-the-horizon transmission should contain a term $10 \log_{10} d_{mi}$, while the free space formula (2) indicates that it should contain a term $20 \log_{10} f_{mc}$. For this reason these terms have been subtracted from the observed

median basic transmission loss L_{bm0} before plotting it as a function of the geometrical parameter $(d-d_{Lt}-d_{Lr})$, which is just the distance between the radio horizons of the transmitting and receiving antennas.[22]

The use of this empirical prediction curve may be illustrated by means of an example. Assume (a) a total transmission path length of $d=100$ miles, (b) the distance from the transmitting antenna to its radio horizon $d_{Lt}=42$ miles, and (c) the distance from the receiving antenna to its radio horizon $d_{Lr}=8$ miles. Then $(d-d_{Lt}-d_{Lr})=50$ miles, and we find on Fig. 7 that $(L_{bm}-10\log_{10} d_{mi}-20\log_{10} f_{mc})=109.3$ decibels. If we add $10\log_{10} d_{mi}=20$ and $20\log_{10} f_{mc}$ to both sides of this equation, we obtain $L_{bm}=129.3+20\log_{10} f_{mc}$ as an equation for determining the expected median basic transmission loss over this particular 100 mile path. For example, the expected median transmission loss on 100 megacycles with half-wave dipoles at each end of the path would be $L_m=129.3-2.15-2.15+40=165$ decibels, and on 1,000 megacycles would be $L_m=185$ decibels.

The smooth curve on Fig. 7 is so drawn that the average of deviations of data from the curve is approximately zero. The root-mean-square deviation of these data from the curve is 5.67 decibels. The data represent a total of 136,000 hourly medians, a frequency range from 66 to 1,046 megacycles, and 122 propagation paths.

Field strengths are higher in summer than in winter on an average, and a diurnal minimum is found somewhere between 1 P.M. and 6 P.M. on most daily records. To allow for such effects in our analysis, the data have been grouped into eight "Time Blocks," defined in the following table:

TIME BLOCKS

1. Nov.–Apr.	6 A.M.– 1 P.M.
2. Nov.–Apr.	1 P.M.– 6 P.M.
3. Nov.–Apr.	6 P.M.–12 Mn.
4. May–Oct.	6 A.M.– 1 P.M.
5. May–Oct.	1 P.M.– 6 P.M.
6. May–Oct.	6 P.M.–12 Mn.
7. May–Oct.	12 Mn.– 6 A.M.
8. Nov.–Apr.	12 Mn.– 6 A.M.

Fig. 8 shows an example of a cumulative distribution of hourly medians for station KXYZ-FM, Houston, Texas, as recorded within Time Block 6 by the University of Texas at Austin. Note that these hourly medians are very nearly distributed in a normal probability distribution; i.e. the hourly median field intensities are from log normal distributions.

Each data point in Fig. 7 is a weighted average of six-month medians which correspond either to Time Block 2 or to Time Block 5. The median of each set of hourly medians was weighted in accordance with the number of hours of recording. The derivation of these weights will be described in detail in a future report; each is the reciprocal of the variance of estimates of a time block median obtained from a number of samples of the same size. For sample sizes of 1, 5, 9, 18, 45, 90, 180, 450, and 900 hours, respectively, these weights were 0.046, 0.054, 0.07, 0.1, 0.16, 0.23, 0.32, 0.48, and 0.58; this last weight corresponds to a standard deviation of 1.31 decibels in estimates of a Time Block 2 or 5 median where all possible hours (approximately 900) are recorded. Over some paths observations were made for several years, and over other paths, for a much shorter period.

A recent report by Rice and Daniel[23] indicates the differences that may be expected between time blocks for 100 mc transmissions.

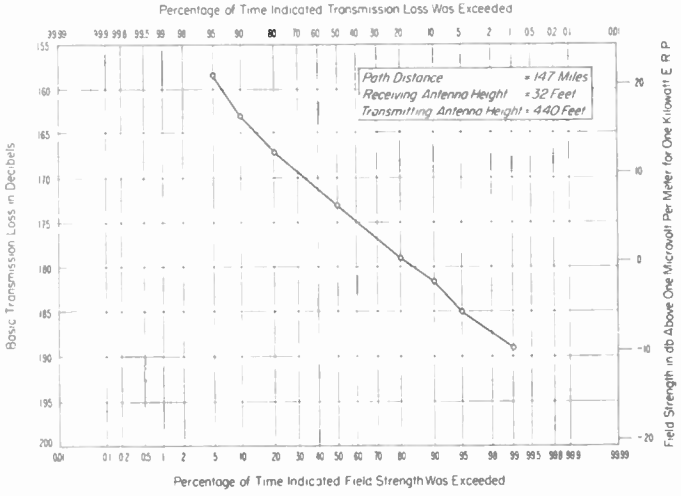

Fig. 8—Cumulative distribution of hourly median transmission loss recorded at Austin, Texas from KXYZ-FM, Houston, Texas, between June 14, 1951 and October 31, 1951. 6 P.M.–11 P.M., C.S.T.

Although the empirical prediction curve on Fig. 7 is much easier to use than the theoretical formulas given in the following sections of this paper, the latter provide a better understanding of the various phenomena involved and provide a much safer basis for extrapolation of the experimental data to other conditions. As an example, the theory indicates that the $20\log_{10} f_{mc}$ term in the empirical formula becomes $30\log_{10} f_{mc}$ at frequencies higher than 1,000 mc. Actually, when an empirical curve similar to that on Fig. 7 was developed using $30\log_{10} f_{mc}$ as the basis, the root-mean-square deviation of the data from the curve only increased from 5.67 db to 6.30 db.

V. The Dependence of Transmission Loss over a Model Smooth Earth on the Angular Distance θ

In this section diffraction and scattering theories will be used to show how the transmission loss may be expected to vary with angular distance, frequency, dis-

[22] When terrain profiles are not available, so that d_{Lt} and d_{Lr} cannot be determined by the methods in the previous section, but estimates of the effective transmitting and receiving antenna heights h_{te} and h_{re} are obtainable, use may be made of the smooth four-thirds earth relations, $d_{Lt}=\sqrt{2h_{te}}$ and $d_{Lr}=\sqrt{2h_{re}}$, where distances are in miles and heights in feet.

[23] P. L. Rice and F. T. Daniel, "Radio transmission loss versus distance and antenna height at 100 mc," *Trans. IRE, PGAP*, vol. AP-3, pp. 59–62; April, 1955. Fig. 2 in this reference compares with Fig. 7 in the present report, with $(d-d_{Lt}-d_{Lr})$ set equal to $(d-\sqrt{2h_{te}}-\sqrt{2h_{re}})$, and the differences between time blocks are essentially a function of this latter parameter. In Fig. 2 the standard deviation of points about the curve was given erroneously as 2.78 decibels and should have been 4.5 decibels.

tance, antenna height, and the assumed linear refractivity gradient ΔN of the earth's atmosphere.

The curves presented in this section are intended to be representative of over-land transmission paths. Thus the fact that the horizon for an over-land propagation path is systematically higher than the adjacent terrain is accounted for in our smooth-earth model by increasing the curvature of the earth somewhat between the radio horizons. An analysis of the values of the effective earth's radius factors for more than 130 different terrain profiles has led us to choose $k_t = k_r = 1$ [see (16) (17)] and $k_{te} = k_{re} = 4/3$ [see (20), (21)] as being representative of an average over-land path.

At small angular distances the transmission loss is calculated by means of the van der Pol-Bremmer[1] diffraction theory using the equations described in Appendix I. This is shown on Fig. 9 for 100 megacycle waves transmitted between antennas at 1,000 feet and 30 feet (a) in free space and (b) over our smooth-earth model.

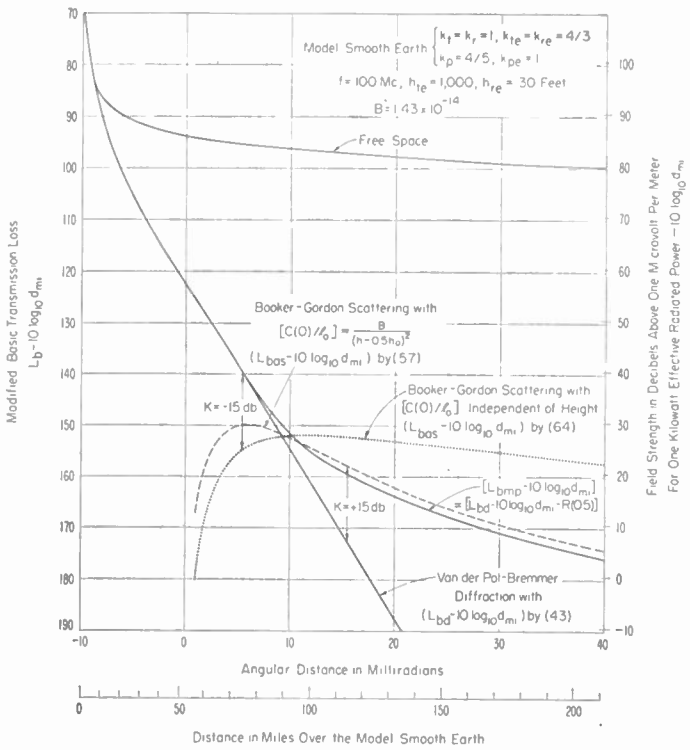

Fig. 9—Illustration of the method of combining the calculated diffracted and scattered fields.

Note that two abscissa scales are shown on Fig. 9, one giving the angular distance in milliradians and the other the transmission path length in statute miles. Note also that the relation between the distance and angular distance scales is different for positive and negative angular distances. This is characteristic of our model smooth earth for which the radius of curvature is smaller between the radio horizons ($k_t = k_r = 1$) than it is from the antennas out to their respective horizons ($k_{te} = k_{re} = 4/3$). Thus for the model smooth earth $d = d_{Lt} + d_{Lr} + 5{,}280\ \theta$ when θ is negative and $d = d_{Lt} + d_{Lr} + 3{,}960\ \theta$ when θ is positive.

Two ordinate scales are given on Fig. 9. The one on the right decreases downwards and gives the field strength E in decibels above one microvolt per meter for one kilowatt of effective radiated power, minus 10 $\log_{10} d_{mi}$, while the one on the left increases downwards and gives the basic transmission loss L_b for the path minus 10 $\log_{10} d_{mi}$.

At large angular distances the transmission loss is calculated as described in Appendix II by means of the Booker-Gordon scattering theory.[24,25] Booker and Gordon based their development of tropospheric scattering theory on the exponential correlation function:

$$C(R) = C(0) \exp(-R/l_0) \qquad (22)$$

where $C(R)$ is the cross correlation between the variations of refractive index, n, at points within the scattering volume separated by a distance R, $C(0)$ is the mean square departure $[\overline{(\Delta n/n)^2}]$ of the refractive index from its mean value, and l_0 is a scale length representative of this isotropic model of atmospheric turbulence. Meteorological data[26–29] appear to indicate that the parameter $[C(0)/l_0]$ decreases rapidly with increasing height at large heights. By assuming that the Booker-Gordon scattering theory is correct and that $[C(0)/l_0]$ varies in inverse proportion to the square of the height above the earth's surface, we may use our radio data obtained at large angular distances to determine the magnitude of $[C(0)/l_0]$ at height of one kilometer above the surface; this value of $[C(0)/l_0]$ at one kilometer is designated by B. Two values of B have been used for the calculations and illustrative graphs in this section of the paper: 1.43×10^{-14} and 8.07×10^{-14} since they lead to results which correspond approximately to our radio data obtained in different parts of the United States. In particular, the value $B = 1.43 \times 10^{-14}$ gives results in good agreement with data obtained in the NBS Cheyenne Mt. experiment.[30] When these radio estimates of $[C(0)/l_0]$ are extrapolated to heights well below one kilometer, they indicate values which are much larger than have been observed. Furthermore, the use of these radio estimates of $[C(0)/l_0]$ at very low heights yields

[24] H. G. Booker and W. E. Gordon, "A theory of radio scattering in the troposphere," PROC. IRE, vol. 38, pp. 401–412; April, 1950.

[25] W. E. Gordon, "Radio scattering in the troposphere," PROC. IRE, vol. 43, pp. 23–28; January, 1955.

[26] G. Birnbaum, H. E. Bussey, and R. R. Larson, "The microwave measurement of variations in atmospheric refractive index," *Trans. IRE Professional Group on Antennas and Propagation*, vol. PGAP-3, pp. 74–78; August, 1952.

[27] C. E. von Rosenberg, C. M. Crain, and A. W. Straiton, "Atmospheric refractive-index fluctuations as recorded by an airborne microwave refractometer," *Elec. Eng. Res. Lab.*, Univ. of Texas, Rep. No. 6-01, February 6, 1953. Data shown in Figs. 10 and 11 were measured in Ohio in July and August, 1952.

[28] C. M. Crain, "Survey of airborne microwave refractometer measurements," p. 1405, this issue. There is a summary and bibliography of more recent data in this paper.

[29] G. Birnbaum and H. E. Bussey, "Amplitude, scale and spectrum of refractive index inhomogeneities in the first 125 meters of the atmosphere," p. 1412, this issue.

[30] A. P. Barsis, J. W. Herbstreit, and K. O. Hornberg, "Cheyenne Mountain tropospheric propagation experiments," NBS Circular 554, January 3, 1955, available from the Superintendent of Documents, Government Printing Office, Washington 25, D. C.

scattered radio fields comparable to the diffracted fields at very small angular distances, and this implies very much larger fading ranges than have been observed. Thus we are led to consider (see Fig. 10) a model of the atmosphere in which $[C(0)/l_0]$ is independent of height up to 2,250 feet, and then decreases in inverse proportion to the square of the height. The method of calculation of scattered fields at large heights is discussed in Appendix II(a), while the method for low heights is discussed in Appendix II(c). The scattered fields calculated by these two methods are shown on Fig. 9 by the dashed and dotted curves. Throughout this paper we have used the lower of these two curves, at any given angular distance, to represent the scattered field for the Booker-Gordon model.

It is also necessary to know the value of the scale of turbulence, l_0, in order to carry out the scattered field calculations in Appendix II(a) and (c). Fig. 11 gives some values of l_0 as a function of height above the surface as determined from the measurements reported.[26,27]

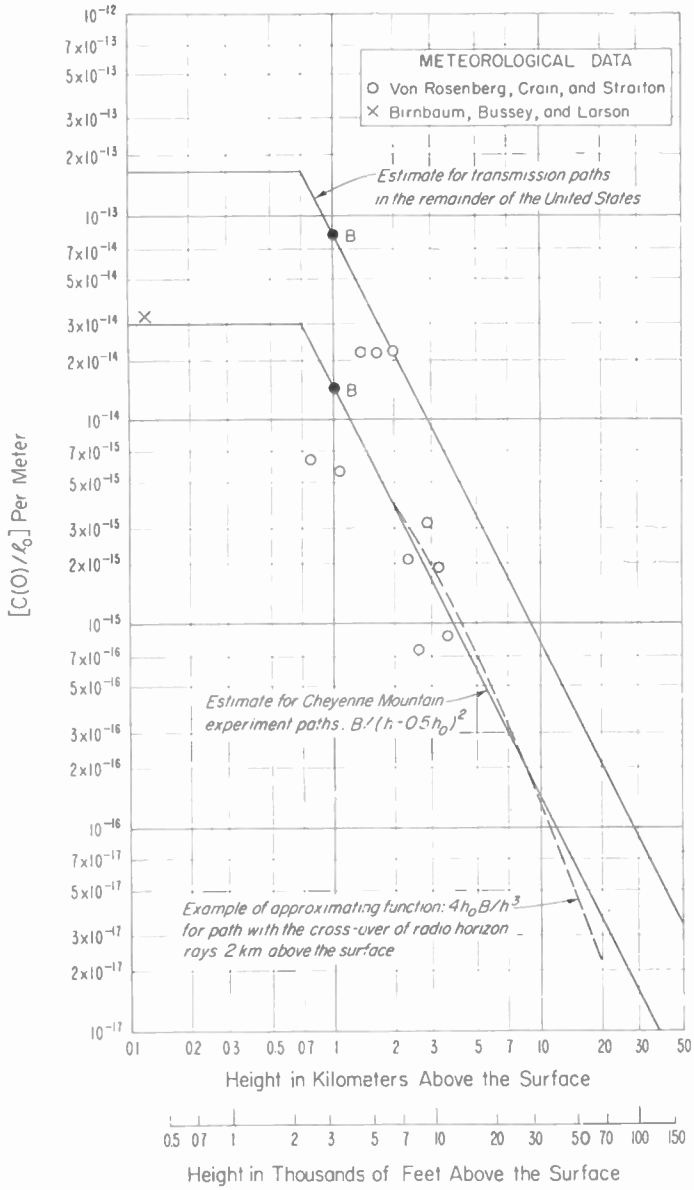

Fig. 10—Estimates of $[C(0)/l_0]$ obtained from radio transmission loss data assuming $C(R) = C(0) \exp(-R/l_0)$ where $C(0) = [(\Delta n/n)^2]$.

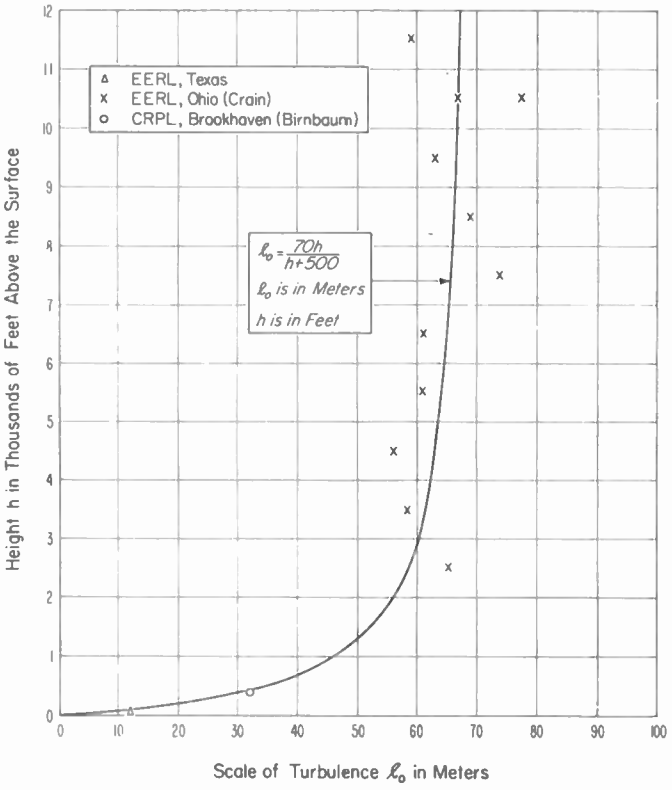

Fig. 11—Scale of turbulence versus height.

It has been established both experimentally[31,32] and theoretically[33] that the instantaneous power received via the scattering mode of propagation is Rayleigh distributed in time. Thus at intermediate angular distances the received field consists of two components, a slowly varying diffracted ground wave component, and a rapidly varying Rayleigh distributed scattered component. Formulas and graphs are given in a companion paper[34] in this issue which may be used to determine the median level, $R(0.5)$, and distribution of the sum of two such components. The procedure is as follows. First the transmission loss, L_{bd}, for the diffracted mode and the average transmission loss L_{bas} for the scattered Rayleigh distributed mode are calculated by the methods in Appendices I and II. Then we may determine $K = L_{bd} - L_{bas}$. The calculated, or predicted, median transmission loss may then be determined from:

$$L_{bmp} = L_{bd} - R(0.5), \tag{23}$$

[31] K. A. Norton, "Extension of FM broadcast range," *NBS Tech. News Bull.*, vol. 32, pp. 37–39; April, 1948.

[32] H. B. Janes, "An analysis of within-the-hour fading in 100–1,000 mc transmissions," *NBS Jour. Res.*, vol. 43, pp. 231–250; April, 1955.

[33] H. Staras, "Forward scattering of radio waves by anisotropic turbulence," p. 1374, this issue.

[34] K. A. Norton, L. E. Vogler, W. V. Mansfield, and P. J. Short, "The probability distribution of the amplitude of a constant vector plus a Rayleigh distributed vector," p. 1354, this issue.

or

$$L_{bmp} = L_{bas} + K - R(0.5). \quad (24)$$

When K is less than -16.5 decibels, L_{bmp} differs from L_{bd} by less than 0.1 decibel, and when K is greater than $+19.5$ decibels, L_{bmp} differs from $(L_{bas}+1.6)$ by less than 0.1 decibel. These formulas were used to determine the curve labelled $[L_{bmp}-10 \log_{10} d_{mi}]$ on Fig. 9 which is the calculated, or predicted, value of the median basic transmission loss minus $10 \log_{10} d_{mi}$. The determination of the level of this curve is illustrated on Fig. 9 by an example at $\theta = 15.5$ milliradians where $K \equiv L_{bd} - L_{bas} = 15$ decibels. Referring to Fig. 6 in reference 34 we find that $R(0.5) = 13.6$ decibels for $K = 15$ decibels so that $[L_{bmp} - 10 \log_{10} d_{mi}] = [L_{bd} - 10 \log d_{mi} - R(0.5)] = [172.6 - 13.6] = 159.0$ decibels.

Eqs. (36) and (43) in Appendix I for the basic transmission loss for the diffracted mode of propagation contain a term $10 \log_{10} d_{mi}$ which reflects the fact that the ground wave is propagated as though guided by the surface[1,35] in such a way that the spatial decay of its energy with distance is as $1/d$ rather than as $1/d^2$, as would be the case in free space. A similar resolution of the transmission loss for the scattered mode of propagation into terms dependent separately upon the physical distance, d, and the angular distance, θ, may be found in (57) and in (64) in Appendix II.

Over rough terrain the angular distance, θ, and the distance, d, are no longer uniquely related as they are over a smooth earth. Thus it is convenient to use theory to predict a "modified median basic transmission loss," $(L_{bm} - 10 \log_{10} d_{mi})$ and to compare predicted values with the corresponding measured values of the same quantity.

Fig. 12 gives $(L_{bm} - 10 \log_{10} d_{mi})$ at 100 megacycles for a wide range of transmitting antenna heights over a smooth four-thirds earth. The small circle on each curve in Fig. 12 indicates the angular distance at which the diffracted and scattered powers are equal. The scattered power was calculated for $B = 1.4 \times 10^{-14}$ so that comparison could be made with the Cheyenne Mountain data. *The important thing to notice in this figure is the very small variation in the expected values of transmission loss for a wide range of transmitting antenna heights at all positive angular distances.* A discussion of the data shown on this figure is given in the next section.

The discussion so far has neglected the effects of atmospheric absorption. This will be denoted by the symbol A_a, a positive quantity expressed in decibels. Unfortunately, there appears to be no information on atmospheric absorption effects over long transmission paths. At frequencies above uhf such effects are important even over small distances. Bussey[36] has shown that the expected additional absorption loss per kilometer is somewhat different over a 50-kilometer path than over a 1-kilometer path. Values taken from Kerr[37] based on the Van Vleck-Weisskopf absorption equation[38] indicate that the water-vapor absorption at 3,000 megacycles is of the order 0.2 decibels for a 500-mile path over the great plains of Colorado and Kansas, and to this must be added oxygen absorption of the order of 6.6 decibels.

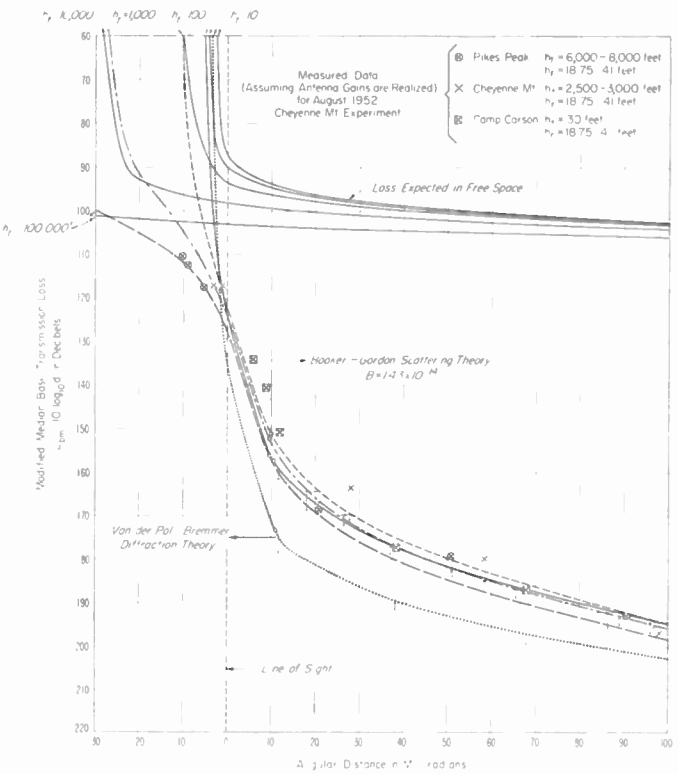

Fig. 12—Modified median basic transmission loss expected for 100 mc propagation over a model smooth earth; transmitting antenna heights as indicated, receiving antenna height 30 feet; $k_t = k_r = 1$; $k_{te} = k_{re} = 4/3$.

The influence of atmospheric absorption has not been included in the theoretical estimates of modified median basic transmission loss shown in the next figure, Fig. 13, where $(L_{bm} - 10 \log_{10} d_{mi} - A_a)$ is plotted versus θ for propagation over a smooth earth between transmitting and receiving antennas at 1,000 feet and at 30 feet and for 100, 1,000, and 10,000 megacycles. Two sets of curves are given on Fig. 13 for the expected transmission loss in the scattering region, one set based on the Booker-Gordon model and the other based on the Weisskopf-Villars model. These curves and the experimental data shown on them will be discussed more fully in later sections of the paper.

Fig. 14 indicates the expected influence at 100 megacycles of changing the value of the linear gradient of

[35] H. G. Booker and W. Walkinshaw, "The mode theory of tropospheric refraction and its relation to wave-guides and diffraction," pp. 80–127 of a report of a conference held on April 8, 1946: Meteorological Factors in Radio-Wave Propagation, published by the Phys. Soc. and the Roy. Met. Soc., London, Eng.

[36] H. E. Bussey, "Microwave attenuation statistics estimated from rainfall and water vapor statistics," PROC. IRE, vol. 38, pp. 781–785; July, 1950.

[37] D. E. Kerr, "Propagation of Short Radio Waves," MIT Rad. Lab. Series, vol. 13, p. 647, McGraw-Hill Book Co., Inc., New York, N. Y., 1951.

[38] J. H. Van Vleck and V. F. Weisskopf, "On the shape of collision-broadened lines," *Rev. Mod. Phys.*, vol. 17, pp. 227–236; April–July, 1945.

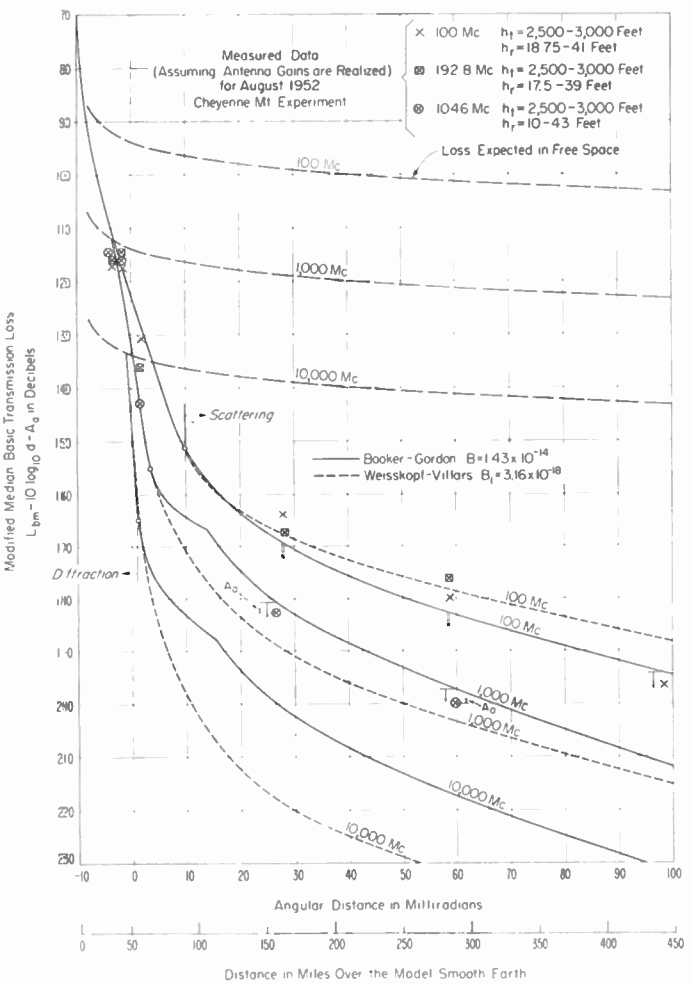

Fig. 13—Modified basic transmission loss expected for propagation over a model smooth earth; transmitting antenna height 1,000 feet; receiving antenna height 30 feet; frequency as indicated; $k_t = k_r = 1$; $k_{te} = k_{re} = 4/3$.

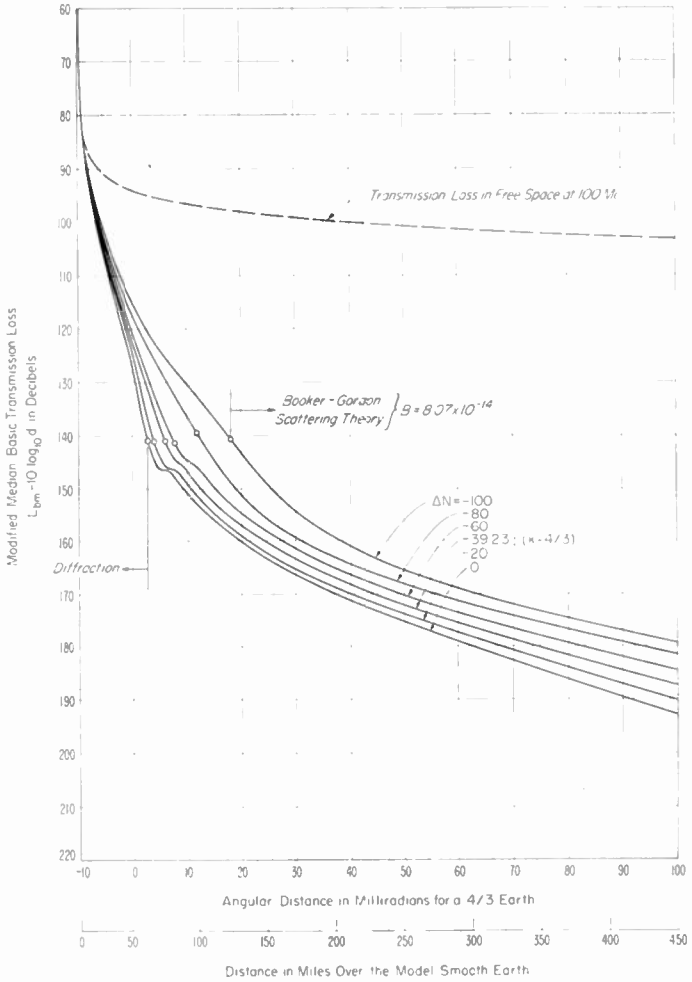

Fig. 14—Modified basic transmission loss expected for 100 mc propagation over a model smooth earth; transmitting antenna height 1,000 feet; receiving antenna height 30 feet; $k_p = 4/5$, $k_{pe} = 1$; curves allow only for refraction in a linear gradient atmosphere. Gradient ΔN in N-units per kilometer as indicated.

refractive index over a range of values of ΔN from 0 to 80 N-units per kilometer. Eq. (5) in reference 14 shows that the effective earth's radius factor k' which includes both the effective radius $k_p a'$ of the terrain and a factor k [see (10) above] to allow for the systematic effects of refraction in the atmosphere, may be calculated from the following formula:

$$\frac{1}{k'} = \frac{1}{k_p} + \frac{1}{k} - 1. \tag{25}$$

If we set $k = 4/3$ in the above, then we find that the values of effective earth's radius factors $k' = k_t = k_r = 1$ and $k' = k_{te} = k_{re} = 4/3$ describing our model earth correspond to $k_p = 4/5$ between radio horizons and $k_{pe} = 1$ from each antenna to its radio horizon. Eq. (25) was used with (10) to determine appropriate pairs of values of k' used in calculating the transmission loss on Fig. 14 as a function of ΔN.

In a paper appearing in this issue, Bean and Meaney[19] study the correlation between transmission loss and the gradient ΔN of refractivity in the first kilometer above the surface. Assuming a relation of the form $L_{bm} = a + b\Delta N$, they have estimated from their data the parameter b. If we assume that the only influence of ΔN on transmission loss is an increase in refraction which may be accounted for by a change in the effective radius of the earth, then the results shown on Fig. 14 may be used to estimate the theoretical value of b expected to account for these effects of refraction. This theoretical value of b is designated by the symbol b'. The lower curves on Fig. 15 (next page) show b' vs θ obtained by dividing by 40 difference of L_b values shown on Fig. 14 for $\Delta N = -20$ and $\Delta N = -60$, respectively, while the upper curves were obtained by use of the values of L_t on Fig. 14 corresponding to $\Delta N = -39.23$ and -80. The dashed curves on Fig. 15 were calculated assuming $B = 1.43 \times 10^{-14}$, while the solid curves correspond to $B = 8.07 \times 10^{-14}$. The unusual shape of the curves on Fig. 15 requires some explanation. For angular distances below 5 milliradians the received field is primarily a diffracted field and, by substituting (10) in (11) and then substituting the resultant expression in the exponential term in (36), we find that b' is very nearly directly proportional to the value of θ for $k = 4/3$. The influence of

changes in refraction on the scattered fields, however, is much smaller. Consequently, as we increase the angular distance from 5 to 15 milliradians, b' increases to a maximum value which is reached when the increasing relative magnitude of scattered to diffracted fields begins to suppress the influence of ΔN on the diffracted field. The secondary maximum on one of the curves on Fig. 15 near $\theta = 12$ milliradians is caused by the somewhat arbitrary method we have adopted for describing the variation of $[C(0)/l_0]$ with height. The fact that b' is larger when the scattered fields are weaker; i.e., when $B = 1.43 \times 10^{-14}$, is caused by smaller suppression in this case of the effects of ΔN on the diffracted field.

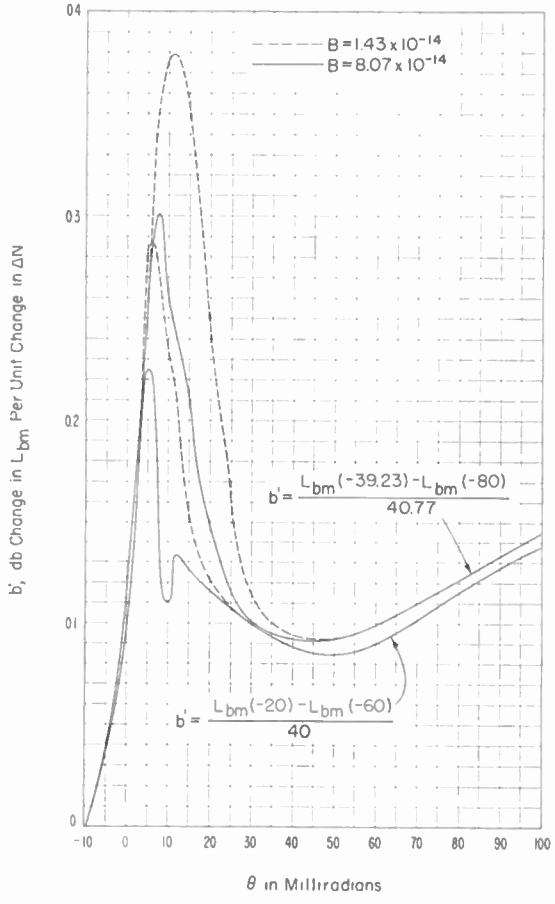

Fig. 15—Theoretical dependence on ΔN of the transmission loss for diffracted plus scattered fields; $L_{bm}(\Delta N) - L_{bmp} = b'(\Delta N + 39.23)$ decibels. Curves allow only for refraction in a linear gradient atmosphere.

When the theoretical values of b' on Fig. 15 are compared with the observed values of b on Fig. 4 in reference 19, we find that these observed values are usually very much larger than the theoretical values, particularly in the scattering region at large angular distances. This suggests that some mechanism other than refraction in a linear gradient atmosphere is responsible for most of the correlation of L_{bm} with ΔN. In the Booker-Gordon theory the values of the parameter $[C(0)/l_0]$, averaged over a period of a month, might very well be expected to be correlated with changes in the monthly median values of ΔN. If we assume that this is, in fact, the case, then use may be made of the empirical data in reference 19 and the theoretical curves on Fig. 15 to determine the relation between ΔN and $10 \log_{10} [C(0)/l_0]$. Since the transmission loss in the scattering region is a linear function of $-10 \log_{10} [C(0)/l_0]$ we may assume a relation of the form:

$$-10 \log_{10} [C(0)/l_0] = a + b''(\Delta N + 39.23) \quad (26)$$

where a is the value of $-10 \log_{10} [C(0)/l_0]$ for a radio standard atmosphere. The values of b in reference 19 represent the total decibel change in L_{bm} per unit change in ΔN and thus $b = b' + b''$.

When the appropriate theoretical values of b' from Fig. 15 are subtracted from each of the measured values of b in the scattering region as given in Table II of reference 19 for the combined 0300 and 1500 observations we obtain 21 estimates of b''. The weighted mean of these values and its estimated standard error are 0.372 and 0.030, respectively. Using this mean value of $b'' = 0.372$ in (26), we have determined from our radio data that $a = -10 \log_{10} B = 134.7$ is an appropriate value for a radio standard atmosphere for use in (57) while $a = -10 \log_{10} [C(0)/l_0] = 131.5$ is the appropriate value for a radio standard atmosphere for use in (64). Using these values and the relation (26), a new set of theoretical curves, showing now the total dependence of L_{bm} on ΔN, have been calculated and are given on Fig. 16.

Fig. 17 gives a theoretical curve for b, the total decibel change in L_{bm} for a unit change in ΔN, as derived from the theoretical curves on Fig. 16. Thus, for a given value of θ, b was determined from the curves on Fig. 16 by dividing by 40 the difference in transmission loss levels corresponding to $\Delta N = -20$ and $\Delta N = -60$. Although these theoretical curves were calculated for 100 megacycles and for terminal antenna heights of $h_t = 1{,}000$ feet and $h_r = 30$ feet, they should, in accordance with their method of derivation, be approximately applicable for frequencies ranging from well below 50 to well above 10,000 megacycles and also for wide ranges of antenna heights when angular distance is used as a parameter. The companion paper in this issue by Bean and Meaney[19] provides the expected monthly median values of ΔN for the United States in the form of isopleths for several months of the year. Thus Figs. 16 and 17 provide a means for determining the expected time and geographic variance of transmission loss in the scattering region.

Thus we have illustrated in this section the theoretical dependence of median basic transmission loss over a model smooth earth on the angular distance, antenna height, frequency, and the effect of the meteorological parameter ΔN.

VI. Comparison of Data with the Model Smooth Earth Predictions

In connection with the National Bureau of Standards Cheyenne Mountain experiment, continuous measurements have been made of the transmission loss on sev-

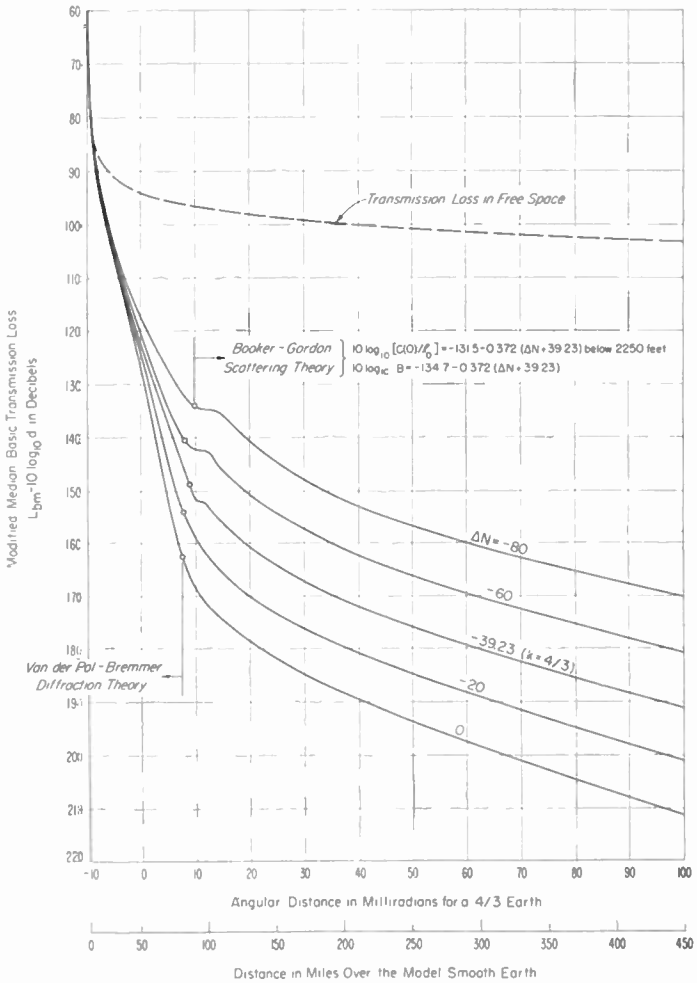

Fig. 16—Modified median basic transmission loss expected for 100 mc propagation over a model smooth earth; transmitting antenna height 1,000 feet; receiving antenna height 30 feet; gradient ΔN in N-units per kilometer as indicated. Curves allow for empirical estimates of climatological differences in $[C(0)/l_c)]$ as well as for refraction in a linear gradient atmosphere ($k_p = 4/5$; $k_{pe} = 1$).

eral different frequencies and over several transmission paths involving a wide range of angular distances and transmitting antenna heights.[30] The measured median transmission loss for the month of August, 1952 has been chosen for comparison with the calculated values given in this paper, since for this month the median value of ΔN for the Cheyenne Mountain paths approximated the value (-39.23 N units) corresponding, if the gradient were linear, to $k = 4/3$. The median basic transmission loss for each path L_{bm0} was estimated from the corresponding measured median transmission loss by adding the free space antenna gains; thus the measured median basic transmission losses determined in this way are a little too large, possibly as much as 2 or 3 decibels at the larger angular distances. Terrain profiles, such as those shown on Fig. 5, were determined for each propagation path, and (14) and (15) used for determining θ. The values of $(L_{bm0} - 10 \log_{10} d_{mi})$ as measured at 100 mc are plotted as a function of θ for comparison with the corresponding theoretical values shown as a function of θ on Fig. 12. A wide range of transmitting and receiving antenna heights is involved with these measurements. Since there is no precise way of determining the effective values of these antenna heights over such irregular terrain, it is fortunate that accurate values are not required for predicting the transmission loss by this angular distance method. This effective suppression of the influence of antenna height is, in fact, the most important advantage of analyzing propagation data in terms of the angular distance, θ.

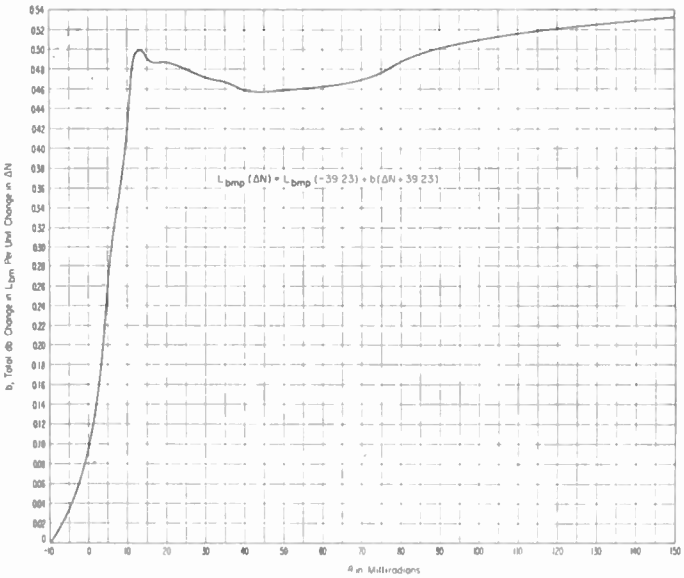

Fig. 17—The theoretical dependence on ΔN of the transmission loss for diffracted plus scattered fields. Curve allows for changes in the magnitude of the scattering cross section due to correlation between ΔN and $[C(0)/l_0]$ as well as for refraction in a linear gradient atmosphere.

Over rough terrain the angular distance, θ, and the distance, d, are no longer uniquely related as they are over a smooth earth. In an attempt to separate the influence of these two variables, we have predicted by our theory a "modified median basic transmission loss," $(L_{bm} - 10 \log_{10} d_{mi})$ so as to be able to compare these predicted values with the corresponding measured values of the same quantity. In the diffraction region this separation of the influence of θ and d is quite effective. On the other hand, the Booker-Gordon model scattering formula (57) for the modified average basic transmission loss $(L_{bas} - 10 \log_{10} d_{mi})$ contains a term $20 \log_{10} d_{mi}$; this term, together with a term $20 \log_{10} \theta_{mr}$, accounts for the particular height dependence we have assumed for $[C(0)/l_0]$. For our model smooth earth ($k_t = k_r = 1$ and $k_{te} = k_{re} = 4/3$), this term $20 \log_{10} d_{mi}$ is equal to $20 \log_{10} [3.96\theta_{mr} + \sqrt{2h_{te}} + \sqrt{2h_{re}}]$ where h_{te} and h_{re} are the assumed values of the effective heights of the transmitting and receiving antennas expressed in feet. Thus, for comparison with values of modified median basic transmission loss observed at a distance d_{mi} and angular distance θ_{mr}, a correction factor $20 \log_{10} [(3.96\theta_{mr} + \sqrt{2h_{te}} + \sqrt{2h_{re}})/d_{mi}]$ should be subtracted from the Booker-Gordon model curves shown on Figs. 12 and 13 before comparison with the data. Such corrections are shown by the arrows on these two figures. Since the scattering formula (63) of the Villars-

Weisskopf theory contains a term 10 $\log_{10} d_{mi}$, this correction is of the same form but only half as large for the theoretical curves based on this model.

The Cheyenne Mountain data on 100, 192.8, and 1,046 mc are shown on Fig. 13. Estimates were made of the atmospheric absorption to be expected on two of the 1,046 mc paths, taking account of the actual characteristics of the atmosphere; thus $A_a = 1.06$ decibels for the path corresponding to $\theta = 26.7$ milliradians, and A_a 1.2 decibels for the path corresponding to $\theta = 60$ milliradians. These values are shown by small arrows labelled A_a associated with the 1,046 mc data. These arrows adjust these data to the values expected with no atmospheric absorption so that they may be compared with the theoretical curves.

The 1,046 megacycle data lie between the theoretical curves based on the Booker-Gordon and Weisskopf-Villars scattering theories but nearer to the former. It should be noted, however, that the constant B_1 in the Weisskopf-Villars theory was determined by adjusting the theoretical curve for 100 megacycles so that it would agree well with the 100 megacycle data. Had a similar procedure been adopted for the constant B in the Booker-Gordon theory, then their 1,000 megacycle curve would not agree as well with the 1,046 megacycle data. This question of frequency dependence is treated more adequately in Section IX.

VII. Within-the-Hour Fading Range

Studies of the cumulative distribution of the instantaneous transmission loss over periods of an hour's duration or less[31,32] have established that Rayleigh distributions of the type discussed in a companion paper[34] appearing in this issue are representative of our data. Fading range is defined as the difference in decibels, $R(0.1) - R(0.9)$ between the instantaneous transmission loss levels exceeded 90 per cent and 10 per cent of the time during a period of one hour. This interdecile range of the cumulative distribution is shown in Fig. 6 of reference 34 as a function of K, the decibel ratio of the average power in the Rayleigh distributed component to the power in the steady component of the received field.

Using the values of K determined from the theoretical values of the transmission loss corresponding to the diffracted and scattered fields; i.e., $K = L_{bd} - L_{bas}$, and the relation between fading range and K shown in Fig. 6 of reference 34, we obtained the curves in Fig. 18 and Fig. 19 showing the expected fading range versus θ as a function of antenna height and frequency, respectively. The experimental data shown on these figures are discussed in detail in reference 32. They represent the median values of a large number of individual hourly fading ranges for several transmission paths. The 418 mc data were obtained on an Iowa-Illinois path, while the remaining data correspond to Cheyenne Mountain paths in Colorado and Kansas.

It should be mentioned that the experimentally-determined fading ranges would usually be expected to be larger than the theoretical values, since the average energies of both the steady and scattered components will vary to some extent during the period of an hour, and this variance would add to that shown by the curves in Figs. 18 and 19. Under certain circumstances, however, these average energy changes may actually reduce the fading range, as in the case where a duct may increase the level of the diffracted ground wave to a very large value for a period of an hour or more.

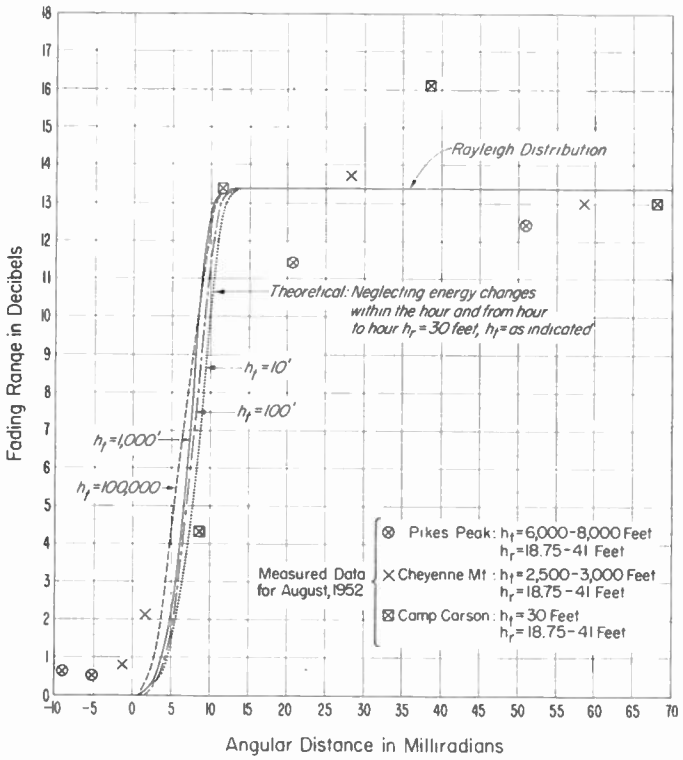

Fig. 18. Within-the-hour fading range at 100 mc. Fading range is defined to be the difference between instantaneous transmission loss in decibels exceeded 90 per cent and 10 per cent of the time.

VIII. Obstacle Gain in the Diffraction Region

In this section a new theory of obstacle gain will be developed, and it will be shown that the very large obstacle gains, observed in propagation over mountain peaks and explained in terms of propagation over a knife edge,[39,40] may be considered as limiting cases of our more general formula.

Before discussing this new method of obstacle gain calculation in more detail, it will be desirable to review briefly the theory of knife-edge diffraction which originally led to this concept. It is well known[41,42] that the

[39] F. H. Dickson, J. J. Egli, J. W. Herbstreit, and G. S. Wickizer, "Large reductions of vhf transmission loss and fading by the presence of a mountain obstacle in beyond-line-of-sight paths," Proc. IRE, vol. 41, pp. 967–969; August, 1953. A discussion of this paper is given by J. H. Crysdale in Proc. IRE, vol. 43, p. 627; May, 1955.

[40] R. S. Kirby, H. T. Dougherty, and P. L., McQuate, "Obstacle gain measurements over Pikes Peak at 60 to 1046 mc," p. 1467, this issue. Additional references are given in this paper.

[41] J. C. Schelleng, C. R. Burrows, and E. B. Ferrell, "Ultra-short-wave propagation," Proc. IRE, vol. 21, pp. 427–463; March, 1933.

[42] K. Bullington, "Radio propagation at frequencies above 30 megacycles," Proc. IRE, vol. 35, pp. 1122–1136; October, 1947.

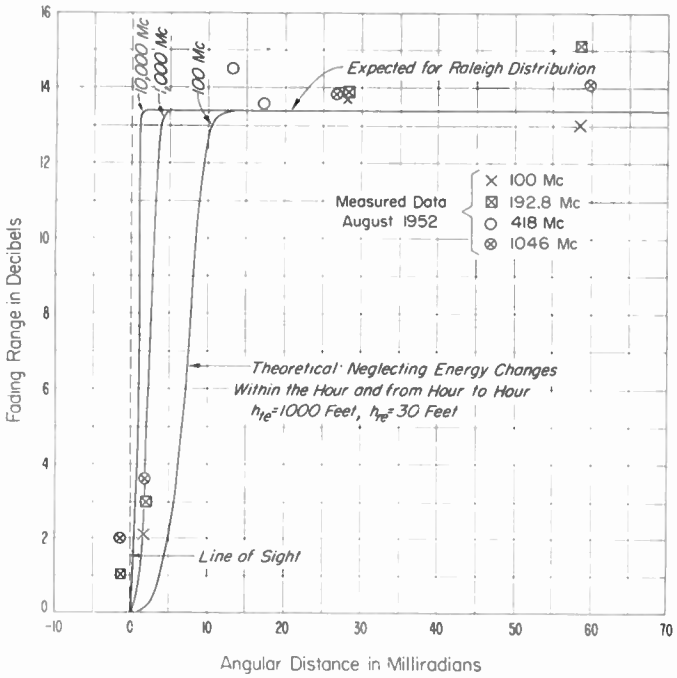

Fig. 19 —Within-the-hour fading range at frequencies from 100 to 10,000 mc. Fading range is defined to be the difference between instantaneous transmission loss in decibels exceeded 90 per cent and 10 per cent of the time.

transmission loss over very rough terrain may often be calculated approximately by assuming that a single perfectly absorbing knife-edge obstacle is situated at an appropriate location along the transmission path. The formulas appropriate for this special case are given in Appendix III. If we compare the formula (36) for the transmission loss expected for waves propagated by diffraction over a smooth sphere with the formula (70) for diffraction over a knife edge, we find that the transmission loss over a knife edge is systematically less than that for propagation over a sphere. The significant difference between smooth earth (36) and knife-edge (70) diffraction is that the transmission loss increases linearly with angular distance in (36) and only as $20 \log_{10} \theta$ in (70).

These large differences between the basic transmission losses calculated for these two extreme cases indicate the desirability for developing a method of calculation applicable more generally to situations involving obstacles of intermediate shapes or involving multiple obstacles along the path. The method illustrated on Figs. 20 and 21 appears to provide a reasonably good solution to this problem. This method depends upon the fact that the expected transmission loss in propagation over a smooth sphere decreases rapidly with a decrease in the value $k'a'$ of the effective radius of the earth when both the distance, d, and the angular distance, θ are kept constant.[43] The smooth sphere calculations shown on Figs. 20 and 21 were made by means of (36) in Appendix I, while the knife-edge basic transmission loss values were obtained by (67) in Appendix III.

One would not ordinarily expect transmission paths with very small values of k' except in mountainous terrain. However, we see by Figs. 20 and 21 that even moderate reductions in k' lead to very large reductions in L_b; i.e., lead to large "obstacle gains." However, in the case where the same obstacle determines both the transmitting and receiving antenna horizons, the effective radius of curvature may be quite small and effectively equal to zero. It should be noted that our spherical obstacle is obviously not suitable as a model in the limit as k' approaches zero; for treating these limiting cases of very small radii of curvature it would be better to develop a theory for propagation over a parabolic cylinder since such a cylinder approaches a knife edge as its radius of curvature approaches zero. S. O. Rice[18] has developed such a theory, but he considers only the case of plane waves incident on the cylinder, and his results have not yet been translated in detail to the case of the transmission loss expected in propagation over a path of finite length. It is of interest to note, however, that Rice's exponential term in his equations (2.26) agrees exactly with the corresponding term in our (36) for propagation over a perfectly conducting sphere with the same radius of curvature; this agreement suggests that the shape of the obstacle in the great circle plane alone is of primary importance in transmission loss calculations, the shape of the obstacle in the plane normal to the path evidently being of less importance.

We see by Fig. 20, p. 1504, that use of (36) does provide an estimate of transmission loss which merges smoothly, for small radii of curvature, with the value expected for a knife edge; i.e., for a parabolic cylinder with an effective radius of curvature $k'a' = 0$. Thus even though (36) is strictly valid, in accordance with the assumptions made in its derivation, only for radii of curvature such that $\theta_{t,r} \ll \pi/3$, it evidently provides a semi-empirical method of calculation of the expected transmission loss over obstacles with small effective radii of curvature which may be used until such time as a more effective solution becomes available.

Fig. 21, p. 1504, shows the theoretical average transmission loss for the scattered component as determined from (57). Here it was assumed that $l_0 = 70$ meters, independent of height. It is evident that the shape of the obstacle has much less influence on the scattered power than it does on the diffracted power. Most of the variation with k' shown on Fig. 21 arises from changes in the heights of the transmitting and receiving antennas as k' is varied with d fixed. Note that the scattered power decreases in importance relative to the diffracted power as the radius of curvature of the obstacle decreases with θ and d fixed. In fact it appears from Fig. 21 that, when the terrain is such that the propagation may be characterized by knife-edge diffraction, the expected scattered component is so low that the fading expected from this

[43] Note the difference in this situation and that shown on Fig. 14 where the transmission loss increases as $k'a'$ decreases; this difference in behavior comes about by virtue of the fact that the θ used in the calculations shown on Fig. 14 increases as k decreases rather than remaining constant as in the present case for which $k = 4/3$ and k_p varies.

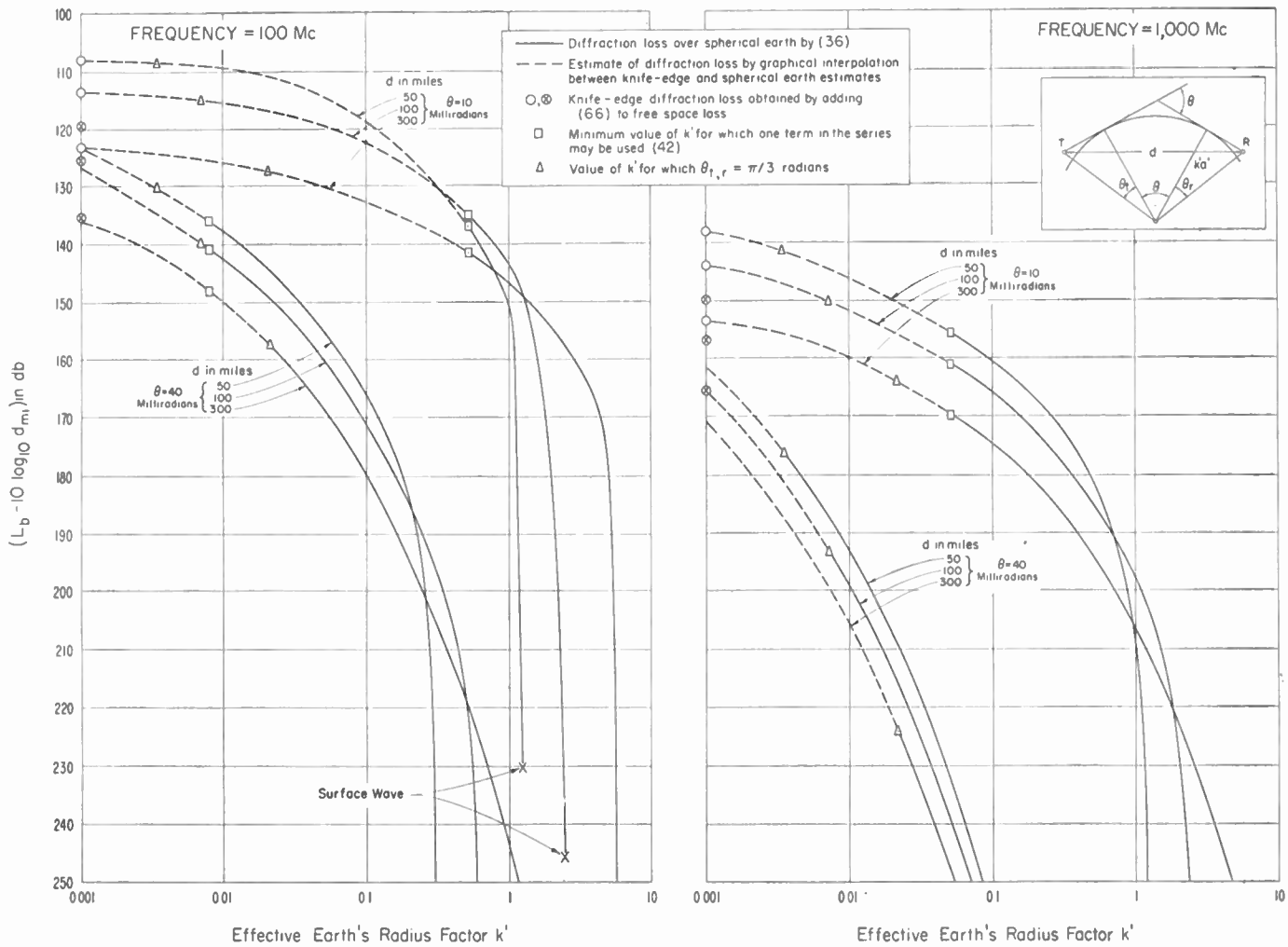

Fig. 20—Dependence of transmission loss on the effective radius $k'a'$ of the obstacle. (The distance d and angular distance θ are kept constant; $a'=3{,}960$ miles.)

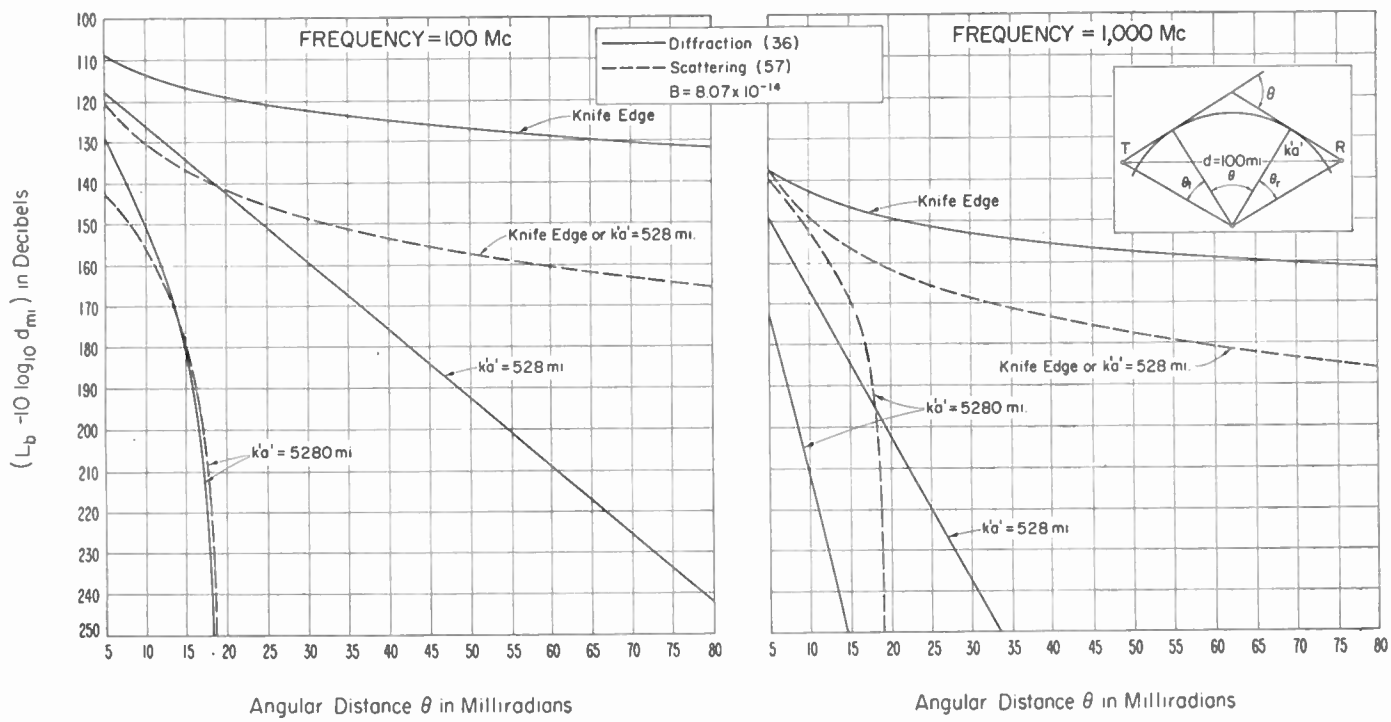

Fig. 21—Dependence of transmission loss on the effective radius $k'a'$ of the obstacle.

cause should be negligible. There is some experimental data to confirm this expectation (see the discussion in reference 39). Some more recent observations of the knife-edge diffraction loss over Pikes Peak reported by Kirby, Dougherty and McQuate[40] also provide further confirmation of this conclusion relative to fading.

Use has been made of the above described method of obstacle gain calculation in the model smooth earth calculations in Section V by taking $k_p = 4/5$ and thus k' equal to 1; i.e., $k_t = k_r = 1$, for the portion of the transmission path between the radio horizons. In Section X use will be made of the four earth-curvature model to calculate the transmission loss expected on particular transmission paths for comparison with the values of median transmission loss observed over these paths.

IX. Tropospheric Forward Scattering Theory and Climatological Predictions

In this section we will review some of the current theories of tropospheric forward scattering in the light of our radio observations. Such theories are useful for extrapolating our already extensive experimental data to other frequency bands and to other climatological conditions. The theory may also be used as a guide in antenna design.

Booker and Gordon[24,25] based their development on a phenomenological theory of scattering by atmospheric turbulence. Thus they chose, somewhat arbitrarily, to describe the fluctuations in the refractivity of the atmosphere by the exponential correlation function (22). The radio wave scattering cross section, σ, is uniquely determined by this assumption:

$$\sigma_{BG} = \frac{2C(0)\,\sin^2\chi}{\pi l_0(\alpha+\beta)^4}\cdot f[(l_0/\lambda)\cdot(\alpha+\beta)] \qquad (27)$$

$$f[(l_0/\lambda)\cdot(\alpha+\beta)] = \{1+\lambda^2/[2\pi l_0(\alpha+\beta)]^2\}^{-2}. \qquad (28)$$

The term $\sin^2\chi$ in (27) allows for polarization effects and is present in the same form in all formulas for the scattering cross section. It is set equal to unity in this report. $(\alpha+\beta)$ is the scattering angle and λ is the wavelength of the radio waves. The function $f[(l_0/\lambda)\cdot(\alpha+\beta)]$ in (27) may be set equal to unity when the product of radio frequency and scattering angle is sufficiently high. For several of our transmission paths this factor became quite large; an approximate allowance for its effect was made by use of the function $F[(l_0/\lambda)\cdot\theta]$ which was derived in reference 15 and is given graphically on Fig. 37 in Appendix II.

As the product $(\theta\cdot f_{mc})$ is lowered, $F[(l_0/\lambda)\cdot\theta]$ increases the transmission loss. In our analysis of individual transmission paths, this term increased the calculated transmission loss of the scattered component of the field by a maximum, on the transmission paths investigated, of 33.3 decibels (see item No. 3 in Appendix IV). Considering only paths for which scattering is the dominant mode of propagation ($K > 3$ db), the increase in transmission loss of the scattered component caused by this term was a maximum of 1.2 decibels (see items 21 and 22 in Appendix IV).

Although the available meteorological data on the magnitude of $[C(0)/l_0]$ (see Fig. 10) appear to agree qualitatively with our radio estimates of this parameter, the latter are much better suited in several respects for the analysis of $[C(0)/l_0]$ since they provide data over a greater range of heights averaged over longer periods of time. The following procedure was adopted in order to obtain an estimate of the average value of $[C(0)/l_0]$, normalized to one kilometer above the surface, for each of the radio transmission paths for which scattering was considered to be the dominant mode of propagation and for which reliable data on ΔN were available near the transmission path. In order to eliminate most of the transmission paths for which the received field was influenced to some extent by diffraction, the transmission loss, L_{bd}, was calculated for each path in Appendix IV by the four earth curvature method and compared with the observed median transmission loss, L_{bm0}, for each of these paths. When $(L_{bd}-L_{bm0}) > 3.4$ decibels, we may expect K to be greater than 3 decibels (see Fig. 6 in reference 34), and thus expect the influence of diffraction to be negligible; 80 of our transmission paths satisfied this criterion as well as the criterion that reliable information on ΔN be available, and these 80 were used to determine estimates of the average transmission loss,

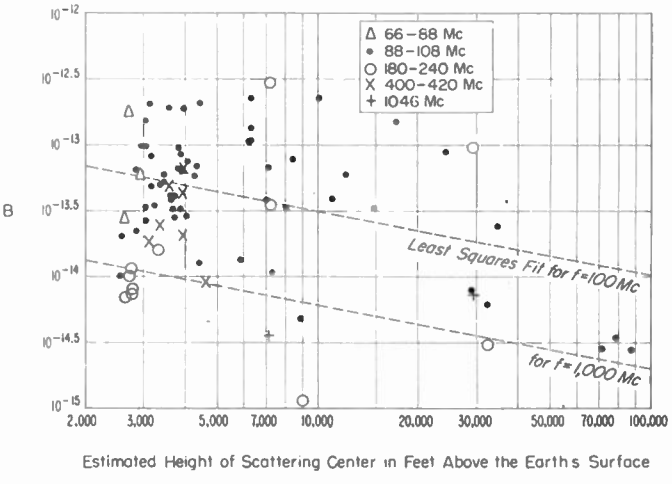

Fig. 22—Estimates obtained from radio transmission loss data of long-term average values for the constant B in the equation $[C(0)/l_0] = B/(h-0.5\ h_0)^2$. $B = [C(0)/l_0]$ per meter at a height of one kilometer above the surface.

L_{bas}, of the scattered field. These observed values of L_{bas} were first adjusted to the values expected by a standard atmosphere by using the theoretical value of b on Fig. 17 together with the values of ΔN in Appendix IV. By equating these adjusted values of L_{bas} to the theoretical values given by (57), we obtained estimates of B, the only unknown factor in (57). The values of B obtained in this way are shown in Fig. 22 as a function of the estimated value of the height of the "center" of scattering above the earth's surface. Methods for estimating the height of the "center" of scattering are given

in a companion paper[44] appearing in this issue. In the present application only very rough estimates of these heights are required, and we have taken them to be 1.5 h_0 above the chord joining the transmitting and receiving antennas (see Fig. 36) and thus, on the average, at a height h_0 above the surface of the earth. The latter result follows since we have determined empirically that the earth's surface is, on the average, midway between the chord and the cross-over of the radio horizon rays.

If $[C(0)/l_0]$ actually varied inversely as the square of the height above the surface as we have assumed, and if the scattering cross section, σ_{BG}, were actually independent of frequency as required by the Booker-Gordon theory, then the values of B shown on Fig. 22 should not vary with either height or radio frequency. They were found to vary with both and a least squares fit yields the following formula:

$$-10\log_{10}B = (101.7 \pm 6.9) + (4.77 \pm 1.41)\log_{10}h_0\ (\text{feet}) + (7.14 \pm 2.15)\log_{10}f_{mc}. \quad (29)$$

The error terms for each of the coefficients in (29) are standard errors estimated by the usual procedure[45] giving equal weight to each of the 80 observed values and with the assumption that h_0 and f_{mc} are free of error. Since the coefficient of $\log_{10}f_{mc}$ deviates from zero by more than three times its standard error, we are forced to reject the Booker-Gordon formula (27) for the scattering cross section.

In an addendum to a paper appearing in this issue Weisskopf and Villars[46] suggest that the scattering cross section may be expressed as follows in terms of the variance $V = \{[\overline{(dn/dh)^2}] - [\overline{(dn/dh)}]^2\}$ of the vertical gradient of the refractive index relative to its mean value:

$$\sigma_{WV} = \frac{4\pi^2\lambda V}{\{2\sin[(\alpha+\beta)/2]\}^5}. \quad (30)$$

In addition to having a somewhat more satisfactory physical basis, the above formula for the scattering cross section differs in form from the Booker-Gordon model by having the additional frequency dependence arising from the wavelength factor λ, and this is in just the right direction to explain the frequency term in (29).

If now we use (63) for determining the values of B_1 in the Weisskopf-Villars scattering formula in exactly the same way and for the same 80 transmission paths used in testing the Booker-Gordon theory, we obtain the following least squares solution:

$$-10\log_{10}B_1 = (141.0 \pm 7.7) + (9.15 \pm 1.57)\log_{10}h_0\ (\text{feet}) - (2.47 \pm 2.40)\log_{10}f_{mc}. \quad (31)$$

If V actually varied inversely as the height above the surface, as was assumed in deriving (63), and if (30) actually has the correct frequency dependence, then the values of B_1 given by (31) should be independent of both height and frequency. The frequency dependence indicated by (31) is quite small and, in fact, the coefficient of $\log_{10}f_{mc}$ deviates from zero only by its standard error. The height dependence in (31) is quite large and indicates that we should have assumed in deriving (63) that V varies on the average inversely as the square of the height above the surface. If the latter assumption had been used, the frequency gain factors H_{0t} and H_{0r} would have been somewhat larger and the coefficient of the frequency term in (31) would have been still smaller. Unfortunately the results in (29) and (31) were obtained much too late to make such a revision of the paper in time for its inclusion in this issue of the PROCEEDINGS, and the authors believed that the readers would prefer to have these preliminary results now rather than a more comprehensive treatment later. If we assume the Weisskopf-Villars formula (30) is correct and that the small frequency dependence indicated by (31) arises because of our incorrect assumption as to the height dependence of V or simply because of random sampling errors, then we obtain, by suppressing this frequency variation:

$$-10\log_{10}B_1 = (136.0 \pm 5.95) + (9.10 \pm 1.57)\log_{10}h_0\ (\text{feet}). \quad (32)$$

When this is combined with the height dependence already assumed in (58) we obtain:

$$-10\log_{10}V = 168.0 + 19.1\log_{10}h_0\ (\text{km}). \quad (33)$$

This height dependence of V is shown on Fig. 23 together with the 80 estimates of V obtained, as above described, from our radio data. Although the authors are not aware of any experimental meteorological studies made specifically for the purpose of studying the variance of the vertical gradient of refractive index, estimates of this parameter from index of refraction profiles, such as those presented by Crain in this issue,[28] are of the same order of magnitude as the values required to explain the radio data.

Further indirect evidence of the possible validity of the Weisskopf-Villars approach to this problem, which they originally based on the Kolmogoroff model of isotropic turbulence, comes from the recent direct measurements of refractivity reported by Birnbaum and Bussey[29] in this issue and the indirect measurements of Herbstreit and Thompson[47] also reported in this issue.

[44] K. A. Norton, P. L. Rice, H. B. Janes, and A. P. Barsis, "The rate of fading in propagation through a turbulent atmosphere," p. 1341, this issue.

[45] W. E. Deming, "Statistical Adjustment of Data," John Wiley and Sons, Inc., New York, N. Y.; 1943. See Chapter IX.

[46] F. Villars and V. F. Weisskopf, "On the scattering of radio waves by turbulent fluctuations of the atmosphere," p. 1232, this issue.

[47] J. W. Herbstreit and M. C. Thompson, Jr., "Measurements of the phase of radio waves received over transmission paths with electrical lengths varying as a result of atmospheric turbulence," p. 1391, this issue.

The least squares curve fit to the data on Fig. 23 indicates that V is very large at low heights. If such large values of V are used for calculating the scattered fields for transmission paths with small angular distances, these calculated values are much larger than those observed. This suggests that V may reach a maximum value at low heights as was assumed (see Fig. 10) for the parameter $[C(0)/l_0]$ of the Booker-Gordon theory.

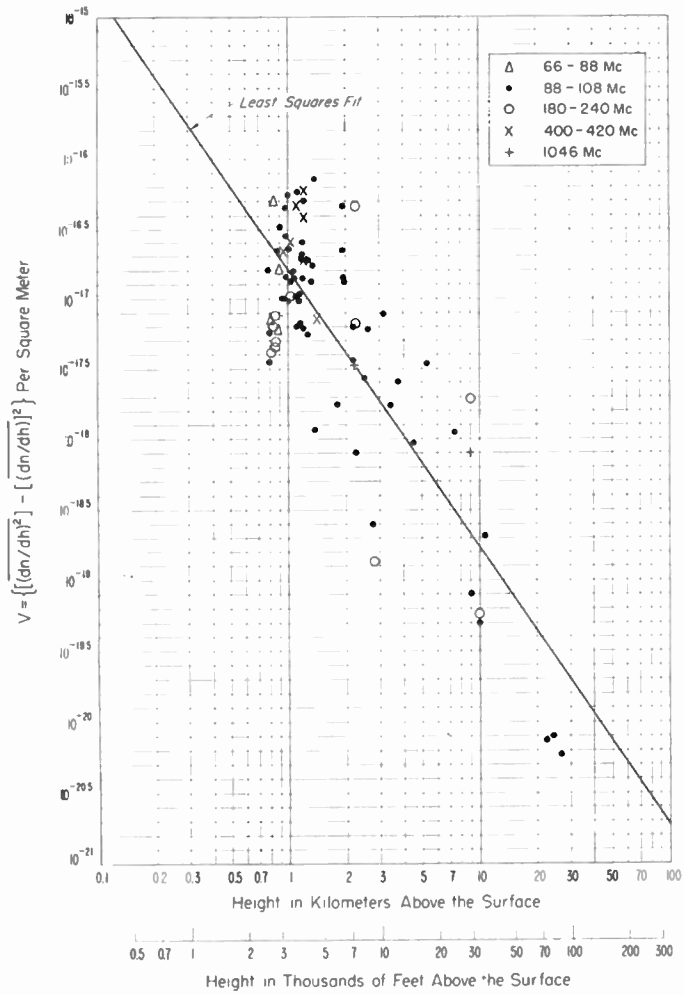

Fig. 23—Estimate of $V=\{[\overline{(dn/dh)^2}]-[\overline{(dn/dh)}]^2\}$ obtained from radio transmission loss data.

Also we may expect a factor in the Weisskopf-Villars theory which is the counterpart of the factor $F[(l_0/\lambda)\cdot(\alpha+\beta)]$ in the Booker-Gordon theory. If we somewhat arbitrarily introduce the term $\{1+\lambda^2/[l_0\cdot(\alpha+\beta)]^2\}^{-5/2}$ as a factor in (30), then this has the effect of reducing the intensity of the scattered fields at low frequencies or at small angular distances; in the limiting case as $(l_0/\lambda)\cdot(\alpha+\beta)$ approaches zero, the scattering cross section (30) including such a factor would approach the familiar Rayleigh scattering cross section which is proportional to the fourth power of the frequency and independent of scattering angle. The scale l_0 is to be identified with the largest eddies in the progressive turbulence decay scheme of the Kolmogoroff theory of isotropic turbulence which is the basis of the scattering theory of Weisskopf and Villars. It should be noted, furthermore, that these largest eddies will no longer be isotropic. Thus, in the range of frequencies below, say 200 megacycles, some aspects of the theory of scattering by anisotropic turbulence, presented in this issue by Staras,[33] should be applicable. Finally, note that frequency gain factors will play a larger role at these small angular distances when calculated on the basis of the correct height dependence (33). Presumably all of the above postulated factors play a role in reducing the scattering at small angular distances, but much further theoretical and experimental work needs to be carried out in this range before reliable predictions can be made. In a paper appearing in this issue Janes and Wells[48] report some new techniques of measurement applicable in this range of angular distances.

In a paper appearing in this issue Trolese[49] reports that his observations of radio scattering over a short path with an angular distance of about 7.8 milliradians indicate an 8 decibel increase in transmission loss relative to free space when the frequency is increased from 1,250 to 9,375 megacycles. These results are consistent with observations at lower frequencies and provide further confirmation of Weisskopf-Villars formula (30).

We have indicated above how the intense forward scattering observed on frequencies of the order of 100 megacycles and above deteriorates into isotropic Rayleigh scattering at very low frequencies. Conversely, at extremely high frequencies, it is expected that the scattering cross section will depart from the form given by (30) as the wavelength becomes sufficiently small with respect to a smallest scale of turbulence. In a paper appearing in this issue Wheelon[50] discusses this aspect of forward scattering.

X. Comparison of Transmission Loss Data with Predictions Based on the Smooth Earth Model Involving Four Earth-Curvatures and the Weisskopf-Villars Theory of Tropospheric Forward Scattering

In this section we will compare our theoretical calculations of transmission loss with the median values observed over long periods of time on 122 transmission paths. The table in Appendix IV lists the significant geometrical parameters of these transmission paths together with the differences between calculated and observed median basic transmission losses. Items in the table are listed in order of increasing angular distance θ. The median basic transmission losses, L_{bm0}, listed as observed values, were determined on the assumption that the measured free space gains were realized. It would have been somewhat more logical to have com-

[48] H. B. Janes and P. I. Wells, "Some tropospheric scatter propagation measurements near the radio horizon," p. 1336, this issue.
[49] L. G. Trolese, "Characteristics of tropospheric scattered fields," p. 1300, this issue.
[50] A. D. Wheelon, "Note on scatter propagation with a modified exponential correlation," p. 1381; this issue.

pared the actual observed transmission loss with the calculated transmission loss including the calculated path antenna gain. Since the gains used in all of our experiments were relatively small—the largest being 26 decibels—this more logical approach was not adopted since it has the practical disadvantage of introducing an additional variable into the transmission loss levels under discussion. An estimated weight, W, associated with each of the observed values of the transmission loss, is also listed. The weight, W, is so defined that its reciprocal represents an estimate of the square of the standard error of the observed transmission loss expressed in decibels.

The following description of the method of calculation used in obtaining the predicted values, L_{bmp}, in Appendix IV provides at the same time a summary of the method of transmission loss calculation recommended for interim use in engineering applications. The authors plan to incorporate what has been learned in the present study into a revised formula for the transmission loss of the scattered mode of propagation, but it is not anticipated that such a revised formula will give very different results except in the region near the radio horizon.

First, the geometrical parameters required to describe the transmission path in terms of our four earth-curvature model are determined by the method given in Section III. Next, the basic transmission loss, L_{bd}, of the diffracted wave is calculated by (43) in Appendix I. If the transmission path is characterized by having a common horizon for both the transmitting and receiving antennas, L_{bd} is to be calculated by (71) instead of (43). Unless a large obstacle gain is suspected, L_{bd} need not be calculated when the angular distance for the path exceeds 15 milliradians since the scattered fields will usually have a much higher level than the diffracted fields in this case.

The average basic transmission loss for the scattered field is computed next by means of the formula:

$$L_{bas} = -14.85 + 30 \log_{10} f_{mc} + 49.1 \log_{10} \theta_{mr} + 29.1 \log_{10} d_{mi} - F(s) - H_{0t} - H_{0r} - F[(l_0/\lambda)\cdot\theta]. \quad (34)$$

The asymmetry function $F(s)$ is shown on Fig. 24 vs the asymmetry factor $s=(\alpha_0/\beta_0)$. The frequency gain functions H_{0t} and H_{0r} are given on Fig. 38, while the function $F[(l_0/\lambda)\cdot\theta]$ is given on Fig. 37.

Now we may determine $K=L_{bd}-L_{bas}$, and, using this value of K, $R(0.5)$ may be determined from the formulas or graphs in reference 34. The median basic transmission loss predicted for a radio standard atmosphere is then given by $L_{bmp}=L_{bd}-R(0.5)=L_{bas}+K-R(0.5)$. Finally, the predicted median basic transmission loss for an atmosphere characterized by a vertical gradient of refractive index ΔN may be determined:

$$L_{bm}(\Delta N)=L_{bmp}-D(\Delta N)\equiv L_{bmp}-b(|\Delta N|-39.23). \quad (35)$$

Appropriate values for ΔN may be determined from reference 19, and b is given graphically as a function of θ on Fig. 17. Values for the correction D listed in the table in Appendix IV are small, but it should be remembered that our data were chosen for "quiet" periods of the day when the correction D would naturally be small.

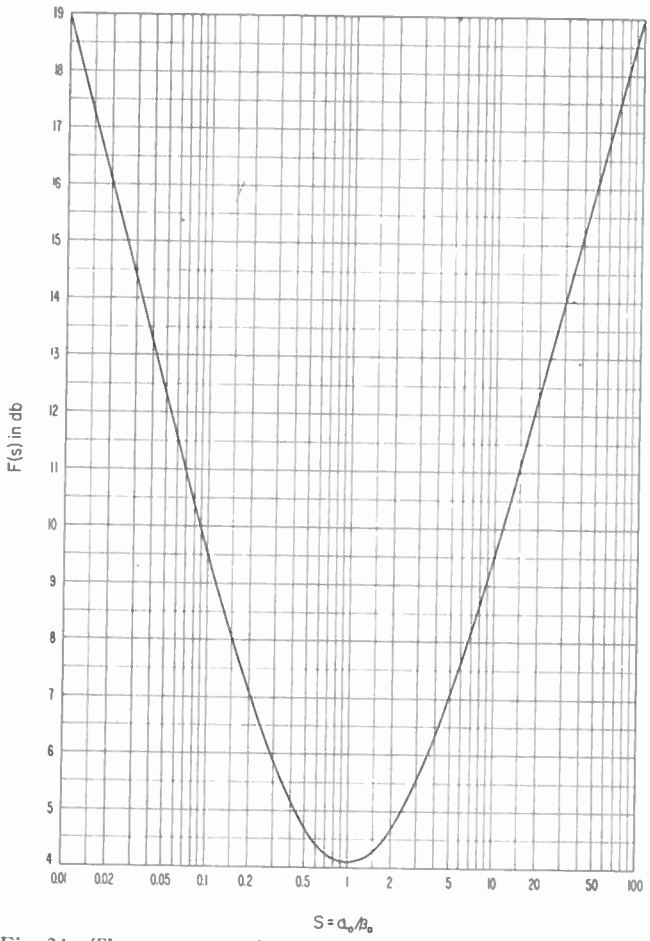

Fig. 24—The asymmetry function $F(s)$ for use in the Weisskopf-Villars prediction formula (34).

The above formulas were used for the predictions given in Appendix IV. Fig. 25 summarizes the degree of success achieved by the use of these formulas. Negative values of Δ mean that the observed transmission loss was less than the predicted value, or that the observed field intensity is greater than the predicted value. Thus we see that our predicted fields are about correct on the average in both the diffraction ($\theta<15$ milliradians) and scattering ($\theta>15$ milliradians) regions, and are about as widely scattered in both regions. Actually these data are somewhat misleading in the diffraction region, since we have over-estimated the intensity of the scattered fields—as discussed in Section IX—and this compensated for an under-estimation of the intensity of the diffracted fields.

It is desirable to discuss some of the reasons for the large departures from theory observed on several of the transmission paths. For items 6, 14, and 15, calculated scattered fields are much too large, and this we attribute to our present (presumably faulty) assumption regarding the height dependence of V at low heights; h_0 is less than 800 feet for these paths, all of which are between

Colorado Springs and Haswell, Colorado. On the other hand, in what is normally the diffraction region, there are two instances of fields exceptionally high compared to the theory; these are items 13 and 17. These are both 100 megacycle recordings where the transmitter was at Camp Carson, Colorado. When the effective transmitting antenna height $h_{te}=40$ feet was determined at Camp Carson, it was found that the first Fresnel zone lay entirely on a portion of the terrain sloping down away from the antenna in such a fashion as to direct the ground reflection lobery at the radio horizon instead of above it. No provision is made in our theoretical formulas to correct for such effects, but it may be readily appreciated that the frequency gain factors $-H_{0t}=26.1$ decibels and $-H_{0t}=15.8$ decibels which we used for items 13 and 17, respectively, are certainly too large. Later versions of these prediction methods should take better account of such terrain effects.

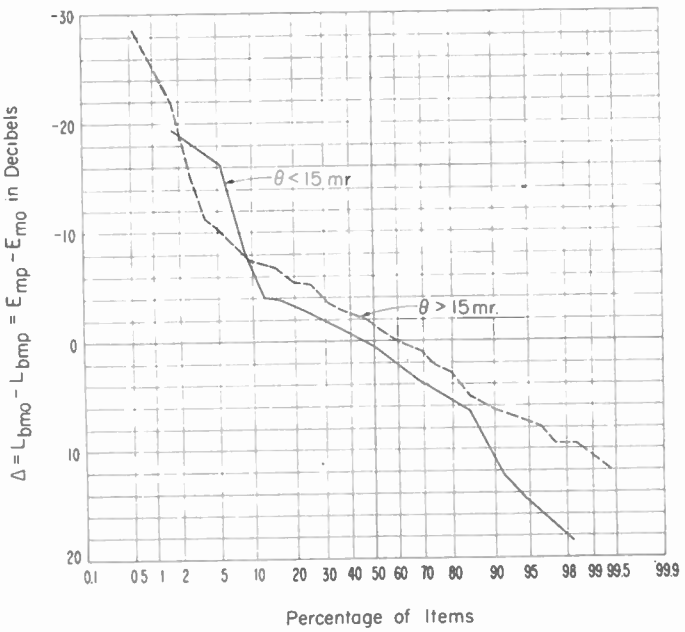

Fig. 25—Distributions of the differences between the observed and predicted transmission loss.

Items 102 and 110 show observed fields more than 20 decibels in excess of the theoretical values. Item 102 corresponds to a path where superrefraction effects may explain the high fields. Item 110 corresponds to a path where obstacle gain was so large that the theoretical diffracted field strength exceeded the theoretical scattered field strength; our formulas apparently systematically underestimate the obstacle gain.

Fig. 26 shows distributions of obstacle gain $G_0=L_{bd}(4/3)-L_{bd}$ which is the decibel ratio between transmission loss for a four-thirds earth and for our four earth-curvature model. Of the fourteen obstacle gains exceeding 50 decibels, eleven were for paths over rough terrain on the Pacific coast. The upper part of the dashed curve in Fig. 26 corresponds to diffracted fields for θ greater than 15 milliradians, that is, in what is

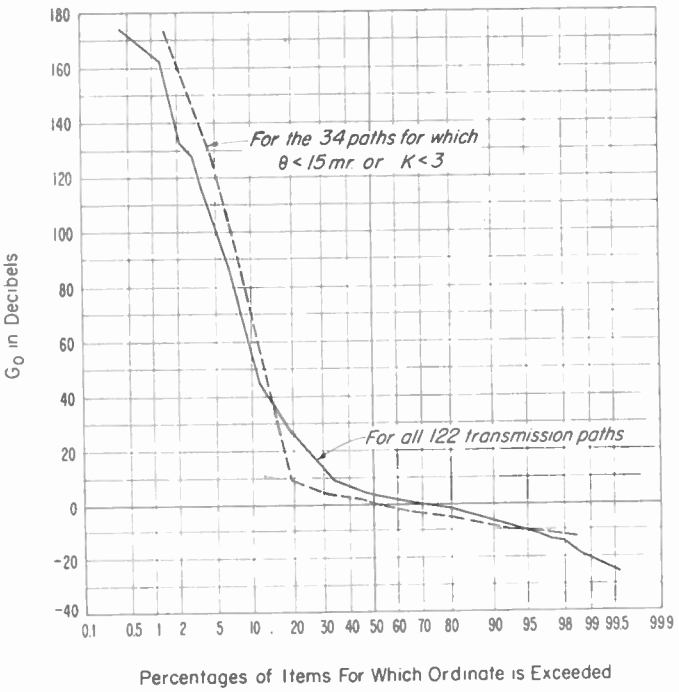

Fig. 26—Distributions of obstacle gain $G_0=L_{bd}(4/3)-L_{bd}$.

normally the scattering region. The largest calculated obstacle gain was 173 decibels for item 110, a path from Sacramento to Livermore, California.

XI. Path Antenna Gain in the Scattering Region

It is well known[51] that the sum (G_t+G_r) of the measured free space gains of the transmitting and receiving antennas are not always fully realized at large angular distances in the scattering region. This loss in path antenna gain $(G_t+G_r-G_p)$ has been explained qualitatively in a paper by Booker and de Bettencourt[52] in terms of the ratio of the antenna beamwidth to a beamwidth characteristic of the forward scattering. (Following Gordon[25] they define the forward scattering beamwidth α_e to be simply two-thirds of the angular distance θ.) When this ratio is very small they predict a large loss in path antenna gain referred to in their paper as "aperture to medium coupling loss." This latter designation may possibly be misleading since two antenna apertures are always involved and their effects on loss in path antenna gain are far from being independent.

Experimental evidence of the loss in path antenna gain has always been obtained by making simultaneous measurements of transmission loss on closely adjacent transmission paths using antennas with different free space gains. Since the fading due to phase interference would be expected to be more or less uncorrelated on the adjacent paths, it is customary to compare the

[51] F. W. Schott, "On the response of a directive antenna to incoherent radiation," Proc. IRE, vol. 39, pp. 677–680; June, 1951.

[52] H. G. Booker and J. T. de Bettencourt, "Theory of radio transmission by tropospheric scattering using very narrow beams," Proc. IRE, vol. 43, pp. 281–290; March, 1955.

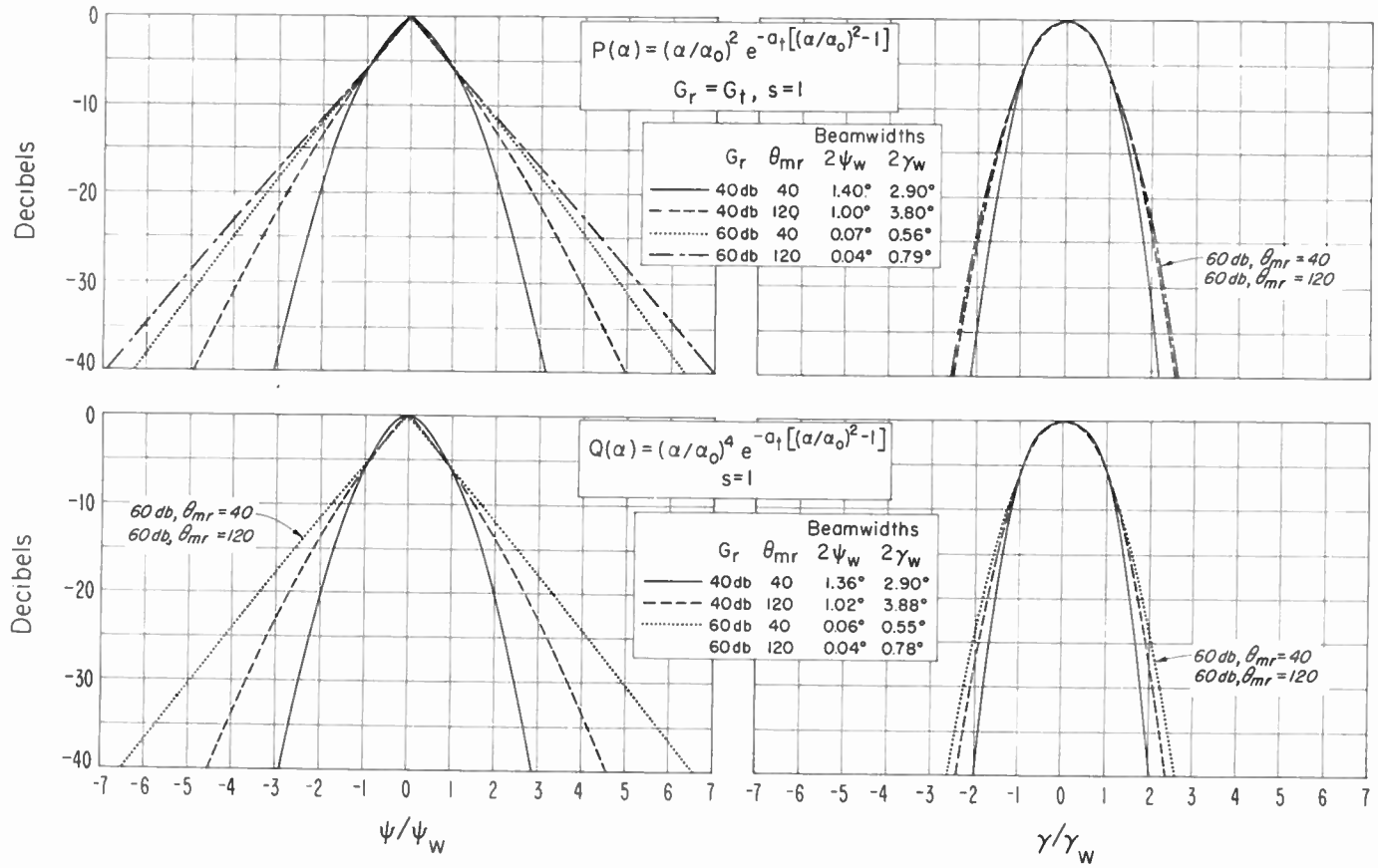

Fig. 27—Assumed transmitting or receiving antenna patterns.

average or median signal levels obtained for periods of time of the order of several minutes up to as much as one hour. Surprisingly enough, even these hourly median fields, recorded on closely adjacent transmission paths, are not well correlated. Data illustrating this point have been presented by Barsis[53] and by Barghausen, Decker, and Maloney.[54] No satisfactory explanation of these unusual phenomena has been made. The theoretical calculations presented below are not compatible with these observations and are presented primarily because the authors believe they probably represent at least an upper bound to the useful path antenna gain realizable with tropospheric forward scatter.

In order to obtain quantitative results with a minimum effort, we have chosen antenna patterns which have a somewhat unusual shape although conforming sufficiently well to the shape of actual antenna patterns so that our conclusions should not be appreciably affected. Fig. 27 shows these assumed antenna patterns, together with the formulas used for their computation. The patterns on the left are for the vertical plane while the patterns on the right are for the horizontal plane. The vertical plane beamwidth is $2\psi_w$ while the horizontal plane beamwidth is $2\gamma_w$. Patterns are shown for antennas with free space gains of 40 and 60 decibels; the patterns differ more in the vertical than in the horizontal plane as the angular distance is changed. These particular patterns were chosen so as to facilitate the evaluation of the scattering integral with these factors in the integrand. As described in an earlier paper[15] the loss in path antenna gain may be calculated from:

$$G_t + G_r - G_p = 10 \log_{10} (I/I')$$

where I denotes the value of the scattering integral (48) with $g_t g_r = 4$ and I' denotes the value of the scattering integral (48) with $g_t g_r = 4P(\alpha)P(\beta)$ in the case where the transmitting and receiving antennas have the same gain, and with $g_t g_r = 4Q(\alpha)$ in the case where the receiving antenna has a gain pattern sufficiently non-directional so that it does not appreciably affect the magnitude of the scattering integral.

The patterns in Fig. 27 are plotted vs ψ/ψ_w and γ/γ_w so that their shapes may more easily be compared. From the beamwidths as listed on the figure, it may be seen that much more directivity has been assumed in the vertical plane than in the horizontal plane, especially at the higher values of G_t and α_0. Most of the loss in gain, then, must be attributed to the vertical plane directivity. This would not be the case for an-

[53] A. P. Barsis, "Comparative 100 mc measurements at distances far beyond the radio horizon," 1954 IRE Convention Record, Part 1, "Antennas and Propagation," vol. 2.

[54] A. F. Barghausen, M. T. Decker, and L. J. Maloney, "Measurements of correlation, height gain, and path antenna gain at 1,046 megacycles on spaced antennas far beyond the radio horizon," 1955 IRE Convention Record, Part 1, "Antennas and Propagation," vol. 3.

tenna patterns with equal directivity in vertical and horizontal planes.

Fig. 28 shows estimates of path antenna gain G_p versus the sum G_t+G_r of free space gains, assuming $G_t=G_r$. Fig. 29 shows estimated of path antenna gain where a half-wave dipole is assumed at one end of the path and a high gain antenna at the other end.

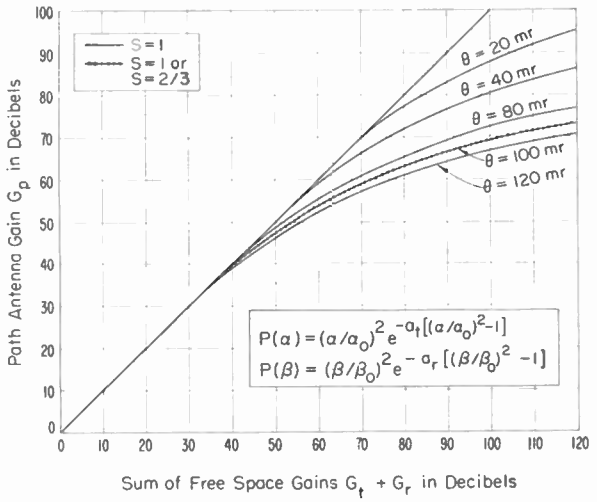

Fig. 28—Path antenna gain, using antennas with the same gain at each end of the path.

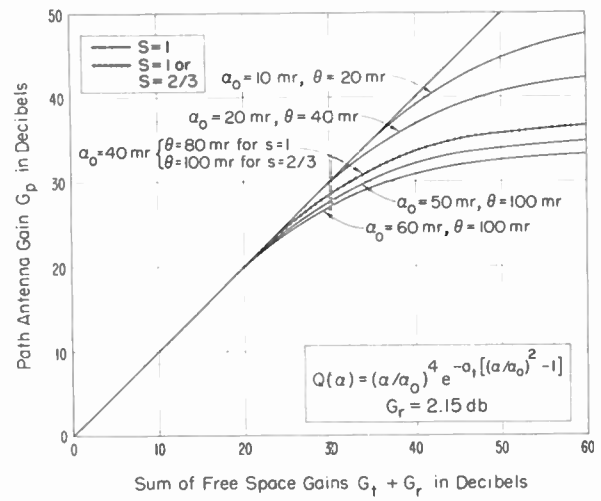

Fig. 29—Path antenna gain, using a half-wave dipole at one end of the path and a high gain antenna at the other end.

A comparison of these two figures reveals several striking features of this phenomenon of loss in antenna gain. First, it may be seen that with a given sum G_t+G_r, more gain is realized over a forward scatter circuit if $G_t=G_r$ than if $G_t>G_r$. This is inevitable; if energy is directed primarily forward (G_t large), little loss in gain can result from its being received over a narrow angle ($G_r=G_t$). But if one antenna has a wide beam and the other a narrow beam, there is less advantage in the concentration of energy by the narrow beam antenna. (The lowest curve on Fig. 29 is not properly labeled; it should read $\alpha_0=60$ mr, $\theta=120$ mr.)

Also, a comparison of Figs. 28 and 29 shows that the path antenna gain G_p decreases more rapidly with an increase in G_t+G_r when $G_t>G_r$ than when $G_t=G_r$. (Reciprocity holds here, of course.)

If a path is somewhat asymmetric ($s=2/3$) and equal free space gains are assumed at the two ends of a path, then G_p is essentially a function of the angular distance, θ, and does not differ appreciably from the gain realized in the symmetric case ($s=1$). If, however, $G_t>G_r$ and the gain pattern at the receiving end is sufficiently non-directional to have little effect on the magnitude of the scattering integral, then it may be seen from Fig. 29 that G_p is the same function of α_0 (rather than of θ) for both the symmetric and asymmetric cases. Additional curves could easily have been added to Fig. 29 for $G_r>2.15$ decibels by considering that the loss in gain ($G_t+G_r-G_p$) is virtually independent of the almost non-directional pattern associated with values of G_r up to about 20 decibels.

Some of these conclusions may be greatly modified when scattering is not isotropic, as for instance where there is scattering from "hot spots" in the atmosphere. Results reported by Trolese,[49] however, indicate less path antenna gain than the average estimates given by the method explained in this report, though his measurements were obtained with a well mixed and nearly standard atmosphere.

XII. Conclusions

In this paper we have described methods for transmission loss and fading range calculations suitable for use on over-land paths and using angular distance as a parameter. It is shown that the terrain profile along the transmission path can have a very large influence on the calculated value of the diffracted field and this may, in some cases, extend well into what would normally be expected to be the scattering region.

A relatively simple formula, based on the new Weisskopf-Villars scattering theory, is presented for the calculation of transmission loss in the scattering region. It is shown that this formula provides an explanation for the observed values over a very wide range of frequencies, angular distances, and antenna heights.

Acknowledgment

All of the staff of the Tropospheric Propagation Research Section of the NBS Boulder Laboratories played some part in developing either the theory or the supporting data presented in this paper. Furthermore, as may be seen in Appendix IV, much of the data was obtained in various laboratories under contract to CRPL. The computations for most of the graphs in the paper were performed under the supervision of Mrs. Frances T. Daniel, Lewis E. Vogler, and Ruth Knopf. The data for the table in Appendix IV were organized and checked by Perry H. Elder and Mrs. Elizabeth B. Sprecker. Methods for obtaining the frequency gain function in Appendix II and the estimates of path antenna gain in

Section XI were organized by Mrs. Daniel, Albrecht P. Barsis, Eugene Barrows, Leon Steinert, and William Hartman. Mr. Barsis checked the derivation of all the formulas used in Appendix II and in Section XI. Other calculations were performed by Robert Wilkerson, Anton Ozanich, Lloyd Yates, James Householder, and Marlon Fowles.

Appendix I

Transmission Loss for the Diffracted Mode of Propagation over a Smooth Earth

Using the relation (5) between basic transmission loss, L_b, and E, in decibels above one microvolt per meter for an effective radiated power of one kilowatt, the van der Pol-Bremmer equations in references 1 and 2 may be used directly to determine the transmission loss expected in propagation over a smooth spherical earth. In particular (33) and (34) of reference 2 may be used with (5) to derive the following simple formula for the expected modified basic transmission loss at large angular distances beyond the radio horizon:

$$\begin{aligned} L_b - 10 \log_{10} d_{mi} &= C[K(k'), b^\circ] + 16.667 \log_{10} f_{mc} \\ &\quad - G[\bar{h}_t(k')] - G[\bar{h}_r(k')] + 20 \log_{10} C_0(k') \\ &\quad + 488.69\, \beta_0(K, b^\circ) C_0(k') f_{mc}^{1/3} \theta \end{aligned} \tag{36}$$

where

$$C_0(k') = (3k'/4)^{1/3} \tag{37}$$

$$\begin{aligned} C[K(k'), b^\circ] &\equiv 17.879 - 20 \log_{10} \gamma - 40 \log_{10} \delta \\ &\quad + 10 \log_{10} \beta_0(K, b^\circ). \end{aligned} \tag{38}$$

The parameters $K(k)$ and b° allow for the effects of the conductivity and dielectric constant of the earth's surface and are somewhat different for horizontal and vertical polarization as may be seen on Fig. 30 and Fig. 31.

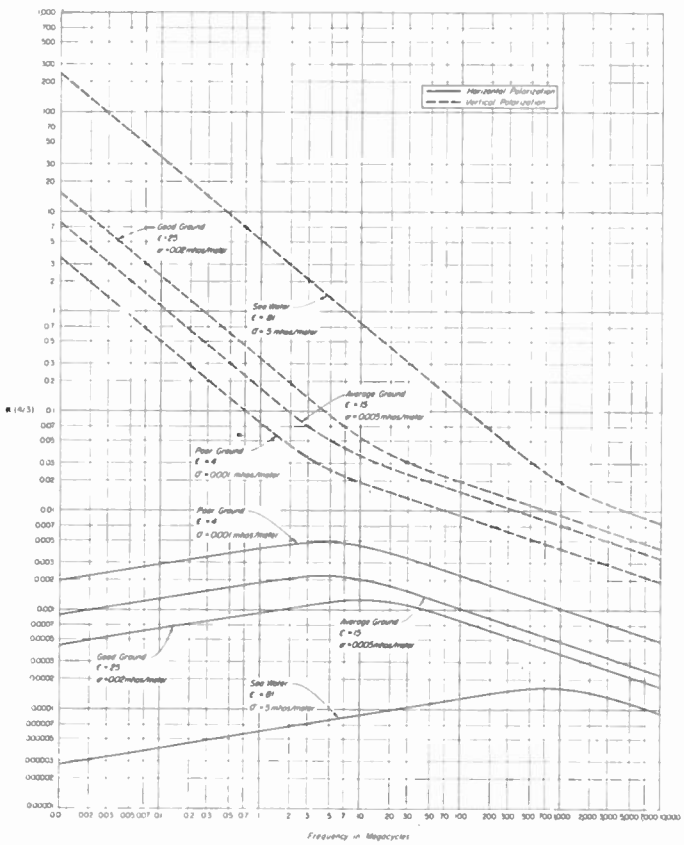

Fig. 30—The parameter $K(k')$ in ground wave propagation over a spherical earth. Values are given for an effective earth's radius 4/3 of its actual value a'; for an earth of effective radius $k'a'$, $K(k') = [4/3k']^{1/3} K(4/3)$.

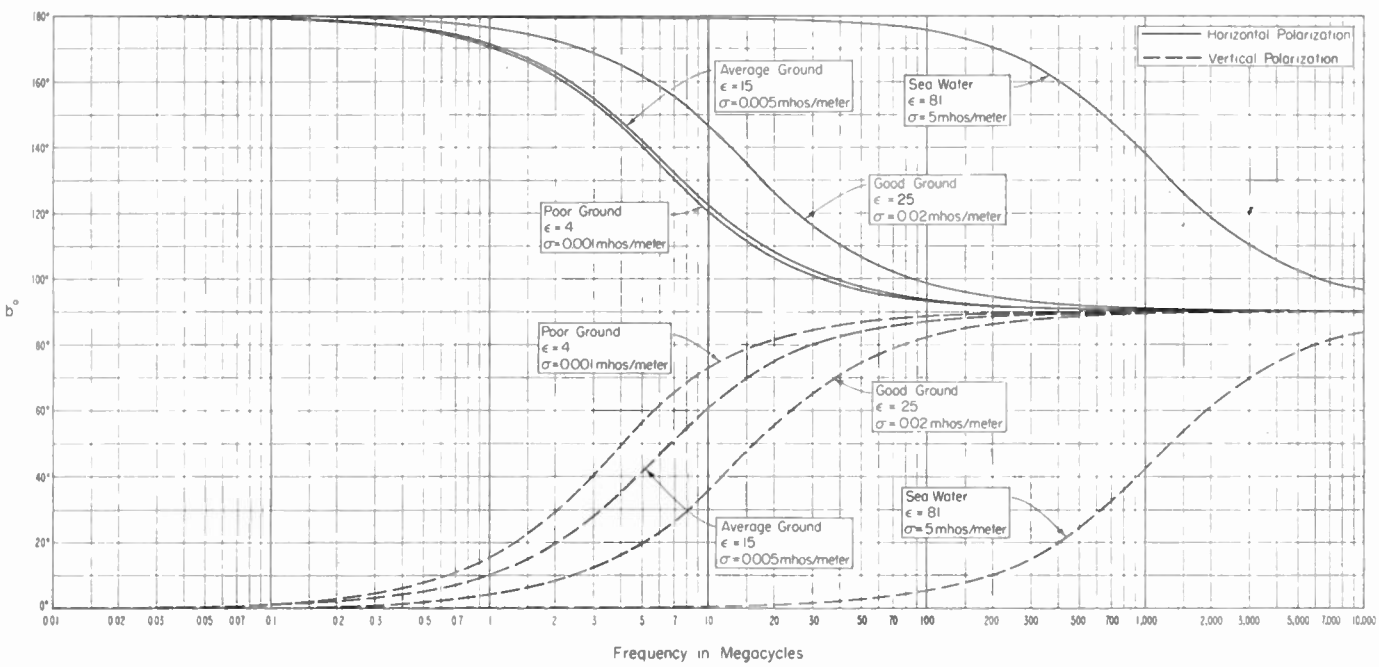

Fig. 31—The parameter b° in ground wave propagation.

These parameters have the following definitions:

$$K(k') = \left[\frac{\lambda}{2\pi k' a'}\right]^{1/3}\left[\frac{x\cos b'}{\cos^2 b''}\right]^{1/2} \quad \text{(Vertical polarization)}$$

$$K(k') = \left[\frac{\lambda}{2\pi k' a'}\right]^{1/3}\left[\frac{\cos b'}{x}\right]^{1/2} \quad \text{(Horizontal polarization)}$$

$$b^\circ = 2b'' - b'$$

$x = 60\lambda\sigma$, $\tan b' = (\epsilon - 1)/x$, $\tan b'' = \epsilon/x$, λ is the free space wavelength in meters, σ is the ground conductivity in mho's per meter, and ϵ is the dielectric constant of the ground referred to air as unity.

The parameters $\gamma(K(k'), b^\circ)$ and $\delta(K(k'), b^\circ$ are defined,[2] but these quantities are not required for use in this appendix since $C[K(k'), b^\circ]$ and $20\log_{10}\delta(K(k'), b^\circ)$ are given on Figs. 33 and 34 (next page). In fact this entire appendix is intended to be sufficiently complete so that it may be used without reference to other papers. Note that $C_0(k') = 1$ for the important case of propagation in a standard atmosphere over a smooth earth with normal

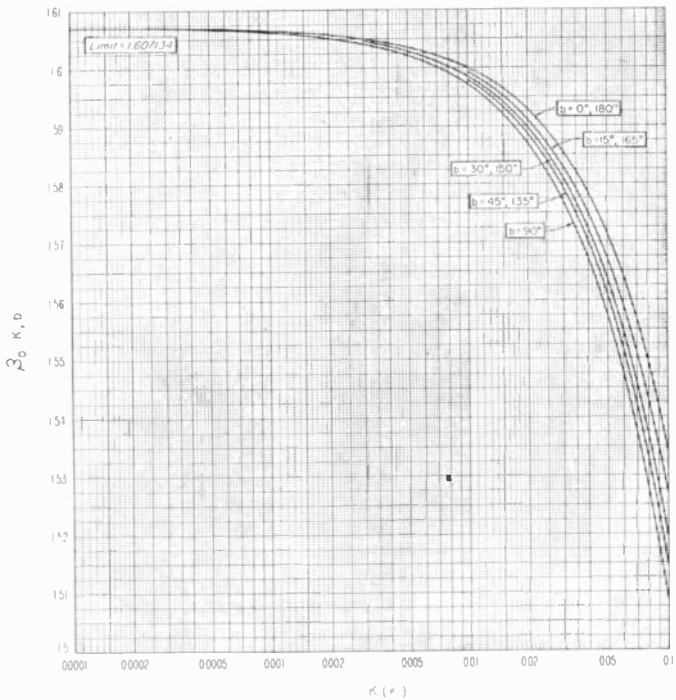

Fig. 32(a)—The parameter $\beta_0[K(k'), b^\circ]$ in ground wave propagation over a spherical earth.

radius $k_e a' = 3{,}960$ miles for which $k' = k = 4/3$. The parameter $\beta_0(K(k'), b^\circ)$ is shown graphically as a function of $K(k')$ and b° on Figs. 32(a), 32(b) and 32(c). $C[K(k'), b^\circ)$ is shown graphically as a function of $K(k')$ and b° on Fig. 33; at frequencies above 30 megacycles over land we may take $C[K(k'), b^\circ]$ to be equal to 61.7 decibels with less than 0.1 decibel error.

The height-gain functions $G[\bar{h}_r(k')]$ and $G[\bar{h}_t(k')]$ corresponding to the receiving and transmitting antennas are defined by:

$$G[\bar{h}(k')] = 20\log_{10} f(\bar{h}) - 22.66675\sqrt{\bar{h}} \qquad (39)$$

$$\bar{h}_{t,r}(k') = [\beta_0(K, b^\circ)\eta_0]^2\, k' a' h_{te,re}$$

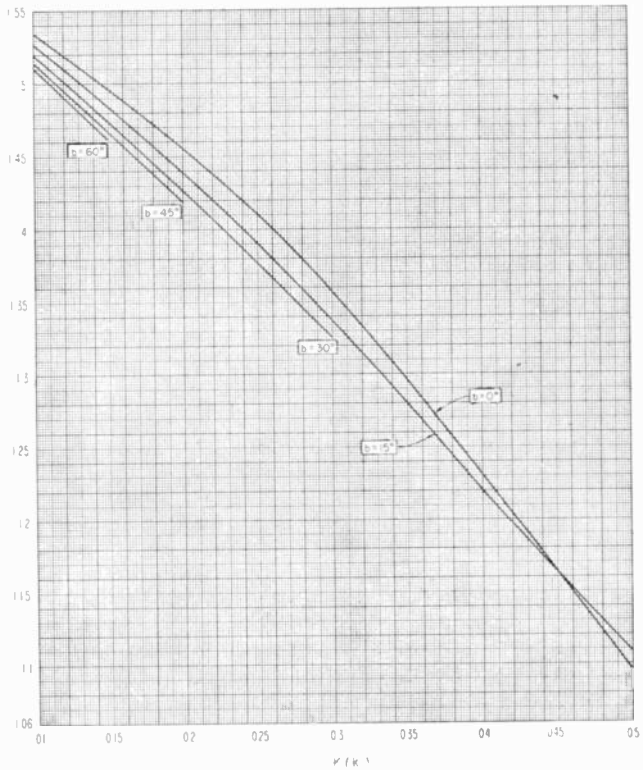

Fig. 32(b)—Same as Fig. 32(a).

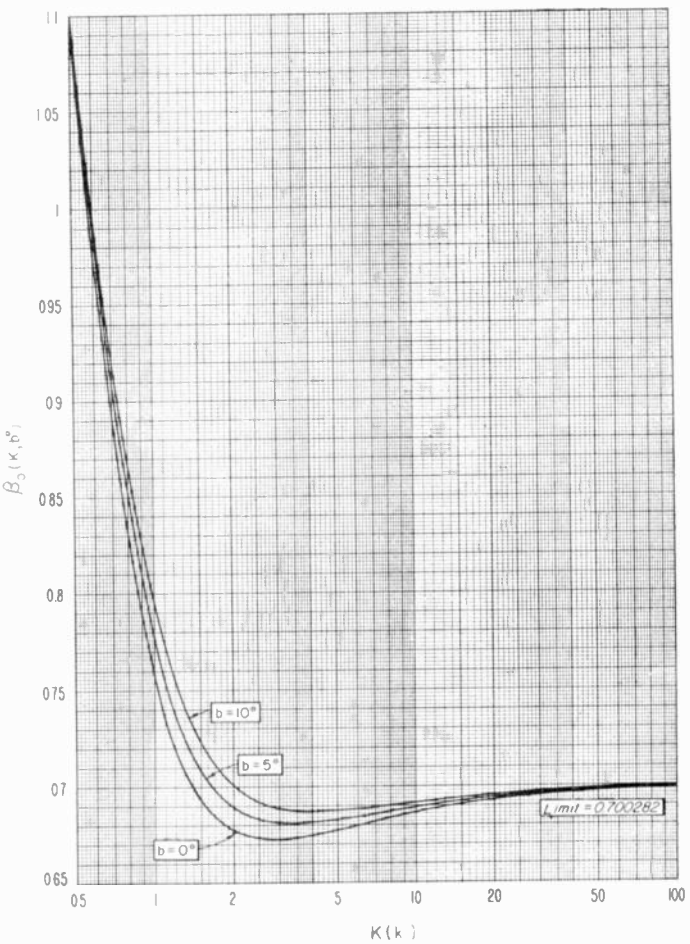

Fig. 32(c)—Same as Fig. 32(a).

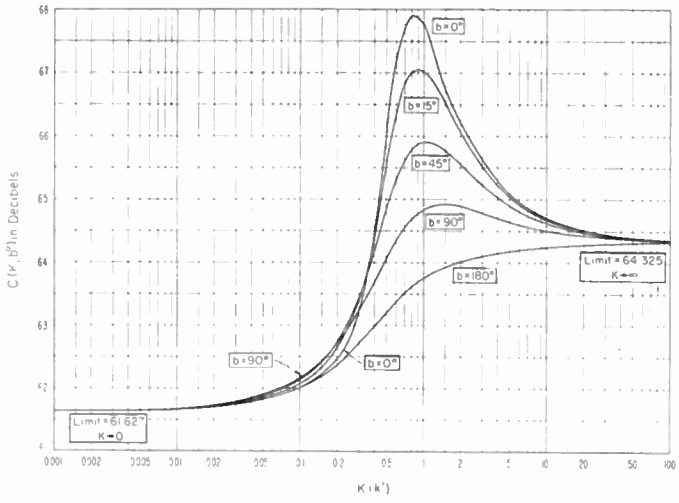

Fig. 33—The parameter $C[K(k'), b°]$ in ground wave propagation over a spherical earth.

$$= 3.33460 \times 10^{-5} h_{te,re} \text{ (feet) } \beta_0^2(K, b°) f_{mc}^{2/3} / C_0(k'). \quad (40)$$

In the above $\eta_0 = (k'^2 a'^2 \lambda)^{-1/3}$. $f(\bar{h})$ is shown graphically on Fig. 11 of reference 2, while $G[\bar{h}(k')]$ is shown graphically with $K(k')$ and $b°$ as parameters on Figs. 34, 35(a), 35(b), and 35(c) of this paper. Since $G[\bar{h}(k')]$ varies only a few decibels for wide ranges of $\bar{h}(k')$, it is clear that the effect of antenna height on L_b is largely absorbed in θ. The diffracted surface wave is obtained by setting $\bar{h}_r(k') = \bar{h}_t(k') = 0$. In order to facilitate calculations of the surface wave, $G(0) \equiv -20 \log_{10} \delta$ is shown graphically as a function of $K(k')$ with $b°$ as a parameter on Fig. 34.

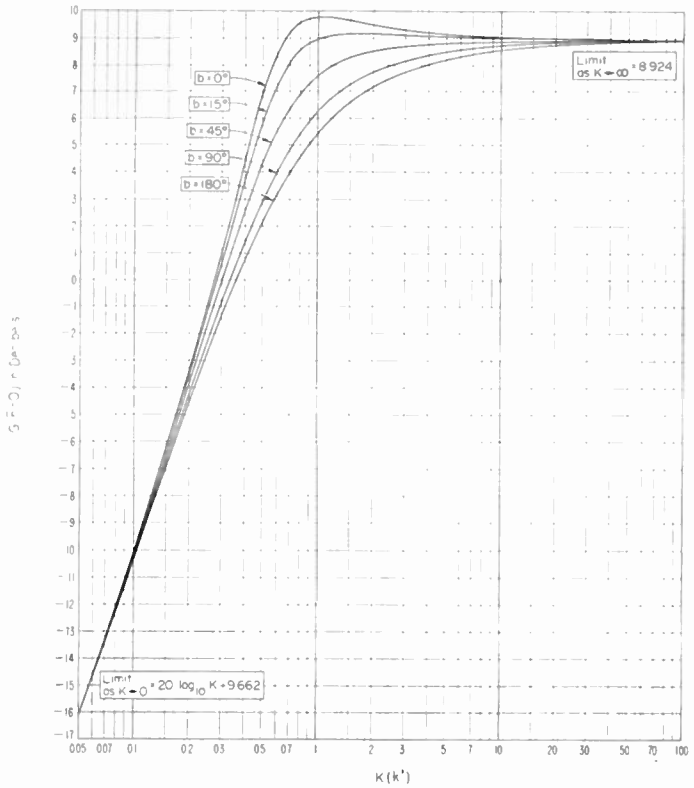

Fig. 34—The residual height-gain function $G(\bar{h} = 0)$ for the surface wave.

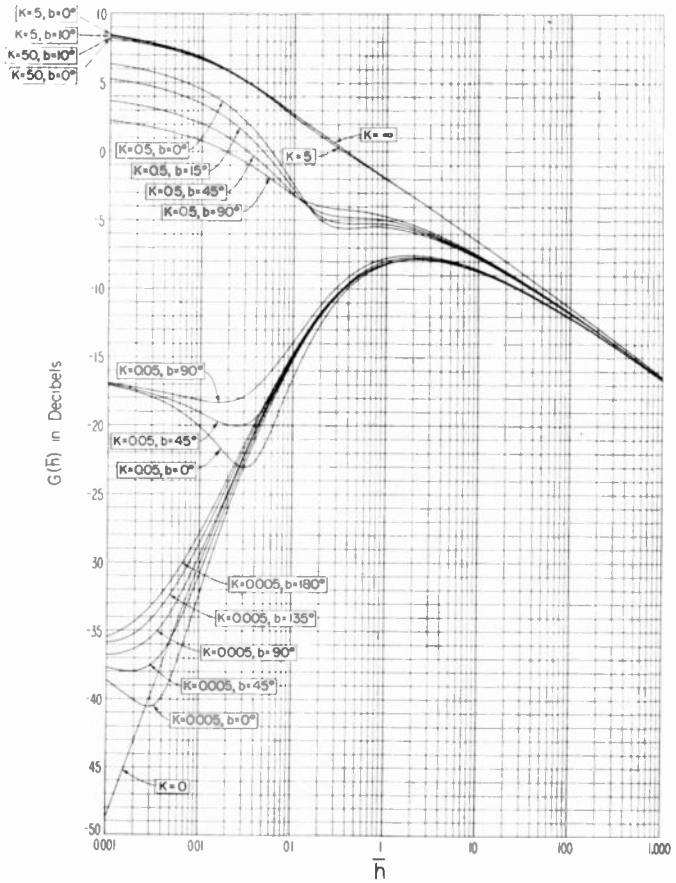

Fig. 35(a)—The residual height-gain function $G(\bar{h})$. Most of the height-gain is included in the dependence of the transmission loss on the angular distance.

$$\bar{h} = 3.3346 \cdot 10^{-6} h_{t,t} \beta_0^2 f_{mc}^{2/3} (4/3k')^{1/3}$$

In deriving (36) use is made of the relation:

$$\begin{aligned} \beta_0(K, b°)\eta_0 d - \sqrt{2\bar{h}_t} - \sqrt{2\bar{h}_r} &= \beta_0(K, b°)\eta_0(d - \sqrt{2k'a'h_{te}} - \sqrt{2k'a'h_{re}}) \\ &= \beta_0(K, b°)\eta_0 k'a'\theta. \end{aligned} \quad (41)$$

Since (36) was derived using only the leading term in the series expansion for field beyond horizon,[1,2] it will be applicable only for large angular distances such that:

$$\theta > 0.03/C_0(k') f_{mc}^{1/3}. \quad (42)$$

For shorter angular distances the procedure of reference 2 is recommended, namely, compute L_b for negative values of θ; i.e., within line of sight, and draw a smooth curve between these values of L_b corresponding to negative values of θ and the values of L_b determined by (36) for θ greater than the limit (42).

The formula (36) involves few approximations and is applicable to calculating the smooth earth diffracted wave (neglecting atmospheric absorption) for any frequency, any set of ground constants, for both vertical or horizontal polarization and with antenna heights varying from zero (surface wave) up to almost arbitrarily large heights. The height-gain function $G[\bar{h}(k')]$ is strictly applicable, in accordance with the assumptions made in its derivation, only for heights which are

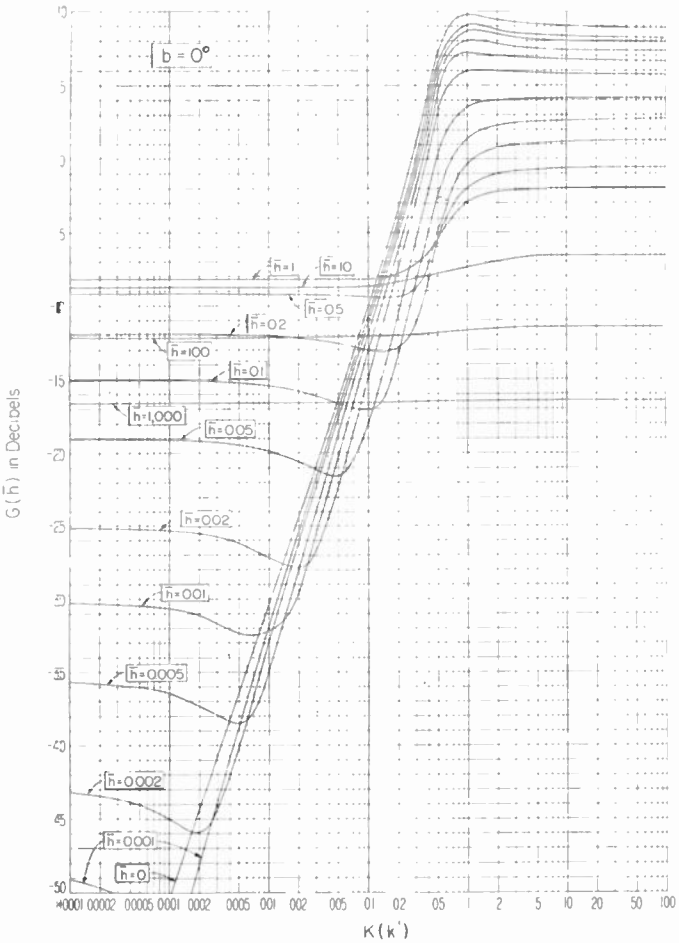

Fig. 35(b)—Same as Fig. 35(a).

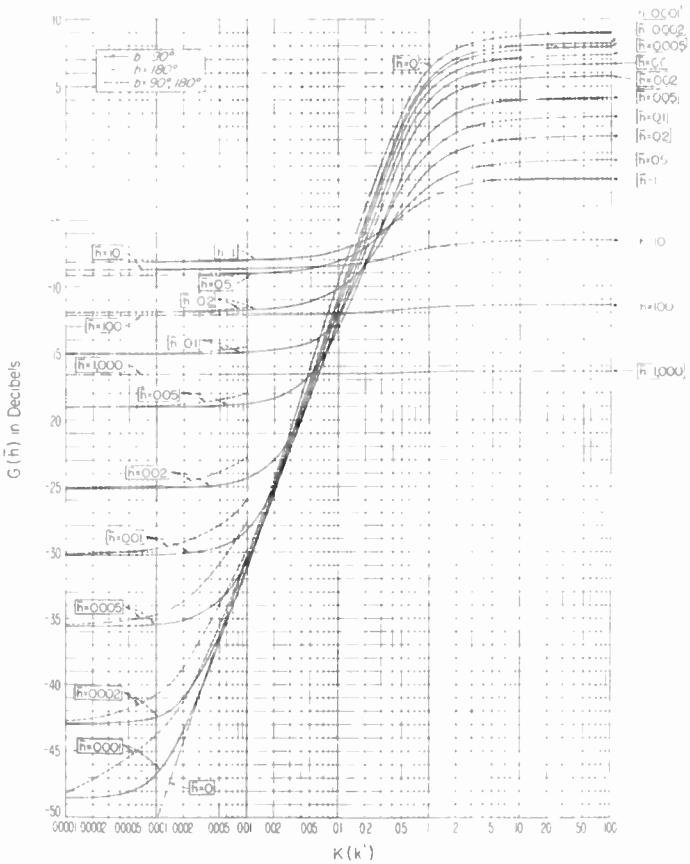

Fig. 35(c)—Same as Fig. 35(a).

sufficiently low so that $\sqrt{2k'a'h_{t,r}} \simeq k'a'\theta_{t,r}$; i.e., for values of $\theta_{t,r} \ll \pi/3$; nevertheless, we see on Figs. 20 and 21 that L_b as computed by (36) approaches the expected knife-edge values even for values of k' for which $\theta_{t,r} > \pi/3$. This circumstance provides a semi-empirical method of calculation of expected transmission loss over obstacles with small effective radii of curvature that may be used until solution for a parabolic cylinder is developed in a form convenient for use.

It should be noted that the θ used in (36) depends upon the linear gradient of atmospheric refractive index assumed; i.e., is the function of k given by (10). When (36) is expressed in terms of the standard atmosphere value of θ with d, h_{te} and h_{re} constant, then the exponential term in (36) is approximately proportional to $[C_0(k')]^{-2}$ rather than proportional to $C_0(k')$; such an expression was used in obtaining the results shown on Fig. 14. On the other hand, the results shown on Figs. 20 and 21 were obtained by using (36) directly since, in these latter calculations, a radio standard atmosphere was assumed for determining θ and the actual radius of curvature of the obstacle was varied.

We turn now to a generalization of the above smooth spherical earth solution to our smooth earth model involving four different radii of curvature. The first four terms on the right-hand side of (36) may be approximately identified with height-gain effects over the terrain to the radio horizons from each antenna. The last two terms in (36) may be approximately identified with the attenuation between the radio horizons. In this way we have arrived at the following formula for the smooth earth model involving the four effective radii of curvature $k_{te}a'$, $k_{re}a'$, k_ta', and k_ra':

$$\begin{aligned} L_b - 10\log_{10} d_{mi} &= \tfrac{1}{2}C[K(k_{te}), b^\circ] + \tfrac{1}{2}C[K(k_{re}), b^\circ] \\ &\quad + 16.667\log_{10} f_{mc} - G[\bar{h}_t(k_{te})] - G[\bar{h}_r(k_{re})] \\ &\quad + 10\log_{10} C_0(k_t) + 10\log_{10} C_0(k_r) \\ &\quad + 488.69 f_{mc}^{1/3}\{\beta_0[K(k_t), b^\circ]C_0(k_t)\alpha_1 \\ &\quad + \beta_0[K(k_r), b^\circ]C_0(k_r)\beta_1\}. \end{aligned} \tag{43}$$

The angles α_1 and β_1, whose sum is equal to the angular distance θ, are defined by (18) and (19) in Section III.

Appendix II

Tropospheric Forward Scatter

Booker-Gordon Model When the Scattering Volume is at Large Heights Above the Earth's Surface

The development in references 15 and 44 of the scattering theory outlined by Booker and Gordon[24,25] and by Staras[33,55] is here simplified and further extended. In

[55] H. Staras, "Scattering of electromagnetic energy in a randomly inhomogeneous atmosphere," *Jour. Appl. Phys.*, vol. 23, p. 1152; October, 1952.

reference 44 a discussion is given of some other aspects of the theory, including a discussion of the shape of the scattering volume.

It may be shown that the attenuation relative to free space may be expressed as the following volume integral:

$$I = d^2 \int_v \frac{g_t g_r \sigma dv}{(RR_0)^2} = \frac{2d^2}{\pi} \cdot \int_v \frac{[C(0)/l_0] g_t g_r f[(l_0/\lambda)\cdot(\alpha+\beta)] \sin^2 x \, dx \, dh \, dw}{(RR_0)^2(\alpha+\beta)^4} \cdot \quad (44)$$

In this paper a rectangular coordinate system is used to locate the volume element dv, as shown in Fig. 36. In reference 15 the volume element dv was located with three angular coordinates, α, β, and ϕ. The coordinate systems are related by the identity $(dx\ dh\ dw)\cdot d \equiv (d\alpha\ d\beta\ d\phi)\cdot(RR_0)^2$. The coordinate w measures the distance from the great circle plane defined by the transmission path terminals A_1 and A_2.

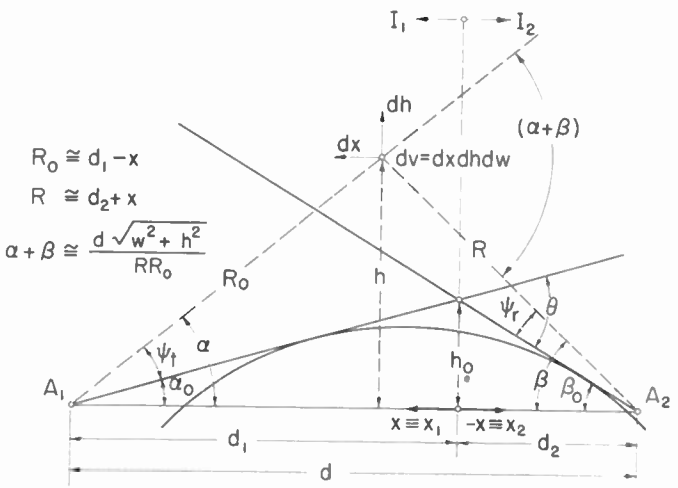

Fig. 36—Geometry for the scattering integral.

The form used for the scattering cross-section, σ, including its parameters $C(0)$, l_0, $\sin^2\chi$, and the function $f[(l_0/\lambda)\cdot(\alpha+\beta)]$ is discussed in Section IX of this paper. An earth is assumed with a radius equal to k times its actual value, a', in order to allow for the average effects of refraction in a linear gradient atmosphere. Transmitting and receiving antennas of heights h_{te} and h_{re} above the earth are located a distance d miles apart. Transmitting and receiving antenna gains, including the effects of earth reflection, are set equal to g_t and g_r, respectively. Here, isotropic antennas are assumed, so g_t and g_r actually allow only for the effects of ground reflection:

$$g_t = 4\sin^2\left[2\pi \frac{h_{te}}{\lambda}\psi_t\right] = 2 - 2\cos\left[\frac{4\pi}{\lambda}h_{te}\left(\frac{h}{d_1 - x} - \alpha_0\right)\right] = 2 - 2C_t \quad (45)$$

$$g_r = 4\sin^2\left[2\pi \frac{h_{re}}{\lambda}\psi_r\right] = 2 - 2\cos\left[\frac{4\pi}{\lambda}h_{re}\left(\frac{h}{d_2 + x} - \beta_0\right)\right] = 2 - 2C_r. \quad (46)$$

These are the usual expressions for ground reflection lobery over a plane reflecting surface. The parameters ψ_t, ψ_r are grazing angles, as shown in Fig. 36, and λ is the wavelength. These expressions also give good results for reflection on the spherical surface of the earth.

When the transmitting and receiving antennas are both sufficiently high so that the oscillations of the sine-squared factors in (45), (46) occur within very small intervals of ψ_t, ψ_r, then each of these factors may be replaced by its average value 1/2. The product $g_t g_r$ in (44) thus becomes equal to 4; this factor arises due to the assumption, implicit in (45) and (46), that the earth is perfectly reflecting and thus doubles the scattered power available to the receiver twice; i.e., the power incident on the scatterers is doubled since it is confined to the half plane above the earth, and the power reradiated from the scatterers is again doubled at the receiving antenna for the same reason.

In the symmetrical smooth earth situation with zero antenna heights, the case, considered in most treatments of the theory of tropospheric forward scatter, the surface of the earth at the distance to the crossover of radio horizons is at a height 0.5 h_0 above the reference axis A_1A_2 from transmitter to receiver. It has been determined from more than 130 terrain profiles that the height of terrain above this reference happens to average out to this same figure, 0.5 h_0. In order to allow for an observed decrease of $[C(0)/l_0]$ with height at large heights[56] above the surface we have assumed, somewhat arbitrarily, the following function:

$$[C(0)/l_0] = \frac{B}{(h - 0.5\,h_0)^2} \cong \frac{4h_0 B}{h^3} \cdot \quad (47)$$

The above is to be used for $(h - 0.5h_0) > 2{,}250$ feet. In the above, $[C(0)/l_0]$ per unit length at a height $(h - 0.5\,h_0)$ one unit above the earth's surface has the value B, and we have approximated this height dependence in our evaluation of the scattering integral by the second expression in (47). The adequacy of this approximation is in Fig. 10 where we note[44] most of the value of the integral is obtained for values of h less than, say, 5 h_0.

In our calculation of scattered fields, the function $f[(l_0/\lambda)\cdot(\alpha+\beta)]$ has been removed from under the sign of integration, and the correction $F[(l_0/\lambda)\cdot\theta]$ derived in reference 15 and shown on Fig. 37 was used. With $F[(l_0/\lambda)\cdot\theta] = 0$, (44) becomes:

$$I = \frac{8h_0 B}{\pi d^2} \cdot \int_{-d_2}^{d_1} \int_{h_m}^{\infty} \int_{-\infty}^{\infty} \frac{(d_1 - x)^2 (d_2 + x)^2 \, g_t g_r \, dx \, dh \, dw}{h^3 (w^2 + h^2)^2}, \quad (48)$$

[56] Part (c) of this appendix deals with the case of scattering at low heights where $[C(0)/l_0]$ is assumed to be independent of height.

where

$$h_{1m} = \beta_0(d_2 + x) = \beta_0(d_2 + x_1) \qquad \text{for } x > 0,$$
$$h_{2m} = \alpha_0(d_1 - x) = \alpha_0(d_1 + x_2) \qquad \text{for } x < 0.$$

The lower limits h_{1m} and h_{2m} for the integration with respect to h are the locations of the horizon rays in the great circle plane between A_1 and A_2 and at distances $x \equiv x_1$ and $-x \equiv x_2$ from the origin of coordinates. Because these limits are different, it is convenient to introduce subscripts 1 and 2 to refer to integration on the left- and right-hand sides, respectively, of the crossover of

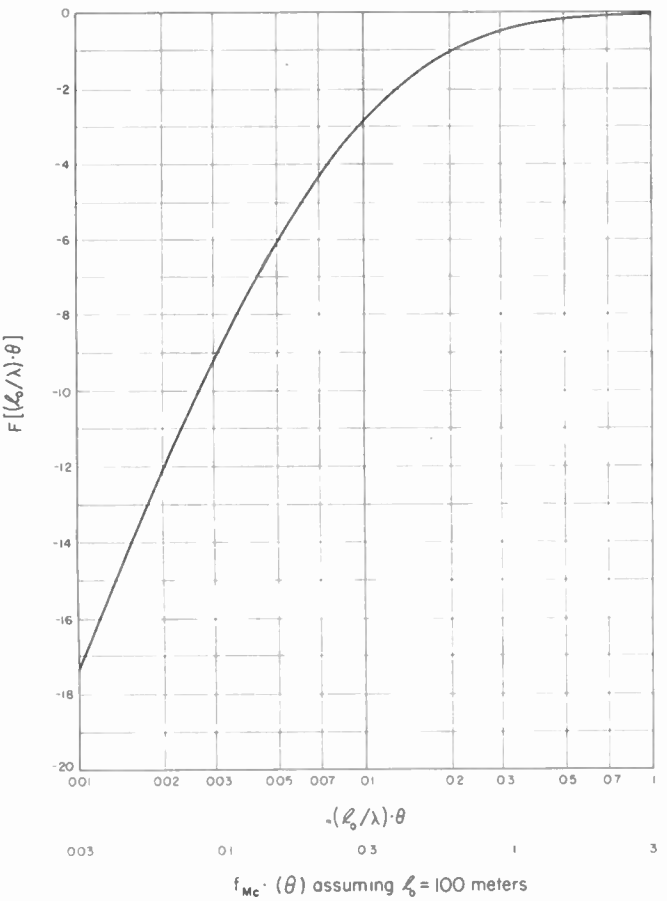

Fig. 37—The function $F[(l_0/\lambda)\cdot\theta]$.

radio horizons. The same thing was done in reference 44, where the integral I is evaluated for the case of very high antennas so that the product $g_t g_r$ may be replaced by its mean value 4. For this case,

$$I = I_1 + I_2 = \frac{16B}{5\theta^4 d}\,[A(s) + A(1/s)\,], \qquad (49)$$

where the asymmetry factor $s = (\alpha_0/\beta_0)$, and

$$A(s) = (s+1)^3[s \log_e ([s+1]/s) + 1/2s - 1].$$

Use will be made of the following terminology:

$$C_t = \cos(u_t - v_t),\ u_t = \frac{4\pi h_{te}}{\lambda(d_1 - x)}h,\ v_t = 4\pi\left(\frac{h_{te}}{\lambda}\ \alpha_0\right),$$

$$C_r = \cos(u_r - v_r),\ u_r = \frac{4\pi h_{re}}{\lambda(d_2 + x)}h,\ v_r = 4\pi\left(\frac{h_{re}}{\lambda}\ \beta_0\right),$$

$$C_{t\pm r} = \cos(u_{t\pm r} - v_{t\pm r}),\quad u_{t\pm r} = u_t \pm u_r,\quad v_{t\pm r} = v_t \pm v_r.$$

With this terminology we obtain:

$$g_t g_r = 4(1 - C_t - C_r + C_t C_r)$$
$$\equiv 4(1 - C_t - C_r + \tfrac{1}{2}C_{t-r} + \tfrac{1}{2}C_{t+r}), \qquad (50)$$

and performing the indicated integration with respect to w, (48) may be written as a double integral:

$$I = \frac{16h_0B}{d^2}\int_{-d_2}^{d_1}(d_1 - x)^2(d_2 + x)^2dx \int_{h_m}^{\infty}\frac{(1 - C_t - C_r + \tfrac{1}{2}C_{t-r} + \tfrac{1}{2}C_{t+r})dh}{h^6}$$
$$= (I_1 + I_2) - I_t - I_r + \tfrac{1}{2}I_{t-r} + \tfrac{1}{2}I_{t+r}, \qquad (51)$$

where $g_t g_r$ has been replaced by the expression given in (50). A change of variable in (51) from x to u will introduce different dependences upon x into the final integration, depending upon whether the subscripts are t, r, $t-r$, or $t+r$ and upon whether integration is performed to the left of the crossover of radio horizons or on the right-hand side. For instance:

$$I_t = \frac{16h_0B}{d^2}\int_0^{d_1}(d_1 - x_1)^2(d_2 + x_1)^2dx_1 \int_{\beta_0(d_2+x_1)}^{\infty}\frac{\cos(u_t - v_t)dh}{h^6} + \frac{16h_0B}{d^2}\int_0^{d_2}(d_1 + x_2)^2(d_2 - x_2)^2dx \int_{\alpha_0(d_1+x_2)}^{\infty}\frac{\cos(u_t - v_t)dh}{h^6}$$
$$= \frac{2B}{15\theta^4 d}\left[\frac{(s+1)^3v_t^3}{s}\int_{v_t}^{\infty}\frac{P_1(v_t, y)dy}{y^3(v_t + sy)} + P_2(v_t)A(1/s)\right], \qquad (52)$$

where

$$P_1(v, y) = 120y^5\int_y^{\infty}\frac{\cos(u - v)du}{u^6}$$

and

$$P_2(v) = P_1(v, y = v).$$

[Here, $y = (h_{1m}/h_{2m})v_t$. Integrating I_r, set $y = (h_{2m}/h_{1m})v_r$.] The integration with respect to y was performed numerically.

The expression for I_r is of exactly the same form as (52) with v_t replaced by v_r and s replaced by $1/s$. If $v_r > 20$, then $I = I_1 + I_2 - I_t$, and if $v_t > 20$, then $I = I_1 + I_2 - I_r$. Otherwise, the cross-product terms I_{t-r} and I_{t+r} should be taken into account. This may be seen from the mathematics in the fact that I_r or I_t approaches zero as v_r or v_t, respectively, becomes large, or it may be seen from the physics by assuming that a very fine lobe structure is equivalent to no lobe structure at all.

Fig. 38 shows for different values of the asymmetry factor $s=(\alpha_0/\beta_0)$ the frequency gain correction H_{0t}, defined as

$$H_{0t} = 10 \log_{10} \frac{I_1 + I_2 - I_t}{I_1 + I_2}. \tag{53}$$

Where a frequency gain correction H_{0r} for the receiving antenna side is required, this same graph is used, replacing the parameter s by $1/s$ and the frequency gain factor $(h_{te}/\lambda)\alpha_0$ by $(h_{re}/\lambda)\beta_0$.

The function H_{0t} shown on Fig. 38 is called a frequency gain function rather than a height-gain function since an increase in antenna height increases the received field more than is indicated by Fig. 38 by virtue of the fact that an increase in height, at a fixed distance, also decreases the angular distance, θ.

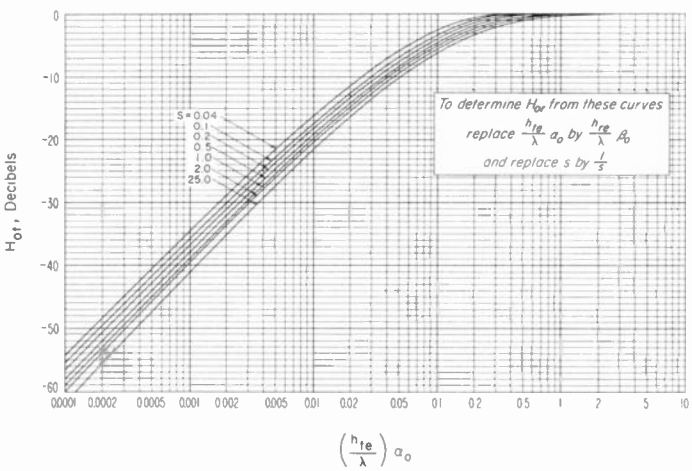

Fig. 38—The frequency-gain function H_{0t}.

For the calculations in this paper, the cross-product terms were neglected, as if H_{0t} and H_{0r} were independent, and use was made of the simple relation:

$$10 \log_{10} I = 10 \log_{10} (I_1+I_2) + H_{0t} + H_{0r} + F[(l_0/\lambda)\cdot\theta]. \tag{54}$$

The correction $F[(l_0/\lambda)\theta]$ mentioned earlier has been included in order to complete the expression used to calculate transmission loss relative to free space. For this purpose, l_0 was assumed to have the value shown on Fig. 11. Since l_0 varies with height above the surface, it should have been considered as one of the integration variables. In order to simplify these integrations, l_0 has been considered constant and equal to its value at the height of the "center" of scattering. In a companion paper[44] the height of the "center" of scattering was shown to be of the order of 1.5 h_0 above the chord A_1A_2 (see Fig. 36) where $h_0=\alpha_0\beta_0 d/\theta$. Since we have determined empirically that the earth's surface is of the order of 0.5 h_0 above the chord A_1A_2 we have the convenient result that the "center" of scattering may be considered to be at a height approximately equal to h_0 above the earth's surface. This height may be used in the following formula to calculate a value of l_0 for use in determining $F[(l_0/\lambda)\cdot\theta]$.

$$l_0 = \frac{70\, h_0}{h_0 + 500} (l_0 \text{ in meters, } h_0 \text{ in feet}). \tag{55}$$

For $v_t=0.05$, $v_r=0.1$, $s=0.2$, approximating the values of these parameters for that particular propagation path where neglect of I_{t-r} and I_{t+r} should be most serious, the error involved was found to be less than two decibel. To determine the correct value of $H_0=10 \log_{10} [I/(I_1+I_2)]$, (51) was used to determine I, and the following integration was performed numerically in order to determine $I_{t-r}+I_{t+r}$:

$$I_{t-r}+I_{t+r} = \frac{2B(s+1)^3}{15\theta^4 ds}\left[v_t^3 \int_{v_+}^{\infty} \frac{P_1(v_{t-r}, y_1)+P_1(v_{t+r}, y_3)}{y^3(sy+v_t)}\, dy + v_r^3 \int_{v_-}^{\infty} \frac{P_1(v_{t-r}, y_2)+P_1(v_{t+r}, y_4)}{y^3(sy+v_r)}\, dy\right], \tag{56}$$

where

$$y_1 = mv_t - v_r,\ y_2 = v_t - v_r/m,\ y_3 = mv_t + v_r,\ y_4 = v_t + v_r/m,$$

and $m=h_{1m}/h_{2m}$. Where $y<0$,

$$P_1 = -120y^5 \int_{-y}^{\infty} \frac{\cos(u+v)du}{u^6}.$$

To complete this development of the Booker-Gordon theory, (54) may now be combined with (6) to give our expression for the modified *average* basic transmission loss due to tropospheric forward scatter, expressed in decibels:

$$\begin{aligned}(L_{bas} - 10 \log_{10} d_{mi}) &= -116.40 + 20 \log_{10} f_{mc} + 20 \log_{10} d_{mi} + 40 \log_{10} \theta_{mr} \\ &\quad - 10 \log_{10} [A(s) + A(1/s)] - H_{0t} - H_{0r} \\ &\quad - F[(l_0/\lambda)\cdot\theta] - 10 \log_{10} B,\end{aligned} \tag{57}$$

where f_{mc} is the radio frequency in megacycles, d_{mi} is the path distance in miles, θ_{mr} is the angular distance in milliradians, and B is the value of $[C(0)/l_0]$ per meter at one kilometer above the earth's surface. To get general agreement with the CRPL Cheyenne Mountain 100 megacycle data, we have chosen a value $-10 \log_{10} B = 138.4$ decibels. This is the value used in plotting the curves on Fig. 9 and curves for the Booker-Gordon theory on Figs. 12 and 13 in Section V. The value of $-10 \log_{10} B$ representative of the data for transmission paths in the remainder of the United States is equal to 130.9 decibels, as may be seen on Fig. 10. This latter value was used in plotting the curves on Fig. 14 in Section V and on Fig. 21 in Section VIII. The analysis in Section V indicates that B depends upon the gradient ΔN of refractivity of the earth's atmosphere and may be determined from the equation

$$-10 \log_{10} B = 142.9 + 0.372\ (\Delta N + 39.23).$$

This equation may be used with the climatic maps of ΔN in the Bean and Meaney paper[19] published in this is-

sue to estimate the value of B to be expected for transmission paths anywhere in the United States.

Weisskopf-Villars Model

As discussed in Section IX, the Weisskopf-Villars theory is based on a form of the scattering cross section which differs from the Booker-Gordon model only by the addition of a λ factor, an additional $(\alpha+\beta)^{-1}$, and the use of $V=\{[(dn/dh)^2]-[dn/dh]^2\}$ instead of $[C(0)/l_0]$.

In order to approximate the θ-dependence observed in our data, we have assumed that

$$V=\frac{B_1}{(h-0.5h_0)}\cong\frac{2h_0B_1}{h^2}, \tag{58}$$

and have approximated this height dependence in our evaluation of the scattering integral by using the second expression in (58). In the above, V per unit length squared at a height $(h-0.5\ h_0)$ one unit above the earth's surface has the value B_1.

The attenuation relative to free space may then be expressed as

$$J=d^2\int_V\frac{g_tg_r\sigma dv}{(RR_0)^2}=\frac{8\pi^2\lambda h_0B_1}{d^3}\int_{-d_2}^{d_1}\int_{h_m}^{\infty}\int_{-\infty}^{\infty}\frac{(d_1-x)^3(d_2+x)^3g_tg_r\,dx\,dh\,dw}{h^2(w^2+h^2)^{5/2}}. \tag{59}$$

Integrating with respect to w, we obtain

$$J=\frac{32\pi^2\lambda h_0B_1}{3d^3}\int_{-d_2}^{d_1}(d_1-x)^3(d_2+x)^3dx\int_{h_m}^{\infty}\frac{g_tg_r dh}{h^6}. \tag{60}$$

Let us assume that the transmitting and receiving antennas are very high, so that the product g_tg_r may be replaced by its mean value 4. For this case:

$$J=\frac{128\pi^2\lambda B_1}{15\theta^4}[A_1(s)+A_1(1/s)], \tag{61}$$

where the asymmetry factor $s=(\alpha_0/\beta_0)$ and

$$A_1(s)=s(s+1)^3\left[\frac{3}{2}+3\log_e\left(\frac{s}{s+1}\right)+\left(\frac{s+1}{s}\right)-3\left(\frac{s}{s+1}\right)+\frac{1}{2}\left(\frac{s}{s+1}\right)^2\right]. \tag{62}$$

Comparing (60) and (51), it may be seen that they differ only in their dependence on x. Consequently we would expect only small differences in the frequency gain functions for the Weisskopf-Villars and Booker-Gordon models described above, since these models lead to integrands with the same dependence on the height h. Assuming the same frequency gain function, then, for the present model, we may write for the modified average basic transmission loss due to tropospheric forward scatter:

$$(L_{bas}-10\log_{10}d_{mi})=-157.44+30\log_{10}f_{mc}+40\log_{10}\theta_{mr}+10\log_{10}d_{mi}-10\log_{10}[A_1(s)+A_1(1/s)]-H_{0t}-H_{0r}-10\log_{10}B_1\text{ decibels}, \tag{63}$$

where f_{mc} is the radio frequency in megacycles per second, d_{mi} is the transmission path length in miles, θ_{mr} is the angular distance in milliradians, H_{0t} and H_{0r} are read from Fig. 38, and B_1 is the value of V per (meter)^2 at one kilometer above the earth's surface. To obtain general agreement with the CRPL Cheyenne Mountain 100 megacycle data, we have chosen a value $-10\log_{10}B_1=175$ decibels. This is the value used in plotting the curves for the Weisskopf-Villars theory on Fig. 13 in Section V.

It is shown in Section IX that (58) assumes the wrong dependence of V on height according to our data, and a correction for this is incorporated into (34), which is the formula used to compare scattering theory with the data. See also the addendum, end of Appendix IV.

Booker-Gordon Model When the Scattering Volume is Near the Earth's Surface

Both meteorological and radio transmission loss data indicate that $[C(0)/l_0]$ does not continue to increase at very low heights as was assumed in (47) for the theory in the first section of Appendix II. In our earlier paper[15] allowance was made for this different behavior of $[C(0)/l_0]$ at low and at high heights by assuming that $[C(0)/l_0]$ varies exponentially with increasing height. In the present paper we have approximated this height dependence by assuming that $[C(0)/l_0]$ is independent of height up to about 2,250 feet and subsequently decreases in inverse proportion to the square of the height above the surface. The method of calculation of radio transmission loss when $[C(0)/l_0]$ is independent of height was discussed in some detail in our earlier paper[15] and will be only briefly reviewed here.

The formula for the modified average basic transmission loss when $[C(0)/l_0]$ is assumed independent of height may be expressed:

$$(L_{bas}-10\log_{10}d_{mi})=-53.73+20\log_{10}f_{mc}+20\log_{10}\theta_{mr}-10\log_{10}[C(0)/l_0]-F[(l_0/\lambda)\cdot\theta]-H_0[(h_{te}/\lambda)\cdot\theta]-H_0[(h_{re}/\lambda)\cdot\theta]. \tag{64}$$

In the above l_0 is expressed in meters and may be determined from (55) using the approximate height h_0 of the "center" of scattering above the earth's surface.

The frequency-gain function $H_0[(h/\lambda)\cdot\theta]$ to be used for this case is given on Fig. 39 (next page). Note that there is no asymmetry factor for this case in which $[C(0)/l_0]$ is assumed independent of the height.

Appendix III

Knife-Edge Diffraction

Use will be made of results based on physical optics and given in reference 41. The parameter v in that paper may be expressed as follows:

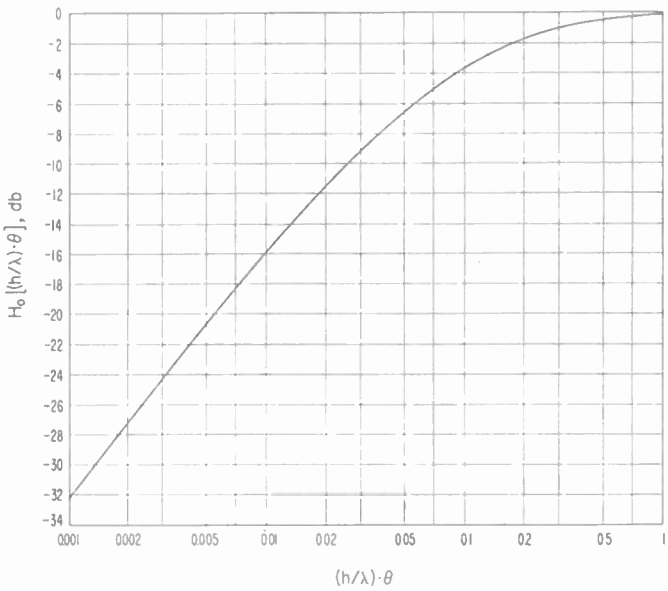

Fig. 39—The frequency-gain function for $[C(0)/I_0]$ independent of height.

$$v = \sqrt{\frac{2d}{\lambda}} \tan \alpha_0 \tan \beta_0. \tag{65}$$

Note on Fig. 40 that v is positive when α_0 and β_0 are positive but negative when α_0 and β_0 are negative. The knife-edge attenuation relative to the free space attenuation, $A(v)$, may then be expressed:

$$A(v) = -10 \log_{10} \frac{1}{2} \left[\left(\int_v^\infty \cos \frac{\pi x^2}{2}\, dx \right)^2 + \left(\int_v^\infty \sin \frac{\pi x^2}{2}\, dx \right)^2 \right]. \tag{66}$$

$A(v)$ is shown graphically on Fig. 40 as a function of v.

Our formula for the basic transmission loss in propagation over a knife edge, neglecting the effects of ground reflection on both sides of the knife edge, may be written:

$$L_b = 20 \log_{10} d_{mi} + 20 \log_{10} f_{mc} + A(v) + 36.581. \tag{67}$$

When v is sufficiently large, say $v > 3$, $A(v) = 12.953 + 20 \log_{10} v$ and, when this is added to the transmission loss in free space, we obtain the following formula for the basic transmission loss expected for propagation over a knife edge:

$$L_b = 30 \log_{10} d_{mi} + 30 \log_{10} f_{mc} + 10 \log_{10} \tan \alpha_0 + 10 \log_{10} \tan \beta_0 + 59.843. \tag{68}$$

The above equation is accurate only when $(d/\lambda) \tan \alpha_0 \tan \beta_0 > 4$; furthermore, (66), (67), and (68) may be expected to be useful only when $d \gg \lambda$, $\tan \alpha_0 \ll 1$, and $\tan \beta_0 \ll 1$.

When $\alpha_0 = \beta_0$ and these angles are sufficiently small so that the tangents may be replaced by the angles, we obtain from (68):

$$L_b = 30 \log_{10} d_{mi} + 30 \log_{10} f_{mc} + 20 \log_{10} \theta + 53.822. \tag{69}$$

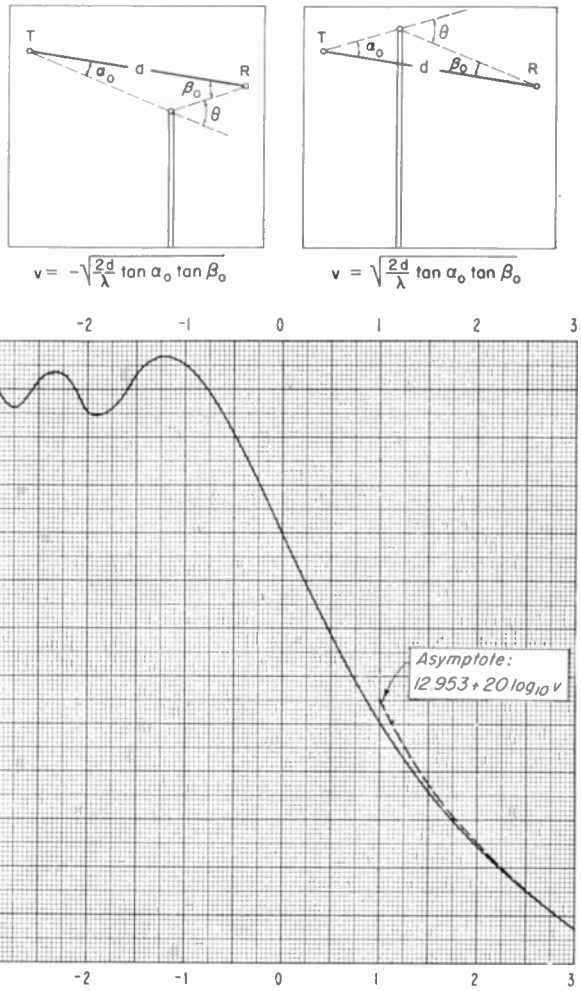

Fig. 40—The parameter $A(v)$ used in the knife-edge diffraction formula (67) and in (71).

If we assume ground reflections on both sides of the knife edge, then four transmission paths are involved as discussed in reference 41.

If the antenna heights are properly adjusted so that the waves arriving along these four paths are approximately in phase, it is possible in the case of perfect ground reflections to increase the received power by a factor of 16. In this case (69) becomes:

$$L_b = 30 \log_{10} d_{mi} + 30 \log_{10} f_{mc} + 20 \log_{10} \theta + 41.781. \tag{70}$$

Eqs. (69) and (70) are accurate only when $(d/\lambda) \tan^2 (\theta/2) > 4$. The above assumptions obviously represent a considerable idealization of the actual problem of knife-edge diffraction. The proper solution of any particular case requires the addition of four vectors, each with proper magnitude and phase, and this process does not lend itself to much simplification except with assumptions such as those made above.

A good example of the applicability of the above formulas is presented in a paper in this issue by Kirby, Dougherty and McQuate.

We have found that a combination of the above theory with some of the results given in Appendix I often provides a useful method of calculation. Thus, in

those cases where the transmitting and receiving antenna have a common horizon so that $(d-d_{Lt}-d_{Lr})=0$, (43) no longer provides a solution, and the effects of ground reflection are difficult to allow for in using (67). In this case we have found that the following formula is useful:

$$L_b = 20\log_{10} d_{mi} + 20\log_{10} f_{mc} + A(v) + 36.581 - G[\bar{h}_t(k_{te})] - G[\bar{h}_r(k_{re})]. \quad (71)$$

The above should be used only for common horizon cases and $G[\bar{h}_t(k_{te})]$ and $G[\bar{h}_r(k_{re})]$ are determined by the methods discussed in Appendix I. This provides an alternative to the methods used in reference 41 to allow for ground reflection. The above formula has given good results when the rays from the antennas to their common horizon are not far from the earth's surface throughout most of their lengths.

Appendix IV

An Explanation of the Symbols Used in the Paper and a Table of Radio Transmission Loss Data

λ Free space radio wavelength.

f_{mc} Radio frequency in megacycles per second.

θ Angular distance; when used as a prediction parameter, this is always to be determined for a radio standard atmosphere ($k=4/3$) with an actual terrain profile.

d, d_T Distance between transmitting and receiving antennas. (In Figs. 1 and 3 the symbol D is used for the path distance.)

p_r Power available for radiation from a transmitting antenna.

p_a Power available from a receiving antenna.

L Transmission loss, expressed in decibels; $L=10\log_{10}(p_r/p_a)$. See (1).

L_f Transmission loss for propagation in free space; see (2).

L_b Basic transmission loss is the transmission loss expected if isotropic transmitting and receiving antennas were used.

L_{bf} Basic transmission loss in free space.

G_p The path antenna gain expressed in decibels; see (3).

G_t, G_r Transmitting and receiving antenna free space gains expressed in decibels relative to an isotropic antenna; see (7); for a half-wave dipole $G_t=2.15$ decibels.

g_t, g_r Transmitting and receiving antenna gain patterns, including the effects of earth reflection. See Appendix II.

L_{bd} Theoretical basic transmission loss using the four earth-curvature diffraction formula (43).

$L_{bd}(4/3)$ Theoretical basic transmission loss using the diffraction formula (36) with $k'a'=5{,}280$ miles.

L_{bas} Theoretical average basic transmission loss for the Weisskopf-Villars scattering theory and a radio standard atmosphere. In the development of the Booker-Gordon scattering theory (64) is used at small angular distances, and at large angular distances calculations are made using both (64) and (62), and the larger of the two values of transmission loss is used.

K $L_{bd}-L_{bas}$.

L_{bmp} Predicted median basic transmission loss for a standard atmosphere. $L_{bmp}=L_{bd}-R(0.5)$. $R(0.5)$ is shown graphically as a function of K on Fig. 6 of reference 34.

$R(0.5)$ The level, in decibels above the amplitude of a constant vector, of the median value of the resultant amplitude of this constant vector added to a Rayleigh-distributed vector.

$R(0.1)-R(0.9)$ Fading range is the interdecile range of the cumulative distribution of instantaneous transmission loss in decibels as recorded for a specified period of time.

$L_{bm}(\Delta N)$ Predicted value of median basic transmission loss for an atmosphere with a refractive index gradient ΔN.

$[L_{bm}-10\log_{10} d_{mi}]$ Modified basic transmission loss in decibels.

E Field strength in decibels above one microvolt per meter for one kilowatt effective power radiated from a half-wave dipole.

E_{mp} Predicted median field intensity.

E_{m0} Observed median field intensity.

L_{bm0} Observed median basic transmission loss for the period indicated, assuming antenna gains are realized.

Δ $L_{bm0}-L_{bmp}+D(\Delta N)=E_{mp}-E_{m0}$

G_0 Theoretical obstacle gain in decibels. $G_0=L_{bd}(4/3)-L_{bd}$.

A_a Atmospheric absorption for the transmission path, expressed in decibels.

A_e Effective absorbing area of an antenna.

Item N°	NBS Path N°	Transmitter	Receiver	Freq (Mc)	θ (mr)	s a_o/β_d	d (miles)	h_{te} (feet)	h_{re} (feet)	$k_{te}a'$ (miles)	$k_{re}a'$ (miles)	k_1a' (miles)	k_Fa' (miles)	h_o (feet)	bmo	Period covered by the data (dates)	(hours)	Total no. of hours	W	G_o (db)	-ΔN	D(ΔN) (db)	Weisskopf-Villars K (db)	Δ (db)
1	350	CRPL, Colo. Springs, Colo.	CRPL, Kendrick, Colo.	210.4	0.934	0.1740	49.4	1396	36	2936	3293	24169	426.9	30.86	140.1	2/52–3/52	1300–1800	91	0.226	3.4	36.6	−0.34	−18.0	− 0.6
2	370	CRPL, Colo. Springs, Colo.	CRPL, Kendrick, Colo.	236	0.934	0.1741	49.4	1396	36	2936	3293	24169	426.9	30.86	142.6	2/54	1300–1800	57	0.179	3.9	36.7	−0.33	−16.6	0.1
3	330	CRPL, Colo. Springs, Colo.	CRPL, Kendrick, Colo.	92	0.934	0.1810	49.4	1376	37	2978	3426	12166	736.8	38.00	134.3	2/52–6/53	1300–1800	940	1.127	3.1	39.0	−0.04	−28.8	− 2.5
4	274	CRPL, Colo. Springs, Colo.	CRPL, Haswell, Colo.	192.8	1.672	0.3682	96.6	2321	18	5670	99146	0	0	167.5	160.2	2/52–4/53	1300–1800	112	1.225	−10.2	40.7	0.21	4.8	0.4
5	294	CRPL, Colo. Springs, Colo.	CRPL, Haswell, Colo.	230	1.672	0.3682	96.6	2321	18	5670	99146	0	0	167.8	157.1	2/54	1300–1800	157	0.300	− 9.8	36.7	−0.38	7.0	− 2.6
6	314	CRPL, Colo. Springs, Colo.	CRPL, Haswell, Colo.	1046	1.744	0.3678	96.6	2226	43	5911	41503	0	0	176.9	170.3	2/52–6/53	1300–1800	1333	0.637	− 5.9	42.4	0.46	20.2	15.5
7	254	CRPL, Colo. Springs, Colo.	CRPL, Haswell, Colo.	100	1.795	0.3603	96.6	2271	19	5794	93928	0	0	180.4	155.2	2/52–6/53	1300–1800	1270	0.923	− 9.8	42.1	0.42	− 2.6	− 3.7
8	56	WKBN-TV, Youngstown, O.	United Broadcasting Co. Hudson, Ohio	98.7	3.637	0.3566	44.9	592	30	4880	12253	0	0	167.1	147.3	8/50–11/53	11:00–1800	2134	2.053	4.0	43.2	0.85	−11.1	3.2
9	39	WFMJ-FM, Youngstown, O.	UBC, Hudson, Ohio	105.1	3.770	0.3937	45.7	395	30	5935	13098	4134	233.0	184.4	148.0	11/52–6/53	1300–1800	1071	0.925	4.2	38.9	−0.09	−13.3	− 0.2
10	352	CRPL, Colo. Springs, Colo.	CRPL, Karval, Colo.	210.4	4.012	0.8871	70.2	1436	36	2544	79360	0	0	370.4	141.3	1/53–4/53	1300–1800	267	0.387	0.2	36.9	−0.54	6.1	− 3.2
11	372	CRPL, Colo. Springs, Colo.	CRPL, Karval, Colo.	230	4.012	0.8871	70.2	1436	36	2544	79800	0	0	370.4	142.9	2/54	1300–1800	36	0.141	1.0	36.7	−0.58	6.7	− 2.7
12	332	CRPL, Colo. Springs, Colo.	CRPL, Karval, Colo.	92	4.108	0.8870	70.2	1416	37	2530	77702	0	0	379.3	144.7	2/52–7/53	1300–1800	1164	0.247	− 1.4	39.9	0.34	− 0.9	− 3.1
13	390	CRPL, Camp Carson, Colo.	CRPL, Kendrick, Colo.	100	5.905	0.2672	46.6	s 40	19	61312	6808	451.8	1285	241.7	123.4	8/52–2/53	1300–1800	26	0.167	− 0.3	43.1	1.14	− 8.6	−16.3
14	354	CRPL, Colo. Springs, Colo.	CRPL, Haswell, Colo.	210.4	6.380	.6456	96.8	1502	36	2781	49573	7717	3059	777.4	175.7	2/52–4/53	1300–1800	580	0.735	− 5.3	36.6	−0.85	16.9	12.4
15	374	CRPL, Colo. Springs, Colo.	CRPL, Haswell, Colo.	236	6.380	0.6456	96.8	1502	36	2784	49573	7717	3059	777.4	178.7	2/54	1300–1800	53	0.171	− 5.2	36.7	−0.82	17.7	11.7
16	334	CRPL, Colo. Springs, Colo.	CRPL, Haswell, Colo.	92	6.402	.6543	96.8	1482	37	2822	48234	7308	3142	790.4	165.5	2/52–6/53	1300–1800	821	0.135	− 5.6	39.0	−0.10	8.2	4.3
17	392	CRPL, Camp Carson, Colo.	CRPL, Karval, Colo.	100	8.527	0.2766	68.0	s 40	19	67584	133528	542.4	633.9	765.3	159.8	8/52–2/53	1300–1800	15	0.130	− 4.8	43.1	1.43	7.9	−19.2
18	302	CRPL, Colo. Springs, Colo.	CRPL, Marble, Colo.	230	9.152	.4328	141.0	2321	32	6061	4641	5087	3590	1419	177.1	2/54	1300–1800	39	0.148	− 2.9	36.7	−1.03	21.9	1.7
19	262	CRPL, Colo. Springs, Colo.	CRPL, Marble, Colo.	100	9.282	.4247	141.0	2271	32	6195	4641	4896	8677	1446	172.1	2/54	1300–1800	16	0.094	− 2.2	36.7	−1.04	11.6	3.1
20	223	WXYZ-TV, Detroit, Mich.	UBC, Hudson, Ohio	179.75	10.288	1.0340	111.8	•• 485	33	4268	2333	3995	14535	1518	171.8	5/50–6/53	1300–1800	5388	0.765	− 5.7	41.1	0.78	24.1	0.6
21	28	WJR, Detroit, Mich.	UBC, Hudson, Ohio	96.3	10.176	1.0171	112.8	•• 480	31	4626	2483	3951	11448	1545	168.0	6/50–6/53	1300–1800	5417	0.794	− 0.5	42.0	1.19	10.2	− 1.4
22	35	WENR-FM, Chicago, Ill.	FCC, Allegan, Mich.	94.7	11.194	0.4770	100.5	• 618	30	5233	16038	8098	2665	1299	169.9	6/51–7/52	1300–1800	995	1.249	2.1	42.6	1.62	11.0	2.8
23	394	CRPL, Camp Carson, Colo.	CRPL, Haswell, Colo.	100	11.432	0.9281	93.8	s 40	19	79929	86842	2044	4328	1414	180.6	6/52–2/53	1300–1800	32	0.187	−12.5	43.1	1.87	21.6	− 4.0
24	52	WIP-FM, Philadelphia, Pa.	FCC, Laurel, Md.	93.3	12.042	0.9123	104.1	555	30	2387	126.7	419	10113	1651	172.8	3/51–10/52	1300–1500	2829	2.088	8.9	42.5	1.58	5.5	4.7
25	3	KDKA-FM, Pittsburg, Pa.	UBC, Hudson, Ohio	92.9	12.151	1.4883	98.7	736	30	3742	1704	3571	6827	1496	172.0	2/52–6/53	1300–1800	2220	1.923	5.7	41.0	0.84	10.4	9.3
26	22	KYEM/KTSA, San Antonio, Texas	University of Texas Austin, Texas	101.5	12.878	0.6152	78.1	472	32	4575	4765	2902	3648	1252	166.8	9/42–4/50	1300–1800	780	0.874	7.4	42.6	1.63	13.8	1.2
27	23	KTSA, San Antonio, Texas	U. Texas, Austin, Texas	101.5	13.967	0.7014	74.2	322	32	4528	4765	2699	3528	1326	169.0	4/50–10/50	1500–1800	527	0.554	9.2	49.2	4.80	14.7	3.6
28	342	CRPL, Colo. Springs, Colo.	CRPL, Marble, Colo.	92	11.285	0.7213	141.1	1400	32	2323	4641	6260	7595	2591	180.1	2/54–8/54	1300–1800	102	0.335	− 2.8	40.8	0.78	22.7	6.4
29	5	KFOR-FM, Lincoln, NEB.	FCC, Grand Island, Neb.	102.9	11.592	0.8304	93.2	411	45	2151	8732	4659	3963	1780	174.4	2/51–7/52	1300–1800	1628	1.764	3.5	42.2	1.42	21.4	6.2
30	451	Collins Radio Company Cedar Rapids, Iowa	Collins, Waukon, Ia.	410	15.023	1.0970	98.2	s 40	10	5228	53233	5101	4899	1943	193.7	10/49–11/49	1300–1800	30	0.179	− 6.9	43.4	1.92	>50	2.0
31	462	Collins, Cedar Rapids, Ia.	Collins, Quincy, Ill.	418	15.698	1.5563	134.0	s 41	665	7791	2788	4623	8174	1625	180.8	8/52	1300–1800	53	0.172	− 4.4	53.2	6.82	>50	0.6
32	57	WMBI, Chicago, Ill.	University of Illinois Urbana, Ill.	95.5	16.133	0.6615	126.0	440	90	8125	11269	5510	3378	2572	175.2	7/50–6/52	1300–1800	3422	2.611	0.7	47.0	1.80	24.9	9.6
33	60	WTIC, Hartford, Conn.	FCC, Millis, Mass.	96.5	16.292	0.7171	80.7	• 875	30	3426	1704	1187	5762	1688	167.0	7/51–7/52	1300–1800	1930	1.565	19.4	43.0	1.80	20.2	− 1.7
34	206	WBKB-TV, Chicago, Ill.	U. Illinois, Urbana, Ill.	71.75	16.294	0.7090	126.6	•• 595	90	4629	9504	5667	3870	2644	173.2	5/51–6/53	1300–1800	2836	2.234	0.0	39.9	0.34	21.3	5.3
35	210	WENR-TV, Chicago, Ill.	U. Illinois, Urbana, Ill.	179.75	16.374	0.7085	126.3	•• 660	90	4096	9504	5683	3821	2650	177.9	7/51–6/53	1300–1800	2973	2.529	1.9	47.7	4.14	36.9	7.6
36	34	WEEU-FM, Reading, Pa.	FCC, Laurel, Md.	92.9	16.405	0.5444	95.4	534	30	6989	2239	2722	3792	1886	167.4	9/51–11/52	1300–1800	1435	1.627	11.6	42.1	1.36	16.9	− 1.8
37	215	WGN-TV, Chicago, Ill.	U. Illinois, Urbana, Ill.	191.75	16.529	0.7633	127.0	•• 585	123	5095	6954	4743	4392	2719	176.9	9/51–6/53	1300–1800	3081	2.495	3.3	44.7	2.68	38.1	5.6
38	219	WNBQ-TV, Chicago, Ill.	U. Illinois, Urbana, Ill.	81.75	16.659	0.7310	126.3	•• 595	110	4544	7776	5310	3951	2710	164.8	10/50–5/51	1300–1800	908	1.012	2.0	40.0	0.39	23.0	− 3.4
39	214	WGN-TV, Chicago, Ill.	U. Illinois, Urbana, Ill.	191.75	16.782	0.7492	127.0	•• 585	98	5095	8728	4815	4193	2755	177.1	7/51–6/53	1300–1800	3417	2.604	2.8	45.4	2.82	39.1	4.9
40	213	WGN-TV, Chicago, Ill.	U. Illinois, Urbana, Ill.	191.75	17.056	0.7353	127.0	•• 585	72	5095	11880	4887	3999	2793	180.0	7/51–6/53	1300–1800	3320	2.607	1.9	45.0	2.32	40.4	6.4
41	216	WGN-TV, Chicago, Ill.	U. Illinois, Urbana, Ill.	191.75	17.056	0.7353	127.0	•• 585	72	5095	11880	4887	3999	2793	179.6	11/51–11/52	1300–1800	1497	1.147	1.9	46.8	1.51	40.4	6.7

Fig. 41

Item No	NBS Path No	Transmitter	Receiver	Freq (Mc)	θ (mr)	s (α_o/β_o)	d (miles)	h_{te} (feet)	h_{re} (feet)	$k_{te}a'$ (miles)	$k_{re}a'$ (miles)	k_1a' (miles)	k_2a' (miles)	h_o (feet)	L_{bmo}	Period ed by the data (Local)	Cover - the data (hours)	Total no. of hours	W	G_o (db)	-ΔN	D(ΔN) (db)	Weiss-kopf-Villars K (db)	Δ (db)
42	222	WOW-TV, Omaha, Neb.	FCC, Grand Island, Neb.	87.75	17.415	0.6432	130.7	570	30	13757	26950	2507	4532	2863	172.0	7/51-1/53	1300-1600	1434	1.364	0.0	46.5	1.56	26.0	5.2
43	202	KMTV, Omaha, Neb.	FCC, Grand Island, Neb.	65.75	17.607	0.6672	131.4	629	30	8843	21968	3542	4424	2732	177.6	7/51-2/53	1300-1600	1425	1.323	- 0.9	41.8	1.27	23.0	2.0
44	459	Collins, Cedar Rapids, Ia.	Collins, Quincy, Ill.	418	17.812	1.2697	134.0	s 41	365	7791	5079	5361	5456	3111	179.8	3/52	1300-1800	50	0.167	- 1.6	53.2	6.82	>50	- 0.9
45	158	WHKC-FM, Columbus, Ohio	UBC, Hudson, Ohio	98.7	18.330	0.8349	118.8	•• 560	30	1848	1704	4677	5708	2348	176.2	7/51-6/52	1300-1600	52	0.289	5.9	41.6	1.17	26.4	- 0.1
46	145	WHKC-FM, Columbus, Ohio	UBC, Hudson, Ohio	98.7	18.700	0.8288	123.8	•• 560	30	3386	44155	4840	3288	3029	176.2	7/51-6/52	1300-1600	52	0.293	- 0.1	41.9	1.31	33.8	2..
47	159	WHKC-FM, Columbus, Ohio	UBC, Hudson, Ohio	98.7	19.247	0.7458	118.8	•• 560	30	1806	3383	5189	4461	2934	176..	7/51-6/52	1300-1600	60	0.293	6.0	41.6	1.17	30.2	- 2.2
48	458	Collins, Cedar Rapids, Ia.	Collins, Quincy, Ill.	418	17.271	1.1393	134.0	s 41	165	7791	11230	5704	1351	3394	187.2	1/52-2/53	1300-1800	34	0.137	5.2	38.1	-0.54	>50	- 2.3
49	19	KXOK-FM, St. Louis, Mo.	U. Illinois, Urbana, Ill.	93.2	19.344	0.7988	11.6.5	657	90	6049	542.4	3752	7615	3694	75.7	1/52-6/52	1300-1800	330	2.609	6.5	42.0	1.36	27.0	2.9
50	44	WHKC-FM, Columbus, Ohio	UBC, Hudson, Ohio	98.7	19.422	0.7724	124.9	718	30	1700	38072	6193	2921	3140	178.9	5/50-6/53	1300-1800	5422	3.798	0.3	41.7	1.22	35.5	- 2.2
51	144	WHKC-FM, Columbus, Ohio	UBC, Hudson, Ohio	98.7	19.617	0.7606	123.8	•• 560	30	3386	35200	5101	3020	3146	173.0	7/51-6/52	1300-1600	47	0.275	1.0	41.9	1.31	35.5	- 1.1
52	28	WCAC, Anderson, S.C.	FCC, Powder Springs, Ga.	101.1	19.814	0.6596	127.5	412	30	3569	9702	6245	3558	3194	176.9	4/51-9/52	1300-1800	1833	1.763	2.0	45.5	3.02	35.9	0.7
53	150	WHKC-FM, Columbus, Ohio	UBC, Hudson, Ohio	98.7	19.826	0.7974	124.2	•• 560	30	1981	25432	4636	4125	3243	150.2	7/51-6/52	1300-1600	50	0.283	0.9	42.1	1.41	36.2	2.3
54	29	WCOL-FM, Columbus, Ohio	UBC, Hudson, Ohio	92.3	20.122	0.9093	121.2	402	30	3783	37707	4054	3565	3212	172.6	4/50-6/53	1300-1800	5039	3.766	-1.1	41.6	1.17	35.5	- 5.2
55	457	Collins, Cedar Rapids, Ia.	Collins, Quincy, Ill.	418	20.292	1.0626	134.0	s 41	30	7791	52822	5882	4006	3586	181.8	1300-1800 8/52		55	0.175	- 4.6	53.2	6.82	>50	- 5.3
56	20	KXYZ-FM, Houston, Texas	U. Texas, Austin, Tex.	96.5	20.318	0.7476	147.8	442	32	5740	557.7	4966	6361	3881	76.1	6/51-12/52	1300-1800	2653	2.071	5.9	50.5	5.49	31.0	2.7
57	416	CRPL, Pikes Peak, Colo.	CRPL, Garden City, Kans.	100	20.444	0.2806	237.1	7800	19	4399	135.1	4467	4009	4416	178.7	2/52	1300-1700	'	0.051	9.2	49.5	5.01	28.6	0.1
58	63	WYKQ-FM, Columbia, Ohio	UBC, Hudson, Ohio	94.7	20.941	0.9504	118.9	335	30	6401	35908	2884	3897	3234	179.6	1/50-1/53	1300-1800	133	0.275	3.5	37.4	-0.87	35.6	- 1.6
59	13	KPRC-FM, Houston, Texas	U. Texas, Austin, Texas	102.9	20.995	0.7876	147.8	348	32	5490	557.7	5028	6315	4038	179.7	5/49-6/53	1300-1800	3114	2.459	5.1	50.2	5.35	34.5	2.8
60	147	WHKC-FM, Columbus, Ohio	UBC, Hudson, Ohio	98.7	21.233	0.7343	123.5	•• 560	30	3696	3383	3943	4486	3380	176.8	7/51-6/52	1300-1800	52	0.288	3.6	41.6	1.17	33.5	0.5
61	148	WHKC-FM, Columbus, Ohio	UBC, Hudson, Ohio	98.7	21.834	0.7225	123.5	•• 560	30	3591	5632	4053	3999	3467	177.6	7/51-6/52	1300-1800	67	0.323	7.7	41.6	1.07	36.4	0.2
62	149	WHKC-FM, Columbus, Ohio	UBC, Hudson, Ohio	98.7	21.908	0.6913	124.4	•• 560	30	2079	4950	5307	3611	3478	173.0	7/51-6/52	1300-1800	72	0.334	6.8	41.6	1.16	36.8	- 0.4
63	204	WAFM, Birmingham, Ala.	FCC, Powder Springs, Ga.	215.75	22.183	0.5720	122.0	•• 808	30	1204	45333	7497	2137	3327	174.7	2/51-6/53	1300-1800	3063	2.763	11.7	43.1	1.89	>50	1.7
64	453	Collins, Cedar Rapids, Ia.	Collins, Quincy, Ill.	418	22.469	0.8104	134.0	s 41	10	7791	129.4	5786	5121	3931	190.1	5/51-12/53	1300-1800	431	0.613	9.7	45.5	3.06	>50	- 2.1
65	454	Collins, Cedar Rapids, Ia.	Collins, Quincy, Ill.	418	22.469	0.8104	134.0	s 41	10	7791	129.4	5786	5121	3931	190.0	5/51-12/53	1300-1800	438	0.657	9.7	45.5	3.06	>50	- 7.2
66	452	Collins, Cedar Rapids, Ia.	Collins, Quincy, Ill.	412	22.469	0.8104	134.0	s 41	10	7791	129.4	5786	5121	3931	194.3	4/50-5/53	1300-1800	142	0.267	9.4	40.3	0.58	>50	- 5.3
67	151	WHKC-FM, Columbus, Ohio	UBC, Hudson, Ohio	98.7	22.781	0.6765	123.5	•• 569	30	1067	2960	5195	3486	3607	180.4	7/51-6/52	1300-1600	72	0.339	9.4	41.6	1.16	36.9	1.1
68	200	KFMB-TV, San Diego, Calif.	FCC, Santa Ana, Calif.	185.75	23.435	0.1638	72.3	989	30	10129	8500	89.78	9.938	1082	151.1	11/51-10/53	1300-1800	3042	2.185	86.1	53.3	6.82	-11.5	- 2.0
69	59	WMRC-FM, Greenville, S.C.	FCC, Powder Springs, Ga.	94.9	23.453	0.4036	151.5	1167	30	8418	29276	5266	1978	3344	177.5	3/51-12/51	1300-1800	67	1.120	9.4	45.6	3.09	37.9	- 0.7
70	153	WHKC-FM, Columbus, Ohio	UBC, Hudson, Ohio	98.7	23.551	0.6636	124.9	560	30	1886	5632	5419	3124	3724	182.4	7/51-6/52	1300-1600	66	0.317	9.3	41.6	1.16	39.5	2.7
71	156	WHKC-FM, Columbus, Ohio	UBC, Hudson, Ohio	98.7	23.684	0.6352	124.0	•• 560	30	1981	1400	5477	3233	3650	180.7	7/51-6/52	1300-1600	71	0.330	13.0	41.6	1.16	36.0	4.2
72	152	WHKC-FM, Columbus, Ohio	UBC, Hudson, Ohio	98.7	24.664	0.5516	124.0	•• 560	30	1.47	1.7[illegible]	5252	2767	3604	180.3	7/51-6/52	1300-1600	69	0.329	16.1	41.6	1.15	36.9	.7
73	155	WHKC-FM, Columbus, Ohio	UBC, Hudson, Ohio	98.7	25.772	0.5192	124.0	•• 560	30	1931	2200	5542	2501	3502	178.1	7/51-6/52	1300-1800	65	0.317	16.4	41.6	1.15	38..	- 2.3
74	316	CRPL, Colo. Springs, Colo.	CRPL, Garden City, Kans.	1040	28.017	.6440	226.5	2321	18	5669	1320	6663	4470	7857	185.2	2/52-1/53	1300-1800	593	0.848	3.9	44.7	1.24	>50	-11.2
75	276	CRPL, Colo. Springs, Colo.	CRPL, Garden City, Kans.	192.8	28.036	.6467	166.7	•• 340	30	1701	17744	8281	2913	5805	192.1	9/52-5/53	1300-1800	1004	1.102	32.5	39.8	0.24	>50	4.8
76	37	WEVD-FM, New York, N.Y.	FCC, Millis, Mass.	107.5	28.054	.4329	123.0	•• 560	30	2302	2200	6774	1725	3842	176.8	7/51-6/52	1300-1600	44	0.264	22.5	42.4	1.47	41.6	- 3.3
77	142	WHKC-FM, Columbus, Ohio	UBC, Hudson, Ohio	98.7	28.088	0.4699	226.5	2271	19	5794	1250	6549	4525	7305	198.3	2/52-1/53	1300-1800	836	1.083	4.0	40.7	0.66	>50	6.3
78	256	CRPL, Colo. Springs, Colo.	CRPL, Garden City, Kans.	100	28.373	0.3972	118.4	•• 560	30	2282	88.00	6493	1740	3502	178.3	7/51-6/52	1300-1800	62	0.329	32.1	41.4	1.00	32.6	- 6.4
79	160	WHKC-FM, Columbus, Ohio	UBC, Hudson, Ohio	98.7	28.840	.4588	226.5	2226	43	5911	552.6	6579	4273	7437	209.0	6/52-10/52	1300-1800	315	0.415	- 1.0	45.9	3.15	>50	0.2
80	6	KSFD-FM, San Diego, Calif.	FCC, Santa Ana, Calif.	94.1	29.037	0.1427	81.7	465	30	25258	8977	4215	17.57	1119	155.5	3/51-6/53	1400-1800	2830	2.752	77.9	52.9	6.45	- 9.7	- 3.9
81	40	WFRO-FM, Fremont, Ohio	FCC, Allegan, Mich.	99.3	29.096	0.7234	169.5	215	30	4912	44550	7029	2710	6343	172.7	1/51	1300-1800	149	0.293	1.4	48.4	4.36	>50	- 4.9
82	41	WHDL-FM, Olean, N.Y.	Pennsylvania State College State College, Pa.	95.7	29.418	0.3099	90.8	640	63	1069	1222	7797	711.7	2547	176.2	5/51-1/53	1300-[illegible]	2229	2.251	12.1	[illegible]	0.33	26.6	2.1

Fig. 42

Item N°	NBS Path N°	Transmitter	Receiver	Freq (Mc)	θ (mr)	s (α_o/β_o)	d (miles)	h_{te} (feet)	h_{re} (feet)	$k_{te}a^2$ (miles)	$k_{re}a^2$ (miles)	$k_t a^2$ (miles)	$k_r a^2$ (miles)	h_o (feet)	L_{bmo}	Period covered by the data (dates)	Coverage (hours)	Total no. of hours	W	G_o (db)	$-\Delta N$	$D(\Delta N)$ (db)	Weisskopf-Villars K (db)	Weisskopf-Villars Δ (db)
83	157	WHKC-FM, Columbus, Ohio	UBC, Hudson, Ohio	98.7	29.616	0.4315	123.9	560 ••	30	2020	254.3	6331	1855	4077	179.5	7/51-6/52	1300-1800	62	0.329	29.4	41.4	1.04	38.9	- 2.4
84	143	WHKC-FM, Columbus, Ohio	UBC, Hudson, Ohio	98.7	29.872	0.3946	124.1	560 ••	30	2302	106.9	6643	1718	3971	175.0	7/51-6/52	1300-1800	49	0.275	33.0	41.9	1.28	36.4	- 6.5
85	154	WHKC-FM, Columbus, Ohio	UBC, Hudson, Ohio	98.7	30.302	0.4620	124.0	560 ••	30	2001	88.00	5682	2010	4256	180.7	7/51-6/52	1300-1800	65	0.321	32.5	41.4	1.04	38.3	- 4.1
86	54	WJAS-FM, Pittsburg, Pa.	Penn St., St. College, Pa.	99.7	30.444	0.4015	117.1	596	63	1092	513.3	7262	1424	3347	176.3	6/51-4/53	1300-1800	32.7	2.240	32.8	40.0	0.38	39.0	- 2.2
87	336	CRPL, Colo. Springs, Colo.	CRPL, Garden City, Kans.	92	31.496	0.6487	226.6	1482	37	2654	642.2	6738	5121	8993	201.6	2/52-4/53	1300-1800	296	0.493	3.4	37.3	-0.94	>50	9.7
88	356	CRPL, Colo. Springs, Colo.	CRPL, Garden City, Kans.	210.4	31.706	0.6558	226.6	1502	36	2619	660.0	6609	5151	9074	211.1	12/52-4/53	1300-1800	182	0.321	1.8	37.4	-0.89	>50	12.2
89	205	WATV, Newark, N. J.	FCC, Millis, Mass.	215.7	31.949	0.6491	179.4	595 ••	30	1920	1862	6425	3616	7223	194.0	11/52-4/53	1300-1800	880	0.571	10.4	37.2	-0.94	>50	- 2.8
90	8	KIXL-FM, Dallas, Texas	U. Texas, Austin, Texas	104.5	31.158	0.6328	175.9	553	32	2984	2496	5931	3404	7133	184.4	6/50-6/53	1300-1800	4922	3.642	10.1	45.4	2.91	>50	- 2.5
91	38	WFAA-FM, Dallas, Texas	U. Texas, Austin, Texas	97.9	32.536	0.6252	174.2	488	32	4031	2406	5617	3358	7084	186.6	11/49-8/50	1300-1800	1112	0.999	10.7	45.0	2.73	>50	0.3
92	16	KREM-FM, Fresno, Calif.	FCC, Livermore, Calif.	93.7	34.095	0.0597	135.3	1925 ••	30	20379	4312	1728	20.39	1296	158.0	6/52-9/52	1300-1800	[illegible]	0.371	95.2	46.0	3.14	- 9.3	- 7.4
93	58	WMIT-FM, Clingmans Peak N. C.	FCC, Powder Springs, Ga.	106.9	34.145	0.6050	189.5	3618	30	1318	11436	4999	3155	8024	189.2	5/52-7/53	1300-1800	17.3	1.507	11.1	45.3	2.85	>50	0.2
94	146	WHKC-FM, Columbus, Ohio	UBC, Hudson, Ohio	98.7	35.238	0.3370	124.1	560 ••	30	2179	88.00	6792	1224	4353	181.0	7/51-6/52	1300-1800	24	0.301	45.4	41.6	1.12	43.4	- 2.6
95	36	WEST-FM, Easton, Pa.	Penn St., St. College, Pa.	107.9	36.666	0.6309	139.3	247 •	63	10740	10198	3520	1789	6397	180.8	8/51-4/53	1300-1800	2040	2.158	27.6	39.5	0.14	>50	- 5.3
96	396	CRPL, Camp Carson, Colo.	CRPL, Garden City, Kans.	100	37.906	0.8007	223.6	40	19	96825	1250	4256	5463	11031	203.1	8/52-2/53	1300-1800	22	0.250	- 1.3	43.1	1.76	>50	-0.4
97	15	KRBC-FM, Abilene, Texas	U. Texas, Austin, Texas	96.9	39.110	0.5630	177.1	231	32	1358	139.4	6910	2573	8428	185.7	4/50-6/50	1300-1800	1200	0.462	27.8	45.8	3.04	> 50	- 3.7
98	53	WJAS, Pittsburg, Pa.	FCC, Laurel, Md.	99.7	40.136	1.0144	191.3	686	30	8683	7287	1826	6167	10134	187.9	11/52-5/53	1300-1800	552	0.790	23.4	36.7	1.15	> 50	- 6.3
99	9	KLTI-FM, Longview, Texas	U. Texas, Austin, Texas	105.9	40.398	0.8828	227.2	305	32	3673	3070	4945	4981	12000	191.2	5/51-12/52	1300-1800	2138	1.582	- 3.1	47.0	1.59	> 50	- 2.8
100	2	KCRA-FM, Sacramento, Cal	FCC, Livermore, Calif.	96.1	40.854	0.0475	63.6	392 •	30	23842	594.9	158.9	8.485	593.4	147.6	7/53-9/53	1300-1800	419	0.460	127.8	46.8	3.44	-18.5	- 7.2
101	50	WHO-FM, DesMoines, Ia.	FCC, Grand Island, Neb.	100.3	42.681	0.7848	267.4	647 •	30	2758	11142	6420	4363	14946	197.4	5/53-6/53	1300-1800	274	0.390	- 3.4	44.5	2.43	> 50	- 0.3
102	201	KGO-TV, San Francisco	FCC, Livermore, Calif.	179.75	43.252	0.2650	38.2	1310 •	30	1270	425.9	221.4	286.9	1445	118.4	7/51-9/52	1300-1800	1989	1.585	132.4	42.6	1.51	22.7	-27.6
103	7	KING-FM, Seattle, Wash.	FCC, Portland, Ore.	98.1	45.650	0.5663	144.9	720	30	14461	14650	2354	339.7	8097	176.3	3/51-8/53	1300-1800	291.	2.818	69.2	41.9	1.19	49.0	-11.5
104	11	KMJ-FM, Fresno, Calif.	FCC, Livermore, Calif.	97.9	45.922	0.2128	117.8	1042	30	21305	6062	170.0	883.7	4133	180.4	2/53	1300-1800	140	0.285	99.0	38.6	-0.32	24.1	- 6.4
105	18	KWKH-FM, Shreveport, La	U. Texas, Austin, Texas	94.5	47.361	0.8346	277.4	399	32	5337	3171	5246	5010	17201	191.7	8/51-6/53	1300-1800	3253	2.512	-25.8	45.4	2.83	> 50	- 7.0
106	12	KOIN-FM, Portland, Ore.	U. Wash., Seattle, Wash.	101.1	49.498	0.4548	149.1	1812	94	3512	112.3	2370	1654	8373	184.4	6/51-3/53	1300-1800	2543	2.114	60.7	41.9	1.19	> 50	- 3.9
107	1	KARM-FM, Fresno, Calif	FCC, Livermore, Calif.	101.9	50.888	0.1292	121.3	374	30	15774	5632	22371	125.3	3315	181.6	7/51-10/52	1300-1800	1553	1.471	115.0	42.7	1.56	25.4	- 7.0
108	418	CRPL, Pikes Peak, Colo.	CRPL, Anthony, Kans.	100	50.941	0.5176	404.1	7800	39	6168	1692	5124	5246	24427	196.0	8/52	1100-1700	7	0.062	4.7	49.4	4.68	> 50	- 5.1
109	141	WHKC-FM, Columbus, Ohio	UBC, Hudson, Ohio	98.7	52.029	0.1099	120.5	560 ••	30	6281	3520	5925	419.2	4439	178.8	9/51-6/52	1300-1800	1.	0.182	84.6	40.4	0.55	> 50	- 9.0
110	66	KXOA-FM, Sacramento, Cal	FCC, Livermore, Calif.	107.9	57.325	0.0423	62.0	187 •	30	42706	2851	560.8	14.42	737.7	152.1	9/53	1300-1800	142	0.287	173.2	44.2	2.26	- 0.5	-21.7
111	278	CRPL, Colo. Springs, Colo.	CRPL, Anthony, Kans.	192.8	58.410	0.6721	393.5	2321	39	6229	1692	5671	5112	29173	201.4	7/52-8/52	1300-1800	1.	0.163	1.2	49.1	4.53	> 50	- 8.9
112	318	CRPL, Colo. Springs, Colo.	CRPL, Anthony, Kans.	1046	58.501	0.6797	393.5	2226	8	6494	3250	5586	5174	29282	227.2	7/52-8/52	1300-1800	2.	0.137	- 4.6	49.1	4.53	> 50	- 5.1
113	258	CRPL, Colo. Springs, Colo.	CRPL, Anthony, Kans.	100	58.538	0.6746	393.5	2271	39	6366	1692	5634	5124	29253	211.8	2/52-3/53	1300-1800	112	0.351	2.5	42.8	1.62	> 50	4.9
114	61	WTOP, Arlington, Va.	Penn St., St. College, Pa.	96.3	61.865	0.2025	136.8	515	63	15620	704.4	3874	405.1	6288	180.7	8/51-4/52	1300-1800	1127	1.010	105.6	39.9	0.32	> 50	-10.0
115	62	WTOP, Washington, D. C.	Penn St., St. College, Pa.	96.3	63.470	0.2001	134.1	387	63	3995	670.5	7958	349.8	6243	183.7	4/52-4/53	1300-1800	179	1.330	112.8	44.2	0.93	> 50	- 6.8
116	338	CRPL, Colo. Springs, Colo.	CRPL, Anthony, Kans.	92	63.474	0.7829	393.6	1383	39	2844	1692	5985	5081	32469	216.8	2/53	1300-1800	30	0.129	4.7	36.7	-1.21	> 50	6.1
117	358	CRPL, Colo. Springs, Colo.	CRPL, Anthony, Kans.	210.4	63.548	0.7855	393.6	1403 s	39	2804	1692	5956	5093	32540	224.2	2/53-3/53	1300-1800	30	0.129	0.3	36.6	-1.25	> 50	5.4
118	398	CRPL, Camp Carson, Colo.	CRPL, Anthony, Kans.	100	67.997	0.8941	390.7	40 s	39	79929	1692	4932	5400	34959	212.9	8/52-2/53	1300-1800	24	0.161	3.2	43.1	1.77	> 50	- 0.7
119	17	KVCI, Chico, Calif.	FCC, Livermore, Calif.	101.1	32.968	0.1766	138.5	482	30	6942	609.9	5507	264.3	7740	182.0	7/51-8/51	1300-1800	530	0.500	162.2	48.1	6.20	> 50	-10.3
120	420	CRPL, Pikes Peak, Colo.	CRPL, Fayetteville, Ark.	100	90.754	0.6715	628.1	7800	38	6168	10004	5311	5292	72336	224.9	3/52	1100-1700	9	0.070	-11.1	42.4	5.07	>50	7.3
121	260	CRPL, Colo. Springs, Colo.	CRPL, Fayetteville, Ark.	100	98.276	0.7930	617.1	2271	38	6366	10004	5596	5219	78984	228.4	8/52-2/53	1100-1800	35	0.181	-13.4	43.1	1.93	> 50	[illegible]
122	400	CRPL, Camp Carson, Colo.	CRPL, Fayetteville, Ark.	100	107.734	0.9494	614.0	40 s	38	96815	10004	5041	5426	87300	232.9	8/52-2/53	1500-1700	8	0.106	-19.3	43.1	1.95	> 50	7.3

Fig. 43

R Distance between any two points in space in (22) and distance from the receiving antenna to an element of the scattering volume in (44).

R_0 Distance from the transmitting antenna to an element of the scattering volume in (44).

α_0 The angle, in the great circle plane, between the radio horizon ray of the transmitting antenna and the line A_1A_2 between the transmitting and receiving antennas.

β_0 The angle, in the great circle plane, between the radio horizon ray of the receiving antenna and the line A_1A_2 between the transmitting and receiving antennas.

α, β Angles from the transmitting and receiving antennas determining the location of an element of the scattering volume relative to the line joining these antennas. Their sum is the scattering angle $(\alpha+\beta)$.

α_1, β_1 See Fig. 6.

θ_t, θ_r See Fig. 4.

ψ_t, ψ_r Angles of elevation, defined in Fig. 36.

γ_t, γ_r Azimuth angles showing deviation from the great circle plane.

ψ_w, γ_w Symbols used in Section XI to denote the angles of elevation and azimuth at which the radiation is 6 decibels down from its maximum at $\psi=0$, $\gamma=0$. Beamwidths are $2\psi_w$ and $2\gamma_w$.

d_{Lt}, d_{Lr} Distances from the transmitting and receiving antennas to their respective horizons; see Figs. 4 and 5.

d_1, d_2 Distances from transmitting and receiving antennas to the crossover of radio horizon rays in the great circle plane.

s Asymmetry factor $=\alpha_0/\beta_0=d_2/d_1$.

h_{Lt}, h_{Lr} Height above mean sea level of the terrain determining the radio horizons for a standard atmosphere.

h_{ts}, h_{rs} Height of transmitting and receiving antennas above mean sea level.

h_{te}, h_{re} Effective transmitting and receiving antenna heights. The receiving antennas were low enough so that their structural heights above ground were taken to be their effective heights in every case. Transmitting antenna effective heights are heights above a curve fit to part of the terrain between the antenna and its four-thirds earth radio horizon unless one of the following symbols is used:

s · · · structural height.

* · · · height above 2 to 10 mile average terrain in direction of the other antenna.

** · · · height above 2 to 10 mile average surrounding terrain.

h_t, h_r Transmitting and receiving antenna heights over a smooth earth.

h In Section III, the height of terrain above mean sea level; in Appendix II and elsewhere the height of a scattering element above a plane through the transmitting and receiving antennas and perpendicular to the great circle plane.

h_0 Height above the chord joining the transmitting and receiving antennas of the crossover of radio horizon rays in the great circle plane; also the approximate height of the "center" of scattering above the earth's surface.

a' The actual radius of the earth, 3,960 miles.

ka' An effective radius of the earth which allows only for the systematic effects of a linear gradient of refractive index; see (10).

k_pa' An actual radius of curvature for that portion of the terrain along the great circle path and between the radio horizons; assumed to be equal to (4/5)á for our model smooth earth.

$k_{ps}a'$ An actual radius of curvature for those portions of the terrain along the great circle path between the antennas and their radio horizons; assumed to be equal to á for our model smooth earth.

$k'a'$ An effective radius of curvature which allows not only for the systematic effects of a linear gradient of refractive index but also for the actual radius of curvature of the portion of terrain under consideration; see (25).

k_ta', k_ra' Effective radii of curvature for portions of the terrain along the great circle path and between the radio horizons; assumed to be equal to á for our model smooth earth.

$k_{te}a'$, $k_{re}a'$ Effective radii of curvature for those portions of the terrain along the great circle path between the antennas and the radio horizon; assumed to be equal to (4/3) á for the model smooth earth.

$C(R)$ Cross correlation between variations of refractive index at points separated by a distance R.

$C(0)=[(\overline{\Delta n/n})^2]$ Variance of the refractive index of the atmosphere about its mean value; a parameter in the Booker-Gordon scattering theory.

l_0 Scale of turbulence in the Booker-Gordon theory; defined by (22).

V The Weisskopf-Villars scattering parameter $\{[\overline{(dn/dh)^2}]-[\overline{dn/dh}]^2\}$, which is the variance of the vertical gradient of the atmosphere about its mean value.

σ_{BG} Radio wave scattering cross section for the Booker-Gordon theory.

σ_{WV} Radio wave scattering cross section for Weisskopf-Villars theory.

B The magnitude of $[C(0)/l_0]$ per meter normalized to a height of one kilometer above the surface.

B_1 The magnitude of $\{[\overline{(dn/dh)^2}]-[\overline{(dn/dh)}]^2\}$ per square meter normalized to a height of one kilometer above the surface.

$N=(n-1)\cdot 10^6$ Scaled up refractivity of the atmosphere with refractive index n.

ΔN Difference in the values of N at surface and at a height of one kilometer above surface; also a measure of a linear atmospheric refractive index gradient in (10).

b' Decibel change in L_{bm} per unit change in ΔN and caused only by the effects of refraction in a linear gradient atmosphere.

b Decibel change in L_{bm} per unit change in ΔN including both the effects of refraction in a linear gradient atmosphere and the effects of changes in the magnitude of the scattering cross section.

$D(\Delta N)$ Empirical correction in decibels to be subtracted from the transmission loss for a standard atmosphere to obtain monthly median values of L_{bm} for a given geographical area or season of the year. Isopleths of ΔN are in.[19]

$f[(l_0/\lambda)\cdot(\alpha+\beta)]$ A correction factor to scattering cross section required at low frequencies, small angular distances.

$F[(l_0/\lambda)\cdot\theta]$ A correction factor to transmission loss of scattered mode of propagation required at low frequencies or small angular distances.

H_{0t}, H_{0r} Frequency gain factors to allow for the increase of transmission loss caused by correlation between the direct and ground reflected fields for low antenna heights. This frequency gain correction is shown in Fig. 38 where $[C(0)/l_0]$ varies with height above earth's surface.

$H_0[(h_{te}/\lambda)\cdot\theta]$ $H_0[(h_{re}/\lambda)\cdot\theta]$ Frequency gain factors based upon the assumption that $[C(0)/l_0]$ does not vary with height above the earth's surface.

W The weight of an observed median value of transmission loss. The reciprocal of W is an estimate of the square of the standard error of the observed median transmission loss expressed in decibels. These standard errors were estimated from a study of the time variance of the hourly medians and thus do not include the effects of systematic errors of measurement.

ADDENDUM

New frequency gain functions and asymmetry functions have been computed by the method of Appendix II for the Weisskopf-Villars model using the more nearly correct height dependence $V=B_2/(h-0.5\ h_0)^2$ which was approximated by $V\cong 4\ h_0B_2/h^3$. Using these revised functions and the same 80 measured values of transmission loss used in determining (29) and (31),we obtained the following least squares solution for B_2.

$$-10\log_{10}B_2=$$

$$(162.5+7.8)+(1.20\pm 1.60)\log_{10}h_0(\text{feet})-(0.44\pm 2.44)\log_{10}f_{,mc}$$

Since the coefficient of $\log_{10}f_{,mc}$ now departs from zero by only a very small fraction of its standard error, our confirmation of the Weisskopf-Villars model is greatly strengthened. It would appear that we are now definitely justified in suppressing the very small frequency dependence indicated by the above formula. When this is done we obtain as our final estimate of the dependence on the height of V for a radio standard atmosphere:

$$-10\log_{10}V=(161.8\pm 6.02)+(21.2\pm 1.59\log_{10}h(km)$$

These new frequency gain functions and asymmetry functions will be published shortly. In the meantime (34) may be used for calculations and will give results within a very few db of these new formulas for the transmission loss expected in the scattering region.

Correspondence

On Node and Mesh Determinants*

S. Seshu[1] has shown that mesh determinants are not invariant under mesh transformation. This note gives some additional properties of mesh and node determinants, as well as of incidence matrices, and presents results of a more general nature.

Denote a matrix P of k rows and n columns with $P_{k,n}$. Then the Binet-Cauchy theorem[2] gives us the expansion of the determinant of a product of matrices:

$$\left| \underset{k,n}{P}\ \underset{n,n}{Y}\ \underset{n,k}{Q} \right| = \sum_{{}_nC_k} \sum_{{}_nC_k} |P||Y||Q|, \quad k \leqq n, \quad (1)$$

One must take double summations for minors of P, Y and Q of the kth order. Combination of k rows of Y should be identical with k columns of minors of P and combination of k columns of Y should be identical with the k rows of minors of Q.

As is well known in topology, all minor determinants of $\alpha^0-1=\rho^1$ order of node branch incidence matrices are ± 1 for minors associated with a set of branches forming a tree and zero when the branches concerned do not constitute a tree. (A "tree" is a set of ρ^1 branches which do not form any closed loops.) α^0 is the number of vertices or nodes in the network. Therefore by (1), the node admittance determinant gives the total number of all possible trees when each branch admittance is given unit value.[3] If $k=\alpha^1-\rho^1$ independent meshes are chosen in a network of $\alpha^1=n$ branches by the "tree" method (each mesh has one branch exclusive to itself), then all its minor determinants of order k are ± 1 for minors associated with a set of branches excluded from a tree (we define this is a "cotree"), and zero when the branches concerned do not constitute a cotree. Therefore, if we apply (1) to the determinant of the mesh impedance matrix

$$BZB' = Z_m \quad (2)$$

it follows that *all mesh determinants formed by the tree method in a given network are equal.* This is actually the dual of a case discussed by Shekel[4] in which all node admittance determinants formed by choosing a common datum vertex are invariant. It should be pointed out that other choices of independent nodal potentials lead to node determinants which are not invariant. Thus referring to Fig. 1, if we adopt the sum $V_{1'}=V_1+V_2$ and the difference $V_{2'}=V_1-V_2$ instead of the usual node potentials V_1 and V_2, as our variables with

$$\begin{bmatrix} I_{1'} \\ I_{2'} \end{bmatrix} = Y_{n'} \begin{bmatrix} V_{1'} \\ V_{2'} \end{bmatrix}$$

and

$$\begin{bmatrix} I_1 \\ I_2 \end{bmatrix} = Y_n \begin{bmatrix} V_1 \\ V_2 \end{bmatrix}$$

where Y_n is the usual nodal admittance matrix, it is readily shown that

$$|Y_{n'}| = 4, \qquad |Y_n| = 1.$$

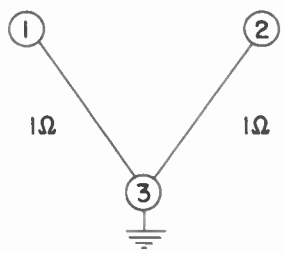

Fig. 1.

Thus it can be seen that the node admittance determined does not remain invariant when general nodal variables are used.

Seshu has shown an example of a linear graph of nullity 3 and rank 3 to demonstrate the change in mesh determinant when the meshes are chosen so as to form a projective plane. A simpler example of nullity 2, rank 0 pointed out by Prof. B. Hoffmann[5] of Queens College is easily demonstrated with Figs. 2 and 3. If we adopt the set of meshes

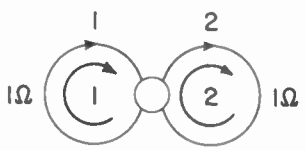

Fig. 2.

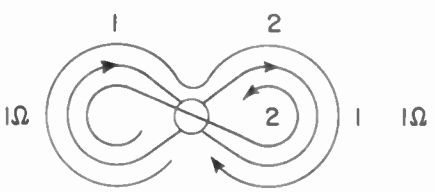

Fig. 3.

of Fig. 3 instead of Fig. 2, then the mesh impedance determinant $|Z_m|$ becomes

$$|Z_m| = \begin{vmatrix} 2 & 0 \\ 0 & 2 \end{vmatrix} = 4.$$

However for the choice of meshes of Fig. 2,

$$|Z_m| = \begin{vmatrix} 1 & 0 \\ 0 & 1 \end{vmatrix} = 1.$$

In general, we can apply the results of algebraic topology by (1) to the node admittance and mesh impedance matrices. Eq. (1) is a bridge between network equations and algebraic topology. We can assume a surface for each mesh by regarding each mesh as a boundary of a surface. Then we can apply 2-dimensional topology.[6] From this we know that if a set of meshes forms a nonorientable manifold such as the projective plane of Fig. 2 of Seshu's paper, then the elementary divisors of 2-dimensional incidence matrices include 2 and in general 2^i, i an integer. Therefore, if as in Seshu, Δ_1 and Δ_2 are any two mesh determinants of a given network, $\Delta_1=2^{2i}\Delta_2$, if the 2-chain of Δ_2 has no torsion ($r=2^i$, $k=2^{2i}$ in Seshu's notation). r may change to a more general value, if we adopt a more general transformation. *k cancels out in the driving point impedance, because k appears simultaneously in the denominator and numerator.*

In a paper which will be presented shortly,[7] I will show that the determinant of a nodal admittance can be regarded as the total number of all possible trees in a network with weight y_i (number of parallel elements, if y_i is an integer) for the branch i. Also the mesh impedance determinant can be interpreted as the total number of cotrees with "co-weight" Z_i (number of series elements, if Z_i is an integer) for the branch i.

S. Okada
Microwave Research Inst.
Polytechnic Inst. of Brooklyn
Brooklyn, N. Y.

* Received by the IRE, June 8, 1955.

[1] S. Seshu, "The mesh counterpart of Shekel's theorem," PROC. IRE, vol. 43, p. 342; March, 1955.

[2] A. C. Aitken, "Determinants and Matrices," The Interscience Publisher, New York, N. Y., p. 86; 1939.

S. Okada and T. Huzi, "Topology and networks, no. 3," *Jour. Inst. Elec. Com. Eng. Japan*, no. 237, pp. 794–796; December, 1942. (In Japanese.)

S. Okada and R. Onodera, "On network topology," *Bull. Yamagata Univ. Nat. Sc.* vol. 2, pp. 89–117; November, 1952 and p. 98 (25) (In English.)

[3] S. Okada and T. Huzi, "Topology and networks, no. 4," *Jour. Inst. Elec. Com. Eng. Japan*, no. 237, pp. 806–809; December, 1942. (In Japanese.)

S. Okada and R. Onodera, "Algebraic electromagnetism, no. 1," *Bull. Yam. Univ. Eng.*, no. 2, pp. 423–425; October, 1951. (In English.)

S. Okada and R. Onodera, "On network topology," *Bull. Yam. Univ. Eng.*, vol. 2, pp. 112–115; November, 1952. (In English.)

H. M. Trent, "Note on the enumeration and listing of all possible trees in a connected linear graph," *Proc. Nat. Acad. Sci.*, vol. 40, pp. 1004–07; October, 1954.

[4] J. Shekel, "Two theorems concerning charge of voltage reference terminal," PROC. IRE, vol. 42, p. 1125, July, 1954.

[5] B. Hoffmann, "Mutual of the primitive systems in Kron's theory," to appear in *Amer. Jour. Phys.*, 1955.

[6] S. Lefschetz, "Algebraic Topology," *Amer. Math. Soc. Col. Pub.*, vol. 27; 1942.

[7] S. Okada, "Algebraic and Topological Foundations of Network Synthesis," Symposium on Modern Network Synthesis by M.R.I. and P.G.C.T., April 13–15, 1955. Proceedings of this will appear in October, 1955.

Cathode-Coupled Phase-Shift Oscillators*

Professor Reich[1] and Mr. Fleming[2] have recently discussed phase-shift oscillators employing cathode-follower isolation of RC phase-shifting sections. Certain advantages result as compared to oscillators with a single tapered filter, such as operation to higher frequencies and the production of multi-phase outputs. A few comments regarding such oscillators bear mentioning. When three cathode followers are employed, the gain of the single amplifying tube must be approximately 8, which means that the upper-frequency limit of oscillations is approximately $\frac{1}{8}$ the gain-bandwidth product of the amplifying tube. (The exact value de-

* Received by the IRE, June 24, 1955.

[1] H. J. Reich, PROC. IRE, vol. 43, p. 229; February, 1955.

[2] L. Fleming, PROC. IRE, vol. 43, p. 754; June 1955.

pends upon the gain loss of the cathode followers and the amount of lagging phase shift contributed by the amplifying tube and can be as much as $\frac{1}{4}$ the gain-bandwidth product of the amplifying tube.)

However, the real value of the cathode follower arrangement seems to have been missed. That is, voltage tuning over an appreciable frequency range (about 3 to 1) can be obtained.[3] The output impedance of a cathode follower is approximately $1/g_m$, which can be varied in accordance with plate voltage or grid voltage. If this output impedance is the effective resistive element of each of the three cathode-follower sections, and if it is assumed that the amplifying tube does not provide appreciable phase shift, then the oscillation frequency is approximately $\omega = 3^{1/2} g_m/C$, where C is the interstage shunt capacitance and where it is assumed that $R_k \gg 1/g_m$, where R_k is the physical cathode-to-ground resistor of each cathode-follower section. The extent of tuning is dependent upon the allowable variation of g_m, the minimum frequency for a given capacitance C being limited by the value of the physical cathode resistor R_k, and the maximum frequency limited by the maximum obtainable value of g_m. A grid return to a positive voltage helps in maintaining the maximum value of g_m large with a large R_k. The coupling capacitors and grid-leak resistors are assumed to be large.

Performance characteristics for the oscillator circuit of Fig. 1 are shown in Fig. 2.

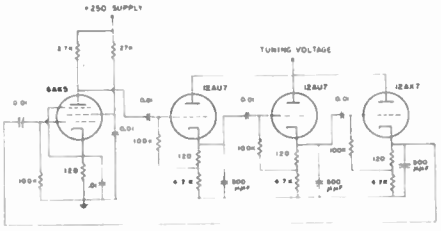

Fig. 1—Circuit of cathode-follower, phase-shift oscillator.

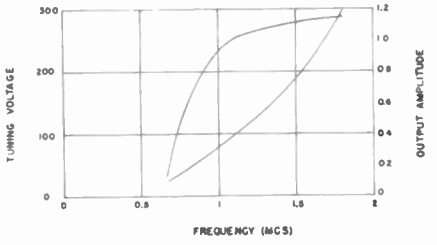

Fig. 2—Oscillator tuning characteristics.

It should be mentioned that shunt capacitance is preferable to series capacitance (that is, lag rather than lead interstage networks) not only because it permits operation to higher frequencies, but because harmonics introduced by nonlinearities tend to be reduced by filtering.

Operation to slightly higher frequencies at the cost of a slightly reduced tuning range can be realized by also obtaining some phase shift in the plate circuit of the amplifying tube. This enables a less distorted high-level waveform to be obtained than is otherwise possible.

J. L. Stewart
K. S. Watkins
University of Michigan
Ann Arbor, Michigan

[3] J. L. Stewart and K. S. Watkins, "Wide-Range Electrically Tunable Oscillators," 1955 Convention Record of the IRE, Part 3, pp. 89–96.

Magnetic Focusing of Electron Beams*

In a recent paper J. T. Mendel[1] discusses an approximation for the variations of the radius of a cylindrical electron beam in a constant or periodic magnetic field. The maximum radius r_{max} is not given in his analysis. In the following it is shown, that by introduction of an appropriate reference radius relations can be obtained which are at the same time simpler and more general.

From the force equation for the boundary electrons[1]

$$\frac{d^2r}{dt^2} + r\left(\frac{\eta B}{2}\right)^2 - r\left(\frac{\eta B_c}{2}\frac{r_c^2}{r^2}\right)^2 - \frac{\eta I}{2\pi\epsilon_0 v r} = 0 \qquad (1)$$

we get a reference radius $r = r_m$, determined by $d^2r/dt^2 = 0$,

$$r_m = r_B\left\{\frac{1}{2} + \frac{1}{2}\left[1 + 4\left(\frac{r_c^2}{r_B^2}\frac{B_c}{B}\right)^2\right]^{1/2}\right\}^{1/2}. \qquad (2)$$

Here

$$r_B = \left(\frac{\eta I}{2\pi\epsilon_0 v \omega_L^2}\right)^{1/2} \qquad (2a)$$

is the Brillouin-radius. We put

$$r = r_m(1+\delta)$$

and for $\delta \ll 1$ we get a linear differential equation which does not contain a space charge parameter, e.g. the plasma frequency:

$$\frac{d^2\delta}{dt^2} + \omega_L^2 2(1+K)\delta = 0 \qquad (3)$$

with

$$\omega_L = \frac{\eta}{2}B, \qquad K = \left(\frac{B_c}{B}\frac{r_c^2}{r_m^2}\right)^2. \qquad (4)$$

For the initial conditions

$$r = r_1, \quad \gamma_1 = \tan^{-1}\left(\frac{dr}{dz}\right) \quad \text{at} \quad z = 0$$

the solution of (3) gives

$$\frac{r_{max}}{r_m} = 1 + \frac{r_1}{r_m}\left[\left(\frac{r_m}{r_1} - 1\right)^2 + \frac{1}{2(1+K)}\left(\frac{v\tan\gamma_1}{\omega_L r_1}\right)^2\right]. \qquad (5)$$

Fig. 1 shows $r_{max}/r = f(r_1/r_m)$, for different values of the parameter

$$p = \frac{1}{2(1+K)}\left(\frac{v\tan\gamma_1}{\omega_L r_1}\right)^2.$$

For $\tan\gamma_1 = 0$, $r_1 = r_m$ the maximum radius $r_{max} = r_m$ decreases with increasing K. These conditions with $K = 0$ give the Brillouin flow with r_{max} having its minimum $r_{max} = r_B$ according to (2a). The larger K for $\tan\gamma_1 \neq 0$ the more r_{max}/r_m approaches 1.

* Received by the IRE, May 16, 1955.

[1] J. T. Mendel, "Magnetic focusing of electron beams," Proc. IRE, vol. 43, pp. 327–331; March, 1955.

For a periodic field

$$B(z) = B_0 \cos \kappa z \qquad (6)$$

we get from (2), replacing B by $B_0/\sqrt{2}$,

$$\frac{d^2\delta}{dx^2} + \alpha[2(1+K)\delta + \cos 2x] = -\delta\alpha\cos 2x \qquad (7)$$

with

$$\alpha = \frac{\omega_{L,eff}^2}{\omega^2}, \qquad \omega_{L,eff} = \frac{\eta}{2}\frac{B_0}{\sqrt{2}},$$

$$x = \omega t = \kappa v t = \kappa z.$$

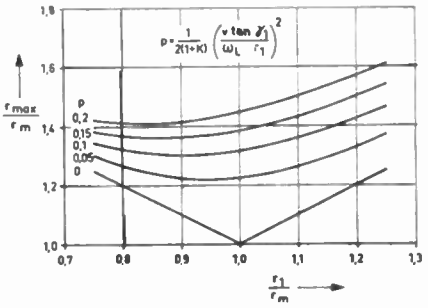

Fig. 1

Here again δ does not depend on the plasma frequency. Suppose $\alpha < 1$ (first stability region). To solve (7) we use an iteration process, at first putting to zero the right-hand side of (7). The solution so obtained is then introduced in this term. In the second approximation we get a correction of r_m

$$r_m' = r_m\left(1 - \frac{\alpha}{4(1+K)[4 - 2\alpha(1+K)]}\right).$$

With

$$r = r_m'(1+\delta')$$

the approximate solution of (7) is

$$\delta' = c_1\cos\sqrt{2(1+K)\alpha}\,x + c_2\sin\sqrt{2(1+K)\alpha}\,x + \frac{\alpha}{4-2\alpha(1+K)}\left[\cos 2x + \frac{\alpha}{2}\frac{\cos 4x}{16-2\alpha(1+K)}\right]. \qquad (8)$$

The constants c_1 and c_2 are given by the initial conditions at $z = 0$

$$c_1 = \delta_1' - \mu, \qquad c_2 = \frac{1}{\sqrt{2(1+K)}}\frac{v\tan\gamma_1}{\omega_{L,eff} r_m},$$

$$\mu = \frac{\alpha}{4-2\alpha(1+K)}\left(1 + \frac{\alpha/2}{16-2\alpha(1+K)}\right).$$

Eq. (8) gives us the upper limit of r_{max}

$$\frac{r_{max}}{r_m'(1+\mu)} \leqq 1 + \frac{r_1}{r_m'(1+\mu)}\left[\left(\frac{r_m'(1+\mu)}{r_1} - 1\right)^2 + \frac{1}{2(1+K)}\left(\frac{v\tan\gamma_1}{\omega_{L,eff} r_1}\right)^2\right]. \qquad (9)$$

This value can be read from Fig. 1, too, by introducing $r_m'(1+\mu)$ instead of r_m and $\omega_{L,eff}$ instead of ω_L in the parameter p.

For fuller details see[2]. There it is shown that our results correspond to those obtained in[3].

W. Kleen and K. Pöschl
Siemens & Halske AG.
Munich, Germany

[2] W. Kleen and K. Pösche, *Archiv. elektr. übertr.*, vol. 9, pp. 295–298; July, 1955.
[3] A. M. Clogston and H. Heffner, *Journ. Appl. Phys.*, vol. 25, pp. 436–447, April, 1954.

Temperature Coefficient of AT Cut Quartz Crystal Vibrators*

It is well known that the temperature-frequency characteristic of a vibrating quartz crystal plate depends upon its orientation with respect to the crystallographic axes of the crystal. Plates vibrating in a thickness shear mode which are used for frequencies above 500 kc have two orientations, called AT and BT cut, where their frequency temperature coefficients assume very small values. However, other parameters also influence the frequency temperature behavior of these two cuts; it is especially the geometry of the crystal plate which has to be taken into account. Fig. 1 shows for the AT orientation the optimum angle of cut as a function of the order of the harmonic mode of the vibration times the ratio diameter /thickness of the crystal plate. The optimum angle of cut is the orientation of the crystal plate which gives the smallest frequency excursion for a defined temperature range.

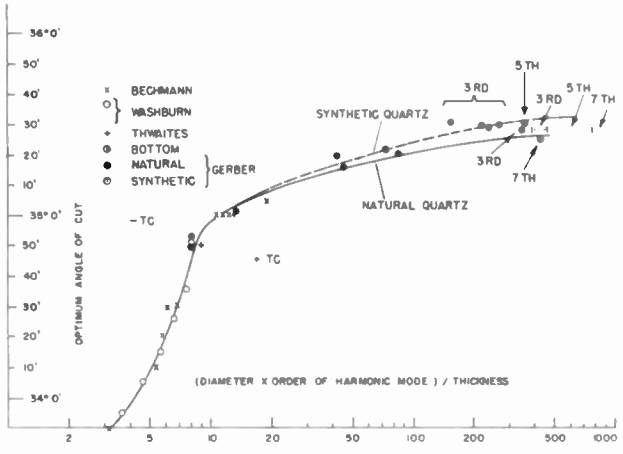

Fig. 1.

All known measurements made by various investigators in the past are plotted in the graph, in addition to results on natural and synthetic quartz vibrators obtained by the author. The synthetic material was grown by the Brush Laboratories Co. Most investigators measured the temperature coefficient in the temperature range from −55 degrees to +90 degrees C., except Bechmann, who used a smaller range. It is surprising how well the various measurements fit one curve, in spite of the above fact and despite wide variations in contour applied to the crystal plates with a low diameter/thickness ratio. As it can be readily seen, the optimum angle of cut is for larger dimensional ratios approximately 7 feet higher in the case of synthetic than in the case of natural quartz. The optimum angle decreases with decreasing dimensional ratio; thus, in the case of an angle of 35 degrees, for instance, the temperature coefficient would be negative for low frequency crystals with dimensional ratios below $10/h$ and would be positive for higher frequency crystals with dimensional ratios above $10/h$. This is due to a change of the value for the effective elastic stiffness coefficient with decreasing diameter/thickness ratio which is accompanied by a change of its temperature coefficient.

* Received by the IRE, June 8, 1955.

Bibliography

1. Bechmann, R. "Eigenschaften von Quarzoszillatoren und Resonatoren im Bereich von 300 bis 5000 kHz." *Hochfrequenztechnik und Elektroakustik*, Vol. 59 (April, 1942), pp. 97–105.
2. Washburn, E. *Research Investigations Pertaining to Low Frequency Contoured AT-Cut Quartz Plates*, RCA Final Rep. on Contract No. DA36-039 sc-5460, pp. 22–25 (January, 1953.)
3. Washburn, E. *Investigation of Mechanical Overtone Crystals, 50 mc to 150 mc or Higher*, RCA Final Rep. on Contract No. W36-039 sc-38265, p. 28 (October, 1950.)
4. Thwaites, J. E., Morton W. D., Davies, A. O. *Development of Miniature Bevelled AT-Cut Quartz Discs for the Frequency Range 500 to 2000 kc/sec*, Post Office Engrg. Dept., Radio Report No. 2108, August, 1951.
5. Bottom, V. E., Murphy, E. S., Arthur, M. G., Hammond, D. L., Tyler, L.C. *Research Investigations on Fundamental and Overtone Crystal Units*, Colorado A&M College, Fourth Quarterly Rep. on Contract No. DA36-039 sc-66, p. 18 (July, 1951.)

E. A. Gerber
Signal Corps Engrg. Labs.,
Fort Monmouth, N. J.

Variation of Juntcion-Transistor Current-Amplification Factor with Emitter Current*

In a recent article,[1] W. M. Webster presented the theory for the variation of the junction-transistor current-amplification factor as a function of emitter current. His experimental verification of the theory was very good in the case of the *p-n-p* transistor, but not as good in the case of the *n-p-n* transistor. It turns out that with a slightly different choice of constants, satisfactory verification can also be obtained for an *n-p-n* transistor.

According to theory by Webster,

$$\frac{1}{\alpha_{cb}} = \frac{sA_e W}{D_e A}\, g(Z) + \left[\frac{\sigma_b W}{\sigma_e L_e} + \frac{1}{2}\left(\frac{W}{L_b}\right)^2\right](1+Z)$$

for an *n-p-n* transistor where

$$Z = \frac{W\mu_p I_E}{D_e A \sigma_b}.$$

* Received by the IRE, May 31, 1955.

[1] W. M. Webster, "On the variation of junction-transistor current-amplification factor with emitter current," Proc. IRE, vol. 42, pp. 914–920; June, 1954.

The constants entering into the determination of Z are known so Z as a function of I_E, $g(Z)$, and $(1+Z)$ can be determined.

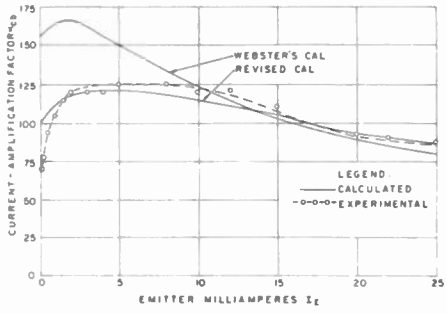

Fig. 1.

The coefficients of $g(Z)$ and $(1+Z)$ cannot be readily evaluated. In fact, the process of curve fitting to be described represents one of the few means for determining these coefficients. For the *n-p-n* transistor, Webster used the coefficient values of

$$\frac{sA_e W}{D_e A} = 5 \times 10^{-3}$$

and

$$\frac{\sigma_b W}{\sigma_e L_e} + \frac{1}{2}\left(\frac{W}{L_b}\right)^2 = 1.53 \times 10^{-3}.$$

If instead, the coefficient values of

$$\frac{sA_e W}{D_e A} = 9 \times 10^{-3}$$

and

$$\frac{\sigma_b W}{\sigma_e L_e} + \frac{1}{2}\left(\frac{W}{L_b}\right)^2 = 1 \times 10^{-3}$$

are used, the check between theory and measurement becomes considerably better as is noted in Fig. 1. The fit to the experimental data is accomplished by a few trials at curve fitting. With the aid of Webster's data, the new coefficient values can be used to obtain new values of $sA_e = 0.2$ cm³/second ($s = 370$ cm/second) and $\sigma_e L_e = 1.5$ mho (neglecting the volume recombination term).

The additional experimental verification of Webster's alpha fall-off theory makes it possible to proceed with assurance in applying the theory to both *n-p-n* and *p-n-p* transistors. As a consequence of his theory, it is noted that it is possible to design junction transistors with constant alphas over a wide current range or even slightly rising alphas with current. These desirable objectives can be obtained by making

$$\frac{sA_e W}{DA} \gg \left[\frac{\sigma_b W}{\sigma_e L_e} + \frac{1}{2}\left(\frac{W}{L_b}\right)^2\right]$$

as, for instance, by purposely making the surface recombination velocity, s, large near the emitter periphery. This mode of treatment flattens off the otherwise sharply peaked alpha characteristic curve and has pronounced effects on the linear behavior of the device as a power transducer.

L. J. Giacoletto
RCA Laboratories
Princeton, N. J.

On the Maximum Signal-to-Noise Ratio Realizable from Several Noisy Signals*

In a diversity receiving system, one usually has available at the detector outputs a number of coherent signal sources, each of which has been additively corrupted by noise. In certain cases, e.g. when the noise in each channel is largely due to the receiver, the noise voltages in the several channels are mutually incoherent. It may then be possible to form a linear combination of the corrupted signals such that the resultant signal will have a higher signal-to-noise ratio than any of the components. In the context of diversity systems, this fact was first pointed out in an important note by Kahn,[1] though it has been used in radar and other applications for some time.

When the average signal power and the average noise power in each channel are known, it is in fact possible to maximize the resultant signal-to-noise ratio. This was indicated by Kahn, who proved it, under restricted conditions, for the case of two channels. However, Kahn used a method of proof that is not well suited to generalization. Object of present note is to sharpen Kahn's result, and to extend to general case.

In what follows, we shall write a bar over a quantity to denote the average value (mean) of the quantity. Also, in speaking of a "signal-to-noise ratio," we shall invariably mean a signal-to-noise *power* ratio.

Let there be given m functions $f_i(t)$ of the form $f_i(t)=s_i(t)+n_i(t)$. Let the signals $s_i(t)$ be of the form $s_i(t)=k_i s(t)$, where the k_i are positive real numbers; i.e., we assume the $s_i(t)$ are mutually coherent. We may let $\overline{s^2}=1$. Let the "noises" $n_i(t)$ have zero means (no dc components) and be incoherent, i.e. uncorrelated, so that $\overline{n_i n_j}=\overline{n_i}\,\overline{n_j}=0$ if $i\neq j$. We assume that the $\overline{s_i^2}$ and $\overline{n_i^2}$ are known, and that $\overline{s_i^2}>0$, $\overline{n_i^2}>0$. Write

$$F(t)=\sum a_i f_i(t)=S(t)+N(t), \qquad (1)$$

where $S(t)=\sum a_i s_i(t)$, $N(t)=\sum a_i n_i(t)$. Let $p_i=\overline{s_i^2}/\overline{n_i^2}$ be the signal-to-noise ratio of f_i, and $P=\overline{S^2}/\overline{N^2}$ be the signal-to-noise ratio of F. We state our result as:

Theorem. For any choice of coefficients a_i,

$$P\leqq\sum p_i, \qquad (2)$$

and if the a_i are chosen so that $a_i=\sqrt{\overline{s_i^2}/\overline{n_i^2}}$, then equality holds. In words: The maximum signal-to-noise ratio that can be realized from any linear combination of the f_i is equal to the sum of the individual ratios, and this maximum is obtained by taking $a_i=\sqrt{\overline{s_i^2}/\overline{n_i^2}}=p_i\sqrt{\overline{s_i^2}}$.

Proof. To illustrate the nature of the situation more clearly, we shall first prove this for the special case where the signals s_i have all been normalized, so that $s_1(t)=s_2(t)=\cdots=s_m(t)=s(t)$, and $\overline{s^2}=1$. Then

$$\overline{S^2}=\overline{(\sum a_i s_i)^2}=\overline{s^2}(\sum a_i)^2=(\sum a_i)^2, \qquad (3)$$

and

$$\overline{N^2}=\overline{(\sum a_i n_i)^2}=\overline{(\sum a_i^2 n_i^2+\sum_{i\neq j} a_i a_j n_i n_j)}=\sum a_i^2\overline{n_i^2}+\sum_{i\neq j} a_i a_j\overline{n_i}\,\overline{n_j}=\sum a_i^2\overline{n_i^2}=\sum a_i^2/p_i, \qquad (4)$$

using the incoherence of the n_i. Now, by the Schwarz inequality,

$$(\sum a_i)^2\leqq[\sum (a_i/\sqrt{p_i})^2][\sum(\sqrt{p_i})^2], \qquad (5)$$

so that

$$P=\frac{(\sum a_i)^2}{\sum (a_i^2/p_i)}\leqq\sum p_i, \qquad (6)$$

which proves (2). We also see that equality holds if $a_i=p_i$.

For the general case, where the s_i have arbitrary magnitudes, we write $a_i=b_i c_i$, and take $c_i^2=1/\overline{s_i^2}$, so that $c_1 s_1(t)=c_2 s_2(t)=\cdots=c_m s_m(t)=s(t)$, and $\overline{s^2}=1$. Then for $F(t)=\sum b_i(c_i s_i(t))+\sum b_i(c_i n_i(t))$, we have $\overline{S^2}=(\sum b_i)^2$, and

$$\overline{N^2}=\sum b_i^2(c_i^2\overline{n_i^2})=\sum(b_i^2/p_i),$$

as before, and

$$P=\frac{(\sum b_i)^2}{\sum (b_i^2/p_i)}\leqq\sum p_i, \qquad (7)$$

with equality holding if $b_i=p_i$. Hence equality holds when $a_i=b_i c_i=p_i/\sqrt{\overline{s_i^2}}$, and the theorem is proved.

The significance of the relation $a_i=\sqrt{\overline{s_i^2}/\overline{n_i^2}}$ is that to maximize the resultant signal-to-noise ratio, one should make the gain of each channel directly proportional to the rms signal (voltage or current) and inversely proportional to the mean-square noise (voltage or current) in that channel. The constant of proportionality must, of course, be the same for each channel. The relation $P=\sum p_i$ enables one to decide, in some given set of circumstances, whether or not the addition of another channel is worth while. It should be clear that the "averages," e.g. $\overline{s_i^2}$, may be only short-term averages; in fact, the only applications presently known to the writer are those in which the a_i change with time, but at a rate that is slow in comparison to the instantaneous variations of the signal and noise. Specific applications and techniques have been given by Kahn[1] and Mack,[2] who treat special cases: Kahn considers equal $\overline{n_i^2}$, and Mack deals with equal s_i. These applications were of course motivated by the work of Kahn.

The writer is indebted to C. L. Mack, Jr., for pointing out this problem.

D. G. Brennan
Lincoln Laboratory, M.I.T.
Lexington 73, Mass.

* Original manuscript received by the IRE, August 1, 1955. This research was supported jointly by the Army, Navy, and Air Force under contract with the Massachusetts Institute of Technology.

[1] L. R. Kahn, "Ratio squarer," PROC. IRE, vol. 42, p. 1704; November, 1954.

[2] C. L. Mack, Jr., "Diversity reception in uhf long-range communications," p. 1281, this issue.

A Note on Tee-Pi Transformations*

The possibility of a transformation between Tee and Pi structures is well known in the analysis of electric networks at a single frequency, but an exact transformation for networks operating over a range of frequencies is not possible in general. The purpose of this note is to give several simple conditions which are sufficient to ensure the physical realizibility of the Pi network obtained by transformation from a realizable Tee network without mutual coupling. By duality the discussion will apply also to Pi-Tee transformations if impedances are replaced by admittances.

Letting primed impedances be those in the Pi, one form of the transformation is

$$\begin{aligned} Z_a' &= Z_b+Z_c+Z_bZ_c/Z_a \\ Z_b' &= Z_c+Z_a+Z_cZ_a/Z_b \\ Z_c' &= Z_a+Z_b+Z_aZ_b/Z_c. \end{aligned} \qquad (1)$$

Appropriate tests can be applied to the primed impedances to test for their positive realness in any given example. However, inspection of (1) shows the sufficiency of any of the following conditions for a realizable Pi:

1. Z_a, Z_b and Z_c have the same form (same poles and zeros).
2. Two of the three impedances, say Z_a and Z_b are resistances. In this case

$$\begin{aligned} Z_a' &= R_b+\left(1+\frac{R_b}{R_a}\right)Z_c \\ Z_b' &= R_a+\left(1+\frac{R_a}{R_b}\right)Z_c. \\ Z_c' &= R_a+R_b+\frac{R_aR_b}{Z_c}. \end{aligned} \qquad (2)$$

These are all realizable if Z_c is realizable. Eqs. (1) can be rewritten in the form

$$Z_a'=\frac{Z_a(Z_b+Z_c)+Z_bZ_c}{Z_a}, \qquad (3)$$

etc. It is evident that the transformation is certainly possible if the numerator is a constant, which will be the case if:

3. One impedance (Z_b) is inverse to the second (Z_c), and the third (Z_a) is inverse to the sum of the first two.

If the Tee is symmetrical, this condition cannot be satisfied unless all arms are resistances.

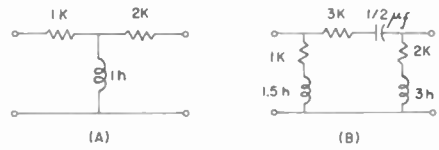

Fig. 1

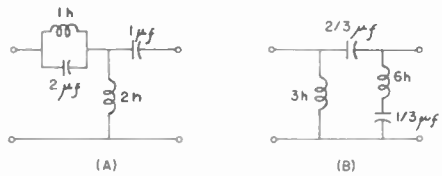

Fig. 2

An interesting illustration of Case 2 is shown in Fig. 1. The need for a lossless inductor is eliminated by the transformation at the expense of additional elements. An illustration of Case 3 is shown in Fig. 2.

N. Balabanian and C. R. Cahn
College of Engrg., Syracuse Univ.
Syracuse, New York

* Received by the IRE, June 20, 1955.

Designing Crystal-Controlled Oscillator Circuits*

With the development of Military Standard specifications for quartz crystals used in U. S. military equipment, the design of crystal-controlled oscillator circuits has undergone a drastic change in point of view. No longer can the designer provide circuitry to the crystal manufacturer and instruct him to produce crystals to yield an over-all characteristic. Today the circuit designer is provided a set of specifications for crystals and is, himself, instructed to produce circuitry to yield the over-all characteristic with any crystal meeting the specification. The rational nature of this approach is now displaying a pronounced effect upon the design of commercial equipment as well.

One item in the crystal specification is the maximum effective resistance which the crystal vendor may supply. The designer must assure himself that his circuit will function properly when equipped with crystals of this maximum resistance, but his chance of having available a set of limit crystals is very small indeed. If his circuit uses series-resonant crystals, a resistor of the specified maximum resistance, shunted by the nominal crystal capacitance, can be substituted. In the commonly-used antiresonant case, however, no simple procedure has been generally available. This communication proposes to offer one.

The designer will have in hand some specimen crystals in the frequency band of interest which are, in general, better than limit crystals. With these crystals he can determine the rf voltage appearing across a good crystal. In the antiresonant case, this will be greater than the voltage across a poorer crystal. The current in the load capacitance at this voltage and frequency is the circulating current in the crystal. The product of the square of this current with the crystal effective resistance is the crystal dissipation. The product of the square of this current with the maximum effective resistance gives an approximation (including a safety factor) of the power dissipated in a limit crystal, which can be compared with the allowed dissipation.

For every oscillator there is a criterion of satisfactory performance (CSP) usually expressed in terms of signal out of the oscillator. Here is offered a technique for determining the maximum effective resistance *Rem* to satisfy this CSP or, conversely, a technique for determining if a crystal of given effective resistance *Rem* will satisfy the CSP. It is assumed that a specimen crystal of known effective resistance *Re* less than this given value is available.

A crystal unit of maximum effective resistance *Rem* (or of minimum allowable Q) may be simulated by the artifice of shunting a better-than-limit unit with a resistor of such value that the Q is degraded as required. (If a dc potential appears across the crystal it will be necessary to block the dc current path through the shunting resistor with a high capacitance.)

The antiresonant resistance of the crystal unit when loaded by the (known) external circuit capacitance C is called the performance index PI. The magnitude of the PI is given by the equation

$$PI = \frac{1}{\omega^2 C^2 Re},$$

where ω is the angular frequency of resonance. The PI of the shunted crystal is simply the parallel combination of the shunting resistance R and the PI of the crystal itself. If the shunting resistor is of such a value as to degrade the circuit exactly to its CSP, then

$$Rem = Re + \frac{1}{\omega^2 C^2 R}.$$

This equation may, of course, be inverted to determine the value of R necessary to degrade a better than limit crystal to be equivalent to a unit of effective resistance equal to *Rem*, yielding

$$R = \frac{1}{\omega^2 C^2 (Rem - Re)}.$$

Measurement of the rf crystal voltage when loaded in this manner will yield a more accurate determination than the previously discussed approximation of the dissipation in a limit crystal. If the circuit is degraded all the way to its CSP, a large discrepancy between this determination and the approximation will probably be observed. If, on the other hand, there is a comfortable margin between the operating conditions with a crystal of specified *Rem* and the CSP, the approximation will prove to be quite good. Indeed, the quality of the initial approximation will serve as a figure of merit for the design as a whole.

The procedure just described of shunting antiresonant crystals with resistance to simulate limit crystals, has proved to be an accurate and convenient means for determining the behavior of a circuit under limit-crystal conditions when the designer has for test purposes only crystals of *Re* less than *Rem*. The scheme has been applied with success at various frequencies through the range from 1.5 megacycles to 51 megacycles and has given uniformly consistent results wherever applied.

J. H. Sherman, Jr
General Electric Co
Syracuse, N. Y

* Received by the IRE, July 29, 1955.

Contributors

W. G. Abel (A'55) was born in Louisville, Ky., on March 3, 1915. He received the B.S. degree in physics from Catholic University in Washington, D.C. in 1939, and the M.S. degree in physics from Fordham University in 1947. From 1947 to 1952, he was employed by the Raytheon Manufacturing Co. in research involving radio communications and propagation. Since 1942, he has been a staff member of the M.I.T. Lincoln Laboratory where he is engaged in radio propagation research.

W. G. Abel

❖

L. A. Ames was born in East Waterford, Maine, on December 13, 1907. He graduated from the Lowell Institute School in 1931. He spent fourteen years in the power metering field, including seven years as assistant in charge of the meter department of the Malden Electric Co. Following ESMWT radio courses at Tufts and Harvard he joined the staff of the Radiation Laboratory of MIT in 1943 where he was engaged in radar systems work.

L. A. Ames

Mr. Ames joined the Air Force Cambridge Research Laboratory, Cambridge, Mass., in November, 1945 and has since been associated with this organization. As a member of the Communications and Relay Laboratory he engaged in research in the fields of microwave relay, data transmission and storage systems. On special assignment to the Lincoln Laboratory of MIT he engaged in research on digital coding and storage.

Mr. Ames is a member of the fraternity of radio amateurs having been assigned the call letters W1GFF in 1933 by the FCC.

❖

D. K. Bailey was born in Clarendon Hills, Ill., on November 22, 1916. After receiving the B.S. degree in astronomy at the University of Arizona in 1937, he went to Oxford as a Rhodes scholar. He received the B.A. degree in physics in 1940, and the M.A. degree in 1943. From 1940 to 1941, he was in Antarctica as a physicist with the U. S. Antarctic expedition to make cosmic ray observations.

D. K. Bailey

Mr. Bailey served with the Signal Corps from 1941 to 1946. From 1941 to 1943, he was in England with the Royal Air Force, and acted as the Air Ministry representative in the Inter-Services Ionosphere Bureau (I.S.I.B.) For the next twenty months, he was assigned to the War Department where he established the Radio Propagation Unit (now the Radio Propagation Agency). From April, 1945 to June, 1946, he served in Manila, Leyte, and Tokyo, Japan in connection with Signal Corps ionosphere stations. In Tokyo, he assisted the Japanese in reestablishing a radio research program.

In December, 1946, Mr. Bailey was associated with the RAND project at the Douglas Aircraft Co., where he worked in the communication and electronic field. From 1948 to 1950, he was a member of the U. S. delegation in Geneva, Switzerland, serving as chairman of the propagation working group of the Provisional Frequency Board. Since then, he has been a member of the U. S. delegation at five international conferences. He has been actively engaged as a senior member of a research group, in the investigation of regular long-distance vhf ionospheric propagation, and related communications matters. His present capacity is consultant to the chief of the radio propagation physics division.

Mr. Bailey holds the Legion of Merit and belongs to Phi Beta Kappa. He is a fellow of the Royal Astronomical Society and the Royal Geographical Society, and is a member of the American Astronomical and Physical Societies.

❖

A. P. Barsis (S'48–A'49–M'53) was born in 1916 in Vienna, Austria. He graduated from the Realgymnasium in 1935, and attended the Technische Hochschule in Vienna. He came to the United States in 1939, and from 1940 to 1942, and 1946 to 1952 was employed with George C. Davis, Consulting Radio Engineer, Washington, D. C., where he worked on broadcast allocations, and directional antenna design.

A. P. Barsis

During World War II, Mr. Barsis served as a radio technician with the psychological warfare branch of the Army. He attended George Washington University, and received the B.E.E. degree in 1948. In 1952, he joined the Boulder Laboratories of the National Bureau of Standards, and has been employed in tropospheric propagation research, especially in the analysis and evaluation of long-distance tropospheric propagation data provided by the Cheyenne Mountain recording project.

Mr. Barsis is a member of Sigma Tau.

R. Bateman (A'42) was born in Toledo, Ore., on July 22, 1912. He received the B.S. degree in electrical engineering from Oregon State College in 1934. From 1934 to 1937, he was employed by the American Pacific Whaling Co., and the Alaska Steamship Co., in connection with the installation and operation of land and ship radio stations. From 1937 to 1942, he was associated with the Federal Communications Commission.

R. Bateman

Mr. Bateman joined the staff of the operational research group in 1942, in the office of the chief signal officer, serving there until 1945. He is now employed by the National Bureau of Standards as chief of ionospheric research at Washington, D. C.

❖

B. R. Bean was born on September 14, 1927, in Boston, Mass. He attended the University of New Hampshire, receiving the B.S. degree in meteorology in 1949. He worked for the Weather Bureau Station at Durham, N.H., from 1945 to 1949.

B. R. Bean

Mr. Bean transferred to the Central Radio Propagation Laboratory of the National Bureau of Standards in 1950. Since that time he has been engaged in radio-meteorological research.

Mr. Bean is a professional member of the American Meteorological Society.

❖

G. Birnbaum (A'43–M'55) was born in Brooklyn, N. Y., on July 16, 1919. He received the A.B. degree in chemistry from Brooklyn College in 1941, and the M.S. degree in physics from George Washington University in 1949.

G. Birnbaum

From 1942 to 1943, he was an instructor in radio engineering with the Air Force Technical Training Command. He served as an officer in the United States Naval Reserve from 1943 to 1946, working with radio and radar aids to air navigation. In 1946, Mr. Birnbaum joined the staff of the National Bureau of Standards in the dielectric and magnetic measurements project of the microwave standards section, and was project leader from 1949 to

1954. At present, he is chief of the microwave frequency and spectroscopy section at the Bureau's Boulder Laboratories.

He is a member of the American Physical Society, Sigma Xi, and U.S.A. Commission II of URSI.

❖

K. Bullington (A'45–SM'53–F'55) was born in Guthrie, Oklahoma on January 11, 1913. He attended the University of New Mexico, receiving the B.S. in E.E. degree in 1936. He received his M.S. in 1937 from MIT.

K. Bullington

He joined the technical staff of Bell Telephone Laboratories after his graduation. He was engaged primarily with wire transmission problems connected with voice frequency and carrier telephone systems. Later, he began working on the engineering of mobile telephone and microwave relay systems. An important aspect of his work has been in radio propagation.

❖

H. E. Bussey was born in Tabor, S. D., in 1917. He attended Yankton College in S. D. and George Washington University, receiving from the latter the B.A. degree in mathematics in 1941, and the M.S. degree in physics in 1951. His military service included meteorological and radar-weather courses, weather engineering, and survey and weather forecasting.

H. E. Bussey

In September, 1946, Mr. Bussey joined the Central Radio Propagation Laboratory of the National Bureau of Standards to do tropospheric propagation research. In 1951, he joined the microwave standards branch of the National Bureau of Standards Boulder Laboratories, to work on microwave dielectric and magnetic measurements.

He is a member of the American Physical Society, the American Meteorological Society, Sigma Pi Sigma, and an associate member of Sigma Xi.

❖

T. J. Carroll (M'44) was born in Pittsburgh, Pa., on April 26, 1912. He received an A.B. degree from the University of Pittsburgh in 1932, and a Ph.D. in physics from Yale University in 1936. From 1936 to 1941, he taught at the College of New Rochelle.

T. J. Carroll

He was a radio propagation and air defense consultant to the Signal Corps and Air Force from 1941 to 1946, and a member of the NDRC Committee on Propagation from 1944 to 1945.

From 1946 to 1951, he was a researcher on microwave propagation at the National Bureau of Standards. Since 1952, as a staff member of the M.I.T. Lincoln Laboratory, he has been engaged in the tropospheric propagation theory.

He was a member of the Ad Hoc Committee formed in 1948 to advise the F.C.C. on propagation questions affecting TV allocations.

❖

J. H. Chisholm was born in Byron, Ga., on February 8, 1913. He received the B.S. degree in electrical engineering from the Georgia Institute of Technology in 1934. He was associated with the Masonite Corp. until his entry into active service with the Signal Corps in 1941 where he attended successively Harvard University, Massachusetts Institute of Technology, and the Air Warning School at Fort Monmouth, N. J. He was assigned to the Air Force School at Orlando, Fla. in 1942 where he was engaged in studies of the tactical use and technical performance of various radar and communications equipment in air defense systems. After serving as chief of the ground communication section of the school, he was assigned as signal officer of the 5th Air Force fighter command in the Pacific theater from 1945 to 1946.

J. H. Chisholm

In 1947, Mr. Chisholm joined the Central Radio Propagation Laboratory of the National Bureau of Standards where he was engaged in research in tropospheric propagation. Since 1951, he has been a staff member of the Lincoln Laboratory of MIT.

❖

C. M. Crain (S'42–M'49) was born in Goodnight, Tex., on September 10, 1920. He received the B.S., M.S. and Ph.D. degrees at the University of Texas in 1942, 1947 and 1952 respectively. After graduation from the University of Texas in 1942 he worked on airborne radar developments with the Philco Corporation in Philadelphia, Pa. In 1943 he returned to the University of Texas as an instructor; in 1944 he was called to active duty in the Naval Reserve, where he served with the Bureau of Ordnance in the influence mine program and the Office of Research and Inventions. In 1946 he returned to the University of Texas, where he is now an associate professor of electrical engineering and a member of the staff of the Electrical Engineering Research Laboratory.

C. M. Crain

Dr. Crain is a member of the AIEE, Sigma Xi, Tau Beta Pi, Eta Kappa Nu, and Commission II, URSI.

❖

M. R. Currie (A'55) was born in Spokane, Wash., on March 13, 1927. From 1944 to 1947 he served with the U. S. Navy. He received the A.B. degree in physics from the University of California in 1949 and the M.S. and Ph.D. degrees from the same institution in 1951 and 1954.

M. R. Currie

Dr. Currie was associated with the Microwave Laboratory at the University of California from 1949 to 1951. From 1952 to 1954, he was a research assistant in the Electronics Research Laboratory. He was an instructor in the Department of Electrical Engineering during 1953 and 1954. As a member of the technical Staff in the Electron Tube Laboratory, Hughes Aircraft Co., he is concerned with problems in microwave electronics.

Dr. Currie is a member of Sigma Xi and Phi Beta Kappa.

❖

A. P. Deam (M'51) was born in Dallas, Tex., on December 10, 1917. He received the B.S.E.E. degree from the Agricultural and Mechanical College of Texas in 1940, and the M.S.E.E. degree from the University of Texas in 1949.

A. P. Deam

During 1941 and 1942 he was employed by the Dallas Power and Light Co.

Since then, he has been employed by the University of Texas, both in a teaching and research capacity. Presently he is a radio engineer at the Electrical Engineering Research Laboratory of the University of Texas.

❖

For a photograph and biography of J. T. de Bettencourt, see page 345 of the March, 1955 issue of the PROCEEDINGS OF THE IRE.

❖

H. T. Dougherty (A'49) was born in Brooklyn, New York, on April 30, 1922. He served with the U. S. Army from 1942 to 1946 and received his B.S. degree in E.E. from the College of the City of New York in 1949.

H. T. Dougherty

In 1949 Mr. Dougherty joined the staff of the Central Radio Propagation Laboratory of the National Bureau of Standards in Washington, D. C. as an

electronic engineer for the Frequency Utilization Research Section. Since 1953 he has been a member of the National Bureau of Standards Boulder Laboratories in Colorado where he is engaged in tropospheric propagation research.

❖

A. L. Durkee (A'31–VA'39) was born in Cambridge, Mass., On August 24, 1905. He was graduated from Harvard University in 1930 with the B.S. degree in engineering. After graduation, he joined the development and research department of the American Telephone and Telegraph Co., in July, 1930.

A. L. Durkee

In 1934, Mr. Durkee left ATT and transferred to the Bell Telephone Laboratories. His work there has been concerned largely with problems connected with the development of radio communication systems.

At present, he is engaged in studies relating to radio relay systems engineering.

❖

V. R. Eshleman (S'48–A'53) was born in Darke County, Ohio, on September 17, 1924. After serving three years in the U. S. Navy, he attended George Washington University and received the B.E.E. degree in 1949. He received the M.S. and Ph.D. degrees in electrical engineering from Stanford University in 1950 and 1952 respectively. From 1951 to 1952, he held an Atomic Energy Commission Fellowship in the Physical Sciences.

V. R. Eshleman

Since 1952, he has been a research associate with the Radio Propagation Laboratory at Stanford University.

Dr. Eshleman is a member of Sigma Tau and Sigma Xi, and the U.S.A. Commission 3 of URSI.

❖

B. M. Fannin (A'49–M'55) was born June 9, 1922, in Midland, Tex. He received the B.S. and M.S. degrees in electrical engineering from The University of Texas in 1944 and 1947, respectively. In 1948 he became a research associate in the Electrical Engineering School of Cornell University.

B. M. Fannin

Mr. Fannin, since 1951, has been with the Electrical Engineering Research Laboratory, University of Texas, as a research engineer.

R. M. Gallet was born in Paris, France, on January 1, 1923. He received degrees in philosophy, physics, and mathematics, with specialized certificates in astronomy and theory of atomic and molecular spectra from the University of the Sorbonne in 1942 and 1943.

R. M. Gallet

During the German occupation, he worked for two years in the laboratories of St. Française Radioelectrique, and in 1943 in the laboratory of the School of Physics and Industrial Chemistry of Paris. He entered active duty in the French Navy and was attached to the Scientific Research Organization. He was in Germany on intelligence work at the end of the war.

In 1946, he took an active part in the creation of SPIM (French Ionospheric Military Service) and was a civilian scientist attached to the French Navy Scientific Research Group until 1954. His work was principally connected with ionospheric and solar physics. He took part in expeditions to Brazil in 1947, and Indochina in 1950 where he was in charge of building an ionospheric field station. In 1950, he was responsible for the development of computing automatic machine methods for radio propagation and ionospheric data processing. His group was the only one using electronic computing methods for regular ionospheric applications.

In 1955, he joined the Boulder Laboratories of the National Bureau of Standards in the field of upper atmosphere physics. His most recent work was on absorption by cosmic noise measurements, absorption during the solar eclipse of June 20, 1955, in the Philippines, and on the theory of sporadic E and turbulence. At present, he is directing plans for computing facility for radio propagation studies.

Mr. Gallet is a member of the French Physical Society, the French Astronomical Society, and the American Astronomical Society.

❖

I. H. Gerks (A'32–M'41–SM'43) was born in New London, Wis., in 1905. He received the B.S. degree from the University of Wisconsin in 1927, and the M.S. degree from the Georgia School of Technology in 1932, both in electrical engineering.

I. H. Gerks

From 1927 to 1929, Mr. Gerks was employed by Bell Telephone Laboratories, where he developed and tested various special equipment for telephone centrals, such as tone signaling and centralized time announcing. He then became an instructor and later, an assistant professor of communication and electronic engineering at the Georgia School of Technology, where he remained until 1940. At present Mr. Gerks is employed by the Collins Radio Company, where he is engaged in radio wave-propagation studies.

❖

J. Granlund (S'47–A'51–M'55) was born in Oakland, Calif., in 1924. He graduated from the Massachusetts Institute of Technology in 1944 with the degree of B.S. in electrical engineering. After service in the U. S. Navy during World War II, he returned to M.I.T. for graduate study, and to work on frequency modulation and multipath transmission in the Research Laboratory of Electronics. He received the M.S. degree in 1947, and the D.Sc. degree in 1950, both in electrical engineering. While with the Research Laboratory of Electronics, he participated in two field tests of transatlantic frequency modulation transmission at shortwave frequencies. Since 1952 he has been with M.I.T.'s Lincoln Laboratory.

J. Granlund

Dr. Granlund is a member of Sigma Xi.

❖

D. J. Gray (S'49–A'53) was born in Yonkers, N. Y., in 1929. He entered the Massachusetts Institute of Technology in 1946 and received the Bachelor of Science and Master of Science degrees in electrical engineering, in 1950 and 1952.

D. J. Gray

From 1950 to 1952 Mr. Gray was a research assistant in the Research Laboratory of Electronics at MIT. In 1952 he was called to active duty with the United States Air Force and spent the next two years as an electronics development officer at the MIT Lincoln Laboratory. He was released from active duty in 1954 and since that time has been on the staff of the Lincoln Laboratory.

Mr. Gray is an associate member of the Society of the Sigma Xi.

❖

J. W. Herbstreit (A'40–SM'45) was born in Cincinnati, Ohio, on September 7, 1917. He received the E.E. degree from the University of Cincinnati in 1939. From 1939 to 1940 he was associated with the Crosley Corp. in Cincinnati, Ohio, as transmitter engineer for stations WSAI, W8XAL and 500-kw WLW.

J. W. Herbstreit

In 1940 Mr. Herbstreit joined the Federal Communications Commission National Defense Opera-

tions in Marietta, Ga., later acting as Radio Inspector at the Atlanta Office. In 1941 he was transferred to the Federal Communications Commission Engineering Department in Washington, D. C. as radio engineer in the Safety and Special Services Division.

He joined the Operational Research Staff in the Office of the Chief Signal Officer, Department of the Army, in 1942. While with this group he made numerous operational radio systems studies including measurements of atmospheric noise levels and the attenuation of radio signals by jungles in Panama and the southwest Pacific, measurements and analyses of experimental low frequency loran in the Western Hemisphere, and frequency requirements for low-power radio communications and navigation equipment.

In 1946 he joined the Central Radio Propagation Laboratory of the National Bureau of Standards conducting research on cosmic radio noise and vhf and uhf propagation. He served as technical advisor to the International High Frequency Broadcast Conference held in Mexico City in 1948 and was responsible for the preparation of radio propagation information used by the conference. He served in a similar capacity in in 1950 when the Conference convened in Florence and Rapallo, Italy. Since 1949 he has been in charge of the tropospheric propagation research work being conducted at the National Bureau of Standards now centered at Boulder, Colo.

Mr. Herbstreit is a member of Tau Beta Pi, Eta Kappa Nu, Phi Eta Sigma, AAAS, Engineering Society of Cincinnati, and is a registered professional engineer.

❖

W. J. Inkster was born on June 30, 1920, in Collingwood, Ontario, Canada. He attended the University of Toronto, where he received his B.A.Sc. degree in electrical engineering in 1943.

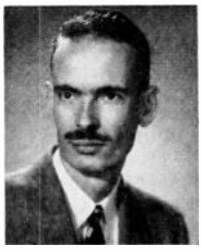

W. J. INKSTER

As a member of the Royal Canadian Navy he served as an Air Radio Officer, on loan to the Royal Naval Fleet Air Arm from 1943 to 1946. In 1946, he joined the transmission department of the Bell Telephone Co. of Canada where he has had experience in engineering mobile, point-to-point, and radio relay systems. He is presently engaged as a radio systems engineer in the special contract department of the Bell Telephone Co. in Montreal, P.Q.

Mr. Inkster is a member of the Association of Professional Engineers of the Province of Ontario.

❖

H. B. Janes (M'53) was born in Medford Ore. on July 13, 1924. During World War II he served in the Armored Force of the U. S. Army in the European theatre. In 1948 he received the B.A. degree in mathematics and physics from Hanover College, Indiana, and subsequently took graduate work in mathematics at Indiana University.

H. B. JANES

During 1949 and 1950 he worked at the U. S. Naval Research Laboratory on the research and development of broadband communication antennas for shipboard use. Since 1950, he has been with the Tropospheric Propagation Research Section of the Boulder Laboratories, National Bureau of Standards. He is in charge of the data analysis group of the Cheyenne Mountain project, which has performed numerous large-scale propagation measurements in the vhf and uhf frequency range.

❖

G. H. Keitel (S'49–M'55) was born on February 16, 1930, in Chicago, Ill. He received his B.S.E.E. in 1952 and M.S.E.E. in 1954 from the University of Washington, and a Ph.D. in electrical engineering in 1955 from Stanford University.

G. H. KEITEL

During the summer of 1952, he worked at the RCA Laboratories with the antenna development group, and at the Applied Physics Laboratory of the University of Washington on instrument development in the summer of 1953. Until the time of his departure for England in September, 1955, to study under a Fulbright grant at the Cavendish Laboratory, Cambridge, he devoted his time to the study of meteor-scattered signals at the Radio Propagation Laboratory, at Stanford University.

Dr. Keitel is a member of Tau Beta Pi, Sigma Xi, and Phi Beta Kappa.

❖

R. C. Kirby (A'44–SM'54) was born in Galesburg, Ill., on November 22, 1922. He received the B.E.E. degree from the University of Minnesota.

R. C. KIRBY

From 1940 to 1942, he worked in the Western Union Telegraph Co. in Minnesota and South Dakota. He served in the Signal Corps from 1942 to 1946 as a member of the radio propagation unit, and later, as an assistant radio officer in the Pacific war theater. He was officer in charge of the Signal Corps ionosphere observatory at Tolosa, Leyte. From 1946 to 1948, he was assistant chief engineer at KFEQ, Inc., in St. Joseph, Mo.

In June, 1948, Mr. Kirby joined the staff of the radio division of the National Bureau of Standards. He was a member of the U. S. delegation to the provisional frequency board (ITU) at Geneva, Switzerland from 1948 to 1950. Since 1951, he has been a member of the ionospheric research section, and has been engaged in research on vhf ionospheric propagation. He was a member of the U. S. delegation to the London assembly of the International Consultative Radio Committee in 1953.

In June, 1955, Mr. Kirby was appointed chief of ionospheric research at the National Bureau of Standards, Boulder, Colo.

❖

R. S. Kirby (M'50) was born in Lawrence, Kans., on July 31, 1920. He received the B.S. degree in engineering in 1943 from the U. S. Naval Academy. He served as an officer on Pacific Fleet destroyers from 1943 until 1946, his duties including those of communications officer, navigator, and executive-officer afloat.

R. S. KIRBY

In 1947 Mr. Kirby joined the staff of the National Bureau of Standards, and has been engaged in propagation studies at the Central Radio Propagation Laboratory. In 1948 he acted in an advisory capacity on propagation tests of air-to-ground communications, conducted at the Naval Air Test Center, Patuxent River, Md. Since 1951 he has been working with the Laboratory in Boulder, Colorado.

He is a member of study group V of the International Radio Consultative Committee.

❖

Y. Kurihara (S'52–A'53) was born on November 30, 1923 in Tokyo, Japan. He received the B.S. degree in electrical engineering from Tokyo University in 1948. In the same year he joined the Radio Research Laboratories, Ministry of Postal Services, Japan, where he was engaged in development of instruments for ionospheric observation and for short-wave radio measurement.

Y. KURIHARA

From 1952 to 1954, Mr. Kurihara attended the Graduate School, Cornell University, on leave from the Radio Research Laboratories, where he made theoretical and experimental studies of radio-wave scattering. He received the M.S. degree from Cornell in 1955.

At present, Mr. Kurihara is engaged in research of tropospheric radio wave propagation at the Radio Research Laboratories, Japan.

C. L. Mack, Jr. (A'55) was born in Cleveland, Ohio, on July 20, 1926. He received the B.S. degree in physics from Harvard University in 1948. From 1948 to 1953, while a graduate student in physics at the University of Pennsylvania, he was engaged in research work. Mr. Mack also taught in the physics department, the Johnson Foundation, the electrical engineering department, and the medical school of the University of Pennsylvania.


C. L. Mack Jr.

In 1953, he joined the staff of the systems engineering group in communications of Lincoln Laboratory at MIT.

❖

L. A. Manning (S'43–A'45–SM'54) was born in Palo Alto, Calif., on April 28, 1923. After receiving the A.B. degree in electrical engineering from Stanford University in 1944, he joined the wartime Radio Research Laboratory at Harvard University as a special research associate. The following year he returned to Stanford, and received the M.Sc. and Ph.D. degrees in 1948 and 1949.


L. A. Manning

He is now an associate professor of electrical engineering; his principal interests are in the field of ionospheric radio propagation.

Dr. Manning is a member of Sigma Xi, Phi Beta Kappa, the American Geophysical Union, the American Meteorological Society, and is serving on the U.S.A. National Committee of the URSI.

❖

W. V. Mansfield was born in New London, Conn., on August 24, 1927. He received his B.A. degree from the College of the University of Chicago in 1948 and has done additional graduate work in mathematics.


W. V. Mansfield

His research associations have included radio sonde evaluation tests, high-altitude oxygen equipment development in the Aeronautic Instruments section of the National Bureau of Standards, and studies of the strain characteristics of high-purity single crystals of aluminum at the Institute for the Study of Metals in Chicago.

In 1951 Mr. Mansfield joined the Tropospheric Propagation Research Section of the Central Radio Propagation Laboratory of the Boulder Laboratories of the National Bureau of Standards. His chief contributions have been in mathematical problems associated with the engineering application of radio physics.

He is a member of the National Speleological Society and of the American Association for the Advancement of Science.

❖

P. L. McQuate was born in Osborn, Mo., on June 5, 1913. He served as a radio technician on a destroyer from 1943 through 1945. He received the B.S. degree in electrical engineering from the University of Denver in 1949. Following graduation he was employed by the Bureau of Reclamation as a transmission line and substation control engineer. In 1951 he was recalled to active duty with the navy as an electronic technician. Late in 1952 he joined the staff of the Boulder Laboratories of the National Bureau of Standards, where he is engaged in tropospheric propagation research.


P. L. McQuate

❖

F. M. Meaney was born October 4, 1927, in Hempstead, N. Y. After receiving the B.A. degree in meteorology from the University of Washington in 1948, she joined the Central Radio Propagation Laboratory of the National Bureau of Standards working in radio-noise research. After a two year leave of absence she rejoined the CRPL in 1952 and engaged in radio-meteorological research until early in 1955. Miss Meaney is now with the Army Special Services Division in Paris, France.


F. M. Meaney

She is a member of the American Meteorological Society.

❖

G. L. Mellen was born in Toledo, Ohio, on February 1, 1914. He attended California Institute of Technology in 1933 and Lowell Institute at M.I.T. from 1937 to 1938.


G. L. Mellen

He was employed by IBM from 1933 to 1943 as a serviceman and later as customer servicer manager of the Worcester, Mass. office. From 1943 to 1950 he worked for National Research Corp. in Boston with a final position as director of the applied physics department. Here he developed vacuum equipment components, controls, and instruments such as the "Alphatron" vacuum gauge.

Mr. Mellen was associated with the aeronautical research department of General Mills, Inc. from 1950 to 1952 as the instrument engineer on a "crash" program involving "skyhook" balloons.

Since 1952 he has been in the systems engineering group of Lincoln Laboratory, implementing systems for the study of ionospheric and tropospheric scatter propagation.

❖

W. E. Morrow, Jr. (S'48–A'41) was born in Springfield, Mass. on July 24, 1928.

He received the S.B. degree from M.I.T. in 1949 and the S.M. degree from the same institution in 1951. Since that time he has been associated with M.I.T. Lincoln Laboratory as a staff engineer and, more recently, as a group leader.


W. E. Morrow, Jr.

While at Lincoln Laboratory, he has done research and development on transistor circuit design, vhf ionospheric scatter communication systems, and vhf tropospheric scatter communication systems.

❖

R. B. Muchmore (S'39–A'40–SM'49) was born July 8, 1917, in Augusta, Kan. He attended the University of California at Berkeley, receiving the B.S. degree in electrical engineering in 1939. He received the E.E. degree in communications engineering from Stanford in 1942.


R. B. Muchmore

From 1942 to 1946, Mr. Muchmore was employed by the Sperry Gyroscope Co. as a project engineer working in the fields of antennas and microwave test equipment. In 1946 he joined the staff of the Guided Missile Laboratory at the Hughes Aircraft Co., where he did systems and noise analysis. Since 1954 he has been with the Ramo-Wooldridge Corp. as a senior member of the technical staff doing systems analysis and also work in the field of radio propagation.

Mr. Muchmore is a member of Sigma Xi, RESA, and the Acoustical Society of America.

❖

Philip Newman (SM'55) was born June 23, 1904 in New York, N. Y. He received the B.S. degree from the City College of New

York in 1924 and the M.A. in physics from Columbia University in 1925. He received a Ph.D. in mathematics from Columbia University in 1940. From 1925 to 1942 he taught mathematics at the City College of New York. From 1942 to 1944, he was a physicist in the Sound Ranging Section at the Signal Corps Laboratory, in New Jersey.

PHILIP NEWMAN

In 1944–1945, he served on the Wave Propagation Group of OSRD at the Columbia University Division of War Research. Since 1945, he has been employed by the Air Force. At present he is chief of the Propagation Laboratory at the Air Force Cambridge Research Center.

Dr. Newman is a member of Resa, Phi Beta Kappa, the American Physical Society and the American Mathematics Society.

❖

K. A. Norton (A'29–M'38–SM'43–F'43) was born on February 27, 1907, in Rockwell City, Ia. He received the B.S. degree in physics from the University of Chicago in 1928. During 1929, he was with the Western Electric Co. in Chicago. From 1929 to 1934 he was in the radio section of the National Bureau of Standards. He attended Columbia University from 1930 to 1931, and then joined the technical information section of the F.C.C. from 1934 to 1942.

K. A. NORTON

From 1942 to 1946, he was assistant director of the operational research group and a consultant on radio propagation in the office of the Chief Signal Officer. He also served as a radio and tactical countermeasures analyst in the operational research section of the Eighth Air Force in England. Since 1946, he has been in the Central Radio Propagation Laboratory of the National Bureau of Standards, as chief of the Frequency Utilization Research Section. At present, he is chief of the Radio Propagation Engineering Division at Boulder, Colo.

Mr. Norton has been a delegate to several international radio conferences, including the Provisional Frequency Board at Geneva, Switzerland in 1948, and the High-Frequency Broadcasting Conference at Mexico City in 1948. He was vice-chairman of the U. S. delegation to the 1950 meetings of Study Group 11 of the International Radio Consultative Committee in the United States, France, The Netherlands, and in the United Kingdom. This study group was concerned with television standards. Mr. Norton was a delegate to the eleventh general assembly of URSI at The Hague, Netherlands, in 1954.

In 1954, Mr. Norton was awarded the Stuart Ballantine medal by the Franklin Institute for his work on radio propagation and fm and television frequency allocations.

Mr. Norton is a Fellow of the American Physical Society, and of the American Association for the Advancement of Science; a member of the Scientific Research Society of America, the American Institute of Electrical Engineers, the American Geophysical Union, the American Mathematical Society, the Institute of Mathematical Statistics, and the American Statistical Association.

❖

A. M. Peterson was born at Santa Clara, Calif., on May 22, 1922. He attended San Jose State College from 1939 to 1942 He was associated with the Electronics Group of Sacramento Air Service Command from 1942 to 1944. He was on active duty with the U. S. Army Air Forces from 1944 to 1946. He received the B.Sc. degree in 1948, the M.Sc. in 1949, and the Ph.D. in 1952 from Stanford University. He is at present a Research Associate and Lecturer in the Electrical Engineering Department at Stanford University and a Senior Research Engineer at the Stanford Research Institute.

A. M. PETERSON

Dr. Peterson is a member of Sigma Xi and the Commission 3 of the United States Committee of (URSI).

❖

P. A. Portmann (M'46) was born in Tavannes, Switzerland, on January 29, 1920. He received the B.S. degree from the Massachusetts Institute of Technology in 1947, and the M.S. degree from the University of Maryland in 1951. From 1941 to 1945, he was engaged in the design of microwave standards and microwave measuring equipment at the Sperry Gyroscope Co. Research Laboratories.

P. A. PORTMANN

From 1947 to 1950, at the Naval Research Laboratory, he was engaged with design of automatic microwave measuring instruments and broad band microwave networks. He was associated with the Johns Hopkins University Applied Physics Laboratory and was engaged in the design of microwave components, antennas and radar test equipment from 1950 to 1952. Since 1952, he has been a staff member of the M.I.T. Lincoln Laboratory, where he has been engaged in tropospheric propagation research.

❖

A. J. Poté (A'51–SM'48) was born in Boston, Mass., on February 9, 1904. He received a B.S. degree in electrical engineering from the Massachusetts Institute of Technology in 1926.

From 1927 to 1928, Mr. Poté was head of the Circuits Laboratory at Raytheon Manufacturing Co. where he invented and developed the saturable core voltage regulator. During World War II, he held a senior post with the Radiation Laboratory at MIT where he was prominent in the research and development leading to the loran system of navigation. From 1946 to 1950, as a research fellow in electronics at Harvard University he was assistant director of the cyclotron laboratory.

A. J. POTÉ

After serving as a consultant for radio communication with several study committees for the U. S. Department of Defense, he joined the M.I.T. Lincoln Laboratory in 1952 as head of the communication system design group.

Early this year, Mr. Poté helped organize Hycon Eastern, Inc., in Cambridge, Mass., and he now holds the position of vice-president and chief engineer with that organization.

Mr. Poté is the holder of numerous patents and is a member of Sigma Xi.

❖

W. H. Radford (A'41–SM'45–F'54) was born in Philadelphia, Pa., on May 20, 1909. He received the B.S. degree in electrical engineering from the Drexel Institute of Technology in 1931 and the M.S. degree from the Massachusetts Institute of Technology in 1932. He is at present a member of the faculty of the department of electrical engineering and a division head of Lincoln Laboratory at MIT.

W. H. RADFORD

Professor Radford has been active as a government and industrial consultant on radio communication facilities and specialized electronic applications since 1935. He served as a section member and consultant to the National Defense Research Committee from 1940 to 1943. In 1941, he assisted in establishing the MIT radar school and became associate director in 1944.

At Lincoln Laboratory, Mr. Radford is engaged in the planning and supervision of a substantial portion of a classified air defense research and development program.

He is a registered professional engineer, a Fellow of the American Institute of Electrical Engineers, and of the American Association for the Advancement of Science, and a member of the American Society of Engineering Education, Sigma Xi, Tau Beta Pi, and Eta Kappa Nu.

❖

P. L. Rice (M'52) was born in Washington, D. C. on December 25, 1922. He went to Lawrence College, in Appleton, Wis. in 1941,

and to the Principia College in Elsah, Ill., from 1946 to 1948. He received the B.S. degree in 1948.

P. L. RICE

During World War II he was commissioned at the Yale University Air Force Communications School, and spent eighteen months in Brazil setting up and operating blind-landing systems for aircraft.

In 1948 and 1949 he was employed by the firm of Raymond M. Wilmotte, Inc., in Washington, D. C. Since that time he has been a staff member of the Central Radio Propagation Laboratory of the National Bureau of Standards. He is now with the Tropospheric Propagation Research Section at Boulder, Colo.

❖

R. M. Ring was born in Norwood, Mass., on August 12, 1924. She received the A.B. degree in mathematics from Emmanuel College in 1945, the M.A. degree in mathematics from Boston College in 1947, and the Ph.D. in applied mathematics from Brown University in 1954.

R. M. RING

From 1946 to 1948, she was an instructor in the physics department at Emmanuel College, and from 1948 to 1951, worked as a research assistant in the graduate division of applied mathematics at Brown University. Since 1951, she has been a staff member of the MIT, Lincoln Laboratory.

❖

J. F. Roche (M'52) was born in Lynn, Mass., on July 27, 1923. He received a B.S. degree in electrical engineering from the University of Rhode Island in 1943. From 1943 to 1946, Mr. Roche served with the Signal Corps, primarily with the Radio Propagation Unit. He became a civilian engineer with the Signal Corps in 1946, and was engaged in radio wave propagation studies pertaining to Army communication circuits. In September 1951, he joined Aeronautical Radio Inc., Washington, D. C., as a frequency and radio wave propagation engineer. Since July 1953, he has been a member of the staff of Lincoln Laboratory engaged in radio wave propagation research.

J. F. ROCHE

Mr. Roche is a registered professional engineer in the District of Columbia.

T. F. Rogers (M'50) was born in Providence, R. I., August 11, 1923. He received the B.S. degree in physics from Providence College in January, 1945 and the M.A. degree, also in physics, from Boston University in 1949. From January, 1945, until the end of the war, he was a research associate on the staff of the Radio Research Laboratory, Harvard University, engaged in radar-countermeasures work. For the next year he worked on television circuit design at the Bell and Howell Co. in Chicago.

T. F. ROGERS

Mr. Rogers joined the staff of the Air Force Cambridge Research Center, Cambridge, Mass. in 1946 and has since been associated with this organization. On assignment to Massachusetts Institute of Technology as a staff member in 1950, he assisted in organizing one of the original MIT Lincoln Laboratory groups, and continued as an associate group leader there for some two years. He returned to Cambridge Research Center to assist in forming an Electromagnetic Propagation Laboratory of which he is the assistant head. While at Cambridge and M.I.T. he has done research work on electronic memory devices, ultrasonics, magnetism, molecular spectra, radio communication and electromagnetic propagation.

Mr. Rogers is a member of the American Physical Society, the Physical Society (England), the American Geophysical Union, and the Scientific Research Society of America.

❖

P. J. Short was born on March 2, 1927, in Mangum, Okla. He served with the Air Force from June, 1945 to March, 1947, and then attended the University of New Mexico from September, 1949 to June, 1950. In 1952, he received the B.S. degree in physics from the University of Colorado.

P. J. SHORT

Since 1951, Mr. Short has been engaged in tropospheric propagation research work at the National Bureau of Standards in Boulder, Colo. He is presently doing graduate work in physics at the University of Colorado.

❖

R. A. Silverman (M'54) was born on June 29, 1926, in Boston, Mass. He received his A.B. degree, magna cum laude, from Harvard University in 1946, his M.A. from Columbia in 1948, and his Ph.D. in theoretical physics from Harvard in 1951.

R. A. SILVERMAN

Dr. Silverman worked in solid-state physics at the Philco Corp. from 1951 to 1952. From 1952 to 1955 he was at MIT, first as a staff member of the Lincoln Laboratory, and then as a research associate in the department of electrical engineering. His recent research has been in the fields of statistical communication theory and radio wave propagation. He is now at the Institute of Mathematical Sciences of New York University in the division of electromagnetic research.

He is a member of Phi Beta Kappa, Sigma Xi, and the American Physical Society.

❖

H. Staras (M'50-SM'53) was born in New York, N. Y., on December 24, 1922. He was graduated from the City College of New York with the B.S. degree in January, 1944. After graduation he worked as a junior physicist for the National Advisory Committee for Aeronautics at Langley Field, Va. where he was engaged in the development of electronic instruments for use in aeronautical research. He then entered the Army and served as a Counter-Intelligence Corps officer.

H. STARAS

After separation from active military duty in 1947, Dr. Staras returned to full-time graduate study at New York University obtaining the M.S. degree in physics in 1948.

He joined the Central Radio Propagation Laboratory of the National Bureau of Standards where he was engaged in the study and analysis of the vagaries of tropospheric propagation. During this time, he continued his graduate studies in physics at the University of Maryland, obtaining his Ph.D. degree in 1955. In April, 1954, Dr. Staras joined the Analytical Engineering Group of RCA, Camden where, in addition to continuing his work in scatter propagation, he is engaged in the analysis of automatic detection and tracking for radar applications.

Dr. Staras is a member of the American Physical Society, Sigma XI, and the National Committee of URSI Commission II.

❖

G. R. Sugar (A'45–S'48–A'51–M'53) was born in Winthrop, Mass., on October 12, 1925. He received the B.S. degree in physics

from the University of Maryland in 1950. From 1950 to 1951 he was a graduate assistant at the Institute for Fluid Dynamics and Applied Mathematics, at the University of Maryland where he attended graduate courses in mathematics and electrical engineering and developed electronic, optical, and mechanical instrumentation for a shock tube research program.

G. R. SUGAR

Since 1951 he has been a member of the staff of the Central Radio Propagation Laboratory of the National Bureau of Standards, where he is engaged in experimental research in specific aspects of ionospheric radio propagation.

Mr. Sugar is a member of Sigma Pi Sigma and Phi Kappa Phi.

❖

W. H. Tidd (SM'45) was graduated from Cornell University in 1929 with a degree in Electrical Engineering, and at once joined the Development and Research Department of A.T.&T., where he was engaged in the development of carrier telephone systems. With the merger of the Development and Research Department with the Bell Telephone Laboratories in 1934, this work was continued. It included the design and development of cable carrier, open-wire carrier, and coaxial systems, and field tests in connection with them.

W. H. TIDD

During the war he was engaged in the development of radio countermeasures equipment for the Signal Corps. After the war he returned to carrier telephone work, specializing in development of transmission testing equipment. Currently he is interested in investigations of extended range radio propagation and the engineering of military radio communication systems.

❖

M. C. Thompson, Jr. was born March 19, 1923, in Punxsutawney, Pa. After receiving the B.E.E. degree from Cornell University in 1944, he worked at the Naval Ordnance Laboratory, Washington, D. C., and later with the Stromberg-Carlson Co., Rochester, N. Y., and the Standard Oil Company of Ohio, Cleveland, Ohio. In July, 1947, he joined the National Bureau of Standards, X-ray Section, Washington, D. C. He transferred in 1949 to the Sound Section and in 1952 to the Tropospheric Propagation Research Section of the Bureau. In 1950, he received the M.S. in physics and in 1952 the Ph.D. in physics from the Catholic University of America, Washington, D. C.

M.C. THOMPSON, JR.

Dr. Thompson has taught in the electrical engineering departments of Cornell University and the University of Colorado, Boulder, Colo. He is a member of Sigma Xi, Tau Beta Pi, and Eta Kappa Nu.

❖

L. G. Trolese (A'42–SM'47) was born in Sonora, Calif., in 1908. He received the B.S. degree in electrical engineering from the University of California in 1930. He was associated with the RCA Victor Co. for a year and with the General Air Conditioning and Heating Co. for five years.

L. G. TROLESE

From 1936 to 1949, he was affiliated with the Navy Electronics Laboratory where he was engaged in wave propagation research and radar development. He is now with Smyth Research Associates where he is a member of the board of directors.

Mr. Trolese is a member of Commission II of the U.S.A. national committee of URSI, and is a registered professional engineer in California.

❖

O. G. Villard, Jr., (S'38–A'41–SM'51) was born at Dobbs Ferry, N. Y., on September 17, 1916. He received the B.A. degree from Yale University in 1938, and the E.E. and Ph.D. degrees from Stanford University in 1943 and 1949, respectively.

O. G. VILLARD

Dr. Villard has been a member of the staff of the Department of Electrical Engineering at Stanford University since 1941, with the exception of the years 1942 to 1946 when he served as a special research associate at the Radio Research Laboratory, Harvard University.

He is now a professor of electrical engineering and is engaged in research and in undergraduate instruction. He is a member of Sigma Xi and Phi Beta Kappa, and the U.S.A. Commission 3 of the International Scientific Radio Union.

❖

F. M. H. Villars was born in Biel-Bienne, Switzerland, in 1921. He received the D.Sc. degree from the Federal Institute of Technology in Zurich in 1946, and remained at Zurich for three years as a research assistant.

In 1949, Dr. Villars came to America and studied for one year at the Institute for Advanced Study in Princeton. Since 1950, he has been at MIT. He served two years as a research associate. became an assistant professor in 1952, and in July, 1955 was made an associate professor. His research subjects are quantum electrodynamics and nuclear physics.

F. M. H. VILLARS

❖

L. E. Vogler was born in Yuma, Ariz., on February 28, 1926. He received the B.S. degree from the University of Oregon in 1946. Following graduation, he served with the armed forces and received his discharge in 1947.

L. E. VOGLER

Mr. Vogler was a graduate student at the University of Washington from 1947 to 1948. He then transferred to Oregon State College for a year of graduate work in 1949.

Since 1952, he has been with the Tropospheric Propagation Research Section at the National Bureau of Standards Laboratories in Boulder, Colo.

❖

J. B. Wiesner (S'36–A'40–SM'48–F'52) was born in Detroit, Mich., in 1915. He received the B.S. degree in 1937, and a year later, the M.S. degree, both from the University of Michigan. In 1950, he was awarded his Ph.D. degree from the same university.

J. B. WIESNER

From 1940 to 1942, Dr. Wiesner was chief engineer of the Library of Congress. In 1942, he was appointed as a staff member of the MIT Radiation Laboratory, and in 1945, joined the University of California Los Alamos Laboratory.

He is presently a professor of communications engineering at MIT, director of the Research Laboratory of Electronics, and a member of the Lincoln Laboratory staff.

He is a member of Sigma Xi, Phi Kappa Phi, Eta Kappa Nu, and the Acoustical Society of America.

❖

V. F. Weisskopf was born in Vienna, Austria, in 1908. He received his doctorate degree in 1931 from the University of

Göttingen in Germany. After completing one year as a research assistant at the University of Berlin. he was awarded a fellowship in Copenhagen, Denmark by the Rockefeller Foundation.

V. F. WEISSKOPF

From 1933 to 1937, Dr. Weisskopf was a research associate at the Federal Institute of Technology in Zurich, and later, at the University of Copenhagen.

He left Europe in 1937 and taught at the University of Rochester until 1943. During the war, he was a group leader in the Manhattan District at Los Alamos. He has been a professor at MIT since 1946.

His research work has included studies in theoretical physics, physics of elementary particles, and the structure of the nucleus.

P. I. Wells (A'54) was born in Onawa, Ia., on March 8, 1925. During World War II he attended State Teachers College, Maryville, Mo. on the Navy V-12 program. He received the B.S.E.E. degree from the University of Missouri in 1949.

P. I. WELLS

During 1949 and 1950 Mr. Wells was with the Naval Research Laboratory, Washington, D. C. While at NRL he did circuit development applied to facsimile communications. Since 1950 he has been associated with the Tropospheric Propagation Research Section, Central Radio Propagation Laboratory, National Bureau of Standards. At present he is engaged in special instrument development associated with propagation studies.

A. D. Wheelon was born in Moline, Ill., on January 18, 1929. He received the B.S. degree in engineering science from Stanford University in 1949. He was a teaching fellow in the physics department of MIT until 1952, when he received the Ph.D. degree in physics. He was also a research assistant in the Laboratory of Electronics.

A. D. WHEELON

He worked on missiles systems at the Douglas Aircraft Co. for one year, and then joined the Research Laboratory of the Ramo-Wooldridge Corp. He has worked primarily on electromagnetic propagation and scattering, and on nonlinear filters and applied mathematics.

Dr. Wheelon is a member of the American Physical Society and Sigma Xi.

IRE News and Radio Notes

Washington Symposium on Scatter Techniques Meets February 28 and 29

A symposium on "Communication by Scatter Techniques" will be held in Washington, D. C., November 14 and 15. The symposium will be sponsored by the IRE Professional Group on Antennas and Propagation, the IRE Professional Group on Communications Systems, and George Washington University.

The technical program, which is to be held in Lisner Hall at George Washington University, will include four sessions. The first will be devoted to propagation mechanisms. Spokesmen on auroral, tropospheric, ionospheric, and meteoric ionization propagation will discuss the mechanics of each of these modes of transmission. The remaining three sessions of the program will include practical and descriptive discussions concerning communication systems, antennas, and propagation studies.

On the evening of November 14, Allen B. Dumont will address a combined meeting of symposium visitors and the IRE Washington Section on commercial aspects of scatter techniques.

Chairman of the Steering Committee is Kenneth S. Kelleher, Melpar, Incorporated, and Chairman of the Technical Program Committee is John J. Renner, Jansky and Bailey.

Advance registration fee will be $2.50. Registration should be made, before October 31, by mailing check or money order to Scatter Symposium, George Washington University, School of Engineering, Washington 6, D. C. Please be sure to include your return address. Members wishing to attend are requested to make their own hotel reservations.

Scintillation Counter Symposium To Meet In February

Plans are now being formulated for the Fifth Scintillation Counter Symposium which will be held in Washington, February 28 and 29. The symposium is sponsored by the National Bureau of Standards, American Institute of Electrical Engineers, and the P.G. on Nuclear Science.

Topics tentatively selected for discussion are Multipliers and Circuitry, Scintillators, Spectroscopy and Particle Identification, and Special Problems and Techniques. Those wishing to contribute papers please write J. B. Horner Kuper, Ch., Program Planning Brookhaven National Laboratory, Upton, L.I., New York.

Eisenhower Appoints Quarles New Secretary of Air Force

Donald A. Quarles, IRE Fellow, has been made Air Force Secretary by Pres. Eisenhower. Prior to his appointment Mr. Quarles was Assistant Secretary of Defense in Charge of Research and Development.

D. A. Quarles

On joining the government, Mr. Quarles resigned as President of Sandia Corporation, a subsidiary of Western Electric of which he was a Vice-President. Previously, he had been with the Bell Telephone System, where, in 1947 he was appointed a Vice-President, a post he kept until joining Sandia in 1952.

Final Call for Papers

IRE National Convention, March 19–22, 1956

Prospective authors are requested to submit all of the following information:
(1) 100-word abstract in triplicate with title, name and address of author.
(2) 500-word summary in triplicate with title, name and address of author.
(3) Indicate the technical field in which your paper falls:

Aeronautical & Navigational Electronics
Antennas & Propagation
Audio
Automatic Control
Broadcast & Television Receivers
Broadcast Transmission Systems
Circuit Theory
Communications Systems
Component Parts
Electron Devices
Electronic Computers
Engineering Management
Industrial Electronics
Information Theory
Instrumentation
Medical Electronics
Microwave Theory & Techniques
Nuclear Science
Production Techniques
Reliability and Quality Control
Telemetry & Remote Control
Ultrasonics Engineering
Vehicular Communications

Deadline for acceptance of papers: November 4, 1955

Address all material to: Russel R. Law
1955 Technical Program Committee
Institute of Radio Engineers, Inc.
1 East 79 Street, New York 21, N. Y.

Calendar of Coming Events

International Analogy Computation Meeting, Société Belge des Ingenieurs des Télécommunications et d'Electronique, Brussels, Belgium, Sept. 27–Oct. 1.
National Electronics Conference Hotel Sherman, Chicago, Ill., October 3–5
Audio Engineering Society Convention, Hotel New Yorker, New York City, Oct. 12–15
Second Symposium on Vacuum Technology, Mellon Inst., Pittsburgh, Pa., Oct. 13–15
IRE-RETMA Radio Fall Meeting, Hotel Syracuse, Syracuse, N. Y., Oct. 17–19
Conference On Electrical Insulation, Pocono, Pa., Oct. 17–19
Eighth Annual Gaseous Electronics Conference, General Electric Res. Lab., Schenectady, N. Y., Oct. 20–22
PG on Electron Devices Annual Technical Meeting, Shoreham Hotel, Washington, D. C., Oct. 24–25
GAMM and NTG-VDE International Conference on Electronic Digital Computers, and Data Processing, Darmstadt, Germany, Oct. 25–27
IRE East Coast Conference on Aeronautical and Navigational Electronics, Lord Baltimore Hotel, Baltimore, Md., Oct. 31–Nov. 1.
Symposium on Applied Solar Energy, Westward Ho Hotel, Phoenix, Ariz., Nov. 1–5
Kansas City Section Electronics Conference, Kansas City, Kansas, Nov. 3–4
IRE-AIEE-ACM Eastern Joint Computer Conference, Hotel Statler, Boston, Nov. 7–9
IRE—George Washington University Symposium on Communications by Scatter Techniques, Lisner Hall, George Washington U., Washington, D. C., Nov. 14–15
IRE-AIEE-ISA Electrical Techniques in Medicine and Biology, Shoreham Hotel, Washington, D. C., Nov. 14–16
Society for Experimental Stress Analysis National Meeting Sheraton Hotel, Chicago, Ill., Nov., 16–18
IRE-PGCS Symposium on Aeronautical Communications—Civil and Military; Utica, New York, Nov. 21–22
PGI and Atlanta Section Data Processing Symposium, Hotel Biltmore, Atlanta, Ga., Nov. 28–30
Engineers Joint Council Nuclear Engineering and Science Congress, Cleveland, Ohio, Dec. 12–16
IRE-ASQC Second National Symposium on Reliability and Quality Control, Hotel Statler, Washington, D. C., Jan. 9–10
IRE National Simulation Symposium, Dallas, Tex., Jan. 19–21
IRE Symposium on Microwave Theory and Techniques, U. of Pennsylvania, Philadelphia, Pa., Feb. 2–3
IRE Annual Southwestern Conference, Oklahoma City, Okla., Feb. 9–11
IRE-AIEE Scintillation Counter Symposium, Shoreham Hotel, Washington, D. C., Feb. 28–29

Harvard To Develop Radio Telescope for Solar Research

Development and construction of a radio telescope for solar research has recently been announced by Donald H. Menzel, Director of Harvard College Observatory. This radio telescope, technically known as the dynamic spectrum analyzer, will be used to further knowledge of the sun by studies of the radio emission from active sunspots and other solar disturbances.

The radio telescope will consist of an antenna 28 feet in diameter, used in conjunction with highly sensitive receivers, which scan the frequency range from 100 to 600 megacycles at the rate of ten times per second. The first of its type in this country, the radio telescope should surpass all equipment now existing in other countries. Henry Jasik will serve as electronics consultant to the project and will be responsible for carrying out the antenna development in his laboratory. The parabolic reflector and its equatorial mounting will be constructed by the D. S. Kennedy Co. of Cohasset, Mass. The high performance, frequency-scanning receivers will be constructed by the Airborne Instruments Laboratory.

The equipment will be placed in operation at the Upper Air Research Observatory at Sacramento Peak, New Mexico in the early part of 1956. This observatory, a joint operation of Harvard and the Air Force, is now devoted largely to optical observations of the sun with coronagraphs and other specialized optical instruments. Addition of the radio instruments will be used to supplement the present optical observations. Financial support of the project has been provided by the Geophysical Directorate of the Air Force Cambridge Research Center.

The astronomer who will be in charge of the solar radio telescope will be Alan Maxwell, lately of the Jodrell Bank Experimental Station of the University of Manchester, England, who joined the Harvard College Observatory scientific staff in August. Richard N. Thomas, of the observatory staff, will direct the project in conjunction with Dr. Menzel.

Terhune Made Fellow of the Standards Engineers Society

H. R. Terhune, Manager of Standards and Components at Federal Telecommunication Laboratories, Nutley, N. J., a division of International Telephone and Telegraph Corporation, has been elected a Fellow of the Standards Engineers Society, national organization of standards engineers. Formal presentation of the award was made at the Standard Engineers' annual convention on September 30 in Hartford, Connecticut.

H. R. Terhune

Mr. Terhune, was one of the society's founders and has been active in its affairs since 1947. He was formerly editor of the organization's publication, *Standards Engineering*, and is now serving as Chairman of the Rules Committee and Treasurer of the New York Section.

Prior to his association with FTL, Mr. Terhune was Vice-President of Engineering for the Mycalex Corporation of America and Manager of the Electrical Standards Section of the RCA Victor Division. He was given special recognition by the American Standards Association for his work in formulating U. S. military standards during World War II. He is a Senior Member of the IRE, a member of the Montclair Society of Engineers, and the American Ordnance Association.

Dinner Honors W. C. White of General Electric

William C. White, consulting engineer for the General Electric Company research laboratory, retired this spring after serving with the company 43 years. At a dinner given in his honor he was lauded by Albert W. Hull, GE scientist, who said Mr. White "as much as any man was responsible for the beginning of GE's electronics tube activities." Other speakers included Lawrence A. Hawkins, master of ceremonies, who recently retired as executive engineer of the Research Laboratory, and John H. Payne, scientist Knolls Atomic Power Laboratory.

A native of Brooklyn, Mr. White was graduated from Columbia in 1912 and joined GE the same year. Throughout his career he was actively engaged in electronic tube developments. In 1930 he was appointed head of the vacuum tube engineering department. Twelve years later he became engineer of the electronics laboratory, and in 1944 he was named electronics engineer of the GE research laboratory.

A Fellow of the IRE, he also has served as Treasurer and on the Board of Directors. Mr. White has served as Chairman of the Board for the National Electronics Conference, is a fellow of the American Institute of Electrical Engineers. He also holds the Columbia University medal for excellence, awarded him in 1948.

Dr. Albert W. Hull (*standing*) was principal speaker at a dinner honoring W. C. White (*left*) who retired this spring after 43 years of service with the General Electric Company. In the center is Lawrence Hawkins who recently retired as executive engineer of the General Electric Research Laboratory.

OBITUARY

Ralph S. Hayes (J'15–A'18–VA'39), U.S.N.R., died suddenly on June 9.

Captain Hayes was born in Germantown, Philadelphia, and was graduated from Germantown Friends School, Phillips Exeter Academy, Dartmouth College, and Massachusetts Institute of Technology. He served in the United States Navy during World War I and remained active in the organized Naval Reserve thereafter.

Recalled to active duty in 1939, he served in the Navy throughout World War II, attaining the rank of captain. For this service he was awarded a commendation by the Secretary of the Navy.

Captain Hayes joined the Bell Telephone Company in 1922 and, except for the period of his World War II Naval service, was associated with that organization until 1952 when he retired with 30 years service. At one time he had been head of the company's Transmission School. At retirement he was inventory and costs engineer.

He was a member of the Telephone pioneers of America, the Franklin Institute, and the Retired Officers Association.

TECHNICAL COMMITTEE NOTES

The **Electronic Computers** Committee met at IRE Headquarters on July 18 with Robert Serrell presiding. The committee discussed and amended the proposed *Standards on Electronic Computers: Definitions of Electronic Computer Terms*. This standard will be completed and approved at the next committee meeting.

Chairman J. E. Ward presided at a meeting of the **Feedback Control Systems** Committee on August 4 at the MIT Faculty Club. Mr. Ward reported on the acceptance of 55 IRE 26. PS1, proposed *Standards on Graphical and Letter Symbols for Feedback Control Systems* at the June 9 meeting of the Standards Committee. The chairman prepared and submitted final copies of the figures, and has been informed that the standard is scheduled for printing in the November issue of the PROCEEDINGS. The remainder of the meeting was devoted to discussing and amending the proposed *Standard on Terminology for Feedback Control Systems*, which will be submitted for final approval at the next meeting of the Standards Committee.

Books

Electronische Halbleiter by E. Spenke

Published (1955) by Springer-Verlag, Reichpietschufer 20, Berlin W 35, Germany. 368 pages+xx pages+10 page index. Illus. 6¼×9¼.

I was brought up in solid state physics on a varied collection of almost good books that never quite covered the things I wanted to know most. At last an adequate text on semiconductors, Spenke's "Electronische Halbleiter," appears. This is a comprehensive treatment of the basic theory of semiconductors and its application to transistors and rectifiers.

A less ambitious author under the shield of the subtitle "Introduction to the Physics of Rectifiers and Transistors" would have tossed off a few physical analogies and half-hearted derivations connected with the underlying physics, in order to get on with the main business of device operation. Not so Spenke. Here we find a thorough review of band theory using the standard approach, conduction and transport mechanisms, Fermi statistics, relaxation time, lifetime, impurity states, all excellently integrated into the general story of solid state devices.

He has not limited his discussion to germanium and silicon, in spite of the fact that these are the "wonder boys" of the present. There are many references to compound semiconductors and the older arts of selenium and copper oxide rectifiers. Thus the advanced student gets a balanced picture of the field.

If Spenke had been more ambitious still, he might have pushed his theoretical discussion to the point where the newer developments in band theory such as non-spherical energy surfaces would become more understandable. Even so, the student can't ask for everything. Already this book is far ahead of the "good old days."

ARNOLD MOORE
RCA Laboratories
Princeton, N. Y.

Approximations for Digital Computers by Cecil Hastings, Jr. with Jeanne T. Wayward and James P. Wong, Jr.

Published (1955) by Princeton University Press, Princeton, N. J. 201 pages+vii pages. 9¼×6¼. $4.00.

This book contains two sections. The first section includes a discussion of such topics as best fit, linear weights, solution of equations, Tchebycheff polynomials, notes of convergence, choice of form, etc. Each topic is well illustrated by examples with brief and sometimes humorous personalized text. The second section consists of polynomial approximations of twenty three often used functions. Approximations are given to various precision limits. Each approximation is accompanied by a carefully drawn error curve and a comment as to the use of the approximation. The error curves are sometimes given in absolute value and at other times in relative value.

The approximations have been available in a very limited distribution for a few years, but have already been widely used in the computing field. All users of computing machines are anxious to reduce the size of a program, the number of instructions executed, and the corresponding computing time. The numerical methods previously used were series expansion or table look-up with various degrees of interpolation. Mr. Hastings' approximations require a minimum of computing and storage space in a stored program machine, and are, therefore, very valuable.

The book is not complete in that it does not describe other methods of approximation and curve fitting which are sometimes useful. The best fit as defined and used by Mr. Hastings produces the minimum of the absolute deviation.

This book should be available to and read by all engineers who have the opportunity of working with digital computing machines.

G. T. HUNTER
IBM Corporation
New York City

RECENT BOOKS

Automatic Record Changer Service Manual with Tape Recorder Service Data, Howard W. Sams and Co., Inc. 2201 East 46 St., Indianapolis 5, Ind. $3.00.

Ball, John, and Williams, Cecil B., *Report Writing*. The Ronald Press Co., 15 East 26 Street, New York 10, N.Y. $4.75.

Beitman, M. N., compiler, *Additional 1955 Television Servicing Information*, Supreme Publications, 1760 Balsam Road, Highland Park, Illinois. $3.00.

Hickey, Henry V., and Villines, William M., *Elements of Electronics*, McGraw-Hill Book Company, Inc., 330 West 42 St., N.Y. 36, N.Y. $5.00.

Knight, Stephen A., *Fundamentals of Radar*, Pitman Publishing Corp., 2 West 45 St., New York 19, N.Y. $3.00.

Picture Book of TV Troubles: Vol. Four, Automatic Gain Control Circuits, John F. Rider Publisher, Inc., 480 Canal St., New York 13, N.Y. $1.80.

Proceedings of the Symposium on Information Networks, Polytechnic Institute of Brooklyn, 99 Livingston St., Brooklyn 1, N.Y. $5.00.

Proceedings of the Symposium on Printed Circuits, Engineering Publishers, GPO Box 1151, New York, N.Y. $5.00.

Renne, Harold S., *Atomic Radiation Detection and Measurement*, Howard W. Sams and Co., Inc., 2201 East 46 St., Indianapolis 5, Ind. $3.00.

Saunders, Albert C. W., *Color Television for the Service Technician*, Howard W. Sams and Co., Inc., 2201 East 46 St., Indianapolis 5, Ind.

THE EAST COAST CONFERENCE ON AERONAUTICAL AND NAVIGATIONAL ELECTRONICS

WASHINGTON, D. C.

OCTOBER 31 AND NOVEMBER 1

October 31

10:00 a.m.–12:00 noon
Chesapeake Lounge

ANTENNAS AND RADOMES

Moderator: Harald Schutz, Glenn L. Martin Co.

"A Pencil Beam Cosecant Squared Ferrite Antenna Using No Moving Parts," Tore N. Anderson, Airtron, Inc.

"A Microwave Antenna Feed for Circular Polarization," E. G. Shelor, Bendix Radio Division.

"Techniques for the Mechanical Scan of Flush-Type Antennas," W. Cox, Glenn L. Martin Co.

"A Solution of the Beam Synthesis Problem for Circular Arrays," D. A. Cope, Glenn L. Martin Co.

"Alternate Solutions to Broad Band Radome Problems," F. Cunningham and K. Tomkawa, Glenn L. Martin Co.

10:00 a.m.–12:00 p.m.
Caswell Room

TESTING TECHNIQUES

Moderator: Ray Wells, Aircraft Armaments, Inc.

"A Wide Bandwidth Measurement Technique," R. Strazzulla, Sperry Gyroscope Co.

"Determination of Noise Level in Radar Receivers—Superheterodyne and T.R.F.," Donald W. Haney, Glenn L. Martin Co.

"Design of a Stabilized Turntable for Testing Integrating and Rate Gyroscopes," P. G. Spink, Westinghouse Electric Corp.

"A Measuring Set for MTI Radar Evaluation," B. F. McCall, Bendix Radio Division.

"An Evaluation of Automatic Performance Testing of Airborne Electronic Equipment," Lester E. McCabe, General Electric Co.

1:30 p.m.–4:30 p.m.
Caswell Room

SYMPOSIUM—COMPARISON OF DESIGN FEATURES REQUIRED FOR MILITARY AND CIVIL AIRBORNE EQUIPMENTS

Moderator: N. Caplan, Bendix Radio Division.

This subject will be discussed by an 8 man panel of scientists and engineers from military and civilian organizations.

November 1

9:00 a.m.–12:00 noon
Caswell Room

AIRBORNE NAVIGATION EQUIPMENT

Moderator: D. M. Allison, Bendix Radio Division.

"Private Flyer TACAN," N. H. Young, Federal Telecommunication Labs.

"Airborne Transponder Unit," V. Johnson, Federal Telecommunication Labs.

"A Subminiature Automatic Direction Finder," E. B. Moore, H. H. Benning, A. Noyes, Aircraft Radio Corp.

"Design Features of Computer Set, Navigational, AN/ASN-7," S. Frangoulis, Ford Instrument Co.

"The Operational Problems of Airborne Radar and the Training Methods of Flight Crews Using This Equipment," M. E. Balzer, United Airlines

"Navigation and Traffic Control with Black Boxes," H. Davis and, F. Moskowitz, Rome Air Development Center.

"Recent Developments in the Simulation of Terminal Area and En Route Area Traffic Control Problems," Tirey K. Vickers, CAA Technical Development & Evaluation Center. Roger S. Miller, Franklin Institute.

9:00 a.m.–12:00 noon
Chesapeake Lounge

CIRCUIT DESIGN TECHNIQUES

Moderator: C. E. McClellan, Westinghouse Electric Corp , Air Arm Division.

"Video Pulse Stretching Using Artificial Delay Lines, Stephen N. Broady, Westinghouse Electric Corp., Air Arm Division.

"Line-Type Pulse Generator Circuit Analysis and Design by Analogue Computer Techniques," M. Gray and S. Baida, Westinghouse Electric Corp., Air Arm Division.

"Spurious Suppression Techniques in a Modern VHF Airborne Transmitter," R. B. Seals, Collins Radio Co.

"Beam Deflection Tube Helps to Simplify ADF for Private Aircraft," J. M. Tewksbury, Bendix Radio Division.

"Transistor Circuits," T. L. Slater, Farnsworth Electronics Co.

"Transistorized Voltage Regulators," Gentry L. Shelton, General Electric Co.

"Optimum Signal-Noise Ratio and Effect of Signal Pulse Width on Signal Detectability," Stephen E. Bederka, General Electric Co.

2:00 p.m.–4:30 p.m.
Caswell Room

RELIABILITY AND COMPONENTS

Moderator: William Bender, Glenn L. Martin Co.

"NRL Vortex Thermometer," Robert E. Ruskin, Naval Research Lab.

"A Comparison of the Thermal Efficiencies of Subminiature Tube Shields Using a New Method of Measurement," L. C. Calhoun, Westinghouse Electric Corp., Air Arm Division.

"Reliability Through Redundancy," R. Hershey, Sperry Gyroscope Co.

"Automatic Component Assembly System," Earl W. Siegel, General Electric Co.

"Long Life Performance of Filamentary Subminiature Tubes," M. Bassett and R. J. E. Whittier, Raytheon Manufacturing Co.

"Contributing to Reliability Through Heat Transfer Without Blowers in a Pressurized Piece of Airborne Electronic Equipment," J. A. Hohos, Melpar, Inc.

"The Effect Upon Calculated Reliability of Errors in Field Malfunction Data," Mark H. Smith, Sperry Gyroscope Co.

2:00 p.m.–4:30 p.m.
Chesapeake Lounge

SYSTEMS

Moderator: S. W. Herewald, Westinghouse Electric Corp., Air Arm Division

"Integrated Instrument System," C. Fragola and, C. Hecker, Sperry Gyroscope Co.

"NAVATEC—The Practical Combination of Navigation Techniques," Hugh J. Galbraith, Wright Air Development Center.

"Homing Systems for Slow Aircraft," L. P. Reiche, Stanford Res. Inst.

"Rate Gyroscope Characteristics Required for Modern Fire Control Systems," R. Hauser and G Shumway, Westinghouse Electric Corp., Air Arm Division.

"An Improved Medium-Range Navigation System for Aircraft," C. G. McMullen, Bendix Radio Division.

"Rotor Modulation in Typical Helicopter Communication and Navigation Systems," R. B. Battelle, Stanford Res. Inst.

"Precision Aerial Mapping Using Radio Phase Comparison Techniques," Joseph T. Bradbury, Raydist Navigation Corp

EASTERN JOINT COMPUTER CONFERENCE

HOTEL STATLER, BOSTON, MASSACHUSETTS
NOVEMBER 7, 8, 9, 1955

Monday, November 7

Morning

GENERAL SESSION

Chairman: Irven Travis, Vice-President, Burroughs Corporation.

Keynote Speaker: J. G. Brainerd, Director, Moore School of Electrical Engineering, University of Pennsylvania.

Address: John S. Coleman, President, Burroughs Corporation.

Afternoon

THE ROLE OF COMPUTERS IN BUSINESS

Chairman: Harry T. Larsen, Ramo-Wooldridge Corp.

"Computers in Basic Business Applications," F. J. Porter, Consolidated Edison Company.

"Operations Control with an Electronic Computer," Benjamin F. Butler, General Electric Company.

Evening

COCKTAIL PARTY AND RECEPTION

Tuesday, November 8

Morning

CARDS, TAPES AND OTHER RECORDS IN ELECTRONIC ACCOUNTING SYSTEMS

Chairman: E. L. Harder, Director, Analytical Section, Westinghouse Electric Corporation.

"Manual Use of Automatic Records," Anthony Oettinger, Harvard University Computation Laboratory.

"Evaluation of Sorting Methods," James C. Hosken, A. D. Little, Inc.

"Document Processing," R. H. Gregory, Massachusetts Institute of Technology.

Afternoon

TRENDS IN SYSTEM DESIGN

Chairman: Alston Householder, Senior Mathematician, Oak Ridge National Laboratory.

"The Computer and its Peripheral Equipment," N. Rochester, International Business Machines Corp.

"Computers with Remote Data Input," Edward L. Fitzgerald, duPont Company.

"Developments in Programming Research," Charles W. Adams, Westinghouse Electric Corp.

"Storage and Retrieval of Information," Louis N. Ridenour, Lockheed Aircraft Corp.

Wednesday, November 9

Morning

COMMUNICATION AND COMPATIBILITY AMONG ELECTRONIC COMPUTERS IN BUSINESS AND INDUSTRIAL USE

Chairman: to be announced.

"The Role of Communications Networks in Digital Data Systems," R. C. Matlack, Bell Telephone Laboratories

"Standardization of Computer Intercommunication," H. R. J. Grosch, General Electric Company.

Statements from Manufacturers on Standardization of Magnetic Tape Records.

Luncheon Meeting

Chairman: J. H. Felker, Radio Development Engineer, Bell Telephone Laboratories.

"Implementing an Industry Wide Standardization Program," W. R. G. Baker, General Electric Company.

Conference Summary, Jay Forrester, Massachusetts Institute of Technology.

Abstracts of IRE Transactions

The following issues of *Transactions* have recently been published, and are now available from the Institute of Radio Engineers, Inc., 1 East 79 Street, New York 21, N. Y. at the following prices. The contents of each issue and, where available, abstracts of technical papers are given below.

Sponsoring Group	Publication	Group Members	IRE Members	Non-Members*
Aeronautical and Navigational Electronics	Vol. ANE-2, No. 2	$1.55	$2.30	$4.65
Antennas and Propagation	Vol. AP-3, No. 3	$2.05	$3.10	$6.15
Electron Devices	Vol. ED-2, No. 3	$1.10	$1.65	$3.30
Microwave Theory and Techniques	Vol. PGMTT-3, No. 4	$1.60	$2.40	$4.80
Nuclear Science	Vol. NS-2, No. 1	$0.55	$0.85	$1.65
Telemetry and Remote Control	Vol. TRC-1, No. 2	$0.95	$1.40	$2.85

* Public libraries and colleges may purchase copies at IRE Member rates.

AERONAUTICAL AND NAVIGATIONAL ELECTRONICS

VOL. ANE-2, NO. 2, JUNE, 1955

Report—Recent PGANE meetings

Elements of the Air Traffic Control Problem
—P. C. Sandretto

This paper's object is to convey broad outlines of the air traffic control problem and various solutions proposed. Problem is defined as procedure of providing safe and expeditious flow of air traffic. Since aircraft are essentially constant speed devices, control is not possible by varying speed of aircraft, but rather must be attained by preventing aircraft from flying into each other, under all weather conditions, without in any way impeding their progress to destinations. Paper points out roles played in air traffic control by type of legal provisions governing flight; by dispositions of airports around metropolitan centers; by landing acceptance rate of airports; by surface movement capacity of airports; and by technical capabilities of instrument low approach and landing aids. Other factors considered are collision warning devices, approach and departure scheduling, and the whole concept of airways.

An Analytic Approach Toward Air Traffic Control—L. J. Fogel

The impending increase in magnitude and complexity of the air traffic control problem makes it necessary to consider a general formulation which would provide the basis for the analysis and evaluation of newly designed equipments or systems. Comparison of the qualities of pictorial and symbolic models leads to a direct analogy which permits aircraft motion to be considered as communication. Various aspects of the symbolic-communication model are then indicated. These include the application of the extended sampling theorem for airpath definition and the discrete probability distribution for establishing the minimum flight safety criterion as well as a measure for air path tracking efficiency in terms of successful mission accomplishment. The purpose of this paper is to stimulate the development of a general analytic technique which would act as a common language for both operations and laboratory personnel and, in this manner, aid in the future development of safe and efficient systems for air traffic control.

A System Plan for Air Traffic Control Embodying the Cursor-Coordinated Display—W. O. Arnold and R. R. Hoefle

This paper describes a system plan for utilizing radar as a primary source of position information for the control of air traffic. Through the specific arrangements suggested, this information is integrated with certain additional flight control data so as to present the controller with a coordinated picture of the air traffic situation in his area. The composite picture for each control area or sector is presented by means of 2 two-dimensional displays which have one dimension in common and are coordinated through the use of a movable cursor. The resulting presentation is known as the Cursor-Coordinated Display.

An air traffic control system performs three fundamental functions that are common to all control systems; namely, information processing, decision making, and effecting. Of these, only the decision-making function requires human intelligence. The efficiency of a manual air traffic control system is directly related to the proportionate amount of time the controller can devote to this paramount function of decision making. It is, therefore, a fundamental requirement that the system gather, process, and display the necessary information in the manner most useful to the controller in decision-making. The Cursor-Coordinated Display accomplishes this through the application of certain fundamental human engineering and industrial design principles.

The general plans and requirements of a system for controlling air traffic, together with its associated displays and equipment, are presented. The plans are set forth in a manner which will permit a smooth transition from the present manual posting methods to a fully coordinated automatic future system of air traffic control.

Notes on the Flow of Scheduled Air Traffic—R. B. Adler and S. J. Fricker

Some of the effects upon air traffic of scheduling the aircraft and of controlling them en route are presented quantitatively in this report in the form of theoretical studies of four problems: (1) relations between the random en route deviations of aircraft from their schedules, and the resulting stack and total delays; (2) effectiveness of a single en route control point when (a) it reschedules the aircraft in an attempt to reduce terminal congestion; (b) it attempts to bring each plane back onto its original schedule; (3) congestion caused by relaxing the schedule; (4) effect of a sudden shutdown of the terminal. The limiting cases of random arrival and continuous control are discussed briefly, and some aspects of multipoint discrete en route control are treated.

Numerical analysis, using IBM punched-card machines, is employed extensively in the first three problems. The fourth problem has been simplified enough so that purely analytic methods could be applied. It is presented merely for comparison purposes.

Problems and Applications of the ATC Radar Beacon System—T. K. Vickers and D. S. Crippen

This paper describes the characteristics of the new ATC radar beacon system. It discusses the operational problems caused by target overlaps, airborne antenna shadowing, secondary radar reflections, sidelobe interrogations and interference, together with some of the methods proposed for alleviating these difficulties. The paper points out specific applications of the beacon system, including its ability to extend radar coverage, to provide continuous target tracking through heavy clutter, to filter the controller's traffic display, and to provide identity for specific aircraft targets in the traffic situation.

Current RTCA Studies which Concern Air Traffic Control.—L. M. Sherer

In a narrow sense, a definition of an Air Traffic Control study probably would be confined to procedures and equipments used solely for take-off, en route navigation, approach, landing and taxiing. In a broader sense, however, Air Traffic Control can be considered to include all means of increasing accuracy and the scope of application of any electronic device employed in aeronautical operation. The Radio Technical Commission for Aeronautics (RTCA) is currently conducting nearly a dozen technical studies relating to one or the other of the above categories. The majority of RTCA's studies are performed by Special Committees. This presentation, therefore, comprises a summary statement of the current status of the activities of those Special Committees whose work relates either directly or indirectly to Air Traffic Control.

Special Committee 54 (SC54) "Operational Analysis of the Need for and Use of Course Line Computers and Pictorial Displays in Air Traffic Control"
Special Committee 56 (SC56) "Implementation of the VHF Utilization Plan and Review of Transition Period Communication Requirements"
Special Committee 57 (SC57) "High Altitude Grid Plan for VOR/DME Frequency Pairing"
Special Committee 62 (SC62) "Re-evaluation of VOR Airways Lateral Separation Procedures"
Special Committee 63 (SC63) "Helicopter Air Navigation, Communication and Traffic Control"
Special Committee 64 (SC64) "Radar Safety Beacons"
Special Committee 69 (SC69) "Remoting of Long Range Radar Displays"
Special Committee 70 (SC70) "Altimetry."

ANTENNAS & PROPAGATION

VOL. AP-3, NO. 3, JULY, 1955

Proceedings or Transactions?—J. R. Pierce

Back-Scatter from Perfectly-Conducting Doubly-Trochoidal and Doubly-Sinusoidal Surfaces—W. C. Hoffman

Expressions are developed by means of the "current-distribution" method for the far-zone energy back-scattered from large perfectly-conducting doubly-trochoidal and doubly-sinusoidal surfaces.

On Nonuniform Dielectric Media—R. B. Barrar and R. M. Redheffer

A theory of nonuniform dielectric media should prove valuable to people engaged in the design of antenna housings or radomes and to those designing absorbers. Such a theory is herein developed. The problem of inhomogeneous media is treated first by means of differential equations and then as a limiting case of an array of panels. Various equivalences such as behavior of a panel at arbitrary incidence angle with that at normal incidence are also discussed.

A Dual-Standard for Radar Echo Measurements—M. H. Cohen and R. C. Fisher

A description is given of a corner-sphere, an aluminum sphere with an excised octant, which serves as a dual-standard echoing body. Its measured and calculated echo patterns are shown. An optical derivation is given for the echo area of the circular corner.

Folded Unipole Antennas—J. Leonhard, R. D. Mattuck and A. J. Pote

Folded unipole antennas less than a quarter wavelength long are used to transform the input resistance of short vertical antennas to a more acceptable value by effecting a transformation within the antenna itself. An equivalent circuit of the folded unipole is derived. The transformation of input impedance is shown to be due to two factors: (1) the division of radiation mode currents between the driven and undriven portions of the antenna, and (2) the flow of currents in a nonradiating transmission-line mode. The effect on the input impedance of reactive elements inserted between the unfed portion and ground is investigated. The theory is verified with an experimental antenna whose input impedance is measured as a function of tuning reactance. The experimental curve is found to be in good agreement with the theory. Two methods of operating the folded unipole are proposed. In the first, only the division of radiation mode currents is utilized to effect the input impedance transformation. This method is applicable to antennas close to a quarter wave. The second method transforms the input impedance by utilizing the transmission-line mode only. It is applicable to short antennas.

Characteristics of Tropospheric Scattered Fields—L. G. Trolese

Experimental results obtained with transmissions at wavelengths of 3.2, 9.3, and 24 cms over a 46.3-mile path are presented. With low terminal heights the scattered field was dominant on this path. Tests with a narrow beam antenna indicate that the scattered field arrives at the receiver spread over an appreciable angle. This angle is some five to seven times as large as the Booker-Gordon theory predicts on the assumption that the scale of turbulence is large compared to the wavelength. Loss in ability to receive power in proportion to antenna gain was encountered for antennas with aperture diameters greater than about 20 wavelengths. This loss occurs for aperture sizes considerably smaller than the Booker-Gordon theory predicts.

The speed of fading of the scattered field signal increases almost linearly with frequency. This agrees fairly well with the concept (due to Ratcliffe and applied to trospheric scattering by Booker and Gordon) that fading is due to beating between various scattered field components whose frequencies differ by a fractional Doppler shift due to motion of the scatterers. The speed of fading always increases, during the day, with time of day and does not correlate with mean upper wind speed. This increase with time of day is probably connected with the repetitive diurnal meteorological cycle prevalent in Arizona.

Use of Folded Monopoles in Antenna Arrays—J. B. Lewis

The use of folded elements in antenna arrays is reviewed and then discussed with regard to an array of vertical monopoles to which an improved impedance match of the feed system is required. A method of calculating the driving point impedances from the self and mutual impedances of related unfolded elements is given

A New Interpretation of the Integral Equation Formulation of Cylindrical Antennas—C. T. Tai

The validity of the conventional integral equation formulation of cylindrical antennas is often criticized because of an approximation of the kernel of the integral equation. If the antenna is of the form of a cylindrical tube there is an exact integral equation formulation. By means of the variational technique the integral equation for the cylindrical tube can be solved approximately. When the length of the tube is large compared to its diameter, the input impedance of the structure is found to be the same as if one had used the approximate integral equation at the very beginning of the analysis. This new procedure therefore clarifies one main ambiguity involved in the early works of the theory of cylindrical antennas based upon the approximate integral equation. It also enables us to treat the problem of relatively thick cylindrical antennas.

The Radiation Field Produced by a Slot in a Large Circular Cylinder—L. L. Bailin

General results obtained previously by Silver and Saunders for slots of arbitrary shape are applied to the cases of narrow-width half-wavelength slots oriented transverse and parallel to the axis of infinite cylinders with fairly large radii. Sufficient theoretical data are given to describe accurately the major portion of the three-dimensional pattern of both the principal and cross-polarized components of the radiation fields of these slots. Perfectly conducting cylinders of circumferences of 8 and 12 wavelengths are considered.

Fresnel Antenna Patterns—L. W. Lechtreck

Parasitic Arrays Excited by Surface Waves—R. S. Elliott and E. N. Rodda

Tropospheric Refraction Near Hawaii—Grote Reber

Effect of Arbitrary Phase Errors on the Gain and Beamwidth Characteristics of Radiation Pattern—D. K. Cheng

Simple expressions have been obtained for predicting the maximum loss in antenna gain when the peak value of the aperture phase deviation is known. It is not necessary to know the exact amplitude or phase distribution function as long as the phase errors are relatively small; and the same expressions may be used for both rectangular and circular aperture cases. Relations have also been established such that the maximum change in the main-lobe beamwidth can be predicted from the knowledge of the amplitude distribution function and the peak phase deviation.

Abstracts of Papers From the IRE-URSI Symposium Held May 2–5, 1955—Washington, D. C.

ELECTRON DEVICES

Vol. ED-2, No. 3, July, 1955

A Broadband RF Noise Generator—M. I. Skolnik

A simple broadband noise generator was constructed which produced substantial noise power over the frequency range from 10 mc to 1000 mc. The measured noise factors were 90 db or better over this range. The noise was generated by an electric arc discharge which operated in a conventional RC relaxation oscillator circuit. A continuous spectrum was produced because of the natural incoherence in the pulse repetition rate of such a circuit. The mechanism of operation is described along with an experimental tube which was constructed for the purpose of demonstrating the principle.

Accelerated Power Aging with Lithium-Doped Point Contact Transistors—L. E. Miller and J. H. Forster

A point contact transistor with electrical properties similar to those obtained using phosphor-bronze collectors can be made by forming a lithium-doped collector point in a conventional manner. The use of lithium-doped points enables the observation of significant changes in transistor parameters during short periods of moderate power aging. In particular, n-type transistors exhibit a large decrease in reverse current with accompanying loss of alpha. It is proposed that changes in the effective donor concentration in the formed region are responsible for these decreases, in view of the high diffusion rate and low solubility of lithium in germanium.

These results emphasize that point contact collector characteristics can change appreciably as a result of surface independent mechanisms.

Integral Equation Solution for Traveling Wave Tube Parameters—P. Parzen

An integral equation method for evaluating the electronic behavior of traveling wave amplifiers is given. This method is utilized to obtain the effects of a thick beam and variations in dc density and dc velocity across the beam. Curves of the space charge parameter $4QC$ and impedance K are obtained for thick beams, which compare favorably with those of Pierce.

A Design of Triode Electron Gun—Kuo-Chu Ho

A theoretical study has been made of the focusing of high current electron beams by means of the aperture effect. The aperture effect is obtained by a triode electron optical system. An equation for describing the beam profile in the system has been described. Both the condition for obtaining the minimum radius of the beam and the condition for optimum focus have also been worked out. Two numerical examples are treated to illustrate the triode focusing of electron beams with two different total current magnitudes of 50 and 250 μ-amp. It is found that by using this triode system the final energy of the electrons and the total current of the electron beam may be controlled separately.

Coupled Helices for Use in Traveling-Wave Tubes—G. Wade and N. Rynn

Previous theoretical treatments concerning coupled helices in the absence of a beam, while useful for predicting approximate behavior, are not satisfactory for many tube applications because the presence of a beam can modify the behavior substantially. This paper presents a theory of propagation for coupled concentric helices in the presence of a coaxial beam and computes therefrom properties pertaining to coupler and attenuator applications.

Included are curves of the propagation constants as functions of coupling coefficient and beam velocity, curves of the inner and outer helix voltages as functions of the physical dimensions, and curves which permit the frequency response for various designs of input and output couplers to be calculated.

Sample calculations show that the proper length for input and output couplers is greater than the length for complete energy transfer between helices in the absence of the beam (a criterion commonly used in design work). Calculations also illustrate the related fact that the frequency for maximum transmission through a coupler is lower when the beam is turned on than when off.

Only preliminary work has been done to date in computing the properties of a coupled-helix attenuator.

The Utilization of Positive Ions for Investigations of Stray Field Effects in Electrostatic Lenses—R. Azud and W. F. Niklas

The paper described a method for the investigation of stray fields caused by surface charges on the glass supports of cathode ray tube guns. These stray fields may penetrate into the gap of an unshielded electrostatic lens and contribute to the astigmatic distortions of the entire electron optical system. The focused spot on the screen of the tube then shows deviations from the ideal circular shape.

The investigation of the stray field influences was carried out utilizing the positive ion component of the electron beam. Discoloration patterns on the second grid aperture due to ion bombardment indicated the expected distortion of the focused spot. Various gun designs were tested in this manner.

MICROWAVE THEORY & TECHNIQUES

PGMTT-3, No. 4, July, 1955

Double-Ridge Waveguide for Commercial Airlines Weather Radar Installation—T. N. Anderson

This paper describes the design and development of a double-ridge waveguide designed to propagate both C-b and X-band (5,400 and 9,300 mc) so as to allow for a common waveguide installation in commercial airliners which could use either a C-band or an X-band weather penetration radar. This double-ridge waveguide is capable of propagating over the desired frequency range with single mode operation only; it yields attenuation at C-band which is only slightly higher than that of normal C-band waveguide and has somewhat reduced attenuation at X-band compared to standard $1\times\frac{1}{2}$ rectangular waveguide. This double-ridge guide has been adopted by Aeronautical Radio, Inc. and is specified in their Characteristic No. 529 entitled "5.7 Cm Weather Penetration Airborne Radar."

This paper also gives an analysis of the calculated guide wavelength in this double-ridge guide, attenuation, and peak power-handling capabilities; and compares the results of these calculations with measured data. Peak power-handling capability for this double-ridge guide is well within the requirements of this application. The testing procedures used for high-power breakdown measurements are described. This paper also covers the development of double-ridge waveguide flanges, elbows, bends, twists, transitions, and flexible waveguide for use over this extremely broad band.

Simplified Calculation of Antenna Patterns, with Application to Radome Problems—J. H. Richmond

Generally, the calculation of antenna far-field patterns from known near-field distributions is tedious and may require the use of a large computer. The calculations are simplified for certain types of antennas having separable near fields. This simplifying assumption is found to yield satisfactory results with pyramidal horns and parabolic reflector antennas. Calculations are further simplified by approximating a complex line integral with two real summations.

Measured and calculated far-field patterns are included to indicate the accuracy of the calculations. Results are presented for horns and parabolic antennas and for a horn covered with a hollow dielectric wedge. The method is applicable to both E-plane and H-plane pattern calculations. The main lobe of a far-field pattern is calculated in less than one hour on a desk calculating machine by the simplified method. In radome work an important feature is that it permits rapid evaluation of the far-field distortion associated with any given near-field distortion in any given small region in the near field.

A Modulated Scattering Technique for Measurement of Field Distributions—J. H. Richmond

Electric field distributions can be measured accurately by passing a short metal dipole through the field and recording the wave scattered by the dipole. Ordinarily the method is difficult to use since the scattered signal is small, critical tuning adjustments are required, and careful attention to stability is necessary. However, by placing a nonlinear impedance

at the center of the dipole and applying an audio voltage through slightly conducting threads, the scattered wave can be modulated. This makes it possible to relax the tuning and stability requirements and at the same time to increase the sensitivity of the measurements.

Potential Solution of a Homogeneous Strip-Line of Finite Width—W. H. Hayt, Jr.

The exact potential solution for a zero-thickness strip centered between two ground planes of finite width is outlined. For unit separation of the ground planes, the solution is applied to obtain curves of capacitance per unit length for several representative ground plane widths as a function of strip width. The results are valid for all strip widths, including the case in which the strip is wider than the ground planes. The validity of assuming infinite ground plane width is investigated and it is found that such an assumption leads to little error providing the ratio of ground plane width to separation is at least 2.5, and also providing the difference between ground plane and strip width is at least one-half of the ground plane separation.

Resonant Frequencies of Higher-Order Modes in Radial Resonators—D. C. Stinson

A summary of the relevant work on radial line discontinuities and radial line resonators is presented. A step-type discontinuity is analyzed using an integral equation formulation and the results are applied to the calculation of the resonant frequencies of a radial resonator. This method is verified by experiment and compared with the foreshortened-line approximation and with the methods of Marcuvitz and Goddard, whose work is satisfactory for the lowest-order TM mode. However, the present method is the only one which is equally applicable to the calculation of the resonant frequencies of TM modes possessing higher-order radial variations.

A Shunt Technique for Microwave Measurements—H. M. Altschuler and A. A. Oliner

A new method of measuring low-loss quantities at microwave frequencies, which employs a lossy shunt structure, is described. The additional loss introduced thereby reduces the excessively high VSWR's to values lying in the measurable range. The relevant information is abstracted from the data in a precision manner independent of the parameters of the shunt structure itself. Applications are made to the meaurement of low-loss dielectric constants, structures with shunt representations such as certain bolometer elements, attenuation constants, and VSWR's of slightly lossy variable short circuits. Physical realizations of such shunt structures are discussed.

A Rotary Joint for Two Microwave Transmission Channels of the Same Frequency Band—H. P. Raabe

This paper describes a rotary joint for two microwave transmission channels of the same frequency band. It consists of two pairs of rectangular waveguide terminals, a circular waveguide which transmits both channels, and coupling elements between the rectangular waveguide terminals and the circular waveguide which convert the rectangular H_{10} mode into the circular H_{01} and E_{01} modes. If pure H_{01} and E_{01} modes can be excited, perfect separation of the channels as well as constant amplitudes and phases can be obtained when the joint rotates. While the conversion into the circular E_{01} mode is performed by a conventional method, a new method had to be developed for the conversion of the rectangular H_{10} into the circular H_{01} mode.

Transverse Electric Resonances in a Coaxial Line Containing Two Cylinders of Different Dielectric Constant—J. W. Carr

A coaxial line containing a medium of propagation consisting of two coaxial cylindrical cylinders of different dielectric constant is considered for the special case of TE_{nm} resonances, and numerical calculations are carried out for a few cases of the TE_{11} type resonance. A reference paper called to the attention of the author by the reviewer treats the general condition of propagation in such a line. The numerical solutions to the cases of interest in this application were not performed, however, presumably since the interest was in propagating modes and since the general characteristic equation is quite complicated. It is shown here that consideration of transverse boundary conditions only leads to an equation which is much less complicated and which is equivalent to the reduction of the general characteristic equation (of the reference paper) when cutoff is approached.

NUCLEAR SCIENCE

Vol. NS-2, No. 1, June, 1955

Rapid Placement of a Synchrotron Beam on an Internal Target—W. F. Stubbins

Two methods of placing high-energy electrons in a synchrotron on an internal target within one microsecond are proposed. One method uses the forced radial oscillations that occur at $n=0.75$ in the presence of a first harmonic azimuthal variation in the magnetic field which gives rise to a Mathieu equation. The effect of the first harmonic in general and at $n=0.75$ is examined. The requirements for changing the radial field gradient to $n=0.75$ are determined. An operating cycle is suggested. The second method proposes the application of a radio frequency electric field resonant with the radial oscillation thus producing blow-up in an unmodified magnetic field. The axial and radial oscillation frequencies are not commensurable, thus resonance blow-up is avoided in the axial direction. The conditions to accomplish these are determined in general and specifically for the Berkeley synchrotron.

Some Remarks on Data Handling Systems—R. L. Chase

Three classes of nuclear data handling problems are discussed, and three output devices are described. These include a card punching system for a neutron diffraction spectrometer, an electric typewriter system for a large counting room, and a proposed magnetic drum storage system for a time-of-flight analyzer.

An Alignment Procedure for an Electrostatic Analyzer—R. R. Weeks

A procedure is described which electrically checks the entrance and exit tangents of an electrostatic analyzer. Audio frequency modulation of the direction of the incident beam is used to fill the aperture of the analyzer. Alignment adjustments may be made while observing signals delivered to oscilloscopes.

News and Views

The Secretary's Notebook

TELEMETRY & REMOTE CONTROL

Vol. TRC-1, No. 2, May, 1955

Analog Simulation of Sampled-Data Systems—R. C. Klein

The importance of analog simulation to control system analysis and synthesis increases as a function of system complexity. Adaptation of these techniques to sampled-data systems is particularly useful since, in addition to establishing control parameters, determination of proper sampling rate is often critical to system stability.

Sampled-data systems are considered which use discontinuous amplitude modulated data as well as digital processing units. Simulation is determined on the basis of theoretical considerations and relay circuitry is presented which has found effective utilization in analog simulation of sampled-data systems.

Image Converter—A New High-Speed Photographic Device—R. W. King

A Complete System for the Flight Testing of Piloted Aircraft—M. L. Van Doren

A Transistorized FM/FM Telemetering System—R. E. Colander and C. M. Kortman

IRE COMMITTEES—1955

Executive

J. D. Ryder, *Chairman*
W. R. G. Baker, *Vice-Chairman*
Haraden Pratt, *Secretary*

W. R. Hewlett
A. G. Jensen
A. V. Loughren
J. R. Pierce

Admissions

G. M. Rose, Jr., *Chairman*

H. S. Bennett
*T. M. Bloomer
*H. A. Brown
C. M. Burrill
L. A. Byam, Jr.
L. J. Castriota
*W. E. Darnell
*E. T. Dickey
*J. S. Donal, Jr.
*E. E. Ecklund
*A. D. Emurian
*Jerome Fox
L. O. Goldstone
J. A. Hansen
M. B. Kline
F. S. Mabry
G. P. McCouch
H. G. Miller
*C. R. Muller
*O. D. Perkins
W. L. Rehm
N. B. Ritchey
L. M. Rodgers
J. L. Sheldon
*W. B. Sullinger
*Eugene Torgow
*J. G. Weissman

* Alternates.

Appointments

J. W. McRae, *Chairman*

J. F. Byrne
J. N. Dyer
J. T. Henderson
A. G. Jensen
L. E. Packard
J. D. Ryder (*ex-officio*)

Awards

Irving Wolff, *Chairman*

R. D. Bennett
R. M. Bowie
H. Busignies
J. F. Byrne
E. B. Ferrell
L. R. Fink
D. E. Foster
H. E. Hartig
J. F. Jordan
A. B. Oxley
W. M. Rust, Jr.

Awards Coordination

W. L. Everitt, *Chairman*

A. V. Loughren
W. M. Rust, Jr.

Constitution and Laws

A. W. Graf, *Chairman*

S. L. Bailey
I. S. Coggeshall
J. B. Coleman
R. A. Heising
J. V. L. Hogan

Editorial Board

J. R. Pierce, *Chairman*

D. G. Fink
E. K. Gannett
W. R. Hewlett
T. A. Hunter
J. A. Stratton
W. N. Tuttle

Editorial Reviewers

W. R. Abbott
M. A. Acheson
R. B. Adler
Robert Adler
H. A. Affel
H. A. Affel, Jr.
W. J. Albersheim
B. H. Alexander
A. E. Anderson
J. A. Aseltine
W. S. Bachman
H. G. Baerwald
E. M. Baldwin
J. T. Bangert
W. L. Barrow
J. M. Barstow
B. L. Basore
B. B. Bauer
W. R. Beam
L. L. Beranek
P. P. Beroza
F. J. Bingley
J. T. Bolljahn
H. G. Booker
J. L. Bower
W. E. Bradley
J. G. Brainerd
D. R. Brown
J. H. Bryant
Werner Buchholz
Kenneth Bullington
J. H. Burnett
R. P. Burr
C. R. Burrows
W. E. Caldes
H. J. Carlin
T. J. Carroll
J. A. Chambers
H. A. Chinn
Marvin Chodorow
J. W. Christensen
L. J. Chu
J. K. Clapp
Edward Clarke
L. E. Closson
J. D. Cobine
R. E. Colander
J. W. Coltman
J. M. Coombs
P. W. Crapuchettes
A. B. Crawford
M. G. Crosby
C. C. Cutler
G. C. Dacey
Sidney Darlington
B. J. Dasher
W. B. Davenport, Jr.
A. R. D'Heedene
A. C. Dickieson
Milton Dishal
Wellesley Dodds
Melvin Doelz
W. H. Doherty
R. B. Dome
H. D. Doolittle
J. O. Edson
W. A. Edson
C. H. Elmendorf
D. W. Epstein
Jess Epstein
W. L. Everitt
R. M. Fano
L. M. Field
J. W. Forrester
W. H. Forster
G. A. Fowler
A. G. Fox
R. W. Frank
G. L. Fredendall
H. B. Frost
E. G. Fubini
I. A. Getting
L. J. Giacoletto
E. N. Gilbert
M. J. E. Golay
Bernard Gold
W. M. Goodall
A. W. Graf
J. V. N. Granger
V. H. Grinich
A. J. Grossman
R. A. Gudmundsen
E. A. Guillemin
A. V. Haeff
N. I. Hall
W. W. Harman
D. B. Harris
A. E. Harrison
L. B. Headrick
P. J. Herbst
J. K. Hilliard
C. J. Hirsch
Gunnar Hok
J. L. Hollis
J. H. Howard
W. H. Huggins
Joe Hull
R. G. E. Hutter
D. D. Israel
E. T. Jaynes
A. G. Jensen
R. L. Jepsen
Harwick Johnson
E. C. Jordan
Robert Kahal
Martin Katzin
W. H. Kautz
R. D. Kell
C. R. Knight
H. S. Knowles
W. E. Kock
Rudolph Kompfner
J. B. Horner Kuper
A. E. Laemmel
H. B. Law
R. R. Law
Vincent Learned
M. T. Lebenbaum
W. R. Lepage
F. D. Lewis
W. D. Lewis
J. G. Linvill
F. B. Llewellyn
S. P. Lloyd
A. W. Lo
J. R. MacDonald
Nathan Marchand
Nathan Marcuvitz
F. L. Marx
W. P. Mason
G. L. Matthaei
W. J. Mayo-Wells
E. D. McArthur
D. O. McCoy
Knox McIlwain
Brockway McMillan
R. E. Meagher
T. H. Meisling
Pierre Mertz
H. R. Mimno
S. E. Miller
A. R. Moore
Norman Moore
G. E. Mueller
E. J. Nalos
H. Q. North
K. A. Norton
W. B. Nottingham
B. M. Oliver
H. F. Olson
G. D. O'Neill
P. F. Ordung
Dale Oyster
C. H. Page
R. M. Page
R. C. Palmer
C. H. Papas
M. C. Pease, III
R. W. Peter
A. P. G. Peterson
H. O. Peterson
W. H. Pickering
J. A. Pierce
W. J. Poch
A. J. Pote
R. L. Pritchard
C. F. Quate
W. H. Radford
J. R. Ragazzini
J. A. Rajchman
Simon Ramo
H. J. Riblet
D. H. Ring
Stanley Rogers
T. A. Rogers
H. E. Roys
V. H. Rumsey
J. D. Ryder
R. M. Ryder
Vincent Salmon
A. L. Samuel
H. A. Samulon
O. H. Schade
S. W. Seeley
Samuel Seely
O. G. Selfridge
Samuel Sensiper
R. F. Shea
R. E. Shelby
Donald Shuster
W. M. Siebert
D. B. Sinclair
George Sinclair
David Slepian
R. W. Slinkman
C. E. Smith
P. T. Smith
O. J. M. Smith
L. D. Smullin
R. A. Soderman
A. H. Sommer
R. C. Spencer
J. R. Steen
Leo Storch
A. W. Straiton
D. E. Sunstein
Charles Susskind
G. C. Sziklai
G. K. Teal
J. C. Tellier
E. R. Thomas
H. P. Thomas
H. E. Tompkins
J. G. Truxal
D. F. Tuttle, Jr.
L. C. Van Atta
K. S. Van Dyke
E. K. Van Tassel
S. N. Van Voorhis
O. G. Villard, Jr.
R. L. Wallace, Jr.
L. G. Walters
C. C. Wang
D. A. Watkins
D. K. Weaver, Jr.
S. E. Webber
W. M. Webster
P. K. Weimer
Louis Weinberg
J. R. Weiner
H. G. Weiss
J. O. Weldon
J. M. West
G. W. Wheeler
H. A. Wheeler
J. R. Whinnery
W. D. White
W. B. Wholey
J. B. Wiesner
Irving Wolff
G. O. Young
L. A. Zadeh

Education

J. M. Pettit, *Chairman*

G. R. Arthur
V. A. Babits
A. B. Bereskin
W. L. Cassell
D. H. Ewing
R. M. Fano
C. L. Foster
A. W. Graf
Ferdinand Hamburger, Jr.
A. E. Harrison
H. E. Hartig
G. B. Hoadley
A. H. Howell
F. S. Howes
T. A. Hunter
Glenn Koehler
H. A. Moench
P. H. Nelson
R. E. Nolte
J. L. Potter
Albert Freisman
L. R. Quarles
J. R. Ragazzini
J. D. Ryder
Samuel Seely
F. R. Stansel
A. W. Straiton
W. M. Tuttle
David Vitrogan
D. L. Waidelich
L. E. Williams
D. G. Wilson
A. H. Wing, Jr.
A. L. Winn
M. E. Zaret

Finance

W. R. G. Baker, *Chairman*

W. R. Hewlett
A. V. Loughren
Haraden Pratt
J. D. Ryder

History

Haraden Pratt, *Chairman*

Melville Eastham — Keith Henney
Lloyd Espenschied — H. W. Houck

Membership

Kipling Adams, *Chairman*

F. W. Albertson — A. B. Oxley
A. R. Beach — George Rappaport
T. H. Clark — D. B. Sinclair
G. R. Town

(*Chairmen of Section Membership Committees Ex Officio*)
(*Regional Directors Ex Officio*)

Nominations

J. W. McRae, *Chairman*

G. H. Browning — F. H. R. Pounsett
W. R. Hewlett — F. E. Terman
C. J. Marshall — D. J. Tucker
H. W. Wells

Policy Advisory

J. T. Henderson, *Chairman*

J. M. Dyer — A. G. Jensen
A. W. Graf — J. M. Pettit
Ferdinand Hamburger, Jr. — J. R. Ragazzini
H. W. Wells

Professional Groups

W. R. G. Baker, *Chairman*
A. W. Graf, *Vice-Chairman* (*Central Div.*)
M. E. Kennedy, *Vice-Chairman* (*Western Div.*)
Ernst Weber, *Vice-Chairman* (*Eastern Div.*)

J. L. Callahan — J. C. McPherson
A. G. Clavier — Leon Podolsky
J. J. Gershon — W. M. Rust, Jr.
R. A. Heising — W. E. Shoupp
J. T. Henderson — C. E. Smith
F. S. Hird — L. C. Van Atta

(*Professional Group Chairmen Ex Officio*)

Tellers

B. F. Tyson, *Chairman*

W. F. Bailey — David Sillman
P. G. Hansel — N. A. Spencer
C. M. Veronda

Special Committees

Armed Forces Liaison Committee

G. W. Bailey, *Chairman*

IRE-IEE International Liaison Committee

F. S. Barton — F. B. Llewellyn
Ralph Bown — C. G. Mayer
R. H. Davies — R. L. Smith-Rose
Willis Jackson — J. A. Stratton

Professional Recognition

G. B. Hoadley, *Chairman*

C. C. Chambers — W. E. Donovan
H. F. Dart — C. M. Edwards

Technical Committees

20. Standards Committee

E. Weber, *Chairman*
M. W. Baldwin, Jr., *Vice-Chairman*
R. F. Shea, *Vice-Chairman*
L. G. Cumming, *Vice-Chairman*

J. Avins — J. G. Kreer, Jr.
W. R. Bennett — E. A. Laport
J. G. Brainerd — A. A. Macdonald
P. S. Carter — Wayne Mason
P. S. Christaldi — D. E. Maxwell
A. G. Clavier — K. R. McConnell
J. E. Eiselein — H. R. Mimno
A. W. Friend — M. G. Morgan
V. M. Graham — G. A. Morton
R. A. Hackbusch — H. L. Owens
H. C. Hardy — C. H. Page
P. J. Herbst — P. A. Redhead
Hans Jaffe — R. Serrell
Henry Jasik — R. M. Showers
A. G. Jensen — H. R. Terhune
J. L. Jones — J. E. Ward
W. T. Wintringham

20.5 Definitions Coordinating

M. W. Baldwin, Jr., *Chairman*

P. S. Carter — J. G. Kreer, Jr.
E. A. Laport

20.8 Basic Terms

J. G. Brainerd, *Chairman*

M. W. Baldwin, Jr. — C. H. Page

2. Antennas and Waveguides

Henry Jasik, *Chairman*
G. A. Deschamps, *Vice-Chairman*
R. L. Mattingly, *Secretary*

P. S. Carter — D. C. Ports
H. A. Finke — W. Sichak
W. C. Jakes, Jr. — G. Sinclair
E. T. Jaynes — P. H. Smith
P. A. Loth — K. Tomiyasu
A. A. Oliner — W. E. Waller
K. S. Packard, Jr. — M. S. Wheeler

2.2 Waveguide and Transmission Line Definitions

G. Deschamps, *Chairman*
W. Sichak

2.3 Antennas and Waveguides West Coast Subcommittee

E. T. Jaynes, *Chairman*

S. Cohn — T. Moreno
R. S. Elliott — S. Silver
S. Kerber — V. Twersky
R. S. Wehner

2.4 Waveguide and Waveguide Component Measurements

A. A. Oliner, *Chairman*

P. A. Loth — K. Packard
W. E. Waller

3. Audio Techniques

D. E. Maxwell, *Chairman*
I. M. Kerney, *Vice-Chairman*

C. A. Cady — F. L. Hopper
L. H. Good — R. C. Moody
G. H. Grenier — L. D. Runkle
F. K. Harvey — F. H. Slaymaker
H. O. Saunders

3.1 Audio Definitions

L. D. Runkle, *Chairman*

W. E. Darnell — C. W. Frank
D. S. Dewire — G. H. Grenier
W. F. Dunklee — R. E. Yaeger

3.2 Methods of Measurement of Gain, Loss, Amplification, Attenuation and Frequency Response

I. M. Kerney, *Acting Chairman*

3.3 Methods of Measurement of Distortion

R. C. Moody, *Chairman*

L. H. Bowman — J. J. Noble
F. Coker — G. Sawyer
J. French — E. Schreiber
L. D. Grignon — R. Scoville
F. Ireland — K. Singer
E. King — A. E. Tilley

4. Circuits

W. R. Bennett, *Chairman*
W. A. Lynch, *Vice-Chairman*

J. T. Bangert — J. C. Logue
J. G. Brainerd — P. F. Ordung
A. R. D'Heedene — C. H. Page
T. R. Finch — E. H. Perkins
R. M. Foster — E. J. Robb
W. H. Huggins — W. N. Tuttle
H. L. Krauss — L. Weinberg
J. G. Linvill — F. H. Williams

4.1 Transistor Circuitry

T. R. Finch, *Chairman*

R. H. Baker — J. G. Linvill
R. L. Bright — A. W. Lo
E. Gonzalez — J. C. Logue
R. A. Henle (alternate) — S. J. Mason
J. J. Suran
F. P. Keiper, Jr. — L. Weinberg
F. H. Williams

4.2 Linear Lumped-Constant Passive Circuits

L. Weinberg, *Chairman*

J. A. Aseltine — G. L. Matthaei
R. Kahal — J. G. Truxal

4.3 Circuit Topology

R. M. Foster, *Chairman*

R. L. Dietzold — E. A. Guillemin
S. Goldman — J. Riordan

4.4 Linear Varying-Parameter and Non-Linear Circuits

W. R. Bennett, *Chairman*

J. G. Kreer, Jr. — C. H. Page
J. R. Weiner

4.5 Time-Constant Network Analysis and Synthesis

W. H. Huggins, *Chairman*

S. Goldman — J. G. Linvill
W. H. Kautz — S. J. Mason
D. F. Tuttle, Jr.

4.7 Linear Active Circuits Including Networks with Feedback Servomechanism

W. A. Lynch, *Chairman*

E. J. Angelo, Jr. — J. M. Manley
H. Levenstein — E. H. Perkins
J. G. Linvill — C. F. Rehberg

4.8 Circuit Components

A. R. D'Heedene, *Chairman*

4.9 Fundamental Quantities

H. L. Krauss, *Chairman*

P. F. Ordung — J. D. Ryder

6. Electroacoustics

H. C. Hardy, *Chairman*

H. L. Barney — W. F. Meeker
B. B. Bauer — H. F. Olson
M. Copel — V. Salmon
W. D. Goodale, Jr. — E. S. Seeley
H. S. Knowles — P. B. Williams

7. Electron Tubes

P. A. Redhead, *Chairman*

E. M. Boone — L. S. Nergaard
W. J. Dodds — G. D. O'Neill
G. A. Espersen — A. C. Rockwood
P. A. Fleming — H. Rothe
T. J. Henry — W. G. Sheperd
E. O. Johnson — R. W. Slinkman
W. J. Kleen — K. R. Spangenberg
P. M. Lapostolle — R. G. Stoudenheimer
C. G. Lob — M. A. Townsend
R. M. Matheson — R. R. Warnecke

7.1 Tubes in Which Transit-Time is not Essential

T. J. Henry, *Chairman*

T. A. Elder — R. W. Slinkman
W. R. Ferris — E. E. Spitzer
W. T. Millis — A. K. Wing
A. H. Young

7.2 Cathode-Ray and Television Tubes

C. G. Lob, *Chairman*

J. R. Adams — R. Koppelon
R. Dressler — J. C. Nonnekens
L. T. Jensen — G. W. Pratt
D. Van Ormer

7.2.2 Storage Tubes

A. S. Luftman, *Chairman*

A. Bramley — M. Knoll
J. Buckbee — C. C. Larson
A. V. Haeff — W. E. Mutter
M. D. Harsh — D. S. Peck
R. B. Janes — R. W. Sears
B. Kazan — P. Youtz

7.3 Gas Tubes

M. A. Townsend, *Chairman*

J. H. Burnett — D. E. Marshall
A. W. Coolidge — G. G. Riska
E. J. Handley — W. W. Watrous
R. A. Herring — H. H. Wittenberg

7.3.1 Methods of Test for TR and ATR Tubes

K. Garoff, *Chairman*
J. Schussele, *Secretary*

I. Birnbaum — F. McCarthy
H. Heins — L. W. Roberts
F. Klawsnik — R. Scudder

7.4 Camera Tubes, Phototubes, and Storage Tubes in which Photo-Emission is Essential

R. G. Stoudenheimer, *Chairman*

B. R. Linden — B. H. Vine

7.4.1 Subcommittee

B. H. Vine, *Chairman*

B. R. Linden — D. H. Schaeffer

7.5 High-Vacuum Microwave Tubes

E. M. Boone, *Chairman*

J. H. Bryant — R. A. LaPlante
H. W. Cole — R. R. Moats
G. A. Espersen — C. R. Moster
L. M. Field — M. Nowogrodzki
M. S. Glass — S. E. Webber

7.5.1 Non-Operating Characteristics of Microwave Tubes

M. Nowogrodzki, *Chairman*
R. L. Cohoon, *Secretary*

M. S. Glass — E. D. Reed
R. C. Hergenrother — F. E. Vaccaro

7.5.2 Operating Measurements of Microwave Oscillator Tubes

R. R. Moats, *Chairman*
R. A. LaPlante, *Secretary*

R. S. Briggs — G. I. Klein
T. P. Curtis — B. D. Kumpfer
C. Dodd — E. C. Okress
W. W. Teich

7.5.3 Operating Measurements of Microwave Amplifier Tubes

S. E. Webber, *Chairman*

J. Berlin — A. W. McEwan
H. W. Cole — C. R. Moster
H. J. Hersh — R. W. Peter
P. M. Lally — G. Weibel

7.6 Physical Electronics

R. M. Matheson, *Chairman*

J. G. Buck — C. T. Goddard
H. B. Frost — P. N. Hamblenton
J. M. Lafferty

7.6.1 Electron Emission

R. M. Matheson, *Chairman*

F. G. Buck — P. N. Hamblenton
H. B. Frost — J. M. Lafferty

7.7.4. Methods of Test for Transistors for Pulse Service

W. H. Lapham, *Chairman*
R. L. Trent, *Secretary*

A. W. Berger — C. Huang
R. L. Wooley

8. Electronic Computers

R. Serrell, *Chairman*
D. R. Brown, *Vice-Chairman*

S. N. Alexander — G. W. Patterson
W. T. Clary — J. A. Rajchman
R. D. Elbourn — R. L. Snyder, Jr.
M. K. Haynes — W. H. Ware
L. C. Hobbs — C. R. Wayne
J. R. Johnson — J. R. Weiner
M. Middleton, Jr. — C. F. West
C. D. Morrill — Way Dong Woo

8.3 Static Storage Elements

M. K. Haynes, *Chairman*

A. O. Black — T. C. Chen
T. H. Bonn — E. Gelbard
H. R. Brownell — W. M. Papian
J. Rajchman — R. Stuart-Williams
E. A. Sands — D. H. Toth

8.4 Definitions (Eastern Division)

L. C. Hobbs, *Chairman*

R. D. Elbourn — R. P. Mayer
J. R. Johnson — G. W. Patterson

8.5 Definitions (Western Division)

W. H. Ware, *Chairman*

H. T. Larson — W. S. Speer
W. E. Smith — R. Thorensen

8.6 Magnetic Recording for Computing Purposes

S. N. Alexander, *Chairman*

9. Facsimile

K. R. McConnell, *Chairman*
D. Frezzolini, *Vice-Chairman*

H. F. Burkhard — L. R. Lankes
J. Callahan — S. A. Lawson
C. K. Clauer — P. Mertz
A. G. Cooley — M. P. Rehm
J. Hackenberg — H. C. Ressler
M. F. Hodges — R. B. Shanck
J. V. Hogan — G. S. Thompson
B. H. Klyce — R. J. Wise
K. Woloschak

26. Feedback Control Systems

J. E. Ward, *Chairman*
E. A. Sabin, *Vice-Chairman*

M. R. Aaron — D. L. Lippitt
G. S. Axelby — J. C. Lozier
G. A. Biernson — T. Kemp Maples
V. B. Haas, Jr. — W. M. Pease
R. J. Kochenburger — P. Travers
D. P. Lindorff — R. B. Wilcox
W. K. Linvill — S. B. Williams
F. R. Zatlin

26.1 Terminology for Feedback Control Systems

M. R. Aaron, *Chairman*
V. Azgapetian, *Secretary*

G. R. Arthur — J. C. Lozier
G. S. Axelby — C. F. Rehberg
T. Flynn — F. Zweig

10. Industrial Electronics

J. E. Eiselein, *Chairman*
E. Mittelmann, *Vice-Chairman*

W. H. Brearley, Jr. — J. H. Mennie
G. P. Bosomworth — P. E. Ohmart
Cledo Brunetti — H. W. Parker
J. M. Cage — S. I. Rambo
E. W. Chapin — W. Richter
D. Cottle — W. C. Rudd
J. L. Dalke — E. H. Schulz
C. W. Frick — C. F. Spitzer
H. C. Gillespie — W. R. Thurston
A. A. Hauser, Jr. — L. P. Tuckerman
T. P. Kinn — M. P. Vore
H. R. Meahl — J. Weinberger
S. L. Yarbrough

10.1 Definitions

D. Cottle, *Chairman*
C. F. Spitzer, *Vice-Chairman*

G. P. Bosomworth — J. Dalke
J. M. Cage — E. Mittelmann
W. Richter

10.4 METHODS OF MEASUREMENTS

E. Mittelmann, *Chairman*

J. M. Cage — S. I. Rambo
J. L. Dalke — E. H. Schulz
W. R. Thurston

11. INFORMATION THEORY AND MODULATION SYSTEMS

J. G. Kreer, Jr., *Chairman*
M. J. E. Golay, *Vice-Chairman*

P. L. Bargellini — H. W. Kohler
W. R. Bennett — E. R. Kretzmer
T. P. Cheatham, Jr. — V. D. Landon
L. A. DeRosa — N. Marchand
P. Elias — L. Meacham
D. Pollack

11.1 MODULATION SYSTEMS

D. Pollack, *Chairman*

11.2 EAST COAST INFORMATION THEORY

P. Elias, *Chairman*

11.3 WEST COAST INFORMATION THEORY

25. MEASUREMENTS AND INSTRUMENTATION

P. S. Christaldi, *Chairman*
J. H. Mulligan, Jr., *Vice-Chairman*

M. J. Ackerman — W. J. Mayo-Wells
J. L. Dalke — G. A. Morton
G. L. Fredendall — C. D. Owens
W. D. George — A. P. G. Peterson
G. B. Hoadley — J. G. Reid, Jr.
R. Showers

25.1 BASIC STANDARDS AND CALIBRATION METHODS

W. D. George, *Chairman*

S. L. Bailey — G. L. Davies
F. J. Gaffney

25.2 DIELECTRIC MEASUREMENTS

J. L. Dalke, *Chairman*

C. A. Bieling — F. A. Muller

25.3 MAGNETIC MEASUREMENTS

C. D. Owens, *Chairman*

W. E. Cairnes — R. C. Powell
G. I. Gordon — J. H. Rowen
P. H. Haas — E. J. Smith

25.4 AUDIO-FREQUENCY MEASUREMENTS

A. P. G. Peterson, *Chairman*

R. Grim — R. A. Long

25.5 VIDEO FREQUENCY MEASUREMENTS

G. L. Fredendall, *Chairman*

J. F. Fisher — H. A. Samulon
C. O. Marsh — W. R. Thurston

25.6 HIGH FREQUENCY MEASUREMENTS

R. V. Lowman, *Chairman* Joint AIEE-IRE Committee High Frequency Measurements
G. B. Hoadley, *Chairman*, IRE Subcommittee 25.6

R. A. Braden — E. W. Houghton
I. G. Easton — D. Keim
F. J. Gaffney — B. M. Oliver
B. Parzen

25.8 INTERFERENCE MEASUREMENTS

R. Showers, *Chairman*

H. E. Dinger — F. M. Greene
C. W. Frick — A. W. Sullivan

25.9 MEASUREMENTS OF RADIO ACTIVITY

G. A. Morton, *Chairman*

25.10 OSCILLOGRAPHY

M. J. Ackerman, *Chairman*

F. J. Bloom — G. R. Mezger (alternate)
P. S. Christaldi — T. B. Perkins
C. F. Fredericks — A. L. Stillwell
H. M. Joseph — H. Vollum

25.13 TELEMETERING

W. J. Mayo-Wells, *Chairman*

J. L. Blackburn — F. W. Lehan
J. F. Brinster — E. E. Lynch
R. E. Colander — M. G. Pawley
A. P. Bruer — W. E. Phillips
R. L. Harding — G. M. Thynell
C. H. Hoeppner — F. L. Verwiebe
M. V. Kiebert — G. F. C. Weedon
W. A. Wildhack

25.14 ELECTRONIC COMPONENTS

J. G. Reid, Jr., *Chairman*

M. B. Carlton — W. G. James
G. B. Devey — A. E. Javitz
J. W. Gruol — J. H. Muncy
J. N. Hall — F. A. Paul
F. E. Wenger

16. MOBILE COMMUNICATION SYSTEMS

A. A. Macdonald, *Chairman*
D. Talley, *Vice-Chairman*

N. Caplan — N. H. Shepherd
D. B. Harris — T. W. Tuttle
N. Monk — A. Whitney
J. C. O'Brien — P. D. Wickersham

12. NAVIGATION AIDS

H. R. Mimno, *Chairman*
W. Palmer, *Vice Chairman*

R. E. Gray — A. G. Richardson
H. I. Metz — L. M. Sherer

12.2 STANDARDS DF MEASUREMENTS

E. D. Blodgett, *Chairman*
J. Kaplan, *Vice-Chairman*
R. Silberstein, *Secretary*

A. D. Bailey — W. M. Richardson
H. I. Butler — J. A. Solga
J. J. Kelleher — J. O. Spriggs
F. M. Kratokvil — C. A. Strom, Jr.
A. A. Kunze — S. R. Thrift
J. T. Lawrence — J. H. Trexler
H. R. Mimno — H. W. von Dohlen

12.3 MEASUREMENT STANDARDS FOR NAVIGATION SYSTEMS

F. Moskowitz, *Chairman*
S. B. Fishbein, *Secretary*

P. Adams — G. Litchford
R. Alexander — J. T. MacLemore
S. Anderson — G. E. Merer
R. Battle — J. S. Pritchard
S. D. Gurian — P. Ricketts
P. Hansel — Abe Tatz
V. Weihe

13. NUCLEAR TECHNIQUES

G. A. Morton, *Chairman*

R. L. Butenhoff — Louis Costrell
D. L. Collins — M. A. Schultz

14. PIEZOELECTRIC CRYSTALS

H. Jaffe, *Chairman*
P. L. Smith, *Vice-Chairman*

H. G. Baerwald — W. D. George
R. Bechmann — E. Gerber
W. G. Cady — R. L. Harvey
W. A. Edson — W. P. Mason
I. E. Fair — R. A. Sykes
K. S. Van Dyke

27. RADIO FREQUENCY INTERFERENCE

R. M. Showers, *Chairman*
S. J. Burruano, *Vice-Chairman*

C. C. Chambers — A. E. Kerwien
L. E. Coffey — W. Mason
M. S. Corrington — J. B. Minter
E. W. Chapin — W. E. Pakala
H. E. Dinger — R. F. Shea
A. B. Glenn — D. Talley
J. A. Hansen — W. A. Shipman

27.1 BASIC MEASUREMENTS

M. S. Corrington, *Chairman*

S. J. Burruano — A. B. Glenn
H. R. Butler — F. M. Greene
E. W. Chapin — W. R. Koch
H. E. Dinger — A. A. Macdonald
C. W. Frick — A. W. Sullivan
D. Talley

27.2 DEFINITIONS

W. Mason, *Chairman*
C. W. Frick

27.3 RADIO AND TV RECEIVERS

A. B. Glenn, *Chairman*

A. Augustine — W. R. Koch
S. J. Burruano — C. G. Seright
E. W. Chapin — P. Simpson
M. S. Corrington — W. S. Skidmore
R. J. Farber — A. E. Smoll
A. M. Intrator — J. W. Stratman
E. O. Johnson — R. S. Yoder

27.4 RADIO TRANSMITTERS

A. E. Kerwein, *Chairman*

27.5 INDUSTRIAL ELECTRONICS

S. J. Burruano, *Chairman*

27.6 RECORDING EQUIPMENT

M. S. Corrington, *Acting Chairman*

27.7 MOBILE COMMUNICATIONS EQUIPMENT

W. Shipman, *Chairman*

27.8 CARRIER CURRENT EQUIPMENT

27.9 COMMUNITY ANTENNAS

27.10 TEST EQUIPMENT

J. B. Minter, *Chairman*

27.11 ATMOSPHERICS

H. E. Dinger, *Chairman*

E. W. Chapin — F. H. Dickson
W. Q. Critchlow — M. M. Newman
A. W. Sullivan

17. RADIO RECEIVERS

J. Avins, *Chairman*
D. E. Harnett, *Vice-Chairman*

K. A. Chittick — J. K. Johnson
L. E. Closson — W. R. Koch
D. J. Healey III — I. J. Melman
K. W. Jarvis — G. Mountjoy

F. R. Norton
L. Riebman
J. D. Reid
L. M. Rodgers
S. W. Seeley
W. O. Swinyard
F. B. Uphoff
R. S. Yoder

17.8 Television Receivers

W. O. Swinyard, *Chairman*

J. Avins
E. C. Freeland
W. J. Gruen
I. J. Melman
B. S. Parmet
E. Pufahl
G. F. Rogers
S. P. Ronzheimer

17.9 Loop Receivers

L. E. Closson, *Chairman*

V. Beck
R. A. Bell
R. J. Farber
W. R. Koch
J. R. Locke
C. G. Seright

17.10 Automatic Frequency and Phase Control

F. B. Uphoff, *Chairman*

R. Davies
W. R. Koch
D. N. Larky
D. Richman

L. Riebman

15. Radio Transmitters

P. J. Herbst, *Chairman*
H. Goldberg, *Vice-Chairman*

T. E. Ahlstedt
J. H. Battison
F. J. Bias
M. R. Briggs
A. Brown
H. R. Butler
W. R. Donsbach
L. K. Findley
H. E. Goldstine
J. B. Heffelfinger
A. E. Kerwien
L. A. Looney
J. F. McDonald
S. M. Morrison
J. Ruston
G. W. Sellers
B. Sheffield
I. R. Weir

V. Ziemelis

15.1 FM Broadcast Transmitters

J. Ruston, *Chairman*

J. Bose
J. R. Boykin
N. Marchand
P. Osborne

H. P. Thomas

15.2 Radio-Telegraph Transmitters up to 50 MC

B. Sheffield, *Chairman*

H. R. Butler
J. L. Finch
J. F. McDonald
F. D. Webster

I. R. Weir

15.3 Double Sideband AM Transmitters

J. B. Heffelfinger, *Chairman*

R. B. Beetham
W. T. Bishop, Jr.
L. K. Findley
D. H. Hax
L. A. Looney
E. J. Martin, Jr.

15.4 Pulse-Modulated Transmitters

H. Goldberg, *Chairman*

R. Bateman
L. L. Bonham
G. F. Montgomery
W. K. Roberts

B. D. Smith

15.5 Single Sideband Radio Communication Transmitters

Adamant Brown, *Chairman*

W. B. Bruene
J. P. Costas
H. E. Goldstine
L. Kahn
A. E. Kerwien
E. A. Laport

J. B. Singel

15.6 Television Broadcast Transmitters

F. J. Bias, *Chairman*

E. Bradburd
L. A. Looney
J. Ruston
F. E. Talmage

19. Recording and Reproducing

A. W. Friend, *Chairman*
M. S. Corrington, *Vice-Chairman*

S. J. Begun
M. Camras
F. A. Comerci
E. W. D'Arcy
S. M. Fairchild
R. M. Fraser
C. J. LeBel
R. C. Moyer
C. B. Pear
A. P. G. Peterson
H. E. Roys
L. Thompson
T. G. Veal
R. A. VonBehren

C. F. West

19.1 Magnetic Recording

R. C. Moyer, *Chairman*

J. S. Boyers
M. Camras
F. A. Comerci
E. W. D'Arcy
W. H. Erikson
C. B. Pear

R. A. VonBehren

19.2 Mechanical Recording

L. Thompson, *Chairman*

W. S. Bachman
S. M. Fairchild
A. R. Morgan
R. C. Moyer
F. W. Roberts
M. F. Royston
R. A. Schlegel
A. S. R. Tobey

19.3 Optical Recording

T. G. Veal, *Chairman*

P. Fish
R. M. Fraser
J. A. Maurer
E. Miller

C. Townsend

19.4 Distortion

A. P. G. Peterson, *Chairman*

M. S. Corrington
C. J. LeBel

19.5 Flutter

H. R. Roys, *Chairman*

F. A. Comerci
S. M. Fairchild
U. Furst
C. J. LeBel

CCIR Liaison Group of IRE Committee 19

H. E. Roys, *Chairman* (*Representative*)
A. W. Friend (*Alternate*)

W. S. Bachman
R. M. Fraser
R. C. Moyer
L. Thompson

28. Solid State Devices

H. L. Owens, *Chairman*

J. B. Angell
S. J. Angello
A. C. Clarke
A. Coblenz
J. J. Ebers
R. S. Fallows
J. R. Flegal
H. Goldberg
J. R. Hyneman
J. P. Jordan
A. W. Lampe
L. T. MacGill
W. J. Mayo Wells
C. W. Mueller
H. Q. North
W. J. Pietenpol
R. L. Pritchard
J. R. Roader
B. J. Rothlein
R. M. Ryder

S. Sherr

28.1 Methods of Test for Transistors for Linear CW Transmission Service

C. L. Rouault, (AIEE) *Chairman*

D. A. Alsberg
A. E. Anderson
A. Coblenz
L. J. Giacoletto

A. W. Lampe

28.2 Semiconductors—Definitions

S. J. Angello, *Chairman*

J. M. Early
M. F. Lamorte
B. J. Rothlein
J. S. Schaffner

K. Uhler

21. Symbols

H. R. Terhune, *Chairman*
R. T. Haviland, *Vice-Chairman*

K. E. Anspach
F. M. Bailey
M. C. Cisler
W. A. Ford
O. T. Laube
C. D. Mitchell
C. Neitzert
M. B. Reed
A. C. Reynolds, Jr.
M. P. Robinson
M. S. Smith
R. M. Stern

H. P. Westman

21.2 Graphical Symbols for Semiconductors

M. P. Robinson, *Chairman*

H. E. Corey
R. A. Henle
R. F. Merrithew
W. H. Miller
C. D. Mitchell
J. G. Weissman

H. J. Woll

21.3 Functional Representation of Control, Computing and Switching Equipment

A. C. Reynolds, Jr., *Chairman*

T. G. Cober
C. W. Frank
J. W. Gorgas
H. F. Herbig
C. W. Hobbs
H. P. Kraatz
F. T. Meyer
E. W. Olcott
J. S. Osborne
G. Patterson
S. W. Roberts
F. J. Roehm

F. M. Sokol

21.5 New Proposals and Special Assignments

M. P. Robinson, *Chairman*

21.7 Letter Symbols

C. Neitzert, *Chairman*

22. Television Systems

W. T Wintringham, *Chairman*
W. F. Bailey, *Vice-Chairman*

M. W. Baldwin, Jr.
J. E. Brown
K. A. Chittick
C. G. Fick
D. G. Fink
P. C. Goldmark
R. N. Harmon
J. E. Hayes
J. L. Hollis
A. G. Jensen
I. J. Kaar
R. D. Kell
D. C. Livingston
J. T. Lyman
L. Mautner
J. Minter
A. F. Murray
D. W. Pugsley
D. B. Smith
M. E. Strieby

22.2 Television Picture Element

D. C. Livingston, *Chairman*

J. S. Bryan (Alternate for Chatten)
J. B. Chatten
P. Mertz
H. A. Samulon
O. H. Schade

23. Video Techniques

J. L. Jones, *Chairman*
S. Doba, Jr., *Vice-Chairman*

S. W. Athey
A. J. Baracket
J. M. Barstow
J. H. Battison
E. E. Benham
K. B. Benson
E. M. Coan
J. R. DeBaun
V. J. Duke
G. L. Fredendall
J. R. Hefele
R. T. Petruzzelli
C. G. Pierce
W. J. Poch

H. O. Saunders

23.1 Definitions

G. L. Fredendall, *Chairman*

R. F. Cotellessa — J. M. Eglin
S. Deutsch — W. C. Espenlaub

23.2 Utilization, Including Video Recording: Methods of Measurement

S. W. Athey, *Chairman*

K. B. Benson — V. J. Duke
J. M. Brumbaugh — G. Gordon
H. Milholland

23.3 Video Systems and Components: Methods of Measurement

J. Hefele, *Chairman*

I. C. Abrahams — E. Stein
A. Lind — J. F. Wiggin
N. E. Sprecher — W. B. Whalley

23.4 Video Signal Transmission: Methods of Measurement

J. M. Barstow, *Chairman*

K. B. Benson — M. H. Diehl
R. I. Brown — H. P. Kelly
R. D. Chipp (Alternate for R. I. Brown) — R. S. O'Brien (Alternate for K. B. Benson)
E. E. Gloystein — E. B. Pores
R. M. Morris — E. H. Schreiber

24. Wave Propagation

M. G. Morgan, *Chairman*

E. W. Allen, Jr. — M. Katzin
S. L. Bailey — M. Kline
A. R. Beach — R. K. Moore
H. G. Booker — K. A. Norton
K. Bullington — H. O. Peterson
C. R. Burrows — G. Sinclair
T. J. Carroll — N. Smith
A. B. Crawford — R. L. Smith-Rose
A. Earl Cullum, Jr. — H. Staras
W. S. Duttera — A. W. Straiton
H. E. Dinger — A. H. Waynick
I. H. Gerks — J. W. Wright
F. M. Greene — T. A. Wright

24.1 Standard Practices

H. O. Peterson, *Chairman*

W. S. Duttera — G. Sinclair
F. M. Greene — J. W. Wright

24.2 Theory and Application of Tropospheric Propagation

T. Carroll, *Chairman*

H. G. Booker — A. B. Crawford
A. W. Straiton

24.3 Theory and Application of Ionospheric Propagation

M. G. Morgan, *Chairman*

R. Bateman — R. A. Helliwell
K. L. Bowles — C. W. McLeish
J. H. Meek

24.4 Definitions and Publications

H. Staras, *Chairman*

A. B. Crawford — I. H. Gerks
J. E. Eaton — M. Katzin
E. G. Fubini — D. E. Kerr
G. Sinclair

24.6 Radio Astronomy

C. R. Burrows, *Chairman*

A. E. Covington — F. T. Haddock, Jr.
J. P. Hagen

24.7 Terrestrial Radio Noise

H. Dinger, *Chairman*

IRE REPRESENTATIVES IN COLLEGES*

*Agricultural and Mechanical College of Texas: H. C. Dillingham
*Akron, Univ. of: P. C. Smith
*Alabama Polytech. Inst. R. M. Steere
Alabama, Univ. of: P. H. Nelson
*Alberta, Univ. of: J. W. Porteous
Arizona State College: C. H. Merritt
*Arizona, Univ. of: H. E. Stewart
*Arkansas, Univ. of: W. W. Cannon
*British Columbia, Univ. of: A. D. Moore
*Polytech. Inst. of Bklyn. (Day Div.): M. V. Joyce
*Polytech. Inst. of Bklyn. (Eve. Div.): G. J. Kent
Brooklyn College: E. H. Green
*Brown Univ.: C. M. Angulo
*Bucknell Univ.: D. L. Bowler
Buffalo, Univ. of: W. Grestbatch
*Calif. Inst. of Technology: H. C. Martel
*Calif. State Polytech. College: C. Radius
*Calif., University of: H. J. Scott
California, Univ. of at L.A.: E. F. King
Capitol Radio Eng'g. Institute: E. Radabaugh
*Carnegie Institute of Technology: J. B. Woodford, Jr.
*Case Institute of Technology: J. R. Martin
Central Technical Institute: J. E. Lovan
*Cincinnati, Univ. of: A. B. Bereskin
*Clarkson College of Tech.: R. J. Reich
Clemson Agricultural College: L. C. Adams
*Colorado Agri. and Mech. College: C C. Britton
*Colorado, Univ. of: W. G. Worchester
*Columbia University: P. Mauzey
*Connecticut, Univ. of: J. L. C. Löf
*Cooper Union School of Eng'g.: J. B. Sherman
*Cornell University: T. McLean
Dartmouth College: M. G. Morgan
*Dayton, Univ. of: L. H. Rose
*Delaware, Univ. of: H. S. Bueche
*Denver, Univ. of: R. C. Webb
*Detroit, Univ. of: G. M. Chute
*Drexel Inst. of Technology: R. T. Zern
Duke University: H. A. Owen, Jr.
*Fenn College: K. S. Sherman
*Florida, Univ. of: M. H. Latour
Franklin University: D. F. Yaw
*George Washington Univ.: G. Abraham
*Georgia Institute of Technology: B. J. Dasher
Harvard University: C. L. Hogan
Houston, Univ. of: T. N. Whitaker
Idaho, Univ. of: L. B. Craine
*Illinois Inst. of Technology: G. T. Flesher
*Illinois, Univ. of: P. F. Schwarzlose
Instituto Tecnologico de Aeronautica: D. K. Reynolds
*Iowa State College: G. A. Richardson
*Iowa, State Univ. of: E. M. Lonsdale
*Johns Hopkins University: W. H. Huggins
*Kansas State College: J. E. Wolfe
*Kansas, Univ. of: D. Rummer
*Kentucky, Univ. of: N. B. Allison
*Lafayette College: F. W. Smith
Lamar State College of Tech.: L. Cherry
Laval University: L. Boulet
*Lehigh University: H. T. MacFarland
*Louisiana State Univ.: L. V. McLean
*Louisville, Univ. of: S. T. Fife
*Maine, Univ. of: C. Blake
*Manhattan College: C. J. Nisteruk
Manitoba, Univ. of: H. Haakonsen
*Marquette University: E. W. Kane
*Maryland, Univ. of: H. W. Price
*Mass. Inst. of Technology: J. F. Reintjes
*Mass. University of: J. W. Langford
McGill Univ.: F. S. Howes
*Miami, Univ. of: F. B. Lucas
*Michigan College of Mining and Tech.: R. J. Jones
*Michigan State University: I. O. Ebert
*Michigan, Univ. of: J. F. Cline
Milwaukee School of Eng'g.: W. A. Van Zeeland
*Minnesota, Univ. of: L. Anderson
*Mississippi State College: D. E. Fisher
*Missouri School of Mines & Metallurgy, Univ. of: R. E. Nolte
*Missouri, Univ. of: J. C. Hogan
*Montana State College: R. C. Seibel
*Nebraska, Univ. of: C. W. Rook
*Nevada, Univ. of: W. Garrott
*Newark College of Eng'g.: D. W. Dickey
*New Hampshire, Univ. of: F. A. Blanchard
*New Mexico College of Agriculture & Mechanic Arts: H. A. Brown
*New Mexico, Univ. of: R. K. Moore
*New York, College of City of: H. Wolf
*New York University (Day Div.): S. Shamis
*New York University (Eve. Div.): S. Shamis
*North Carolina State College: E. G. Manning
*North Dakota Agricultural College: E. M. Anderson
*North Dakota, University of: C. Thomforde
*Northeastern University: J. S. Rochefort
*Northwestern University: C. W. McMullen
Norwich University: R. F. Marsh
*Notre Dame, Univ. of: H. E. Ellithorn
*Ohio State University: C. E. Warren

*Colleges with Approved Student Branches.

*Ohio University: D. B. Green
*Oklahoma Agri. and Mech. College: H. T. Fristoe
Oklahoma Inst. of Technology: H. T. Fristoe
*Oklahoma, Univ. of: C. E. Harp
*Oregon State College: A. L. Albert
*Pennsylvania State University: H. J. Nearhoof
*Pennsylvania, Univ. of: E. I. Hawthorne
*Pittsburgh, Univ. of: J. Brinda, Jr.
*Pratt Institute: D. Vitrogan
*Princeton University: N. W. Mather
Puerto Rico, Universidad de: J. L. Garcia de Quevedo
*Purdue University: W. H. Hayt, Jr.
Queen's University: H. H. Stewart
RCA Institutes, Inc.: P. J. Clinton
*Rensselaer Polytechnic Institute: H. D. Harris
*Rhode Island, Univ. of: R. S. Haas
*Rice Institute: C. R. Wischmeyer
*Rose Polytechnic Institute: H. A. Moench
*Rutgers University: C. V. Longo

* Colleges with Approved Student Branches.

*Saint Louis University: G. E. Dreifke
*San Diego State College: D. C. Kalbfell
*San Jose State College: H. Engwicht
Santa Clara, Univ. of: H. P. Nettesheim
*Seattle University: F. P. Wood
South Dakota State College of Agriculture and Mechanic Arts: J. N. Cheadle
*South Dakota School of Mines & Technology: D. R. Macken
*Southern Calif. Univ. of: G. W. Reynolds
*Southern Methodist University: P. Harton
Southern Technical Institute: R. C. Carter
*Stanford University: J. Linvill
*Stevens Inst. Tech.: L. L. Merrill
Swarthmore College: C. Barus
*Syracuse University: H. Hellerman
*Tennessee, University of: S. King
*Texas, University of: W. H. Hartwig
*Texas College of Arts and Industries: J. R. Guinn
*Texas Technological College: H. A. Spuhler
*Toledo, University of: D. J. Ewing
*Toronto, Univ. of: G. Sinclair
*Tufts College: A. L. Pike
*Tulane University: J. A. Cronvich

*U. S. Naval Postgraduate School: G. R. Giet
*Utah State Agricultural College: C. Clark
*Utah, Univ. of: C. L. Alley
Valparaiso Tech. Institute: E. E. Bullis
Vanderbilt University: F. Schumann
*Vermont, Univ. of: W. L. Steinmann
*Villanova University: J. A. Klekotka
*Virginia Polytechnic Institute: R. R. Wright
*Virginia, Univ. of: O. R. Harris
Washington, State College of: R. D. Harbour
*Washington University: H. Crosby
*Washington, University of: F. D. Robbins
*Wayne University: D. V. Stocker
Wentworth Institute: T. A. Verrechhia
Wesleyan University: K. S. Van Dyke
Western Ontario, Univ. of: E. H. Tull
*West Virginia University: C. B. Seibert
*Wisconsin, University of: G. Koehler
Witwatersrand, University of: G. R. Bozzoli
*Worcester Polytechnic Institute: H. H. Newell
*Wyoming, Univ. of: W. M. Mallory
*Yale University: J. G. Skalnik

IRE REPRESENTATIVES ON OTHER BODIES

ASA Conference of Executives of Organization Members: G. W. Bailey, L. G. Cumming, alternate
ASA Standards Council: E. Weber, A. G. Jensen, alternate, L. G. Cumming, aternate
ASA Electrical Standards Board: E. Weber, A. G. Jensen, L. G. Cumming
ASA Graphic Standards Board: H. R. Terhune, R. T. Haviland, alternate
ASA Sectional Committee (C16) on Radio; A. G. Jensen, Chairman, J. Avins, E. Weber, L. G. Cumming, Secretary
ASA Sectional Committee (C39) on Electrical Measuring Instruments: P. S. Christaldi, F. J. Gaffney, alternate
ASA Sectional Committee (C42) on Definitions of Electrical Terms: M. W. Baldwin, Jr., J. G. Brainerd, A. G. Jensen, H. Pratt, E. Weber
ASA Subcommittee (C42.1) on General Terms: J. G. Brainerd
ASA Subcommittee (C42.6) on Electrical Instruments: Ernst Weber
ASA Subcommittee (C42.13) on Communications: J. C. Schelleng
ASA Subcommittee (C42.14) on Electron Tubes: W. Dodds
ASA Sectional Committee (C60) on Standardization on Electron Tubes: L. S. Nergaard, C. E. Fay
ASA Sectional Committee (C61) on Electric and Magnetic Magnitudes and Units: S. A. Schelkunoff, J. W. Horton, E. S. Purington
ASA Sectional Committee (C63) on Radio-Electrical Coordination: C. C. Chambers, R. M. Showers
ASA Sectional Committee (C67) on Standardization of Voltages—Preferred Voltages—100 Volts and Under: No IRE Voting Representative; Liaison: J. R. Steen
ASA Sectional Committee (C83) on Components for Electronic Equipment: P. K. McElroy
ASA Sectional Committee (C85) on Terminology for Automatic Controls: R. B. Wilcox, J. E. Ward
ASA Sectional Committee (Y1) on Abbreviations: H. R. Terhune, R. T. Haviland, alternate
ASA Sectional Committee (Y10) on Letter Symbols and Abbreviations for Science and Engineering: H. R. Terhune, R. T. Haviland, alternate
ASA Subcommittee (Y10.9) on Letter Symbols for Radio: A. Pomeroy, Chairman
ASA Subcommittee (Y10.14) on Nomenclature for Feedback Control Systems: J. E. Ward, W. A. Lynch, G. A. Biernson
ASA Sectional Committee (Y14) on Standards for Drawing and Drafting Room Practices: Austin Bailey, K. E. Anspach, alternate
ASA Sectional Committee (Y15) on Preferred Practice for the Preparation of Graphs, Charts and Other Technical Illustrations: C. R. Muller, M. P. Robinson, alternate
ASA Sectional Committee (Y32) on Graphical Symbols and Designations: Austin Bailey, A. G. Clavier, A. F. Pomeroy, alternate
ASA Sectional Committee (Z17) on Preferred Numbers: A. F. Van Dyck
ASA Sectional Committee (Z24) on Acoustical Measurements and Terminology: H. S. Knowles, H. F. Olson, alternate
ASA Sectional Committee (Z57) on Sound Recording: Neal McNaughten, Chairman, H. E. Roys, Representative, A. W. Friend, alternate
ASA Sectional Committee (Z58) on Standardization of Optics: T. Gentry Veal, E. Dudley Goodale, alternate
American Association for the Advancement of Science: J. C. Jensen
International Radio Consultative Committee, Executive Committee of U. S. Delegation: A. G. Jensen, Ernst Weber; L. G. Cumming, alternate
International Scientific Radio Union (URSI) Executive Committee: S. L. Bailey, Ernst Weber, alternate
IRE-RETMA-SMPTE-NARTB Committee for Inter-Society Coordination: W. J. Poch; M. W. Baldwin, Jr., alternate
Joint IRE-AIEE Committee on High Frequency Measurements: G. B. Hoadley (IRE Chairman), R. A. Braden, I. G. Easton, Willard H. Fenn, F. J. Gaffney, H. W. Houghton, J. W. Kearney, David Y. Keim, B. M. Oliver, B. Parzen
National Electronics Conference: A. W. Graf
National Research Council—Division of Engineering and Industrial Research: F. B. Llewellyn
U. S. National Committee, International Electrotechnical Commission, Advisers on Symbols: Austin Bailey, A. G. Clavier; A. F. Pomeroy, alternate
U. S. National Committee, International Electrotechnical Commission, Advisers on Electrical Measuring Instruments: P. S. Christaldi; F. J. Gaffney, alternate
U. S. National Committee of the International Electrotechnical Commission: A. G. Jensen, Ernst Weber, L. G. Cumming.

Abstracts and References

Compiled by the Radio Research Organization of the Department of Scientific and Industrial Research, London, England, and Published by Arrangement with that Department and the *Wireless Engineer*, London, England

NOTE: The Institute of Radio Engineers does not have available copies of the publications mentioned in these pages, nor does it have reprints of the articles abstracted. Correspondence regarding these articles and requests for their procurement should be addressed to the individual publications, not to the IRE.

The number in heavy type at the upper left of each Abstract is its Universal Decimal Classification number and is not to be confused with the Decimal Classification used by the United States National Bureau of Standards. The number in heavy type at the top right is the serial number of the Abstract. DC numbers marked with a dagger (†) must be regarded as provisional.

The Index to the Abstracts and References published in the PROC. IRE from February, 1954 through January, 1955 is published by the PROC. IRE, April, 1955, Part II. It is also published by *Wireless Engineer* and included in the March, 1955 issue of that journal. Included with the Index is a selected list of journals scanned for abstracting with publishers' addresses.

ACOUSTICS AND AUDIO FREQUENCIES

534.2+538.566 2492

Note on the Propagation of Normal Modes in Inhomogeneous Media—I. Tolstoy. (*Jour. Acous. Soc. Amer.*, vol. 27, pp. 274–277; March, 1955.) Analysis is presented for propagation in ducts with stratified media.

534.2 2493

Studies on Acoustic Radiation Pressure—J. Awatani. (*Jour. Acous. Soc. Amer.*, vol. 27, pp. 278–286; March, 1955.) General expressions are derived for the acoustic radiation pressure on rigid and nonrigid surfaces. The pressure on objects in motion is treated, using moving coordinates. The case of a thin rigid disk is examined in detail, and numerical examples are given.

534.23–8 2494

Underwater Ultrasonic Scattering by a Radial Cylindrical Temperature Gradient—P. E. Grant. (*Jour. Acous. Soc. Amer.*, vol. 27, pp. 287–291; March, 1955.)

534.232–8:546.431.824–31 2495

Electrostrictive Vibrations of Barium Titanate Tubes—M. Federici. (*Alta Frequenza*, vol. 24, pp. 5–11; February, 1955.) Radial and longitudinal vibrations are discussed and the equations of the equivalent circuit are developed in terms of the tube dimensions and the density and elastic modulus of the material. Curves show the observed variation of impedance with frequency. The coupling coefficients for the two types of vibration are deduced.

534.24:526.956.5 2496

Reflection of Sound in the Ocean from a Continuous Stratum containing a Velocity Extremum—E. O. Cook and H. S. Heaps. (*Jour. Appl. Phys.*, vol. 26, pp. 429–433; April, 1955.) Discussion indicates that reflection from layers of this type may be significantly higher than for a layer producing abrupt or monotonic velocity variation [3463 of 1953 (Carhart)]. Numerical results are tabulated for various types of layers, of thickness from 0 to 10λ, producing a total velocity variation of ±5 and ±10 feet per second.

534.3 2497

Studies of the Science of Music—É. de Blavette. (*Rev. Sci.*, (Paris), vol. 91, pp. 163–211; May/June 1953.)

534.32 2498

Note on Standard Pitch—W. Lottermoser and H. J. von Braunmühl. (*Akust. Beihefte*, no. 1, pp. 92–97; 1955.) Orchestra leaders in Western Germany have been questioned regarding their practice in respect of standard pitch; the results indicate that a high proportion of them are not interested, but the most important conductors accept the 440 cps standard. A method is described which has been used to record the standard pitch as rendered by some instruments and orchestras; this involves filtering the signal through a narrow-band filter, modulating a 5440 cps carrier, filtering out the 5000 cps signal and feeding it to a pen recorder; the accuracy of the method is within about ±0.25 cps.

534.42:534–8:621.395.623.7 2499

Some New Data on the Demodulation in Air of Two Ultrasonic Waves of Different Frequency, at least One of which is a Stationary Wave—S. Klein. (*Ann. Télécommun.*, vol. 10, pp. 26–29; February, 1955.) A series of experiments is described designed to verify earlier demonstrations reported by Maulois (958 of 1954). Two ionophone units arranged face to face some 10 cm apart, and with reflecting surfaces around the apertures, radiate acoustic waves at 30 and 32 kc, with acoustic pressure not exceeding 100 db above 2×10^{-4} dynes/cm². Stationary waves are detected by a hot-wire instrument; an audible 2 kc note is picked up by a stethoscope at intervals of half the ultrasonic wavelength between the apertures, or by using a microphone connected to a cro. Tests out of range of the ultrasonic waves and the cessation of the audible signal when a thin card is placed between the sources indicate that the phenomenon is not due to the nonlinearity of the ear or of the detecting system.

534.6 2500

An Acoustic Intensity Meter—S. Baker. (*Jour. Acous. Soc. Amer.*, vol. 27, pp. 269–273; March, 1955.) An instrument is described using a crystal microphone as a pressure transducer, a directional hot-wire anemometer as a velocity transducer and an electronic multiplier and integrator. The response can be made level to within ±1 db over the frequency range 60–7,000 cps, and the directional pattern is nearly circular.

534.6:519.272 2501

The Application of Correlation Techniques to Some Acoustic Measurements—K. W. Goff. (*Jour. Acous. Soc. Amer.*, vol. 27, pp. 236–246; March, 1955.) Application of the correlator described in 2542 below to measurement of the transmission loss of structures, location of sound sources, etc., is discussed.

534.6:681.142:519.272 2502

An Analog Electronic Correlator for Acoustic Measurements—Goff. (See 2542.)

534.61–8 2503

Investigation of a Probe for Ultrasonic Power—M. Degrois. (*Ann. Télécommun.*, vol. 10, pp. 2–7; January, 1955.) A simply constructed instrument is described in which the temperature gradient in a rod of absorbent material (picein $C_{14}H_{18}O_7$) is measured by a thermocouple. The rod is secured to the end of a glass rod the other end of which is immersed in a liquid under ultrasonic excitation from a crystal. Calibration methods are described.

534.75 2504

Abnormal Amplitude Variation of Nonlinear Distortion by the Ear—E. Zwicker. (*Akust. Beihefte*, no. 1, pp. 67–74; 1955.) Measurements of the quadratic and cubic distortion were made by applying compensation so as to eliminate a subjectively perceived difference tone. The difference in the amplitude variation of the effect for the two types of distortion is interpreted as indicating that the pressure response characteristic of the ear exhibits an inflection region at about ±0.1 μbar.

534.75 2505

Distribution of Audibility Threshold in Man—E. Zwicker and W. Heinz. (*Akust. Beihefte*, no. 1, pp. 75–80; 1955.) Measurements were made on about 100 men and women students; results are shown graphically. The binaural threshold lies a little below the monaural for frequencies <500 cps; at frequencies >500 cps hearing at the threshold is by the two ears alternately.

534.75 2506

Masking by a Periodically Interrupted Noise—I. Pollack. (*Jour. Acous. Soc. Amer.*, vol. 27, pp. 353–355; March, 1955.)

534.75 2507

Perceptibility of Flutter in Speech and Music—F. A. Comerci. (*Jour. Soc. Mot. Pict. & Telev. Eng.*, vol. 64, pp. 117–122; March, 1955.) Preference tests were conducted with twelve subjects listening to pure tone, a sustained chord of eight tones, piano and orchestral music, and male speech subjected to flutter of different types and degree. Comparisons

with results of objective measurements show that data obtained on pure tones can be used to predict the effect of flutter on musical programmes, and that the reading of a rms meter with a flutter-rate weighting network provides an index directly related to subjective quality.

534.78 2508
An Analysis of Perceptual Confusions among some English Consonants—G. A. Miller and P. E. Nicely. (*Jour. Acous. Soc. Amer.*, vol. 27, pp. 338–352; March, 1955.)

534.78 2509
Calculations on a Model of the Vocal Tract for Vowel /i/ (Meat) and on the Larynx—J. van den Berg. (*Jour. Acous. Soc. Amer.*, vol. 27, pp. 332–338; March, 1955.)

534.79 2510
Objective and Subjective Measurements of Loudness—G. Quietsch. (*Akust. Beihefte*, no. 1, pp. 49–66; 1955.) Subjective measurements were made using 37 different noises, and the results compared with objective measurements made by three different methods, including in particular an eight-octave summation method. A 1,000 cps tone was used as comparison standard. Deviations between the subjective and objective assessments are investigated. Masking in the lower octaves and subjective increase of loudness in the eighth octave can be allowed for. An objective loudness meter operating on the summation principle should have six bands, with the five upper bands of equal width of the "mel" scale and the lowest band of greater width.

534.79 2511
The Apparent Reduction of Loudness: a Repeat Experiment—S. S. Stevens, M. S. Rogers, and R. J. Herrnstein (*Jour. Acous. Soc. Amer.*, vol. 27, pp. 326–328; March, 1955.) Experiments by Laird et al. (*Jour. Accous. Soc. Amer.*, vol. 3, pp. 393–401; 1932.) on the relation between sound intensity and loudness indicated that an intensity reduction of 20 db brought the loudness to half-level; this result is at variance with results of other workers. New experiments with similar apparatus, a Type-2A audiometer, indicate that the original method may have been excessively sensitive to the level and order of presentation of the stimuli.

534.79 2512
On the Halving and Doubling of the Loudness of White Noise—E. C. Poulton and S. S. Stevens. (*Jour. Acous. Soc. Amer.*, vol. 27, pp. 329–331; March, 1955.) "The decibel changes required to halve and to double the apparent loudness of a white noise were determined at nine sound pressure levels by 36 subjects. The subjects adjusted the level of the noise by means of an improved control—a "sone potentiometer" whose angular turn is roughly proportional to the loudness produced. An attempt was also made to measure and control some of the biasing factors that affect loudness estimations. Results: the median decibel changes required to produce a 2:1 loudness ratio ranged from 6 to 10 db, approximately."

534.84 2513
Interference Patterns in Reverberant Sound Fields—R. V. Waterhouse. (*Jour. Acous. Soc. Amer.*, vol. 27, pp. 247–258; March, 1955.) Expressions are derived for the distribution of sound pressure, particle velocity and energy density in the interference field resulting from reflection at a plane surface large compared with λ, and for systems of mutually perpendicular reflectors. The largest departure from uniform distribution occurs in corners. The interference patterns do not vary greatly over the frequency range usually considered in room acoustics. Experimental results confirming the calculations are presented.

534.84 2514
Experiments for the Determination of Optimum Reverberation Time for Large Music Studios—T. Somerville and W. Kuhl. (*Akust. Beihefte*, no. 1, pp. 99–100, 1955.) Comment on 620 of March (Kuhl), author's reply, and further comment.

534.85 2515
The Mechanical Input Impedance of Gramophone Pickups—R. Kaiser. (*Akust. Beihefte*, no. 1, pp. 81–92; 1955.) The forces acting on the tip of the stylus are determined by making separate measurements of the lateral and vertical input impedance, using vibrometers specially designed for the two purposes. Results are given for several commercial pickups in the form of the locus diagram of the input impedance in the complex impedance plane.

534.85:621.396.677.833.2 2516
Parabolic Reflector for Sound Recording—F. A. Everest. (*Tele-Tech.*, vol. 14, pp. 77–128; March, 1955.)

621.395.61 2517
Microphones—J. K. Hilliard. (*Proc. IRE* (Australia), vol. 16, pp. 70–73; March, 1955. *Convention Record, IRE.*, vol. 2, part 6, pp. 42–44; 1954.) The properties of carbon, capacitor, moving-coil, ribbon, piezoelectric and differential microphones are outlined; a note on calibration and rating is included.

621.395.623.7:621.396.621 2518
Stereophonic Sound Receiver—Limann. (See 2731).

621.395.625.3 2519
Midget Tape Recorder—(*Prod. Eng.*, vol. 26, pp. 148–149; February, 1955.) By applying techniques used in the manufacture of hearing aids, a recorder has been designed weighing just over 3 lb and measuring $8\frac{1}{2}$ by $3\frac{7}{8}$ by $1\frac{7}{8}$ inches. The twin-track tape accommodates a half-hour record on each track. A 0.003-hp motor drives the tape at a speed of $1\frac{7}{8}$ inches per second. Output is 3 mw at 2000Ω, with signal-noise ratio of 35 db and overall gain of 70 db.

ANTENNAS AND TRANSMISSION LINES

621.372+621.396.677.75 2520
Azimuthal Surface Waves on Circular Cylinders—R. S. Elliott. (*Jour. Appl. Phys.*, vol. 26, pp. 368–376; April, 1955.) "Solutions of Maxwell's equations are presented which satisfy the boundary conditions for corrugated and dielectric-clad circular conducting cylinders. These solutions have the physical interpretation of leaky azimuthal surface waves. Values of the complex propagation constant are given as functions of the geometry. For large cylinders the leakage is small and the transmission properties are approximately those of a trapped wave on a flat surface. A coarse experiment gives reasonable agreement with the theory. Some possible applications to transmission lines and antennas are indicated." See also 2853 of 1954.

621.372 2521
An Experimental Investigation of Axial Cylindrical Surface Waves supported by Capacitive Surfaces—H. E. M. Barlow and A. E. Karbowiak. (*Proc. I. E. E.* (London), part B, vol. 102, pp. 313–322; May, 1955.) A solid perspex rod was used as the waveguide, the diameter being reduced in stages to enable the transition from inductive to capacitive surface impedance to be observed. The measurements confirm the theoretical prediction [624 of 1954 (Barlow and Cullen)] that an axial cylindrical surface wave (E_{0x} mode) having a phase velocity greater than that of light can be supported by such a capacitive surface.

621.372.2 2522
Coupled Transmission Lines as Symmetrical Directional Couplers—G. D. Monteath. (*Proc. I.E.E.*, part B, vol. 102, pp. 383–392; May, 1955.) Symmetrical directional couplers produced by coupling together two similar unbalanced transmission lines by sharing a common outer conductor for part of their length have a characteristic impedance independent of frequency. Two forms are described; one, for laboratory measurements of power at frequencies up to 1 kmc, consists of two parallel strips enclosed in a square-section outer conductor; the other, for monitoring transmitter power, consists of two lead-covered coaxial cables grafted together. Possible uses in filters and antenna systems are also mentioned.

621.372.2.012 2523
Graphical Representation of the Impedance of a Loss-Free Line—A. Ascione. (*Alta Frequenza*, vol. 24, pp. 64–84; February, 1955.) The relations between the methods of Smith, Carter, and Hazeltine, and Deschamps are discussed.

621.372.8 2524
The Anisotropic Waveguide—M. A. Gintsburg. (*Zh. Tekh. Fiz.*, vol. 25, pp. 358–363; February, 1955.) A general equation of the 4th order with one unknown function is derived for propagation in a waveguide filled with an anisotropic medium. Propagation modes and the internal field are determined for the case of a rectangular waveguide. The interaction of the modes is discussed and conditions are established determining the possibility of the propagation of particular modes. A geometrical interpretation of the results is given, and reference is made to waveguides of other cross sections.

621.372.8:621.372.413 2525
The Excitation of Circular Polarization in Microwave Cavities—Tinkham and Strandberg. (See 2557.)

621.372.8.012.8 2526
Circular and Rectangular Waveguides and their Equivalent Circuits—O. Zinke. (*Arch. Elektrotech.* vol. 41, pp. 364–384; February 10, 1955.) Equivalent circuits are deduced from Maxwell's equations for waveguides with TE or TM fields. The circuits comprise three reactive components whose values are independent of frequency, and one or two resistive components. The equivalence is exact in both rejection and pass bands in respect of attenuation, phase constant and characteristic impedance.

621.396.67:621.396.822 2527
Thermal [fluctuation] Radiation from a Thin Straight Aerial—M. L. Levin and S. M. Rytov. (*Zh. Tekh. Fiz.*, vol. 25, pp. 323–332; February, 1955.) On the basis of the general theory of electrical fluctuations and the theory of thin antennas, the thermal [fluctuation] radiation of a cylindrical conductor is considered. Spectral intensities are found for the densities of the energy flow and for the total radiated power. An expression is derived for the directivity diagram. The distribution of the fluctuation current along the antenna and the radiation resistance are calculated. The results are generalized to cover the case of a conductor of nonuniform cross section.

621.396.67.012 2528
The Vertical Radiation Patterns of Medium-Wave Broadcasting Aerials—H. Page and G. D. Monteath. (*Proc. I. E. E.* (London), part B, vol. 102, pp. 279–295; May, 1955. Discussion, pp. 295–297.) It is common practice to use vertical antennas of height 0.5 λ–0.6 λ so as to reduce the strength of the wave reflected by the ionosphere and thus increase the

fading-free range. Results of experiments on small-scale and full-scale radiators indicate that, for an antenna on a flat uniform site, if the ionosphere behaved like a smooth reflector a larger service area would result from loop feeding than from base feeding; further improvement is obtainable by double feeding, the magnitude of the improvement being greater the lower the ground conductivity. The effect of earth systems is mainly to improve efficiency. Irregularity of the ground at the transmitter site causes distortion of the vertical radiation pattern, while diffuse reflection at the ionosphere produces an effect equivalent to blurring of the pattern. Computed patterns based on a semi-empirically determined current distribution are in reasonably good agreement with the experimental results.

621.396.67.018.2.011.21 2529

Coupling between Two Thin Straight Aerials carrying Harmonic Currents, in Any Position relative to Each Other—F. Babin. *Ann. Télécommun.*, vol. 10, pp. 8–17; January, 1955.) The mutual-impedance concept applied earlier (2569 of 1953) is invalid except in the case of a sinusoidal current distribution. Formulas are modified and extended by considering active and reactive power, and are applied in calculating the radiation resistance (*a*) for unattenuated progressive waves in a parallel-wire feeder, and (*b*) for a rhombic antenna, taking account of ground reflection.

621.396.67.029.62:624.07 2530

Disturbing Effects of Guys on Metre-Wave Radiation—E. Paolini. (*Alta Frequenza*, vol. 24, pp. 33–47; February, 1955.) Guyed antenna towers for multichannel radiotelephony systems are discussed in relation to the cost per decibel of the input signal level. The cost is minimum when the uppermost guy attachment point is above the antennas. Measurements have been made of the radiation loss due to the guys with this arrangement. With horizontal polarization it entails no disadvantages, but with vertical polarization the resulting attenuation may not be negligible, and excessive coupling may be introduced between transmitting and receiving antennas. The effect on antenna impedance is generally not great.

621.396.674.3:621.372 2531

The Excitation of Surface Waves by a Vertical Antenna—D. B. Brick. (PROC. IRE, vol. 43, pp. 721–727; June, 1955.) Theory developed previously (2201 of August) is used to investigate the field of a linear antenna over a conducting ground plane with a thin dielectric coating. Experiments were made in a room with walls absorbent for em radiation; polystyrene ground-plane coatings of three different thicknesses were tried, with (*a*) a polyrod and (*b*) a tapered-waveguide antenna. The results confirm that the field of a vertical antenna includes a cylindrical-surface-wave component large compared with the radiation-wave component. Measurements with partially coated surfaces indicate possibilities for directive radiators.

621.396.674.31.011.2 2532

Radiation Resistance of Folded Dipoles—G. C. Corazza. (*Alta Frequenza*, vol. 24, pp. 22–32; February, 1955.) A general method is discussed for determining the ratio of the radiation resistance of the folded dipole to that of the corresponding simple dipole, for elements of arbitrary cross section. The special case of elements with circular cross section is treated.

621.396.677 2533

The Mechanism of Reception by Directional Antennae—E. Istvánffy. (*Acta Tech. Acad. Sci. Hung.*, vol. 11, nos. 1/2, pp. 257–268; 1955. In English.) Hertz's solution of the wave equation implies that the existence of currents in conductors is always associated with radiation; this concept leads to contradictions in the case of highly directive antennas. By consideration of an elementary absorbing dipole it is shown that, under conditions of matching, an incident wave is totally absorbed, without re-radiation, if it has the same configuration as the wave which would be radiated by the dipole.

621.396.677.012.12 2534

Power Density Diagrams of Short-Wave Aerial Arrays—S. Sampath. (*Jour. Inst. Telecommun. Eng.* (India), vol. 1, pp. 27–34; March, 1955.) A method of constructing the power-density diagrams is described based on equal-directivity contours for an equivalent point-source array.

621.396.677.71 2535

Field Radiated by Circular Cylinders with Resonant Slots—J. Munier. (*C. R. Acad. Sci.* (Paris), vol. 240, pp. 1520–1522; April 4, 1955.) Formulas are derived for the field radiated by an array of narrow slots. Polar diagrams calculated from the formulas are in good agreement with diagrams determined experimentally.

621.396.677.71 2536

Field produced by an Arbitrary Slot on an Elliptic Cylinder—J. R. Wait. (*Jour. Appl. Phys.*, vol. 26, pp. 458–463; April, 1955.) Analysis is presented based on a prescribed tangential component of the electric field in the slot. The integrals in the formal solution are evaluated approximately for the far-zone fields by the saddle-point method. On applying the solutions to the case of thin axial or transverse slots in a strip, results are obtained in agreement with experimental results reported by Gruenberg (1914 of 1953).

621.396.677.85 2537

Surface Matching of Dielectric Lenses—E. M. T. Jones and S. B. Cohn. (*Jour. Appl. Phys.*, vol. 26, pp. 452–457; April, 1955.) Two methods of cancelling the surface reflections are described, one using a $\lambda/4$ matching layer and the other a reactive wall embedded within the dielectric. The reactive wall may comprise an inductive array of thin wires or a capacitive array of thin disks. Curves show how the reflection depends on the angles of incidence and polarization. Some measurements on arrays of obstacles in waveguides give results supporting the theory.

621.396.677.85 2538

Investigation of High Gain in Lattice Lenses for Centimetre Waves—J. Moussiegt. (*Ann. Télécommun.*, vol. 10, pp. 19–24; January, 1955.) The design of a lattice-type lens (1595 of 1953 and back references) is discussed, in particular the location of the metal strips, the lens thickness and the number of strips in a given volume. With an experimental model of overall thickness 31.1 cm operating at a wavelength of 3.16 cm and comprising 2213 Al strips 16 mm×4 mm×0.05 mm strung on nylon threads 16 mm apart, half-power beam widths were 2.75 degrees and 3.8 degrees in the horizontal and vertical planes respectively, and gain 34 db. An efficient lens can be designed with strips in only three nodal planes, the lens thickness being only about one wavelength.

621.396.677.85 2539

The Design of a Zoned Dielectric Lens for Wide-Angle Scanning—D. H. Shinn. (*Marconi Rev.*, vol. 18, pp. 37–47; 2nd Quarter 1955.) Details are given of a lens whose performance was described earlier by Cheston and Shinn (731 of 1953).

AUTOMATIC COMPUTERS

681.142 2540

Gating Multipliers—M. Lilamand. (*Onde élect.*, vol. 35, pp. 142–150; February, 1955.) Analog computing equipment on lines proposed by Goldberg (151 of 1953) is described. Economy of materials is achieved by careful design of the switching circuit and by neutralization of the parasitic capacitances of the tubes. An accuracy to within one part in 1,000 at a mean gating frequency of 1.5 kc is obtained.

681.142 2541

A Simplified Method for the Design of Logical Conversion Matrices—M. L. Klein. (*Electronic Eng.* (London), vol. 27, pp. 270–272; June, 1955.) Diode matrix networks are discussed. A numero-graphical method is explained for converting from one numbering system to another. Possible applications for programming sequence control are suggested.

681.142:519.272:534.6 2542

An Analog Electronic Correlator for Acoustic Measurements—K. W. Goff. (*Jour. Acous. Soc. Amer.*, vol. 27, pp. 223–236; March, 1955.) The correlator described is of the class operating directly on the input signals, i.e., using no carrier. The magnetic-drum time-delay system described in 322 of 1954 is used.

681.142:621.383 2543

Photoelectric Reader feeds Business Machines—D. H. Shepard and C. C. Heasly, Jr. (*Electronics*, vol. 28, pp. 134–138; May, 1955.) Ordinary print is scanned by a photocell, and the resulting signals are coded and recorded on punched cards or tape, for input to computers.

681.142:621.395.625.3 2544

Magnetic Recording applied to [digital] Computers—F. H. Raymond. (*Onde élect.*, vol. 35, pp. 89–96; February, 1955.) The basic considerations involved in the design of the magnetic storage drum used in the C.U.B.A. machine are discussed. Optimum dimensions of pole faces for recording and reproducing heads are calculated and design curves are given.

CIRCUITS AND CIRCUIT ELEMENTS

621.3.066.6 2545

Contact Metals and Relay Contacts—Properties and Comparative Investigations—T. Gerber. (*Tech. Mitt. schweiz. Telegr.-Teleph. Verw.*, vol. 33, pp. 89–114; March 1, 1955. In German.) A detailed experimental investigation is reported of the relation between contact resistance and the changes occurring at the contact surfaces. Current-carrying, current-free and sparking contacts are discussed. Photographs are shown of contacts of various metals after service.

621.318.4 2546

Optimum Shape Coils—L. Lewin. (*Wireless Eng.*, vol. 32, pp. 177–178; July, 1955.) Analysis is presented for designing a coil to produce a required field at the center of a cylinder, with a minimum expenditure of power.

621.318.423.013 2547

Calculation of Magnetic Field Strength in Cylindrical Coils—F. H. Schückher. (*Arch. Elektrotech.*, vol. 41, pp. 400–413; February 10, 1955.) Expressions are derived for the axial component of the magnetic field using the fact that the field strength at a given point is proportional to the difference of the solid angles subtended by the end faces of the coil. The expression for the solid angles is obtained in the form of a difference of two double series; this can easily be evaluated approximately. Tables and graphs are given together with numerical examples illustrating the method. The case of a multilayer coil is included.

621.318.5 2548

Parallel-Ferroresonant Feedback-Type Trigger Circuit—J. G. Santesmases and M. R. Vidal. (*Onde élect.*, vol. 35, pp. 165–173; February, 1955.) A self-excited circuit consisting of

an ac winding on a ferromagnetic core, shunted by a capacitance, with auxiliary windings for excitation and polarization, may be adjusted to present two, and in certain conditions, three, stable states. Curves are given showing the influence of the various parameters.

621.318.57 2549
A Design Method for Direct-Coupled Flip-Flops—W. Renwick and M. Phister. (*Electronic Eng.* (London), vol. 27, pp. 246–250; June, 1955.) Design procedure is described securing independence of tube characteristics and achieving stability with resistors and supply voltages which may vary by given percentages from the nominal values. Switching speed for given stability is a function of the supply voltages.

621.318.57:621.387 2550
Reversible Dekatron Counters—L. C. Branson. (*Electronic Eng.*, vol. 27, pp. 266–268; June, 1955.) Bidirectional coupling in multistage counters is achieved without the use of gating circuits by providing the dekatrons with separate terminals for the two transfer electrodes between the ninth and zero cathodes.

621.319.4:537.311.33 2551
The Charging and Discharging of Nonlinear Capacitors—J. R. Macdonald and M. K. Brachman. (PROC. IRE, vol. 43, p. 741; June, 1955.) Correction to paper abstracted in 958 of April.

621.372 2552
Bounds Existing on the Time and Frequency Responses of Various Types of Networks—A. H. Zemanian. (PROC. IRE, vol. 43, p. 738; June, 1955.) Correction to paper abstracted in 2331 of 1954.

621.372:512.8/.9 2553
Tensor Analysis and Linear Network Theory—R. Braae. (*Trans. S. Afr. Inst. Elect. Eng.*, vol. 46, part 3, pp 67–87; March, 1955. Discussion, pp. 87–95.)

621.372:534.2–8 2554
Transducer Design for Ultrasonic Delay Lines—H. J. McSkimin. (*Jour. Acous. Soc. Amer.*, vol. 27, pp. 302–309; March, 1955.) The suitability of quartz and $BaTiO_3$ transducers is considered for use in conjunction with $\lambda/2$ and $\lambda/4$ bonds between transducer and delay medium to widen the pass band. A relative bandwidth of 46 per cent can theoretically be obtained using a transducer composed of $BaTiO_3$ with 12 per cent $PbTiO_3$ and 8 per cent $CaTiO_3$ with a $\lambda/2$ bond to a fused-silica delay line. Using quartz transducers, a relative bandwidth of 20 per cent was obtained experimentally with a $\lambda/2$ plastic bond, and of 85 per cent with a $\lambda/4$ solder bond. Theory based on equivalent circuits is given.

621.372.029.6 2555
The Ultra-bandwidth Finline Coupler—S. D. Robertson. (PROC. IRE, vol. 43, pp. 739–741; June, 1955.) "The finline coupler is a recently developed microwave circuit element with which it has been possible to assemble hybrid junctions, directional couplers, and polarization-selective couplers capable of operating over bandwidths of at least three to one in frequency. Constructional details and experimental results are given."

621.372.413 2556
Effect of Surface Roughness on Losses in Microwave Resonant Cavities—U. Pellegrini. (*Alta Frequenza*, vol. 24, pp. 12–21; February, 1955.) Measurements of Q value were made on a cylindrical TE_{011}-mode cavity specially designed so that the internal surface could be treated in various ways, e.g. by plating or polishing. The magnitude of the discrepancies between the measured values and those calculated for a perfectly smooth surface depends on the dimensions of the surface irregularities and is very small when the surface unevenness is no greater than the skin depth.

621.372.413:621.372.8 2557
The Excitation of Circular Polarization in Microwave Cavities—M. Tinkham and M. W. P. Strandberg. (PROC. IRE, vol. 43, pp. 734–738; June, 1955.) A matrix method is used to study the effect of transition pieces and differential phase shifters on waves propagating in guides with two degenerate orthogonal modes. Three different methods are discussed for generating circularly polarized waves in a cavity coupled to the side wall of a guide; the preferred arrangement uses a square guide with incident wave polarized along one transverse diagonal and reflected wave polarized along the other, and a circular coupling window centered in the width of one wall at an appropriate distance from the reflecting end.

621.372.5 2558
An Approximate Graphical-Analytical Method for plotting the Frequency Characteristics of a Linear System from its Transient Characteristic—D. D. Klovski. (*Zh. Tekh. Fiz.*, vol. 25, pp. 333–338; February, 1955.) The method proposed is based on the approximation of the area under the given curve by a sum of triangles. It is of importance in the design of automatic regulation systems.

621.372.5 2559
Transient Response Calculation: Approximate Method for Minimum-Phase-Shift Networks—D. G. Sarma. (*Wireless Eng.*, vol. 32, pp. 179–186; July, 1955.) "The well-known method of linear segments for the calculation of zero-pole locations of the transfer function corresponding to a given attenuation characteristic is extended by allowing the zeros and the poles to assume complex instead of only real values."

621.372.5:512.831 2560
Matrix Algebra—J. J. Karakash. (*Wireless Eng.*, vol. 32, pp. 190–195; July, 1955.) As a sequel to the quadripole theory presented by Cutteridge (1264 of 1953), special procedures and applications involving the general parameter matrix of passive quadripoles with bilateral circuit elements are discussed.

621.372.5:621.317.729 2561
Electrolyte Tank for solving Network Problems—Met. (See 2702.)

621.372.5.018.7 2562
Synthesis of a Network for a Prescribed Time Function—N. B. Chakrabarty. (*Indian Jour. Phys.*, vol. 28, pp. 473–484; October, 1954.) The moment-generating-function method and the time-series method are discussed; they yield physically realizable networks under general conditions. Three particular types of response are considered as illustrations.

621.372.54 2563
Design of Low-Pass Ladder Networks to work between Unequal Resistances—E. Green. (*Marconi Rev.*, vol. 18, pp. 21–28; 1st Quarter 1955.) Discussion of conversion data to enable formulas established in an earlier paper (1267 of 1953) to be used for cases of unequal terminating resistances. Curves are presented relating the ratio of input and output branch resistances to the ratio of input and output decrement, for up to five branches. See also 370 of February.

621.372.54.029.6 2564
Band-Pass Filters using Strip-Line Techniques—E. H. Bradley and D. R. J. White. (*Electronics*, vol. 28, pp. 152–155; May, 1955.) Practical details are given of materials and dimensions for uhf filters and for matching them to coaxial lines. Typical units have mid-band insertion loss <1 db, with attenuation >40 db at 12 per cent off mid-band frequency.

621.372.543.2 2565
Tchebycheff-Type Band-Pass Filters with Arbitrary Number of Circuits—E. Henze. (*Arch. elekt. Übertragung*, vol. 9, pp. 131–139; March, 1955.) Extension of the method developed by Dishal (3369 of 1949). Undercoupled as well as critically and overcoupled circuits are dealt with.

621.372.543.2.029.6 2566
Coaxial Resonator Filters—R. F. Brown. (*AWA Tech. Rev.*, vol. 9, pp. 293–318; February, 1955.) From an analysis of an equivalent band pass circuit, an expression is derived for insertion loss in terms of the loaded and unloaded Q factors, and the electrical design parameters are related to the dimensions of the resonator and the coupling loops. The insertion-loss characteristic of n identical resonators in tandem is determined by considering shunt susceptances equally spaced along a transmission line. An alignment procedure and arrangements for frequency multiplexing are described.

621.372.543.2.029.6:621.372.2 2567
Microstrip applied to Band-Pass Microwave Filters—M. Arditi and J. Elefant. (*Elec. Commun.*, vol. 32, pp. 52–61; March, 1955.) Impedance measurements are made by connecting the microstrip line through a network to a waveguide or a coaxial slotted line. Characteristics deduced are: (*a*) phase velocity is constant over a wide range of frequencies; (*b*) wavelength in microstrip is greater than the value corresponding to a transverse em mode between infinite parallel plates, approaching this value asymptotically for very wide strips; (*c*) the dominant mode propagated is not a pure transverse em mode; the characteristic impedance of a microstrip line is approximately equal to the reciprocal of the product of capacitance per unit length and phase velocity. The design of resonant sections by placing obstacles such as posts at proper distances is discussed in detail.

621.372.57 2568
Theory of Noisy Quadripoles—H. Rothe and W. Dahlke. (*Arch. elekt. Übertragung*, vol. 9, pp. 117–121; March, 1955.) Analysis is based on equivalent circuits in which the original quadripole is depicted as noise-free, all noise sources being transferred to a separate noise quadripole connected in front of it. The noise figure is found from the equivalent noise resistance, the equivalent noise conductance and a complex correlation admittance. Methods for the experimental determination of the elements of the noise quadripole are outlined. See also *Trans. I.R.E.*, vol. ED-1, pp. 258–259; December, 1954.

621.373 2569
On Asynchronous Action—N. Minorsky. (*Jour. Frank. Inst.*, vol. 259, pp. 209–219; March, 1955.) An analysis is made of quenching and excitation of oscillations by an external oscillation of unrelated frequency. The excitation depends only on the transfer of the position of equilibrium across the bifurcation point in the stability diagram, and is hence observed only in "hard" systems, whereas quenching can occur in "hard" and in "soft" systems.

621.373.4:621.375.232.3 2570
Cathode-Follower-Coupled Phase-Shift Oscillator—L. Fleming. (PROC. IRE, vol. 43, p. 754; June, 1955.) Comment on 1291 of May (Reich).

621.373.421.012 2571
A Graphical Sinusoidal Analysis of a Nonlinear RC Phase-Shift Feedback Circuit—D. Barbiere. (PROC. IRE, vol. 43, pp. 679–684;

June, 1955.) Frequency response curves are discussed of af oscillator circuits including nonlinear, e.g. thyrite, resistors in the feedback loop; over a part of the frequency range the voltage function is triple-valued. The method used involves the graphical superposition of the voltage/resistance characteristic of the nonlinear resistor on that of the parallel circuit.

621.375.13 2572
The Realization of a Given Transfer Coefficient: Feedback Amplifier Systems—F. H. Raymond. (*Onde élect.*, vol. 35, pp. 105–112; February, 1955.) The design of feedback amplifiers using *RC* networks is discussed in general terms and in relation to analog computers, low-frequency filters, servomechanisms, etc.

621.375.225:621.376.3.018.78 2573
Harmonic Distortion in Sinusoidal Frequency Modulation. Case of an Amplifier Stage comprising Pentode Valve and Tuned Transformer—L. Robin. (*C. R. Acad. Sci.* (Paris), vol. 240, pp. 1518–1520; April 4, 1955.) Formulas are presented for calculating the harmonics and the total distortion present in the demodulated voltage. Numerical calculations are performed for five different sets of values of two important circuit parameters.

621.375.23 2574
Electrical Integration Methods—H. Wittke. (*Frequenz*, vol. 9, pp. 49–57; February, 1955.) Following brief theoretical discussions of the *RC*, Miller, and Wiegand-Hansen (772 of 1949) integrators, a new quasi-exact integrator circuit is described and both an approximate and an exact theory are given. The errors inherent in the various methods are discussed and graphs for their estimation are given.

621.375.3 2575
Design of Choke Magnetic Amplifiers with Complex Load—N. P. Vasileva and O. A. Sedykh (*Avtomatika i Telemekhanika*, vol. 16, 47–63; January/February, 1955.) The design of transductors is considered from the practical point of view. The characteristic curves of four core materials of Russian origin are given. To illustrate the method, the design of a transductor with an amplification factor of 20, working into a 50-w load, is worked out in full.

621.375.4:538.632:546.682.86 2576
An Amplifier based on the Hall Effect—I. M. Ross and N. A. C. Thompson. (*Nature*, (London), vol. 175, p. 518; March 19, 1955.) The dc or ac signal is fed to a suitably matched coil wound on a laminated magnetic core having a narrow gap into which is inserted a thin rectangular slice of single-crystal InSb. Dc is passed through the slice, and the Hall emf is picked up and applied to a matched load. High values of power gain are theoretically possible. An upper frequency limit is set by core losses. For comment by H. M. Barbon and author's reply, see *ibid.*, vol. 175, p. 1004; June 4, 1955.

621.375.4:621.314.7 2577
Feedback-Stabilized Transistor Amplifier—D. W. Slaughter. (*Electronics*, vol. 28, pp. 174–175; May, 1955.) Loading of the feedback network is avoided by the use of an emitter-coupled amplifier in the first stage. A three-stage amplifier using Ge transistors gives an overall gain of 10 independent of the transistors used; Si junction transistors give more stable operation at high ambient temperatures. Circuits and component values for typical amplifiers are given.

621.376.223.018.78 2578
Cubic Distortions in Ring Modulators—L. Christiansen. (*Elec. Commun.*, vol. 32, pp. 43–51; March, 1955.) Translation of paper abstracted in 1874 of 1952.

621.376.4.029.64:621.387 2579
An Electronic Phase-Shift Tube for Microwave Frequencies—D. H. Pringle. (*Jour. Sci. Instr.*, vol. 32, pp. 125–127; April, 1955.) "The transmission of microwave radiation through an electron gas supported by a gas discharge plasma situated in a waveguide structure is discussed for the case in which the electron collision frequency is much less than the microwave frequency, and an expression is derived for the phase shift arising from the change in guide wavelength. A gas discharge phase-shift tube has been developed on this principle and efficient action obtained by using the negative glow region of the discharge. The performance of the tube is discussed in detail." See also 1289 of May (Bradley and Pringle).

GENERAL PHYSICS

536.7:621.396.822 2580
Electrical Fluctuations and Thermal Radiation—S. M. Rytov. (*Uspekhi Fiz. Nauk*, vol. 55, pp. 299–314; March, 1955.) Text of a lecture giving a broad nonmathematical review of theoretical work on thermal fluctuations (noise) with particular reference to the uhf region.

537/538 2581
Fundamental Electromagnetic Quantities—P. de Belatini. (*Bull. Tech. Univ. Istanbul*, vol. 6, pp. 11–28; 1953. In German.) Anomalies involved in the generally accepted dual system of electric and magnetic quantities are discussed. A threefold system comprising magnetism, conduction electricity and dielectric electricity is proposed as an improved basis.

537 2582
Study of some Problems of Electrostatics—H. Bonifas. (*Rev. gén. élect.*, vol. 64, pp. 149–158; March, 1955.) Elementary electrostatic phenomena are deduced from the simple electronic theory of metals; the phenomena of conduction in homogeneous metals and from metal to metal, contact potentials and the Peltier effect, are examined. The treatment is essentially non-mathematical.

537/538 (439.1) 2583
Survey of Researches in Physics in Hungary: Part 1—L. Jánossy. (*Nuovo Cim.*, vol. 1, Supplement, pp. 247–272; 1955. In English.) Short surveys by different authors are given on several subjects, including research on ferromagnetics, magnetic moments of atomic nuclei, and the force on polarized media.

537.226 2584
Extension of Fröhlich's General Theory of the Static Dielectric Constant to Dielectrically Anisotropic Materials—J. G. Powles. (*Trans. Faraday Soc.*, vol. 51, Part 3, pp. 377–382; March, 1955.)

537.228.1 2585
Applications of the Piezoelectric Equations of State—R. Bechmann. (*Arch. elekt. Übertragung*, vol. 9, pp. 122–130; March, 1955.) Application of the general linear piezoelectric equations of state (110 of 1954) to plates and thin bars. Particular stress and strain systems are considered. A uniform notation is introduced for the elastic and piezoelectric constants used. The relation between dielectric constant at constant stress and at constant strain is investigated. Electromechanical coupling factor is discussed.

537.311.5 2586
The Resistance of an Elliptic Plate—E. E. Jones. (*Brit. Jour. Appl. Phys.*, vol. 6, pp. 88–90; March, 1955.) Formulas for the resistance are derived in the form of infinite series, capable of numerical evaluation to any degree of approximation, for two different electrode arrangements.

537.52 2587
Dependence of the Electric Strengths of Liquids on Electrode Spacing—A. H. Sharbaugh, J. K. Bragg and R. W. Crowe. (*Jour. Appl. Phys.*, vol. 26, pp. 434–437; April, 1955.) Measurements have been made on hexane, heptane and tetradecane, using electrode spacings of 2–200 μ. The electric strengths are found to vary inversely with the logarithm of the separation, as predicted by theory.

537.52 2588
Constriction of the Positive Column of a Glow Discharge at High Pressure—R. G. Fowler. (*Proc. Phys. Soc.*, (London), vol. 68, pp. 130–136; March 1, 1955.)

537.52 2589
The Growth of Electrodeless Discharges in Hydrogen—G. Francis. (*Proc. Phys. Soc.*, vol. 68, pp. 137–147; March 1, 1955.)

537.525 2590
Electrical Breakdown at Very Low Gas Pressures—J. W. Leech. (*Brit. Jour. Appl. Phys.*, vol. 6, pp. 107–109; March, 1955.) A discussion, in terms of atomic collision data, of problems involved in the interpretation of an observed anomaly in the variation of breakdown strength with pressure and in the estimation of the pressure at which breakdown would occur if it were due solely to ionizing collisions in the body of the gas.

537.525.5:621.385.132 2591
Studies of Externally Heated Hot-Cathode Arcs: Part 3—Plasma Density Distributions in the Anode-Glow Mode—E. O. Johnson and W. M. Webster. (*RCA Rev.*, vol. 16, pp. 82–108; March, 1955.) Analysis of the plasma density distributions indicates that the anode-glow mode can exist only if the emission capacity of the cathode is at least twice as great as the anode current. This is supported by experimental evidence. Part 2: 3068 of 1952 (Webster et al.).

537.533 2592
Experimental Investigations on Electron Interaction—E. A. Ash and D. Gabor. (*Proc. Roy. Soc. A*, vol. 228, pp. 477–490; March 22, 1955.) Certain observations in low-pressure gas discharges and in magnetrons suggest an electron interaction effect several orders of magnitude in excess of the theoretical values based on binary encounters only. The validity of the theory was tested by experiments in which a carefully collimated electron beam was shot through a charge cloud, the scattering of the beam being directly observed. Both plasmas in thermal equilibrium and pure electronic space charges were investigated. In both cases the degree of scattering observed is less than five times the value predicted by theories neglecting simultaneous multiple collisions, hence the latter cannot account for the observed anomalies.

537.533.8 2593
On the Measurement of the Average Time Delay in Secondary Emission—M. H. Greenblatt. (*RCA Rev.*, vol. 16, pp. 52–64; March, 1955.) The time delay of the secondary emission is measured by comparing the duration of short bursts of primary emission with the duration of the corresponding bursts of secondary emission. The primary bursts are produced by deflecting a beam across an aperture at high speed, while the secondary beam is scanned over e.g. a fluorescent screen. The duration of the secondary pulses is longer than that of the primaries by an amount which depends on the accelerating voltage.

537.562:538.566 2594
Fundamental Wave Functions in an Unbounded Magneto-hydrodynamic Field: Part 1—General Theory—A. Baños, Jr. (*Phys. Rev.*, vol. 97, pp. 1435–1443; March 15, 1955.)

537.562:538.6 2595
Particle Transport, Electric Currents, and Pressure Balance in a Magnetically Immobilized Plasma—L. Tonks. (*Phys. Rev.*, vol. 97, pp. 1443–1445; March 15, 1955.) "An analysis of a plasma immobilized by a magnetic field shows that each kind of charged particle has a general drift perpendicular to the gradient of the field, but that there is no corresponding electric current density. There is an exact cancellation arising from the gradient of the Larmor radius. The current density which is present arises exclusively from the particle density gradient and is not associated with any drift of matter."

538.11 2596
Antiferromagnetism—T. Nagamiya, K. Yosida and R. Kubo. (*Advances Phys.*, vol. 4, pp. 1–112; January, 1955.) A survey of theoretical and experimental aspects. The spin-wave approximation is useful, especially for lattices of higher dimensions and for larger magnitudes of spin. This method can be easily generalized, e.g. so as to take second-neighbor interactions and dipole forces into account. Great mathematical difficulties are involved in the refinement of the theory to apply to higher temperatures and the calculation of higher-order quantities such as the fluctuations or the short-range order. Over 100 references. See also 2920 of 1954 (Lidiard).

538.22 2597
Statistical Models of Ferrimagnetism—I. Syozi and H. Nakano. (*Progr. Theor. Phys.*, vol. 13, pp. 69–78; January, 1955.) A theoretical discussion of the properties of some idealized ferrimagnetic crystals, the lattice being considered divided into two sublattices.

538.3 2598
A Short Modern Review of Fundamental Electromagnetic Theory—P. Hammond. (*Proc. IEE*, (London) part B, vol. 102, pp. 298–300; May, 1955.) Further discussion on 97 of January.

538.566:535.4 2599
Diffraction of Electromagnetic Waves by a Metallic Wedge of Acute and Dihedral Angle—W. W. Grannemann and R. B. Watson. (*Jour. Appl. Phys.*, vol. 26, pp. 392–393; April, 1955.) An investigation is made of the field produced by reflections within the space included between two plane conductors set at an angle ≥ 90 degrees. Experimental and theoretical results are given for angles of 90 degrees and 30 degrees. Discussion indicates that the field pattern for angles which are integral fractions of π can be computed on the basis of geometrical optics.

538.566:535.42 2600
The Diffraction of a Non-monochromatic Electromagnetic Wave by a Slit and a Grating—M. H. N. Potok. (*Proc. Phys. Soc.*, (London), vol. 68, pp. 171–176; March 1, 1955.) A general solution is derived from Kirchhoff's solution. Results of calculations and measurements are in good agreement over the range in which Kirchhoff's solution is applicable.

538.566:621.396.96 2601
Elliptically and Circularly Polarized Electromagnetic Waves—M. Bouix. (*Onde élect.*, vol. 35, pp. 126–136; February, 1955.) A general discussion of the subject and its applications in radar technique, with extensive bibliography. See also 2199 of August.

538.569.4 2602
Absorption of 3.18-cm Microwaves in some Aromatic and Aliphatic Compounds in the Liquid State—D. K. Ghosh. (*Indian Jour. Phys.*, vol. 28, pp. 485–489; October, 1954.)

538.569.4:535.33 2603
Microwave Spectroscopy of Gases—J. Sheridan (*Research*, (London), vol. 8, pp. 88–93; March, 1955.) Recent developments in the field are outlined; measurements have been made at wavelengths down to <1 mm. About 80 references.

GEOPHYSICAL AND EXTRATERRESTRIAL PHENOMENA

523.16 2604
Distribution of Radio Brightness across the Andromeda Nebula—J. D. Kraus. (*Nature*, (London), vol. 175, pp. 502–503; March 19, 1955.) Measurements made with the 96-helix antenna and improved receiver at the Ohio State University are reported; the frequency used was 250 mc.

523.72:621.396.822.029.6 2605
Evidence of Limb-Brightening of the Sun at 60 cm Wavelength—G. Swarup and R. Parthasarathy. (*Observatory*, vol. 75, pp. 8–9; February, 1955.) See 2607 below.

523.72:621.396.822.029.6 2606
The Sun in Two Dimensions at 21 cm—W. N. Christiansen and J. A. Warburton. (*Observatory*, vol. 75, pp. 9–10; February, 1955.) See 2607 below.

523.72:621.396.822.029.6 2607
Distribution of Radio-Frequency Brightness across the Solar Disk at a Wavelength of 60 cm—P. A. O'Brien and E. Tandberg-Hanssen. (*Observatory*, vol. 75, pp. 11–13; February, 1955.) Results of three investigations (see also 2605 and 2606 above) indicate appreciable limb brightening, contrary to results reported by Stanier (1401 of 1950). There has been a marked change of brightness during the sunspot cycle. The radial extent of the distribution is greater at the equator than at the poles.

523.74:538.6:550.385.4 2608
Magnetic Field of the Sun—M. Waldmeier. (*Naturwiss.*, vol. 42, pp. 149–151; March, 1955.) The principles of operation of Babcock's Zeeman-effect solar magnetograph (*Astrophys. Jour.*, vol. 118, pp. 387–396; November, 1953.) are described and some experimental results obtained (see e.g. *Astrophys. Jour.*, vol. 119, pp. 687–688; May, 1954.) are shown in the form of magnetograms. The general magnetic-field strength is 1–2 oersted, of polarity opposite to that of the earth. Large local bipolar and unipolar fields have been observed and are shown in several of the magnetograms. The field distribution varies from day to day and fluctuations of the order of 1 oersted are believed to occur in local fields with periods of about 30 minutes. The unipolar fields are probably the sources of corpuscular emission which produce geomagnetic storms with a 27-day recurrence period.

523.78:621.396.11 2609
Some Observations in Bratislava during the Solar Eclipse on 30th June 1954—J. Šimaljak and A. Milerová. (*Bull. mét. tchécosl.*, vol. 7, pp. 132–134; November 30, 1954. In Slovak.) Relative measurements were made of the total radiation (Fig. 1.*a*1), radiation in the red (1.*a*2), yellow (1.*a*3) and ultraviolet (1.*a*4) bands, the air temperature (Fig. 2), detected intensity of broadcast transmissions from Bratislava I (Fig. 3) and the level of cosmic radiation (Fig. 4). The maximum in fig. 3 occurred about 30 minutes before the minima in Figs. 1 and 4.

550.3 2610
Scientific Programme of the International Geophysical Year 1957–58—S. Chapman. (*Nature*, (London), vol. 175, pp. 402–406; March 5, 1955.) An outline is given of comprehensive investigations planned in various branches of geophysics and allied subjects, including geomagnetism, the aurora, airglow, solar activity and ionospheric phenomena.

550.384 2611
Theories of the Earth's Magnetism—D. R. Inglis. (*Rev. Mod. Phys.*, vol. 27, pp. 212–248; April, 1955.)

550.386 2612
A Semi-annual Periodicity in the Beginnings of Recurrent Magnetic Storm Series—J. H. Rush. (*Nature*, (London), vol. 175, pp. 517–518; March 19, 1955.)

551.510.535 2613
A Note on the World-Wide Distribution of the Sporadic-E Ionisation—L. J. Prechner. (*Marconi Rev.*, vol. 18, pp. 1–7; 1st Quarter, 1955.) A discussion based on data obtained during 1944–45 from 31 ionospheric sounding stations, 10 of them in N. America. In geomagnetic mid-latitudes the prevalence of E_s clouds is greatest in local summer daytime. In the northern auroral and the equatorial zones no seasonal variation is apparent. In the auroral zone there is a daytime belt of intense E_s ionization and in the equatorial zone one at night time. These belts have different characteristics and appear to have different causes. Very marked variation with longitude has been noted.

551.510.535 2614
A Particular Feature of the F_2 Layer at Lwiro [Central Africa]—G. Bonnet. (*Ann. Géophys.*, vol. 10, pp. 348–350; October/December, 1954.) Observations over the period January to May, 1953 indicate that at the equinoxes the F_2 layer rapidly drops, sometimes to below 200 km, towards midnight, by an apparent contraction following an equally rapid expansion, often coinciding with the formation of a lower layer of measurable thickness corresponding to a night-time E layer.

551.510.535:523.78:621.396.81 2615
On Radio Measurements at Jabalpur during the Solar Eclipse of 30th June 1954—Ghose, Roy, Gupta, Das Gupta, Sarwate and Mithal. (See 2725.)

551.510.535:550.38 2616
Some Geomagnetic Effects in the Equatorial F_2 Region—N. J. Skinner and R. W. Wright. (*Jour. Atmos. Terr. Phys.*, vol. 6, pp. 177–188; April, 1955.) Observations at Ibadan, Nigeria, during 1952 show that the midday minimum of the maximum concentration of ionization exhibited on magnetically quiet days disappears and is replaced by a maximum as the degree of magnetic disturbance increases. The total ion content below the height of maximum ionization varies similarly. Perturbations due to magnetic disturbance have both diurnal and semidiurnal components. Difficulties in the application of Martyn's theory (3301 of 1953) are discussed and certain modifications are suggested.

551.593.9 2617
On a New Method of Determining the Height of the Nightglow—P. St. Amand, H. B. Pettit, F. E. Roach and D. R. Williams. (*Jour. Atmos. Terr. Phys.*, vol. 6, pp. 189–197; April, 1955.) Nightglow observations taken at two stations separated by a distance comparable with the height of the layer observed will show correlation over a period if both stations observe the same point; the height of the point can hence be deduced. Observations taken during two successive nights give a height between 80 and 100 km for the origin of the 5577 Å radiation.

551.594.221 2618
Equipment for Lightning Research on Monte San Salvatore—K. Berger. (*Bull. schweiz. elektrotech. Ver.*, vol. 46, pp. 193–201; March 5, 1955.) The equipment has been appreciably augmented since the previous report (110 of 1948).

551.594.5:538.69 2619
The Significance of a Nonterrestrial Magnetic Field in Neutral-Stream Theories of the Aurora—B. C. Landseer-Jones. (*Jour. Atmos. Terr. Phys.*, vol. 6, pp. 215–226; April, 1955.) The hypothesis that a neutral stream of ions travels from the sun with a velocity of 10^8 cm in a magnetic field of strength 10^{-5} G fits observed data on aurorae and magnetic storms.

551.594.5:550.385 2620
On the Electric Field Theory of Magnetic Storms and Aurorae—H. Alfvén. (*Tellus*, vol. 7, pp. 50–64; February, 1955.) The electric field theory is further developed. By taking into account the inertia of the beam of ionized gas emitted by the sun, the initial as well as the main phase of storms can be accounted for. See also 2621 below.

551.594.5:550.385 2621
Model Experiments on Aurorae and Magnetic Storms—L. Block. (*Tellus*, vol. 7, pp. 65–86; February, 1955.) Experiments on a magnetized sphere [2426 of 1947 (Malmfors)] were performed to check Alfven's theory (2620 above). Although a proper scaling down is not possible, some confirmation of the theory was obtained; in particular, the space charge accumulated in the discharge region discharges along the lines of magnetic force. Photographs of the discharge patterns produced at various electric and magnetic field strengths are shown and discussed.

551.594.5:621.396.96 2622
Radio Reflections from Aurorae: Part 2—K. Bullough and T. R. Kaiser. (*Jour. Atmos. Terr. Phys.*, vol. 6, pp. 198–214; April, 1955.) Observations made with a meteor-survey apparatus confirm the conclusions drawn previously (125 of January). The mean velocity of the reflecting regions changes from 600 m/s westwards at 1500 ut, with diffuse echoes, to 600 m/s eastwards at 0500 ut, with discrete echoes. There is a diurnal minimum of echo frequency between 2100 and 2200 ut, when the reflecting regions appear to be at rest, and echoes are absent from 0600 to 1300 ut. Correlation is observed between the radio echoes, the occurrence of visual aurorae and magnetic activity.

LOCATION AND AIDS TO NAVIGATION

621.396.93 2623
Use of Phase Measurements in a System for the Guiding and Location of Moving Objects—J. Zakheim. (*Onde élect.*, vol. 35, pp. 137–141; February, 1955.) Discussion of the O.N.E.R.A. radio-alignment system, in which a cw signal radiated by the moving object is received on the ground by a system having two pairs of antennas, one pair spaced $\lambda/2$ apart, the other separated by a distance $\gg\lambda$. The phase difference between signals received by the individual antennas can be measured with high accuracy and the position of the moving object hence determined. More elaborate equipment measures the speed of the object and enables its trajectory to be corrected.

621.396.933 2624
Airborne Interrogator spots Location—A. R. Applegarth. (*Electronics*, vol. 28, pp. 170–173; May, 1955.) Distance-measuring equipment in production as a result of the project described previously [2722 of 1951 (Borden et al.)] is described.

621.396.96 2625
Evaluation of Radar Sea Clutter—A. H. Schooley. (*Tele-Tech.*, vol. 14, pp. 70–71, 132; March, 1955.) A 1954 National Electronics Conference paper. Investigations of the statistical properties of a water surface disturbed by wind are discussed in relation to the design of military search radar.

621.396.96 2626
London Airport New-Type Radar—(*Elect. Jour.*, vol. 154, p. 694; March 4, 1955.) The Type-S.232 radar operates in the 50 cm band, thus retaining full efficiency in bad weather. A moving-target-indicator system is used in which both the reference signal and the stabilization of transmitter and receiver frequencies are crystal-controlled. The one equipment can serve all airport radar requirements except precision approach. The antenna system comprises parabolic reflector with off-set horn.

621.396.96:538.566 2627
Elliptically and Circularly Polarized Electromagnetic Waves—Bouix. (See 2601.)

621.396.96.095.1 2628
A Polarized Mirror Duplexer for use with a Circularly Polarized Lens Aerial—J. F. Ramsay and W. F. Gunn. (*Marconi Rev.*, vol. 18, pp. 29–36; 1st Quarter 1955.) A simple alternative to the waveguide duplexer suggested in an earlier paper [2811 of 1952 (Ramsay)] is to use a closely spaced grating as a polarization-sensitive mirror, to separate two orthogonally polarized waves. A cross-talk factor of −65 db was obtainable for such a duplexer over the band 8.65–8.8 mm., or −75 db over a narrow band. A simple radar equipment incorporating this duplexer is discussed. An overall cross-talk factor of −55 db was obtainable over a 2 per cent bandwidth.

621.396.962.2:621.396.621.54.029.6 2629
Local Oscillator for C. W. Radars—H. B. Goldberg. (*Electronics*, vol. 28, pp. 166–167; May, 1955.) The need for a local X band oscillator valve and special frequency-control circuits is avoided by using a crystal-controlled oscillator operating at the receiver if, which beats with a portion of the transmitter oscillator output, giving sidebands one of which is mixed with the received signal to obtain the desired if.

621.396.962.23 2630
Direction-Sensitive Doppler Device—H. P. Kalmus. (Proc. IRE, vol. 43, pp. 698–700; June, 1955.) Radar cw Doppler method is described in which, as well as the usual Doppler-frequency signal, a second signal with a 90 per cent phase difference is produced, the sign of the phase difference depending on whether the target is approaching or receding. A single antenna with a low-loss duplexing arrangement using a gyrator is used. Various applications are indicated.

621.396.962.3:621.396.822 2631
Signal-Detection Studies, with Applications—E. L. Kaplan. (*Bell Syst. Tech. Jour.*, vol. 34, pp. 403–437; March, 1955.) Curves are given relating the probability of detection of a signal in noise to the signal-noise ratio, to the proportion of false detections which can be tolerated, and to the time available. Three sets of conditions are considered: (*a*) steady sinusoidal signal, (*b*) fading sinusoidal signal, (*c*) signal varying as rapidly as noise. The curves are used to determine the best values of radar parameters, such as pulse energy, scan rate and averaging time.

MATERIALS AND SUBSIDIARY TECHNIQUES

533.583:621.385 2632
Barium Getters in Carbon Monoxide—J. Morrison and R. B. Zetterstrom. (*Jour. Appl. Phys.*, vol. 26, pp. 437–442; April, 1955.) The effectiveness of a 5 mg iron-clad Ba getter for cleaning up CO was studied as a function of pressure, temperature and physical state, using a method based on that of Wagener (122 of 1951). At CO pressures around 10^{-5} mm the getter is exhausted in about 1,000 hours. The gettering rate is nearly independent of pressure over the range 10^{-5} mm -10^{-7} mm. Temperature variation from 25 degrees to 150 degrees C has little effect. Flashing in argon to obtain a diffuse deposit increased the gettering rate by a factor of two or three for the first hundred hours.

535.215:537.224 2633
Persistent Internal Polarization—H. Kallmann and R. Rosenberg. (*Phys. Rev.*, vol. 97, pp. 1596–1610; March 15, 1955.) Experimental studies on the production of polarization in photoconductive fluorescent substances of high dark resistance, by the action of various kinds of wave and particle radiation in the presence of a unidirectional electric field are reported. Effects similar to those in electrets are produced. The polarization is due to a partial separation by the applied field of free charges produced by the radiation, and to their trapping. The mechanisms involved are discussed.

535.215:546.817.231 2634
Preparation of Sensitive PbSe Photoconductors—H. Gobrecht, F. Niemeck and F. Speer. (*Naturwiss.* vol. 42, p. 152; March, 1955.) A brief note on infrared-sensitive PbSe layers prepared by a method similar to that used for InSe by Bode and Levinstein (1777 of 1954). Sensitivity at room temperature is increased to an appreciable level by interrupting the vacuum heat treatment by exposure to air at about 120 degrees C.

535.37 2635
Fundamental Law of Escape from Traps [in phosphors]—D. Curie. (*C. R. Acad. Sci.*, (Paris), vol. 240, pp. 1614–1616; April 13, 1955.)

537.226/.027 2636
Optical Study of $PbZrO_3$ and $NaNbO_3$ Single Crystals—F. Jona, G. Shirane, and R. Pepinsky. (*Phys. Rev.*, vol. 97, pp. 1584–1590; March 15, 1955.) Investigations throwing light on the mechanism of antiferroelectric transitions in perovskite-type crystals are described.

537.227:546.431.824-31:534.2-8 2637
Ultrasonic Attenuation Studies in Biased $BaTiO_3$ Ceramics—T. F. Hueter and D. P. Neuhaus. (*Jour. Acous. Soc. Amer.*, vol. 27, pp. 292–296; March, 1955.) Observations were made of the variation with temperature and with applied field of the ultrasonic attenuation produced by polycrystalline $BaTiO_3$; pulses of 10 mc vibrations were used. Maxima in the attenuation/field-strength curve are observed for those values at which the electromechanical response varies rapidly. The observations are related to domain-wall movements of two kinds. In both cases the losses appear to be caused by elastic hysteresis due to dislocation movement.

537.228.1 2638
Piezoelectric Effect in Wood—V. A. Bazhenov. (*Trud. Inst. Lesa*, vol. 9, pp. 281–314; 1953. *Referativnyi Zh., Fiz*, pp. 172–173; March, 1955. Abstract 4950.) The piezoelectric effect was observed in dried specimens of oak, pine, birch, and beech; the effect was not noticeable in some isotropic woods. The magnitude of the constant $d_{14}(=-d_{25})$ ranged between 0.3×10^{-8} and 0.7×10^{-8} esu, i.e. about one tenth of the constant d_{11} for quartz. The dependence of the piezoelectric properties on the temperature, humidity, and dimensions of specimens was also investigated. The piezoelectric effect in wood is shown to be due to the presence of cellulose.

537.311.3.023:[537.226.2+538.213 2639
Effective Electrical Conductivity of a Medium with Inclusions—I. K. Ovchinnikov and G. G. Kilyukova. (*Bull. Acad. Sci. (URSS), sér. géophys.*, no. 1, pp. 57–59; January/February, 1955. In Russian.) Formulas are given for the conductivities parallel to

the cartesian coordinate axes of a medium with embedded conducting particles in the form of ellipsoids. The formulas also apply to calculations of the dielectric constant and the effective permeability, and can be adapted to deal with particles of other shapes. Calculated and experimental results are tabulated and show good agreement.

537.311.31 2640

Resistivity in Metals. Resistivity Changes by Plastic Deformation of Polycrystalline Metals—H. G. van Bueren and P. Jongenburger. (*Nature*, (London), vol. 175, pp. 544–545; March 26, 1955.) Resistivity measurements have been made on annealed wires of 99.99 per cent pure Cu and Ag plastically deformed in extension and in torsion at 20 degrees K and at 77 degrees K. The results are discussed in terms of dislocations and point defects; the latter are apparently responsible for nearly all the resistivity increase associated with the plastic deformation.

537.311.31 2641

Resistivity in Metals. Extra-Resistivity due to Interstitial Atoms in Copper—P. Jongenburger. (*Nature*, (London), vol. 175, pp. 545–546; March 26, 1955.) An approximate calculation is presented.

537.311.33 2642

Transport Properties of a Many-Valley Semiconductor—C. Herring. (*Bell. Syst. Tech. Jour.*, vol. 34, pp. 237–290; March, 1955.) In the semiconductor conduction-band model discussed, the energy of an electron, considered as a function of its wave-number vector, has a number of minima, or "valleys." For the valence band the conditions are inverted. For models of this type the theory is developed for (*a*) mobility and its temperature dependence, (*b*) thermoelectric power, (*c*) piezoresistance, (*d*) Hall effect, (*e*) hf dielectric constant, and (*f*) magneto-resistance. These phenomena are treated, for the cases to which Maxwellian statistics apply, on the assumption that the scattering of the charge carriers can be represented by a relaxation time which depends on energy only, but is otherwise unrestricted. Special attention is given to the role of intervalley lattice scattering.

537.311.33 2643

Considerations on the Location of Generation and Recombination Phenomena at Contact Barriers and at the Surface of a Semiconductor—N. Nifontoff. (*Compt. Rend. Acad. Sci.*, (Paris), vol. 240, pp. 1634–1636; April 18, 1955.) Assuming that the energy levels of traps are distributed uniformly over the forbidden band, it is shown on the basis of theory developed by Shockley and Read (420 of 1953) that carrier generation and recombination are maximum for traps at the neutral level, i.e. the Fermi level or midway between quasi-Fermi levels. These considerations explain observed phenomena such as high recombination rate near a free surface, the occurrence of Zener current in *p-n* junctions at high reverse voltage, and certain photoelectric effects.

537.311.33 2644

Injected Current Carrier Transport in a Semi-infinite Semiconductor and the Determination of Lifetimes and Surface Recombination Velocities—W. van Roosbroeck. (*Jour. Appl. Phys.*, vol. 26, pp. 380–391; April, 1955.) "With both surface and volume recombination taken into account, time-dependent and steady-state Green's functions are obtained for a point source of added carriers in a semi-infinite semiconductor, and for infinite line and plane sources parallel to the surface. Small-signal theory is employed, and a compact Stieltjes-integral derivation is given. The Green's functions are specialized to provide: the time dependence of surface concentration following the instantaneous injection of carriers at a point on the surface; that following instantaneous injection which is uniform over the surface: and the distance dependences for steady point, infinite-line, semi-infinite plane, and semi-infinite line surface sources. Steady flows of minority carriers from these sources into a *p-n* junction perpendicular to the surface are also calculated. Analytical approximations are found for the steady-source cases. Theoretical and experimental aspects of the determination of lifetimes and surface recombination velocities from data by means of these results are discussed."

537.311.33:535.215 2645

Photoconductivity in Calcium Tungstate—J. R. Cook. (*Proc. Phys. Soc.* (London), vol. 68, pp. 148–155; March 1, 1955.) Measurements on artificial single crystals indicate that photoconductivity is produced on exposure to ultraviolet radiation. The material is an intrinsic semiconductor with an activation energy of 2.1 ev.

537.311.33:535.215:538.63 2646

Photodiffusion Current Hall Effect: Transient Behavior—L. H. Hall. (*Phys. Rev.*, vol. 97, pp. 1471–1474; March 15, 1955.) Theory is developed to account for the voltage peak preceding the steady-state value, as observed by Bulliard (3231 of 1954).

537.311.33:537.52:621.315.61 2647

Space-Charge-Limited Currents in Solids—A. Rose. (*Phys. Rev.*, vol. 97, pp. 1538–1544; March 15, 1955.) Theory is developed for the processes described by Smith and Rose (2666 below). The relation of these processes to breakdown in insulators is discussed.

537.311.33:537.58:[546.28+546.289 2648

Thermal Ionization and Capture of Electrons Trapped in Semiconductors—H. Gummel and M. Lax. (*Phys. Rev.*, vol. 97, pp. 1469–1470; March 15, 1955.) Calculations are made of the ionization and capture probabilities for Si and Ge, using Coulomb wave functions. The results are consistent with the upper limit to to the lifetime of photoconductive carriers determined experimentally by Burstein et al. (*Phys. Rev.*, vol. 89, pp. 331–332; January 1, 1953.)

537.311.33:[546.28+546.289 2649

Theory of the Infrared Absorption of Carriers in Germanium and Silicon—A. H. Kahn. (*Phys. Rev.*, vol. 97, pp. 1647–1652; March 15, 1955.) The Drude-Zener theory is used to study infrared absorption in *n*-type Ge and *p*-type Si. Average values are determined for the effective masses of electrons in Ge and holes in Si. Infrared absorption bands in *p*-type Ge are explained on the basis of transitions of holes among three energy bands lying near the top of the valence band, this structure being suggested by cyclotron resonance experiments. On the basis of this theory, absorption peaks are to be expected at wavelengths near 25 μ and 33 μ for *p* type Si.

537.311.33:546.28 2650

Theory of Donor Levels in Silicon—W. Kohn and J. M. Luttinger. (*Phys. Rev.*, vol. 97, p. 1721; March 15, 1955.) Extension of theory presented by Luttinger and Kohn (1390 of May).

537.311.33:546.28 2651

Excited Donor Levels in Silicon—W. H. Kleiner. (*Phys. Rev.*, vol. 97, pp. 1722–1723; March 15, 1955.)

537.311.33:546.28 2652

On the Measurement of Minority-Carrier Lifetime in *n*-type Silicon—J. B. Arthur, W. Bardaley, A. F. Gibson, and C. A. Hogarth. (*Proc. Phys. Soc.*, vol. 68, pp. 121–129; March 1, 1955.) Four known methods are examined and discrepancies between the results are discussed. Precautions necessary to obtain valid results with the traveling-light-spot method are indicated. Erroneous results may be obtained if methods developed for measurements on Ge are applied indiscriminately to other semiconductors.

537.311.33:546.28 2653

Radioactivation Analysis of Arsenic in Silicon—J. A. James and D. H. Richards. (*Nature* (London), vol. 175, pp. 769–770; April 30, 1955.) Outline of a method for determining sub-microgram quantities of arsenic impurity, involving irradiation of the impure Si specimen with thermal neutrons.

537.311.33:546.28 2654

Densitometric and Electrical Investigation of Boron in Silicon—F. H. Horn. (*Phys. Rev.*, vol. 97, pp. 1521–1525; March 15, 1955.) Results of this investigation confirm that boron resides substitutionally in the Si lattice for concentrations up to 0.3 atom per cent.

537.311.33:546.289 2655

Thermoelectric Power of Germanium at Low Temperatures—E. Mooser and S. B. Woods. (*Phys. Rev.*, vol. 97, pp. 1721–1722; March 15, 1955.) Measurements are reported providing evidence of a contribution to the thermoelectric power due to electron scattering by lattice vibrations with a bias towards the colder end of the sample [3498 of 1947 (Gurevich)].

537.311.33:546.289 2656

Infrared Absorption of Germanium near the Lattice Edge—G. G. Macfarlane and V. Roberts. (*Phys. Rev.*, vol. 97, pp. 1714–1716; March 15, 1955.) Observations are reported giving results in agreement with calculations made by Hall et al. (152 of January) for indirect transitions of valence electrons.

537.311.33:546.289 2657

Measurement of the Lifetime of Minority Carriers in Germanium—W. G. Spitzer, T. E. Firle, M. Cutler, R. G. Shulman, and M. Becker. (*Jour. Appl. Phys.*, vol. 26, pp. 414–417; April, 1955.) Two methods are described, both useful for measuring the lifetime in a small region rather than the average value over the sample. One is a modification of the method described by Haynes and Shockley (1928 of 1951), using pulsed injection of carriers into a filament with detection, after a known delay, at a spaced collector. The other is based on the decay of the spreading resistance resulting from injection of carriers at a point contact, as described by Many (2129 of 1954).

537.311.33:546.289 2658

Breakdown Effect in p-n Alloy Germanium Junctions—R. D. Knott, I. D. Colson, and M. R. P. Young. (*Proc. Phys. Soc.* (London), vol. 68, pp. 182–185; March 1, 1955.) Two forms of breakdown mechanism identified by McKay and McAfee in grown junctions (1079 of 1954) are investigated in relation to alloyed-In junctions. Observed and theoretically predicted results both indicate that for Ge of resistivity $>0.5\Omega$. cm avalanche breakdown occurs, while for resistivity $<0.5\ \Omega$. cm field-emission theory applies.

537.311.33:546.289 2659

Germanium in Power-Station Boiler Plant—J. S. Forrest, A. C. Smith, and J. M. Ward. (*Nature*, (*London*), vol. 175, p. 558; March 26, 1955.) Determinations have been made of the quantity of Ge in over 60 samples of dust and deposits taken from various types of steam-raising plant of the British Electricity Authority. The results indicate that deposits from such sources only occasionally contain useful amounts of Ge. Experiments are planned on the effect of pyrites and chlorides of Na and K on the release of Ge during the combustion of coal.

537.311.33:546.289:621.396.822 2660
Variation of Noise with Ambient in Germanium Filaments—T. G. Maple, L. Bess, and H. A. Gebbie. (*Jour. Appl. Phys.*, vol. 26, pp. 490–491; April, 1955.) An experimental investigation of $1/f$ noise in semiconductors is reported briefly. Noise-power/frequency curves are shown for filaments immersed successively in dry N_2 and in liquid CCl_4, the filament surface being in one case sand-blasted and in the other case etched. The observations for N_2 are consistent with the addition of $1/f$ noise and shot noise, those for CCl_4 are not.

537.311.33:546.368.63 2661
Hall Effect in Cesium Antimonide with Audiofrequency Currents—T. Sakata. (*Jour. Phys. Soc.* (Japan), vol. 9, pp. 1030–1031; November/December, 1954.) Variations in the Hall effect over the temperature range 189 degrees–357 degrees K are investigated for various Cs_3Sb samples; results are tabulated.

537.311.33:546.368.63 2662
On the Thermoelectric Power of Cesium Antimonide—T. Sakata. (*Jour. Phys. Soc.* (Japan), vol. 9, pp. 1031–1032; November/December, 1954.) Thermoelectric power measurements were made over the temperature range 220 degrees–305 degrees K. Values of Hall coefficient computed from these measurements are uniformly higher than those previously measured (2661 above).

537.311.33:546.431–31 2663
On the Optical Absorption of Thin BaO Film in the Ultraviolet Region—K. Takazawa and T. Tomotika. (*Jour. Phys. Soc.* (Japan), vol. 9, pp. 996–1000; November/December, 1954.) A hitherto unreported absorption band with a maximum at about 3000 Å was observed, which coincides with the first maximum of photoconductivity in BaO single crystals. It vanished when the film was exposed to oxygen.

537.311.33:546.482.21 2664
Temperature Dependence of the Hall Effect and the Resistivity of CdS Single Crystals—F. A. Kröger, H. J. Vink, and J. Volger. (*Philips Res. Rep.*, vol. 10, pp. 39–76; February, 1955.) Measurements were made on CdS crystals, pure, and doped with Ga and Cl, in the temperature range 25 degrees–700 degrees K. Peaks in the Hall-constant/temperature curves indicate a double-band conduction mechanism. At room temperature electron mobility in the normal conduction band is about 210 cm per v/cm; mobility in the donor band increases both with the concentration of donors and with the number of electrons. In the case of insulating crystals, the reduction of photocurrent on application of additional infrared irradiation is due to the latter decreasing the concentration of free electrons, mobility being unaffected; If capacitance measurements give a value of 11.6 ± 1.5 for dielectric constant. 51 references.

537.311.33:546.482.21 2665
Properties of Ohmic Contacts to Cadmium Sulfide Single Crystals—R. W. Smith. (*Phys. Rev.*, vol. 97, pp. 1525–1530; March 15, 1955.) Indium and gallium have been found to make good nonrectifying noise-free contact with CdS crystals, thus facilitating experimental investigation of the rectifying and photoconductive properties of the material. Various measurements are reported.

537.311.33:546.482.21 2666
Space-Charge-Limited Currents in Single Crystals of Cadmium Sulfide—R. W. Smith and A. Rose. (*Phys. Rev.*, vol. 97, pp. 1531–1537; March 15, 1955.) Using a pair of the nonrectifying contacts described by Smith (2665 above), currents of 20 A/cm² have been drawn through unilluminated crystals of CdS. Experimental evidence indicates that these currents are space-charge-limited. The value of the current is lower by several orders of magnitude than that obtained with a trap-free solid; hence this type of experiment should be useful for measuring trap concentration.

537.311.33:546.681.86 2667
Electrical Properties of Gallium Antimonide—D. P. Detwiler. (*Phys. Rev.*, vol. 97, pp. 1575–1578; March 15, 1955.) Measurements are reported on some p-type samples and one n-type sample over the temperature range −196 degrees to 650 degrees C. The intrinsic energy gap is 0.78 ev at −198 degrees C. The mobility of electrons in n-type material is several times greater than the hole mobility. The problem of preparing the material with a purity comparable to that of Ge is discussed.

537.311.33:546.817.221 2668
Mobility of Electrons and Holes in the Polar Crystal, PbS—R. L. Petritz and W. W. Scanlon. (*Phys. Rev.*, vol. 97, pp. 1620–1626; March 15, 1955.) Hall coefficient and resistivity values determined experimentally by Brebrick and Scanlon (1410 of May) are used to calculate mobility curves for PbS; these are used as a basis for discussing theoretical work on mobility in polar crystals and to derive estimates of the effective masses of electrons and holes.

537.311.33:621.314.7 2669
Comparative High-Frequency Operation of Junction Transistors made of Different Semiconductor Materials—Giacoletto. (See 2782.)

538.221 2670
Ferromagnetic Resonance Absorption in Colloidal Suspensions—D. M. S. Bagguley. (*Proc. Roy. Soc. A*, vol. 228, pp. 549–567; March 22, 1955.) Suspensions of pure metals and alloys have been investigated at wavelengths of 3.14 and 1.25 cm, at 290 degrees K. The g-factor for Fe is 2.06 ± 0.02 and for Ni 2.22 ± 0.02. In the Ni–Fe alloys anomalous variation of g-factor with Ni content is observed. Except in the case of Ni there is good agreement between results from the microwave measurements and those from gyromagnetic experiments. The half-width of the absorption line for Fe is 700 oersteds[1] ± 10 per cent. For the face-centered alloys the line width varies smoothly with a minimum value of 300 oersteds near 70 per cent Ni.

538.221:537.323 2671
Magneto-thermoelectric Powers of Nickel Single Crystals—N. Miyata and Z. Funatogawa. (*Jour. Phys. Soc.* (Japan), vol. 9, pp. 967–973; November/December, 1954.) The change of thermoelectric power due to magnetization, E_m, was measured on Ni single crystals, and calculated for the [100] and [111] directions; the values obtained at room temperature are 0.57 μV/degrees C and 0.69 μV/degrees C respectively. E_m values reach a maximum around room temperature. E_m is positive except near the Curie point, where it may be negative due to additive magnetization proportional to the external magnetic field.

538.221:538.569.4 2672
The Relaxation Process in Ferromagnetic Resonance Absorption—T. Kasuya. (*Progr. Theor. Phys.*, vol. 12, pp. 802–805; December, 1954.) Results of analysis based on the spin-wave approximation suggest that the line width in ferrites is determined mainly by lattice imperfections causing interaction between spin waves having zero and nonzero vectors. Discussion gives support to the view that in metals such as Ni, as opposed to ferrites, processes involving interaction with conduction electrons are of greater importance than collisions between spin waves.

538.221:538.652 2673
The Temperature Dependence of Magnetostriction in a Nickel Crystal—W. D. Corner and G. H. Hunt. (*Proc. Phys. Soc.*, vol. 68, pp. 133–144; March 1, 1955.) Using the capacitance bridge described in 1752 of June, the longitudinal magnetostriction of prolate-spheroid specimens prepared from a Ni single crystal was measured over the temperature range −180 degrees to 360 degrees C. The results indicate that at low temperatures the magnetostriction below saturation varies with magnetization approximately in accordance with Heisenberg's domain theory; with increasing temperature there is a steady departure from the calculated values. The variation of saturation magnetostriction with temperature did not correspond to any known theory.

538.221:621.318.134 2674
Motion of Individual Domain Walls in a Nickel-Iron Ferrite—J. K. Galt. (*Bell Syst. Tech. Jour.* vol. 34, pp. 439–441; March, 1955.) Correction to paper abstracted in 175 of January.

548.5:549.514.51 2675
Influence of Impurities on the Growth of Quartz Crystals from Flint and Quartzite—C. S. Brown, R. C. Kell, P. Middleton, and L. A. Thomas. (*Nature* (London), vol. 175, pp. 602–603; April 2, 1955.) Processes are described by means of which quartz crystals can be grown from readily available flint and quartzite, having properties similar to those of crystals grown from melting-quality quartz.

621.315.5/.6+621.318.22 2676
The Development of New Materials—F. E. Robinson. (*Marconi Rev.*, vol. 18, pp. 60–68; 2nd Quarter 1955.) The review presented earlier (3166 of 1949) is brought up to date. Permanent-magnet materials are included.

621.315.6 2677
Dielectric Properties of Pinacol Hydrate: Application to Temperature Measurement—J. S. Dryden and R. J. Meakins. (*Nature* (London), vol. 175, p. 603; April 2, 1955.) This material is found to have a permittivity variation of 5.5 per cent per degree C at a dispersion region centered about a frequency of 80 kc at 20 degrees C.

621.315.616 2678
Conductivity induced in Unplasticized 'Perspex' by X-Rays—J. F. Fowler and F. T. Farmer. (*Nature*, (London), vol. 175, pp. 516–517; March 19, 1955.) Differences from the behavior of the plasticized material (2153 of 1954) are noted. Unplasticized perspex is grouped with polyethylene, polytetrafluorothene and polystyrene, all of which display an exponential distribution of traps in depth.

621.315.616.9 2679
Conductivity Induced by X-Rays in Polyethylene Terephthalate: a Possible Insulator for Radiological Apparatus—J. F. Fowler and F. T. Farmer. (*Nature* (London), vol. 175, pp. 590–591; April 2, 1955.)

621.315.616.9.011.5 2680
Dependence of Coefficient of Dielectric Losses ϵ'' of Polar Polymers on Temperature—P. F. Veselovski. (*Zh. Tekh. Fiz.*, vol. 25, pp. 266–269; February, 1955.)

621.318.134:538.566.029.6:538.6 2681
On the Microwave Cotton-Mouton Effect in Ferroxcube—F. K. du Pré. (*Philips Res. Rep.*, vol. 10, pp. 1–10; February, 1955.) The effect investigated is the splitting of a microwave beam traversing a ferrite to which a transverse magnetic field is applied. Measurements were made at 9.35 kmc on a sample of ferroxcube IVB held between two glass plates, to determine the phase difference of the emergent waves as a function of the field intensity. Results are in fair agreement with theory for the simplified case of plane wave transmission through a ferrite with small damping loss.

Considerable phase differences can be produced by small applied fields.

669.046.54 2682
Cage Zone Refining—P. H. Brace, A. W. Cochardt, and G. Comenetz. (*Rev. Sci. Instr.*, vol. 26, p. 303; March, 1955.) Need for a crucible is avoided by preparing the specimen in an elongated form with polygonal cross section. On passing such a specimen longitudinally through a short induction coil, a short length of the specimen can be kept molten throughout its interior while the edges, or attached fins, remain solid and constitute the "cage." The method is not suitable for growing single crystals.

MEASUREMENTS AND TEST GEAR

531.76:621.318.57 2683
Short-Interval Timer—N. A. Moerman. (*Electronics*, vol. 28, pp. 168–169; May, 1955.) The timer comprises a counter circuit in which delay in registering the stop pulse of a period is eliminated by a bypass circuit.

621.3.018.41(083.74):621.373.4 2684
High-Stability Bridge-Balancing Oscillator—P. G. Sulzer. (PROC. IRE, vol. 43, pp. 701–707; June, 1955.) A frequency-standard unit in which the frequency varies by only a few parts in 10^{10} over a day has a 1-mc GT-cut crystal serving as resonator both for the oscillator and for the bridge from which the automatic frequency control voltage is obtained. See also 1726 of June (Lea).

621.314.5.024.12:621.317.3 2685
A Generator for Very Small Direct Currents—K. D. E. Crawford. (*Jour. Sci. Instr.*, vol. 32, pp. 128–131; April, 1955.) A linearly changing voltage with rate of change controlled by a differentiating circuit is applied to a specially constructed, cylindrical capacitor. The output current can be varied between 2×10^{-17} and 2×10^{-10} A. Source resistance is $>10^{16}\Omega$. Applications in calibrating current measuring devices and in measuring high resistance and possibly capacitance are noted.

621.314.7.001.4 2686
The Measurement and Display of the Current Gain (α) of a Transistor as a Function of Emitter Current—Hilbourne. (See 2784.)

621.317.328 2687
Visual Display of Electromagnetic Waves—H. Kleinwächter. (*Arch. elekt. Übertragung*, vol. 9, pp. 154–156; March, 1955.) The method described is suitable for observing microwave radiation fields with large intensity variations, such as the diffraction field behind a conducting screen. A test signal from a klystron modulated at 5 kc is compared for phase and amplitude with that picked up by an electric-dipole probe carrying a lamp controlled by the detector. The probe is guided along concentric arcs and the fluctuations of lamp brightness are recorded photographically.

621.317.328:621.372.413 2688
A Method of Measuring the Intensity Distributions of Radio-Frequency Electric and Magnetic Fields in Resonant Cavities—J. G. Linhart and T. H. B. Baker. (*Brit. Jour. Appl. Phys.*, vol. 6, pp. 100–103; March, 1955.) The method is based on changes in resonance frequency and Q factor caused by introduction of a small sphere of dielectric or ferromagnetic material. See also 2265 of 1952 (Maier and Slater).

621.317.329:621.385.029.6 2689
A Proposed Method of investigating the Field Distribution in a Magnetron—Aikin. (See 2792.)

621.317.331:537.311.33 2690
Theoretical Bases of the Probe Method of Measurement of Resistivity and Hall Constant—J. Laplume. (*Onde élect.*, vol. 35, pp. 113–125; February, 1955.) Theory of the method described by Pistoulet (*ibid.*, vol. 35, pp. 82–87; January, 1955.) See also 1502 of 1954 (Valdes).

621.317.333.6 2691
Solid-Dielectric Breakdown Techniques—J. J. Chapman, L. J. Frisco, and J. S. Smith. (*Jour. Electrochem. Soc.*, vol. 102, pp. 67–72; February, 1955.) Solder sprayed from a gun into a properly shaped cavity in the specimen under test formed an embedded electrode which was found satisfactory for breakdown-strength measurements at frequencies between 60 c/s and 100 mc and at temperatures between −55 degrees and 125 degrees C. The technique used is described.

621.317.333.8 2692
Automatic Control and Display in Impulse Testing—R. F. Saxe. (PROC. IRE, part B, vol. 102, pp. 371–374; May, 1955.) Circuits are described for triggering the impulse generator automatically at a preset charging voltage, enabling the peak voltage and duration of the waveform to be displayed on ordinary meters rather than on a cro.

621.317.337:621.372.412 2693
Determination of Quality Factor of Quartz Crystals in Parallel Resonance—G. Brunner and A. Lösche. (*Z. angew. Phys.*, vol. 7, pp. 67–71; February, 1955.) An analysis is made of the response of a parallel-tuned circuit to a voltage whose frequency varies linearly with time; the differential equation involved is solved by suitable transformations. The final expression gives the instantaneous voltage across the tuned circuit in terms of the instantaneous value of the driving current and of a function of the circuit parameters; this latter function, the Fresnel function [671 of 1949 (Hok)], is shown graphically. In the experimental arrangement described, the Fresnel function is displayed on a cro screen and hence by comparison with the plotted function the quality factor can be deduced. See also 2058 of July (Mayer).

621.317.35:621.3.018.78 2694
Measurement of Nonlinearity Distortion—M. G. Scroggie. (*Wireless World*, vol. 61, pp. 317–323; July, 1955.) The degree of distortion caused by sound-reproducing equipment should be expressed simply and so as to correspond with aural judgment. Various methods of measurement are discussed; adoption of a fixed distortion-product frequency between 1,000 and 2,000 cps is suggested, with two input signals whose amplitudes are in the ratio 4:1.

621.317.361:621.396.822 2695
Mean Frequency Determination of Narrow-Band Noise Spectra—W. W. H. Clarke and R. F. Nikkel. (*Proc. I.E.E.*, part B, vol. 102, pp. 364–370; May, 1955.) The design is discussed of a magnetic-amplifier servo-loop system for continuously measuring the mean frequency of a signal whose energy/frequency characteristic approximates to a symmetrical Gaussian distribution. Spectra of this type can be obtained by passing white noise through two Π sections of a constant-k filter. The effect of signal deviation from the assumed characteristics is discussed, and the degree of signal asymmetry which can be tolerated without undue loss of accuracy is indicated.

621.317.7 2696
Considerations of Mechanical Shock in the Loading and Testing of Instruments—K. Hintermann. (*Bull. schweiz. elektrotech. Ver.*, vol. 46, pp. 201–206; March 5, 1955.) The subject is discussed with reference to a vibrating-plate frequency meter.

621.317.7:778.3 2697
Equipment of Instrumental Accuracy for Recording and Reproduction of Electrical Signals, using Cinematographic Film—H. McG. Ross. (*Proc. I.E.E.*, part B, vol. 102, pp. 323–339; May, 1955. Discussion, pp. 339–342.) A description is given of apparatus designed as an adjunct to electrical measuring equipment, covering the frequency range 0–1 kc; the errors are about 1 per cent over most of the range. The film records are reproduced by means of a photocell arrangement. Comparison is made between disk, magnetic-tape and kinematographic recording systems for this application.

621.317.7.029.6:621.372.8 2698
The Squeeze Section, a Simple and Universal Measurement Apparatus for Centimetre Wavelengths—H. Severin. (*Tech. Mitt. schweiz. Telegr.-Teleph. Verw.*, vol. 33, pp. 130–135; March 1, 1955. In German.) Impedance measurements can be made conveniently using a waveguide having a region with adjustable cross section. The geometrical length from the test object to the probe remains fixed, the determination being based on the relation between the mechanical deformation and the electrical length of the line. The device is also useful as a precision phase shifter. See also 21 of January.

621.317.725.082.72 2699
An Attracted-Disc Absolute Voltmeter—G. W. Bowdler. (*Proc. I.E.E.*, part B, vol. 102, pp. 301–309; May, 1955. Discussion, pp. 310–312.) Details are given of the design and performance of an instrument operating in compressed gas. Measurement accuracy is within about 1 per cent at 1 kv and about 0.1 per cent at 30 kv and above.

621.317.726 2700
Automatic Slide-Back Voltmeter—H. J. Fraser. (*Wireless Eng.*, vol. 32, pp. 187–189; July, 1955.) The instrument described was designed to indicate directly the peak voltage of recurring positive pulses as used, e.g. for valve testing. The pulses are applied to a diode detector which is automatically biased so that the difference between the input voltage and the slide-back bias is small. The slide-back bias is obtained by integrating the output pulses of a multivibrator which is triggered by this difference voltage. Experimental results are presented for pulse widths of 0.5–50 μs and repetition rates of 10–20000 pulses/s. The maximum error is ±2 v over the range 0–100 v.

621.317.726 2701
A Transient-Voltage Measuring Instrument—*Electrotech. Jour.*, vol. 154, p. 917; March 18, 1955.) Description of a commercially available peak voltmeter in which the control grid of a thyratron is connected to a tapping switch on a noninductive potentiometer across which the transient is applied. Indication of the firing of the thyratron is given by a neon lamp. The maximum permissible continuous input voltage, either alternating or direct, is 2.24 kv. Voltages >35 kv can be measured.

621.317.729:621.372.5 2702
Electrolyte Tank for solving Network Problems—V. Met. (*Frequenz*, vol. 9, pp. 57–63; February, 1955.) The tank described is of a form which is the result of a reflection and two different conformal transformations of the complex frequency plane, by means of which the positive $j\omega$ axis is reproduced on the circular perimeter of the trough. This reduces the errors due to inaccurate electrode positioning. Measurements are limited to the determination of potential; the current function is determined by graphical integration. The accuracy of the method is illustrated by a simple example.

621.318.4.013.2:621.317.4 2703
A Screened Uniform Magnetic Field—E. G. Schlosser. (*Z. angew. Phys.*, vol. 7, pp. 59–61; February, 1955.) The production is considered of a highly uniform magnetic field by means of

a pair of Helmholtz coils symmetrically placed inside a high-permeability cylindrical container witl end plates. The optimum dimensions of the system are stated and the experimentally determined radial variation of the field parallel to the axis is shown graphically, both for the screened arrangement and the usual Helmholtz coil arrangement. The calculated characteristics agree well with those determined experimentally.

621.385.001.4 2704
An Inflection-Point Emission Test—Hopkins and Shrivastava. (See 2787.)

621.385.001.4 2705
Subminiature-Tube Reliability Testing—Bickel. (See 2788.)

OTHER APPLICATIONS OF RADIO AND ELECTRONICS

534.2-8 2706
A Method of Transducing an Ultrasonic Shadowgraph or Image for Display on an Oscilloscope—E. E. Suckling and W. R. MacLean. (*Jour. Acous. Soc. Amer.*, vol. 27, pp. 297–301; March, 1955.) A pattern of piezoelectric voltage set up on the surface of a quartz plate, corresponding to the pattern of an exciting ultrasonic field, is scanned capacitively.

534.222.2:621.396.96 2707
Measurement of Detonation Velocity by Doppler Effect at Three-Centimeter Wavelength—M. A. Cook, R. L. Doran, and G. J. Morris. (*Jour. Appl. Phys.*, vol. 26, pp. 426–428; April, 1955.) The ionized wave front of the detonation wave acts as a moving reflector for em waves directed against it. Results are reported for four solid explosives. Complexities in the observed Doppler patterns occur because the cylindrical charges act as multimode dielectric waveguides.

621.317.083.7 2708
Data Reduction for Missile Telemetering—E. M. McCormick. (*Electronics*, vol. 28, pp. 126–130; May, 1955.) Fm/fm telemeter signals recorded on magnetic tape produce a pulse train proportional to the original function which is recorded on punched cards for processing.

621.317.39:531.714.7 2709
Design Criteria for Mutual-Inductance Transducers—(*Tech. Bull. Nat. Bur. Stand.*, vol. 39, pp. 36–37; March, 1955.) Developments in the design of Greenough's electronic micrometer (1129 of 1948) are embodied in a series of recommendations. The reference plate should be as nearly a perfect conductor as possible; the primary coil should be as large as possible and should be coplanar with the secondary coil, or should be the further of the two from the reference plate; leads to the coils should be shielded from one another; excitation frequency should be as high as possible.

621.317.39:531.78:537.228.1 2710
Piezoelectrical Measurement of Force—H. H. Rust and J. Krohn. (*Z. angew. Phys.*, vol. 7, pp. 61–67; February, 1955.) The charge which appears on a stressed quartz plate is converted into an alternating voltage by means of a variable capacitor comprising a modified telephone receiver vibrating at a few tens of cycles per second. The theory and the electrical and mechanical design are discussed. If no corrections are made, the error in the determination of force over a period of 30 seconds is about 2.5 per cent. Forces down to 0.01 pond (9.81 dynes) can be measured.

621.317.39:621.317.755:621.43 2711
A Versatile Electronic Engine Indicator—R. K. Vinycomb. (*Jour. Brit. I.R.E.*, vol. 15, pp. 235–246; May, 1955.) Trolley-mounted cro equipment is described, for use with several types of transducer, permitting a wide range of measurements.

621.384.622:621.385.833 2712
Lateral Stabilization of the Ion Beam in a Linear Accelerator by Grid-Type Electrostatic Lenses—M. Y. Bernard. (*Compt. Rend. Acad. Sci.* (Paris), vol. 240, pp. 1636–1638; April 18, 1955.)

621.385.833 2713
Recent Developments in Electron Microscopy—V. E. Cosslett. (*Research* (London), vol. 8, pp. 48–56; February, 1955.) Advances in lens design, the production of commercial instruments, and techniques for the preparation of specimens are reviewed. 51 references.

621.385.833 2714
A Reflexion Electron Microscope—V. E Cosslett and D. Jones. (*Jour. Sci. Instr.*, vol. 32, pp. 86–91; March, 1955.) Description of apparatus for examining solid surfaces illuminated by an electron beam at grazing incidence; magnification is continuously variable from ×500 to ×10,000.

621.385.833 2715
Two New Simplified Systems for the Correction of Spherical Aberration in Electron Lenses—G. D. Archard. (*Proc. Phys. Soc.* (London), vol. 68, pp. 156–164; March 1, 1955.)

621.385.833 2716
Precise Determination of Cardinal Elements in Strongly Converging [electron] Lenses—M. Y. Bernard. (*Compt. Rend. Acad. Sci.* (Paris), vol. 240, pp. 1612–1614; April 13, 1955.)

621.396.934 2717
Information required for Missile Guidance—F. P. Adler. (*Jour. Appl. Phys.*, vol. 26, p. 492; April, 1955.) Calculations and discussion indicate that the amount of information and the information rates required for guiding a missile are quite small, so that it should be possible to guide it by talking to it slowly.

PROPAGATION OF WAVES

538.566+534.2 2718
Note on the Propagation of Normal Modes in Inhomogeneous Media—I. Tolstoy. (*Jour. Acous. Soc. Amer.*, vol. 27, pp. 274–277; March, 1955.) Analysis is presented for propagation in ducts with stratified media.

538.566.029.4 2719
More Exact Theory of Propagation of Long Electric Waves around the Earth—J. Weidner. (*Z. angew. Phys.*, vol. 7, pp. 77–82; February, 1955.) Schumann's simplified approximation (802 and 1772 of 1953) to the general solution given by Watson (*Proc. Roy. Soc. A*, vol. 95, pp. 546–563; July 15, 1919) is made more exact by means of an extension to two terms. The formula for the effective field strength is valid in the wavelength range from 40 to 180 km, breaking down for $\lambda < 40$ km and changing into Schumann's formula for $\lambda > 180$ km. Field-strength/distance curves are given for 40 and 130 km λ, and field-strength/wavelength curves for distances of 5,000, 7,500 and 10,000 km.

621.396.1.029.63:621.397.5 2720
U.H.F. Television Broadcasting—Smith-Rose and Saxton. (*See* 2762.)

621.396.11 2721
Doppler Spectrum of Sea Echo at 13.56 Mc/s—D. D. Crombie. (*Nature*, (London), vol. 175, pp. 681–682; April 16, 1955.) A typical record of the Doppler frequency shift of radio waves reflected from the sea surface shows the frequency of the principal component to be about 0.38 cps, irrespective of the state of the sea, and the range of frequencies to be small. An explanation of these features is presented based on the diffraction-grating effect due to the sea waves.

621.396.11:523.78 2722
Some Observations in Bratislava during the Solar Eclipse on 30th June 1954.—Šimaljak and Milerová. (*See* 2609.)

621.396.11:551.510.535 2723
Determination of the Energy Paths of a Wave propagated in the Ionosphere. Study of Two Particular Cases (Transparent Medium)—É. Argence. (*Ann. géophys.*, vol. 10, pp. 249–253; July/September, 1954.) The method used gives directly the differential equations for the phase and energy paths. The case of normal incidence is discussed in detail and numerical results are given for the lateral deviation of ordinary and extraordinary rays at Freiburg and Dakar. Application of the method to propagation along the magnetic equator is dealt with briefly.

621.396.11:551.510.535 2724
Research on the Interaction and on the Self-Demodulation of Electromagnetic Waves—E. Carlevaro. (*Ricerca sci.*, vol. 25, pp. 521–531; March, 1955.) Work carried out at the Radio-Propagation and Radio-Navigation Study Centre at Naples is briefly surveyed, with particular attention to Cutolo's investigations of self-demodulation (see e.g. 1167 of 1954).

621.396.81:551.510.535:523.78 2725
On Radio Measurements at Jabalpur during the Solar Eclipse of 30th June 1954—A. K. Ghose, K. M. Roy, S. K. Gupta, S. M. Das Gupta, V. V. Sarwate, and G. K. Mithal. (*Jour. Inst. Telecommun. Engr. India*, vol. 1, pp. 20–26; March, 1955.) Measurements were made of the strength and angle of incidence of 15.17-mc signals from Moscow, and of the intensity of atmospheric noise on 0.6 mc received from the direction of the belt of totality. The observed angle of incidence indicated two-hop transmission as the normal mode, with the second point of reflection from the F layer in the shadow belt. Rapid fluctuations of field strength around the period of the eclipse are associated with transitions from double-hop to single-hop transmission and back. The direction of the downcoming ray varied more widely during the eclipse period than during the same hours on the preceding and following days, and the atmospheric noise was higher, indicating reduction of attentuation by the E layer.

621.396.812 2726
An Analysis of Within-the-Hour Fading in 100- to 1000-Mc/s Transmissions—H. B. Janes. (*Jour. Res. Nat. Bur. Stand.*, vol. 54, pp. 231–250; April, 1955.) A detailed analysis is presented of measurements made during August 1952 on transmissions from sites in the Cheyenne Mountain area and at Cedar Rapids, over paths of lengths ranging from 70 to 393 miles. Fading range is defined as the ratio in decibels of the signal levels exceeded during 10 per cent and during 90 per cent of the hour. A special study is made of the variation of fading range with time of day and with the angular distance, defined as the angle in the great circle plane between the horizon rays from the transmitting and receiving antennas as determined for a standard atmosphere. Beyond the region where diffraction is considered to be the dominant mechanism, the signal-level distributions closely resemble the Rayleigh distribution in both fading range and general shape. Deviations from the 13.4-db fading range of a Rayleigh distribution are attributed to changes in the average signal power. See also 2399 of August (Barsis et al.).

621.396.812 2727
Tropospheric Refraction of Ultrashort Waves (Diurnal Variation of Field Strength)—

O. Heer. (*Fernmeldetech. Z.*, vol. 8, pp. 129–138; March, 1955.) The fine structure of the lower atmosphere is studied using meteorological data for heights of 2, 10 and 70 m; estimates are made of the resulting refraction of radio waves. Field-strength records for the 213-km Berlin/Harz usw radio link for a period of a year are compared with values calculated from the meteorological data; the observed diurnal variations of field strength are consistent with the temperature-gradient variations, but the effect of water vapor is not clear.

621.396.812.029.55 2728

Field-Strength Measurements in the Short-Wave Band—J. Grosskopf. (*Fernmeldetech. Z.*, vol. 8, pp. 114–118; 146–152; February/March 1955.) Measurements reported previously (513 of 1954) were given in terms of receiver input voltage relative to 1 μV. An absolute method has since been developed; the receiver is calibrated from the known angle of arrival of the wave and the gain/angle-of-arrival characteristic of the rhombic antenna, the calculations being checked by measurements using an auxiliary local transmitter and auxiliary dipole transmitter and receiver antennas. Measurements of the strength of WWV 15-mc signals received at Darmstadt over a period of a year are analysed statistically in relation to the period of the sun's rotation and to the terrestrial seasons. Comparison of the measurements with values calculated by the S.P.I.M. and C.R.P.L. methods indicates that attenuation must be caused not only by D layer absorption but also by scattering at the surface of the earth and of the ionosphere.

621.396.812.3.029.55 2729

Statistical Investigations of Short-Wave Transmission Paths—W. Kronjäger and K. Vogt. (*Fernmeldetech. Z.*, vol. 8, pp. 165–167; March, 1955.) The validity of results of previous statistical investigations [513 of 1954 (Grosskopf)] is examined in the light of further measurements made at Eschborn on signals received from Daventry, Rome, Ankara, Cairo, New York, Tokyo and Buenos Aires. The distribution of field-strength obeys a log-normal law for 98 per cent of the observations. A well defined value of 6 db is found for the monthly median value of the hourly scatter, and a mean value of 15 db for the scatter of the hourly median values, independent of frequency and of path length and direction.

RECEPTION

621.376.232.2 2730

Analysis of a Broadband Detector Circuit—M. H. Brockman. (Proc. IRE, vol. 43, pp. 715–720; June, 1955.) The bandwidth of a diode AM detector with an output circuit containing resistance shunted by capacitance is increased by inserting an inductance L of appropriate value. The detection efficiency is calculated by successive approximations, assuming first an infinite and then a finite value of L.

621.396.621:621.395.623.7 2731

Stereophonic Sound Receivers—O. Limann. (*Elektrotech. Z.*, Edn B, vol. 7, pp. 75–79; March 21, 1955.) Loudspeaker arrangements used in some West-German commercial high-fidelity receivers are described. In addition to a large-diameter central moving-coil loudspeaker, smaller moving-coil loudspeakers are mounted so as to produce ellipsoidal equal-pressure surfaces at about 100 cps and 8 kc. A lf attenuator is included in the ancillary loudspeaker circuits. Experimentally determined polar sound-pressure diagrams are shown.

621.396.621.54:621.314.7 2732

A Developmental Pocket-Size Broadcast Receiver employing Transistors—D. D. Holmes, T. O. Stanley, and L. A. Freedman. (Proc. IRE, vol. 43, pp. 662–670; June, 1955.) Details are given of the construction and performance of a superheterodyne AM receiver using eight junction transistors. A single transistor acts as oscillator and mixer. The overall dimensions are $5\frac{1}{8}$ inches × $2\frac{3}{4}$ inches × $1\frac{1}{4}$ inches, and the weight is 17 oz.

621.396.621.54:621.314.7 2733

An Experimental Automobile Receiver employing Transistors—L. A. Freedman, T. O. Stanley, and D. D. Holmes. (Proc. IRE, vol. 43, pp. 671–678; June, 1955.) Details are given of the construction and performance of a superheterodyne receiver using nine Ge *p-n-p* alloy-junction transistors. The current drain, including that for two pilot lights, is about a tenth of that of a conventional receiver. Particular attention has been paid to obtaining satisfactory operation over a wide temperature range.

621.396.828 2734

Suppression of Interference—(*Elec. Times*, vol. 127, p. 411; March 10, 1955.) A note on two Statutory Instruments laid before the British Parliament on March 1, 1955 and coming into force on September 1, 1955, covering regulations to be complied with by (*a*) suppliers of refrigerators and (*b*) users of motors.

621.396.828 2735

How to suppress Radio Interference—J. D. Cooney. (*Elec. Mfg.*, vol. 54, pp. 109–128; September, 1954.) This review covers (*a*) USA regulations, (*b*) sources of interference, (*c*) measurement, and (*d*) suppression. Methods of reducing interference by means of suitable design of equipment are particularly stressed. The equipment considered includes electrical motors, switches and regulators as well as various mechanical-drive elements where interference may be produced by discharge of the large electrostatic charges built up by friction.

STATIONS AND COMMUNICATION SYSTEMS

621.376.3:621.396.822 2736

The Power Spectrum of a Carrier Frequency-Modulated by Gaussian Noise—R. G. Medhurst and J. L. Stewart. (Proc. IRE, vol. 43, pp. 752–754; June, 1955.) Critical comment on 259 of January and author's reply.

621.376.5:621.39 2737

Pulse Slope Modulation—a New Method of modulating Video Pulses and its Possible Application on Line Circuits—J. Das. (*Indian Jour. Phys.*, vol. 28, pp. 449–462; October, 1954.) Pulse-slope modulation is achieved by applying a rectangular gating pulse to an integrating circuit, the charging current to the integrating capacitor being made to vary with signal voltage. Demodulation is performed by differentiating the slope-modulated pulses and passing the resulting pulses through a memory circuit and low-pass filter. Successful transmission has been achieved over a 100-mile open-wire circuit. Signal/noise ratio and modulation linearity are satisfactory; the system may be be useful for time-division multiplex.

621.376.5:621.39 2738

Pulse Space Modulation—G. X. Potier. (*Onde élect.*, vol. 35, pp. 159–164; February, 1955.) A variation of ppm in which the position of any pulse in one channel of a multiplex system is determined by the instantaneous values of the signals in the other channels. In a given bandwidth four times as many communication channels can be accommodated as in a normal ppm system. Liability to crosstalk is eliminated by the use of storage devices.

621.376.5:621.396.41 2739

A 24-Channel Pulse-Time Modulation System—R. F. B. Speed. (Proc. IRE, part B, vol. 102, pp. 375–382; May, 1955.) A system for use with a 2-kmc/s radio link is described.

621.39.001.11 2740

On the Definition of Entropy in Information Theory—A. Tortrat. (*Ann. Télécommun.*, vol. 10, pp. 39–47; February, 1955.) From the definition of entropy based on a coordinate system representing the number of degrees of freedom, two different expressions are obtained in information theory according as the distribution considered is continuous or discontinuous. The restrictions on applying the definition generally adopted for the former case are examined and functions are discussed applicable in defining entropy when the number of parameters is infinite.

621.39.001.11 2741

Coding for Constant-Data-Rate Systems: Part 2—Multiple-Error-Correcting Codes—M. Balser and R. A. Silverman. (Proc. IRE, vol. 43, pp. 728–733; June, 1955.) Continuation of the study described previously [3674 of 1954 (Silverman and Balser)]. A simple pulse model of the system is presented which is easier to visualize than the correlation-detection scheme. The Wagner code is extended to two multiple-error-correcting schemes. The efficiency of the Wagner code is evaluated by comparing it with Shannon's ideal coding.

621.39.001.11:519.2 2742

Information, Selection, Selective Information. Is Certainty a Universal Constant?—M. Laloe. (*Ann. Télécommun.*, vol. 10, pp. 31–38; February, 1955.) Discussion, with reference to probability theory [1724 of 1952 (Woodward and Davies)], of a definition of information equivalent to entropy; selection is defined as an operation consuming information in accordance with the risk of error. By assessing a communication system on a cost/time basis results are brought into line with those of Shannon's theory.

621.394 2743

Functional-Diagram Approach to Electronics in Telegraphy—E. P. G. Wright and D. S. Ridler. (*Elec. Commun.*, vol. 32, pp. 26–42; March, 1955.) Functional diagrams developed in connection with digital computers are explained and applications to telegraph systems are illustrated. Counter, gating and trigger circuits, and applications for avoiding the effects of interference, are discussed. Error indicating and correcting systems which do not require the use of signal storage are based on the fact that a large percentage of all errors are isolated and may be corrected automatically. Such a system is described in detail. Storage systems have advantages in flexibility and control and may be desirable on economic grounds.

621.395.44 2744

Construction of the Carrier-Frequency System Z12N: a System for Short- and Long-Distance Communication—O. Schmitt, R. Stecher, and W. Zitzmann. (*Frequenz*, vol. 9, pp. 33–41; February, 1955.)

621.396 2745

The Argentine Telecommunication Network—H. B. R. Boosman. (*Commun. News.*, vol. 15, pp. 60–70; March, 1955.) A radio network for telegraph and telephone traffic is being set up for use during extensive line modernization. Hf ssb connection between Buenos Aires and the more important inland towns will be provided. There will also be zonal networks, rural networks and press and mobile maritime services.

621.396:621.376 2746

A Phase-Rotation Single-Sideband Generating System—J. R. Hall. (*RCA Rev.*, vol. 16, pp. 43–51; March, 1955.) A system is described in which a single control in one phase branch of the af modulating circuit is used to maintain the amount of sideband suppression constant when the output frequency is varied.

621.396.3/.5 (931) 2747

A Survey of Radio Progress in the New Zealand Post-Office—G. Searle. (*Radio elec. Rev.*, (Wellington, N.Z.), vol. 9, pp. 33–35, 50; February 1, 1955; vol. 10, pp. 36–39; March 1, 1955.) Text of a recent conference address outlining important developments since 1944 and covering frequency allocations and the production of crystals, and long-distance and short-distance communication services including a microwave system. Equipment operated by the Air and Marine Departments, and Post Office equipment for inspection and measurement are noted.

621.396.712 2748

Spurious Radiation from Wrotham—J. R. Brinkley. (*Wireless World*, vol. 61, p. 325; July, 1955.) Cases of unwanted radiation, particularly of third-order intermodulation products, due to direct coupling between co-sited transmitters sharing an antenna are reported. The importance of using separate antennas, suitably spaced to avoid this trouble, is emphasized. A letter from Pawley (*ibid.*, vol. 61, p. 367; August, 1955) points out that the fault discussed will not arise with the Wrotham installation in its final form.

621.396.712:621.376.3 2749

Inauguration of V.H.F.-F.M. Service in Great Britain. (*Jour. Brit. IRE*, vol. 15, pp. 269–270; May, 1955.) The station networks under construction and under consideration are briefly indicated, and some details are given of the transmitting equipment at Wrotham.

621.396.97 2750

Sound Broadcasting in North America—R. H. Tanner. (*Jour. IEE*, (London), vol. 1, pp. 341–346; June, 1955.) A survey indicating how the existing stage of development has been influenced by the earlier stages.

SUBSIDIARY APPARATUS

621–526 2751

Time-Scale and Gain Influence on Servo Performance—D. Graham and R. C. Lathrop. (*Trans. AIEE*, part II, *Applications and Industry*, vol. 73, pp. 173–178; July, 1954. Digest, *Elec. Eng., N.Y.*, vol. 73, p. 995; November, 1954.) The criterion previously applied in determining normalized transfer function coefficients (2433 of August) can also usefully be applied in the selection of optimum gain or time scale for second- or third-order servomechanisms.

621–526:519.272 2752

The Use of Correlation Techniques in the Study of Servomechanisms—T. M. Burford, V. C. Rideout, and D. S. Sather. (*Jour. Brit. IRE*, vol. 15, pp. 249–257; May, 1955.)

621–526:621.387 2753

The Dynamic Behaviour of Servomechanisms using Thyratrons—P. Bonnet. (*Onde élect.*, vol. 35, pp. 97–104; February, 1955.) If the response of the servomechanism is linear the self-inductance of the motor armature may be ignored in calculating the transfer constant of the system for discontinuous operation; in continuous operation it must be taken into account. A method of calculating the transfer function is presented for the general case of nonlinear operation, but the formulas involved are cumbersome and an experimental approach may be preferable.

621.311.6:621.314.7 2754

The Economics of the Transistor D.C. Transformer—G. Grimsdell. (*Electronic Eng.* (London), vol. 27, pp. 268–269; June, 1955.) Hv supply units using power junction transistors are compared with conventional hv sources.

621.314.63:546.824–3 2755

Electrical Properties of Titanium Dioxide Rectifiers—T. S. Shilliday and C. S. Peet. (*Elec. Mfg.*, vol. 54, pp. 102–105; September, 1954.) Results obtained are similar to those reported earlier by Breckenridge and Hosler (229 of 1953). The conversion efficiency of a Bi-TiO_2 rectifier remained constant during operation for 515 h at 125 degrees C and during most of the 320 h test at 150 degrees C, but decreased rapidly during operation at 200 degrees C, failure occurring after 60 h. The spread of the rectification characteristics of 92 Bi-TiO_2 rectifiers is presented graphically, as well as the distribution of peak dynamic current/voltage characteristics in 54 specimens.

621.316.721 2756

A Precision Direct-Current Stabilizer—M. W. Jervis. (*Proc. IEE*, part B, vol. 102, pp. 274–277; May, 1955. Discussion, pp. 277–278.) "A dc stabilizer is described which delivers 50–150 ma stable to a few parts in 10^6. A degenerative feedback system is used with a contact-modulator amplifier, self-oscillation being prevented and the frequency response improved by an auxiliary ac feedback loop. Facilities for monitoring the stability are provided."

621.316.722.1:621.3.027.3.029.5 2757

A Voltage Stabilizer for a Radio-Frequency Extra-High-Tension Set—R. B. D. Knight, K. M. Poole, and J. H. Sanders. (*Jour. Sci. Instr.*, vol. 32, pp. 134–136; April, 1955.) The voltage to be stabilized is applied across a 250-$M\Omega$ bank of resistors, and a fraction is balanced against a 120 v reference voltage, the difference being converted, in a circuit comprising two valves Type 12SA7, to a 2 kc signal which is amplified, rectified in a phase-sensitive circuit, and applied to control the screen voltage of the main oscillator. Curves show the variation with load current up to 450 μA for nominal output voltages of 7.5, 10, 15 and 20 kv.

621.316.722.1:621.311.6 2758

Heavy-Duty, High-Stability D.C. Power Supplies—D. M. Neale. (*Jour. Brit. IRE*, vol. 15, pp. 271–280; May, 1955.) "Series-valve stabilizers are considered as a simple step-by-step development of the cathode follower. By shunting a resistor or barretter across the series valve, substantially constant loads of several amperes can be stabilized to ± 0.01 per cent. . . . Full circuits are given of two typical units providing outputs of 250 and 500 watts with efficiencies of 35 and 65 per cent respectively. The latter includes a device providing audible warning when supply-voltage variations exceed the range stabilized automatically."

621.316.722.1:621.311.6.027.3:621.385.833 2759

The Use of an Electron Velocity Analyser to Stabilize a 50-kV Direct-Voltage Source to a Few Parts in a Million—M. E. Haine and M. W. Jervis. (*Proc. IEE*, (London) part B, vol. 102, pp. 265–273; May, 1955. Discussion, pp. 277–278.) A degenerative-feedback stabilizer circuit is used in which the signal to the feedback amplifier is obtained by accelerating a beam of electrons by the voltage to be stabilized and measuring the velocity by deflection in a fixed magnetic field. Much larger signals can be obtained in this way than by use of the usual resistance-type potential divider.

TELEVISION AND PHOTOTELEGRAPHY

621.397.5 2760

The 625-Line C.C.I.R. System: an Investigation by a Mobile Laboratory—D. Bauer, E. Ribchester, and G. B. Townsend. (*Jour. Telev. Soc.*, vol. 7, pp. 369–377; January/March, 1955.) Tests on a British-designed 625-line receiver were made in Holland. The results indicated that (*a*) positive modulation is preferable to negative, (*b*) a 625-line system is a useful compromise as between quality and cost, (*c*) fm is desirable provided the deviation is not less than about 50 kc, (*d*) there is little to choose between horizontal and vertical polarization, (*e*) nonsynchronous mains operation may be desirable from the point of view of international program exchanges, but may lead to more costly receivers.

621.397.5:535.623(083.71) 2761

I.R.E.Standards on Television: Definitions of Color Terms, 1955—(PROC. IRE, vol. 43, pp. 742–748; June, 1955.) This Standard, 55 IRE 22.S1, is an expanded and revised version of one presented previously (1817 of 1953).

621.397.5:621.396.1.029.63 2762

U.H.F. Television Broadcasting—R. L. Smith-Rose and J. A. Saxton. (*Wireless World*, vol. 61, pp. 343–346; July, 1955.) From experimental evidence it is inferred that in mixed urban and rural areas a range of 60 km obtained on a frequency of 50 mc will be reduced to 30 km on 500 mc for equal effective radiated power, or to 36 km with a tenfold increase in power; the type of polarization of the radiated waves does not affect the received field strength.

621.397.5:[778.5+621.395.625 2763

A Short History of Television Recording—A. Abramson. (*Jour. Soc. Mot. Pict. & Telev. Eng.*, vol. 64, pp. 72–76; February, 1955.) A review of past and present techniques including notes on magnetic recording systems for monochrome and color television and the application of television techniques in kinematography.

621.397.5:778.5 2764

Recording Television Pictures on Cinematograph Film—R. Theile and A. Brosch. (*Arch. elekt. Übertragung*, vol. 9, pp. 141–154; March, 1955.) Known methods for operating with continuous or intermittent film motion are discussed and their suitability for operation with different television standards compared. An experimental arrangement for suppressed-frame recording on 16-mm film is described; this uses spot wobbling to eliminate the line structure revealed by blanking out alternate frames. In considering the further development of recording systems, attention is directed to the advantages of picture storage with long-persistence fluorescent screens, and of medium-fast pull-down with intermittent film motion.

621.397.6 2765

Combat Television—E. L. Scheiber and H. C. Oppenheimer. (*Jour. Soc. Mot. Pict. & Telev. Eng.*, vol. 64, pp. 129–132; March, 1955.) Requirements for a transportable television unit for military operations are discussed. Successful demonstrations staged in 1954 using standard broadcast-type and airborne equipment showed 525 line definition to be adequate.

621.397.6:535.317.001.4 2766

Equipment for Evaluating Lenses of Television Systems—E. Hutto, Jr. (*Jour. Soc. Mot. Pict. & Telev. Eng.*, vol. 64, pp. 133–136; March, 1955.) Description of a test bench with cro equipment for rapid determination of the response of lenses, of focal length up to 24 inches, at different apertures and field angles.

621.397.6:621.397.8 2767

Control of [brightness] Levels in Television Transmission Installations—W. Dillenburger. (*Frequenz*, vol. 9, pp. 42–49; February, 1955.) Brightness control in a negative-modulation system is discussed in which the black level is kept constant both at the transmitter and the receiver and the white level is controlled by agc. This produces less distortion of brightness

gradation than a limiter system. A suitable circuit is given.

621.397.6.001.4 2768
Testing International Television Transmission Lines—J. Müller and E. Demus. (*Fernmeldetech. Z.* vol. 8, pp. 141–143; March, 1955.) Procedure and equipment developed in Germany for testing the performance of television links under operating conditions are briefly described. A sawtooth voltage is used for adjusting levels and checking linearity, and a square-wave voltage for testing transient response.

621.397.6.001.4 2769
Video-Frequency Signal-Level Measurements on Television Transmissions—H. Bödeker. (*Fernmeldetech. Z.*, vol. 8, pp. 143–145; March, 1955.) Cro equipment and procedure developed by the Federal German Post Office are described. The voltages under test are compared with an adjustable known direct voltage by rapid commutation.

621.397.62:535.623 2770
Simplified RCA Color Receiver—W. H. Buchsbaum. (*Radio and Telev. News*, vol. 53, pp. 37–39; 124; March, 1955.) The circuits used in this 28-valve television receiver are briefly described, with emphasis on new features. Circuit diagrams given include one of the double-triode demodulator which supplies the color-difference voltages to the 21-inch three-gun cr tube.

621.397.621.2:535.623:621.385.832 2771
Development of a 21-Inch Metal-Envelope Color Kinescope—H. R. Seelen, H. C. Moodey, D. D. VanOrmer, and A. M. Morell. (*RCA Rev.*, vol. 16, pp. 122–139; March, 1955.) The Type-21AXP22 shadow-mask tube is described in some detail.

621.397.621.2:535.623:621.385.832 2772
Deflection and Convergence of the 21-Inch Color Kinescope—M. J. Obert. (*RCA Rev.*, vol. 16, pp. 140–169; March, 1955.) Details are given of the deflection and convergence systems for the Type-21AXP22 tube. The method used to investigate the field distribution of the deflection yoke is described. Typical performance data are presented.

TRANSMISSION

621.396.61:621.373.42 2773
A Variable-Frequency Drive of High Stability for Aircraft Use—T. T. Brown. (*Marconi Rev.*, vol. 18, pp. 8–20; 1st Quarter, 1955.) Difficulties in the design of aircraft transmitters, due to exacting physical conditions, are overcome by an equipment in which the output of an *LC* oscillator is mixed with that of an 11-step crystal oscillator and followed by a frequency multiplier to give a range of 2–12 mc. The first models produced had an average temperature coefficient of ± 2 parts in 10^6 per degree C over the temperature range -40 degrees C to $+55$ degrees C. The tuning scale enables frequencies to be set with an error of the order of 1 part in 10^4. Production of spurious frequencies in the mixer stage is reduced by the choice of appropriate frequency ratios and other precautions.

621.396.66:621.316.726 2774
Automatic Frequency Control for Centimetre-Wave Communication Transmitter—J. Cayzac. (*Onde élect.*, vol. 35, pp. 151–158; February, 1955.) Two resonant cavities tuned to symmetrically offset frequencies are sampled alternately by a crystal detector whose output provides a control voltage for maintaining, to an accuracy of one part in 10^5 the frequency of the oscillator, which may be either frequency or amplitude modulated. The frequency-determining and -correcting elements may be mounted together in a position remote from the power-consuming parts of the system.

TUBES AND THERMIONICS

621.314.63 2775
A Possible Explanation of Flicker Effect in Crystal Rectifiers—N. Nifontoff. (*Compt. Rend. Acad., Sci.*, (Paris), vol. 240, pp. 1695–1697; April 25, 1955.) An explanation consistent with experimental results obtained previously (1047 of 1953) is based on fluctuations of currents across the potential barrier due to generation and recombination of carriers. See also 2643 above.

621.314.63:537.311.33 2776
Rectifiers with *p-i-n* or *p-s-n* Structure under D.C. Loading—A. Herlet and E. Spenke. (*Z. angew. Phys.*, vol. 7, pp. 99–107; 149–163; 195–212; February/April, 1955.) Rectifiers with an intrinsic-conduction intermediate layer (*p-i-n*), discussed earlier by Prim (2689 of 1953), and those with a "soft" intermediate layer (*p-s-n*), having an impurity-introduced carrier concentration of the order of 10^{-3} times that of the *n* or *p* layers, are considered theoretically with particular reference to their behavior under conditions of no-load, light forward or blocking load, and heavy blocking load. The *p-i-n* type is considered to be a physically unattainable limiting case.

621.314.63:546.28 2777
A Method of making Silicon Junction Diodes—J. W. Granville. (*Brit. Jour. Appl. Phys.*, vol. 6, p. 109; March, 1955.) Brief details are given of a *p-n* junction diode made by oxidizing the surface of a Si crystal, pressing a probe of suitable material on to the oxide layer, and passing a short pulse pulse of large amplitude through the contact so that the oxide layer is pierced and the probe is welded to the crystal.

621.314.63:621.396.822 2778
Experimental Confirmation of the Schottky Noise Formulae for Recently Developed Semiconductor Junction Diodes over the White-Noise [frequency-independent noise] Spectrum—W. Guggenbühl and M. J. O. Strutt. (*Arch. elekt. Übertragung*, vol. 9, pp. 103–108; March, 1955.) Formulas for the available noise power, derived from Schottky's equation for the saturated thermionic diode, on the assumption of two uncorrelated noise currents associated respectively with forward and reverse junction currents, are found to be valid for the frequency range from about 1 kc upwards over which the noise is frequency independent. Measurements are reported of the current dependence and frequency dependence of noise in point-contact and junction diodes; the difference between the frequency dependent characteristic at low af and the frequency independent characteristic at the higher frequencies is observed.

621.314.7 2779
Stabilizing Transistors Against Temperature Variations—S. Sherr and T. Kwap. (*Tele-Tech.*, vol. 14, pp. 74–76; 147; March, 1955.) Application of direct-coupled feedback enables the operating temperature range of transistors to be extended by as much as 40 degrees C.

621.314.7 2780
Diffusion Capacitances and High-Injection-Level Operation of Junction Transistor—T. Misawa. (PROC. IRE, vol. 43, pp. 749–750; June, 1955.) Calculations are made of the diffusion capacitances. Even at high injection level the ratio of collector-junction diffusion capacitance to depletion-layer capacitance serves as a measure of injection level.

621.314.7 2781
Delayed Collector Conduction, a New Effect in Junction Transistors—M. C. Kidd, W. Hasenberg, and W. M. Webster. (*RCA Rev.*, vol. 16, pp. 16–33; March, 1955.) Examination of the family of I_c/V_c characteristics of junction transistors for a wide range of values of base current I_b indicates that, in the regions where I_b exerts a blocking influence on emitter current, collector current cannot flow until collector voltage reaches a certain value; this is the "delayed collector conduction" effect. The I_c/V_c characteristic rises steeply, with positive slope over part of the region and negative slope over the remainder. The transistor then has high input impedance and low output impedance. Theory of the effect is discussed and applications in amplifiers, voltage regulators and switching devices are described.

621.314.7:537.311.33 2782
Comparative High-Frequency Operation of Junction Transistors made of Different Semiconductor Materials—L. J. Giacoletto. (*RCA Rev.*, vol. 16, pp. 34–42; March, 1955.) Discussion indicates that mobilities of minority and majority carriers have about equal influence on the high-frequency performance of junction transistors; hence the *n-p-n* type should give about the same performance as the geometrically identical *p-n-p* type. The suitability of semiconductors for use in transistors can be assessed in terms of a figure of merit given by the product of the two drift mobilities divided by the square root of the dielectric constant.

621.314.7:621.375.4 2783
Transistor Circuit Analysis—B. Millar. (*Wireless Engr.*, vol. 32, p. 196, July, 1955.) Formulas for the operating impedances are derived from consideration of the equivalent circuits for earthed-base, earthed-emitter, and earthed-collector amplifiers.

621.314.7.001.4 2784
The Measurement and Display of the Current Gain (α) of a Transistor as a Function of Emitter Current—R. A. Hilbourne. (*Jour. Sci. Instr.*, vol. 32, pp. 83–85; 87; March, 1955.) Cro apparatus is described, with particular reference to the amplifier bandwidth requirements for the accurate display of the rapid variations of α.

621.383 2785
Calculation of Radiant Photoelectric Sensitivity from Luminous Sensitivity—R. W. Engstrom. (*RCA Rev.*, vol. 16, pp. 116–121; March, 1955.)

621.383.2:537.311.33 2786
Variation of the Conductivity of the Semitransparent Cesium-Antimony Photocathode—W. Widmaier and R. W. Engstrom. (*RCA Rev.*, vol. 16, pp. 109–115; March, 1955.) The response of photocells with this type of cathode may be limited at low and even at normal temperatures by the resistance of the cathode. The conductivity falls while the cell is out of use but recovers during operation.

621.385.001.4 2787
An Inflection-Point Emission Test—E. G. Hopkins and K. K. Shrivastava. (PROC. IRE, vol. 43, pp. 707–711; June, 1955.) A rapid method of testing tubes is described in which a single triangular current pulse is passed through the tube and the anode voltage is differentiated twice; the time taken for the second differential to reach zero is indicated on a meter calibrated to give a direct reading of the inflection-point emission. In the experimental equipment used, the pulse current varied at a rate of 4 A/ms. It is suggested that tests of this type would be useful for investigating emission variations during operation, even if the particular tube has no definite inflection point at the normal operating temperature of the cathode.

621.385.001.4 2788

Subminiature-Tube Reliability Testing—S. Bickel. (*Elect. Commun.*, vol. 32, pp. 11–18; March, 1955.) Description of acceptance tests on tubes used in applications such as guided missiles where mechanical stresses are high. In the vibration test tubes are subjected to an acceleration of 15*g*, at 40 cps. Emphasis is placed on microscope inspection, and a series of photographs shows typical faults detected in this way.

621.385.002.2 2789

Thermionic Valves of Improved Quality for Government and Industrial Purposes—E. G. Rowe, P. Welch, and W. W. Wright. (*Proc. IEE*, (London) part B, vol. 102, pp. 343–357; May, 1955. Discussion, pp. 357–363.) Reliability requirements of tubes for computers, aircraft equipment, etc. are discussed. Work done on the design of tubes to give trouble-free service under conditions of vibration and shock is described. Future trends are outlined. 102 references. For a short progress report see also *Wireless World*, vol. 61, pp. 18–20; January, 1955.

621.385.029.6 2790

Backward-Wave Oscillators—H. R. Johnson. (PROC. IRE, vol. 43, pp. 684–697; June, 1955.) " The Pierce traveling-wave tube theory is modified to apply to the backward-wave oscillator. Theoretical dependence of both starting current and frequency upon space charge and circuit loss is calculated, as is the dependence of efficiency upon these parameters. Good experimental confirmation is obtained with two tubes, one of which was of adjustable length. Pushing, pulling, stability, frequency gaps, and spurious oscillations are described and explained. Lack of oscillation at low-voltage end of tuning range of some tubes is tentatively assigned to a velocity-distribution effect."

621.385.029.6 2791

Amplification of the Traveling-Wave Tube at High Beam Current—S. Olving. (*Chalmers tek. Högsk. Handl.*, no. 157, 11 pp., 1955. In English.) A method for evaluating the gain explicitly as a function of the tube parameters is based on solutions of the equation for the wave propagation constants involving asymptotic expansions of the modified Bessel functions for large arguments. The solutions are valid only when the beam circumference is large compared with the axial wavelength. When the beam is in step with the unperturbed helical wave, the gain is $\propto i_0^{1/3}$ for small values of beam current i_0; as i_0 increases the gain becomes independent of its value over a wide range; for high values of i_0 the gain is $\propto i_0^{-1/2}$. This result is compared with that of Friedman (2579 of 1951).

621.385.029.6:621.317.329 2792

A Proposed Method of investigating the Field Distribution in a Magnetron—A. W. Aikin. (*Jour. Sci. Instr.*, vol. 32, p. 152; April, 1955.) A rotating cathode is fitted with a disk at each end, and two thin fibres stretched between the disks support a small dielectric needle of high permittivity. The deviation of the resonance frequency of the cavity is proportional to the square of the component of electric field strength in the direction of the needle. A complete plot can be made of the field in the anode bore.

621.385.029.6:621.318.2 2793

Optimum Design of Periodic Magnet Structures for Electron-Beam Focusing—K. K. N. Chang. (*RCA Rev.*, vol. 16, pp. 65–81; March, 1955.) Design curves are given for ring magnets combining low weight with maximum focusing effect. Results of some measurements are compared with calculated data.

621.385.029.6:621.396.822 2794

Correlation Conditions for the Shot Effect—H. W. König. (*Arch. elekt. Übertragung*, vol. 9, pp. 109–116; March, 1955.) The experimental results obtained by Cutler and Quate on noise in electron beams (1274 of 1951) have been interpreted on the assumption that under space-charge conditions there are uncorrelated noise contributions due to a velocity fluctuation and a current fluctuation at the potential minimum. This view cannot be reconciled with the theory developed by Rack (*Bell Syst. Tech. Jour.*, vol. 17, pp. 592–619; October, 1938). Better agreement is established on the assumption of partial correlation between the two contributions. A value is determined for the real part r of the complex correlation factor. The product of maximum and minimum noise-current values investigated by Pierce (304 of January) is independent of r but is dependent on the imaginary part of the correlation factor.

621.385.029.6:621.396.822 2795

Theory of Frequency-Modulation Noise in Tubes employing Phase Focusing—J. L. Stewart. (*Jour. Appl. Phys.*, vol. 26, pp. 409–413; April, 1955.) Discussion of noise resulting from fluctuations in magnetron oscillation frequency due to random distribution of electron velocities. The noise bandwidth is estimated. The theory is applied to a particular wide-band magnetron.

621.385.029.63 2796

A Medium-Power Travelling-Wave Tube for 2,000 Mc/s—R. B. Coulson and F. N. H. Robinson, (*Marconi Rev.*, vol. 18, pp. 48–59; 2nd Quarter, 1955.) Description of design and construction of valve Type N1001. Low-level gain is >40 db with an operating voltage of 2200 V and 40 ma beam current; saturation output power is 20 w, with 2600 v.

621.385.032.21 2797

Field Emission from Rhenium: Emission Pattern corresponding to Hexagonal Crystal Structure—G. Barnes. (*Phys. Rev.*, vol. 97, pp. 1579–1583; March 15, 1955.) Initial results are reported of a study of rhenium needle-shaped cathodes. Some advantages over tungsten are noted.

621.385.032.213 2798

Ionic Bombardment Heating of Magnetron Cathodes—A. E. Barrington. (*Brit. Jour. Appl. Phys.*, vol. 6, pp. 96–98; March, 1955.) A method is described in which hydrogen from a heated replenisher, consisting of an indirectly heated Ni pellet coated with a suspension of zirconium hydride, is introduced into the tube. A low-pressure gas discharge is initiated and the cathode is heated by positive-ion bombardment. When the cathode temperature reaches the level required for operation, the hydrogen is reabsorbed by the replenisher.

621.385.032.216 2799

On the Electron Bombardment Effect for Deposited Barium Oxide Films—T. Imai. (*Jour. Phys. Soc.* (Japan), vol. 9, p. 1037; November/December, 1954.) Correction to paper abstracted in 2819 of 1954.

621.385.032.216 2800

On the Electron Bombardment Effect for Deposited Barium Oxide Films: Part 2—T. Imai and Y. Mizushima. (*Jour. Phys. Soc.* (Japan), vol. 9, pp. 1032–1034; November/December, 1954.) Continuation of work reported previously [2819 of 1954 (Imai)]. The film containing an extremely small quantity of free Ba showed a large increase in emission under bombardment, while the film containing a large quantity of free Ba showed a marked tendency to deactivation. The temperature effect and its inhibition are also considered.

621.385.032.216 2801

Effect of the Base Metal on the Electron Dissociation of Deposited Barium Oxide Films—T. Imai and N. Shibata. (*Jour. Phys. Soc.* (Japan), vol. 9, pp. 1034–1035; November/December, 1954.) Measurements were made on films deposited on Ti and Ni anodes under electron-bombardment. A greater evolution of gas and higher rate of release of Ba atoms were observed from the Ti anode.

621.385.2+621.385.029.6 2802

Electron Temperature in the Parallel Plane Diode—T. N. Chin. (*Jour. Appl. Phys.*, vol. 26, pp. 418–423; April, 1955.) Analysis is based on introduction of a relaxation time defined previously in work on stellar clouds. The electron flow is designated as isotropic if the relaxation time t_R is very much smaller than the mean electron transit time t_T and anisotropic if $t_T \ll t_R$. Equations are derived expressing the velocity dependence of the electron temperature for both types of flow; in the parallel plane diode the electron temperature along the flow decreases as the mean electron velocity increases. The theory is applied to the case of a travelling-wave-tube under conditions assumed by Parzen and Goldstein (2580 of 1951).

621.385.3.032.24.029.6 2803

Producing Formed and Inside-Out Grids for U.H.F. Pencil Tubes—H. J. Ackerman. (*Electronics*, vol. 28, pp. 270–278; May, 1955.) To ensure that the grid-cathode spacing is not limited by the thickness of the supports, the grid wires are either formed against an internal mandrel so as to encircle the supports, or else wound directly on the mandrel with the supports placed outside.

621.385.832+621.383.2 2804

An Electron Tube for High-Speed Teleprinting—W. H. Bliss and J. E. Ruedy. (*RCA Rev.*, vol. 16, pp. 5–15; March, 1955.) The tube described combines features of the image converter with those of the ordinary cr tube, and simulates electronically the operations of selecting type characters from a font and arranging them in lines. The characters are on a slide which is projected on to the photoemissive cathode and reproduced on a fluorescent screen which can be photographed. The cross-sectional region of the beam corresponding to a desired character is selected by magnetic deflection controlled by a coded input; a second deflection system controls the arrangement of the characters on the screen. A line of 150 characters is considered feasible.

621.387:537.531 2805

X-Ray Emission from High-Voltage Hydrogen Thyratrons—S. Schneider and B. Reich. (PROC. IRE, vol. 43, pp. 711–715; June, 1955.) Beam pattern, energy and intensity are investigated for the X rays emitted by three types of thyratron during the breakdown of pulses and as a result of grid emission between pulses.

621.387:621.318.57 2806

Reversible Dekatron Counters—Branson. (*See* 2550.)

MISCELLANEOUS

413-20-50 2807

Technical Dictionary English-Italian Italian-English. [Book Review]—G. Marolli. Publishers: F. Le Monnier, Florence, 1954, 5th edn revised and extended, 1075 pp., 7500 L. (*Alta Frequenza*, vol. 24, pp. 86–87; February, 1955.)

621.3.049.7 2808

Automation at Work in Production of Electronic Equipment—(*Elec. Jour.*, vol. 154, pp. 1848–1850; June 10, 1955.) A description of the National Bureau of Standards Tinkertoy production system. See also 693 of 1954 (Henry and Rayburn).